

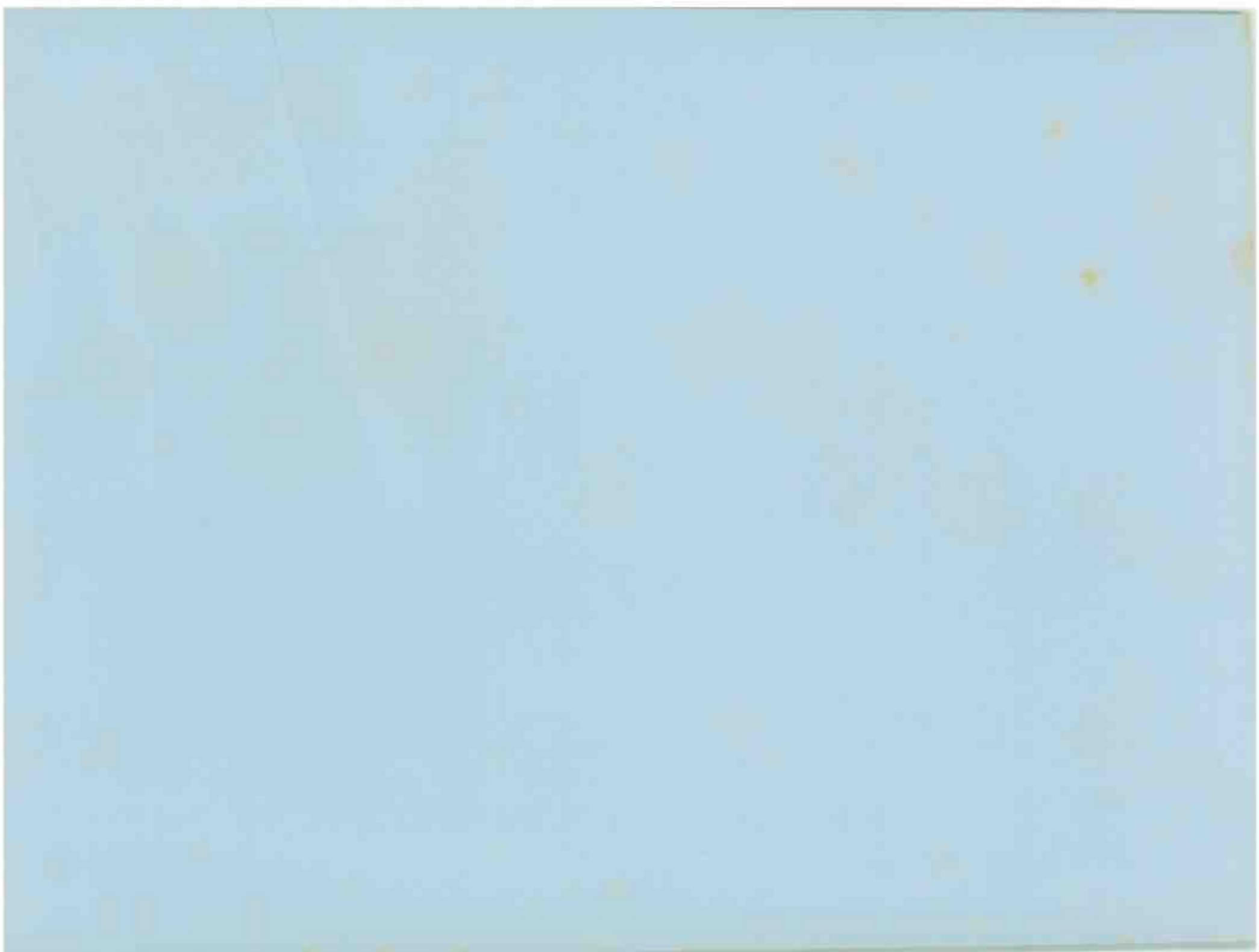
Proceedings

RF expo

EAST

*November 13-15, 1990
MARRIOTT's
Orlando World Center
Orlando, Florida*

Sponsored by
RF design
Magazine



Alan Victor
11-13-90
RF 8000
burst

Proceedings

RF expo --- ***EAST*** *November 13-15, 1990* *MARRIOTT's* *Orlando World Center* *Orlando, Florida*

Copyright © 1990 by
Cardiff Publishing Company
All rights reserved.

RF design

6300 S. Syracuse Way
Suite 650
Englewood, Colorado 80111

TABLE OF CONTENTS

Session A-1 - Receivers I (Tutorial) Chair: Peter Chadwick, Plessey Semiconductor

Design of Receivers for Electronic Warfare
Sherman R. Vincent, Raytheon.....1

Session A-2 - Power Amplifiers Chair: Stephen J. Samay, Trontech Corp.

VSWR Performance of Transistor RF Power Amplifiers
Richard W. Brounley, RF Engineering Consultant.....41

A Novel Technique for Analyzing High-Efficiency
Switched-Mode Amplifiers
Kazimierz "Kai" Siwiak, Motorola.....49

RF Power Transistors for 200-W Multicarrier
Cellular Base Stations
Korne Vennema, Philips Components.....57

Session A-3 - PLLs and Synthesizers Chair: Rob Gilmore, QUALCOMM, Inc.

The "Approximation Method" of Frequency Synthesis
Albert D. Helfrick, Consulting Engineer.....67

Ten-bit 350-MHz DAC for Direct Digital Synthesis
Perry Jordan, Analog Devices.....73

A Comparison of Techniques for Phase-Stability Measurement
Lisa M. Moder, Erbtec Engineering.....81

Session A-4 - Microwaves Chair: Robert M. Livingston, Rockwell International

System Design Considerations for Line of Sight
Microwave Radio Transmission
George M. Kizer, Rockwell International.....89

Phase Shifter Based Upon Reflectively Terminated
Multi-Port Coupler
M. H. Kori, Centre for Development of Telematics.....119

Instrumentation for Radar Reflectivity Measurement
D. J. Kozakov, C. W. Sirles, R. S. Banks,
and D. A. Thompson, Millimeter Wave Technology.....125

Session B-1 - Receivers II (Spread-Spectrum) Chair: David Krautheimer, RHG Electronics Laboratory

Spread Spectrum Design Using Digital ASICs
Robert J. Zavrel, Jr., Gwyn Edwards, and David Tahmassebi,
Stanford Telecommunications.....131

GPS and GLONASS Spread-Spectrum Navigation Systems
James Danaher, Structured Systems.....141

Detection and Sorting of Frequency-Hopped Signals
Eric Dunn and Steve Russell, Iowa State University.....157

Session B-2 - MMICs Chair: Sheryl S. Johnson, Motorola

Ku-band MMIC Transceiver for Mobile Satellite Communication
Rob Gilmore, Clarence Bruckner, and Doug Dunn, QUALCOMM.....169

Silicon MMICs: 35 dB - 35 dBm - \$35
T. E. Boles and D. Osika, SGS-Thomson.....179

Some Design Considerations for L-band Power MMICs
Robert J. Weber, ISU Microelectronics Research Center.....187

Session B-3 - Filters Chair: Maura Fox, Thomson-ICS

Capabilities and Applications of SAW Coupled-Resonator Filters
Allan Coon, RF Monolithics.....201

At Long Last; Modular, Digitally Tuned RF Filters
as Easy as Amplifiers and Mixers
Eugene A. Janning, Pole-Zero Corp.....215

Narrowband SAW Filters for IF Applications
B. Horine and S. Gopani, Sawtek.....227

Session B-4 - Antennas and Propagation

Chair: Alan Victor, Monicor Electronics Corp.

Large Loop Antennas
R. P. Haviland, MiniLab Instruments.....243

VHF Multipath Propagation: Causes and Cures
D. R. Dorsey, Jr. DocSoft Enterprises.....255

Radio-Frequency Identification Systems --
Industrial and Commercial Applications
James Eagleson, Allen-Bradley.....273

Session C-1 - Receivers III (Digital)

Chair: Madjid A. Belkerdid, University of Central Florida

IF Frequency-Response Considerations for the Digital-Radio Environment
Richard D. Roberts, Harris Corp., GCSD,
and Mark A. Webster, Florida Institute of Technology.....285

DSP Demodulation
Steve F. Russell, Iowa State University.....293

A DSP PSK Modem for SATCOM SCPC Data/Voice
Y. S. Rao, R. Asokan, and K. Reeta,
C-DOT Telecom Research Centre.....303

Session C-2 - Transmitters

Chair: Michael B. Steer, North Carolina State University

High Efficiency RF Power Amplifier Combiner With
Integrated Adaptive Interference Canceler
Paul F. Finman, LCF Enterprises.....311

Digital Feedback Techniques for a Pulse-Width-Modulated
RF Power Amplifier
Harry Direen, Ehrhorn Technological Operations.....319

High-Frequency, High-Power Operation of Static Induction
Transistors at Cryogenic Temperatures
M. Abdollahian, R. Regan, S. Butler, R. Gage,
and E. Bulat, GTE Laboratories.....331

Session C-3 - SAW Tutorial

Chair: James Yolda, U. S. Army Center for Signals Warfare

Surface Acoustic Wave (S.A.W.) Technology
Carl A. Erikson, Jr., Oakmont Enterprises, Messiah College.....341

Session C-4 - RF Systems for Research in Particle Physics

Chair: Otward Mueller, General Electric Company

Overview of RF Systems for the Advanced Photon Source
J. F. Bridges, Argonne National Laboratory.....367

RF Applications in Particle Accelerators
C. Hovater and R. Abbott, Continuous Electron Beam
Accelerator Facility.....405

A Fully Digital RF-Signal Synthesis and Phase Control
for Acceleration in the Cooler Synchrotron COSY
P. Shirkey, H. Meuth, and H. Rongen,
Forschungszentrum KFA Julich.....417

Session D-1 - Receivers IV (Applications)

Chair: Mahesh Kumar, AEL

Dynamic Evaluation of High-Speed, High-Resolution
D/A Converters
James Colotti, CSD/Telephonics.....427

A High Performance Low Cost T.V. Demodulator
Paulo R. M. A. Correa (BRAZIL).....439

Digital-Signal-Processing-Based Spectrum-Monitoring System
Used for the European Broadcasting Area
Istvan Novak, Design Automation/Technical Univ of Budapest.....449

Session D-2 - Components

Chair: S. M. Richie, University of Central Florida

Impedance-Matching Transformers for RF Power Amplifiers
David N. Haupt, Erbtac Engineering.....459

Temperature-Compensating Attenuators
Perry F. Hamlyn, ANZAC.....471

Useful Network Transformations in Filter Design
William B. Lurie, Consultant.....477

Session D-3 - Quartz Crystals and Applications
Chair: Murat Eron, Compact Software

Vibrational Sensitivity and Phase Noise
in Crystal Oscillators
Glenn R. Kurzenkabe, Piezo Crystal.....491

Quartz-Crystal Filters: A Review of Current Issues
M. D. Howard and R. C. Smythe, Piezo Technology.....501

Frequency Correlation of Quartz-Crystal Resonators
Bruce R. Long, Piezo Crystal.....515

Session D-4 - Modulation
Chair: Brian D. May, NASA Lewis Research Center

New Method of Linear Amplitude Modulation
Li Minggang, Gan Liangcai, and Zhang Suwen, Wuhan University.....527

4-GHz Multiplied Source
R. Daniel Balusek, Rockwell International.....533

Techniques in Voice Compression and Synthesis
Paul G. Beaty, Erbttec Engineering.....543

Session E-1 - Noise Tutorial
Chair: Michael J. Willis, Georgia Tech Research Institute

RF System Noise Basics
Frank H. Perkins, Jr., RF Monolithics.....551

RF System Noise Basics, Part II
Al Ward, AvanteK.....563

Session E-2 - CAD and Simulation
Chair: Mehdy Abdollahian, GTE

Spice Modeling and Simulation of an 800-MHz, Class-AB
Push-Pull Amplifier
Richard Y. LaLau, Mobile Data.....575

Computer Programs Design and Optimize High-Efficiency
Switching-Mode (Class E) RF Power Amplifiers
Nathan O. Sokal and Istvan Novak, Design Automation.....585

A Quasi-Linear Determination of UHF Power Device Operation
from a Spice-Simulated Nonlinear BJT Model
Pablo E. D'Anna, Microwave Modules & Devices.....613

Session E-3 - PLLs and Synthesizers II
Chair: William A. Davis, Virginia Tech

Designing with Direct Digital Frequency Synthesizers
Francisco A. B. Cercas, M. Tomlinson,
and A. A. Albuquerque, Instituto Superior Tecnico.....625

Direct-Digital Waveform Generation Using Advanced
Multi-Mode Digital Modulation
Bar-Giora Goldberg, Sciteq Electronics.....635

Optimum PLL Design for Low Phase-Noise Performance
Stanley Goldman, E-Systems, Garland Div.....641

Session E-4 - Test and Measurement
Chair: Sara Mussman, Wavetek RF Products

Design and Development of an RF Data-Acquisition System
Thomas H. Jones, Dynetics, and Madjid A. Belkerdid,
University of Central Florida.....649

Handheld Probing Techniques for RF-PCB and
Hybrid-Circuit Characterization
Young Dae Kim, Hewlett-Packard.....661

Using VXIBus-Based Products for RF Test Systems
Malcolm E. Levy, Raca-Dana Instruments.....673

BIOGRAPHIES OF THE CHAIRMEN

Program Chairman

Frederick H. Raab is President and Owner of Green Mountain Radio Research Company. He received BS, MS and Ph.D. EE degrees from Iowa State University in 1968, 1970 and 1972. Dr. Raab is coauthor of Solid State Radio Engineering and over fifty technical papers. His professional interests include RF power, communications systems, signal processing. He is a senior member of IEEE and a member of HKN, $\Sigma\alpha$ and IuA. "Fritz" is extra-class amateur radio operator WA1WLW, licensed since 1961.

Session Chairmen

Peter Chadwick (Session A-1) is a Senior Principal Engineer at Plessey Semiconductor (UK). He is the author of 23 papers, has chaired two international conferences, and has 10 patents. Mr Chadwick's professional interests include product definition, applications, and specifications. He is a member of the RSGB and is amateur radio operator G3RZP.

Stephen J. Samay (Session A-2) is an electronics engineer with Trontech Corporation. Mr Samay received his BSEE degree from Trenton State College in 1974. His professional interests include amplifiers, filters, diplexers, splitters, and combiners from HF through C band.

Rob Gilmore (Session A-3) is the Engineering Director at QUALCOMM, Inc. He received the BSEE and MSEE degrees from Massachusetts Institute of Technology in 1977. He has authored five technical publications and his professional interests include communication systems, RF/microwave systems, and synthesizers. Mr. Gilmore is a member of TB π , HKN, and $\Sigma\alpha$, and is amateur radio operator WA8YTJ.

Robert M. Livingston (Session A-4) is with Rockwell International, Collins Network Transmission Systems Division. Mr. Livingston received his BSME from Yale in 1957 and his MSEE from Rice in 1962. His professional interests include troposcatter and line-of-sight systems as well as microwave components.

David Krautheimer (Session B-1) is Director of Marketing for RHG Electronics Laboratory. He received the BSEE degree from New York Institute in 1972 and the MS in 1975 from Post (L.I.U.). his professional interests include transmitters, receivers, and components. He is the author of over twenty technical publications, a senior member of IEEE, and a member of the Association of Old Crows and AFCEA.

Sheryl S. Johnson (Session B-2) is a Product Development and Applications Engineer at Motorola in Phoenix. She received the BSEE from Arizona State University in 1982. Her professional interests include microwave power transistors and RF ICs.

Maura Fox (Session B-3) is Director of Marketing with Thomson-ICS and was previously an applications engineer at Phonon Corporation. Ms. Fox received her BSEE from the University of Maryland in 1982. Her professional interests include surface-acoustic-wave, bulk-acoustic-wave, acousto-optic, and integrated-optic technologies. She is a member of IEEE.

Alan Victor (Session B-4) is Vice President and co-founder of Monicor Electronics, which is involved in the design and manufacture of equipment for RF data communications. His BSEE and MSE degrees were received from the University of Florida and Florida Atlantic University in 1980. He holds six patents in signal generation, synthesis, and receivers and is a member of IEEE.

Madjid A. Belkerdid (Session C-1) is an Associate Professor of Electrical Engineering at the University of Central Florida. He received the BS, MS and Ph.D. EE degrees from UCF in 1978, 1980, and 1984, respectively. He is an active consultant in communication and the author of over thirty technical papers. His professional interests include RF measurement, receivers, crystal oscillators, and SAW technology. Dr. Belkerdid is a senior member of IEEE and a member of TB π and HKN.

Michael B. Steer (Session C-2) is an Assistant Professor in the Department of Electrical and Computer Engineering at North Carolina State University. He received the BE and Ph.D. from the University of Queensland (Australia) in 1976 and 1983, respectively. His professional interests include simulation and CAD of nonlinear microwave circuits and systems, delta sigma modulators, high frequency limits of transistors, microwave measurements, and simulation of high performance digital circuits. Dr. Steer has published over twenty papers, is a senior member of IEEE, and is active in the MTT Society. In 1987, he was named a Presidential young investigator.

James Yolda (Session C-3) is a Supervisory Electrical Engineer with the U.S. Army CECOM Center for Signals Warfare. He received a BSEE degree from Virginia Military Institute in 1972, an MS in Business Administration from Boston University in 1980, and an MSEE from the U.S. Naval Postgraduate School in 1983. His professional interests include spread-spectrum electronic countermeasures, electronic warfare applications for power amplifiers, transmitters, antennas, and ESM receiver technology.

Otward Mueller (Session C-4) is a Staff Member in General Electric Company Corporate Research & Development, Magnetic Resonance Imaging (MRI). He received the Dipl.-Eng. in EE from the Technical University of Munich and the Ph.D. in EE from the Technical University of Stuttgart in 1962. Dr. Mueller has authored over thirty papers and holds seven patents. His professional interests include semiconductor electronics, communication systems, RF power, NMR electronics, RF signal processing, and low-noise design. He is member of IEEE.

Mahesh Kumar (Session D-1) is Manager for Design Engineering for the Microwave Hybrid Division of American Electronic Laboratories, Inc. He received the Ph.D. EE degree from the Indian Institute of Technology in 1977. Dr. Kumar is the author of 45 technical papers, holds 14 patents, and has contributed to two books. His professional interests include MIC and MMIC components and subsystems for electronic warfare and he is a senior member of IEEE.

Sam M. Richie (Session D-2) is an Assistant Professor of Electrical Engineering at the University of Central Florida. He received his BS, MS, and Ph.D. degrees from UCF in 1980, 1983, and 1989, respectively. His professional interests include CAD for SAW filters and computer-generated imagery. He is a member of IEEE, TB π , and HKN.

Murat Eron (Session D-3) is the MMIC Activities Manager for Compact Software. He received the BSEE degree from Bogazici University on 1978, the MSEE and Ph.D. degrees from Drexel University on 1980 and 1984. He has published over a dozen papers and holds four U.S. patents. His professional interests include MMICs, GaAs/Si technology, modeling, design and development. He is an IEEE member.

Brian D. May (Session D-4) is an Electronics Engineer with NASA Lewis Research Center. He holds a BSEE from Purdue University (1982) and an MSEE degree from the University of Toledo (1986). His professional interests include satellite communications and microwaves, and he is a member of the IEEE.

Michael J. Willis (Session E-1) is a Research Engineer at the Georgia Tech Research Institute. He received the BEE and MSEE degrees from the Georgia Institute of Technology in 1981 and 1982, respectively. His professional interests include analog and RF design to 400 MHz, especially receivers and detectors. He has published three technical papers and is a member of IEEE, HKN, TB π , *K*, and the Association of Old Crows.

Mehdy Abdollahian (Session E-2) is a Member of the Technical Staff at GTE Laboratories Inc. in Waltham, Mass. He received his BSEE degree from the Wentworth Institute of Technology and his MSEE degree from the University of Lowell. Mr. Abdollahian has published five technical papers and holds one patent. His professional interests are microwave and RF amplifier and oscillator design and device modeling.

William A. Davis (Session E-3) is an Associate Professor in the EE Department at Virginia Polytech Institute and State University ("Virginia Tech"). He received his BS, MS, and Ph.D. EE degrees from the University of Illinois (Urbana) in 1969, 1970, and 1974. His professional interests include electromagnetics (numerical methods), thick-film RF hybrids, modeling of RF circuits, and S-parameter measurements.

Sara Mussman (Session E-4) is the T&M Product Line Manager for Wavetek RF Products. She received her BSEE and MSIE degrees from Purdue University in 1978 (honors program) and 1988, respectively. She holds four patents and has authored eight papers. Ms. Mussman's professional interests include digital design, software, digital applications to RF, and marketing. She is a member of IEEE, HKN, and a senior member of SWE.

The papers contained in these Proceedings represent the views of the authors and/or their employers, and have been presented by them as original works. While an attempt has been made to assure accuracy, Cardiff Publishing Company and RF Design will not be responsible for any copyright, trademark or patent infringement that may be contained in these papers.

DESIGN OF RECEIVERS FOR ELECTRONIC WARFARE

SHERMAN VINCENT
RAYTHEON COMPANY
6380 HOLLISTER AVENUE
GOLETA, CA 93117

DESIGN OF RECEIVERS FOR ELECTRONIC WARFARE

SHERMAN VINCENT
RAYTHEON COMPANY
6380 HOLLISTER AVENUE
GOLETA, CA 93117

ABSTRACT

The purpose of this tutorial is to provide an introduction to electronic warfare microwave receivers. The sophistication of the radar and weapons guidance systems requires quick detection of possible threats at the earliest stage of a military mission. Frequency, angle of arrival, amplitude, pulse width, and polarization may be measured on each received radar pulse. Collection of multiple pulses allows determination of pulse PRI and radar scan rates which leads to platform identification.

This tutorial is divided into 2 parts: a review of the characteristics of the five basic EW receiver architectures and a review of the basic analysis equations and calculations used by the EW receiver designer.

The material in this tutorial is from the presenter's experience, many technical articles, and James Baw-Yen Tsui's book Microwave Receivers With Electronic Warfare Application published by Wiley - Interscience.

The tutorial outline and a reproduction of the viewgraphs follows.

OUTLINE

- 1. RECEIVER ARCHITECTURE COMPARISON SUMMARY
 - 1.1 SUPERHETRODYNE RECEIVERS
 - 0 PRINCIPLE OF OPERATION
 - 0 MIXER INTERMODULATION PRODUCTS
 - 0 DOWNCONVERSION MIXER SPUR CHART
 - 0 MIXER THIRD ORDER TWO TONE INTERMODULATION
 - 0 PRESELECTION
 - 0 MIXER TYPES
 - 0 AM NOISE REJECTION OF MIXERS
 - 0 HOMODYNE RECEIVER
 - 0 ADVANTAGES AND DISADVANTAGES
 - 1.2 CRYSTAL VIDEO RECEIVERS
 - 0 PRINCIPLE OF OPERATION
 - 0 CVR CHARACTERISTICS
 - 0 COMPRESSION TYPES
 - 0 TRF CVR
 - 0 ADVANTAGES AND DISADVANTAGES
 - 1.3 IFM RECEIVERS
 - 0 PRINCIPLE OF OPERATION
 - 0 SINGLE CORRELATOR
 - 0 MULTIPLE CORRELATOR
 - 0 CW SIGNAL PROBLEM
 - 0 SIMULTANEOUS SIGNAL PROBLEM
 - 0 ADVANTAGES AND DISADVANTAGES
 - 1.4 CHANNELIZED RECEIVERS
 - 0 PRINCIPLE OF OPERATION
 - 0 DESIGN CONSIDERATIONS
 - 0 SINGLE LEVEL CHANNELIZED RECEIVER
 - 0 THREE LEVEL CHANNELIZED RECEIVER
 - 0 ADVANTAGES AND DISADVANTAGES
 - 1.5 COMPRESSIVE RECEIVERS
 - 0 PRINCIPLE OF OPERATION
 - 0 CHIRP AND COMPRESSIVE FILTER RELATIONSHIP
 - 0 DESIGN PARAMETERS AND TRADEOFFS
 - 0 ADVANTAGES AND DISADVANTAGES
- 2.0 RECEIVER ANALYSIS EQUATIONS
 - 0 THERMAL NOISE AND NOISE FIGURE
 - 0 OUTPUT S/N OF LIMITER
 - 0 TANGENTIAL SENSITIVITY
 - 0 FALSE ALARM RATE AND PROBABILITY OF DETECTION
 - 0 EXAMPLE OF RECEIVER SENSITIVITY CALCULATION
 - 0 THEORETICAL CALCULATION OF POST DETECTION FALSE ALARM RATE
 - 0 TWO TONE SPUR-FREE DYNAMIC RANGE AND THIRD ORDER INTERMODULATION.
 - 0 SECOND AND THIRD ORDER INTERCEPT POINTS FOR A CASCADE CHAIN OF AMPLIFIERS
 - 0 REVIEW OF MEAN VALUE, RMS, AND STANDARD DEVIATION

1. RECEIVER ARCHITECTURE COMPARISON SUMMARY

SUPERHETRODYNE RECEIVER

- o HIGH SENSITIVITY
- o WIDE DYNAMIC RANGE
- o SELECTIVITY IMPROVES SIMULTANEOUS SIGNAL PROCESSING
- o LOW POI TO LOW DUTY CYCLE SIGNALS

CRYSTAL VIDEO RECEIVER

- o SIMPLE STRUCTURE
- o SENSITIVITY AND DYNAMIC RANGE IS LOW
- o WIDE INSTANTANEOUS BANDWIDTH
- o DOES NOT PROVIDE FREQUENCY INFORMATION (UNLESS TRF IS ADDED)
- o CANNOT SEPARATE SIMULTANEOUS SIGNALS
- o HIGH POI
- o DETERMINE AOA THROUGH AMPLITUDE COMPARISON SCHEME

1

3

INSTANTANEOUS FREQUENCY MEASUREMENT RECEIVER

- o SIMPLE STRUCTURE
- o SENSITIVITY AND DYNAMIC RANGE IS LOW
- o WIDE INSTANTANEOUS BANDWIDTH
- o CAN MEASURE SHORT PULSES AND HIGH FREQUENCY RESOLUTION
- o PROBLEMS WITH CW CAPTURE AND SIMULTANEOUS SIGNAL PROCESSING

CHANNELIZED RECEIVER

- o VERY COMPLICATED STRUCTURE - MANY PARALLEL OUTPUTS
- o SENSITIVITY AND DYNAMIC RANGE IS HIGH
- o WIDE INSTANTANEOUS BANDWIDTH
- o SELECTIVITY ALLOWS PROCESSING OF SIMULTANEOUS SIGNALS
- o CAN MEASURE SHORT PULSES WITH HIGH TO MEDIUM FREQUENCY RESOLUTION

2

COMPRESSIVE RECEIVER

- o VERY HIGH SPEED ANALOG AND DIGITAL PROCESSING REQUIRED
- o WIDE INSTANTANEOUS BANDWIDTH
- o CAN PROCESS SIMULTANEOUS SIGNALS, CW, AND CHIRP

ACOUSTO-OPTIC

- o VERY COMPLICATED STRUCTURE
- o FURTHER DEVELOPMENT IS REQUIRED FOR EW APPLICATIONS

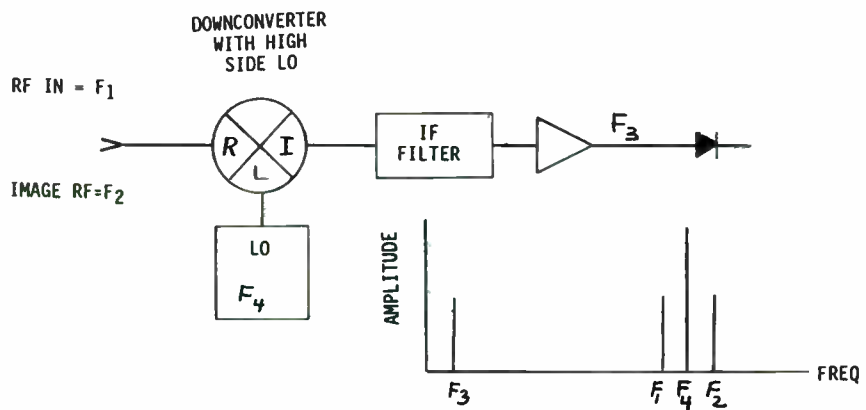
3

4

1.1 SUPERHETRODYNE RECEIVER

PRINCIPLE OF OPERATION

- o DOWN CONVERSION $F_4 - F_1 = F_3$ AND $F_2 - F_4 = F_3$



- o UP CONVERSION
 - $F_1 + F_4 = F_3$
 - IMAGE OF $F_1 = (F_1 + F_4) + F_4 = F_2$
 $= 2 F_4 + F_1$

4

MIXER INTERMODULATION PRODUCTS

- o THE MIXER IS A NON-LINEAR DEVICE, THEREFORE V_o IS REPRESENTED AS A POWER SERIES = $a_1V_1 + a_2V_1^2 + a_3V_1^3$
 - o $f_o = MF_1 + Nf_2$ o M AND N ARE INTEGERS (ANY SIGN).
 - o f_o MUST BE POSITIVE.

- o M AND N ARE +1 OR -1 FOR NORMAL MIXING.

- o THE SUM OF M AND N IDENTIFIES SPURIOUS ORDER

5

5

- o PREDICTING INTERMODULATION SUPPRESSION IN DOUBLE BALANCED MIXERS FOR RF INPUT LEVEL OTHER THAN 0 AND -10 dBm REF 3

(LO) <u>N</u>	(RF) <u>M</u>	SUPPRESSION <u>(dBc)</u>	(LO) <u>N</u>	(RF) <u>M</u>	SUPPRESSION <u>(dBc)</u>
1	1	0	3	3	2P-18
1	2	P-41	4	1	-35
1	3	2P-28	4	2	P-39
2	1	-35	5	1	-14
2	2	P-39	5	3	2P-14
2	3	2P-44	6	1	-35
3	1	-10	6	2	P-39
3	2	P-32	7	1	-17
			7	3	2P-11

FORMULAS FOR APPROXIMATING SUPPRESSION OF CERTAIN IM PRODUCTS:

$$P = P_{RF} \text{ (dBm)} - P_{LO} \text{ (dBm)}$$

DOWNCONVERSION MIXER SPUR CHART

- o PREDICT SPURIOUS FREQUENCIES AND ORDER THAT FALL IN IF PASSBAND

$$f_I = f_2 - f_1 \text{ SPUR CHART}$$

- o $f_I = f_{IF} = Mf_1 + Nf_2$

$$\frac{f_I}{f_2} = M\frac{f_1}{f_2} + N$$

6 x 6 ORDER NORMALIZED TO RF INPUT FREQ

- o FOR DOWNCONVERSION EXAMPLE

$$M = -1, N = 1 \quad F_I = -f_1 + f_2$$

$F_1 = \text{LOCAL OSCILLATOR} \quad F_2 = \text{RF INPUT}$

DOWNCONVERSION EXAMPLE WITH

LOW SIDE LOCAL OSCILLATOR

BOUNDARY CONDITIONS

FOR $f_1 \geq 0$

$$0 < \frac{f_I}{f_2} < 1 \quad \boxed{1 - \frac{f_I}{f_2} = \frac{f_1}{f_2}}$$

AND

$$0 < \frac{f_1}{f_2} < 1 \quad \boxed{\frac{f_I}{f_2} = -\frac{f_1}{f_2} + 1}$$

ASSUMES $f_1 < f_2$ $L = f_1$
 $H = f_2$

7

6

- o THE REGIONS ON THE OUTPUT LINE (H-L) WHERE THERE ARE NO LINES INTERSECTING ARE PREFERABLE SINCE THERE IS NO SPUR IN THIS REGION.

- o THE HIGHER THE ORDER OF SPURS, THE SMALLER THEIR AMPLITUDE.

- o EXAMPLE: INPUT = 450 - 550 MHz
IF = 100 MHz
BW = 10 MHz
LO = LOW SIDE, 350 ----> 450

TO FIND SPURS AT CENTER OF IF PASSBAND FOR 500 MHz INPUT:

$$\frac{L}{H} = \frac{400}{500} = 0.8$$

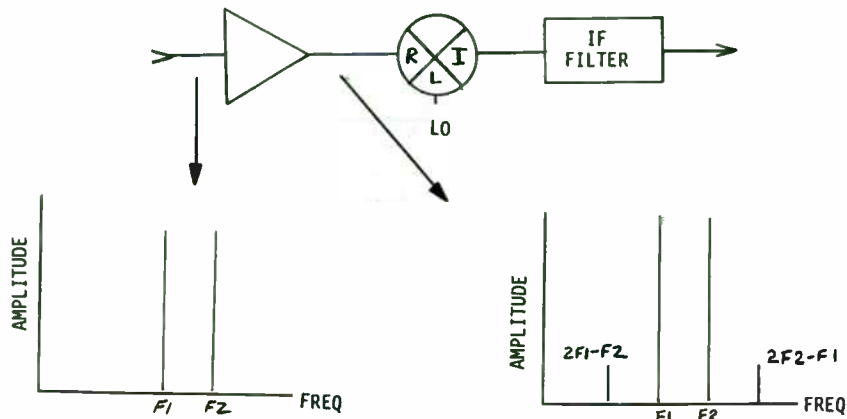
$$\frac{f_I}{H} = \frac{100}{500} = 0.2$$

$$\begin{array}{l} 5H - 6L \\ \hline 75 \text{ dBc} \end{array}$$

$$\begin{array}{l} 4L - 3H \\ \hline 55 \text{ dBc} \end{array}$$

FOR LO = +7 dBm
RF = 0 dBm

THIRD ORDER TWO TONE INTERMODULATION

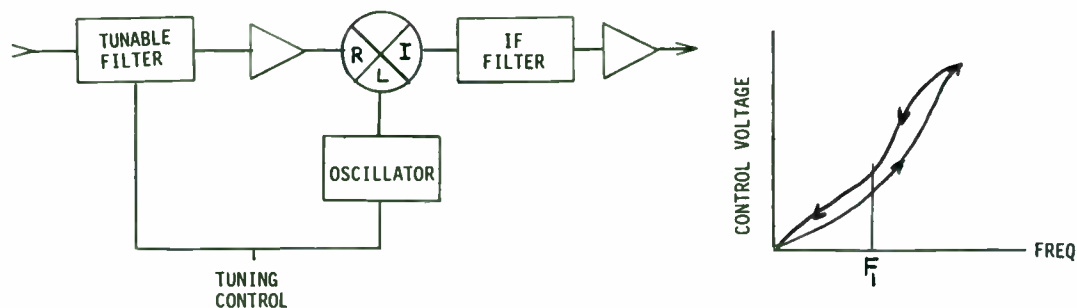


- o THIRD ORDER MODULATION TERMS ($2F_1-F_2$; $2F_2-F_1$) ARE UP CONVERTED TO THE IF FREQUENCY.
- o GIVEN AN INPUT THIRD ORDER INTERCEPT POINT OF 0 dBm AND TWO INPUT SIGNALS (BOTH AT -10 dBm) THE RESULTING OUTPUT INTERMODULATION RATIO IS 20 dB.
- o WITH A 10 dB INCREASE IN THE INPUT THIRD ORDER INTERCEPT POINT THE RESULTING INTERMODULATION RATIO IS 40 dB

7

PRESELECTION

- o REQUIRED TO REJECT IMAGE FREQ AND MINIMIZE THE CREATION OF TWO TONE MIXER SPURIOUS SIGNALS
- o USE SWITCHED BPFs AND SWITCHED LOCAL OSCILLATOR FREQUENCIES
- o USE YIG BPFs (ALSO ACT AS FRONT END LIMITERS)
 - OPEN LOOP TUNING: ± 10 MHz LO TRACKING (FILTER AND OSC INDEPENDENTLY TUNED)
 - CLOSED LOOP TUNING: ± 1 MHz LO TRACKING (FILTER AND OSC TUNED WITH COMMON MAGNET)



TUNING HYSTERESIS/NONLINEARITY

MIXER TYPES

o SINGLE DIODE MIXER

o RF INPUT

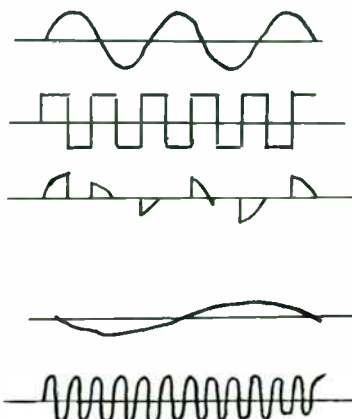
o LO SIGNAL

o OUTPUT

o OUTPUT

LO - RF

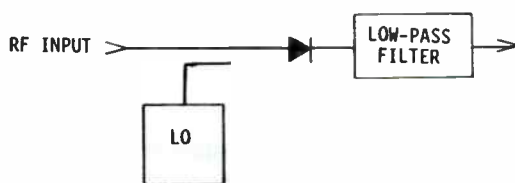
LO + RF



11

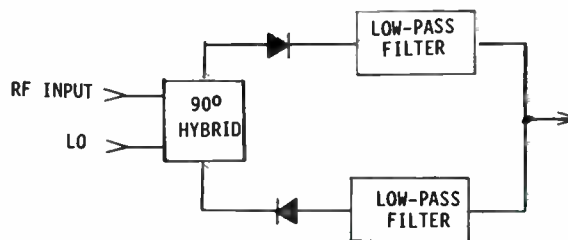
∞

SINGLE DIODE MIXER



- o DOWNCONVERSION APPLICATION ONLY
- o HIGH LO POWER REQUIRED TO OVERCOME COUPLER LOSS
- o NO CIRCUITRY TO NULL SPURIOUS RESPONSES
- o THIS CONFIGURATION IS SELDOM USED

SINGLE BALANCED MIXER

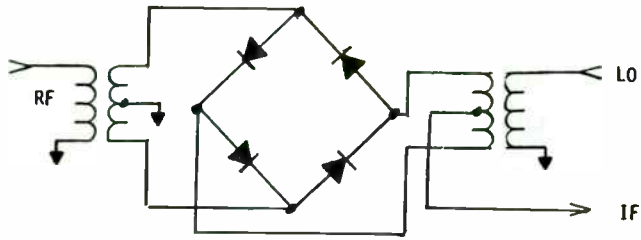


- o LOW INPUT SIGNAL VSWR - REFLECTED RF SIGNAL WILL EMERGE FROM LO PORT
- o POOR LO TO RF ISOLATION
- o HARMONICS AND INTERMODULATION OF RF AND LO ARE SUPPRESSED

12

DOUBLE BALANCED MIXERS

- o THE SYMMETRY PROVIDED BY THE FOUR DIODE ARRAY WILL:
 - SUPPRESS SPURIOUS RESPONSES
 - ENSURE GOOD ISOLATION BETWEEN RF, LO, AND IF PORTS



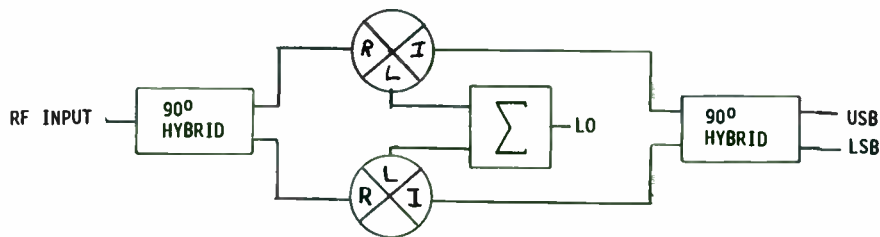
- o HIGH LEVEL MIXERS ALLOW MUCH HIGHER RF DYNAMIC RANGE BUT REQUIRE LO POWER LEVELS UP TO +27 dBm:
 - ADD 2 OR 3 DIODES IN SERIES
 - COMBINE 2 DIODE RINGS
 - USE 2 DBMs, 2 90° HYBRIDS, AND ONE 180° HYBRID AS SHOWN

13

9

IMAGE REJECTION MIXER

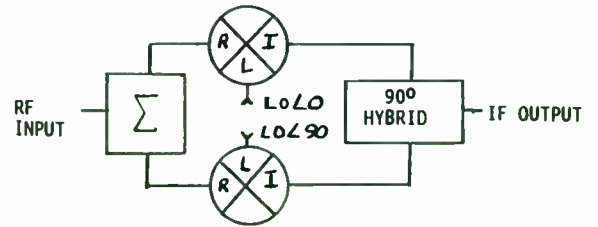
- o DOUBLES INSTANTANEOUS RF BW OF RECEIVER UTILIZING DUAL IF CHANNELS.
- o PROVIDES 20 dB REJECTION OF IMAGE FREQ WITHOUT RF FILTERING.



14

IMAGE-ENHANCED MIXER

- o DECREASES MIXER CONVERSION LOSS 1 TO 2 dB (BY RECONVERSION OF THE REFLECTED IMAGE) WITH NO DEGRADATION TO DYNAMIC RANGE (RGH'S QUIET MIXER).



- o MIXING F_R WITH $2F_{LO}$ PRODUCES ENERGY AT THE INPUT IMAGE FREQUENCY:

$$2F_{LO} - F_R = 2F_L - (F_{LO} \pm F_{IF}) = F_L \pm F_{IF}$$

- o THEORY OF OPERATION:

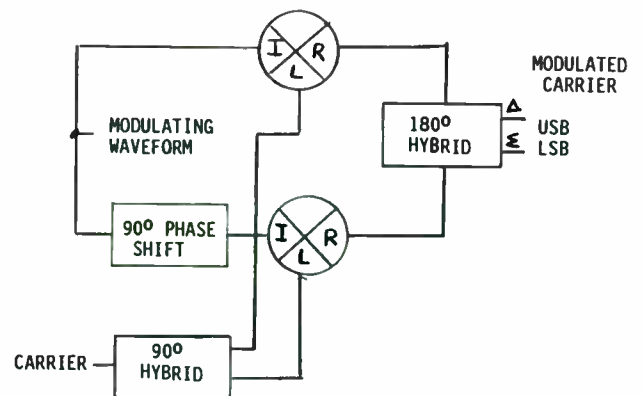
- THE IMAGE FREQUENCIES GENERATED IN THE MIXERS REFLECTED TOWARD THE RF SOURCE ARE 180° OUT OF PHASE.
- THE MAXIMUM IMAGE CURRENT AT THE RF INPUT PORT IS EQUIVALENT TO A SHORT CIRCUIT CONDITION FOR THE IMAGE CURRENT THUS REFLECTING THE POWER BACK TO THE MIXERS TO ENHANCE THE DESIRED OUTPUT.

15

10

SSB MIXER

- o USE FOR UP CONVERSION APPLICATIONS.
- o CARRIER (LO) SUPPRESSION IS DETERMINED BY THE LO TO RF ISOLATION OF MIXERS.
- o THE UNWANTED SIDEBAND SUPPRESSION DEPENDS UPON THE GAIN AND PHASE BALANCE OF THE TWO CHANNELS.
- o ACHIEVEMENT OF CONSTANT 90° PHASE SHIFT AT MOD FREQ IS DIFFICULT TO IMPLEMENT. SOLUTION IS TO DIGITIZE MOD WAVEFORMS THEN USE D/A.



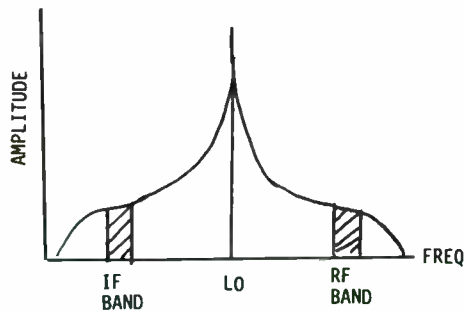
16

SUBHARMONICALLY PUMPED MIXER

- o USE FOR MILLIMETER WAVE MIXER APPLICATIONS.
- o BEST PERFORMANCE ALTERNATIVE WHEN COMPARED WITH FUNDAMENTAL MIXER WITH INADEQUATE LO LEVEL.
- o MIX RF WITH SECOND OR FOURTH HARMONIC OF LO.
- o FEATURES:
 - LO NOISE AT FUNDAMENTAL IS BALANCED OUT. LO NOISE AT SECOND HARMONIC IS LOW.
 - REJECTS SPURIOUS RESPONSES ASSOCIATED WITH THE ODD HARMONICS OF THE LO WITH EVEN HARMONICS OF RF.

AM NOISE REJECTION OF MIXERS

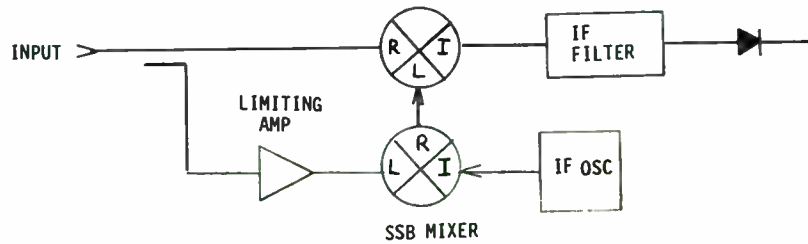
- o LOCAL OSCILLATOR AM NOISE RESULTS FROM:
 - OSCILLATOR RESONATOR Q
 - POST OSCILLATOR RF AMPLIFIER SELF NOISE
- o LO AM NOISE INCREASES MIXER NOISE TEMPERATURE RESULTING FROM IF NOISE FEEDTHROUGH PLUS CONVERSION OF RF NOISE TO THE IF.



- o A DOUBLE BALANCED MIXER WILL PROVIDE 10 TO 20 dB OF LO AM NOISE REJECTION. REF 4
- o ADDITIONAL LO AM NOISE REJECTION CAN BE OBTAINED WITH USE OF A BPF IN THE LO OUTPUT.

HOMODYNE RECEIVER

- o A SUPERHETRODYNE RECEIVER WHICH DERIVES ITS LO FROM THE RECEIVED SIGNAL
- o DOES NOT PROVIDE FREQUENCY INFORMATION
- o DOES PROVIDE DETECTION OF CHIRP AND SPREAD SPECTRUM SIGNALS
- o THE CHIRP SIGNAL IS DETECTED AS AN ORDINARY PULSED SIGNAL WITH A FIXED FREQUENCY CARRIER.



19

12

SUMMARY OF FEATURES AND LIMITATIONS

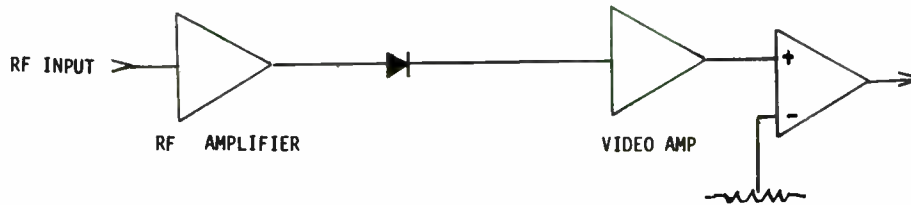
SUPERHETRODYNE RECEIVER

FEATURES	LIMITATIONS
<ul style="list-style-type: none"> o FREQUENCY RESOLUTION o SENSITIVITY o WIDE DYNAMIC RANGE o RETENTION OF SIGNAL CHARACTERISTICS o SIMULTANEOUS SIGNAL CAPABILITY o IMMUNITY FROM JAMMING 	<ul style="list-style-type: none"> o SIGNAL ACQUISITION TIME o INSTANTANEOUS ANALYSIS BANDWIDTH o CANNOT PROCESS FREQUENCY CHIRP SIGNALS (EXCEPT HOMODYNE CONFIGURATION)

20

1.2 CRYSTAL VIDEO RECEIVERS

PRINCIPLE OF OPERATION



- o DETECTION OCCURS WHEN THE INPUT SIGNAL EXCEEDS THE COMPARATOR THRESHOLD.

21

CVR CHARACTERISTICS

- o WIDE RF INPUT BANDWIDTH
- o HIGH PROBABILITY OF SIGNAL INTERCEPTION
- o DYNAMIC RANGE TYPICALLY 50 dB
- o POOR SENSITIVITY WITHOUT RF PREAMPLIFIER
- o SIMPLE; SMALL SIZE, LOW POWER, HIGH RELIABILITY, LOW COST
- o COMPRESSION TRANSFER CHARACTERISTIC
- o CONSISTS OF DETECTOR AND VIDEO AMPLIFIER (TYPICALLY)
- o DYNAMIC RANGE LIMITED TO THAT OF DETECTOR(S)
- o LOW END OF DYNAMIC RANGE SET BY TANGENTIAL SIGNAL SENSITIVITY (TSS) OF DETECTOR AND VIDEO AMPLIFIER.
- o TSS CAN BE IMPROVED BY ADDING A RF AMPLIFIER IN FRONT OF DETECTOR, PROVIDED THAT THE RF AMPLIFIER HAS A GOOD ENOUGH NOISE FIGURE.
- o EFFECTIVE NOISE BANDWIDTH IS APPROXIMATELY $\sqrt{2B_v B_{RF}}$

13

COMPRESSION TYPES

1. LOGARITHMIC COMPRESSION

$$E_{OUT} = A + B (P - P_R)$$

P = RF POWER IN dBm
 P_R = A REFERENCE LEVEL IN dBm

WITH LOG COMPRESSION, A PAIR OF SIGNALS WHICH ARE A GIVEN NUMBER OF dB APART WILL HAVE A CONSTANT DIFFERENCE OF THEIR CVR OUTPUT VOLTAGES (ANYWHERE IN THE DYNAMIC RANGE).

2. POWER COMPRESSION

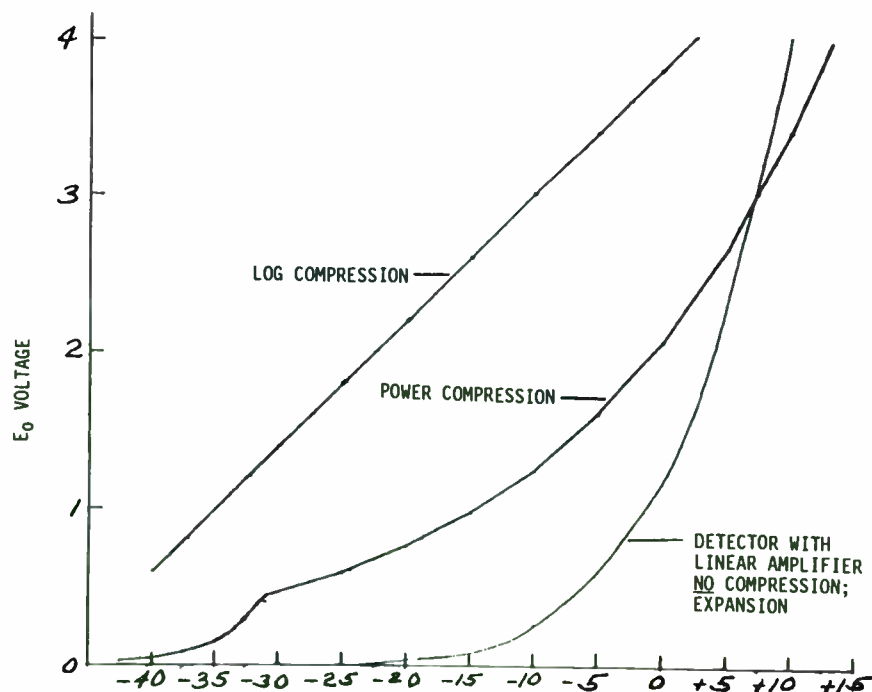
$$E_{OUT} = E_R 10^{K(P-P_R)}$$

P = RF POWER IN dBm
 P_R = A REFERENCE LEVEL IN dBm
 E_R = A REFERENCE OUTPUT LEVEL
 K = COMPRESSION FACTOR

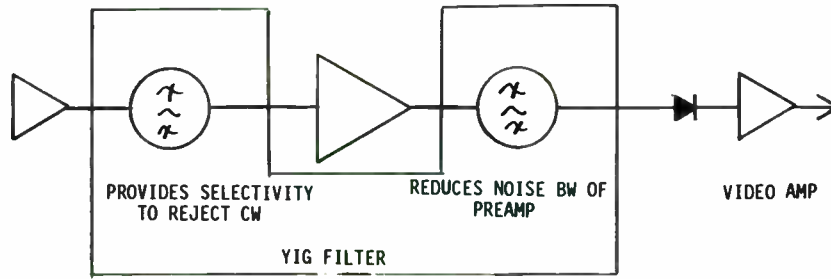
WITH POWER COMPRESSION, A PAIR OF SIGNALS WHICH ARE A GIVEN NUMBER OF dB APART WILL HAVE A CONSTANT RATIO OF THEIR DVCA OUTPUT VOLTAGES (ANYWHERE IN THE DYNAMIC RANGE).

FOR K = .05, LINEAR OPERATION RESULTS
 FOR K > .05, EXPANSION INSTEAD OF COMPRESSION
 FOR K = .1, SQUARE-LAW EXPANSION OCCURS; dB OUTPUT CHANGE IS TWICE THE dB INPUT CHANGE

COMPRESSION TYPES



TRF CVR



- o TUNABLE BPF ----> FREQUENCY MEASUREMENT CAPABILITY
- o RF AMP + BPF ----> IMPROVED SENSITIVITY
- o A SWEPT YIG FILTER WILL PRODUCE A PULSE OUTPUT FOR EACH CW SIGNAL DETECTED.

25

15

SUMMARY OF FEATURES AND LIMITATIONS

CRYSTAL VIDEO RECEIVER

FEATURES	LIMITATIONS
<ul style="list-style-type: none"> o INSTANTANEOUS ANALYSIS BANDWIDTH o SIGNAL ACQUISITION SPEED o SMALL SIZE o LOW COST 	<ul style="list-style-type: none"> o FREQUENCY RESOLUTION o SENSITIVITY o SIMULTANEOUS SIGNAL CAPABILITY o IMMUNITY FROM JAMMING

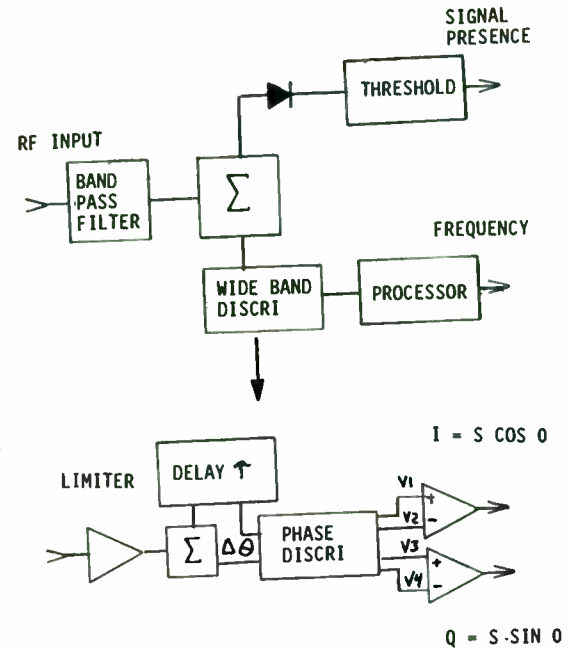
26

1.3 IFM RECEIVERS

PRINCIPLE OF OPERATION

- o INPUT SIGNAL PROCESSING
 - THRESHOLD FOR SIGNAL PRESENT
 - WIDEBAND DISCRIMINATOR
- o WIDEBAND DISCRIMINATOR PROCESSING
 - DELAY PATH
 - UNDELAYED PATH
- o CALCULATE UNAMBIGUOUS PHASE FROM I AND Q OUTPUTS
- o CALCULATE FREQUENCY AS SHOWN ($PW > \gamma$) -

$$f = \frac{\Delta \epsilon}{2 \pi \gamma}$$

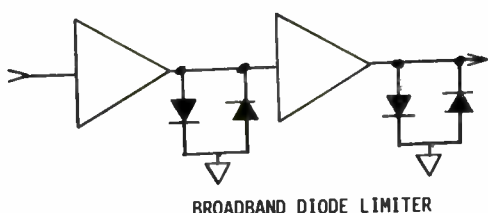


27

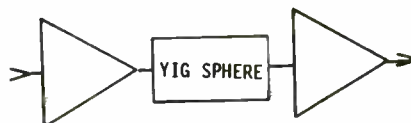
16

- o GAIN OF LIMITER SHOULD BE SUFFICIENT TO LIMIT ON WEAKEST SIGNAL.
- o $\left(\frac{S}{N}\right)_{\text{OUTPUT}} = \left(\frac{S}{N}\right)_{\text{IN}} \left[\frac{1 + 2(S/N)I}{4/\pi + (S/N)I} \right]$
 MORE THAN 2 dB IMPROVEMENT IN (S/N) OUTPUT IS POSSIBLE.
- o THE LIMITING AMPLIFIER IS DESIGNED TO PRODUCE A CONSTANT OUTPUT LEVEL AFTER SATURATION. A STANDARD LINEAR AMPLIFIER'S OUTPUT MAY DROP SLIGHTLY AFTER SATURATION. A TRUE LIMITER MAKES THE WIDEBAND DISCRIMINATOR OUTPUT INDEPENDENT OF INPUT RF LEVEL.
- o LONG LEADING AND TRAILING EDGES ON THE INPUT PULSE WILL BE SHORTER AT THE OUTPUT ----> PW INCREASE.
- o THE OUTPUT IS RICH IN HARMONICS. A LOW PASS FILTER IS REQUIRED TO RESTORE SINUSOIDAL WAVE.

- o FOR SIMULTANEOUS INPUTS - THE LIMITING AMPLIFIER CAPTURE EFFECT WILL CAUSE SUPPRESSION OF THE WEAKER SIGNALS UP TO 6 dB.
- o CAPTURE EFFECT REDUCES PROBABILITY OF GENERATING ERRONEOUS FREQUENCIES.
- o IF LIMITER CONFIGURATIONS:



BROADBAND DIODE LIMITER



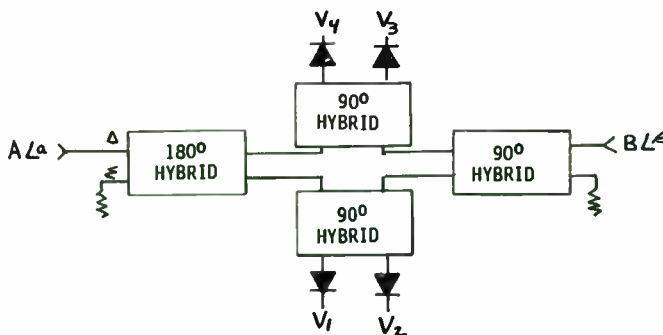
NARROWBAND YIG LIMITER

29

17

PHASE DISCRIMINATOR NETWORKS

- o PROVIDES FOUR DETECTED RF OUTPUTS WHICH ARE USED TO DETERMINE THE PHASE DIFFERENCE BY INTERFEROMETRY BETWEEN THE TWO RF INPUT SIGNALS.



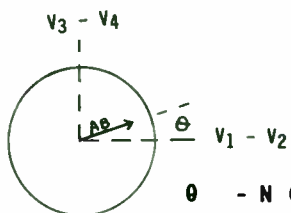
- o POLAR DISPLAY:

- Θ = PHASE DIFFERENCE BETWEEN RF INPUTS
- LENGTH OF AB REPRESENTS SIGNAL STRENGTH

$$\Theta = \angle a - \angle b$$

$$\begin{aligned} V_1 &= (A^2 + B^2) + 2 AB \cos \theta \\ V_2 &= (A^2 + B^2) - 2 AB \cos \theta \\ V_3 &= (A^2 + B^2) + 2 AB \sin \theta \\ V_4 &= (A^2 + B^2) - 2 AB \sin \theta \end{aligned}$$

MICROWAVE NETWORK IMPLEMENTATION

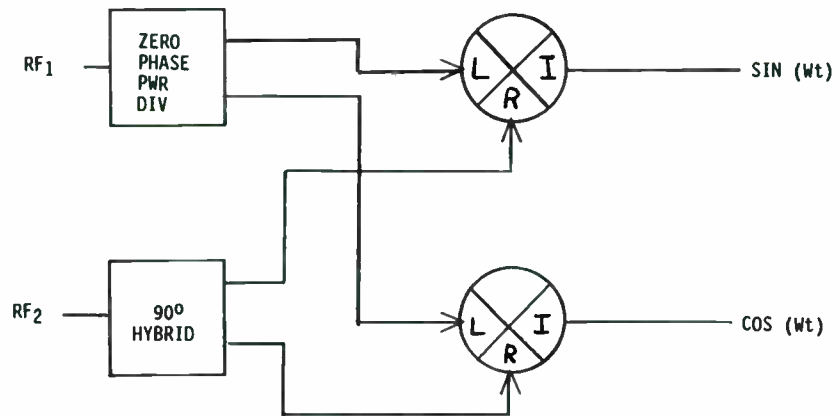


$$\theta = N (360^\circ) + \text{RESIDUAL PHASE}$$

THE PHASE ENCODER OUTPUTS RESIDUAL PHASE

30

ALTERNATE CONFIGURATION

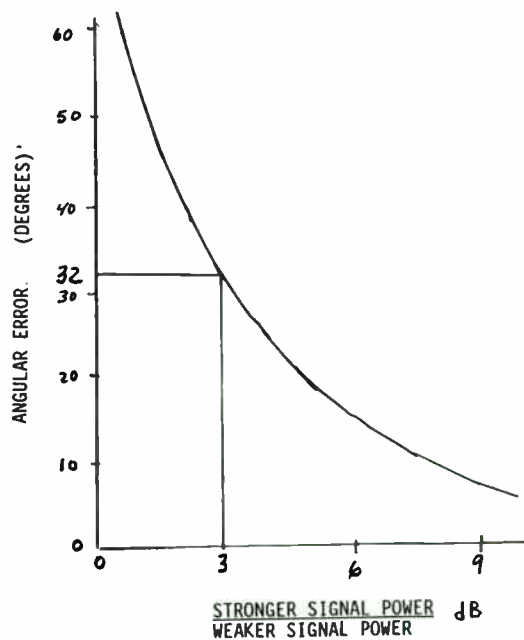


- o THE MIXER I PORT IS DC COUPLED AND PROVIDES SIN/COS OUTPUTS. NO VIDEO SUBTRACTION IS REQUIRED.

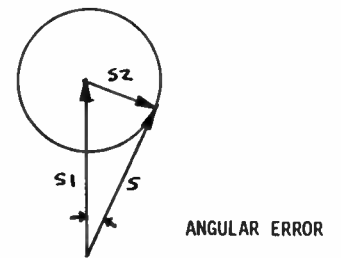
31

18

SIMULTANEOUS SIGNAL PROBLEM



$$\Delta\theta \text{ MAX} = \sin^{-1}(S_2/S_1)$$



REF 5

32

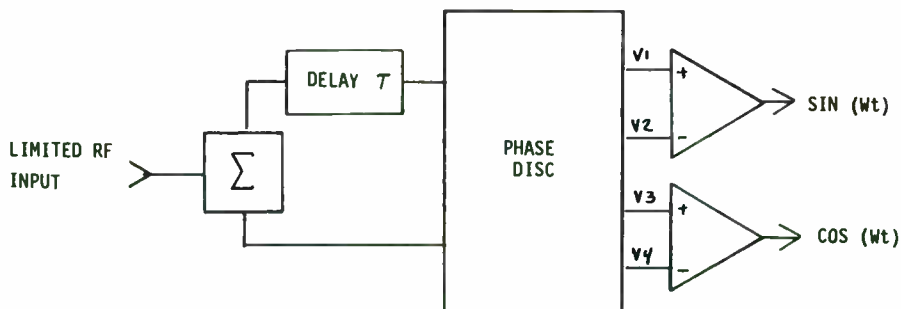
CW SIGNAL PROBLEM

- o ONE CW SIGNAL MAY RESULT IN SIMULTANEOUS SIGNAL FREQUENCY ERRORS ON ALL PULSES.
- o USE AC COUPLED VIDEO CIRCUITRY TO REMOVE BIAS RESULTING FROM WEAK CW TO ALLOW ACCURATE ENCODING OF STRONGER PULSE SIGNALS.
- o STRONG CW INTERFERENCE PROBLEM SOLUTIONS:
 - 1 - CHOP CW WITH RF SWITCH AHEAD OF LIMITER
 - MEASURE FREQUENCY OF CW SIGNAL
 - TUNE YIG NOTCH FILTER (AHEAD OF LIMITER) TO REJECT CW SIGNAL
 - 2 - USE SCANNING NARROWBAND FILTER TO CONVERT CW SIGNALS TO PULSE SIGNALS FOR FREQUENCY MEASUREMENT
 - TUNE YIG NOTCH FILTER TO SAME FREQUENCY TO REJECT CW SIGNAL

33

19

SINGLE CORRELATOR DESIGN EXAMPLE



GIVEN - RF INPUT FREQ RANGE 3 TO 4 GHz

DETERMINE τ TO ALLOW UNAMBIGUOUS FREQ ENCODING (DESIGN FOR ± 50 MHz FREQ EXTENSION) AND MIN RF PULSE WIDTH THAT CAN BE PROPERLY ENCODED. DESIGN FOR MORE THAN 180° PHASE CHANGE AS FREQUENCY IS INCREASED FROM 3 TO 4 GHz.

SOLUTION

$$f = \frac{\Delta\phi}{2\pi\tau} \quad f_{\text{MIN}} = 2,950 \text{ MHz}, \quad f_{\text{MAX}} = 4,050 \text{ MHz}$$

- o IF ONE LIMITS THE MAX PHASE DELTA TO 2π THEN $\tau = \frac{2\pi}{2\pi f_{\text{max}}} = 0.24 \text{ NSEC}$

FREQ	$\tau = 0.24 \text{ NSEC}$ PHASE Δ	$\tau = 0.85 \text{ NSEC}$ PHASE Δ	$\tau = 0.51 \text{ NSEC}$ PHASE Δ
2,950	261	926 = 720 + 206	556 = 360 + 196
3,000	265	942 = 720 + 222	565 = 360 + 205
3,500	309	1,099 = 1,080 + 19	659 = 360 + 299
4,000	354	1,256 = 1,080 + 176	753 = 720 + 33
4,050	360	1,271 = 1,080 + 191	763 = 720 + 43
PHASE DELTA 3,000 --> 4,000	89°	PHASE MARGIN = 15° 314°	PHASE MARGIN = 153° 188°

- o CHOOSE $\tau = 0.51 \text{ NSEC}$ - OFFERS HIGHEST MARGIN FOR AMBIGUITY RESOLUTION AND MIN PULSE PROCESSING CAPABILITY.
- o FOR $\tau = 0.51 \text{ NSEC}$ - THE MINIMUM PULSE WIDTH IS 0.51 NSEC (FOR DELAY LINE) + $1/2.5 \text{ BV} = 0.51 + 1/(2.5)(10 \text{ MHz}) = \underline{40.51 \text{ NSEC}}$

35

20

- 2 - USE SCANNING NARROWBAND FILTER TO CONVERT CW SIGNALS TO PULSE SIGNAL FOR PROPER FREQUENCY ENCODING
- TUNE YIG NOTCH FILTERS TO APPROPRIATE FREQUENCIES TO REJECT MULTIPLE CW SIGNALS

SUMMARY OF FEATURES AND LIMITATIONS

INSTANTANEOUS FREQUENCY MEASUREMENT RECEIVER

FEATURES	LIMITATIONS
o INSTANTANEOUS ANALYSIS BANDWIDTH	o SENSITIVITY
o FREQUENCY RESOLUTION	o RETENTION OF SIGNAL CHARACTERISTICS
o DYNAMIC RANGE	o SIMULTANEOUS SIGNAL CAPABILITY
o SIGNAL ACQUISITION SPEED	o IMMUNITY FROM JAMMING

37

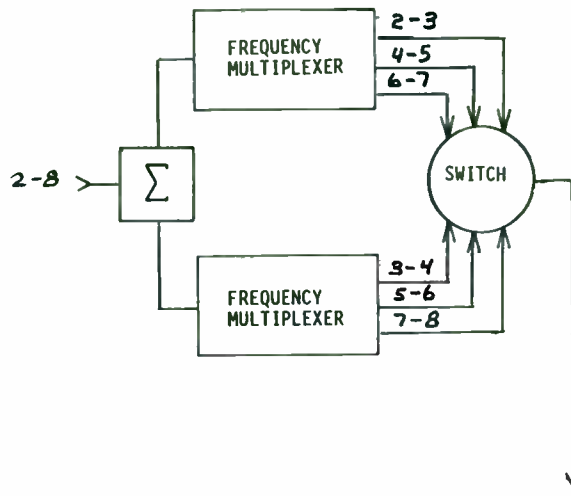
21

1.4 CHANNELIZED RECEIVER

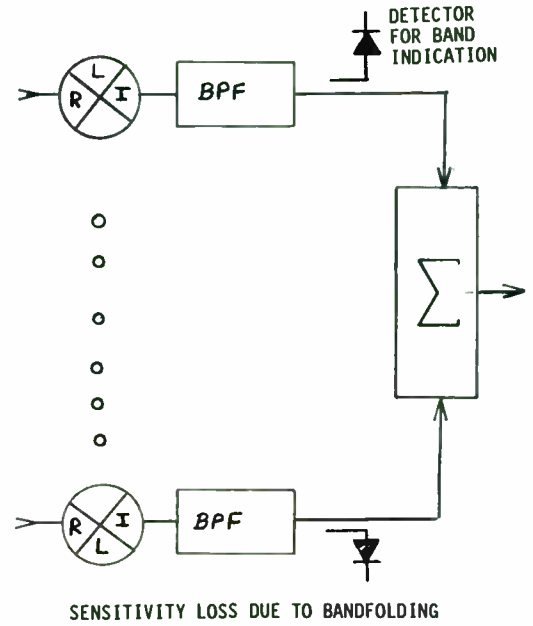
PRINCIPLE OF OPERATION

- o USES A LARGE NUMBER OF CONTIGUOUS FILTERS TO SORT THE INPUT SIGNALS.
- o SAMPLE FILTER OUTPUTS TO DETERMINE SIGNAL FREQUENCY.
- o PROVIDES 100% POI WHEN ALL CHANNELS ARE PROCESSED IN PARALLEL.
- o TO REDUCE VOLUME OF RECEIVER TWO SOLUTIONS ARE:
 - TIME SHARING - WILL REDUCE POI UNLESS CHANNEL SAMPLING IS SYNCHRONIZED WITH EMITTER'S PULSE ARRIVAL TIME.
 - BAND FOLDING - WILL REDUCE SENSITIVITY AND ABILITY TO CORRECTLY IDENTIFY EMITTER FREQUENCY IN A DENSE SIGNAL ENVIRONMENT.

TIME MULTIPLEXING



BAND FOLDING



OUTPUT TO CVR TO MEASURE PULSE AMPLITUDE AND WIDTH

OUTPUT TO FREQ CONVERTER WHICH DRIVES IFM TO MEASURE PULSE FREQ

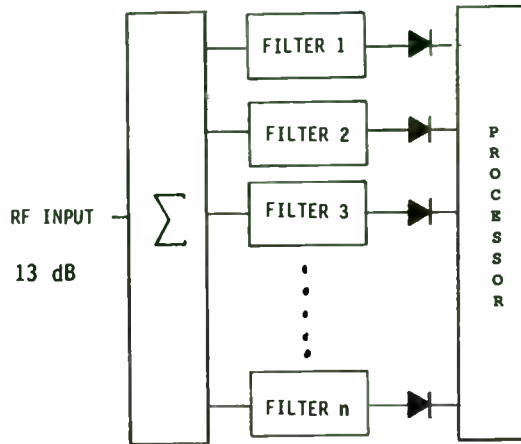
39

DESIGN CONSIDERATIONS

- o TWO CONFLICTING REQUIREMENTS - SELECTIVITY AND TRANSIENT RESPONSE
- o FILTER SELECTIVITY SHOULD BE SUFFICIENT TO ENSURE THAT A STRONG SIGNAL DOES NOT INTERFERE WITH THE SIMULTANEOUS MEASUREMENT OF A WEAK SIGNAL IN AN ADJACENT FILTER.
- o FILTER TRANSIENT RESPONSE SHOULD BE MINIMIZED - FEWER FILTER SECTIONS AND WIDER BANDWIDTH.

SINGLE LEVEL CHANNELIZED RECEIVER

- o BAND OF CONTIGUOUS FILTERS PROVIDE 100% POI OVER INPUT BANDWIDTH.
- o SENSITIVITY IS POORER THAN A SINGLE CHANNEL SUPERHET WITH SAME SLOT BANDWIDTH.
 - SUPERHET
 $P_{DET} = 90\%$, $P_{FA} = 10^{-6}$ ----> $S/N|_{RF} = 13$ dB
 - 100 SLOT CHANNELIZER
 EACH CHANNEL MUST HAVE $P_{FA} = 10^{-8}$
 THEREFORE, $S/N|_{RF} = 14.3$ dB

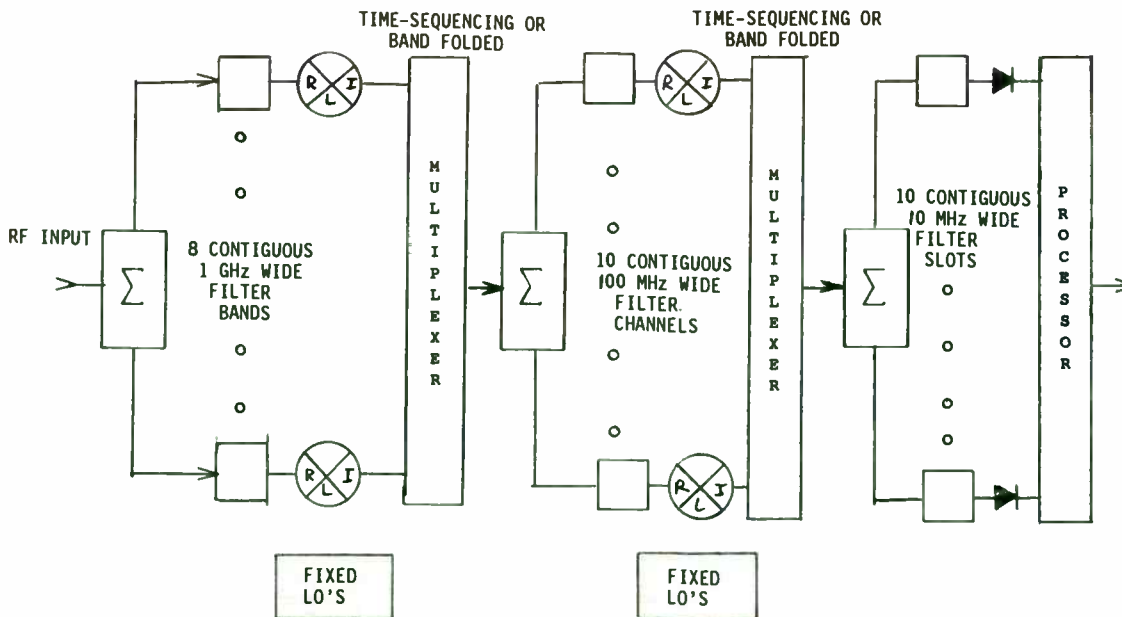


- o SLOT BANDWIDTH $\geq \frac{3.2}{\text{MIN PULSE WIDTH}}$ 100 NSEC PW REQUIRES 32 MHz SLOT BW
- o TO MINIMIZE FILTER TRANSIENT RESPONSE - USE GAUSSIAN RESPONSE WITH MINIMUM NUMBER OF SECTIONS.

41

23

THREE LEVEL CHANNELIZED RECEIVER



- o EACH MULTIPLIER INPUT HAS A CVR TO RESOLVE FREQ AMBIGUITIES WHEN BAND FOLDING IS SELECTED.

42

SUMMARY OF FEATURES AND LIMITATIONS

CHANNELIZED RECEIVER

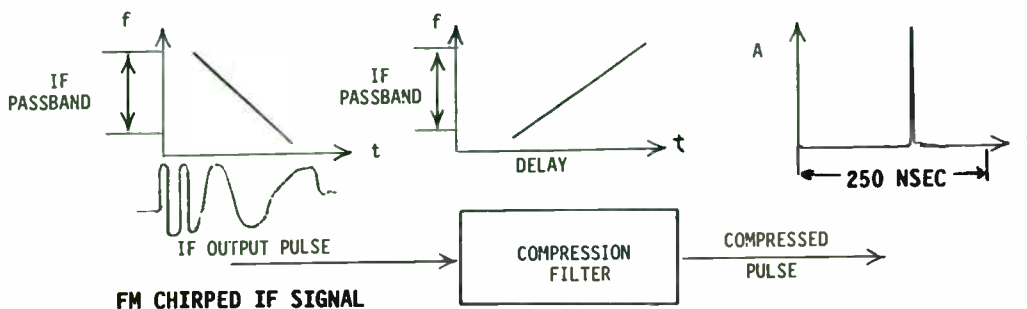
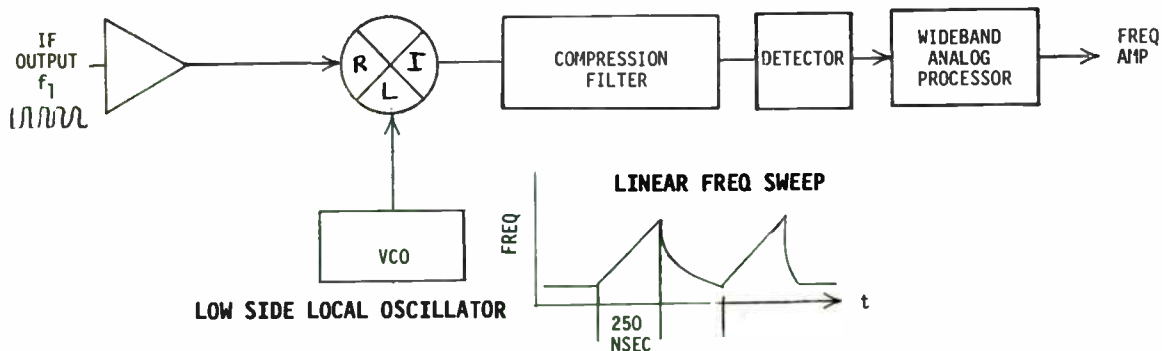
FEATURES	LIMITATIONS
<ul style="list-style-type: none"> o INSTANTANEOUS ANALYSIS BANDWIDTH o SENSITIVITY o DYNAMIC RANGE o SIGNAL ACQUISITION SPEED o RETENTION OF SIGNAL CHARACTERISTICS o SIMULTANEOUS SIGNAL CAPABILITY o IMMUNITY FROM JAMMING 	<ul style="list-style-type: none"> o COST o SIZE o POWER REQUIREMENTS

43

24

1.5 COMPRESSIVE RECEIVER / LINEAR FM PULSE COMPRESSION RECEIVER

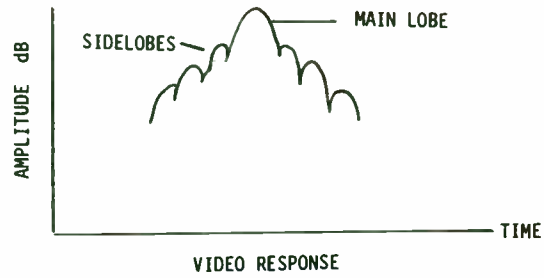
PRINCIPLE OF OPERATION



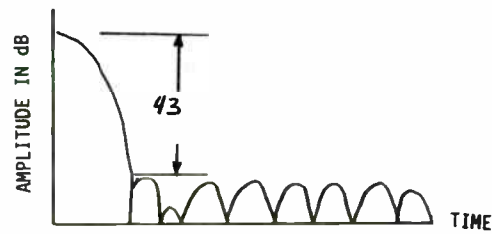
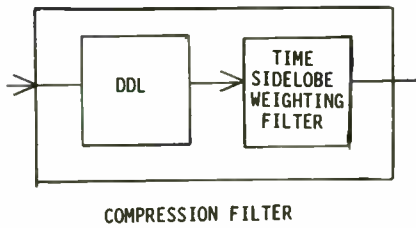
44

COMPRESSIVE RECEIVER OUTPUT

- o WITH NO SIDELobe WEIGHTING FILTER - OUTPUT IS SINX/X WITH FIRST SIDELobe DOWN 13 dB



- o WITH HAMMING WEIGHTING FILTER - FIRST SIDELobe DOWN 43 dB



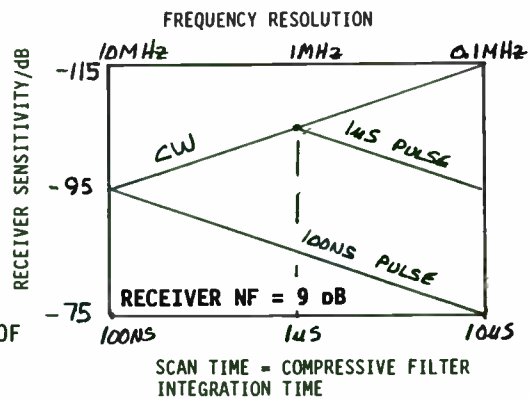
45

25

DESIGN PARAMETERS AND TRADEOFFS

- o SENSITIVITY

- FOR SIGNAL POWER = NOISE POWER
 $-114 \text{ dBm/MHz} + \text{NF} + 10 \text{ LOG } (1/T)$
 $T = \text{DDL DIFFERENTIAL DELAY TIME IN } \mu\text{SEC}$
- IF INPUT PULSE IS LESS THAN T, SENSITIVITY WILL BE DEGRADED BY 10 LOG OF THE RATIO.
- INCREASING THE DDL DIFFERENTIAL DISPERSION DELAY WILL IMPROVE CW SENSITIVITY AND FREQUENCY RESOLUTION AND ACCURACY BUT REQUIRES LONGER INPUT PULSES TO OBTAIN THE BENEFITS OF RECEIVER COMPRESSIVE GAIN.



46

DESIGN PARAMETERS AND TRADEOFFS

o BANDWIDTH DDL

- SAW DDL PRACTICAL LIMIT IS 1,000 MHz
- OUTPUT PULSE WIDTH = K/B_{DDL}
- MAXIMUM OUTPUT PULSE RATE = B_{DDL}/K

o BANDWIDTH RECEIVER

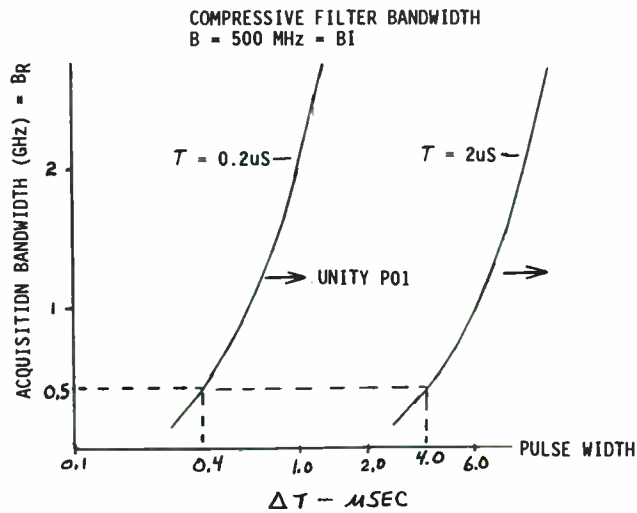
- FOR $B_R = B_I$, MAXIMUM POI AND FULL SENSITIVITY
 - LO SCAN TIME = $2T$
 - LO TUNING RANGE = $2B_I$
 - MINIMUM INPUT PULSE WIDTH = $2T$
- FOR $B_R \neq B_I$ THEN
 - LO SCAN TIME = $[(B_R+B_I)/B_I]T$
 - LO TUNING RANGE = B_R+B_I

47

26

DESIGN PARAMETERS AND TRADEOFFS

o PULSE WIDTH RANGE



FOR UNITY POI AT FULL SENSITIVITY $\Delta T \geq \text{LO SCAN TIME}$
 $\geq T_{DDL} [1+B_R/B_I]$

48

DESIGN PARAMETERS AND TRADEOFFS

o FREQUENCY RESOLUTION

THEORETICAL LIMIT (WITHOUT WEIGHING FACTOR) = $1/T_{DDL}$

PERCENTAGE RESOLUTION = $1/B_I T_{DDL}$ - 0.1% PRACTICAL

o ACCURACY

FUNCTION OF LO TUNING LINEARITY AND SIGNAL PROCESSING CIRCUITS

o PROBABILITY OF INTERCEPT - POI

LIMITED BY INPUT SIGNAL PULSE

PULSES $< T_{DDL}[1 + B_R/B_I]$ WILL STILL BE DETECTED AT NEAR 100% POI BUT AT REDUCED SENSITIVITY

49

DESIGN PARAMETERS AND TRADEOFFS

o DYNAMIC RANGE

LIMITED BY CHARACTERISTIC OF THE COMPRESSIVE FILTER

IF BPF IS RECTANGULAR THE OUTPUT PULSE (FOURIER TRANSFORM OF BPF) HAS SIDELOBES.

UNWEIGHTED SIDELOBES HAVE SINX/X RESPONSE - FIRST SIDELOBE IS 13 dB DOWN

WITH HAMMING OR TRUNCATED GAUSSIAN WEIGHTING FUNCTION - SIDELOBES ARE 40 TO 50 dB DOWN

50

27

SUMMARY OF FEATURES AND LIMITATIONS

COMPRESSIVE RECEIVER

FEATURES	LIMITATIONS
<ul style="list-style-type: none"> o INSTANTANEOUS ANALYSIS BANDWIDTH o SENSITIVITY o SIGNAL ACQUISITION SPEED o FREQUENCY RESOLUTION o SIMULTANEOUS SIGNAL CAPABILITY o IMMUNITY FROM JAMMING 	<ul style="list-style-type: none"> o RETENTION OF SIGNAL CHARACTERISTICS o PROCESSING COMPLEXITY

51

28

2.0 RECEIVER ANALYSIS EQUATIONS

THERMAL NOISE

- o $N_f = KTB$ NOISE POWER
 $K =$ BOLTZMANN'S CONSTANT = $1.38 (10^{-23})$ J/°K
 $T =$ TEMP OF RESISTOR IN °K
 $B =$ BANDWIDTH IN HERTZ
- o $P_{dBm} = 10 \text{ LOG } (P \text{ IN MILLIWATTS})$
- o FOR $T =$ ROOM TEMP = 290°K and $B = 1$ Hz
INPUT THERMAL NOISE = -174 dBm/Hz
= -114 dBm/MHz
- o IF RECEIVER INPUT IS AN ANTENNA FACING A COLD SKY, T COULD BE MUCH LESS THAN 290°K.
- o THERMAL NOISE GOES TO ZERO AS T GOES TO 0.

52

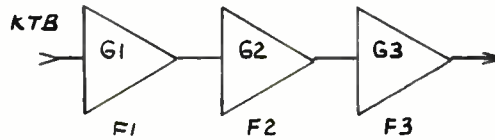
NOISE FIGURE

o $F = \frac{\text{NOISE OUTPUT OF PRACTICAL RECEIVER}}{\text{NOISE OUTPUT OF IDEAL RECEIVER AT TEMP} = 290^{\circ}\text{K}}$

$= \frac{N_o}{GN_i} = \frac{N_o}{GKTB}$ G = GAIN OF RECEIVER

o $G = \frac{S_o}{S_i}$ THEREFORE $F = \frac{S_i/N_i}{S_o/N_o}$

o $F_{RCV} = F_1 + \frac{F_2-1}{G_1} + \frac{F_3-1}{G_1G_2}$



53

29

(S/N) OUTPUT OF RF LIMITER AMP

$\left(\frac{S_o}{N_o}\right) = \left(\frac{S_i}{N_i}\right) \left[\frac{1 + (S_i/N_i)^2}{4/\pi + S_i/N_i} \right]$

ASSUMES AMPLIFIER IS LIMITING ON N_i

EXAMPLE -

$(S/N)_{INPUT} = 5.42 \text{ dB (3.483)}$

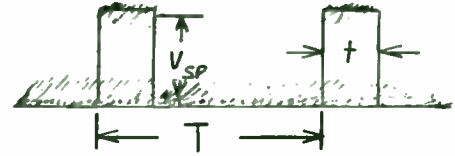
CALCULATE S_o/N_o

$S_o/N_o = 3.483 \frac{1 + 3.483}{4/\pi + 3.483} = 5.833 \text{ 7.7 dB}$

TANGENTIAL SENSITIVITY

- o OSCILLOSCOPE METHOD - APPROXIMATELY 8 dB S/N with $\sigma = 0.4$ dB
- o RMS VOLTMETER METHOD - $V_{sp} = 2.5 V_n$

V_{sp} = PEAK AMPLITUDE OF SIGNAL
 V_n = RMS NOISE VOLTAGE



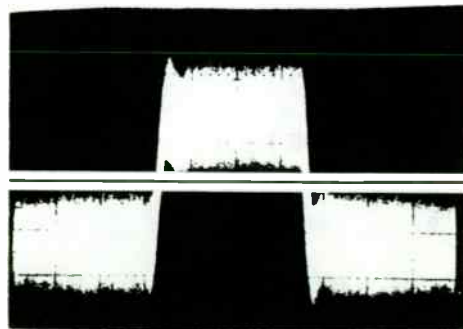
- o FOR $\delta = t/T =$ DUTY CYCLE, THE dB CHANGE ON THE RMS VOLTMETER FROM THE NOISE LEVEL TO THE TANGENTIAL CONDITION IS

$$\Delta \text{ dB} = 10 \text{ LOG } (1 + 6.25 \delta (1 - \delta))$$

FOR 10% DUTY CYCLE -

$$\Delta \text{ dB} = 10 \text{ LOG } (1.5625) = 1.94 \text{ dB}$$

55



DETECTOR OUTPUT AT TANGENTIAL SENSITIVITY

56

- o TSS IS FUNCTION OF B_R , B_V = RCV NF, CHARACTERISTICS OF DETECTOR
- o TSS OF VIDEO DETECTOR AND VIDEO AMPLIFIER

$$TSS = -110 + 10 \text{ LOG } \sqrt{AB_V} \quad (\text{UNITS ARE dBm})$$

A = f (DIODE, VIDEO AMP)

$$A = \frac{4 F_V (10^{-6})}{KTM^2}$$

$$M = \text{DIODE FIGURE OF MERIT} = \frac{\text{DET SENSITIVITY (VOLTS/WATT)}}{\sqrt{\text{DYNAMIC R OF DET}}}$$

57

- o ADD A RF AMPLIFIER AHEAD OF THE DETECTOR THEN

$$TSS = -114 + 10 \text{ LOG } F_T + 10 \text{ LOG } \left[3.15 B_R + 2.5 \sqrt{2 B_R B_V - B_V^2 + AB_V / (G_T F_T)^2} \right]$$

FOR $B_V \leq B_R < 2B_V$

$$TSS = -114 + 10 \text{ LOG } F_T + 10 \text{ LOG } \left[6.31 B_V + 2.5 \sqrt{2 B_R B_V - B_V^2 + AB_V / (G_T F_T)^2} \right]$$

FOR $B_R \geq 2B_V$

G_T AND F_T ARE OVERALL GAIN AND NF FROM RCV INPUT TO DETECTOR

B_R AND B_V ARE IN MHz

F_T AND G_T ARE LINEAR NOT LOG VALUES

58

31

VIDEO S/N CALCULATION BASED ON RF S/N

FOR OPERATION IN SQUARE LAW REGION OF DETECTOR (ASSUMES $B_{RF} \geq 2B_V$)

$$S/N \left| \begin{array}{l} \text{SQ LAW} \\ \text{VIDEO} \end{array} \right. = \frac{(S/N)_{RF}^2}{2 B_V/B_R - (B_V/B_R)^2 + 4 (B_V/B_R) (S/N)_{RF}}$$

FOR OPERATION IN LINEAR REGION OF DETECTOR

$$S/N \left| \begin{array}{l} \text{LIN} \\ \text{VIDEO} \end{array} \right. = \text{TWICE } S/N \left| \begin{array}{l} \text{SQ LAW} \\ \text{VIDEO} \end{array} \right.$$

60

32

- o DETERMINE RECEIVER RF GAIN REQUIRED TO MAKE THE RECEIVER SENSITIVITY NOISE LIMITED.

$$G_T \geq T_d - (-114 + 10 \text{ LOG } F_T + 10 \text{ LOG } \sqrt{2B_R B_V - B_V^2})$$

$T_d = \text{TSS OF DETECTOR}$

BRINGS NOISE FLOOR OF RECEIVER TO T_d

THEN THE TSS OF THE RECEIVER CAN BE CALCULATED WITH LESS THAN 0.4 dB ERROR AS SHOWN -

- o FOR $B_R \geq 2B_V$

$$TSS = -114 + 10 \text{ LOG } F_T + 10 \text{ LOG } (6.31 B_V + 2.5 \sqrt{2B_R B_V - B_V^2})$$

- o IF $B_R \gg B_V$ THEN (FOR $B_R \geq 1000 B_V$, ERROR IS LESS THAN 1 dB)

$$TSS = -114 + 10 \text{ LOG } F_T + 4 + 10 \text{ LOG } \sqrt{2B_R B_V}$$

THE TERM $\sqrt{2B_R B_V}$ CAN BE REFERRED TO AS EFFECTIVE BW.

RF S/N CALCULATION BASED ON VIDEO S/N

FOR A SQ LAW DETECTOR GIVEN THE (S/N) VIDEO IS -

$$\left. \frac{S}{N} \right|_{RF} = 2 \left[(B_V/B_R) (S/N)_V + \sqrt{(B_V/B_R)^2 (S/N)_V^2 - 1/4 (B_V/B_R)^2 (S/N)_V + 1/2 (B_V/B_R) (S/N)_V} \right]$$

ASSUMES $B_{RF} \geq 2 B_V$

61

FALSE ALARM AND PROBABILITY OF DETECTION

- o ASSUME RF GAIN AHEAD OF THE DETECTOR IS SUFFICIENT TO BRING THE NOISE FLOOR UP TO THE TSS LEVEL OF THE DETECTOR (NOISE LIMITED CASE).
- o FIGURES 2.11 TO 2.35 SHOW THE PROBABILITY OF DETECTION FOR A SINE WAVE IN NOISE AS A FUNCTION OF $S/N|_{RF}$ AT THE DETECTOR INPUT FOR RATIOS OF B_R/B_V FROM 1 THROUGH 3000. REF 1

62

33

EXAMPLE OF RECEIVER SENSITIVITY CALCULATION

IFM RECEIVER WITH $B_R = 2000$ MHz, $B_V = 1$ MHz, $G_T = 51$ dB, $F_T = 10$ dB (10)

1. DETERMINE TSS - INPUT RF POWER WHICH PRODUCES 0dB VIDEO S/N
DETERMINE IF RF GAIN IS SUFFICIENT TO MAKE RECEIVER SENSITIVITY NOISE LIMITED

$$\text{NOISE FLOOR} = -114 + 10 \text{ LOG } B_R + F_T = -71 \text{ dBm}$$

THE GAIN (51 dB) WILL AMPLIFY NOISE FLOOR TO -20 dBm WHICH IS $>T_d$.

SINCE B_R IS $\gg B_V$

$$\begin{aligned} \text{TSS} &= -114 + 10 \text{ LOG } F_T + 4 + 10 \text{ LOG } \sqrt{2B_R B_V} \\ &= -114 + 10 + 4 + 10 \text{ LOG } 63.2 \\ &= -82 \text{ dBm} \end{aligned}$$

2. DETERMINE SENSITIVITY ASSUMING $P_D = 99\%$ AND $T_{FA} = 100$ SEC

$$P_{FA} = \frac{1}{T_{FA} B_{RF}} = \frac{1}{(100)(2000)(10^6)} = 5 (10^{-12})$$

T_{FA} = TIME BETWEEN NOISE CROSSING OF THRESHOLD

63

THE REQUIRED PREDETECTION S/N FROM FIG 2.34 IS - 5.6 dB, REF 1.
THE CORRESPONDING SIGNAL LEVEL AT THE RECEIVER INPUT IS

$$-114 + 10 \text{ LOG } B_R + F_T + (-5.6) = \underline{-76.6 \text{ dBm}}$$

WHICH IS 5.4 dB ABOVE RECEIVER TSS.

TWO-TONE SPUR-FREE DYNAMIC RANGE AND THIRD ORDER INTERMODULATION

- o WHEN STRONG INPUT SIGNALS DRIVE RECEIVER COMPONENTS INTO THE NONLINEAR REGION, THE RELATIONSHIP BETWEEN INPUT AND OUTPUT CAN BE WRITTEN AS

$$V_o = a_1V_i + a_2V_i^2 + a_3V_i^3 \dots$$

THIRD ORDER INTERMOD PRODUCTS ARE PRODUCED BY TWO SIMULTANEOUS INPUT SIGNALS OF DIFFERENT FREQUENCIES.

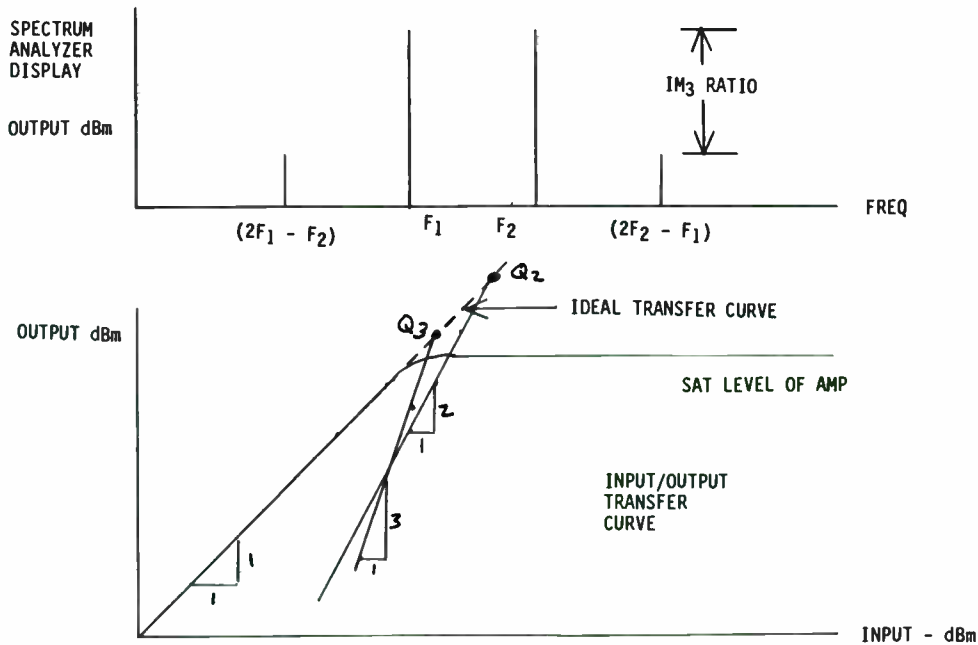
$$V_i = \cos(w_1t) + \cos(w_2t)$$

THE THIRD TERM OF V_o ($a_3V_i^3$) GENERATES TERMS CONTAINING

$$\cos(2w_1t - w_2t) \text{ AND } \cos(2w_2t - w_1t)$$

65

35



SECOND AND THIRD ORDER INTERCEPT POINTS

66

o LEVEL OF SECOND ORDER TERM

$$IM_2 = 2 (P_i + G) - Q_2 \text{ dBm}$$

P_i = INPUT POWER IN dBm

G = GAIN OF AMPLIFIER IN LINEAR REGION

Q_2 = SECOND ORDER INTERCEPT POINT REFERENCED TO THE OUTPUT

o LEVEL OF THIRD ORDER TERM

$$IM_3 = 3(P_i + G) - 2Q_3 \text{ dBm}$$

o ONE COULD DEFINE THE MAXIMUM INPUT LEVEL FOR TWO TONES WHICH PRODUCE IM_3 PRODUCTS EQUAL TO THE NOISE LEVEL OF THE RECEIVER

$$N_i G = IM_3 = 3(P_i + G) - 2Q_3 \text{ dBm}$$

$$\text{THEN } P_i = 1/3(N_i - 2G + 2Q_3) \text{ dBm}$$

67

36

AND DYNAMIC RANGE = $P_i - N_i$

$$= 2/3(Q_3 - G - N_i) \text{ dB } (IM_3)$$

TWO TONE THIRD ORDER SPUR FREE DYNAMIC RANGE

$$= 1/2(Q_2 - N_i - 2G) \text{ dB } (IM_2)$$

TWO TONE SECOND ORDER SPUR FREE DYNAMIC RANGE

ACTUAL RECEIVER DYNAMIC RANGE IS ALWAYS LESS SINCE THE RECEIVER THRESHOLD IS SET HIGHER THAN THE NOISE FLOOR.

68

TWO-TONE THIRD ORDER INTERMOD LEVELS FOR UNEQUAL INPUTS

$F_1 \text{ ----> } P_1 \text{ dBm}$ $F_2 \text{ ----> } P_2 \text{ dBm}$

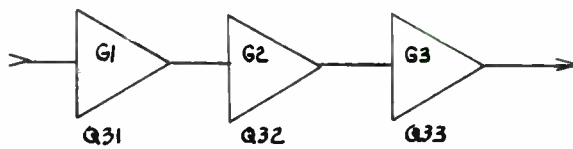
$$IM_3 = 2P_1 + P_2 - 2 Q_3 + 3G \text{ dBm (} 2F_1-f_2 \text{ SPUR)}$$

$$IM_3 = 2P_2 + P_1 - 2 Q_3 + 3G \text{ dBm (} 2f_2-f_1 \text{ SPUR)}$$

69

37

INTERCEPT POINTS OF CASCADE AMPLIFIERS



NOTE $Q_{3Xi} = Q_{3X} - G_X =$ THIRD ORDER INTERCEPT POINT REF TO INPUT

$$\sqrt{1/Q_{2iT}} = \sqrt{1/Q_{2i1}} + \sqrt{G_1/Q_{2i2}} + \sqrt{G_1G_2/Q_{2i3}}$$

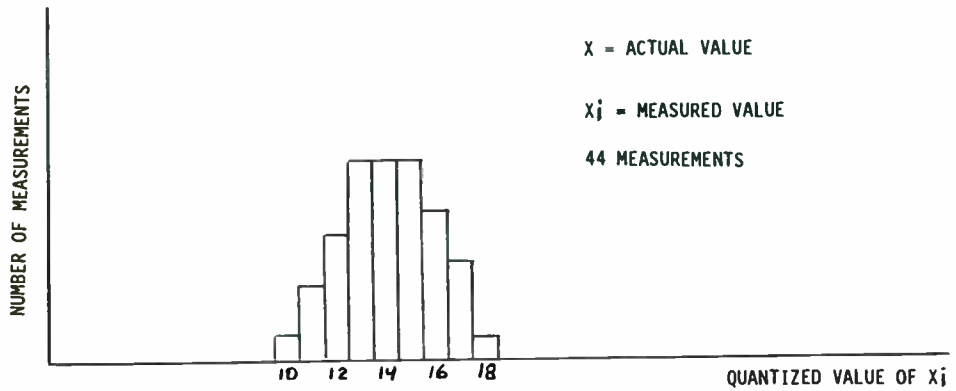
AND

$$1/Q_{3iT} = 1/Q_{3i1} + G_1/Q_{3i2} + G_1G_2/Q_{3i3}$$

70

RESOLUTION, ACCURACY, MEAN VALUE, RMS, STD DEV

- o RESOLUTION ≠ ACCURACY; RESOLUTION = PARAMETER LSB
- o ACCURACY IS THE DIFFERENCE BETWEEN MEASURED VALUE AND ACTUAL VALUE
- o HISTOGRAM OF MEASUREMENT ERROR



71

- o $\text{RMS OF DATA} = \sqrt{\frac{1}{N} \sum (x_i)^2}$ $\text{RMS OF ERROR} = \sqrt{\frac{1}{N} \sum (x_i - x)^2}$

- o AVE VALUE OF MEASUREMENT DATA = MEAN VALUE

$$\bar{x} = \frac{\sum_{i=1}^N x_i}{N} \quad x_i = \text{MEASURED VALUE}$$

- o AVE ERROR OF MEASUREMENT DATA = MEAN VALUE OF ERROR

$$\bar{x}_e = \frac{\sum_{i=1}^N (x_i - x)}{N} \quad \begin{array}{l} x = \text{ACTUAL VALUE} \\ x_i = \text{MEASURED VALUE} \end{array}$$

- o STD DEVIATION OF THE DATA = 1σ VALUE

$$\sigma = \sqrt{\frac{1}{N} \sum_{i=1}^N (x_i - \bar{x})^2}$$

- o STD DEVIATION OF THE ERROR = 1σ VALUE

$$\sigma_e = \sqrt{\frac{1}{N} \sum_{i=1}^N (x_{ie} - \bar{x}_e)^2} \quad x_{ie} = x_i - x$$

- o $\text{STD}^2 = \text{RMS}^2 - (\text{MEAN VALUE})^2$

EXAMPLE #1 ACTUAL VALUE = 3 5 MEASUREMENTS MADE

DATA = 2, 2, 3, 4, 4

o RMS DATA = 3.13

o $\bar{X} = \frac{15}{5} = 3$

o STD DEV OF DATA = 1σ

$$= \sqrt{\frac{(1+1+0+1+1)}{5}} = 0.89$$

CHECK EQUALITY

$$\text{STD}^2 = \text{RMS}^2 - \bar{X}^2$$

$$(0.89)^2 = (3.13)^2 - (3)^2$$

$$0.8 = 9.8 - 9$$

$$0.8 = 0.8$$

$$\text{RMS OF ERROR} = \sqrt{1/5 (1 + 1 + 0 + 1 + 1)} = 0.89$$

$$\bar{X}_e = \frac{(2-3) + (2-3) + (3-3) + (4-3) + (4-3)}{5}$$

$$\bar{X}_e = 0$$

STD DEV OF ERROR = 1σ

$$= \sqrt{\frac{(1+1+0+1+1)}{5}} = 0.89$$

CHECK EQUALITY

$$\text{STD}_e^2 = \text{RMS}_e^2 - (\bar{X}_e)^2$$

$$(0.89)^2 = (0.89)^2 - 0$$

73

39

EXAMPLE #2 ACTUAL VALUE = 0 5 MEASUREMENTS MADE

DATA = 2, 2, 3, 4, 4

o RMS, \bar{X} , STD DEV OF DATA IS SAME AS EXAMPLE NUMBER 1

o RMS OF ERROR = $\sqrt{(1/N)\sum (x_i - X)^2} = \sqrt{(4 + 4 + 9 + 16 + 16)/5} = 3.13$

o $\bar{X}_e = (2 + 2 + 3 + 4 + 4)/5 = 15/5 = 3$

o STD DEV OF ERROR (1σ) = $\sqrt{1/N\sum (X_{ie} - \bar{X}_e)^2} = \sqrt{(1 + 1 + 0 + 1 + 1)/5} = 0.89$

CHECK FOR EQUALITY

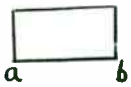
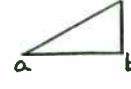
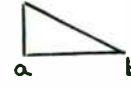
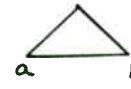

$$\text{STD}^2 = \text{RMS}^2 - \bar{X}_e^2$$

$$(0.89)^2 = (3.13)^2 - (3)^2$$

$$0.8 = 0.8$$

74

STANDARD DEVIATION OF COMMON DISTRIBUTIONS

DISTRIBUTION	STANDARD DEVIATION	
	$\frac{b-a}{3.5}$	QUANTIZING ERROR
	$\frac{b-a}{4.2}$	A SMALL σ VALUE ----> CONSISTENT MEASUREMENTS
	$\frac{b-a}{4.2}$	LARGE σ VALUE
	$\frac{b-a}{4.9}$	<ul style="list-style-type: none"> o X_i HAS WIDE VARIATION OR o MOST OF THE DATA IS CONSISTENT WITH A FEW POINTS WELL OUTSIDE THE MAJORITY WINDOW
	$\frac{b-a}{6}$	GAUSSIAN (NORMAL) DISTRIBUTION FOR 100% OF DATA AND SMALL SAMPLE SIZE USE THE FOLLOWING: $\sigma = \text{RANGE}/C_n$

n	2	3	4	5	10	20	30	50	100
C_n	1.13	1.69	2.06	2.33	3.08	3.73	4.09	4.50	5.02

75

40

REFERENCES

1. JAMES BAO - YEN TSUI, "MICROWAVE RECEIVERS WITH ELECTRONIC WARFARE APPLICATIONS," JOHN WILEY & SONS INC, 1986.
2. STEPHEN J. ERST, "RECEIVING SYSTEMS DESIGN," ARTECH HOUSE INC., 1984.
3. BERT C. HENDERSON, "PREDICTING INTERMODULATION SUPPRESSION IN DOUBLE BALANCED MIXERS", 1998/89 WJ RF AND MICROWAVE COMPONENT DESIGNER HANDBOOK.
4. STEPHEN A. MAAS, "MICROWAVE MIXERS", ARTECH HOUSE INC., 1986.
5. RICHARD G. WILEY, "ELECTRONIC INTELLIGENCE: THE INTERCEPTION OF RADAR SIGNAL", ARTECH HOUSE INC., 1985.

VSWR PERFORMANCE OF TRANSISTOR RF POWER AMPLIFIERS

by

Richard W. Brounley, P.E., RF Engineering Consultant
10341 Nicaron Court, Largo, Florida 34648 U.S.A.
1-813-393-8177

2.

Introduction

The operation of high power RF solid-state power amplifiers under mismatched conditions is one of the most important and difficult parts of amplifier design. A design which is too conservative can be overly expensive and complex, while one which is overstressed can have an excessive rate of failure. The object of this paper is to explore the various factors which must be considered when specifying the mismatched performance of an amplifier. The test data and conclusions are primarily for power levels of 500 watts and higher, operated as saturated Class B amplifiers below 100 mhz. Other frequencies and classes of operation may have similar characteristics but are not specifically addressed.

I. Basic Characteristics of a Mismatched Transmission Line

A transmission line which has a matched source impedance but a mismatched load impedance will have a constant developed output power versus the phase angle of the reflection coefficient

ρ . The output power will be:

$$P_o = P(1 - \rho^2) \text{ where } P = 50 \text{ ohms power}$$

While this is well documented, it can be demonstrated using

the simple equivalent circuit shown in Figure 1. Here the power output has been chosen to be 500 watts and the mismatched load to have a VSWR of 5.9:1. The value of Z_L can be found for 20° steps of θ , for $\rho = .71L\theta$ using a Smith Chart. The output power, current and power dissipated in the source impedance can then be calculated. Figures 2, 3, and 4 display these three parameters.

In similar fashion, the source impedance can be lowered and the parameters recalculated. Figures 2, 3, and 4 display the output power, current and power dissipated for a source impedance of 21.53 ohms. This is more representative of a saturated power amplifier whose collector or drain efficiency is nearer 70% rather than the 50% of the 50 ohm source impedance example.

Figure 2 demonstrates the variation in power developed as the phase angle of ρ is varied over a range of ± 180 degrees for these two cases. The highest power for the lower impedance case is near 500 watts while the lowest is only about 160 watts. In contrast, the 50 ohm source delivers a constant 250 watts.

Figure 4 is important since it displays the power dissipation in the source versus the phase angle of ρ . The maximum allow-

3.

able junction temperature of the RF transistors will determine the range over which mismatched performance can be specified.

Included in Figures 2 through 4 is the mismatched performance of a 500 watt bipolar amplifier using four transistors in the final. The offset phase from the models is a function of the amplifier's output matching circuits. It can be concluded that the source impedance of the amplifier is lower than 50 ohms but higher than the 21.53 ohm model. It has been estimated to be about 28 ohms.

This amplifier is used to drive a laser which has a VSWR of 5.9:1 before it strikes. In order to strike the laser effectively, the amplifier is phased with the laser's reflection coefficient before striking so as to generate maximum power. This results in the maximum DC input current being drawn as well as the maximum power being dissipated in the transistors. Figures 2 through 4 illustrate these parameters at a phase angle of about -60 degrees.

In the case of lasers, it is not possible to protect the transistors by reducing the B+ voltage through fast-acting current limiting or by reducing the drive to the final transistors because ineffective striking will result due to the reduced peak power. Reduced B+ voltage, coupled with additional transistors to achieve the same power rating, is not a

4.

practical solution either due to both cost and size limitations. With the heatsink and temperature specifications, the power dissipation for the four transistors is limited to about 400 watts. The dissipation into the mismatch at $\theta = -60^\circ$ is about 950 watts. The 28v B+ voltage would then have to be reduced to about 18 volts to keep the dissipation below 400 watts. The matched power would then be reduced to about 200 watts, thereby requiring an additional 6 transistors to be added to regain the 500 watts of matched output power. In general, this is not a practical means of mismatch protection for amplifiers of this power level and higher.

In lieu of the above, a pulsed format is used which delivers full peak power into the mismatch until striking occurs at which time normal pulsed or CW operation commences. This pulsed format must have both a limited pulse length and duty cycle to adequately protect the transistor against excessive power dissipation. A pulse length of 2 msec and a duty cycle of 20% has proven to provide reliable operation for the transistors as well as striking the laser effectively.

II. VSWR Characterization

In order to characterize the VSWR performance of an amplifier, a family of curves is plotted as shown in Figures 5 through 7. The amplifier used here is a 4 transistor FET design using broadband transformers for both matching and the combining

of the two push-pull pairs. The tests are conducted at a low duty cycle in order to protect the amplifier. The real power developed is measured directly rather than by using the forward and reflected power on the transmission line. A series of VSWR loads is constructed by locating on the Smith Chart appropriate reactances in parallel with 50 ohms which provide the desired VSWR. The phase is then varied through 180 degrees by means of calibrated coaxial cables. These curves can then be used to analyze the mismatch capabilities of the amplifier.

Figures 8 through 10 characterize the amplifier with 90° delay networks placed in series with the input of one push-pull pair and in series with the output of the other pair. These 90° networks have a major effect upon the VSWR characterization and basically make the amplifier appear to have an output source impedance closer to 50 ohms. Isolation is also provided to a driver stage thereby resulting in easier cascadeability. The power dissipation curve in Figure 10 is misleading, however, because the two push-pull pairs see reflection coefficients 180 degrees apart and, while one is delivering maximum power, the other is delivering minimum power. VSWR derating must take this into account; otherwise, one pair can be overstressed while the other dissipates only low power. The condition can then reverse when θ changes by 180 degrees.

In addition, less maximum peak power is generated than when the 90 degree networks are not used and laser striking may not be as effective. The characteristics have value, however, for some applications since they offer a relatively flat developed power versus phase angle as well as a relatively constant current demand from the DC power supply.

These tests also demonstrate the stability of the amplifier under mismatched conditions. Spurious oscillations can be observed on an oscilloscope and should be corrected since they can increase the failure rate and inhibit protection methods. In general, FET amplifiers give superior mismatched stability performance over those using bi-polar transistors. Also, the 90 degree delay networks enhance stability and can make a significant improvement, particularly for bi-polar designs.

III. Matched Power Characterization

In order to use the VSWR curves to evaluate the amplifier's mismatched performance, it is necessary to determine the matched power capability of the amplifier. This depends on a number of factors such as the type of heatsinks, the amplifier efficiency, the maximum allowable junction temperature, etc. The performance of the FET amplifier is shown below and is used as an example. This is a pulsed amplifier whose average

7.

output power is determined by the duty cycle. The heatsink is liquid cooled in combination with forced air. The thermal resistance from the heatsink coolant connection to the transistors' junction has been measured to be .8° C/W. Also, the system is duty cycle limited at 70%.

Table 1

Duty Cycle %	P _o wpk	P _o w avg	P _D w avg	P _D /Trans. w avg	Eff %	T inlet °C	T j °C
10	970	97	48	12	67	27	37
25	958	240	116	29	67	27	50
50	911	456	240	60	66	27	75
70	860	602	324	81	65	27	92
70	819	573	352	88	62	40	110

It is observed that both the peak output power and efficiency drop as the transistor junction temperature is increased. This should be considered when using the VSWR curves since these tests are conducted at a low duty cycle. The VSWR curves are valuable in estimating the power developed versus the phase angle of the reflection coefficient as well as the maximum dissipation. Tests under average power conditions should then be conducted to verify performances by measuring transistor dissipation and estimating junction temperature.

8.

As an example, Figure 5 shows a developed power that varies from a minimum of 760 watts peak to a maximum of 1080 watts peak for a VSWR of 1.5:1. Figure 7 shows a dissipation of 550 watts peak for $\theta = +120$ degrees. At a 70% duty cycle, this would be 385 watts average and would raise the junction temperatures to about 120° C. If a maximum of 140° C. is used for reliability purposes, this amplifier would be operating safely under these conditions. For VSWR's in excess of 1.5:1, however, the dissipation quickly exceeds the safe dissipation level and protection methods should be employed. For instance, at a VSWR of 2.7:1, the dissipation is 1025 watts peak and the duty cycle would have to be limited to about 38% or the dissipation reduced by some other means.

IV. Protection Methods

The goal in the design of high power amplifiers is to achieve as much power per transistor as possible without sacrificing reliability. The VSWR performance, in conjunction with protection techniques, is important in achieving this goal. In the example discussed, a maximum operating VSWR of 1.5:1 is specified and the amplifier is capable of 600 watts of average power under this and the thermal conditions described. The amplifier must be able to survive VSWR's in excess of 50:1, however. There are two techniques used to achieve this requirement which are discussed below.

1. VSWR Detection

In this method the forward and reflected voltages on the transmission line are detected and a voltage comparator is used to shut down the amplifier when the ratio indicates an excessive VSWR. Periodic resetting is used to determine if the VSWR is still present. If it has been removed, the amplifier is automatically restored to normal operation. If not, the cycle of shut down and reset continues with a duty cycle low enough to provide protection under any mismatched condition.

2. Current Limit

Figure 5 demonstrates that the power developed from $\theta = +20^\circ$ to 170° is actually higher than the matched power. If the DC power supply is set to current limit at about 35 amps peak, or 24.5 amps average for 70% duty cycle, protection for VSWR's in excess of 1.5:1 will be achieved. For the protection to be effective, the response time of the current limiter should be less than 2 msec; otherwise, the junctions of the transistors can rise to an excessive temperature before the current limiter can reduce the dissipation. The current limiter combined with the VSWR detection method is particularly effective because setting the VSWR activation point too close to the operating VSWR can result in a critically performing system. A VSWR setting of 3:1 with reliance on the current limiter for protection up to that point has been

a reliable combination.

SUMMARY

The preceding has been an effort to explore the various factors contributing to power amplifier design under mismatched conditions. The methods developed maximize the power output per transistor while retaining reliable operation. While the examples used are for a particular design, the principles should be appropriate for designs with different requirements and classes of operation.

FIGURE 1 MISMATCHED TRANSMISSION LINE EQUIVALENT CIRCUIT MODEL

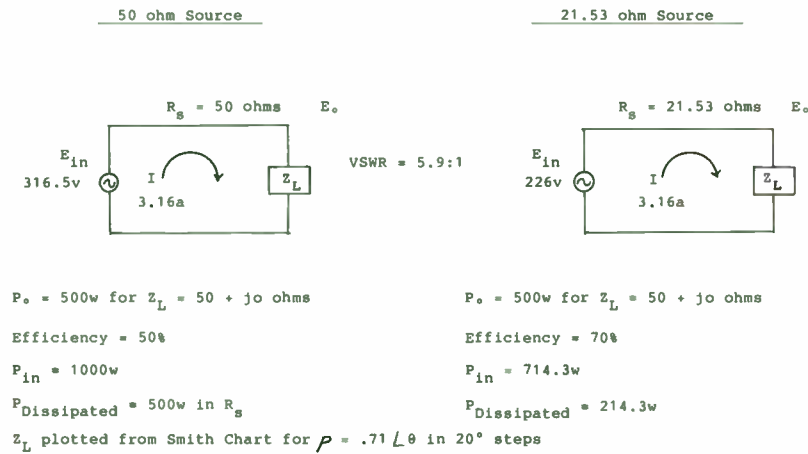


Figure 3 Current vs Phase Angle for Various Sources

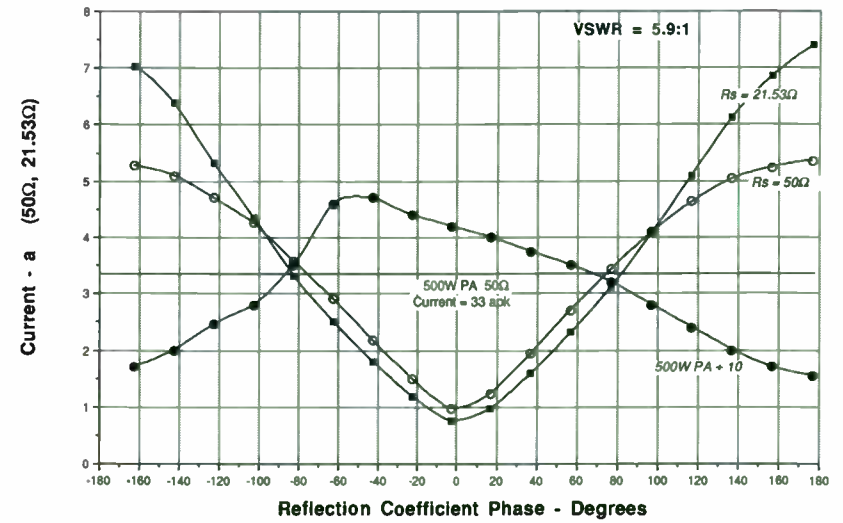


Figure 2 Power Developed vs Phase Angle for Various Sources

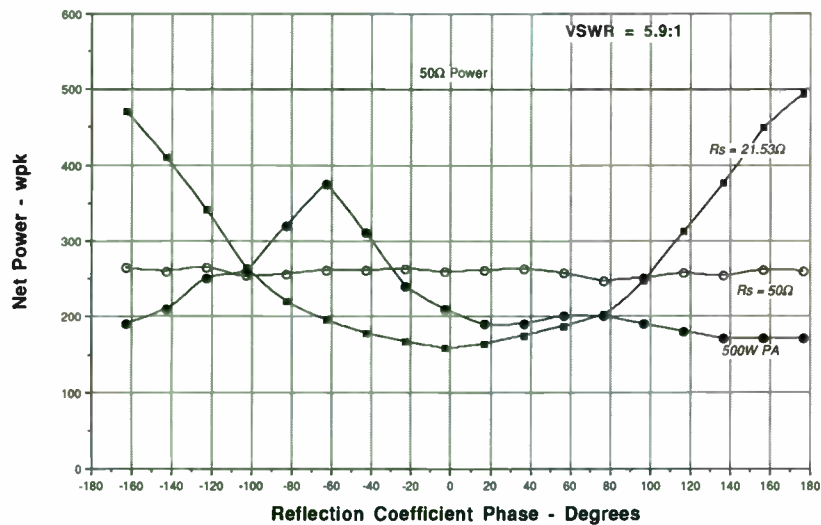


Figure 4 Power Dissipation vs Phase Angle for Various Sources

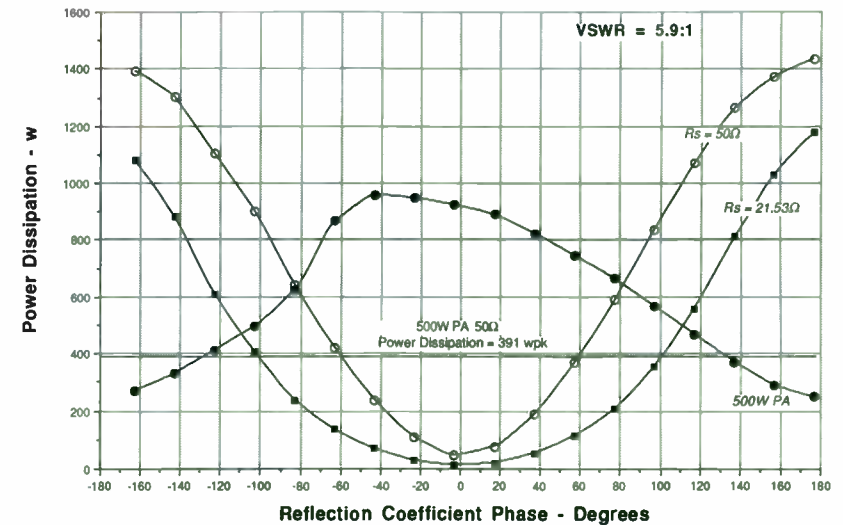


Figure 5 Power Developed vs Phase Angle for Various VSWR's

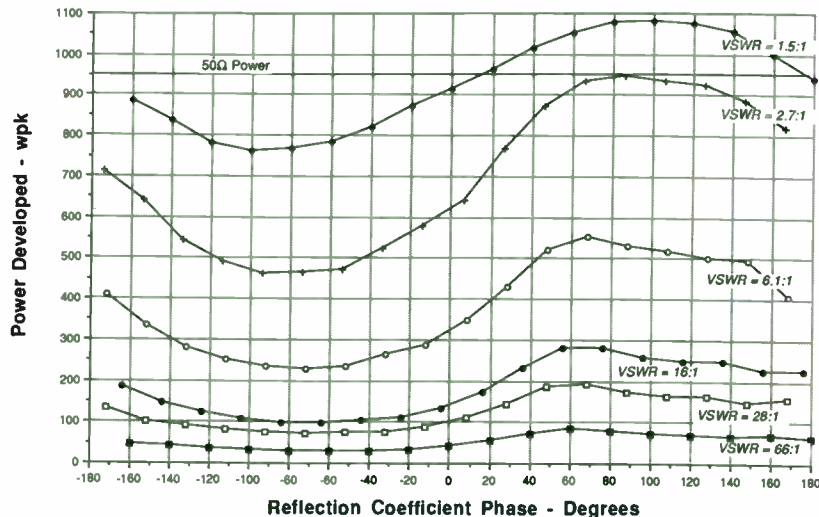


Figure 7 Power Dissipated vs Phase Angle for Various VSWR's

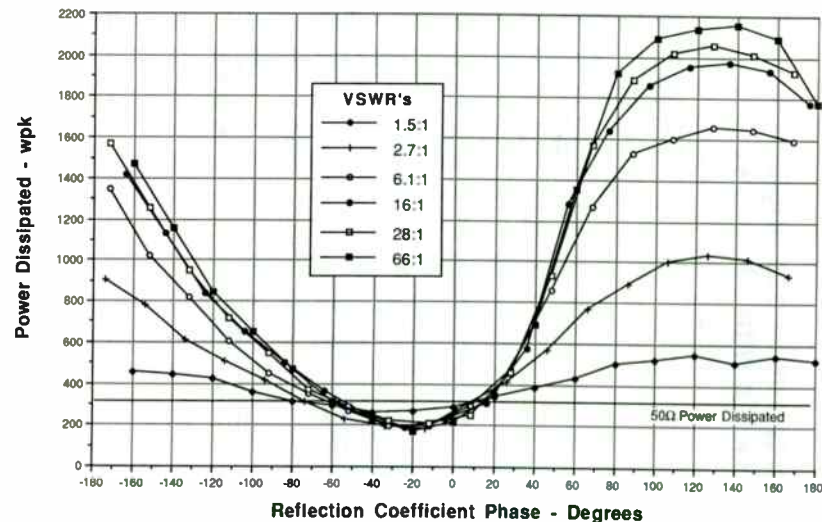


Figure 6 Peak DC Input Current vs Phase Angle for Various VSWR's

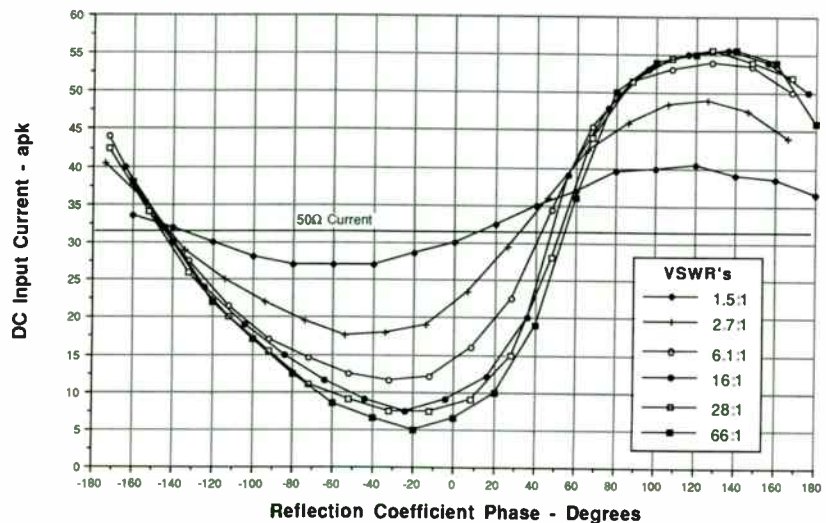


Figure 8 Power Developed vs Phase Angle for Various VSWR's with 90° Delays

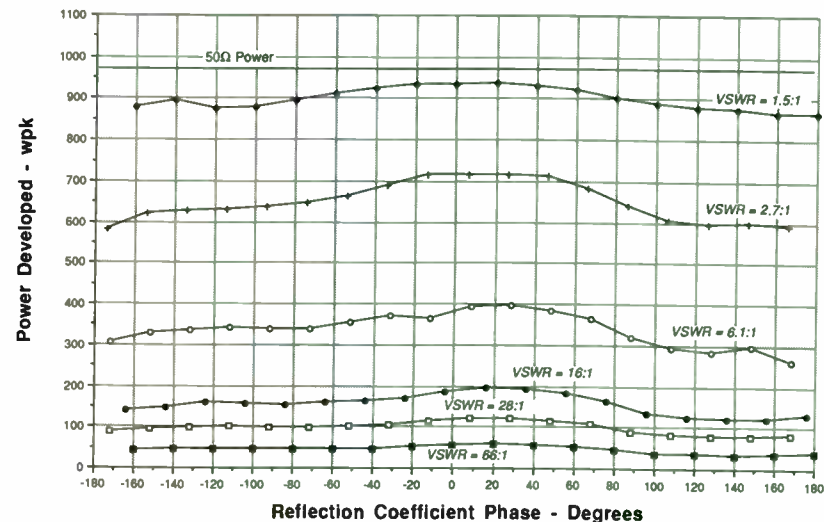


Figure 10

Power Dissipated vs Phase Angle for Various VSWR's with 90° Delays

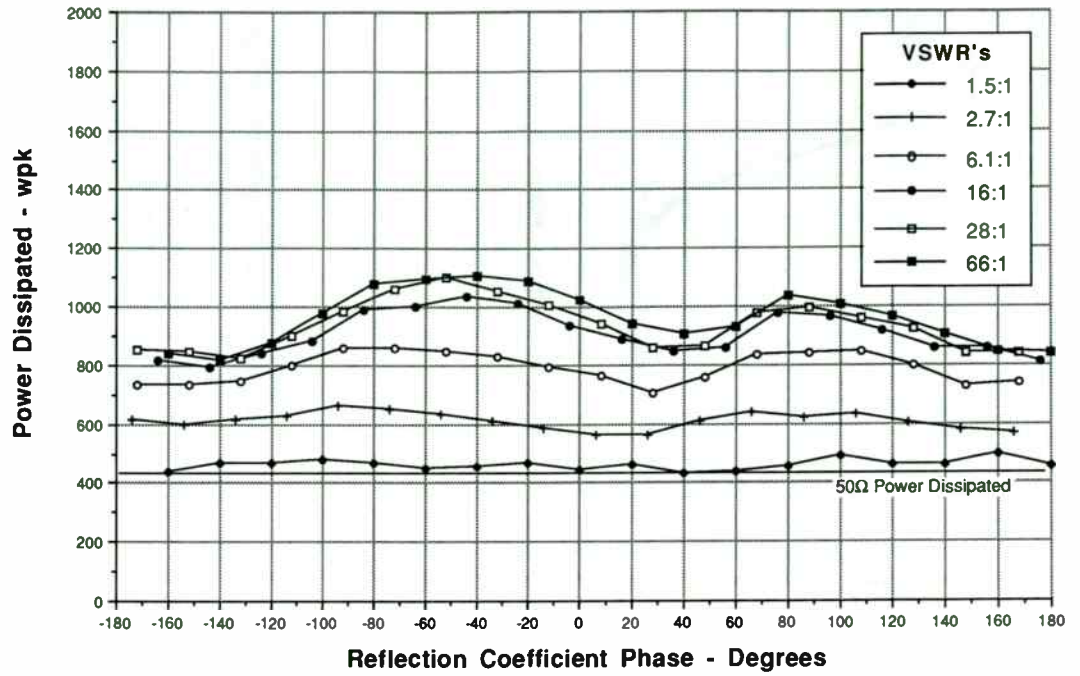
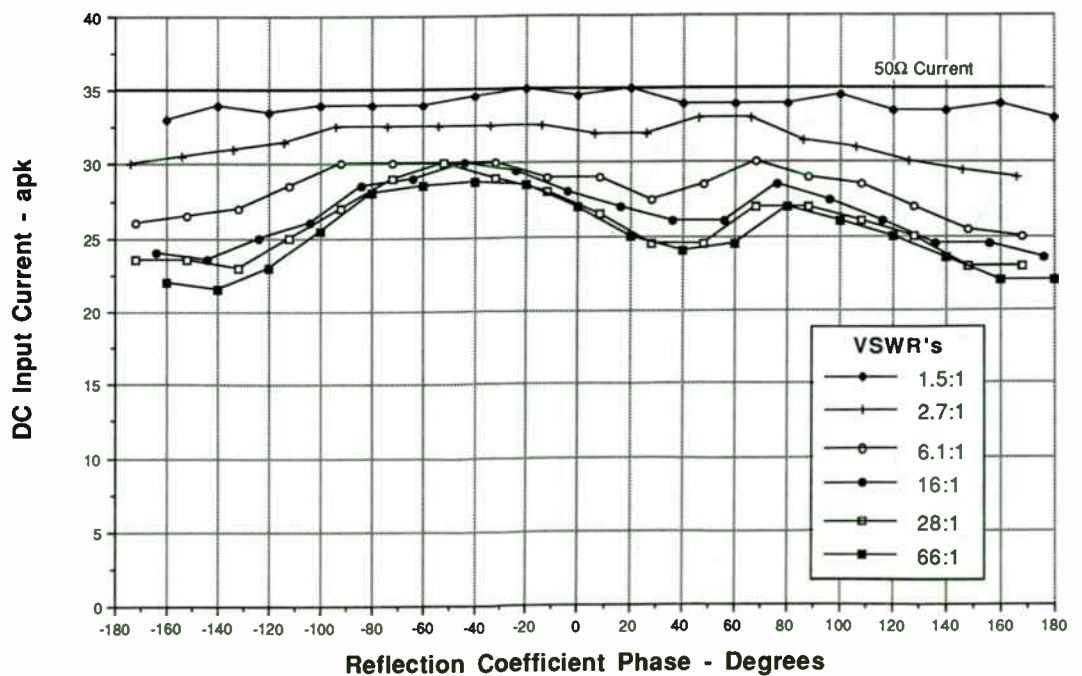


Figure 9

Peak DC Input Current vs Phase Angle for Various VSWR's with 90° Delays



A Novel Technique for Analyzing High Efficiency Switched Mode Amplifiers

Kazimierz (Kai) Siwiak

Motorola, Inc., Paging Division, Boynton Beach, FL.

Introduction

A novel circuit analysis technique was developed for investigating the efficiency performance of high efficiency amplifiers operating in the switched mode. The approximate technique is based on a simple but realistic model of a non-ideal switch. Within the limits of the approximation, the optimum operating parameters for several circuit configurations are derived in terms of the switch damping factor D (analogous to Q in resonant circuits). The efficiency performance of a current driven switch terminated in a fundamentally resonant tuned load (of which the class E mode amplifier [1] is a particular example) is contrasted with that of the switch terminated with harmonically tuned loads (of which the class F amplifiers [2] are particular examples).

It is shown that, neglecting switching transient losses, the losses in switched mode amplifiers having a non-ideal switch are proportional to circuit configuration dependent constants divided by the switch damping factor D . The constants depend on the particular form of the reactive load, and will be derived for the cases of a fundamentally resonant and for harmonically tuned loads. Voltages across and currents through the switch are derived and voltages are shown for the different load configurations. The resulting analysis gives insight into the practical implementations of high efficiency RF amplifiers, particularly at high frequencies. Different modes of switching amplifier operation can easily be compared with respect to efficiency, switch device capability requirements, voltage and current wave forms and load mismatch effects.

High efficiency switched mode amplifier operation

There are several necessary conditions that must be satisfied for 100% efficient conversion of DC to RF power. These include:

- i) voltage and current may not appear across the switch simultaneously,
- ii) the time derivative of the voltage wave form must be zero at each switch transition.

Condition [i] implies that the switch resistance is zero when conducting and infinite when off, while condition [ii] implies a particular value of switch capacitance or tuned load. It has been shown that [ii] can not be satisfied simultaneously for both switch transitions [3]. This analysis ignores the switching transient, that effect is studied in [4] and [5], and assumes that the desired switch duty cycle actually exists. The effect on efficiency of the non-ideal switch, that is, the switch resistance and capacitance is then studied.

This analysis was motivated by observing that the capacitances for some practical high power devices used as switches at VHF and UHF often exceed the optimum capacitance value [6] required for class E mode operation. The analysis explores, then, the limit of the optimum efficiency under those circumstances.

Current driven switch terminated in a fundamentally tuned load

Amplifier devices operating in the switched mode can be represented by a periodically operated ideal switch S , as shown in Figure 1, having a parallel capacitance C_S and switch resistances R_S and R_C . The switch-leg series resistance R_S and the common series resistance R_C are ignored for the moment. Since the voltage source V_O supplies a constant current I_O through the choke coil L_O and the load R_L passes only a fundamental frequency current because of the (high Q) series combination C_1 and L_1 , the switch/capacitor current must be:

$$i(t) = I_O + I_A \cos \omega_0 t + I_B \sin \omega_0 t \quad (1)$$

where $\omega_o = 2\pi f_o$ is the radian frequency. A 50 percent duty cycle for the switch is chosen for convenience. The switch is open from $t = -\pi/2$ to $\pi/2$. The average DC current through the switch must be I_o so the integral of $i(t)$ over the conducting interval of the switch gives $I_A = -\pi I_o/2$. The average voltage across the switch in a period must be V_o so:

$$V_o = \frac{\omega_o}{2\pi} \int_{-\pi/2\omega_o}^{\pi/2\omega_o} v(t) dt \quad (2)$$

where the switch voltage:

$$v(t) = \frac{1}{C_s} \int_{-\pi/2\omega_o}^t i(t') dt' \\ = \frac{I_o}{\omega_o C_s} \left[\omega_o t - \frac{\pi}{2} \sin \omega_o t \right] - \frac{I_B}{\omega_o C_s} \cos \omega_o t \quad (3)$$

which, with equation (2) gives $I_B = -\pi V_o \omega_o C_s$. The switch voltage $v(t)$ normalized by the source voltage is:

$$\frac{v(t)}{V_o} = \frac{(\omega_o t - \frac{\pi}{2} \sin \omega_o t)}{x} + \pi \cos \omega_o t, \quad (4)$$

over the interval $-\pi/2 \leq \omega_o t \leq \pi/2$ when the switch is open, and zero with the switch conducting, and where $x = V_o \omega_o C_s / I_o$. The switch current, normalized to the DC current, is continuous,

$$\frac{i(t)}{I_o} = (1 - \frac{\pi}{2} \cos \omega_o t) - x \pi \sin \omega_o t \quad (5)$$

and flows either through the switch S when the switch conducts or, otherwise, through the capacitor C_s . The power delivered to

the load resistor R_L must equal $V_o I_o$, and the r.m.s. current through the load is $(I_A^2 + I_B^2)/2$ so substituting for I_A and I_B , the load resistance is written in terms of the source voltage and current (hence DC power) and the switch capacitance C_s :

$$R_L = \frac{V_o}{I_o} \frac{8}{\pi^2} \left[\frac{1}{1 + (2x)^2} \right] \quad (6)$$

Given a source voltage V_o and a current I_o , the required load resistance can be found once the parallel capacitance of the non-ideal switch is known.

If we set the derivative of the voltage to zero when the switch closes $t = \pi/(2\omega_o)$, then differentiating (4), we get $x = x_E = (1/\pi)$ and, hence, the required switch capacitance for that case must be, $C_E = I_o / (V_o \omega_o \pi)$, which is the condition for the class E mode switching amplifier. C_E , of course, can be realized by adding parallel capacitance to C_s if C_s is smaller than C_E . Now using equation (6), $\omega_o C_E R_L = 0.1836$, which is the value for class E operation [7] when the Q of the load circuit filter (L_1, C_1) is assumed to be infinite.

The expression for efficiency can be found by perturbing the above results, letting R_s and R_c take on small (with respect to R_L) non-zero values. The power lost in R_s and R_c is found by integrating the square of the current $i(t)$ flowing in the respective resistors over a complete period (current flows in R_s only when the switch conducts), and multiplying by the resistance in which the current flows. The fraction of total power lost in resistors R_s and R_c , after integration and sufficient algebraic manipulation is:

$$p = R_s \omega_o C \left[\frac{a_s}{x} + x b_s \right] + R_c \omega_o C \left[\frac{a_c}{x} + x b_c \right] \quad (7)$$

where the circuit constants are,

$$a_s = (3/2 + \pi^2/16) \quad a_c = (1 + \pi^2/8)$$

$$b_s = \pi^2/4 \quad b_c = \pi^2/2$$

For convenience we let the damping factor D of the switch be, in turn, $D_s=1/(\omega_0 R_s C_s)$, and $D_c=1/(\omega_0 R_c C_s)$. Efficiency is now written as:

$$u = 1 - p \quad (8)$$

for which an optimized value of x can obviously be found for best efficiency by minimizing p with respect to x in (7). That optimized efficiency in terms of the circuit constants and the switch damping factors is:

$$u_{opt} = 1 - 2\sqrt{(a_s/D_s + a_c/D_c)(b_s/D_s + b_c/D_c)} \quad (9)$$

The value of x for optimizing efficiency is:

$$x_{opt} = \sqrt{\frac{(a_s/D_s + a_c/D_c)}{(b_s/D_s + b_c/D_c)}} \quad (10)$$

Note that the optimum efficiency and the optimum value of x differ from those found above for the class E mode. This is because we have not imposed conditions on the wave forms at the switching transitions.

Since x is proportional to the DC load resistance of the harmonically operated switch, it fixes the optimum relationship between the power and the source voltage. In other words, for a given source voltage V_o , and a given switch damping factor D , there is an optimum power level for maximum efficiency.

Current driven switch terminated in a harmonically tuned load

Harmonic tuning of the load is an effective method of achieving enhanced efficiency operation, particularly at frequencies in the

several GHz range [8]. The analysis of this paper is readily extended to harmonically tuned load circuits such as shown in Figure 2. Compared with Figure 1, in Figure 2 there is an additional inductor L_2 and capacitor C_2 chosen to series resonate at the second harmonic of the operating frequency f_o . In addition, the ratio of L_2 to C_2 is chosen, in this example, to parallel resonate with switch capacitance C_s at the third harmonic of f_o . L_2 and C_2 have a zero at $2f_o$, while L_2 , C_2 and C_s have a pole at $3f_o$. Thus the circuit is representative of a class F circuit in which the second and third harmonics are tuned. The switch is again operated with a 50% duty cycle at frequency f_o . As in Figure 1, only fundamental frequency currents flow in the load R_L and only DC flows through choke L_o , hence the total switch current is again given by equation (1). Now, however, capacitor C_s current is $i_1(t)$, and the L_2 , C_2 leg current is $i_2(t)$, both of which include DC and fundamental frequency currents (forcing functions) as well as third harmonic components (transient solution) when the switch is open because L_2 , C_2 and C_s are a series resonant loop at the third harmonic:

$$i_1(t) = I_A + I_C \cos \omega_0 t + I_E \sin \omega_0 t \dots$$

$$+ I_G \cos 3\omega_0 t + I_I \sin 3\omega_0 t \quad (11)$$

and

$$i_2(t) = I_B + I_D \cos \omega_0 t + I_F \sin \omega_0 t \dots$$

$$+ I_H \cos 3\omega_0 t + I_J \sin 3\omega_0 t \quad (12)$$

The two current expressions include unknowns I_A through I_J . When the switch is closed, $i_3(t)$ flows through the switch leg. DC and fundamental frequency currents are again the forcing functions, while the second harmonic zero allows a second harmonic transient solution, so:

$$i_3(t) = I_A + I_B + (I_C + I_D) \cos \omega_0 t + \dots$$

$$+ (I_E + I_F) \sin \omega_0 t + I_K \cos 2\omega_0 t + I_L \sin 2\omega_0 t \quad (13)$$

and two additional unknowns I_K and I_L are introduced. The DC terms $I_A + I_B$ of $i_3(t)$ add up to I_O . Additional conditions such as the average voltage across the switch is V_O and $i(t) = i_1(t) + i_2(t) + i_3(t)$ along with some very dense algebra yields the expression for the normalized switch voltage as:

$$\frac{v(t)}{V_O} = \left(\frac{4\omega_0 t}{9} - \frac{3\pi}{16} \sin \omega_0 t + \frac{5\pi}{144} \sin 3\omega_0 t \right) \frac{1}{x} + \dots + \frac{27\pi}{32} \cos \omega_0 t - \frac{15\pi}{32} \cos 3\omega_0 t \quad (14)$$

during the switch open interval and zero otherwise. The switch current is continuous,

$$\frac{i(t)}{I_O} = 1 - \frac{\pi}{2} \cos \omega_0 t - \frac{9\pi}{4} x \sin \omega_0 t \quad (15)$$

for all t . Efficiency is again calculated using equations (7) and (8), using the new circuit coefficients a_s , b_s , a_c and b_c found for this circuit configuration. Omitting the tedious integrations and algebra, the new circuit coefficients are:

$$\begin{aligned} a_s &= 2.3792 & a_c &= 2.3939 \\ b_s &= 12.4912 & b_c &= 19.1272 \end{aligned}$$

The optimum efficiency is given by equation (9), and the optimum value of x is from (10), both with the above coefficients.

The efficiencies of switched mode circuits

It is interesting to look at the efficiency of these circuits under the conditions that the losses are due to either the switch leg resistance R_s or the combined path resistance R_c . With those simplifications, the efficiency expression (9) is:

$$u = 1 - \frac{2\sqrt{ab}}{D} \quad (16)$$

where D is D_s or D_c as appropriate. In Table 1 six cases are compared with respect to efficiency and peak switch voltage:

TABLE 1. Efficiency and Peak Switch Voltages for Six Cases.

Case:	$2\sqrt{ab}$	V_{peak}	$V_{\text{peak}} \sqrt{x}$
a. Fig 1., opt, $R_c=0$	4.57	3.200	3.08
b. Fig 1., opt, $R_s=0$	6.64	3.250	2.67
c. Fig 1., class E, $R_c=0$	7.44	3.562	2.01
d. Fig 1., class E, $R_s=0$	8.59	3.562	2.01
e. Fig 2., class F, $R_c=0$	10.90	3.016	1.99
f. Fig 2., class F, $R_s=0$	13.53	3.027	1.80

Losses for each case are proportional to the number in the second column. Evidently, as shown by cases (a) and (b), the simplest circuit configurations having the simplest conditions give the best efficiency according to (16) when only the switch damping factor D is considered. Cases (c) and (d) show that imposing a condition on the voltage at the switch transition (reducing a transient loss not considered here) results in slightly sub-optimum efficiency when compared to cases (a) and (b). Figure 3 shows the voltage wave forms of the switch voltage for case (a) with the optimum value of x (solid line) and for case (c), the class E mode (dotted line) of the circuit in Figure 1 with $R_c=0$. Only slight differences are seen, chiefly that the class E mode results in a slightly higher peak voltage for a fixed source voltage V_O , and that the slope of the class E mode voltage is zero when the switch closes.

Finally, attempting to shape the switch peak voltage with a class F circuit costs additional efficiency degradation as shown by cases (e) and (f), but slightly lowers the switch peak voltages for a given source voltage. Figure 4 shows the voltage wave form for the class F case (e). We note that output power is equal to $V_O^2 \omega_0 C_S / x$, so the peak of the voltage wave form must be multiplied by the square root of x to compare voltages at the

same output power for a given device capacitance. When the peak voltage is normalized to a constant output power (by multiplying by the square root of x), the lower peak voltage advantage of class F largely vanishes as seen in the last column of Table 1, while the optimum efficiency cases (a) and (b) have the highest peak voltages. This is reasonable, since for a constant power output the current, and hence switch losses, go down as voltage increases. The peak voltages were obtained numerically from equations (4) and (14) using the MathCAD [9] analysis program.

An "ideal" class F circuit can be modelled as an ideal switch driven by a voltage source through a quarter wave transmission line and has a perfect square wave voltage across the switch. The peak value of the switch voltage is equal to twice the source voltage [10]. Clearly, more than two harmonics must be controlled to approach the "ideal" class F square wave, however, the overshoot, evident in Figure 4, giving rise to Gibbs [11] phenomenon must be controlled.

Peak voltages under load mismatch conditions

Let's examine the peak voltage when the load R_L is disconnected. For the circuit of Figure 1, we then have a capacitor C_S charged periodically by a constant current source. The charge is dumped when the switch S conducts. The capacitor voltage wave form in that case is a ramp when the switch is open. Since the average voltage must still be V_O , it follows that the peak voltage is $4V_O$. A practical switching device needs to survive that open circuit condition. This is not necessarily the worst peak voltage condition, simply one that is likely with an open load.

The circuit of Figure 2 is not as readily amenable to an open load peak voltage analysis when L_2 and C_2 are present, but with the load open, the switch-open impedance can be shown to be:

$$Z(\omega) = \left(\frac{4}{9} \right) \left[\frac{1 - \left(\frac{\omega}{2\omega_O} \right)^2}{1 - \left(\frac{\omega}{3\omega_O} \right)^2} \right] \quad (17)$$

compared with $1/(j\omega C_S)$ for the Figure 1 case. To first order, the load circuit looks like a somewhat larger capacitor than in Figure 1. The pole at the third harmonic will simply introduce a slight third harmonic ripple onto a ramp shaped voltage wave form. The peak open load voltage will thus again be in the neighborhood of $4V_O$ as before.

The efficiency of RF switched mode amplifiers compared

The efficiency versus source voltage of four RF amplifiers operated as switches is shown in Figure 5. The DC input power is chosen as 2 watts and the operating frequency is 900 MHz. Fixing the power at 2 watts and varying the source voltage means that the RF load resistance must be varied with source voltage according to equation (6) since x changes with V_O . Two switch devices are modelled: a GaAs FET represented by $C_S=5\text{pF}$ and $R_S=0.36$ ohms having a $D_S=100$, and a silicon BJT represented by $C_S=5\text{pF}$ and $R_S=0.72$ ohms for a $D_S=50$. Figure 5 shows that for the circuit of Figure 1 (solid curves) the optimum efficiency design voltage for the $D_S=100$ device as well as for the $D_S=50$ device is about 8.1 volts. In both cases, operating in the class E mode requires that the design voltage be 4.75 volts as marked by the X's on the solid curves.

The dotted curves of Figure 5 show the efficiency performance versus source voltage for the circuit of Figure 2 with $D_S=100$ and $D_S=50$ devices. It is seen that the highest efficiency for a given device is achieved with the circuit of Figure 1. Additionally, operating in the class E mode does not necessarily result in the optimum efficiency when a non-ideal switch is considered.

Conclusions

A novel analysis was developed to study the efficiency performance of amplifiers operating in the switched mode. Losses were demonstrated to depend on circuit dependent constants and on the inverse of the switch damping factor D. When switching transients are not considered, it was shown that the optimum efficiency is achieved with a class E-type circuit. The class E mode operating point, however, resulted in degraded performance. Harmonic tuning in the case studied resulted in further degradation of performance when compared with both the optimum and class E mode operating points for a given switch damping factor D. Open load switch voltages were shown to be similar at four times the source voltage for both circuits.

Acknowledgement

The author is deeply indebted to the late Robert Francis Steel who suggested this analysis technique and critiqued the earlier work.

References:

1. N. O. Sokal, A. D. Sokal, "Class E - a new class of high efficiency tuned single-ended switching power amplifiers," IEEE Journal of Solid State Circuits, Vol. SC-10, No. 3, June 1975.
2. V. J. Tyler, "A new high efficiency high power amplifier," Marconi Review, Vol. 21, No. 130 pp.96-109, 3rd Quarter, 1958.
3. F. H. Raab, "Analysis of second-harmonic-peaking power amplifiers," RN82-26, Green Mountain Radio Research Company, Winooski, VT, 1 April 1982.
4. F. H. Raab, N. O. Sokal, "Transistor power losses in the class E tuned power amplifier," IEEE Journal of Solid State Circuits, Vol. SC-13, No. 6, Dec. 1978.
5. M. Kazimierczuk, "Teoria wzmacniacza mocy wielkiej czestotliwosci klasy E," (Theory of high efficiency Class E amplifiers) Rozprawy Elektrotechniczne, 1979, 25, z. 4, ss.957-986, 1979.
6. M. Kazimierczuk, "Effects of the collector current fall time on the class E tuned power amplifier," IEEE Journal of Solid State Circuits, Vol. SC-18, No. 2, April 1983.
7. **Solid State Radio Engineering**, H. L. Krauss, C. W. Bostian, F. H. Raab, John Wiley & Sons, New York, 1980, p. 452.
8. T. Nojima, S. Hishiki, "High efficiency microwave harmonic amplifier," 1988 IEEE MTT-S Digest, pp 1007-1010, June 1988. Originally presented (in Japanese) at the 1986 Electronic Communication Conference, Japan.
9. **MathCAD**, version 2.53, MathSoft, Inc., Cambridge MA.
10. D. M. Snider, "A theoretical analysis and experimental confirmation of the optimally loaded and overdriven RF power amplifier," IEEE Transactions on Electron Devices, Vol. ED-14, No. 12, Dec. 1967.
11. **An Introduction to Statistical Communication Theory**, J. B. Thomas, John Wiley & Sons, New York, 1969.

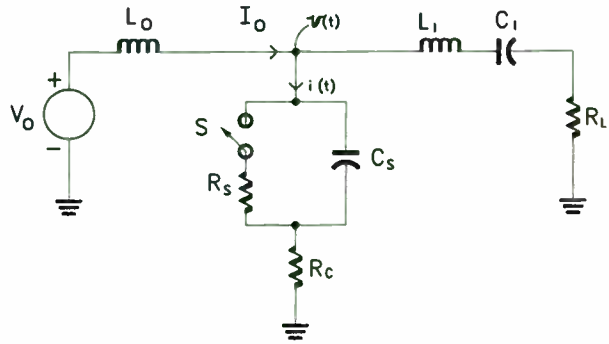


Fig. 1. Switched mode amplifier with a fundamental frequency resonant load.

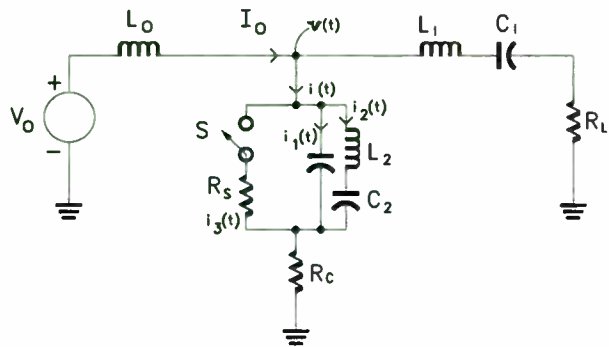


Fig. 2. Switched mode amplifier with a harmonically tuned load.

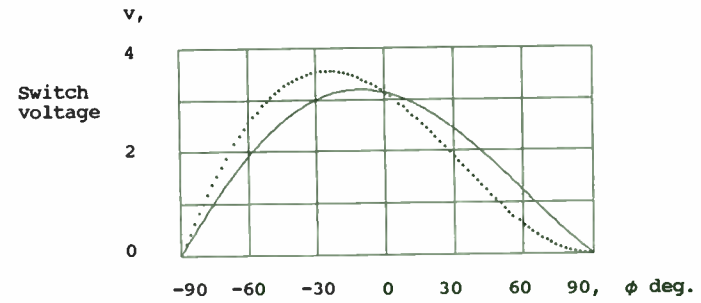


Fig. 3. Voltage waveform on the switch for the optimum case (a) (solid) and for the class E mode case (b) (dotted) of Table 1.

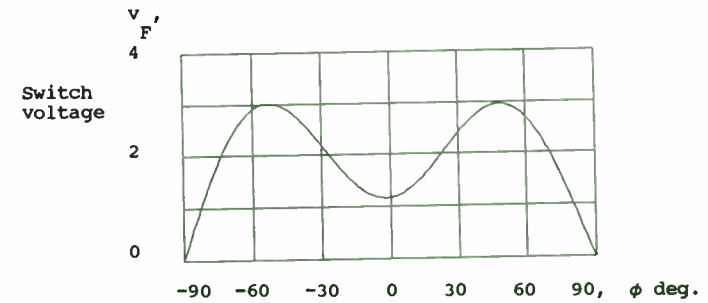


Fig. 4. Voltage waveform on the switch for the class F case (e) of Table 1.

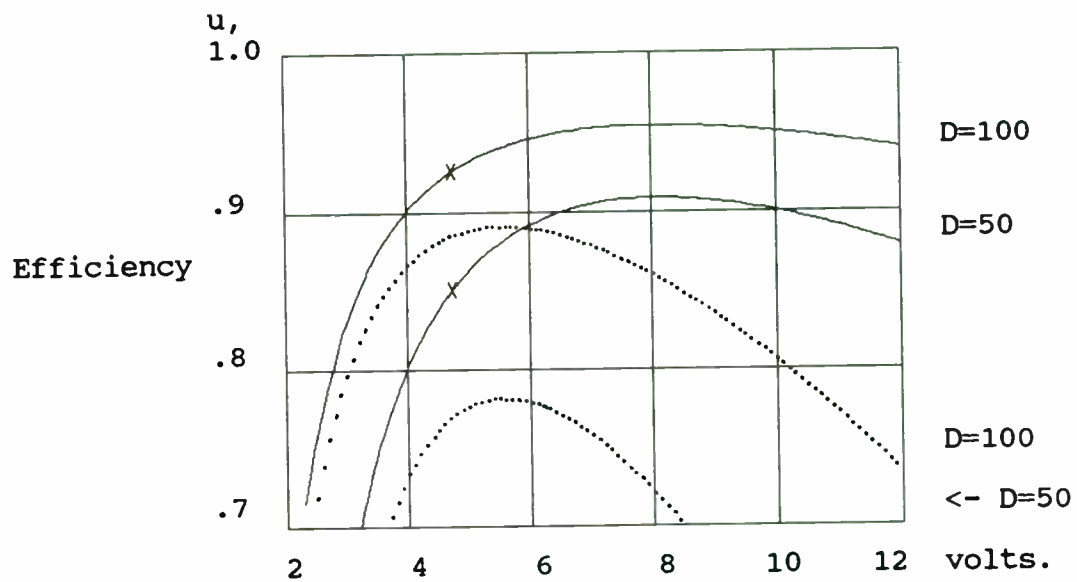


Fig. 5. Efficiency as a function of source voltage, circuits of Fig. 1 (solid) and Fig. 2 (dotted) for $D=100$ and $D=50$ and the DC input power set to 2 watts. The class E mode operating point is marked (x).

by

Korné Vennema
PHILIPS COMPONENTS
Gerstweg 2
6534 AE Nijmegen
The Netherlands

INTRODUCTION

Today's market for mobile telephone systems is increasing very rapidly. System designs require active devices for the transmitter portions of handheld units, mobile equipment (car radio's), and the base-stations. This paper addresses the design and application of several new 900MHz base-station transistors, having linear power output capabilities up to 120W PEP. Main emphasis will be on the design of the internal matching configuration of a transistor and its influence on the total RF performance of an amplifier. A complete description of a 50W broadband amplifier is given, first along with measured data, followed by the design of a 120W PEP broadband amplifier. The results of linearity measurements are given for this amplifier, since multi-channel operation is a key performance issue for new generation base-stations.

DESIGN PARAMETERS FOR A BIPOLAR CHIP

In a bipolar transistor, the resistivity and thickness of the epitaxial layer have a large influence on most electrical parameters such as frequency band, operating voltage, power gain, efficiency, ruggedness and maximum power handling. The layout of U.H.F. transistors, is an interdigitated structure with an emitter pitch of 8 - 10 μm and emitter width of 1.5 μm . The layout is designed to minimize parasitic capacitance while allowing the required current to be handled safely. Emitter and base regions are formed by shallow implantations of arsenic and boron, which results in a narrow basewidth and therefore high transition frequency. Depending on the transistor, diffused or poly-silicon emitter ballasting resistors are used to be sure of an excellent current distribution. The negative feedback, provided by those resistors, takes care of a uniform heat distribution over the chip. Infrared scans in practical situations (under nominal and mismatch conditions) have been done for each transistor to optimize the R_e value. All PHILIPS base-station transistor dies utilize titanium-platinum-gold top metallization to ensure long lifetime and an excellent reliability. In this metallization system, the gold layer serves as a conductive layer with a high electromigration resistance. The platinum and titanium layers provide adhesion and an efficient barrier layer to prevent Au-Si eutectic formation. Reliability tests, extrapolated to standard D.C. adjustments and temperatures, predict a lifetime over 15 years. A silicon nitride sealing on

the active die area prevents moisture penetration and improves the resistance against electro-migration. The use of gold bonding wires in combination with the TiPtAu-metallization is required to deter the on-set of the purple plaque phenomena, which strongly influences MTBF performance.

MATCHING CONFIGURATIONS INSIDE THE TRANSISTOR PACKAGE

Every design of a bipolar transistor starts with a selection of the active element. The choice of a package is the next step. Factors which should be taken into account are: - should it be a single ended or push-pull transistor; what is the dimension of the silicon inside; is the package able to take care of the dissipated power (thermal resistance); is any kind of internal matching required and so on. In practice, a high power transistor is fabricated by incorporating more than one active die in a given package. Paralleling dies will irrevocably introduce losses inside the transistor, i.e. one cannot expect the same RF performance at the double output power by paralleling two equal dies. One of the problems inside a transistor package is to offer each area on the die the same load. Figure 1 shows the schematic diagram of a common emitter transistor with 5 active areas. L1 - L5 represent the emitter bonding wires, L6 - L8 represent the inductances caused by the metallized emitter bridge of the package. Assuming L6, L7 and L8 are equal, it is clear that the voltage drop at the center of the

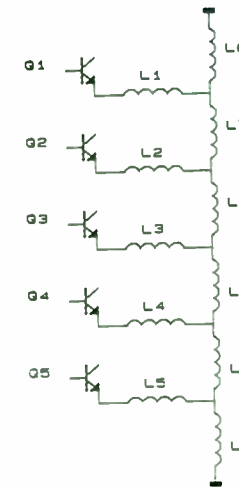


FIGURE 1

internal bridge has the highest value. So, the allowed voltage swing over active area 3 is the lowest, followed by the active areas 2/4 and 1/5. A direct influence on parameters such as lower saturated power and decreased collector efficiency can be noticed. This results in a higher junction temperature and less linearity. An emitter bridge with through metallized holes to the flange of the package is a good solution and provides an excellent and equal grounding for every active area. Through metallized holes also imply a low emitter inductance, resulting in a high power gain. Besides unequally loaded active areas on a chip, paralleling dies will cause unacceptably low transistor input and output impedances. Low transistor impedances will result in large losses in the

matching network outside the transistor (see section "LOSSES IN EXTERNAL MATCHING NETWORKS"). To increase the transistor impedances, a matching network inside the package is required.

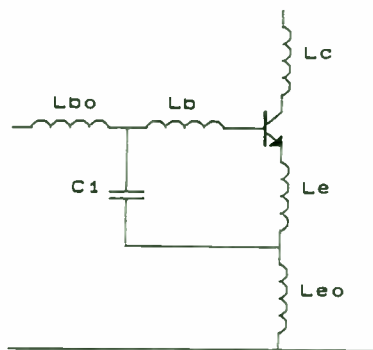


FIGURE 2

The most familiar internal matching configuration is the one with a low-pass characteristic at the input side of the transistor, created by means of a MOS capacitor C1 and the base bonding wires Lb (see figure 2). Besides taking care of a higher input impedance, input match (or pre-matching) also affects the power gain of the transistor. Normally the power gain roll-off is 6dB/octave (see figure 3, dashed line).

Pre-matching provides a more constant power gain in the operating frequency band. Resonance occurs, but in case of a well behaved match, this resonance is far above the

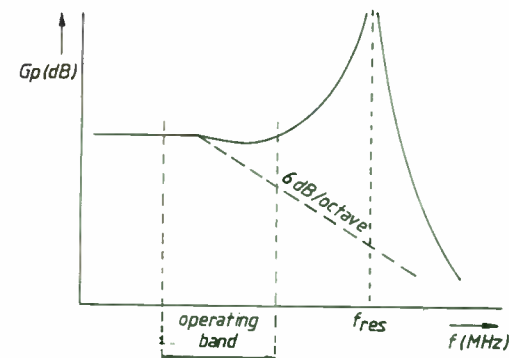


FIGURE 3

operating band. Pre-matching effects also parameters such as efficiency and stability.

At the output side of a transistor, internal matching configurations can also be used. Losses in the external matching network, due to a low output impedance of the transistor, will decrease powergain and efficiency of an amplifier. This can be improved by internally matching at the outputside of the transistor, which in principle can be achieved by using a low-pass or a high pass matching circuit. Using internal output matching with a low pass characteristic in a common emitter device is in most cases not the correct way. This can be explained as follows: Looking to the output side of a conventional transistor, the load impedance (conjugate of the output impedance) has an inductive imaginary part (the imaginary part of the output impedance is

capacitive). It is only useful to use low-pass output matching when the load impedance at the connecting point of this output matching already has a capacitive imaginary part. This condition can only be created by means of bonding wires inside the transistor package. In most cases there is not sufficient space inside the transistor package to transform the load impedance from a inductive to a capacitive imaginary part, by means of the inductance of the collector bonding wires. So, in this case, a matching configuration with a high-pass characteristic is the solution. At the output of the transistor, a shunt inductor is created by means of bonding wires. To prevent a short circuit of the supply voltage to ground, a DC-blocking capacitor with a large value is used. In this way, the output capacitance of the active dies is tuned out (parallel resonance), resulting in a higher real part of the output impedance of the device. The shunt inductor reduces losses caused by the device output capacitance as well. Reduced internal and external matching losses result in an overall efficiency improvement of 10 - 15%. The high-pass configuration is formed by the combination of the shunt inductor and the feedback capacitor of the active dies. In figure 4, the schematic diagram of the base-station transistor BLV101 is given. At the input, two low pass pré-matching sections are present, and at the output the high pass section (C_{cb} in combination with L_s). The design of such a complicated transistor is only allowed when full automatic bonding wire equipment can be used, to be sure of a minimum spread in transistor impedances and RF performance.

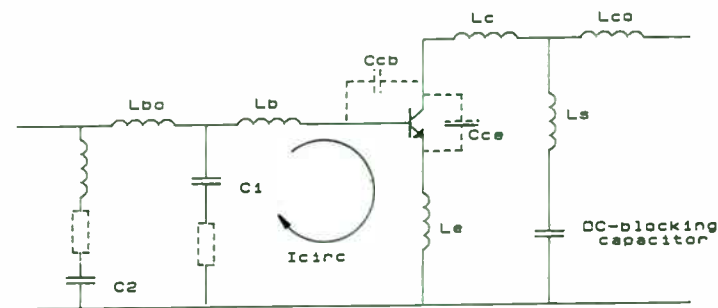


FIGURE 4

LOSSES IN EXTERNAL MATCHING NETWORKS

Losses in the matching networks outside a transistor are related to the impedances of a device. These network losses can directly be translated into a decrease of power gain and efficiency. For instance higher transistor impedances will cause lower network losses. This can be explained as follows. Figure 5 shows a schematic diagram of a transistor impedance

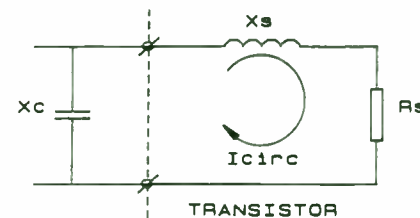


FIGURE 5

in combination with the first section of a matching network. R_s is the real part and X_s is the imaginary part of the transistor impedance. X_c is the impedance of the matching capacitor. Series to parallel conversion gives figure 6.

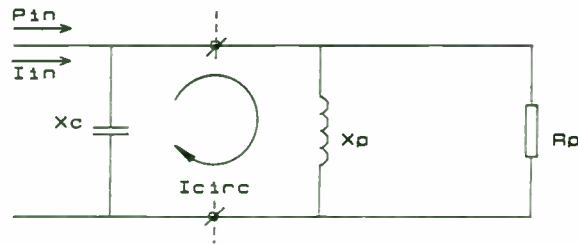


FIGURE 6

In case of resonance the loaded Q is equal to:

$$Q_L = \frac{R_p}{X_p} = \frac{R_p}{X_c} = \frac{X_s}{R_s}$$

I_{in} can be derived from the formula:

$$I_{in} = \sqrt{\frac{P_{in}}{R_p}}$$

The loaded Q of the network gives the relationship between I_{in} and I_{circ} :

$$I_{circ} = Q_L * I_{in}$$

The matching capacitor introduces introduces losses which are equal to:

$$P_{diss} = I_{circ}^2 * R_c$$

in which R_c is the loss resistance of the capacitor (see figure 7). R_c can be determined from the formula:

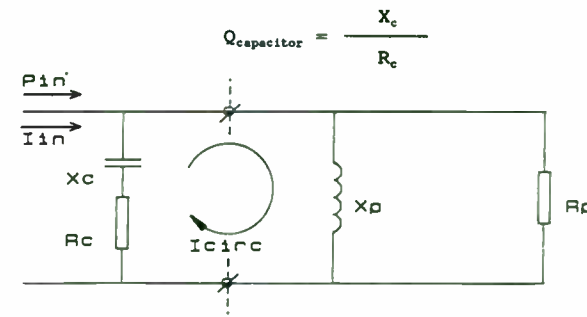


FIGURE 7

So, the total required input power, assuming no losses in X_s , is equal to the addition of the power dissipated in R_c and the transistor input power ($P_{transistor} = I_{circ}^2 * R_{in}$).

$$P_{in} = P_{transistor} * \frac{R_c + R_{in}}{R_{in}} \quad (\text{in Watt})$$

So, the dissipation loss in the matching capacitor, due to R_c , is equal to:

$$P_{loss} = 10 \log_{10} \frac{R_c + R_{in}}{R_{in}} \quad (\text{in dB})$$

From the formula above, it can be concluded that a transistor with a higher impedance will cause less losses in your matching network.

PRACTICAL AMPLIFIER EXAMPLES INCLUDING MEASUREMENT RESULTS

PHILIPS offers a wide range of 900MHz base-station transistors for analog as well as digital systems. Our knowledge and experience with linear TV transistors was used to design new devices for the next generation multi-channel base-stations. This section describes two practical wideband base-station applications. Both amplifiers are designed in close cooperation with the German company SSB-Electronic.

A 50W wideband amplifier with the BLV101A

The BLV101 is a 50W single ended common emitter transistor with double input and output matching. The internal matching networks provide high input and output impedances, resulting in high power gain and collector efficiency. The BLV101 is available in two versions: - the BLV101A, optimized for 850-900MHz and the BLV101B for the 935-960MHz band. The BLV101A, intended for the USA market, has a 50W (continuous wave) output power capability ($V_{ce}=26V$). A load mismatch of $V_{SWR}=5$ (0-360°) is allowed at the same output power. Due to the high input and output impedances, it was very easy to match the transistor to 50Ω. A wide stripline ($Z_0=9\Omega$) together with a trimming capacitor is the only thing needed to run into the 50Ω system.

In figure 8 the schematic diagram of the amplifier is given. The great advantage of this kind of matching configurations is that it is no longer necessary to use external matching

capacitors near the edge of the device. So, no mechanical forces are exerted on the capacitors when the transistor is heating up and cooling down. Looking to the application in which the transistor is used this will improve the reliability and the number of field rejects. In addition, system costs will be reduced.

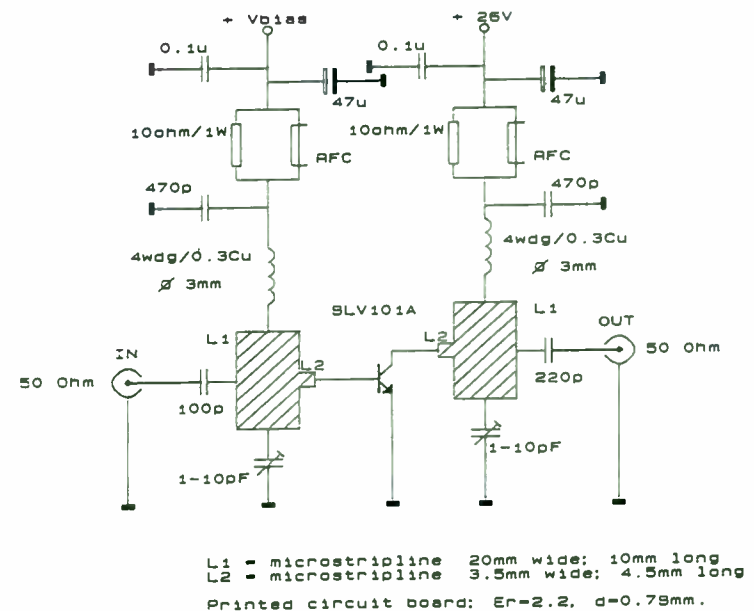


FIGURE 8

Figure 9 shows the RF performance at full output power.

A 120W PEP wideband amplifier with the BLV102A

Looking into the future, multi-channel amplifiers with output power levels up to 200W PEP and intermodulation products below -30dBc will be needed. PHILIPS designed a new class-AB die with a good linear performance, especially for high power and high frequency. These dies are used in the BLV102A. Emitter ballasting resistors and epi-material are selected, to optimize power capability, power gain, linearity, thermal behaviour and ruggedness. The BLV102A is a push-pull transistor, intended for the 865-900MHz band. Internal input and output matching, resulting in high input and output impedances, allow a simple external matching configuration. The schematic diagram of the amplifier is given in figure 10, and the layout of the printed circuit board in figure 11. The simple matching networks provide less field rejects. At an output power of 120W PEP (two tones: $f_1=880\text{MHz}$ and $f_2=880.1\text{MHz}$) and a supply voltage of 28V, all intermodulation distortion products are below -35dBc (see figure 12). The quiescent current in this case is 5mA per transistor section which is an advantage as regards the current consumption of the amplifier in the standby situation. Power gain under the conditions mentioned above is 9dB (!). Of course a higher quiescent current will result in an increase in power gain. Line-up proposals for a 200W PEP multi-carrier amplifier will be given during the presentation.

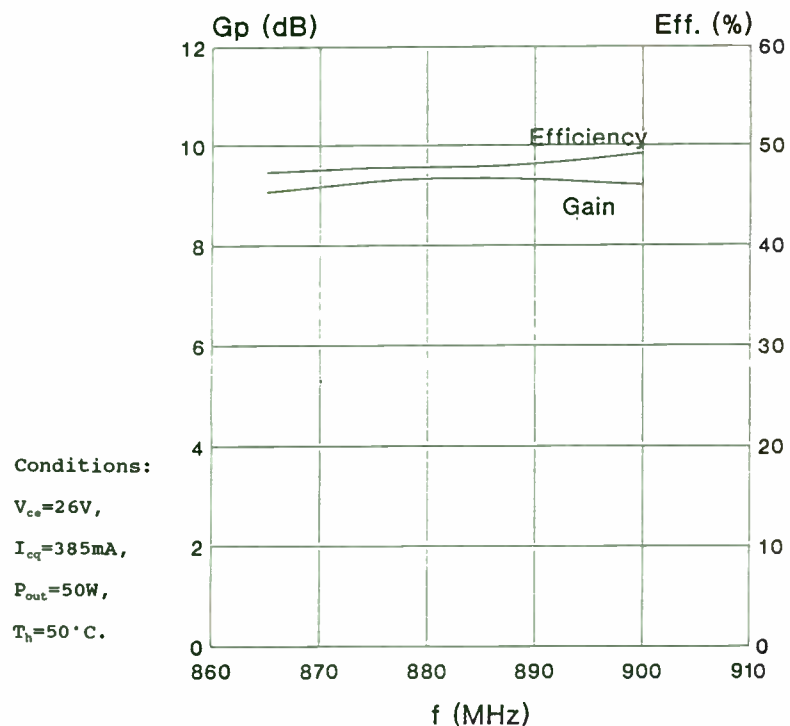


FIGURE 9

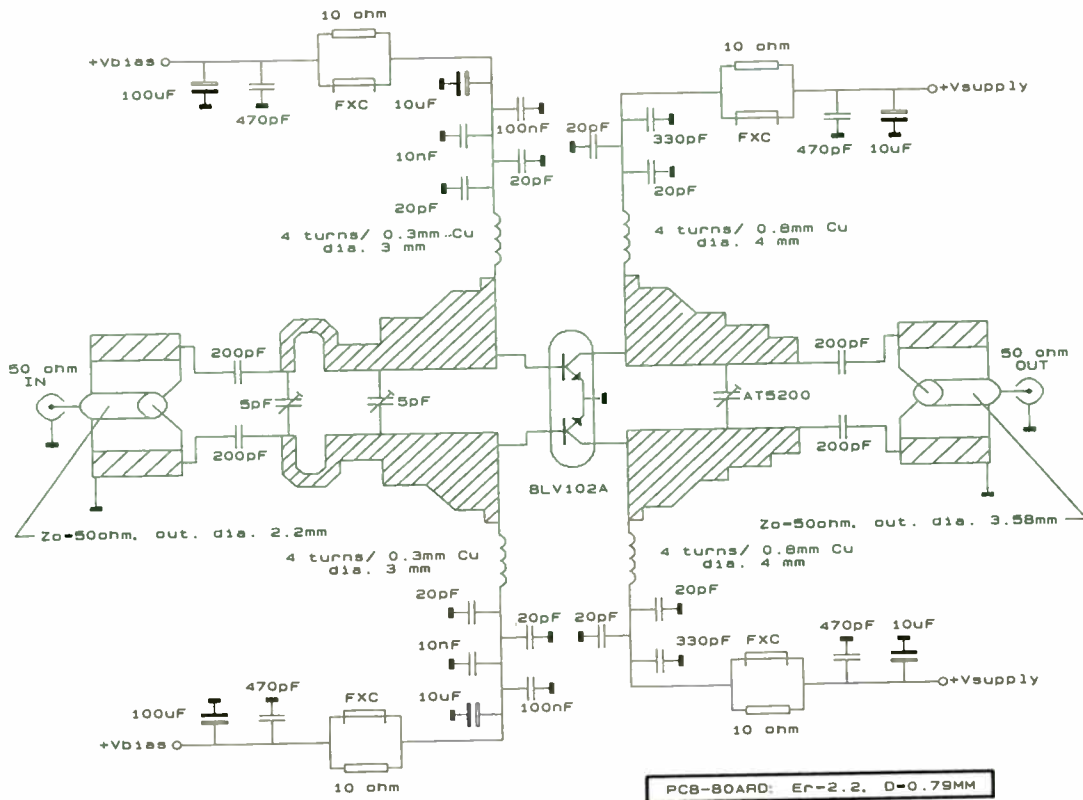


FIGURE 10

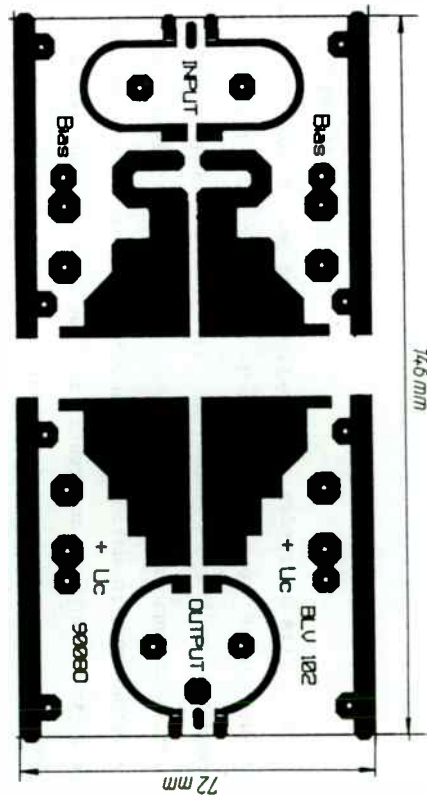


FIGURE 11

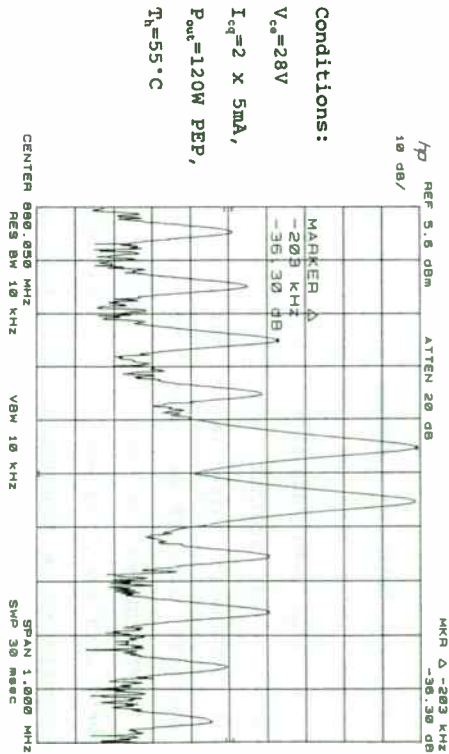


FIGURE 12

CONCLUSIONS

Today's generation 900MHz base-stations requires linear class-AB RF-power amplifiers with high peak power capability. High transistor impedances will be helpful to improve the overall amplifier performance, i.e. powergain, efficiency, linearity, MTBF figures etc., since high impedances allow the application engineer to design rather simple and low loss external matching networks. Complicated matching configurations inside the transistor, as applied in PHILIPS' base-station transistors BLV101 and BLV102, create those high impedance levels which guarantee an optimum RF performance.

REFERENCES

- Chris Bowick, "RF circuit design", Howard W. Sams & Co., 1986
- Richard S. Muller and Theodore I. Kamins, "Device electronics for integrated circuits", John Wiley and sons, 1986
- Private contact with: Rolf Albert, director and application engineer from SSB-Electronic, Panzermacherstraße 5, 5860 Iserlohn, Germany

THE "APPROXIMATION METHOD" OF FREQUENCY SYNTHESIS

Albert Helfrick

CONSULTING ENGINEER
5 BANTA ROAD
KINNELON, N.J. 07405

Probably the most widely used form of frequency synthesis is the phase locked loop. One of the more significant problems associated with the phase locked loop arises when this method of frequency synthesis is called upon to provide narrow frequency resolution. This is when the loop suffers from a number of problems.

Usually, a narrow frequency resolution implies the synthesizer is used for a narrow band application where phase noise and discrete sideband energy are of importance. For a simple, single-loop synthesizer, the frequency step is equal to the reference frequency of the loop. The reference frequency, on the other hand, is an indication of the phase locked loop's ability to reduce phase noise. The digital phase detector is, essentially, a sampled system and the more often a waveform is sampled the more is known about that waveform. As with any sampled system, the frequency range of the sampled waveform is directly proportional to the sampling rate and, thus, the higher this rate, the more phase noise may be reduced. This sampling

results in sidebands to the carrier which are reduced with the loop filter. The amount of sideband energy can be reduced by simply increasing the amount of loop filtering with the undesirable result of slowing of the loop and thus increasing the lock-up time between frequency changes. In addition, reducing the bandwidth of the loop reduces the ability of the phase locked loop to reduce the phase noise of the VCO.

To insure adequate frequency resolution without increasing the phase noise or the lock-up time to an unacceptable amount, various multiple loop and hybrid systems have been generated. Some systems use several phase locked loops where one loop provides a coarse frequency control with a second loop providing a fine frequency resolution. Other techniques involve a mix of direct and indirect frequency synthesis where the advantages of both are exploited to provide a broad frequency range with narrow resolution.

The technique described in this paper is a combination of multiple loops and a simple form of direct frequency synthesis.

Figure 1 shows a simple single-loop synthesizer with a variable reference frequency. By changing the value of N , the output frequency varies by NF_{ref} . If, by some method, the reference frequency could be changed by a small amount, ΔF_{ref} the output frequency would change, due to this reference frequency change by $N \Delta F_{ref}$. Therefore, the output frequency is a function of N , ΔF_{ref} and F_{ref} . The ability of the phase locked loop to reduce phase noise is a function of F_{ref} , while the frequency of the output is mostly a function of N . The change

in reference frequency, ΔF_{ref} could be small so that additional frequency steps could be provided between those provided by changes of N. Several small changes of the reference frequency could provide increased frequency resolution and "fill in" the space between the nominal frequency steps provided by changes in N. There is no limit to how small the output frequency resolution may be set by simply choosing a small ΔF_{ref} . The disadvantage of this method is that the change of output frequency as a function of ΔF_{ref} is proportional to N, which is not a constant. This may require some clever manipulations of ΔF_{ref} .

However, if the variation of N were restricted to be small, the change in the output frequency as a function of ΔF_{ref} could be made to be nearly constant.

To give an example of how this technique can provide a phase locked loop with narrow frequency resolution yet with a relatively high reference frequency, consider a 100 to 101 MHz phase locked loop with a nominal F_{ref} of 10 kHz. Therefore, the range of N is from 10000 to 10100. Consider that the loop is to provide a frequency resolution of 250 Hz. Therefore if a nominal ΔF_{ref} of $250/10000 = .025$ Hz is provided, at 100 MHz the actual frequency resolution is exactly 250 Hz. However, when the loop division is set to 10100 the actual frequency resolution is $(.025 \times 10100)$ or 252.5 Hz, which is 2.5 Hz too large. The obvious choice in this case is a ΔF_{ref} of 250 Hz divided by the mean value of N or $250/10050 = 0.024875622$ Hz. When N is at a minimum, the frequency resolution at the output is 248.7565 Hz which is slightly short of the desired 250 Hz and is 251.25 Hz or slightly greater than the desired when N is at it's maximum.

Due to these small errors I have called the technique the "approximation" method.

The frequency change error for the example is only about 1 Hz for each frequency step. However, each frequency step provided by a variation of the reference frequency is in error and the error accumulates and thus after several steps provides a much larger absolute frequency error.

In this example, to provide 250 Hz resolution, an additional 39 frequency steps are required between the nominal 10 kHz steps provided by a change in the value of N. To calculate the total frequency error due to the application of reference frequency shifting, the actual values of the example are inserted into the equation and the error calculated.

The frequency of the VCO is

$$(F_{\text{ref}} + M \Delta F_{\text{ref}}) N = F_{\text{out}} \quad 1.1$$

where M is an integer and lies between -19 and +20.

If the value of ΔF_{ref} is chosen to provide the correct frequency step at the mean value of N, 10050, the worst case frequency error will occur when both M and N are at either their maximum or minimum values. Thus, the worst case errors are when $M = -19$ and N is 10000 and when $N = +20$ and $N = 10099$. Numerically, the lower frequency is 100.00052732 MHz and 100.9950244 MHz. The frequency error at the lower frequency is 23.2 Hz and at the upper frequency is 24.4 Hz. This represents an error of less than 1/4 parts per million.

A serious disadvantage of this technique is the need to generate an accurate but very small change in the reference frequency. If this were achieved with a phase locked loop, we would have the very same problems we set out to solve. These small changes in F_{ref} must be generated with a form of direct digital synthesis.

A very simple technique of direct digital synthesis is shown in fig. 2. In this method of direct synthesis, a relatively high frequency is divided both by a fixed amount, Q and a variable amount, M. The value of Q is chosen to be considerably less than P. The two divided frequencies are mixed and the sum frequency is chosen and divided by a factor of X which is fixed.

The frequency of F_{ref} is

$$F_{ref} = \frac{F_i}{X} \left(\frac{1}{P} + \frac{1}{Q} \right) \quad 1.2$$

Because the value of P is to be changed by only a small amount, set $P = K - M$, where K is much greater than M. Therefore 1.2 becomes

$$F_{ref} = \frac{F_i}{X} \left(\frac{1}{K-M} + \frac{1}{Q} \right) \quad 1.3$$

To determine the frequency change of F_{ref} as a function of changes in M, the partial derivative is taken

$$\frac{\partial F_{ref}}{\partial M} = \frac{F_i}{X} \left(\frac{1}{K-M} \right)^2 \quad 1.4$$

Since K is set to be much greater than M, only the first two terms of the binary expansion of equation 1.4 may be used as in equation 1.5

$$\begin{aligned} \frac{\partial F_{ref}}{\partial M} &= \frac{F_i}{XK^2} \left[1 - \frac{2M}{K} + 3\left(\frac{M}{K}\right)^2 \dots \right] \\ &\approx \frac{F_i}{XK^2} \left[1 - \frac{2M}{K} \right] \end{aligned} \quad 1.5$$

Thus the change in the reference frequency is approximately directly proportional to changes in M. This is the second approximation of this method of frequency synthesis.

Just how do these approximations affect the frequency accuracy of a frequency synthesizer? Returning to the example synthesizer, using the described method reference frequency generation values are provided for K, M, Q, and X as shown on the following page.

K = 2000
M = 0 to 39
Q = 10
X = 1005

A spread-sheet program was used to calculate the frequency error for these parameters and is shown in fig. 3. As this figure shows, the error is quite respectable being a maximum of only 1.5 parts per million. This synthesizer has a frequency resolution of 250 Hz with a nominal reference frequency of 10 kHz. This would be an approximate 40-fold improvement in performance over a phase locked loop using a 250 Hz reference frequency.

What is evident from the error frequency plot is the discontinuities at those frequencies where the value of M changes from 39 to 0 and N is incremented by one. In the example the error is -150 Hz just before N is incremented and exact at the next frequency giving rise to a 400 Hz step rather than a 250 Hz step. It must be understood the frequency accuracy is 1.5 parts per million but the frequency step is in error by 60%

These discontinuities can be reduced by choosing a different range for N or some other parameter. To have a zero discontinuity the frequency error for M = 39 must be equal to the frequency error at M = 0. The frequency error is given by

$$\text{Freq error} = 10^4 N + 250M - \frac{F_1 N}{X} \left(\frac{1}{k-M} + \frac{1}{Q} \right) \quad 1.6$$

Using the parameters given, the error is zero for M = 0 and thus equation 1.6 is set to zero with M = 39 and solved for N.

$$10^4 N + 250 \times 39 - \frac{10^8 N}{1005} \left(\frac{1}{2000-39} + \frac{1}{10} \right) = 0$$

1.7

$$N = 9850$$

Thus, a frequency range from 98.0 MHz to 99.0 MHz would provide a reduction in discontinuity when the value of N changes. Fig. 4 shows the spread-sheet graph of the error for this frequency range. As it can be seen, the frequency discontinuity is essentially non-existent in the mid-frequency range and has been reduced to less than 50 Hz at the upper and lower extremes. The maximum frequency error as shown in the figure is 0.8 parts per million.

The frequency error of the "approximation" synthesizer can be reduced even further by the application of a microprocessor-controlled error reduction system. The frequency error due to the approximations in this synthesizer may be calculated. Therefore, corrections to the master reference oscillator may be provided to further reduce the frequency error. Since the errors in this example synthesizer are only on the order of 0.5 parts per million, only small corrections are required and thus the overall stability of the synthesizer is not compromised.

To give one example of an application for the 98-99 MHz synthesizer described, figure 5 shows the example synthesizer used for an ACSB transceiver in the 30 - 50 MHz frequency range.

Two phase locked loops are used in this application. The wide band loop has a 1 MHz reference frequency and would add very little phase noise to the system.

SOME NOTES ON THE HARDWARE

At first glance it may appear that some of the hardware shown in figure 2 is difficult to find or expensive. This is not the case.

The 100 MHz oscillator should be a TCXO if the accuracy of the synthesizer is to be realized. Without correction, the synthesizer is capable of better than one part per million and this necessitates a TCXO. If correction is to be employed, a voltage controlled TCXO would be required. These are both readily available items.

The two frequency dividers operating with the 100 MHz frequency, P and Q are implemented simply with common ECL. The mixer can be any common balanced mixer. The sum frequency filter must be a quartz crystal filter as the image frequency is removed by only 100 kHz. This may appear to be a major stumbling block for this technique. Not at all. The total frequency variation of the 10.05 MHz sum is only 1 Hz. Therefore, a simple one pole-one zero filter using two quartz crystals is more than adequate.

The remaining circuits, the divide by N, divide by 1005 and the associated phase detector is implemented with one LSI chip.

Note: Some of the specific techniques outlined in this paper are covered by a recent U.S. Patent. Basic reference pulling techniques are not new and are not covered under this patent.

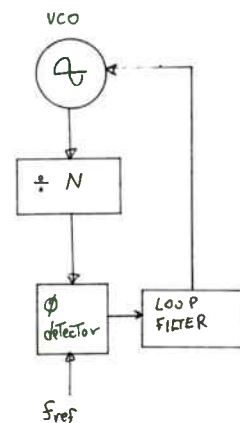


Figure 1

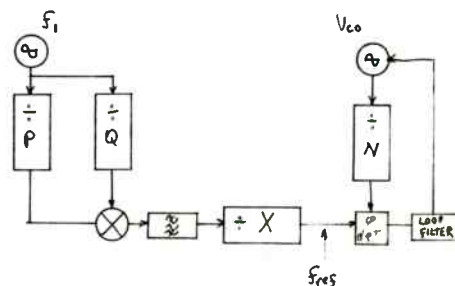
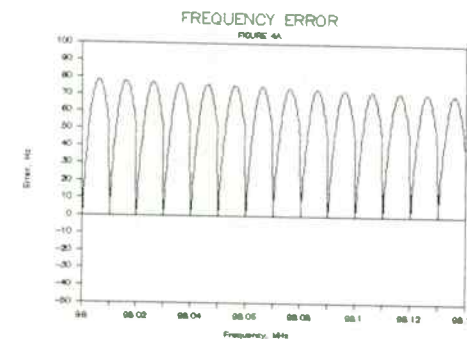
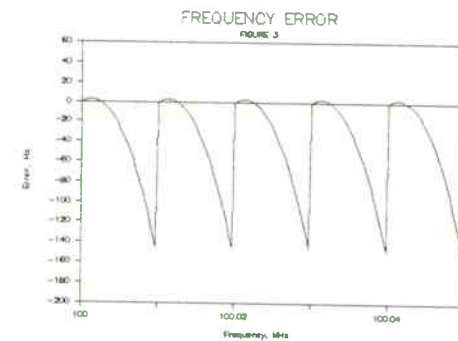
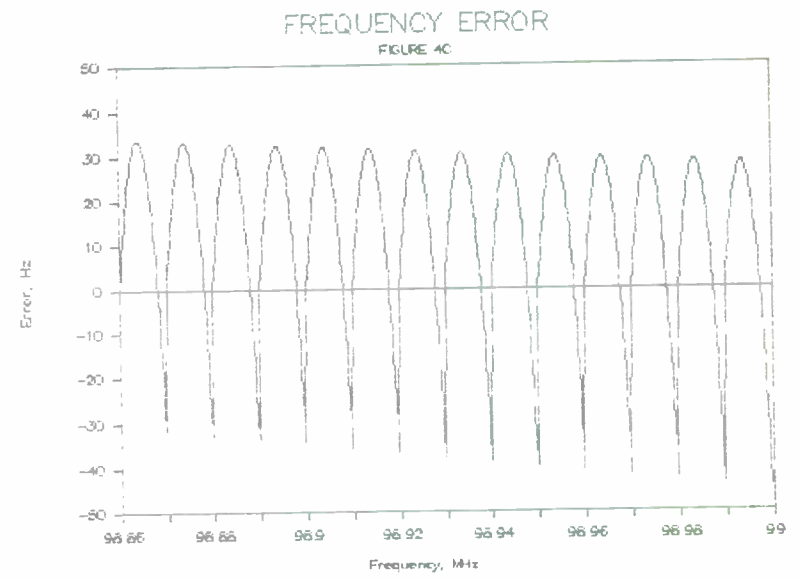
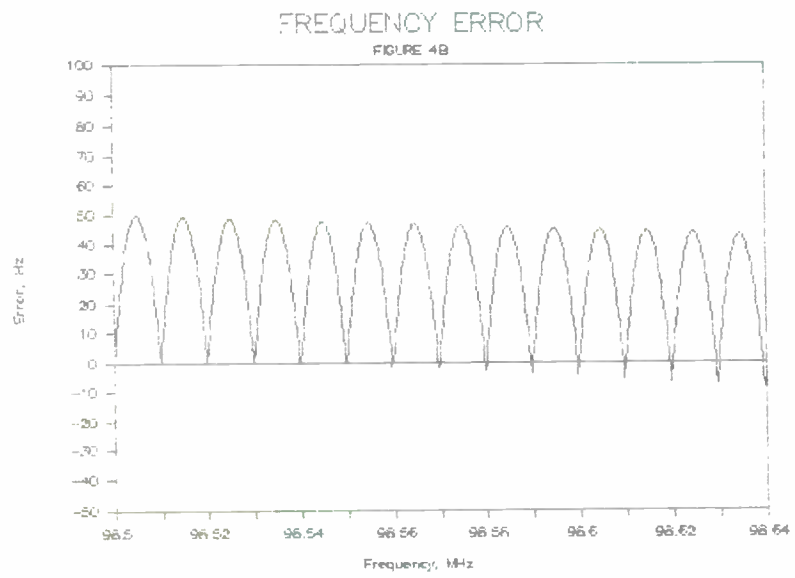


Figure 2





Perry Jordan
Analog Devices, Inc.
7910 Triad Center Drive
Greensboro, NC 27409

INTRODUCTION

In recent years the field of DDS (direct digital synthesis) has expanded greatly due to faster integrated circuit processes. It is now possible to digitally generate signals well into the RF signal range. A signal generator can be implemented with a fast phase accumulator, sufficient RAM to store 360 degrees of phase information, an invert circuit, and a DAC (digital to analog converter).

There are several key parameters that the system designer must understand and utilize to design an efficient DDS system. The DAC is the critical component in any DDS system. If the DAC is less than optimum, a clean spectrum is impossible to generate even with an "ideal phase accumulator" and an ideal RAM. This paper will outline a new 350Mhz DAC. This DAC, the AD9720 (or the AD9721 TTL version of this DAC) has been optimized for high speed, low glitch, and 90 degree phase data.

AN EFFICIENT DDS SYSTEM

A DDS system can be implemented by noticing the repetitive nature of a 360 degree cycle of a sine wave. The first 90 degrees of a sine wave contains all of the important phase information of the signal. The portion of the sine wave from 90 to 180 degrees is nothing more than a mirror image of the wave from 0 to 90 degrees. Finally, the portion of the wave from 180 to 360 degrees is no more than the negative of the signal from 0 to 180 degrees phase shifted by 180 degrees. If the proper counter is utilized, and

the proper logic is implemented, the RAM size can be reduced by 75% of the original required RAM. For this reason specialized DDS counters have been designed. One example is the 350 Mhz AD9950 phase accumulator (figure 1). This phase accumulator has 32 inputs which provide $(2e32)-1$ possible phase increments. The output frequency is determined by equation 1.

$$F_{out} = F_{clock}(M)/2e32 \quad (1)$$

F_{out} = output frequency

F_{clock} = update frequency of the AD9950

M = step size from $2e0$ to $(2e32)-1$

The AD9950's output consists of 12 data bits. The 10 LSB's can be used to access RAM locations which have 90 degrees of sine wave phase information. With the AD9950 in the quad enable mode, the output will count from 0 to $2e10$. At this point, bit 11 goes high and the DDS chip counts down to 0. This allows the system to generate 180 degrees of digital phase data from 90 degrees of phase data stored in the RAM.

At this point it would be advantageous to be able to generate the negative of this data but 180 degrees out of phase. If we feed the first 180 degrees of phase information into a DAC from mid-scale to full scale (IE the DAC's MSB is on), we can generate one half of a sine wave. If we invert the data into the DAC, and we use the DAC's mid-scale to zero scale (IE the DAC's MSB is off), we can generate the final 180 degrees of the sine wave. Bit 12 (MSB) of the phase accumulator is high for the first count up and count down cycle of the 10 LSB's. At this point the MSB is set to zero. For the next count up and down cycle of the 10 LSB's, the MSB is low. By inverting the phase information into the DAC, a complete sine wave can now be generated. The circuit that will accomplish this inversion is shown in figure 2. This

(3)

one's complement circuit is placed between the RAM and the DAC (as in figure 3).

IMPORTANT DAC SPECIFICATIONS

There are many important specifications that must be met to generate high frequency DDS sine waves. A clean frequency spectrum up to the Nyquist frequency is the required result. However understanding the parameters that effect the DAC's performance can aid in the choice of a correct DAC.

DAC ARCHITECTURE

There are three basic high speed DAC architectures. The R-2R DAC, current weighted DAC, and the segmented DAC. The current weighted DAC is potentially the fastest of the three DAC types. However this DAC usually has high glitch (due to the binary switching of the current sources) and it is hard to match the current sources above about three or four bits without doubling the number of current sources with each additional bit (figure 4).

The R-2R is difficult to match integrated resistors above about 6 bits without expensive laser trimming (figure 5). The final major architecture is a segmented architecture. It consists of turning on an additional current source each time another data bit turns on. This type of DAC is limited to lower order DACs. A 10 bit segmented DAC requires $2e10$ current switches and requires a 10 to $2e10$ decode section. The DAC's output capacitance would be excessive ($IE (Cjs+Cjc) \times 2e10$). For a good high speed process the DAC's output capacitance could vary from 20pf to 50pf. This would limit the slew rate of any high speed DAC.

(4)

AD9720

Due to the strong points and weak points of each architecture, a hybrid architecture for the AD9720 was chosen (see fig 6). This architecture has the advantage of a much reduced decode section, a reduced number of latches, and fewer current switches than a segmented DAC. The resistor matching requirements are reduced versus a 10 bit R-2R DAC, and a fewer number of current sinks than would be required by a current weighted DAC.

One advantage of the segmented DAC is its glitch performance. The "thermometer code" of the segmented DAC activates one LSB for each binary input code. Since only one "LSBs worth" of current is switched with each binary input step, the glitch performance of a well designed segmented DAC will be good. Large glitches at data transitions add to the AC nonlinearity (and degrade the spurious free dynamic range) of a DAC's output. Using the hybrid architecture of the AD9720, a compromise was made. A maximum of six LSB's current are switched at one time (versus one half scale current in the current weighted DAC). Careful consideration was given to the speed at which the R-2R can switch. If the R-2R switches slowly, there will be a large glitch every 64 codes. Due to a modern process with a four micron metal pitch, low diffusion capacitances, an optimized R-2R ladder, and differential logic the AD9720 has impressive glitch performance (see figure 7). These measures also aide the output slew rate and settling time of the DAC to 10 bits (less than 800ps and 10ns respectively).

Measuring settling time and low levels of glitch impulse is an art in itself. The AD9720 specifies glitch and settling time by measurement. To measure levels this low, specialized equipment must be used. Standard high speed scope probes are fine for measuring fast edges. However, probe

(5)

capacitances and reflections in most probes distort measurements. A Data Precision 6100 digitizing oscilloscope with its electronics in the probe tip (thus eliminating the reflections from its coaxial cable) was used to measure the output performance of the AD9720 DAC. This measurement technique gives accurate settling data. Specifying the settling time of a DAC by the output slew rate and a simple R-C time constant ignores the reality of the wire bond inductance and package inductance. This adds an L-C ringing which adds to the output settling time. Using the AD9720's output slew rate and calculating the settling time would yield a settling time of 2ns instead of the measured 10ns.

$$V = Vfs(1 - e^{-Ts/t}) \quad \text{equation 2}$$

T_s = settling time

$$t = R_{out} \times C_{out} = 40.74\text{ohms} \times 6.5\text{pf}$$

V = 90% of full-scale

T_r = AD9720 rise time into 50 ohm load

$$V/Vfs = 1 - (2e^{-11}) = 0.9995 \text{ (10 bit settling)}$$

substitute into equation 2

$$T_s = 7.6t \quad \text{equation 3}$$

$$T_r/t = 0.8\text{ns}/(40.74\text{ohms} \times 6.5\text{pf}) = 3.02$$

$$T_r/3.02 = t$$

substitute into equation 3

$$T_s = (7.6/3.02)0.8\text{ns} = 2\text{ns}$$

The AD9720 can be used as a standard DAC. Also, by using the one's complement inputs which have been included on the DAC (figure 2), the DAC can be used to generate sine waves with an appropriate phase accumulator and

(6)

enough RAM (room for 90 degrees of a digitized sine wave data). This gives the system of figure 3 without the one's complement circuit.

Another important feature of any high quality signal is phase noise. There are several things that the circuit designer can do to improve the switching characteristics in a DAC. Differential logic versus single ended logic effectively doubles the slew rate and the noise margin of the AD9720. When the output current switches of the DAC switch, there is a very fast transition through the "linear region" of the DAC switches. This improves the signal quality (phase noise) of the output signal. Glitch performance, and the maximum speed of the DAC is also improved. IC layout is also important. The placement of the DAC, data latches, logic circuits, current reference circuits, and substrate contacts are important. Substrate contacts must be placed in strategic locations. They should be placed to remove substrate noise but not increase the noise on the DAC outputs. Thermal gradients from the logic circuits must be accounted for. If one portion of the DAC is "hotter" than another, the DAC's linearity will degrade.

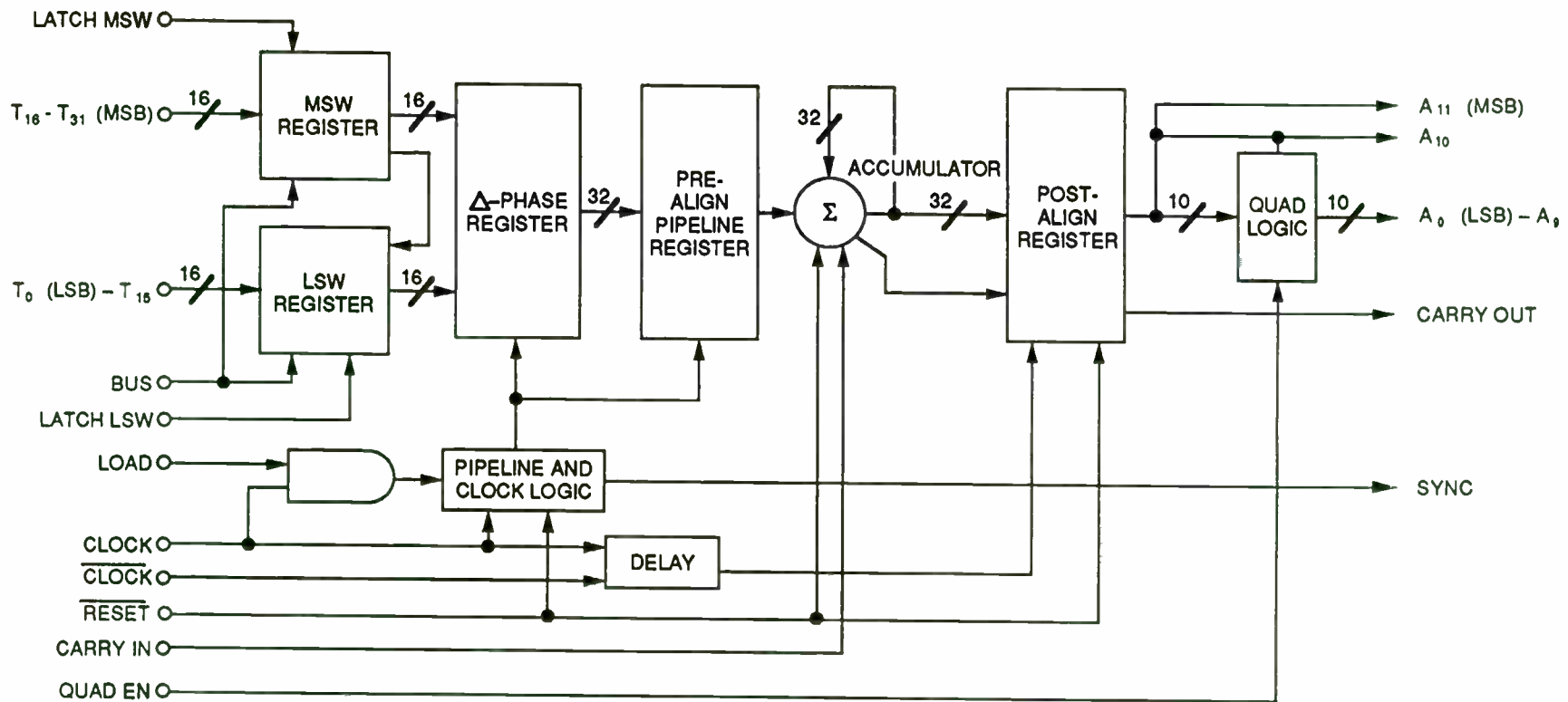
Figures 8, 9, 10, and 11 demonstrate the output response of the AD9720 at selected different outputs. As the figures show, the AD9720's output harmonics and spurious response is degraded at higher clock rates and higher output frequencies. The DAC's nonlinearities become a larger portion of the output signal at higher speeds. These plots show the importance of the DAC specifications at higher clock rates. Even with the settling time, output slew rate, glitch performance, and linearity of the AD9720, the output performance will degrade at higher update rates and output frequencies. At higher output frequencies the DAC will use less codes per cycle. Thus the DAC's non linearities such as glitch settling time, and slew rate become a

(7)

larger portion of the output waveform. A lower frequency signal with a fixed clock rate usually will give a cleaner signal than a higher output signal with the same clock rate. The more steps that are used in the output signal, the less slew rate is a factor. Also, if every code is used, the next step will start at almost the same point each time. This helps to negate the effects of the settling time on the output waveform.

CONCLUSION

A DDS system capable of 350Mhz update rates with a minimum of external components has been explained. DAC specifications that are important to DDS were discussed. Also, the design of the AD9720 and how its performance specifications were geared to the high speed DDS market were also discussed.



AD9950 DDS Phase Accumulator Block Diagram

Figure 1

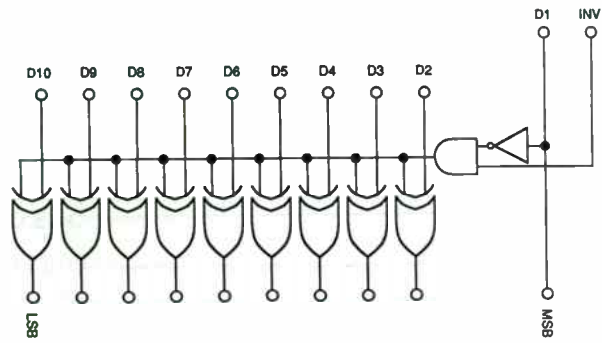
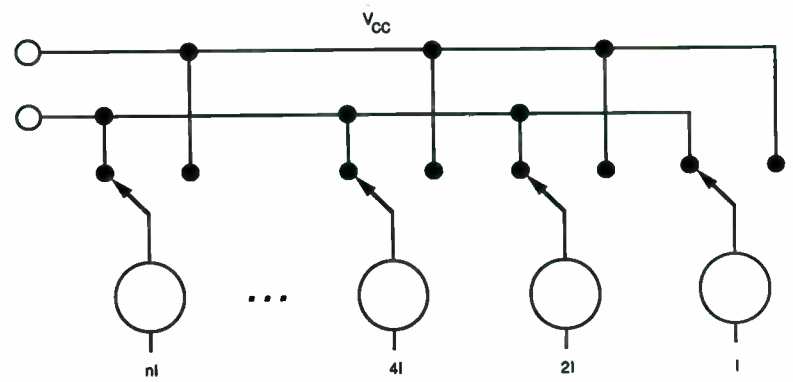


Figure 2



Current-Weighted DAC
Figure 4

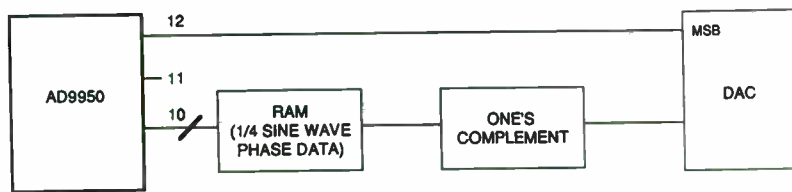


Figure 3

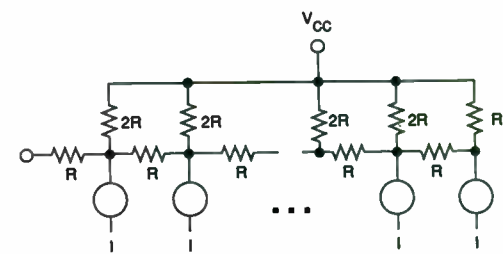


Figure 5

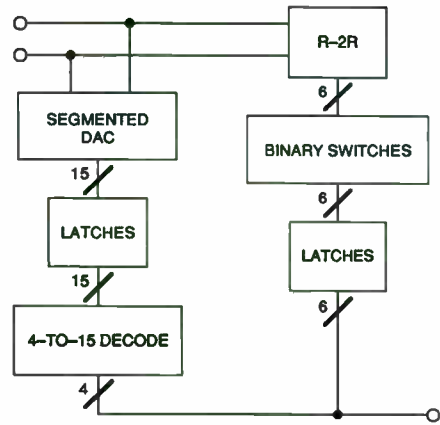
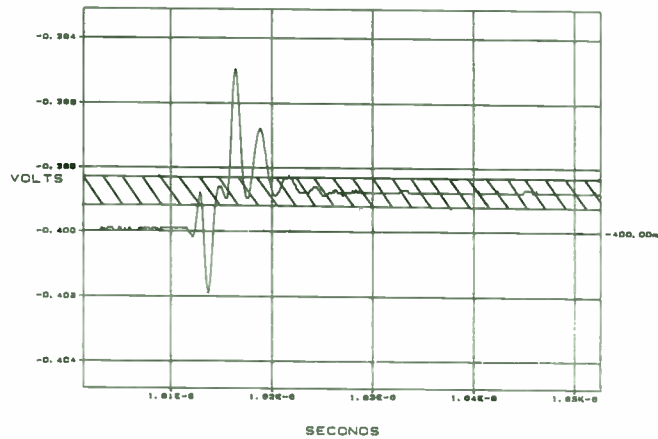


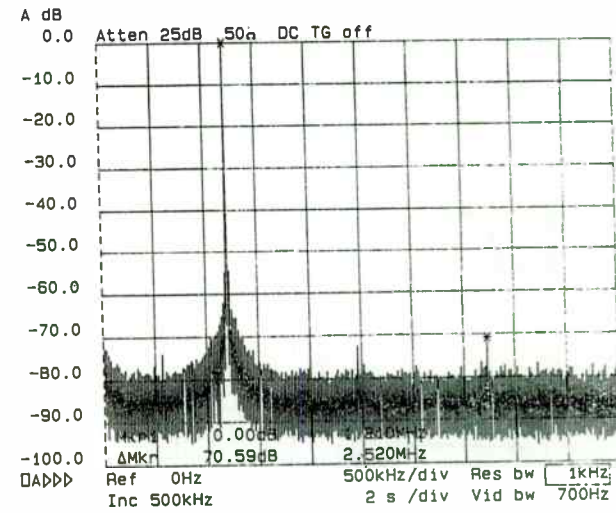
Figure 6



Total Glitch
100Vs
Peak Glitch
3.4pVs
Net Glitch
4pVs
Settling
10ns

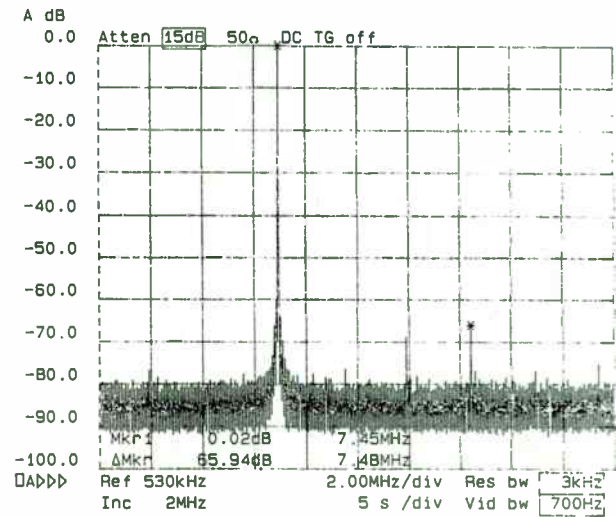
AD9720 Settling and Glitch

Figure 7



Fclock
10 MHz
Fout
1.21 MHz

FIGURE 8



Fclock
50 MHz
Fout
7.45 MHz

FIGURE 9

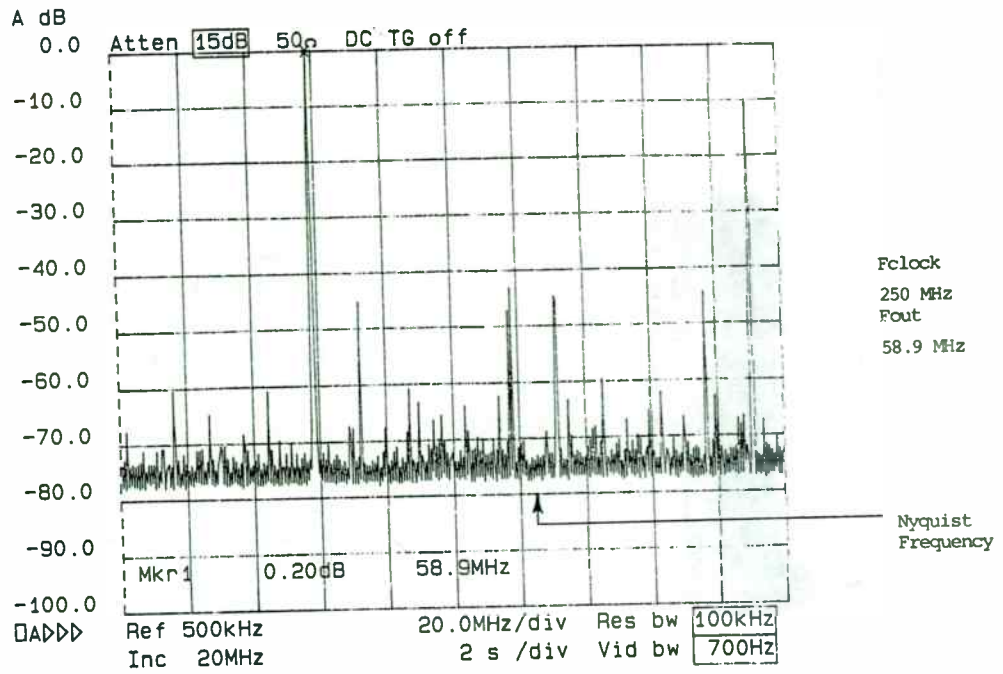


FIGURE 11

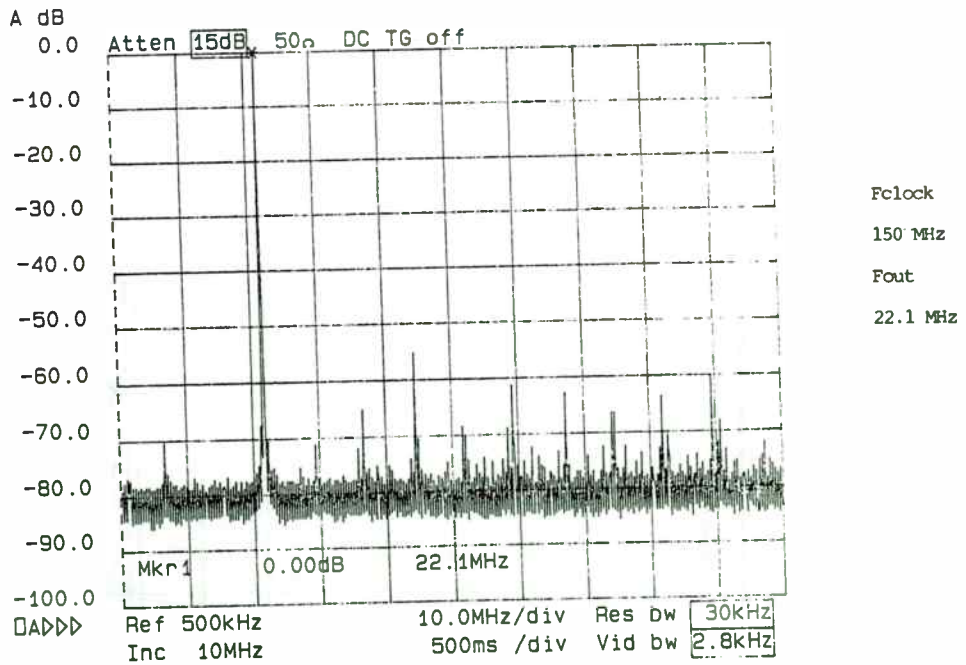


FIGURE 10

Lisa Moder
 Erbtec Engineering
 2760 29th St
 Boulder, CO. 80301

INTRODUCTION:

Measuring phase drift across a RF pulse in an amplifier can sometimes be very difficult to accomplish due to all of the different factors involved. This paper intends to show three of the possible techniques for measuring this drift in an amplifier.

Phase stability as discussed in this paper is different from phase noise. Phase noise is measured over a very short period of time, whereas phase stability as discussed in this paper is the long term drift across a RF pulse. This paper deals with the long term drift in an amplifier over a 10 to 20 minute period.

The reasons for measuring phase stability in an amplifier are different for each specific application. One reason that is common to all projects is amplifier stability. Phase stability is just one of the factors in making sure that the system being built is a stable one.

At Erbtec Engineering, we are concerned with the stability of our amplifier because our amplifier is used in the medical field for Magnetic Resonance Imaging (MRI). MRI is based on the ability to flip an atom 180° . The atoms need to be flipped exactly 180° for the image to be created. If any part of the MRI system has phase instability, the atom does not flip exactly 180° and the image is not accurate.

Three methods for the measurement of phase drift across a RF pulse will be described, along with a discussion of the relative advantages and disadvantages of each technique.

SINGLE RF MIXER METHOD:

Fig. 1 shows a block diagram of a single mixer arrangement for measuring phase drift across a RF pulse in an amplifier. This particular technique utilizes a double balanced mixer and samples one point on the RF pulse. For single mixer measurements it is first necessary to determine the sensitivity of the system through calibration.

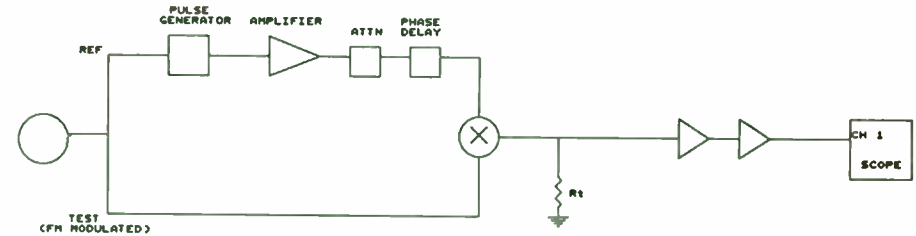


Fig. 1 Block Diagram of Single Mixer arrangement

K_d is measured using an oscilloscope to measure the slope of the beat frequency (See Fig. 2). The frequency is adjusted so that there is about a 1kHz beat frequency. EQ(1) shows how to determine K_d once the system is set up as shown in Fig 3. The phase delay line is adjusted before K_d is determined, to achieve quadrature at the input.

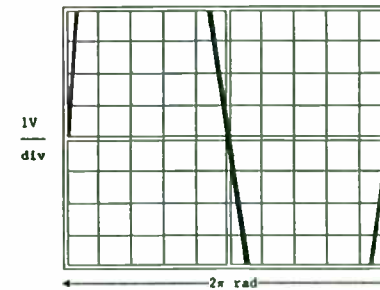


Fig. 2 Scope trace of 1kHz beat frequency.

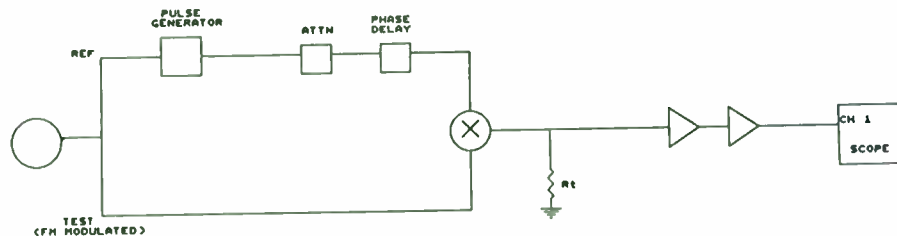


Fig. 3 Set up for calibration of single mixer method.

$$K_d = \frac{\text{volts}}{\text{Num div}} * \frac{100 \text{ div}}{2 \pi \sqrt{1000}} \quad \text{EQ(1)}$$

The phase drift can now be measured over time using K_d as the reference value. Using the oscilloscope, or a spectrum analyzer, it can be determined what the voltage change is over time. Thus using K_d , the designer can determine the resultant phase change. For example, if $K_d = 0.83$ volts/rad is the sensitivity factor, and after 10 minutes the voltage changed by 2 volts, by simple arithmetic it would be concluded that the phase drifted by 1.67 radians (0.26 deg).

A simple computer program can be written to collect the phase data into an array. This array could then be graphed versus time to show how the phase has drifted. An example of this is shown in Fig. 4.

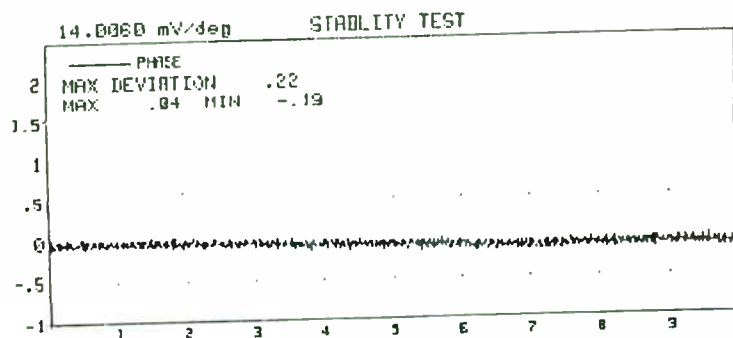


Fig. 4 Single mixer phase drift of an amplifier.

One of the major advantages of this method is cost. It only requires one signal source and has only one mixer. It also is much easier to implement than the dual mixer method discussed below. A disadvantage of the single mixer technique is that it is extremely sensitive to outside noise. For example, it does not permit the filtering of stray RF, which may degrade the measurement.

Another problem encountered with single mixer methods is that they need to be calibrated before each use to account for the differences in cable length and possible equipment changes. Also, when adjusting the phase delay for quadrature and in determining K_d , it is up to the operator's discretion as to where the measurement lies on the scope grid.

DUAL MIXER METHOD:

The dual mixer method takes a reference and a test signal from 2 signal sources and applies each one to a mixer. These mixer signals are then downconverted to a reference frequency which can be measured on an oscilloscope. This measurement technique is similar to the single RF mixer method except that there is no need for a phase delay adjustment. Fig. 5 is a block diagram of the system.

As in the single mixer approach, K_d needs to be determined for the system. After K_d has been determined, the amplifier is placed into the circuit between the reference signal and the attenuation. The reference signal is set to about 100Hz away from the test signal. Each signal is passed through a set of mixers and downconverted to 100Hz (see Fig. 5).

The dual mixer method digitizes the data using a digital oscilloscope. To convert this data back into meaningful analog phase data, it is necessary to extract the amplitude and phase out of each pair of data points. Fig. 6 and 7 show the output of the mixers across the RF pulse. Since the data is digitized it is preferable to sample the data in the manner shown in Fig. 6, rather than in Fig. 7. If the data points are sampled too close together, there will be a lot of noisy data present. The oscilloscope has certain points on the screen that it takes measurements from and if the designer wishes to sample at points 1 and 2 on Fig. 7, the worst case is that the

scope could measure at 3 and 4 or 5 and 6 on the same figure. If the data points were spread out as in Fig. 6, there is less room for error.

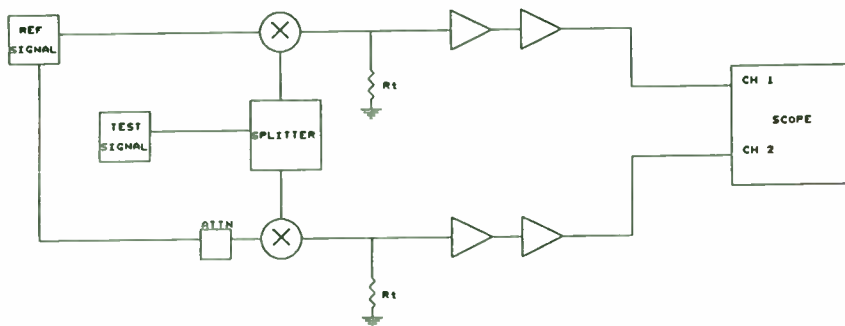


Fig. 5 Block Diagram of Dual Mixer Calibration

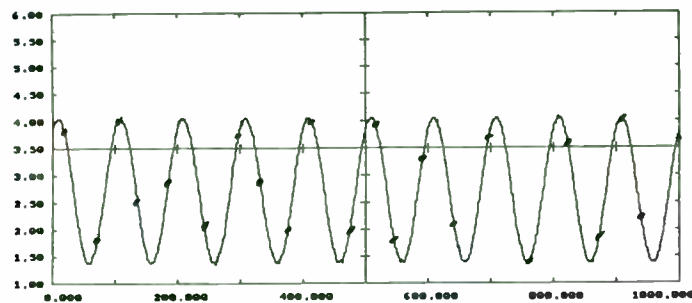


Fig. 6 Samples across the RF pulse.

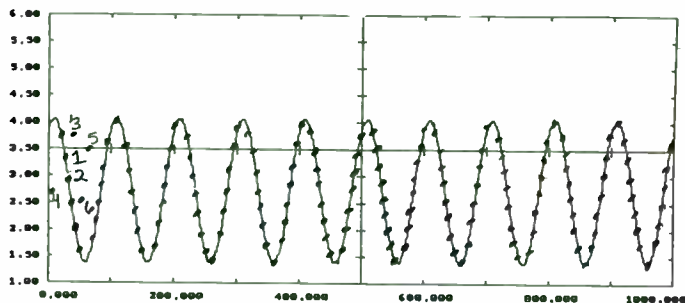


Fig. 7 Samples across the RF pulse.

This technique samples 1000 data points on the oscilloscope and stores them into an array. These 1000 data points are sampled on the RF pulse. Each pair has an amplitude and a phase that need to be extracted using EQ(2).

$$y_x = A \sin(\omega t_x + \phi) + \beta \quad \text{EQ(2)}$$

For each pair of data points we have a time (t_x) and a y-axis value (y_x) where x is the data point number. Assuming that ω is some constant frequency and β is some constant, the β term falls out when all of the data points are added up and β is subtracted as a whole. With 2 data points there are 2 equations and 2 unknowns (see EQ(3) & EQ(4)). It is clear that if EQ(4) is subtracted from EQ(3), EQ(5) results. Taking the sine of each side of EQ(5) and doing some mathematics results in EQ(6).

$$\sin^{-1}\left(\frac{y_1}{A}\right) = \omega t_1 + \phi \quad \text{EQ(3)}$$

$$\sin^{-1}\left(\frac{y_2}{A}\right) = \omega t_2 + \phi \quad \text{EQ(4)}$$

$$\sin^{-1}\left(\frac{y_1}{A}\right) - \sin^{-1}\left(\frac{y_2}{A}\right) = \omega(t_1 - t_2) \quad \text{EQ(5)}$$

$$\sin(\sin^{-1}\left(\frac{y_1}{A}\right)) \cdot \cos(\sin^{-1}\left(\frac{y_2}{A}\right)) - \sin(\sin^{-1}\left(\frac{y_2}{A}\right)) \cdot \cos(\sin^{-1}\left(\frac{y_1}{A}\right)) = \sin(\omega(t_1 - t_2))$$

$$\frac{y_1}{A} \cdot \cos(\sin^{-1}\left(\frac{y_2}{A}\right)) - \frac{y_2}{A} \cdot \cos(\sin^{-1}\left(\frac{y_1}{A}\right)) = \sin(\omega(t_1 - t_2)) \quad \text{EQ(6)}$$

This is a 4th order equation. The mathematics are shown in the APPENDIX. The result of the mathematics for the first pair of data points is shown in EQ(7). Any root finder program can solve this problem for A and consequently ϕ .

$$\begin{aligned} & \sin^4[\omega(t_1-t_2)]A^8 - \{2(y_1^2 + y_2^2)(\sin^2[\omega(t_1-t_2)])\}A^6 \\ & + \{(y_1^2 + y_2^2)^2 + 4y_1^2y_2^2\sin^2[\omega(t_1-t_2)] - 4y_1^2y_2^2\}A^4 \\ & - \{4y_1^2y_2^2(y_1^2 + y_2^2) - 8y_1^4y_2^4\}A^2 \\ & + \{4y_1^4y_2^4 - 4y_1^6y_2^6\} = 0 \end{aligned} \quad \text{EQ(7)}$$

If each of the 500 pairs is averaged in this manner and put into yet another array, the result is noise of about 5 degrees or so. If every 20 points is averaged, there tends to be only 2-3 degrees of noise. This is accomplished with a least squares fit. To do this, a computer program is necessary to solve for the values of A , ω , and ϕ . Fig. 8 shows a typical graph of phase drift using the dual mixer approach.

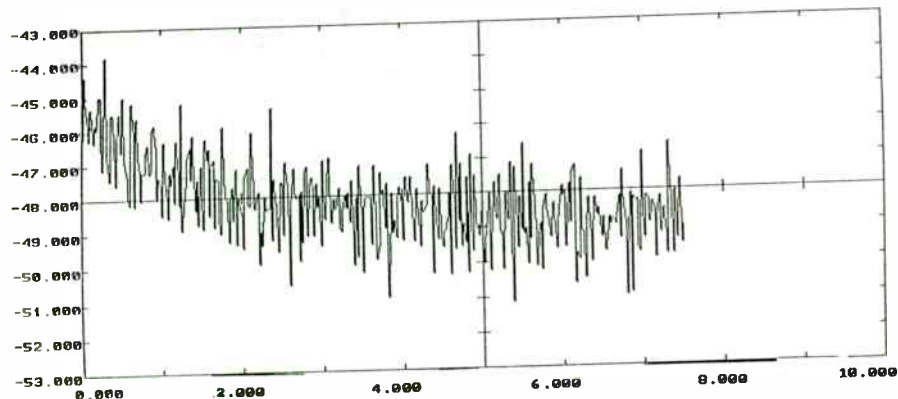


Fig. 8 Phase drift using the dual mixer method.

Aside from the obvious physical differences, the one major difference between this technique and the previous one is that there is no need for a phase delay circuit. It is not necessary to have the dependence on the phase coherence in this method.

One disadvantage of this method is that the sources are not phase locked and they should be for the best performance. Also if the system setup is changed a

recalibration must be done. Another pitfall of this technique is that a person must take the data, increasing the chance for operator error.

NETWORK ANALYZER METHOD:

The network analyzer method is the easiest method discussed in this paper and probably the most accurate in terms of less operator error. The network analyzer eliminates the need for much of the setup required by the previously discussed methods. For instance, the network analyzer has a 4kHz sampling frequency and is limited to a 3kHz bandwidth, whereas in the dual mixer method mentioned above it is up to the designer to determine these parameters. The network analyzer also has an internal source, so the need for external signal sources is gone. EQ(7) from the dual mixer method is calculated by the network analyzer, which displays the amplitude in dBm and the phase in degrees.

Erbtec has written a computer program to utilize the network analyzer method to determine both the magnitude and phase stability of a RF pulse in an amplifier. This program is available upon request. The program configures the network analyzer and the pulse generator, collects the data into arrays, does some statistical analysis on the data, and then stores the data into files.

The network analyzer setup is shown in Fig. 9. Port 1 is the frequency source, and also supplies the RF power to the amplifier. The pulse generator is used to generate the RF pulse at an apparent duty cycle. This particular application uses a 3ms pulse with a 5% duty cycle. This means that about every 60ms or so a 3ms RF pulse is generated to the amplifier. We wish to measure the drift across a 3ms pulse over a 10 minute time span.

The pulses are sampled for a 10 minute timed test, 6 data points per pulse. These 6 data points are spaced approx. 0.52ms apart on the 3ms pulse (See Fig. 10). Each of these data points goes into a separate data file, for a total of 6 files. These measurements are taken at port 2 of the network analyzer.

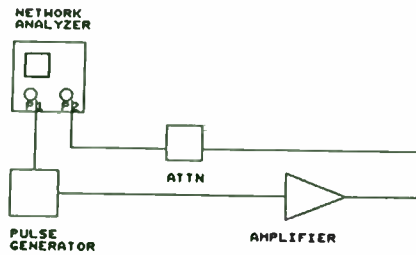


Fig. 9 Block Diagram of network analyzer method.

Attenuation is included in the path to protect the network analyzer from the high power out of the amplifier. The attenuation is accounted for in the calibration procedure.

The configuration of the network analyzer is as follows: A Smith Chart format is used to get both phase and magnitude data. The frequency is set to a predetermined CW value, 64MHz for this application. The power at port 1 is set such that the amplifier is at maximum power out to make the stability measurements. The network analyzer is triggered externally via the pulse generator. The smallest distance that can be achieved between markers in this application is 0.52ms, so in order to get 6 data points across the pulse and keep the duty cycle the same a sweep time of 13ms is required.

The data is collected for 10 minutes into 6 data files. These files are then graphed and analyzed. Fig. 11 shows a typical 10 min phase stability run on an amplifier set up to operate at 64MHz.

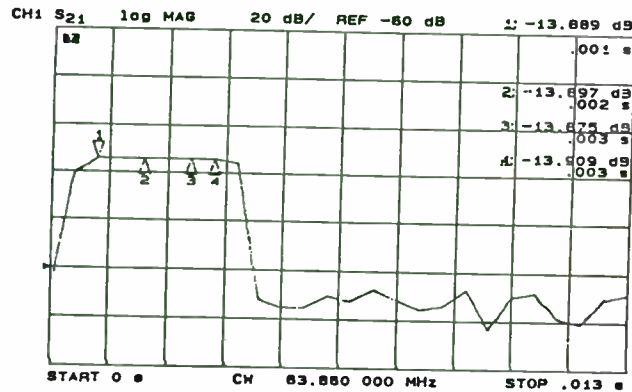


Fig. 10 3ms RF pulse with markers.

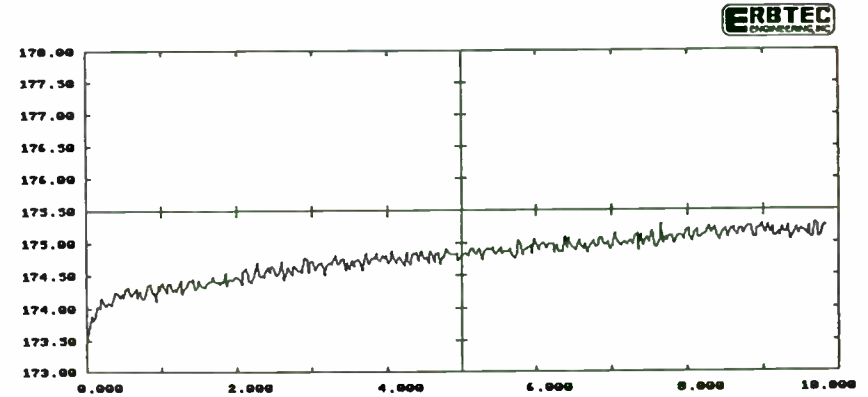


Fig. 11 Phase drift of 64MHz amplifier.

The chances of error are reduced with the computer taking all of the data. Also, the network analyzer permits the designer to collect both magnitude and phase data

which can be beneficial in determining the stability of the system.

The network analyzer also has its limitations, most of which are internal and thus cannot be changed. For instance, the sampling frequency is set to 4kHz in a 3kHz bandwidth. This means that the smallest distance that is obtainable between markers is approximately 0.50ms. Ideally it would be nice to have as many points across the pulse as possible. The 3kHz bandwidth means that any fast phase changes will not be detected. Fast phase changes are typically on the order of less than 0.20ms.

CONCLUSIONS:

Three techniques for phase stability measurement of a RF pulse in an amplifier have been described. These are only a sample of the many different techniques for measuring phase drift across a pulse over an extended period of time.

There are numerous reasons for measuring phase drift. Most reasons are application specific, but all realize that characterization of phase drift is necessary in determining phase stability.

APPENDIX

Substitutions:

$$x = y_1 \quad C = y_1^2 + y_2^2$$

$$y = y_2$$

$$t_3 = t_1 - t_2 \quad D = \sin(\omega(t_1 - t_2))$$

$$B = y_1^2 y_2^2$$

$$x = A \sin(\omega t_1 + \phi)$$

$$y = A \sin(\omega t_2 + \phi)$$

$$\sin^{-1}\left(\frac{x}{A}\right) = \omega t_1 + \phi$$

$$\sin^{-1}\left(\frac{y}{A}\right) = \omega t_2 + \phi$$

$$\sin^{-1}\left(\frac{x}{A}\right) - \sin^{-1}\left(\frac{y}{A}\right) = \omega t_3$$

$$\sin[\sin^{-1}\left(\frac{x}{A}\right) - \sin^{-1}\left(\frac{y}{A}\right)] = \sin(\omega t_3)$$

$$\sin[\sin^{-1}\left(\frac{x}{A}\right)] \cos[\sin^{-1}\left(\frac{y}{A}\right)] - \sin[\sin^{-1}\left(\frac{y}{A}\right)] \cos[\sin^{-1}\left(\frac{x}{A}\right)] = \sin(\omega t_3)$$

$$\frac{x}{A} \cos[\sin^{-1}\left(\frac{y}{A}\right)] - \frac{y}{A} \cos[\sin^{-1}\left(\frac{x}{A}\right)] = \sin(\omega t_3)$$

$$\frac{x}{A} \left[\frac{\sqrt{A^2 - y^2}}{A} \right] - \frac{y}{A} \left[\frac{\sqrt{A^2 - x^2}}{A} \right] = \sin(\omega t_3)$$

$$\left[x \sqrt{A^2 - y^2} - y \sqrt{A^2 - x^2} \right]^2 = \left[A^2 \sin(\omega t_3) \right]^2$$

$$x^2 \sqrt{A^2 - y^2} - 2xy \sqrt{A^2 - y^2} \sqrt{A^2 - x^2} + y^2 \sqrt{A^2 - x^2} = A^4 \sin^4(\omega t_3)$$

$$x^2A^2 - 2x^2y^2 + y^2A^2 - A^4\sin^2(\omega t_3) = 2xy\sqrt{A^2 - y^2}\sqrt{A^2 - x^2}$$

$$[CA^2 - 2B - D^2A^4]^2 = [2xy\sqrt{A^2 - y^2}\sqrt{A^2 - x^2}]^2$$

$$C^2A^4 - 2CBA^2 - CD^2A^6 - 2CBA^2 + 4B^2 + 2BD^2A^4 - CD^2A^6 + 2BD^2A^4 + D^4A^8 = 4B(A^2 - y^2)(A^2 - x^2)$$

$$D^4A^8 - (CD^2 + CD^2)A^6 + (C^2 + 2BD^2 + 2BD^2)A^4 - (2CB + 2CB)A^2 + 4B^2 = 4B(A^4 - 2BA^2 + B^2)$$

$$D^4A^8 - 2CD^2A^6 + (C^2 + 4BD^2)A^4 - 4CBA^2 + 4B^2 = 4BA^4 - 8B^2A^2 + 4B^3$$

Replacing all variables:

$$[\sin^4[\omega(t_1 - t_2)]] A^8 - [2(y_1^2 + y_2^2)\sin^2[\omega(t_1 - t_2)]] A^6$$

$$+ [(y_1^2 + y_2^2)^2 + 4y_1^2y_2^2\sin^2[\omega(t_1 - t_2)] - 4y_1^2y_2^2] A^4$$

$$- [4y_1^2y_2^2(y_1^2 + y_2^2) - 8y_1^4y_2^4\sin[\omega(t_1 - t_2)]] A^2$$

$$+ [4y_1^2y_2^2 - 4y_1^6y_2^6] = 0$$

System Design Considerations for Line of Sight Microwave Radio Transmission

George Kizer

Network Transmission Systems Division
Rockwell International
P. O. Box 568842
Mail Stop 406-158
Dallas, Texas 75356-8842

INTRODUCTION

Microwave system design is a tradeoff of many factors. Some of those are a function of state of the art equipment parameters. Other factors are independent of equipment design. Considerable attention is placed on transmission bandwidth and system gain. However, it is often the equipment independent factors which dominate overall system performance. Those factors are overviewed in this paper.

SYSTEM DESIGN

Detailed radio system design is done on the basis of interference noise limits and transmission path loss objectives. The data necessary to estimate terrestrial microwave interference is listed in Table 1. Based on this data, carrier to interference objectives are established. The estimation of interference noise requires a knowledge of the desired signal (carrier) power, C, and the undesired interfering signal power, I. If the desired signal originates at station A, transmitting toward station B, and the interfering signal originates at station C, transmitting toward D, then the C/I observed at station B is given by

$$C/I(\text{dB}) = P(\text{dB}) + G(\text{dB}) + L(\text{dB}) + D(\text{dB})$$

$$P(\text{dB}) = \text{transmitter power differential}$$

$$= P_c(\text{dBm}) - P_i(\text{dBm}) - L_c(\text{dB}) + L_i(\text{dB})$$

$$G(\text{dB}) = \text{antenna gain differential}$$

$$= G_c(\text{dB}) - G_i(\text{dB})$$

$$L(\text{dB}) = \text{free space loss differential}$$

$$= 20 \log (d_i/d_c)$$

$$D(\text{dB}) = \text{antenna discrimination}$$

$$= D_c(\text{dB}) + D_i(\text{dB})$$

$$P_c = \text{transmitter power of desired signal}$$

$$P_i = \text{transmitter power of undesired signal}$$

$$L_c = \text{power loss of desired signal between transmitter and transmit antenna}$$

$$L_i = \text{power loss of undesired signal between transmitter and transmit antenna}$$

$$G_c = \text{gain of transmit antenna at site A toward site B}$$

$$G_i = \text{gain of transmit antenna at site C toward site D}$$

$$D_c = \text{discrimination (relative to main lobe power) of receive antenna at site B toward site C}$$

$$D_i = \text{discrimination (relative to main lobe power) of transmit antenna at site C toward site B}$$

$$d_c = \text{distance from site A to site B}$$

d_i = distance from site C to site B

For adjacent channel interference noise calculations on a multiline parallel route system, the C/I equation reduces to the combined cross-polarization discrimination (XPD) of the transmit and receive antennas. The combined XPD is never better than the worse of the two antennas. Based on a calculated C/I, an estimate is made of interference noise. The interference depends on both the desired signal as well as the interfering signal. Figures 1 and 2 show examples of noise produced in an FM radio from FM or digital signal interference. The preceding formula assumed free space transmission. Some interference cases may require calculation of obstruction or rain scatter loss. Adjacent channel interference requires an estimate of relative fading of the C and I signals. Obviously antenna and transmission path performance is crucial to optimizing the C to I objectives. Tables 2 and 3 list typical ranges of C/I for interfering signals which have the same (cochannel) or slightly different (adjacent channel) interfering frequency. These tables are based on Interference Objective Tables, Issue 7, revised August 1989, of Working Group 5 of the National Spectrum Managers Association. The FM or SSB system objectives are based on a foreign system interference allocation of 4 dBmC0 (5 pwC0) per exposure for carrier-sideband interference and 17 dBmC0 (50 pwC0) per exposure for carrier-beat interference (with an assumed 10 dB burble factor). Digital C/I objectives are based on a allocation of 30 dB C/I per exposure for foreign system interference. Paths below 10 Ghz have an assumed 40 dB (multipath) fade margin while those above 10 GHz have a 50 to 55 dB (multipath plus rain) fade margin. Objectives are to be met when the desired signal is in a deep fade and the foreign interference is experiencing an correlated 10 dB fade.

ANTENNA RADIATION PATTERNS

Frequency reutilization and interference reduction is directly related to antenna radiation pattern performance. An antenna is a device for transmitting or receiving electromagnetic signals through space. In discussions of antenna gain, the concept of an isotropic radiator (isotrope) is fundamental. Essentially an isotrope is an antenna that radiates uniformly in all directions of space. Its pattern is a perfect spherical surface in space; that is, if the electric intensity of the field radiated by an isotrope is measured at all points on an imaginary spherical surface with the isotrope at the center (in free space), the same value will be measured everywhere.

A nonisotropic antenna will radiate more power in some directions than in others and therefore has a directional pattern. Any directional antenna will radiate more power in its direction (or directions) of maximum radiation than would an isotrope (with both radiating the same total power). The

directive gain of an antenna is defined, in a particular direction, as the ratio of the power density radiated in that direction, at a given distance, to the power density that would be radiated at the same distance by an isotrope radiating the same total power.

At microwave frequencies, the main type of antenna for transmission is a large parabolic reflector feeding or feed by a small horn antenna. The horn is constructed and placed in such a way that the energy field across the parabolic reflector is greatest at the center of the reflector and tapers to a lower value (typically -10 dB) at the reflector edge. Although this illumination tapering reduces antenna efficiency, it also reduces the side lobe level (spurious responses) which make frequency reuse more difficult. Passive flat plane reflectors, either elliptical or rectangular shaped, may be used in the path to change direction of transmission. The field across the passive reflector is uniform. This causes the reflector to have high efficiency but poor side lobe performance. Sometimes the relatively inefficient parabolic antennas are used back to back as a passive repeater to avoid this side lobe (frequency reuse) problem.

The far field relative radiation pattern of a circular parabolic antenna (circular aperture) is a function of the illumination of the circular reflector. Sciambi [29] used Silver's [30] uniform and fully tapered parabolic illumination results to develop field patterns for arbitrarily tapered illuminations. The circular antenna patterns are given in Fig. 3. The 10dB tapered pattern is typical of commercial parabolic antennas.

G_0 = normalized power intensity

D = diameter of the circular aperture

λ = free space wavelength

= $1/[1.0167 f(\text{GHz})]$ in feet

= $1/[3.3356 f(\text{GHz})]$ in meters

f = radio frequency of operation

θ = azimuth of measurement relative to path of maximum transmission

The far field relative radiation pattern for a circular reflector can be obtained directly from the results for a parabolic antenna with uniform illumination. The far field relative radiation pattern of a rectangular passive reflector can be obtained from Silver's results [30]. The far field radiation patterns for circular and square passive reflectors (uniformly illuminated apertures of projection) are plotted in Figs. 4 and 5.

L = width of the reflector

ϕ = rotation of the passive reflector in the plane orthogonal to the direction of wave propagation ($\phi = 0$ when the width dimension is parallel to the earth)

Note in Figure 5 as the rectangular reflector is rotated from the parallel to the earth position, the nulls move to the right and the side lobe peak levels are reduced. The side lobe reduction is a complicated function of the amount of rotation. If ϕ is zero, the pattern is not a function of the height/width ratio. As noted in Fig. 6, for ϕ of 45 degrees, the pattern is only mildly sensitive to the passive height/width ratio R . Fig. 4 shows that for $\phi = 0$, the far field radiation pattern of a rectangular reflector is significantly worse than that of a circular reflector antenna. However, comparison of Figs. 4 and 5 shows that if the rectangular reflector is rotated, its far field radiation pattern (in one plane) can be significantly better than a similarly sized circular reflector antenna.

The preceding antenna far field radiation patterns were based on assumed field amplitude distributions across the antenna aperture. For a passive reflector, the radiation patterns for uniform illumination are generally accurate since the reflectors are usually in a far field condition. These patterns can be distorted by secondary reflections due to terrain as well as moving the reflector into the near field of the illuminating antenna. For center-fed parabolic antennas, these patterns are never quite achieved. The aperture illumination distribution is complicated by the feedhorn design necessary to achieve that distribution. In addition, the near side lobe level (as well as overall gain) is affected adversely by blockage of the aperture by the feedhorn mechanical assembly. The low level wide-angle side lobe level is generally dominated by feedhorn spillover, rim diffraction, and reradiation and diffraction by the feedhorn support structure.

The results for the passive reflectors were developed assuming the passives to be oriented directly orthogonal to the path of transmission (uniform phase illumination). If the passive is rotated in a plane which includes the line of maximum power transmission, a linear phase error is introduced onto the aperture illumination. This causes the main beam to rotate and broaden relative to the

uniform phase case. From the point of view of an observer, the result is exactly the same as a passive reflector oriented directly orthogonal to the path of transmission but which has the area of the projection of the original passive into that orthogonal plane of reference.

FREE SPACE TRANSMISSION LOSS

An isotropic source is a hypothetical radiator which transmits or receives power equally in all directions. In an infinite homogeneous lossless medium, the power density P at a distance d from an isotropic source is the total power transmitted W_t divided by the surface area of a sphere with radius d . The power received W_r , by a receiving antenna with effective area A_r , is the product of A_r and P . The free space loss is defined as W_r/W_t .

$$L(\text{dB}) = 10 \text{ Log } (W_r/W_t)$$

The formula is more commonly expressed in decibels in one of the following ways:

$$\begin{aligned} L(\text{dB}) &= -74.3 + 20 \log f(\text{GHz}) - 20 \log d(\text{miles}) \\ &\quad + 10 \log A_t(\text{ft}^2) + 10 \log A_r(\text{ft}^2) - T_t(\text{dB}) - T_r(\text{dB}) \\ &= -49.5 + 20 \log f(\text{GHz}) - 20 \log d(\text{km}) \\ &\quad + 10 \log A_t(\text{m}^2) + 10 \log A_r(\text{m}^2) - T_t(\text{dB}) - T_r(\text{dB}) \end{aligned}$$

Transmission line losses are significant at microwave frequencies and must be accounted for. T_t is the transmission line loss between transmitter and transmit antenna and T_r is the transmission line loss between receive antenna and the receiver. A_x is the effective area of projection of the antenna aperture in the direction of transmission and δ be the antenna efficiency. If the transmit antenna has axial gain (relative to an isotropic radiator) G_t and effective area A_t and the receiving antenna has axial gain G_r (relative to an isotropic radiator) and effective area A_r , the free space transmission loss formula [10] becomes

$$\begin{aligned} L(\text{dB}) &= -96.6 - 20 \log f(\text{GHz}) - 20 \log d(\text{miles}) \\ &\quad - T_t(\text{dB}) + G_t(\text{dB}) + G_r(\text{dB}) - T_r(\text{dB}) \end{aligned}$$

$$= -92.4 - 20 \log f(\text{GHz}) - 20 \log d(\text{km})$$

$$- T_t(\text{dB}) + G_t(\text{dB}) + G_r(\text{dB}) - T_r(\text{dB})$$

where antenna gain is given by

$$G_x(\text{dB}) = +11.1 + 20 \log f(\text{GHz}) + 10 \log A(\text{ft}^2) + 10 \log (\delta)$$

$$= +21.5 + 20 \log f(\text{GHz}) + 10 \log A(\text{m}^2) + 10 \log (\delta)$$

The typical value of δ varies from 0.45 to 0.55 for commercial parabolic antennas and 0.90 to 1.0 for passive reflectors. For parabolic antennas, A is merely the frontal area ($\pi \times \text{diameter}^2 / 4$) of the reflector since the antenna is aligned in the direction of transmission. For passive reflectors, A is the area of the passive projected onto a plane passing through the passive which is orthogonal to the direction of transmission. For a passive reflector, the effective area is the total surface frontal area multiplied by $\cos (C/2)$ where C is the angle formed by the two transmission paths which converge at the reflector.

The above loss formulas are commonly written as the following:

$$L(\text{dB}) = - T_t(\text{dB}) + G_t(\text{dB}) + \alpha(\text{dB}) + G_r(\text{dB}) - T_r(\text{dB})$$

$\alpha(\text{dB})$ = free space loss

$$= -96.6 - 20 \log f(\text{GHz}) - 20 \log d(\text{miles})$$

$$= -92.4 - 20 \log f(\text{GHz}) - 20 \log d(\text{km})$$

It is quite common to use one, two, or more passive reflectors between a transmitter and a receiver. One can treat each path independently. The reflector acts as a receiver in one direction and a transmitter in the other. The gain is, of course, the same in either case. The 2-way repeater gain referred to by some authors is the sum of the receive and transmit gain (expressed in dB) of the repeater.

The preceding formulas assume that all antennas are far enough from each other that far field conditions apply. Lewis, as reported by Friis [10], suggested that far field conditions exist as long as

$$\delta > 2 a^2 / \lambda$$

where d is the distance between the antennas, a is the largest linear dimension (in the plane of projection of the wave) of the larger antenna, and λ is the wavelength of the radio wave. As the antennas are moved closer together, the gain of the two antennas is reduced compared to the far field gain. The case of parabolic antennas was addressed by Bickmore and Hansen [2] for the case where one antenna is much larger than the other (only the large antenna is in the near field). Pace [28] gives an approximation for parabolic antennas of similar size. Based on these results, Fig. 7 was produced. This figure graphs the loss in composite antenna gain relative to far field gain as a function of D_a and D_b , the diameters of the two parabolic antennas. $D_a \geq D_b$ and the above parameter definitions apply.

It is common to estimate total path loss through a passive repeater as two independent paths. Often one end of the path has the reflector and/or parabolic antenna in the near field reducing effective free space gain. Jakes [13] considered the case of a parabolic antenna and elliptical (circular projection) reflector. Medhurst [24] produced a result for both the elliptical (circular projection) and rectangular (square projection) reflector cases. Based on Medhurst's results, Figs. 8, 9, 11 and 12 were produced. They represent the loss in composite antenna and reflector gain when the two approach each other. D_r is the diameter or width of the projection of the reflector in a plane parallel to the parabolic antenna. D_a is the diameter of the primary parabolic antenna.

Sometimes a pair of rectangular passive reflectors are used to go over or around obstructions. Although this case may be analyzed as three independent paths, typically the two passive reflectors are in each others near field. Wang [34] analyzed this case of two rectangular (square projection) passive reflectors in the transmission path. Figs. 10 and 13 show the loss in combined far field gain (relative to the gain of a single smaller reflector) as the two passive reflectors are moved close together. It is assumed that the projection of each rectangular passive in the plane orthogonal to the direction of transmission is square. A is the width of the square projection of the smaller reflector and B is the width of the square projection of the larger reflector. To use Fig. 10, work the problem as the loss of two independent paths with the smaller reflector as a single reflector and add the loss from Fig. 10. Many engineers prefer to treat passive reflector or double reflector problems as a combined gain problem. That may be accomplished through the use of Figs. 11, 12 and 13.

Note that all rectangular reflectors are assumed to have a square shape when projected into the path of transmission. If they are rectangular, the width used in the figures is the larger of the two rectangular dimensions. All elliptical reflectors are assumed to have a circular projection. If they are elliptical, the large dimension is used for the diameter. In all cases, however, the actual projection area is to be used to calculate far field gain.

PATH LOSS CALCULATION EXAMPLES

The general expression for path loss between transmitter T and receiver R may be written as follows:

$$Pr = Pt + L$$

$$Pr(\text{dB}) = \text{power received at R}$$

$$Pt(\text{dB}) = \text{power transmitted at T}$$

$$L(\text{dB}) = \text{path loss (expressed as gain) between T and R}$$

Direct Path Loss

Consider a typical 30 mile 6.2 GHz path with 10 foot parabolic antennas and 100 feet of elliptical waveguide at each site.

$$L = -Tr + Gt + \alpha + Gr - Tr$$

$$Tr = Tt = 1.2 \text{ dB}/100 \text{ ft} \times 100 \text{ ft} = 1.2 \text{ dB using the data in Table 5.}$$

$$Gt = Gr = 43.1 \text{ dB using data from Table 4 since we are not sure of the parabolic antenna efficiency (52% in this case).}$$

$$\alpha = -96.6 - 20 \log(6.2) - 20 \log(30) = -141.9 \text{ dB}$$

$$L = -1.2 + 43.1 - 141.9 + 43.1 - 1.2 = -58.1 \text{ dB}$$

Single Passive Repeater Loss (back to back parabolic antennas)

Let us suppose that the above 30 mile path must have a passive repeater. Let us further assume the passive is a pair of back to back parabolic 10 foot antennas in the middle of the path.

$$L = -Tt + Gt + \alpha 1 + Grr - Trr + Gtr + \alpha 2 + Gr - Tr$$

$$Grr(\text{dB}) = \text{passive receive antenna gain}$$

$$Gtr(\text{dB}) = \text{passive transmit antenna gain}$$

$$Trr(\text{dB}) = \text{line loss between the passive repeater antennas}$$

$$\alpha 1 = \text{free space loss between the transmitter site and the passive site}$$

$$\alpha 2 = \text{free space loss between the passive site and the receiver site}$$

$$Tt = Tr = 1.2 \text{ dB as before.}$$

$$Trr = 0.5 \text{ dB (assumed value)}$$

$$Gt = Gr = Grr = Gtr = 43.1 \text{ dB since all antennas are 10 foot parabolics.}$$

$$\alpha 1 = \alpha 2 = -96.6 - 20 \log(6.2) - 20 \log(15) = -135.9 \text{ dB}$$

$$L = -1.2 + 43.1 - 135.9 + 43.1 - 0.5 + 43.1 - 135.9 + 43.1 - 1.2 = -102.3 \text{ dB}$$

This is quite an increase in path loss. Overall loss becomes less as the passive repeater is moved toward one end of the path. Therefore, let's assume the passive is 500 ft from the receive site. The loss formula is the same except we have a near field correction term $N_a(\text{dB})$.

$$L = -Tt + Gt + \alpha 1 + Grr - Trr + Gtr + \alpha 2 + N2 + Gr - Tr$$

$$\alpha 1 = -96.6 - 20 \log(6.2) - 20 \log(29.9) = -141.9 \text{ dB}$$

$$\alpha 2 = -96.6 - 20 \log(6.2) - 20 \log(0.0947) = -91.9 \text{ dB}$$

$$\lambda(\text{ft}) = 1 / [1.02 \times 6.2] = 0.158$$

Da(ft) = diameter of (larger) parabolic on the short path

Db/Da = 1 since both antennas are the same size.

$$10 \log(d / [2Da^2 / \lambda]) = 10 \log(500 / [2 \times 10^2 / 0.158]) = -4.0$$

N2(dB) = -2.3 dB from Figure 7.

$$L = -1.2 + 43.1 - 141.9 + 43.1 - 0.5 + 43.1 - 91.9 - 2.3 + 43.1 - 1.2 = -66.6 \text{ dB}$$

This is much better. The loss is much closer to the free space loss of the direct path. This points out the necessity of limiting the use of back to back parabolic antennas to short paths or locations near one end of a long transmission path.

Single Passive Repeater Loss (rectangular reflector)

For long paths, a physically large reflector is an improvement from a path loss perspective. Let's replace the 10 foot parabolic antennas of the previous example with a rectangular flat metal plate 10 feet by 14.1 feet tilted 45 degrees relative to each path of transmission (C = 90 degrees). The reflector's projection on each path would appear as a 10 foot square sheet. That projection is used to calculate area.

Consider the case treated previously of a 30 mile path with the passive rectangular reflector in the middle of the path. The path loss is similar to the previous case except there is no loss between the reflector receiving antenna and transmitting antenna - they are the same object.

$$L = -T_t + G_t + \alpha_1 + G_{rr} + G_{tr} + \alpha_2 + G_r - T_r$$

All terms are the same as previously except

$$G_{rr} = G_{tr} = +11.1 + 20 \log(6.2) + 10 \log(10 \times 10) + \log(1) = 46.9$$

δ is 1 since in the far field a uniform field exists over the entire surface of the passive reflector.

$$L = -1.2 + 43.1 - 135.9 + 46.9 + 46.9 - 135.9 + 43.1 - 1.2 = -94.2 \text{ dB}$$

Now let's move the reflector to a hill 500 feet from the receive end.

$$L = -T_t + G_t + \alpha_1 + G_{rr} + G_{tr} + \alpha_2 + N_2 + G_r - T_r$$

where, as before, N2 is the near field correction term.

Da = diameter of the parabolic receive antenna

Dr = width of the (square) reflector projection onto the transmission path

$$Da / Dr = 10 / 10 = 1$$

$$10 \log(d / [2Dr^2 / \lambda]) = 10 \log(500 / [2 \times 10^2 / 0.158]) = -4.0$$

N2 = -3.2 dB from Figure 9.

Using the calculations from the previous examples

$$L = -1.2 + 43.1 - 141.9 + 46.9 + 46.9 - 91.9 - 3.2 + 43.1 - 1.2 = -59.4 \text{ dB}$$

A popular alternate procedure is to calculate the path loss ignoring the reflector and then add a correction factor N to account for the introduction of the reflector into the path.

$$L = -T_t + G_t + \alpha + N + G_r - T_r$$

$$= -58.1 \text{ dB} + N \text{ from our first example.}$$

$$N = -1.1 \text{ dB from Figure 12.}$$

$$L = -58.1 - 1.1 = -59.2 \text{ which is in reasonable agreement with the previous result.}$$

Double Reflector Passive Repeater Loss

Sometimes it is necessary to use two passive reflectors in a back to back configuration to make sharp bends not possible with a single reflector (eg, sending a signal over a hill). These two reflectors will usually be so large and so close that they will be in the near field of each other. It is possible to perform the calculations for the three paths and calculate the loss using the correction factor from Figure 10. A faster way is to calculate the loss using a single passive (using the smaller of the two rectangular reflectors) and adding a correction factor from Figure 13.

Let's consider the previous example of a single 10 foot square passive reflector at the midpoint of a 30 mile path. As we noted previously, the combined path loss for this case is

$$L = -94.2 \text{ dB}$$

Now let's replace the single 10 foot passive by a pair of 10 foot square passives separated by 500 feet.

$$D_b/D_a = 10/10 = 1$$

$$10 \log(d / [2D_a^2 / \lambda]) = 10 \log(500 / [2 \times 10^2 / 0.158]) = -4.0$$

per the previous calculations. Therefore, the combined loss taking the N factor from Figure 13 is

$$L = -94.2 + N = -94.2 - 2.6 = -96.8 \text{ dB}$$

RECEIVED SIGNAL VARIATION (FADING)

The predicted values of received radio signal strength are usually based on a standard atmosphere (one which has no ducts, no refractive index discontinuities, and no turbulence). Natural variations from the standard atmosphere that occur at various times and places are produced chiefly by variations in the temperature and water vapor content of the actual atmosphere. They can cause considerable variation (fading) in the actual signal strength received compared to that predicted from a theory which assumes a static standard atmosphere. These variations in the predicted

values of signal strength produced by natural phenomena should be considered in the design of a radio communication system.

Predicting fades is not an exact science. Throver [31] observed,

"On the philosophical side of the dB ledger, one doesn't like to see a fade but, being practical, you can't make absolute predictions as to whether a path will fade or not, since we live in a terrestrial environment, rather than in theoretical free space. Even path testing is not an absolute way of establishing the reliability of a path, since to do it properly, one would have to run a propagation test over the path, with the planned tower height and with the planned antenna sizes for a minimum of a year in order to obtain data under all environmental conditions, and even that will vary from year to year, witness the drought stricken areas of the country for 1976 - 1977. Tests made, for example, in the Pacific Northwest during that winter, would result in totally different results compared to normal wet years in that region and a planned 11-GHz radio path would be defective when weather conditions return to their more normal saturated state.

It is for these reasons that one cannot, and should not, guarantee a path and the potential system user should be wary of those who offer to guarantee the path because it just can't be done. The experienced systems manufacturer and the experienced consultant don't and won't and shouldn't. The user should always be cautioned that there is always the possibility of fading although the path will be designed using the techniques that have been found to offer best protection against fading."

Most fading can be categorized as atmospheric absorption (including rain attenuation), multipath, diffraction (shadow), loss (earth bulge), antenna decoupling, and ducting. Often, fading is a combination of these types. A general introduction is given in the following paragraphs.

ATMOSPHERIC ABSORPTION

Path loss caused by atmospheric absorption is primarily due to atmospheric gases and rain. At frequencies below 60 GHz, attenuation due to frozen moisture (eg, snow or ice crystals) can be neglected. The only significant loss due to precipitation is caused by liquid raindrops. This loss will be overviewed later. Atmospheric gas absorption is due to resonance of various molecules and a broad nonresonant loss due to oxygen and water vapor. Below 100 GHz, the only significant resonances [3] are due to water vapor (H₂O) at 22 and 68 GHz, ozone (O₃) at 67 and

96 GHz, and a broad band of oxygen (O²) resonances from 61 to 68 GHz. Due to atmospheric pressure, the absorption resonances are broadened so that significant absorption is observed near the resonance frequencies. Oxygen attenuation is sensitive to temperature variations but its contribution is masked by water vapor loss. Water vapor loss is a moderate function of temperature above roughly 26 GHz. With little loss of accuracy, the loss dependency on temperature can be ignored. The above losses have been plotted in Fig. 15. As point of reference, in fog a visibility distance of 10 meters equates to about 10 gm/m³ of water. Likewise, 50 meters indicates 1 gm/m³, 100 meters indicates 0.4 gm/m³, and 500 meters indicates 0.04 gm/m³.

RAIN LOSS

At higher radio frequencies, large amounts of rain can have a significant effect on system radio interference, cross-polarization discrimination, and path attenuation. The interference and cross-polarization discrimination effects are short lived and generally are not a significant degradation to terrestrial paths. Path attenuation, however, has a significant impact on path design. Tillotson [32] observed the considerable effect rain can have on path design. He observed that for a rain rate of 100 mm (4 in)/hr, a normal 4- or 6-GHz path of 30 to 60 km (20 to 30 mi) designed for a 40-dB fade margin would be unaffected by rain. However, to maintain the path within the 40-dB fade range, the path length would have to be reduced to 9.2 km (5.7 mi) at 11 GHz, 3.7 km (2.3 mi) at 18 GHz, or 2.1 km (1.3 mi) at 30 GHz.

The rain attenuation observed on a radio path is a function of the following three variables:

$$\alpha(\text{dB}) = \beta \gamma L$$

$$\beta(\text{dB/km}) = \text{attenuation of a signal in rain of constant density and rate (attenuation due to point rain rate)}$$

$$\gamma = \text{path correction factor (conversion factor from point rain rate to path averaged rate)}$$

$$L = \text{path length}$$

The attenuation of a signal due to rain is a function of the size distribution of raindrops as well as a function of rain rate and the terminal velocity of the drops. The size distribution is a function of the type of rain (eg, thunderstorm, drizzle), and terminal velocity is a function of raindrop shape which is a function of rain type and wind. Olsen, Rogers, and Hodge [27] suggest that the Laws and Parsons [18] size distribution and the Gunn and Kinzer [14] terminal velocity results are the most reliable data to date. If the raindrops are assumed to be spherical, β is given by Olsen, Rogers, and Hodge [27] as

$$\beta(\text{dB/km}) = a R^b$$

$$R(\text{mm/hr}) = \text{rain rate}$$

where a and b must be calculated. Based on an assumed spherical shape for raindrops and various rain distributions and rates, Olsen, Rogers, and Hodge [27] calculated the theoretical values for a and b for various atmospheric temperatures. Rain attenuation is a moderate function of temperature. Comparing attenuation of 0° and 20°C, attenuation is slightly greater at 0° for frequencies below 10 GHz or greater than 20 GHz. Table 7 lists values for a and b for 20°C and spherical rain with the Laws and Parsons distribution. These results are in excellent agreement with Medhurst's results [25] for rain rates of 5 mm/hr or greater. Photographs have shown that rain, rather than being spherical, is actually flattened or concave. A slightly better approximation is to assume that raindrops are elliptical. Based on this approximation, vertically polarized signals experience less attenuation than do horizontally polarized signals. Horizontally polarized signals experience attenuation slightly greater than the attenuation predicted by spherical raindrops [25]. Based on Lin's data [19] [21] for 11, 18.1, and 30 GHz and Nowland, Olsen, and Shkarofsky [26] for 13 and 19.3 GHz, Table 8 was produced. The table lists the percentage that vertical attenuation $\beta_v(\text{dB/km})$ is less than horizontal attenuation $\beta_h(\text{dB/km})$. The table lists the values of $(100[\beta_h - \beta_v]/\beta_h)$ as a function of rain rate. Rain rate data is taken by measuring the total rain accumulated in a rain gauge in a period of time (integration period) and dividing by the integration time. The measured rain rate varies considerably with rain gauge integration time. A very short integration time produces widely varying results due to wind and spatial variations. A long integration time reduces the effect of short duration high rain rate. Fig.16, based on Lin's results [20] [23], shows the effect of gauge integration time. Bussev [5] observed that a rain rate of 1 mm/hr represented light rain, 4 mm/hr moderate rain, 16 mm/hr heavy rain, and 100 mm/hr represented a cloudburst.

The attenuation measured at one point of a radio path is not totally representative of the attenuation of the path taken as a whole. The relationship between point rain rate attenuation is a complex function of rain gauge integration time and probability of rain cell size and occurrence. Lin [21] [23] suggests that if the point rain rate R is measured with 5-minute integration time, γ is given by

$$\gamma = L' / [L' + L]$$

$$L(\text{km}) = \text{path length}$$

$$L' = 2636 / [R - 6.2]$$

$$R(\text{mm/hr}) \leq 10$$

Crane [7] suggests a slightly more complicated model. Lin's model yields a γ factor less than unity. His model is accurate primarily for high rain rates (R greater than 25 mm/hr). Crane's model yields a γ factor less than unity for high rates and greater than unity for low rain rates. This accounts for the observation that although the rain rate at one location may be low, it may be much higher elsewhere. High rain rates, however, indicate that the observation point is near the center of maximum rain intensity. Either Lin's or Crane's result is reasonable for the high rain rates that dominate short high frequency path design. Lin's requires the use of a 5-minute rain rate; Crane's uses a 1-minute rate. Lin, Bergman, and Pursley's results in Fig.16 can be used to convert between rain rates.

The previous calculations have assumed a point rain rate R which will not be exceeded more than a percent of the time. The actual rain rate at any instant is quite erratic. Long-term rain rate data gathered from a single rain gauge requires a very long time base (several years) to yield stable statistics. If the time base is not sufficiently long, the short-term results tend to underestimate (or occasionally overestimate) the long term, large sample average. Data taken over a period of less than 10 years [7] is generally unreliable for moderate rain rates. Incidence of high rain rates at a single point is so low that a much longer time base (a few decades) is required to obtain stable statistics [12]. Fig. 17, based on Lin's 20 years of United States data [23], shows the range of rain rates for various cities. Crane [7] gives estimated rain rates for various locations of the world.

The preceding rain rate data is based on distributions measured over one or two decades. The rain rates obtained from this data represent the rates that would have been measured if the radio path

had been operating over the previous long time period. Exactly the same data will probably not be obtained if measurements are made over the next couple of decades. However, this data represents the best estimate of the rain rate which would not be exceeded over any 1 year. The actual rain rate measured over any one specific year will be different than the average value. Average values should not be confused with worst-case values. Osborne [28] observed that the worst-case 1-year rain rates can exceed long-term averages by 2.5 to 10 times. Worst-case month or hour rates can exceed long-term averages by extremely large factors. Engineering paths based on worst-case statistics lead to very uneconomical radio systems. As Osborne [28] observed, at the present time there is no definitive proven solution to this problem. There is no practical method to limit the worst-case outage time for radio paths with loss dominated by rain attenuation.

It should be noted that it is the rainfall rate that determines outage time, not the total annual amount of water that falls. The northwest coast of the United States is a primary example of a very wet region where there are virtually no rain-related path outages. Large-scale climatological factors [28] which seem to bear some relation to high rain rates are number of thunderstorms, late summer humidity, and total July precipitation. These are probably related because most of the rain rates large enough to cause an outage are due to thunderstorms. Terrain should also be considered since rough terrain and mountains contribute to the formation of thunderstorms. In mountainous regions, precipitation tends to increase with altitude. When moist winds are lifted by a mountain chain, the windward slope tends to have heavier precipitation than the lee side. One side of a hill exposed to prevailing winds may have very heavy rainfall while areas on the other side may be quite dry.

In addition to losses in the path, rain on antenna radomes and passive reflector surfaces can increase losses at higher frequencies. Blevis [4] derived the loss of a thin sheet of water. He then related hemispherical radome dimensions to water thickness based on rain rates. He observed that a thickness of 0.010 inch of water would be produced by 50 mm/hr of rain on a radome of 2.5-foot radius or 12.5 mm/hr on a radome of 10-foot radius. This water layer would produce 2.5-dB loss at 3.7 GHz and 8.7-dB loss at 16 GHz. Lin [21] also reported experimental results. At 12 GHz, the loss of a 10-foot diameter, 10-year old conical radome varied from 2.5 dB for a light water sprinkle to 7.0 dB for a heavy sprinkle. At 20 GHz with a 10-mm/hr water rate, a new radome caused about 2.5-dB loss while a month old radome caused 8-dB loss. Weathering of the radome caused it to hold more water than the new radome. Hogg [12] observed that during heavy rain, each antenna radome would cause 3- to 6-dB attenuation at 11 GHz and 4- to 8-dB attenuation at 20 GHz. The variation was a function of radome material, shape, age, wind velocity

Atmospheric multipath fading is relatively independent of path clearance. The fading becomes more frequent, faster, and deeper as distance or frequency is increased [10]. As frequency or distance is increased, the statistics of the received signal approach the distribution of Rayleigh. After the multipath fading has reached the Rayleigh distribution, further increase in either distance or frequency increases the number of fades to a given depth but decreases the duration so that the product is essentially constant [4].

If a received signal envelope voltage, V , at an instant of time has a Rayleigh distribution (as measured over a long period of time), the probability, p , that it has a value less than or equal to L is given by

$$p(v \leq L) = 1 - e^{-L^2}$$

v^2 = instantaneous received signal power relative to unfaded power

L^2 = specific faded power level relative to unfaded power

The instantaneous fade depth in dB is $-20 \log(v) = -10 \log(v^2)$. The specific fade depth in dB is $-20 \log(L) = -10 \log(L^2)$. For L smaller than 0.1 (fade greater than 20 dB)

$$p(v \leq L) \approx L^2$$

To account for the fact that fading is not as severe as Rayleigh for short, low-frequency paths, Barnett [1] modified the probability to

$$p = r L^2$$

where r is a correction factor to account for path variables. As implied by Barnett's figure 8 [1], r should be limited to the range 0.01 to 1.0 (1.0 indicating full Rayleigh fading). Lin's results [22] indicate fading is only worse than Rayleigh for paths with a relatively constant interfering reflection (such as over water paths). Fading is generally much better than Rayleigh for relatively short paths. Barnett [1] suggests r is given by

$$r = 2.50 \times 10^{-6} c f D^3$$

and direction, and rain rate. At 11 GHz, total path loss due to two wet radomes is sometimes estimated at 4 dB [21] [28] for path design purposes.

ATMOSPHERIC MULTIPATH FADING

Multipath fading generally takes one of two forms. The first, atmospheric multipath, is caused by the received signal being composed of several signals arriving at the receive site by slightly different paths from the transmitter. The different transmission paths are caused by slight time and space dependent variations in the atmospheric refractive index. This phenomenon is the same one that causes stars to twinkle at night. Since the relative time delay of the various received signals will change as the atmosphere varies randomly, the composite received signal will vary widely and rapidly. This fading will be worse if obstruction (earth bulge) or reflective fading has already reduced the level of the dominant received signal. Figure 19 shows typical received signal variation during multipath fading.

DeLange [8] noticed that for a 22-mile path operating at 4 GHz, path differences were from a fraction of 1 foot to 7 feet with 3 feet being the most common. Kaylor [14] made several observations on a typical 31-mile, 4-GHz path with no significant ground reflections. He observed that deep multipath fades (greater than 20 dB relative to normal propagation conditions) always showed definite frequency selectivity (great loss only occurred over a relatively narrow frequency range). The deep fading was caused by at least four to six different component rays.

The amplitude of the short path signals was larger than longer path signals, but depth of fade was primarily a function of long path signal amplitude. Deep fading was largely uncorrelated for frequencies separated by more than 160 MHz (4 percent separation) but was highly correlated for frequencies within 80 MHz (2 percent) of the deep fade notch. Deep fading usually occurred with a wide frequency loss of at least 10 dB (for deep fades of 30 to 40 dB, broadband losses were typically 10 to 20 dB).

Most multipath fading occurs between midnight and 9:00 am [1] during the summer and early fall [6]. Frequency diversity helps reduce deep fading but has no effect on shallow fades. The space correlation of fading signals is large in the horizontal plane. However, it is small in the vertical plane under severe fading conditions. Therefore, vertically spaced (transmit or receive) space diversity antennas can be used to reduce fading. Space diversity is as good or better than frequency diversity for multipath or reflective fading [33] and sometimes better for long, slow fades due to defocusing and ducting [35].

for f , the operating frequency in GHz, and D , the path length in miles. For D in kilometers

$$r = 6.00 \times 10^{-7} c f D^3$$

The c factor is a function of path location. For good paths, c is 0.25; for average paths, 1.0; and for bad paths, 4.0. Some sources have expanded the range of c to 0.1 to 10. A good path would generally occur in an area characterized by dry climate, hilly or mountainous country with rough terrain, rare occurrence of calm weather or atmospheric stratification, or launch angles exceeding one-half degree. Average paths would be hilly or flat country (not marsh or salt flats) with occasional calm weather or atmospheric stratification; coastal areas with moderate to low temperatures (not Gulf Coast or over water); or hot, tropical regions with steep launch angles. Bad paths would have low launch angles over flat ground or in warm coastal regions or tropical regions, humid areas where ground mist forms, wet or swampy terrain (eg, irrigated fields), conditions favorable for atmospheric stratification (eg, broad protected river valleys, moors), or over water (eg, inland lakes, sea). Vigants [33] suggested that c could be modified to account for terrain roughness by making

$$c = 0.5 (w/50)^{-1.3} \text{ for good paths}$$

$$c = 1.0 (w/50)^{-1.3} \text{ for average paths}$$

$$c = 2.0 (w/50)^{-1.3} \text{ for bad paths}$$

where w is a path roughness factor in rms averaged feet. This factor is introduced to quantify the observation that paths over rough terrain fade less than paths over smooth. Presumably this happens because stable atmospheric layering is less likely to occur over rough terrain. Figure 20 shows the calculated and observed received signal level statistics of a 30 mile path in the Dallas area.

REFLECTION (FRESNEL ZONE) FADING

The second form of multipath fading is reflective fading (sometimes called Fresnel zone fading). This fading, like that caused by atmospheric multipath, is due to the reception of several signals from several different paths. The concept is exactly the same used in optics. Indirect signals arrive

due to reflections from the ground, water, nearby objects, or stable atmospheric layers. Unlike atmospheric multipath, fading due to these reflective signals is relatively slow-changing since the secondary paths are relatively stable. If the fading is due to cancellation between the main signal and a single reflected signal, the composite signal will be a minimum when the reflected signal is reflected from an obstacle an even Fresnel zone radius from the main path. The composite signal will be a maximum if the radius is odd. Generally, reflective fading is not a problem for paths over heavily wooded terrain or for paths so far above the reflecting surfaces that the transmit and receive patterns discriminate against reflections. Flat paths can have reflections. Paths over water or salt flats almost always have reflections. Reflections can be reduced by blocking the reflection (using screen or high-low path design), tilting the antenna, or using spaced antennas. It is common to use two receive antennas (space diversity) to combat the effect of multipath. Another method is to reduce antenna height at one end of the path while raising it at the other end to block the reflection or move it to a location less likely to be reflective (high-low path design). This technique makes one site elevated so as to provide the required clearance; the other site is located near ground level. The reflection point can be placed at a selected location by slight changes in the lower antenna height and geographical location. Even if the path is reflective, this technique reduces the difference between the direct and reflected paths when compared to midpath reflection.

OBSTRUCTION (DIFFRACTION) FADING

Radio waves normally travel outward along radial lines from their source, except when deviated by refraction or reflection. Another condition under which radio waves deviate from a straight line is called diffraction. Whenever radio waves encounter an obstructing object, some of the energy of the wave is diffracted at the edges of the object and becomes bent around the edge. This is a direct result of Huygens' principle of secondary radiation. This reduces the shadowing effect of objects which are opaque to radio waves. Diffraction fills part of the shadow area with some energy from the wave. The curved surface of the earth is the edge of one such object. Other objects may be buildings, trees, hills, or mountains, or structural parts of a ship or airplane. If the obstructing object is small and subtends only a small angle, as seen from the source of radiation, the region at a considerable distance behind the object may become filled in and suffer little or no shadowing effect. Close behind the object, however, shadowing will be observed. Shadowing due to the earth causes the field strength to decrease rapidly with distance beyond the radio horizon. In general, an exact determination of signal strength for various path clearances is difficult. The obstruction loss generally falls somewhere between the knife-edge diffraction and flat-sheet reflection cases shown in Fig. 14.

The first Fresnel zone radius F1 at any point on the radio path is given by the following:

F1 = first Fresnel zone radius

d1 = distance from one end of path to reflection point

d2 = distance from other end of path to reflection point

do = total length of path

$$= d1 + d2$$

f = frequency of operation

For F1 in feet, do, d1, and d2 in miles and f in GHz:

$$F1 = 72.1 (d1 d2 / f do)^{1/2}$$

For F1 in meters, do, d1, and d2 in kilometers and f in GHz:

$$F1 = 17.3 (d1 d2 / f do)^{1/2}$$

From a classical physics point of view, the quantity $(h/F1)^2$ defines the Fresnel zone (or fraction of the zone) clearance of an obstacle as measured perpendicular to the line of wave propagation. In practice it is measured in a line perpendicular to the earth. For normal microwave paths, there is no significant difference. Bullington [4] used $(h/F1)$ to define path clearance. Since that time, common usage has been to define $(h/F1)$ as Fresnel zone clearance rather than $(h/F1)^2$.

A particular form of diffraction loss is called obstruction fading. When the K factor becomes less than one (see Fig. 18), the radio wave is bent upward. Under extreme cases the receive path can be partially or completely blocked. This type of loss is called "Earth bulging" because the Earth appears to bulge up into the radio path. The power fades that occur due to diffraction by the earth's surface are generally supported by a subrefractive (positive) gradient of refractive index. This type of fading can persist for several hours to depths of 20 or 30 dB. The fading is essentially independent of small scale changes of frequency, but may be reduced or avoided by a proper choice of terminal antenna heights.

In mountainous terrain where terminals are located on dominating ridges or peaks, a single Fresnel zone clearance, or even less, will usually be sufficient to avoid this effect. If only a limited range of refractive index gradients is encountered, a first Fresnel zone clearance, or less, is sufficient. For those microwave paths where subrefractive index gradients are encountered, increased clearances are required. Diffraction fading in the sense used earlier may also occur when a strong super-refractive layer is positioned slightly below the terminal antennas. The severity of this type of fading will be reduced somewhat by terrain reflections or contributions from subrefractive layers positioned below the diffracting layer which can direct energy back toward the receiver. These contributions are a function of the gradients within and below the diffracting layer and also of the terrain roughness.

From experience, various rules of thumb have been developed to reduce obstruction fading to an insignificant effect. CCIR [13] suggests the following guidelines for line-of-sight radio paths (where F1 is the first Fresnel zone radius):

For frequencies below 1 GHz, allow obstruction clearance of

$$1.00 F1 \text{ for } K = 4/3$$

For frequencies between 1 and 7 GHz, allow obstruction clearance of

$$0.30 F1 \text{ for } K = 2/3$$

For frequencies greater than 7 GHz, allow obstruction clearance of

$$0.8 F1 \text{ for } K = 7/10$$

White [41] of GTE Lenkurt proposed the following guidelines for highest reliability (heavy route) systems:

For areas of good-to-average propagation conditions, allow obstruction clearance of

$$0.30 F1 \text{ for } K = 2/3, \text{ or}$$

$$1.00 F1 \text{ for } K = 4/3,$$

whichever is greater

For areas of difficult propagation conditions, in addition to the above clearance criteria, add the following

For 2-GHz paths longer than 8 km (36 miles), allow obstruction clearance of 0.60 FI for $K = 1$

For all other paths, allow obstruction clearance of 0.00 FI (grazing) for $K = 1/2$

For moderate reliability (light route) systems, allow obstruction clearance of

3 meters (10 feet) plus 0.60 FI for $K = 1.00$

White observes that clearance evaluations should be carried out along the entire path, not just the center. Often, one criterion is controlling for obstacles near the center of the path and another is controlling near the end. Near the path ends, the Fresnel zone radius and earth bulge are negligible. However, it is good practice to maintain a minimum obstacle clearance of 15 to 20 feet. The heavy-route criteria are conservative guidelines and often result in clearance heights required only in the more difficult propagation areas. Even these criteria, however, are not adequate to protect against fading due to severe surface ducts (blackout fading). If blackout fading is expected, 150 feet of clearance above the earth at all path points for $K = 1$ should be imposed.

Vigants [33] of American Telephone and Telegraph (Bell System) and other Bell sources suggest the following guidelines:

For good propagation areas, allow obstruction clearance of

0.60 FI for $K = 1$, or
0.00 FI (grazing) for $K = 2/3$,
whichever is greater

For average propagation areas, allow obstruction clearance of

0.30 FI for $K = 2/3$ or,
1.00 FI for $K = 4/3$,

whichever is greater

For difficult propagation areas, allow obstruction clearance of

0.00 FI (grazing) for $K = 1/2$

For very difficult propagation areas, allow obstruction clearance of

0.00 FI (grazing) for $K = 5/12$

The preceding guidelines apply to the normal or main antennas. If space diversity is used, the criterion for diversity antenna clearance is less stringent.

For the diversity antenna path, allow obstruction clearance of

0.60 FI for $K = 4/3$ with at least 10 feet in the first 500 feet from the antenna.

This usually permits placement of the diversity antenna at an appropriate level below the main antenna. If the path terrain is nonreflective, multipath fading improvement is achieved by placing the diversity antenna at least 200 wavelengths below (or above) the main antenna.

To analyze a microwave path for conformance to the above guidelines, the profile of the earth along the transmission path is plotted on rectangular graph paper. The microwave beam is then shown as a straight line between the two points. This represents the radio or light ray for K of infinity. An h value is then subtracted from the ray height to show beam bending due to various potential K values. The h correction value is given by the following:

h = the change in vertical distance from a horizontal reference line

p = location where h is determined

d_1 = distance from p to one end of path

d_2 = distance from p to other end of path

K = effective earth radius factor

For h in feet and d_1 and d_2 in miles

$$h = [d_1 d_2] / [1.50 K]$$

For h in meters and d_1 and d_2 in kilometers

$$h = [d_1 d_2] / [12.74 K]$$

To adjust for ray curvature, subtract the above h value from the height of the ray above a flat earth or add the h value to the height of the earth below a straight ray.

In unusually severe propagation areas (such as southern United States coastal areas) path lengths are often limited to 20 miles to reduce the occurrence of obstruction fading to a reasonable level. Good propagation areas are regions with low humidity and/or temperatures and significant turbulence (eg, mountainous regions). Mountainous areas such as the Alps, Andes, Atlas, Himalayas, and Rockies are good examples. Average propagation areas include most of continental Europe and North America and most tropical and cold maritime countries. Difficult propagation conditions are related to high humidity and/or temperature area where atmospheric turbulence is not prevalent (layering is prevalent). In the United States, this includes the south eastern coastal region (Texas through North Carolina), Southern California, and the Great Lakes region. Most subtropical and warm maritime countries fall into this category. Very difficult propagation conditions are usually associated with high humidity and temperature and frequent, severe, extensive atmosphere layering. Tropical coastal areas and most desert regions are in this category.

POWER FADING

Power fading due to antenna decoupling refers to the loss of signal that occurs for transmission and reception of the signal outside of, or at the extremities of, the main lobe of the antenna pattern. Variation of atmospheric refraction can cause changes in the apparent angle-of-arrival of the line-of-sight ray, particularly in the vertical plane, and can therefore effectively cause a reduction in gain in the antennas used at the radio path terminals. Measurements made in the United States over a path of 28 kilometers, at frequencies of 4 and 24 GHz, show that the angle-of-arrival can change rapidly by as much as 0.75 degree above and below the normal line of sight. Another

source observed 0.5 degree of angle-of-arrival variation on a 39 kilometer path. Variations in the vertical angle-of-arrival of up to one-half degree have been observed on a 40-kilometer path. This effect is proportional to the path length and can introduce several decibels of loss for high gain antennas and long line-of-sight paths. Because of the vertical variations in angle-of-arrival, antennas having half-power beam widths less than 0.5 degree should generally be avoided for line-of-sight paths. This limitation can be used as one criterion to determine maximum aperture size for antennas and the maximum vertical dimension for passive repeaters. This loss may be minimized by specifying a sufficiently broad antenna beam so that the expected variations of the angle of arrival are matched or exceeded.

DUCT FADING

Refraction (bending) of a radio wave occurs when the wave speed on one side of the beam is reduced below that on the other. The bending is in the direction of the reduced speed, and its degree is directly proportional to the amount of speed reduction with distance (ie, the gradient of wave speed) normal to the beam axis. Since refractivity N is a ratio of wave speeds, it follows that the gradient of refraction normal to the radio wave axis indicates the direction and amount of the resultant radio refraction. Refraction is a function of the gradient and not of discrete values of N . Significant gradients of N in the atmosphere normally occur only in the vertical, and these are specified as positive or negative (ie, increasing or decreasing N -values with height respectively). Positive N -gradients cause subrefraction (ie, upward bending of a radio wave), and negative N -gradients cause superrefraction (ie, bending downward toward the curvature of the earth's surface). Extreme superrefraction is called ducting or trapping, since it results in the wave following a path which approximates the curvature of the earth. Gradients of N averaged over a world wide basis are shown in Fig. 15. This figure also related N gradient to K factor. Gradients of N , which result in gradients of wave speed and refraction of a radio beam, are in turn the results of characteristics of the atmosphere. The significant atmospheric properties in this respect are water vapor content and density. Of these, water vapor content is, in general, the most important.

Whenever a horizontal layer of air has its normal properties altered so that the refractive index decreases rapidly with increase in height, strong downward bending of any nearly horizontal rays traversing the layer will occur. The curvature of these rays often exceeds the curvature of the earth's surface. A layer of air having this property is called a duct. Ducts may be divided into two types, ground (surface) and elevated. The underside of a ground based duct is in contact with the earth's surface while the underside of an elevated duct is above the earth's surface and overlies a layer of normal air. Prolonged fading, or signal enhancement, can result from propagation through

ducts, especially when either the transmitter or the receiver is located within the duct. Signals may be trapped within the duct and propagated far beyond the horizon. Ducts may also cause multipath fading. Two conditions are necessary to form a duct. The first is for the refractive index gradient to be equal to or more negative than -1.67 N per kilometer (-23 N per mile). This means that K must be infinite (flat earth) or negative (extreme superrefractivity). The second necessary condition is that the gradient must be maintained over a height of several wavelengths. For ducts 100 to 30 feet thick, trapping will occur for frequencies between 2 and 13 GHz respectively. Of course, this cutoff relationship is only approximate since ducts have vague boundaries.

Because the energy within the duct spreads with distance in the horizontal but is constrained in the vertical direction, it is possible in principle that the field strength within a duct may be greater than the free-space field strength for the same distance. The transmission power loss might be expected to be proportional to the distance d , instead of following the free space d^2 law (power loss in dB a function of $10 \log [d]$ rather than $20 \log [d]$). Some energy will steadily pass out of the top of the duct, thereby adding to the transmission loss within the duct. A consequence of this leakage is that the field strength just above a duct at a distance well beyond the normal horizon may be higher than if the duct were not present. The signal level within the duct would be higher than normal even if the transmitter were just outside the duct. Conversely, the duct may cause much lower signal strength above the duct top if the transmitter is within the duct, or much lower signal strength within the duct if the transmitter is above the duct. Normally, the refractive index gradient will not be constant with horizontal distance, so a duct will have horizontal limits beyond which the radio energy reduces rapidly. Also, the transmission loss within a duct will change considerably as a function of time as the duct characteristics change. This type of fading mechanism is the likely source of many so called space wave fadeouts. The fading is not generally sensitive to small changes of frequency or of spatial position of the antennas and cannot be remedied by commonly used diversity techniques.

Ground-based ducts may be formed by an unusually rapid decrease of water vapor with height, or an increase in temperature with height, or both effects together. Two causes associated with the sea or large areas of water are evaporation and advection. Evaporation of water vapor from the surface of the sea may cause a zone of high humidity (ie, high refractive index) below a region of drier air. Such ducts are particularly likely to occur in the afternoon due to prolonged solar heating. The duct thickness is typically 15 m. Over tropical seas, the high humidity existing near the surface produces almost permanent ducts that may contain a change of some 40 N-units. Advection, the movement of one air type over another, may cause hot dry air (from the land) to be blown over cold wet air, producing a region of low refractive index about a region of high

refractive index. This is most marked at evening with the onset of a land breeze. The duct thickness is typically 25 meters. Such a duct may also form when warm dry air is blown over cold ground. Radiation cooling may also produce temperature gradients which cause ground based ducting. This occurs when the ground cools at night due to the absence of cloud cover. Air next to the ground becomes colder than that higher up, and the process continues as the ground continues cooling. The duct becomes thicker as the night continues. This phenomenon is fairly commonplace in desert and tropical climates.

There is no comprehensive data available to permit calculation of duct fading statistics for a particular path. It is generally unwise to extrapolate fading statistics for one area to apply to some other part of the world. Fading is related to local conditions and refractive index.

A severe form of fading produced by surface ducts has been termed blackout fading [17]. Low clearance paths traversing areas supporting superrefractive ground-based layers have experienced complete loss of signal for periods of up to 24 hours due to the blackout phenomenon. The fades are sudden, catastrophic, and nonselective (although widely spaced antennas are sometimes effective). A rising atmospheric layer (usually not visible, but sometimes associated with visible steam fog formed over warm water or moist ground) may intercept and trap the path. The failure is occasionally preceded by reflection fades (reflection path from the layer) and an obstruction fade.

CONCLUSION

For the last few pages the nonequipment related system design considerations have been overviewed. Radio system performance is highly dependent of the choice of proper antennas and careful path design. No single article can begin to treat the topics adequately. However, the various topics are pursued in considerable detail in [16]. The intent of this article is to acquaint the reader with the most significant system design topics.

REFERENCES

- [1] Barnett, W. T., "Multipath Propagation at 4, 6, and 11 GHz," *Bell System Technical Journal*, pp. 321-361, February 1972.
- [2] Bickmore, R. W. and Hansen, R. C., "Antenna Power Densities in the Fresnel Region," *Proceedings of the IRE*, pp. 2119-2120, December 1959.
- [3] Blevis, B. C., Dohoo, R. M., and McCormick, K. S., "Measurements of Rainfall Attenuation at 8 and 15 GHz," *IEEE Transactions on Antennas and Propagation*, pp. 394-403, May 1967.
- [4] Bullington, K., "Radio Propagation Fundamentals," *Bell System Technical Journal*, pp. 593-626, May 1957.
- [5] Bussey, H. E., "Microwave Attenuation Statistics Estimated From Rainfall and Water Vapor Statistics," *Proceedings of the IRE*, pp. 781-785, July 1950.
- [6] Crane, R. K., "Attenuation Due to Rain—A Mini-Review," *IEEE Transactions on Antennas and Propagation*, pp. 750-752, September
- [7] Crane, R. K., "Prediction of Attenuation by Rain," *IEEE Transactions on Communications*, pp. 1717-1733, September
- [8] DeLange, O. E., "Propagation Studies at Microwave Frequencies by Means of Very Short Pulses," *Bell System Technical Journal*, pp. 91-103, January 1952.
- [9] Egli, J. J., "UHF Radio-Relay System Engineering," *Proceedings of the IRE*, pp. 11124, January 1953.
- [10] Friis, H. T., "Microwave Repeater Research," *Bell System Technical Journal*, pp. 183-246, April 1948.
- [11] Gunn, R. and Kinzer, G. D., "The Terminal Velocity of Fall for Water Droplets in Stagnant Air," *Journal of Meteorology*, pp. 243-248, August 1949.
- [12] Hogg, D. C., Giger, A. J., Longton, A. C., and Muller, E. E., "The Influence of Rain on Design of 11-GHz Terrestrial Radio Relay," *Bell System Technical Journal*, pp. 1575-1580, November 1977.
- [13] International Telecommunication Union (ITU), Propagation, Appendix to Section B.IV.3 of *GAS 3 Manual, Transmission Systems. Economic and Technical Aspects of the Choice of Transmission Systems*, Geneva: ITU, 1971.
- [14] Jakes, W. C., Jr., "A Theoretical Study of an Antenna—Reflector Problem," *Proceedings of the IRE*, pp. 272-274, February 1953.
- [15] Kaylor, R. L., "A Statistical Study of Selective Fading of Super-High Frequency Radio Signals," *Bell System Technical Journal*, pp. 1187-1202, September 1953.
- [16] Kizer, G. M., *Microwave Communication*, Ames: Iowa State University Press, pp. 315-440, 1990.
- [17] Laine, R. U., "Blackout Fading in Line-of-Sight Microwave Links," *PIEA-PESA-PEPA Conference Presentation*, Dallas, Texas, April 1975.
- [18] Laws, J. O. and Parsons, D. A., "The Relation of Raindrop-Size to Intensity," *American Geophysical Union Transactions of 1943, Part II* (April 1943), pp. 452-460, January 1944.
- [19] Lin, S. H., "A Method for Calculating Rain Attenuation Distributions on Microwave Paths," *Bell System Technical Journal*, pp. 1051-1086, July-August 1975.
- [20] Lin, S. H., "Dependence of Rain-Rate Distribution on Rain-Gauge Integration Time," *Bell System Technical Journal*, pp. 135-141, January 1976.
- [21] Lin, S. H., "Nationwide Long-Term Rain Statistics and Empirical Calculation of 11-GHz Microwave Rain Attenuation," *Bell System Technical Journal*, pp. 1581-1604, November 1977.
- [22] Lin, S. H., "Statistical Behavior of a Fading Signal," *Bell System Technical Journal*, pp. 3211-3269, December 1971.

- [23] Lin, S. H., Bergmann, H. J., and Pursley, M. V., "Rain Attenuation Distributions on Earth-Satellite Paths—Summary of 10-Year Experiments and Studies," *Bell System Technical Journal*, pp. 183-228, February 1980.
- [24] Medhurst, R. G., "Passive Microwave Mirrors," *Electronic and Radio Engineer*, pp. 443-449, December 1959.
- [25] Medhurst, R. G., "Rainfall Attenuation of Centimeter Waves: Comparison of Theory and Measurement," *IEEE Transactions on Antennas and Propagation*, pp. 550-564, July 1965.
- [26] Nowland, W. L., Olsen, R. L., Shkarofsky, I. P., "Theoretical Relationship Between Rain Depolarization and Attenuation," *Electronics Letters*, pp. 676-678, October 1977.
- [27] Olsen, R. L., Rogers, D. V., and Hodge, D. B., "The aR^b Relation in the Calculation of Rain Attenuation," *IEEE Transactions on Antennas and Propagation*, pp. 318-329, March 1978
- [28] Osborne, T. L., "Applications of Rain Attenuation Data to 11-GHz Radio Path Engineering," *Bell System Technical Journal*, pp. 1605-1627, November 1977.
- [29] Sciambi, A. F., "The Effect of the Aperture Illumination on the Circular Aperture Antenna Pattern Characteristics," *The Microwave Journal*, pp. 79-84, August 1965.
- [30] Silver, S., *Microwave Antenna Theory and Design*, New York: McGraw-Hill, pp. 169-199, 413-542, 574-592, 1949.
- [31] Thrower, R. D., "Curing the Fades, Part III," *Telephone Engineer and Management*, p. 82, September 1, 1977.
- [32] Tillotson, L. C., "Use of Frequencies Above 10 GHz for Common Carrier Applications," *Bell System Technical Journal*, pp. 1563-1576, July-August 1969.
- [33] Vigants, A., "Space-Diversity Engineering," *Bell System Technical Journal*, pp.103-142, January 1975.
- [34] Wang, H.S.C., "Distortion of FM Signals Caused by Channel Phase Nonlinearity and Amplitude Fluctuations," *IEEE Transactions on Communication Technology*, pp. 440-448, August 1966
- [35] White, R. F., "Space Diversity on Line-of-Sight Microwave Systems," *IEEE Transactions on Communication Technology*, pp. 119-133, February 1968.
- [36] White, R. F., *Engineering Considerations for Microwave Communications Systems*, San Carlos: GTE Lenkurt, pp. 51-52, 1975.

Table 2 Typical Radio Carrier to Interference Objectives (Cochannel Interference)

Interfered System	C/I Objective (dB) Frequency Band		
	4 GHz	6 GHz	11 GHz
1200 Channel FDM-FM	63-76	62-81	61-89
1800 Channel FDM-FM	65-85	63-83	64-94
2400 Channel FDM-FM	-	62-80	64-92
2700 Channel FDM-FM	-	63-84	73-96
5400 Channel SSB	-	54-90	-
525 Line NTSC Video	66-68	54-68	62-70
45 Mb/sec 8 PSK	65	-	75
45 Mb/sec 16 QAM	65	-	75
90 Mb/sec 8 PSK	-	65	75
90 Mb/sec 16 QAM	-	65	75
90 Mb/sec 64 QAM	72	-	-
135 Mb/sec 16 QAM	-	-	75
135 Mb/sec 64 QAM	-	72	81

Table 3 Typical Radio Carrier to Interference Objectives (Adjacent Channel Interference)

Interfered System	C/I Objective (dB) Frequency Separation				
	15 MHz	20 MHz		30 MHz	40 MHz
	6 GHz	4 GHz	11 GHz	6 GHz	11 GHz
1200 Channel FDM-FM	37-69	27-48	38-60	20-35	20-37
1800 Channel FDM-FM	57-77	35-54	49-72	20-49	20-43
2400 Channel FDM-FM	63-78	-	57-77	20-57	20-53
2700 Channel FDM-FM	-	-	58-80	-	-
5400 Channel FDM-SSB	60-90	-	-	20-51	-
525 Line NTSC Video	35-57	22-35	20-52	20	20
45 Mb/sec 8 PSK	-	25-56	20-75	-	20-45
45 Mb/sec 16 QAM	-	25	20-59	-	20
90 Mb/sec 8 PSK	60-71	-	60-75	23-66	20-34
90 Mb/sec 16 QAM	53-61	-	30-67	20-44	20-33
90 Mb/sec 64 QAM	-	32	-	-	-
135 Mb/sec 16 QAM	-	-	75	-	45
135 Mb/sec 64 QAM	67-69	-	75	20-45	20-40

Table 1 Terrestrial Frequency Planning Data

1. Site name (with user identification).
2. Latitude: degrees, minutes, seconds, north or south.
3. Longitude: degrees, minutes, seconds, east or west.
4. Site elevation (meters or feet) above mean sea level.
5. Antenna center line (meters or feet) above site elevation - include data for both main and diversity antennas if appropriate.
6. Antenna description (manufacturer, type number (eg, UHX-10), type (eg, shrouded parabolic), feed type (eg, dual polarization horn), aperture diameter (eg, 10 feet) for main and diversity antennas.
7. Antenna discrimination curves for both copolarization and orthogonal polarization (cross-polarized) signals.
8. Passive repeater size and type (eg, 10 feet by 10 feet, single billboard) and manufacturer and type number.
9. Equipment transmitter power and transmission line loss (or waveguide type and length) or transmitter power delivered to the transmit antenna.
10. Receiver transmission lines loss (or waveguide type and length).
11. Transmitter frequency in MHz to nearest kHz (eg, 5945.200 MHz).
12. Transmitter frequency stability (eg, 0.005 percent).
13. Traffic type (video, telephony, data) and specific loading. If video, specify 525-line or 625-line, NTSC, SECAM, or PAL. If FDM telephony, indicate number of channels (eg, 1800) and multiplexing plan (eg, CCITT Plan 2, 15 SGA). If data indicate bit rate and modulation method (eg, 135 Mb/s, 64 QAM) and if transmitter spectrum meets any emission mask.
14. Receiver interference susceptibility curves relating C/I to performance degradation for various cochannel and adjacent interfering signals.

Table 4 Typical Worst-case Commercial Parabolic Antenna Gain (dB Relative to Isotropic Radiator)

Diameter m (ft) Frequency (GHz)	0.6(2)	1.2(4)	1.8(6)	2.4(8)	3.0(10)	3.7(12)	4.6(15)
1.9	-	25.0	28.5	31.0	32.9	34.5	36.4
2.1	-	25.8	29.3	31.9	33.8	35.4	37.3
2.2	-	26.3	29.3	32.2	34.2	35.7	37.6
2.4	-	27.2	30.9	33.3	35.2	36.9	-
2.5	-	-	31.0	33.5	-	-	-
2.6	-	27.9	31.1	33.6	35.4	37.4	-
3.7	-	-	-	36.8	38.8	40.4	42.3
3.9	-	-	-	36.8	38.8	40.4	42.3
4.0	-	31.4	34.9	37.3	39.0	41.0	42.7
4.7	-	33.0	36.4	38.9	40.8	42.4	44.3
5.9	-	-	-	-	42.9	44.5	-
6.2	-	35.0	38.5	41.3	43.1	44.8	46.4
6.8	-	36.0	39.4	42.0	43.8	45.4	46.9
7.4	-	36.5	40.0	42.5	44.5	46.0	47.7
8.0	-	37.1	40.7	43.3	45.2	46.7	48.6
8.1	-	37.2	40.8	43.3	45.2	46.7	48.6
8.4	-	-	41.0	43.5	45.4	47.0	48.8
10.6	34.1	39.6	43.1	-	-	-	-
11.2	34.5	40.5	44.0	46.4	47.8	49.8	12.5
12.5	35.4	40.7	44.8	47.3	48.5	50.6	51.6
12.7	35.5	40.8	45.1	47.6	48.8	50.9	51.9
13.0	35.6	41.0	45.1	47.6	48.8	50.9	-
14.9	36.5	42.5	46.1	48.6	50.5	-	-
18.7	38.5	44.7	-	-	-	-	-

Table 5 Typical Copper Corrugated Elliptical Waveguide Loss

Frequency (GHz)	Waveguide Type	Loss	
		dB/100 m	dB/100 ft
1.9	EW20	2.0	0.60
2.1	EW20	1.7	0.52
2.2	EW20	1.6	0.49
2.4	EW20	1.5	0.45
2.5	EW20	1.4	0.44
2.6	EW20	1.4	0.43
3.7	EW37	3.1	0.94
3.9	EW37	2.9	0.87
4.0	EW37	2.8	0.85
4.7	EW44	4.0	1.2
5.9	EW52	4.0	1.2
6.2	EW52	3.9	1.2
6.8	EW63	4.4	1.4
7.4	EW64	4.8	1.5
8.0	EW77	5.8	1.8
8.1	EW77	5.8	1.8
8.4	EW77	5.6	1.7
10.6	EW90	10.5	3.3
11.2	EW90	10.0	3.1
12.5	EW127	11.8	3.6
12.7	EW127	11.7	3.6
13.0	EW127	11.5	3.5
14.9	EW132	15.4	4.7
18.7	EW180	19.4	5.9

Table 6 Typical Copper Circular Waveguide Loss

Frequency (GHz)	Waveguide Type	Loss	
		dB/100 m	dB/100 ft
4.0	WC-281/-269	1.2/1.3	0.36/0.41
4.7	WC-281/-269	1.0/1.1	0.32/0.35
5.9	WC-281/269	0.91/0.99	0.28/0.30
6.2	WC-281/-269/-205	0.91/0.98/1.6	0.28/0.30/0.50
6.8	WC-281/-269/-166	0.89/0.97/2.5	0.27/0.30/0.76
7.4	WC-281/-166	0.89/2.3	0.27/0.70
8.0	WC-281/-166	0.89/2.1	0.27/0.65
8.1	WC-281/-166	0.89/2.1	0.27/0.64
8.4	WC-281/-166	0.89/2.1	0.27/0.64
10.6	WC-281/-166/-109	0.91/1.9/4.5	0.28/0.57/1.4
11.2	WC-281/-166/-109	0.92/1.9/4.3	0.28/0.57/1.3
12.5	WC-281/-109	0.95/4.2	0.29/1.30

Table 7 Rain Attenuation Coefficients

F (GHz)	a	b	F (GHz)	a	b
1.0	0.0000317	0.945	11	0.0167	1.181
1.5	0.0000675	0.972	12	0.0233	1.142
2.0	0.000115	1.007	15	0.0459	1.076
2.5	0.000173	1.049	20	0.0859	1.044
3.0	0.000239	1.096	25	0.143	1.007
3.5	0.000311	1.151	30	0.228	0.955
4.0	0.000378	1.219	35	0.337	0.904
5.0	0.000515	1.377	40	0.452	0.864
6.0	0.00106	1.393	50	0.648	0.815
7.0	0.00204	1.380	60	0.775	0.794
8.0	0.00378	1.342	70	0.850	0.785
9.0	0.00674	1.285	80	0.902	0.780
10	0.0111	1.229	100	0.958	0.774

Table 8 Relative Rain Attenuation for Vertical and Horizontal Signals

f (GHz)	R (mm/hr)					
	5	12.5	25	50	100	150
11	15	16	16	16	17	18
13	11	13	15	16	18	19
18.1	12	14	16	18	19	20
19.3	11	14	16	19	21	22
30	12	12	12	12	12	12

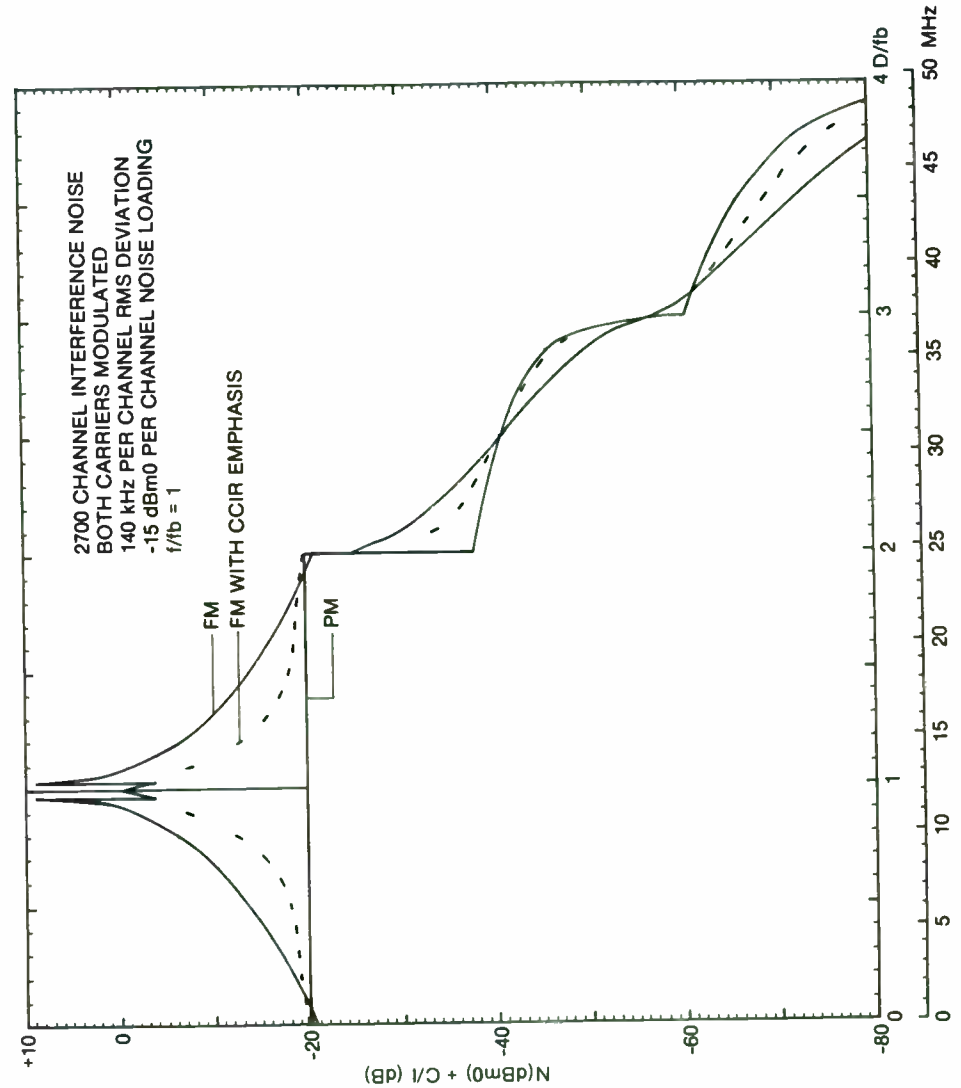


Figure 1 Analog into Analog Interference

Angle Modulation is 2400 Channel FDM
 Interference is 3 DS-3 64 QAM

Noise (dBm0) - C/I (dB)

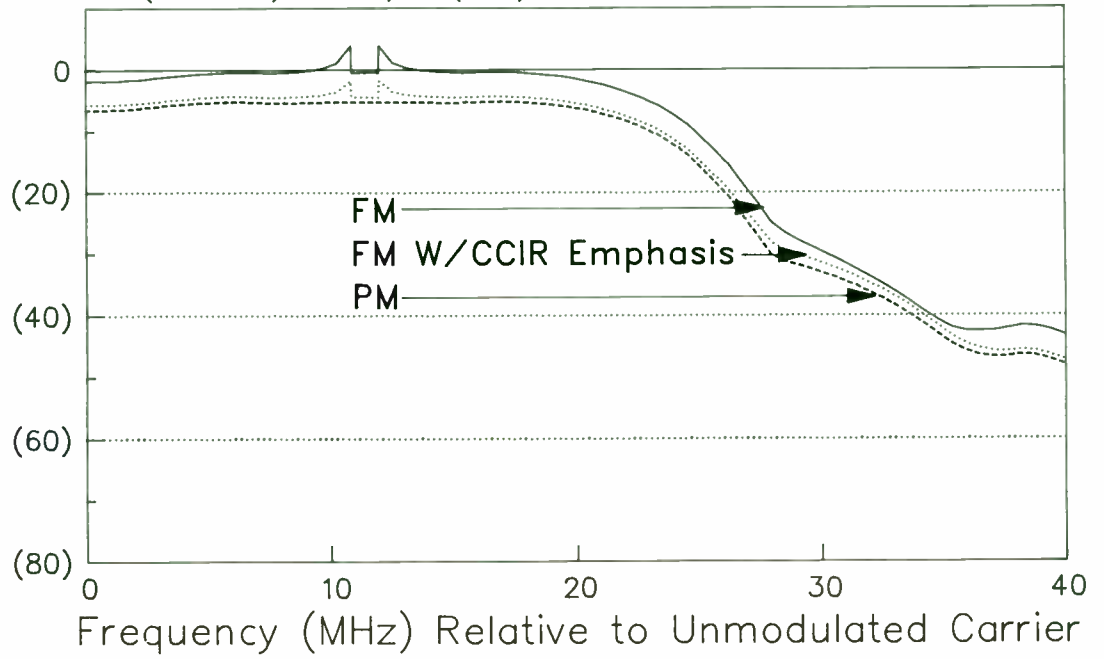
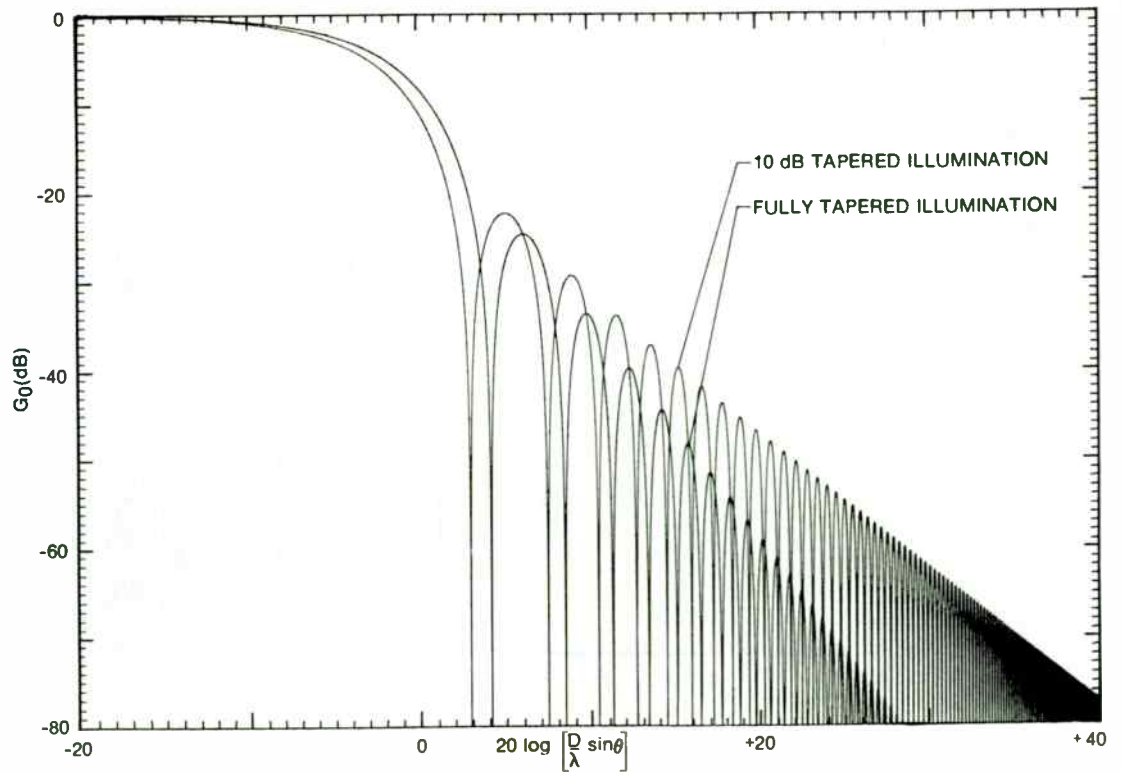


Figure 2 Digital into Analog Interference

Figure 3 Circular Aperture Far Field Radiation Patterns



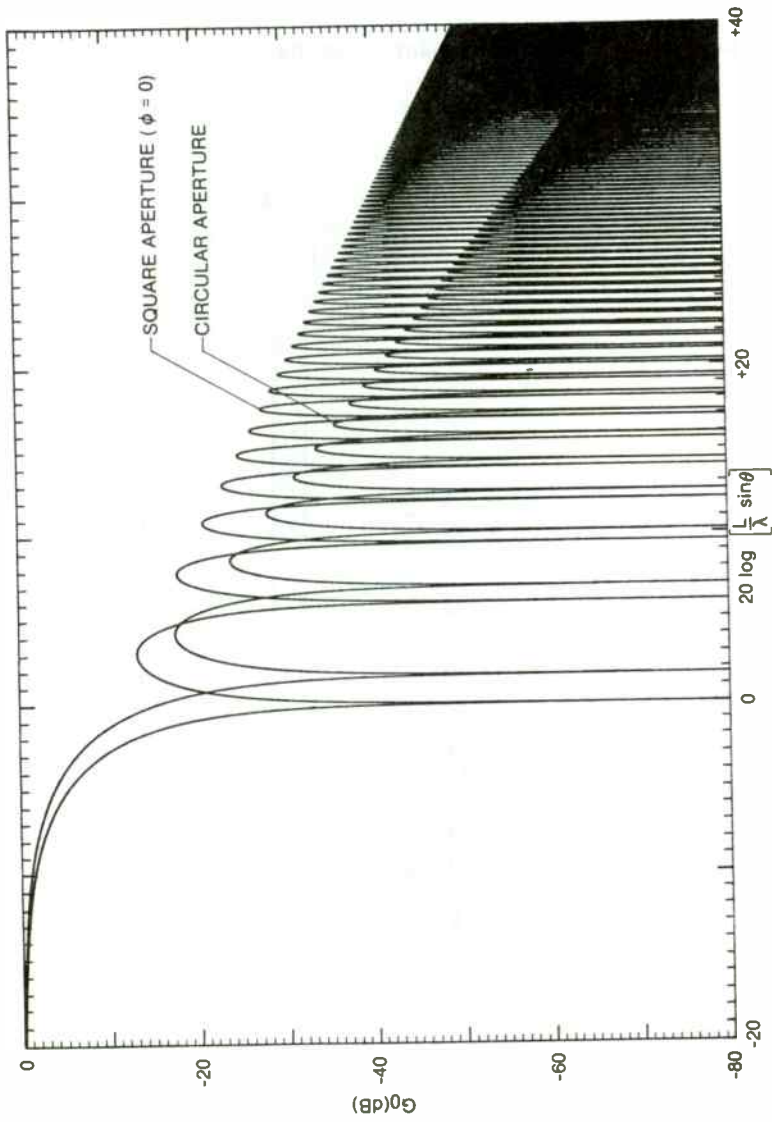


Figure 4 Uniformly Illuminated Apertures Far Field Radiation Patterns

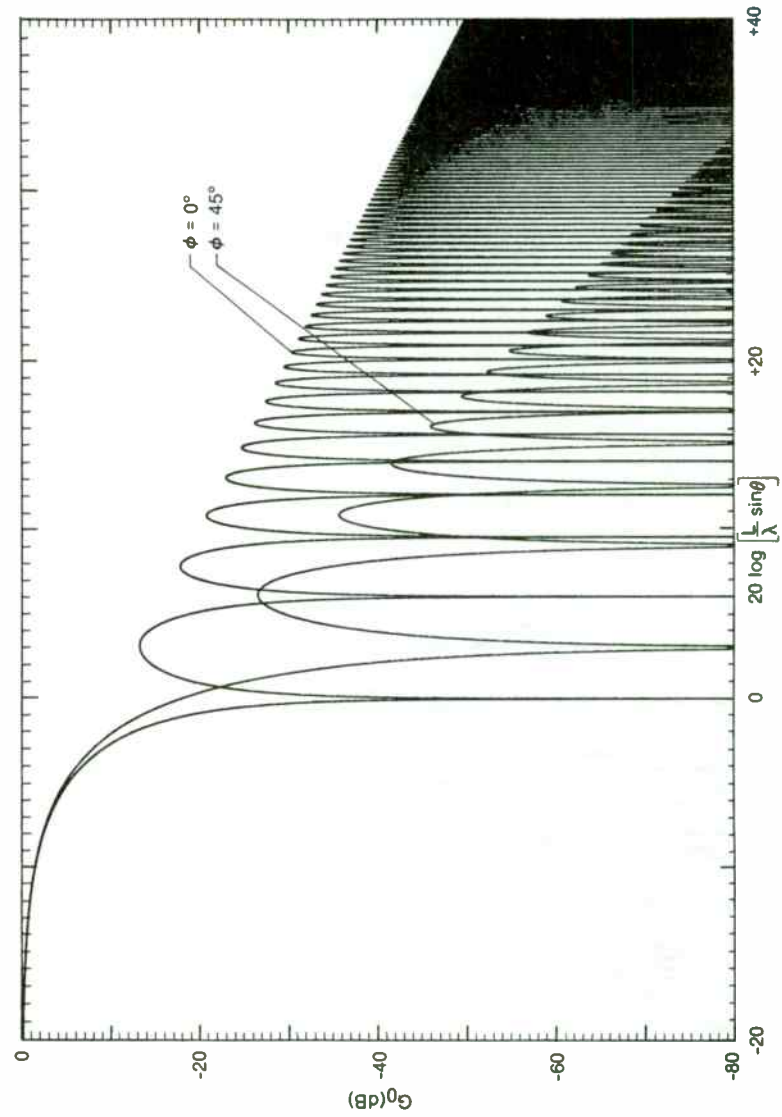


Figure 5 Uniformly Illuminated Square Aperture Far Field Radiation Patterns

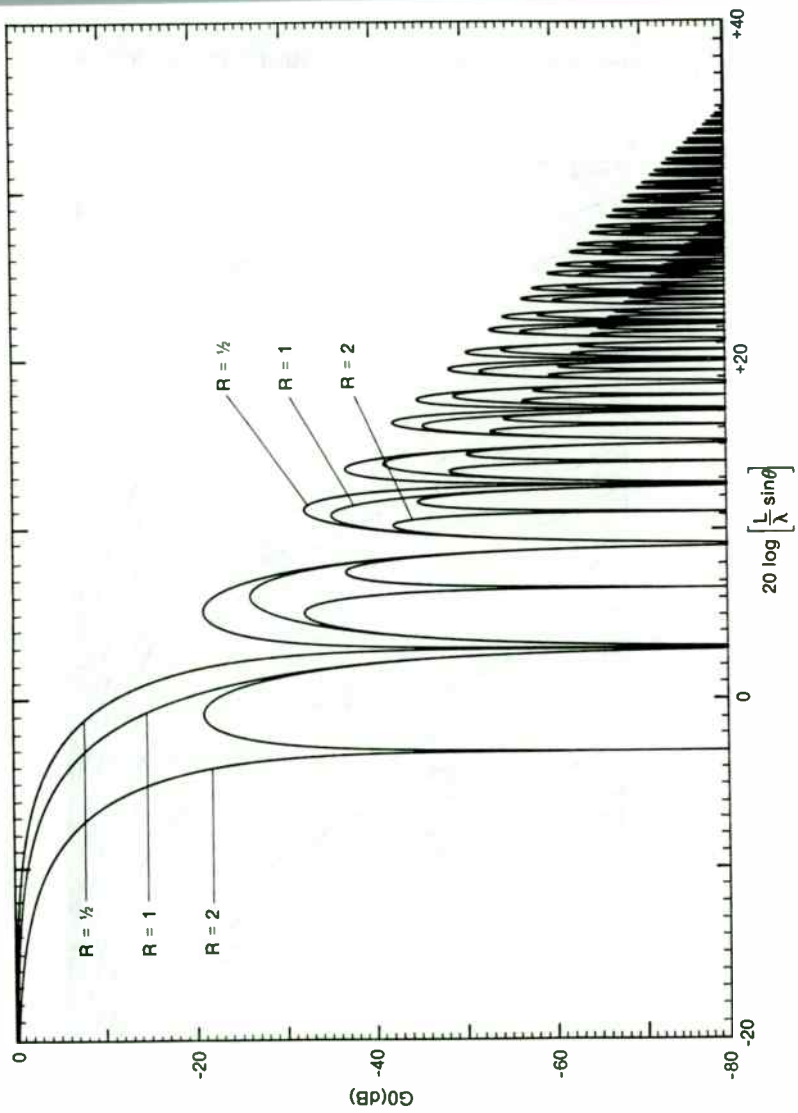


Figure 6 Uniformly Illuminated Rectangular Aperture Far Field Radiation Patterns

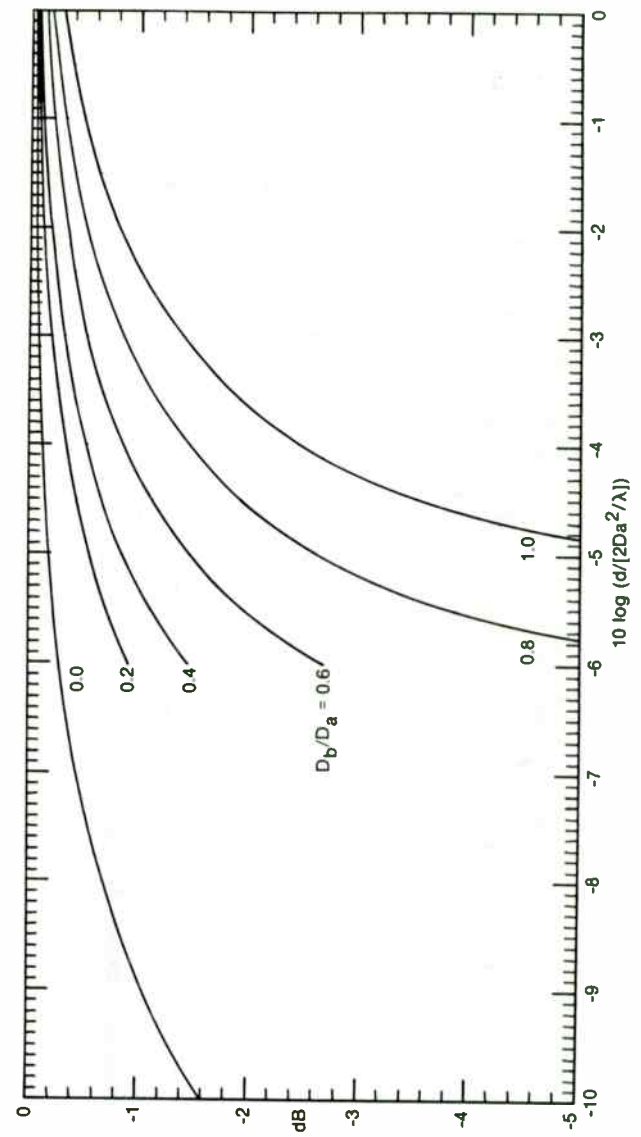


Figure 7 Dual Parabolic Antennas Near Field Correction Term

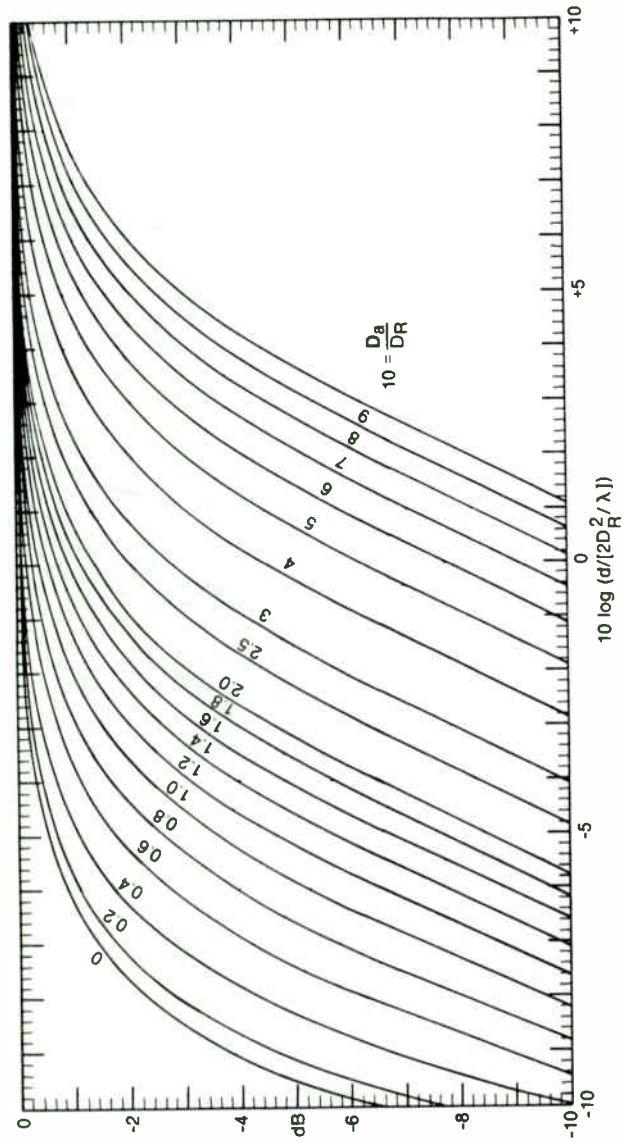


Figure 8 Circular Reflector Near Field Correction Term

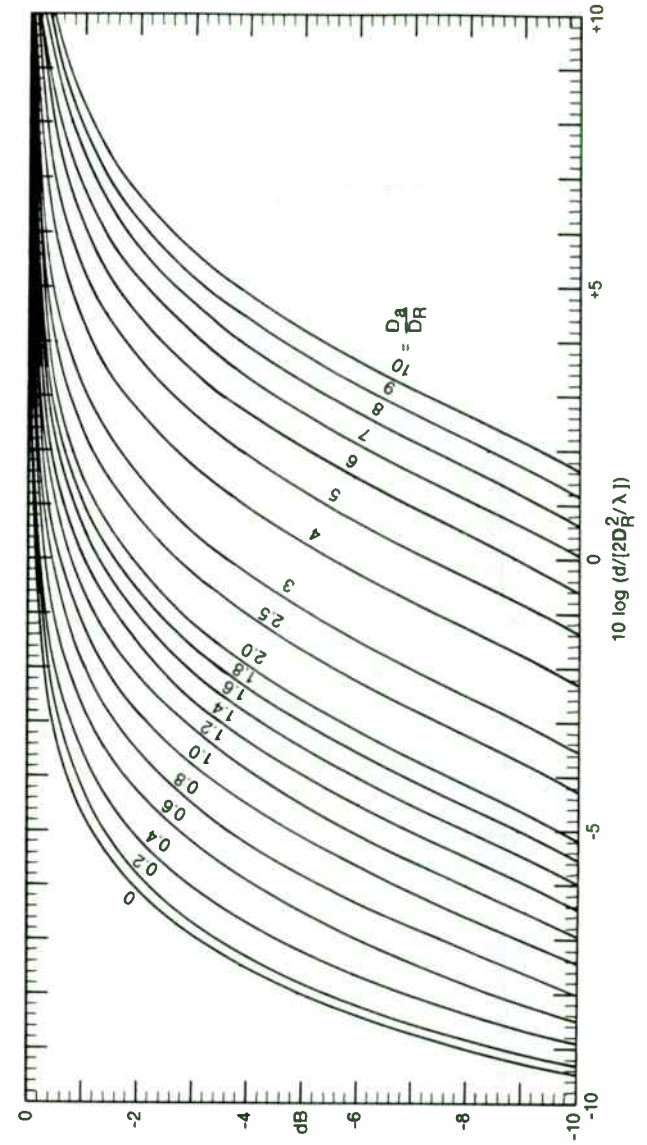


Figure 9 Square Reflector Near Field Correction Term

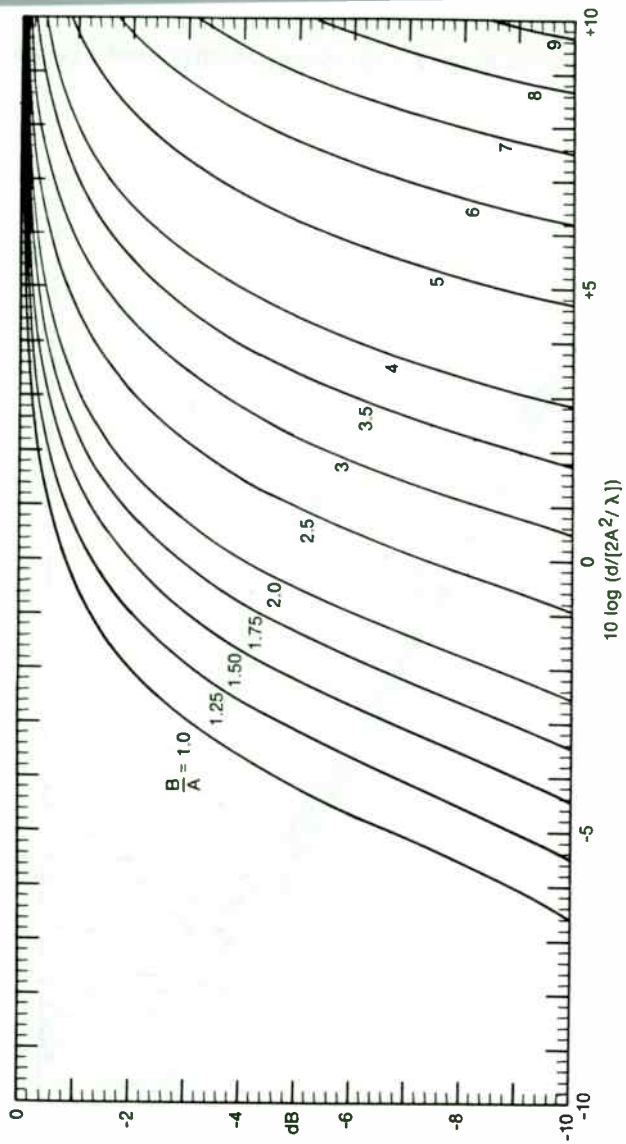


Figure 10 Dual Square Reflectors Near Field Correction Term

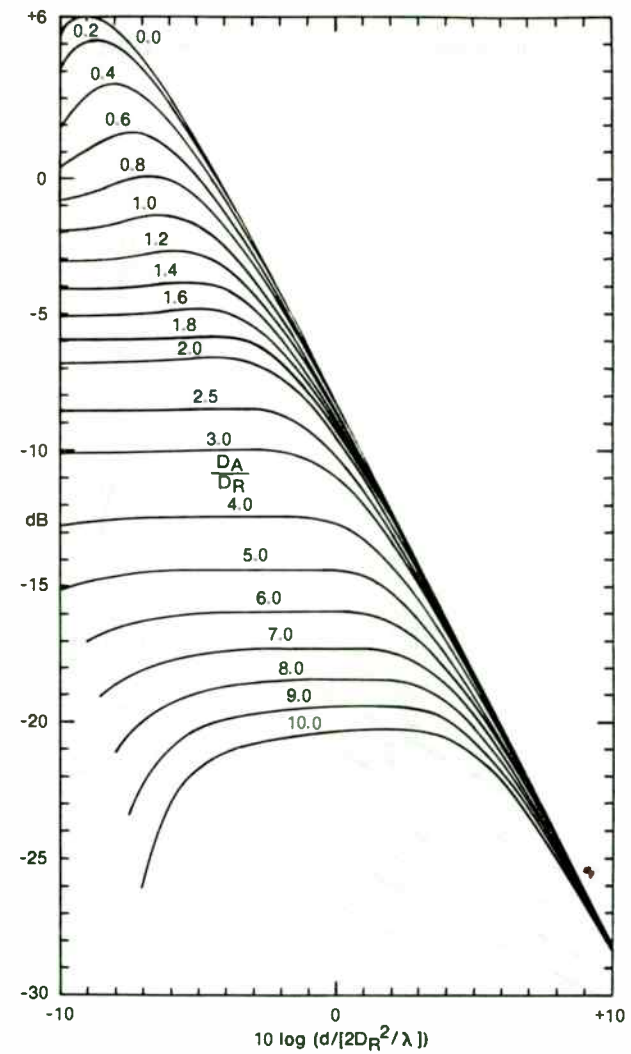


Figure 11 Circular Reflector and Parabolic Antenna Combined Gain

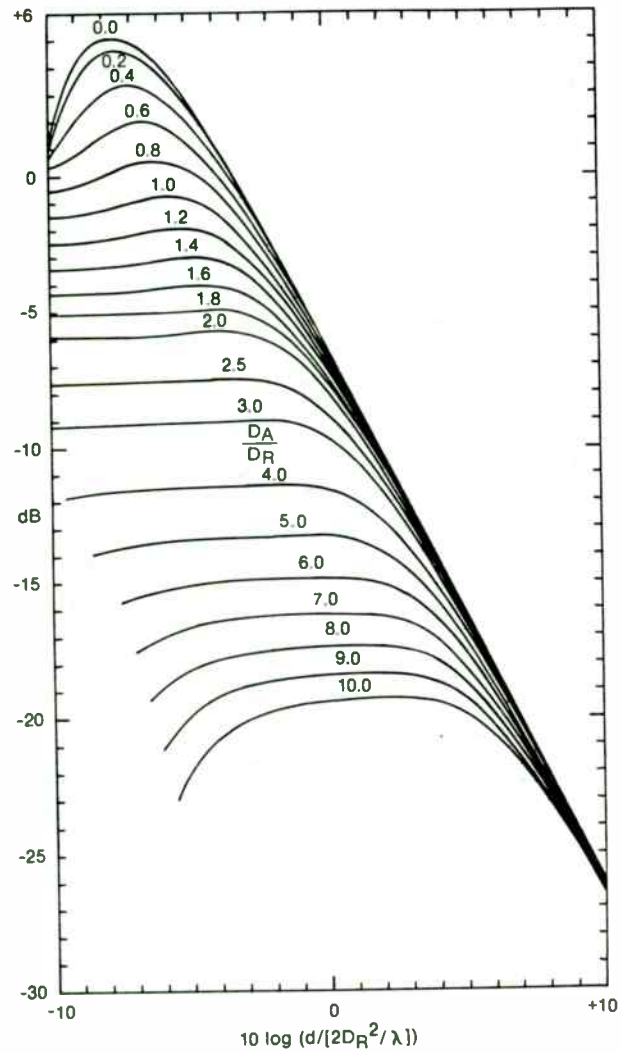


Figure 12 Square Reflector and Parabolic Antenna Combined Gain

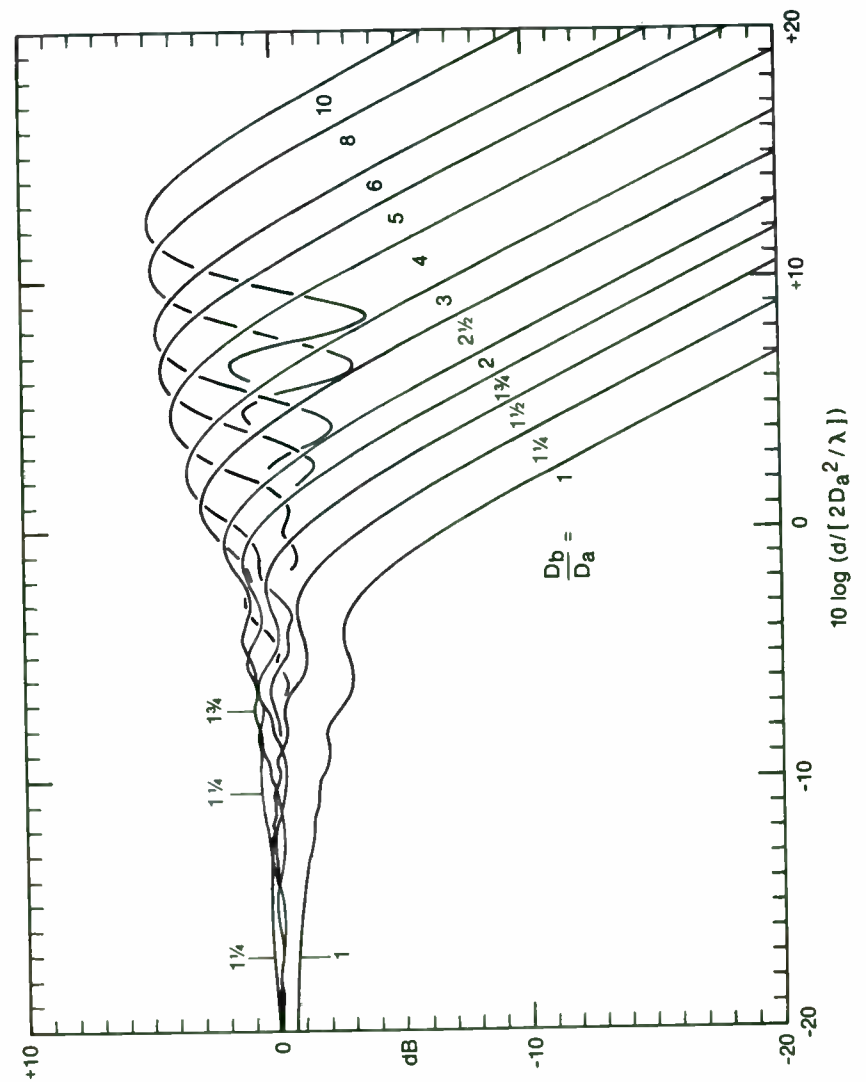


Figure 13 Dual Square Reflectors Combined Gain

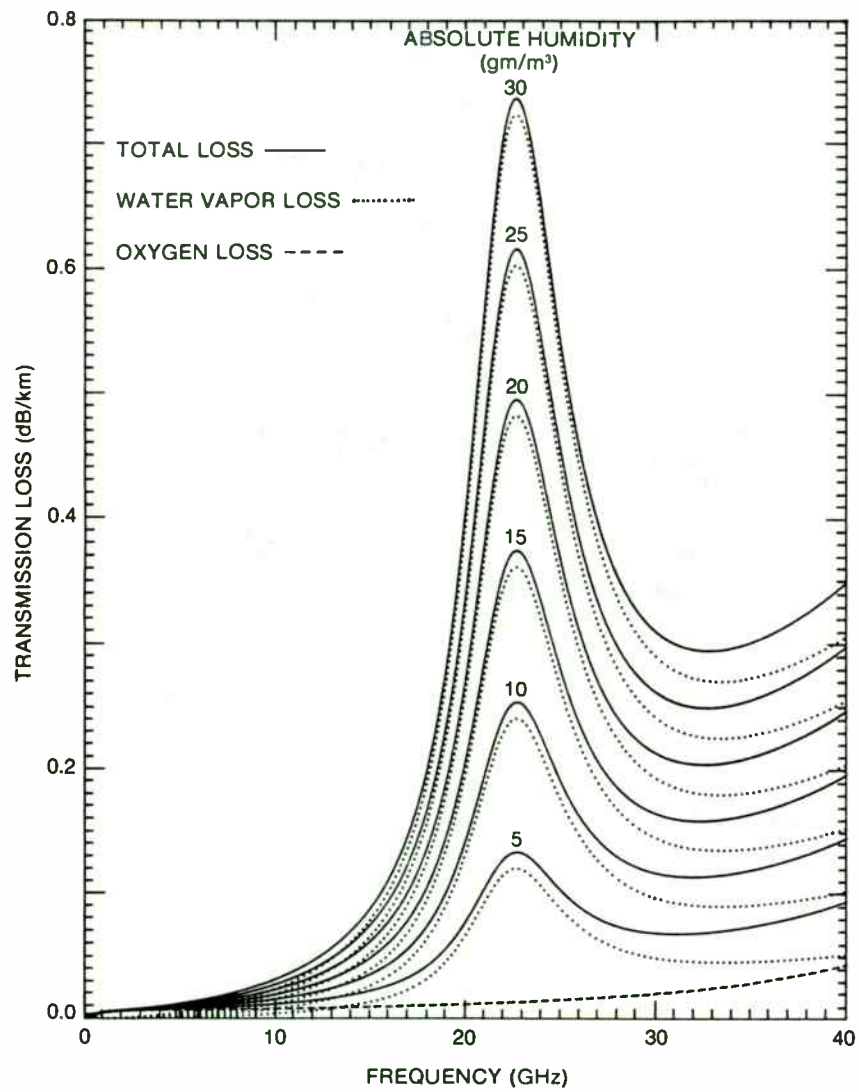


Figure 15 Nonrain Atmospheric Transmission Loss

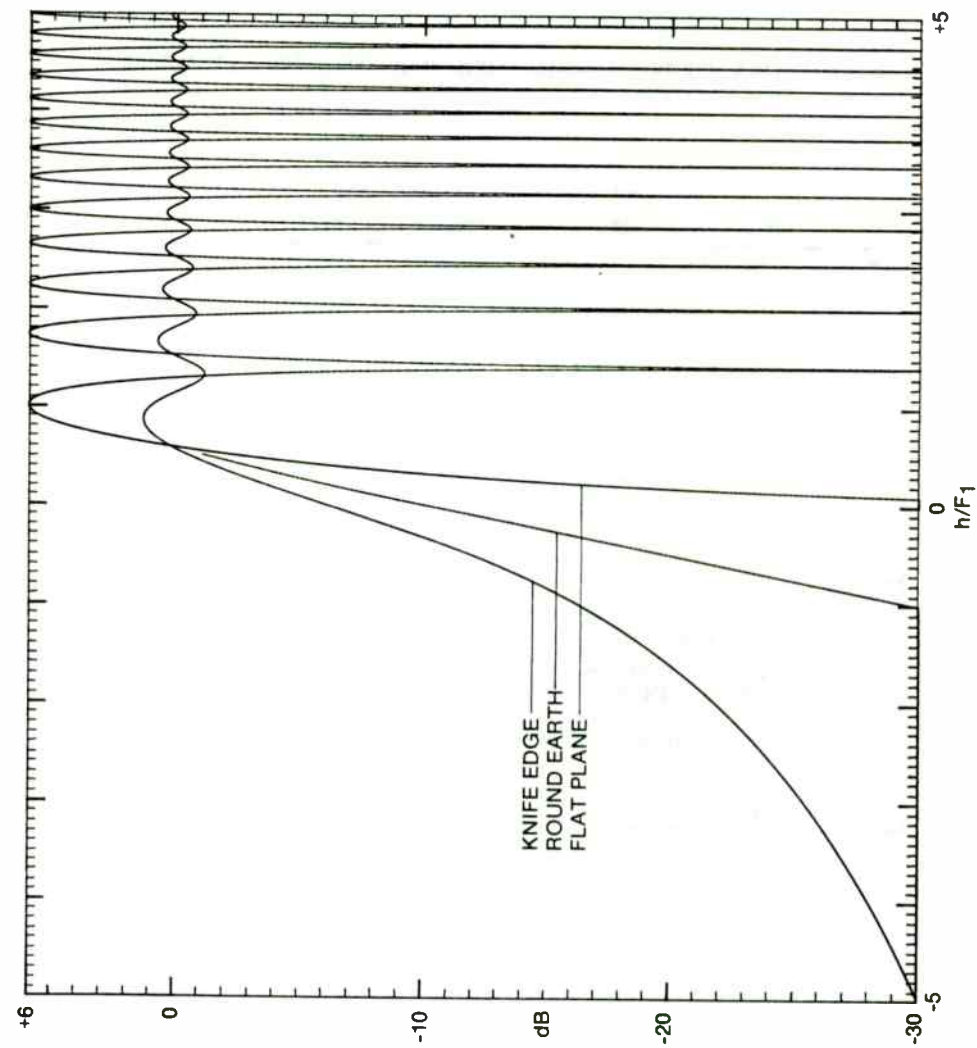


Figure 14 Obstruction Gain

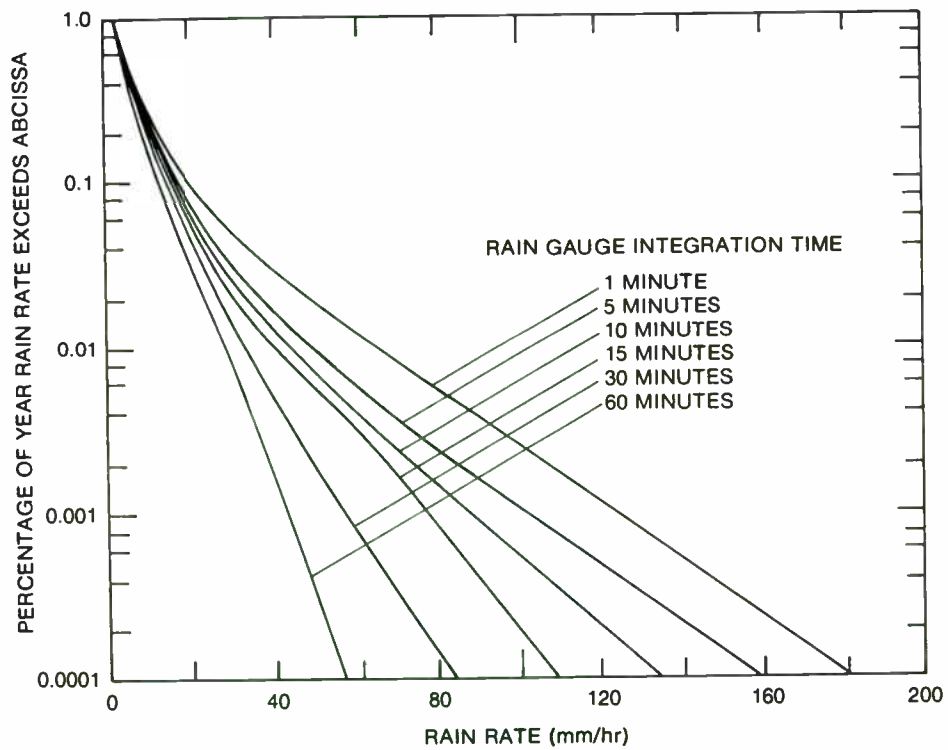


Figure 16 Averaged Rain Rates for the New York Area

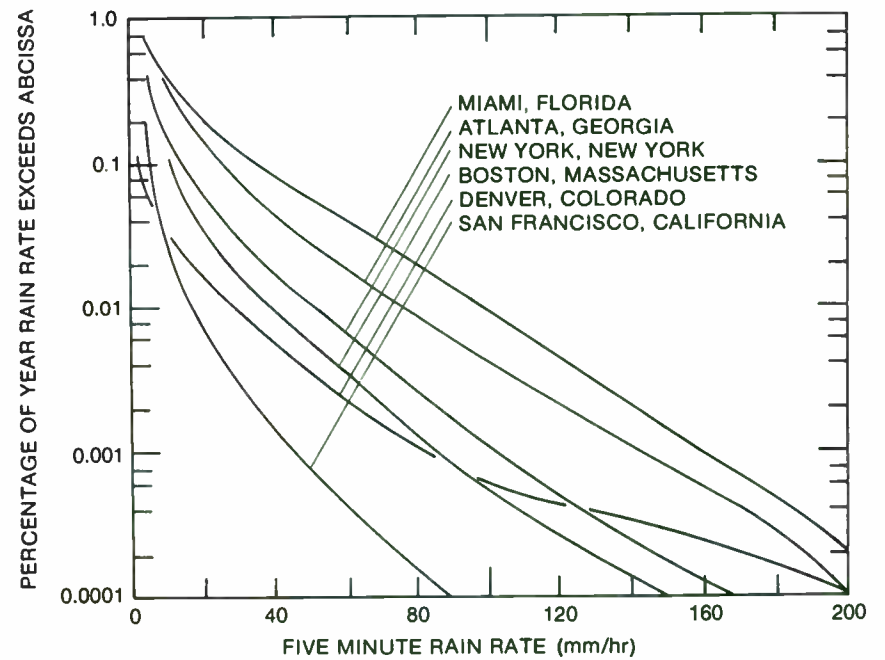


Figure 17 Long Term Rain Rates Distributions for Various Cities

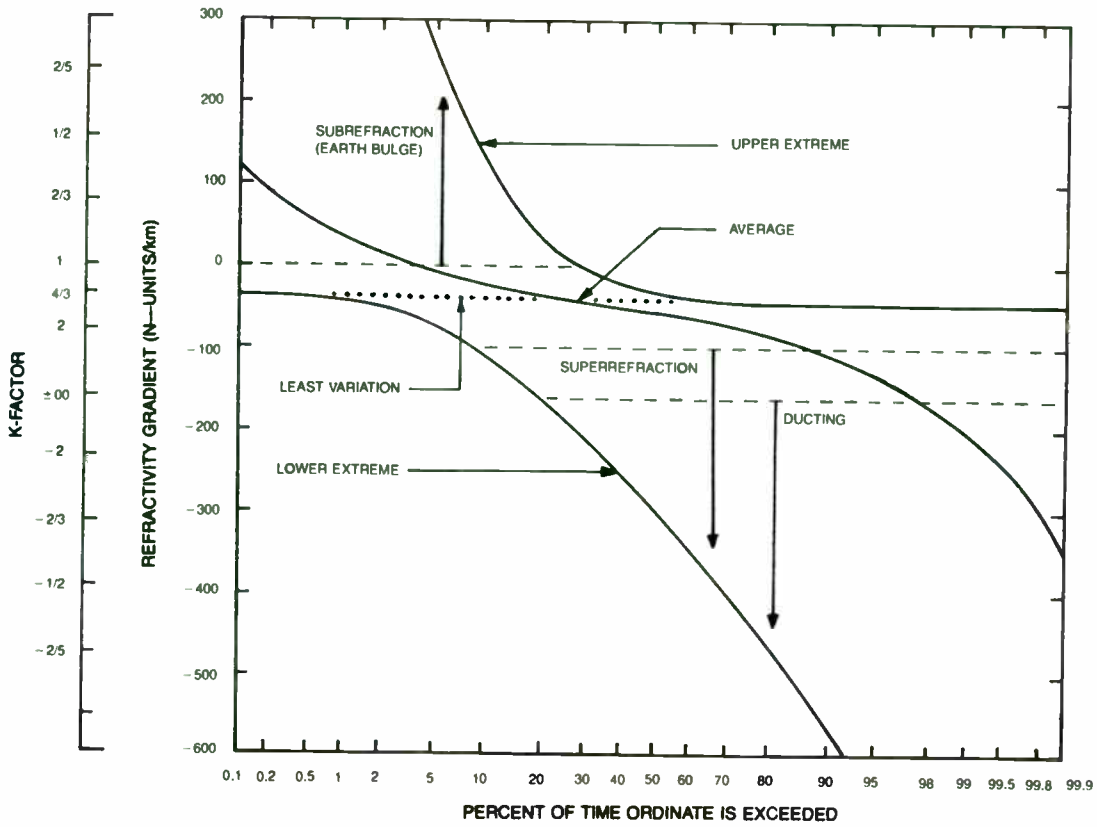


Figure 18 World Wide Refractivity Gradient (K Factor) Variation

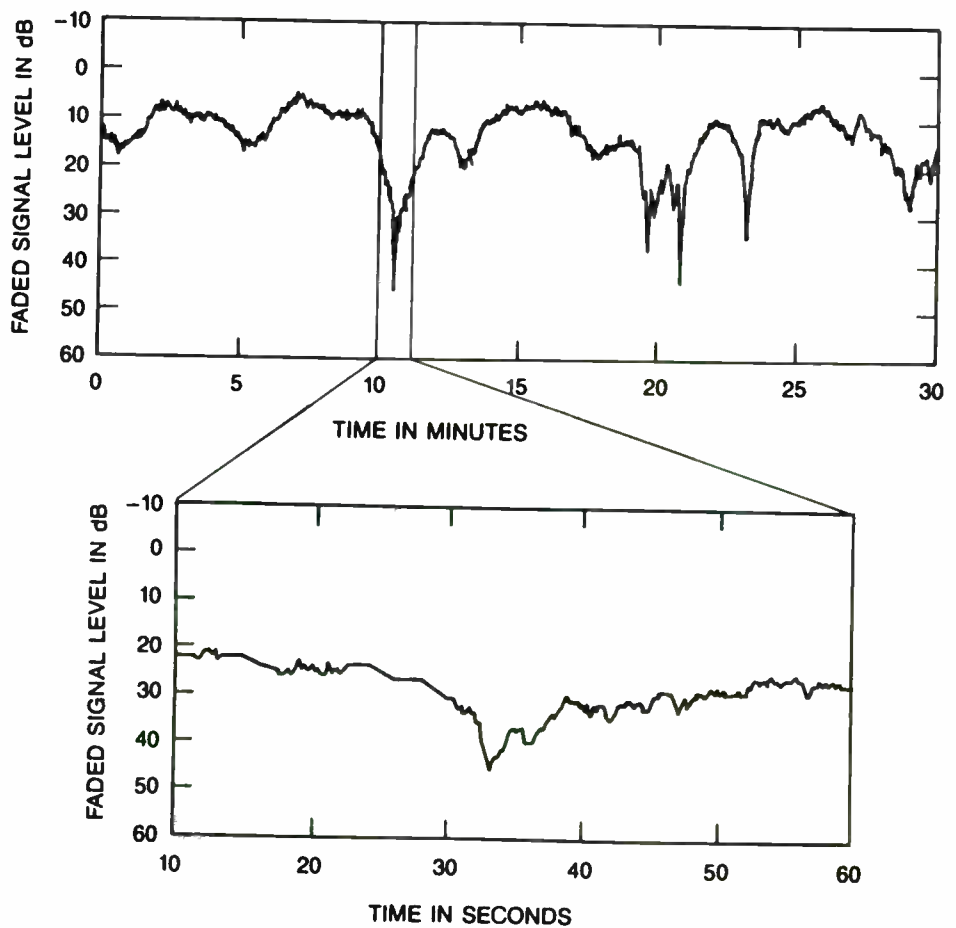


Figure 19 Typical Received Signal Variation during Fading

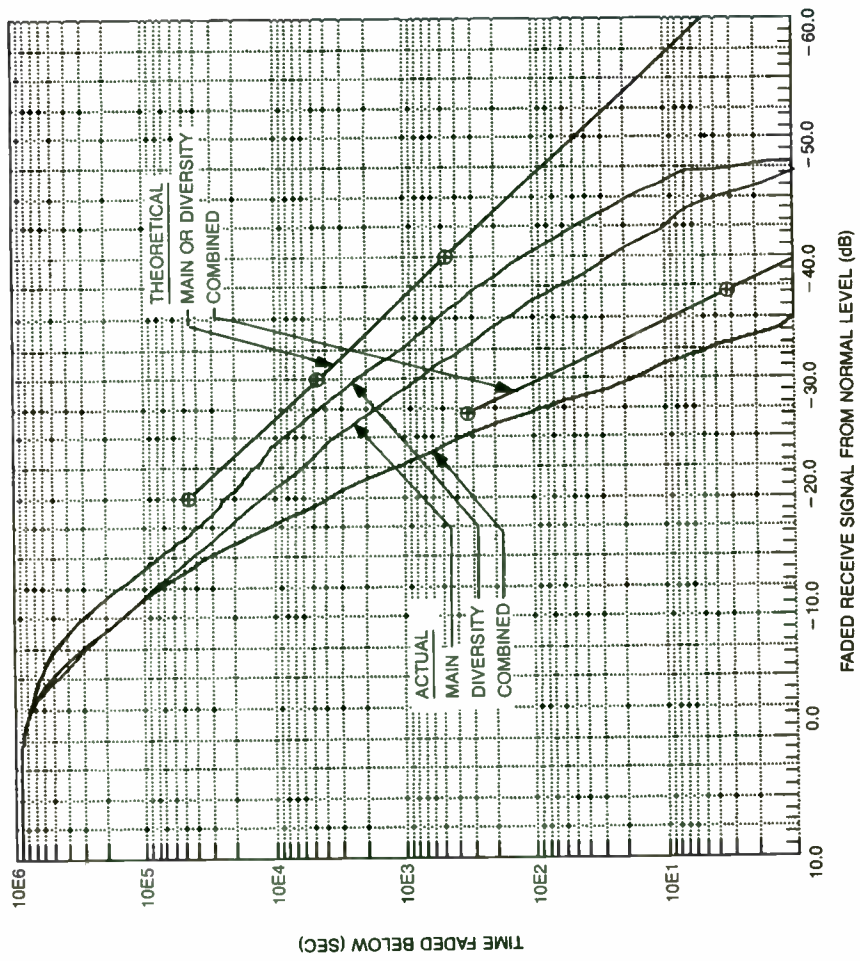


Figure 20 Year Long Received Signal Fading Statistics on Texas Path

PHASE SHIFTER BASED UPON
REFLECTIVELY TERMINATED MULTI-PORT COUPLER

M.H.KORI
CENTRE FOR DEVELOPMENT OF TELEMATICS
MILLER ROAD, BANGALORE 560052, INDIA

ABSTRACT

Reflection phase shifter, which comprises the reflection circuit and the coupler, is conventionally designed by designing the two parts separately. But a comprehensive analysis which takes both the units together reveals that the coupler also introduces phase error which is a function of the argument of the reflection coefficient (Γ) of the reflection circuit. The overall input VSWR is also a function of Γ . The reflection circuit also contributes to the phase error at frequencies other than centre frequency. Hence the design of a reflection phase shifter for a given bandwidth is a delicate task of balancing the various parameters to obtain optimal performance. The guidelines needed for obtaining this is described in this paper. Also a novel technique is developed for analysis of reflectively terminated multiport couplers, which is used in the analysis of reflection phase shifter.

INTRODUCTION

Phase shifter finds extensive applications in phased arrays and communication systems. Semiconductor phase shifter, which uses PIN diode or GaAs FET as the switching device, can be realised either in transmission configuration or reflection configuration. Branch line hybrid coupled phase shifter is the commonly used reflection version.

The theory and design aspects of hybrid coupled phase shifter have been dealt in detail in literature [1,2,3]. But the analysis and design is on the basis of separating the reflection circuit from the hybrid branch line coupler. This has an implicit assumption that coupler is ideal and does not affect the reflection circuit performance, and only route the input signal to the reflection circuit and reroute the reflected signal to the output. This is true, even in an ideal coupler, only at the centre frequency. As certain bandwidth requirement is always present, designer has to take into consideration the effect of coupler also.

A comprehensive analysis which takes both coupler and reflection circuit was first reported in [4], where using a novel technique closed form expressions for the total reflected signal and transmitted signal were derived. Using these relations the complete reflection circuit was

analysed. In this paper the analysis has been further extended to analysis of reflective terminated multi-port coupler in terms of generalized S-parameters. These relations are used for the specific case of 4-port hybrid coupler whose two ports are terminated by reflection circuits, to identify the crucial aspects affecting the performance of reflection phase shifter. It is clearly shown that the argument of the reflection coefficient of the reflection circuit plays a significant & conflicting role in the overall phase error & the input VSWR. On this basis the guidelines for an optimal synthesis has been evolved. The optimal design methodology is presented.

REFLECTIVELY TERMINATED MULTI-PORT COUPLER ANALYSIS

This approach is based on finding the total transmitted and reflected signals at the matched external ports in terms of the S-matrix of the coupler and the reflection coefficients Γ of the terminating circuits at other ports. Expressions developed for a 4-port case [4] is generalised to an m-port case.

Consider a 4-port coupler. If ports 1 & 2 are external matched ports & ports 3 & 4 are terminated with circuits of reflection coefficients Γ_3 & Γ_4 . $[S]$ is the 4 x 4 S-matrix of the coupler & $[S']$ is the 2 x 2 S-matrix of the overall

circuit. Considering a unit input at port 1 and accounting for all the multiple reflections one can obtain the expression as [4]

$$S'_{11} = S_{11} + [\Gamma_3 S_{13} \quad \Gamma_4 S_{14}] \left[\begin{array}{cc} 1 & 0 \\ 0 & 1 \end{array} \right] - \left[\begin{array}{cc} \Gamma_3 S_{33} & \Gamma_4 S_{34} \\ \Gamma_3 S_{43} & \Gamma_4 S_{44} \end{array} \right]^{-1} \begin{bmatrix} S_{31} \\ S_{41} \end{bmatrix}$$

Similarly expressions for S'_{21}, S'_{12} & S'_{22} can be obtained. Extending it to an m-port coupler whose 1 to n ports are matched external ports and (n+1) to m-ports are terminated with loads whose reflection coefficients are $\Gamma_{n+1}, \Gamma_{n+2}, \dots, \Gamma_m$, respectively, the modified matrix is given by

$$[S'_1] = [S_1] + [S_2] [\Gamma] [[I] - [S_4] [\Gamma]]^{-1} [S_3]$$

where $[S_1]$ to $[S_4]$ are submatrices & $[\Gamma]$ is the diagonal reflection coefficient matrix.

COMPREHENSIVE ANALYSIS OF REFLECTION PHASE SHIFTER

Fig 1. shows an example of a 2-branch line hybrid coupled reflection phase shifter. Most of the analysis, design & optimisation information reported in the literature pertains only to the reflection circuit. But to get the overall performance analysis, the complete circuit, which includes the coupler and the transmission line connecting

the coupler to the reflection circuit, has to be considered. The details of the technique adopted for analysis is available elsewhere [4]. Only the inferences drawn on the basis of the study are given below.

1. The phase shifter performance over a bandwidth is dependent on the performance the phase shifting reflection circuit as well as on the performance of the coupler.

2. The two important performance parameters, input VSWR and phase shift error are dependent on the coupler directivity and the argument of the reflection coefficient (Γ) of the reflection circuit. For a given configuration of the coupler, the directivity is a fixed quantity at any given frequency. Hence the only other variable available for designer is Γ .

3. Coupler induced phase error study indicates that the variation of phase error with frequency is different for different values of ϕ_0 .

(If Γ is changed from $\phi_1 = \phi_0 - \Delta\phi/2$ to $\phi_2 = \phi_0 + \Delta\phi/2$, then the phase shift obtained at the reflection circuit is $\Delta\phi$. If the phase shift obtained at the output of the coupler is $\Delta\phi_1$ then the error is $\Delta\phi_1 \sim \Delta\phi$. This error is also dependent on the value of ϕ_0 . A plot of error vs

frequency for various values of ϕ_0 is given in Fig 2.)

4. Input VSWR is also a function of Γ (Fig 3.)

5. Reflection circuit also has a phase frequency characteristics and this too has to be considered while designing.

DESIGN METHODOLOGY

The design of a phase shifter involves a careful study of various factors. If the phase accuracy over the bandwidth is the primary concern, then only the phase error introduced by the coupler and the phase shift produced by the reflection circuit, over the bandwidth, are to be considered. Even if the reflection circuit has a large variation of phase shift with frequency, by properly choosing the value of ϕ_0 , the overall phase shift error can be reduced by compensating one error with the other. Significant reduction in error is possible by this technique.

If input VSWR is also an important factor, then choice of ϕ_0 becomes more critical. Hypothetically it is possible to reduce the overall phase error for extreme bandwidths by synthesising a reflection circuit whose phase frequency curve can be designed to nullify the coupler induced phase

error, over this bandwidth. But it is not so in case of input VSWR. No matter what exotic reflection circuit is designed, VSWR has absolute limits. This is apparent from Fig 3. For a 180° phase shifter bit, for example, ϕ_1 & ϕ_2 have to be 180° apart. Over the 20% bandwidth shown in the plot, only $\phi = 180^\circ$ has least VSWR. If this is chosen as ϕ_1 , then ϕ_2 is automatically fixed to 0° . It has a VSWR of 1.8 at band edges. If one chooses any other ϕ_1 or ϕ_2 values, they have higher VSWR at one band edge or other. Thus VSWR limits are fixed. Hence after fixing the VSWR limits the phase error compensation techniques have to be implemented to obtain an optimal solution.

EXAMPLES

Using the guidelines developed, circuits have been designed, analysed and experimentally fabricated. Experimental results are shown in Fig 4.

CONCLUSION

A comprehensive analysis of the complete circuit of reflection circuit has indicated that input VSWR & phase error are primarily dependent on the argument of the reflection coefficient of the reflection circuit. With a right choice of ϕ_0 , the phase error induced by the coupler

can be made to compensate the phase frequency response of the reflection circuit to obtain large bandwidths. But limiting factor is imposed by the input VSWR.

REFERENCES

1. White J.F 'Semiconductor Control' (Artech 1977)
2. Garver R.V 'Microwave Diode Control Devices' (Artech 1976)
3. Starski P.J 'Optimization of matching network for a hybrid coupled phase shifter' IEEE Trans. MTT, 25, PP 662-666 (1977)
4. Kori & Mahapatra 'An integral analysis of hybrid coupled semiconductor phase shifter' IEE Proc. - H (1986)

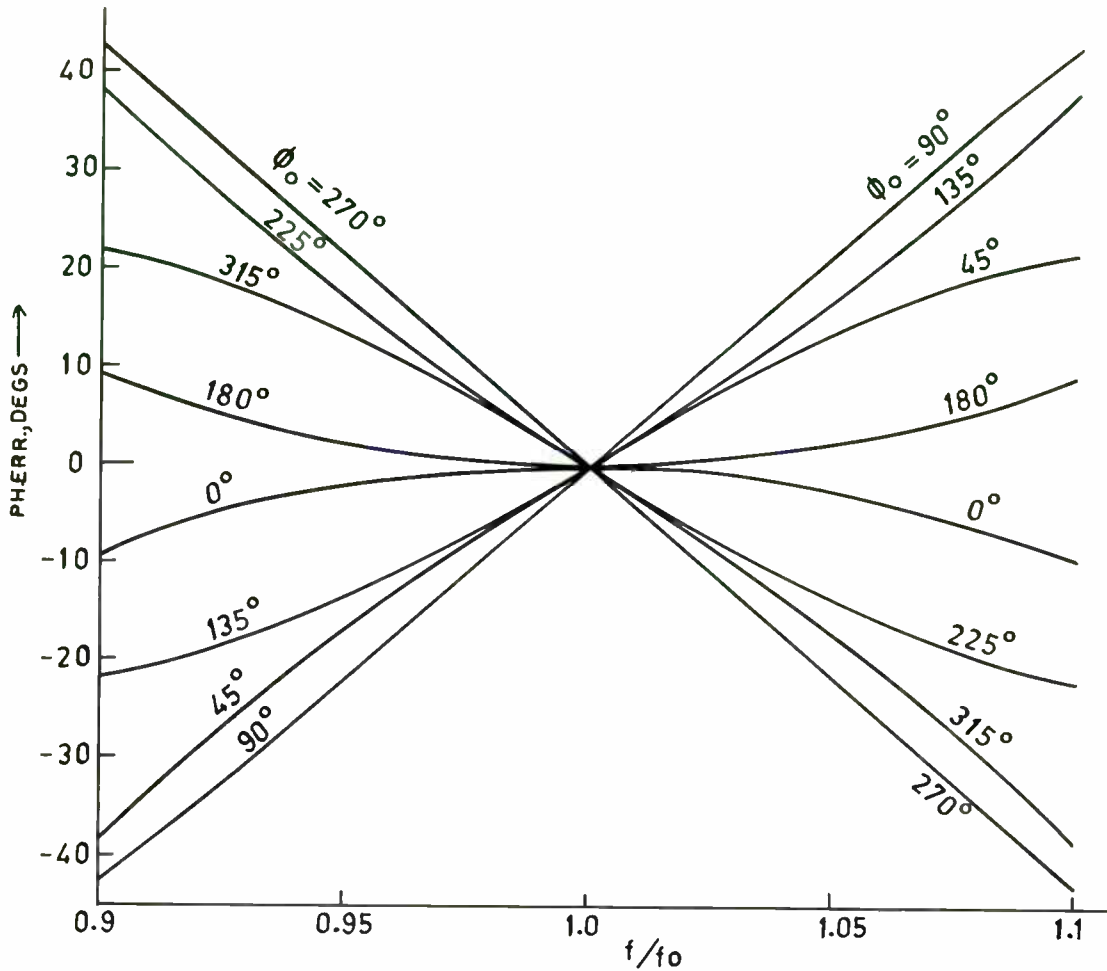


FIG. 2 - COUPLER INDUCED PHASE ERROR VS FREQUENCY FOR VARIOUS ϕ_o . $\Delta\phi = 180^\circ$, 2 BRANCH COUPLER

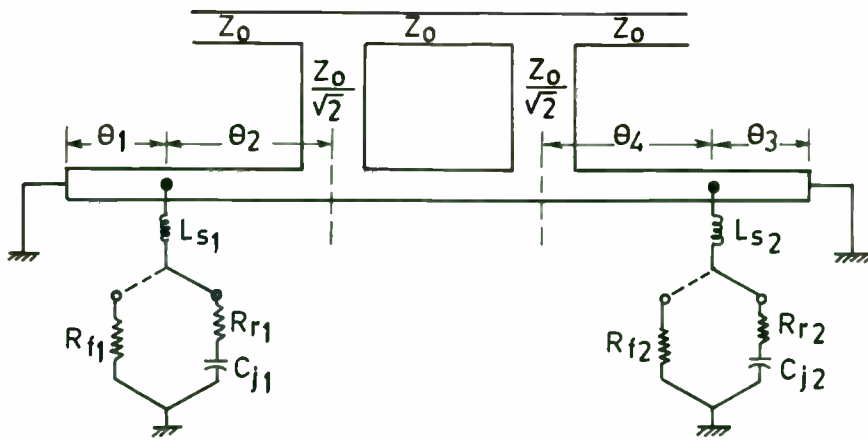


FIG. 1 - SHUNT MOUNTED SHORT CIRCUIT TERMINATED HYBRID COUPLED PIN DIODE REFLECTION PHASE SHIFTER

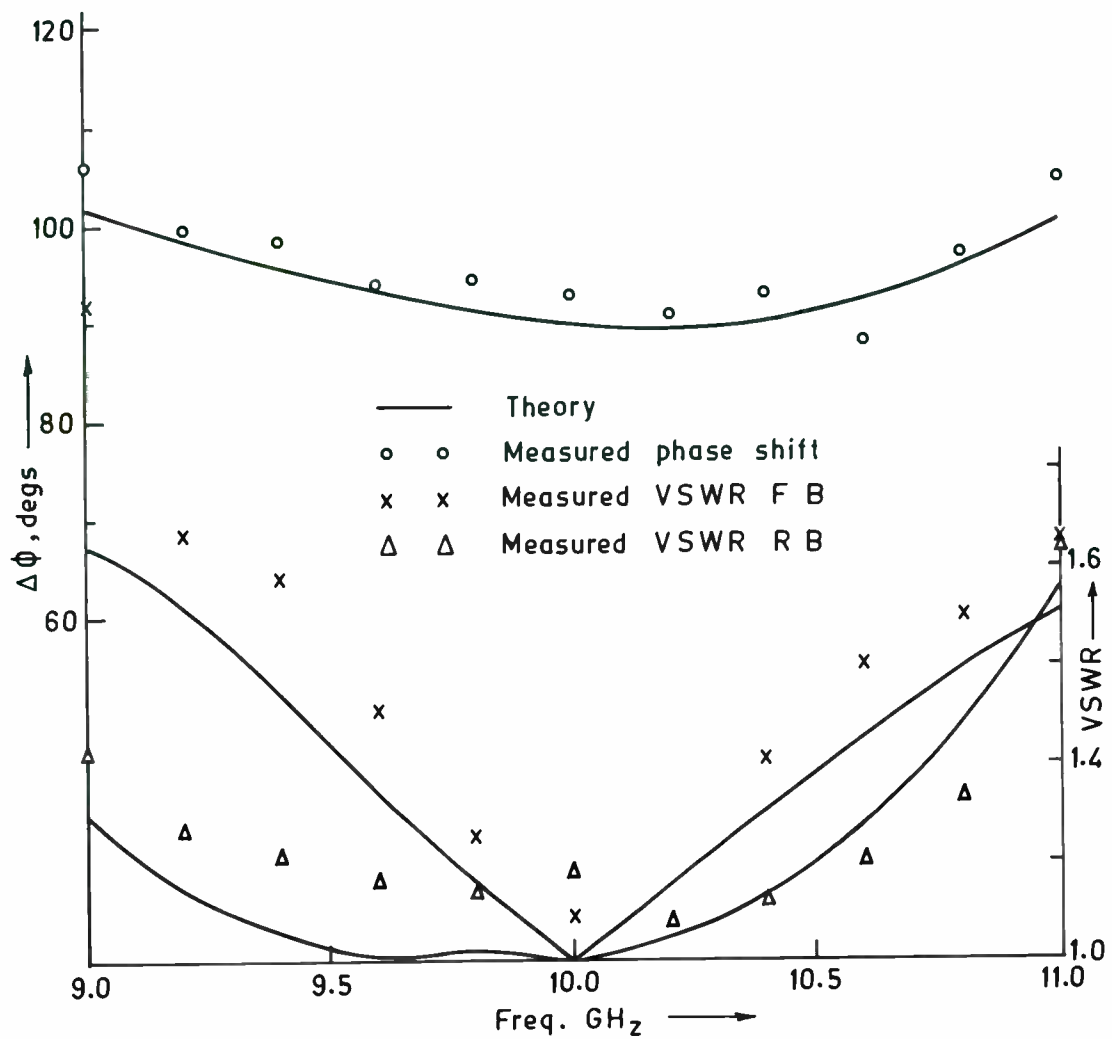


FIG. 4 -HYBRID COUPLED PHASE SHIFTER PERFORMANCE, EXPERIMENTAL RESULTS, 2 BRANCH COUPLER, $\Delta\Phi = 90^\circ$

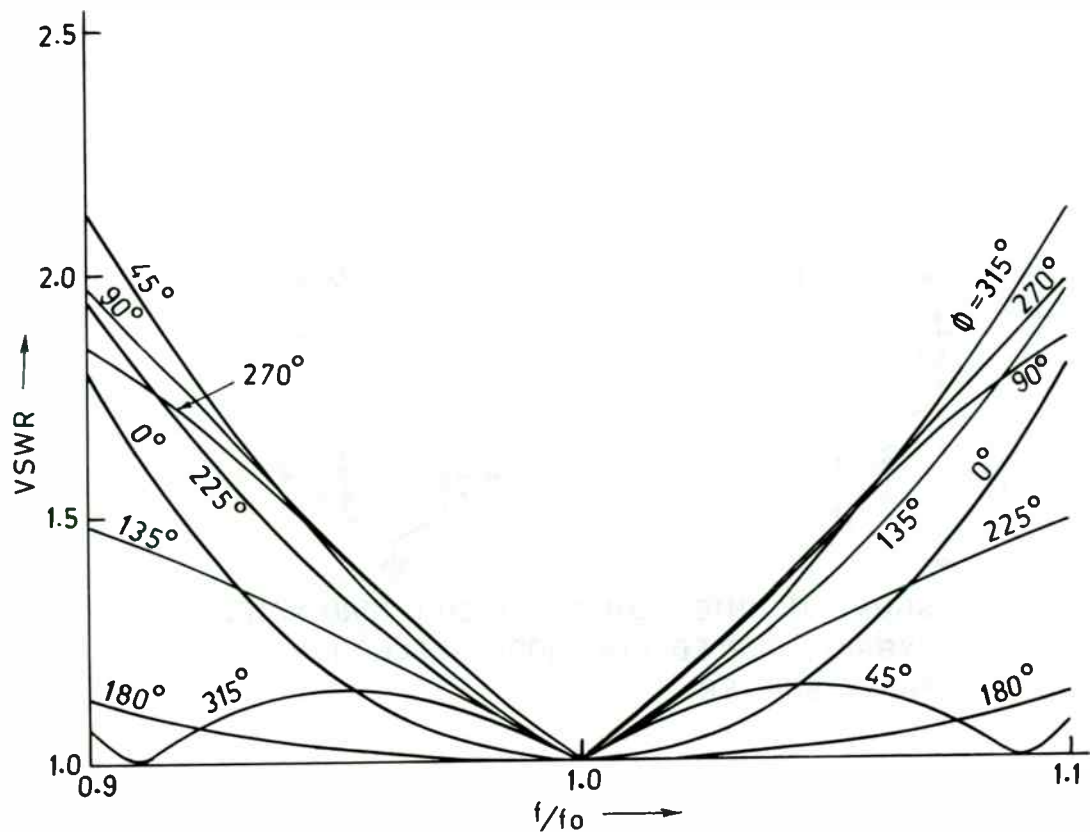


FIG.3 -VSWR Vs FREQUENCY FOR DIFFERENT Φ , 2 BRANCH COUPLER

INSTRUMENTATION FOR RADAR REFLECTIVITY MEASUREMENT

D.J. Kozakoff, C.W. Sirls, R.S. Banks and D.A. Thompson
Millimeter Wave Technology, Inc.
1395 S. Marietta Parkway, Building 700
Marietta, Georgia 30067

INTRODUCTION

This article describes RF reflectometer instrumentation useful for performance evaluation of sheet microwave absorber, absorptive coatings and RCS reduction structures. Two approaches are investigated: 1) a quasi-far-field method using separate transmit and receive antennas, and 2) a near-field approach using a single axially scanned sensor antenna. For both approaches we considered measurement errors and data validation.

QUASI FAR-FIELD INSTRUMENTATION

Bistatic surface reflectivity is generally measured with the so-called NRL Arch [1] shown in Figure 1. In our portable unit, termed the PR-11, we miniaturize the antenna spacing and distance to the sample in accordance with the following design approach:

- o Broadband performance achieved with custom designed ridge horn antennas;
- o Antenna design to satisfy $r = D^2/\lambda$ criterion at highest frequency;
- o Antenna-to-antenna isolation (crosstalk) below -35 dB;
- o Data normalization to reference measurements to metal plate reflection.

With this approach, the differences between NRL Arch and PR-11 measurements appear in Table 1.

System Description

The system design shown in Figure 2 consists of a hand held gun with LCD readout connected via a cable to a base unit, which contains a microcomputer, control electronics and thermal printer. The gun assembly contains the microwave electronics and both transmit and receive dual ridged horn antennas set at a fixed ± 15 degree bistatic angle. A plastic rod standoff assembly establishes the

measurement distance. The specifications for the base unit and gun assembly are shown in Tables 2 and 3.

Under microprocessor control, frequency can be set to any desired CW value from 8 to 18 GHz. Alternatively, the unit can staircase any segment of the 8 to 18 GHz range in increments as small as 100 MHz. Various other microwave/mmw band guns are available as options. A remote power unit option is available for portable operation where AC power is not available. The batteries will provide for up to three (3) hours of operation of the instrument before recharging. The average time for recharging is 8 hours. Table 4 lists Battery Pack Specifications.

The device is packaged in a militarized aluminum carrying case and is useful for absorber material development, laboratory tests, production line tests, field tests, and quality assurance (QA) tests to determine the effectiveness of composite absorber materials. The reflectometer can also be used for evaluating absorber degradation due to weather, cracking or abrasion.

Operation of the reflectometer was designed to be simple and straightforward. When power is applied to the unit, the user is automatically prompted by the microprocessor to set all reflectometer parameters such as single frequency, staircase sweep, etc. Subsequently, the user is prompted for a calibration in air and of a metal plate to establish a reflective zero loss reference. Once a zero reference is taken, the operator can take reflectivity measurements by simply placing the guns standoff rods on the surface to be measured and pulling the trigger. The surface attenuation can be read (in dB) from an LCD display mounted on the front panel of the base unit. The user also has the option of recording measured data via the thermal printer or storing data on a 3.5 inch floppy disc. This is valuable for QA testing where hard copies of measured data must be provided. Output data is also available at an RS232 port for other computer peripheral devices.

After initialization, each time the trigger is pulled a three-digit running counter index is incremented. Thus, each data output is associated with a unique index number. This is convenient in applications where many measurement points must be examined over a surface. Time and date are also automatically recorded on all hard copy data outputs.

The user-interactive setup menu allows the operator to set a "fail test" value (in dB). Whenever a measurement is above the "fail test" level, a beeper is activated and the data is printed

[1] See Appendix to MIL-STD 17161D, 3 June 1985.

by the thermal printer. Measurement points which are acceptable are not printed out.

Measurement Errors

There are several sources of measurement error which must be considered in the design and operation of a free-space reflectometer. The most significant error sources result from finite antenna-to-antenna isolation and antenna mismatch.

Antenna isolation produces a constant level interference signal which adds randomly in phase with the desired signal reflected from the sample under test. This effect produces larger errors as the measured reflected signal becomes small (i.e., when the absorber sample is less reflective). Figure 3 shows the effect of antenna isolation on measurement accuracy for an antenna-to-antenna isolation of -45dB.

Unlike isolation, antenna mismatch affects reflection measurement accuracy more seriously when the reflected signal level is high. Small antenna-to-sample spacing produces multiple bounce energy between the two antennas, resulting in a periodicity in the measured absorber reflectivity as a function of frequency. Peaks and valleys occur as the multi-bounce energy adds in- and out-of-phase, respectively.

Isolation and mismatch errors can be essentially eliminated from the reflection measurement through the use of time gating. The time gate can be realized in hardware with a fast RF switch, or in software if a phase-amplitude receiving system is available. However, gating techniques are typically costly to implement, particularly when the electrical path length is small.

In order to minimize cost, an amplitude only receiver is employed in the PR-11. Further, the total measurement path length is less than two feet, rendering gating impractical for this instrument. As an effective alternative the system utilizes a smoothing algorithm based on techniques used in precision transmission line reflectometers to reduce mismatch errors. For higher levels of reflection, agreement of measured PR-11 data to NRL Arch data where software gating was employed has been within ± 1.0 dB. The effect of the smoothing algorithm is illustrated in Figure 4.

Two second order error sources exist in the PR-11 system implementation and should be

mentioned. First, the system utilizes a stabilized but non-coherent YIG oscillator as the signal source. The source is isolated from the transmit antenna to eliminate load-pull effects, and is characterized point-by-point over its frequency range to achieve tuning accuracy and repeatability of ± 5 MHz at 25°C. Frequency variation versus temperature is 40 MHz maximum from 0 to 65°C, 25 MHz typical. This drift can cause slight errors in the measured frequency of the reflectivity null of resonant absorbers and should be considered when the PR-11 is used in outdoor environments.

A final source of measurement error exists in the A/D processing of the reflected signal energy. Twelve bit A/D converters are employed to reduce this error source to less than 1.0 dB at a reflected signal level of -30 dB.

Maximum measurement error of the PR-11 system due to all sources cumulatively is ± 1 dB at 0 dB reflectivity and ± 2.5 dB at -25 dB reflectivity.

Data Validation

Primary measurement differences between the PR-11 and the NRL Arch result from the variation in measurement spot size on the sample-under-test. When the illumination encompasses the entire test sample, edge effects can produce significant differences from measurements over a small spot area. Also, the smaller measurement spot size of the PR-11 often reveals RAM inhomogeneities from spot to spot.

The basic electronics of the PR-11 System have been validated by connecting the transmit and receive antennas to a phase-amplitude receiving system (HP 8510) used with the NRL Arch. The reflectivity of test samples measured with the PR-11 and the 8510 using the same antenna assembly agree within ± 1 dB for reflectivity levels from 0 to -10 dB, and with ± 1.5 dB from -10 to -30 dB. Figure 5 shows measured data on a typical test sample using both measurement systems.

NEAR-FIELD INSTRUMENTATION

System Description

The near-field instrument illustrated in Figure 6, termed the BEKISCAN-CP[2], utilizes an

[2]BEKISCAN CP and BEKI-SHIELD are registered trademarks of N.V. Bekaert S.A., Zvevegem, Belgium.

internal microwave circulator to measure the power reflected from a surface. However, because the field intensity in the near-field varies (Figure 7), we use a spring loaded movable antenna assembly and a peak detector circuit to detect and measure the peak field intensity when a sample is moved through the rear field of the antenna assembly.

As with the case of the PR-11, this unit references the unknown reflection to that of a flat metal plate. The voltage reflection coefficient is displayed on a large 3 digit LCD on a separate remote display unit. The electrical specifications are shown in Table 5.

The BEKISCAN-CP is useful to characterize microwave absorption of RAM composites, paint and/or coatings on surfaces in laboratory research or quality assurance (QA) tests. But more interestingly, this instrument has been found to be a state-of-the-art method for quantifying the shielding effectiveness of conductive stainless steel fibre (BEKI-SHIELD[2]) loaded plastic parts, D-4935[3] and provides excellent measurement correlation with ASTM.

Measurement Errors

There exist two potential sources of error in the BEKISCAN-CP: The microwave near field reflectometer, and the analog processing and display unit. By scanning the reflectometer antenna to locate the peak reflection point, errors due to near field intensity variation, antenna match, and finite circulator isolation are effectively eliminated. The error of the LCD display is .1% of the reading and is negligible.

The major source of error remain in the BEKISCAN-CP is the Analog Devices AD538 Real-Time Analog Computational Unit. The AD538 is set up to perform the mathematical operation

$$V_o = \left(\frac{V_s}{V_x} \right)^{\frac{1}{2}} \tag{1}$$

where

- V_s = Transmitted signal level (Reference)
- V_x = Reflected signal level
- V_o = Output Voltage (Voltage Reflection Coefficient)

[3]Comparison of Testing Methods for Shielding Effectiveness of Materials Against Electromagnetic Waves*, N.V. Bekaert Report, Prof. ir. J. Catrysse, KIH.WV/Oostende, Belgium, 1990.

When the unit is displaying a voltage reflection coefficient of .500, the AD538 is approximately processing V_s = 125 mV and V_x = 500 mV. The error, Ve, of the AD538 [4] is typically

$$Ve = \pm 0.5\% \text{ of reading} \pm 200 \text{ uV} \tag{2}$$

$$Ve = \pm [(500)(.005)] \pm .2 \text{ mV} \tag{3}$$

Ve will range from +2.7 mV to -2.7 mV of the displayed reading. This makes Vo and the displayed voltage reflection coefficient range from .497 to .503 volts.

When Vz goes below 100 mV a new error equation is used [4]. Assume the voltage reflection coefficient is .200, Vz = 20 mV and Vx = 500 mV. The new error equation is

$$Ve = \pm 1\% \text{ of reading} \pm 0.2 \text{ mV} \pm (0.1 \text{ mV}) \left(\frac{1 + V_s}{V_x} \right) \tag{4}$$

The displayed reading will range from .198 to .202.

The display error is typically $\pm .003$ down to a voltage reflection coefficient of about .100.

Data Validation

Using the same antenna assembly, a number of materials were characterized using a range gated HP8510 Network Analyzer and the BEKISCAN CP. Under all conditions, data has compared well within ± 0.5 dB tolerance. BEKAERT, S.A., of Zwevegem, Belgium, has also compared our measurements with their own instrumentation, and has confirmed the accuracy.

ACKNOWLEDGEMENT

The authors are grateful to Steve Kidd and Paul Deceunick of Bekaert Fibre Technologies for their assistance and data.

CONCLUSIONS

We have examined two novel approaches for measurement of material microwave absorption. In both cases, accurate and acceptable performance is achieved in cost effective portable instrumentation.

[4]Analog Devices Linear Products Databook, 1988, Page 6-24.

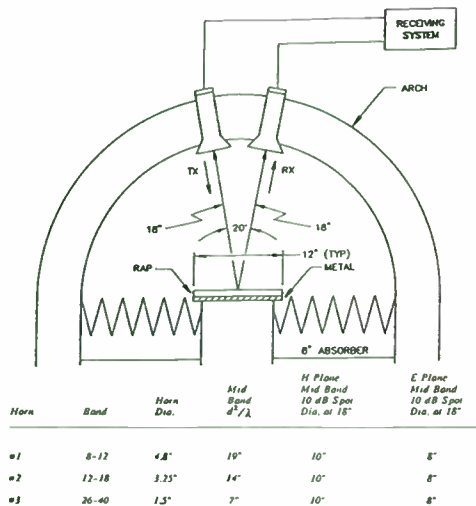


FIGURE 1. NRL Arch Reflectivity Test Fixture

Table 1. Comparison of PR-11 and NRL Arch Measurements

PARAMETER	DIFFERENCES
Measurement spot size	More localized measurement with PR-11.
Edge diffraction from measurement surface	Almost non-existent with PR-11; full NRL Arch tends to illuminate more of plate.
Plane wave criterion	NRL Arch is true plane wave; PR-11 is quasi-plane wave.
Secondary reflections	Can be range-gated out with NRL Arch/Phase-amplitude receiver. These result in data errors in PR-11.
Antenna-to-Antenna isolation	Smaller with NRL Arch since antennas are physically spaced further apart.

TABLE 2. Base Unit Specifications

BASIC UNIT: Includes portable instrument case containing microcomputer, discdrive, printer and storage provision for gun assembly and cables, operating system software and 6 ft. AC power cord.

INTEGRAL MICROCOMPUTER: 512K bytes RAM, 8 MHz clock, 3.5 inch floppy drive, 12 button keypad, 16 character display.

SOFTWARE: User prompted input menu for all modes, data smoothing algorithm, automatic calibration.

MEASUREMENT OUTPUTS: Visual LCD, 16 character readout on control panel and/or remoteterminal readout via RS232 or HPIB interface. Internal thermal printer, 24 characters. Serial Data, RS232 or HPIB to computer peripheral device/plotter option. Also, data can be accessed and recorded on a 3.5 inch floppy.

POWER REQUIREMENTS: 120 VAC/60 Hz or 220 VAC/50 Hz. 38 watts standby, 86 watts under measurement conditions.

BATTERY PACK (OPTIONAL): Sealed lead acid, provides power for 3 hours maximum, 8 hours average recharge.

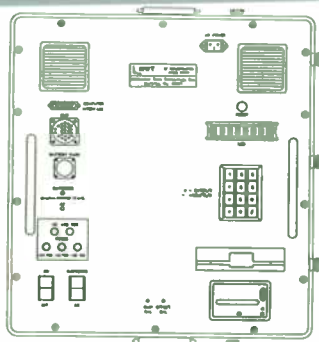
WEIGHT: Base Unit, 61 lbs. Battery Pack, 55 lbs. Sturdy carrying case meets MIL-STD-108 specifications.

TABLE 3. Gun Specifications

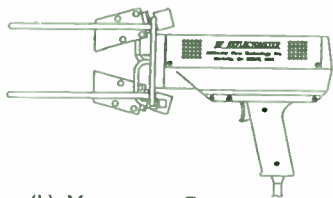
	PH-818 GUN	PH-28 GUN
Source	YIG: 8-18 GHz	YIG: 2.6-8 GHz
Polarization	Linear	Linear
Sweep Mode	100 MHz Min Stepsize	100 MHz Min Stepsize
Manual Mode	Operator Set Frequency	Operator Set Frequency
Cable Length	4m Standard 10m Optional	4m Standard 10m Optional
Weight	10 lbs. (including cable)	17 lbs. (including cable)

TABLE 4. Remote Power Unit Specifications

Physical Size:	15" x 20" x 8"
Weight:	55 pounds
Output Voltage:	+24, -24, +12
Operating Time:	3 hours
Recharge Power:	120 volts A.C.
Recharge Time:	8 hours
Accessories:	6 conductor power cable 10 feet long
Batteries:	- 6 volt Sealed Rechargeable type, 10 AH 4 each - 6 volt Sealed Rechargeable type, 10 AH 4 each - 12 volt Sealed Rechargeable type, 15 AH, 1 each



(a) Measurement Unit



(b) Measurement Gun



(c) Photograph

FIGURE 2. PR-11 System Packaging

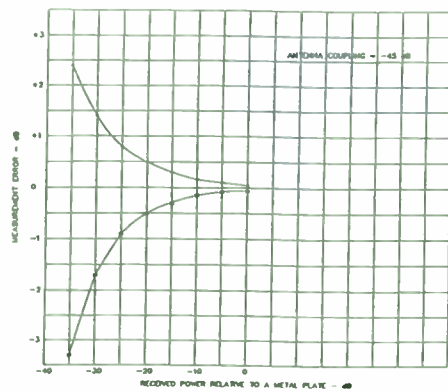


FIGURE 3. Reflectivity Measurement Error Resulting From Finite Antenna-To-Antenna Isolation

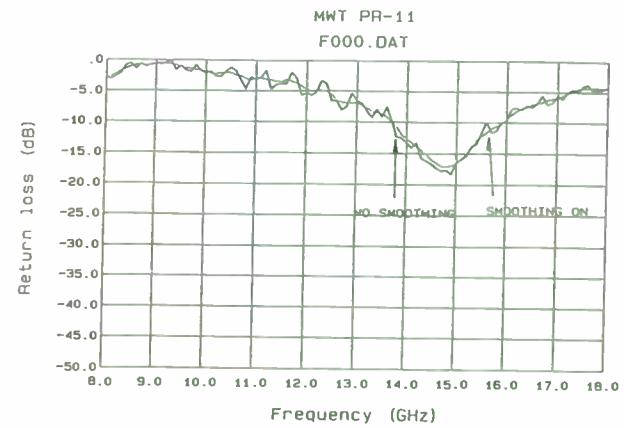


FIGURE 4. Effect Of Smoothing Algorithm On PR-11 Measured Data

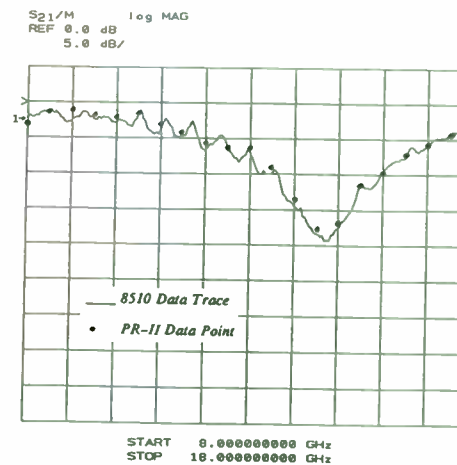


FIGURE 5. Comparison OF HP-8510 And MWT PR-11 Measured Data. PR-11 Antenna Assembly Common to Both Tests.

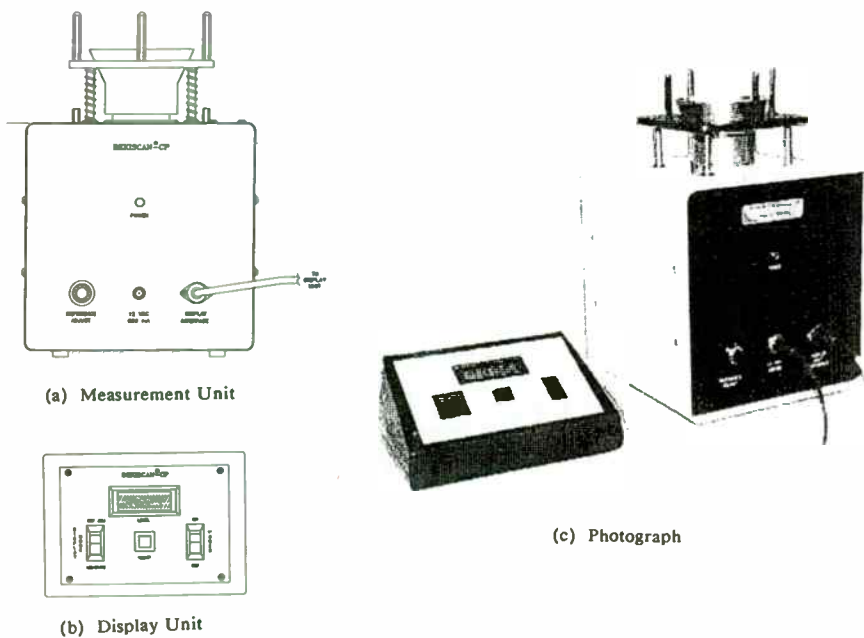


FIGURE 6. BEKISCAN Microwave Reflection Analyzer

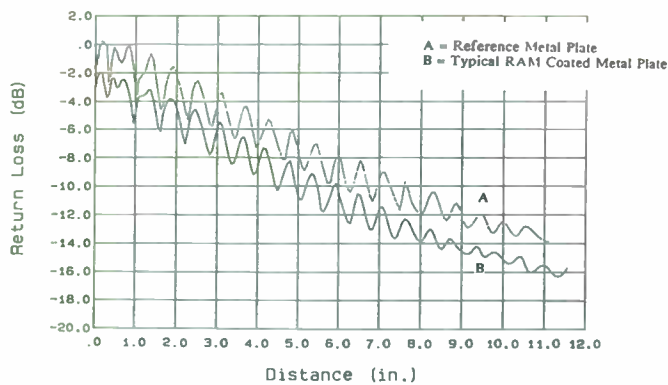


FIGURE 7. Detected Reflected Signal Level Versus Sample Plate Axial Distance From Horn Antenna

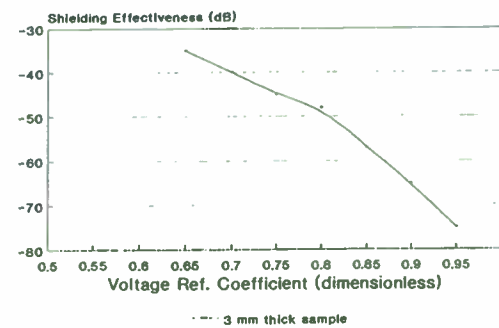


FIGURE 8. Shielding Effectiveness of Conductive Plastic Versus Voltage Reflection Coefficient

TABLE 5. BEKISCAN-CP Electrical Specifications

Operating Frequency:	10.525 GHz
Frequency Stability:	±25 MHz
Dynamic Range:	10 dB min. Standard Model 20 dB min. Extended Range Option Model CP-A
Measurement Accuracy:	$P \pm 0.05$ ($0.32 \leq P \leq 1.00$) $P \pm 0.06$ ($0.10 \leq P \leq 0.32$)
Measurement Stability:	$P \pm 0.02$
Analog Output:	0- 1 Volt for $0 \leq P \leq 1$
Input Power:	+12 Volts DC, 0.5 A (Supplied by wall plug-in power transformer)
Operating Temperature:	0 to 50°C
Measurement Spot Size Area:	8.6 cm (3.4 inches) diameter using flared horn section or 4.6 cm (1.8 inches) diameter with flared horn section removed.

Spread Spectrum Design Using Digital ASICs

Robert J. Zavrel Jr.

Gwyn Edwards

David Tahmassebi

Stanford Telecommunications, Inc.

1. INTRODUCTION

Until just a few years ago, spread spectrum techniques were rarely found in commercial applications; indeed, spread spectrum was considered only for military and aerospace applications. Recently the FCC opened the 902-928MHz band for license-free operation, permitting up to 1 watt of RF transmitter power. This allocation instantly became a very attractive solution to a wide range of wireless communications problems, from cordless telephones to wireless modems, to name but two. The "catch" to this spectral jewel is that the user *must* employ spread spectrum techniques. There is also growing interest in spread spectrum for cellular radio and a host of other established and new wireless applications. The purpose of this paper is to discuss the basics of spread spectrum and then show how a new set of specialized digital ASIC devices can be configured to perform the necessary functions found in spread spectrum systems.

The traditional methods of synthesizing and demodulating the spread spectrum signal utilize analog techniques. Now, a complete set of highly sophisticated digital ASICs is available for spread spectrum system designs. These ASIC devices were designed

primarily for the "direct sequence" method of spread spectrum. However, since many of the problems associated with spread spectrum are common to all techniques, these devices can also be used in frequency hopping and chirp systems.

2. PRINCIPLES OF SPREAD SPECTRUM SYSTEMS

Spread spectrum systems "spread" the transmitted signal energy over a much wider frequency band than is required for the information being sent. There are several potential advantages to be realized by resorting to the greater circuit and system complexity of spread spectrum systems. This explanation represents a simplification of a very complex subject, but is valid to gain a basic understanding of spread spectrum system architectures. These advantages are:

- A. Potentially greater immunity from interference, noise, and multi-path distortion
- B. Inherent greater security or "privacy" of the transmitted information
- C. Permits non-coordinated random multiple access to the medium by non-coordinated users

A. Greater immunity from interference and noise is not synonymous with *complete* immunity as some literature states. The degree of *increased* immunity from interference in a spread spectrum system is defined as:

$$(PG)_{db} = 10 \log (BW/R_b)$$

where PG is the spread spectrum "processing gain", BW is the main lobe spread spectrum bandwidth and R_b is the minimum required signal bandwidth necessary for

the transmitted symbol rate. Notice that there are two modulating signals in a spread spectrum system: the spreading signal which corresponds to the bandwidth BW , and the symbol rate which corresponds to the bandwidth R_b . The rate of the spreading signal is referred to as the "chip rate" in direct sequence systems and "hop rate" in frequency hopping systems. The chip or hop rate and the exact method of spreading will determine BW . For a given type of interference, the immunity will increase as the bandwidth is increased, consequently chip or hop rates are much higher than symbol rates in spread spectrum systems.

The level of interference needed to disrupt a spread spectrum signal with reference to the desired carrier strength is called the jamming margin, or M_j .

$$M_j = PG - (L + (S/N)) \quad (\text{units in dB})$$

where L is the system loss and S/N is the required signal-to-noise ratio at the information output. S/N refers to the necessary signal-to-noise level required for a specified bit error rate. This equation shows that the amount of interfering signal necessary to disrupt a spread spectrum signal is not only finite, but indeed less than the processing gain of the system. The notion that an infinite number of stations can use a spread spectrum channel simultaneously is incorrect.

B. Secure communication is inherent since the receiver despreader and transmitter spreader must synchronize to some predetermined code. The *degree* of security is determined by the sophistication of the coding system used and, of course, the sophistication of the would-be eavesdropper.

C. Multiple access requirements are easily met by using code division multiplexing, or CDMA. With CDMA a multitude of users can use the same band simultaneously if they are all using different codes. Mutual interference is reduced by the processing gain equation stated above. This same equation will also dictate the maximum permissible number of transmitters and their relative field strengths at a given receiver. Indeed, all system performance calculations are derived from this basic equation.

3. TYPES OF SPREAD SPECTRUM TECHNIQUES

"Spreading" the spectrum of a transmitted signal must be realized through one or more of the generic modulation techniques: FM, PM, and/or AM. There are numerous possible variations of spread spectrum as there are innumerable variations of modulation techniques. However, several basic schemes have evolved, each based on one of the generic modulation types. The following is a list of the most widely used schemes and the generic modulation technique involved:

1. Direct Sequence (PSK)
2. Frequency Hopping (multi-frequency FSK)
3. Pulsed Chirp (FM)

The Stanford Telecom ASIC line was developed specifically for the most common spread spectrum technique, direct sequence. However, many of these devices can be put to good use in other types of spread spectrum systems. After direct sequence, the most common techniques are frequency hopping and pulsed chirp. Consequently, our discussion will focus on only these three system types with emphasis on direct sequence.

Modulation typically is defined in the time domain. The frequency domain spectral distribution of the resultant "spread" can be predicted from the time domain modulation by Fourier analysis. The Fourier integrals are very well documented with specific relevance to spread spectrum in References 1 and 2. The particular spectrum distribution will depend upon the particular modulation type employed i.e.. BPSK, QPSK, MSK or PM or a wide range of FM types.

4. DIRECT SEQUENCE SYSTEMS

Papers which treat practical spread spectrum construction techniques are rare since much of this technology remains classified. Reference 6 explains a practical yet simple analog direct sequence (DS) spread spectrum system. Figure 1 shows a simple diagram of this direct sequence spread spectrum system. A narrow-band transmitter is modulated with the digital waveform. The signal is then modulated again by the spreader at the chip rate. In this case the spreader is a double-balanced mixer which inverts the phase of the signal by 180 degrees (BPSK). The chip rate is considerably higher than that of the baseband data and therefore spreads the carrier over a much wider spectrum (BW). Figure 2 shows the $(\text{SIN}(X)/X)^2$ spectrum of the direct sequence spread spectrum signal. The sequence of chipping modulation states (1 or 0) is determined by a pseudo-random noise generator or "PRN" source. Sequence lengths can range from microseconds to one month or longer! Indeed, coding is a complex science unto itself. The reader is advised to consult References 1, 2, and 7 for more details.

At the receiver, the incoming signal is despread by the same coding sequence used in

the transmitter. This can be done either at the RF frequency using another double-balanced mixer, or in the LO circuitry. In either event, synchronized identical modulation will cause the spectrum to collapse and reproduce the original waveform. When the received signal and receiver reference sequences are locked in time, "synchronization" is achieved. Perhaps the most difficult practical problems associated with spread spectrum systems are achieving initial synchronization and then maintaining it. The analog method used for sync in the Reference 6 article is the "synchronous oscillator" discussed in detail in Reference 8. For relatively simple systems, these analog techniques can be quite effective. However, for designs with higher performance design objectives (higher data rates, QPSK, fast correlation, etc..) the builder must choose between very complex analog and RF designs, or perform all the basic spread spectrum functions in the digital domain.

5. A DIGITAL DIRECT SEQUENCE SPREAD SPECTRUM SYSTEM

Figure 3 shows a completely digital direct sequence spread spectrum receiver using custom ASIC devices. All the necessary functions: synthesis, correlation, code generation, bit synchronization, and demodulation are performed in the digital domain. The result is a high performance receiver which is repeatable in a manufacturing environment and stable over a wide range of environmental conditions. The receiver is treated first since it is more complicated than the transmitter and many of the transmit functions are simply reciprocal of the receive functions.

A. Local Oscillator Synthesizer

The IF signal is converted to baseband and simultaneously split into I and Q channels.

The LO is synthesized using a combination of PLL and DDS techniques in the frequency synthesizer module. For a detailed description of DDS techniques please consult Reference 4, published by Stanford Telecom. DDS techniques allow very fine frequency resolution with direct digital control. Consequently, DDS is used in the LO synthesizer AFC loop. Quadrature LO synthesis is easily realized using the DDS technique. The baseband signals are then passed through low-pass filters and converted to digital words by the two A/D converters. This clock is generated via the synthesizer module using the reference signal, appropriate dividers and PLL techniques.

B. Digital Spectrum Despreading (sliding correlator)

Following baseband quantization, the despreading circuit must provide initial synchronization and code tracking. The digitized I and Q signals are applied to the inputs of three STEL-2410 correlator/accumulator ASIC devices. The STEL-2410s perform late, early, and punctual correlations. The PRN code from an STEL-1032 PRN sequence generator is applied to the multiplier sections of the STEL-2410 along with the I and Q signals. The outputs of these multipliers are then summed in the STEL-2410 adders. When the timing between the local PRN generator and the received signal is punctual, high correlation is achieved. The punctual STEL-2410 is used in conjunction with an external tracking microprocessor to lock the AFC loop thereby synchronizing the LO frequency. Synchronizing the LO will compensate for any frequency differences between the transmitter and receiver master clocks and/or Doppler effects.

The STEL-2410 is referred to as a "sliding" correlator. The PRN code is clocked by a

digital AFC loop. Before synchronization the transmitted code sequence "slides" against the receiver code sequence since they are not yet locked, and consequently not the same frequency. While the two sequences approach an in-phase condition, the correlation value on either the early or late correlator increases. Then the acquisition processor can begin to lock the NCO-driven PRN clock to the transmitter's PRN clock. To maintain sync the receiver and transmitter code clocks must be locked in frequency at the same location along the PRN sequence. The analog spread spectrum system in Reference 6 is also a sliding correlator.

Once synchronization has been achieved the punctual correlator maintains the highest possible correlation value. The timing differences between the punctual correlator and the early and late correlators are 1/2 chip, therefore the clocking rate of the correlators must be twice the system chip rate. The acquisition microprocessor continuously adjusts the timing frequency of the PRN generator to maintain synchronization. This digital AFC loop therefore maintains sync for the despreading function. The clock signal for the three correlators is synchronized to the LO synthesizer. Finally, a divider and MUX is included to accommodate multiple sample rates.

The despreader outlined above is adequate in systems where the chip rate is synchronous to the symbol rate. In more complex asynchronous systems, a fourth STEL-2410 can be used, deriving its clock from the bit synchronizer which is found in the circuitry that follows.

C. Digital Bit Synchronization and Demodulation

The punctual STEL-2410 correlator is used to provide a despread baseband signal for data recovery. This correlator uses a clock provided by the STEL-2110A bit synchronizer to recover the symbol edges. Bit synchronization is also required to provide a proper clock for the desreading correlator.

After the baseband signal has been despread, coherent data must be recovered. The several functions necessary to realize this coherent signal recovery are performed by the STEL-2110A bit synchronizer and STEL-2210 block phase estimator. The bit synchronization portion of the STEL-2110A operates by integrating the input signals in both the I and Q channels over one symbol period. This is performed three times; in addition to the nominally "on time" integration, quarter period early and quarter period late integrations are performed. The difference between the last two gives an indication of the timing error, since the averaged difference will be zero when the timing is correct. The signal is then used to drive an NCO contained within the STEL-2110A which produces the clock signals. The signals are also integrated prior to the main timing integrators to improve the performance. The STEL-2110A can be configured to provide a PLL or AFC discriminator for a receiving system.

Finally the STEL-2210 provides a phase reference to compensate for phase rotation and/or the effects of noise on the despread symbol. The STEL-2210 facilitates quick acquisition and should be used wherever fast acquisition is a requirement. The output of the STEL-2210 is the recovered baseband data.

D. Digital Matched Filter/Correlator

An alternative approach to the sliding correlator for synchronization is the digital

matched filter. In the STEL-3310 digital matched filter the digitized spread spectrum signal is clocked down a shift register/delay line so that the samples are passed from one filter tap to the next in a manner similar to a shift register. With each clock cycle the values stored in the register are multiplied with stationary code values and then summed to derive the correlation value. When the correlation value goes high, it indicates that sync is established. The acquisition time is much faster with the matched filter than with the sliding correlator because the sequence progresses at the system clock rate rather than a rate which is the difference between the transmitter and receiver code rates. The primary disadvantage of the matched filter approach is that the length of the filter must be equal to the code length, which limits the code length to 256 chips with the STEL-3310.

The STEL-3310 digital matched filter/correlator can be used in a variety of applications that require rapid acquisition of spread spectrum signals, radar detection or frame synchronization applications. Matched filters remove excess noise without introducing inter-symbol-interference (ISI). In general a matched filter is used to receive a pulse with known shape $p(t)$. The pulse amplitude (A_r) and time of arrival $t(o)$, however, are usually unknown. The pulse shape information makes it possible to design optimum receiving filters for detecting pulses buried in the noise of known spectral density.

The pulse shape can be represented as follows:

$$X(t) = A_r p(t-t(o))$$

Where A_r =Amplitude
with Fourier transform

$$X(f) = A \rho(f) e^{-j\omega t(d)}$$

The optimum filter $H_{opt}(f)$ that will detect the band-limited pulse $X(f)$ has the impulse response:

$$H_{opt}(t) = K \rho(t_d - t)$$

Where K = an arbitrary constant

and t_d = an arbitrary constant

Thus the name "matched filter" comes from the fact that $H_{opt}(t)$ has the same shape as the pulse $\rho(t)$ reversed in time and shifted by $t(d)$. The value $t(d)$ equals the delay between the pulse and the output peak, and may be chosen by the designer.

In each application the user will configure the matched filter by loading the I and Q relay register blocks, threshold values and the expander block if necessary (64 taps per device, cascaded up to 4 devices). The configured matched filter will now have a transfer function equivalent to:

$$H(f) = K \rho(f) e^{-j\omega t_d}$$

where $H(f)$ is the Fourier transform of $H_{opt}(t)$, and

$$(H_{opt}(t) \Rightarrow H(f))$$

At the output the system will receive the vector magnitude of the I and Q channel

correlator sums on a cycle by cycle basis as well as other pertinent signal parameters useful to the end user.

E. STEL-3310 Functions

Figure 4 shows a simple block diagram of the complex STEL-3310. The front-end processor allows for signal averaging when two samples per chip are taken. The front-end processor will automatically average two samples and then begin a new sequence. If one sample per chip is taken, the processor can be disabled.

The samples of the digitized signals propagate down the filter register blocks. During each chip, the complex products of the filter coefficients and signal samples are summed. When correlation occurs the sums of the adder circuits go to high values, and the symbol state can thus be ascertained. Although the symbol state is valid for only one chip period, processing gain is maintained because time integration is being performed by virtue of the register block delays. Therefore, the computed time integral of the signal is available only during one chip period, and appears on the I SUM and Q SUM busses.

The I OUT, Q OUT, I CASC, and Q CASC busses are used when cascading devices. The IX and QX input and output busses are used in QPSK applications. The expander block contains a delay circuit and adders that permit easy cascading of up to four filters. The post processor block performs the three final functions. It calculates the absolute value of the two's complement data, calculates signal magnitude, and performs a comparison of the magnitude with a programmable threshold. This comparison function allows the detection level to be optimally set for a given

signal-to-noise ratio, flagging loss of sync, or other signal level functions.

F. STEL-3310 Applications

Figure 5 shows a typical application of the STEL-3310 used in conjunction with the STEL-2110A PSK demodulator. In this application we can assume that a known PN sequence of 64 chips needs to be detected (time of arrival unknown). Detection must take place before the STEL-2110A can demodulate the data. To configure the STEL-3310 matched filter chip, the control processor can be programmed by the user to set a pre-defined threshold value. A detailed description of STEL-3310 operation is beyond the scope of this paper, but it is useful to illustrate the very high performance systems possible with only two CMOS ASIC devices. In addition to this basic circuit, four STEL-3310s can be cascaded to form a 256-tap filter. Also, two STEL-3310s can be combined to configure a QPSK filter.

G. Direct Sequence Transmitter

One of the distinct advantages of the direct sequence spread spectrum technique is that transmitter circuitry is rather simple. This is shown in Figure 1 where the "spreader" is nothing more than a double-balanced mixer. The use of DDS techniques offers a comparable simple solution in the digital domain for BPSK, QPSK, 8PSK, as well as higher PSK levels. Furthermore, the digital control bus for the modulator links directly to the NCO, making designs much easier to realize.

6. FREQUENCY HOPPING SPREAD SPECTRUM SYSTEMS

Unlike direct sequence spread spectrum, frequency hopping spread spectrum uses multiple discrete frequencies. Frequency hopping systems also use a coding sequence to provide the hop information. The system sequences the discrete frequencies by means of synthesizers in the transmitter and receiver. The transmitter and receiver LO synthesizers must sequence in sync to allow despreading in a manner not unlike the direct sequence technique. The need for fast-settling synthesizers makes direct digital synthesis (DDS) an attractive technique for frequency hopping systems. For extensive information regarding DDS Reference 4 is recommended.

Figure 6 shows how a hopping system might be configured by using the STEL-1177, STEL-1032 PRN code generator, and a memory interface. The data can be either analog FM, PM or AM, FSK, PSK, and/or ASK. In this case five bits of the PRN code generator are used simultaneously to define one of 32 discrete frequencies. The transmitter then "hops" among these frequencies according to the PRN code.

7. PULSE CHIRPED SPREAD SPECTRUM SYSTEMS

Pulse Chirped spread spectrum is most commonly found in radar systems. Code generation is not required if linear sweeps are used. Outstanding sweep linearity is obtained using digital counters to "sweep" the tuning word on a DDS NCO. Figure 7 shows a sweep system diagram. Again, for details of generating sweep signals through numeric modulation techniques please refer to Reference 4.

8. CONCLUSIONS

A basic review of spread spectrum techniques has been presented with emphasis on the unique digital spread spectrum approaches. Much of the required sophisticated circuitry associated with digital spread spectrum is now available as specialized spread spectrum ASIC devices. The digital approach will result in only a slight performance reduction from theoretical optimums while offering the advantages traditionally associated with digital over analog techniques.

9. REFERENCES

1. Spread Spectrum Systems, Robert C. Dixon, John Wiley & Sons, 1984
2. Spread Spectrum Communications, Volumes 1, 2, & 3., Marvin K. Simon, Jim K. Omura, Robert A. Scholtz, Barry K. Levitt, Computer Science Press, 1985
3. Presampling Filtering, Sampling and Quantization Effects on the Digital Matched Filter Performance, Horen Chang, "Proceedings of the International Telecommunications Conference", 1982
4. The DDS Handbook, Robert J. Zavrel Jr., Gwyn Edwards, Stanford Telecommunications, Inc., 1990
5. The ARRL Handbook, American Radio Relay League, 1990
6. A Practical Direct-Sequence Spread-Spectrum UHF Link, Andre Kesteloot, "QST", May, 1989, American Radio Relay League
7. Digital Communications by Satellite, James J. Spilker Jr., Prentice-Hall, 1977
8. The Synchronous Oscillator: A Synchronization and Tracking Network, Vasil Uzunoglu and Marvin H. White, IEEE Journal of Solid State Circuits, Dec. 6, 1985
9. Communication Systems, Bruce Carlson, McGraw-Hill, 1986
10. Digital Matched Filter ASIC, D. T. Magill & Gwyn Edwards, Proceedings of 1990 IEEE MILCOM Conference, September 30 - October 3, 1990

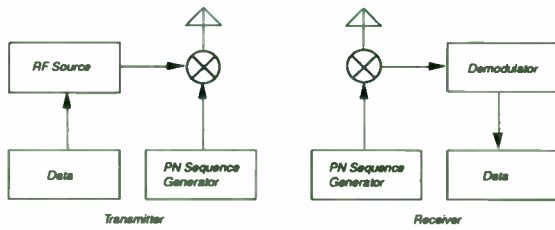


Figure 1. Simplified form of a spread spectrum system

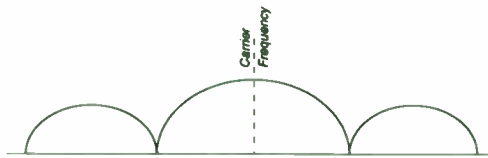


Figure 2. $(\text{SIN } X/X)^2$ spectrum of a spread spectrum BPSK signal

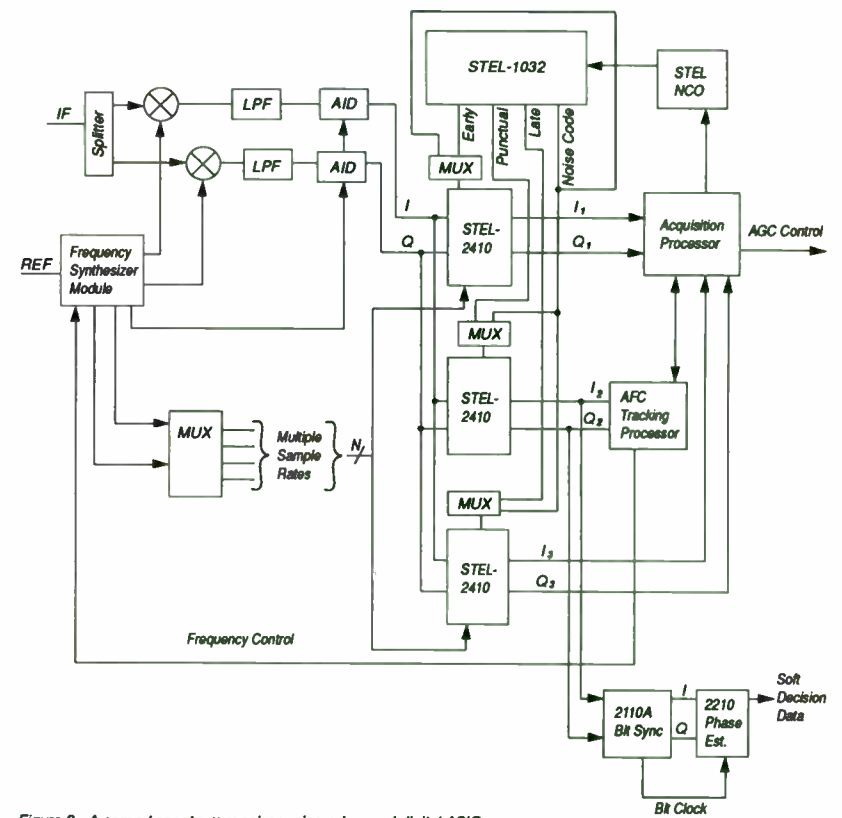


Figure 3. A spread spectrum receiver using advanced digital ASICs

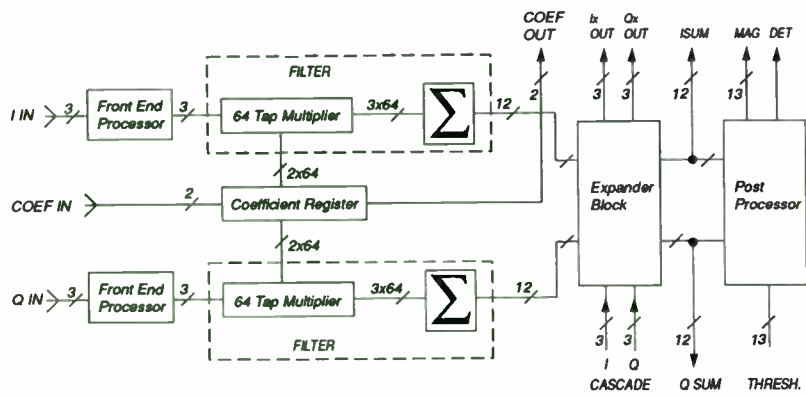


Figure 4. Simplified block diagram of the STEL-3310 digital matched filter

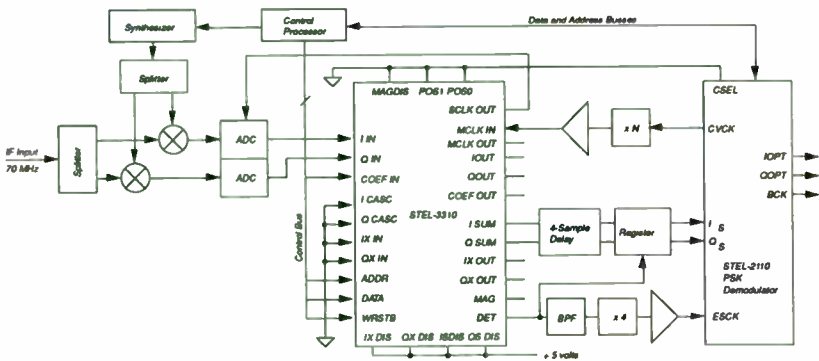


Figure 5. Typical application using the STEL-3310 and STEL-2110 for spread spectrum synchronization

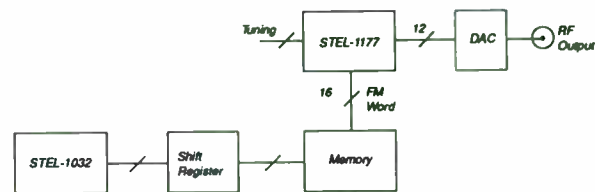


Figure 6. Frequency hopping transmitter using the STEL-1032 generator and STEL-1177 NCO

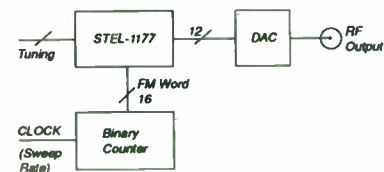


Figure 7. Sweep synthesizer

GPS and GLONASS Spread-Spectrum Navigation Systems

by

James Danaher
3S Navigation
23141 Plaza Pointe Drive
Laguna Hills, California 92653
Phone: (714) 830-3777 FAX: 830-8411 BBS: 830-3794

Abstract

The United States Global Positioning System (GPS) and the Soviet Global Navigation Satellite System (GLONASS) will both provide precise, world-wide position and timing information when their respective satellite constellations are complete in the mid-1990's. These systems will each consist of over twenty satellites. GPS and GLONASS satellites transmit spread-spectrum signals at adjacent L-band frequencies. GLONASS satellites transmit signals similar to but simpler than those from GPS satellites. Mathematical methods used by a receiver to compute position and timing from GPS and GLONASS satellite signals are practically identical. Thus a single receiver can be developed to use signals from both GPS and GLONASS. Such a receiver will have a greater degree of accuracy and availability than can be achieved using either GPS or GLONASS alone.

This paper describes the GPS and GLONASS systems, details of the GPS and GLONASS spread-spectrum signal structures, and innovations in GPS/GLONASS receivers being developed by 3S.

Introduction

The United States and the Soviet Union are both rapidly implementing independent satellite navigation systems that each allow an L-band (1215 to 1620 MHz) receiver to accurately estimate the current time and the position of the receiver antenna. Although primarily intended for military purposes, these systems both have extensive civil uses. For specialized applications, a receiver can synchronize itself to universal time with an accuracy of a few nanoseconds and can find its own position relative to the world geodetic coordinate system to an accuracy of better than a centimeter. For more general applications, receivers routinely produce results with time accuracy of tens of nanoseconds and a position accuracy of a few meters.

As the U.S. GPS and the Soviet GLONASS systems become operational, the deployed receivers are expected to number in the hundreds of thousands. These receivers will be used in applications that range from surveying to locating a wide variety of moving vehicles on or above the surface of the Earth.

Thus GPS and GLONASS receivers will be an increasingly important focus of L-band RF hardware development over the next decade. With this in mind, this paper introduces the RF engineer to the operation of GPS and GLONASS and describes key features of GPS/GLONASS receivers.

GPS/GLONASS Receiver Basics

GPS and GLONASS receivers compute their own position by comparing the transit time of RF signals from multiple satellites [1]. The satellites generate spread-spectrum RF signals by binary phase-shift keying (BPSK) modulation of a carrier with a predictable sequence of bits known as the code. A receiver generates a replica of the code and shifts the replica until maximum correlation is achieved between the locally generated code and the code present in the received RF signal. The relative shift of the code for each of the satellites under observation provides a measure of the relative transit time to those satellites. This relative transit time is referred to as the pseudo-range, and is equivalently expressed as time-of-travel (ns) or distance (m).

Typically signals from four satellites are required in order to compute the position of a receiver in three dimensions. Three satellites are needed to compute the position of a receiver in two dimensions. A receiver sitting at a fixed location can use the signal from a single satellite to set its clock to an accuracy of tens of nanoseconds. The number of satellites in each of the constellations and the orbits of the satellites have been selected to provide practically continuous world-wide visibility of five or six satellites from either constellation.

The precision of the receiver computation of its own position depends upon the relative position of the satellites observed. For example, if all the satellites are in approximately the same region of the sky, the geometry for a position computation

is poor and the precision of the position estimate is degraded. This degradation is commonly referred to as dilution of precision (DOP).

Frequency Standards on the Satellites

Signals transmitted by the satellites in a constellation must be precisely synchronized in order to compute pseudo-range to each satellite. A cesium or rubidium atomic frequency standard on board each GPS satellite provides the basis for synthesizing all carrier and clock frequencies. The operation of the frequency standards on all of the GPS satellites is observed from control stations on the ground. The GPS satellite controllers use these observations both to apply tuning adjustments to the frequency standard on each satellite and to compute clock corrections that are transmitted by the satellite. A receiver uses clock corrections transmitted by a GPS satellite to correct its measure of the pseudo-range to that satellite. The clock corrections also allow a GPS receiver to synchronize itself to coordinated universal time (UTC).

Observations of signals broadcast from the GLONASS satellites reveal that highly accurate cesium or rubidium atomic frequency standards are present [2]. The GLONASS satellites also transmit clock corrections similar in operation to those transmitted by the GPS satellites. These clock corrections allow a receiver to compute pseudo-range to that satellite and to synchronize to coordinated universal time, Soviet Union (UTC-SU)

Benefits of an Integrated GPS/GLONASS Receiver

Interchangeable use of GPS and GLONASS signals in a single receiver has a number of significant advantages over a receiver that can only receive signals from one of the constellations. An integrated GPS/GLONASS receiver would always have far more satellites in view than are required to compute the position of the receiver. This eliminates periods when there are an insufficient number of satellites. The increased number of visible satellites also will allow a receiver to select satellites that are spread out in the sky and reduce DOP and produce a more accurate position estimate. The larger number of visible satellites will also increase the probability of maintaining track on sufficient satellites when a ground-vehicle borne receiver moves through urban canyons, forests or mountainous terrain.

An integrated GPS/GLONASS receiver also has advantages in autonomously verifying the integrity of its position solution [3]. This is called receiver autonomous integrity monitoring (RAIM) and is important when the receiver is used as a primary means of determining the position of an aircraft.

Interchangeable Use of GPS and GLONASS Signals

RF and code replica generator hardware functions in a GPS receiver are somewhat different from the same functions in a GLONASS receiver. The correlation measurement hardware is identical, however. The software used to

interpret digital data transmitted by the satellites is, of course, different for GPS vs. GLONASS. Once the receiver measurements and the satellite digital data are converted to a common reference and format, the software used to compute the position of the receiver can be identical.

Contrary to frequently expressed opinion in the satellite navigation community, no coordination or contact of any kind should be necessary between the operators of the GPS and GLONASS constellations for receivers to use these satellites as if they formed a single integrated constellation. While such contact should not be discouraged, it is simply not required since the satellites already transmit adequate data for combined use.

Both GPS and GLONASS are tied to precise time and geodetic references. If a receiver knows the transformation between the GPS and GLONASS references, the receiver can autonomously resolve the differences and use all of the satellites in view as if they formed a part of a single constellation.

Considerable progress has been made in resolving differences between the time references used by the GPS and GLONASS constellations [2]. An important feature of these observations is that the time reference of the GLONASS constellation has a fairly constant rate of drift relative to the international time standard that is the time reference for GPS. This means that a receiver can autonomously determine the relative offset and rate of drift of the GPS vs. GLONASS time references and subsequently freely convert between the two. The only problem with this approach is that the developmental GLONASS

constellation has occasionally undergone large jumps in its time reference. Perhaps these jumps will be eliminated in the operational GLONASS constellation. Otherwise signals from the GLONASS satellites will be unusable for a few days after each time reference jump.

The geodetic reference of GPS is the World Geodetic Survey 1984 (WGS-84), whereas GLONASS is referenced to the Soviet Geocentric System 1985 (SGS-85). These both define a reference standard for the shape of an Earth surface ellipsoid, the position of the rotational axis of the Earth, the rate of rotation of the Earth, and the rotational position of the Earth at a specific epoch. WGS-84 and SGS-85 have differences in each of these terms which must be resolved in order to interchangeably use the satellite position data transmitted by each satellite. Several organizations are currently planning efforts to determine these differences. This final roadblock in developing integrated GPS/GLONASS receivers can be expected to be cleared by the time full GPS and GLONASS satellite constellations become operational in the mid-1990's.

GLONASS Satellite Constellation

The operational GLONASS system will have 24 satellites orbiting the Earth in three planes, inclined 64.3 ± 0.3 degrees to the equator [4]. Each of the three planes will contain 8 satellites evenly separated by 45 degrees. The orbit of GLONASS satellites is nominally circular, with an altitude of approximately 19,150 km and a period of 11 hours 15 minutes and 44 seconds ± 5 seconds.

As of 27 September 1990, the GLONASS satellite constellation consisted of 8 satellites, located in 2 orbital planes as shown in Figure 1. An additional 6 GLONASS satellites are due to be launched by the end of 1990. An operational constellation of 24 satellites is planned by 1993. These plans assume that the Soviets solve the severe reliability problems that have shortened the life of many of the GLONASS satellites.

GPS Satellite Constellation

The operational GPS system will have 21 satellites plus 3 spare satellites orbiting the Earth in six planes, inclined 55 degrees to the equator. (For the next few years some of the satellites will be in planes inclined 64 degrees to the equator; these are remaining satellites from the original test constellation.) Each of the six planes will contain 4 satellites separated to optimize signal coverage on the Earth's surface. The orbit of GPS satellites is nominally circular, with an altitude of approximately 20,200 km and a period of 11 hours 58 minutes.

As of 27 September 1990, the GPS satellite constellation consisted of 14 satellites, located in 6 orbital planes. An additional 2 satellites are due to be launched by the end of 1990 and a full constellation of 24 satellites is expected to be operational in 1992. The reliability record of the GPS satellites has been excellent, so there is little doubt that the full GPS constellation will be achieved in the early 1990's.

GLONASS Transmission Frequencies

GLONASS satellites transmit L band signals that are BPSK modulated by pseudo-random number (PRN) bits at 0.511 MHz and 5.11 MHz clock rates. Each GLONASS satellite transmits the 0.511 MHz clock rate signal on a single frequency and the 5.11 MHz clock rate signal on dual frequencies.

The signal structure of the 0.511 MHz clock rate signals has been officially released by the Soviet Union for international use [4]. This signal is referred to as the GLONASS coarse/acquisition-code (C/A-code) in this paper, due to its similarity to the GPS C/A-code.

The signal structure of the 5.11 MHz clock rate signals has not been announced by the Soviets, but was empirically determined by Lennen [5]. This signal is referred to as the GLONASS precision-code (P-code) in this paper, since it is analogous to the GPS P-code.

Each GLONASS satellite transmits both C/A-code and P-code signals at an L1 band carrier frequency of:

$$f_k = 1602 + 0.5625 k \quad (\text{MHz})$$

where $k = 1, 2, \dots, 24$; k is the carrier frequency channel number given in the almanac data transmitted by each GLONASS satellite. Thus GLONASS satellites

use frequency division multiple access (FDMA) to allow a receiver to separate signals from different GLONASS satellites.

Each GLONASS satellite also transmits the P-code signal at an L2 band carrier frequency of:

$$f_k = 1246 + 0.4375 k \quad (\text{MHz})$$

GLONASS apparently has a second transmission frequency for the same reason as GPS. Observations of the relative phase of signals at two different frequencies allows a receiver to autonomously estimate the amount of ionospheric delay that is present on the downlink from a satellite.

GPS Transmission Frequencies

GPS satellites transmit L band signals that are BPSK-modulated at 1.023 MHz and 10.23 MHz clock rates. Each GPS satellite transmits the 1.023 MHz clock rate signal on a single frequency and the 10.23 MHz clock rate signal on dual frequencies [6].

Each GPS satellite transmits both C/A-code and P-code signals at an L1 band carrier frequency of 1575.42 MHz and P-code only signals at an L2 band carrier frequency of 1227.6 MHz.

Each GPS satellite uses a different sequence of PRN code chips to modulate the carrier frequency. This allows a receiver to separate signals from the different GPS satellites by use of code division multiple access (CDMA).

GLONASS Code Generation

The GLONASS C/A-code transmission signal is created by BPSK-modulating the GLONASS L1 carrier frequency for the particular satellite with a repeating PRN sequence of 511 bits at a clock rate of 0.511 MHz [4]. Thus the 511 bit sequence repeats 1000 times per second. The 511 bits are generated by the 9-bit shift register with feedback taps as shown in Figure 2.

The GLONASS C/A-code PRN sequence is itself modulated by a 100 bits/s stream of digital data, which includes precision position and timing information for the particular satellite transmitting the data as well as an approximate orbit description for all satellites currently in the GLONASS constellation.

The GLONASS P-code transmission signals are created by BPSK-modulating the GLONASS L1 and L2 carrier frequencies for the particular satellite with a repeating PRN sequence of 5,110,00 bits at a clock rate of 5.11 MHz [5]. Thus the 5,110,000 bit sequence repeats once per second. The P-code PRN sequence is generated by the 25-bit shift register with feedback taps as shown in Figure 3.

Digital data modulation of the GLONASS P-code has been observed, but the format and content of this data have not yet been announced by the Soviets.

GPS Code Generation

The GPS C/A-code transmission signal is created by BPSK-modulating the GLONASS L1 carrier frequency of 1575.42 MHz with a repeating PRN sequence of 1023 bits at a clock rate of 1.023 MHz [6]. Thus the 1023 bit sequence repeats 1000 times per second. The 1023 bit sequence is different for each GPS satellite and is generated by combining the outputs from two 10-bit feedback tap shift registers.

The GPS C/A-code PRN sequence is itself modulated by a 50 bits/s stream of digital data, which includes precision position and timing information for the particular satellite transmitting the data as well as an approximate orbit description for all satellites currently in the GPS constellation.

The GPS P-code transmission signals are created by BPSK-modulating the GPS L1 and L2 carrier frequencies for the particular satellite with a PRN sequence at a clock rate of 10.23 MHz. This sequence is one week in duration and is different for each GPS satellite. It is generated by combining outputs from four 10-bit feedback tap shift registers [7].

At L1, the P-code is in fact modulated in phase quadrature with the C/A-code signal, thus resulting in quadriphase shift keying (QPSK) modulation of the L1

carrier. This can be ignored in a practical receiver, however. The difference between C/A-code and P-code clock rates and PRN sequences ensures that only one code is visible to a receiver channel at any time. The selected code appears as a BPSK modulated signal.

The GPS P-code is modulated by exactly the same digital data transmitted on the C/A-code.

The signals transmitted by the GPS satellites show two important characteristics not seen in the GLONASS system. Selective Availability (SA) is the intentional degradation of the precision position and timing information transmitted by the GPS satellites. SA is implemented both by dithering the satellite reference frequency and by adjusting the transmitted digital data in order to cause errors in the results produced by a receiver. These errors can, however, be avoided by correcting the received signal using a decryption algorithm and key provided by the US Government. SA is intended to limit the accuracy of results produced by a receiver that does not have this decryption key.

Anti Spoofing (AS) is the replacement of the GPS P-code with a code that is encrypted and cannot be received without a decryption key provided by the US Government. AS is intended to prevent an unauthorized receiver from using the 10.23 MHz P-code whenever the US Government decides to make it unavailable. As the name implies, AS also makes it difficult for an adversary to transmit a P-code signal that might spoof receivers deployed by the US Government.

The US Government policy on when SA and AS will be applied is currently in a state of flux. The fact that these forms of intentional signal degradation do not seem to be present on GLONASS signals is one of the reasons for interest in the use of GLONASS.

GPS/GLONASS Frequency Spectrum

The satellites perform BPSK modulation by inverting the carrier whenever there is a change in the value of the modulating signal. BPSK modulation suppresses the carrier and spreads the transmitted energy over a bandwidth that has its first nulls at \pm the code clock frequency [8]. The power density of the transmitted signal is defined by a $(\sin(x)/x)^2$ curve as shown in Figure 4.

A higher resolution look at the spread-spectrum power density shown in Figure 4 reveals that it is composed of individual spectral lines with a spacing equivalent to the repetition frequency of the modulating PRN code. For both GPS and GLONASS C/A-codes, this line spacing is 1000 Hz, for GLONASS P-code it is 1 Hz, and for GPS P-code the spacing is 1.7×10^{-6} Hz. As a practical matter this fine detail of the spread-spectrum signal has no effect on the receiver RF design.

The L1 and L2 frequency spectrum occupied by GPS and GLONASS signals are shown in Figures 5 and 6. The vertical scale is relative to GLONASS C/A-code, which is the strongest of the various signals. The typical strength of the GLONASS C/A-code signal is roughly -124 dBm-Hz when viewed from the surface

of the Earth with the satellite at the zenith using a 3 dBi right-hand circularly polarized antenna. This is the approximate level of the signal at the output of the antenna and is well below the level of background thermal noise. The manner in which the spread-spectrum receiver detects this weak signal is the topic of the remainder of this paper. Table I contains a list of the approximate strength of each type of signal received from GPS and GLONASS satellites.

Integrated GPS/GLONASS Receiver

The block diagram of a one-channel GPS/GLONASS receiver is shown in Figure 7. This receiver can observe one type of signal (i.e. C/A-code or P-code) from a single GPS or GLONASS satellite at one time. With a temperature-controlled crystal oscillator, a one channel stationary receiver can observe in sequence the four satellites required to compute a position solution.

The antenna has hemispherical coverage and right hand circular polarization. A preamplifier compensates for cable losses if there is a long cable run from the antenna to the receiver. The RF/IF section converts the selected L-band frequency to low IF and provides filtering to exclude signals out of the selected passband. The digital correlator performs digital sampling of the IF signal, code correlation, and carrier phase detection [9]. The computer completes the phase lock loops that track the code and carrier and computes the navigation solution.

3S Research Receiver Design

The design of the 3S GPS/GLONASS research receiver is shown in Figure 8. This receiver observes all of the navigation signals transmitted by GPS and GLONASS satellites. The 3S receiver is somewhat more complex than a receiver that would only observe a subset of the GPS and GLONASS signals. For example a GPS/GLONASS receiver that only tracks L1 C/A code signals would have a single passband antenna/RF and lower clock rate digital processing, compared to the receiver described below, which has a dual passband and high clock rate.

GPS and GLONASS signals are located in two different regions of the L-band spectrum. These are from 1217.6 to 1256.5 Mhz in the L2 band and from 1565.4 to 1620.6 MHz in the L1 band. An antenna to receive these signals should have right-hand circular polarization, moderate frequency selectivity and uniform hemispherical coverage. Quadrifilar helix [10] and patch antennas perform well against these criteria and are commonly used.

A broad-band low-noise preamplifier is located at the antenna unless the cable length to the receiver is short. This preamplifier compensates for losses in the cable run to the receiver and is a primary factor in establishing the noise figure of the receiver. The spread-spectrum receiver has considerable immunity to interfering signals, however it is important that the preamplifier not be saturated. Thus, depending upon the level of ambient interference, a carefully designed low insertion loss filter is sometimes placed between the antenna and

the preamplifier in order to reject out-of-band interference. The insertion loss of this filter is important because it adds directly to the noise figure of the receiver.

After the preamplifier, a bandpass filter passes a 44 MHz bandwidth centered at 1240 MHz and a 55 MHz bandwidth centered at 1593 MHz. In the 3S receiver this filter is located in the receiver, although in other designs it can be co-located with the antenna and preamplifier. The purpose of this filter is to prevent wideband noise from saturating the subsequent RF amplifier.

The 3S receiver uses a double-balanced mixer to convert the RF signal to the selected IF. The local oscillator is a digital synthesizer tied to the 10 MHz master reference. The phase noise of the local oscillator is minimized to avoid disrupting the operation of the Costas carrier phase lock loop that follows it. The local oscillator frequency is different (typically lower) than that of the spread-spectrum signal by an amount that defines the IF center frequency. The local oscillator is set to translate the nominal, i.e. without doppler, spread-spectrum carrier frequency. Doppler shift is accounted for later in the carrier numerically controlled oscillator (NCO).

The double-balanced mixer also converts an image to the same IF as the desired signal. This results in a 3 dB signal-to-noise ratio (S/N) degradation that will be eliminated by future use of an image rejection mixer. This 3 dB degradation is not present for those signals, such as L2 GPS, where the image frequency is attenuated by prior filtering.

The IF signal is then bandpass-filtered to restrict its -3 dB bandwidth to 1.4 times the spread-spectrum modulation code clock frequency. Although this is narrower than the first nulls of the BPSK spectrum at 2 times the clock frequency, the narrower bandwidth improves system S/N [11]. There is a separate linear-phase filter for each of the four types of spread-spectrum signals processed by the receiver.

Digital Correlation Processing

Details of the digital correlation processing performed by the 3S research receiver are shown in Figure 9.

The filtered IF signal is sampled by a 1-bit A-D, which is simply a fast comparator. A disadvantage of 1-bit digitization is the 1.5 dB S/N loss as compared to 2-bit digitization. Also, a 1-bit digitized signal is more easily jammed by extraneous signals. The major advantage is simplification of the subsequent digital processing, which was considered the priority in the present design.

The A-D sampling clock rate is 2.5 MHz for GPS or GLONASS C/A code, 10 MHz for GLONASS P-code, and 20 MHz for GPS P-code. The sampling clock is locked to the 10 MHz reference and clocks the operation of the digital correlator application-specific integrated circuits (ASIC) described below.

Replicas of the carrier and code clocks are generated by dual Stanford Telecom 32 bit NCOs. These will, however, soon be replaced by a Qualcomm part that has two NCOs in a single chip. The dual NCOs are directly clocked by the 10 MHz master reference for GPS or GLONASS C/A-code. When processing GPS or GLONASS P-code the NCOs are clocked at a 30 MHz rate that is phase-locked to the 10 MHz reference.

The replica of the carrier is set to the center frequency of the spread-spectrum signal in the IF, as corrected for the downlink doppler shift caused by the relative motion between the transmitting satellite and the receiver antenna. The one-bit sine carrier is mixed (exclusive or'ed) with the data sample to create the in-phase (I) signal, which is fed into the I shift register. The 90 degree phase-shifted cosine carrier is mixed with the data sample to create the quadrature-phase (Q) signal, which is fed into the Q shift register.

The replica of the code clock drives one of two 3S-developed code generation ASICs. These ASICs use Altera "MAX" programmable logic devices (PLD). One ASIC produces GPS C/A-code, GLONASS C/A-code and GLONASS P-code, while the other generates GPS P-code. The selected code is clocked at the rate of the code clock on the satellite, with correction for downlink doppler shift.

Carrier Tracking

A Costas phase locked loop is used to adjust the carrier replica NCO to match the carrier frequency and phase of the spread-spectrum signal carrier received from the satellite [11]. The following description assumes that the replica code is a priori phase-locked to the received code. The I and Q shift registers can be ignored because an identical time delay is applied to the I on-time and Q on-time signals that are used for carrier tracking.

The I signal was created by mixing the received signal with the sine carrier replica. The I signal is then mixed with the replica code. The resulting number of 1's detected over a fixed period of one millisecond are counted by the I on-time counter. If the sine carrier replica and the received signal are in-phase then a the number of 1's detected will be somewhat more or somewhat less than half the number of sample ticks during the one millisecond correlation period.

The Q signal was created by mixing the received signal with the cosine carrier replica. The Q signal is then mixed with the replica code. If the cosine carrier and the received carrier replica is 90 degrees shifted in phase then the resulting Q on-time counts will be approximately equal to half the number of sample ticks during the correlation period. This indicates that no correlation, only noise, was measured by the counter.

As the replica carrier phase begins to drift relative to the received carrier then a signal will be seen in the Q on-time counter. The I on-time and Q on-time counts

provide an estimate of the replica carrier phase error as $\arctan ((Q_{ot-ticks}) / (I_{ot-ticks}))$, where Q_{ot} is the number of counts in the Q on-time counter, I_{ot} is the number of counts in the I on-time counter, and ticks is half the number of A-D samples during the correlation period. The computer performs a low pass filter on the estimated replica carrier phase error and sends corrections to the replica carrier NCO to close the Costas loop. Thus the receiver maintains coherent track of the frequency and phase of the spread-spectrum signal carrier.

Code Tracking

A separate phase lock loop is used to adjust the code replica NCO to match the frequency and phase of the spread-spectrum modulating code received from the satellite [6].

The I signal is fed into a shift register. The shift register is tapped at points before and after the tap for the I on-time signal used in the carrier tracking loop described above. These I-early and I-late tap points are selected by the digital correlator ASIC so that they sample the I signal approximately one-half of a code clock period before and after the I on-time tap.

If the replica code phase perfectly matches the received code phase at the I on-time tap, the number of correlations detected at the I-early and I-late taps will be about equal. As the replica code phase begins to drift relative to the received code, then there will be a difference in the number of correlations detected at the I-early

and I-late taps. The I-early and I-late counts provide an estimate of the replica code phase error as simply $I_e - I_l$ where I_e is the number of I-early counts and I_l is the number of I-late counts. The computer performs a low pass filter on the estimated replica code phase error and sends corrections to the replica code NCO to close the loop. Thus the receiver maintains track of the frequency and phase of the spread-spectrum signal code.

Data Demodulation

The above description of code and carrier tracking ignores the effects of the low-bandwidth data signal that is modulated on the spread-spectrum signal. The demodulation of this signal is entirely handled in software and has only minor effect on the operation of the tracking loops [9]. When both loops are phase-locked, the sign of the signal in the I on-time channel provides data bit values and is used to correct the direction of the phase errors estimated by the code and carrier loops. The data bits detected in this manner may be inverted. This is easily detected and corrected as the computer interprets the data in accordance with the GPS or GLONASS specifications.

Receiver Navigation Processing

The receiver detects the frequency and phase of both the carrier and code that comprise the spread-spectrum signal from a GPS or GLONASS satellite.

Multiple receiver channels detect these data synchronously and provide the data to a navigation processor. The navigation processor uses these data to compute the position of the receiver, but the techniques for this computation are beyond the scope of the present paper.

Conclusion

The receiver described in this paper can track all navigation signals transmitted by the GPS and GLONASS satellites. The digital design is largely built from PLDs and is amenable to VLSI implementation. This technology will result in miniaturized high-precision GPS/GLONASS digital receivers. These receivers will become an increasingly important area of RF and digital engineering during the current decade.

Information Resources

The Institute of Navigation is the premiere U.S. civil organization with an interest in GPS and GLONASS technology. ION can be contacted at 1026 16th Street, N.W., Suite 104, Washington, D.C. 20036, telephone (202) 783-4121.

Navtech Seminars has a wide variety of publications and tutorials regarding GPS and GLONASS. Navtech Seminars is located at 2775 S. Quincy Street, Suite 610, Arlington, Virginia 22206, telephone (703) 931-0500.

The U.S. Coast Guard has a free electronic bulletin board system (BBS) that provides current information regarding the GPS satellites. The USCG GPS BBS can be reached at (703) 866-3890 at 300, 1200 or 2400 baud, or (703) 866-3894 at 1200, 2400, 4800 or 9600 baud.

The author of this paper operates a free BBS that provides current information regarding the GLONASS satellites. This information collected from the GLONASS satellites by the 3S research receiver described in this paper. The 3S GLONASS BBS can be reached at (714) 830-3974 at 1200 or 2400 baud.

References

1. Milliken, R.J. and C.J. Zoller. "Principle of Operation of NAVSTAR and System Characteristics." *GPS Papers*, Volume I, ION, 1980.
2. Daly, P. and I. D. Kitching. "Characterisation of Navstar GPS & GLONASS On-board Clocks." *IEEE PLANS '90 Position Location and Navigation Symposium Record*, IEEE Catalog No. 90CH2811-8, March 1990.
3. Sturza, M. A. and A. K. Brown. "Integrated GPS/GLONASS for Reliable Receiver Integrity Monitoring (RAIM)." *Proceedings of the Forty-Sixth Annual Meeting of the Institute of Navigation*, ION, June 1990.

4. *Global Satellite Navigation System GLONASS Interface Control Document*, 90-100/GPS-31, Airlines Electronic Engineering Committee (AEEC) of Aeronautical Radio, Inc. (ARINC), Annapolis, Maryland, June 1990.
5. Lennen, G.R. "The USSR's GLONASS P-code - Determination and Initial Results." *Proceedings of the Second International Technical Meeting of the Satellite Division of the ION*, September 1989.
6. Spilker, J.R. Jr. "GPS Signal Structure and Performance Characteristics." *GPS Papers*, Volume I, ION, 1980.
7. Ould, P.C. and R. J. VanWechel. "All-Digital GPS Receiver Mechanization." *GPS Papers*, Volume II, ION, 1984.
8. Stansell, T.A. "The WM 102 P Code Channel Beats a Full House of Squared Channels." *IEEE PLANS '90 Position Location and Navigation Symposium Record*, IEEE Catalog No. 90CH2811-8, March 1990.
9. Lennen, G.R. and P. Daly. "A Navstar GPS C/A Code Digital Receiver." *Navigation: Journal of The ION*, Vol. 36, No. 1, Spring 1989, pp. 115-126.
10. Kilgus, C. C. "Resonant Quadrifilar Helix Design." *Microwave Journal*, pp. 49-54, December 1970.
11. Gibson, J.D. *Principles of Digital and Analog Communications*. Macmillan, New York, 1989.

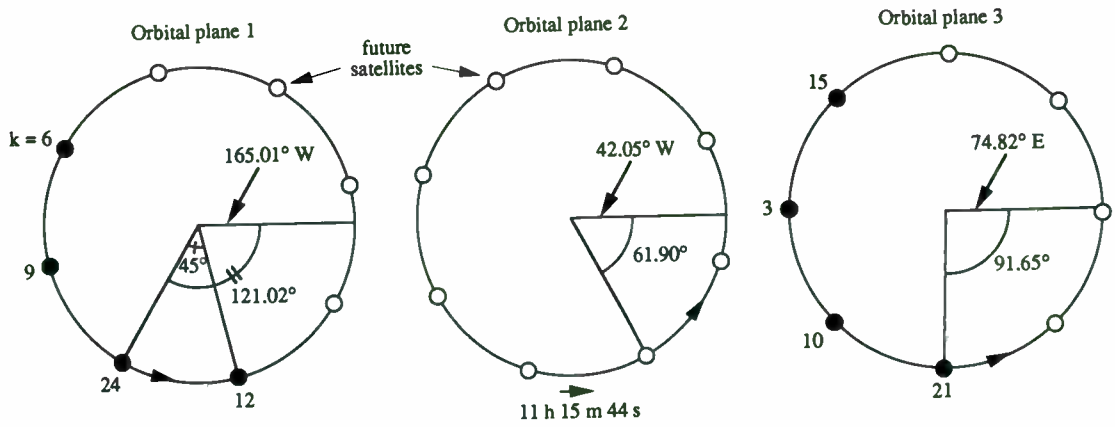


Figure 1 — GLONASS Constellation at 0300 UT on 27 September 1990

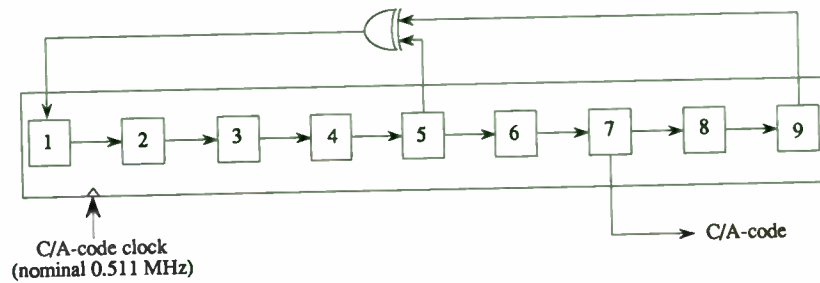


Figure 2 — GLONASS C/A-code Generator

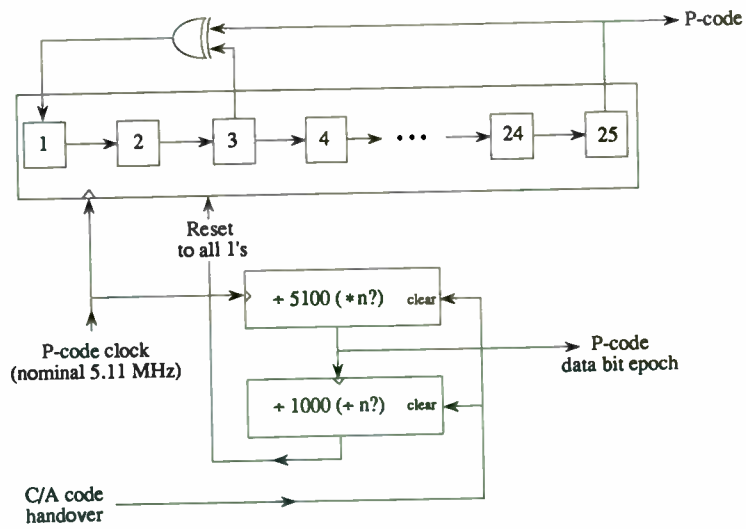


Figure 3 — GLONASS P-code Generator

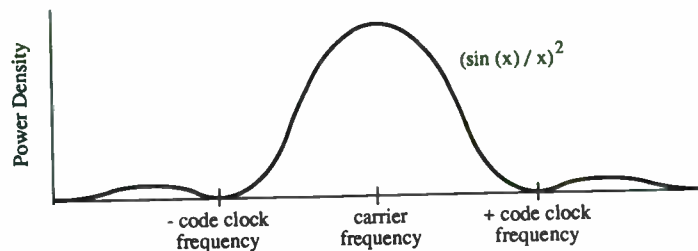


Figure 4 — BPSK Power Density

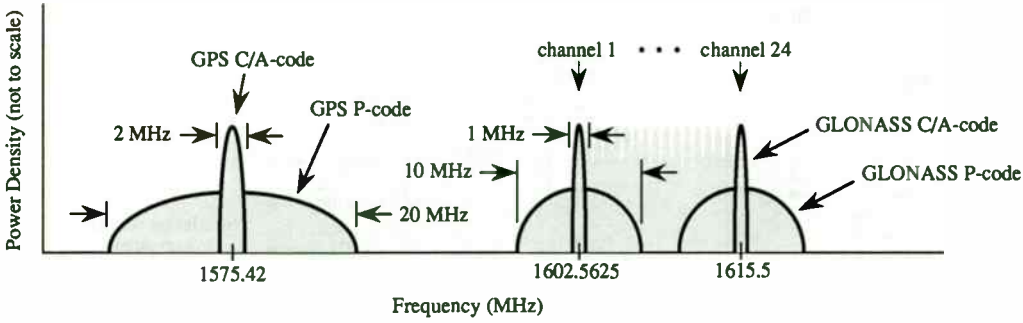


Figure 5 — GPS/GLONASS L1 Spectrum Utilization

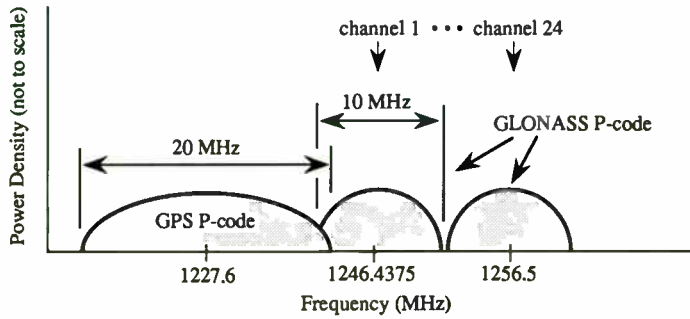


Figure 6 — GPS/GLONASS L2 Spectrum Utilization

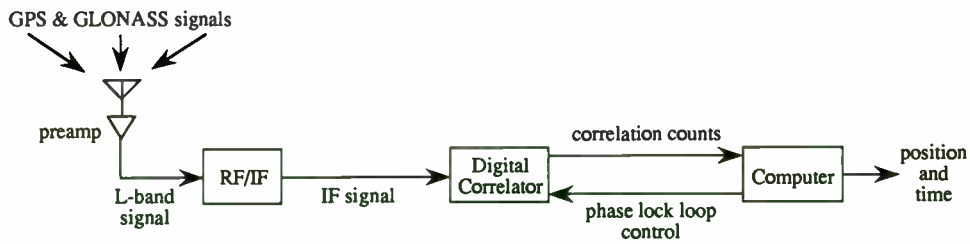


Figure 7 — GPS/GLONASS Receiver

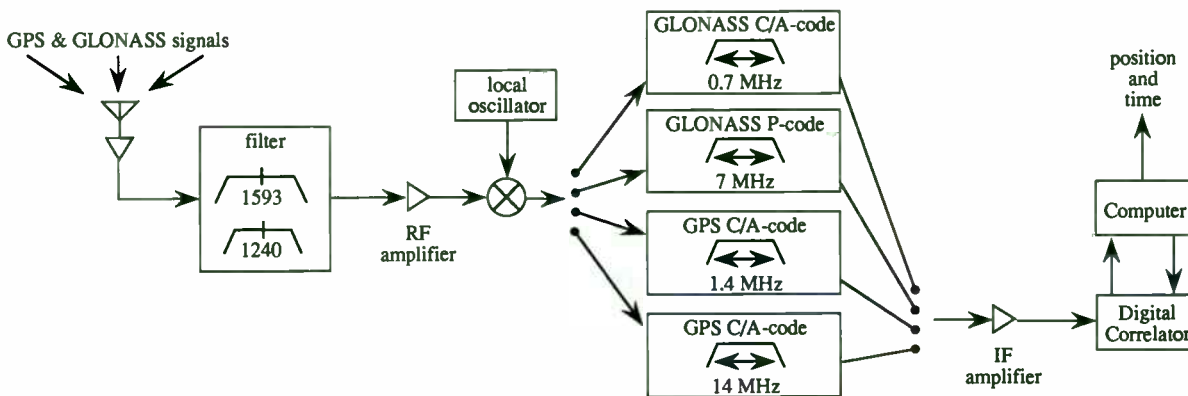


Figure 8 — 3S Research Receiver

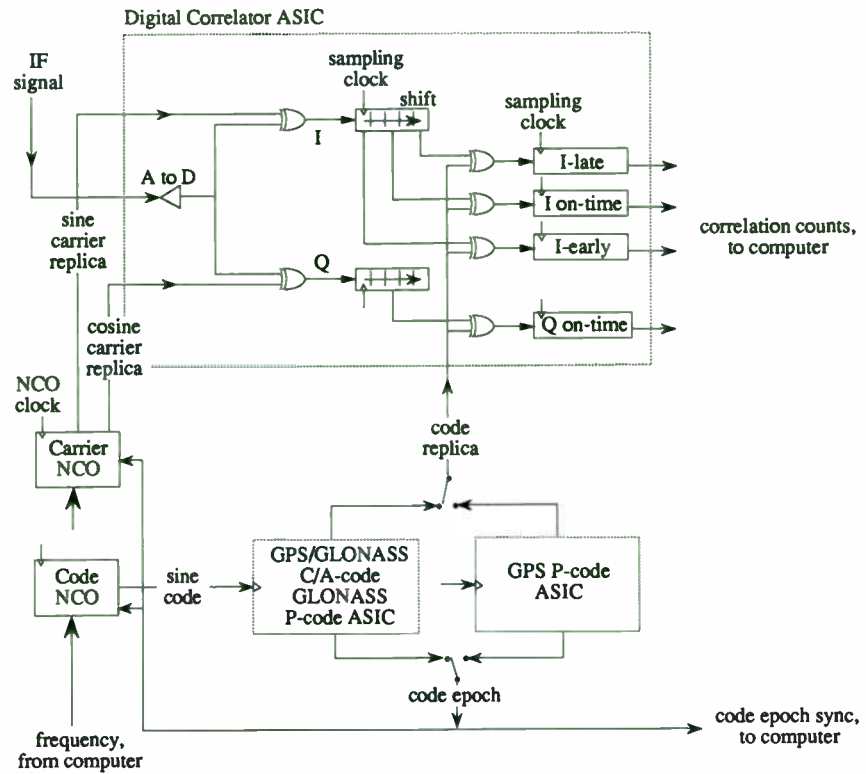


Figure 9 — 3S Research Receiver Digital Processing

Table I — Approximate Strength of GPS and GLONASS Signals [5, 8]

	Signal Power (dBm-Hz)	C/N ₀ (dB-Hz)
GLONASS		
C/A-code	-121	+40
P-code, L1	-132	+41
P-code, L2	-142	+31
GPS		
CA-code	-126	+38
P-code, L1	-129	+45
P-code, L2	-130	+45

Detection and Sorting of Frequency-Hopped Signals

by

Eric Dunn, Steve Russell
Department of Electrical and Computer Engineering
Iowa State University
Ames, Iowa 50011

COPY FROM PAGES 157 THRU 168 HAVE BEEN WITHDRAWN FROM PROCEEDINGS

Ku-Band MMIC Transceiver for Mobile Satellite Communications

Rob Gilmore, Clarence Bruckner, and Doug Dunn

QUALCOMM, Inc.
10555 Sorrento Valley Road
San Diego, CA 92121
(619) 587-1121

Introduction

A fully integrated Ku-Band transceiver utilizing state-of-the-art GaAs MMIC components has been developed for use in a commercial two-way mobile satellite communication system. The current transceiver, with over 500 discrete components requiring an area of 50 square inches, has been reduced to six MMIC chips and an area of 4.2 square inches. The extensive use of integration maximizes the inherent advantages of size, weight, cost, and reliability. The MMIC's are integrated onto an alumina substrate to eliminate the cost associated with individual microwave quality packages. To further reduce the cost, state-of-the-art techniques in thick film are being used for the metallization of the substrate. After a brief description of the OmniTRACS® mobile communication system, this paper will describe the Ku-Band transceiver, the alumina substrate, and the individual GaAs MMIC's.

The OmniTRACS® System

The OmniTRACS® Ku-Band Mobile Communication System became fully operational in August, 1988 to provide reliable, low cost, two way satellite communications and position location to mobile units anywhere in the continental United States. Today the system is in operation in several nations world-wide utilizing Ku-Band transponders on existing satellites. Specifically, the system is in use in the U.S., Canada, and throughout Europe, and in preliminary operational stages in Japan, Mexico, and Australia. Although the principal market to date has been the trucking industry, OmniTRACS® terminals have been installed on tractor-trailers, automobiles, marine vessels, aircraft, fixed sites, and in at least one instance a bicycle. The

OmniTRACS® components consist of the Mobile Terminal installed in each vehicle and the Network Management equipment at a Network Management Center. As shown in Figure 1, individual customer dispatch facilities connect to the Network Management Center to send messages or receive messages from any mobile terminal in their fleet.

The Mobile Terminal consists of three units as shown in Figure 2: the Outdoor Unit (ODU), the Communication Unit, and the Display Unit. The Outdoor Unit consists of a mechanically-steered Ku-Band antenna, LNA, HPA, Ku-Band up and down conversion circuitry, and various control functions. Since the ODU is mounted on the outside of the vehicle, it is subjected to severe environmental extremes as well as significant vibration. As part of a continuing effort to refine the electronics for lower cost, improved versatility, reliability, and manufacturability, plus reduced size and weight, the ODU has recently been re-designed using the latest in GaAs MMIC and thick film process technology. Improved versatility permits a single design to cover the world-wide Ku-Band frequencies, in contrast with three separate versions using the older technology. This paper describes the MMIC Ku-Band transceiver now being phased into production for the OmniTRACS® system. Variations of the OmniTRACS® substrate are currently under development for use in VSAT (Very Small Aperture) Terminals.

The OMNITRACS® Outdoor Unit

Figure 3 is a block diagram of the OmniTRACS® ODU. The world-wide transmit band for the OmniTRACS® system is 14.0-14.5 GHz, and the receive band is one of the following: 10.95-11.7 GHz, 11.7-12.2 GHz, or 12.25-12.75 GHz. The IF passband is 900-1400 MHz for both transmit and receive. The system is half-duplex; the transmitter and the receiver are not active simultaneously. Receive-only and transmit-only substrates are available for VSAT or other full-duplex applications. The diplexer at the left of Figure 3 serves as a low loss connection to the antenna for both Rx and Tx, with the additional benefit of out-of-band filtering.

The transmit section produces 1 Watt of Ku-Band output power over a -15 dBm to +5 dBm range of input IF power without the use of AGC. This is

accomplished using the limiting amplifier and low pass filter at the right of Figure 3. The selection of the OmniTRACS® constant-envelope transmit waveform makes this approach possible. Harmonic generation caused by the limiter, as well as resultant intermodulation products, are reduced to below specification levels by the filters in the transmit chain.

The specifications of the OmniTRACS® front-end over the operating temperature range of -40 to +85° C are:

Receiver

Noise Figure:	2.7 dB max.
Conversion Gain:	45 - 55 dB
IP3:	0 dBm min.
1 dB Compression:	-15 dBm min.

Transmitter

Output Power:	1 Watt (-1, +2 dB)
IF Input Power:	-15 to +5 dBm
Spurious Output:	-45 dBc max.

A single synthesized local oscillator is shared between the transmit and receive functions. This LO is generated directly at 12.0 - 13.9 GHz, and phaselocked to a 10 MHz reference using a 14 GHz +8 prescaler and the QUALCOMM Q3036 PLL Frequency Synthesizer IC. The LO can be set to a fixed frequency, or switched between fixed Tx and Rx frequencies, to support 900 - 1400 MHz block up and down conversion. In a frequency agile mode, the LO can be commanded in 40 MHz steps to support narrowband receive and transmit IF's. The synthesizer settling time is under 50 usec. The phase noise is better than -75 dBc/Hz at 100 KHz offset, and a DRO version is approximately -90 dBc/Hz at 100 KHz offset.

Two coaxial cables connect the ODU to the Communications Unit. One cable carries the transmit and receive IF signals. Also multiplexed onto this cable is DC power, and a subcarrier containing antenna pointing commands and synthesizer frequency commands. The second cable carries the 10 MHz reference to the ODU, and a status/handshake signal from the ODU. A microprocessor in the new ODU design interprets the commands from the

Communications Unit, and sends the status and handshake information to the Communications Unit.

The OmniTRACS® system has to date used a discrete implementation of the ODU, with over 11000 of these units shipped. Although this ODU design has proven to be exceptionally reliable, there are several motivations for a re-design. As OmniTRACS® becomes increasingly international, it is desirable to have a single design which supports all frequency plans worldwide with no component changes. The older design required filter, LO, and LNA changes for different frequency bands. The re-design with GaAs MMIC's also provides lower cost and easier assembly. Finally, the MMIC version affords a major size and weight advantage. The older design is 6.7 inches high, 11.4 inches in diameter, and weighs approximately 9 lbs. The re-design is 4.5 inches high, 11.1 inches in diameter (established by the antenna aperture), and weighs 5.5 lbs. The microwave circuitry in the older design contains over 500 discrete components and occupies an area of 50 square inches. The re-design has been reduced to six MMIC chips, a HEMT LNA stage, and a +8 prescaler, which occupies a total area of 4.2 square inches.

The Transceiver Hybrid

The microwave circuitry is implemented on a 2.0" by 2.1", 25-mil thick alumina substrate. The substrate is 99.6% alumina with thick film gold, thick film silver where appropriate, and thick film resistors and capacitors. Thick film techniques were selected over thin film for cost reasons, and proprietary processing has been developed to achieve the tolerances and edge definition required at Ku-Band. A hybrid approach using chips rather than packaged devices was chosen due to the high cost of Ku-Band packages for MMIC's. The hybrid is coated with Paralene™ to protect against moisture, and a 0.25" high plastic cover is attached. The hybrid has leads spaced 0.1" on center, and may be mounted in a socket or soldered (using flux-less solder) to a printed circuit board. The IF transitions to and from the substrate exhibit excellent return loss through 2.0 GHz, even when socketed.

A block diagram of the transceiver hybrid with the MMIC's highlighted is presented in Figure 4. The active components consist of the HEMT LNA (a

discrete GaAs FET design), MMIC LNA, MMIC Down-converter, MMIC Ku-Band VCO, MMIC Dual IF Amp/Switch, MMIC Upconverter, MMIC 1 Watt HPA, and a 14 GHz GaAs +8 prescaler. Closely associated with the substrate is the QUALCOMM Q3036 PLL IC which phaselocks the Ku-Band VCO. This PLL chip is located on the ODU printed circuit board adjacent to the hybrid. The substrate is designed so that the HEMT GaAs FET LNA in conjunction with the MMIC LNA may both be replaced with a single HEMT MMIC LNA when the appropriate technology becomes available. With the exception of the Downconverter MMIC (a commercially available component), each of the MMIC's was developed specifically for this application.

Each MMIC is RF and DC tested on wafer prior to scribing. Before substrate assembly, the substrate itself is tested for proper ϵ_r , trace integrity, and thickness by characterizing a test filter. After assembly, the complete substrate is RF tested. This is facilitated by extensive Built-In-Test. Most of the MMIC's provide a detected output voltage indicating signal strength, and coupled samples of various RF signals are brought to the edge for test.

The substrate layout is presented in Figure 5. Brief descriptions of the passive circuitry are provided below. Each passive circuit is a distributed design. Thick film resistors and capacitors are used only for bias circuits and for terminations. A typical 24 pf bypass capacitor measures .02" x .02" and has a self-resonant frequency of approximately 8 GHz.

The diplexer is a bandpass/bandstop approach with a receive bandpass of 10.95-12.75 GHz and a transmit-arm bandstop filter centered around the receive passband. The transition from the antenna feeds the diplexer approximately at the center of the substrate. The receive arm has an additional notch at the upper stopband edge to enhance image rejection.

The HEMT LNA stage follows the receive section of the diplexer. A discrete GaAs FET design uses a FET with a noise figure below 1.0 dB. The discrete LNA is followed by a MMIC LNA. As previously mentioned, the intent is to replace both of these LNA stages with a single HEMT MMIC as the technology becomes available. Prior to downconversion by the MMIC downconverter, the image is rejected by a coupled line microstrip bandpass

filter. This is a wideband design with a passband of 10.95 - 12.75 GHz. Two additional notches are provided on the upper stop band to enhance image rejection. The signal is then processed by the Downconverter MMIC and the Dual IF Amp/Switch MMIC. The Downconverter provides broadband conversion to the 900-1400 MHz IF. The Dual IF Amp/Switch provides 15 dB of IF gain, and also an IF T-R switch.

The transmit section begins with 30 dB of IF gain and a hard limiting function in the Dual IF Amp/Switch. The limited output is filtered by a 7-section elliptical lowpass filter to reduce harmonic content. After conversion to Ku-Band in the Upconverter MMIC, the signal is filtered by a 14.0 - 14.5 GHz coupled line microstrip bandpass filter. The difference between the even mode and odd mode impedances results in dispersion in this filter, a problem which is solved by inclusion of a partial cover over the coupled lines. The cover effects the even and odd mode impedances differently, which permits the velocities to be equalized. (No dispersion would have resulted if this particular filter was constructed on thinner material with a lower ϵ_r .) An additional notch is added to the upper stop band of this filter to improve the 2 x IF + LO rejection at 14.9 GHz. The Ku-Band signal is then applied to the 1 Watt HPA, and then on to the diplexer.

The GaAs MMIC's

Six GaAs MMIC's are used on the transceiver substrate (seven if the +8 prescaler is considered a MMIC). Of the six, two were designed in-house at QUALCOMM - the Upconverter and the Dual IF Amp/Switch, and two more (the HPA and the LNA) were designed at Hughes Microwave Products Division (Torrance, CA) with the participation of QUALCOMM personnel. The Downconverter MMIC is a commercially available design, and the VCO is a custom version of an off-the-shelf design. Block diagrams and performance data for the Dual IF Amp/Switch, Upconverter, LNA, and HPA are given in Figures 6 - 9 respectively. Brief descriptions of these designs are given below.

Dual IF Amplifier/Switch

The Dual IF Amplifier/Switch is comprised of three components, an IF receive amplifier, an IF limiting amplifier, and a single pole double throw switch.

To meet the IF receive amplifier specifications of gain, gain flatness, and input and output VSWR, a three stage feedback amplifier was used. Employing feedback provides extremely flat gain, good VSWR, and a very stable amplifier. Perhaps most important, the feedback topology will provide an amplifier with a high yield.

The transmit IF limiting amplifier is designed to have a saturated output of +9 dBm with an input level of -15dBm. In order to assure the amplifier is saturated, four 600um MESFET's are used to drive a 240um output MESFET. Simple reactive matching is used at the input and output of the amplifier, while the interstages employ lossy matching. The resulting amplifier has a gain of 30 dB in-band and is very flat. A feedback approach was not selected because it would have required one additional gain stage, and the stability of the amplifier would have been degraded.

The single pole double throw switch provides a common point for the input of the limiting amplifier and the output of the receive amplifier. The switch prevents the amplifiers from interacting by providing greater than 25dB of isolation between the on port and the off port, and it introduces only 0.5dB of insertion loss. The switch is realized with two 500um x 1.0um MESFET's used as series switches.

The Dual IF Amplifier/Switch is 2291um x 2455um x 100um. It was fabricated using 0.5um and 1.0um MESFET structures on selectively ion implanted material.

Upconverter

The MMIC upconverter was one of the most challenging devices to develop because of the required output power. The upconverter specification was derived by determining the IF power level which would be available from the Dual Amplifier/Switch limiting amplifier, the available LO drive level from the VCO and the power level needed to drive the power amplifier into compression. The specifications of all four MMIC's had to be examined so that the best trade-offs for performance and yield could be made for all the

devices. The upconverter can be divided into three functions, LO amplifier, RF amplifier, and mixer.

The LO amplifier was determined to need a minimum of 6dB gain from 12.5GHz to 13.8GHz. This is possible to achieve with a single stage amplifier using single stub matching circuits on the input and output. A self bias FET was used to simplify the bias of the complete chip. The resulting amplifier has 10dB gain with an input VSWR of better than 2:1.

The RF amplifier must provide 20.5dBm of output power with the input available from the mixer. This requires that it have 28 dB of gain. In order to meet this goal a four stage amplifier employing a broadband matching topology was designed. To allow for process variations, the amplifier was designed to have 32 dB of small signal gain.

The mixer was considered to be the highest risk item because it was desired to keep the spurious levels to a minimum. Two approaches were considered, the balanced passive FET mixer and the balanced diode mixer. The balanced FET mixer is known to have superior spurious rejection, however it requires an IF balun and was found to have a slightly higher conversion loss than the diode mixer. An active FET balun was designed for use with the FET mixer. It was found that the IF drive level required to get the lowest conversion loss was much higher than for the diode mixer which has no balun.

Two MMIC upconverters were fabricated, one with the FET mixer and one with the diode mixer. It was found that the diode upconverter produced 20.5dBm output power, while the FET version produced 19dBm. The spurious output of both versions were almost identical. The diode upconverter has been chosen for use in the system because it requires lower drive levels and less current than the FET version.

The upconverter is 2838um x 2436um x 100um. It was fabricated using 0.5um MESFET structures on selectively ion implanted material.

LOW NOISE AMPLIFIER

The low noise amplifier is a two stage amplifier employing two 300um x 0.5um FET's. The circuit makes use of self biasing so that only a single supply voltage is needed. The amplifier has a gain of 14dB with 4dB noise figure.

High Power Amplifier

Two topologies were explored for the HPA, a single-ended topology and a balanced topology. The single-ended amplifier has slightly higher gain and output power since there is no loss due to input and output couplers. The balanced design was selected due to superior input and output match and excellent stability. The balanced power amplifier consists of two three-stage amplifiers combined with Lange couplers. The amplifier produces 31dBm minimum saturated output power with a 16dBm input drive.

The HPA is 3912um x 2819um x 100um. It was fabricated using 0.5um MESFET structures on selectively ion implanted material.

Conclusion

A fully integrated Ku-Band transceiver has been described which represents the latest in MMIC and thick film technology. The design incorporates single chip implementations of a Ku-Band upconverter, a Ku-Band downconverter, Ku-Band HPA, LNA, VCO, and a dual IF amp/switch. In addition, the design implements a Ku-Band frequency agile local oscillator using 4 active devices: a MMIC VCO, a 14 GHz +8 prescaler, the QUALCOMM Q3036 PLL, and an op amp loop filter. Thick film techniques, formerly used only at the lowest microwave frequencies, have been successfully employed at Ku-Band to achieve significant cost savings. The extensive use of integration maximizes the inherent advantages of size, weight, cost, and reliability. The design also increases the versatility of the product by providing an agile outdoor LO, and also by providing a single design for world-wide coverage.

Acknowledgement

The Ku-Band ODU re-design effort has been a team effort involving many individuals. In particular, the authors wish to thank Bill Johnston, Rick Dewey, Bill Schoenbeck, and Doug Moe of QUALCOMM, Inc., and Leo Fong of Hughes MPD.

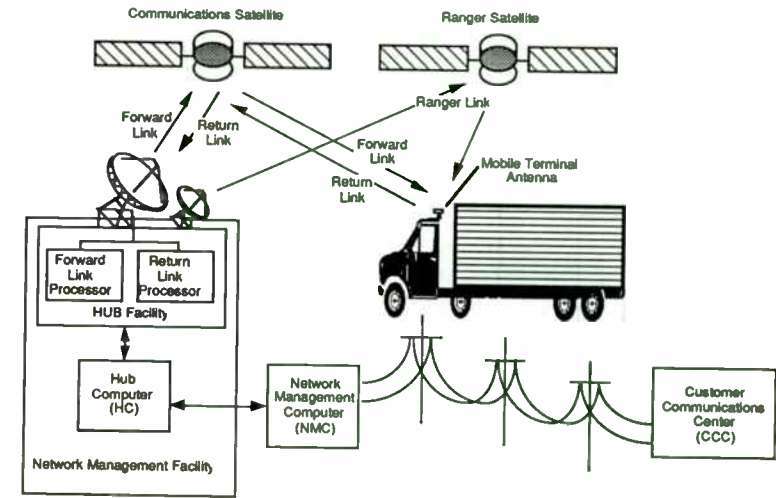


Figure 1: The OmniTRACS® System

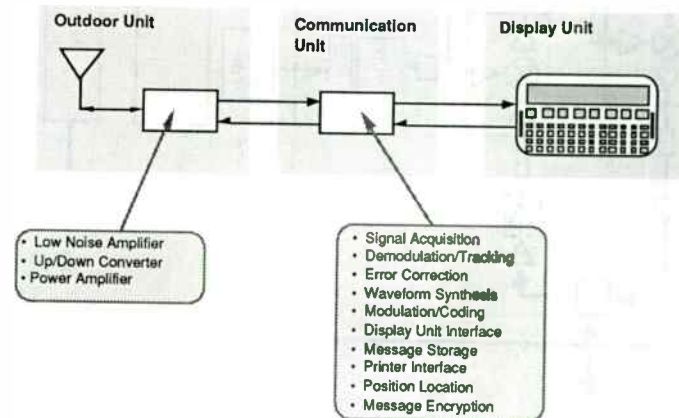


Figure 2: The OmniTRACS® Mobile Terminal

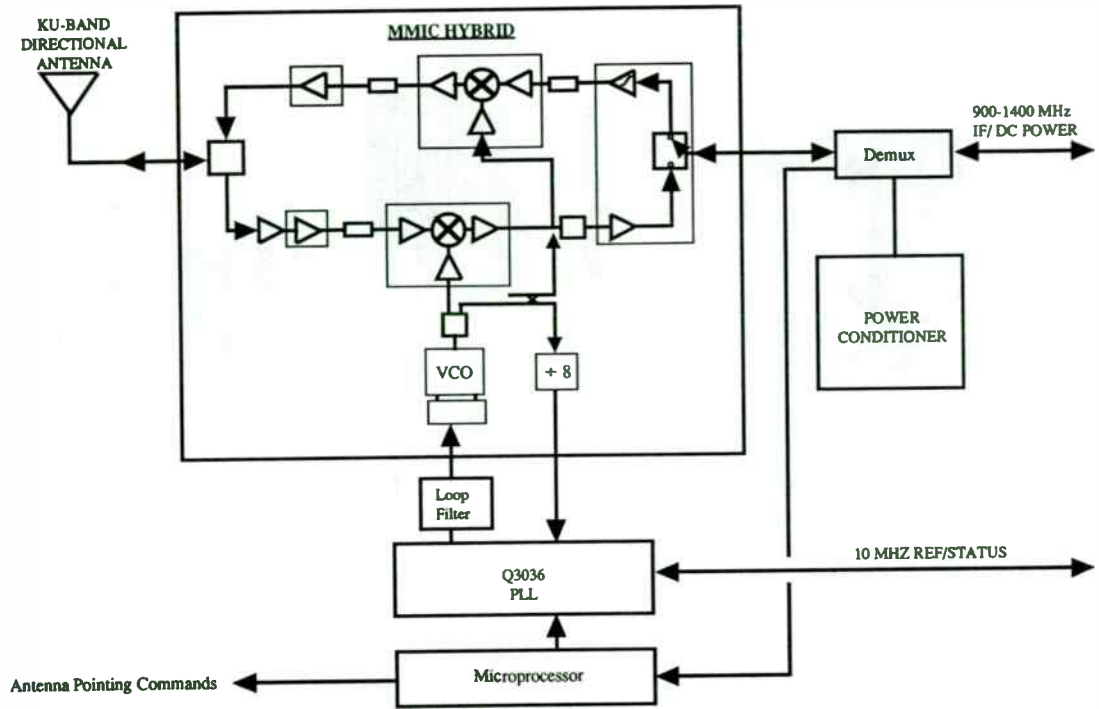


Figure 3: OmniTRACS® Outdoor Unit Block Diagram

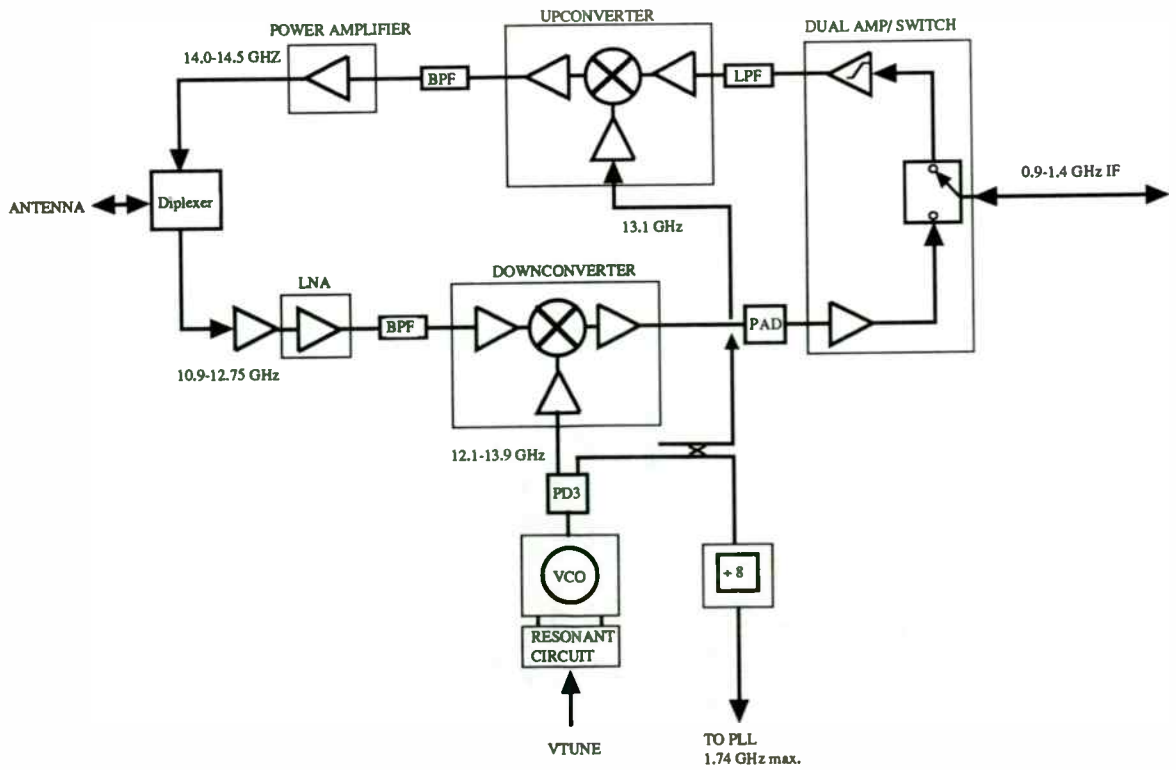


FIGURE 4: TRANSCEIVER HYBRID BLOCK DIAGRAM

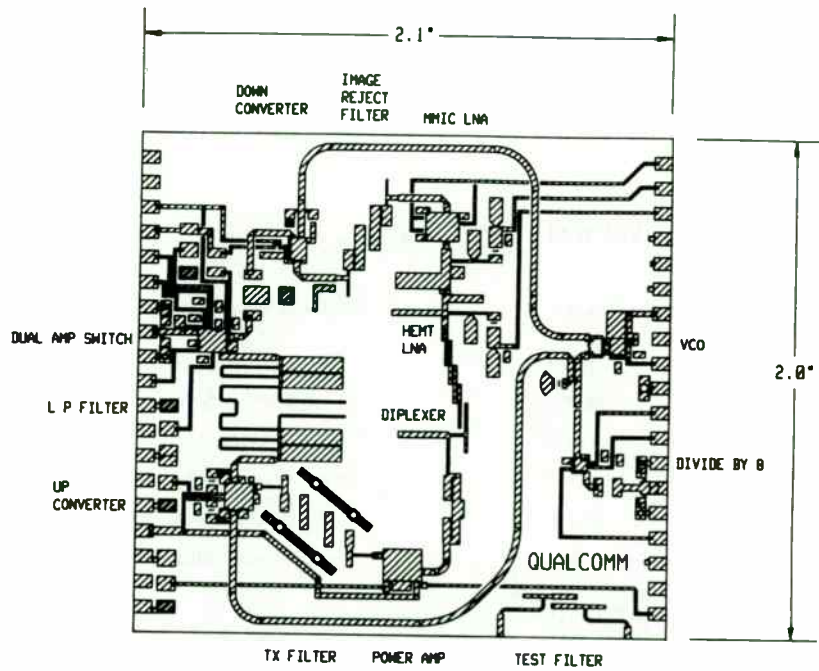
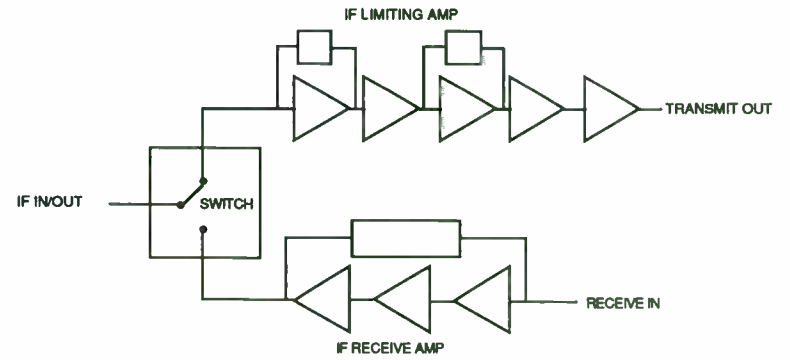
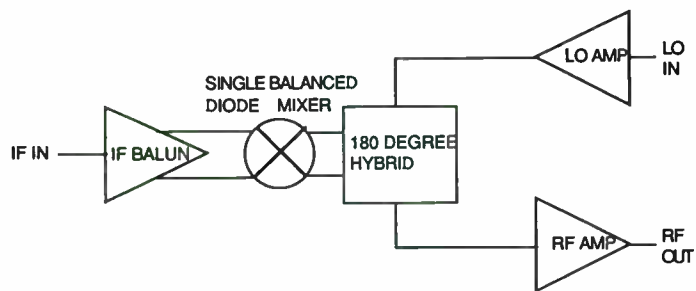


FIGURE 5: TRANSCEIVER SUBSTRATE



ALL PORTS:	PERFORMANCE
FREQUENCY	0.7-1.7GHz
VSWR	<2.0:1
RECEIVE PATH:	
GAIN	14.5 dB
GAIN VARIATION	± 0.5 dB
NOISE FIGURE	4 dB MAX.
IP3	>10 dBm
1 DB COMPRESSION	+0 dBm
TRANSMIT PATH:	
LIMITED OUTPUT	+9 dBm ± 1 dB -15 to +5 dBm INPUT
HARMONICS	> 14 dBc (SECOND) > 17 dBc (THIRD)
DC POWER CONTROL:	
OPERATING TEMPERATURE RANGE:	ABILITY TO TURN OFF POWER IN UNUSED PATH -40 TO +85 DEG. C

FIGURE 6: DUAL IF AMP/SWITCH MMIC



FREQUENCY

RF PORT
LO PORT
IF PORT

IF INPUT POWER:

RF OUTPUT POWER:

POWER OUT VARIATION:

LO DRIVE:

LO-RF ISOLATION

VSWR (ALL PORTS)

OPERATING
TEMPERATURE RANGE:

PERFORMANCE

13.5 - 15 GHz
12.5 - 13.8 GHz
700 - 1700 MHz

+8 dBm MIN.

20.5 dBm

± 1.2 dB VS TEMP

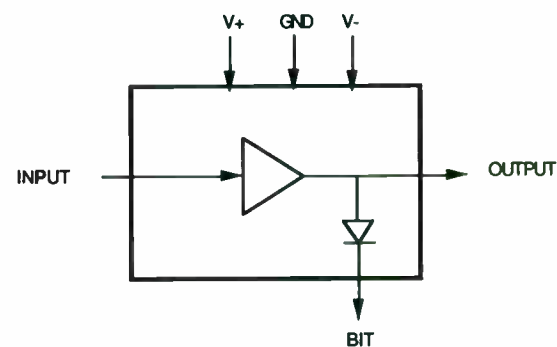
0 ± 2 dBm

>20 dBc

<2.0:1

-40 TO +85 DEG. C

FIGURE 7: UPCONVERTER MMIC



PERFORMANCE

FREQUENCY:

10.5-13.0 GHz

GAIN:

13.5 ± 1.5 dB

NOISE FIGURE:

3.5 dB NOM

IP3:

5 dBm

1 dB COMPRESSION:

0 dBm

VSWR:

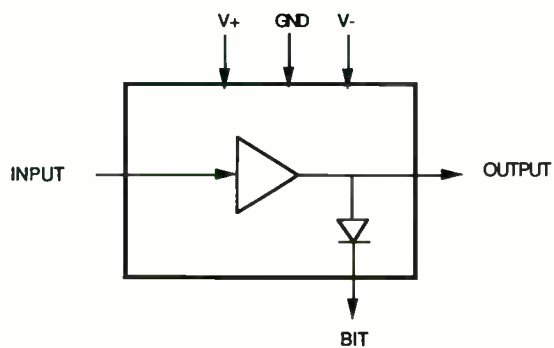
INPUT
OUTPUT

<2.5:1
<2.0:1

OPERATING
TEMPERATURE RANGE:

-40 TO +85 DEG. C

FIGURE 8: LNA MMIC



	PERFORMANCE
FREQUENCY	14.0-14.5 GHZ
POWER OUT	31.5 ±1.5 DBM (INTO 1.5:1 VSWR) (INPUT POWER=+16±2 DBM) (-40 TO +70 C) 28.5-33 DBM (+70 TO +85 C)
LINEAR GAIN	17 DB MIN.
GAIN VARIATION	± 0.25 DB OVER ANY 40 MHZ
INPUT VSWR	<2.0:1
BUILT-IN-TEST(BIT)	DC OUTPUT PROPORTIONAL TO POWER OUT (Vo> 50 mV into 10K ohms, Po> +30 dBm)
DC POWER	8 ± 0.8 VDC @ 1 AMP MAX. -5 ± 0.5 VDC @ 20 MA. MAX.
OPERATING TEMPERATURE RANGE:	-40 TO +85 DEG. C

FIGURE 9: HPA MMIC

SILICON MMIC'S
35 dB - 35 dBm - \$35

by

T. BOLES, M. DIESS, D. OSIKA
SGS-Thomson Microelectronics
Commerce Drive
Montgomeryville, Pennsylvania, 18936

Introduction

Over the last several years, the demands placed on the frequency band from 800 MHz to 1.0 GHz have grown in both usage and complexity. The usages vary from commercial mobile communications, i.e. cellular radio; fixed special remote services, i.e. meter reading, anti-intrusion alarms, etc.; amateur radio; aeronautical communication and navigation, i.e. DME/IFF; and scientific and space applications. The complexity of specific performance requirements is vastly different from one application to another and ranges from relatively low power, CW needs of a handheld mobile radio to the multihundred watt, low duty, pulsed power requirements of DME/IFF systems.

One area of the above frequency usages which has undergone a large change from a device requirement point-of-view, centers on applications which need low to medium, CW output power. The changes in the required devices have been driven by the volume/cost constraints placed by the various end marketplaces. The major end-use area that comes to mind lies in cellular radio, which has shown large growth in its usage while simultaneously driving ambitious cost goals to further enhance the system customer base. A second market which is somewhat less glamorous but has

the same type of both RF performance requirements and volume/cost objectives lies in the area of remote automatic meter reading.

Initial device/system design approaches for both of these applications started with a lineup of discrete packaged devices which were further assembled into a high frequency amplifier to achieve the RF performance levels required by the operating system. Cost and manufacturing volume factors, especially in the area of cellular radio, has rapidly driven the packaged device amplifier design approach to the present hybrid chip and wire module concept.

In response to the above needs for moderate power level amplifiers, both from an ease of manufacturability and cost reduction considerations, an internal program at SGS-Thomson has developed a medium power, CW lineup of devices which will deliver approximately 35 dBm (3.1 watts) of RF output power with a minimum gain of 35 dB at 900 MHz utilizing monolithic circuits in place of discrete devices whenever possible. While the internal development work was performed using packaged circuits and devices, the conversion to a chip and wire hybrid should be significantly less difficult when compared to the same type of assembly using discrete transistors. This lineup consists of a combination of two silicon Monolithic Microwave Integrated Circuits (MMIC) and a discrete NPN bipolar transistor as the output stage. Details of the design approach are presented below.

MMIC Design

Each of the silicon MMIC's, which constitute the initial two stages of the amplifier, consist of a Darlington coupled pair of high frequency bipolar transistors which have an on-chip biasing and resistive feedback network. A typical schematic configuration is shown in Figure 1. The transistor geometry employed on the silicon MMIC's is a fine line interdigitated structure having one micron metal fingers with a 4.8 micron emitter-to-emitter "pitch". A sub-half micron ($0.4 \mu\text{m}$) emitter width is utilized to minimize emitter-base capacitance and its associated "shot-noise" and maximize the device frequency response. These device dimensions translate to an EP/BA figure-of-merit for the individual transistor stages of approximately $0.41 \mu\text{m}^{-1}$ (10.5 mil^{-1}). A collector field build-up utilizing LOCOS technology to reduce parasitic stray MOS capacitances has been integrated into the device design and circuit fabrication. The device cross-sectional profile is obtained entirely by ion implantation, utilizing boron to form the base and P+ junctions, while arsenic is used as the emitter dopant. The result of the above design parameters is a minimum device f_t of 7.0 GHz.

A proprietary, RF lifetested, refractory barrier/gold metallization system to insure reliable, long term operation (a MTF greater than 10^6 hours at a T_j of 150°C is projected) is employed for all circuit and device interconnections. For added reliability and circuit ruggedness, thin film metals are NOT USED to form the resistive feedback and biasing elements, instead arsenic ion implanted polycrystalline

silicon is exclusively utilized for all resistive elements. The use of this material reduces the current density in the resistor films by at least a factor of five, which coupled with the intrinsic high temperature properties of the material itself, greatly increases the reliability of the overall circuit.

Referring to Figure 1, the actual circuit values for the resistive feedback elements, R_f and R_e , are chosen, using a "SPICE" optimization routine to provide both a resistive match to 50 ohms on the circuit input and output, and the obtain the desired overall circuit gain and gain versus frequency characteristics. Once the specific R_f and R_e resistor values are chosen, the remaining circuit elements, R_b and R_{bias} , are fixed simply by DC biasing requirements. The overall circuit -1dB compressed output power is determined by a combination of the emitter periphery (physical size) of the output stage of the Darlington pair, the chosen DC bias point, and the resistive RF feedback networks. Overall circuit noise figure for the MMIC's is limited not only by the intrinsic noise of the two devices in the Darlington pair but also by the total circuit current that is flowing through the input DC biasing/feedback leg, $\{R_f + R_b\}$.

In order to further optimize the total RF performance of the silicon MMIC's, an additional resistive component can be added to allow the DC bias point to be optimized independent of some of the required RF feedback considerations. This circuit concept is shown in Figure 2. As can be seen the additional elements are

labeled R_{fb} and C_{fb} . The C_{fb} element, which is provided external to the MMIC die but within the high frequency package, is simply a DC blocking capacitor which allows the R_f resistor to serve only as part of the voltage divider network needed to set the first and second stage DC bias points. The required RF feedback is provided by the additional resistive element R_{fb} , which is incorporated on the MMIC die and electrically connected to C_{fb} via bond wires. The value of this resistive feedback element is chosen as described previously by using "SPICE" to model the active and passive circuit components. With this approach, the overall circuit gain, gain flatness, compressed output power, DC bias point, and noise figure can be more easily and independently optimized.

The silicon MMIC's, which are used as the predriver and driver stages for the medium power cascaded amplifier, are constant current structures as opposed to operating from a fixed voltage supply. If the devices are not operated from a constant current source, the proper Class A, DC bias point will not be obtained on either device in the Darlington pair. This will be demonstrated, in terms of RF performance, by large variability both in gain and saturated output power from unit to unit.

Since resistive feedback elements are the only components used to obtain a 50 ohm input and output match, the silicon MMIC's are extremely broadband devices. Typical bandwidths for these structures range from virtually DC to 1.5 GHz, the

only limitation at lower frequencies being the value of the external DC blocking/RF coupling capacitors which are used between amplifier stages.

A consequence of using the resistive match/multi-octave bandwidth approach is that it requires the circuit be operated in a Class A mode. Operation in Class AB, Class B, or Class C is possible, but because there are no reactive components used in the output circuit, the stored energy within the device during the "off" half-cycle cannot be extracted. This essentially limits the circuit compressed output power to one half or less when compared to Class A operation.

MMIC Predriver/MMIC Driver Stages

The predriver stage of the medium power cascaded amplifier is a modified SGS-Thomson AMP0910 silicon MMIC, which is configured as shown in the schematic in Figure 2. This device operates at a fixed current of 45 mA and at a supply voltage of approximately 6.5 volts. The AMP0910 was chosen as the first stage of the amplifier line-up because it exhibits both high small signal gain (≈ 15 dB) and a moderate level of -1 dB compressed output power (≈ 14 dBm) over the 800 MHz to 1.0 GHz band. Typical RF performance data from 300 MHz to 1.0 GHz is presented in Figure 3.

The AMP0910 modification occurred "off-chip" during the assembly of the packaged device. In this case the C_{fb} is eliminated, which RF isolates the R_{fb} feedback

resistor and causes the R_f resistor to serve as both a feedback and bias element. The net result of the elimination of the $\{C_{fb}$ to $R_{fb}\}$ feedback path is that the low frequency gain of the AMP0910 is increased at the expense of gain flatness below 500 MHz. However, with the AMP0910 device there is little noticeable effect over the 800 MHz to 1.0 GHz band as can be seen in Figure 3.

The second stage of the amplifier chain is a standard SGS-Thomson AMP0520 silicon MMIC, which is again configured as shown in the schematic in Figure 2. This device operates at a fixed current of 165 mA and at a supply voltage of approximately 12.5 volts. The AMP0520 enables output power levels of approximately 0.25 watts (23.5 dBm) with approximately 8.5 dB of power gain to be readily obtained over the desired 800 MHz to 1.0 GHz band with no external matching required other than 50 ohm lines. Also, because the dissipated power levels within this second stage are reaching moderate levels, heat sinking of the device through a BeO based package is required. Typical RF performance data, again from 300 MHz to 1.0 GHz, is presented in Figure 4.

Operational Modes For Discrete Output Device

A discrete NPN power transistor is used as the third stage in this amplifier chain and the bias point for the transistor has to be provided external to the die. The final stage of this cascaded amplifier can be optimized for the users specific application or their specific system requirements. By changing its mode of operation, bonding

configuration, or power capability a final custom design could be monolithized or hybridized into one multi-lead package or module.

The four major amplifier classes which will be discussed are Class A, Class B, Class AB, and Class C. These various groups of amplifier classes are described and contrasted in the following section.

A Class A amplifier requires that a DC voltage is placed across the base to emitter junction which causes a base current to flow raising the collector output current to a desired quiescent point (I_{CQ}). A RF signal swings around this input bias point and is translated to the output with an associated gain. When the RF output current swing is equal to I_{CQ} in amplitude the device goes into -1dB power gain compression and distortion occurs.

To compensate for variations in temperature or H_{fe} , typically some emitter resistance is introduced to provide stability and prevent oscillations or thermal runaway. Some emitter resistance is even introduced at the chip level to enhance current sharing in the device through debiasing effects. Class A operation offers an inherent linearity advantage over the other classes but may put unsatisfactory conditions on system power requirements and thermal management. If signal purity is a prime requirement Class A will provide the best low distortion amplification with a minimum of circuit design and construction.

Amplifiers can be operated in a Class B mode where the input of the device is biased off or no bias is applied and the input RF signal is used to provide the necessary voltage swing to drive the device into conduction. A Class B amplifier will have lower gain than that of an equivalent Class A one and the output signal will contain more harmonic power. These spurious signals are generated by the nonlinear turn on characteristics of the transistor and the nonsinusoidal output waveform due to halfwave amplification. A lack of signal clarity is an obvious disadvantage when operating in this mode. A major reason for Class B operation is to achieve RF power levels not possible in devices having low RF conversion efficiency thus leading to unacceptable levels of power dissipation. The DC operating point of a RF power transistor biased for Class A mode has a theoretical collector efficiency of 50% whereas one in Class B mode is 78% and if the output waveform is squared-off, even higher efficiencies are possible.

In Class AB the input bias point of the transistor is placed between the above two modes. This allows the user to achieve some of the desired properties of both modes. Allowing a small bias current to flow can improve the gain of the transistor without a large impact on the collector efficiency of the device; however, stability requirements will be increased.

Class C operation of a transistor has a period of amplification which is less than 180° of a full cycle. The RF input signal is used to turn on the device which is normally not in conduction. The device is not consuming power when no input

signal is applied; therefore, the highest efficiencies and power levels are achieved in this class of operation. Reactive tuned matching circuits must be used to remove signal distortion and to provide power to the load while the device is not conducting. The disadvantage of Class C operation is the lack of linearity and reduced gain when compared to Class B and Class AB amplifiers.

Amplifier Output Stage Performance

The first design approach utilized the SGS-Thomson 80725 linear power transistor as the output device for the two stage MMIC drivers. This part was designed and has been used for linear power generation up to 4.0 GHz in other applications. Using microstrip circuit boards with variable trim capacitors, a good interstage and output load match to 50 ohms was achieved at 920 ± 20 MHz. This common emitter device was operated Class A and from an 18 volt collector supply. The quiescent bias current was 450 mA and the associated total system gain and -1db compressed power are shown in Figure 5. Collector efficiency was 20% at 900 MHz for the output device, which is essentially the total amplifier power added efficiency, and could be improved by using fix tuned matching circuits. This cascaded amplifier had an overall noise figure of 2.8 dB at 900 MHz which was largely due to the high gain and low noise figure of the first stage.

A second approach, aimed at improving the -1dB compressed output power level and overall power added efficiency, was to use a Class C output stage in the cascaded amplifier. Using SGS-Thomson's common base NPN transistor 82003,

developed for Class C operation at 28 volt, additional data over the 920 ± 20 MHz range was taken. Figure 6 shows the -1dB compressed output power versus frequency for a range of voltages from 18 to 28 volts. Since this part was operated Class C the overall system power gain reflects a decrease in power gain when compared to the complete amplifier chain being operated in a Class A mode. However, higher power levels of up to 35 dBm (3.1 watts) were now achieved with the goal of 35 db total system gain still being met. The Class C operation of the output stage of this cascaded amplifier also enabled the amplifier conversion efficiency at 900 MHz to be improved from approximately 18% to 43%, but with a trade off in signal linearity.

The above three stage line-up of devices was chosen not only to meet the given RF performance level, which was achieved, but also had a cost objective that would allow the entire chain to be sold for a maximum of \$35. The complete "packaged" set of silicon MMIC's and a discrete power transistor, with some difficulty, met this goal. For chip and wire hybrid/module amplifier applications, the device line-up is available in die form, which should enable the same RF performance levels to be achieved and the above target price improved.

Conclusion

Long term, end users of 900 MHz medium power amplifiers should not be surprised when they read about the entire power/gain block being available in a truly monolithic form on one piece of semiconductor material. Advances which have

already occurred in isolation techniques now allow multi-stage, small signal, monolithic amplifiers to be realized. The only technology development that remains is to incorporate the required large element values needed for reactive matching circuits and the interstage coupling capacitors for the Class A/Class AB/Class B/Class C power output stages. Whether this occurs first and most economically on III-V compounded material or silicon is the only remaining question.

FIGURE 1 – SILICON MMIC DARLINGTON CIRCUIT DIAGRAM

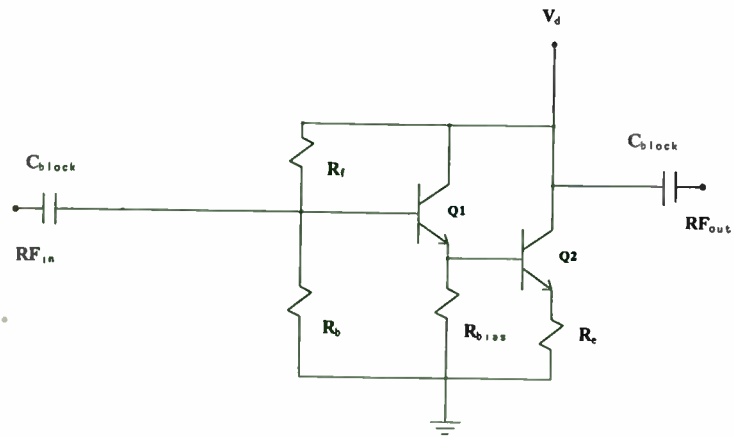
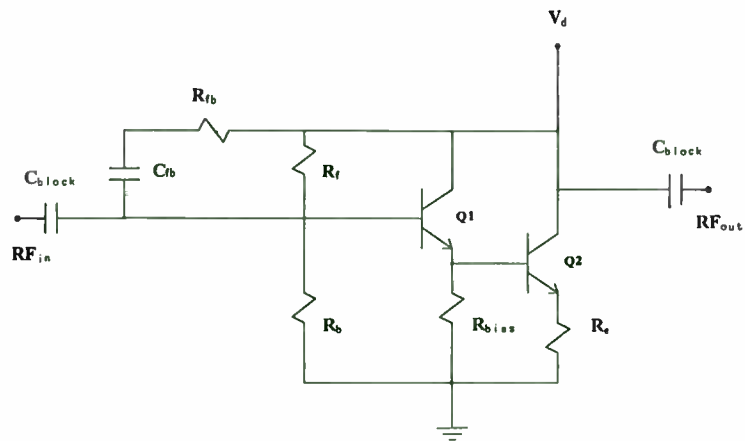
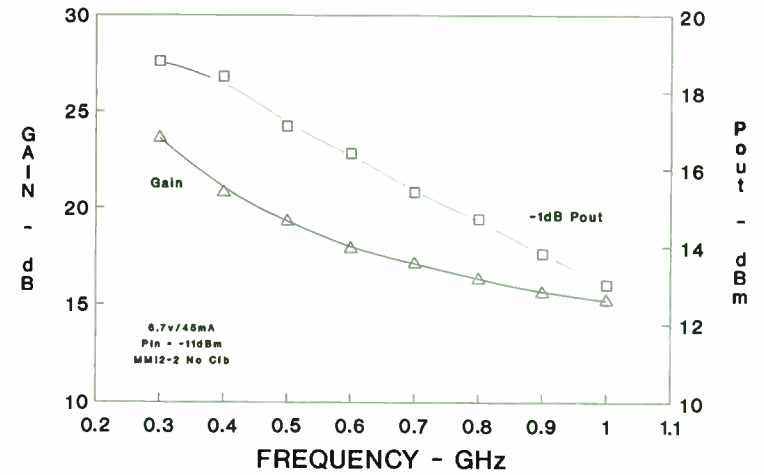


FIGURE 2 – SILICON MMIC DARLINGTON CIRCUIT DIAGRAM WITH BIAS AND FEEDBACK OPTIONS



**FIGURE 3
AMP0910 RF PERFORMANCE DATA**



**FIGURE 4
AMP0520 RF PERFORMANCE DATA**

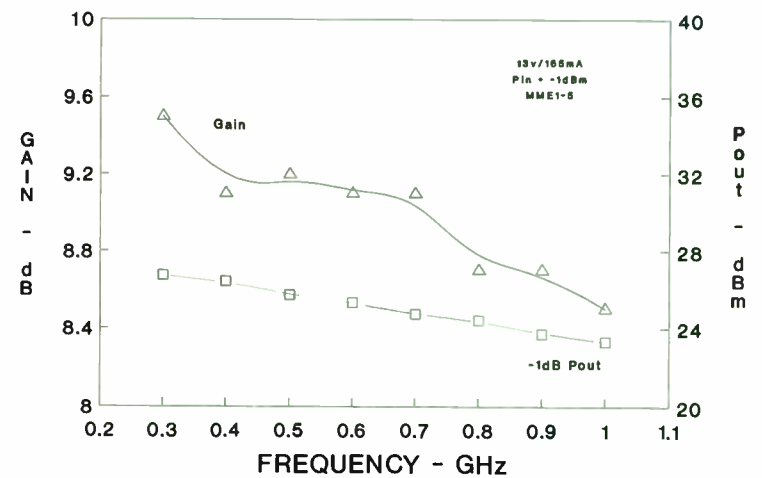
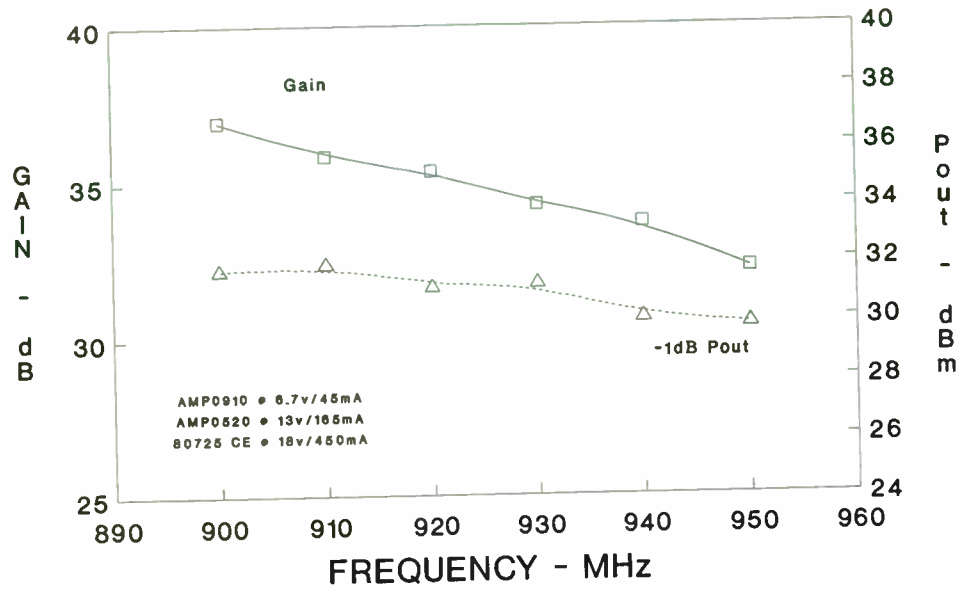
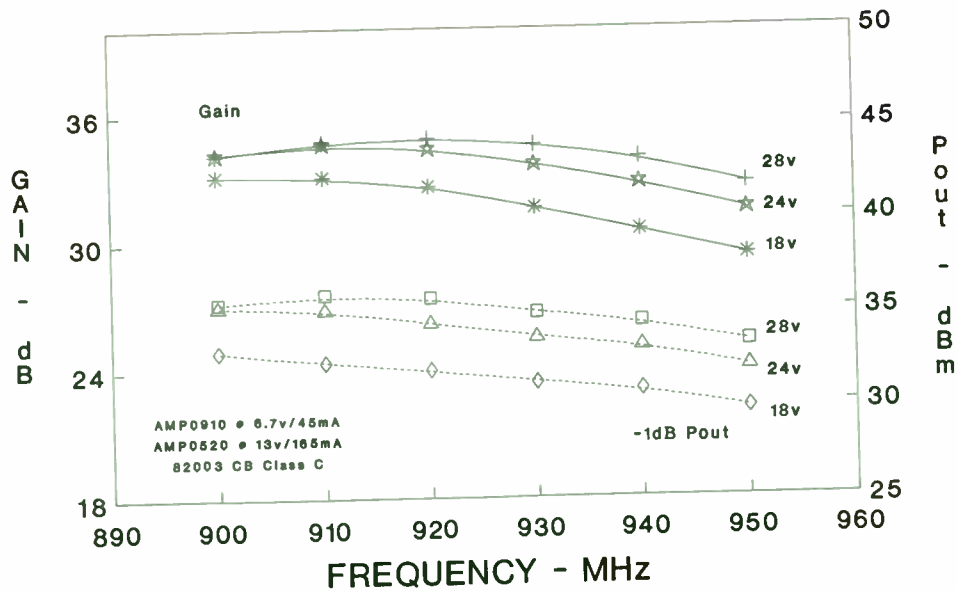


FIGURE 5
CASCADED AMPLIFIER RF PERFORMANCE DATA
(CLASS A OUTPUT)



186

FIGURE 6
CASCADED AMPLIFIER RF PERFORMANCE DATA
(CLASS C OUTPUT)



by

Robert J. Weber
Department of Electrical Engineering and Computer Engineering
and
Microelectronics Research Center
Iowa State University
Ames, Iowa 50011

Abstract

Technology advances over the past decade have resulted in a large number of small signal MMICs (monolithic microwave integrated circuits) becoming commercially available. It is also possible to produce high power (>10 watts) MMICs. However, several design constraints and tradeoffs concerning thermal limitations, chip size, available components, market, etc. are variables which must be considered whenever a power MMIC is considered.

This paper discusses:

- Power Capabilities
- Circuit Types/Stability
- Inductor availabilities, limitations, and alternatives
- Thermal considerations
- Device Isolation Techniques

for L-Band power MMICs in the range of tens of watts for CW devices and several 100s of watts for pulse power devices.

Introduction

This paper will address one small segment of the monolithic circuit technology - that of power microwave monolithic integrated circuits (MMICs). Specifically, the technology to be discussed is that of L-band (nominally 1 GHz) power MMICs. The technology covered in this paper is applicable to

either silicon or gallium arsenide semiconductor based integrated circuits. However, most of this paper will discuss silicon MMICs. Many of the design considerations are equally valid for GaAs and other III-V semiconductor device MMICs.

Many analog monolithic integrated circuits have been introduced to the industry during and since the decade of the 1960s. The industry standard 741 operational amplifier was introduced to the industry in 1966 and has been a "standard" integrated circuit for many years. It contains several transistors, resistors, and a capacitor. The technology available during that decade produced an integrated circuit with megahertz bandwidths. Over the intervening two decades, monolithic integrated circuit technology has continued to develop. Advances in lithography, etching, and implantation have been just some of the technologies which have helped the industry advance the monolithic integrated circuit technology. The early monolithic circuits were high impedance, low power, low frequency circuits. Parasitic inductance becomes very important in low impedance power circuits. Parasitic capacitance becomes very important in high frequency microwave circuits.

There are several conferences addressing the various technology issues of monolithic integrated circuits in the various semiconductor technologies. Just within the various societies of the Institute of Electrical and Electronic Engineers, there are the IEEE Bipolar Circuits and Technology Meeting, the IEEE Gallium Arsenide IC Symposium, the IEEE International Solid-State Circuits Conference, the Microwave and Millimeter-Wave Monolithic Circuits Symposium, etc. addressing the various monolithic circuit developments of the industry.

The issues are very basic considerations. The correct implementation of these considerations contributes greatly to the success of any MMIC. The design of an L-band power MMIC is the design of lumped constant circuitry with circuit elements having a significant amount of parasitics. At 1 GHz, distributed effects are minimal for nominal chip sizes on MMICs.

Five areas will be discussed. These are 1) Power Capabilities of Active Devices, 2) Some Types of Amplifier Circuits, 3) Inductor Characteristics, 4) Thermal Considerations, and 5) Device Isolation Types. This paper will discuss self-contained monolithic integrated circuits. Integrated circuits which require most or all of the bypassing and tuning circuit elements to be mounted "off chip" are not really monolithic for the purposes of this paper. These are hybrid integrated circuits even if the semiconductor chip contains several active devices and circuit elements.

Figure 1 shows a general diagram which uses a single ended part. This circuit topology will be used to describe most of the circuits and devices to be discussed.

Power Capabilities

Power capabilities of devices need to be considered in power MMIC design. Just as in hybrid circuit design, the power amplifier is not conjugately matched but is power matched. Figure 2 shows a general active device set of V-I curves. It is generally recognized in the industry, that the circuit of Figure 3 operating in the linear (Class A) range of operation will generate up to:

$$P = \frac{V^2}{2R}; \text{ where } V = V_{dc} - V_{sat} \quad (1)$$

watts of power.

However, an equally valid limitation on power which must be considered is given by:

$$P = \frac{I^2}{2} R; \text{ where } I = I_{dc} - I_{min} \quad (2)$$

These formulae contain V_{sat} and I_{min} . The active device will not act as a short at saturating drive levels nor will it completely shut off at cut-off drive levels.

The simple matching circuit shown in Figure 4 presents a pure resistance to the device at the design center frequency. However, the slope of the resistance seen by the device versus frequency is negative at the match frequency. This means that the value of R to be used in the equations above will increase below band center and will decrease above band center. The device will be voltage limited below band center and current limited above band center. The voltage formula must be used below band center and the current formula must be used above band center. For a broadband linear power MMIC, a significant amount of design margin must be built into the part to ensure that the required amount of linear power is available across the total bandwidth. A capacitively coupled matching section will exhibit the opposite slope and opposite power saturation conditions.

Added power margin means added power dissipation in the MMIC. Power dissipation considerations will be discussed later. Another implication of the simple analysis discussed above is that the device will put out the required power with lower supply voltages at one end of the band but more input power will be required since the resulting current required is higher. In effect, the gain of the device is reduced in the current controlled region for a bipolar device which is current gain controlled. Circuit topology must

be carefully chosen to minimize the amount of gain margin that must be included.

Class C devices respond with similar matching requirements but require lower values of load impedances than that calculated above for Class A devices. The value of impedance will be on the order of 35 percent lower than the value of the Class A impedance calculated (1).

The MMIC circuitry must perform this impedance matching within the bounds of the chip and without the trimmers that are easily available in hybrid circuits. Since all devices exhibit parasitic capacitance, an inductance is needed to resonate out the effect of any parasitic capacitance which can not be absorbed into any matching circuit. The various matching techniques used in hybrid integrated circuits can be used on a power MMIC. However, severe limitations are imposed by the parasitics of circuit elements available on a MMIC. Inductor parameter limitations will be discussed in a later section of this paper.

Circuit Types

Although many system applications can be satisfied with Class A and Class C amplifiers, optimal power conversion occurs with other types of circuit operation. This section will address a few considerations of switching amplifiers as they apply to power generation at L-band.

Switching amplifier devices require higher cutoff frequencies than do Class A or Class C devices. A switching amplifier must support at least some of the harmonics of the amplified frequency. Figure 5 shows the velocity versus electric field curve for silicon and GaAs. The saturation velocity for

carriers in these semiconductors is on the order of 100,000 m/s. Using this value for saturation velocity and a relation derived from a single sided breakdown versus depletion width curve (2) one can derive that:

$$\tau = 0.136 V^{1.25} \quad (3)$$

where V is the breakdown voltage in volts and τ is the carrier drift time in ps across the collector depletion region as shown in Figure 6.

Using $f = 1/(2 * \pi * \tau)$ one can calculate the frequency degradation to the first order approximation resulting from increasing the breakdown voltage of a part. A part with a 6 GHz cutoff frequency would have a total time delay of 26.5 ps. If this part has a 10 V breakdown originally and the collector region is changed to a higher resistivity allowing a 100 V breakdown, the part would degrade to a 2.37 GHz cutoff. This assumes that the collector base junction remains approximately the same in the base region and that the only deterioration is due to the extra drift time in the collector region.

Using these assumptions and assuming that the current capability remains the same per unit area whenever the collector region is extended in length, Figure 7 shows a plot of cutoff frequency versus breakdown voltage normalized to a part with a 6 GHz cutoff frequency at 10 V breakdown. The power variation that could also be expected is shown normalized to one watt at a frequency of 6 GHz. The power plot assumes a saturation voltage of 2.0 volts at all breakdown voltages.

It is therefore readily evident that the geometry for high power switching L-band MMICs would require geometries expected of small signal C-band devices. In order to make a switching amplifier, the cutoff frequency should be a factor of four to ten higher than the frequency of operation of the

device in order for the collector to base junction to respond quickly with respect to the total switching time. For operation up to 1.5 GHz, the part then needs to have a cutoff frequency somewhere around 4 to 6 GHz. This means that the total time delay (using a 5 GHz cutoff) needs to be less than 31.8 ps. Assuming that a 15 GHz small signal geometry for a 10 V breakdown is possible, the time delay of the small signal part would be equal to 10.6 ps. For 31.8 ps (a 5 GHz cutoff), the added time delay for added collector drift time is $31.8 - 10.6 = 21.2$ ps.

Using the above formula for time delay in a drift region, a drift time of 2.42 ps is calculated for a 10 V junction. Adding 21.2 ps to 2.42 ps gives 23.62 ps. This implies that the highest voltage part with a 5 GHz cutoff frequency would be a part with a breakdown voltage of 62 V in silicon. It should be possible to make a switching amplifier with a 60 V breakdown for operation at 1 to 1.5 GHz with the same geometry used in small signal 15 GHz devices. The switching amplifier would be able to operate in class D or other modes of switching operation. However, the part would have to be prevented from entering into heavy collector saturation to keep the switching speeds high. Remember that the calculations were done assuming that the carrier drift velocity was saturated at 100,000 m/s and no time delay for collector base saturation was included in the calculations.

A power MMIC designed in GaAs rather than in Si would have a faster response time in that portion of the time that the device is at low voltage (fields less than 20,000 V/cm shown in Figure 5) but a slower response time than Si during the time the carrier velocities are saturated. The circuit topology (circuit elements etc.) would determine whether a GaAs part or Si part would respond faster in a switching amplifier. The other characteristics of GaAs

versus Si, e.g. parasitic capacitance and resistance of the two different substrates, would also determine whether a complete amplifier would be faster in GaAs or Si.

Efficient switching amplifiers require low loss inductors. Some comments about inductors will be given in a later section of this paper. Lossy inductors will limit the magnitude of inductive voltage multiplication that can be obtained.

Stability

Figure 8 shows a block diagram of a MMIC that is bonded into some external circuit. This diagram will be used to describe three different types of stability criteria for a MMIC to determine whether the circuit will be stable in linear two port, overload, and cascaded operation. Stability criteria connected with parametric effects will not be discussed in this paper but also need to be considered for successful MMIC operation.

It can be shown that a necessary and sufficient condition for linear two port unconditional stability is (3):

$$| |DET| * |DET| - L | + L < 1 ; \text{ where} \\ L = |S12 * S21| + \frac{|S11| * |S11| + |S22| * |S22|}{2} \quad (4)$$

DET = determinant of the scattering matrix

This calculation is an easy calculation and is done using alternative sets of criteria in circuit analysis programs. It is well known that if two port circuits which are unconditionally stable are cascaded, then the resulting two port circuit is unconditionally stable. However, from Figure 8(a), it is seen that cascading circuits on a MMIC or hybrid with the same power supply

yields cascaded three ports, not two ports. The net cascade of the three ports may not be stable when cascaded with the same power supply even though the circuits calculated as two ports are unconditionally stable. This is one of the common problems unsuspectingly appearing in multistage circuits on a MMIC.

Figure 8(b) also shows the common mode inductance of the MMIC for the whole packaged device. The packaged device may not be stable even though the circuit is built up of unconditionally stable two ports. The net circuit on the MMIC is not a cascade of two ports but two ports coupled through a common ground return. It is easy to get an rough estimate of allowable gain in such a single ended MMIC circuit.

Consider that a bond wire has roughly 10 nH/inch of inductance. At 1 GHz, this is 62.8 ohms/inch. For a 0.050 inch bond wire, the inductive reactance of the bond wire is approximately three ohms. Notice that the input and output currents must flow through this bondwire. Then:

$$I_{in} = \frac{E}{(2 \cdot Z_0)}$$

$$I_{out} = G \cdot I_{in} ; \text{ where } G \text{ is current gain} \quad (5)$$

$$I_{ind} = I_{out} ; \text{ for large } G$$

$$|G| \cdot |I_{in}| \cdot |X_L| = \frac{E}{2} = I_{in} \cdot Z_0$$

For $Z_0 = 50$ ohms, $X_L = 3$ ohms, $G_{max} = Z_0/3 = 16.6 = 24$ dB.

The amount of gain allowed will go up as the value of the inductance is reduced. More bond wires could be added in parallel and positioned such that the output current tends to flow down a different ground path than the input ground current does. However, it is hardly possible to reduce the inductance

value by an order of magnitude which limits the L-band gain to under approximately 30-40 dB of gain when bond wire grounds are used on the MMIC. If the MMIC has gain possible at higher frequencies, then similar calculations need to be performed at those frequencies to check parasitic high frequency gain (gain needs to be checked up beyond the f_{max} of the active devices). If back vias (equivalent to plated through holes in a printed circuit board) are used for ground, then the value of inductance drops from .5 nH to under .05 nH making it possible to develop in excess of 40 dB of gain in a single ended grounded MMIC at 1 GHz and fifty ohms Z_0 .

Notice that a balanced circuit such as shown in Figure 9 reduces the magnitude of current in the common ground inductance. However, a balanced circuit requires that the input drive source and output loads also be balanced. If the balance is only on the order of 10 dB, then a balanced circuit will be able to have only 10 dB more gain capable than a single ended circuit. However, it is necessary to provide this balance at all frequencies where the part has potential gain. If the output load is not well balanced at some out of band frequency, the circuit may tend to oscillate in the even mode of excitation at that frequency.

Figure 8 shows several cascaded stages. Consider what happens when the stages are driven into saturation for power amplifier operation at overdrive conditions. For analysis purposes the first two stages of the amplifier will be considered. The current in the first stage is proportional to the input power (typical Class C or saturated operation). The power out of the first stage is a function of the supply voltage for a saturated amplifier. The current in the second stage is a function of this output power. When the second stage current increases due to the first stage power increasing, the

voltage to the first stage is reduced by the effect of the bias supply impedance. This reduces the power to the second stage reducing the current in the second stage. This increases the voltage to the first stage of the amplifier increasing the power to and thus the current in the second stage of the amplifier etc. It is seen that a stable limit cycle oscillation is possible via power supply feedback. This type of oscillation has been termed motorboating or squegging due to the sounds this phenomena makes in audio amplifiers which are limit cycle oscillating. This is a serious potential problem in linear circuits which suddenly get overdriven.

Limit cycle oscillation usually catches a MMIC designer unaware because normally testing and analysis are done in a linear sense. However, the first time the "stable" MMIC is installed in a system which encounters a momentary overload, the part will start oscillating and continue oscillating even when the overload disappears. This type of oscillation tendency can be minimized by designing with devices which have only enough DC beta to work adequately in RF operation, but not so large as to aggravate the nonlinear feedback limit cycle oscillation. Designing with bias supply circuits which have different cutoff frequencies tends also to minimize this problem.

Oscillations due to momentary overloads can also occur in MMICs which have frequency conversion in them. Consider a circuit as described in Figure 10 with a 1.0 GHz amplifier driving a mixer and down converting to 200 MHz. Whenever the 200 MHz amplifier is overloaded, it will generate harmonics with the odd harmonics likely being the largest. The fifth harmonic of the 200 MHz amplifier is at 1.0 GHz. This signal can feed back to the input stages via the common mode inductance discussed above, via the power supply leads, or other feedback paths. If the signal feedback is sufficiently

large, the MMIC will oscillate under overload conditions and then continue to oscillate even when the momentary overload is withdrawn similar to the motorboating oscillation described above. MMIC layout and chip/system architecture can be altered to minimize these problems.

Inductor Availabilities, Limitations, and Alternatives

Many of the GaAs circuits shown in the literature use inductors in the matching circuits. These circuits are predominantly operating at frequencies an order of magnitude higher than L-band. The use of inductors at L-band is limited by Q and by the magnitude of inductance available. Low values of inductance can be used in high power circuits but the Q of the inductor is low. High values of inductance for high impedance circuits cannot be built at 1 GHz. At 1 GHz, the inductance reactance is 6.28 ohms/nH. Several hundred ohms of inductance requires in excess of 30 nH of inductance. Inductors of this size are larger than 250 microns square and exhibit low Q at 1 GHz.

Consider an active device operating at a power supply voltage of 28 Volts and putting out 50 watts. According to the equations shown above and using a V_{sat} of 3 Volts, the device requires a load of 6.25 ohms. The part would operate with a DC current of 4.0 Amperes. Assuming the Q of the match required for the load is on the order of one, the inductive reactance would also be 6.25 ohms. This requires an inductance of approximately one nH. Published data (4) shows that the Q at 1 GHz for this inductor would be at somewhere between 2 or 6. The series resistance of the inductor would be on the order of 1 to 3 ohms depending on the thickness of the metal. If this inductor is used to bring power supply voltages up to the part, at four amps of current, the inductor will drop 4 to 12 volts of the power supply voltage.

Some other approach needs to be found to bring voltage into the active device. If the inductor is used to tune out the capacitance of the device, it would be in parallel with the load resistance. As shown in Figure 11, it would put a 15.6 ohm load in parallel with the load using a Q of 2 at 1 GHz. This requires a load of 10.4 ohms. The inductor would dissipate thirty percent of the power reducing the device efficiency to seventy percent of its net value.

The DC bias current can be provided to a device with an integrated current device such as shown in Figure 12. However, this method as opposed to the use of an inductor will increase the Q of the match required and limit the bandwidth of the MMIC circuit. The current sources could best be provided in silicon by using a FET structure similar to the current source used in GaAs MESFET circuits such as shown in Figure 12. However, in silicon bipolar MMICs, this requires the addition of MOS or other types of structures to the process. One alternative, is to recognize that the majority of MMICs will be bonded into the external packages using bond wires. This bond wire in addition to an external inductor will serve as the feed inductor of a circuit as shown in Figure 13. It must be remembered that when the current source bias is used, the device load line is reduced to 1/2 the value that it has with an inductor bias. The same power output requires twice the size of active devices.

It is possible to synthesize inductances for matching on a MMIC. Figure 14 shows the passband of a hybrid amplifier matched with inductance synthesized from transimpedance amplifiers (5). Further work is progressing on these synthesized inductors and overall efficiency and effective Q of these circuits are yet to be characterized. However, it appears that with these

circuits or variants of them a completely integrated monolithic microwave integrated circuit for moderately high powers is possible.

Thermal Considerations

Pulsed and CW operation power MMICs have different thermal considerations. State of the art heat fluxes being studied suggest that 1000 W/cm² should be possible for power dissipation in fluid cooled circuits such as shown in Figure 15 (6). This means that a 1 KW transmitter would be possible with 50% power added conversion efficiency in a package 1 cm square. Typical power dissipations are closer to 100 W/cm² in microwave packages used today.

Figure 16 shows the cross section of a configuration that has been proposed to dissipate powers up to 1000 W/cm². These techniques use high thermal conductivity thin films.

In addition to the heat dissipation in the package, the instantaneous power dissipated in matching inductors, active matches, and supply circuits need to be analyzed for high peak power low duty factor circuits.

Circuit effects and reliability due to high thermal gradients also need to be considered in power MMIC design.

Device Isolation Techniques

For a power amplifier MMIC, device isolation techniques have to be considered in conjunction with power dissipation. The various isolation techniques have to be considered in regard to the amount of parasitic capacitance each device subcell presents to the circuit. Figure 17 shows some of the isolation techniques used in silicon bipolar technologies. Many of the various

technologies require trench filling techniques and reactive ion-etching techniques. One of the most promising techniques for medium power MMICs at L-band is shown in Figure 18. The technology for doing this process is available. Films of AlN, SiC, and diamond are also being studied for new semiconductor applications. Figure 19 shows a layout of a three stage L-band circuit capable of ten watts pulse power output. That circuit uses on chip coupling capacitors but requires off chip bias and tuning inductors. Future work is planned for eliminating the need for all of these external components.

Conclusion

Different design considerations have been discussed which need to be considered for successful power MMIC design. Careful application of these considerations makes high power (100 watt level) etc. MMICs possible. The use of appropriate grounding, power supply isolation, low loss biasing, and adequate inductors are some of the important considerations for successful MMIC design.

References

1. Krauss, Bostian, and Raab, "Solid State Radio Engineering," Wiley, c1980, p 405.
2. Sze, "Physics of Semiconductor Devices," Wiley, c1981, p 78.
3. R.J. Weber, RF/Microwave Class, University of Iowa, 1987.
4. Pettenpaul, et al., "CAD Models of Lumped Elements on GaAs up to 18 GHz," IEEE-MTT36 (2), 294 (1988).
5. C. Campbell and R.J. Weber, to be published.
6. D.B. Tuckerman and F.W. Pease, "High-Performance Heat Sinking for VLSI," IEEE Electron Device Letters, EDL-2 (5), 126 (1981).

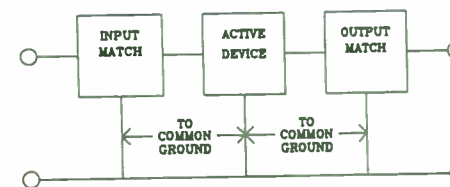


FIGURE 1 - SINGLE ENDED AMPLIFIER

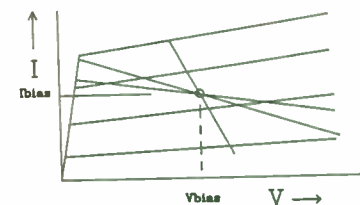


FIGURE 2 - TYPICAL V-I CURVES

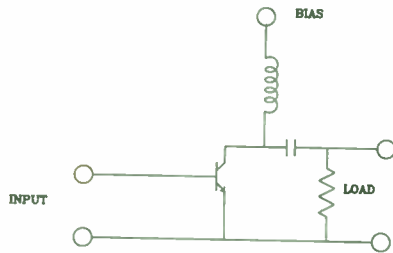


FIGURE 3 - INDUCTIVELY BIASED DEVICE

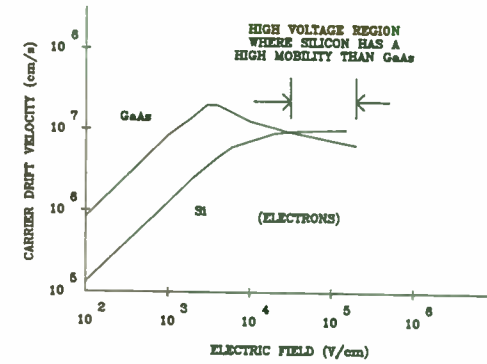


FIGURE 5 - MOBILITY COMPARISON OF GaAs AND Si FOR POWER AMPLIFIER VOLTAGES

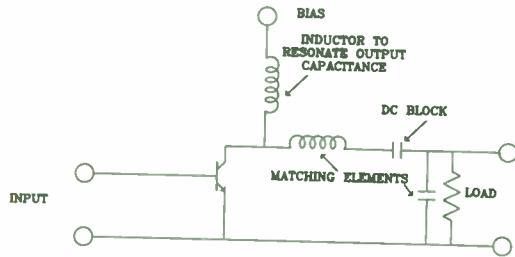


FIGURE 4 - SIMPLE OUTPUT MATCHING CIRCUIT

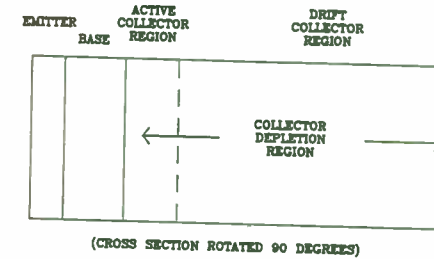


FIGURE 6 - CROSS SECTION OF A BIPOLAR DEVICE

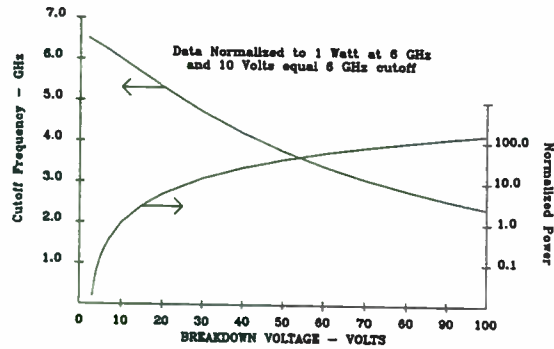


FIGURE 7 - POWER AND CUTOFF FREQUENCY VERSUS BREAKDOWN VOLTAGE

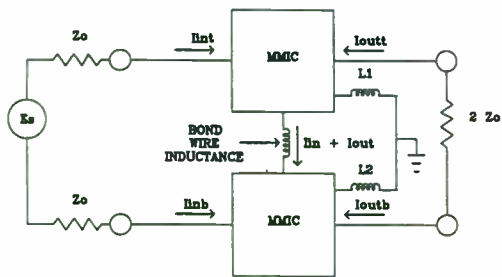


FIGURE 9 - BALANCED MMIC GROUNDED WITH TWO DIFFERENT VALUES OF INDUCTANCE

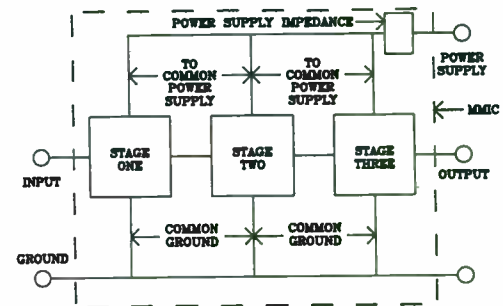


FIGURE 8(a) - MMIC STAGES WITH COMMON POWER SUPPLY

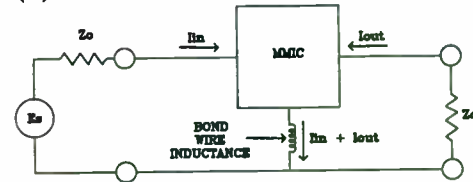


FIGURE 8(b) - MMIC GROUNDED WITH BOND WIRES

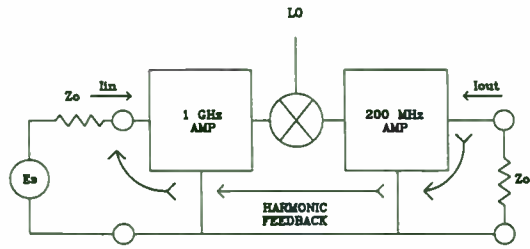


FIGURE 10 - HARMONIC FEEDBACK CAUSING INSTABILITY

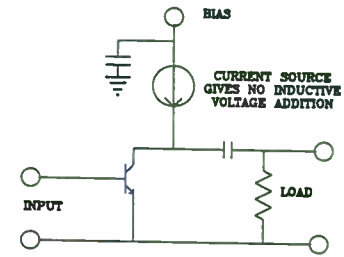


FIGURE 12 - POWER STAGE BIASED WITH A CURRENT SOURCE

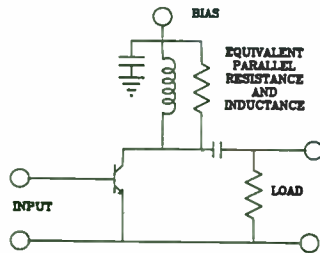


FIGURE 11 - INDUCTIVELY BIASED DEVICE USING A LOSSY INDUCTOR

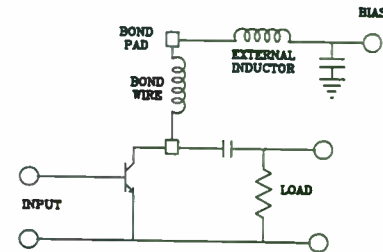


FIGURE 13 - INDUCTIVELY BIASED DEVICE USING AN EXTERNAL INDUCTOR

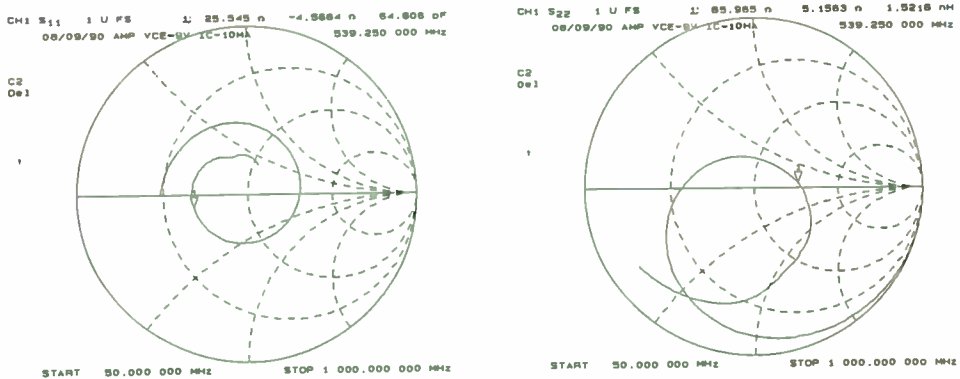


FIGURE 14 - PASSBAND OF AN AMPLIFIER USING TRANSCONDUCTANCE AMP INDUCTORS

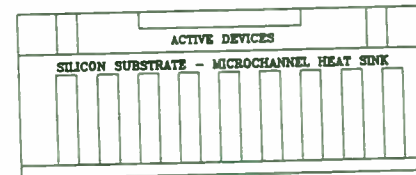
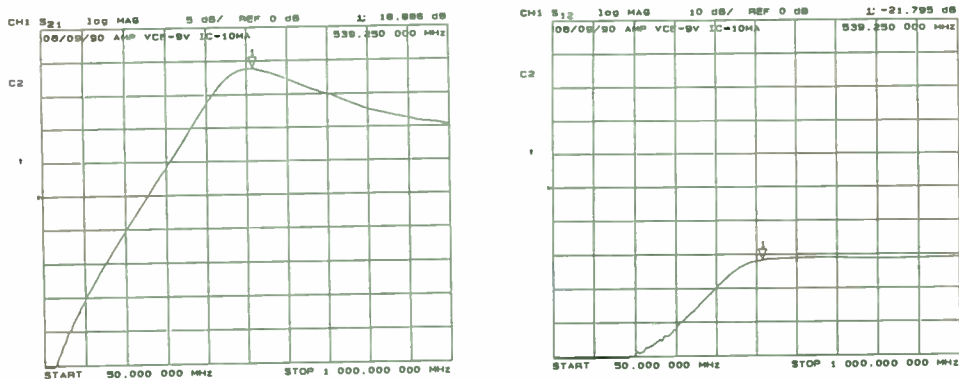


FIGURE 15 - HIGH THERMAL DISSIPATION SILICON MICROCHANNEL HEAT DISSIPATORS

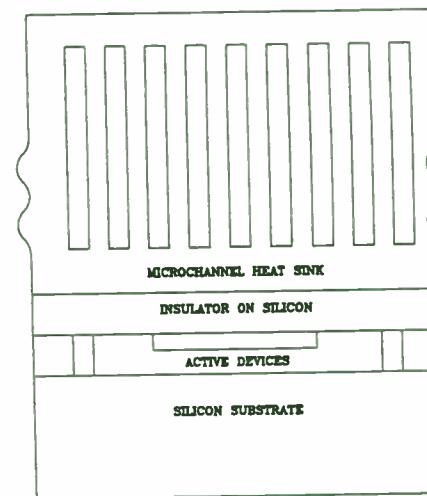


FIGURE 16 - HIGH THERMAL DISSIPATION THIN FILM HEAT SINK WITH FLUID CHANNEL HEAT SINK

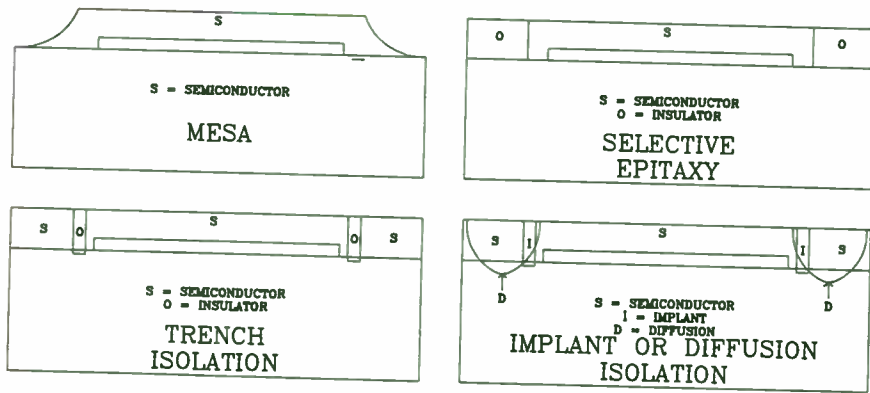


FIGURE 17 - SOME TYPES OF DEVICE ISOLATION

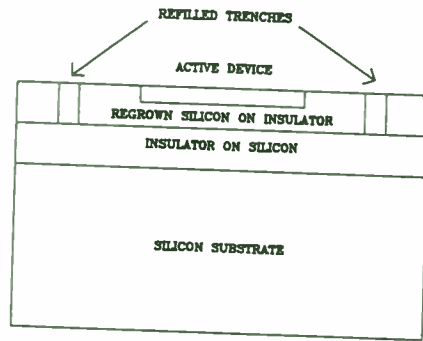


FIGURE 18 - CONFIGURATION FOR A MEDIUM POWER MMIC

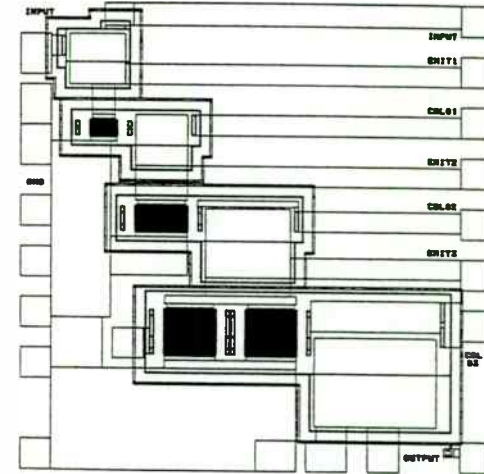


FIGURE 19 - THREE STAGE AMPLIFIER FOR ON CHIP COUPLING CAPS AND OFF CHIP TUNING INDUCTORS

Capabilities And Applications of SAW Coupled-Resonator Filters

Allan Coon

RF Monolithics, Inc.
4441 Sigma Road
Dallas, TX 75244

ABSTRACT

Although Surface Acoustic Wave Coupled-Resonator (SAW CR) filters have been readily available for several years, two issues currently inhibit the effective use of this technology: 1) Rapidly evolving technical performance has resulted in a lack of awareness by the design community of current capabilities, and 2) Systems originally designed for conventional filtering technologies, often *cannot* achieve optimum performance and cost because SAW CR filters were not considered in the initial system design. These problems are addressed with a practical selection guide of filter technologies in the VHF and UHF frequency ranges. Current practical capabilities are reviewed. Guidelines are developed as an aid in the optimal selection of filter technology during system design. SAW CR filters are emphasized and compared with other bandpass filter technologies. Finally, typical applications of SAW CR filters are illustrated with examples.

INTRODUCTION

Single-pole resonators using SAW cavities were first proposed in 1970. [1, 2] By the mid 1970's, single-pole resonators were becoming practical and multi-pole SAW CR filters were shown to be feasible. [3, 4] In the early 1980's, CR filters of up to six poles were demonstrated [5-7] and two-pole SAW CR filters became readily available in quantity and at reasonable cost. SAW CR filters at frequencies as high as 1500 MHz were demonstrated in the mid 1980's. [8]

In spite of the knowledge of SAW CR filter capabilities in the ultrasonics community and the availability of practical devices in production volumes, this particular technology is still not well known among RF circuit and system designers. From the author's perspective as an applications engineer, a surprisingly large percentage of RF design engineers seem unaware of the capabilities presently available and the design possibilities made viable by this technology.

SAW CR filters possess narrow bandwidths (typically 0.03% to 0.6%), low insertion losses (as low as 2 dB), and good ultimate rejection *without* harmonic spurious responses. Combined with center frequencies up to 1650 MHz, this type of filter is ideal for many consumer, industrial, and military applications in signal selection and frequency control. In addition, SAW CR filters often offer the smallest size and lowest unit cost of any of the alternatives.

In this paper, a brief overview of basic SAW CR filter concepts is followed by a description of current practical performance capabilities important to the RF design engineer. The capabilities of SAW CR filters are then compared with other passive bandpass filter technologies with an emphasis on optimizing the selection process at the system design level. As a design aid, a reference chart is presented covering practical, passive devices in the frequency range of 10 MHz to 10 GHz. Several application examples of SAW CR filters are also presented.

THE BASIC CONCEPT

Theory of operation is not the subject of this paper. However, a very brief review and description of the basic concepts is in order as a point of reference for the RF design engineer.

In and near the passband, the SAW CR filter may be modeled by the two-pole lumped element bandpass filter model shown in Figure 1. In this model, R_m , L_m , and C_m are the motional resistance, inductance, and capacitance values of each acoustic resonant cavity. C_0 is static capacitance which includes both case parasitic capacitance and capacitance between electrodes. C_{12} represents the acoustic coupling between the two resonant cavities, and as a practical matter, also includes parasitics. (This model is not valid in the reject band, however.) [9]

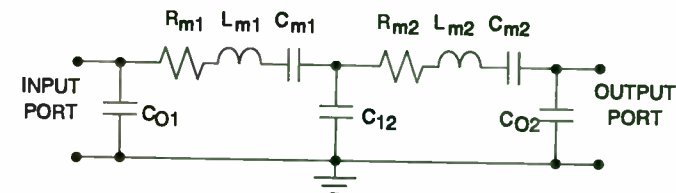


Figure 1: 2-Pole CR Equivalent LC Circuit Model

The SAW CR filter relies on the piezoelectric effect. Electric waves are converted into surface acoustic waves at the input of the device by an Inter-Digital Transducer (IDT) composed of metal electrodes on, or recessed into, the surface of a substrate material. These acoustic waves excite a

half wavelength ($\lambda/2$) resonant acoustic cavity formed between the transducer and a reflective grating, or within the transducer itself. Energy is then coupled to another $\lambda/2$ resonant acoustic cavity and converted back to electric waves at another IDT at the output. Impedance matching between the IDT's and the external electrical circuit is usually required for optimum insertion loss.

There are three principal methods of coupling the two acoustic cavities. One common method relies on the evanescent field between two side-by-side cavities. This coupling mode is referred to variously as evanescent coupling, waveguide coupling, transducer coupling, or proximity coupling. The resulting "double-mode" or "multi-mode" CR filters provide good performance in a practical design and are presently manufactured in high volume for pager receiver front-end applications [10, 11]. Coupling may also be directional via a multistrip coupler or the cavities can be in-line (collinear) with the surface wave. Each of these methods offers some advantages. [4] However, in-line acoustic coupling results in the simplest and most compact structure, which is desirable for practical volume manufacturability. In-line coupling may be accomplished with a metal grating on the surface or with grooves. A generalized schematic representation of an in-line acoustically coupled filter is shown in Figure 2.

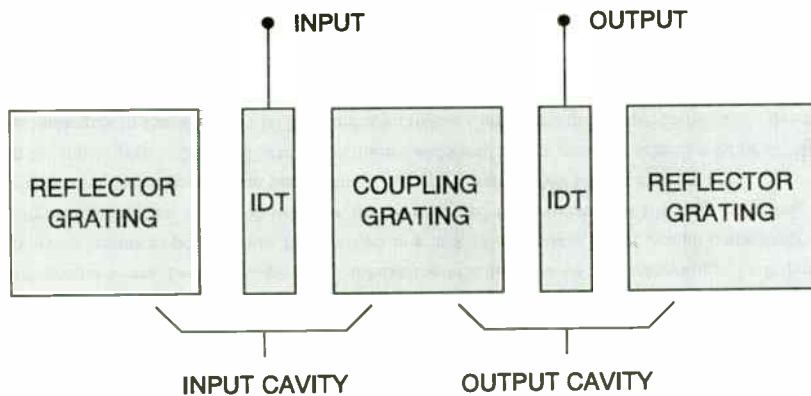


Figure 2: Schematic of Collinear CR Filter

Several substrate materials are possible, but quartz is by far the most common because it results in the best temperature characteristic. Also, various metals may be used for the metal electrodes. The most common is aluminum or an alloy of aluminum and copper.

State-of-the-art insertion loss, out-of-band spurious responses, and best symmetry in the frequency domain require minimized reflections internal to the transducers and maximized coupling between transducers and the acoustic standing wave. Traditionally, this has been accomplished with electrodes recessed in grooves or by the use of various "split electrode" arrangements using transducer electrodes narrower than $\lambda/4$. These techniques have resulted in high performance with regard to the parameters mentioned above, but with some significant practical limitations. These limitations include limited practical upper frequencies (about 800 MHz), high manufacturing costs, and various design complications (i. e., the design is not "well behaved"). Consequently, these high-performance designs have only been suitable for high-budget applications. They have never been available in significant production volumes for commercial applications.

Likewise, CR filters with three and more poles, for improved selectivity, have been successfully designed and fabricated. To date, these designs have not gained widespread acceptance due to considerable manufacturing fabrication difficulties.

Developments in two-pole SAW CR filter technology at RF Monolithics have eliminated the need for either recessed or split electrodes in high-performance SAW CR filters. Internal transducer reflections can be eliminated and acoustic coupling maximized by one or more of several other methods. One uses special quartz crystal orientations to achieve the Natural Single-Phase Unidirectional Transducer (NSPUDT). The other employs a "hiccup" in the transducer for the resonant cavity. [12-16] Figure 3 shows the configuration of a typical two-pole SAW CR filter with a single "hiccup" cavity. Typically, various weighting functions (not shown here) are designed into the transducers.

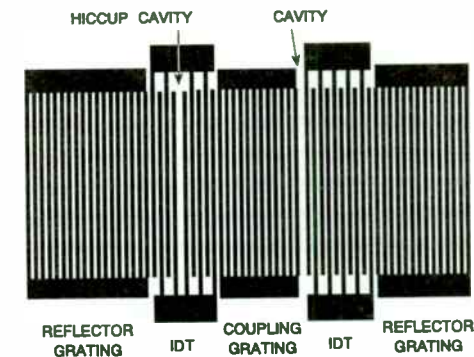


Figure 3: Configuration of SAW CR with "Hiccup"

One or both IDT's may employ a "hiccup" cavity. A SAW CR filter employing only one "hiccup" has almost symmetrical out-of-band response. CR filters with a "hiccup" in both transducers have exceptionally good rejection below the passband frequency but slightly worse passband flatness and worse high-side rejection. A common variation on this theme is the use of a "hiccup," as shown above, in one transducer and a "conjugate hiccup" cavity in the other transducer. In the "conjugate hiccup" cavity, electrode polarity is reversed on each side of the cavity.

These "hiccup" cavity designs are readily modelled and designed by Coupling-Of-Modes (COM) theory. [17, 18] Two-pole "hiccup" SAW CR filters have been proven to be well-behaved and are very manufacturable in high volume for reasonable costs. This is the type of practical design whose performance capabilities are discussed in the following sections.

CURRENT PERFORMANCE CAPABILITIES

In this section, we will first consider the performance limitations of the basic parameters of center frequency and bandwidth. The discussion of bandwidth necessarily requires a detailed explanation of practical production tolerances and temperature characteristics. Next, insertion loss and impedance matching are discussed. This is followed by rejection and passband characteristics. Finally, several other performance issues are covered.

The type of SAW CR filter described in the previous section is presently available in center frequencies as high as 1650 MHz. (Note that not all SAW CR filter designs are capable of this high of a center frequency.) Although technically feasible down to frequencies below 30 MHz, the limitations of size and cost set a practical lower limit of about 70 MHz. An optimum mix of small size and lowest manufacturing costs occurs approximately in the frequency range of 200 to 1200 MHz.

The most readily achievable pass bandwidths (3 dB) fall in the range of approximately 0.03% to 0.2%. The upper limit currently feasible is 0.6%. Bandwidths narrower than 0.03% are possible, but are seldom practical due primarily to center frequency manufacturing tolerances and drift with temperature. The region of practical SAW CR filters is plotted on a plane of fractional bandwidth versus center frequency in Figure 4. Note that the highlighted central region indicates the region where SAW CR filters are likely to be superior to any other bandpass filter technology in most applications. SAW CR filter technology is *not* suitable for any combination of frequency and bandwidth outside of the outer boundaries shown. Since there are so many parameters that may be specified for a filter, a requirement within the outer boundary may or may not be suitable for SAW

CR technology. However, this chart is an excellent starting place in determining whether or not SAW CR technology should be considered for any given application.

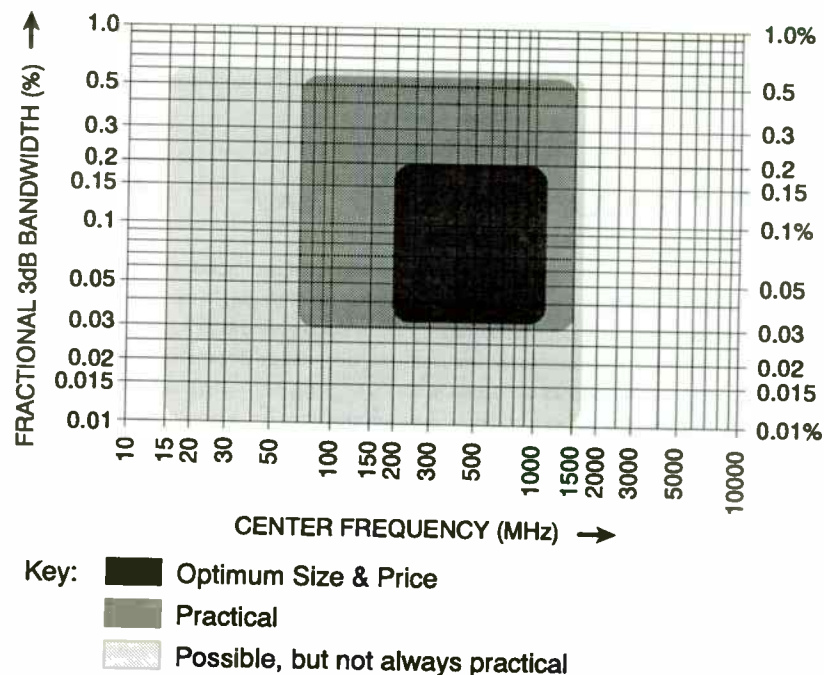


Figure 4: Frequency and Bandwidth Capabilities

Temperature is usually a major factor in determining the minimum practical bandwidth. The temperature characteristic of center frequency versus temperature for all SAW devices on conventional cuts of quartz is parabolic. A point of highest frequency occurs at one particular temperature defined as the "turnover" temperature, T_0 . The turnover temperature may be set in the design process to anywhere in the 0°C to 100°C range. The relationship of center frequency vs. temperature may be described by either of the following two equations which are also plotted in Figure 5.

$$(1) f_A = f_O [1 - 0.032 (\Delta T)^2]$$

$$(2) \Delta f / f_O \text{ (in ppm)} = - (\Delta T / 5.6)^2$$

Where: T_O = Turnover Temperature in °C
 f_O = Turnover Frequency in Hz
 T_A = Ambient Temperature in °C
 f_A = Center Frequency (at T_A) in Hz
 ΔT = $T_O - T_A$
 Δf = $f_O - f_A$

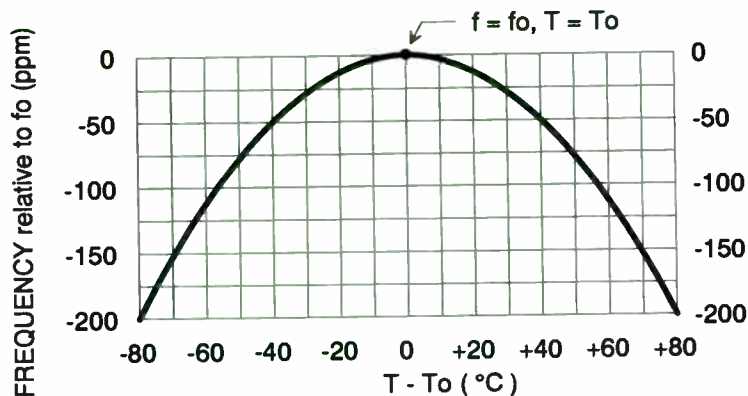


Figure 5: Quartz SAW CR Temperature Characteristic

The other major factor limiting minimum practical bandwidth is the production frequency tolerance (at fixed temperature). Typical practical center frequency tolerances range from about 100 ppm to 500 ppm. (This parameter affects the unit cost and should not be specified more tightly than necessary!)

Additionally, the turnover temperature has a tolerance associated with it. Any variation of T_O from the center of the operating temperature range worsens the overall worst case temperature variation of center frequency. Typically, the turnover temperature can be set in the design process to within about $\pm 10^\circ\text{C}$. The production variation in T_O is typically well within about $\pm 5^\circ\text{C}$ but is usually

specified at $\pm 15^\circ\text{C}$ to eliminate unnecessary testing of this parameter and to minimize unit cost. All of the above considerations determine the minimum practical bandwidth of a SAW CR filter.

As an example, consider a SAW CR filter with a center frequency of 500 MHz which will be used over an ambient temperature range of -40°C to $+85^\circ\text{C}$. To minimize temperature variation, T_O is designed to be at the center (22.5°C) of the operating temperature range. With a T_O tolerance of $\pm 15^\circ\text{C}$ assumed, the maximum possible ΔT is 77.5°C . This worst case ΔT results in a worst case frequency variation of about 190 ppm. Once the minimum practical production variation of 100 ppm is added, the minimum practical 3 dB bandwidth is about 290 ppm (0.029%), or 145 kHz, for this particular filter. In an actual design, this minimum practical bandwidth would be added to the system signal bandwidth (plus its tolerance, if any) in order to arrive at the nominal bandwidth of the filter.

As shown above, the minimum practical bandwidth is a function of both operating temperature range and permissible unit cost which both vary with the situation. Increasing the allowed production tolerance, and hence the minimum bandwidth, would result in a more economical filter. A smaller minimum bandwidth would be possible at significantly increased unit price (tighter production tolerance) and/or by the use of an oven for temperature stabilization. If the absolute minimum bandwidth is required at the expense of cost, size, insertion loss, and power consumption, then about 0.01% (100 ppm) bandwidth is possible.

The insertion loss of a SAW CR filter with impedance matching can be less than 2 dB for fractional bandwidths between 0.03% and 0.15%. (A typical maximum production specification might be about 4 or 5 dB.) Depending on size, cost, and other tolerance constraints, the required impedance matching can usually be provided either internally (inside the filter's hermetic case) or externally (provided by the user). Typically, the required matching consists of a series inductor or series inductor and shunt capacitor per port. This is shown in Figure 6.

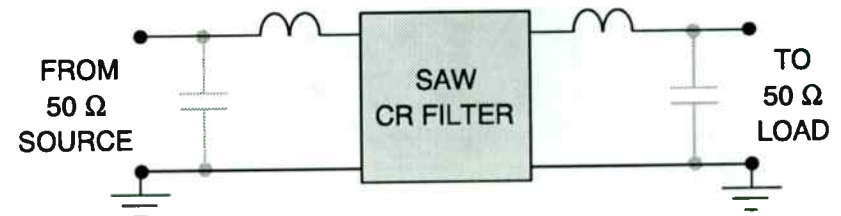


Figure 6: Typical SAW CR Impedance Matching Networks

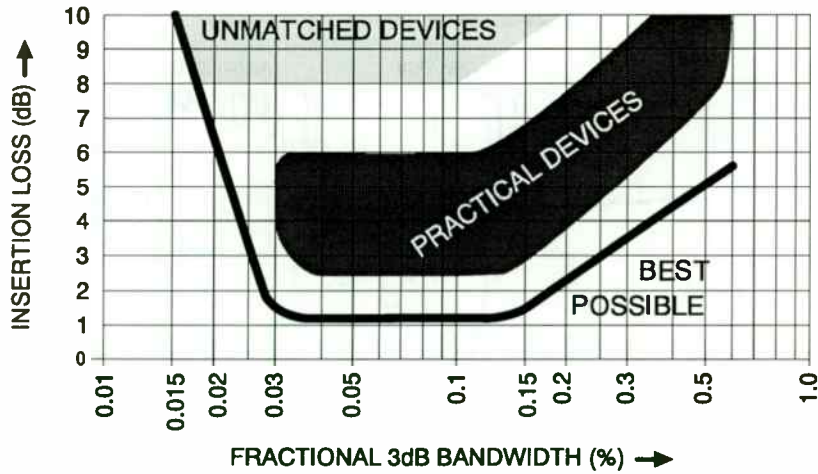


Figure 7: Insertion Loss Characteristics

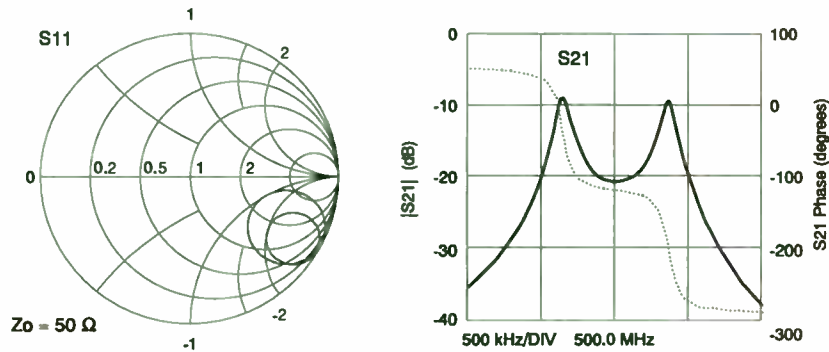


Figure 8: Typical Unmatched Impedance and Response

In some situations, size, cost, or component count may be more important than insertion loss. Without any matching networks, insertion losses as low as 7 dB are possible. (A typical maximum specification might be 10 dB.) The best possible and typical insertion losses are illustrated in Figure 7 for both matched and unmatched devices. The input/output impedances of a typical unmatched SAW CR filter along with an unmatched frequency response are shown in Figure 8 as S_{11} (or S_{22}) and S_{21} in a 50Ω system. Note that the s-parameters shown are for an unmatched device that was designed to be matched externally. Devices designed for unmatched applications have optimum passband ripple when terminated in the design impedance.

Typical resonator unloaded Q's can range from 4000 to over 10,000. The 15/3 dB shape factor is typically about 2:1 for the main center response. Close-in spurious sidelobes can vary from 10 to 25 dBc. Ultimate rejection (typically 60 to 80 dB) is usually limited only by the parasitic electric coupling around the SAW device in the small package. One very useful characteristic of this type of filter is the complete absence of harmonic spurious responses. The frequency response of a representative device is illustrated in Figures 9 through 11. One conventional "hiccup" cavity (as shown in Figure 3) and one conjugate "hiccup" cavity are employed. This filter is representative of a SAW CR filter designed to meet specific rejection requirements (shown).

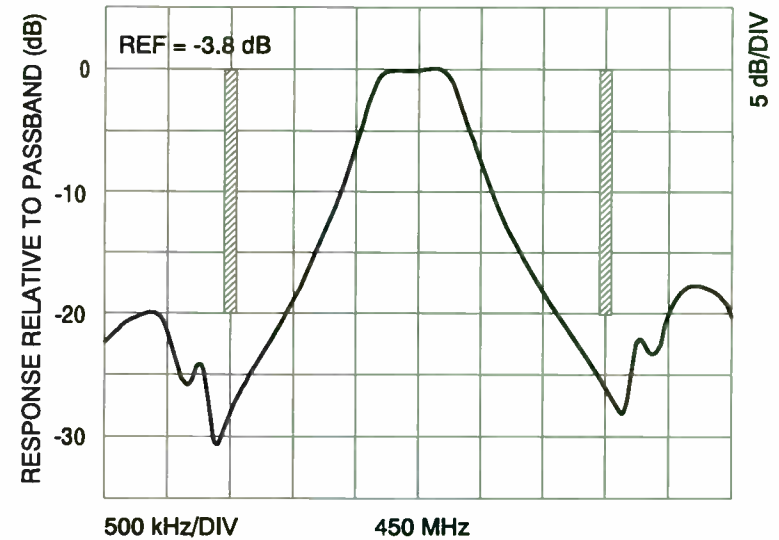


Figure 9: Typical SAW CR Passband Response

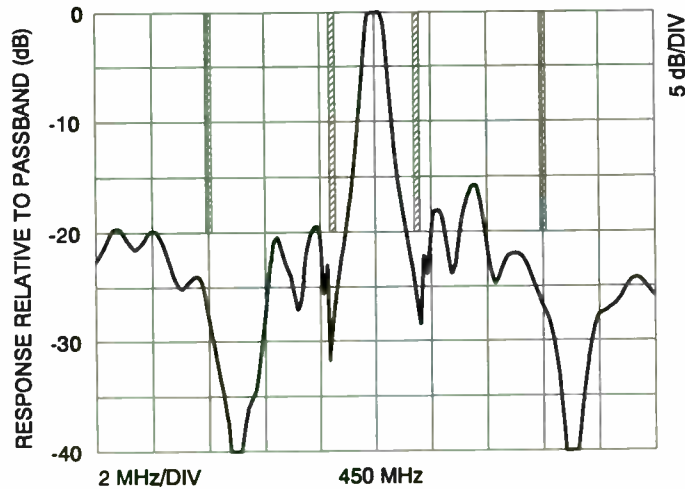


Figure 10: Typical SAW CR Frequency Response

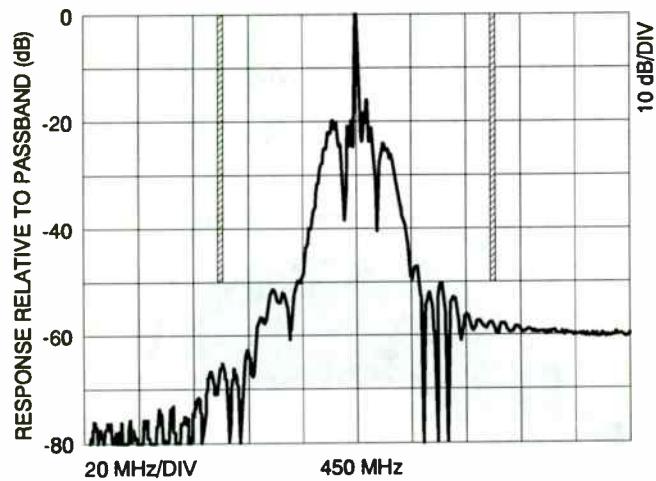


Figure 11: Typical SAW CR Rejection Response

Please note that bandwidth, passband amplitude ripple, and phase linearity are highly dependent on the interaction between the SAW CR filter and the impedances presented to it by the source and load and the matching networks coupling to the source and load. Unlike conventional transversal SAW filters, amplitude and phase characteristics are *not* independently controllable. They are interdependent in the same manner as in an LC or other electromagnetic cavity coupled-resonator filter. (Remember that the equivalent model of Figure 1 is a good approximation near the passband.) However, this also means that conventional coupled-resonator responses (e. g., butterworth, chebyshev, gaussian, etc.) can be approximated in and near the passband of the SAW CR filter.

The positions of the nulls shown in the response can be controlled. The responses of Figures 9-11 are good examples of selective null placement on either side of the passband. The use of two conventional "hiccup" transducers, as described in the previous section, results in exceptional rejection on the low side at the expense of high-side rejection. An example of this type of response is shown in Figure 12.

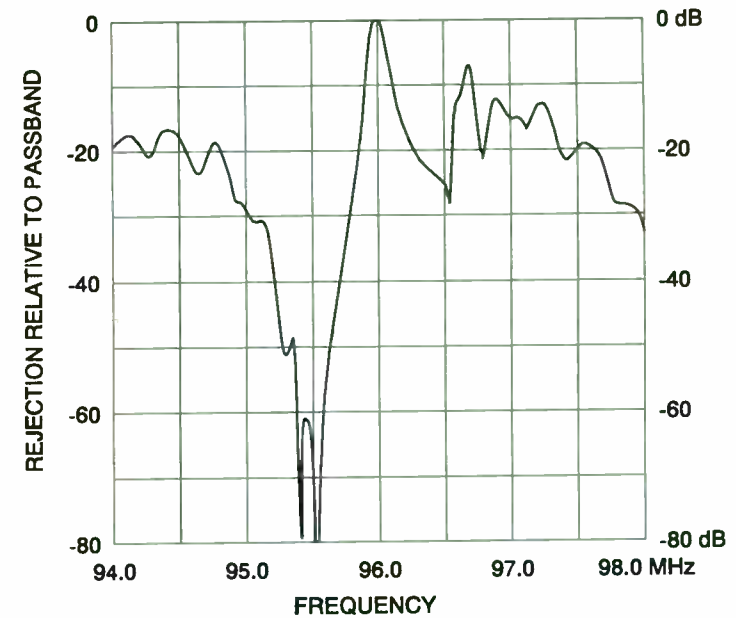


Figure 12: Response of Dual "Hiccup" SAW CR Filter

SAW CR filters are nearly always supplied hermetically packaged due to the extreme sensitivity of performance to surface contamination. Cleanliness inside that hermetic package and the type of packaging affect aging performance, which is typically well under 10 ppm per year. (Current state-of-the-art aging is less than 1 ppm per year. [19]) Typically, the SAW CR filter is packaged in a metal TO-39, Dual Inline Package (DIP), or flatpack. These may range in size from a 0.18" × 0.18" × 0.07" 8-lead flatpack at the highest frequencies to a 1.5" × 1" × 0.25" DIP at the lower end of the practical frequency scale. The most common and least expensive package is the TO-39 for frequencies from 200 MHz to 1650 MHz. Although numerous parameters affect the exact size of the SAW die, frequency is by far the primary factor. The lower frequencies result in larger package sizes which impact the unit cost. Some of these practical considerations are shown versus frequency in Figure 13.

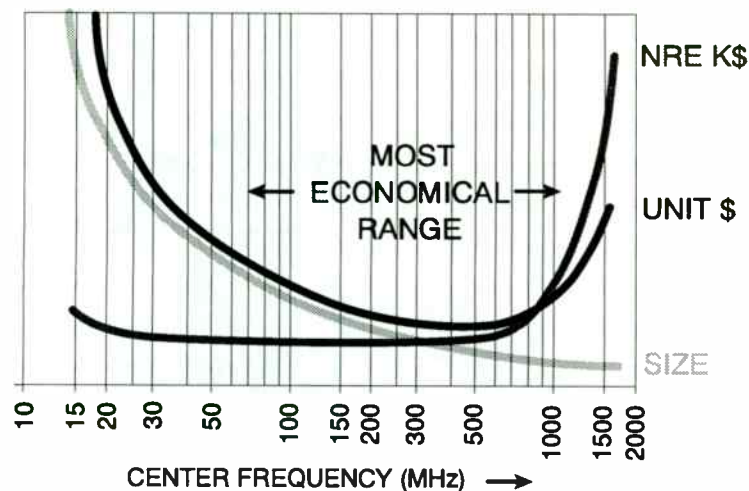


Figure 13: Practical Considerations vs. Frequency

What about costs? Unless an appropriate off-the-shelf design is available, Nonrecurring Engineering Charges (NRE) may be required. These charges start at several thousand dollars. Recurring costs can be less than \$10 in high volume for loosely specified consumer parts in TO-39 packaging with no internal matching. Low volume, tightly specified, internally matched, SAW CR filters can cost several hundred dollars. Figure 13 illustrates *relative* recurring and nonrecurring costs as a function of frequency with *all other parameters constant*. This graph can be used to help optimize system frequencies for lowest SAW CR filter costs.

COMPARISON WITH OTHER FILTER TECHNOLOGIES

SAW CR filter technology is complimentary to many other types of bandpass filters, including SAW transversal filters, in the frequency range of 40 MHz to 1.6 GHz. The other major types of practical bandpass filters in this frequency range include (but are not limited to) crystal, LC, helical, tubular, cavity, interdigital, combline, and dielectric-resonator types. In this section some of the key characteristics, advantages, and disadvantages of these different bandpass filter technologies are briefly reviewed. Active filters and very specialized devices with limited availability are not considered here. Some examples of alternate technologies not covered here are: 1) Thin Film Resonator (TFR) crystal filters for monolithic applications, 2) Bias tunable Yttrium Iron Garnet (YIG) filters for microwave frequencies, 3) all filters below 10 MHz, and 4) all filters above 10 GHz.

A generalized map of frequency and bandwidth capabilities is shown in Figure 14 for the frequency range of 10 MHz to 10 GHz and for fractional bandwidths of 0.01% to 100%. This chart can be used as a guide in determining which bandpass filter technologies should be considered for any particular project. A filter type should be seriously considered if the frequency and bandwidth fall within the boundaries shown. Please note that typically, the optimum ranges of frequency and bandwidth for a given filter type are the central areas of the regions shown in Figure 14. It is generally wise to assume that points near the boundaries may be possible but may not be entirely practical for every application in terms of size, cost, manufacturability, or availability. Points outside of the boundaries for a particular filter type indicate that it is probably unsuitable. Although often possible, these are likely to be expensive laboratory curiosities.

Of course, since there are many more filter parameters than frequency and bandwidth, the identification of a candidate filter type with the chart of Figure 14 is only the start of the selection process. The boundaries shown are based on reasonably practical ranges and are somewhat subjective. The actual boundaries are certainly a function of which parameters require optimization in a given application. In general, lower frequencies than shown are possible if size and cost are of no concern. Often narrower bandwidths are possible if insertion loss can be sacrificed and temperature is relatively stable. Also, it is apparent that several filter technologies are often possible for any given combination of frequency and bandwidth. More must be known about the available filter types and the intended application.

In this frequency range, bandpass filters can be divided into two broad categories: piezoelectric and electromagnetic. Following is a brief description of some of the major types in these categories.

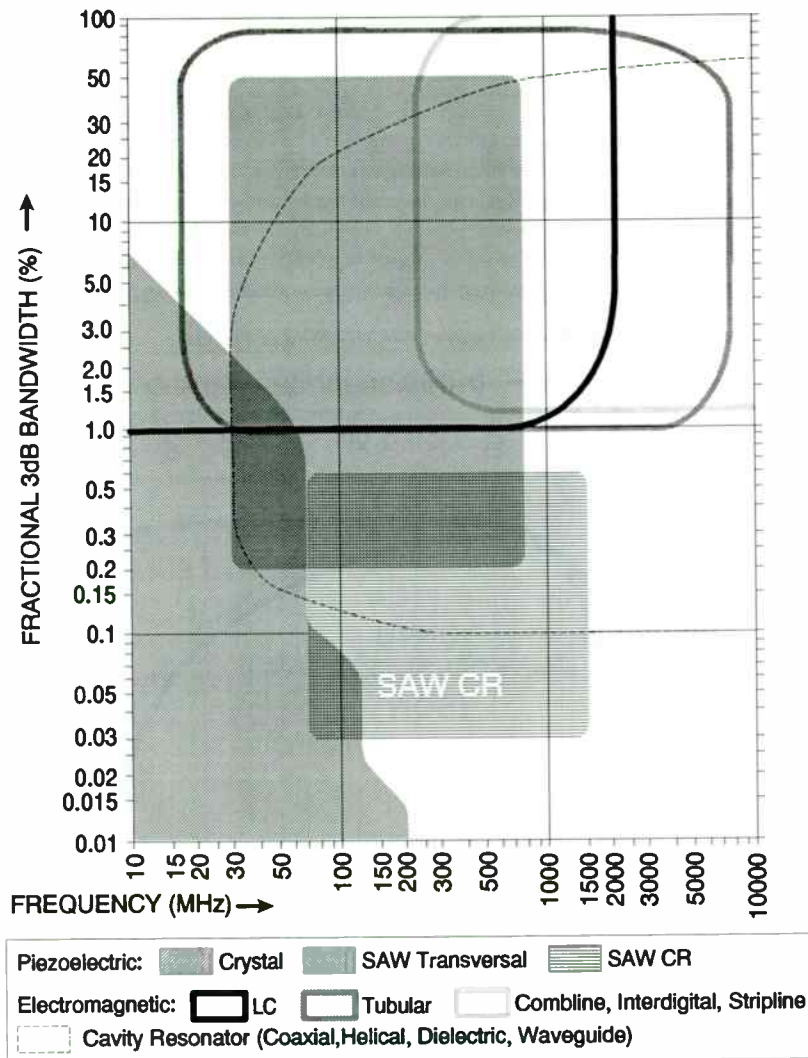


Figure 14: General Bandpass Filters - 10 MHz to 10 GHz

Unless noted otherwise, the piezoelectric filters are generally not tunable and the electromagnetic filters are.

Piezoelectric Bandpass Filters Above 10 MHz

Crystal filters (either discrete or monolithic) are well known and widely used. Topologies include ladder for narrower bandwidths and lattice for wider bandwidths. These devices rely on bulk acoustic waves (generated piezoelectrically) that pass directly through a quartz crystal. They offer excellent Q, selectivity, ultimate rejection, the best temperature stability, and the narrowest bandwidths of all of the filter types being considered here. Key disadvantages include spurious responses, limited power handling, the generation of IM products, and a lack of ruggedness in high shock and vibration environments. For very narrow bandwidths (about 0.01%), fundamental frequencies of up to 200 MHz are possible, although most practical devices are well below 100 MHz. Very narrow bandwidth overtone designs are also possible. At frequencies below 30 MHz, bandwidths as wide as 7% are possible with wideband lattice designs, but most practical devices are well below 1%. In the frequencies that overlap SAW CR filter frequencies (approximately 70 MHz to 100 MHz) the widest practical bandwidths are typically less than 0.1%. These characteristics make them ideal for many narrowband receiver applications, especially 10.7 MHz and 21.4 MHz IF filters. [20]

Ceramic filters are primarily used in receiver IF applications at 10.7 MHz and 455 kHz. This filter is possible, but not common, at frequencies higher than 10.7 MHz. Typical bandwidths range from about 1% to 3%. There is virtually no overlap with SAW CR capabilities.

SAW transversal filters include conventional high-loss (typically more than 20 dB) and newer mid and low-loss (5 to 15 dB) designs using single or multilevel metallizations. The highest center frequency practical for fundamental-mode high-loss designs is about 800 MHz with 1.5 GHz possible. For low and mid-loss designs, frequencies well over 1 GHz are practical, with maximum practical bandwidths up to about 10%. The lower limits of frequency are limited by the same size/cost constraints that affect SAW CR filters. The narrowest practical bandwidth is about 0.2% to 0.3% with 0.1% possible. For conventional high-loss designs, 30% to 50% bandwidths are practical. Bandwidths over 100% are possible with sacrifices in rejection characteristics. Related devices (e. g., those utilizing surface skimming bulk waves, and others) are capable of fundamental mode center frequencies as high as 2.5 GHz. Also, harmonic responses have been utilized as high as 3 GHz

A unique advantage of the transversal SAW filter is the independent control of amplitude and phase characteristics in the passband due to the time domain nature of the design. (This filter is essentially "digital" in nature.) Other advantages include excellent passband group delay and amplitude ripple

characteristics, steep shape factors (typically 1.5:1), small size at higher frequencies, good temperature stability, and excellent manufacturing reproducibility. Disadvantages include substantial NRE costs (higher than for SAW CR's) for designs not available, limited power handling, odd or even harmonic spurious responses, and for high-loss designs, triple transit spurious responses in the time domain. Absolute time delays (which can often be designed to a specific value) range from several hundred nanoseconds to several microseconds. This delay can be desirable or undesirable, depending on the application. These filters find frequent use in signal processing applications and wideband receiver IF sections.

SAW CR filter capabilities were described in previous sections. Key advantages of this type of filter include very low insertion loss, high Q, very narrow bandwidths, selective null placement, and excellent ultimate rejection with no harmonic spurious responses. Additional advantages are good temperature stability, very small size at UHF, and low unit costs at UHF. As shown in Figure 14, this filter technology has little competition for the higher frequencies and narrower bandwidths. Disadvantages include somewhat limited power handling, close-in sidelobe responses, and NRE charges for custom designs. These devices are experiencing increasing application at higher IF frequencies, permitting fewer receiver frequency conversions. Their use is also increasing in UHF frequency control applications.

Electromagnetic Filters, 10 MHz to 10 GHz

The conventional, lumped element LC filter has been improved considerably in the past decade by the development of smaller components with higher Q at high frequencies and by CAD techniques. This type of filter has tremendous design flexibility and has practically no lower limit of frequency or upper limit of bandwidth. The present upper practical limit for frequency is about 2 GHz and the lower bandwidth limit is about 1%. Additional advantages include good power handling and insertion loss at the lower frequencies and small size at the higher frequencies. Custom designs are available with little or no NRE charges and short lead times. Disadvantages include poor Q at high frequencies, moderately high unit costs, and only fair temperature and vibration characteristics. This type of filter is a good general purpose choice excellent for lower frequency and wider bandwidth applications. [20-23]

Combine filters are essentially the same as LC filters but with the inductances distributed instead of lumped. This permits higher Q (about 3500), higher frequencies, and less shock and vibration sensitivity than LC filters. Practical frequencies range from 300 MHz to well over 10 GHz. The most practical bandwidths range from 3% to 20% with 1% to 50% possible. The closest spurious response is just above four times the center frequency. Advantages include low insertion loss (typically under 1 dB), high power handling capability (up to several hundred watts), and small size

at the higher frequencies. Disadvantages include fairly high recurring unit cost and large size at lower frequencies. [24, 25]

Interdigital filters are similar to combline filters, but are made entirely from distributed reactances. Frequency, Q (up to 5500), and bandwidths are all somewhat higher than combline filters, but the size is somewhat larger. The practical limits of frequency are 500 MHz to well over 10 GHz. Bandwidths of 5% to 80% are most practical with 3.5% to 100% possible. Insertion loss, power handling, advantages, and disadvantages are very similar to those of combline filters. Additionally, size can be excessive for the narrower bandwidths as well as for the lower frequencies.

Suspended substrate stripline and/or microstrip bandpass filters can be implemented in a variety of ways but are usually a printed implementation of the interdigital filter described above. This type of filter is feasible down to 100 MHz, but is not usually considered practical below 1 GHz due to size. The upper frequency limit is well over 10 GHz.

Tubular filters are made of direct or capacitively-coupled resonator sections installed in a tube. Practical frequencies range from 15 MHz (with fairly large size) to about 8 GHz. Bandwidths range from 1% to 80%. Advantages include low loss, high power handling at lower frequencies, virtually no spurious responses, and little or no NRE charges for custom designs. Disadvantages include large size at lower frequencies, no method to externally tune, and high unit costs.

Cavity-resonator filters are usually implemented with helical, coaxial, or waveguide resonators. Waveguide filters are feasible down to 1 GHz, but with excessive size. Waveguide filters are not discussed further here since there is essentially no overlap with SAW CR technology. Coaxial and helical filters are essentially the same with $\lambda/4$ resonators in cavity enclosures. The only difference between helical and coaxial cavities is the shape of the resonator, which is compressed into a helical coil for reduced size in helical designs. Coaxial filters are available in frequencies from 30 MHz to over 10 GHz and helical filters from below 10 MHz to 2 GHz. Size is quite excessive for both of these at the lower ends of their frequency ranges. Practical helical filter bandwidths range from 0.2% to 20%. Practical coaxial filter bandwidths range from 0.2% to 3.5%. Advantages include excellent Q (up to 10,000), good selectivity, and low loss. The primary disadvantages are size and cost. (Depending on specifications and frequency, helical filters can be very economical, however.)

Dielectric resonator filters, like SAW CR filters, have been developed fairly recently. They are available for center frequencies from less than 500 MHz to over 10 GHz. Practical bandwidths range from about 0.1% to over 50% with insertion losses in the range of 1 dB to 5 dB. More than two poles are available. The nearest spurious responses are beyond 1.3 times the center frequency. Power handling can be several hundred watts for the lowest frequency devices. The combination of low

loss, wide bandwidth, and good power handling makes this filter ideal for many transceiver duplexer applications.

Note that at comparable frequencies, SAW CR filters are usually considerably smaller in size than any of the electromagnetic filters (except LC) and are usually significantly less expensive (except low cost helicals) in production volumes. However, all of these filters have their application niche and can be considered complimentary to one another. (i. e., No single filter type has all of the advantages that are ideal for every requirement.) The SAW CR filter is one of the newest of these filter types. Consequently, its advantages are not widely known and its niche is not fully established. As a result, many system designers are not getting the most out of their system designs. We will look at this in the next section.

APPLICATIONS

Applications of SAW CR filters fall into two major categories: frequency selection (filtering) and frequency control (oscillator stabilization). The low insertion loss of the SAW CR filter makes it an ideal filter for many receiver front end applications. The narrow bandwidth makes it suitable for many receiver IF applications with some unique benefits. And, as will be shown, its properties make it ideal for stabilization of UHF oscillators.

Receiver Front-End

The combination of small size, low unit cost, and low insertion loss can be used to advantage in receiver front-ends. An additional benefit of SAW CR filter technology in this application is the possibility of the selective null placement described in earlier sections. When the receiver frequency scheme and the SAW CR filter preselector are both designed for each other, it is often possible to place a null in the frequency response at the image frequency. Usually, this would be done with the use of the dual "hiccup" design described earlier. In this SAW CR filter design, a null of 80 dB is often possible at 910 kHz below the center of the receiver passband. This provides excellent image rejection for a conventional 455 kHz IF. Frequently, a dual conversion receiver can be replaced by a single conversion design *with no sacrifice in performance*. An example of this enhancement is the guard receiver portion of the ARC-182 ECCM transceiver developed for the U. S. Navy. (See Figure 15.) The previous versions of this receiver were dual conversion. In this case, small size was the critical design parameter. SAW CR filter technology was the key to meeting that design goal.

If a SAW CR filter is chosen for a receiver front-end only because of size, cost, good ultimate rejection, and low loss, then the receiver designer might not know that he could get by with only a

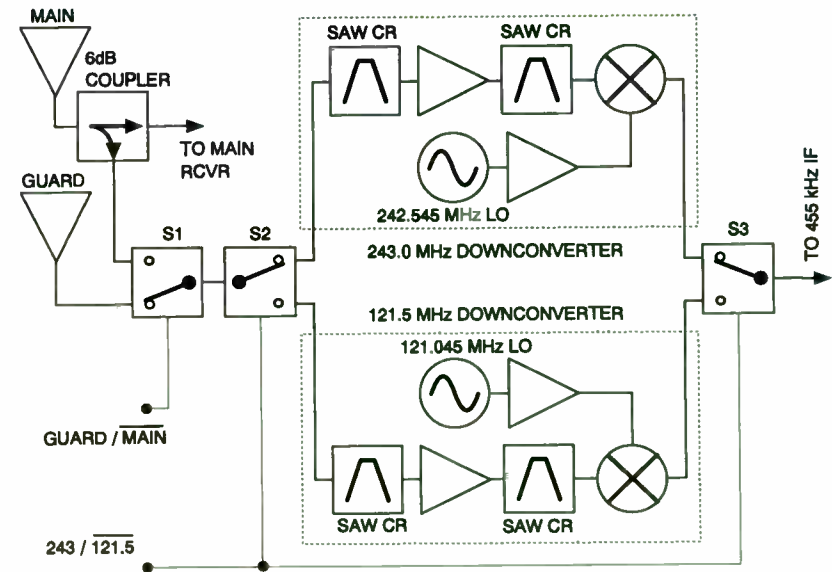


Figure 15: Guard Receiver Front-End

single conversion receiver. If the SAW CR filter is specified and ordered only after committing to a dual conversion receiver design, then considerable price/performance/size advantage might be left untapped! For this reason, the system designer should contact the SAW device manufacturer with details of the application very early in the system design phase of the project. Provide the SAW manufacturer with the system frequency scheme and rejection wish list. Many requests are turned down as not practical, but often that extra bit of knowledge allows the SAW CR filter designer to provide unexpected enhancements in system performance. [26-28]

Receiver IF

The SAW CR filter's small size, low unit cost, and narrow bandwidth make it an excellent candidate for many receiver IF applications. One of many possible receiver IF applications is in the handheld, cellular telephone. Potentially small size and low cost are obviously key to this size and price competitive application. SAW CR filters have been successfully designed for both conventional and the new, wider bandwidth, digital cellular telephones. An example of a SAW CR filter designed for a digital cellular telephone IF is shown in Figure 16.

block diagram.) The SAW CR filter offers the simplest, least expensive, and most reliable method of extracting the clock signal. Once extracted, it is used to retime the data with significantly less jitter. The narrow bandwidth, the regenerative effect of the “ringing” acoustic cavity, and the high frequency of the SAW CR filter make it ideal for this application.

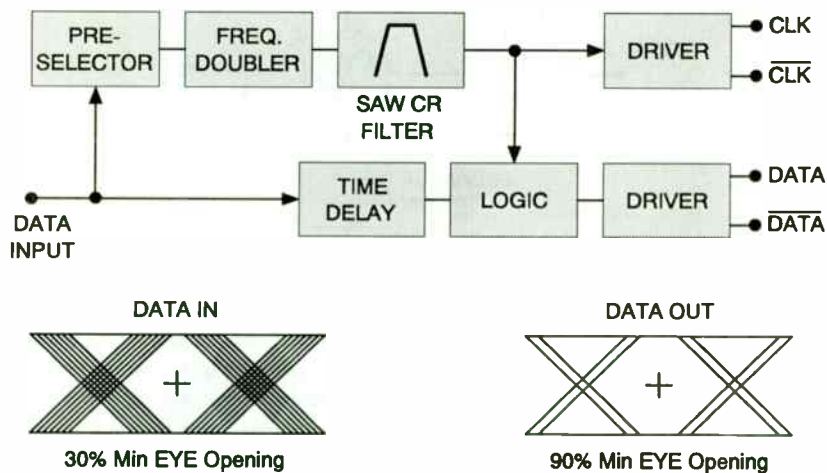


Figure 17: Fiber Optic Clock Recovery & Data Retiming

Multiplier Frequency Selection

This application uses the SAW CR as a filter, but in a novel frequency control application. Multiplied crystal oscillators are sometimes used for stable UHF frequency sources. This may be appropriate when a free running SAW oscillator does not provide sufficient stability and a Voltage Controlled SAW Oscillator (VCSO) phase locked to a stable low frequency crystal oscillator is not appropriate for several possible reasons. In this approach, the crystal oscillator is multiplied by any of many different types of multiplier. Even a step recovery diode multiplier can be used which is rich in harmonics. The absence of any harmonic responses in the SAW CR filter allows the selection of the desired harmonic. This is shown in Figure 18.

22

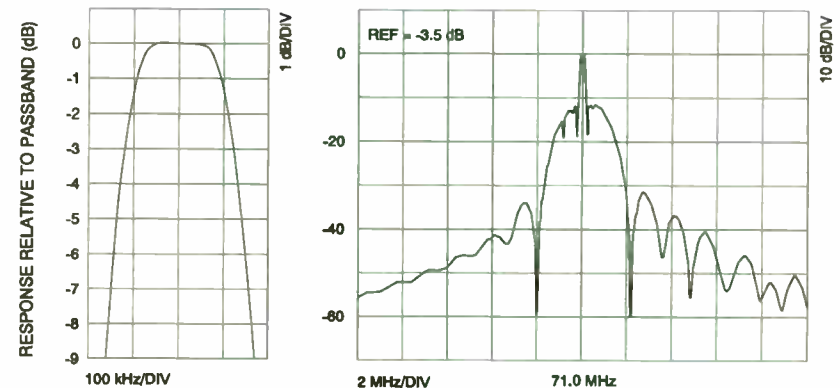


Figure 16: A Digital Cellular Telephone IF Filter

Note that the center frequency of this filter is above 70 MHz. (Some designs use IF's at frequencies above 90 MHz.) These IF frequencies allow the SAW CR filter to be both reasonably small and cost effective while also moving the image frequency of the receiver farther away where the preselector can provide better image rejection. The result is both better performance and lower cost than could have otherwise been achieved. The result is state-of-the-art for this type of product.

Currently, a common mistake in the cellular telephone industry is the choice of 45 MHz for the IF frequency. That frequency was a popular IF frequency in conventional cellular telephones with crystal IF filters. However, that frequency does not permit the performance, size, and cost advantages made possible with a SAW CR filter. The wider bandwidth required by digital cellular is possible, but difficult, with a crystal filter. Some digital telephone manufacturers are moving to the higher IF frequencies and using SAW CR filter technology. Some are trying to stay at 45 MHz. Guess which will have the competitive edge! Tradition and inertia can be terrible things when it comes to applying new technologies. The system should be designed with the available technologies in mind.

Fiber Optic Clock Recovery

A unique application of SAW CR filter technology is clock recovery and data reconditioning in telecommunications fiber optic transmission networks. An example is the recovery of the 155.52 Mb/s clock in the Synchronous Optical Network (SONET). (See Figure 17 for a basic

21

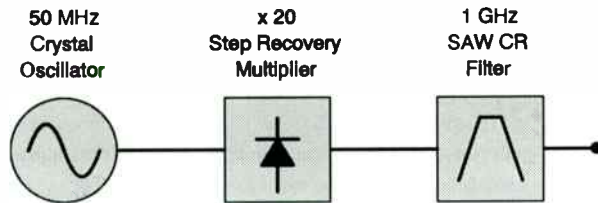


Figure 18: Multiplier Harmonic Selection

Inductorless Oscillators

The phase shift of a two-pole SAW CR filter between the 3 dB points is 180°. This type of phase characteristic provides a very favorable situation when designing a UHF oscillator with either no impedance matching or with no inductors. [30] One application of this technique is the high performance oscillator that cannot have coils because of size or vibration requirements. Another is in low cost, high volume devices where it is desirable to have only a SAW device and an IC to minimize parts count and eliminate production adjustments. An example of such a low cost application is the Microtransmitter manufactured by RF Monolithics. This device is available for frequencies between 200 MHz and 450 MHz and fits in a TO-39 package. It is sold for low cost, high volume consumer remote control applications. This type of device is made possible only by the use of SAW CR filter technology. [31] The block diagram is shown in Figure 19.

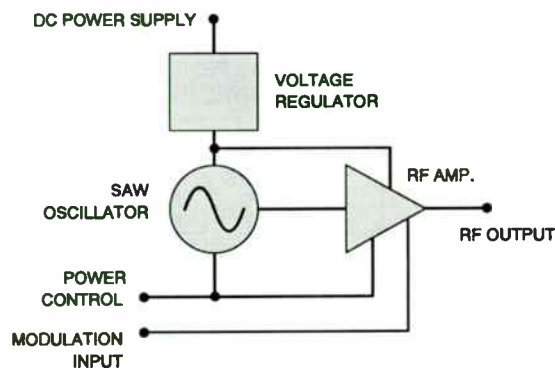


Figure 19: The Microtransmitter

VCSO's

A VCSO is typically phase locked to a stable reference crystal oscillator. The VCSO must be able to tune over a range sufficient to compensate for all frequency variations in the VCSO, which is usually dominated by temperature variations. This tuning range is directly influenced by the bandwidth of the SAW device in the VCSO. Therefore, it is desirable to have a SAW device with a fairly wide bandwidth. Yet the wider the bandwidth, the worse the SSB phase noise. Consequently, it is necessary to carefully balance the bandwidth of the SAW device in a VCSO design for optimum performance. Although possible with a one-pole SAW resonator, [32] the design is somewhat complex. The SAW CR filter allows excellent control of its bandwidth and is therefore an ideal device for VCSO applications. [33] A block diagram of such a VCSO is shown in Figure 20.

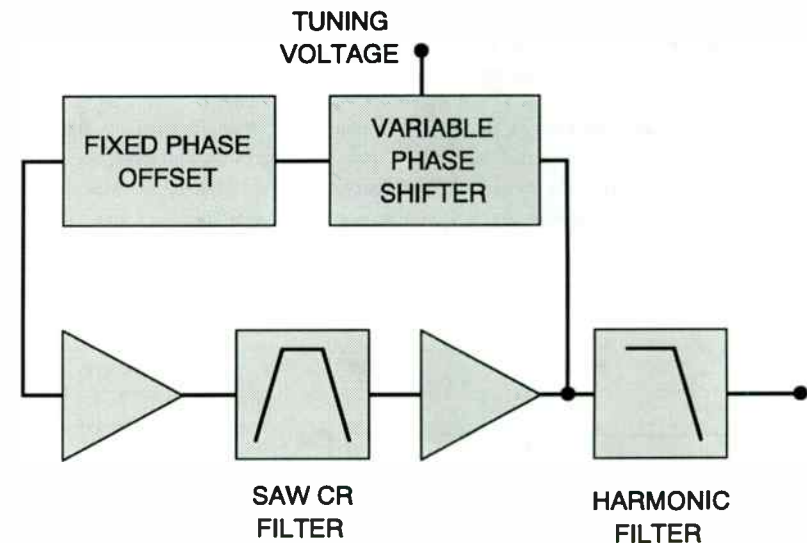


Figure 20: A VCSO Stabilized with a SAW CR

This section has identified only some of the principal applications of SAW CR filters. As this new technology becomes more widely used, it is expected that many more applications will be discovered that offer unique advantages over prior techniques.

SUMMARY

The SAW CR filter was shown to be a valuable addition to the many possible choices of bandpass filtering technologies available in the VHF and UHF frequency ranges. The basic concepts of this filter technology were reviewed specifically to provide background to the RF circuit and system design engineer. Performance capabilities and limitations were summarized, including practical information about cost optimization. SAW CR filter technology was compared with the major types of passive bandpass filter technologies available for the same frequency ranges. Practical reference material was developed as an aid in choosing the optimum bandpass filter technology for any given application. Finally, application examples of SAW CR filters were given. The proper choice of filter technology at the system design phase was emphasized in order to optimize performance and minimize system development time and cost, and recurring system costs.

ACKNOWLEDGEMENTS

The author wishes to express appreciation to Charles Baker, Lon Cecil, Larry Heep, Frank Perkins, Bob Potter, and Dr. Peter Wright for their assistance.

REFERENCES

1. E. A. Ash, "Surface Wave Grating Reflectors and Resonators," *Proceedings IEEE International Microwave Symposium*, May, 1970, pp 385-386.
2. G. L. Mathaei, B. P. O'Shaughnessy, F. Barman, "Relations for Analysis and Design of Surface Wave Resonators," *IEEE Transactions Sonics & Ultrasonics*, SU-23, March 1976, pp 99-107.
3. H. A. Haus, R. V. Schmidt, "Transmission Response of Cascaded Gratings," *IEEE Transactions Sonics & Ultrasonics*, SU-24, March 1977, pp 94-101.
4. P. S. Cross, R. V. Schmidt, "Coupled Surface-Acoustic-Wave Resonators," *The Bell System Technical Journal*, Vol. 56, No. 8, October 1977, pp 1447-1482.
5. W. J. Tanski, "Multipole SAW Resonator Filters: Elements of Design and Fabrication," *Proceedings IEEE Ultrasonics Symposium*, 1981, pp 100-104.
6. T. F. O'Shea, "SAW Resonator Filters with Optimized Transducer Rejection," *Proceedings IEEE Ultrasonics Symposium*, 1981, pp 105-110.
7. P. C. Meyer, D. Gunes, "Design and Fabrication of SAW Multipole Filters," *Proceedings IEEE Ultrasonics Symposium*, 1983, pp 66-71.
8. M. B. King, L. W. Heep, J. C. Andle, "1500 MHz Coupled Resonator Filter," *Proceedings IEEE Ultrasonics Symposium*, 1987, pp 127-130.
9. W. R. Shreve, "Surface-Wave Two-Port Resonator Equivalent Circuit," *Proceedings IEEE Ultrasonics Symposium*, 1975, pp 295-298.
10. M. Tanaka, T. Morita, K. Ono, & Y. Nakazawa, "Narrow Bandpass Filter Using Double-Mode SAW Resonators on Quartz," *Proceedings IEEE Frequency Control Symposium*, 1984, pp 286-293.
11. Y. Ebata & H. Satoh, "Current Applications and Future Trends for SAW in Asia," *Proceedings IEEE Ultrasonics Symposium*, 1988, pp 195-202.
12. P. V. Wright, "Resonator," U. S. Patent No. 4,616,197, Oct. 1986.
13. J. C. Andle, "Doubly Rotated Orientations of Cut Angles for Quartz Crystal for Novel Surface Acoustic Wave Devices," U. S. Patent No. 4,670,680, June 1987.
14. P. V. Wright, "Resonator Structure," U. S. Patent No. 4,731,595, March 1988.
15. P. V. Wright, "Low-cost High-Performance Resonator and Coupled-Resonator Design: NSPUDT and Other Innovative Structures," *Proceedings 43rd Annual Symposium on Frequency Control*, 1989, pp 574-587.
16. P. V. Wright, "Method of Making a Single Phase Unidirectional Surface Acoustic Wave Transducer," U. S. Patent No. 4,910,839, March 1990.
17. P. V. Wright, "A New Generalized Modeling of SAW Transducers and Gratings," *43rd Annual Symposium on Frequency Control*, 1989, pp 596-605.
18. P. V. Wright, "Analysis and Design of Low-Loss SAW Devices with Internal Reflections Using Coupling-of-Modes Theory," *Proceedings IEEE Ultrasonics Symposium*, 1989, pp 141-152.
19. T. E. Parker & G. K. Montress, "Frequency Stability of High Performance SAW Oscillators," *Proceedings IEEE Ultrasonics Symposium*, 1989, pp 37-45.
20. M. D. Howard and R. C. Smith, "Quartz Crystal Filters: A Review of Current Issues," *Proceedings RF Technology Expo 90*, March 1990, pp 275-288.
21. E. Christian, *LC Filters: Design, Testing, & Manufacturing*, John Wiley & Sons, New York, 1983.
22. B. G. Malcom, "The Current State of the Art of Miniature L/C Filters," *Proceedings IEEE Ultrasonics Symposium*, 1985, pp 38-42.
23. R. Levy, "Design Considerations for Lumped-Element Microwave Filters," *Microwave Journal*, February, 1988, pp 183-192.
24. A. I. Zverev, *Handbook of Filter Synthesis*, John Wiley & Sons, New York, 1967.
25. G. L. Mathaei, L. Young, E. M. T. Jones, *Microwave Filters, Impedance-Matching Networks, and Coupling Structures*, Artech House, Dedham, MA, 1980.
26. D. Ash, "Optimal Application of SAW Devices in Spread Spectrum and Other RF Systems," *Proceedings IEEE Ultrasonics Symposium*, 1989, pp 265-274.
27. J. Iseli, "Receiver Design -- Simplified," *Proceedings RF Technology Expo East*, 1988, pp 17-22.
28. P. Zibis, "UHF Low Loss SAW Filters for Front End Applications," *Proceedings IEEE Ultrasonics Symposium*, 1986, pp 293-297.
29. G. Riha, "Saw Devices for Communications Systems," *Proceedings IEEE Ultrasonics Symposium*, 1989, pp 241-250.
30. D. Ash, "Coupled Resonator Phase Shift Oscillator," U. S. Patent No. 4,760,352, June 1988.
31. J. M. Robinson, "A SAW Stabilized Monolithic Pulse Amplitude Modulated Microtransmitter," *IEEE Transactions on Consumer Electronics*, August 1987.
32. M. M. Driscoll, "Linear Frequency Tuning of SAW Resonators," *Proceedings IEEE Ultrasonics Symposium*, 1989, pp 191-194.
33. J. M. Robinson, "SAW Coupled Resonator Oscillator Technology," *Proceedings IEEE Ultrasonics Symposium*, 1989, pp 47-51.

At Long Last: Modular, Digitally Tuned RF
Filters As Easy As Amplifiers And Mixers.

by E. A. Janning

Pole/Zero Corporation
4480 Lake Forest Dr.
Cincinnati, OH 45243

INTRODUCTION

Most RF Systems are a collage of three basic components; amplifiers, mixers, and filters. An endless array of broadband amplifier and mixer modules are available to cover most any frequency band of interest. Filters of the fixed tuned variety are also readily available to cover those applications which do not require tunability. On the other hand, many applications requiring narrowband RF filters tunable over wide frequency ranges have gone begging for readily available, inexpensive solutions. These applications normally require a separate engineering effort to develop independent custom designs for each new requirement.

This paper describes a novel family of filter modules intended to offer the system designer an alternative to custom engineering. Their high power handling capability and rapid digital tuning control make them ideally suited for many applications, including receiver preselection, synthesizer/transmitter noise cleanup, cosine filtering, or for use as the frequency control element in high signal to noise (S/N) oscillators.

BACKGROUND

The quest for such filter modules is not new. As long as twenty years ago such modules were available, using varactors as tuning elements. These filters never gained wide acceptance, primarily because of the vagaries of varactor tuning; the need to generate customized analog tuning voltages (no two modules followed the same "tuning curve"), their low power handling capabilities (in the milliwatt range), and their poor linearity.

In recent years these technical problems have been largely overcome by the utilization of PIN diodes for filter tuning. Indeed, filters which operate at RF power levels of hundreds of Watts with third order intercepts exceeding +100 dBm and microsecond tuning times have been accomplished. However PIN diode switched filters have been limited to more esoteric applications because of their high cost, complexity, size, and power consumption.

The filter modules described in this paper are intended to bridge the gap between these two widely disparate technologies.

DESCRIPTION

Our goal was to develop a family of affordable filter modules in two power ranges; a 1 Watt **MINI-POLE™** series, and a 10 Watt **MAXI-POLE™** series with the characteristics shown in Table 1.

A two pole Butterworth design was chosen as the most efficacious

configuration for an off-the-shelf product, owing to its simple structure, flat passband characteristic, excellent selectivity vs loss tradeoff, and relative immunity from VSWR effects. The **MINI-POLE™** two pole series is available with passbands from 3% to 30%. The **MAXI-POLE™** series will be available with passbands as narrow as 1%. Models will be available in both series with insertion loss of less than 1 dB for the wider bandwidth units.

Standard frequency ranges were established to coincide with existing services, as shown in Table 2. Any other special frequency ranges are easily accommodated with the design, requiring little, if any, engineering time. Thus "custom" digitally tuned hopping filters, tailored for frequency range, selectivity and insertion loss are available essentially "off-the-shelf".

DESIGN APPROACH

Figure 1 shows the standardized configuration for the entire series of filters. Input and output matching networks transform the 50 Ohm input/output impedance to the natural design impedance of each filter. The matching transformation is chosen to hold the singly loaded partial Q of each section equal to a constant fraction of the unloaded Q across each frequency band. This results in a constant insertion loss design, causing the filter bandwidth to vary with frequency. The resulting bandwidth falls between a constant Q (bandwidth proportional to frequency) and a constant bandwidth (Q invariant with frequency). An interstage

coupling network completes the Butterworth structure. These matching networks are easily modified to accommodate the various bandwidth/insertion loss combinations.

Tuning is accomplished via a PIN diode switched binary capacitor array. A unique feature of this particular array is that it is broadband in nature and usable over wide frequency ranges. Thus the same array can serve as a tuning element at widely separated frequencies by simply changing the value of the tank inductor. It is truly a "universal" broadband digital capacitor array.

Shown in Figure 2 is the response of a typical **MINI-POLE™** two pole filter (30 to 90 MHz, 10% bandwidth model) at several tune positions across its operating frequency range.

The digital capacitor arrays are driven by a decoder/driver which contains all of the necessary circuitry to receive digital tuning commands, translate them to the internal filter tuning codes, and drive the PIN diodes with the proper bias. The entire tuning process is accomplished in under 10 microseconds, making the filters suitable for fast hop applications. Programmable logic handles the decoding task, making practically any input format compatible, and compensating for any variation in internal filter tune codes. The standard input format is an 8 bit binary sequence. Each filter has 250 tune positions, linearly spaced over its RF tuning range. For example, the 30 to 90 MHz filter tunes a 60 MHz range in 250 equal steps of $60 \text{ MHz}/250 = 240 \text{ kHz}$ each, as depicted in Table 3.

The six codes which are unused for frequency tuning are used for housekeeping functions, such as a power saver mode in which all PIN diodes are biased off, or an RF blanking mode in which both tank circuits are shorted to ground, providing 60 dB isolation between the input and output at all frequencies.

Forward bias for the diodes is supplied by the decoder/driver from a standard +5 VDC logic supply. Supply current varies with frequency, averaging 100 mA for the complete MINI-POLE™ two pole filter. Reverse bias is also supplied by the decoder/driver from an external +V_b supply. A unique feature of the design is that the value of +V_b is at the total discretion of the user, and may be established at any value between +15 and +150 VDC.

The primary effect of raising the bias is to improve the intermodulation performance. Surprisingly, changing the bias has no adverse effect on power handling capability. This is because the biasing circuitry has been designed to allow the bias to "free wheel", thus allowing the PIN diodes to establish their own value of reverse bias. This turns out to be a very stable method¹ of establishing reverse bias, the only effect of which is to modify the intermodulation performance. Those applications requiring the ultimate in intermodulation performance will still require an external bias, the minimum value of which is a function of the power level at which the filter is operating.

In most applications, adequate performance will be obtained using only the minimum +15 VDC bias, even in high power applications. Thus the need for the usual high voltage supplies is obviated. Current drain from the +V_b supply is less than 100 microamperes. Those familiar with PIN diode drivers will appreciate that no negative voltages are required.

PACKAGING

The MINI-POLE™ two pole filters complete with internal decoder/driver circuitry are supplied as hermetically sealed modules with dimensions of 1.25 X 2.50 X 0.50 inch, a volume of approximately 1.5 in³, or 0.75 in³ per pole. Pins provide all external connections out the bottom of the module. Hermeticity ensures maintenance of the filter performance parameters under all environmental extremes. Internal construction consists of a single circuit board with surface mount components on both sides.

Connectorized versions are also available in 1.50 X 3.25 X 0.75 inch enclosures with SMA, BNC, TNC, or type N connectors. Power and control inputs are via a 15 pin D-microminiature connector.

APPLICATIONS

RECEIVER PRESELECTION

The **MINI-POLE™** filters are ideally suited for wide dynamic range receiver front ends, as shown by the typical block diagram in Figure 3. Placing a low noise RF amplifier module between two **MINI-POLE™** filters followed by a double balanced mixer module provides a high performance receiver front end from standard bolt-together modules. An optional LO tracking filter can be added to improve receiver desensitization caused by noisy or high spurious content LO sources.

In this example a low loss (-2 dB, 8% bandwidth) **MINI-POLE™** is used as the first stage to preserve noise figure, while a higher loss (-4 dB, 4% bandwidth) **MINI-POLE™** is used for enhanced selectivity following the amplifier.

Figure 4 summarizes the overall performance of the preselector; +13 dB overall gain, 6 dB noise figure, and a third order inband intercept point (IP₃) of +17 dBm, truly a wide dynamic range front end.

The performance really shines when we consider that the filters greatly improve the dynamic range performance as interfering signals move away from f_0 . Figure 5, for example, illustrates how the filters dramatically improve the saturation (desensitization) performance for out of band interfering signals. Similar results accrue for intermodulation, crossmodulation, and other

deleterious effects of strong interfering signals. The resultant wide dynamic range front end is a state of the art performer, especially in a dense urban or cosite environment. Figure 5 also illustrates that, for this example, the performance is limited by the amplifiers and mixer. Thus even better performance could be obtained using improved components.

TRANSMITTER NOISE/SPURIOUS CLEANUP

Another excellent application for the **MINI-POLE™** is cleaning up noise and spurious outputs from transmitters, exciters or synthesizers. Simply placing it in line with the output and supplying a digital frequency word can significantly reduce spurious and noise outputs. The fast tuning characteristic of the filters allow them to track even fast frequency hopping sources. Shown in Figure 6 is a typical application, using a low power exciter to generate a clean (S/N=200 dBc/Hz) 100 Watt transmitter output. For even higher performance, a **MAXI-POLE™** filter could be used at the 10 Watt power level in the amplifier chain.

COSITE FILTER/RF POWER BOOSTER

Combining the receiver preselection and transmitter cleanup applications together results in an easy method of increasing the cosite interference tolerance of existing transceivers, especially the frequency hopping variety. Figure 7 depicts a combination cosite filter and RF power output booster.

RF MULTIPLEXER/COMBINER

As with any reactive filter, **MINI-POLE™** filters can be used in banks with a common input or output connection to provide low loss reactive combining of non-coherent (different frequency) signals. Unlike passive non-coherent RF power combining which imposes severe minimum losses (e.g., 3 dB for two signals, 6 dB for 4 signals, etc.), reactive non-coherent combining entails only the losses associated with the filters themselves, plus whatever losses are added by any imperfect impedance matching. For the example shown in Figure 8, each channel suffers only a 2 dB loss, as against a theoretical 6 dB loss with passive combining. An additional advantage of the filter combiner is the selectivity afforded each path by the filters, further reducing noise and spurious content. The circuit is bidirectional: the same comments apply to the RF splitter case.

The multiplexed **MINI-POLE™** filters may cover the same band or different bands. However, they must be ordered as a set so as to control the impedance matching (reactive loading effects) at the common port.

HIGH S/N OSCILLATOR

In addition to being used to clean up existing sources, the **MINI-POLE™** makes an excellent resonator for use in high power, digitally tuned, low noise oscillators. The output S/N ratio of an oscillator may be expressed² as:

$$S/N = 10 \log_{10} \left[\frac{2P_0 Q^2 \omega_m^2}{4KTQ^2 \omega_m^2 + FG\omega_0^2} \right] \quad \text{dBc/Hz}$$

where;

P₀ = Oscillator output power

Q = Resonator loaded Q

K = Boltzmann's constant

T = Temperature (⁰ Kelvin)

ω₀ = RF oscillator frequency

ω_m = frequency removed from ω₀

F = Oscillator active device noise figure

G = Oscillator active device operating gain

For small ω_m,

$$S/N \approx 10 \log_{10} \left[\frac{4P_0 Q^2 \omega_m^2}{FGKT \omega_0^2} \right] \quad \text{dBc/Hz}$$

For large ω_m,

$$S/N \approx 10 \log_{10} \left[\frac{P_0}{KT} \right] \quad \text{dBc/Hz}$$

SUMMARY

Assuming low noise active devices for the oscillator and buffer, the design problem reduces to tuned circuit Q (or, more accurately, the rate of change of phase vs. frequency at f_0), and operating power. Power and Q both control the resultant S/N ratio; in essence, as a squared function of Q and as a linear function of power. Thus, for example, raising the power level of an oscillator by 30 dB increases the S/N ratio (at any frequency removed) just as much as increasing the Q by a factor of 32 !! Often in the quest for higher S/N ratio, only the Q of the oscillator resonator is emphasized, while the operating power of the oscillator is ignored.

In the simple example shown in Figure 9, the oscillator is allowed to operate near the 1 Watt power level, producing an ultimate S/N ratio approaching 200 dBc/Hz. Not only is the ultimate S/N ratio very good, but is achieved relatively close-in. In the example shown, the ultimate S/N would be reached at less than 5% removed from f_0 .

A new digitally tuned filter module is about to join ranks alongside amplifier and mixer modules, complementing the arsenal of tools available to RF System designers. Two-pole models are available to cover octave or greater bands from 10 MHz to 1 GHz, with passbands from 1 to 30 %. Tuning is accomplished in under 10 microseconds from an 8 bit TTL/CMOS compatible input. Two series are presently being offered; the **MINI-POLE™**, a one Watt design packaged in 1.5 in³, and the **MAXI-POLE™**, a ten Watt design packaged in approximately 8 in³.

These digitally tuned hopping filters will find many applications in RF Systems, including Receiver preselection, transmitter noise/spurious cleanup, Cosite filtering, signal multiplexing, and high S/N RF sources.

REFERENCES

- [1] G. Hiller, R. Caverly, "The Reverse Bias Requirement for PIN Diodes In High Power Switches and Phase Shifters", IEEE MTT-S International Microwave Symposium, Dallas, Texas, 1990.
- [2] E.A. Janning, "A Low Noise Oscillator", Master's dissertation, University of Cincinnati, Ohio, 1967.

AUTHOR BIOGRAPHY

Eugene A. Janning received his BSEE from the University of Dayton in 1960, and his MSEE from the University of Cincinnati in 1967. In 1972, he co-founded Xetron Corporation, Cincinnati, OH, where he served in the capacity of Chief Scientist until leaving in January, 1990, to form Pole/Zero Corporation. While at Xetron, Mr. Janning pioneered in the development of high power, high performance PIN diode frequency hopping filters and multicouplers and high S/N ratio RF sources.

	MINI-POLE™	MAXI-POLE™
Frequency Coverage	10 MHz to 1 GHz	
RF Tuning Range	3:1	
RF Power Handling	1 Watt	10 Watts
Third Order IP	+ 40 dBm	+ 60 dBm
Bandwidth	3% to 30%	1% to 30%
Input/Output Z	50 Ohms, VSWR < 1.5:1	
Tuning Control	Digital	
Tuning Speed	10 μS	
Packaged Size	1 in ³ /pole	4 in ³ /pole
DC Power	+ 5 VDC	

TABLE 1: DESIGN GOALS

10 to 30 MHz	200 to 400 MHz
30 to 90 MHz	400 to 700 MHz
90 to 200 MHz	.70 to 1 GHz

TABLE 2: STANDARD FREQUENCY BANDS

TUNE CODE	FREQUENCY (MHz)
00000000	30.000
00000001	30.240
00000010	30.480
00000011	30.720
.....
.....
11110111	89.280
11111000	89.520
11111001	89.760
11111010	90.000
11111011
11111100
11111101
11111110	RF Blanked
11111111	Power Saver

TABLE 3: EXAMPLE FILTER TUNE CODES

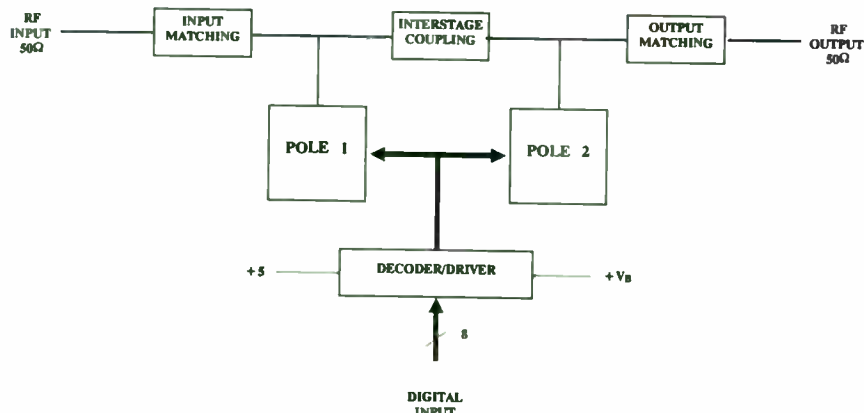


FIGURE 1: FILTER CONFIGURATION

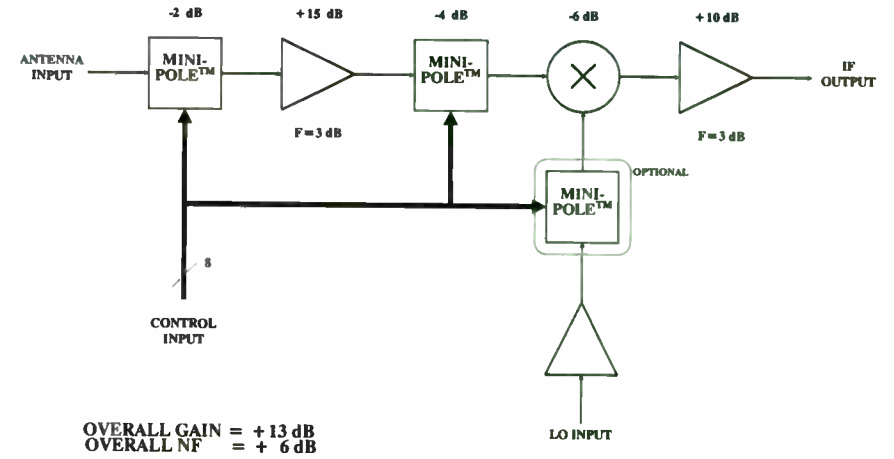


FIGURE 3: WIDE DYNAMIC RANGE FRONT END

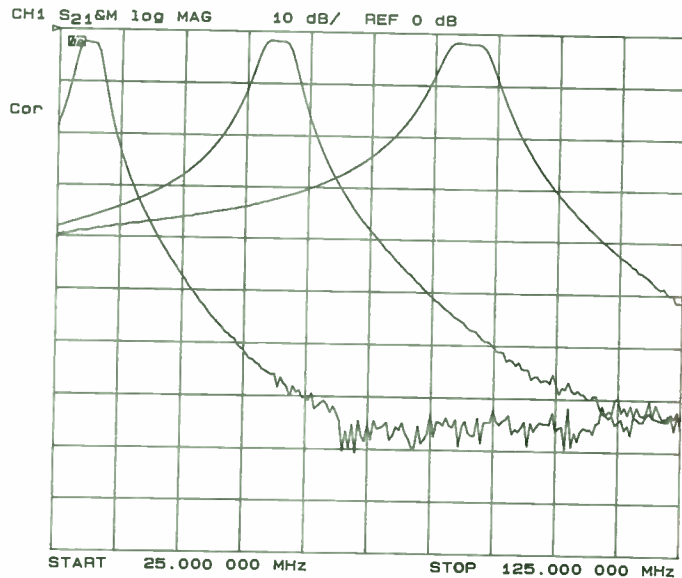
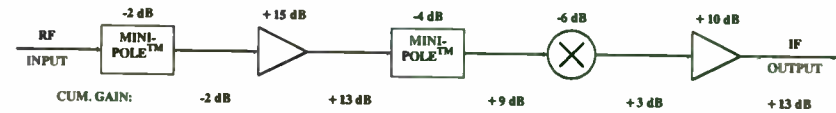


FIGURE 2: TYPICAL MINI-POLE™ RESPONSE



MODULE 1 dB SATURATION (INBAND) REFERENCED TO MODULE INPUT				
+36 dBm	+13 dBm	+36 dBm	+20 dBm	+13 dBm
MODULE 1 dB SATURATION (INBAND) REFERENCED TO RECEIVER INPUT				
+36 dBm	+15 dBm	+23 dBm	+11 dBm	+10 dBm
OVERALL RECEIVER INPUT INBAND 1 dB SATURATION = +7 dBm (rms ADDITION)				

INBAND THIRD ORDER INTERCEPT (IP ₃) OF MODULE REFERENCED TO ITS INPUT				
+46 dBm	+23 dBm	+46 dBm	+30 dBm	+23 dBm
MODULE CONTRIBUTION TO INBAND IP ₃ REFERENCED TO RECEIVER INPUT				
+46 dBm	+25 dBm	+33 dBm	+21 dBm	+20 dBm
OVERALL RECEIVER INPUT INBAND IP ₃ = +17 dBm (rms ADDITION)				

FIGURE 4: RECEIVER INBAND DYNAMIC RANGE PERFORMANCE

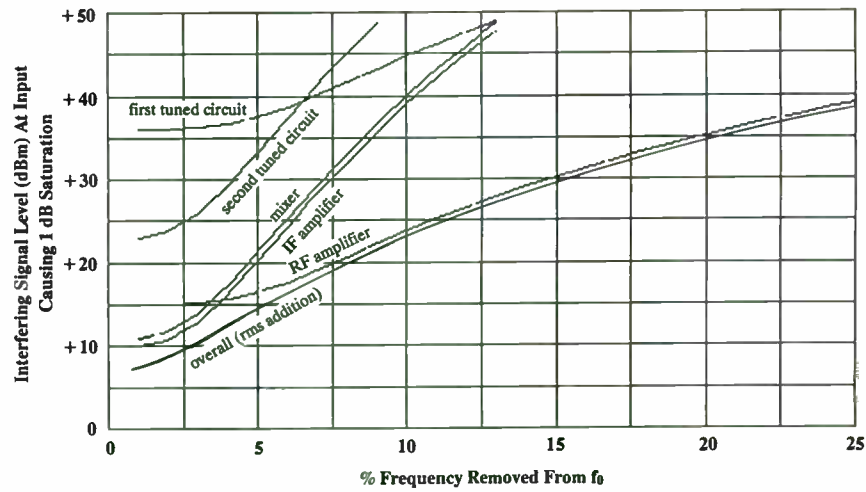


FIGURE 5: SATURATION vs. FREQUENCY REMOVED

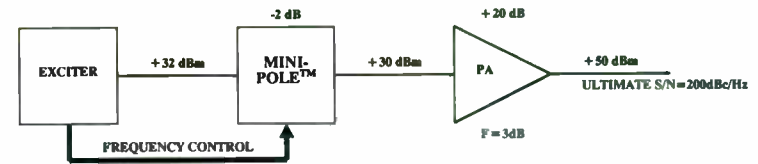


FIGURE 6: TRANSMITTER NOISE CLEANUP

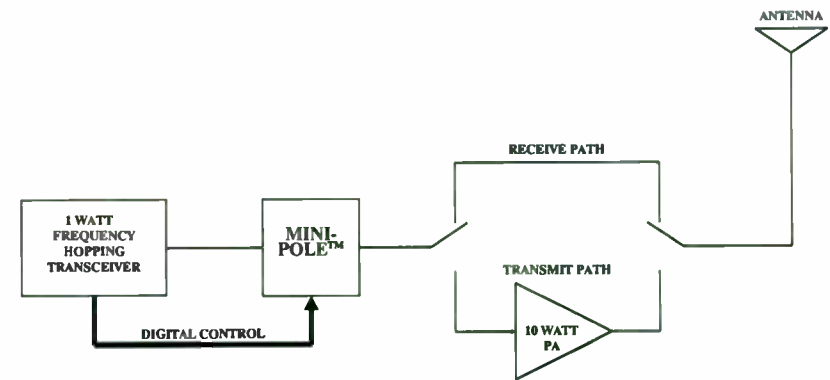


FIGURE 7: COSITE FILTER/RF POWER BOOSTER

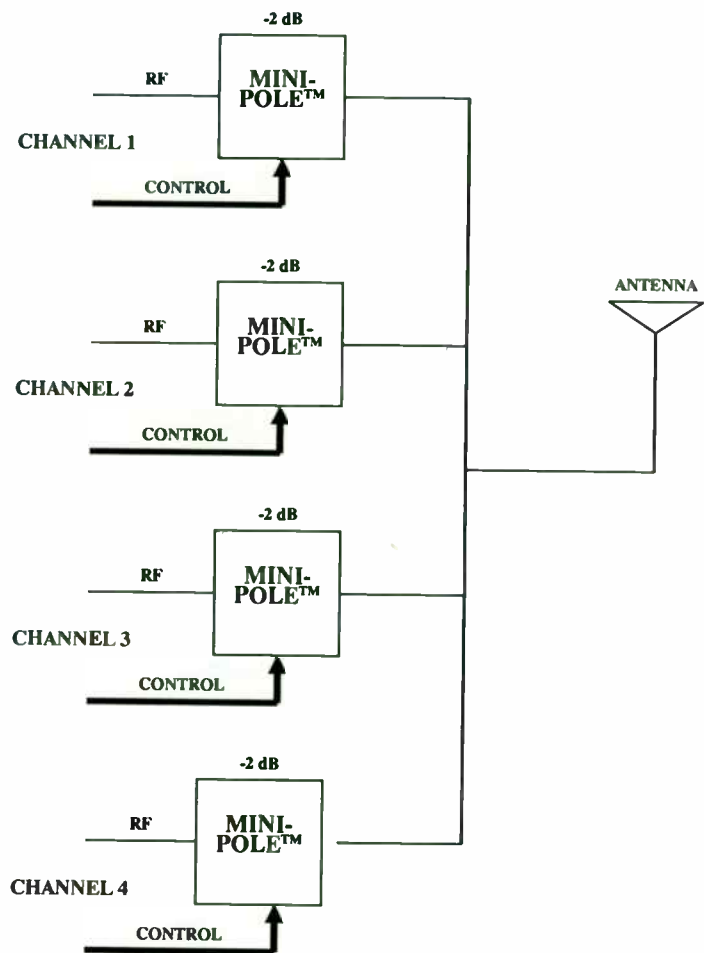


FIGURE 8: RF MULTIPLEXER/COMBINER

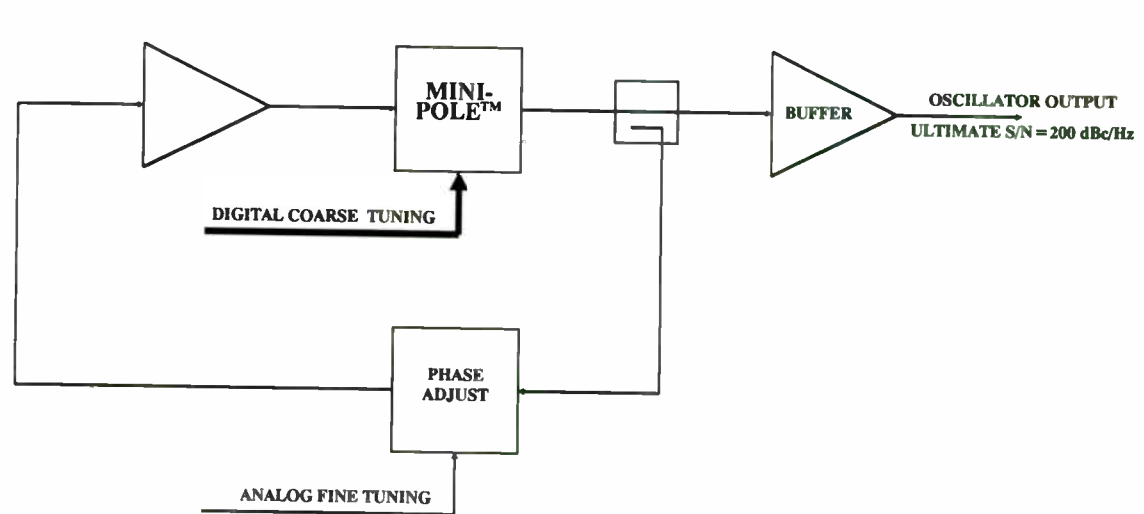


FIGURE 9: HIGH S/N OSCILLATOR

and shapefactor.

Because of the wide selection of narrowband SAW techniques now available, the receiver design can flow smoothly from system requirements to choice of architecture and filter specifications. This paper will start with several different typical receiver requirements, point out the critical factors, and develop the SAW solution for each.

Each example is introduced by studying the general requirements of the system. These general requirements along with available filter technology then determine the actual filter specifications. The choice of a particular SAW filter technology is crucial at this stage. Finally, the actual filter implementation and performance is reviewed.

INTRODUCTION

Narrowband (less than 0.2%) IF filtering in the high VHF and UHF frequency band represents a special challenge although it offers many benefits. Only a few techniques produce high quality responses in a reasonable packaging configuration. Three main types of SAW filters have found common use in this area: the in-line coupled resonator filter (RFI), the waveguide coupled resonator filter (RFW), and the reflective array filter (RAF). Several tradeoffs are involved in designing and selecting a particular filter approach. This paper will review the general concerns of narrowband SAW filtering, the specific characteristics of each approach, and finally study the application of

NARROWBAND SAW FILTERS FOR IF APPLICATIONS

B. Horine and S. Gopani

Sawtek, Inc. PO Box 609501, Orlando, FL 32860-9501

ABSTRACT

Surface acoustic wave (SAW) filters offer Q's comparable to crystal filters from 50 MHz to well over 1 GHz. Resonator filters using in-line coupling are the most familiar SAW approach to narrowband filtering. On the other hand, the newer waveguide coupled resonator filter offers superior close-in rejection. For the same filter size, the RFW achieves 30 to 40 dB of close-in rejection while the RFI achieves 10 to 20 dB. Since both approaches exhibit losses of only 3 to 6 dB, either may be easily cascaded to obtain greater rejection.

For narrowband applications where linear phase or phase tracking is important, resonant type filters may not meet performance requirements and a transversal design may be needed. In normal SAW transversal filter design, however, distortion due to overcoupling becomes a significant design challenge below 0.3% fractional bandwidth. Reflective array filters avoid this pitfall and result in a shorter device with little distortion for the same bandwidth

these filters in particular IF subsystems.

Frequency accuracy is critical in narrowband filtering applications. For SAW devices, the most important sources of frequency error are the manufacturing set accuracy and the temperature stability. Aging is also important but is nearly an order of magnitude smaller. The total required frequency tolerance is added to the information bandwidth in order to determine the passband width required of the filter. The tolerance requirement is also subtracted from the specified rejection bandwidths, thereby narrowing the actual filter rejection skirts. The tolerances required, therefore, for narrowband filters can have a dramatic impact on the shape factor of the filter. Also, the rejection floor tends to degrade at the wider bandwidths needed to cover the tolerances. For these reasons, it is important to maintain a high degree of control over the sources of error and minimize the frequency tolerance required.

The manufacturing set accuracy can range from +/- 30 ppm to +/- 200 ppm. The narrower range is used for low frequency applications where it is more effective to deal with a tight set accuracy rather than be driven to a lower shape factor and higher order filter. The wide end of the range is typically used for the narrowest band signals ($BW3 < 300$ ppm) where the rejection bandwidth is not critical. Most filters are designed assuming a +/- 75 ppm tolerance for manufacturing set accuracy.

ST cut quartz is the most commonly used substrate for narrowband filters, although other singly rotated cuts, particularly those with lower coupling coefficients, are of interest [1,2]. The complexities of beam steering, especially over a large temperature range has slowed the use of these other cuts. ST

quartz exhibits a parabolic frequency versus temperature curve, and by varying the cut angle and metal thickness slightly, the turnover temperature can easily be set within +/- 10°C. Assuming a conservative second order coefficient, this leads to the required tolerances listed in Table 1.

Range	Frequency Drift
0°C to 60°C	-55 ppm
-20°C to 75°C	-113 ppm
-54°C to 85°C	-220 ppm

Table 1: Typical Temperature Stabilities

In order to develop an appreciation for the significance of these frequency tolerances in SAW devices, Figure 1 details an example design. Note that the addition of the individual tolerances is done by adding the peak to peak value of each component. As this example shows, the addition of the required tolerances has increased the number of poles needed to synthesize the filter function.

SAW Resonator Filters

Multipole resonator filters are the workhorse of narrowband filtering in SAW technology. Their center frequencies range from 50 MHz to over 1250 MHz.

At 50 MHz the package required is 2 inches long. At 1250 MHz the line size is about 0.6 μm . Physical size and lithography capabilities therefore set the soft limits on the frequency range.

Bandwidth is limited on the low side to approximately 0.02% by the finite Q of the individual resonant cavities and by the required frequency tolerances. On the other end, 0.2% bandwidth is achievable. Wider bandwidths than this are difficult to impedance match and typically do not provide adequate rejection.

Insertion loss is sensitive to the center frequency and the number of poles. It ranges from 2 dB to 7 dB for most applications. Because this loss is usually easily handled in IF applications, cascading filters is an effective technique to increase the rejection. The filters are simply coupled resonant cavities and they exhibit the familiar Butterworth or Chebychev characteristics. The rejection floor is highly dependent upon the coupling mechanism between poles of the filter. These mechanisms are the basis for the following two resonator filter classifications.

In-Line Coupling

In-line coupling, diagramed in Figure 2, is the most established monolithic coupling technique for SAW resonator filters [3]. In this design, the outside acoustic reflector arrays trap the energy within the device ensuring a low loss and high Q response. A center reflector splits the device into two separate resonant cavities (or poles) and controls the degree of coupling. The interdigital transducers convert the energy from electrical to acoustical and

vice-versa. This configuration results in a monolithic 2 pole building block. Higher order filters are normally implemented by cascading these 2 pole sections by directly connecting the transducers and using a shunt, interstage matching inductor (often referred to as transducer coupling) [3].

The reflectors in the arrays are distributed uniformly on half-wavelength centers and are designed to trap the acoustic energy over a very narrow bandwidth. Beyond their finite bandwidth, the reflectors become essentially transparent so that the filter response is given simply by the transmission from one transducer to the other in a simple delay line configuration. This results in a broad $(\sin x / x)^2$ response, as shown in Figure 3, with a resonance peak at the center where the reflectors trap the energy launched by the transducers. If high selectivity is important, one would cascade the 2 pole sections to achieve better than the 18 - 20 dB near-in rejection shown. On the other hand, where absolute rejection more distant from the frequency of operation is most important as in some synthesizer applications, these filters provide low loss with outstanding rejection floors.

In general, the RFI approach achieves 45 dB to 55 dB of ultimate rejection with 10 dB to 18 dB of near-in rejection per 2 pole section. The near-in rejection degrades with increasing bandwidth resulting in a maximum practical bandwidth of 0.20% for most applications.

Waveguide Coupling

Waveguide coupling alleviates the near-in rejection limitation by coupling the energy transversely to the normal traveling wave direction [4,5]. The topology of the design is illustrated in Figure 4. In this case, a waveguide is formed by embedding a single cavity resonator in a slow wave structure. Because of the boundary conditions, the fundamental mode profile across the beamwidth of the device is cosinusoidal within the guide with an exponential evanescent tail immediately outside the guide. If an identical guide is placed alongside the first one, energy may be transferred from pole to pole via the evanescent tail. The amount of intersection of the evanescent tails determines the coupling and therefore the bandwidth of the resulting filter.

When the reflectors become transparent in this design, outside the narrow stopband, the evanescent tail is no longer supported resulting in zero coupling, and the wave simply propagates to the end of the crystal and is absorbed or dispersed. Since there is no longer any path from input to output, the near-in rejection is excellent. In practice, this level is limited by spurious waveguide modes and electromagnetic feedthrough. The response of this type of filter is plotted in Figure 5. This is a 4 pole filter implemented monolithically using transducer coupling without a coupling inductor by taking advantage of the zero susceptance effect of a long transducer [6]. This direct cascading is typical of RFWs which are normally designed as 4 pole building blocks rather than 2 pole blocks as in the RFI case.

RFWs exhibit 40 dB to 50 dB of rejection with a few narrowband spurs as high

as 30 dB to 40 dB. Because of crosstalk concerns and material property constraints, the bandwidth is currently limited to just over 0.1%. Extending the bandwidth range in order to cover broader applications is the subject of current research.

Transversal Reflective Array Filters

In applications where linear phase and good shape factor filters are required, transversal design is a preferred choice. Figure 6a shows a conventional narrowband transversal filter design. The problem associated with this design is that the transducers are very long and comprised of many electrodes. The interdigitated electrodes of the input transducer generate, sample and perturb the surface wave passing through them. The surface wave is detected and reconverted back to electrical energy by the output transducer. The accumulated perturbations and overcoupling caused by the large number of electrodes in the transducers cause the output to deviate from a desired ideal impulse response. This results in both amplitude and phase distortions in the filter passband response.

One way to avoid these problems is to separate the frequency selection and energy transduction process as indicated in Figure 6b [7]. The reflective array filter (RAF) design approach presents numerous advantages. The launching and receiving transducers have relatively few fingers thereby eliminating the overcoupling in the transduction. Sampling of the propagating wave by the reflective arrays is performed by localized mechanical reflections making the filter more tolerant to defects such as opens and shorts. The total reflective

grating impulse response which determines the filter frequency characteristics can be computed by performing a modified spatial convolution of the two reflective arrays. Since the two arrays are folded, the reflective array filter results in a shorter device for the same bandwidth and shape factor.

APPLICATIONS

IF applications may require a steep shape factor for channel selectivity, high rejection, minimum flyback, or a flat passband. In some applications linear phase and low VSWR may be required. The choice of filter element will be dependent upon these specific requirements. A few examples will clarify this.

ANTI-JAM MODEM

An anti-jam modem is intended to accept a modulated signal from a radio and demodulate and decode the information in the presence of jammers. An example is a Qualcomm modem that accepts a frequency hopped signal centered at 70 MHz. The information bandwidth is hopped over a 40 MHz bandwidth. In this application, good power linearity is important in order to reduce jamming effects. The noise figure is dominated by the radio so the insertion loss of the filter is not critical. Since the signal is M'ary FSK modulated, a flat frequency response is desired.

Figure 7 is a simplified block diagram of the IF section. Up conversion is the obvious choice in view of the large bandwidth. Since IMD is a concern, it is

important to eliminate any extraneous tones as early in the chain as possible. A high resolution synthesizer is used as the first LO and a narrowband filter is used in the first IF. By setting the first IF at 289.368 MHz, a convenient 300 MHz fixed second LO can be used to convert the signal to approximately 10.6 MHz where very inexpensive filters and other components are available. At this point the signal is demodulated.

Clearly, the high frequency of operation, narrow bandwidth, and good IMD rejection suggest a SAW filter. An RFW was designed with ± 77 kHz 1 dB bandwidth. The specified 20 dB bandwidth of ± 215 kHz sets the noise bandwidth of the system while the 45 dB bandwidth of 1 MHz sets the jamming bandwidth of the modem.

Figure 8 is a response plot of the filter showing both the narrowband and wideband response. Note that the narrowband spurious responses on the low side are located just inside the jamming bandwidth. The insertion loss and ripple are 4.5 dB and 0.25 dB respectively.

SATELLITE TRANSPONDER

Satellite transponders have special requirements that are not always as critical in other applications. For example, ruggedness, reliability, small size, and low weight often rank at the top of the requirements list. In addition, loss is important to the extent of avoiding being downlink limited. Finally, the interference needing rejection is mainly comprised of the many other signals used in the satellite.

The Data Collection Platform (DCP) of the GOES satellite built by Ford Aerospace Company for NASA includes both interrogate and reply transponders that communicate between a control station and hundreds of remote stations scattered throughout the footprint of the satellite. In order to transmit the data efficiently, it is frequency and time multiplexed.

Figures 9 and 10 illustrate the simplified block diagrams of the interrogate (DCPI) and reply (DCPR) channel respectively. In both channels, two filters are cascaded in order to meet the ultimate rejection requirements. The DCPI filter is used primarily to reject other incoming signals that are used elsewhere in the communications subsystem. On the other hand, the DCPR filter is more concerned with eliminating unwanted signals coming from the ground and especially reducing the out-of-band noise. Both filters operate in the 400 MHz range with narrow bandwidth, must survive a 1500 G mechanical shock, and be small in size and weight. These requirements suggest a SAW resonator filter.

DCPR

The DCPR channel is specified with a 400 kHz bandwidth at 1.4 dB. Once the appropriate frequency tolerances have been added, the passband width is too large to be implemented using RFW technology. Instead, a 12 pole RFI is used to achieve 60 dB of near-in rejection. These are delivered as a pair of 6 pole devices so that amplifiers may be placed in between them. The noise bandwidth is specified at 500 kHz. The VSWR over the 3 dB bandwidth is important so that the integration of the satellite can proceed smoothly and at a low risk. This is specified at 1.92:1 which will require some resistive padding

inside the device. Finally, because the signal is actually a composite, frequency multiplexed signal, no sharp transitions can be tolerated since they can affect a single channel significantly. This requirement leads to a passband slope specification of 0.1 dB / kHz. The response of a 6 pole unit is plotted in Figure 11. The insertion loss of nearly 17 dB resulted in a VSWR of 1.3 : 1 maximum across the 3 dB bandwidth. This bandwidth is 495 kHz wide.

DCPI

The DCPI channel is specified at only 180 kHz bandwidth at 1.2 dB. This is narrow enough for an RFW approach. In this case 8 poles are required to achieve the 60 dB near-in rejection specification. The filters are delivered as separate 4 pole devices so that amplifiers may be used in between. The specifications are similar to those for the DCPR filter, scaled accordingly for the narrower bandwidth. The response of a single 4 pole device is plotted in Figure 12.

DIRECTION FINDING

Direction finding is required in electronic warfare applications and navigation and landing system applications. The principle is to measure relative phase from multiple sources (antennas). It is obviously important to have linear phase, and in some applications, phase tracking over temperature is required. Normally a calibration signal is used to effectively zero any overall phase offset at any given temperature.

Since linear phase is a major issue, an RAF type filter is normally used. The

IF processing should be done below 600 MHz because of fabrication limitations. Figure 13 and 14 illustrate the measured amplitude and phase response of a 70 MHz filter with a 3 dB bandwidth of 140 KHz. The 40 dB bandwidth is 400 KHz and the near-inrejection is well above 40 dB. The ultimate rejection is limited by electromagnetic feedthrough to 55 dB. The filter has an insertion loss of 20.7 dB with very little amplitude ripple. The filter is externally matched with an inductor on each port. A two element matching network can reduce the insertion loss of the filter to 17 dB, but this is at the expense of increasing the amplitude and phase ripples. The excellent phase characteristics of the filter makes the RAF design an optimum approach for applications where phase linearity and phase tracking are important.

Figures 15 and 16 show the modeled amplitude and phase responses for the same 70 MHz filter. The transfer function of the filter is the product of the individual transfer functions of the input transducer, output transducer, the associated matching networks and the reflecting grating arrays. Table 2 lists the predicted and actual measured parameters of the 70 MHz RAF filter. As can be seen, the simulations are in close agreement with the experimental results. A detailed discussion of the filter design and its modeling approach will be presented in a future paper [8].

Parameters	Actual	Modeled
Insertion Loss(dB)	20.7	19.5
1 dB BW (KHz)	96	101
3 dB BW (KHz)	142	142
40 dB BW (KHz)	396	385
Phase deviation (deg.)	± 1	± 1

Table II : A Comparison of Theoretical Modeled values and Experimental results.

CONCLUSION

From the above discussion, it is clear that SAW filters can and are being used in a wide variety of narrowband IF applications. RFW filters offer the best near-in rejection performance for a given size and insertion loss but are limited to 0.1% bandwidth. When greater bandwidths are called for but low loss is important or near-in rejection is not a concern, RFI filters are effective. Because of their low loss, resonator type filters are often cascaded when greater rejection or steeper shape factors are required. Finally, when linear

phase is required, RAF filters can satisfy the specifications provided a larger size and higher insertion loss can be tolerated.

ACKNOWLEDGMENTS

The authors gratefully acknowledges the contributions of R. Kornfeld of Qualcomm and J. J. MacFarland of Ford Aerospace Company who provided the details of their subsystem designs for this paper. The author also acknowledges the contributions of T. O'Shea, R. Brown, and J. Sunkin who contributed to the design of these filters and R. Hays who contributed much helpful guidance in the preparation of this paper.

REFERENCES

1. R. Webster, "X-cut Quartz for Improved Surface Acoustic Wave Temperature Stability," in the Journal of Applied Physics, vol 56, 1984, pp 1540-1542.
2. B. K. Sinha, "A Stress and Temperature Compensated Orientation and Propagation Direction for Surface Acoustic Wave Devices," in the IEEE Transactions on Ultrasonics, Ferroelectrics, and Frequency Control, vol. UFFC-34, NO1, 1987, pp 64-74.
3. P. S. Cross, R. V. Schmidt, and H. A. Haus, "Acoustically Cascaded ASW Resonator Filters," in the 1976 Ultrasonics Symposium Proceedings, pp. 277-280.
4. H. F. Tiersten and R. C. Smythe, "Guided Acoustic Surface Wave Filters," in the 1975 Ultrasonics Symposium Proceedings, pp. 293-294.
5. M. Tanaka, T. Morita, K. Ono, and Y. Nakazawa, "Narrow Bandpass Filter Using Double-Mode SAW Resonators on Quartz," in the Proceedings of the 38TH Annual Symposium on Frequency Control, 1984, pp 286-293.
6. M. Hikita, Y. Kinoshita, H. Kojima, and T. Tabuchi, "800 MHz Low Loss SAW Filters Using New Phase Weighting," in the IEEE MTT International Microwave Symp. Digest, 1982, pp. 46-48.
7. J. Melngailis, J. M. Smith, and J. H. Cafarella, "Bandpass Surface Wave Filters," in the 1972 Ultrasonics Symposium Proceedings, pp 221-225.
8. S. Gopani, R. Brown, J. Hines, and B. Horine, "Reflective Array SAW Narrowband Filters," to be published in the 1990 Ultrasonics Symposium Proceedings.

Example:

Set accuracy = ± 75 ppm

Temperature stability = -113 ppm

Lifetime aging = ± 20 ppm

Total required tolerance = 303 ppm

Information BW = 400 ppm

Rejection BW = 2000 ppm

Shape Factor = $5 : 1$

(w/o tolerances)

Filter BW = $400 + 303 = 703$ ppm

Rej. BW = $2000 - 303 = 1697$ ppm

Shape Factor = $2.4 : 1$

(w/ tolerances)

Figure 1: Impact Of Frequency Tolerances

Example:

Set accuracy = ± 75 ppm

Temperature stability = -113 ppm

Lifetime aging = ± 20 ppm

Total required tolerance = 303 ppm

Information BW = 400 ppm

Rejection BW = 2000 ppm

Shape Factor = $5 : 1$

(w/o tolerances)

Filter BW = $400 + 303 = 703$ ppm

Rej. BW = $2000 - 303 = 1697$ ppm

Shape Factor = $2.4 : 1$

(w/ tolerances)

Figure 1: Impact Of Frequency Tolerances

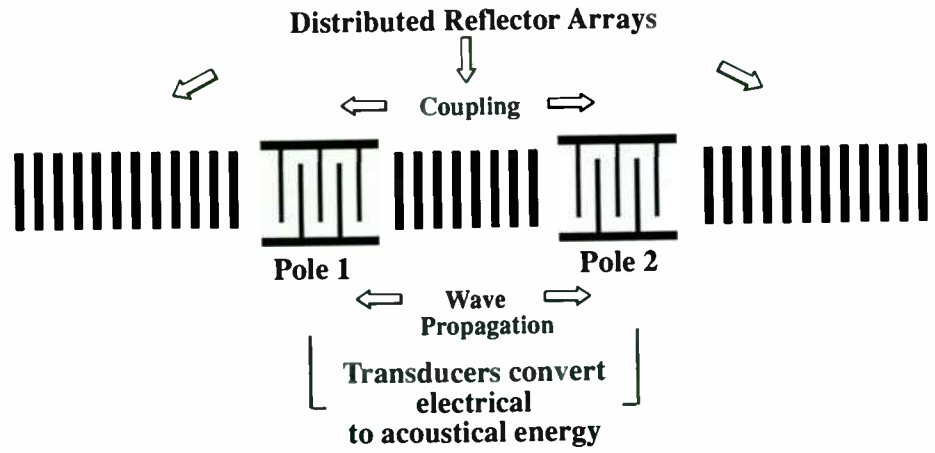


Figure 2. Inline Coupled Resonator Filter Schematic

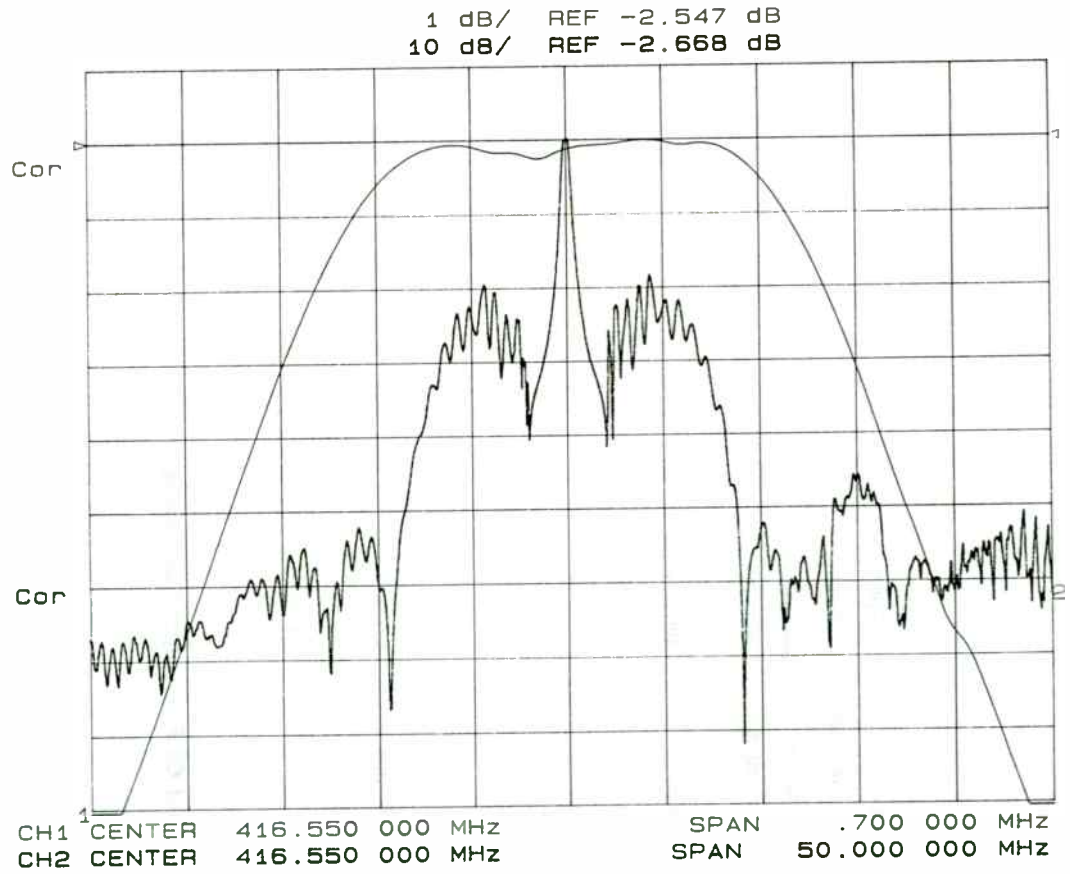


Figure 3. Inline Coupled Frequency Response

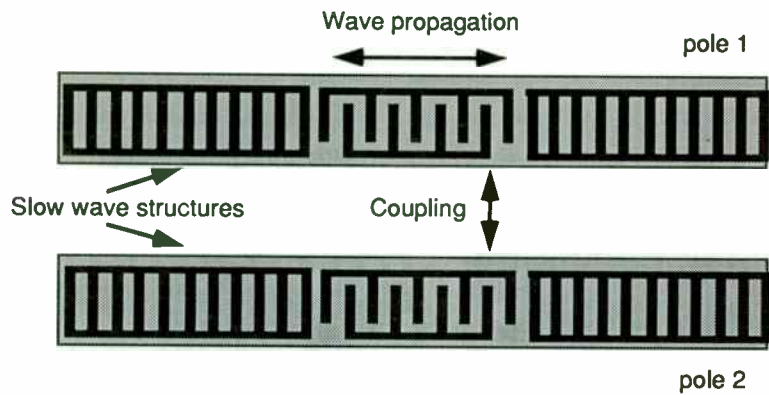


Figure 4. Waveguide Coupled Resonator Filter Schematic

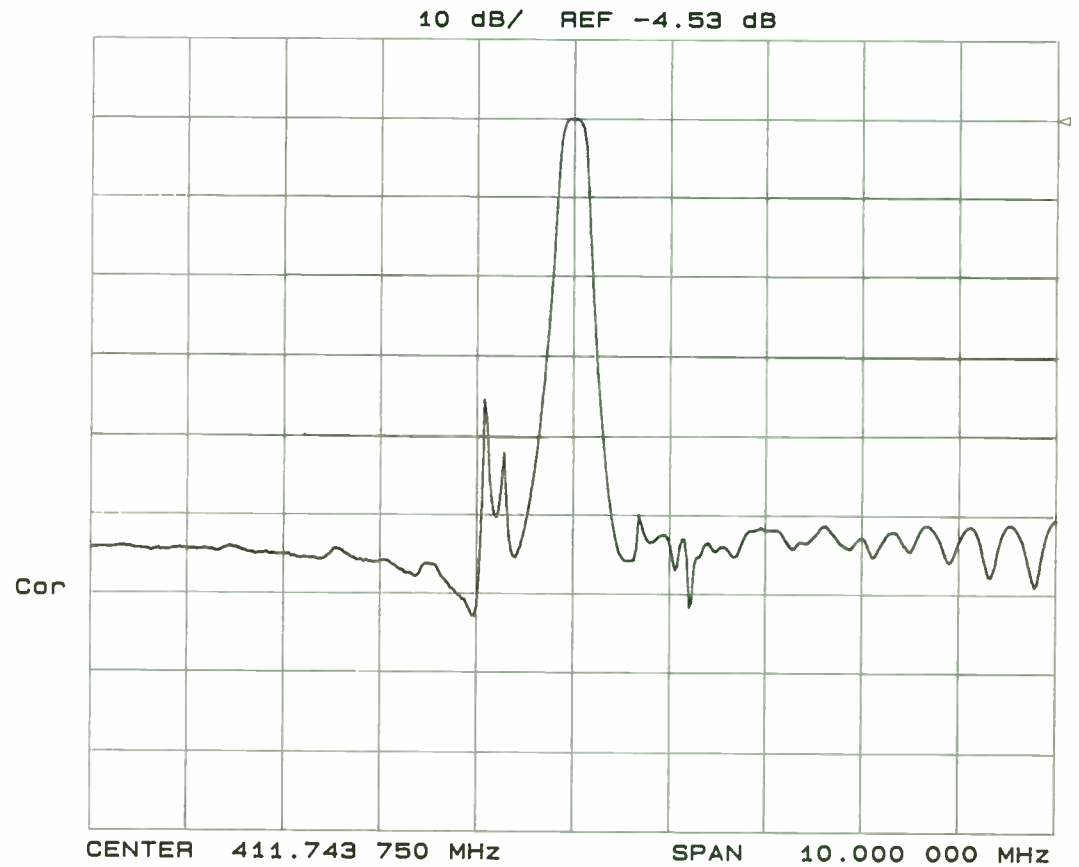


Figure 5. Waveguide Coupled Frequency Response

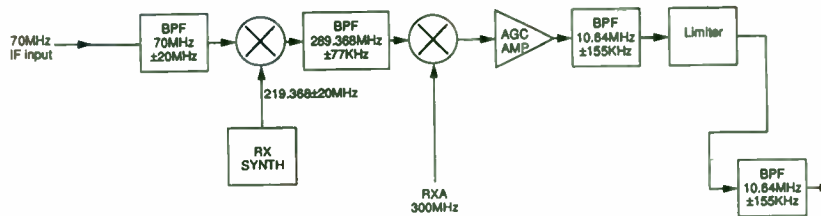


Figure 7. AntiJam Modem IF Section (Qualcomm)



Figure 6a. Traditional SAW Transversal Filter Design

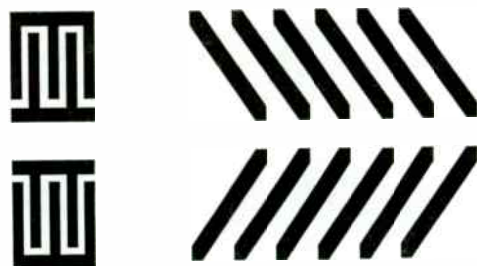


Figure 6b. Reflective Array SAW Transversal Filter Design

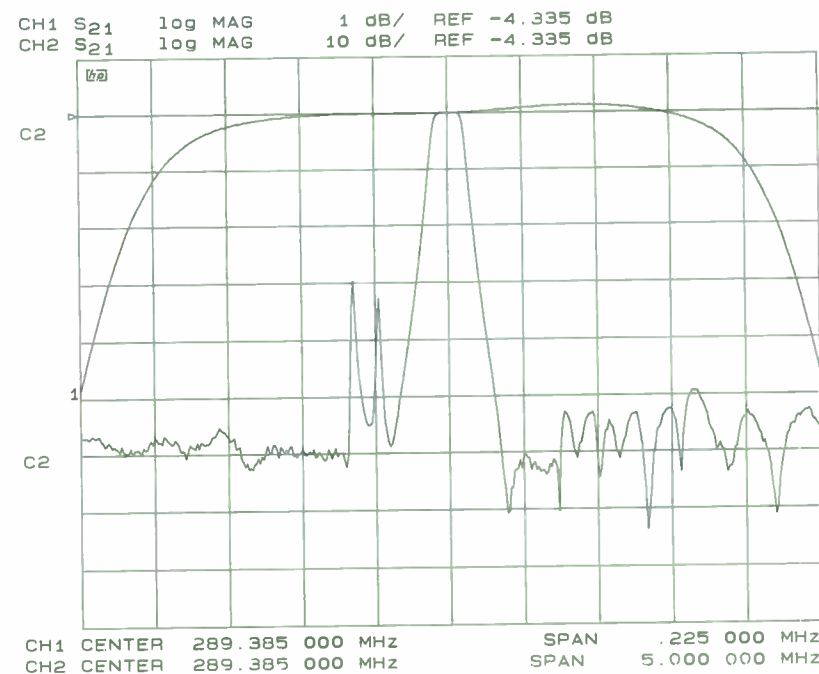


Figure 8. RFW 4-Pole for A-J Modem IF

1685.7 MHz }
1691.0 MHz } ADDITIONAL FREQUENCIES USED

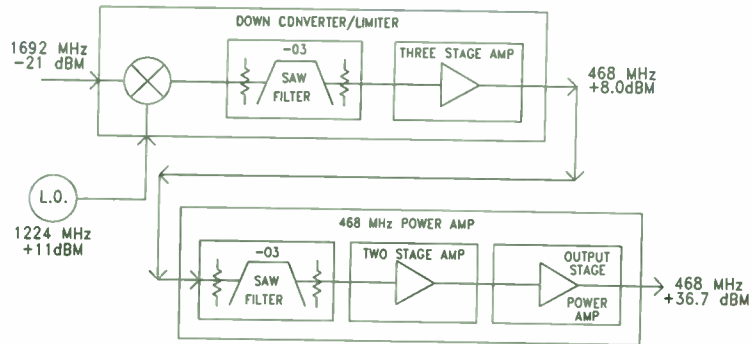


Figure 9: DCPI Transponder (Ford Aerospace)

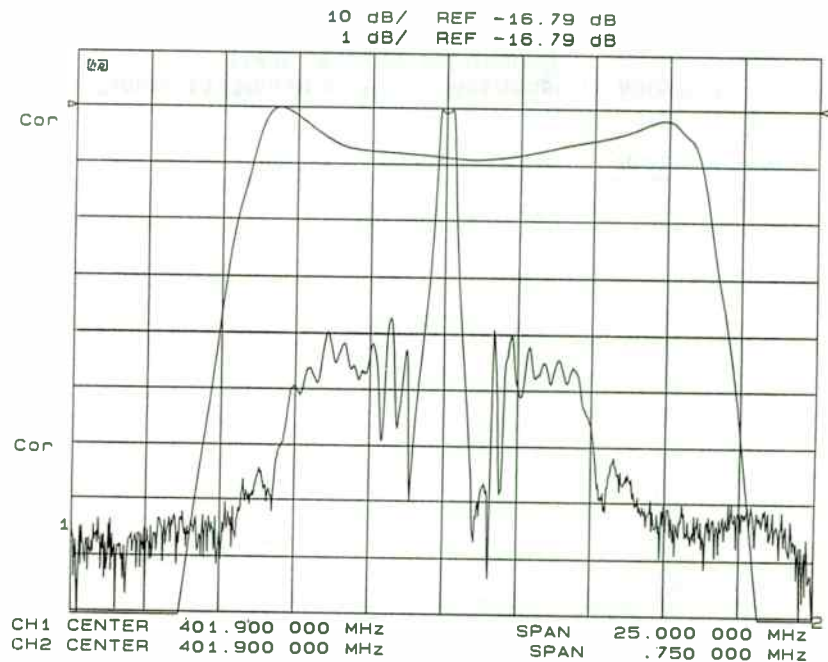


Figure 11: RFI 6-Pole for DCPR Channel

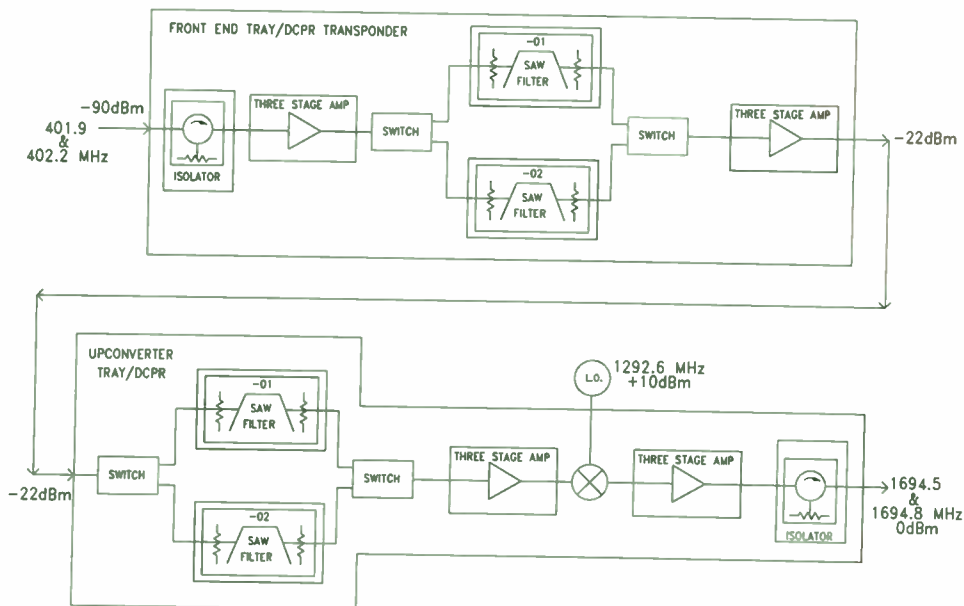


Figure 10: DCPR Transponder (Ford Aerospace)

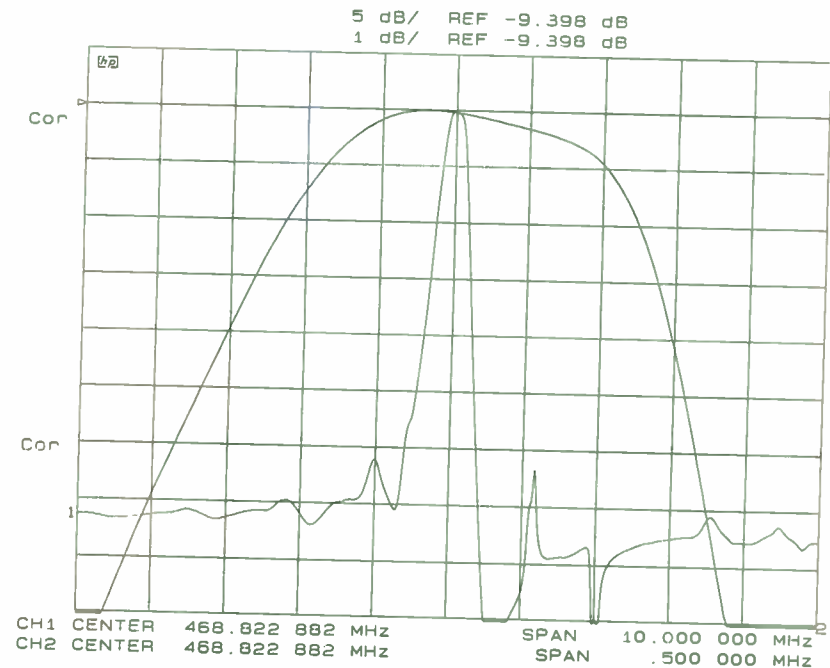


Figure 12: RFW 4 pole for DCPI Channel

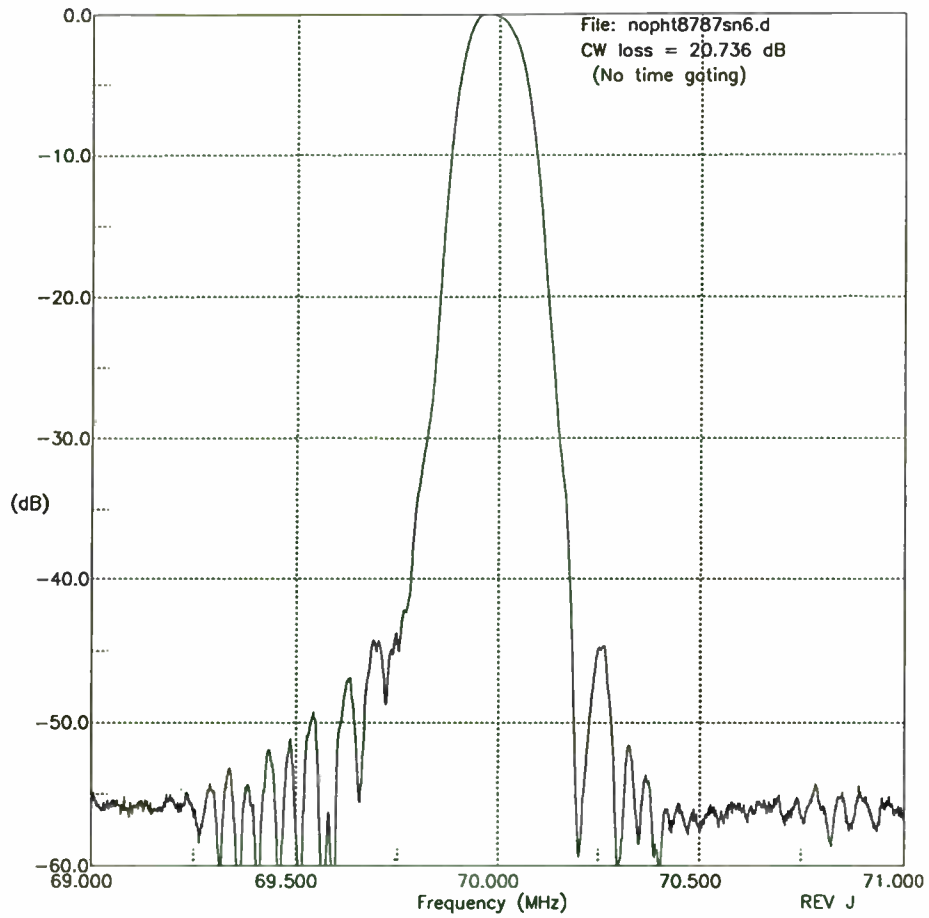


Figure 13: Measured Amplitude Response 70 MHz RAF

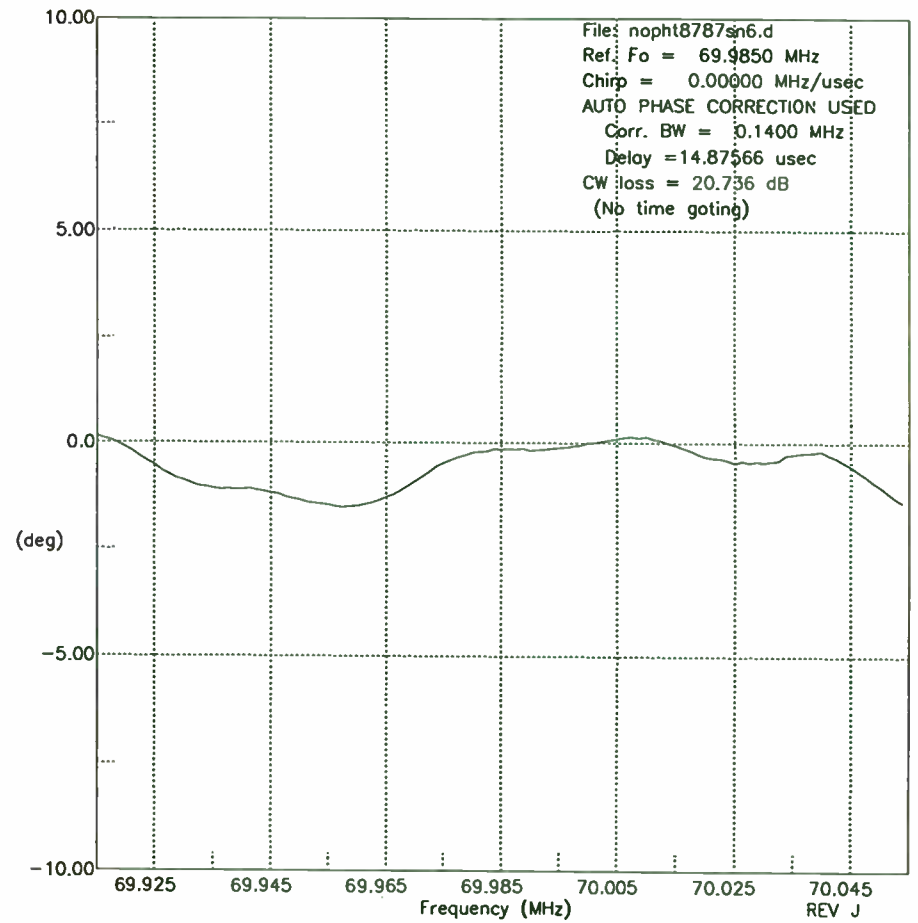


Figure 14: Measured Phase Response 70 MHz RAF
 (14.8 μ s delay subtracted)

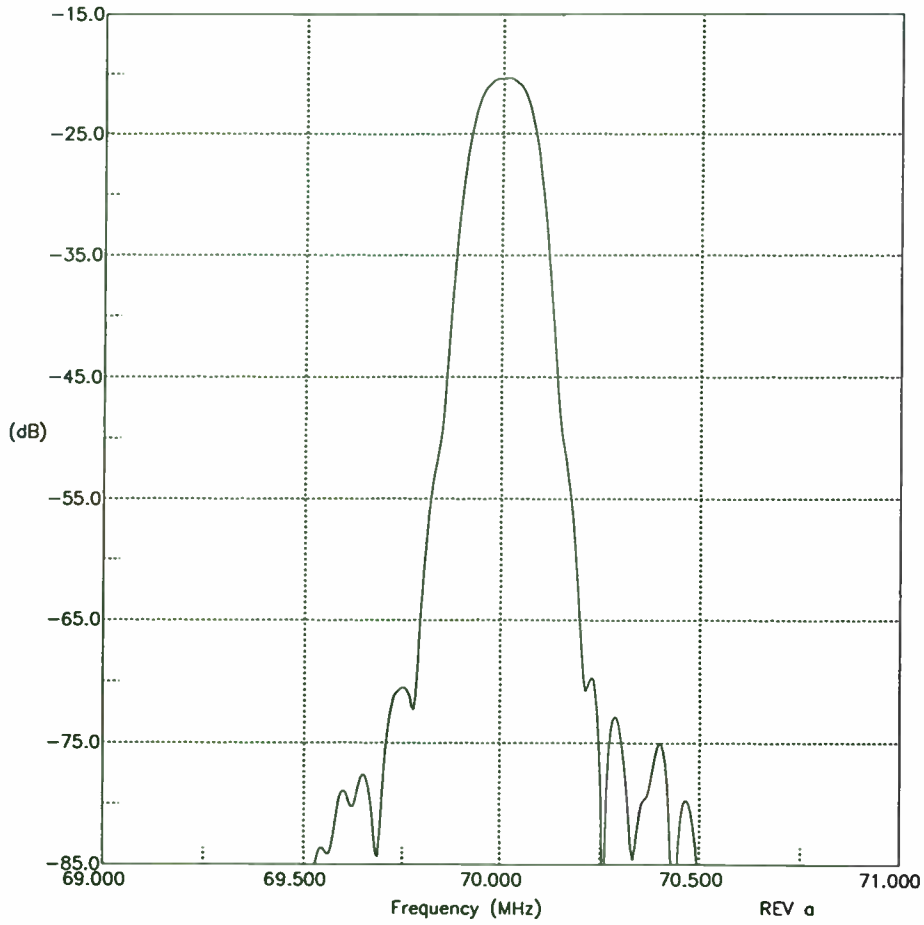


Figure 15: Modeled Amplitude Response 70 MHz RAF

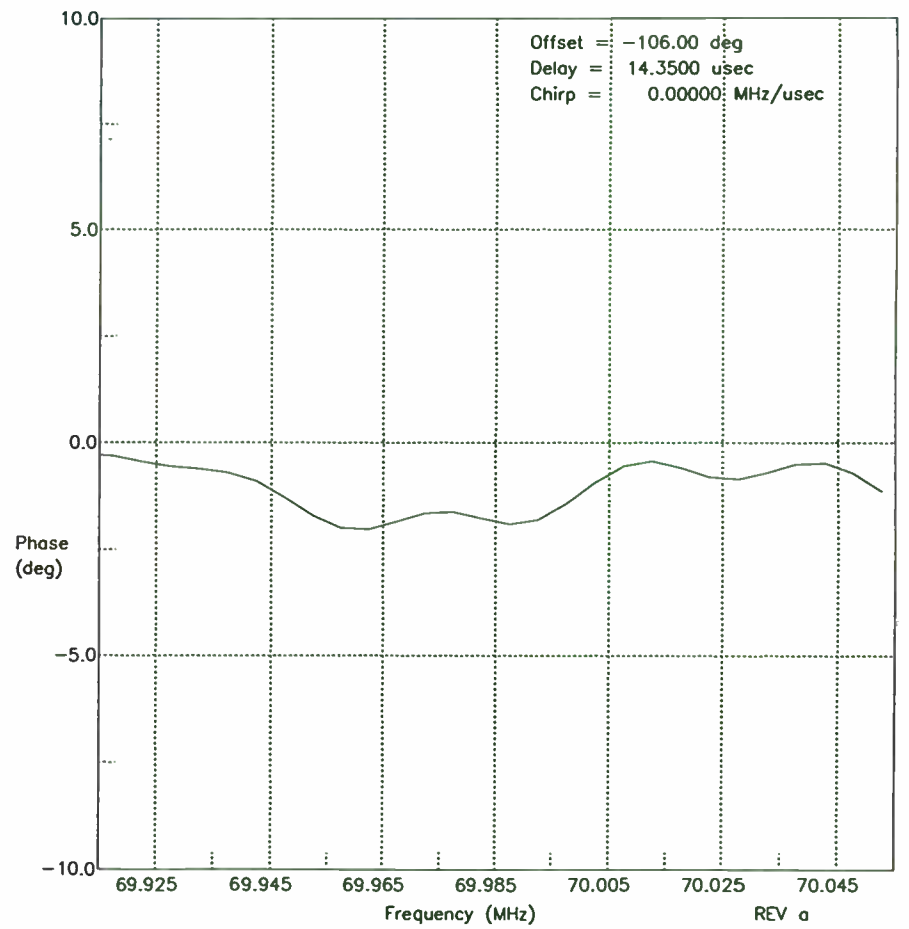


Figure 16: Modeled Phase Response 70 MHz RAF
(14.35 μs delay subtracted)

LARGE LOOP ANTENNAS

R. P. Haviland

MiniLab Instruments

Daytona Beach, Florida

INTRODUCTION

This paper starts with a review of basic principles of loop antennas, then proceeds to some of the characteristics of large loops, especially those which make such loops of use in solving particular antenna problems.

A loop antenna is any of the member shapes generated by forming the antenna conductor so that its ends meet. Small loops are defined as those whose conductor lengths are short compared to a wavelength, 0.3 wavelengths usually being taken as the limit of "small", since analysis equations below this limit give good accuracy with simple approximations. There is no accepted range for "large", but dimensions of a wavelength or more are often used.

GENERAL LOOP CHARACTERISTICS

The general characteristics of the loop family can be developed without mathematical analysis. The square loop can be regarded as a member of a sub-family, as in Fig. 1a, 1b, 1c, with a

transmission line at one end, and a folded dipole at the other. With total conductor length of $1/2$ wavelength, the transmission line will show infinite input impedance. At one wavelength, the line will show essentially zero impedance. Very similarly, the folded dipole will show high input impedance at the $1/2$ wavelength point, and low impedance at the one wavelength point. At one wavelength, the transmission line will show essentially zero resistance input, and the dipole around 300 ohms resistance.

The square loop will show much the same drive reactance characteristic, since it can be regarded as a transmission line with wide spacing. Its drive resistance will be intermediate, around the average of zero and 300 ohms, or 150 ohms.

The pattern of high and low reactance will repeat at successive multiples of $1/2$ and one wavelength of conductor. The pattern will also exist for other shapes, the intermediate rectangles, and triangles, polygons and circles, although there will be magnitude changes with shape change.

The radiation pattern can also be visualized. Suppose the conductor is one wavelength, a square, with a current feed in the center of one side, as in Fig. 1d. The drive current vector and the one opposite to it are in phase, so the radiation normal to the loop will approach that of two half-wave dipole elements spaced one-quarter wavelength. The pattern will not be greatly

QUADS -
Spring '91 Pub.

Drive $Z \sim 150 \Omega$

different from that of a dipole, but will show somewhat greater gain.

With 2 wavelengths of conductor, Fig. 1e, the currents on opposite sides will be out of phase, so the radiation normal to the page will be zero. This cancellation will occur for all integer multiples of one wavelength of conductor.

One way of restoring the normal component is to open the loop opposite to the feed, as for the diamond of Fig. 1f. Now, with high impedance feed, the side current vectors are in phase. The normal lobe will show gain as compared to that of Fig. 1d.

There will be radiation in the plane of the loop. For the one wavelength loop, the current vector is sketched in Fig. 1d1 looking towards the feed point, and in Fig. 1d2 towards the right angle arm. Because of the cancellation in 1d2, ideally there is a minimum or null along this line.

Figs. 1e1, 1e2 and 1e3 are for the two wavelength loop, the first looking towards the feed, the second at right angles and the third along the diagonal. Now there are four lobes, with nulls or minima along the diagonals. Sketches for other conductor lengths show that the number of lobes is twice the conductor length in wavelengths.

It is interesting that this method of consideration of antenna

characteristics by intuitive analysis has led to so many designs, including all of the types in common use.

RESULTS OF LOOP ANALYSIS

The following results are from Mininec analysis, using a minimum of 8 pulses per half-wavelength. Resistance and pattern accuracy with this segmentation are good, and reactance accuracy somewhat lower, but acceptable.

Fig. 2 shows the drive point reactance of a square loop with an omega factor ($2\pi \ln(b/a)=20$, where b is the conductor length and a its radius. (An omega of 20 is a thin conductor).

Resonances occur above the exact multiples of 0.5 wavelengths, in contrast to dipole resonance. Fig. 3 shows the corresponding feed resistance.

The curves for other loop shapes will resemble these, as shown in Fig. 3 for circular loops, (based on circular loop theory). There will be differences in details, of exact location of resonance, and in the magnitude of resistance and reactance at resonance.

There will also be differences as the conductor size changes. Greater conductor diameter will reduce the magnitude of resistance and reactance at odd multiples of $1/2$ wavelength, but have relatively little effect near the even multiples. The effect of conductor size has been largely ignored in the practical loop

antenna literature.

One point of this variation is worth noting. For ω less than 9, the reactance becomes small, negative and essentially constant for any conductor length greater than one wavelength. As the result, a thick conductor loop is a very broad-band antenna. Because of the details of drive impedance change and the associated changes in pattern, specific analysis is required to determine if such a loop is suitable for a particular application.

The lobe patterns normal to an octagon loop are shown in Figs. 4 and 5. For a loop fed at the bottom, these correspond to the the H and V components. The presence of the V component is the main difference from the dipole pattern. It is not known whether this has much practical significance, although it has been suggested that the vertical component reduces the fading in HF communication by polarization diversity.

Fig 6 shows the variation in gain normal to the loop for several shapes, with dipole and area factor for comparison. Again, the value of the loop as a broad-band radiator is evident.

Figs. 7 and 8 show the in-plane radiation pattern for one and 2 wavelength square loops. The 2 and 4 lobes appear, with some radiation in all directions. These antennas and still larger ones can be mounted parallel to the earth, oriented for coverage in

preferred directions. With larger loops, the number of lobes increases, and with thick conductors the nulls fill in, so nearly circular coverage is possible.

One possibility for loop antennas is multiple feeds, for various purposes. For example, a loop in the vertical plane can be fed at the bottom and side, to give choice of vertical or horizontal polarization. Full polarization diversity in reception can be secured with a two receiver voting system. With proper isolators installed, simultaneous feed with 90 degree phase shift will give circular polarization. And addition of a goniometer would permit rotation of a multi-leaved pattern for navigation, or direction finding.

The gain relation of the two wavelength opened loop to that of a closed one wavelength loop is shown in Fig. 9. The "breakeven" gain is almost exactly zero DB isotropic, occurring at 1.35 wavelength of conductor. The open loop shows gain above isotropic to 2.5 wavelengths. A single loop with a relay to switch from open to closed state has isotropic gain or better from 0.5 to 2.5 wavelength. The impedance change is large, but this can be handled with adjustable matching networks.

OTHER SHAPES

All of the above examples used simple shapes. This is not a necessary condition, as shown in Fig. 10. The design at 10a may

be regarded as two one-wavelength loops fed in parallel, or it may be regarded as a two wavelength loop with opposite corners brought towards the center, to bring the phase relations of each half-wave section to the condition for vector addition rather than cancellation. (This system has been called the Doppleloop, but is related to the Chireix-Mesny array of early trans-Atlantic short-wave radio).

The design of Fig. 10b is a specific example of shape modification to control section phasing. With 3 wavelengths of conductor, the top and bottom sections act as half-wave elements spaced one wavelength. The contribution of the sides cancel on the line normal to the paper. There will be a 6-lobed pattern in the plane of the paper.

This antenna can be assembled into a planar array of simple construction, as shown in Fig. 10c. It is unusual in that the additional sections are voltage fed. Array gain can be approximated by conventional array theory, but this will lose accuracy as the number of loops increases. The reason is that the currents in the loops further from the feed will be reduced by the radiation from inner loops, and by ohmic loss. The range of possibilities has not been studied, but some sidelobe control should be possible by conductor size selection. If a reflector is added, the gain can approach that of an aperture antenna of equal area, but usually with simpler construction.

The deforming of the radiator can be extended to three dimensions. This is not common, but it is sometimes done to simplify feed problems. More commonly, the goal is reduction of array dimensions: in essence, the deformed section is used as a capacitative or inductive load, lowering the resonant frequency of the effective radiating section.

As with other antennas, two or more loops can be used to form an array. The gain and drive resistance of the Dopple loop are shown in Fig. 11. For comparison, the gain of separately fed loops is shown in Fig. 12. Since the capture cross-section of a single loop is greater than that of a dipole, separations must be relatively greater to attain maximum gain. The gain is greater than can be developed with the same number of dipoles.

Endfire arrays are equally possible. Hybrid designs based on loop reflector and radiator and dipole (Yagi) directors are used.

CONCLUDING REMARKS

The square loop antenna was developed for the Broadcast Service, in South America, to eliminate the arc problem encountered in high power operation at high altitude with dipoles. Despite this beginning, the antenna has not been popular in commercial services. It is widely used in the Amateur service as the end-fire Cubical Quad, amounting to some 15 percent of all Amateur HF antennas world-wide. It is also used in some military

work, but commonly in the small loop form.

It is hoped that this descriptive paper will serve to invite attention to some of the useful properties of loops, an antenna for use from HF to SHF and above.

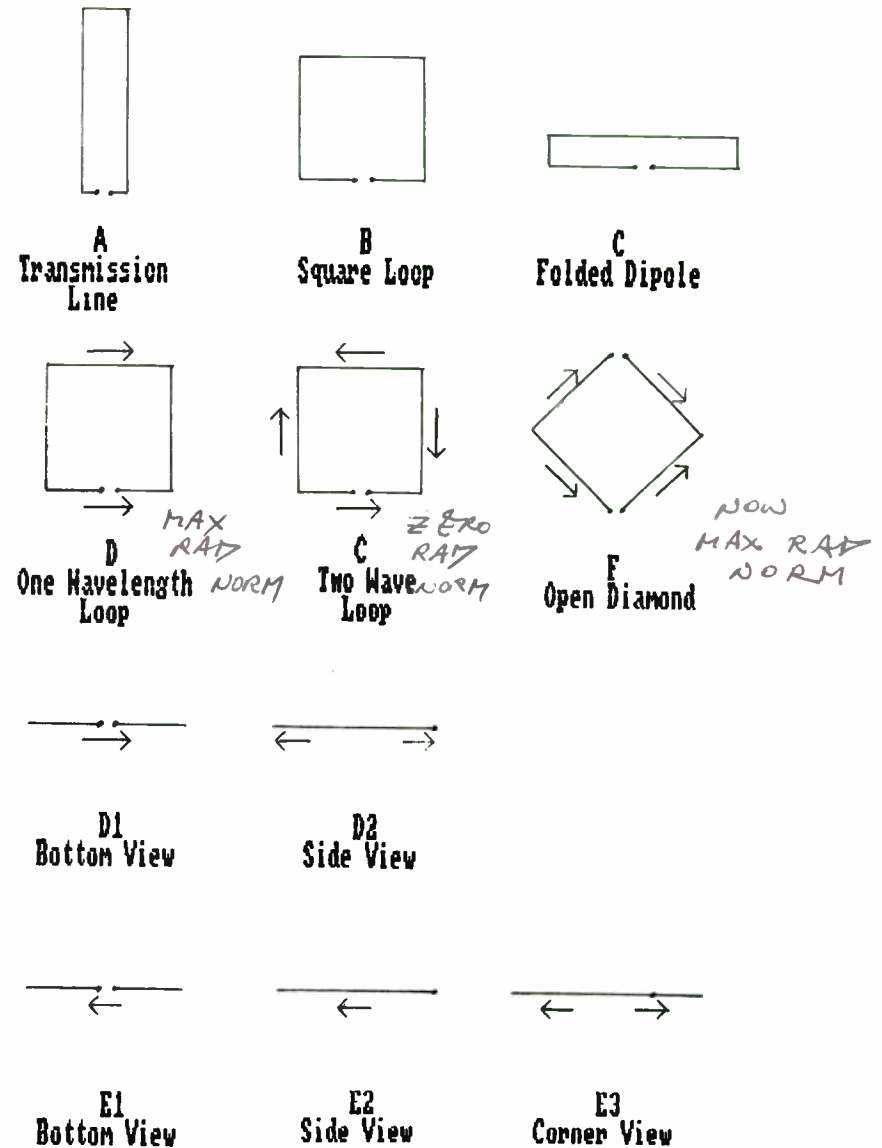
It has been noted that the specific data presented here was derived by Mininec analysis. This is by far the best way of determining the characteristics of specific loop design possibilities, and their application to a specific antenna problem.

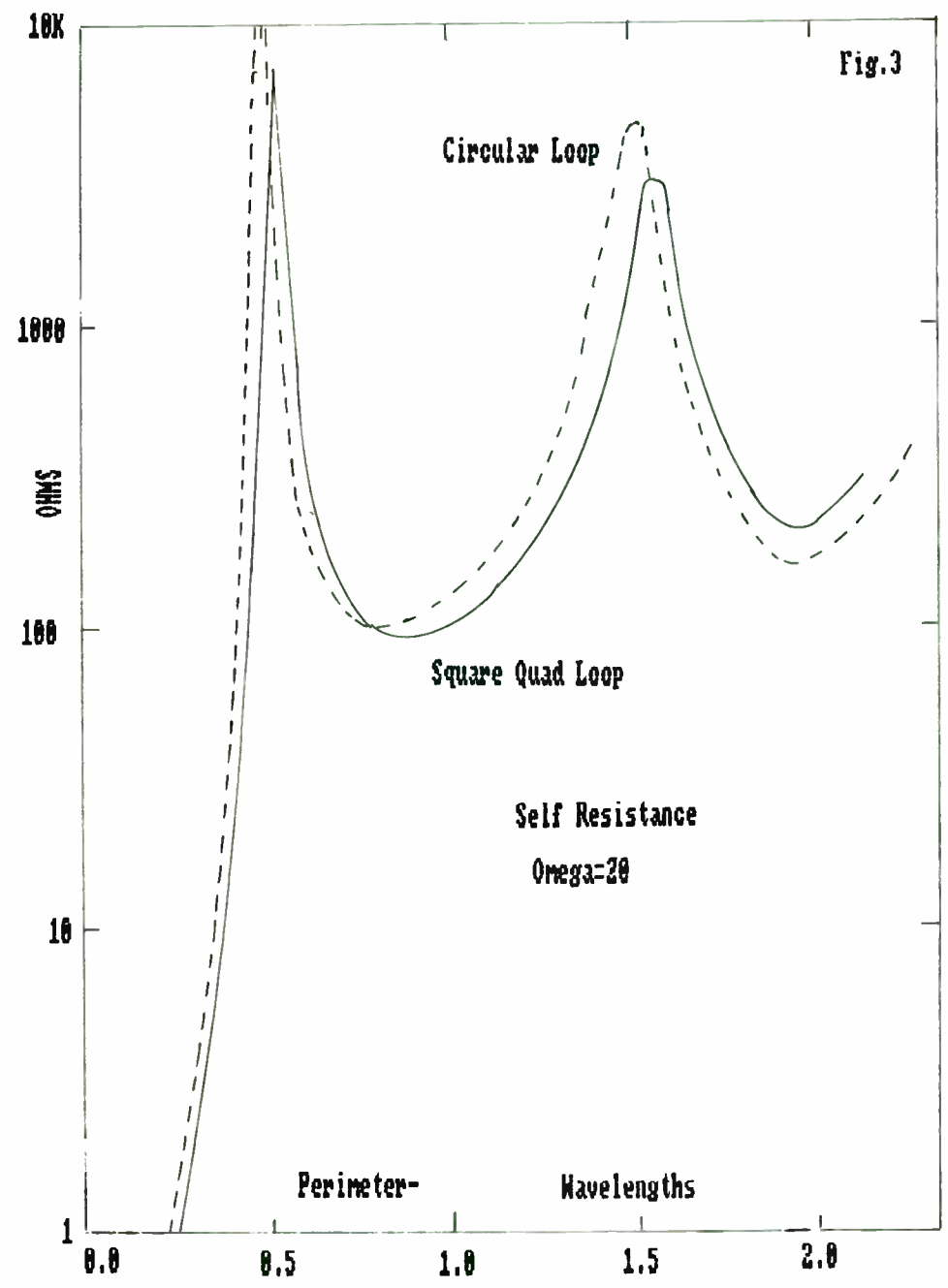
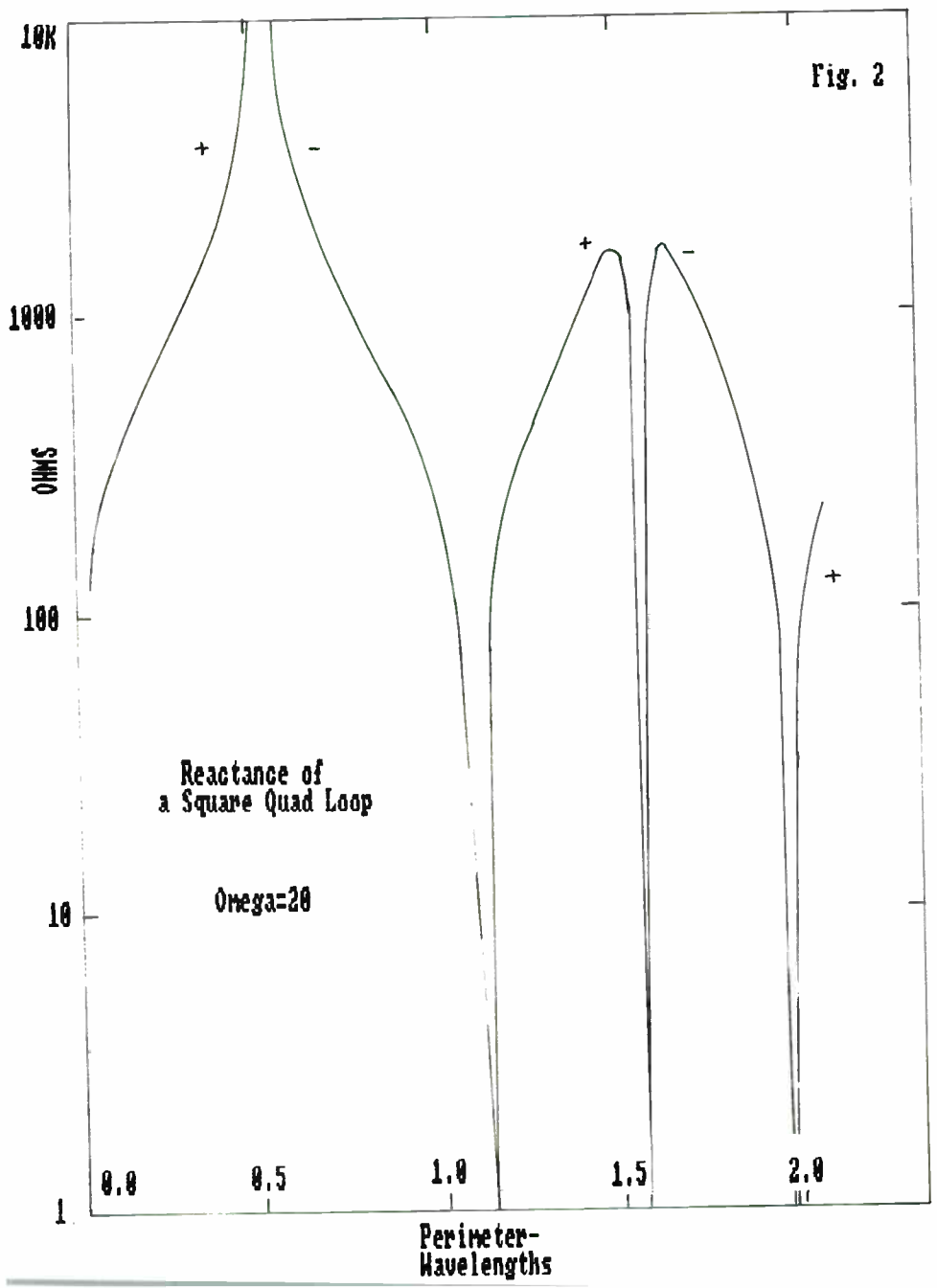
NOTE ON REFERENCES.

The literature on loop antennas and arrays is in two parts. Theoretical analysis is essentially confined to the simpler shapes, and to simple arrays formed of these. The IEEE Transactions on Antennas and Propagation contains or will quickly lead to all of this literature.

Concepts of the more complex shapes and arrays, constructional details and experimental results are essentially confined to the literature supporting the Amateur Radio Service. The magazines QST, CQ and Ham Radio and their associated publications should be consulted.

Fig. 1





HORIZONTAL COMPONENT PATTERN FOR
 10CTO
 PATTERN IS FOR THE
 H-PLANE
 FOR 0
 DEGREES ABOVE HORIZON
 PLOT REFERENCE GAIN=
 3.396611 DB U/V
 = LARGEST LOBE GAIN
 RELATIVE TO ISOTROPIC
 TOP IS NORTH

SCALE, CENTER-OUT
 -100 DB
 -30 DB
 -10 DB
 -3 DB
 0 DB
 RELATIVE TO
 REFERENCE GAIN
 ? |

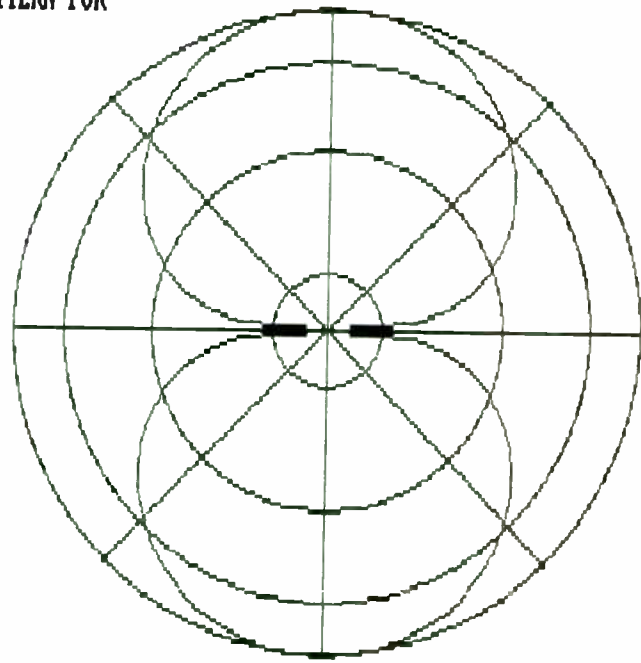


Fig. 4

VERTICAL COMPONENT PATTERN FOR
 10CTO
 PATTERN IS FOR THE
 H-PLANE
 FOR 0
 DEGREES ABOVE HORIZON
 PLOT REFERENCE GAIN=
 3.396611 DB U/V
 = LARGEST LOBE GAIN
 RELATIVE TO ISOTROPIC
 TOP IS NORTH

SCALE, CENTER-OUT
 -100 DB
 -30 DB
 -10 DB
 -3 DB
 0 DB
 RELATIVE TO
 REFERENCE GAIN
 ? |

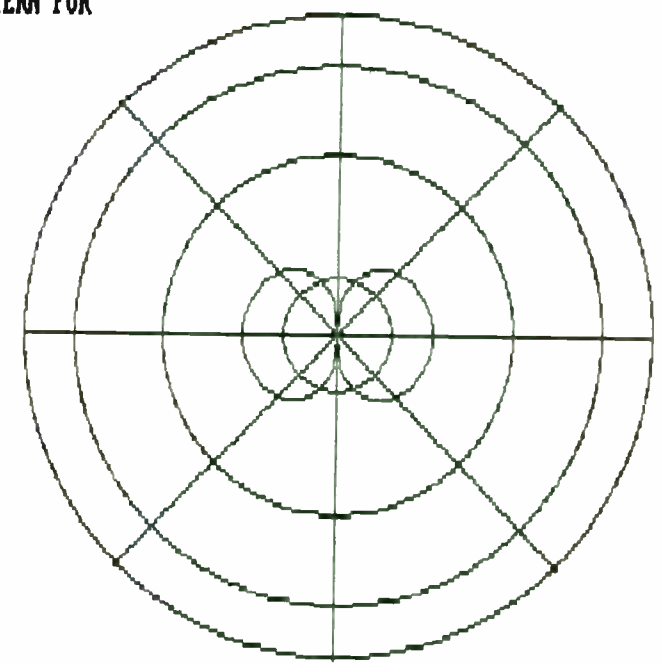


Fig.5

*Horiz
 Dipole = 2.15 dBi
 Loop > Dipole*

Vertical.

Fig. 6

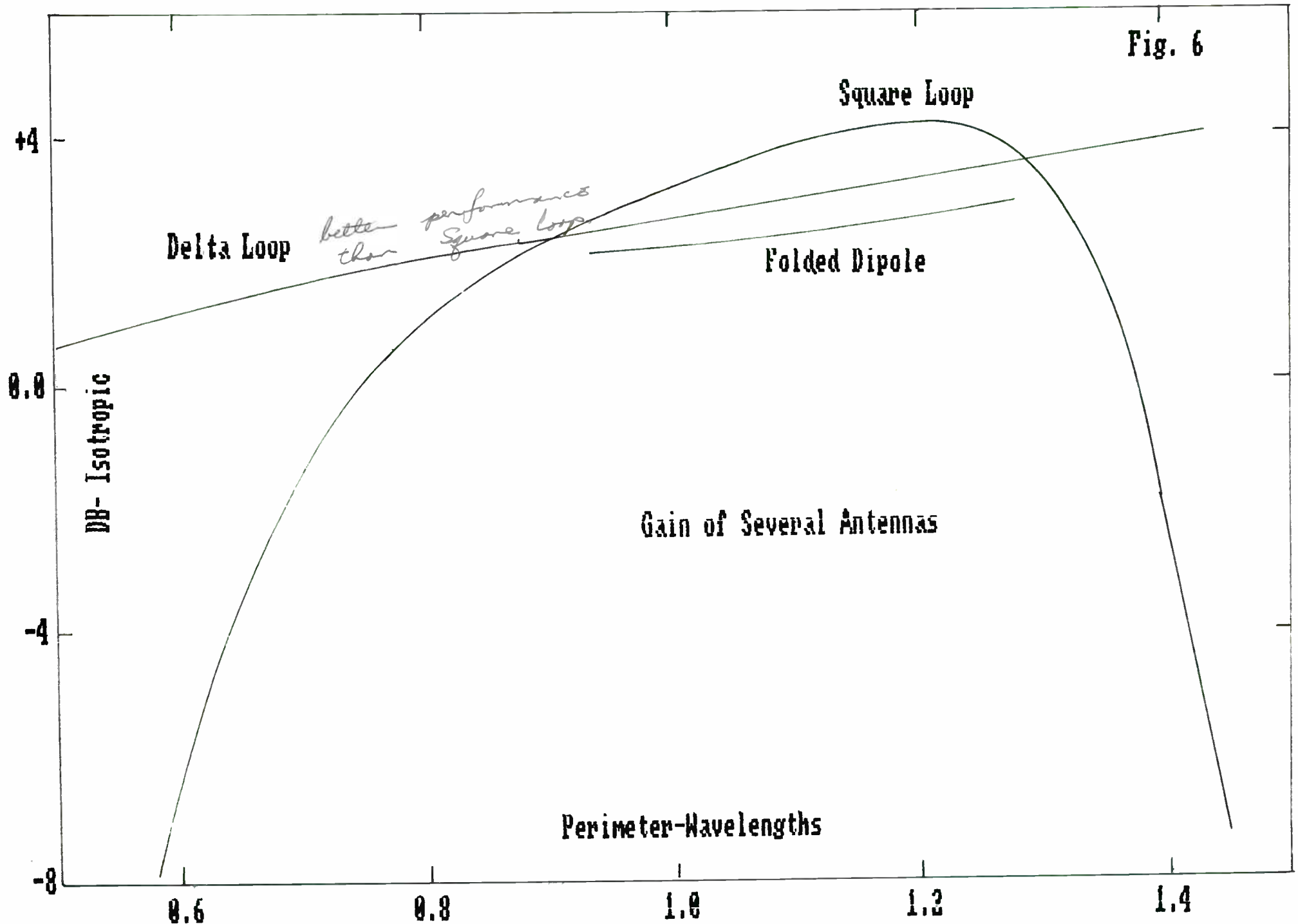


Fig. 7

TOTAL COMPONENT PATTERN FOR
1QUADF1.0
PATTERN IS FOR THE
V-PLANE
AT AN AZMUTH OF
0 DEGREES

PLOT REFERENCE GAIN=
3.0947 DB U/V
= LARGEST LOBE GAIN
RELATIVE TO ISOTROPIC
TOP IS ZENITH

SCALE, CENTER-OUT
-100 DB
- 30 DB
-10 DB
-3 DB
0 DB
RELATIVE TO
REFERENCE GAIN
? |

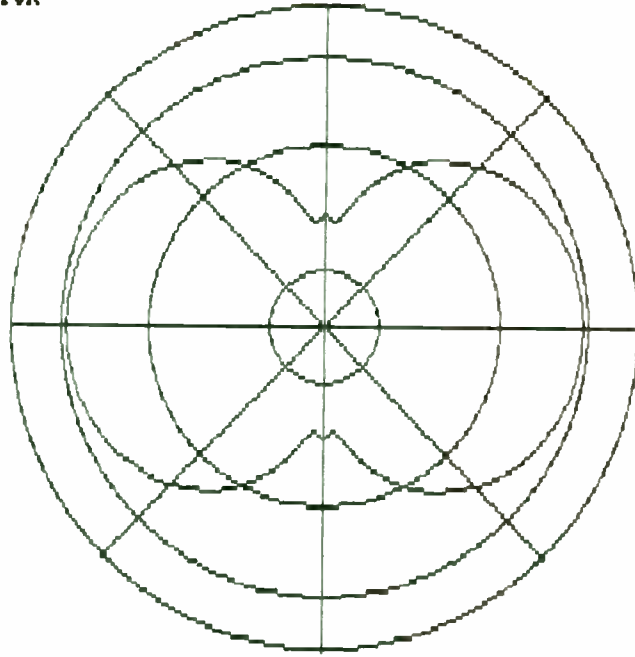
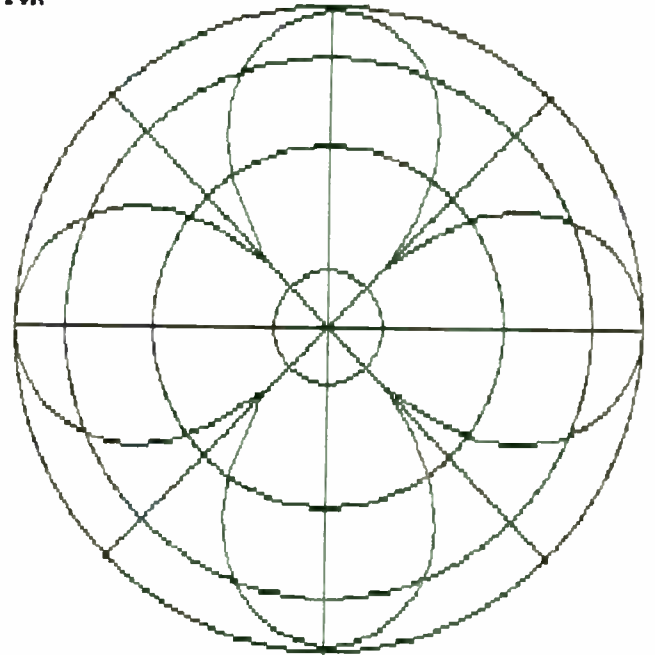


Fig. 8

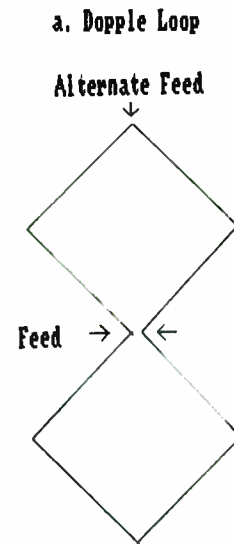
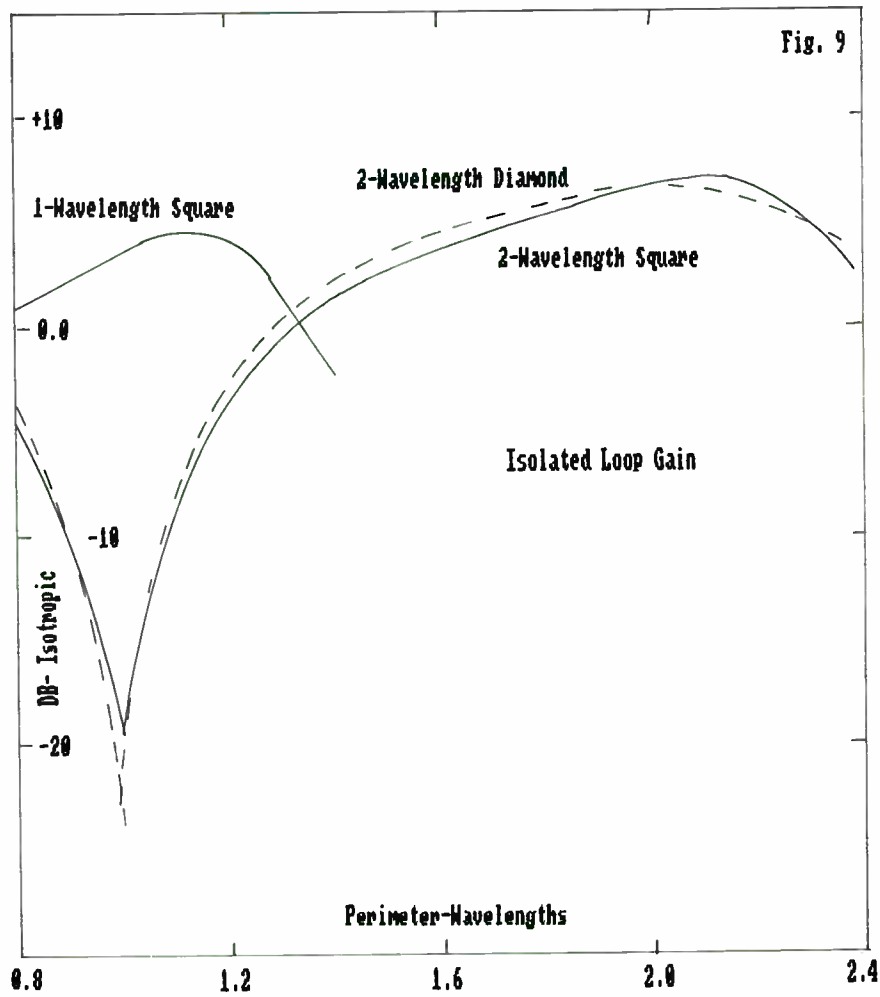
TOTAL COMPONENT PATTERN FOR
XZ1QUADF2.0
PATTERN IS FOR THE
V-PLANE
AT AN AZMUTH OF
0 DEGREES

PLOT REFERENCE GAIN=
2.81051 DB U/V
= LARGEST LOBE GAIN
RELATIVE TO ISOTROPIC
TOP IS ZENITH

SCALE, CENTER-OUT
-100 DB
- 30 DB
-10 DB
-3 DB
0 DB
RELATIVE TO
REFERENCE GAIN
? |



*pattern generated in
the plane of the loop.
proper feeding of loop
gives H/V polarization
and circular polarization.*



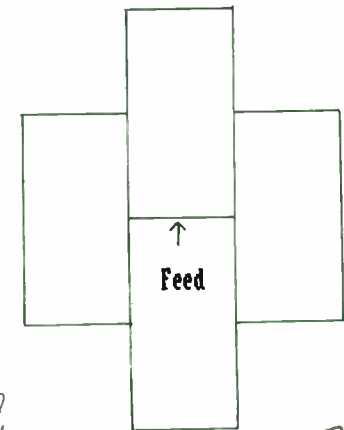
*A z wave
loop corners
pulled in.*

b. 3 wavelength Loop



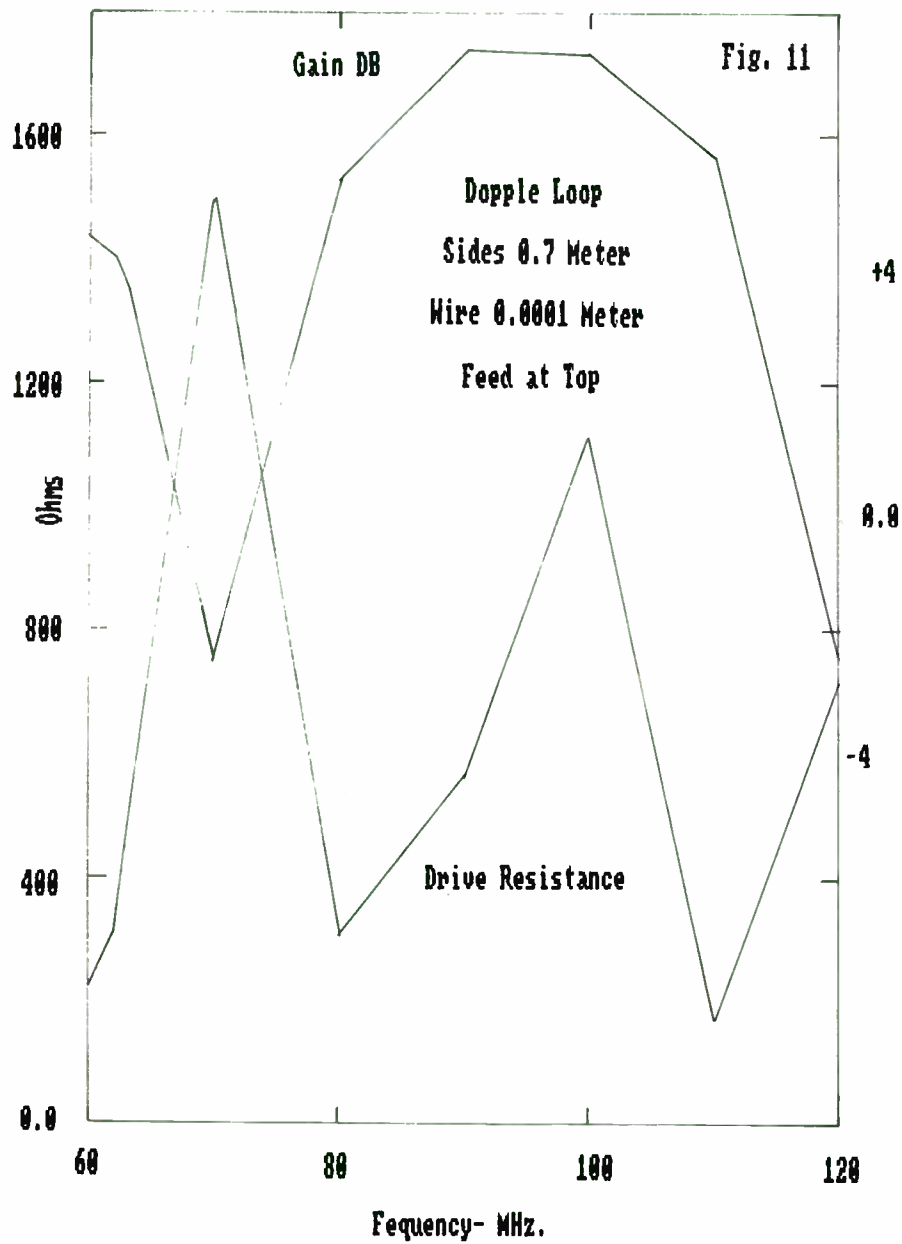
*not real
norm to
paper.
Loop Variations*

c. Curtain Array



*Several 3λ
length loops
over λ/4
ground -
16 dBi*

Fig. 10



VHF MULTIPATH PROPAGATION

CAUSES AND CURES

D. R. Dorsey, Jr.
President
DocSoft Enterprises
Sunnyvale, CA 94087

INTRODUCTION

This paper explores the phenomenon of multipath propagation at VHF frequencies and above. It will define the basic physical causes of multipath propagation and some of the means that may be effectively used to overcome it on line-of-sight radio links. Special attention is paid to digital radio and land mobile radio applications.

MULTIPATH PROPAGATION - WHAT CAUSES IT ?

Multipath propagation is precisely what its name implies -- signals received from one or more paths on a line-of-sight radio link (Figure 1). Several reflected, refracted and/or scattered paths may exist in addition to the primary direct signal path. (1, 2, 3, 4, 5, 6, 7) The receiver will see several signal inputs, most of which are delayed by the extra path length introduced by these extra ray paths. Multipath is a manifestation of the basic principles of wave motion -- constructive and destructive interference. Signals add or subtract according to the phase relationships produced by paths other than the direct signal path. The composite signal will contain the modulation components of all the varying paths, and the amplitude will be determined by the phase relationships of the components. The destructively interfering variations lead to the phenomenon of **fading**, usually in the form of signal strength depressions,

signal-to-noise variations or "jitter". Fortunately, there are ways to keep it under control and manageable in many cases.

Fading is usually defined as a time variation of signal level, phase or polarization (1, 2, 3, 4, 5, 6, 7, 8). It is patently statistical in nature, and in most cases of interest tends to follow a Rayleigh distribution (Gaussian) (4). This is particularly true in the mobile environment, as we shall see shortly. The mechanisms that lead to fading are refraction, diffraction, reflection, attenuation, scattering and/or ducting of a radio wave. Terrain characteristics and local meteorological conditions are definitely also strong determining factors. Fading is highly frequency and path-length dependent.

A classic example of multipath propagation is the "ghosting" experienced in television receivers, particularly in areas where there exist large natural or man-made obstructions interposed in the path between transmitter and receiver. The obstruction can be either stationary or moving --- most of us have experienced temporary multipath propagation on our TV sets due to an airplane flying into the path between the transmitting site and the TV receiver. Under extreme conditions, ghosting could even cause total loss of picture synchronization.

For the VHF and above frequency range, we are normally dealing with a line-of-sight radio link. Even changing location between transmitter and receiver by only a few wavelengths may be sufficient to make the difference in maintaining reliable communications⁽⁴⁾. By definition, then, the path between the transmitting and receiving antennas should be as free as possible of obstructions and the effects of the earth's curvature. But in reality, we must also consider the combined effects of the curvature of the earth's surface and the refractive properties of the atmosphere just above it, since variations in the refractive index of the atmosphere may produce signal ray path curvature. In certain localities, the presence of atmospheric anomalies such as temperature inversions may also have to be considered⁽⁵⁾. In general, transmitter and receiver antenna heights should be high enough to provide at least a tangential path across the earth's surface, with these factors considered.

We will also have to consider the type of link being implemented. Line-of-sight radio links generally fall into three major categories⁽⁵⁾:

Long Overland Links - These links are typically over 50 kilometers in length, and are generally used for radio relay links and radar detection of targets at long distance. The earth's atmosphere plays the predominant role. Atmospheric fluctuations may produce multiple propagation paths and subsequent fades.

Short Overland Links - Common in some radio relay networks, particularly at frequencies above 10 GHz. Multipath fading is then due to earth reflections and attenuation due to atmospheric gases and rain.

Oblique Links - Links in which the elevation angle is fairly large, as in many satellite and radar links. Attenuation due to rain and atmospheric gases are the major factors.

REFRACTIVE EFFECTS

Atmospheric multipath propagation is caused by variations in refractive index ⁽³⁾. In the standard atmosphere, the values of pressure, temperature and humidity all decrease with an increase in altitude. Since the refractive index is a function of these three parameters, it decreases with altitude as well. Defining the parameter **REFRACTIVITY** ⁽³⁾

$$N = (n - 1)10^6$$

we have for the earth's atmosphere

$$N = \frac{77.6}{T} \left(P + 4810 \frac{e_s}{T} \right)$$

where

- P = atmospheric pressure (millibars)
- T = temperature (degrees Kelvin)
- e_s = saturation water vapor pressure (millibars)

For standard atmospheric conditions, N is normally about 300. A closely related parameter is the **REFRACTIVE MODULUS** (M) ⁽²⁾

$$M = N + (h / r_0)10^6$$

where

- r₀ = radius of earth = 6370 km
- h = altitude above sea level

A plot of the vertical distribution of M is commonly called an M-curve or M-profile.

Radio waves will travel at different velocities in different parts of the atmospheric medium, which may contain many areas of varying refractive index, n. Since an electromagnetic wave travels faster in a medium of smaller n, the upper edge of the wavefront moves faster than the lower edge, leading to a net downward deflection of the composite beam. Assuming the vertical decrease in n with altitude is gradual, the deflection is continuous, and the beam tends to follow the curvature of the earth. These refractive effects may allow propagation beyond the optical horizon by as much as 15 percent, to what is called the radio horizon (Figure 2).

It is easy to see that we can get into a complicated situation trying to draw a realistic picture of what these curved ray paths would look like along a real path that considers the curvature of the earth. To simplify the analytical task somewhat, and to characterize the degree of curvature induced in a ray path due to vertical refractive index gradient variations, there exists a widely used scaling factor, K, known as the effective earth radius coefficient. This parameter simplifies the preparation of a path profile chart immensely by allowing a ray path between two points to be

plotted as a straight line. It references the radius of ray curvature to the radius of the earth (Figure 3), and is defined by ⁽²⁾

$$\frac{r}{r_0} = K = \left[1 + \frac{r_0}{n} \frac{dn}{dh} \right]^{-1}$$

where

- r_0 = radius of earth = 6370 km
- n = refractive index
- h = altitude above earth

The M- and K- parameters are related, and can be used to identify several cases of refractive phenomena. For standard refraction, the value of $dM/dh = 0.12$ and corresponds to $K = 4/3$. For the subrefractive case, the refractive gradient is positive and greater than the standard value. These conditions correspond to the range $0 < K < 1.0$, as shown in Figure 3 ⁽³⁾. For a homogeneous atmosphere, $dM/dh = 0.157$, which corresponds to $K = 1$, which in turn defines a direct line-of-sight path, or optical horizon. Should subrefraction become severe enough ($K = 0.33$), difficult problems due to diffraction losses can result if the proximity of terrain and ground features is not allowed for in the design of the link system. In the super-refractive case, dM/dh is less than the standard value and corresponds to $K > 1.0$. For these conditions, the radio beam would tend to bend back toward the earth. Adjustments in take-off angle from the antenna may need to be made, but ground proximity would not likely be a factor. Indeed, the most usual situation we will need to deal with is for $K \geq 1.0$, and usually only in the range $1 \leq K \leq 2$.

The effects of local weather conditions on the refractive properties of the atmosphere should not be under-estimated, as these effects very strongly influence the likelihood of fading. Fading is to be expected more frequently and more severely in summer than in winter (at mid-latitude locations), in calm weather, or across relatively dry ground.

MULTIPATH FADING

Multipath fading is the most common type of fading encountered on line-of-sight radio links. As we saw in the previous section, atmospheric effects can lead to multipath fading due to interference between direct, ground-reflected and other non-reflected ray paths. Many factors may contribute to multipath fading :

- Time of day
 - Temperature Conditions
- Season
- Local climate - vertical refractive index profile
 - Equatorial - Polar - Moderate
- Atmospheric absorption & attenuation
- Local Weather Conditions
- Presence of snow, ice or vegetation
- Reflection and Diffraction from local terrain features :
 - Mountainous or Flat
 - High-Density Urban or Suburban
 - Land and/or Water paths
- Radiation
 - Local stratification of atmosphere
- Mobile Links
 - Doppler effects due to speed and motion of a moving terminal
 - Antenna size and location on vehicle
 - Intervening obstacles

Fading is usually characterized by three main parameters :

DEPTH (Signal strength depression, dB)
RATE
DURATION

On average, signal strength losses up to 20 dB are fairly common in a deep fade, although fade depths of 30 db or more are also quite possible. We

would also be interested in the statistics of the fading envelope ⁽⁴⁰⁾. Points of interest include the average rate at which the envelope crosses a specified level (the level-crossing rate) and the duration for which it stays below that level. The level-crossing rate is defined ⁽⁴⁰⁾ as the average number of times per second that the envelope crosses the specified level in a positive-going direction. The average fade duration is the average amount of time spent below that level.

If we plot the fade depth against frequency (Figure 4), we come up with what is commonly referred to as a multipath notch ⁽⁷⁾. When the notch falls within a desired communications channel, adjacent channel interference problems may result in the crossover regions of the filter responses (Figure 5) ⁽⁷⁾. For digital radio applications, the notch depth directly influences bit error rate (BER). The modeling and characterization of a multipath fading channel, with consideration toward predicting outages, are covered in great detail in several papers included in the references. (10, 11, 19, 22, 23, 25, 29, 30)

Duffy ⁽³²⁾ indicates that severe multipath fading may occur in locations with antennas sited on mountain tops with a deep flat valley in between. For microwave radio applications, the optimum areas are dry, windy and mountainous with uniform air density, while the worst are wet, flat and humid regions such as coastal areas, at least as far as atmospheric conditions are concerned.

MULTIPATH FADING COUNTERMEASURES

There are several means that may be used to combat multipath fading. Some may be obvious -- optimum transmit and receive antenna location and height, the absence of intervening obstacles, improved receiver performance, etc. But in most cases, that will be difficult or impossible to achieve. There are several excellent detailed references for the characterization of fading, estimation of fading parameters, margins and outages, and route and site planning based on those estimations ^(2, 3). These references cover most practical situations of interest, and can be

used almost "cookbook"-style to address the required parameters and computations.

ANTENNA DESIGN CONSIDERATIONS

Proper antenna system design may alleviate some multipath problems. Ensure that transmit and receive antennas are at proper heights to define a reliable radio horizon that will allow coverage over the required range or area. The use of high-gain directive antennas, along with higher transmitter output power, should provide some improvement in received signal strength. In a mobile environment, however, this may not prove entirely fruitful; in this case, an omnidirectional antenna providing a fairly constant signal level and with a radiation pattern at the appropriate elevation angles to serve the mobile environment will achieve better results. Keep track of polarization effects -- in a dense urban environment, most buildings, power lines or other reflecting entities are generally parallel to a vertically polarized wave, so vertical polarization will experience less in the way of cross-polarization effects than would a horizontally-polarized system.

DIVERSITY METHODS

The basic idea of any diversity method is to introduce redundancy by transmitting information over a number of independently fading paths, on the assumption that a deep fade will not occur simultaneously on each path. Of course, the signals from each path must somehow be re-combined at the receiving site, by implementing a selection and combining algorithm to select the best decision branch, usually based on SNR, to minimize the effects of fading. This is usually accomplished by using some appropriate form of signal processing in the receiver. Once the proper branch is selected, phase-lock techniques may be employed to acquire a solid lock onto the received signal. Diversity techniques can add up to 3 dB in total system gain. Several diversity methods are described below. Detailed and highly mathematical treatments of diversity and combining methods are

available in several of the references (3, 4, 6, 7) . Current applications of diversity methods are also to be found in the current literature (31, 42, 43) .

SPACE DIVERSITY

Space diversity uses one transmitting antenna at a single frequency and several receiving antennas spaced so that the fading that appears on each path is uncorrelated. A common way of doing this is to place the receiving antennas at different vertical locations on the same tower (Figure 6a) (3) . Each antenna receives the same information, but hopefully fading will not occur on both paths. Current practice suggests that the antennas should be spaced at least 200 wavelengths apart (3) for best results although separations of 100-150 wavelengths are the norm. At 6 GHz, this would be no more than 33 feet. Signal improvement factors of several hundred over a non-diversity system may be obtained, depending on frequency, antenna spacing, path length and required fade margin.

ANGLE DIVERSITY

Angle (direction) diversity uses several directive antennas, each designed to provide incidence angle discrimination to isolate a signal with a particular angle and direction, independently of the other antennas. However, it is not a commonly used method, as it would require steerable arrays.

POLARIZATION DIVERSITY

Polarization diversity is a particularly effective method that transmits the same information over two orthogonally polarized channels. This method uses "quadruple diversity", i.e., it produces four space paths. At the transmit end are two antennas, one horizontally polarized and the other vertically polarized. A similar arrangement exists on the receiving end. These differently polarized paths are highly uncorrelated, as each path essentially is unaware of the presence of the other. This method is

another form of space diversity, so signal improvement ratios of several hundred should be attainable. This method is good for reducing polarization mismatch problems.

FREQUENCY DIVERSITY

With frequency diversity, the same signal is transmitted at different frequencies. In this case, only one receive antenna is required (Figure 6b). It provides higher diversity gain than the space diversity method, and is generally cheaper to implement. Frequency separation between the transmit frequencies would ideally be 10%, but should be at least 3 to 5 % in order to obtain the best possible signal decorrelation. However, separations of 1-2% are more common in our frequency-congested world. Signal improvements of 15-20 dB are quite achievable. This method is common in spread-spectrum and frequency-hopping systems. In the United States, however, the FCC regulatory position is not to approve the use of frequency diversity unless it is the only way to achieve the needed system reliability, in order to reduce frequency congestion and to conserve available RF spectrum.

TIME DIVERSITY

Time diversity techniques generally apply only to the transmission of digital data. Data is sent across the channel at time intervals on the order of the reciprocal of the baseband fade rate. In a mobile radio environment, the time separation and sampling rates are dependent on the Doppler frequency defined by the speed of the moving vehicle. If the vehicle is not moving, this method becomes useless.

DIVERSITY COMBINING METHODS

Methods of recovering and combining signals transmitted over a diversity path fall into three major classes: Maximal-ratio combining, equal-gain combining and selection.

In maximal-ratio combining (Figure 7a), each signal is weighted for optimum performance and co-phased before combining. Since it

requires the weighting, summing and co-phasing circuitry, it is the most complex method to implement, but it provides the best overall signal improvement performance. It essentially uses the best features of both an equal-gain combiner and a selection combiner. If one signal is zero, it acts like a selection combiner. If both input signals are at the same level, it acts like an equal-gain combiner.

Equal-gain combining is similar to maximal-ratio combining, except that the weighting circuitry is omitted (Figure 7b). A simple phase-locked summing circuit may be used to sum the individual signal branches. The signal improvement realized in the equal-gain combining method is only slightly inferior (about 1 dB) to that of the maximal-ratio combining method, in that noise-corrupted signals may also combine with the noise-free signals. Equal-gain combining is not a good method to use in the land mobile radio environment, owing to the difficulty of designing a co-phasing circuit that is precise and stable enough to properly track the moving vehicle.

In the selection method (Figure 7c), the signal branch containing the highest signal level is the one selected in the pre-detection phase. This method, however, requires the use of a switching or scanning receiver to provide continuous monitoring of all signal branches ⁽⁶⁾. Signal improvement performance may be up to 4 dB less than that provided by the equal-gain combining scheme.

ADAPTIVE EQUALIZATION

Adaptive equalization is another powerful and effective method for combatting multipath fading. The intent is to provide some sort of correlation in the receiver circuitry in order to equalize the effects produced by the communications channel and attempt to correct for the distortions produced. Basically, we would like the receiver to follow or track the variations produced by the channel and correct for them as much as possible. The equalizer should combine all multipath components present and cross-correlate a single mode while attempting to reject all the others in deriving the best final composite signal. Adaptive equalization is very useful in serial communications. Input waveforms on an analog

channel may be corrupted or transformed by frequency translations, time dispersion or harmonic and nonlinear distortions ⁽⁶⁾. In high-speed digital data communications and modems, this type of equalization is used to reduce intersymbol interference (ISI), or symbol overlap, caused by transmission over a time-dispersive channel. ISI can occur in any pulse-modulated system, including FSK, PAM and QAM, and arises due to the symbol over-extending the time slot used to represent it. Today, most any modem capable of 2400 baud or better uses some form of automatic adaptive equalization. At even higher data transmission rates, the use of trellis-coded modulation, a coded form of QAM, is used to provide improved performance in the face of significant noise and channel distortions. In radio work, adaptive equalizers are used to provide diversity combining or interference / jamming cancellation functions.

In general, any equalizer must be able to measure the current channel parameters, set its matched filter elements accordingly and do so often enough to follow the channel variations it encounters. They may be very sensitive to channel variability and may not work well in a fast fade, unless the processor speed is able to keep up with it. Most equalizers are implementable in either the time or frequency domains. The application of adaptive equalization to digital radio systems is discussed in several of the references ^(14, 21, 24, 26, 27, 28).

One of the simplest types of adaptive equalizer is the linear transversal equalizer (Figure 8a), which acts like a tapped delay line or non-recursive digital filter. The current and past values of the received signal are weighted linearly by equalizing gain and then summed to produce the output. The equalization coefficients may be adjusted continuously by comparing an error signal derived from the most current total signal estimate with the input. The least mean-squared (LMS) equalizer is a more robust version of this type of equalizer in that it also accounts for the noise power at the output of the equalizer by choosing the equalizer coefficients in an effort to reduce the mean squared error (MSE).

A decision-feedback equalizer (Figure 8b) is a nonlinear recursive equalizer scheme that is very effective for channels suffering from severe amplitude distortion ⁽⁶⁾. The decision feedback is used to

null out any ISI from symbols which might have already been detected and processed.

A fractionally-spaced equalizer (Figure 8c) is effective for severe distortion delay, and may have better noise performance than a regular transversal filter ⁽⁶⁾. The delay line taps are spaced to be some fraction of the symbol interval.

An adaptive antenna array might also be used before reaching the receiver stage in an attempt to enhance the desired signal interference and/or jamming. These arrays are commonly used to maximize the SNR of the desired signal and to minimize or null undesired signal input power.

CONSIDERATIONS FOR MOBILE RADIO SYSTEMS

In the last 15 years or so, there has been an increasing interest in and demand for communications systems in the mobile environment, the most popular examples of which are paging systems and cellular telephones. The advances in digital technology in that time period have prompted a movement toward the use of digital modulation and transmission schemes at higher frequencies in order to better utilize the RF spectrum that is available and to provide highly reliable transmission. Spectral efficiency involves judicious use of the frequency, time and space elements of the spectrum ⁽⁶⁾, based on the use of narrowband transmission, multichannel access and proper channel spacing. Mobile land radio appears to have entrenched itself firmly in the 800-900 MHz range. The Integrated Services Digital Network (ISDN) is gaining wide acceptance, and promises to provide data and voice services reliably on a world-wide scale for both fixed and mobile services.

However, the mobile environment does present special problems, and the main obstacle is the nature of the propagation path. A fixed base station, usually located at an elevated site to minimize local reflection and scattering effects, must try to communicate with a mobile station that is constantly on the move between varying terrain features, so that in general a direct line-of-sight path may not always be available. The antenna on the vehicle may average only ten feet above ground at most, and it would not need to move very far to introduce a variation of several

dB in signal level. Obstructions in the propagation path may be stationary or moving. Thus, the effects of reflection, scattering and diffraction may all come into play to produce many random propagation paths, leading to fast, deep fades, even up to 30-40 dB in depth. These sorts of problems may become particularly severe in high-density urban environments (Figure 9), where scattering and multiple reflections from buildings and other structures will predominate. Figure 9a shows a typical fading envelope in the urban environment ⁽⁴⁰⁾. In a rapid fade situation, things change so quickly and dynamically that it would be pointless to look at the problem in a deterministic fashion, so we usually view it statistically and look for a mean signal level. In particular, fast fades can lead to significant burst errors ⁽³⁰⁾. The proper method of digital radio modulation scheme ^(33, 34) may help tremendously.

Mobile propagation paths can be characterized by three major phenomena -- envelope fading, shadowing and path loss ⁽⁶⁾. **Envelope fading** is the appearance of fast, deep variations over the entire signal envelope, especially at longer distances. This type of fading is considered the single most important factor in mobile work. The fade rate depends on both the speed of the vehicle and the carrier center frequency. For example, the fade rate may be as much as 30 Hz at a frequency of 900 MHz for a vehicle travelling at 25 miles per hour. Vehicle motion will also introduce Doppler spreading, which shows up as a rapid phase change, or random FM noise, on the carrier. **Shadowing** is due primarily to terrain features or other obstructions, and tends to produce slow variations in the received signal. **Path loss** deals simply with the distance between transmitter and receiver, and may vary anywhere from the inverse square of distance up to the fifth or sixth order of inverse distance.

MULTIPATH EFFECTS DUE TO TROPOSPHERIC DUCTING

At frequencies of interest to satellite communications, tropospheric multipath propagation may be of concern for elevation angles less than about 5 degrees, due to the long length of the propagation path and the possibility of scintillation phenomena from atmospheric turbulence across that path ⁽⁴⁾. For this reason, elevation angles of less than 5 degrees

should be avoided ⁽³⁾. But even at higher elevation angles, multipath propagation may occur from reflections from the surrounding terrain ⁽⁴⁾; this can be virtually eliminated by the use of highly directional antennas, such as are used at most commercial satellite installations. Multipath response differs between analog and digital systems, however; an excellent review of this problem is described in the paper by Siller ⁽⁶⁾. Depolarization effects have been observed in satellite communications due to multipath-induced co-polarized fading ⁽⁶⁾. Such depolarizations may result from tropospheric turbulence along the signal path, reflections from an ionospheric layer, refractive bending or reflections and scattering from earth surfaces.

MULTIPATH PROPAGATION IN BUILDINGS AND FACTORIES

The digital and computer age has given rise to many applications for communications between people and computers and other automated gadgets. Although much of the interconnection of high-tech systems, such as computers in a local area network, is done by coaxial cable or fiber-optic means, it could also be done quite easily by radio. In a factory environment, multipath can be caused by reflection from both the building and its contents (machinery and/or inventory), all of which may have a high metal content ⁽¹⁸⁾; shadowing may also occur from the equipment usually found in a factory. Although general principles may be applied, the conditions prevalent at a given location will determine the measures that must be taken for that particular site. Similar studies for data communications in large buildings and homes have been conducted by Ishii ⁽¹⁵⁾ and Saleh, et. al. ^(16, 17).

MULTIPATH PROPAGATION IN SPREAD SPECTRUM SYSTEMS

Spread spectrum systems tend to be less prone to multipath variations than conventional systems ⁽¹⁾. Direct sequence receivers treat the reflected signal in the same fashion as any other uncorrelated signal. The multipath problem becomes of less concern when a higher code chip

rate is used. Frequency hopping receivers can reduce multipath losses by either transmitting the same data on more than one frequency or by comparing the power available in alternate mark/space channels when making each bit decision. The use of delay-line matched filters, chirp filters or digital matched filters may also help in nulling out the delayed signal inputs. Swept chirp spread-spectrum systems may be effective against moderate multipath conditions, but they require good matched filter systems.

MULTIPATH FADING SIMULATION MODELS

We saw earlier that multipath fading is a statistical process that follows a Rayleigh distribution (Gaussian) ⁽⁴⁾. A basic simulator to reproduce envelope and phase characteristics can be fashioned from either hardware alone (Figure 10) or from a combined hardware-software system. In the hardware simulator, the cutoff frequency of the low-pass filters is based on the center frequency of interest and an assumed average vehicle speed. A software system is described in Lee ⁽⁴⁾. The obvious advantage of the software-based simulator is the speed in which various operational parameters can be varied and the differences quickly noted.

Another popular model is the Rummler model ^(20, 38, 39), a three-path model which characterizes multipath fading according to the multipath notch concept described earlier. This model has a transfer function defined by ^(38, 39)

$$H(j\omega) = a(1 - be^{-j(\omega - \omega_0)\tau})$$

where

- a = attenuation due to flat fading
- b = amplitude ratio, primary beam to secondary beam
- ω_0 = notch center frequency
- τ = IF passband center frequency
- τ = delay time between two signals

For an actual microwave radio link, Rummler indicates a nominal value of $\tau = 6.3$ nanoseconds. This value is best computed on the basis of the actual length of the signal path.

A multipath fading simulator based on the Rummler model is shown in Figure 11 (38). Notch frequency variation is accomplished by varying the amount of phase shift, while notch depth is controlled by varying the ratio between the two attenuator stages. This type of simulator is used to generate M-curves, or outage signature curves, which are a plot of notch frequency versus the notch depth at which the bit error rate (BER) exceeds a pre-defined threshold. Outage signatures are a common criterion for determining the ability of a digital radio to withstand multipath fading effects. This model is used in a commercially available multipath fading simulator, the HP 11757A, which is designed to stress-test digital radio systems under many multipath conditions.

REFERENCES

- (1) Dixon, Robert C., *SPREAD SPECTRUM SYSTEMS*, Second Edition, John Wiley and Sons, 1984.
- (2) Shibuya, S. A., *A BASIC ATLAS OF RADIOWAVE PROPAGATION*, John Wiley and Sons, 1987
- (3) Freeman, R. L., *RADIO SYSTEM DESIGN FOR TELECOMMUNICATIONS (1 - 100 GHz)*, Wiley Interscience, 1987
- (4) Lee, W. C. Y., *MOBILE COMMUNICATIONS ENGINEERING*, McGraw-Hill Book Company, 1982
- (5) Bothias, Lucien, *RADIO WAVE PROPAGATION*, McGraw-Hill Book Company, 1987
- (6) Feher, K., *ADVANCED DIGITAL COMMUNICATIONS - Systems and Signal Processing Techniques*, Prentice-Hall, Inc., 1987
- (7) Hall, M. P. M. and Barclay, L. W., *RADIOWAVE PROPAGATION*, Peter Peregrinus Ltd., 1989
- (8) Dorsey, D. R., "Radiowave Propagation - A Tutorial", *Proceedings, RF Technology EXPO '89*, p. 291-354 (February 1989)
- (9) Siller, C. A., Jr., "Multipath Propagation", *IEEE Communications Magazine*, 22, p. 6-15 (February 1984)
- (10) Lavergnat, J. and Sylvain, M., "Selective Fading Radio Channels", *IEEE JOURNAL ON SELECTED AREAS IN COMMUNICATIONS*, SAC-5, No. 3, p. 378-388 (April 1987)
- (11) Shafi, M., "Statistical Analysis/Simulation of a Three Ray Model for Multipath Fading with Applications to Outage Prediction", *IEEE JOURNAL ON SELECTED AREAS IN COMMUNICATIONS*, SAC-5, No. 3, p. 389-401 (April 1987)
- (12) Pratt, T. and Bostian, C. W., *SATELLITE COMMUNICATIONS*, John Wiley and Sons, 1986
- (13) Ippolito, L. J., *RADIOWAVE PROPAGATION IN SATELLITE COMMUNICATIONS*, Van Nostrand Reinhold Company, 1986
- (14) Turner, S. E., "Multipath Interference in FM Data Transmission", *RF DESIGN*, p. 26-47 (December 1988)
- (15) Ishii, T. K., "RF Propagation in Buildings", *RF DESIGN*, p. 45-49 (July 1989)
- (16) Saleh, A. A. M. and Valenzuela, R. A., "A Statistical Model for Indoor Multipath Propagation", *IEEE JOURNAL ON SELECTED AREAS IN COMMUNICATIONS*, SAC-5, No. 2, p. 128-137 (December 1987)
- (17) Saleh, A. A. M., Rustako, A. J. and Roman, R. S., "Distributed Antennas for Indoor Radio Communications", *IEEE TRANSACTIONS ON COMMUNICATIONS*, COM-35, No. 12, p. 1245-1251 (December 1987)
- (18) Rappaport, T. S., "Factory Radio Communications", *RF DESIGN*, p. 67-73 (January 1989)
- (19) Greenstein, L. J. and Shafi, M., "Outage Calculation Methods for Microwave Digital Radio", *IEEE COMMUNICATIONS MAGAZINE*, p. 30-39 (February 1987)
- (20) Rummler, W. D., Coutts, R. P. and Liniger, M., "Multipath Fading Channel Models for Microwave Digital Radio", *IEEE COMMUNICATIONS MAGAZINE*, p. 30-42 (November 1986)
- (21) Chamberlain, J. K., Clayton, F. M., Sari, H. and Vandamme, P., "Receiver Techniques for Microwave Digital Radio", *IEEE COMMUNICATIONS MAGAZINE*, p. 43-54 (November 1986)
- (22) Bultitude, R. J. C., "Measured Characteristics of 800/900 MHz Fading Radio Channels with High Angle Propagation Through Moderately

- Dense Foliage", *IEEE JOURNAL ON SELECTED AREAS IN COMMUNICATIONS*, SAC-5, No. 2, p. 116-127 (February 1987)
- (23) Oetting, J. D., "The Effects of Fading on Antijam Performance Requirements", *IEEE JOURNAL ON SELECTED AREAS IN COMMUNICATIONS*, SAC-5, No. 2, p. 155-161 (February 1987)
- (24) Kammeyer, K., Mann, R. and Tobergte, W., "A Modified Adaptive FIR Equalizer for Multipath Echo Cancellation in FM Transmission", *IEEE JOURNAL ON SELECTED AREAS IN COMMUNICATIONS*, SAC-5, No. 2, p. 226-237 (February 1987)
- (25) Martin, A. L., "Dispersion Signatures, a Statistically Based Dynamic, Digital Microwave Radio System Measurement Technique", *IEEE JOURNAL ON SELECTED AREAS IN COMMUNICATIONS*, SAC-5, No. 3, p. 427-436 (April 1987)
- (26) Sebald, G., Lankl, B and Nossek, J. A., "Advanced Time- and Frequency-Domain Adaptive Equalization in Multilevel QAM Digital Radio Systems", *IEEE JOURNAL ON SELECTED AREAS IN COMMUNICATIONS*, SAC-5, No. 3, p. 448-456 (April 1987)
- (27) Baccetti, B., Bellini, S., Filiberti, G. and Tartara, G., "Full Digital Adaptive Equalization in 64-QAM Radio Systems", *IEEE JOURNAL ON SELECTED AREAS IN COMMUNICATIONS*, SAC-5, No. 3, p. 466-475 (April 1987)
- (28) Andrisano, O., Bianconi, G. and Calandrino, L., "Adaptive Equalization of High Capacity M-QAM Radio Systems on Multipath Fading Channels", *IEEE JOURNAL ON SELECTED AREAS IN COMMUNICATIONS*, SAC-5, No. 3, p. 457-465 (April 1987)
- (29) Garber, F. D. and Pursley, M. B., "Performance of Differentially Coherent Digital Communications Over Frequency-Selective Fading Channels", *IEEE TRANSACTIONS ON COMMUNICATIONS*, 36, No. 1, p. 21-31 (January 1988)
- (30) Yoshida, S., Ikegami, F. and Takeuchi, T., "Causes of Burst Errors in Multipath Fading Channels", *IEEE TRANSACTIONS ON COMMUNICATIONS*, 36, No. 1, p. 107-113 (January 1988)
- (31) Stuber, G. L., Mark, J. W. and Blake, I. F., "Diversity and Coding for FH/MFSK Systems with Fading and Jamming -- Part I : Multichannel Diversity", *IEEE TRANSACTIONS ON COMMUNICATIONS*, COM-35, No. 12, p. 1329-1341 (December 1987)
- (32) Duffy, T., "Eliminating Multipath Fading in Digital Radios", *MICROWAVES AND RF*, p. 127-134 (June 1988)
- (33) Walker, H., "Modulation Schemes Aid Digital Radio Growth", *MICROWAVES AND RF*, p. 75-84 (February 1987)
- (34) Walker, H., "Gauging Errors Sets Digital Radio Quality", *MICROWAVES AND RF*, p. 89-99 (April 1987)
- (35) Wen, J. H. and Chang, J. F., "The Effect of Multipath Interference on the Performance of Packet Radios", *IEEE TRANSACTIONS ON COMMUNICATIONS*, Vol. 38, No. 6, p. 740-743 (June 1990)
- (36) Elnoubi, S. M., "Probability of Error Analysis of Partial Response Continuous Phase Modulation with Two-Bit Differential Detection and Offset Receiver Diversity in Fast Rayleigh Fading Channels", *IEEE TRANSACTIONS ON COMMUNICATIONS*, Vol. 38, No. 6, p. 782-786 (June 1990)
- (37) Lodge, J. H. and Moher, M. L., "Maximum Likelihood Sequence Estimation of CPM Signals Transmitted Over Rayleigh Flat-Fading Channels", *IEEE TRANSACTIONS ON COMMUNICATIONS*, Vol. 38, No. 6, p. 787-794 (June 1990)
- (38) Romanchik, D., "Getting a Handle on Multipath Fading Tests", *TEST & MEASUREMENT WORLD*, p. 65-68 (May 1990)
- (39) Rummler, W. D., "A New Selective Fading Model: Application to Propagation Data", *Bell Systems Technical Journal* 58, 1979, p. 1073-1100
- (40) Parsons, J. D. and Gardiner, J. G., *Mobile Communications Systems*, Blackie and Son Ltd., 1989
- (41) Devasirvatham, D. M. J., "Multipath Time Delay Jitter Measured at 850 MHz in the Portable Radio Environment", *IEEE Journal on Selected Areas in Communications*, Vol. SAC-5, Number 5, June 1987, p. 855-861
- (42) Bernhardt, R. C., "Macroscopic Diversity in Frequency Reuse Radio Systems", *IEEE Journal on Selected Areas in Communications*, Vol. SAC-5, Number 5, June 1987, p. 862-870
- (43) Winters, J. H., "On The Capacity Of Radio Communication Systems with Diversity in a Rayleigh Fading Environment", *IEEE Journal on Selected Areas in Communications*, Vol. SAC-5, Number 5, June 1987, p. 871-878

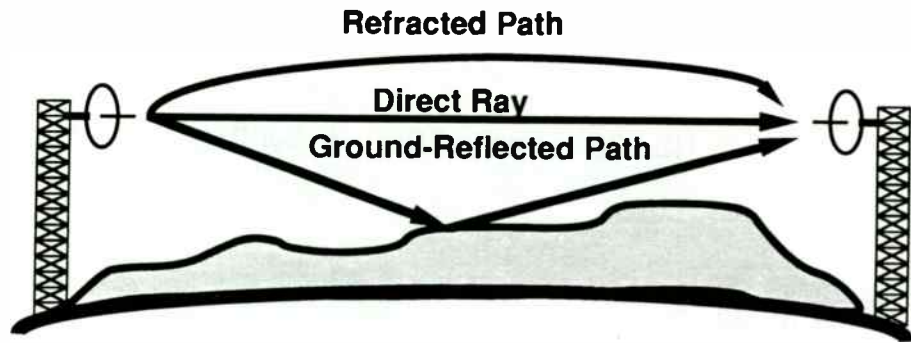


Figure 1. Nature of Multipath Propagation

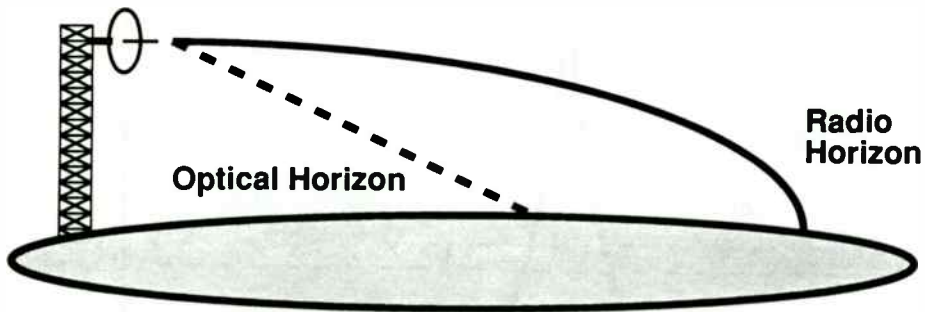


Figure 2. Optical Horizon and Radio Line-of-Sight

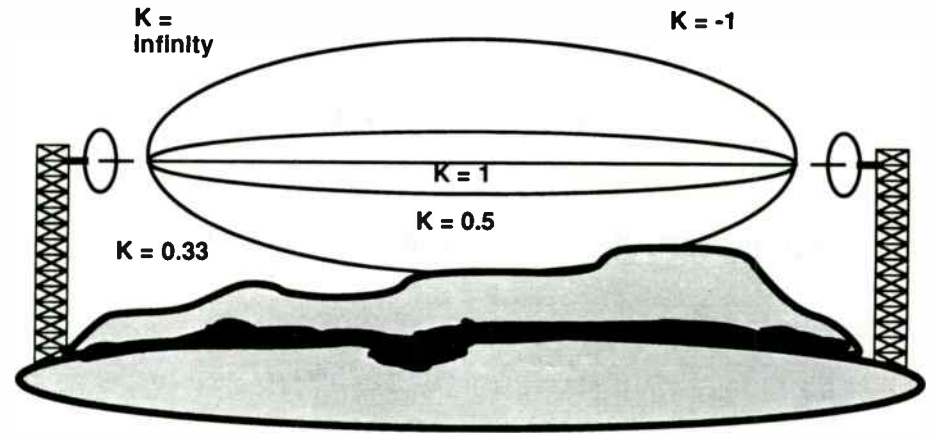


Figure 3. K-Factor and Ray Paths

(From Reference 3 - Freeman)

*HP 11757 - Fading Analyzer.
 LRF 102 - Fading Analyzer.
 Higher code chip rate
 better the multipath
 reduction?*

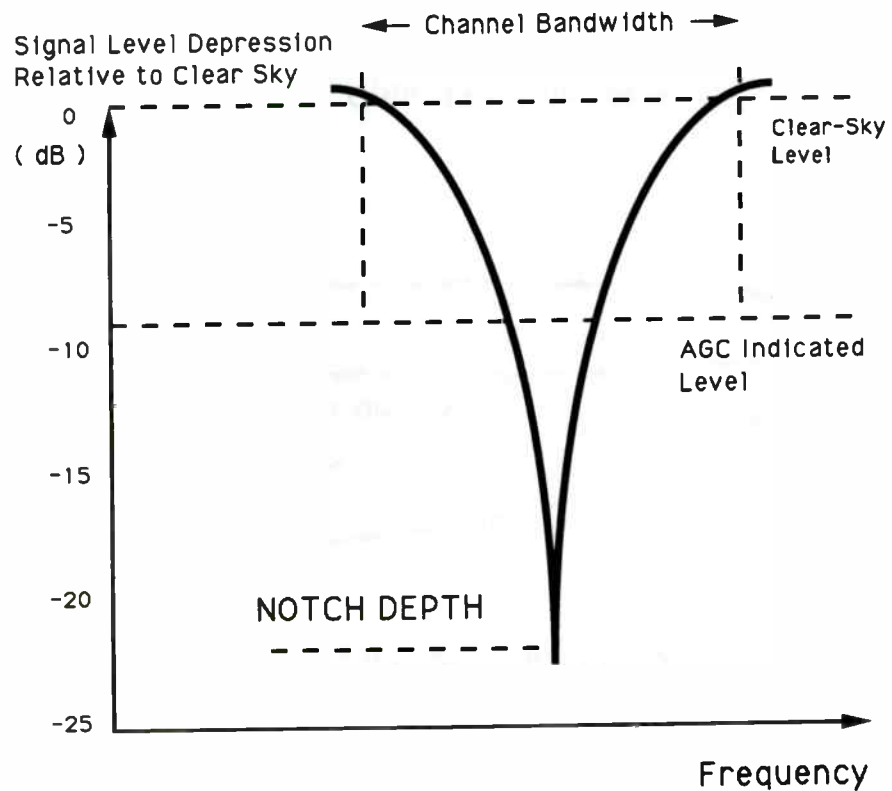


Figure 4. MULTIPATH NOTCH

(From Reference 7 - Hall & Barclay)

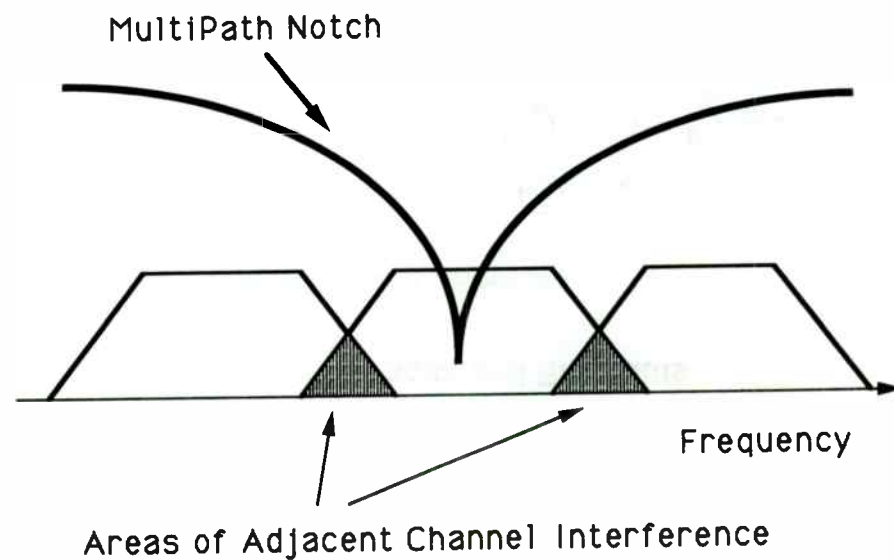


Figure 5. Adjacent Channel Interference

(From Reference 7 - Hall and Barclay)

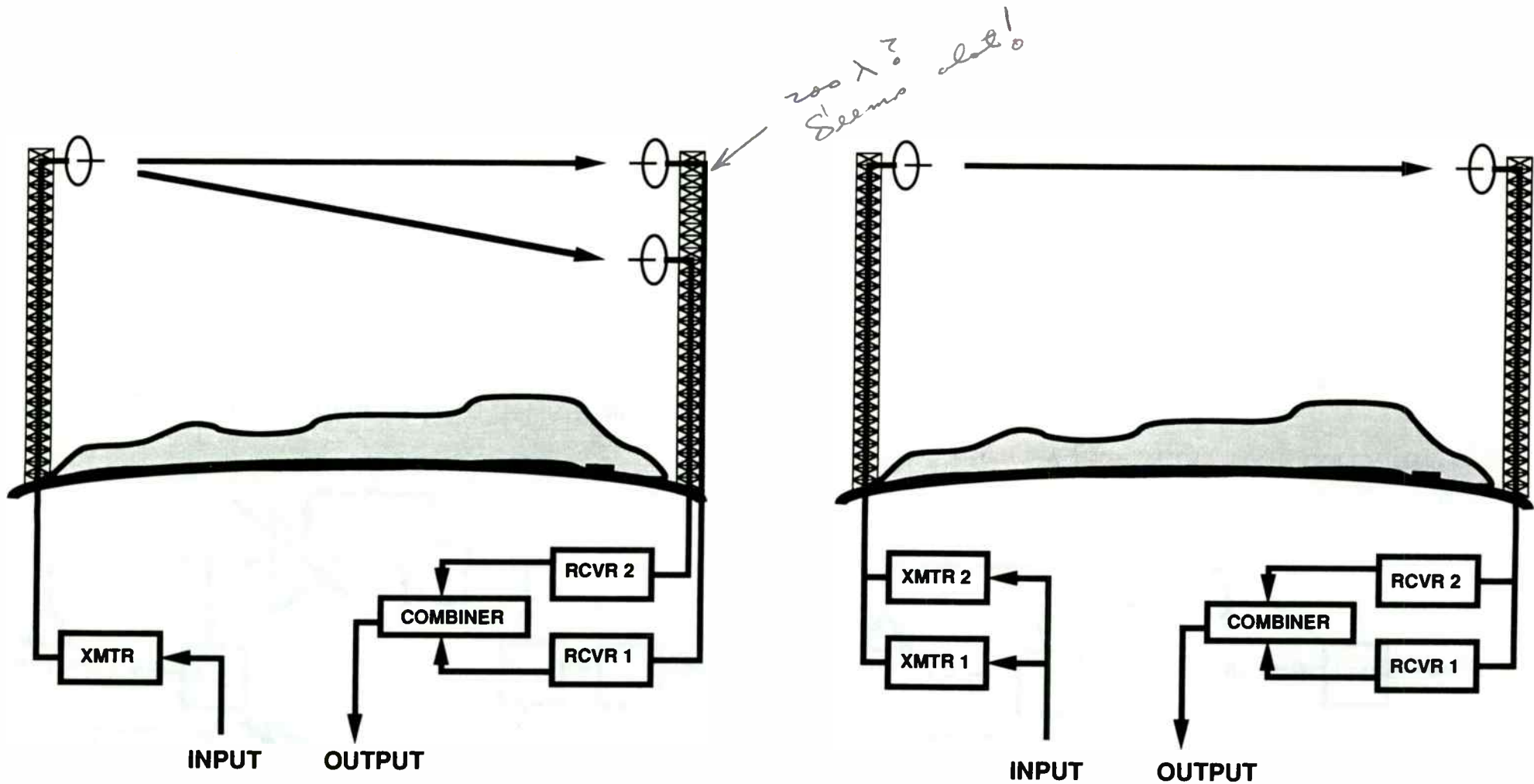


Figure 6(a). SPACE DIVERSITY

(From Reference 3 - Freeman)

Figure 6(b). FREQUENCY DIVERSITY

(From Reference 3 - Freeman)

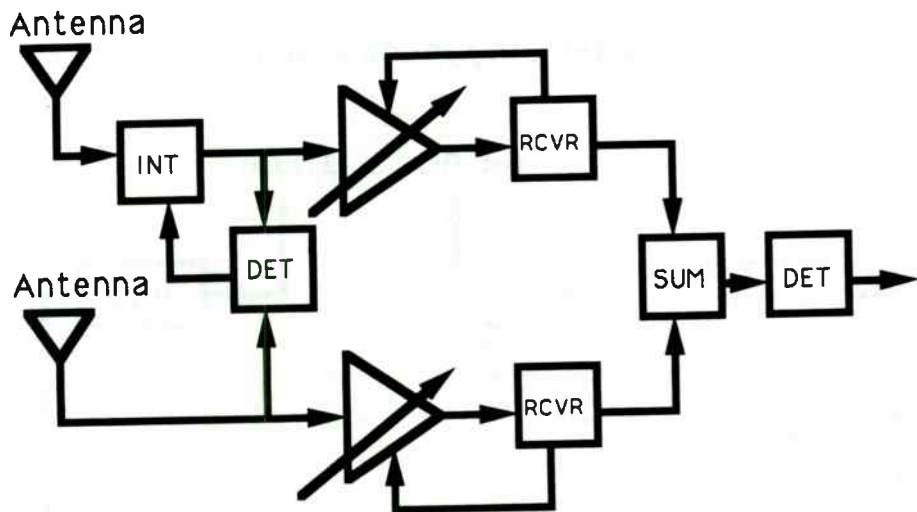


Figure 7(a). MAXIMAL-RATIO COMBINING

(From Reference 6 - Feher)

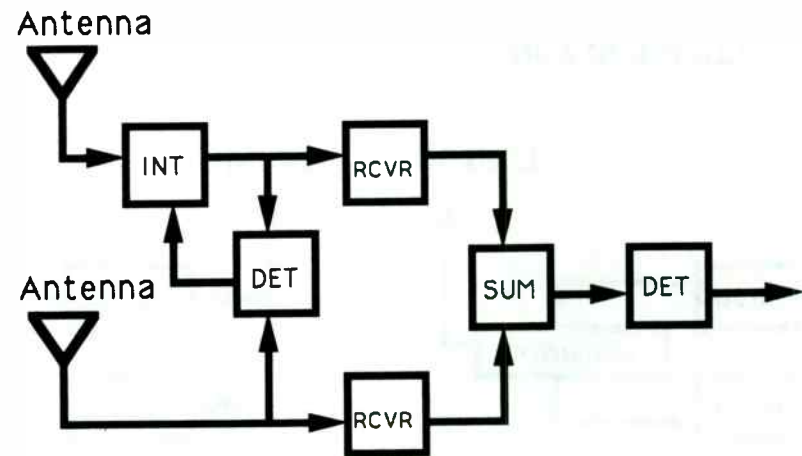


Figure 7(b). EQUAL-GAIN COMBINING

(From Reference 6 - Feher)

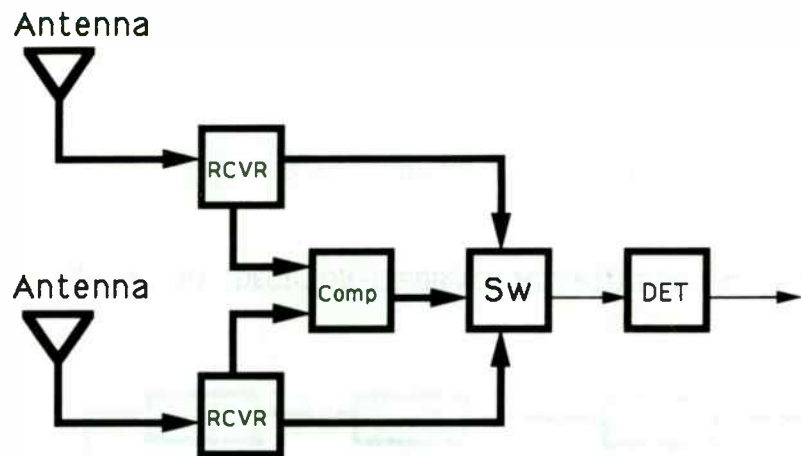


Figure 7(c). SELECTION METHOD

(From Reference 6 - Feher)

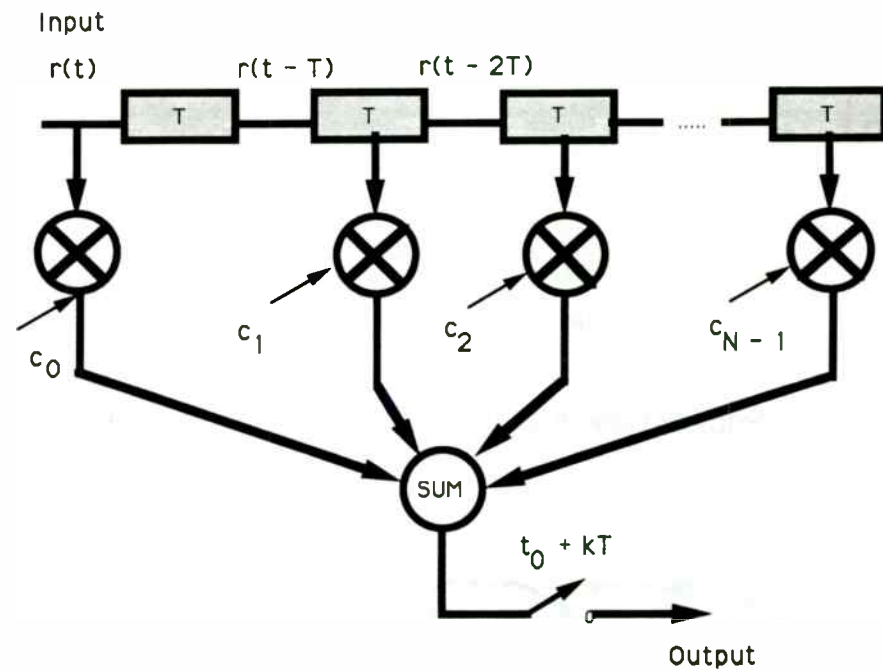


Figure 8(a). LINEAR TRANSVERSAL FILTER
ADAPTIVE EQUALIZER

(From reference 6 - Feher)

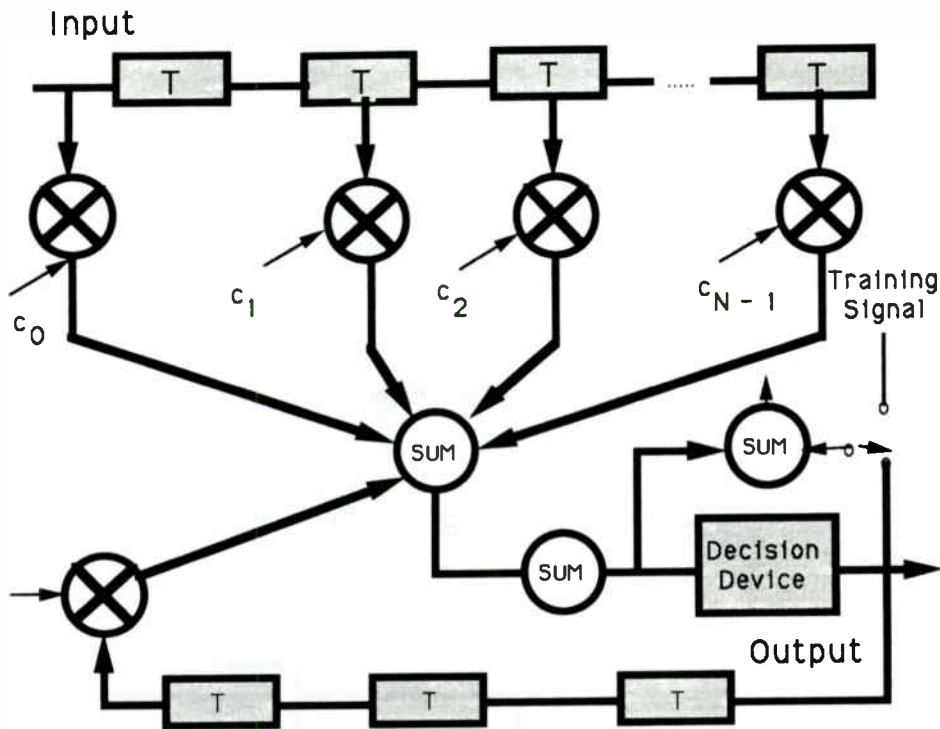


Figure 8(b). DECISION-FEEDBACK ADAPTIVE EQUALIZER

(From Reference 6 - Feher)

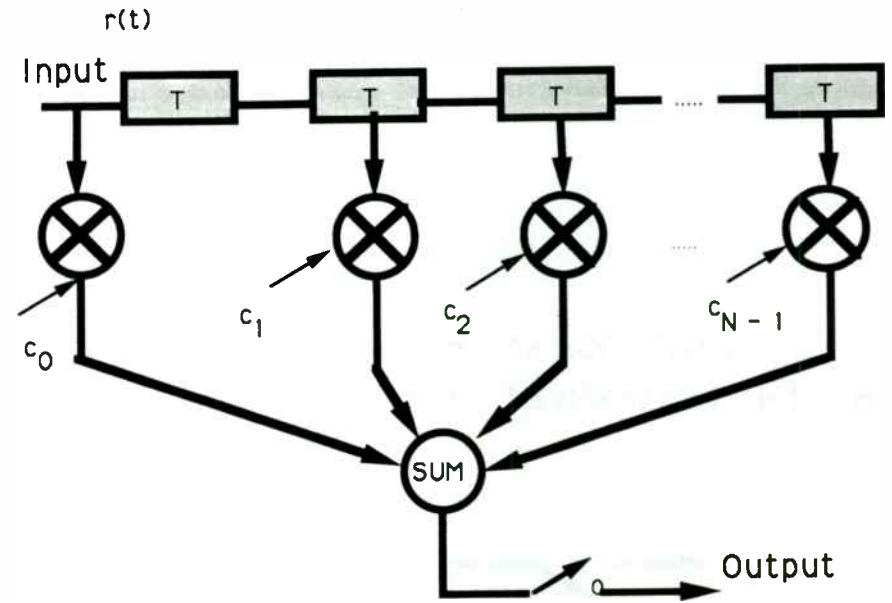


Figure 8(c). FRACTIONALLY-SPACED ADAPTIVE EQUALIZER

(From Reference 6 - Feher)

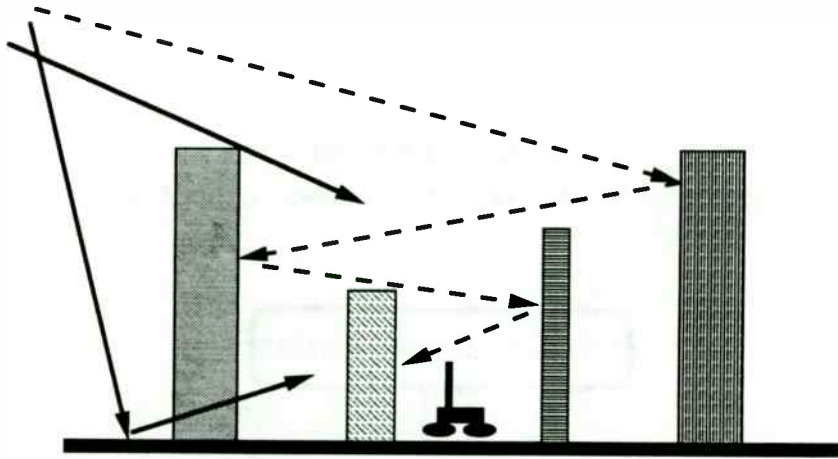


Figure 9. Propagation in Dense Urban Areas

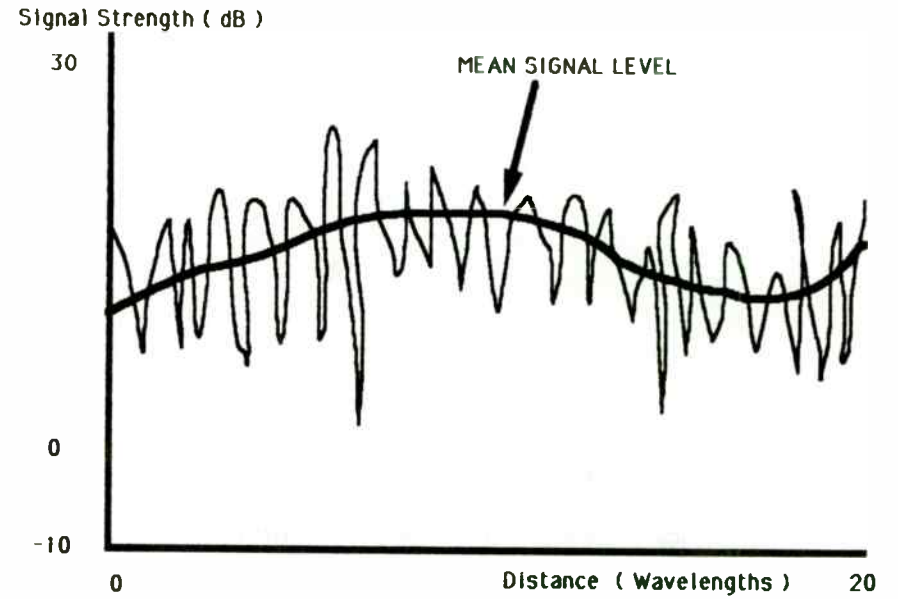


Figure 9a

FADING ENVELOPE STATISTICS
 (From Parsons and Gardiner -- Reference 40)

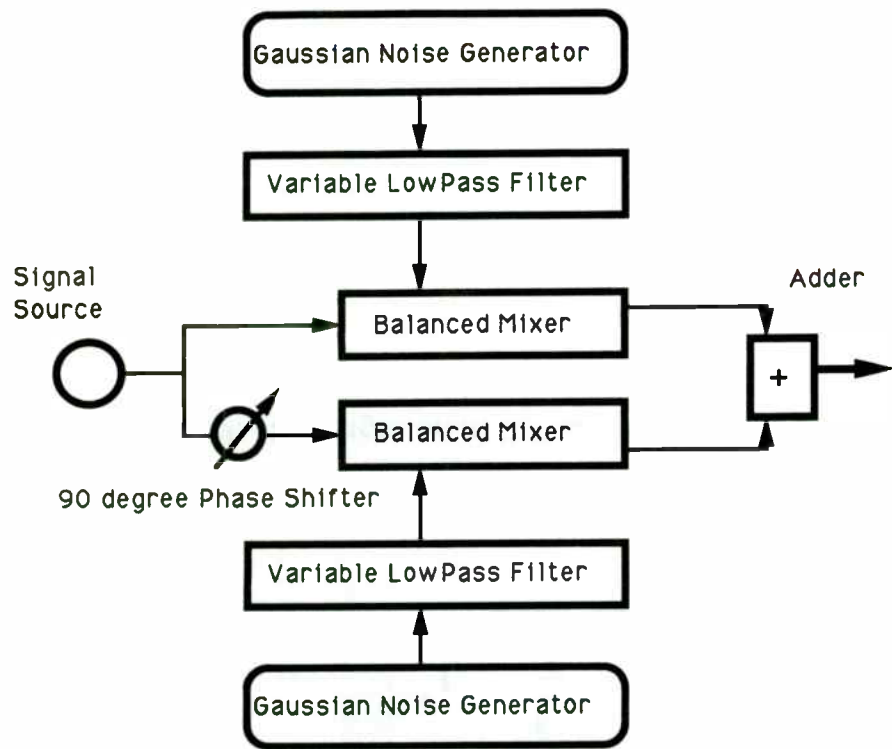


Figure 10. Rayleigh Multipath Fading Simulator
Hardware Implementation

(From Lee - Reference 4)

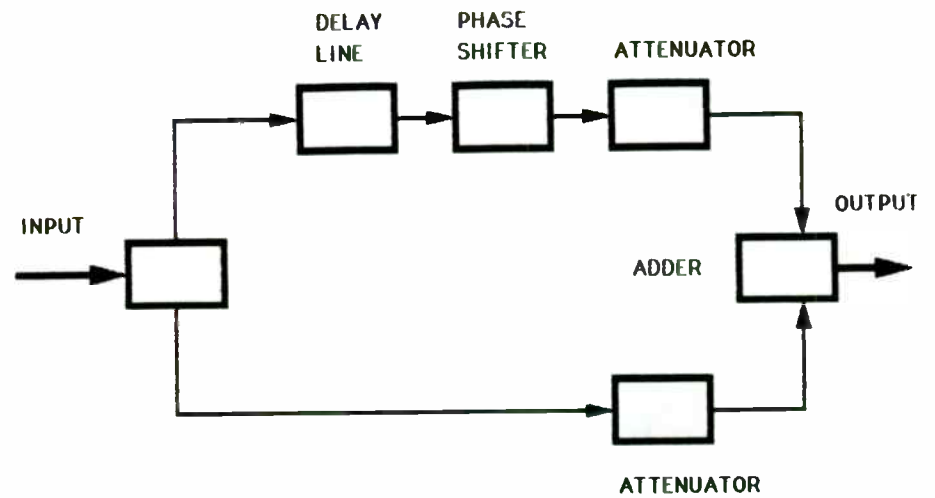


Figure 11
MULTIPATH SIMULATOR BASED ON RUMMLER MODEL

(From Romanchik -- Reference 38)



RADIO FREQUENCY IDENTIFICATION SYSTEMS

INDUSTRIAL AND COMMERCIAL APPLICATIONS

James Eagleson
Senior Development Engineer



RF IDENTIFICATION - WHAT IS IT?

Just about everyone, technically inclined or not, has noticed Bar Code labels on products they buy at their local supermarket or department store. Not always so obvious are the anti-theft tags on clothing and other items which ensure that products don't leave the store unpaid for. Both items represent applications of technology to the problem of tracking and identifying objects without significant human intervention.

Figure 1: BAR CODE LABEL

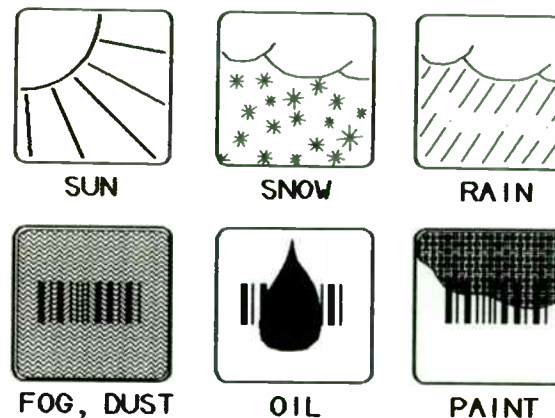


There are applications, however, where neither of these simple, inexpensive techniques will work very well because of the environment

in which the system must operate. Smoke, dust, dirt, grease, or other factors can render laser-based systems either unreliable or impossible to use. The object to be identified may get painted, dipped in chemical baths, or dried at elevated temperatures (200 degrees Celsius).. any of which may destroy or modify normal Bar Code labels.

Outdoor environments present special problems for laser-based technologies since required distances can be 5 to 50 feet, and strong sunlight, ice, rain, snow, fog, dust, oil, and dirt may interfere with the light beam.

Figure 2: Sun, Snow, Rain, Fog...

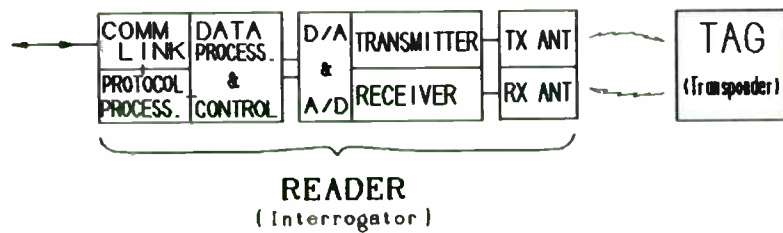


Radio Frequencies, on the other hand, are relatively unaffected by these obstacles and can even penetrate most paints, cardboard, even asphalt or cement so that RF based systems provide a viable alternative to visual light systems for these tougher Auto ID applications.

RF ID SYSTEM DESCRIPTION

There are two basic parts to an RF ID System: the "Reader" and the "Tag".

Figure 3. RF/ID System - Reader



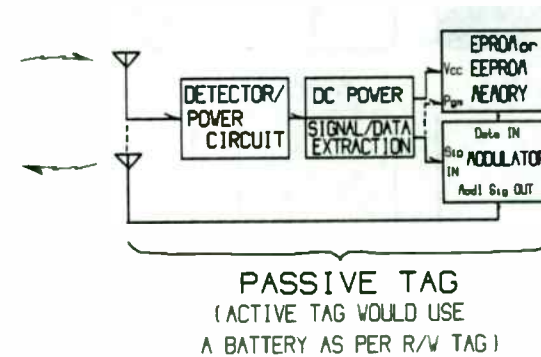
The "reader" consists of:

- 1) Computer/Reader Communications Link
- 2) RF Communications Link
- 3) Data Processing/Control Circuitry
- 4) Protocol Processing
- 5) Transmitter Circuitry
- 6) Receiver Circuitry
- 7) Antennas or Antenna Coils

The reader may also provide some level of "write" capability to the tag as well as being able to read it. Some manufacturers refer to units with this capability as a "reader/writer". At ALLEN-BRADLEY, we refer to our system as an "Intelligent Antenna Unit" since it can be computer configured to work with any of our tags whether Read Only, Programmable, or Read/Write.

Tags also contain a receiver and a transmitter but on a much simpler level than used by the reader. The tag's data circuitry may merely consist of a preprogrammed EPROM-based circuit in which case it is referred to as a "Read Only" tag. One unusual implementation of a read only tag uses tapped SAW delay lines as the method of coding.

Figure 4. Generalized Tag Diagram



Other tags use EPROM technology to allow contact reprogramming or EEPROMs to allow non-contact programmability through an RF or inductive link. These tags are referred to as "Programmable" Tags.

The most sophisticated tag type provides complete data communications in both tag/reader and reader/tag directions using battery backed RAM. These tags are referred to as "Read/Write" Tags.

GENERAL USAGE

Read Only tags, of course, have the identical function to Bar Code Labels. They place a preset serial number on an object through which

it can be identified. The limitation, here, is that no direct correlation between identified object and tag code exists and modification of tag code for specific purposes is not possible.

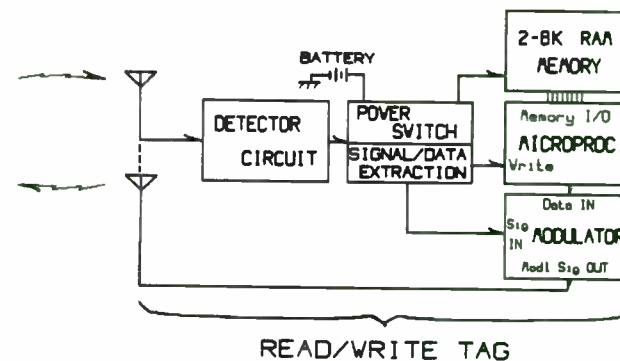
Figure 5. Tag Types

READ ONLY	RF equivalent to Bar Code
PROGRAMMABLE	Able to be user programmed over a moderate lifetime (10,000+ times with up to 1024 bits of data.)
READ/WRITE	Provides full Write and Read capability up to 8K BYTES of block addressable memory. In essence, a portable RAM with an RF Comm Link.

Programmable tags, on the other hand, can be programmed by the user as many times as required up to the limit of EEPROM technology. This allows customization of tag data so that specific information can be placed in the tag as it is attached to an object. In fact, the data can be read back, modified, and reprogrammed into the tag for process control purposes, though use in this manner may be limited by the available memory space up to about 1000 bits and the maximum programming cycle limitations of the particular chip being used.

Read/Write (R/W) tags act as a kind of portable, wireless, non-volatile Random Access Memory. This is ideal for users requiring custom process control, data collection functions, or other kinds of data modification during use. Typical R/W tags have about 1K to 2K bytes of memory though 8K bytes, or more, is available from a few manufacturers. Individual blocks of memory can be independently accessed for reading or writing these tags.

Figure 6. READ/WRITE TAG



APPLICATIONS OF RF ID

RF ID has seen an amazing variety of applications over the past 10 years. To provide a brief overview, consider the following systems:

AUTO ANTI-COLLISION SYSTEM

An early application of RF ID was for an automobile anti-collision system in which a 915 MHz low power carrier from the front of one vehicle would strike passive antenna/diode circuit in the vehicle in front of it (built into the license plate), convert some of the energy to 1830 MHz, then return that signal to the interrogating vehicle. Even at freeway closing speeds, Doppler will be present on the outgoing and incoming signals equal to about four times that which would be present for a one-way transmission since the signal going out is shifted (1x), its frequency is then doubled (2x), and the 2nd harmonic will have twice the Doppler shift on the return trip due to

its frequency. Thus the system has a means of checking proximity and closing rate which are the two essentials for such a system to function.

The system uses only microstrip patch antennas for both frequencies and a diode harmonic generator so that:

- a) Cost is minimal
- b) Complexity is minimal
- c) Range is automatically limited by diode detection sensitivity

The transmitter and an autodyne based receiver system should be economical, as well. Unfortunately, all vehicles must be so equipped for the system to be effective and other "real world" factors such as severely "cluttered" freeways and the political "hard sell" of "universal" anything must be taken into account. As far as I know, no such system is presently being actively pursued.

RETAIL STORE ANTI-THEFT

Store anti-theft systems also use the "cheap diode" technique. When the "transponder" diode, basically a stamped metal resonator with a diode junction, is present, it returns a signal to a receiver tuned to the second harmonic of the transmitter indicating the transponder's presence. Try to leave the store with the "tag" still attached and you'll have alarming results!

Other systems use VHF or UHF resonant circuits printed on plastic or paper substrates with metallized foil. These will reflect sufficient energy to trigger the alarm circuit. They are disabled, in many instances, by blowing a low voltage, printed circuit capacitor to a shorted condition, or simply by being removed from the article.

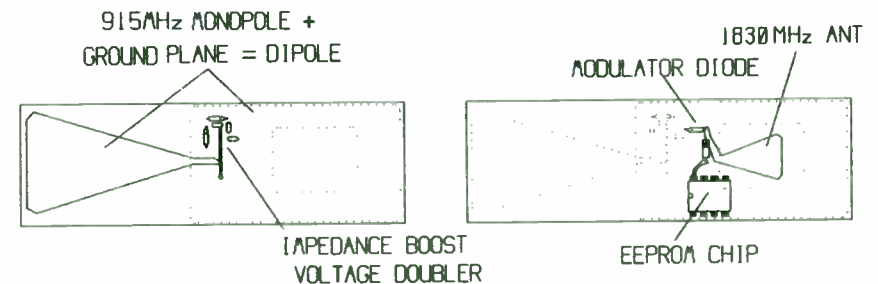
Most of these schemes simply detect the presence of a tag but make no specific attempt to find an identification code. Low cost is the name of the game, both for the reader and the tag.

ANIMAL IDENTIFICATION

One early experiment in animal ID used a 915 MHz / 1830 MHz harmonic generation scheme similar to the Auto Anti-Collision system except that data was added to the return signal by modulating the conversion diode. The advantage, of course, was that "tag" power was derived from the transmitter in the interrogation unit (reader), so that no batteries or other power source was required in the tag. This has obvious advantages in any device implanted inside an animal both from a battery replacement standpoint and to prevent poisoning the animal should the tag leak.

In essence, a harmonic tag consists of a 915 MHz antenna, a microstrip to control the tuning range and boost the impedance to provide the higher voltages required to run EPROM or EEPROM chips, a

Figure 7. 915 Harmonic RF/ID Tag



harmonic generator, a diode modulator, a memory chip with serial output driver, and an 1830 MHz antenna.

VLF systems have supplanted UHF systems for implantables, with tags as small as a large grain of rice having about a six inch range and used to track fish in commercial "fish farms", to somewhat larger tags which can be used for pet or farm animal identification at somewhat longer distances.

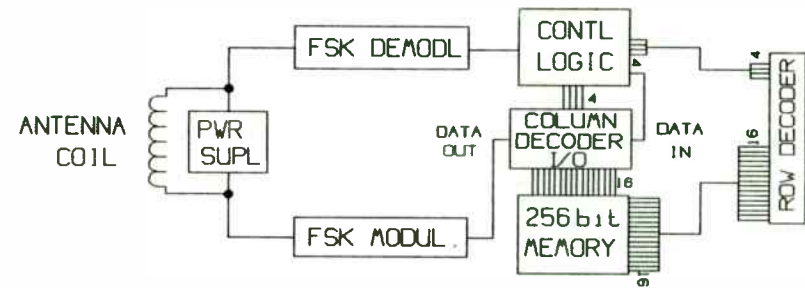
In the case of the fish farm, fish are hatched, released to the open sea, then identified and harvested upon their return to the "spawning grounds". The new hatch is also tagged and monitored. To get around the six inch reader limit caused by the miniature tag size, fish are forced to swim through a 12 inch diameter pipe so that they will never be more than six inches from the reader's antenna coil. This also keeps the fish more or less single file to prevent conflicting reads between fish arriving at the same moment.

VLF TAGS

VLF has the advantage of simplicity and a rapid signal fall off about $60 \text{ LOG (DISTANCE)}$ which allows very close reader/tag spacing and tag-to-tag spacing. This is because these systems are obviously in the near field of the reader antenna (consider the wavelength of 200 KHz).

By the same token, applications having a long distance or varying distance requirement (0.5-50 feet), are often better served by UHF tags because their far field $20 \text{ LOG (DISTANCE)}$ power drop off will provide more consistent signal levels to and from the tag. At VLF 0.5-10 foot level would drop 78 dB compared to only 26 dB at UHF.

Figure 8. Representative VLF Tag



Since VLF tags generally operate in the 50-500 KHz region, they generally use data rates under 10 KHz (3-10 Kb/s). While wider bandwidths could be used to allow higher data rates, the noise in many applications, particularly on the factory floor, presents high levels of RFI in the VLF region so that selectivity is usually required if the reader is to maintain a reasonable signal-to-interference ratio. Most IC's also require 3-5 volts to operate even though only 25-50 microamps of current may be required. Thus boosting the impedance by resonating the circuit and using moderate "Q" is helpful.

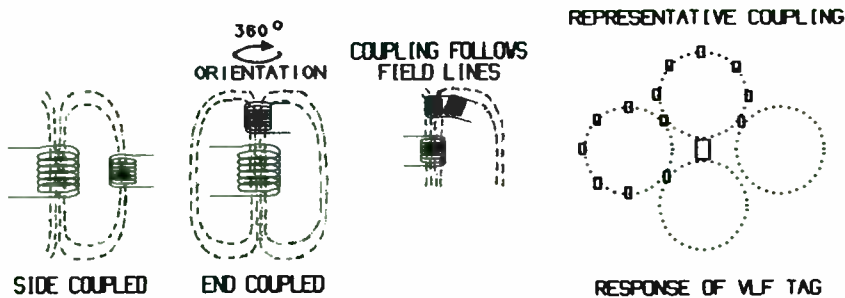
ORIENTATION OF TAGS

Another factor in many applications is the orientation of the tag. One major difficulty with Bar Code labels is the handling of the label's orientation. In the local grocery store, the problem is handled by scanning in several orientations usually with a help from the grocery clerk who just passes it over the scanner again if it doesn't

read the first time. In the factory, however, such orientation problems must be handled without human intervention. For many applications, the tag must be able used even though it may be rotated 360-degrees in a plane parallel to the reader's antenna (or coil).

Obviously, coil coupled devices such as VLF tags, can do this quite readily if their own coil is end on to the reader. For UHF systems, circular polarization can be employed so that though the tag is linearly polarized, it can be read in any orientation due to the reader having circularly polarized response.

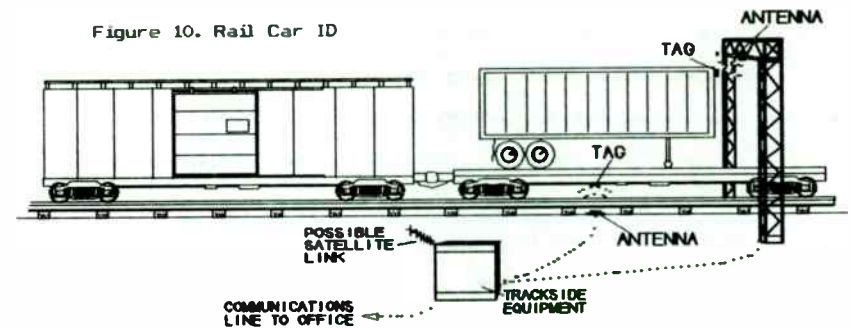
Figure 9. VLF Tag Orientation



Some applications, though, have no orientation problem at all. Railcars, for example, maintain a firmly fixed orientation once the initial installation is made since, unless the car leaves the tracks, objects installed on it should not change orientation. Here, however, data rate (data capture time) is the more serious consideration as is reliability, ruggedness, and security.

RAILROAD CARS

Figure 10. Rail Car ID



At any given time, about 10 percent of the rolling stock in America is "lost". At least, no one knows for certain where boxcar 1234567890 is at that particular moment. While all these cars have 10-digit ID numbers on their sides, some railroad worker using a pencil and clipboard writes down all those numbers as a train sits in a rail yard somewhere. If he gets distracted, isn't at his peak performance that day, or just plain writes down the wrong number, that box car becomes "lost".

Seeing the need for electronic ID, if for no other reason than to back up the human operator, the railroads did an experiment with a Bar Code based system. It was an expensive failure. Not only did rain, snow, sleet, dirt, dust, smoke, oil, and other normal environmental factors prevent reasonable performance, but kids living near railroad tracks love to throw rocks, mudballs, and snowballs at passing trains and disgruntled rail workers aren't always in favor of "automatic" anything! Put another way, it was difficult to keep the labels or trackside equipment in a reasonable state of repair.

With UHF, tags as small as 1 x 2 x 4 inches are practical with optimum performance available from tags in the 1.5 x 2 x 7 inch size range. Their higher data rate (up to 400 Kb/s) allow the required capture window to be smaller with antenna size requirements more in the 6 x 6 x 2 inch region. One manufacturer's reflective tag system, however, uses a high gain antenna in about a 6 x 12 x 30 inch weather proof enclosure in order to optimize performance.

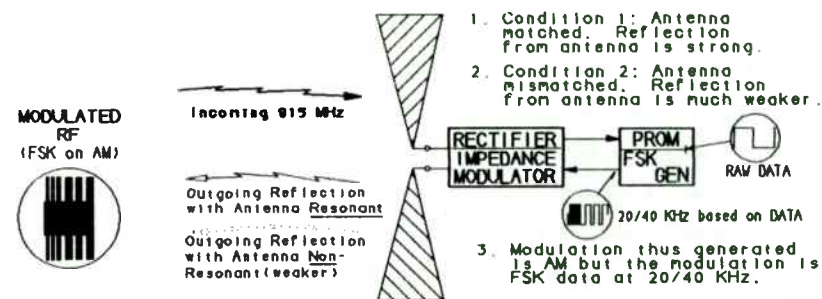
In tags for this application, the ID number is stored in an EPROM or EEPROM so that it can be programmed with the exact ID number of the railcar and/or with other data up to as many as 40 characters. The EEPROM versions can be reprogrammed many times or they can be "locked" after initial programming with a permanent number. This kind of chip can be programmed using the reader's radiated signal so that physical connection to the tag is not required. EPROM versions, obviously, require some kind of physical connection to the tag during programming then some means to seal the tag against the harsh rail environment after programming.

UHF systems can also be used to identify containerized cargo riding on the railcar as well as the railcar, itself, since they operate in the far field with the usual 20 LOG (Distance) signal fall off. Thus, the system can be used at distances from about one-half to fifty feet (in some cases, more) which allows a system to be built which will identify the railcar from underneath the train while separately identifying cargo containers from the top or side of the rail car.

Two approaches are presently in use in the UHF rail ID marketplace.. Reflective and Harmonic tags. Harmonic tags are at 915 MHz with an 1830 MHz return signal modulated with the railcar ID. This was previously described.

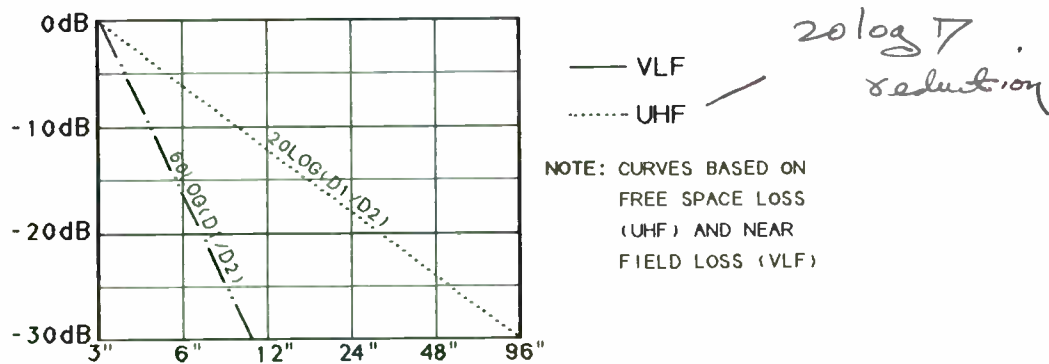
Reflective tags merely absorb or reflect the 915 MHz energy striking them by switching their "receive" antenna in or out of phase so that an autodyne receiver at the "reader" can decode the sidebands of the signal thus generated.

Figure 11. Reflective Tags



UHF systems are favored because their much higher data rates and smaller antenna size are advantageous when speeds up to 120 MPH are contemplated. VLF antenna loops tend to be 3 x 7 feet in order to achieve a large enough capture window to decode tags passing this fast.. Location, spacing, and size of the tag tends to be somewhat more critical compared to UHF tags, as well.

Figure 12. VLF versus UHF "space loss" due to near field versus far field operation.



The 60 LOG (Distance) of VLF systems, which are essentially transformer coupled (loop to loop), restricts tag to antenna placement to relatively short distances and only within the perimeter of the reader antenna coil. This is why the 3 x 7 foot size is required to obtain a 3 x 7 foot response window for rail or truck/car identification systems operating at high speeds.

It is easy to see that it would be difficult to place a set of loops to read both the car and containers for the usual rail situation.

Harmonic systems have shown good performance with the tag mounted under the box car and the antenna between the tracks though the primary supplier of reflective RF ID systems for railroads seems to prefer the side of car mount with the reader's antenna located as much as 50 feet away from the railcar.

Early customer preference seemed to favor an under the car tag location, both from a security standpoint (kids with rocks), and so a single equipment point could be used to scan multiple track locations without reading tags on adjacent tracks. The side-of-car location, however, simplifies mounting of both tag and reader, provides a much larger read window since the antenna can be placed 25-50 feet from the tracks, and should reduce nulling and Doppler effects.

As an aside, one test of the Harmonic system showed the problem of laser based system when used on railcars versus RF based systems. On a run of a hundred loops of the Pueblo, Colorado high speed test track, the RF ID system did not miss tags even once. The test track's own Lazer based lap counter, which merely had to detect light from a reflector mounted under the train, missed the reflection three times during the same run! We're back to dust, dirt, vibrations...

ELECTRONIC SIGN POSTS

Another area of renewed interest in RF ID is in mass transit systems. It is often difficult to get information on location from buses and commuter trains. And, yes, it's usually the human factor at work, again.

Several systems have been developed using line powered and reader powered "sign post" systems which are read from the vehicle then reported automatically, usually by the vehicle's own two way radio system, to the central control point. This provides automatic updating on the location of the vehicle for scheduling and tracking purposes. It can also be used for automatic station announcement systems which will flash the station name on an overhead LED display

and use one of the excellent, modern speech synthesizers to announce the station name on a loud speaker.

The station announcement idea has already been experimented with and is aimed at blind or deaf riders, but should also aid people too short to see which station they are entering over the heads of the "masses" as well as those who are just too deeply engrossed in the Wall Street Journal or other reading material to notice that they have arrived at their destination.

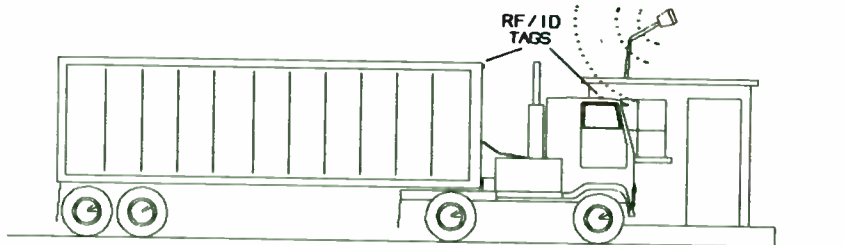
On trains, signposting can also be used as one element of an automatic routing system, as well.

TRUCKING

In our modern era, efficient operation of truck fleets often makes the difference between success and failure. Systems presently exist which record a variety of data about the operation of trucks

TRUCK TRIP DATA / TRACTOR-TRAILER IDENTIFICATION

Figure 13. Trip Recorder Data Link



NOTE: TRACTOR TAG CAN ALSO BE USED AS TRIP RECORDER DATA LINK.
TRAILER TAG CAN BE USED FOR YARD OPERATIONS AND FOR I. D.
WHILE TRAILER IS ON A RAIL CAR

during its trip between terminal "A" and "B".. speed, engine perform-

ance, temperature, and so forth. At the end of the journey, the driver must get out of the cab, open a door on the side of his tractor, remove a heavy duty RS-232 cable with an MS connector, then plug it in to the terminal's cable to dump his trip recorder's data into the terminal's computer.

With UHF RF ID systems, both the tractor and trailer can be tagged for identification purposes while the tractor's tag can be linked to the trip recorder allowing the RF ID link to be used to also dump the trip data. Thus, it is quite possible to automatically identify the tractor, dump its trip data, and identify the attached trailer and even cargo containers which may be on it.. all while the truck drives into the terminal facility. This should be much more convenient for the drivers, particular in the northern states during the winter, and can provide in-terminal tracking of trailers for the terminal operator, as well.

Another use for RF ID on trucks would be for automatic, weigh-in-motion systems. The technology exists to allow truck weigh stations to be automated by burying a reader antenna in the road or placing it overhead so that trucks traveling the highway would no longer have to stop at the weigh station but could just pass by the weigh station at normal speeds. The weighing mechanism can already be placed in the roadbed but unique identification of the truck would be required to make the system practical. RF ID provides the missing link and standardizing on either a UHF or VLF approach is the only real technical question.

Both would work. Both have strengths and weaknesses. The data link function for trip recorders would be more effective at the higher data rates available using a UHF. UHF systems also can have much better reader-to-tag distance capability (over 100 feet, in some cases) compared to the 5-10 foot limit of VLF systems. VLF systems can have their antenna loops buried in roadbed more easily, however, and require less sophisticated maintenance equipment.

Certainly, most truckers would probably prefer to drive by a weigh station at freeway speeds to waiting in line and state governments would like to have weigh stations which can function 24 hours a day with no increase in staffing requirements.

AUTOMATIC TOLL COLLECTION

One frustration of modern life is waiting in line for collection of bridge or tollway tolls. No matter how efficiently the toll collection points are designed or how many stations exist, traffic must still come to a complete stop to get through them. RF ID makes this unnecessary.

Many commuters who use tollways on a regular basis purchase weekly or monthly passes. If an RF ID tag was issued to these commuters, a lane (or lanes) could be set aside to allow them to drive at 45-55 MPH through an automatic toll station. The system could also be programmed to provide automatic monthly billing for those who may prefer to pay on a per-trip basis, yet have the convenience of being able to use the faster, automated toll station. Transit system buses, commercial trucks, police vehicles, and utility operators would also benefit from such a system.

GATE AND PLANT ACCESS

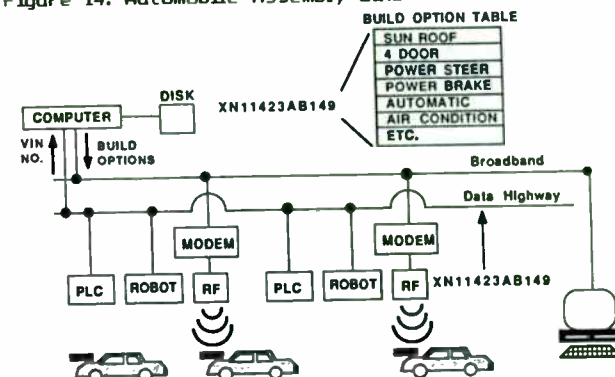
Obviously, anything which can be used for toll collection or weigh-in-motion identification can also be used for gate control. This might be an additional use for the tractor-trailer RF ID system previously described or a system usable for parking lot, plant, or even secured room access. It could be mounted on the vehicle or used for personal ID.

With programmable tags, data and access codes can be changed, as required, for security or billing purposes.

MATERIAL HANDLING WITHIN FACTORIES

Bar code identification is commonly used for material control purposes in factories, but in many cases, they are not practical for one reason or another. Among those reasons are material chemical treatment, painting, high temperature drying in paint ovens, or environments where dirt, dust, grease, oil, or other things would render most bar code labels unusable.

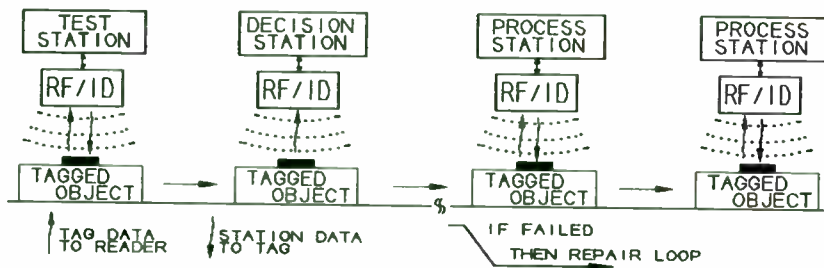
Figure 14. Automobile Assembly Line



A good example is the building of automobiles where all of the above problems exist. One of the major, in-plant uses for RF ID, in fact, is on the auto assembly line. Here, positive ID is required since no one model or even make of auto is produced on a given line but a mixture according to orders received from distributors. The RF tag can hold enough data to allow paint color selection, chassis identification, chassis style, and other data unique to that vehicle. Re-programmable tags are used for this so that they can be used on a couple of hundred vehicles before temperature, paint, and general rough factory handling finally do them in.

A second area where RF ID provides advantages not available from competing technologies is in the area of distributed data within an assembly plant. Several RF tags are available which allow changing a few bits to 8,000 or more bytes of data either all at the same time or in addressable blocks.

Figure 15. Distributed Data Base



Test data can be stored in the tag at each test station for

later retrieval by the main computer or a processing station further along the line. The need for real-time communication is thus eliminated between the station and the main computer which can speed up the line and reduce the impact of main computer or communications failures to the operation of any otherwise self-sufficient loops within the plant.

An example of how such a tag has been used to optimize an already automated line is the use of Read-Write tags to transfer test data down a carburetor assembly line so that appropriate action can be taken. Such actions might include adjustments or custom selection of jet sizes and allows the manufacturer to produce customized carburetors on an automated assembly line.

Both UHF and VLF tags have been used in these applications with UHF tags better able to meet high temperature requirements and VLF better able to meet close spacing and miniature tag uses. Which frequency selection is "best" appears largely to depend on what a given RF tag manufacturer makes or what a given user has chosen to use.

Both have applications not optimum for the other, but both have uses to which they are not well suited. Generally, UHF tags have significantly faster data transfer times for Read-Write applications requiring fast transaction times such as high speed assembly lines. On the other hand, tagging of very small parts can be more readily accomplished using VLF tags since only the distance at which the tag can be read will usually be affected by size reduction. Even machine tools have been tagged using very small VLF transponders.

THE CHALLENGE FOR THE ENGINEER

RF/ID presents the engineer with what he loves most and hates most about his job... multiple challenges. The technology requires mil-spec performance for a product priced more in keeping with consumer electronics. RF/ID tends to be very application specific so that engineers must try to pre-think potential uses in order to be ready to modify existing products in minimal time for minimal cost in order to meet new uses.

Whether at VLF or UHF, these products require interdisciplinary effort involving antennas, coupling coils, receivers, transmitters, power supplies, communications links (both RF and Digital), modulators, demodulators, protocol handling, EMI suppression, and packaging.. all sufficiently well implemented to handle the often severe environment found in industrial settings.

Customers typically expect that the equipment can be installed using a screwdriver and a pair of pliers by a worker who doesn't know what he is installing, probably doesn't care, and has never seen the manual, yet have it perform as if it was "fine tuned" by a master technician. At the same time he usually doesn't even consider RF/ID until other, more familiar technologies been tried but failed to meet the requirements of the application.

The sales force expects it to be "bullet-proof" even though applications and environments often vary widely from customer to customer.

RF/ID is a field both in its infancy yet becoming of age. Some

applications are already becoming commonplace, yet new ones are being discovered as industry pushes towards increased automation and more efficient production and quality controls during the 1990's.

REFERENCES

- (1) G. Schettler, "Developments in Radio Frequency Transponders", paper delivered at Material Handling Focus '88, Material Handling Research Center, Georgia Institute of Technology, Atlanta, GA 30332-0205
- (2) Larry E. Stall, "Parts Tracking in Automated Assembly", p 24, Assembly, August 1990.
- (3) Bernie Knill, editor, "Update on Radio Frequency Identification", p 66, Material Handling Engineering, May 1990.
- (4) Paul Susca, "Airport RF System Reduces Ground Traffic", p22, ID Systems, May 1990
- (5) Bill McIlvaine, "Radio Frequency is Making Some Waves", p32, Managing Automation, December 1988
- (6) J. A Landt, "Multichannel Homodyne Receiver", U.S. Patent #4,360,810; "System For Identifying Particular Objects", U.S. Patent #4,739,328 (Reflective Tags)
- (7) G. Schettler, "Radio Frequency Identification: The Ultimate Distributed Database", p 657, Proceedings IIE Integrated Manufacturing Conference, November 1989, 25 Technology Park, Norcross, GA 30092 (Publication # IIE-P-254)
- (8) Automatic ID News, August 1990 issue:
R. Adams, "RF/ID: Meeting Industry's Needs in Harsh Environments"
M. Gallucci, "RF Tags May be a Dog's (and Cat's) Best Friend"
D. Draxler, "RF/ID: Productivity & Quality on the Assembly Line"
"RF/ID Speeds Fuel Injector Test, Calibration"

Also in this issue: "Buyer's Guide to RF/ID"

IF Frequency-Response Considerations
for the Digital-Radio Environment

Richard D. Roberts and Mark A. Webster
Harris Corporation, GCSD
Melbourne, Florida

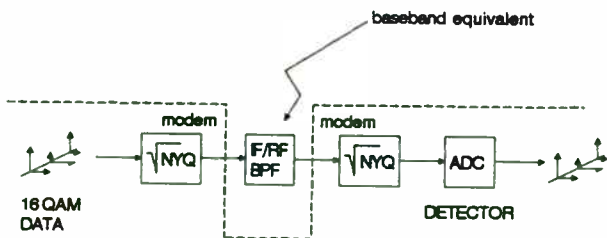
Nazif Tepedelenlioglu
Florida Institute of Technology
Melbourne, Florida

Introduction

The popularity and availability of off-the-shelf digital modems has given the RF engineer an additional challenge in IF/RF filtering. These off-the-shelf modems generate signals that are modulated on low frequency carriers and must be frequency translated before being sent out onto the communications channel. This data communications channel can be modeled as a baseband equivalent filter which is the cascade of all filtering and channel propagation characteristics. For the case of the ideal channel, the baseband equivalent filter consists of only the modem filtering and the IF/RF filtering. The input to this equivalent filter are data impulses which represent the desired message to be sent and the output is an analog impulse response continuum that is quantized by an ADC.

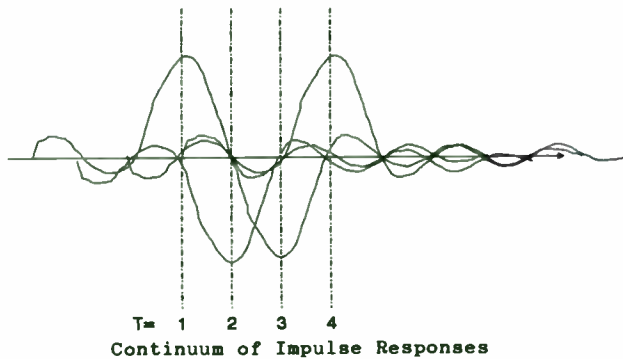
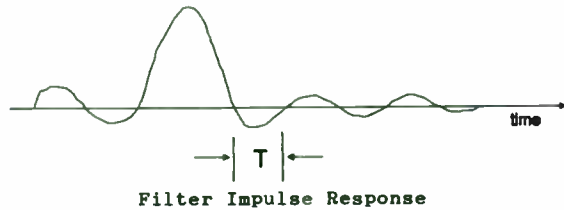
The digital bits are then further processed, including any adaptive equalization. The modem designer strives to form the impulse response of the modem so it has low intersymbol interference and hence a bit error rate near the theoretical curve. He then relies on an adaptive equalizer to compensate for less than ideal channel responses so as to maintain a good bit error rate. It is the job of the RF engineer to RF process the output/input of the modem without disturbing the modem filtering too much, thus allowing the equalizer to compensate for channel impairments instead of bandpass filtering related impairments. This paper provides insight and guidelines to assist an RF engineer to do a good job of RF filtering a digitally modulated signal.

*LP → BP Transform. in
gives asymmetry - origin
zeros.
Can see @ of filter get
better symmetry.*



Nyquist Filtering

Nyquist filtering has the characteristics that the impulse response is controlled so that the zero crossings of the filter "ringing" are separated by T seconds, where T is the baud rate of the data. The super position of a sequence of these impulse responses, generated by some data sequence, is shown below.



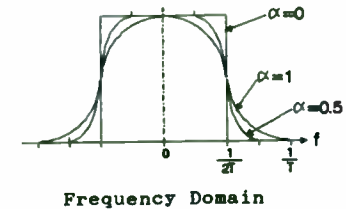
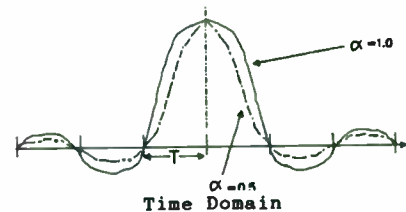
Notice how at each sample time the contribution to the total signal from neighboring symbols is zero. This is the ideal case. In the nonideal case, the contribution from neighboring symbols is not zero and intersymbol interference results. We'll call this

form of intersymbol interference "self-talk". The baseband equivalent impulse response can be real or complex. If it is complex (e.g. a quadriphase signal represented by I/Q vectors), the real part must not "bleed" into the complex part and visa versa. We'll call this part of intersymbol interference "cross-talk". The frequency response of a physical baseband Nyquist filter has an even magnitude and odd phase. A common class of filters are those represented by the "raised cosine", whose time and frequency representations are given below.

$$X(f) = \begin{cases} \frac{T}{2} \left[1 - \sin \left[\frac{\pi T}{\alpha} \left(|2\pi f| - \frac{1}{2T} \right) \right] \right] & 0 \leq |f| \leq (1-\alpha) \frac{1}{2T} \\ 0 & (1-\alpha) \frac{1}{2T} \leq |f| \leq (1+\alpha) \frac{1}{2T} \\ \frac{T}{2} \left[1 + \sin \left[\frac{\pi T}{\alpha} \left(|2\pi f| - \frac{1}{2T} \right) \right] \right] & |f| > (1+\alpha) \frac{1}{2T} \end{cases}$$

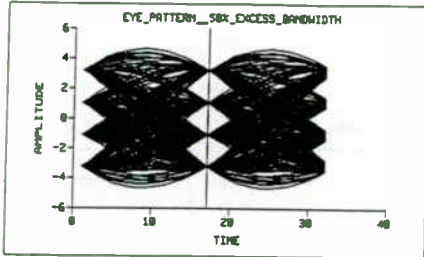
$$x(t) = \left\{ \frac{\sin(\pi t/T)}{(\pi t/T)} \right\} * \left\{ \frac{\cos(\alpha \pi t/T)}{[1 - (2\alpha t/T)^2]} \right\}$$

The term "alpha" is called the excess bandwidth and has a value between 0 and 1. The impulse response and time response for several values of alpha is given below. Observe the odd symmetry of the frequency rolloff about the frequency $1/2T$.

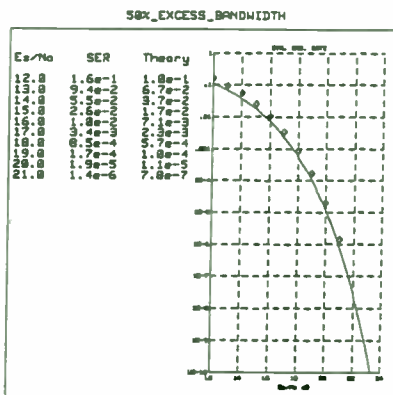


Eye Patterns and SER

If we plot the time varying sum of the impulse responses instead of the super position of these impulse responses, we get the "eye pattern". The eye pattern is sampled in the middle of the eye, and symbol decisions are made on these samples. The eye pattern for 16 QAM with raised cosine filtering of 50% excess bandwidth is presented below.

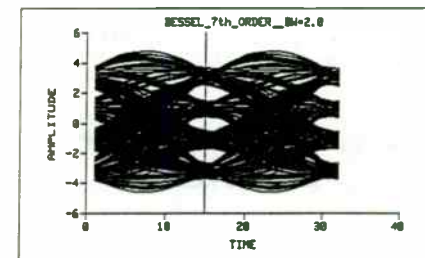
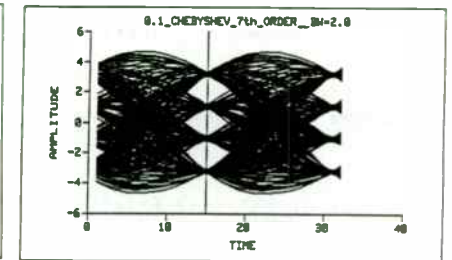
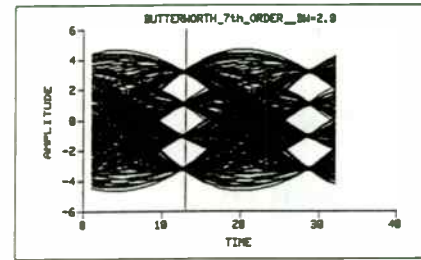


We can plot the symbol error rate (SER) for these decisions versus the signal to noise ratio (in the form of the ratio of the energy per symbol divided by the noise density - e.g. E_s/N_0). Such a plot is shown for the theoretical "ideal" case.

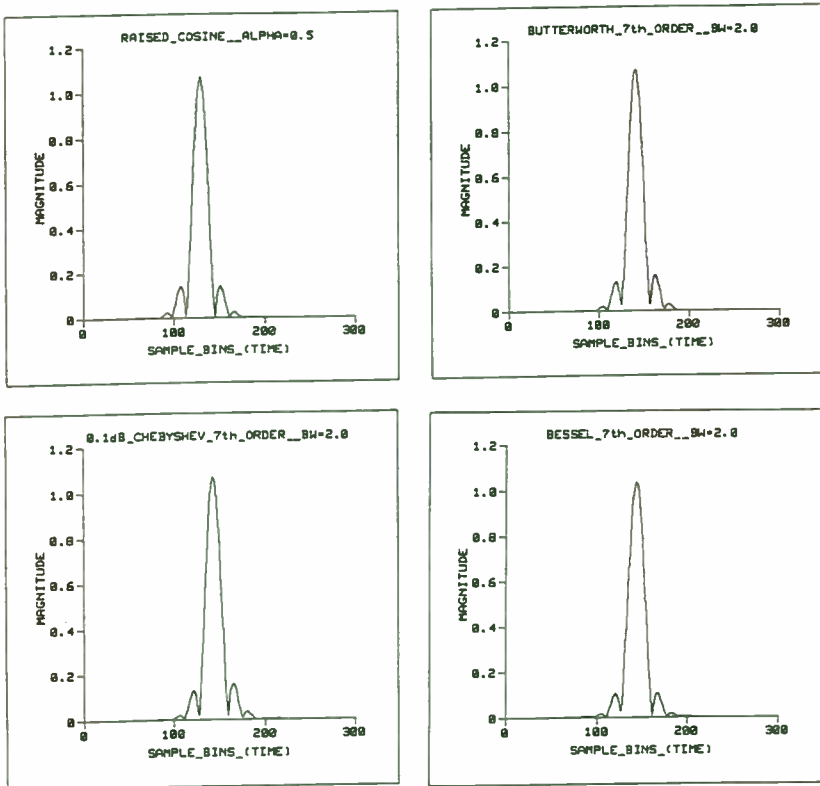


*SER = SIGNAL
ERROR RATE.*

The effect of degradations due to suboptimal bandpass filtering (ignoring the effects of any adaptive equalization) is to cause the actual SER curve to lay above the theoretical curve. The same effects causes the eye pattern to show some "closure". The next figure shows the effect of IF filter on the eye pattern. The data filtering is raised cosine with alpha=0.5 and the IF filtering has a IF center frequency to bandwidth ratio of 10.0 (commonly called Q) with a bandwidth of 2.0. The filter types are 7th order Butterworth, Chebyshev, and Bessel.



The next set of figures illustrates the distortion of the raised cosine impulse (which is shown for comparison, $\alpha=0.5$) after it is convolved with the 7th order Butterworth, Chebyshev and Bessel IF filters respectively. We can see how the nulls in the raised cosine impulse response are "filled-in". (These plots are of the magnitude only).



Bandpass Filter Constraints

A bandpass filter can cause both self-talk and cross-talk; however, we can minimize the effects of both by making the following observations. (We will work with the equivalent baseband filter for the bandpass process, which is basically a non-realizable bandpass filter with a zero Hertz center frequency).

- Observation 1:
If the frequency response of the baseband equivalent filter has an even magnitude and odd phase then the impulse response is real. This filter will not cause cross-talk.
- Observation 2:
If the bandpass filter has little impact on the magnitude of the modem data spectrum then we can expect little self-talk to be generated. If these two observations are satisfied then the IF filtering will be satisfactory.

The first observation can be broken into two parts: generating an IF filter with linear phase, and secondly one with even magnitude. Let's take the second part first. A common way to design bandpass filters is to take a low pass prototype and transform the response to a bandpass filter using the transform $s=p-1/p$. This type of filter does not have an even magnitude response because of zeros introduced at the origin and at infinity by the transformation process, but it can closely approximate an even response for those cases where the IF center frequency to bandwidth ratio (commonly called Q) is large. In order to have an even response, also called arithmetic symmetry, the ratio of the number of zeros at infinity to those at zero must equal three (known as Carassa's ratio). The low pass

Nomographs for Popular Filter Types - 16 QAM Example

prototype transform can not do this in general and other techniques must be applied. An efficient means to design such filters is to specify a topology that yields the correct ratio of zeros and poles then use an optimizing RF analysis program to realize a given response [1]. The other consideration that we stated was necessity for linear phase. Again, the low pass prototype transform does not achieve this but if the IF center frequency to bandwidth ratio is again large, the phase of the filter will closely resemble that of the low pass prototype. For cases where a closer approximation to linear phase is desired, phase compensation techniques can be used [2].

The second observation is more subjective. What we basically want is the classic brickwall filter that just contains all of the modem spectrum. Lacking this type of filter, each of the various low pass filters can be examined to determine where the "flat" part of the response lies for a given shape factor.

The trouble with what we just stated is the lack of analytical results due to the complexity of the problem. A way around this was for us to use a simulation program and generate nomographs for several popular filter types, and chart how the IF bandwidth to center frequency of the IF filter affects the system performance.

The following charts present this data in the form of dBs of degraded performance from theory at a symbol error rate (SER) of 10^{-4} . We used 16 QAM as the waveform because this waveform is complex enough to be interesting yet simple enough to generate. Work has already been presented for BPSK and QPSK [3].

We used a parabolic curve fitting routine to present the data points. The curves strongly show general trends but one should not assume tenths of a dB accuracy. Also, all filter bandwidths are normalized to the single sided spectrum main lobe; for example, a bandpass filter with a bandwidth of 2.0 contains the double sided spectrum main lobe of the unfiltered data.

CHART 1

The first set of tables shows the effects of filter bandwidth on the system performance for three different types of filter responses: Butterworth, Chebyshev, and Bessel. The filter bandwidth was varied from 1.75 (less than the main lobe) to 4.0 (which is twice the main lobe). Filters of order 3, 5 and 7 were investigated. The IF/BW ratio is high enough that the narrowband approximation holds. The results are reported with respect to the

performance at a bandwidth of 4.0. It can be seen from the graphs that the 7th order filter produced the worst degradation, and the Bessel response was the worst. Also, the value of alpha makes a significant difference with a value of 1.0 being the worst.

CHART 2

The second set of tables shows what happens to the system performance as the IF/BW ratio was varied from 1.0 to 10.0 for a given filter bandwidth. The results are reported with respect to the performance for a IF/BW ratio of 10.0. The bandwidths tested where 2.0, 3.0 and 4.0. The alpha factor for the 16 QAM data was fixed at 0.5. The filters with a bandwidth of 2.0 suffered the most degradation as the IF/BW approached 1.0, and the Bessel filter performed the worst overall.

CHART 3

The third table has a graph that shows the system performance when the phase of the IF filter is forced to be linear. The tested filters where 5th order Butterworth, Chebyshev and Bessel. The data filter was raised cosine with alpha set to 0.5, the IF/BW ratio set at 10.0 and the filter bandwidth varied from 1.75 to 4.0. Comparing this graph to the previous performance we can see a dramatic improvement in system performance for the Bessel filter with less difference in the performance for the other two filter types.

The other two graphs on this page show the impact of gain slope and parabolic (nonlinear) phase on the system performance. The data filter is again raised cosine, alpha=0.5.

Conclusions

We have shown that the IF filtering can have a major impact on the digital radio link performance. In general, in order to avoid degraded performance, we would want to keep the IF/BW ratio as large as feasible and make the bandwidth of the filter at least twice as wide as the main lobe of the unfiltered data spectrum. Also, it appears a Bessel response is not a good choice.

Bibliography

- [1] Rhea, Randall W., "Symmetrical Bandpass Filters" Proceedings RF Expo East 89, October 1989
- [2] Williams, Arthur B., "Electronic Filter Design Handbook" McGraw-Hill, 1981
- [3] Jones, J.J. "Filter Distortion and Intersymbol Interference Effects on PSK Signals" IEEE Trans. Comm., April 1971

Keep order of filter as low as possible, $Q > 6$ rel. BW > 4

*Best filter is — Butterworth possibly —
Given a tighter filter requirement, Bessel may not be the best choice.*

CHART 2 (SER=10⁻⁴)
System Performance vs. IF/BW Ratio ($\alpha=0.5$)

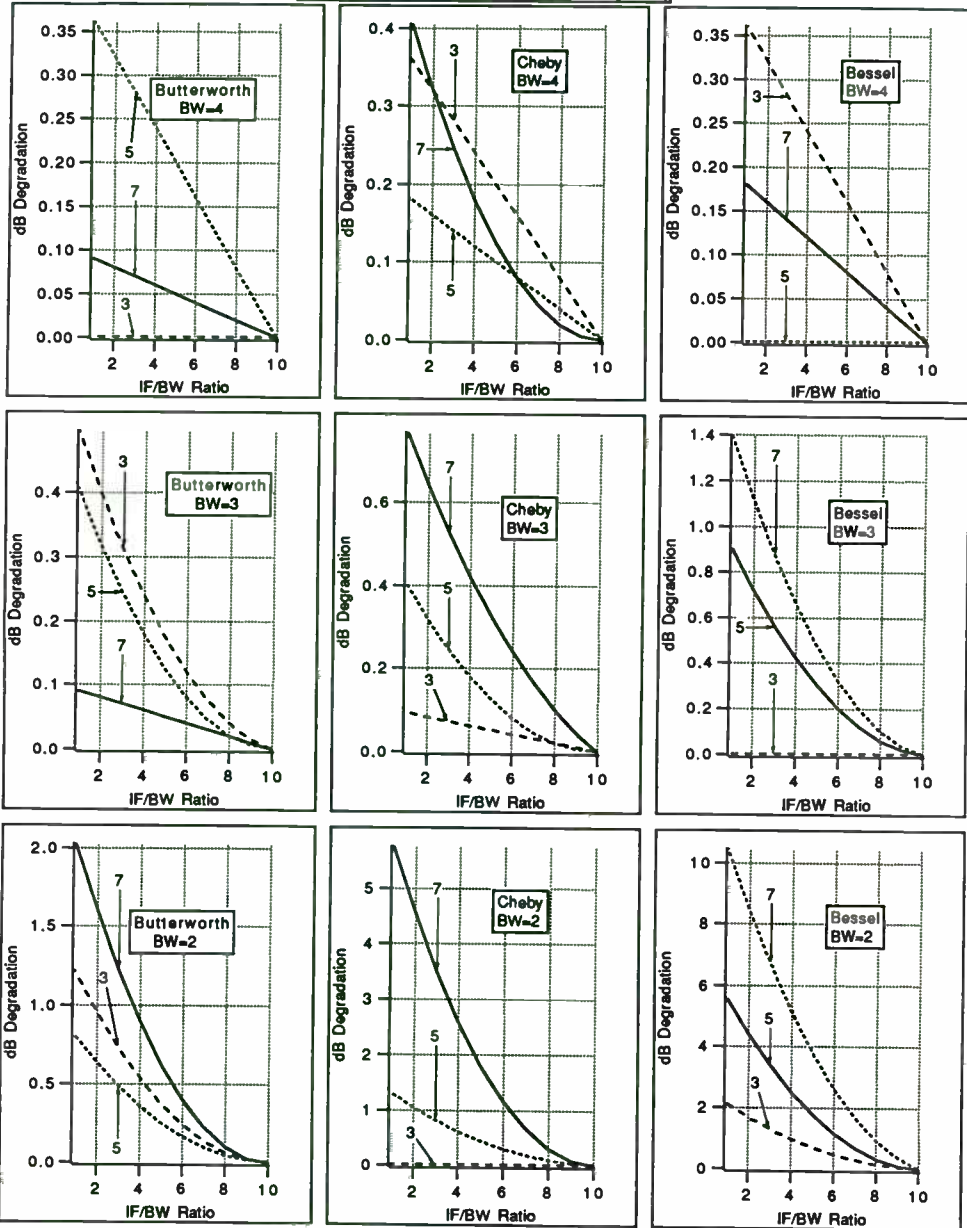
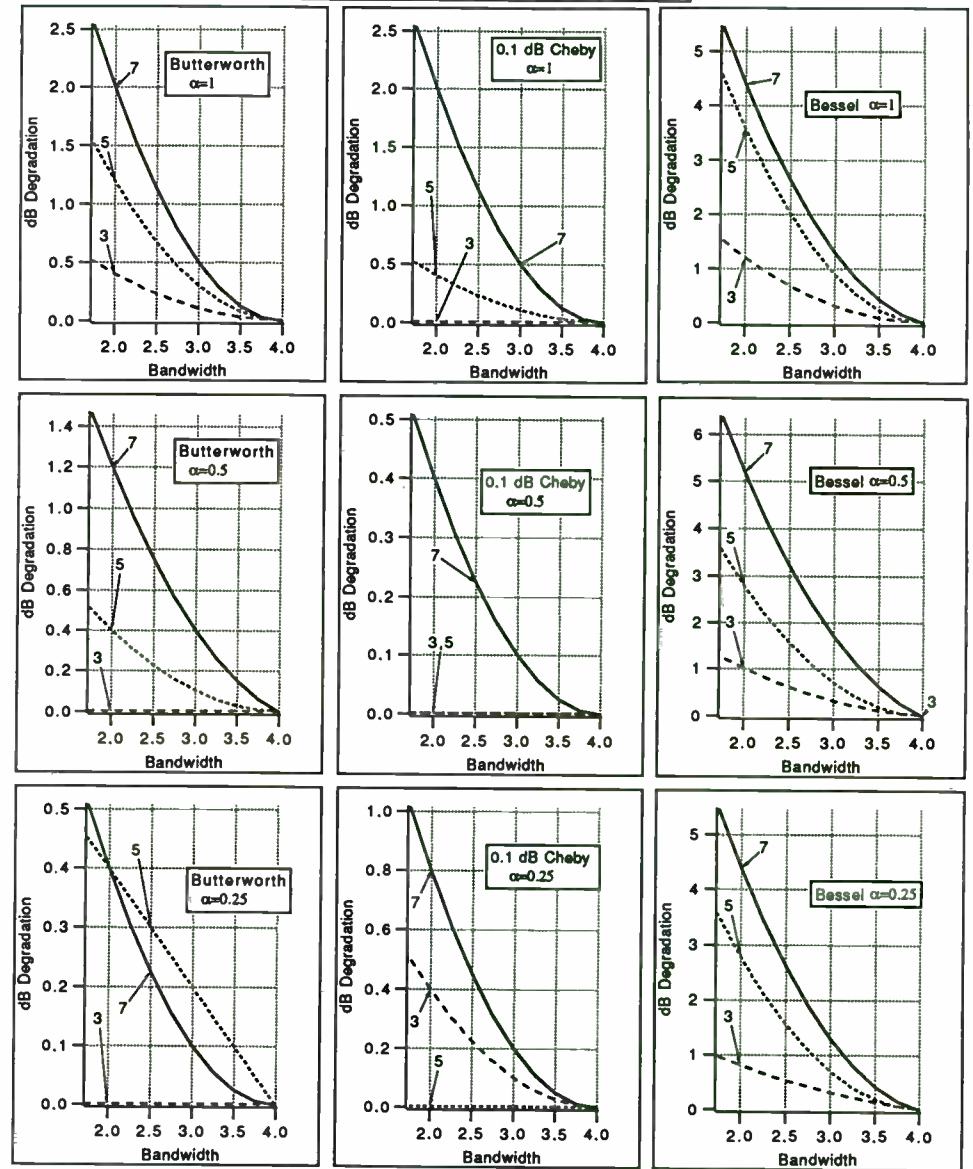


CHART 1 (IF/BW=10)
System Performance vs. Filter Bandwidth (SER=10⁻⁴)

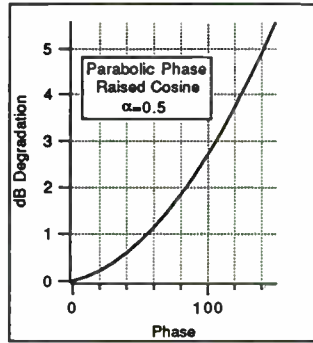
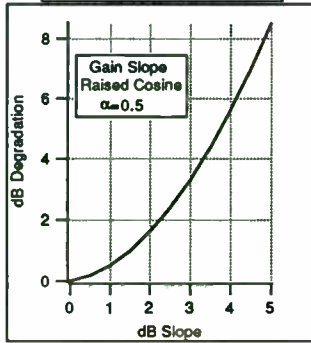
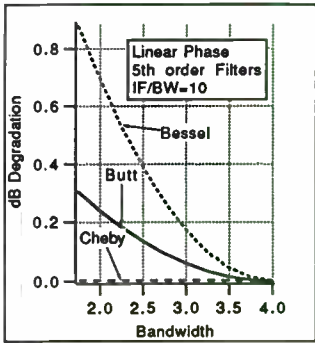


*BW normalization
to
BW/DATA
RATE*

*B.W. - no
actual filter
BW*

*Lower Q
causes
degradation
in SER*

CHART 3
Miscellaneous (SER=10⁻⁴)



DSP Demodulation

by

Steve F. Russell, Ph.D.
Department of Electrical Engineering
Iowa State University
Ames, Iowa 50010

ABSTRACT

With high-speed digital signal processing (DSP) and signal digitization hardware becoming available at a reasonable cost, it is now practical to propose DSP demodulation for future designs. This paper presents the necessary theory and governing equations for practical DSP demodulators that can be implemented for a wide variety of applications. The Generalized Costas Demodulator (GCD) will be emphasized because it is capable of recovering the demodulation functions of an arbitrary bandlimited signal.

1. INTRODUCTION

The use of digital signal processing for modem designs has been very popular the past few years. The effective application of DSP to these designs requires a good understanding of the governing equations associated with modulation/demodulation and the signal digitization process. In particular, a good understanding of quadrature detectors, aliasing, decimation, and the process of carrier recovery is required. This paper has been written to contribute to this understanding by presenting the necessary governing equations.

A good DSP design depends on a good signal digitization technique. The designer must be concerned with the linearity, dynamic range, and noise performance of the digitizer. It is especially difficult to achieve the dynamic range needed for most receiver designs because of 1) digitizer range limitations and 2) quantization noise produced during digitization. Usually, automatic gain control (AGC) or hard limiters are used to reduce the dynamic range requirements for the digitizer. Recently [1] [2] sigma-delta modulation has been

proposed for use in signal digitizers as a method of achieving high dynamic range and good linearity.

The governing equations for modulation/demodulation will now be presented. It will be assumed that adequate signal digitization has been achieved. An illustrative modulation/demodulation example is included in the appendix.

2. CONCEPTUAL SIGNAL MODEL - TRANSMITTER

To adequately describe DSP demodulation, it is first necessary to develop precise conceptual models for the transmitted and received signals. The fundamental model underpinning all analysis is that of a noiseless narrowband signal that can be analytically represented in:

1. amplitude/phase form,

$$s(t) = r(t)A_c \cos[2\pi f_c t + \phi_c + \phi(t)] \quad (1)$$

2. or quadrature form [3],

$$s(t) = a(t)A_c \cos[2\pi f_c t + \phi_c] - b(t)A_c \sin[2\pi f_c t + \phi_c] \quad (2)$$

3. or upper/lower sideband form [4]:

$$s(t) = [u(t) + l(t) + k_c]A_c \cos[2\pi f_c t + \phi_c] - [\bar{u}(t) - \bar{l}(t)]A_c \sin[2\pi f_c t + \phi_c] \quad (3)$$

The signal carrier is modeled as a cosine with amplitude A_c , frequency f_c , and constant phase, ϕ_c . The constant phase will be used to model the effect of an arbitrary reference time at the receiver. The effect of modulation on the carrier is modeled using the envelope and phase functions, $r(t)$ and $\phi(t)$, the quadrature functions, $a(t)$ and $b(t)$, or the upper and lower sideband functions, $u(t)$ and $l(t)$. These modulation functions all represent some coded form of an analog or digital information source. For this narrowband model, the modulation of the carrier must be restricted such that the spectrum of $s(t)$ is zero outside the frequency range f_1 to f_2 where $(f_2 - f_1) \ll f_c$ and all the transmitted spectrum is passed by the preselector and IF filters in the receiver. An unmodulated carrier will be represented by the constants $r(t) = 1$ and $\phi(t) = 0$.

Using trigonometric identities [5], the modulation functions can be related as follows:

$$a(t) = r(t) \cos[\phi(t)] \quad b(t) = r(t) \sin[\phi(t)] \quad (4)$$

$$r(t) = \sqrt{a^2(t) + b^2(t)} \quad \phi(t) = \arctan \left[\frac{b(t)}{a(t)} \right] \quad (5)$$

$$a(t) = u(t) + l(t) + k_c \quad b(t) = \tilde{u}(t) - \tilde{l}(t) \quad (6)$$

$$u(t) = \frac{1}{2}[a(t) - \tilde{b}(t)] \quad l(t) = \frac{1}{2}[a(t) + \tilde{b}(t)] \quad (7)$$

The modulation functions may assume any real value except for the envelope function, $r(t)$, which must always be non-negative.

The amplitude spectrum of $s(t)$, if it exists, can be obtained by applying the Fourier transform to the quadrature form of the signal. Because $s(t)$ is a narrowband signal, the spectrum is nonzero only near the frequencies $\pm f_c$. Furthermore, a sinusoidal carrier frequency component is present only if $A(f \pm f_c)$ or $B(f \pm f_c)$ contains a Dirac delta function [3]. The tilde ($\tilde{}$) denotes the Hilbert transform needed to generate SSB signals. The constant, k_c , represents the magnitude of any carrier that is transmitted with the two sidebands.

3. CONCEPTUAL SIGNAL MODEL - RECEIVER

The simplified signal model at the receiver will include the effects of additive channel noise and carrier phase shift due to propagation delay. Doppler, dispersion, slow carrier amplitude variations, and multipath effects will not be modeled in this paper. The constant phase, ϕ_c , represents the carrier phase shift observed at the receiver due to propagation delay and an arbitrary, but known, local reference time.

Additive channel noise, $n(t)$, can be thought of as an additional source of modulation that is random and unwanted. The composite signal, $s_c(t)$, in a narrowband IF filter is the sum of the noiseless signal and narrowband noise:

$$s_c(t) = r(t) A_c \cos[2\pi f_c t + \phi_c + \phi(t)] + n(t) \quad (8)$$

Since the channel noise is narrowband, it can be represented in quadrature form [6] as:

$$n(t) = n_c(t) \cos[2\pi f_c t + \phi_c] - n_s(t) \sin[2\pi f_c t + \phi_c] \quad (9)$$

The quadrature noise components, $n_c(t)$ and $n_s(t)$, are baseband, zero-mean, uncorrelated, Gaussian noise signals with a spectral shape that is the same as the IF filter.

The quadrature form of the composite IF signal is easily computed as the sum of the quadrature forms of the modulated carrier and the narrowband noise,

$$s_c(t) = \hat{a}(t) A_c \cos[2\pi f_c t + \phi_c] - \hat{b}(t) A_c \sin[2\pi f_c t + \phi_c] \quad (10)$$

where:

$$\hat{a}(t) = a(t) + n_c(t)/A_c = \hat{r}(t) \cos[\hat{\phi}(t)] \quad (11)$$

$$\hat{b}(t) = b(t) + n_s(t)/A_c = \hat{r}(t) \sin[\hat{\phi}(t)] \quad (12)$$

and the "hat" indicates that the function has been corrupted by noise. The relationships among all the noise-corrupted modulation functions are the same as noiseless ones given in (4) through (7).

It is important to note that the channel noise terms are always scaled by the amplitude of the carrier signal, i.e. the representation chosen for this model accounts for the signal-to-noise ratio in a "natural" way. The computation of the sideband signals requires the implementation of a Hilbert transform in the receiver.

4. THE DEMODULATION PROCESS

Demodulation is the process of recovering the noise-corrupted modulation functions from the received signal. It can also be thought of as carrier removal or "carrier stripping". To properly demodulate a signal, the carrier parameters (amplitude, frequency, and phase constant) must be known or estimated by the receiver. In other words, $\{\hat{a}(t), \hat{b}(t)\}$, $\{\hat{l}(t), \hat{u}(t)\}$, or $\{\hat{r}(t), \hat{\phi}(t)\}$ cannot, in general, be extracted from the carrier without a knowledge of the carrier parameters. The carrier amplitude governs the linearity and dynamic range requirements of the receiver as well as the design of the signal digitizer. Carrier frequency changes (not those due to frequency modulation) and/or frequency channelization require that the receiver be precisely tuned. Coherent modulation/demodulation schemes also

require precise estimation (tracking) of both carrier frequency and carrier phase.

The noise-corrupted modulation functions will be called **demodulation functions** and A_c, f_c and ϕ_c will be called **carrier parameters**. To be effective, a receiver must produce good estimates of the carrier parameters and then successfully extract the demodulation functions. However, the original modulation functions can never be exactly recovered because they have been irretrievably corrupted by noise.

The most general approach to demodulation is to implement "I-Q" or quadrature detection and then remove the carrier by obtaining good estimates of the carrier parameters. Figure 1 shows a basic quadrature detector. To begin, the received signal is multiplied by the local-carrier quadrature functions as shown in the following equations:

$$x_1(t) = s_c(t)2A_0 \cos[\theta_0(t)] \quad (13)$$

$$y_1(t) = s_c(t)2A_0 \sin[\theta_0(t)] \quad (14)$$

where:

$$\theta_0(t) = 2\pi f_0 t + \phi_0 - \eta(t) \quad (15)$$

$$\frac{d}{dt}\theta_0(t) = 2\pi f_0 - \frac{d}{dt}\eta(t) \quad (16)$$

The parameters A_0, f_0, ϕ_0 , and $\theta_0(t)$ for the local carrier, represent estimates of A_c, f_c, ϕ_c , and $\theta_c(t)$, respectively. The additive noise term, $\eta(t)$, is the error in the receiver's estimation of the carrier phase function.

When the trigonometric products representing the mixer outputs are expanded using trig identities, the equations representing the mixer outputs can be expressed as:

$$x_1(t) = \hat{r}(t)K_0 \cos[\theta_c(t) + \theta_0(t) + \hat{\phi}(t)] + \hat{r}(t)K_0 \cos[\theta_c(t) - \theta_0(t) + \hat{\phi}(t)] \quad (17)$$

and,

$$y_1(t) = \hat{r}(t)K_0 \sin[\theta_c(t) + \theta_0(t) + \hat{\phi}(t)] - \hat{r}(t)K_0 \sin[\theta_c(t) - \theta_0(t) + \hat{\phi}(t)] \quad (18)$$

Lowpass zonal filtering [7] (an "ideal" lowpass filter) can be applied to the multiplier outputs to reject the "sum" terms and pass the "difference" terms so that the filter outputs

are,

$$x_2(t) = \hat{r}(t)K_0 \cos[\theta_c(t) - \theta_0(t) + \hat{\phi}(t)] = \hat{r}(t)K_0 \cos[\psi(t)] \quad (19)$$

$$y_2(t) = -\hat{r}(t)K_0 \sin[\theta_c(t) - \theta_0(t) + \hat{\phi}(t)] = -\hat{r}(t)K_0 \sin[\psi(t)] \quad (20)$$

where the substitution, $\psi(t) = \theta_c(t) - \theta_0(t) + \hat{\phi}(t)$, will be used to simplify the notation.

This widely-known result is valid only if the received signal is narrowband and the zonal filter passes an undistorted version of the entire spectrum of the difference term. In practical designs, the zonal filter is implemented using a lowpass filter having a stopband attenuation that adequately suppresses the sum-frequency output while still passing the entire frequency spectrum of the difference-frequency output. If the lowpass filter distorts the difference-frequency spectrum, this result assuming zonal filtering is not valid. The technical literature frequently uses the symbols I and Q to represent these quadrature outputs. The quadrature outputs of the lowpass zonal filters contain all of the recoverable information about the transmitted signal as well as the undesired noise caused by both the channel and the imperfect estimation of the local-carrier phase function.

The quadrature detector outputs can be processed using summing, scaling, squaring, square root, inverse tangent, and Hilbert transform operations to estimate all of the modulation functions as follows:

$$r(t) \approx \hat{r}(t) = \frac{1}{K_0} \sqrt{x_2^2(t) + y_2^2(t)} \quad (21)$$

$$\phi(t) \approx \hat{\phi}(t) = \psi(t) = \arctan \left[\frac{-y_2(t)}{x_2(t)} \right] \quad (22)$$

$$a(t) \approx \hat{a}(t) \approx \frac{1}{K_0} x_2(t) \quad (23)$$

$$b(t) \approx \hat{b}(t) \approx \frac{-1}{K_0} y_2(t) \quad (24)$$

$$l(t) \approx \hat{l}(t) \approx \frac{1}{2} [x_2(t) - \bar{y}_2(t)] \quad (25)$$

$$u(t) \approx \hat{u}(t) \approx \frac{1}{2} [x_2(t) + \hat{y}_2(t)] \quad (26)$$

The estimates for the phase function, quadrature functions, and the upper and lower sideband signals are valid only if the receiver is "tracking" the carrier, i.e. only if $\theta_o(t) + \eta(t) = \theta_c(t)$. The double approximations are used to indicate the separate influences of channel noise and local oscillator noise in estimating all the outputs that are dependent on phase.

For specific types of modulation, there can be ways to recover the demodulation functions that avoid the need for a quadrature detector. For example, a square-law-based envelope detector, represented by the following equation, can be used to recover the envelope function without the use of a quadrature detector:

$$x_4(t) = \sqrt{h_L(t) * [s_c^2(t)]} = \frac{1}{2} A_c \hat{r}(t) \quad (27)$$

For phase modulation, a simple phase-locked loop can be used. These two methods are represented by the block diagram of Figure 2. In this figure, x_3 is the output of bandpass limiter which removes the envelope modulation and preserves the phase modulation. The PLL phase output is x_6 which is an estimate of the phase modulation function. The lower branch of the figure represents the processing needed for envelope demodulation.

In summary, a generalized demodulator must: 1) have a prior knowledge of, or estimate, the carrier parameters, 2) generate the estimated carrier for use in an I/Q detector (or a correlator), and 3) recover the demodulation functions.

5. GENERALIZED COSTAS DEMODULATOR

The Generalized Costas Demodulator (GCD) of Figure 3 represents a general method of signal demodulation. Its essential elements are, 1) a quadrature detector, 2) carrier estimation, and 3) a Hilbert transform. The signal processing blocks to the right of the quadrature detector implement Equations 21 through 26.

This general-purpose demodulator block diagram represents all of the governing

equations necessary to demodulate any type of signal. It can be implemented using DSP if proper bandpass signal digitization is used. The next section will discuss various issues for this digital implementation.

6. DISCRETE-TIME DEMODULATION

Discrete-Time (or DSP) demodulation refers the concept of implementing the demodulation process in digital signal processing hardware and software [8] [9] [10] [11] [12]. A successful DSP demodulator design requires the proper use of 1) sampler prefiltering, 2) sampling design (including aliased sampling), 3) digital lowpass filtering, and 4) decimation. In addition, adequate algorithms must be available for the following operations: 1) multiplication, 2) squaring, 3) square root, and 4) arctangent. Care must be taken to insure that the noise caused by number truncation in the algorithms does not degrade the signal-to-noise ratio in the demodulator.

The signal can be sampled 1) after the bandpass filter, 2) after the mixers, or 3) after the lowpass filters. A knowledge of the signal spectrum at each point in the block diagram is necessary if the design is to avoid signal aliasing. Also, this knowledge will help the designer to implement decimation where it will be the most effective.

Sampling after the Bandpass Filter. Baseband or aliased passband sampling [10] can be used after the bandpass filter as long as the sampling frequency, f_s , is chosen such that the spectrum of the "sum" frequency term can be adequately filtered while still passing the "difference" frequency term. This requirement is imposed because of the multiplication that is performed in the sine and cosine mixers. When using the governing equations, the carrier frequency, f_c , must be interpreted as the carrier frequency after aliased sampling. In actual designs, some spectral folding is acceptable as long as the lowpass filter can still effectively remove all of the spectrum associated with the "sum" frequency, i.e., it performs like a zonal filter. Decimation can be applied to the outputs of the lowpass filters to reduce the processing requirements for subsequent DSP operations. Care must be taken not to decimate to the point where subsequent operations might produce undesirable spectral folding.

Sampling after the Mixers. Baseband sampling can be used after the mixers as long as the folding frequency, $f_s/2$, is high enough to prevent the folding of the "sum" frequency terms into the equivalent passband of the lowpass filters. Some decimation can be applied to the outputs of the lowpass filters but the number rate should still be at least four times the cutoff frequency.

Sampling after the Lowpass Filters. If the carrier frequency is too high for adequate-quality aliased sampling, it is still possible to sample after the lowpass filters and then use DSP algorithms for the remaining demodulation processing. Because nonlinear operations such as squaring are used, the sampling rate (number rate) at the filter output must be much higher than the Nyquist rate. For example, Fourier analysis shows that the spectrum of x_2 or y_2 will be doubled after squaring so the number rate must be at least four times the cutoff frequency of the lowpass filter. Designers should carefully analyze the output spectrum for each specific design and choose the number rate accordingly.

To summarize, the signal spectrum at the sampling point and all subsequent numerical operations should be carefully studied before selecting the sampling rate and the amount of decimation to be applied. Many designs can be effective with aliased sampling of the bandpass filter output and a number rate at the quadrature outputs of at least four times the lowpass filter cutoff frequency.

7. CARRIER ESTIMATION

The generation of a local replica for the carrier is required for proper operation of the Generalized Costas Demodulator or any synchronous demodulator. In order to generate a local replica, the receiver must be capable of estimating the carrier parameters A_c , f_c , and ϕ_c by using one or more of the signals represented by equations 10, 19, or 20. The required accuracy of the estimation for each parameter will depend upon the modulation type and the available signal-to-noise ratio.

Carrier estimation is accomplished in a variety of ways using a combination of filtering, phase tracking, and nonlinear operations such as squaring or bandpass limiting. The

governing equations are summarized below.

Narrowband filtering. If a pilot carrier or other carrier frequency component is present and the modulation sidebands are sufficiently separated from the carrier, narrowband filtering can be used:

$$s_c(t) * h_n(t) \approx A_c \cos[2\pi f_c t + \phi_c] \quad (28)$$

In this case, the carrier phase constant also models the delay in the filter.

Bandpass limiter. When only envelope modulation is present, a bandpass limiter (hard limiter followed by a narrowband filter) can be used:

$$\text{sgn}\{s_c(t)\} * h_n(t) = \frac{4a}{\pi} \cos[2\pi f_c t + \phi_c] \quad (29)$$

The signum function, $\text{sgn}\{\}$, [3] represents the action of the hard limiter. The symmetrical limiter clipping levels are $\pm a$.

Phase-locked Loop. For some types of modulation, phase-locked loop can be used to regenerate the carrier. For best performance, a PLL is often used in conjunction with hard limiters and/or filters. The PLL local oscillator produces a waveform with a fundamental frequency component of:

$$s_0(t) = A_0 \sin[2\pi f_0 t + \phi_0 - \eta(t)] \quad (30)$$

where $f_0 = f_c$ and $\phi_0 = \phi_c$ when the loop is properly tracking.

Costas Loop. The Costas loop is similar to the PLL in that it controls a local oscillator that tracks the carrier frequency and phase. The error signal for the loop is obtained by averaging the product of the quadrature outputs as represented below.

$$\begin{aligned} \langle x_2(t)y_2(t) \rangle &= -I^2(t)K_0^2 \cos[\psi(t)] \sin[\psi(t)] \\ &= \frac{-K_0^2}{2} \langle I^2(t) \sin[2\psi(t)] \rangle \\ &\approx -K_2 \langle 2\psi(t) \rangle \approx 0 \end{aligned} \quad (31)$$

The control loop works to keep the average value of $\psi(t)$ at zero.

Squaring Loop. The squaring loop [13] is used for binary phase-shift keyed (BPSK) signals and works by filtering or phase locking to the second harmonic of the squared narrowband signal represented below. Notice that by doubling the phase function, the phase modulation has been removed.

$$s_c^2(t) = \frac{f^2(t) A_c^2}{2} [1 + \cos[2\theta_c(t) + 2\hat{\phi}(t)]] \quad (32)$$

The carrier is regenerated using a divide-by-two on the PLL oscillator output.

Multiplier, m-th order. The squaring loop idea can be applied to m-ary phase modulation by obtaining the m-th harmonic of the narrowband signal as represented by the equation:

$$s_c^m(t) = f^m(t) \cos^m[\theta_c(t) + \hat{\phi}(t)] \\ = f^m(t) [\dots + k_m \cos[m\theta_c(t) + m\hat{\phi}(t)] + \dots] \quad (33)$$

Derivative. An estimate of the carrier frequency can be obtained by applying the derivative to the output of the bandpass limiter [14]. This result is:

$$\frac{d}{dt}[\text{sgn}\{s_c(t)\} * h_n(t)] = -\frac{4a}{\pi} \sin[2\pi f_c t + \phi_c + \hat{\phi}(t)] \left[2\pi f_c + \frac{d}{dt} \hat{\phi}(t) \right] \\ = -\left[8af_c + \frac{4a}{\pi} \frac{d}{dt} \hat{\phi}(t) \right] \sin[2\pi f_c t + \phi_c + \hat{\phi}(t)] \quad (34)$$

The average value of the envelope function of the result is used for the estimate:

$$f_c \approx -\frac{1}{8a} \left\langle -\left[8af_c + \frac{4a}{\pi} \frac{d}{dt} \hat{\phi}(t) \right] \right\rangle \quad (35)$$

For this approach to be valid, the average value of the derivative of the phase modulation function must be zero.

For some types of modulation it is not possible to obtain an estimate of the carrier parameters directly from the signal. Single-sideband modulation is an example of this. For these cases, the receiver must have an accurate prior knowledge of the carrier frequency.

8. CONCLUSIONS

The successful development of hardware and software designs for DSP demodulation requires a good understanding of the governing equations for demodulation and the aliasing problems associated with discrete-time nonlinear operations. Using the governing equations, it is possible to develop one design, the Generalized Costas Demodulator, that will work for any type of modulation. For new designs, aliased sampling at the output of the bandpass prefilter should be considered first. A number rate at least twice the Nyquist rate should be used at the output of the lowpass filters in the quadrature detector.

9. APPENDIX

An example will now be given to illustrate how the modulation functions are selected for a well-known modulation type, Minimum-Shift Keying (MSK). In MSK, one of four possible waveforms are sent using a phase-coherent frequency-shift keying technique. The four possible waveforms are generated by selecting one of two possible frequencies and one of two possible phases. The selections are restricted such that either the slope (MSK-1) or the magnitude (MSK-2) of the transmitted signal is zero at the time the next waveform is selected.

To insure these smooth transitions, the carrier frequencies are restricted to the values,

$$f_c = \frac{n+1}{2T_b} \quad (36)$$

where n is an integer (usually large) and T_b is the interval between data bits. The two frequencies transmitted by MSK are related to T_b and the carrier frequency as follows:

$$f_1 = \frac{n}{2T_b} = f_c - \frac{1}{4T_b} \quad (37)$$

$$f_2 = \frac{n+1}{2T_b} = f_c + \frac{1}{4T_b} \quad (38)$$

For MSK-1, the modulation functions defined for the time interval $kT_b \leq t \leq (k+1)T_b$ are

$$a_k(t) = I_k \cos \left[\frac{\pi t}{2T_b} \right] \quad (39)$$

$$b_k(t) = -Q_k \sin \left[\frac{\pi t}{2T_b} \right] \quad (40)$$

$$r_k(t) = 1 \quad (41)$$

$$\phi_k(t) = - \left[\frac{\pi t}{2T_b} \right] I_k Q_k + \frac{\pi}{2} [1 - Q_k] \quad (42)$$

where the data values, d_k , are used to create two, staggered, $\frac{1}{2}$ -rate sequences as follows:

1) for k even and $0 \leq k \leq N$

$$I_k = I_{k+1} = d_k \quad (43)$$

$$Q_k = d_{k-1}$$

2) for k odd and $1 \leq k \leq N$

$$Q_k = Q_{k+1} = d_k \quad (44)$$

$$I_k = d_{k-1}$$

Since the sequences are staggered, only one of the sequences can change its value at each data epoch, kT_b . The phase functions for odd and even k are,

$$\phi_k(t) = - \left[\frac{\pi t}{2T_b} \right] d_k d_{k-1} + \frac{\pi}{2} [1 - d_{k-1}] \quad \text{for } k \text{ even} \quad (45)$$

$$\phi_k(t) = - \left[\frac{\pi t}{2T_b} \right] d_k d_{k-1} + \frac{\pi}{2} [1 - d_k] \quad \text{for } k \text{ odd} \quad (46)$$

and the waveform for the k -th time interval is:

$$\begin{aligned} s_k(t) &= I_k \cos \left[\frac{\pi t}{2T_b} \right] A_c \cos [2\pi f_c t + \phi_c] \\ &\quad + Q_k \sin \left[\frac{\pi t}{2T_b} \right] A_c \sin [2\pi f_c t + \phi_c] \\ &= I_k A_c \cos \left[2\pi f_c t - \frac{\pi t}{2T_b} I_k Q_k + \phi_c \right] \\ &= A_c \cos \left[2\pi f_c t - \frac{\pi t}{2T_b} I_k Q_k + \frac{\pi}{2} [1 - I_k] + \phi_c \right] \end{aligned} \quad (47)$$

For the demodulation of MSK-1, the phase differences are used to estimate $I_k Q_k$.

$$\Delta \phi_k = \phi_k((k+1)T_b) - \phi_{k-1}(kT_b) = - \frac{\pi}{2} I_k Q_k \quad (48)$$

$$I_k Q_k = - \frac{2}{\pi} \Delta \phi_k \quad (49)$$

$$d_k = I_k Q_k d_{k-1} = - \frac{2}{\pi} \Delta \phi_k d_{k-1} \quad (50)$$

10. ACKNOWLEDGEMENTS

I want to thank Texas Instruments and Iowa State University for their support of this work and to acknowledge the helpful reviews by my graduate students J. Eric Dunn, Michael Komodromos, and Don Yochem.

11. REFERENCES

- [1] Wu Chou, Pin Wah Wong, and Robert M. Gray, Multistage Sigma-Delta Modulation, IEEE Transactions of Information Theory, Vol. 35, No. 4, July, 1989.

- [2] Steven R. Norsworthy, Irving G. Post, and H. Scott Fetterman, A 14-bit 80-Khz Sigma-Delta A/D Converter: Modeling, Design, and Performance Evaluation, IEEE Journal of Solid-State Circuits, Vol. 24, No. 2, April, 1989.
- [3] Leon W. Couch II, Digital and Analog Communication Systems, Second Edition, New York: Macmillan, 1987.
- [4] Donald M. Yochem, Theoretical operation of an independent sideband receiver and sideband correlator, MS Thesis, Iowa State University, 1990.
- [5] Herbert B. Dwight, Tables of Integrals and Other Mathematical Data, New York: MacMillan, 1961.
- [6] Anthony D. Whalen, Detection of Signals in Noise, San Diego, CA: Academic Press, 1971.
- [7] Wilbur B. Davenport, Jr. and William L. Root, An Introduction to the Theory of Random Signals and Noise, New York: McGraw-Hill, 1958.
- [8] Alan V. Oppenheim and Ronald W. Schafer, Discrete-Time Signal Processing, Englewood Cliffs, NJ: Prentice-Hall, 1989.
- [9] Ronald E. Crochiere and Lawrence R. Rabiner, Multirate Digital Signal Processing, Englewood Cliffs, NJ: Prentice-Hall, 1983.
- [10] Douglas F. Elliott, Editor, Handbook of Digital Signal Processing Engineering Applications, New York: Academic Press, Harcourt Brace Jovanovich, 1987.
- [11] Douglas F. Elliott and K. Ramamohan Rao, Fast Transforms: Algorithms, Analysis, Applications, New York: Academic Press, Harcourt Brace Jovanovich, 1982.
- [12] Murat Kunt, Digital Signal Processing, Norwood, MA: Artech House, 1986.
- [13] James J. Spilker, Jr., Digital Communications by Satellite, Englewood Cliffs, New Jersey: Prentice-Hall, 1977.
- [14] A. Bruce Carlson, Communication Systems, Third Edition, New York: McGraw-Hill, 1986.

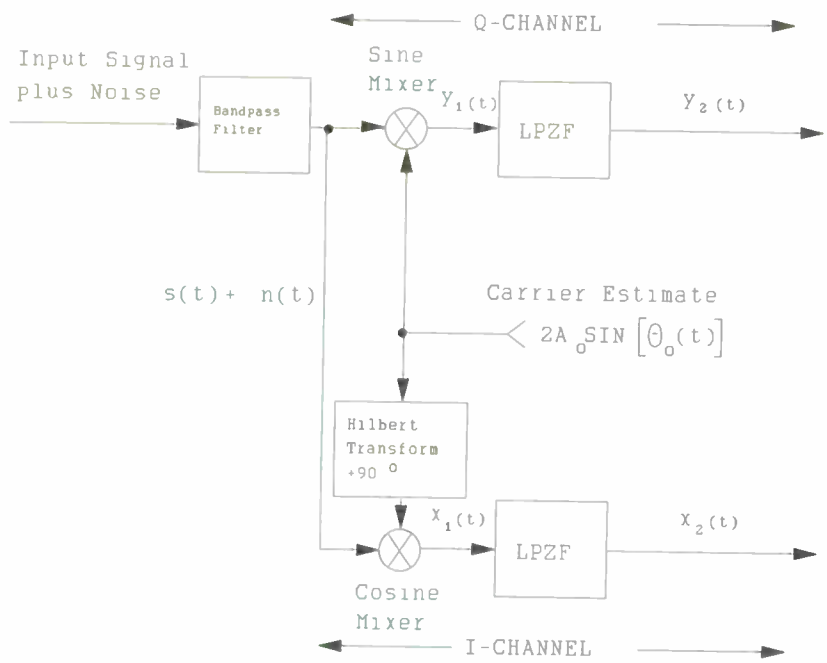


Figure 1. Basic Quadrature Detector.

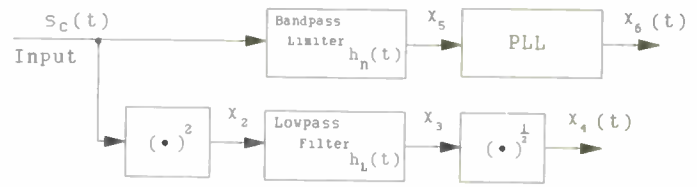


Figure 2. Examples of Simple Demodulation Schemes using a Phase-locked Loop or an Envelope Detector.

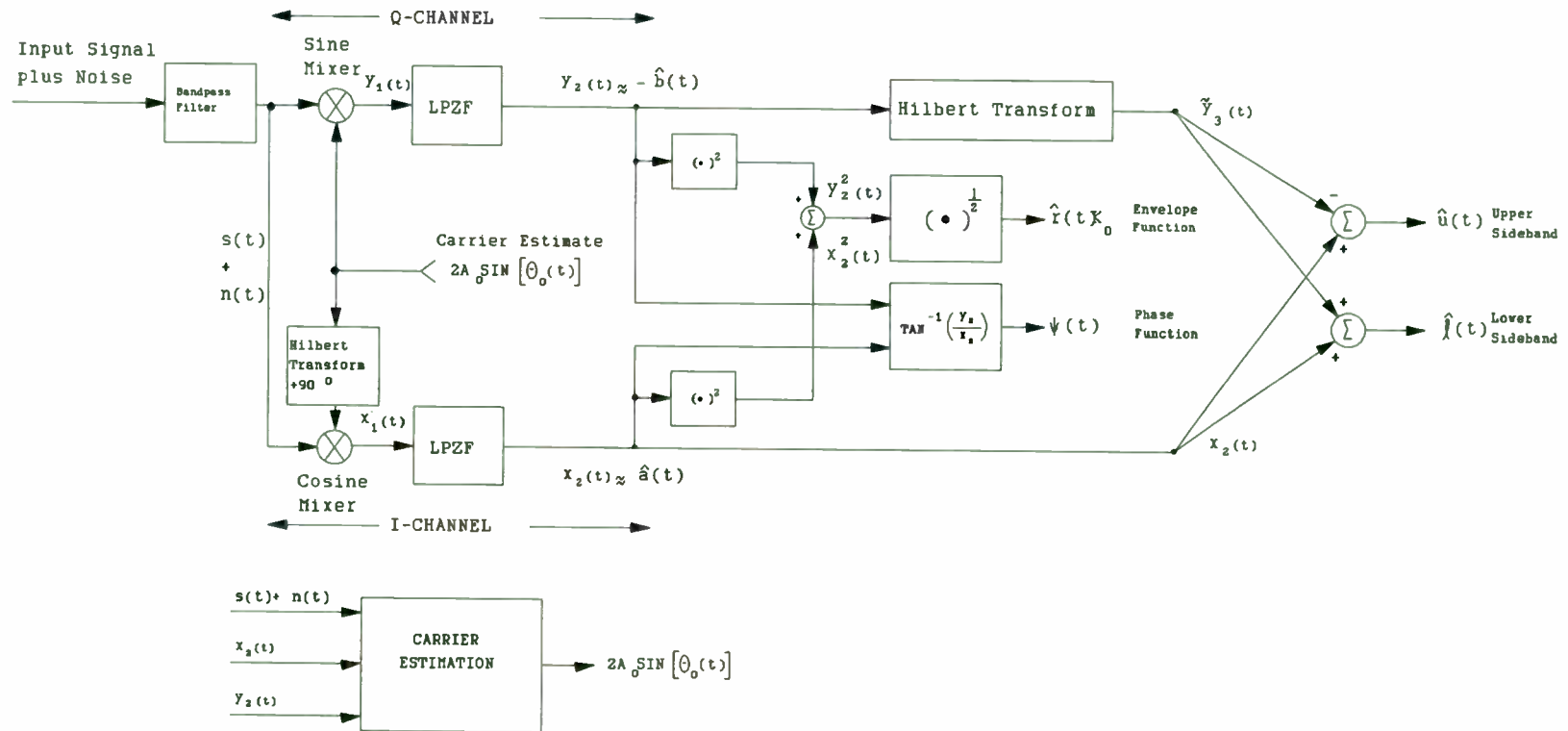


Figure 3. Generalized Costas Demodulator.

A DSP PSK MODEM FOR SATCOM SCPC DATA/VOICE

Mr.Y.S.Rao,Mr.R.Asokan and Ms.K.Reeta
C-DOT Telecom Research Centre
Bangalore INDIA

Abstract

Narrow band PSK modems implemented on Digital Signal Processors (DSP) at low frequencies pose problems with regard to adjacent channel and image rejection when upconverted and worked in the 52-88 MHz Intermediate Frequency (IF) range for Single Channel Per Carrier (SCPC) applications. To avoid these problems, a hybrid approach is presented for implementation of the modulator directly at 45 MHz and brought to 52-88 MHz range (using a synthesizer with a step size of 22.5/45 KHz) and the demodulator through DSP at low IF carrier after single down conversion. A QPSK Demod has been realised using a single TMS 320C25 DSP chip with all digital PLLs for carrier recovery and baud timing. This modem implementation covers a wide range of bit rates viz 9.6 to 32 Kbps suitable for digital data/voice in Satcom SCPC applications.

Introduction

Demands for digital transmission using SCPC carriers in Satellite Networks have increased. In such networks PSK is usually adopted as the modulation method and either SCPC (FDMA) or TDMA is employed as the multiple access technique. An analysis of PSK modulation shows that the theoretical performance of BPSK and QPSK are identical in a channel dominated by Gaussian noise such as a Satellite channel [2].

Two common performance criteria in the adoption of a modulation scheme are the bandwidth efficiency, defined as the ratio of data rate (R_b) to channel bandwidth (w) and the energy efficiency, defined as the bit energy to noise spectral density ratio (E_b/N_0) required to achieve a specified bit error rate P_e , say 1×10^{-5} . The energy efficiency depends mostly on signal space dimension and the correlation receiver which maximizes the probability of correct decision. Band limiting the spectral shape is carefully done by shaping the data pulse so as to satisfy the Nyquist criterion of zero Inter Symbol Interference (ISI).

Digital Signal Processing for data modems is cheaper than analog processing methods and takes up less space. DSP processors also offer the advantage of software reconfigurability by which the software-controlled hardware can be configured for different specifications of modulation, spectral shaping and demodulation. For the purpose of evaluation, an experimental QPSK modem has been developed with a data rate of 9.6/16 Kbps complying with the Satcom SCPC system specifications.

Transmitter

The main functions in the PSK modulator of a baseband signal involve shaping /filtering of an input NRZ data signal for reducing intersymbol interference and frequency conversion for converting the shaped/filtered base band signal to the IF signal [Fig.1].

The binary input data to the modulator is differentially encoded taking successive pair of bits. The spectral shaping of the

modulated signal is done by shaping the base band data bits using square-root raised cosine 60% roll-off FIR filters of Nyquist bandwidth. Since the output sampling rate and the input bit rate are not the same, the transmit filters are interpolating filters with an interpolation factor of $L=fs/f_b$ where f_b is the baud rate and f_s is the sampling frequency. Hence the number of multiplications required to compute the filter output reduces from N to N/L , N is the number of filter taps [3].

The above mentioned functions are implemented on a TMS32010 DSP device which gives out the shaped base band data streams, $D_E(n)$ and $D_O(n)$, through two DACs. The two analogue data streams then modulate a 45 MHz IF signal and brought to 52-58 MHz range using a synthesiser.

Receiver

The coherent demodulation of a PSK signal in the IF band involves frequency down conversion, filtering, carrier and clock recovery, data decision and differential decoding [Fig.2]. In the receive side, the 45 MHz IF signal is down converted to a Sub-IF of 19.2 KHz for 9.6 Kbps data rate before being converted to digital data by an A/D converter.

The digital data streams are supplied to a pair of square root 60% roll-off raised cosine Hilbert transform filters of Nyquist bandwidth for minimum ISI. The coefficients of the filters at the required IF are arrived from the baseband filter coefficients $h(n)$ by frequency transformation [4].

$$h_I(n) = 2h(n) \cos(2\pi f_c n)$$

$$h_Q(n) = 2h(n) \sin(2\pi f_c n)$$

In addition to shifting the baseband spectrum to the appropriate IF frequency, these filters give precise 90° phase difference which avoids distortion caused in the subsequent sections. The input modulated carrier is sampled at four times the carrier frequency (76.8 KHz) which reduces the computation required for the filters by half.

The demodulator operates on the modulated quadrature signals, $S_I(n)$ and $S_Q(n)$, with the help of the recovered carrier. This section removes the second harmonic of the carrier and retrieves the baseband information, $X_I(n)$ & $X_Q(n)$, corresponding to dibit [5].

$$S_I(n) = D_E(n) \cos(2\pi f_c n) + D_O(n) \sin(2\pi f_c n)$$

$$S_Q(n) = D_E(n) \sin(2\pi f_c n) - D_O(n) \cos(2\pi f_c n)$$

$$X_I(n) = D_E(n) \quad , \quad X_Q(n) = D_O(n)$$

Imperfect 90° relative phase difference between $S_I(n)$ and $S_Q(n)$ may require a lowpass filter following the demodulation, to remove the harmonics of the carrier.

The most critical part of the receiver implementation is the carrier recovery loop which comprises phase detection, loop filter and VCO. The phase detector, a hard-limited costas-loop, works on the retrieved baseband information $X_I(n)$, $X_Q(n)$ and generates an error signal that is used to synchronise the local carrier to the incoming carrier [6] [7].

$$\text{Err}(n) = X_I(n) \cdot \text{Sgn}[X_Q(n)] - X_Q(n) \cdot \text{Sgn}[X_I(n)]$$

The error signal $\text{Err}(n)$ is directly proportional to the phase difference between the local and incoming carrier and its derivative with respect to time is proportional to the frequency difference. The VCO generates a local carrier using a Sine table upon which the error signal operates to synchronise the local carrier to the received one. The Loop filter is a first order recursive filter which switches between wide and narrow bandwidth based on the lock-detect information. It is known that wider the loop bandwidth faster the carrier lock and more the phase jitter and hence high error probability (P_e).

Baud time recovery, another closed loop operation, is implemented by Early-Late gate technique. It compares a window of baud duration T_b , early by sample time, with another window late by the same time. The polarity of the difference signal $D(n.T_b)$ given below decides whether the baud time window is leading or lagging.

$$D(n.T_b) = \text{ABS} \left(\sum_{n=1}^{T_b/T} S_I(n) \right) - \text{ABS} \left(\sum_{n=1}^{T_b/T-2} S_I(n) \right)$$

All demodulator functions are implemented on a single TMS 320C25 DSP processor which makes use of 97.5% of processor power. A logic level at BIO pin of the processor can control the software to provide either hard decision or soft decision output.

Processor Utilization

The Table shows per sample processor resource utilization attained in the 9.6 Kbps demodulator implemented at a carrier

frequency of 19.2 KHz sampled at 76.8 KHz.

Sl. No.	Function	No. of Machine Cycles
1.	Receiver Filters	47
2.	Demodulation	09
3.	Phase detector	10
4.	Loop filter	12
5.	VCO	26
6.	Baud time recovery/AGC/Differential Decoding	14
7.	Overhead Instructions	09
Worst case no. of machine cycles required		127

Conclusion

A DSP based differentially encoded coherent QPSK modem has been developed for SCPC systems. Instead of making the modulator fully digital, the hybrid type proposed solves the problem of upconversion. The demodulator which is fully realised on DSP system offers the advantages of ease of implementation and superior performance.

Bit Error Rate (BER) at 9.6 Kbps has been measured under various channel noise conditions (Fig.3) and the resulting BER Vs E_b/N_0 has been found to be within 1db of the theoretical value. Eye patterns (Fig.4) have been presented without noise and under threshold condition ($\text{BER of } 1 \times 10^{-3}$) for comparison sake.

REFERENCES

1. I.R.Corden, R.A.Corrasco Staffordshire Polytechnic, U.K., "A High Speed DSP PSK Modem for Real Time Digital Speech Transmission".
2. Bernard Sklar, "Digital Communication Fundamentals and Applications".
3. Lim, Oppenheim, "Advanced Topics in Signal Processing".
4. Piet J.Van Gerwan et al, "Microprocessor Implementation of High-Speed Data Modems". IEEE Trans. on Commn., Vol. COMM-25, No.2.
5. Susumu Otani et al, "Development of a Variable-Rate Digital Modem for Satellite Communication systems", NEC Res. & Develop, No.92. Jan.1989.
6. Watkins-Johnson Company Tech-notes, "PSK Demodulation".
7. Lindsey W.C., and Simon M.K., IEEE Trans. on Commn. June 1972, 441-454.

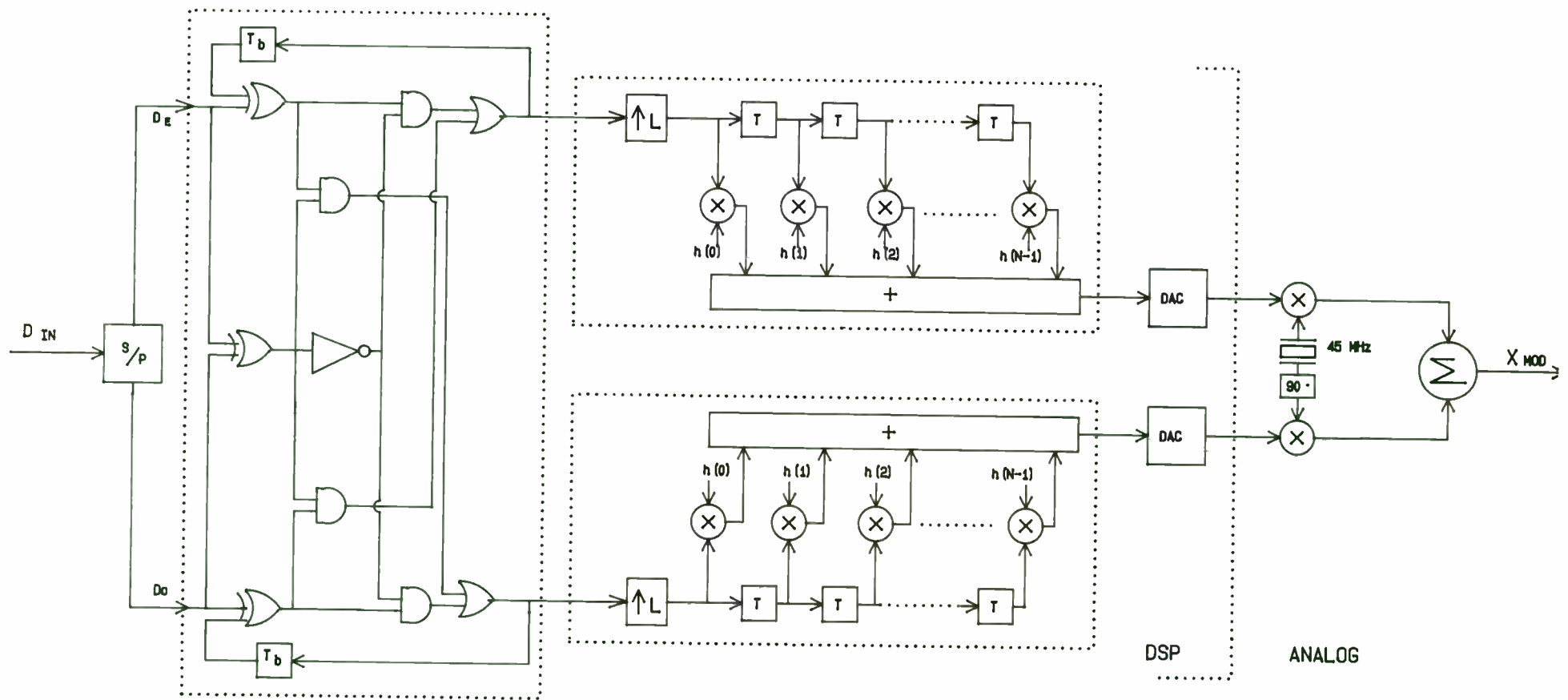


FIG.1 MODULATOR

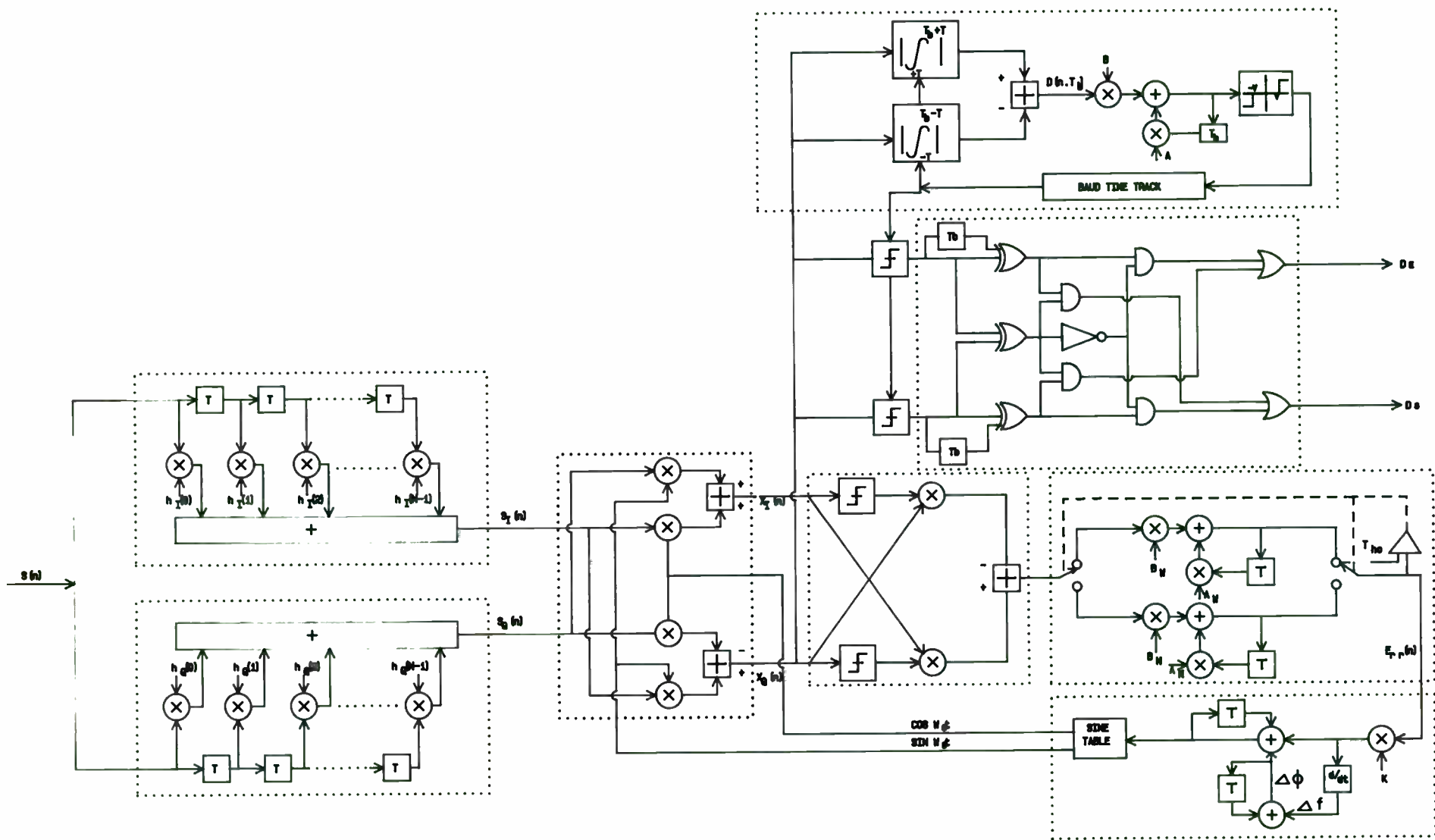


FIG.2 COHERENT DEMODULATOR

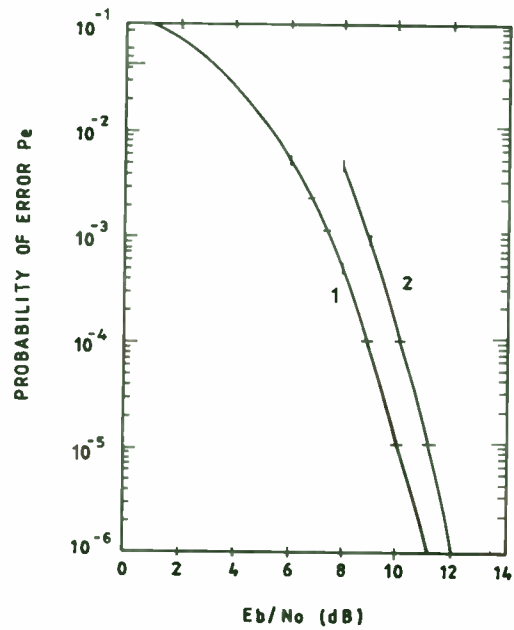


FIG. 3. BIT ERROR RATE PERFORMANCE
1. THEORETICAL 2. EXPERIMENTAL

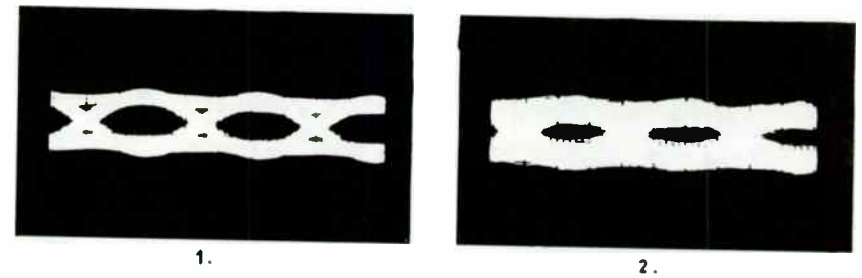


FIG. 4. MEASURED EYE DIAGRAM OF A 60% ROLL-OFF
RAISED COSINE CHANNEL 1. NOISE FREE
2. $E_b/N_0 = 9$ dB

HIGH EFFICIENCY POWER AMPLIFIER COMBINER
WITH INTEGRATED
ADAPTIVE INTERFERENCE CANCELER

Paul F. Finman, PhDEE

LCF Enterprises
651 Via Alondra, #710
Camarillo, CA 93010
Phone: (805)-388-8454

ABSTRACT

Efficient power combining of multiple amplifiers is a key determinant of size, weight, and range in EW and communication systems. However, precise amplitude and phase matching for optimum power combining efficiency is difficult to achieve over broad frequency bandwidths. Also, when a transmitter operates in close proximity to a receiver, a means for isolating the receiver from the high power interference is needed. Adaptive interference cancellation has been used successfully to solve this problem. This paper presents innovative integration of adaptive amplitude and phase control within a power amplifier combiner to achieve both optimum power combining efficiency and cancellation of interference in a nearby receiver. The hardware is small and moderate in cost, and the technology is well suited to upgrade both fixed carrier and frequency hopping communication systems which have interference problems.

Copyright (c) 1990 by LCF Enterprises

All rights reserved. No part of this publication may be reproduced, stored in a retrieval system, or transmitted, in any form or by any means, electronic, mechanical, photocopying, recording, or otherwise, without the written permission of LCF Enterprises.

LCF Enterprises assumes no responsibility for the use of any circuits described herein and makes no representation that they are free of patent infringement.

1. Introduction

Efficient power combining of multiple amplifiers is a key determinant of size, weight, and range in EW and communication systems. However, precise amplitude and phase matching for optimum power combining efficiency is difficult to achieve over broad frequency bandwidths. When amplitude and phase matching over broad bandwidths are not realized, power is lost to the load resistor of a matched and isolated 50 ohm power combiner.

Adaptive interference cancellation is an additional application where precise amplitude and phase matching is required for optimum performance. In this interference reduction approach, a sample signal from an interfering transmitter is adjusted in amplitude and phase and injected into a receiver. When the adjusted sample is equal in magnitude and opposite in phase to the interference in the receiver, the interference is canceled. Interfering signals can be canceled with negligible effect on desired signals even when the interfering and desired signals have common frequencies, so the technology is well suited for frequency hopping applications.

This paper presents innovative integration of adaptive amplitude and phase control within a power amplifier combiner to achieve both optimum power combining efficiency and cancellation of interference in a receiver. This achieves significant improvements in canceler performance over conventional configurations, since the amplitude and phase control is completed at low power levels. Interference problems in both new and existing systems can now be solved simply with a power amplifier which has a cost only moderately higher than a conventional amplifier. As previously stated, this technology is particularly well suited to frequency hopping upgrades.

2. Technical Description

A discussion of the importance of precise amplitude and phase balance for

optimum power combining follows. Also, interference cancellation is reviewed and some problems with the conventional configuration for an interference canceler are discussed. Finally, the new configuration for an interference canceling amplifier is presented along with a discussion of the advantages of integrating adaptive amplitude and phase control within a power amplifier.

2.1 Amplifier Efficiency

Amplifier efficiency is dependent on the active device characteristics and biasing. For Class A biasing, Class AB biasing, and Class C biasing; the ideal efficiency limits are 50%, 78.5%, and 100%, respectively. In practice, the realizable efficiency is typically 25%, 50%, and 75%, respectively. In many cases, it is necessary to sacrifice efficiency in amplifier design to achieve stable, rugged performance, and losses are purposely introduced in the output matching network. When additional lossy circuits must be placed on the output for a specific application (e.g. combining losses), proper integration of the output matching network with the lossy circuits achieves optimum performance. This can match or exceed the performance of a stable, rugged amplifier driving a load through lossless circuits.

2.2. Combiner Losses

The two main losses in a power combiner are resistive and imbalance losses. The resistive losses can in many cases be made small, and can also be integrated into an amplifier output matching network to actually improve stable, rugged performance. Therefore, the most troublesome losses in combiners are due to amplitude and phase imbalances. For a two-way power combiner, common amplitude and phase imbalances are 0.5 dB and 10 degrees, respectively.

An example of the power lost due to a 0.5 dB amplitude imbalance in a power combiner follows. A 0.5 dB amplitude difference corresponds to a 12% power

difference and a 6% amplitude difference. The power loss of two signals coherently combined in a matched system with a 0.5 dB amplitude imbalance is 6% or 0.25 dB. For a four-way combiner, the losses cascade and the total loss for a 0.5 dB amplitude imbalance is 12% or 0.5 dB. For an amplifier with a 60% DC conversion efficiency on the output stage, a 20% increase in DC power is required to compensate for a 12% RF power loss.

An example of the power lost due to a 10 degree phase imbalance in a two-way combiner follows. The cosine of 10 degrees is .985 which corresponds to an amplitude imbalance of 1.5% or 0.13 dB. The power loss of two signals coherently combined in a matched system with a 0.13 dB amplitude imbalance is 0.75% or .07 dB. For a four-way combiner, the losses cascade and the total loss for a 10 degree phase imbalance is 1.5% or .13 dB. For an amplifier with a 60% DC conversion efficiency on the output stage, a 2.5% increase in DC power is required to compensate for a 1.5% RF power loss.

Since amplitude and phase imbalances cascade under worst case conditions, the total imbalance losses in a four-way combiner from amplitude and phase imbalances of 0.5 dB and 10 degrees, respectively, can be 13.5% or 0.63 dB. For an amplifier with 60% DC conversion efficiency on the output stage, a 22.5% increase in DC power is required to compensate for a 13.5% RF power loss. These examples show that optimum amplitude and phase balance is very important for achieving good combining efficiency.

2.3. Conventional Adaptive Interference Cancellation Configuration

A schematic of the circuitry for an interference canceler based on the Least Mean Square (LMS) adaptive algorithm is presented in Figure 1. In this interference reduction approach, a sample of an interferer is adjusted in amplitude and phase to cancel interference in a receiver. A key feature of adaptive interference cancellation is that signals correlated with the

interference are removed while desired signals are virtually unaffected. The adaptive algorithm ensures that optimum amplitude and phase are maintained for varying system conditions.

A brief description of the operation of the circuit in Figure 1 follows. A reference sample of the interfering transmitter is adjusted in amplitude and phase by a Complex Phasor Modulator (CPM) according to control voltage inputs and then injected in the receiver line. An error signal is coupled from the RF output, amplified, and fed to a Phase Comparator (PC). The PC is also fed a reference sample of the interfering transmitter input. The PC multiplies the error signal and the interfering transmitter sample. This generates DC signal outputs which are proportional to the sine and cosine amplitudes of the error components which are frequency and phase correlated with the interference sample. Signals in the error input which are not frequency and phase correlated with the interference sample generate time varying signal outputs. The sine and cosine product outputs are connected to integrators and the results serve as the control voltage inputs to the CPM.

The control voltages converge to values which zero the DC integrator inputs. This occurs when the mean square error of signals in the receive line correlated with the reference interference sample is minimized. The ideal condition for minimizing the mean square error to zero is achieved when the amplitude and phase adjusted sample of the interfering transmitter is equal in magnitude and opposite in phase to the interference in the receive line such that the interference is canceled.

Performance of an adaptive interference canceler utilizing the standard LMS algorithm is presented in Figures 2 - 3. In this experiment, a reference sample of an interfering transmitter is available. The example shows that the interference and the desired signal can be separated with a high degree of accuracy.

2.4. Limitations of Conventional Configuration

The conventional configuration for an adaptive interference canceler has several limitations. The complex phasor modulator (CPM) generally is a passive device to minimize distortion. That is, the CPM operates by splitting an RF input signal into in-phase and quadrature-phase components which are then attenuated by controls to achieve the cosine and sine signals whose vector sum give the required amplitude and phase. The power dividing, power summing, and controlled attenuation within the CPM result in a 10 dB loss typically. Therefore, a 50W interference sample power is required to cancel a 5W interference level at the receiver.

When the required interference sample power is as high as 1W - 50W, system efficiency is sacrificed, and large, costly components must be used, thereby increasing system size, cost, and weight. Therefore, with the conventional canceler configuration, it is difficult if not impossible to retrofit an existing system with a fixed form factor and limited available power. For a new system, the cost and size of including interference cancellation may be prohibitive.

Even with a passive CPM, distortion is a problem when controlling high power signals. In some applications, a booster amplifier can be added after a passive CPM so that the interference sample power is reduced. This reduces distortion within the passive CPM, but the booster amplifier adds distortion. Minimizing total distortion then involves a trade-off between interference sample power, CPM distortion, and amplifier gain and distortion.

Group delay matching over frequency is also a problem using the conventional interference cancellation configuration. To achieve precise cancellation of a broadband signal (e.g. a spread spectrum signal), the group delay of the amplitude and phase adjusted sample must match the group delay of the interference in the receiver. Introducing a CPM by itself or with a booster amplifier in the sample signal path makes group delay matching more difficult.

2.5. Power Combiner/Canceler Integration

The problems of the conventional interference canceler can be solved by innovative integration of a power amplifier combiner with adaptive amplitude and phase control. Figure 4 presents the configuration. A discussion of the operation follows.

A signal source drives two-way combined power amplifiers. One branch of the power amplifiers contains a complex phasor modulator (CPM) for control of the amplitude and phase balance between each amplifier. The two amplifiers feed a 4-port power combiner with one output to the transmit antenna while the remaining output injects a controlled interference sample into the receiver. For optimum power combining, the CPM is adjusted to give precise amplitude and phase matching between the two amplifier branches such that zero power appears at the controlled interference sample output. In this case all the combined power appears at the transmit antenna, and there are no combining losses due to amplitude and phase imbalances.

For adaptive interference cancellation, small amplitude and phase imbalances are introduced to achieve a low power controlled interference sample which cancels the interference in the receiver. In this case virtually all the combined power appears at the transmit antenna, and the power loss from the amplitude and phase imbalances is used productively to cancel interference.

The integrated combiner/canceler has the following key advantages over conventional cancelers:

1. The CPM sees a low power signal so distortion is minimized.
2. Small changes in amplitude and phase balance give good control over the adjusted interference sample.
3. Group delay matching is achieved easily between the controlled interference sample signal path and the receiver interference path, since the number of components in each path is minimized.

4. Only small, inexpensive, low-power components need be added to a two-way combined power amplifier to integrate interference cancellation. Therefore, there is only a small increase in size and cost compared to a standard two-way combined power amplifier.

3. Example Application

Table 1 presents an example of an existing system which is well suited to a low cost upgrade which solves current interference problems. It should be noted that the upgrade size matches the original amplifier, and no additional power is required, so the system retro-fit is accomplished easily.

Table 1. Example Amplifier Upgrade

Frequency: 30 - 88 MHz frequency hopping
Modulation: 25 KHz FM
RF power output: 50W compressed
RF power input: 4W (11 dB compressed gain)
Frequency hopping rate: 111 hops/second
Size: 2" X 12" X 6" (form factor of original amplifier)
Interference level at receiver: 4W
Interference cancellation: 55 dB minimum (60 dB typical)
Cost: approximately 30% - 50% above original amplifier cost

4. Summary and Conclusions

In summary, innovative integration of adaptive amplitude and phase control within a power amplifier combiner yields optimum combining efficiency over broad frequency bandwidths by eliminating combiner losses due to amplitude and phase imbalances. This also yields an adaptive interference canceler with important advantages over conventional cancelers. The hardware is small and moderate in

cost, so the technology is well suited for upgrading existing systems with interference problems. This is particularly true for upgrading frequency hopping systems.

5. References

Additional information on adaptive signal processing can be found in the following references.

1. R.T. Compton, Jr., Adaptive Antennas, Concepts and Performance, Prentice Hall, Inc., Englewood Cliffs, NJ, 1988.
2. Robert A. Monzingo and Thomas W. Miller, Introduction to Adaptive Arrays, John Wiley and Sons, New York, NY, 1980.
3. Leon H. Sibul, editor, Adaptive Signal Processing, IEEE Press, New York, NY, 1987.
4. Bernard Widrow and Samuel D. Stearns, Adaptive Signal Processing, Prentice-Hall, Inc. Englewood Cliffs, NJ, 1985.

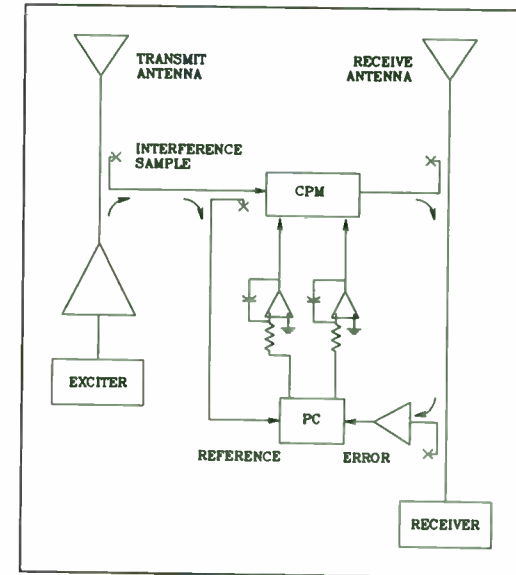


Figure 1. LMS Adaptive Interference Canceller Block Diagram.

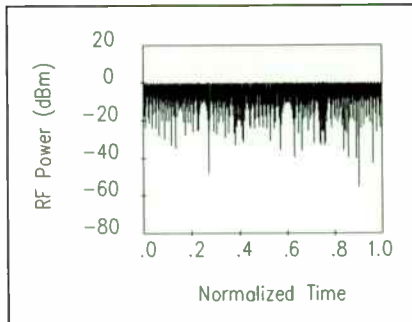


Figure 2a. Interfering transmitter.

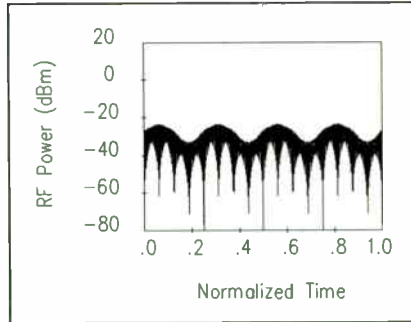


Figure 2b. Desired Signal.

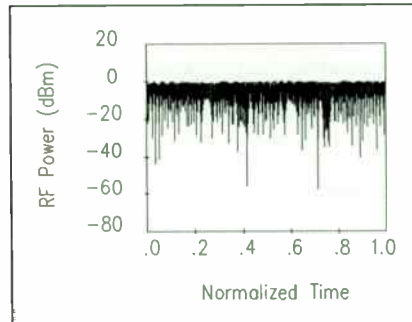


Figure 2c. Interferer and desired signal without interference cancellation.

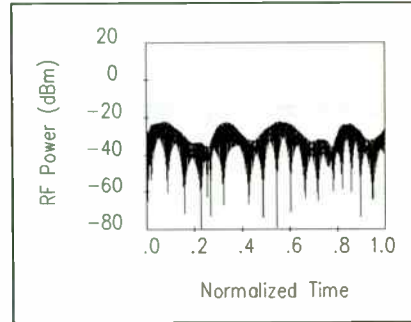


Figure 2d. Interferer and desired signal with interference cancellation.

Figure 2. Adaptive interference cancellation time domain simulations demonstrate separation of the interference from the desired signal with a high degree of accuracy.

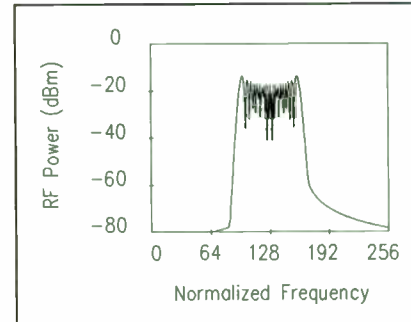


Figure 3a. Interfering transmitter.

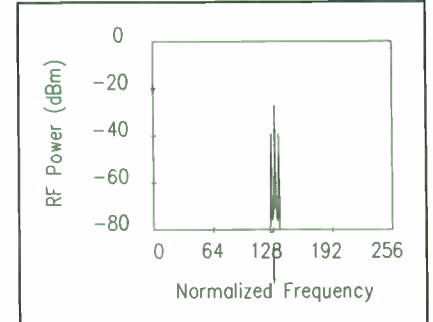


Figure 4b. Desired signal.

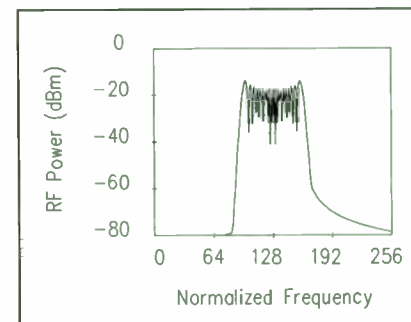


Figure 5c. Interferer and desired signal without interference cancellation.

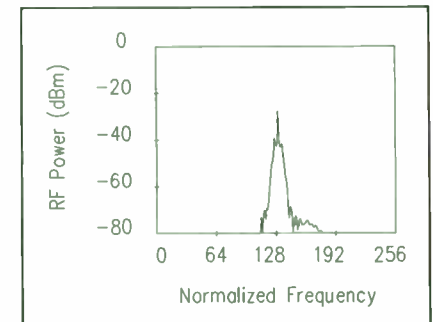


Figure 6d. Interferer and desired signal with interference cancellation.

Figure 3. Adaptive interference cancellation frequency domain simulations demonstrate separation of the interference from the desired signal with a high degree of accuracy.

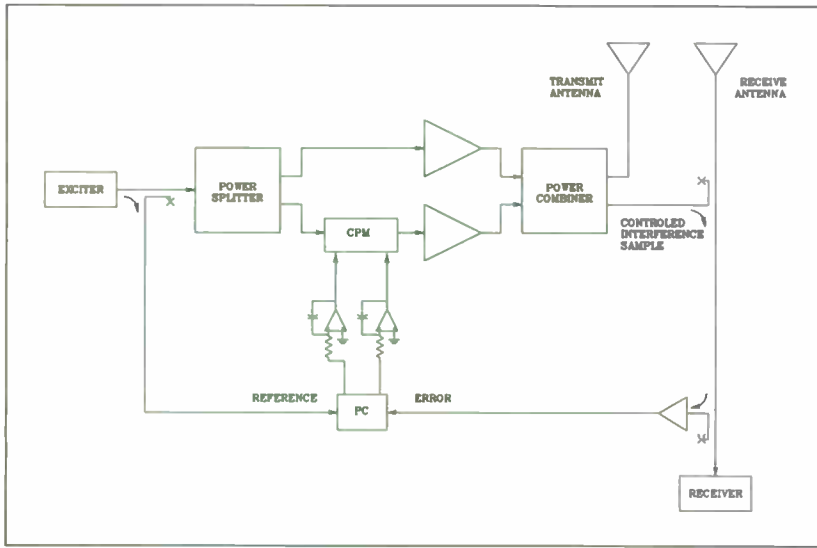


Figure 7. Power Amplifier Combiner with Integrated Interference Canceler.

**DIGITAL FEEDBACK TECHNIQUES
FOR A
PULSE-WIDTH MODULATED RF POWER AMPLIFIER**

by
Harry Direen
Ehrhorn Technological Operations, Inc.
4975 North 30th Street
Colorado Springs, Colorado 80919

ABSTRACT

Certain applications, such as various types of plasma generators, require a pulse-width modulated RF power amplifier, with well regulated output level. The RF power output will tend to vary with: load variations, AC line variations, pulse-width and duty cycle settings, and temperature changes. A feedback loop around the RF power amplifier will correct this problem. This paper discusses a microprocessor-based, digital, feedback loop that corrects the RF output variations.

INTRODUCTION

A microprocessor-based, digital feedback loop around an RF power amplifier (or RF power generator) is presented here. One of the basic assumptions is that the factors which cause RF output to vary, change slowly enough in time that an inexpensive,

8-bit, microprocessor can be used in the feedback loop. Based on results from an evaluation system, this proved to be a good assumption.

In order to gain understanding of the feedback loop, it is important to understand the nature of the control problem. A specific example will be used to describe the problem and its solution. The example may be adapted to a wide variety of applications. A generic set of specifications will be given for a pulse-width modulated RF power amplifier. These specifications will provide an example which can be followed with realistic numbers.

A short discussion of why a digital feedback loop has been chosen rather than an analog feedback loop will be presented. Then, the actual feedback loop circuitry and design will be discussed and analyzed. Finally, the results from a working feedback loop will be covered.

THE CONTROL PROBLEM

The control problem may be presented by a generic set of specifications for the RF amplifier. Only those specifications which affect the feedback loop are needed. In this way a concrete example can be followed with real world numbers. The numbers given here are for purposes of the example only, and do not necessarily reflect any particular amplifier.

EXAMPLE SPECIFICATIONS

RF POWER OUTPUT

10 Kilowatts maximum, continuously controllable over the range of 1 kilowatt to 10 kilowatt.

RF LEVEL CONTROL INPUT

An external input (POWER LEVEL SET) shall be provided to set the amplifier RF output level. A linear control characteristic is desirable.

PULSE-WIDTH MODULATION INPUT

The Pulse-Width Modulation (PWM) input is used to gate the RF output on and off. This digital input signal has the pulse width and pulse rate of the desired RF output signal. It may be changed at any time within the following limits:

Pulse Rate (PWM_f): 0 Hz to 25 KHz

Pulse Width (PWM_ton): 20 μ sec to CW (continuous)

RF POWER LEVEL REGULATION

The allowed variation in the RF output level due to any cause is $\pm 1\%$ of Pout_max, or ± 100 watts.

NOTE: The RF output level will tend to vary with: load variations; AC line variations pulse-width and duty cycle settings; and temperature changes.

ANALOG VERSUS DIGITAL FEEDBACK

The requirement for pulse-width modulation of the RF output, with varying pulse rate and pulse width, makes a strictly analog approach to the feedback loop difficult. One reason for this is each time the amplifier is gated off with the PWM input, the feedback loop, which is monitoring the RF power output, will drive the power level control in such a way as to correct for the "low" power output. When the amplifier is gated back on, the power level control will overdrive the RF output until the control loop has time to lock back onto the RF output and correct it to the proper level. This overshoot is highly undesirable.

In order to correct this problem, the feedback loop must be gated on and off with the PWM input. The power level control voltage must be held constant during the period of time the amplifier is gated off. This can be accomplished by the use of a track-and-hold stage in the feedback loop. However, even with a track-and-hold stage, either high loop gain or an integrator in the loop will tend to drive the feedback stages to one rail when the amplifier is gated off.

With a digital feedback loop, the RF output power can be sampled synchronously with the PWM signal. The gating on and off of the feedback loop becomes natural, and there are no drifts in the feedback loop when the RF output is gated off.

The digital feedback loop also allows another feature not easily implemented in a strictly analog loop. The voltage output of a

power monitor (wattmeter) typically is proportional to the square root of the actual power level. Also, the control voltage that adjusts the RF power output is rarely an inherently linear function. These two functions can easily be linearized by the microprocessor.

MICROPROCESSOR BASED FEEDBACK LOOP TOPOLOGY AND DESCRIPTION

Figure 1 is the overall block diagram of the RF power amplifier with digital feedback loop. The PWM control and Power Level control are inputs to the Low Level RF stages.

A directional coupler with detectors is used to sample the forward and reflected RF power envelopes at the output of the power amplifier (PA). These signals typically are proportional to the square root (or possibly some other non-linear relationship) of the actual forward and reflected power levels. Feedback control of the RF amplifier may be based on the net power out of the amplifier (forward minus reflected power), or simply on the forward power out. The choice is based on the application requirements.

The forward and reflected signals feed sample-and-hold (S/H) devices. Key to the operation of this feedback loop is proper sampling of the forward reflected signals. Sampling must be synchronized with the PWM signal in such a way as to assure that the forward and reflected power samples are not taken dur-

ing amplifier gate-on transients or when the amplifier is gated off. If this occurs, the feedback loop will attempt to correct on erroneous data.

The outputs of the sample-and-hold devices are converted into the digital domain by analog-to-digital converters (A/D). The A/D outputs go to the microprocessor.

The microprocessor is the heart of the feedback loop. Feedback control within the microprocessor uses rather straightforward digital signal processing techniques and code.

POWER LEVEL SET is another input to the microprocessor. This command signal is used to set the desired power output level. It may be an analog signal converted into the digital domain by an A/D converter. Or it may be supplied via an RS-232 interface or other convenient means.

Feedback control signals from the microprocessor feed a digital-to-analog (D/A) converter which converts them back to the analog domain. The output of the D/A converter drives the analog POWER LEVEL CONTROL input of the RF amplifier.

Sample Synchronization Logic (SSL) is digital hardware logic that assures samples of the forward and reflected power are properly synchronized to the PWM control input. The microprocessor has two digital control lines, one (GET SAMPLE) going to the SSL, and one (SAMPLE DONE) coming from the SSL. These control lines determine when samples of the for-

ward and reflected power are to be taken and when sampling is complete. Sample timing of the S/H devices is controlled by the SAMPLE CTRL line.

FEEDBACK LOOP DESIGN DETAILS

Microprocessor and Sample Rate

A basic assumption in the feedback loop design is that the factors which cause the RF output to vary in time are slow enough that an 8-bit microprocessor can handle the task. This is important if the cost of the feedback loop is to be kept low.

It is assumed here that the maximum required sample rate for the feedback loop is 4 KHz (250 microseconds between samples). This will allow the microprocessor enough time to handle the feedback loop as well as other tasks.

From the example specifications, the minimum pulsewidth is 20 microseconds with a maximum pulse rate of 25 KHz (40 microsecond period). It can be seen that with a 250 microsecond sample period and a minimum pulse period of 40 microseconds, not every RF pulse can always be sampled. The microprocessor will have to determine, via the Sample Synchronization Logic, which RF pulses are to be sampled and which are not. The fact that not every RF pulse is sampled does not prevent the control loop from correcting slow RF output variations.

Sample Synchronization Logic

The Pulse-Width Modulation (PWM) control to the amplifier is asynchronous with the feedback loop. It is the job of the Sample Synchronization Logic (SSL) to assure that samples of the forward and reflected power are taken only when the RF output is gated on, after any turn-on transients.

Figure 2 shows a timing diagram for the SSL. The PWM control is used to gate the RF output on and off. The second line of the timing diagram shows the RF output being gated on and off with the PWM control. The RF output signal shows typical turn-on transients for such an amplifier.

The microprocessor signals the SSL that it is ready for the next sample of forward and reflected power via the Get Sample control line. This pulse typically resets the SSL. The SSL does one of two things, depending on the state of the PWM control. If the PWM control is low (RF output off), the SSL waits for the PWM control line to go high. After the PWM line goes high (turning the RF output on), the SSL waits a short period of time for RF turn-on transients to settle out. After this short delay, the SSL signals the S/H devices to take the next forward and reflected power samples. When the S/H devices have acquired the samples, the SSL informs the microprocessor that a valid sample is ready, using the Sample Done control line.

If the PWM control is high (RF output on) when the Get Sample line is pulsed, the SSL pulses the S/H devices immediately and then takes the Sample Done line high. In this way the feedback

loop will continue sampling the RF output during long pulses or CW operation.

Analog-to-Digital and Digital-to-Analog Converters

The A/D converters must have enough resolution to assure that the feedback loop can monitor and hold the RF power output to the required maximum variation. For our particular example, the maximum allowed variation is $\pm 1\%$ of 10 KW, or ± 100 watts. Let us assume that the output of the Coupler /Detectors is approximated by:

$$P_{out} = k * V^2$$

Further, assume that an 8-bit A/D converter is used with an input voltage range of 0-5 volts, and the output of the Coupler/Detector is scaled such that 10 kW = 4.5 volts. Then:

$$k = 10 \text{ kW} / (4.5 \text{ volts})^2 = 0.494 \text{ kW/volt}^2$$

The resolution of a 0 - 5 volt, 8-bit A/D converter will then be:

$$\Delta V_{min} = 5 \text{ volts} / 256 = 20 \text{ millivolts}$$

At 10 kW RF output, ΔV_{min} corresponds to 90 watts. At 1 kW RF output, ΔV_{min} corresponds to 30 watts. This implies that an 8 bit A/D converter is marginal for our amplifier. A 10 or 12 bit A/D converter would be a better choice.

Arguments similar to those used for selection of the A/D converter are used for the selection of the D/A converter.

The sample-and-hold devices (S/H) must have an acquisition

time short enough to assure that a sample can be taken on the shortest RF pulse. The S/H must also be able to hold the signal with a droop of less than one least-significant bit of the A/D converter during the sample period.

SOFTWARE CONTROL LOOP

Figure 3 shows a diagram of the software control loop that is executed by the microprocessor. The control loop shown is by no means the only scheme that would work, however, it has been proven to perform quite well for this application.

The forward and reflected samples from the A/D converters are not linearly proportional to the actual forward and reflected RF power levels. It is necessary first to linearize them such that the resultant signals, P_{fwr} and P_{refl} , are linearly proportional to the actual forward and reflected power levels. This is particularly important if the feedback loop is to correct for net power output.

If the output of the coupler/detectors can be approximated by:

$$V_{fwr} \text{ or } V_{refl} = k * \sqrt{P_{fwr}}$$

then the forward and reflected power samples may simply be squared by the processor. If the power samples follow some other non-linear curve, a table look-up is the fastest way to linearize them. A table can readily be generated from a measured curve of the actual detected voltage out verses RF power. For an

8-bit A/D converter, a table of only 256 bytes of memory is required.

Depending on system requirements, either the net power output (P_{fwr} - P_{refl}) or the forward power can be held constant by the feedback loop. Figure 3 shows net power (P_{net}) control.

Net power, P_{net}, is compared to the Power Set level, P_{set}, resulting in an error signal (P_{err}). The error signal is integrated and summed with the P_{set} signal. Feed forward of P_{set} allows the RF output to be set independent of the feedback loop. The signal P_{err'} then represents the total deviation of power output from the set point. The signal P_{ctrl} (P_{ctrl} = P_{err'} + P_{set}), is used to control the power level out of the amplifier.

The Z⁻¹ block in figure 3 represents a unit delay, where the unit of time is one sample period. The signal P_{err'} is computed as:

$$P_{err'}(n) = P_{err'}(n-1) + P_{err}(n)$$

where "n" is the nth sample and n-1 is the sample just previous to sample n. Using z-transforms gives:

$$P_{err'}(z) = \frac{z}{z-1} * P_{err}(z)$$

The block labeled "Kf" allows the loop gain to be set.

RF output, P_{out}, is typically a non-linear function of the Power Level Control voltage. This non-linear relationship may be lin-

earized by the use of a table look-up in the software control loop. The advantages of linearizing this function are: the RF output will be a linear function of the Power Level Set command; linear analysis of the feedback loop will be valid; and feedback loop gain will not be a function of the RF output level.

ANALYSIS OF THE FEEDBACK LOOP

The feedback loop may be analyzed using z-transform methods. In using the z-transforms we must be careful to remember that our sample periods are irregular. The software control loop will request samples on a regular basis; however, due to the asynchronous PWM, the actual sample period can vary considerably. This means that a frequency interpretation of the z-transformed signals is valid only when the RF output is gated on continuously.

Net power out of the amplifier can be described as a component directly proportional to the control setting P_{ctrl} plus a term that represents the variation in power output from the ideal. Therefore we can represent P_{net} as

$$P_{net} = K_a * P_{ctrl} + P_{var}$$

Where: K_a is the gain from P_{ctrl} to P_{net}.

P_{var} is the difference in P_{net} from the set value.

The transfer function of the feedback loop then is

$$P_{net}(z) = \frac{K_a K_f + K_a(z-1)}{K_a K_f + (z-1)} P_{set}(z) + \frac{z-1}{K_a K_f + (z-1)} P_{var}(z)$$

If the gain K_a from P_{ctrl} to P_{net} is set to 1, then the above equation simplifies giving a closed loop transfer function of

$$P_{net}(z) = P_{set}(z) + \frac{z-1}{z-(1-K_f)} P_{var}(z)$$

The feedback loop will be stable for values of K_f between 0 and 2. For z-transforms, all the poles of a system must be inside the unit circle ($|z| < 1$) for the system to be stable.

The closed loop transfer function has a zero at $z = 1$. This will force the dc components of P_{var} to zero, which is the desired effect of the feedback loop.

Step Response

The response of the feedback loop for a unit step in P_{var} is

$$P_{net}(n) = a^n$$

where: $a = 1 - K_f$ also: $-1 < a < 1$ and n is the sample time

Figures 4 a, b, and c show the unit step response for three different values of K_f . When K_f equals 0.5, the feed-back loop corrects the measured error by 50% each sample time. When K_f equals 1.0, the feedback loop corrects the measured error 100% on the first sample after the unit step. When K_f equals 1.5, the

feedback loop over-corrects the error by 50% each sample time.

Frequency Response

As mentioned above, due to the asynchronous PWM, we must use caution in interpreting the frequency response of the closed loop system. Nevertheless, the frequency response gives some very useful information and it will be accurate when the amplifier is gated on continuously.

The frequency response may be obtained by replacing z in the closed loop transfer function with:

$$z = e^{j2\pi fT}$$

Where: $T = \text{Sample Period} \dots 250 \mu\text{sec}$
 $f = \text{frequency}$

Figures 5 a, b, and c show the frequency response for three different values of K_f . The closed loop frequency response is that of a high pass filter. The frequency response stops at 2 KHz. Due to the 4 KHz sample rate ($T = 250 \mu\text{sec}$), all frequencies above 2 KHz will be mapped back into the frequency range of 0 to 2 KHz. Odd multiples of 2 KHz will map into 2KHz, and even multiples will map into 0 Hz.

Let us assume for the moment that there is 360 Hz ripple on the RF power output, such as due to use of a 3 phase power supply. Figure 5a shows that with $K_f = 0.5$, the feedback loop gives very

little attenuation to 360 Hz ripple. Figure 5c shows that with $K_f = 1.5$, the feedback loop would help reduce the 360 Hz ripple significantly.

On the other hand, when we look at figures 5 a-c, we see that as K_f is increased, the feedback loop amplifies 2KHz noise more and more. The 2 KHz noise will come about naturally when the PWM rate is at 2 KHz, or odd multiples of 2 KHz. From the standpoint of not amplifying higher frequency noise, it is better to keep the loop gain factor K_f lower in value.

RESULTS FROM A WORKING FEEDBACK LOOP AND CONCLUSIONS

A microprocessor-based digital feedback loop has been built, tested, and proved successfully. The microprocessor used is an 8-bit Intel 8031. Due to pre-existing constraints, an 8-bit A/D converter was used to sample the forward and reflected powers.

Two-8 bit D/A converters were summed at their analog outputs to give an effective 10-bit D/A converter for the power level control. The use of 8-bit A/D and D/A converters allowed more time-efficient 8 bit calculations to be used.

Best overall results for the feedback loop were obtained with a loop gain factor, K_f , of 0.25. This gain factor produced a very stable feedback loop which did not show signs of resonance at half the sample frequency.

The fact that an 8-bit A/D converter was used instead of a 10 or 12 bit converter played an important role in forcing K_f to a lower value. One effect not analyzed above is quantization error in sampling and finite-word-length representation of numbers in the microprocessor control loop. This effect can cause low level oscillations in the feedback loop. Designing the hardware such that P_{ctrl} has 4 times the resolution of P_{fwr} and P_{refl} (10-bit D/A verse 8-bit A/D) kept the feedback loop from oscillating around the least-significant-bit (LSB) of the A/D input.

Setting K_f to 0.25 did not give the quick step response that a value of 1.0 would have. Also, there was no improvement in the power supply ripple with this value of K_f . However, the primary goal of the feedback loop was achieved. Under test, the RF power output remained within a ± 0.1 dB window for all combinations of load, AC line, temperature, and PWM variations.

The microprocessor used for the feedback loop is also being used to control and monitor all other aspects of the RF power amplifier.

REFERENCES

Digital Control Systems

Benjamin C. Kuo

HRW Series in Electrical and Computer Engineering. 1980

Digital Signal Processing

Alan V. Oppenheim & Ronald W. Schaffer

Prentice-Hall. 1975

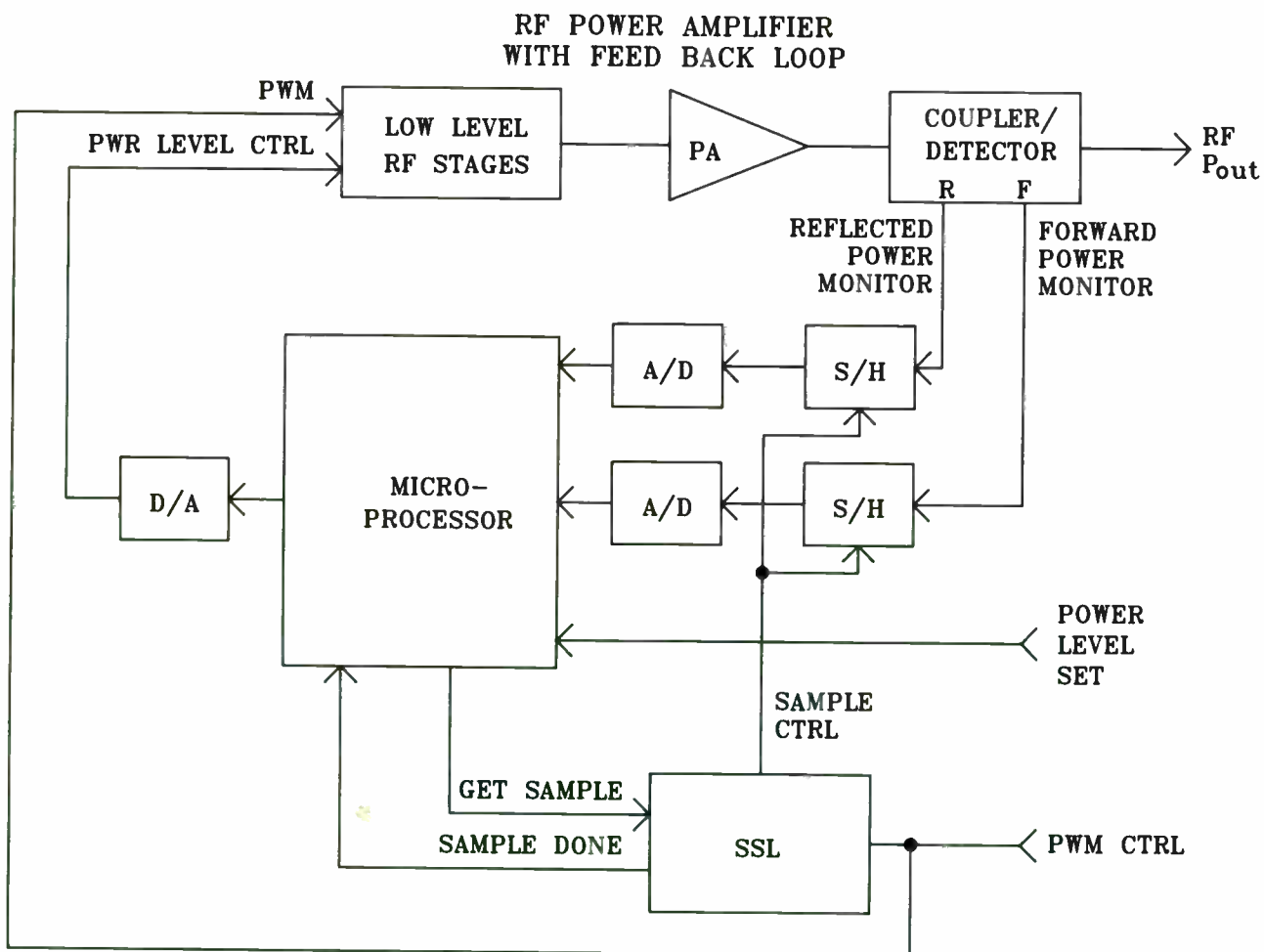


FIGURE 1

TIMING DIAGRAMS FOR SSL

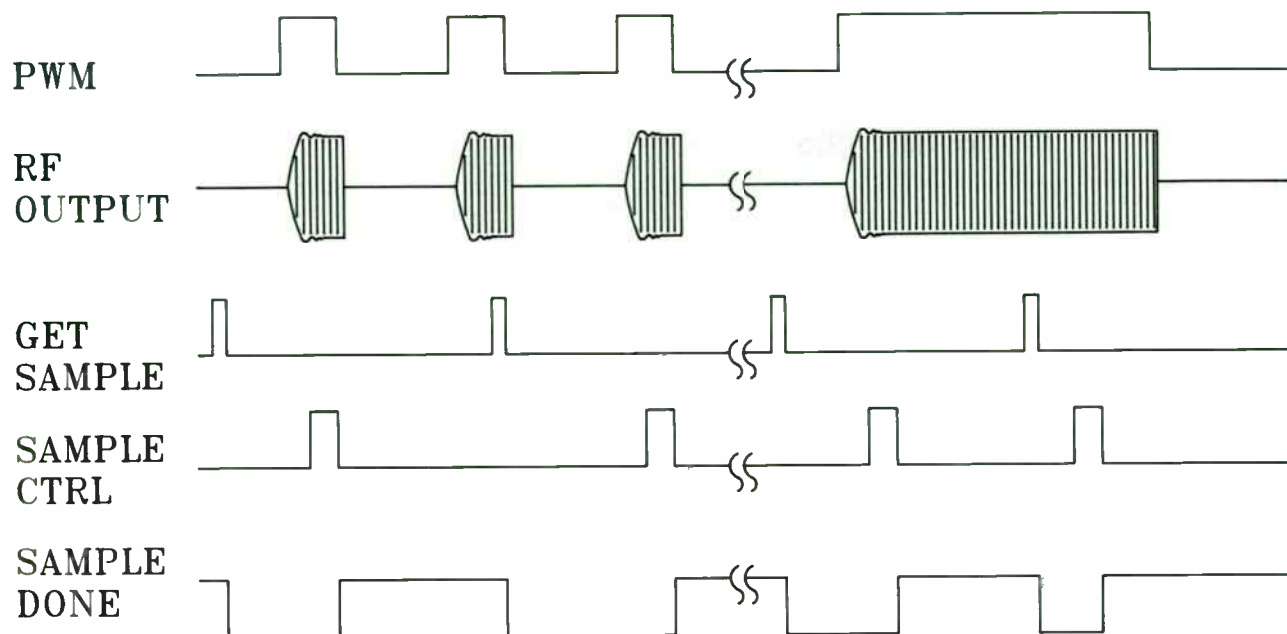


FIGURE 2

328

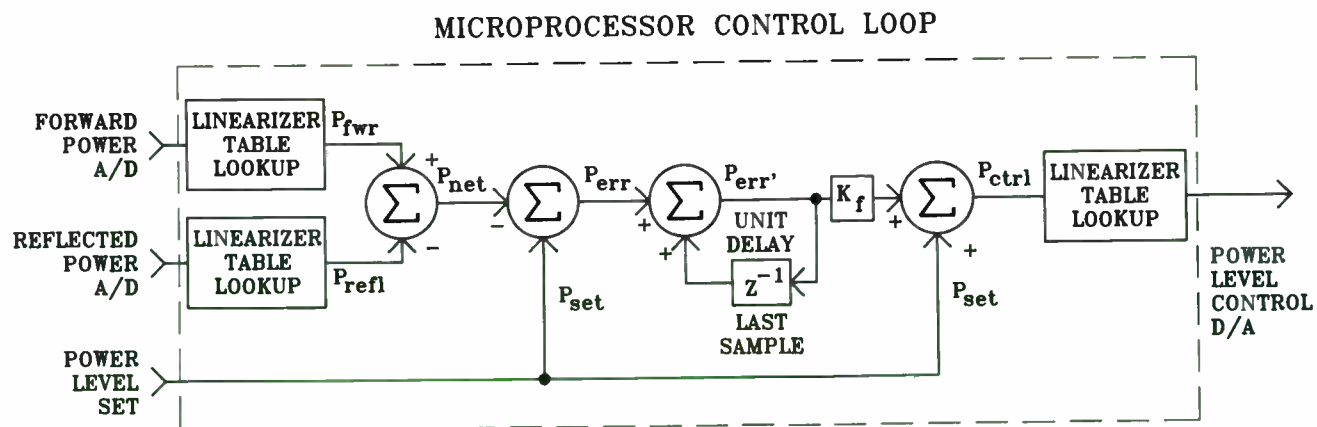


FIGURE 3

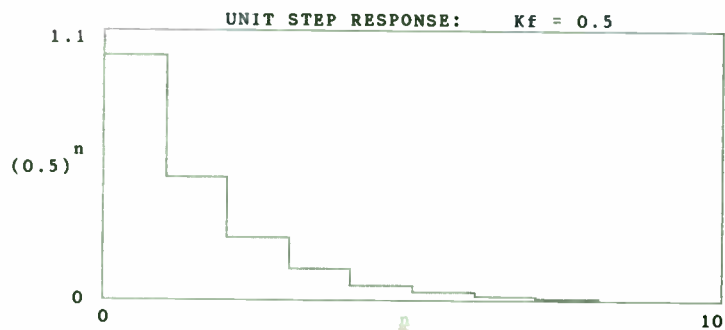


Figure 4a

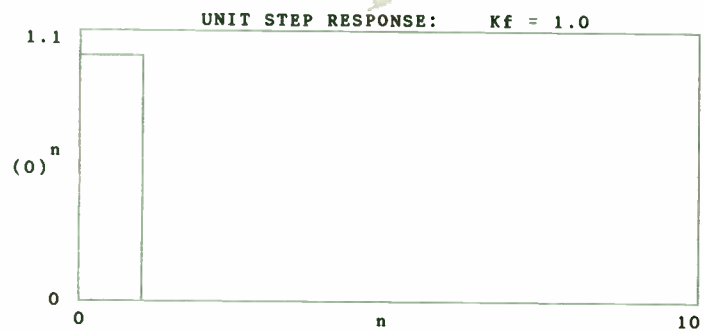


Figure 4b

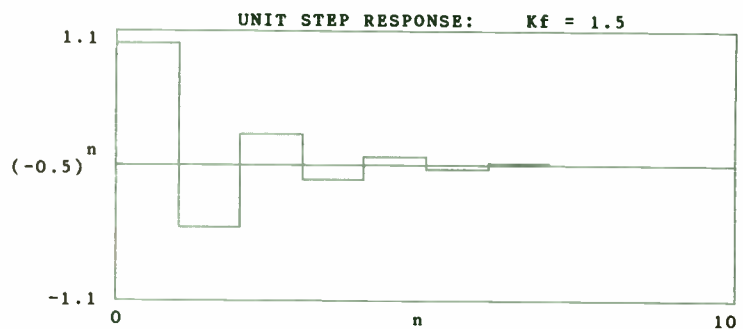


Figure 4c

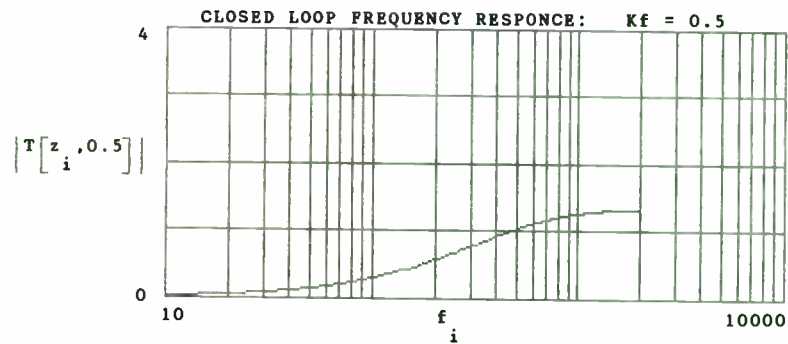


Figure 5a

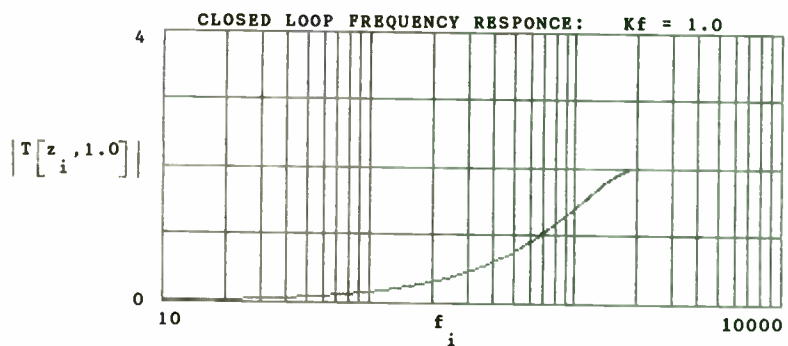


Figure 5b

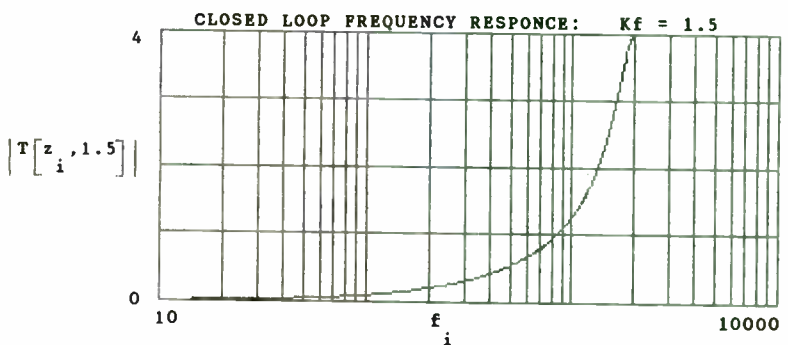


Figure 5c

High-Frequency, High-Power Operation of Static Induction Transistors At Cryogenic Temperatures

M. Abdollahian, R. Regan, S. Butler, R. Gage and E. Bulat
GTE Laboratories Incorporated
40 Sylvan Road
Waltham, MA 02254

Abstract

Silicon static induction transistors (SITs) have proven themselves well-suited for HF, VHF, and UHF applications. Various device designs and amplifier circuit configurations have been implemented to demonstrate high-power (CW and pulsed) UHF performance and broadband HF/VHF performance. This paper describes the results of recent experiments with high-power surface gate SITs operated at and below liquid nitrogen temperatures. The device DC current-voltage characteristics were measured from 4.2 K to 300 K and large-signal parameters such as transconductance (G_m) and on-resistance (R_{ON}) were derived from these measurements to demonstrate their influence on the RF performance of the device. The parameters measured at 30 K were incorporated into a small-signal equivalent circuit model to predict gain-bandwidth performance. The UHF power performance of liquid-nitrogen-cooled SIT power amplifiers is also described. A single-ended power amplifier has been fabricated which exhibits output power levels greater than 350 W cw at 425 MHz with 8 dB gain and nearly 80% drain efficiency. Smaller test devices have been used in an 850 MHz amplifier, which exhibits 30 W cw with 7.8 dB gain and 65% drain efficiency.

Introduction

Silicon static induction transistors (SITs) have been implemented to demonstrate high power (cw and pulsed) UHF performance and broadband HF/VHF power performance at supply voltage levels that are unattainable with other device technologies.¹⁻¹⁶ The attributes of SITs make them attractive for use in a wide array of applications. In particular, the experimental efforts described here are applicable to RF driver amplifiers for particle beam accelerators or nuclear magnetic resonance imaging and spectroscopy systems which require operation of devices at or near cryogenic temperatures. The recent research activity in high temperature superconductor

technology may lead to RF power systems applications where liquid nitrogen would be available as the primary coolant for the entire electronics system. An SIT which exhibits enhanced performance at liquid nitrogen temperature would lead to efficient and compact power module designs.

SIT Operation

SITs are short-channel effect junction FETs in which the current flowing vertically between the source and drain, is controlled by the height of an electrostatically induced potential barrier under the source. Since the channel current is due to majority carriers and the barrier is controlled electrostatically by the reverse-biased gate junction, no minority-carrier charge storage effects are present. The carriers travel at saturated drift velocity in the drift region beyond the potential barrier thereby allowing a relatively long drift region and thus, higher voltage operation.

The short-channel effect in the SIT results in a near exponential dependence of the drain current on the drain voltage, since an increase in drain voltage alters the height of the potential barrier induced by the gate bias. Hence, the SIT exhibits current-voltage characteristics similar to that of a triode vacuum tube. At average and high current density levels, the drain current exhibits a negative thermal coefficient, which makes the SIT suitable for high power operation with no concern for thermal runaway.

SIT Current-Voltage Characteristics Dependence on Temperature

The DC current-voltage (I-V) characteristics for a 7 μm pitch test SIT were measured using a curve tracer, with the device sitting at an ambient temperature of 300 K, when immersed in liquid nitrogen ($T = 77$ K), and when mounted in an exchange-gas cryostat at 30K. Figure 1 shows the I-V characteristics of the device for all three temperature conditions. DC characteristics were measured with a limiting value of source-to-gate bias voltage of 0.7 V (forward biased); this corresponds to the actual saturation condition in a high frequency amplifier utilizing SITs. As shown in the figure a substantial improvement in transconductance and a large reduction in dynamic drain resistance is observed at lower temperatures. These significant improvements are accompanied by a reduction in saturation voltage (directly related to on-resistance), which allows higher efficiency operation at the lower temperatures. The improvements in the DC I-V

characteristics of the device can be attributed to the enhanced mobility and saturated velocity as well as to a reduction in parasitic resistances (metallization and contact) at 77 K. In particular, parasitic source resistance results in substantial degenerative feedback thereby increasing on-resistance and reducing transconductance.¹⁷ Reducing this parasitic resistance has a marked, positive impact on the rf output power, gain, and efficiency performance of the device.

To obtain a more detailed set of dc data, the changes in the I-V characteristics of a 7 μm pitch SIT were measured as a function of surface temperature from 10 K to 300 K. Packaged SITs were mounted in a liquid-helium exchange-gas cryostat and measurements were performed at various temperatures between 4 K and 300 K. A Tektronix/Sony 377 curve tracer was used in a single shot measurement mode to eliminate self heating effects. Figure 2 illustrates the I-V characteristics of a 7 μm pitch SIT at 300 K, 77 K and 11 K. As shown, the saturation voltage, large signal transconductance and small signal transconductance all improve dramatically at 11 K compared to 77 K. Figure 3 illustrates the temperature dependence of two important large signal SIT characteristics. The on-resistance, (measured at Vd=10v) which is directly proportional to the saturation voltage and therefore to the maximum achievable output power and efficiency, and the large signal transconductance which is directly proportional to the gain and power added efficiency. As shown in this figure the characteristics continue to improve as the temperature drops. The improvements in transconductance and on resistance can be attributed primarily to the enhanced mobility and saturated velocity at lower temperatures. Only a slight improvement in the small signal blocking voltage gain is observed at 11 K. This indicates that the improvements in the mobility and saturated velocity have a dominant effect on the device performance compared with carrier freeze-out. At room temperature, the voltage gain of the device is strongly dependent on the carrier concentration and one would expect that the effective carrier concentration at temperatures below 100 K (carrier freeze-out range) would lead to higher blocking voltage gains and higher saturation voltages. Nevertheless, carrier freeze-out does indeed improve the device performance with respect to capacitance-voltage characteristics as shown in Figures 4 and 5. These figures illustrate that the terminal capacitances of the devices at 77 K reach punch-through at much lower voltages than observed at room temperature. This condition should lead to improved linearity in a cryogenically cooled SIT power amplifier. As one would expect the junction breakdown voltage levels are somewhat lower at 77 K. We have observed gate-drain breakdown voltages of 140 V for SITs which typically exhibit 160-165 V breakdown voltages at room temperature.

These measurements were also applied to incremental SIT equivalent circuit models to predict the improvements in frequency response at low temperatures. Figure 6 illustrates the small-signal

frequency response of a common-source SIT at 300 K and at 30 K. This performance improvement can be primarily attributed to higher electron mobility at lower temperatures as well as higher saturated velocity. However, at 30 K electron transport is influenced by an ionization mechanism. This mechanism is caused by a tunneling process due to the induced potential.

SIT RF Performance Improvement at Cryogenic Temperatures

To correlate the RF performance enhancement at lower temperatures to the changes in the device current-voltage characteristics, a 1-cell SIT (Ws=2.3) was used to obtain I-V characteristics at 77 K and 400 K (the surface temperature of the device at maximum output power). These measurements were used to derive the output power and gain for 1-cell common-gate SIT at both 77 K and 400 K. As is the case for BJTs and MOSFETs, the on-resistance of the SIT limits the maximum output voltage swing thus limiting the maximum output power. Saturation occurs when the minimum instantaneous drain voltage is equal to the product of drain current and on-resistance (Vsat). Figure 7 illustrates the DC I-V characteristics at 77 K and 400 K with the corresponding load lines.

Maximum output power is given by:

$$P_{o_{max}} = \frac{(V_{dd} - V_{sat})^2}{2R_L}$$

where,

$$V_{sat} = I_{dmax} \cdot R_{on}$$

Given a constant load line at a drain voltage of 70 V and load resistance of 155 Ω, maximum output power can be calculated using the above expressions for various operating temperatures. For the case where T = 400 K, the on-resistance calculates to be 26 Ω, resulting in a maximum output power of 10.8 W. With the operating temperature at 77 K, the on-resistance calculates to be 9 Ω, resulting in a calculated output power maximum of 14 W, a 30% increase.

For a common-gate configuration, the power gain expression is:

$$G_p = 10 \log(g_m R_L)^2 \frac{R_i}{R_L}$$

Table 1 below presents the performance characteristics for the device at 400 K and at 77 K and makes use of the power gain expression to calculate the gains shown in the last column.

Table 1.

Temperature K	Transconductance gm, mS	Input Resistance Ri, Ω	Load Resistance RL, Ω	Power Gain Gp
400	100	10	155	11.9
77	200	5	155	14.9

As indicated the 77 K data shows a 3 dB increase in gain.

All of the above calculations assume a constant and identical load line at both operating temperatures. As shown in Figure 7, at lower temperatures the load line can be raised by lowering R_L , due to the low saturation voltage levels. This should result in further improvements in the performance of the device.

UHF Power SIT Performance with Liquid Nitrogen Cooling:

The cryogenic power amplifier test chamber shown in Figure 8 has been utilized in the system shown in Figure 9 to test the performance of 425 MHz power SITs. This chamber is constructed primarily of plexiglas and was designed to permit operation of packaged power transistors in a test fixture amplifier cooled with flowing cryogenic liquids. The device under test and all associated circuit components are contained within the plexiglas chamber and continuously pressurized with dry nitrogen so that condensation will not form on the components during testing. In addition, adjustable open ports are designed into the unit to permit both tuning of the input and output impedance matching networks and monitoring of the surface temperature of the semiconductor

while the device is under test.

An experimental single-ended power SIT was tested in this system to observe the performance advantages of this enhanced cooling system. The SIT under test contained 22 cells; each cell containing 2.3 cm of total source length for a total of 50.6 cm. Processing and process development for this type SIT was conducted under both GTE Labs funded research programs and government funded contract research programs aimed primarily at improving cell yield with concomitant high power and efficiency performance. Output power performance at 425 MHz was 280 watts cw ($P_o = 5.5 \text{ W/cm}$) with the flange cooled with water as indicated on Figure 10a. As shown in Figure 10b, the same size device provided 350 watts of cw power ($P_o = 6.9 \text{ W/cm}$) with 8 dB gain and 74 percent efficiency using the liquid-nitrogen-cooled heat-sink. In each case the device was operated at 71 volts dc and biased for class C-operation.

The 850 MHz power performance of several two-cell 7 μm pitch SITs mounted on liquid-nitrogen-cooled heatsinks also have been examined. Load pull measurements were performed with one of these devices using a specially designed test fixture similar to that employed in the 425 MHz measurements described earlier. The load pull measurements resulted in the performance shown in Figures 11 through 13 for common-gate, class B operation with a drain source potential of 70 V. As shown, an output power level of 30 W (= 6.6 W/cm) was achieved with 7.8 dB gain at a drain efficiency of 63%. The measured load and input impedances corresponding to this performance were $3.3 + j 13 \Omega$ and $11 + j 5 \Omega$ respectively. These relatively high impedance levels indicate that larger single-ended cw power SITs with output power performance levels of several hundred watts are possible.

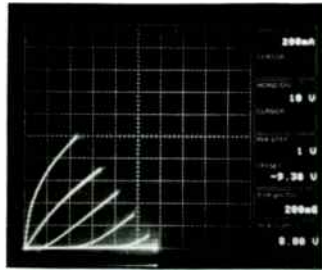
Based on the thermal resistance of the cooling block and transistor package, we estimate that the surface temperature at which the rf data shown in Figures 10b and 11 above was obtained was approximately 175 K. As shown in Figure 3, there is little change in the on resistance from 77 K to 175 K, however, the transconductance of the device improves by nearly 20% as shown in Figure 3. Therefore, the power-added efficiency and gain performance shown in Figures 10b and 11 could be further improved if lower junction temperatures could be maintained in the device under test. This could be achieved by improving the test chamber design and/or perhaps by employing other coolants at lower temperatures such as liquid neon or liquid helium. Preliminary results of dc characterization of SITs at temperatures as low as 4.2 K indicate that substantial performance improvements can be realized at lower temperatures.

Acknowledgements:

The authors gratefully acknowledge M. Delaney for her work in device packaging; P. Palermo for his contributions to the device package and test fixture design; J. Larsen for his contributions in device characterization; and B. Devlin and M. Sullivan for their work in device process engineering and fabrication. Their careful work and dedication have been essential to the realization of these results.

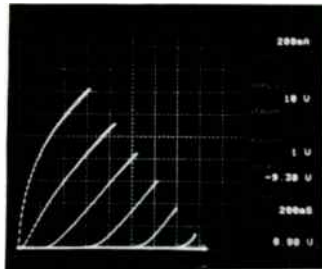
References:

- 1 Yukimoto, Y. Kajiwara, Y. Nakamura, G. and Aiga, M. 1 GHz 20 W Static Induction Transistor Japan. J. Appl. Phys. 17, Supplement 17-1, (1978) 241
- 2 Kajiwara, Y. Yukimoto, Y. and Shirahata, K. High Power Microwave Static Induction Transistor IEEE MTT-S International Microwave Symposium Digest (1977)
- 3 Nishizawa, J. and Yamamoto, K. High-Frequency High Power Static Induction Transistor IEEE Trans. Electron Dev. ED-25 (1978)
- 4 Aiga, M. Higaki, Y. Kato, M. Kajiwara, Y. and Yukimoto, Y. 1 GHz, 100 W Internally Matched Static Induction Transistor Proc. European Microwave Conf., (1979)
- 5 Shino, T. Kamo, H. and Okano, S. New SIT Structure Exceeds 10 W at 2 GHz Microwaves February (1980)
6. Shino, T. Kamo, H. Akoi, K. and Okano S. 2 GHz High Power Silicon SITs Japan. J. Appl. Phys. 19, Supplement 19-1 (1980) 283
- 7 Xian-e, C. Ping-hai, Z. and Wen-rui, Q. L-Band Silicon Power V-FET Proc. IEEE MTT-S (1982) 74
- 8 Cogan, A. Regan, R. Bencuya, I. Butler, S. and Rock, F. High Performance Microwave Static Induction Transistors Int. Electron. Dev. Meeting (1983) 221-224
- 9 Regan, R. Cogan, A. Butler, S. Bencuya, I. and Haugsjaa, P. Improved Performance of High-Voltage Microwave Power Static Induction Transistors Proc. 14th European Microwave Conference (1984)
- 10 Kane, M. and Frey, R. The PSIFET Emerges as a New Contender Microwave Systems News Vol. 14 No. 10 (1984)
- 11 Bencuya, I. Cogan, A. Butler, S. and Regan, R. Static Induction Transistors Optimized for High Voltage Operation and High Microwave Power Output IEEE Trans. Electron Dev. (1985) 32 1321-1327
- 12 Regan, R. Bencuya, I. Butler, S. Stites, F. and Harrison, W. New UHF Power Transistor Operates at High Voltage Microwaves and RF (1985) 24
- 13 Regan, R. and Butler, S. High Voltage UHF Power Static Induction Transistors Proc. RF Technology Expo (1985)
- 14 Butler, S. and Regan, R. High Voltage HF/VHF Power Static Induction Transistor Amplifiers Proc. RF Technology Expo (1986)
- 15 Regan, R. Butler, S. Bulat, E. Varallo, A. Abdollahian, M. and Rock, F. HF/VHF/UHF Power Static Induction Transistor Performance Proc. RF Technology Expo East (1986)
- 16 Regan, R. Butler, S. Armiento, A. and Rock, F. Static Induction Transistors: HF to X-Band Microwave Journal (1987)
- 17 Yamaguchi, K. and Kodera, H. Optimum Design of Triode-Like JFETs by Two-Dimensional Computer Simulation IEEE Trans. Electron. Dev. (1977) 24 1061-1069
- 18 Smith, R. Semiconductors 2nd Edn Cambridge University Press, Cambridge, UK (1978) Ch 5, 143-145



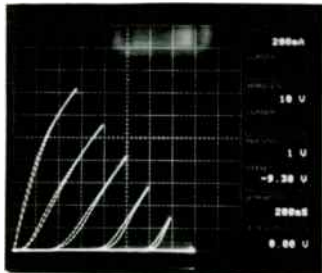
T = 300 K

$G_m = 285 \text{ ms}$
 $\mu = 20$
 $R_{on} = 15 \Omega$



T = 77 K

$G_m = 470 \text{ ms}$
 $\mu = 20$
 $R_{on} = 12 \Omega$

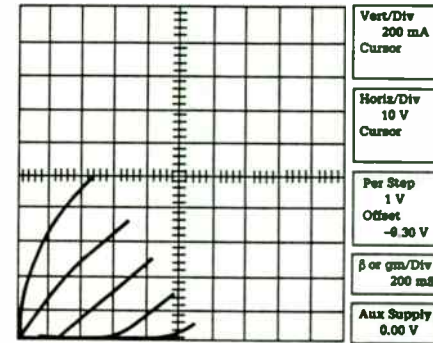


T = 30 K

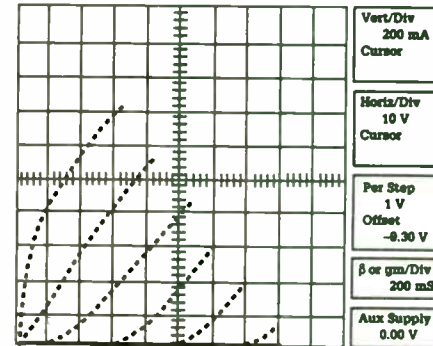
$G_m = 620 \text{ ms}$
 $\mu = 20$
 $R_{on} = 14 \Omega$

G_m measured at $V_D = 40 \text{ V}$ and $I_D = 200 \text{ mA}$; R_{on} measured at $V_D = 10 \text{ V}$.

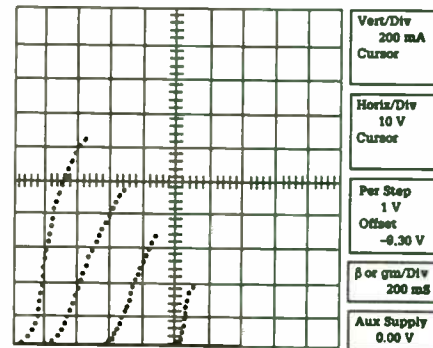
Figure 1. Current-voltage characteristics of two-cell ($W_s = 4.6 \text{ cm}$), $7 \mu\text{m}$ pitch SIT; (a) room temperature ($T = 300 \text{ K}$), (b) immersed in liquid nitrogen ($T = 77 \text{ K}$), and (c) in helium exchange-gas cryostat ($T = 11 \text{ K}$).



T = 300 K



T = 77 K



T = 11 K

Figure 2. Current-voltage characteristics of two-cell, $7 \mu\text{m}$ pitch SIT at 300 K, 77 K, and 11 K.

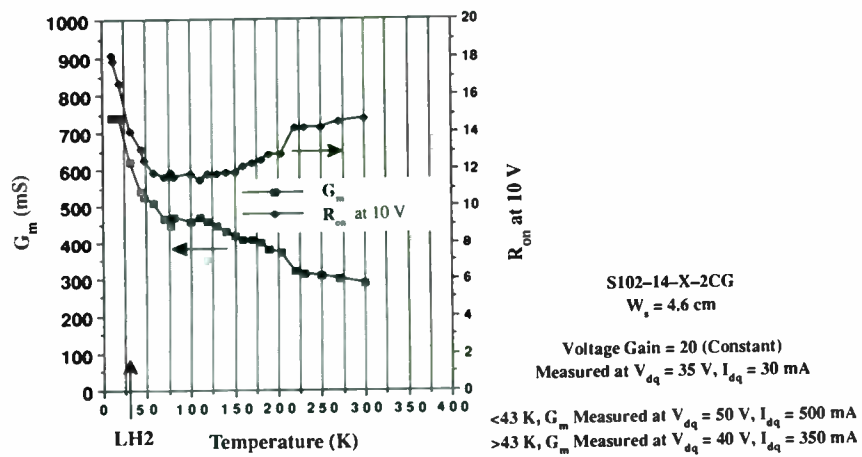


Figure 3. Temperature dependence of large-signal SIT characteristics.

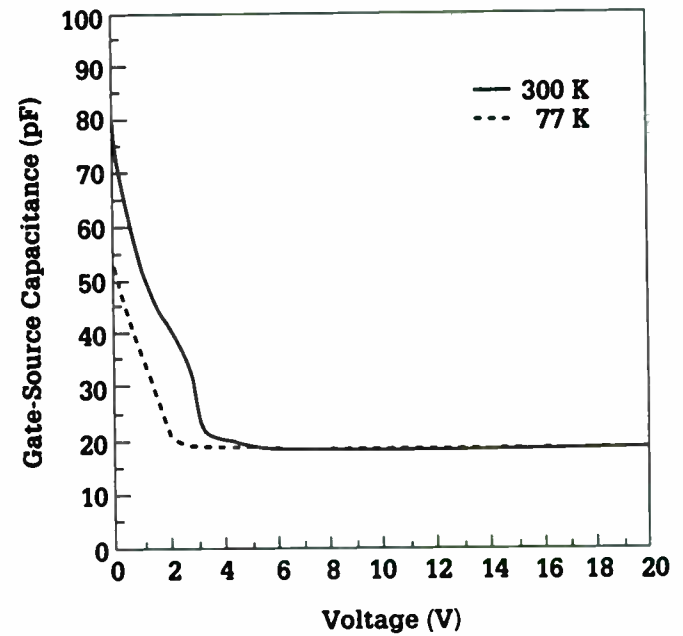


Figure 4. Capacitance-voltage characteristics of SIT gate-source junction at 300 K and 77 K.

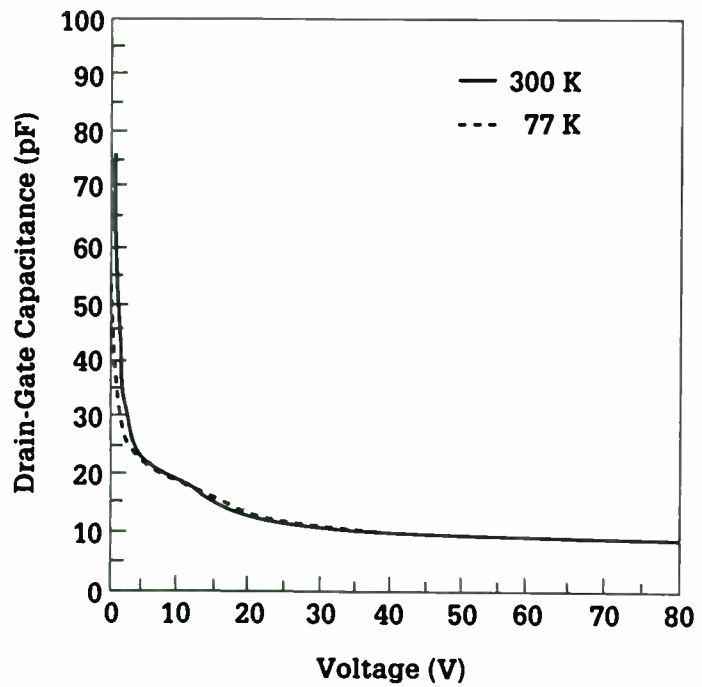


Figure 5. Capacitance-voltage characteristics of SIT drain-gate junction at 300 K and 77 K.

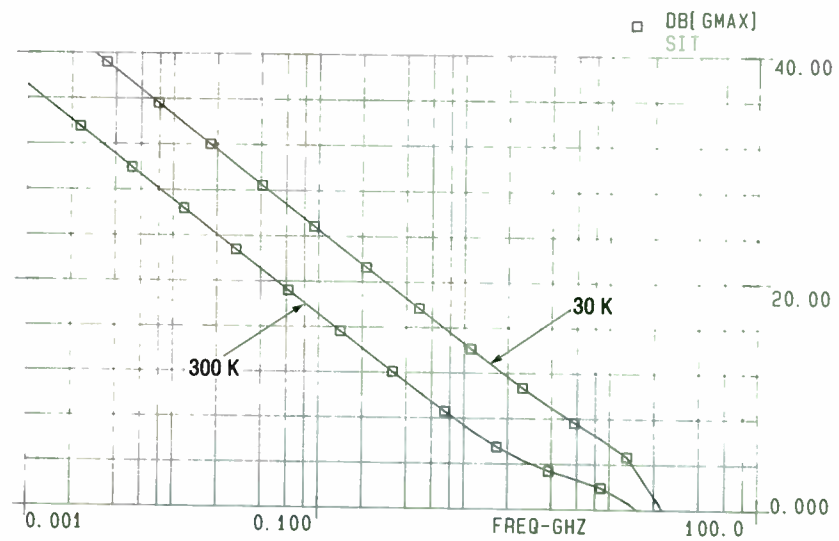
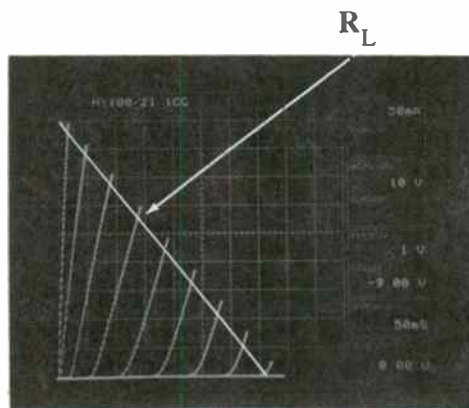
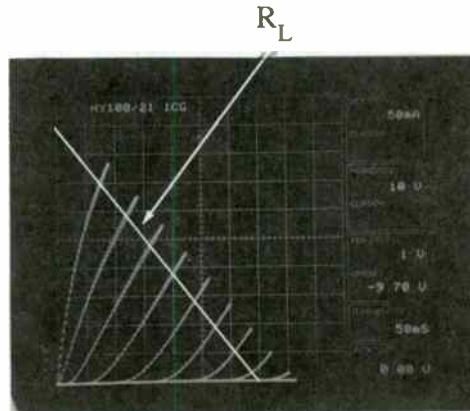


Figure 6. Small-signal gain of a common-source SIT at 300 K and 30 K.



$R_L = 155 \Omega$
 $V_{DG} = 70 \text{ V}$
 $I_{Dmax} = 450 \text{ mA}$
 $V_{sat} = 4 \text{ V}$
 $R_{on} = 9 \Omega$
 $P_{o max} = 14 \text{ W}$

$T = 77 \text{ K}$



$R_L = 155 \Omega$
 $V_{DG} = 70 \text{ V}$
 $I_{Dmax} = 450 \text{ mA}$
 $V_{sat} = 12 \text{ V}$
 $R_{on} = 26 \Omega$
 $P_{o max} = 10.8 \text{ W}$

$T = 400 \text{ K}$

Figure 7. DC-IV characteristics of a 1 cell-SIT at 77 K and 400 K with the corresponding load lines.

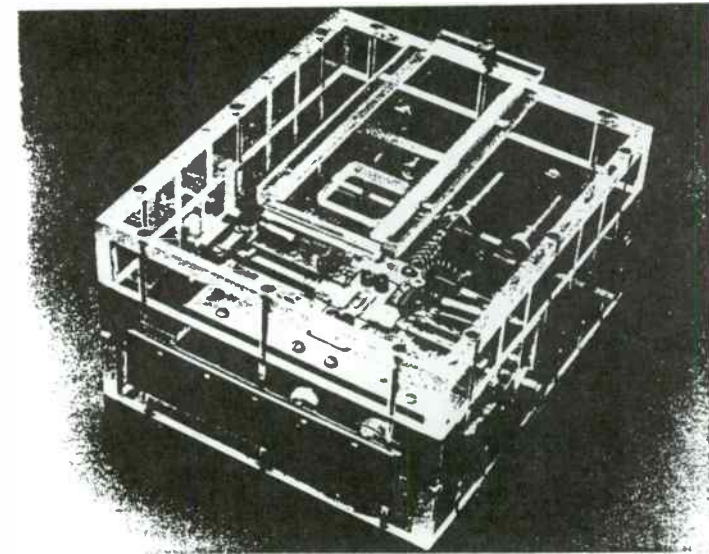


Figure 8. Cryogenic power amplifier test chamber.

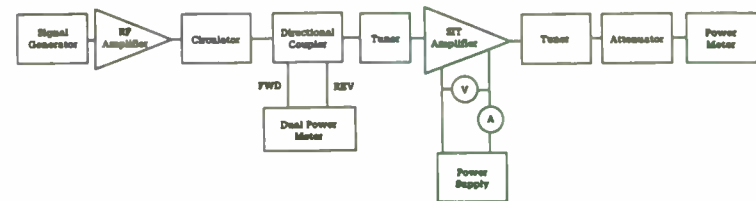
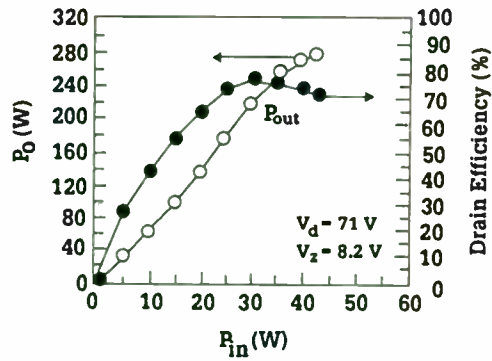
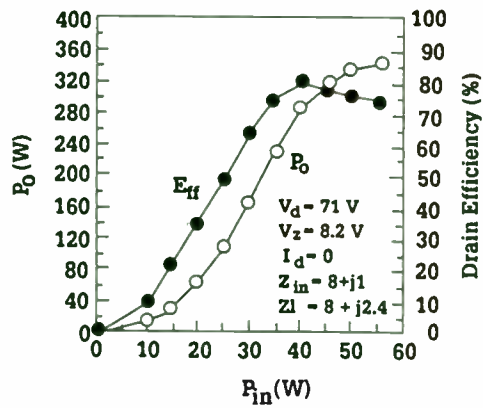


Figure 9. Experimental UHF load-pull instrumentation.



(a)



(b)

Figure 10. 425 MHz output power and efficiency performance of a single-ended SIT test fixture amplifier; (a) with water-cooled heatsink and (b) with liquid-nitrogen-cooled heatsink.

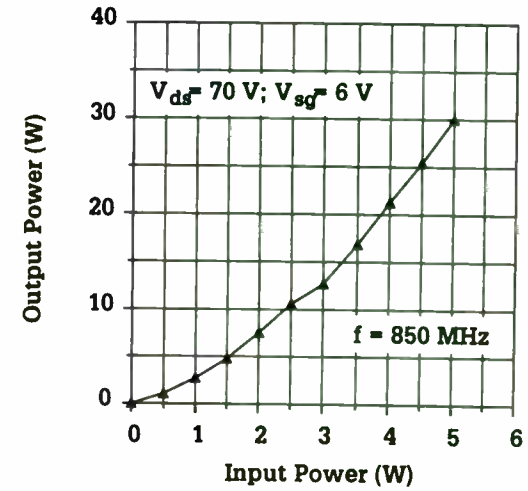


Figure 11. 850 MHz output power performance of a two-cell SIT with liquid nitrogen cooling.

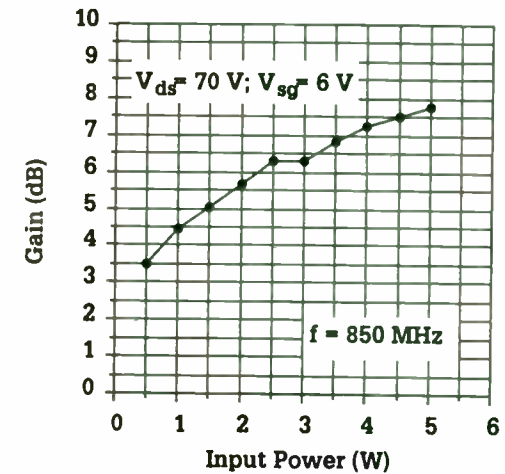


Figure 12. Measured 850 MHz gain characteristics of a two-cell SIT with liquid nitrogen cooling.

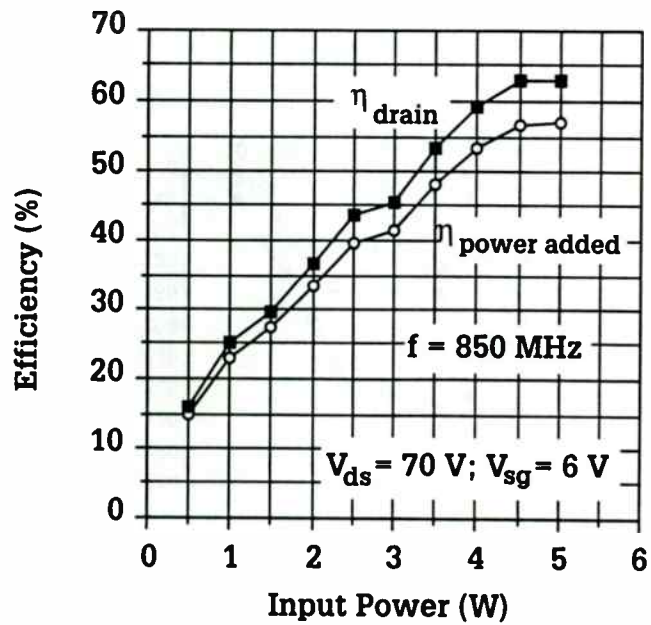


Figure 13. Measured power-added efficiency and drain efficiency of a liquid-nitrogen-cooled two-cell SIT at 850 MHz.

SURFACE ACOUSTIC WAVE (SAW) TECHNOLOGY

A TUTORIAL FOR
RF EXPO EAST 1990

by
Carl A. Erikson, Jr.

Messiah College
Grantham, PA.
&
Oakmont Enterprises
Dillsburg, PA.

Outline for SAW Tutorial

- * Introduction
- * What is a SAW Device?
- * Design
- * Fabrication
- * Testing
- * Future Trends

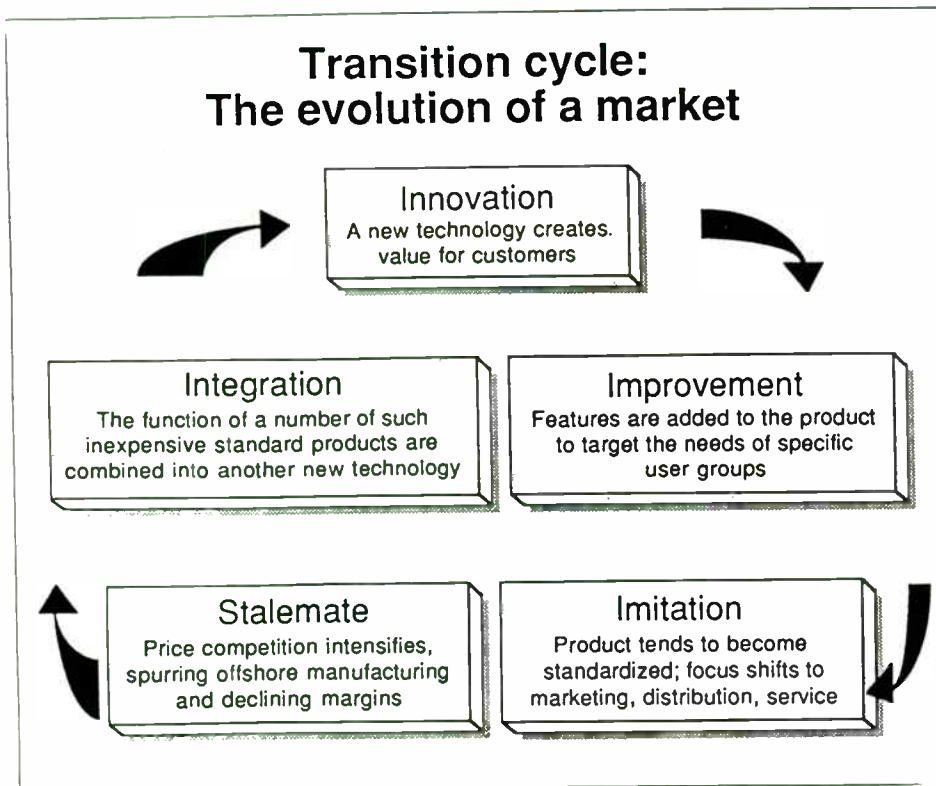
What is a SAW Device?

- *Three Parts of a SAW Device

- *Reasons for Use

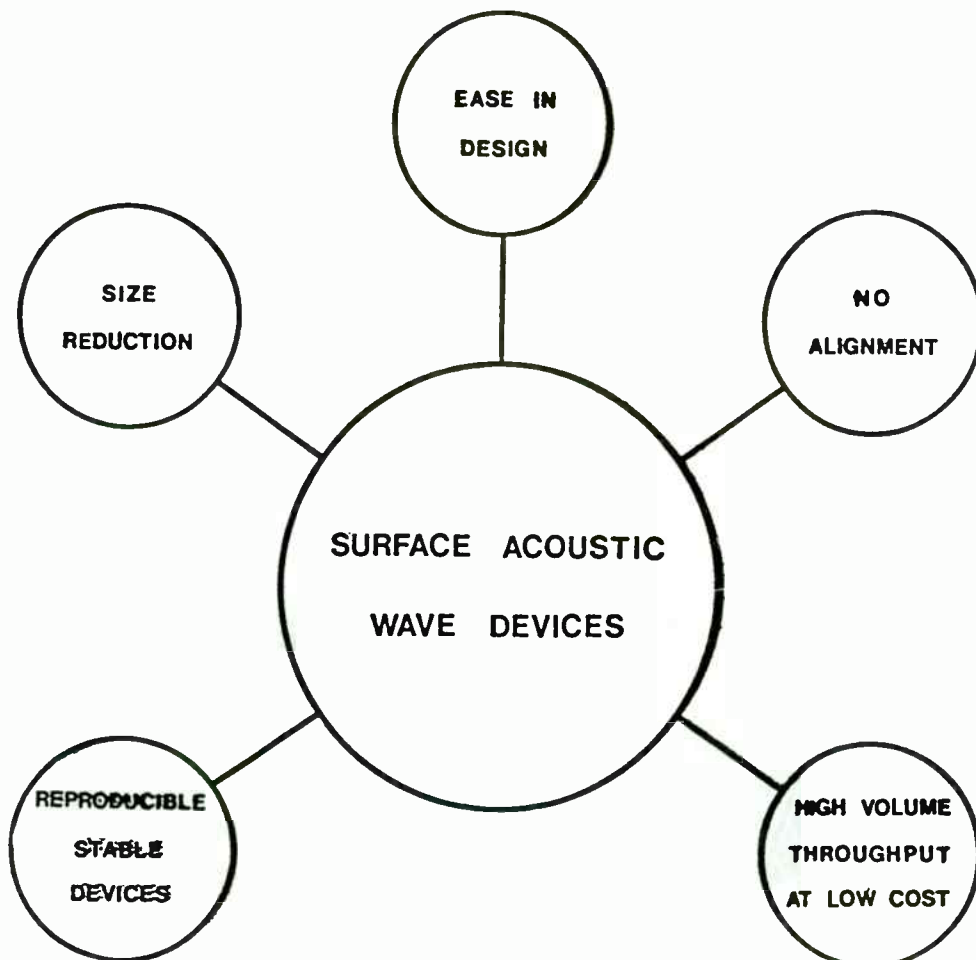
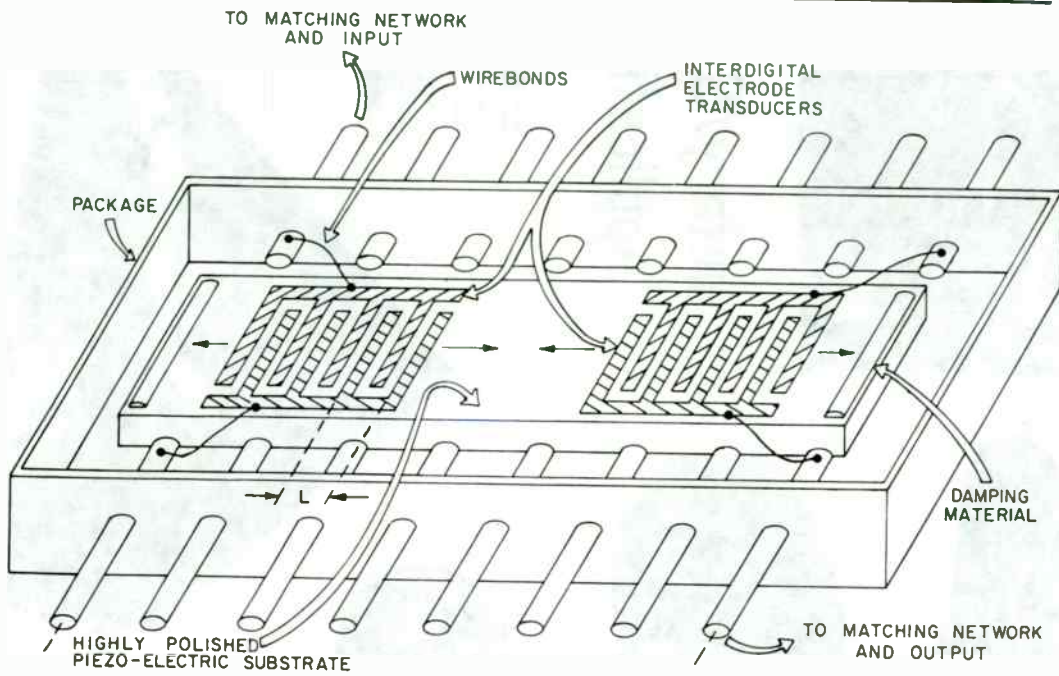
- *Types of Devices

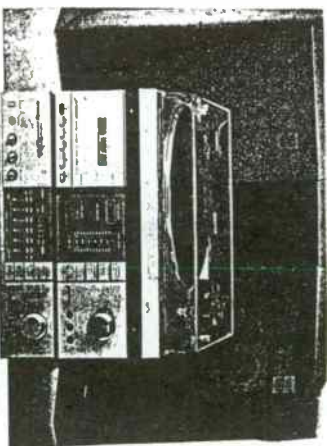
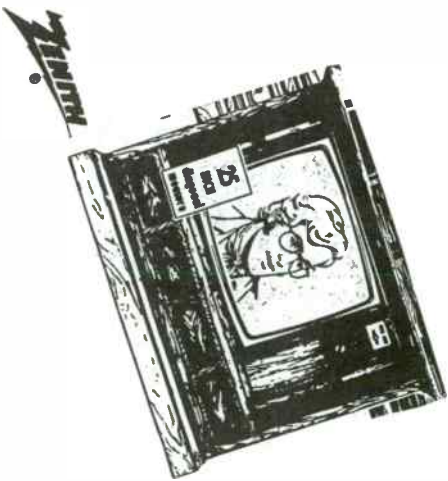
- *Applications



Taken from Electronic Business, May 15, 1986

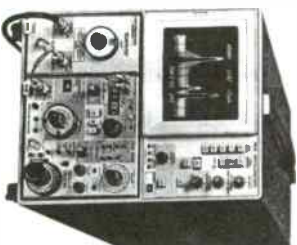
THREE PARTS OF A SURFACE ACOUSTIC WAVE DEVICE



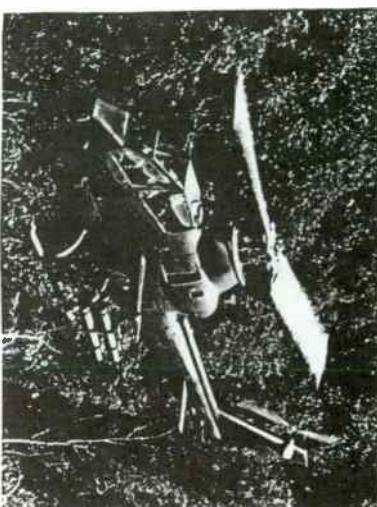


PIONEER STEREO COMPONENTS

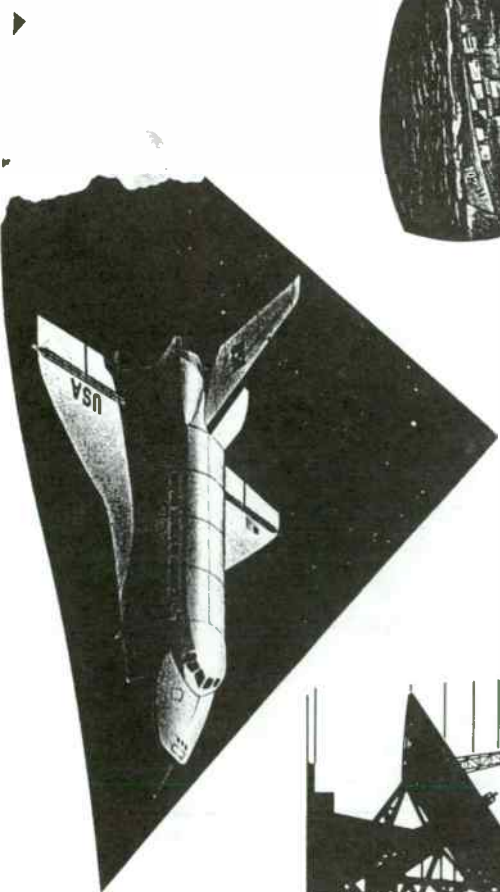
Commercial Applications



Spectrum Analyzer



Military/Space Applications



Some High Volume Commercial SAW Applications

SAW IF Filters

- CATV Converters
- MDS Mini-Hub Control Converters
- Pay TV Converters
- CATV Processors
- Satellite Receivers
- Cordless Phones
- LAN Data Systems
- Data Communication Systems
- Cellular Radio
- TV Tuner
- RF Source

SAW Output Filters

- CATV Converters
- Amplifiers
- PABX
- Data-Voice Distribution
- Satellite Receivers
- Home Computers
- Pay TV Converters

SAW Resonators

- CATV Converters
- Cordless Phones
- Subscription TV Security
- Garage Door Openers

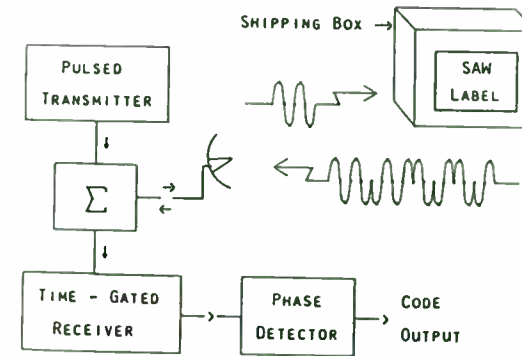


Figure 10: SAW Wireless Label System

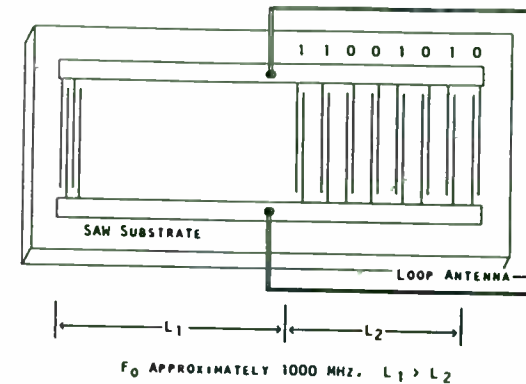


Figure 11: Coded SAW Wireless Label

taken from paper by C. S. Hartmann
 1985 Ultrasonics Symposium
 "Future High Volume Applications of SAW Devices"

SAW SENSORS

Some Physical Parameters Which Can Be Measured:

Pressure

Force

Displacement

Acceleration

Vibration/Shock

Temperature

Measurement is accomplished by noting the change in the transducer characteristics due to mechanically or thermally induced stress.

For SAW resonators and/or delay line oscillators, usually it is the frequency shift.

ADVANTAGES

Fast Response

High Sensitivity

Small Size

Good Output Signal

DISADVANTAGES

Packaging (Environmental)

Sensitive to Shock/Vibration (mounting)

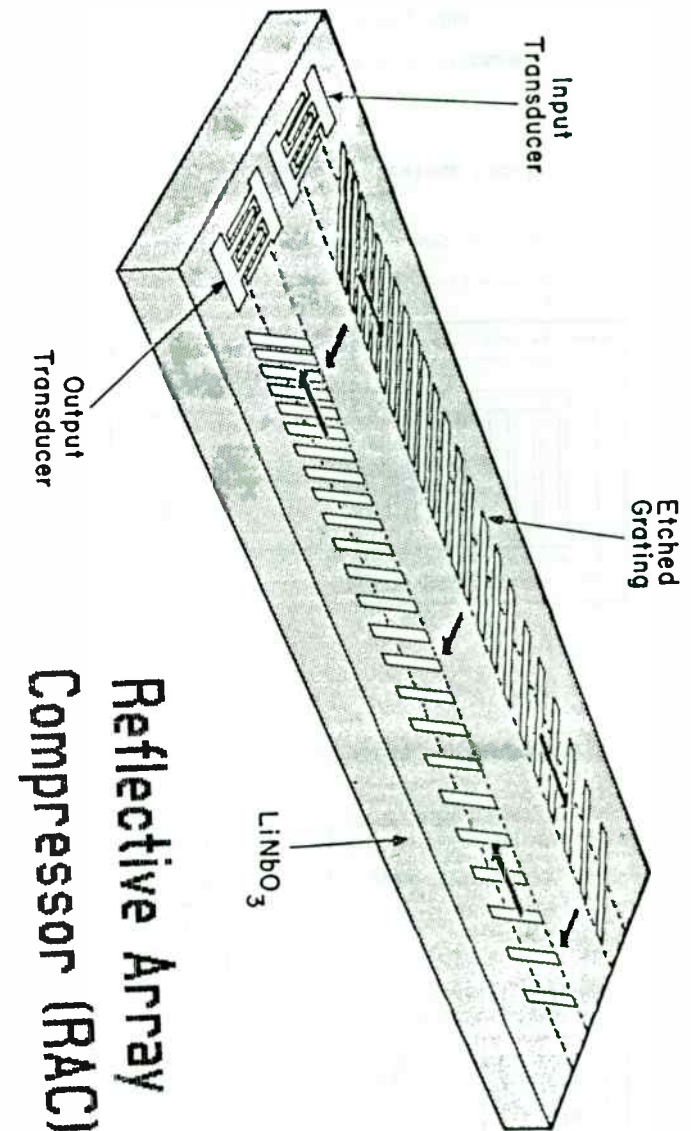
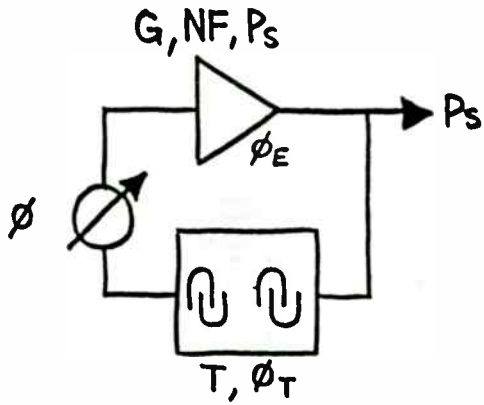


Figure 1

SAW OSCILLATORS

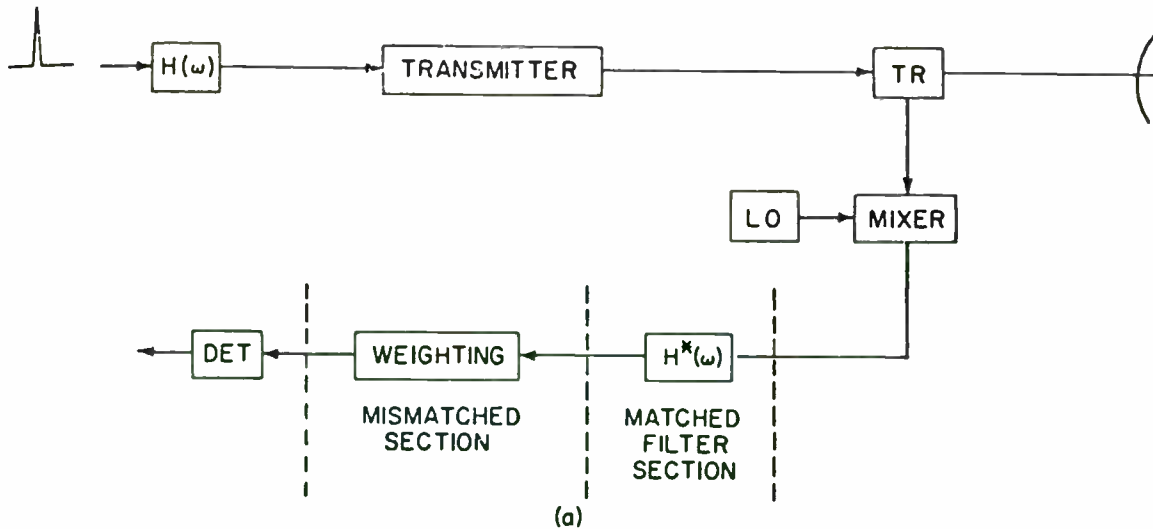
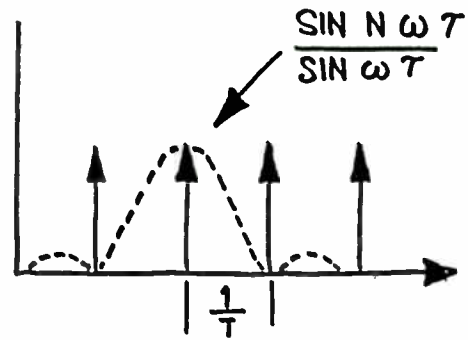
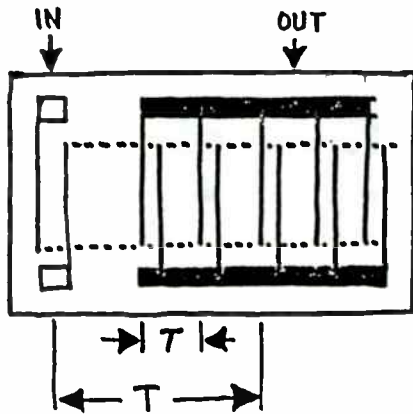


$$\phi_T + \phi_E + \phi = 2n\pi$$

$$\phi_T = 2\pi f_0 T \gg \phi_E$$

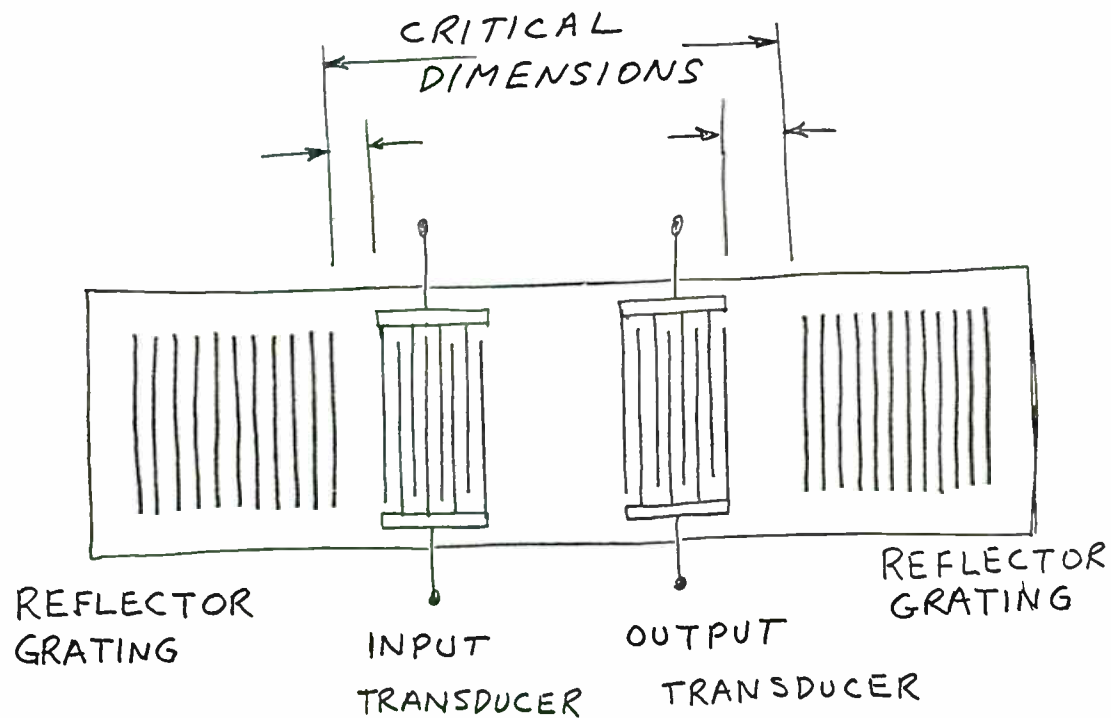
$$\Delta f_0 \leq \frac{1}{2T}$$

$$Q = \pi f_0 T$$



BASIC PULSE COMPRESSION SYSTEM

SAW RESONATOR



Design

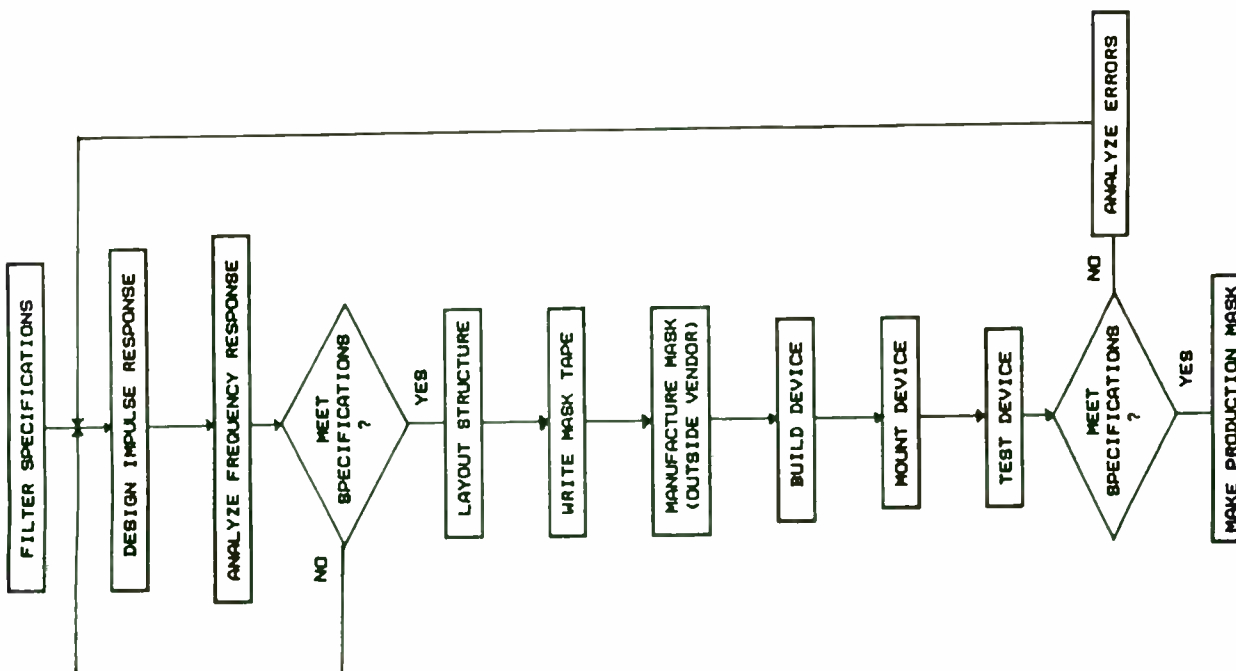
- * Substrate Considerations
- * CAD Techniques
- * Mask Design
- * Package Design

TYPICAL SAW MATERIALS

	YZ LiNbO ₃	"MDC" LiTaO ₃	ST-X QUARTZ	(001) (110) Bi ₂ GeO ₂₀
ELECTRO-MECHANICAL COUPLING CONSTANT k ²	0.044	0.0067	0.0015	0.014
RELATIVE DIELECTRIC CONSTANT	50	48	4.4	38
VELOCITY M/SEC	3488	3378	3156	1681
LINEAR TEMPERATURE COEFFICIENT OF DELAY 1/r dr/dT	94 X 10 ⁻⁶ /°C	64 X 10 ⁻⁶ /°C	0	-
TYPICAL FRACTIONAL BANDWIDTH APPLICABILITY RANGE	> 15%	5 - 15%	≤ 5%	5 - 20%

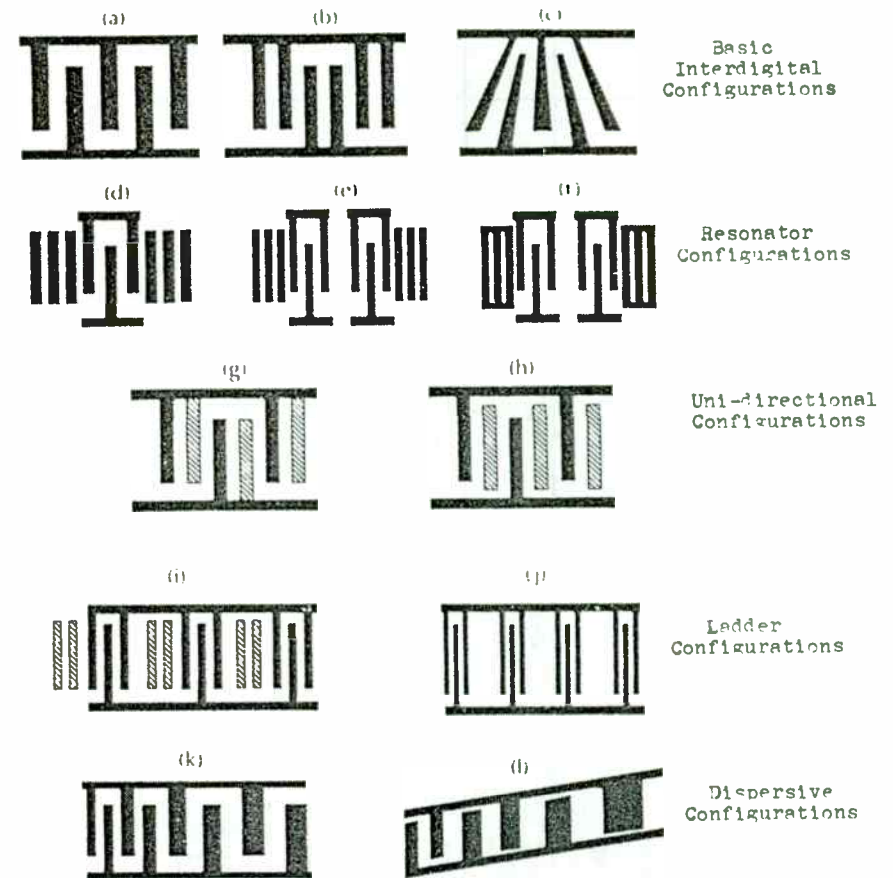
95227-23 (5-1-79)

Courtesy of W.R. Smith, Jr.



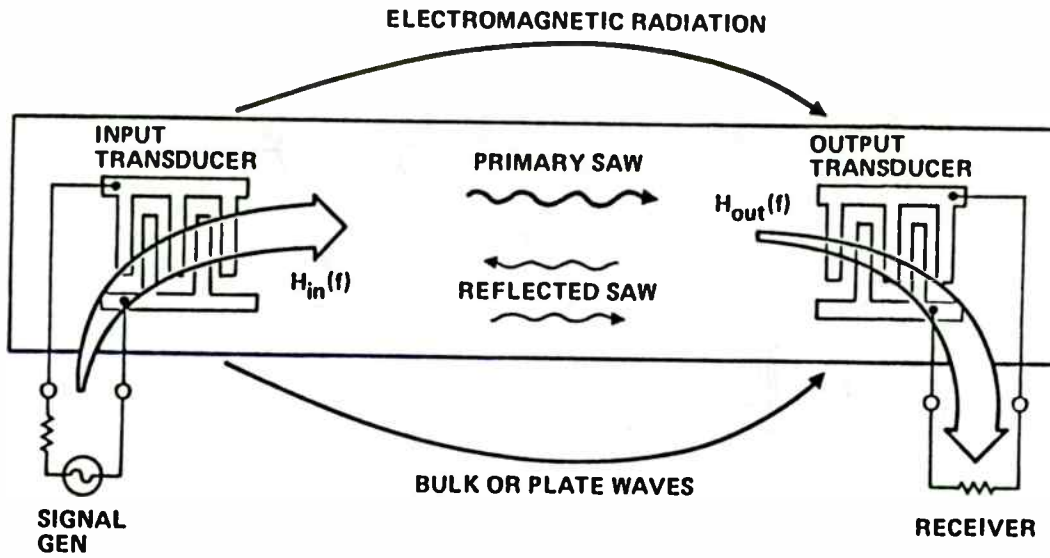
SAW WAVELENGTHS IN QUARTZ

f ₀ MHz	λ ₀ MILS	λ/4		λ/8	
		MILS	μ	MILS	μ
50	2.486	.622	15.55	.311	7.77
60	2.072	.518	12.94	.259	6.47
70	1.776	.444	11.10	.222	5.55
100	1.243	.311	7.76	.155	3.88
150	.8287	.207	5.18	.104	2.59
200	.6215	.155	3.88	.0777	1.94
300	.4143	.104	2.58	.0518	1.29
400	.3108	.0777	1.74	.0388	.971
500	.2426	.0623	1.55	.0311	.777
600	.2072	.0518	1.29	.0259	.647
700	.1776	.0444	1.11	.0222	.555
800	.1554	.0388	.972	.0194	.486
900	.1321	.0345	.864	.0173	.432
1000	.1243	.0311	.776	.0155	.388
1100	.1130	.0283	.706	.0141	.353
1200	.1036	.0259	.648	.0129	.324
1300	.09562	.0239	.598	.0120	.299
1400	.08879	.0222	.554	.0111	.277
1500	.08287	.0207	.518	.0104	.259
1600	.07769	.0194	.486	.00971	.243
1700	.07312	.0183	.458	.00914	.229



Transducer Types

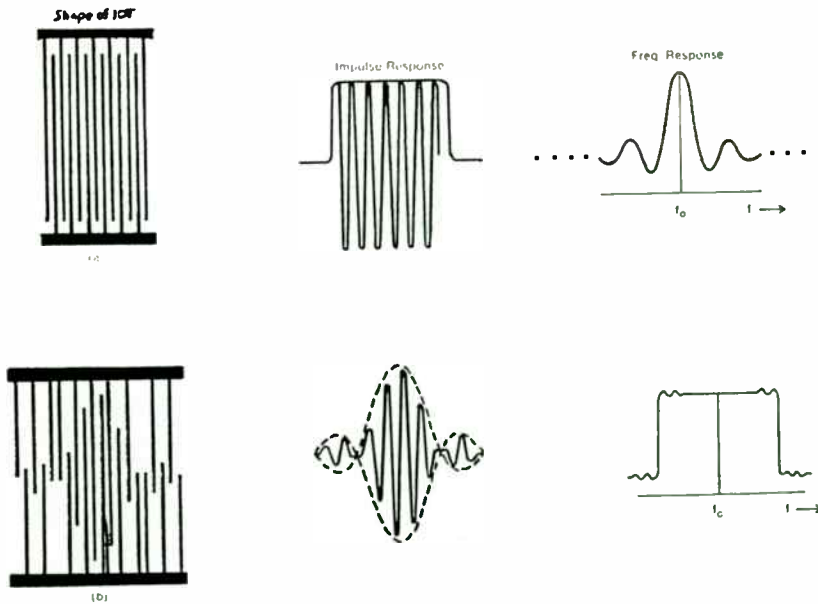
FILTER TRANSFER FUNCTION AS PRODUCT OF TRANSDUCER TRANSFER FUNCTIONS



$$H(f) \cong H_{in}(f) \cdot H_{out}(f) \cdot \exp(-j2\pi fT)$$

95227-10 (9-1-79)

Courtesy of W.R. Smith, Jr.



Two IDT configurations and the corresponding filter characteristics.

PACKAGING'S FUNCTIONS FOR SAW DEVICES

MECHANICAL SUPPORT FOR SAW SUBSTRATE

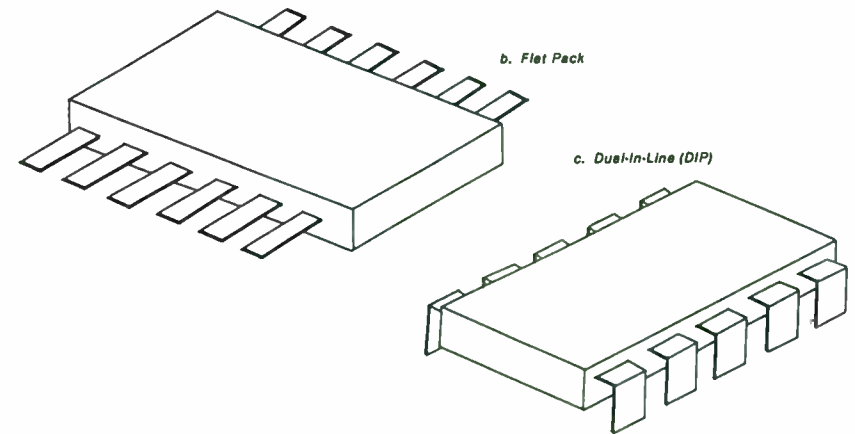
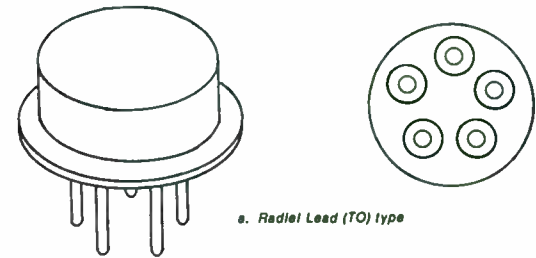
PROTECTS SAW SUBSTRATE'S SURFACE

HOUSES MATCHING NETWORKS

CONTAINS ELECTRICAL INTERCONNECTIONS

MAINTAINS HERMETICITY

Basic Hybrid Circuit Packages



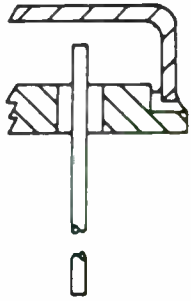
PACKAGE SEALING TECHNIQUES FOR SAW DEVICES

SOLDER	}	Small volume, Prototypes
EPOXY		
CONFORMAL COATINGS	}	High volume, Low cost
ENCAPSULATION		
COLD WELD	-	High volume T0-type
RESISTANCE WELD	-	DIPs
PARALLEL SEAM	-	Flat paks
ELECTRON BEAM	-	Large packages
LASER	-	Minimum fixturing

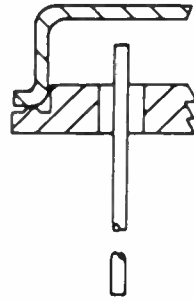
Fabrication

- * Basic Procedure
- * Clean Room Requirements
- * Additional fabrication techniques

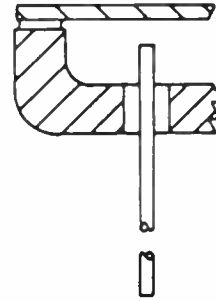
TYPES OF CLOSURES



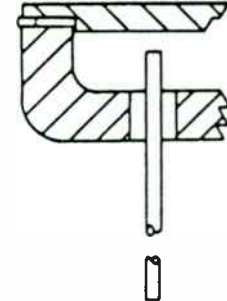
EDGE SOLDER SEAL



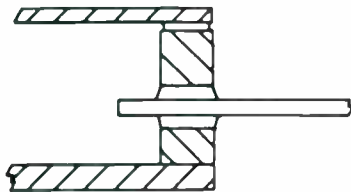
RESISTANCE WELDABLE



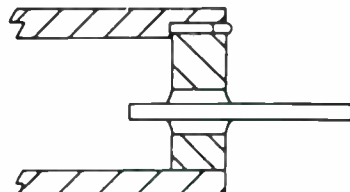
SOLID SIDEWALL SOLDER SEAL



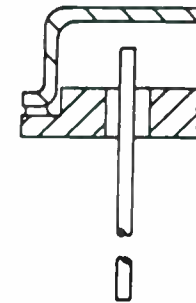
SOLID SIDEWALL SEAM OR STITCH WELD



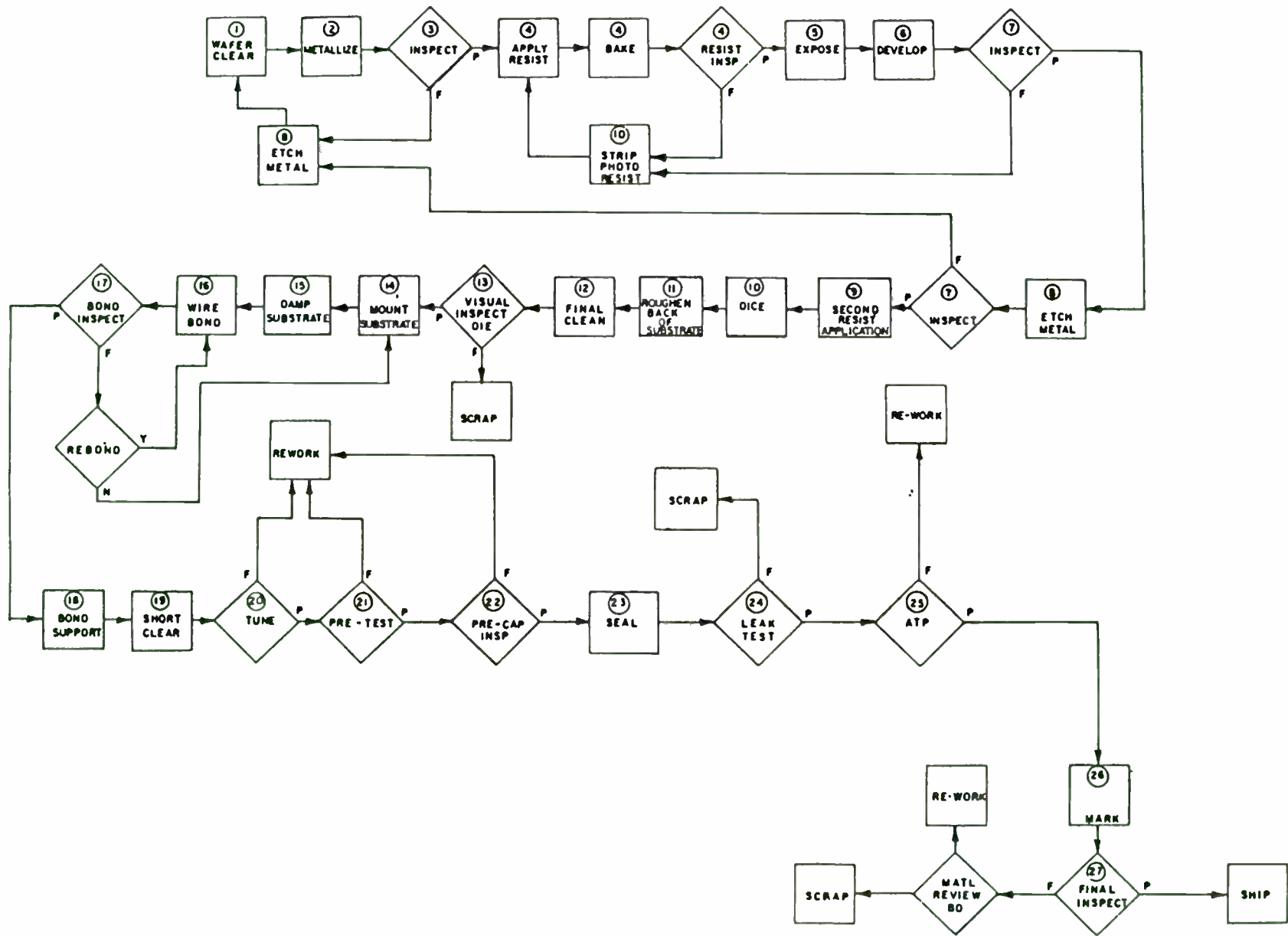
FLAT PACK SOLDER SEAL



FLAT PACK SEAM OR STITCH WELD



FLANGE SOLDER SEAL



Typical SAW Device Manufacturing Flow Diagram

Photolithography

CONTACT PRINTING (2000 - 4000 Å)

- Oldest and most widely used
- Relatively cheap
- Very fast
- Satisfactory for large areas
- Mask life limited
- Slight discrepancies from perfect flatness in the masters or substrate lead to uneven contact, so that highest resolution is not obtained over the entire field

PROXIMITY PRINTING

- Actual physical contact is avoided between mask and substrate
- Increases mask life
- Decreases resolution

PROJECTION PRINTING

- Ratios 1:1, 10:1
- Long mask life
- Can obtain variable ratios for frequency adjustment of SAW devices
- Image quality depends critically on optical alignment and lens quality

ELECTRON BEAM LITHOGRAPHY (500-2000 Å)

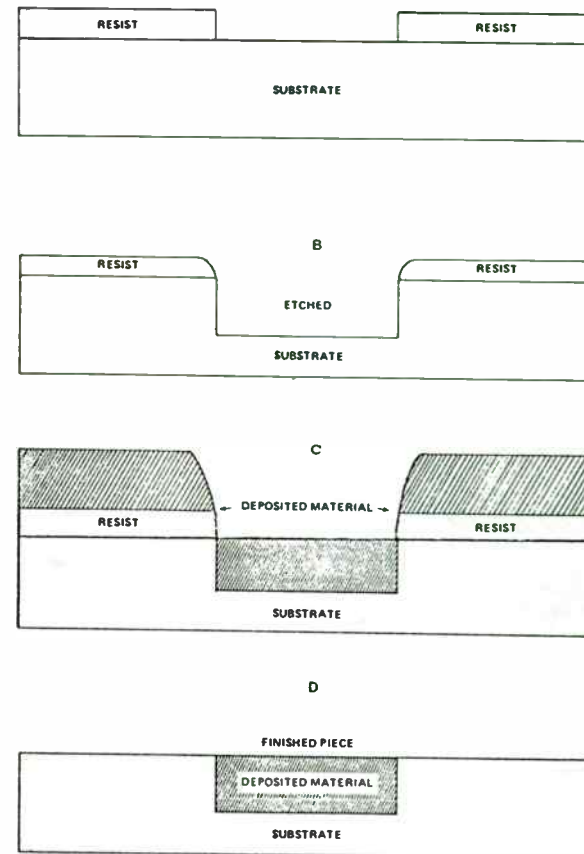
- Better resolution
- Fast turnaround
- Improved alignment capability
- Large pattern capability
- Defect control
- Vector scan vs raster scan

X-RAY LITHOGRAPHY (5 - 500 Å)

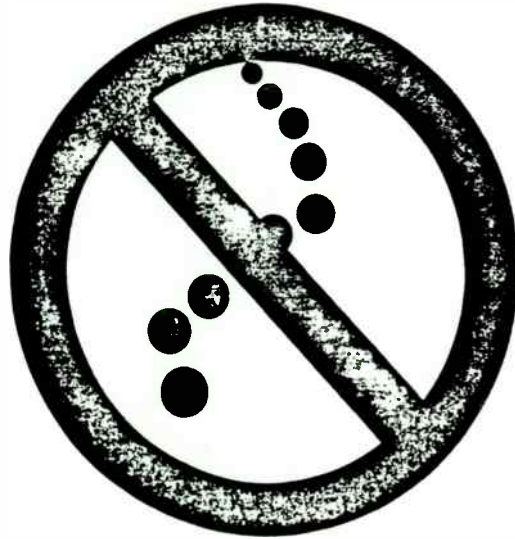
- Unequaled pattern resolution capability
- Absence of significant scattering of X-rays within the resist and substrate material
- Insensitivity to defect generation due to particle contamination
- Need EBL to generate masks

MOST IMPORTANT RESIST PROPERTIES REQUIRED FOR
PRODUCING A MICROLITHOGRAPHIC PATTERN

1. RESOLUTION
2. CONTRAST
3. FREEDOM FROM DEFECTS
4. UNIFORMITY
5. HIGH SENSITIVITY TO THE EXPOSING RADIATION
6. EASE OF PROCESSING
7. ADHESION TO THE SUBSTRATE
8. RESISTANCE TO DEGRADATION BY THE ETCHANT
9. SUBSEQUENT EASE OF REMOVAL



BASIC FABRICATION STEPS TO FORM A
BURIED INTERDIGITAL TRANSDUCER

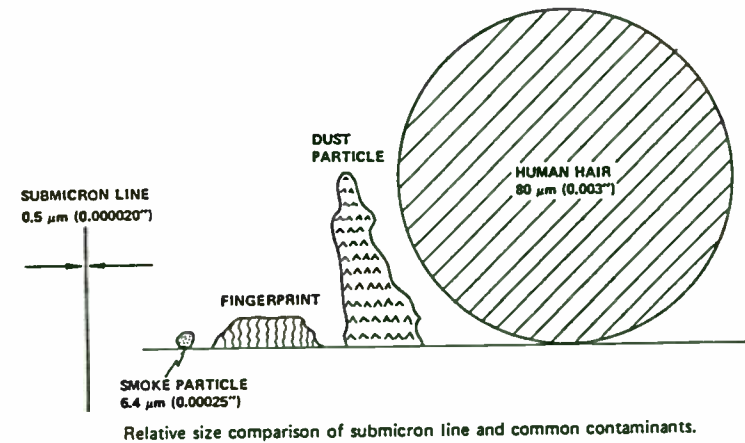


ENTRY RESTRICTED

particle control center

authorized personnel only
clean room conduct enforced
correct gowning required
approved materials only

© 2014, Ametek, Inc. 000000



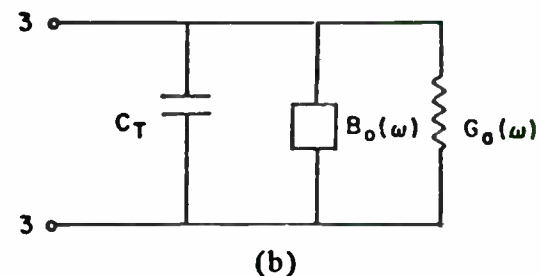
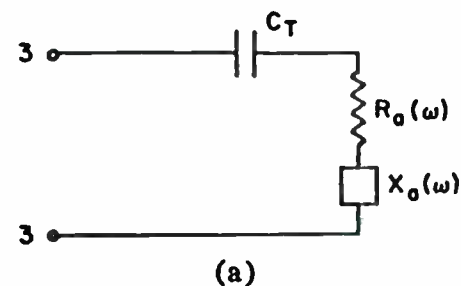
Testing

* Electrical Performance

* Testing Equipment

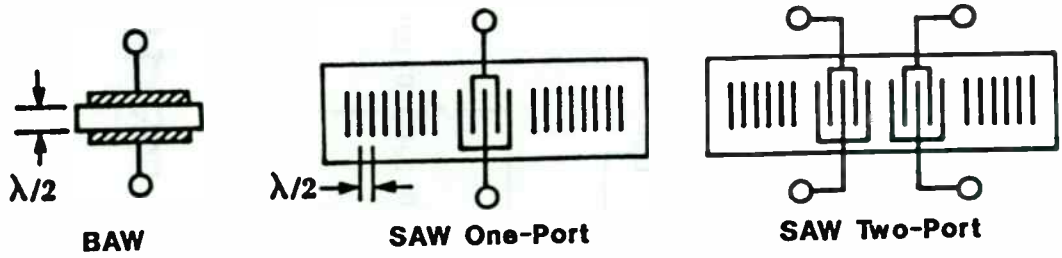
* Environmental Testing

* Military Specifications

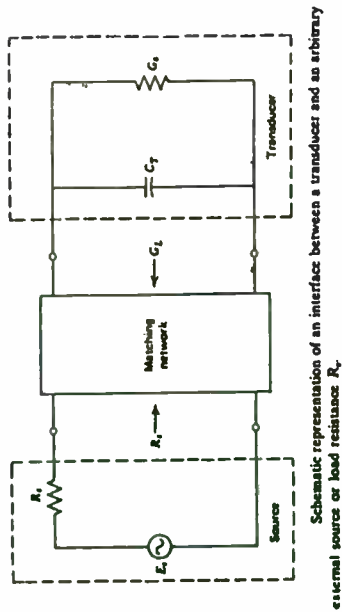
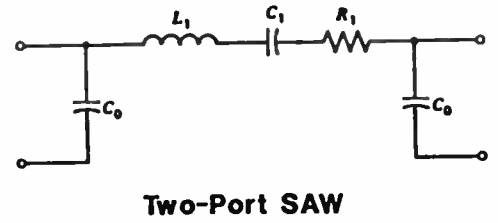
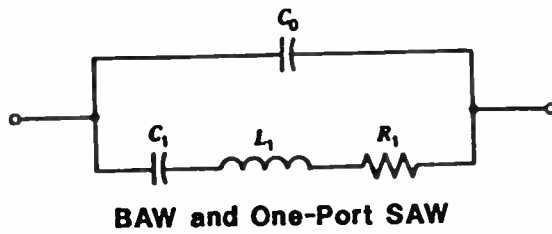


EQUIVALENT CIRCUITS FOR IDT

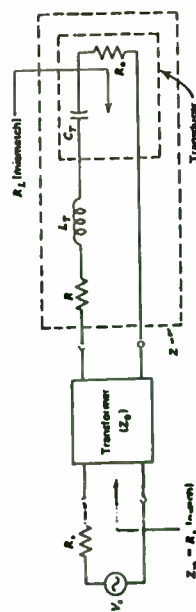
Surface Acoustic Wave (SAW) Devices



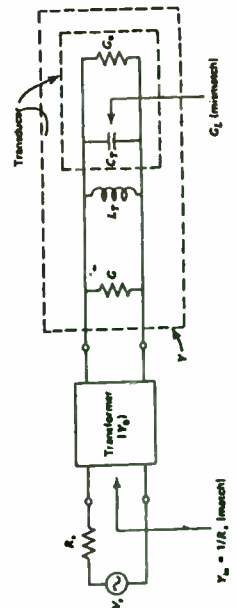
Simplified Equivalent Circuits



Schematic representation of an interface between a transducer and an arbitrary external source or load resistance R_e .



Schematic representation of series matching network.

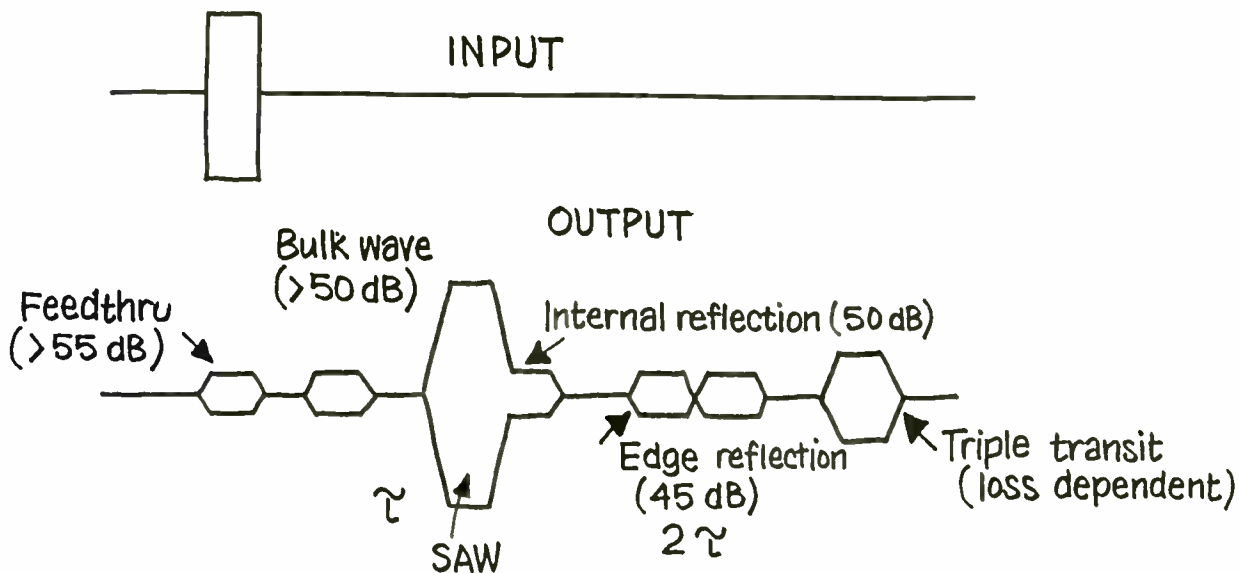


Schematic representation of shunt matching network.

SECOND ORDER EFFECTS

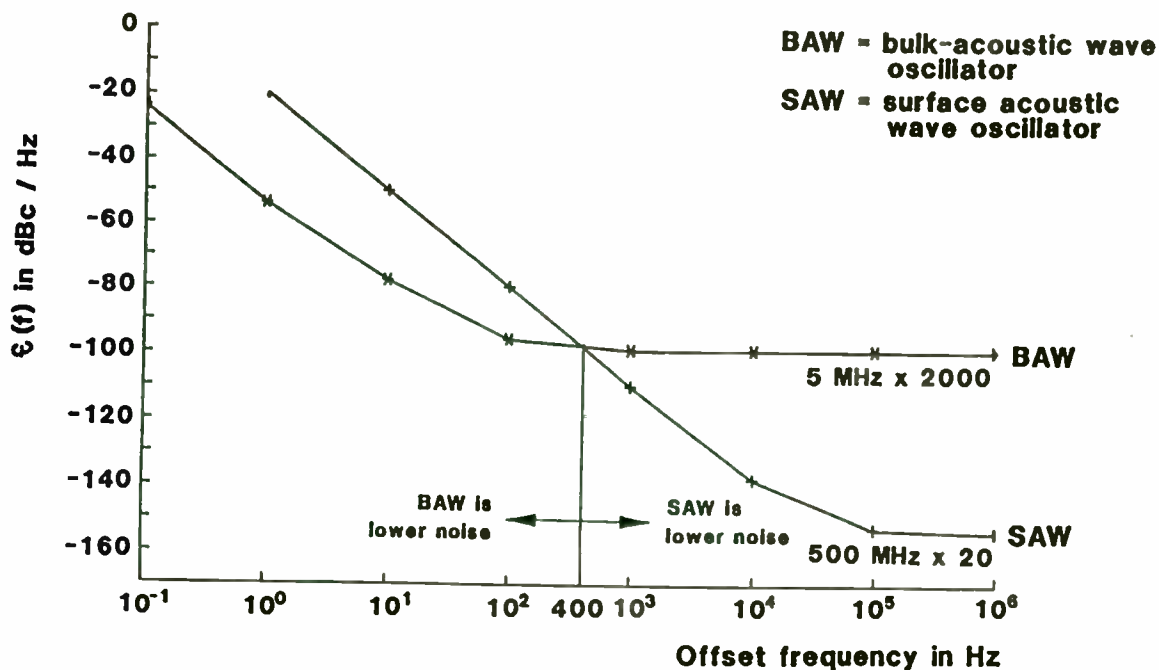
Time domain spurious

- Edge reflections - angle, absorber
- Bulk waves - roughen
- Internal reflections - metal - adjust velocity
- mass - clever design



361

Low-Noise BAW and SAW Multiplied to 10 GHz (in nonvibrating environment)



Based on Draft Spec Rev E (7/86)

MIL-HDBK-217E

SURFACE ACOUSTIC WAVE DEVICES

5.1.2.11 Surface Acoustic Wave (SAW) Devices. The part operating failure rate model (λ_p) is:

$$\lambda_p = \lambda_b \Pi_Q \Pi_E \text{ failures}/10^6 \text{ hours.}$$

where:

$$\lambda_b = \text{base failure rate} \\ = 2.1 \text{ failures}/10^6 \text{ hours}$$

$$\Pi_E = \text{environmental factor (Table 5.1.2.11-1)}$$

$$\Pi_Q = 0.1 \text{ for high quality part, subjected to 10 temperature cycles, } (-55^\circ\text{C to } 125^\circ\text{C}) \text{ with end point electrical test}$$

$$\Pi_Q = 1.0 \text{ commercial part}$$

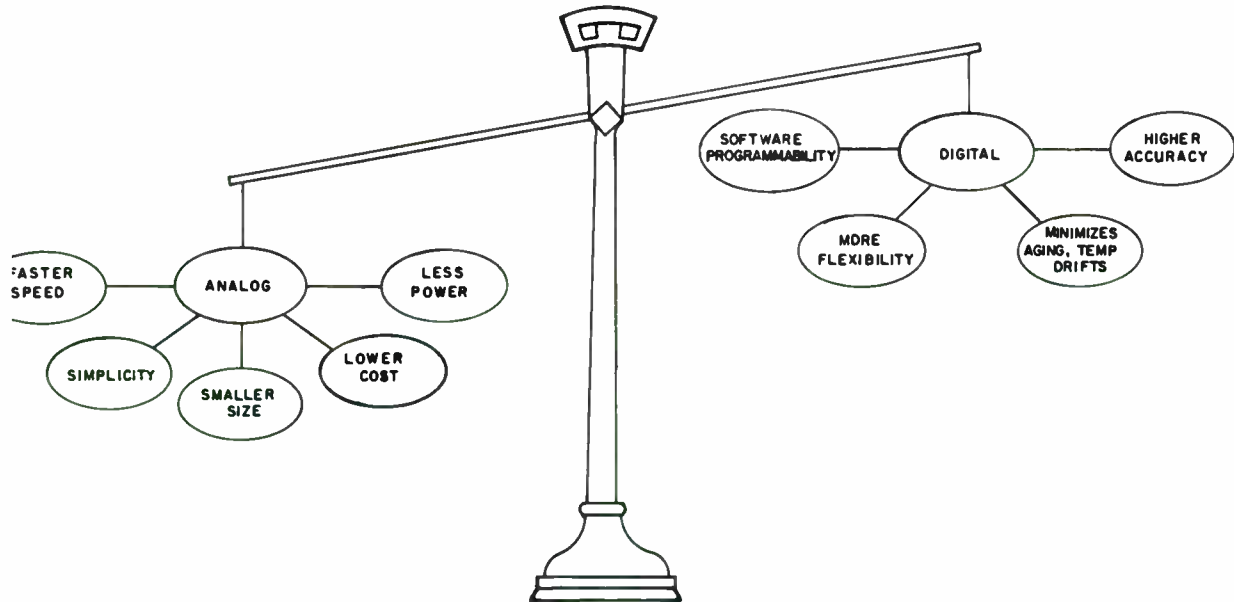
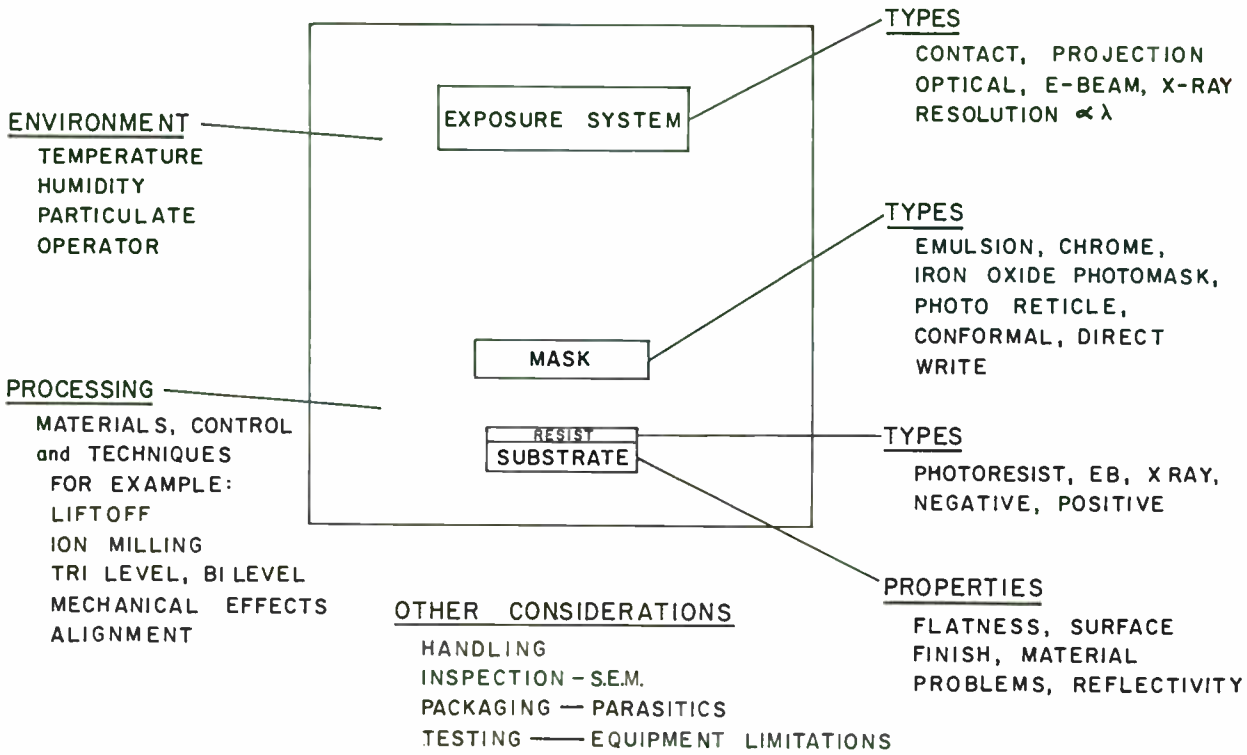
TABLE 5.1.2.11-1: ENVIRONMENTAL MODE FACTOR

ENVIRONMENT	Π_E	ENVIRONMENT	Π_E
G _B	1.0	A _{IB}	13.0
G _{MS}	1.4	A _{IA}	10.0
G _F	3.9	A _{IF}	15.0
G _M	11.0	A _{UC}	13.0
M _P	10.0	A _{UT}	10.0
N _{SB}	5.0	A _{UB}	20.0
N _S	8.5	A _{UA}	15.0
N _U	16.0	A _{UF}	20.0
N _H	16.0	S _F	1.6
N _{UU}	17.0	M _{FF}	11.0
A _{RW}	23.0	M _{FA}	15.0
A _{IC}	7.5	U _{SL}	31.0
A _{IT}	7.5	M _L	35.0
		C _L	600.0

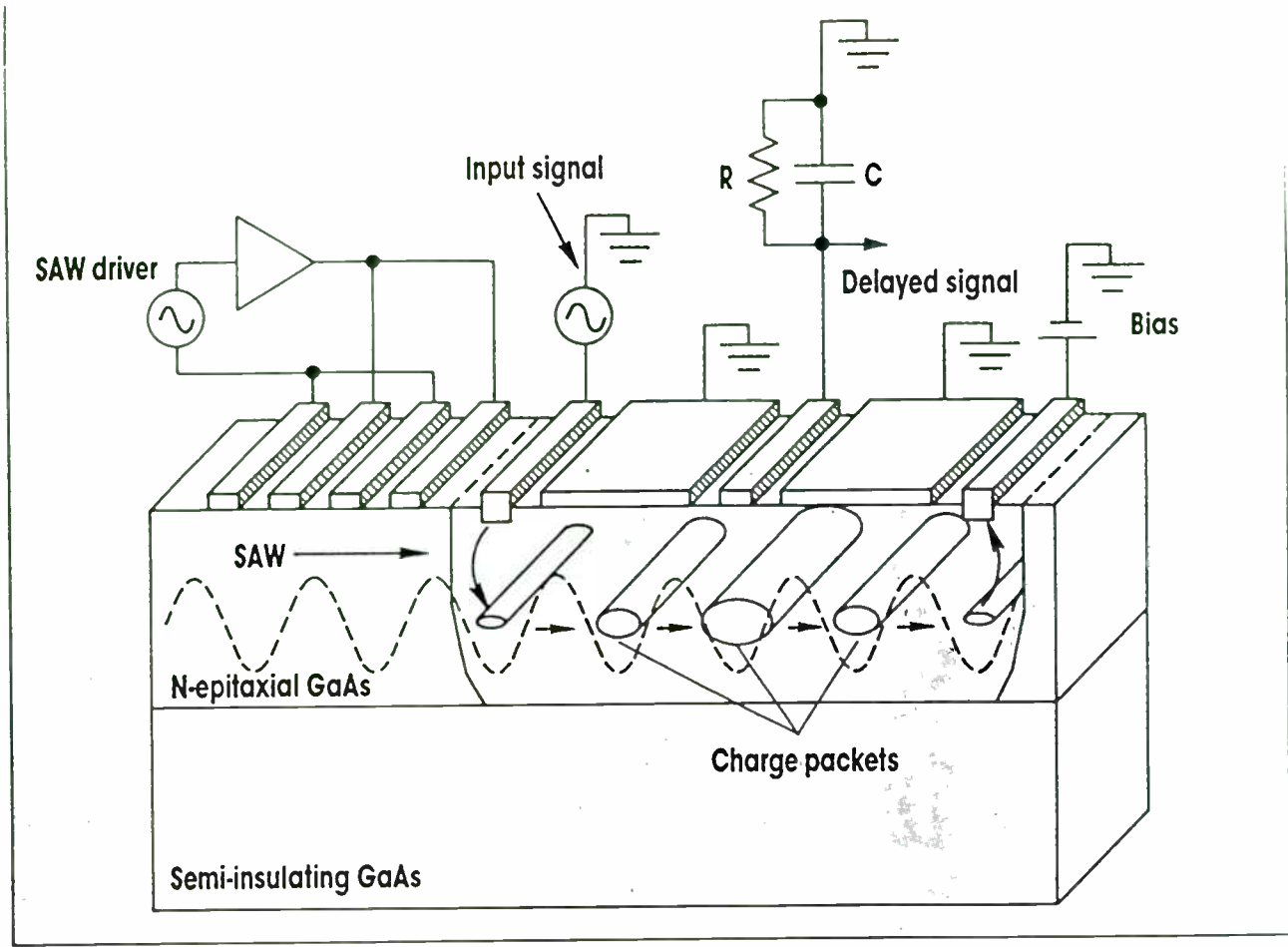
Future Trends

- * New piezoelectric materials
- * Higher Frequency Devices
- * Competitive Technologies
- * Integration with other Technologies

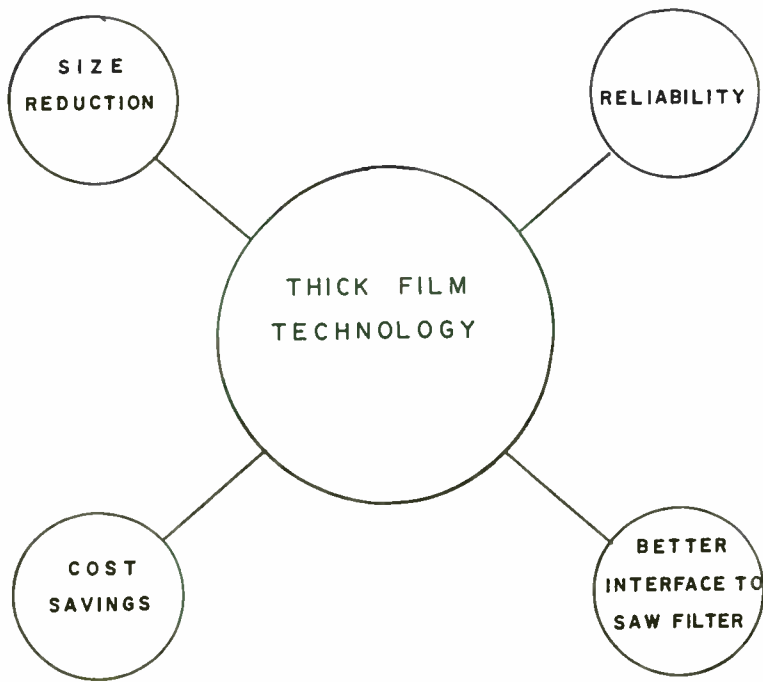
INTEGRATED APPROACH TO FABRICATION OF HIGH FREQUENCY SAW DEVICES



PERFORMANCE CAPABILITIES OF ANALOG
DEVICES OVER THEIR DIGITAL COUNTERPARTS



Utilizing acoustic charge transport (ACT), delay lines are formed on GaAs substrates. Surface acoustic waves (SAWs) create electric fields that transport charge packets along the channel.



ADVANTAGES OF THICK FILM

- (1) SHORT CONDUCTOR PATHS
- (2) MINIMAL STRAY CAPACITANCE
- (3) GROUND PLANES
- (4) SHORT DEVICE LEADS

Conclusions:

1. Mature Technology

2. Real growth will come in the following areas:

- a. Consumer applications
- b. High frequency devices
- c. Integration with other
technologies

3. Education of users still necessary

PUBLICATIONS

- 1.) "Analog Technologies Still have a Place in a Digital World", C.A. Erikson, Jr., Proceedings of RF Technology EXPO 1990, pp. 145 -153.
- 2.) "SAW Accelerometers: Integration of Thick and Thin Film Technologies", T. B. Bonbrake, C.A. Erikson, Jr., and D. Thoma, Proceedings of 1985 Ultrasonics Symposium, pp. 591 - 594.
- 3.) "First Non-Linear FM IMCON: Design and Performance", R.D. Dorman, C.A. Erikson, Jr., D. Carlton, and M. Apter, Proceedings of the Ultrasonics International, July 1985
- 4.) "DDLs Perform Vital Signal-Processing Role", C.A. Erikson, Jr., D. Carlton, R. Dorman, MSN & CT, July 1985, pp. 99-103
- 5.) "Surface Acoustic Wave Device Assembly Techniques", C.A. Erikson, Jr. and L.J. Thurber, Electric-ronics, July 1985, pp. 59-62.
- 6.) "Use of SAW Technology in the RF Systems of the 1980's", C.A. Erikson, Jr., Proceedings of RF Technology Expo 85, pp. 85 - 89.
- 7.) "Dispersive Delay Lines: Key Signal Processing Devices for the 80's", C. A. Erikson, Jr., D. Carlton, and R. Dorman, Conference Proceedings Military Microwave 1984, pp 329-333
- 8.) "Packaging of SAW Devices", C.A. Erikson, Jr., International Journal for Hybrid Microelectronics, March 1984, pp. 10-15.
- 9.) "SAW Prosperity Depends on Production Readiness", C.A. Erikson, Jr., Microwaves & RF, November 1983, pp. 75-83.
- 10.) "Vertical Inline SAW Package(VISP)", C. A. Erikson, Jr. and D. R. LeSeige, Proceedings of the 1983 Ultrasonics Symposium, Vol I., pp.125-128.
- 11.) "The Natural Integration of SAW and Hybrid Technologies", C.A. Erikson, Jr., and R. Vachon, Electric-ronics, June 1983, pp. 46-48.
- 12.) "SAW Devices: A Product Whose Time Has Come", C.A. Erikson, Jr., L. Thurber, and R. Vachon, Proceedings of Circuit Expo 82, October 1982, pp. 5-7.

1. Abstract

James F. Bridges
Argonne National Laboratory
9700 South Cass Avenue
Argonne, IL 60439 USA

The Advanced Photon Source (APS) is being built by Argonne National Laboratory (ANL) near Chicago. The APS is a 7-GeV positron storage ring from which x-ray beams of energies from a few keV to hundreds of keV are emitted as the positrons pass through ring bending magnets and also through special magnets called wigglers and undulators. The present schedule is to be operational in 1995.

The energy emitted from the positron beam as x-rays is replaced through a radio-frequency accelerating system operating at 352 MHz at a maximum power level of 3 MW.

The RF system will be described as well as several lower-power systems at frequencies of 0.8 MHz, 117 MHz and 2.8 GHz. The associated control electronics (phase shifters amplitude control, automatic tuning control, etc.) as well as the computer control architecture will also be described.

2. Introduction

RF systems have been associated with particle accelerators since E. O. Lawrence invented the cyclotron in 1932 at the University of California at Berkeley. Two electrodes, called dees because of their D-like shape, were driven by a high powered, typically 20-40 kW, electron tube used as an oscillator. In the early sixties, frequency synthesizers were used to drive an amplifier chain with the output stage usually a large tetrode of about 100 kW output. The frequency band was about 7-20 MHz, depending on the ion accelerated.

Synchrotrons, having separated magnets and RF systems, overcame the limitations of cyclotrons and could accelerate protons to much higher energies. RF accelerating systems are distributed around the ring of magnets, have swept frequency operation and have output powers of several megawatts.

Electrons, because of their low mass, travel at the speed of light with very little energy, and so electron synchrotrons and storage rings operate at a fixed RF frequency. However, synchrotron light is emitted from the accelerated electrons in the range of infrared (10^{12} Hz) through the visible, ultraviolet and x-ray (2×10^{19} Hz) spectrum.

The energy lost as radiated light must be replaced by the RF System. For an intense light source even more power is needed. The APS storage ring RF power will be 3 M watt for a 300mA, 7 GeV stored beam. Since so much power is needed, the accelerating cavity design is optimized for high voltage with low power, i.e., the shunt impedance is maximized. Cavity optimization leads to higher frequencies, typically 500 MHz range, than previous (proton) accelerators. These higher frequencies are above the usual electron tube (tridodes & tetrodes) capabilities. Klystrons, usually used above 1 GHz, were developed to operate at 500 MHz, then 352 MHz and for CW operation.

For the low-level RF components, both amplitude and phase modulation circuitry is necessary. Maximizing the cavity impedance reduces the power for a given accelerating voltage. And for large beam currents needed for bright light sources, the beam current is larger than the source (Klystron amplifier) current. See Figure 2.1.

3. Project Description

The Advanced Photon Source (APS) at Argonne National Laboratory (ANL) is a high energy synchrotron x-ray source which provides at least a 100-mA beam of low-emittance, 7-GeV positrons capable of being stored for at least 10 hours. The

APS facility is specifically designed to optimize the use of insertion devices (IDs) because of the extremely high brilliance of the radiation produced by these devices. The lattice structure is a 40-sector Chasman-Green lattice which allows the stored beam to pass through insertion devices (undulators and wigglers) in the storage-ring. The photon beams produced in these straight sections contain fundamental x-ray energies up to 20 keV. In addition to these insertion device beams there are also available up to 35 photon beams from the bending magnets in the storage-ring. A layout of the Advanced Photon Source facility is shown in Figure 3-1.

The overall APS anatomy structure, the motion path of the positrons and the production of x-rays, are illustrated in Figure 3-2.

Even though the design energy of the stored positron beam is 7.0 GeV, the technical components of the facility are capable of producing stored beam energies up to 7.7 GeV. The design goals and specifications for the technical/facilities, are listed in Table 3-1. Reliability, stability and flexibility are emphasized in the designs of the components of the APS facility.

The Injector System is designed to fill the storage ring with a 7-GeV positron beam to at least 100 mA, in less than a minute (~ 50 s). The major components of the injector system are:

Linac

Low Energy Transport Line

Positron Accumulator Ring

Injector Synchrotron

High Energy Transport Line

A layout of the injector system is shown in Figure 3-3 and the design performance specifications are listed in Table 3-2.

The APS storage ring lattice is a Chasman-Green type containing dipole magnets for bending and quadrupole magnets for focusing the circulating positrons. Each magnet is individually powered. The ring contains 40 dispersion free straight sections, of which, 34 are available for insertion devices.

The storage ring receives full energy positrons from the injector and stores them as a low emittance beam of more than 100 mA for times greater than 10 hours. During the storage time, the beam is maintained at stable positions in the straight sections that contain insertion devices. A layout of one of the APS storage ring sectors is shown in Figure 3-4.

The function of the storage ring is to confine a 7 GeV positron beam to circulate stably around the ring. The very narrow and high intensity beam radiates synchrotron radiations of high brilliance and over a wide range of wave lengths. The general design performance parameters of the storage ring are given in Table 3-5.

4. X-ray Production

Fast-moving, charged particles, such as electrons traveling very close to the speed of light, radiate energy when an electromagnetic force causes their direction or speed to change. This radiation is emitted in the forward direction in a very intense, narrow beam. In synchrotrons, magnetic fields bend the particles' path, and photons ranging in energy from the infrared to the x-ray region of the electromagnetic spectrum are emitted. See Figure 4 - 1.

Through the use of wigglers and undulators, Argonne's Advanced Photon Source will produce x-ray beams in the energy range from 1 to 100 keV that are 10,000 times more brilliant than those available from bending magnets at Brookhaven National Laboratory's National Synchrotron Light Source (NSLS). Other synchrotron light sources depicted are proposed 1-2 GeV undulators at Lawrence Berkeley Laboratory, NSLS X-1 at Brookhaven, PEP undulator at Stanford University, and the SPEAR 54-pole wiggler at Stanford. See Figure 4-2.

The storage ring receives full energy positrons from the injector and stores them as a low emittance beam of more than 100 mA for times greater than 10 hours. During the storage time, the beam is maintained at stable positions in the straight sections that contain insertion devices. A layout of one of the APS storage ring sectors is shown in Figure 3-4.

The function of the storage ring is to confine a 7-GeV positron beam to circulate stably around the ring. The very narrow and high intensity beam radiates stably around the ring. The very narrow and high intensity beam radiates synchrotron radiations of high brilliance and over a wide range of wave-lengths. The general design performance parameters of the storage ring are given in Table 3-3.

5. Linac

The Linac System consists of three major components:

1. The Electron Linac
2. The Tungsten Positron Production Target
3. The Positron Linac

The general design specifications of the linacs and their beam parameters are set by the requirements of the system and the acceptance of the Positron Accumulator Ring (PAR). A layout of the linac system is illustrated in Figure 5-1. The design performance specifications for the linac system are listed in Table 5-1.

The electron linac accelerates an electron beam to 200 MeV with 1.7 A output at a 60 Hz repetition rate. Each linac macropulse is 30 ns long and contains 50 nC of electrons by the process of multiple nuclear scattering.

Positrons are produced when the 200 MeV electron beam impinges on a 7 mm thick tungsten target. The positrons are focused by a solenoid field magnet and accelerated to 450 MeV in the positron linac. With each pulse of 50 nC of electrons, 0.42 nC of positrons are produced within the acceptance of the positron linac and 0.25 nC (1.5×10^9 positrons) are accelerated to 450 MeV.

The positron accelerating sections are constant-gradient, traveling-wave, exactly like the electron sections. Care has been taken to keep the positron beam diameter smaller than 13 mm by using a focusing system similar to those at DESY and LEP. This ensures that the positron beam is injected into the PAR with minimal loss. Linac parameters are listed in Table 5-2.

The option of injecting into the synchrotron 300 mA of electrons with energies up to 650 MeV can be done by withdrawing the positron target, rephasing the positron linac and reversing the focusing system.

In Figure 5-1, an Energy Compression System is shown as a set of devices forming a small curve in the positron beam line between the linac and PAR.

ENERGY GAIN CALCULATIONS

For - Klystron Peak Power	35 MW
- Frequency of Operation	2856 MHz
- R.F. Pulse Length (Flat-top)	5 μ s
- Fill Time (waveguide) t_f	0.8 μ s
- SLED Energy Gain Factor (with 4 μ s stored and then 180° phase reversal. e^\pm injection between 4.75 μ s + 4.8 μ s)	1.78
- SLED Power Gain	7.9 dB
- Efficiency Factor (for 0.24 dB loss in 30' RFW + 7 flanges)	0.95

Figure 5-2 illustrates the planned power distribution for the e^- and e^+ linacs. Note that Klystrons II, IV, and V utilize SLED resonators.

For Klystrons I & III

Input Power = (35 MW-4MW) (.95) = 29.5 MW
 Note: (4MW to Buncher elements Klystron I)
 (4MW to Energy Compression Klystron III) (if used)

Energy Gain = 58.8 MeV

For Klystron II, IV, and V (SLED):

Input power into each section = $\frac{(35 \text{ MW}) (.95)}{4} = 8.3 \text{ MW}$

Energy Gain of each section = 222 MeV

The accelerating structures to be used will be of the SLAC type. Presently, RF windows will be employed to separate the RF power transmission waveguide vacuum from the accelerator structure vacuum.

To maintain the correct resonant frequency when RF power is applied, the phase of the structure will be measured and the temperature of the cooling water will be varied.

The accelerating structures are traveling wave constant gradient structures consisting of 86 cavities with an overall length of 3.05 m. The accelerating structures will be the same in both the electron and positron linacs. Figure 5-3 shows the preliminary drawing, and Table 5-3 lists the preliminary parameters for an accelerating structure.

The klystron modulators is a "line-type," using a capacitance-inductance network (pulse forming network, or PFN) constructed so as to simulate electrically a transmission line. A block diagram of the modulator is shown in Figure 5-4. The main pulse and charging circuits have been also drawn in schematic form. Table 5-4 lists the major parameters.

After each output pulse the PFN capacitors charge to approximately twice the DC power supply voltage due to the resonant charging characteristics of the charging transformer and the total PFN capacitance. The PFN capacitors retain this voltage level until the hydrogen thyratron tube is triggered. Once this occurs, the PFN capacitors discharge through the primary of the pulse transformer.

The value of the charge placed on the PFN can be regulated either by "Dequing systems" in conjunction with the silicon control rectifier (SCR) and the charging transformer, or by a tetrode vacuum tube switch between the DC power supply and the P.F.N.

6. Position Accumulator Ring (PAR) RF System

There are two RF systems in the PAR. One operates at 9.8 MHz, and the other at 117 MHz. Each consists of one cavity, one RF amplifier, and associated control circuitry. The control system also synchronizes operation with the linac during injection and with the injector synchrotron during extraction.

The linac beam is injected into the 9.8-MHz bucket. The synchronous phase angle is about 175° to compensate for radiation loss while the bunch is damped. When the bunch is damped sufficiently, the 117-MHz system is turned on, and further damping occurs until extraction.

The 117-MHz system is deactivated during the first 450 ms of the 500-ms PAR cycle to prevent self-bunching of the beam at 117 MHz.

The parameters of the PAR RF System are given in Table 6-1.

6.1 Fundamental Frequency RF System

The cavity is a folded quarter-wavelength, coaxial re-entrant type that is capacitively loaded to resonate at a frequency of 9.8 MHz. Figure 6-1 shows a half section of the cavity, and the parameters are listed in Table 6-2.

The cavity is made of aluminum with a ceramic cylinder across the accelerating gap for vacuum isolation. Only the beam tube is evacuated, keeping the vacuum system cost low and avoiding multipactoring problems in the bulk of the cavity. Fine tuning will be done by a capacitive adjustment located at the loading capacitor. No high-order-mode suppression is presently included, although ports are available and could be used for mode-damping circuits.

The power amplifier will be a commercially bought 5 to 10 kW amplifier. Two amplifiers can be used if this saves money and/or increases reliability. The power amplifier is located outside the shield wall but close enough to the cavity to minimize resonances in the transmission line.

Since beam loading is incremental, with 24 linac bunches injected over a 400- μ s period, a modest feedback control system keeps the cavity voltage constant and the power amplifier load impedance real. Programming of the power amplifier input voltage, and cavity fine tuning is included to offset the transient from each injected bunch. Feed-forward techniques can be added if necessary (see Figure 6-2).

Pertinent parameters will be monitored, digitized, and interfaced to the Injector Control System for status monitoring.

Similarly, Control System commands will be interfaced to the various amplifiers for status control and to some extent for synchronization with linac and injector synchrotron.

6.2 Twelfth-Harmonic RF System

The twelfth-harmonic cavity is a half-wavelength coaxial cavity slightly foreshortened by the accelerating gap capacitance. The cavity is made of aluminum with the vacuum seal at the accelerating gap to minimize the vacuum volume and multipactoring difficulties. The cavity is tunable over a range of 1 MHz.

The cavity is electronically adjusted during operation of the 9.8-MHz cavity so as not to interact with the beam, since only the fundamental cavity is used during the injection time of the PAR cycle. PIN diodes are used to connect resistors into the cavity to lower the gap impedance by at least a factor of ten. If needed, the resonance is shifted away from 117 MHz by similar PIN diode switches connecting a reactance into the cavity. Also, higher-order-mode suppression is implemented so that the beam is undisturbed during operation of the cavity (Figure 6-3).

The power amplifier is located outside the shield wall, and power is fed to the cavity via a coaxial cable. This is a 2-kW amplifier (1600 watts for resistive loading). If beam and feedback control circuitry work well enough, the resistive loading may be removed. If RF feedback is needed, this amplifier could be mounted on the cavity to minimize phase delay at 117 MHz.¹

When the cavity is switched from a passive (imitating a beam pipe) to an active state, beam loading is rapid. A fast tuning and voltage control system, including feed-forward techniques, is used. Large induced voltages (224 kV) are avoided with programmed tuning. Figure 6-4 shows the control circuit for the cavity with both feedback signals from the cavity and feed-forward signals from a beam monitor. The amount of circulating beam controls the

program signals to the power amplifier and to the tuning device, so that as the cavity is turned on for the last 50 ms of the PAR cycle, the accelerating voltage has the correct phase with respect to the 9.8-MHz bucket and the power amplifier sees a real load. The program can be a learning (adaptive) program to monitor the feedback error signals and adjust the program to minimize the errors. This correction can be done in several ways: over many PAR cycles, using only the last PAR cycle, or using a weighted running average. Using a correction signal improves the operation of the cavity; thus, for a given tolerance on cavity parameters, the feedback loop dynamic range and gain can be smaller.

The unloaded shunt impedance of the cavity is 2.0 M Ω and the maximum twelfth-harmonic beam current is 112 mA, so the maximum induced voltage without compensation due to the beam is 224 kV. The RF amplifier produces a 30-kV accelerating voltage, and the total current without compensation would cause the voltage to be 82.4° out of phase with the empty 117-MHz buckets and the 9.8-Hz bucket. Since only 222 W is needed to power the empty cavity, resistive loading is added to the cavity to lower the shunt impedance and reduce the phase shift between beam current and generator current. This makes the programming and feedback systems less sensitive to variations in beam loading and increases the stability of the feedback system.

The 352-MHz frequency source is a synthesizer with direct digital synthesis (DDS) capability and resolution of 0.1 Hz. The DDS has phase continuity when switching frequencies so that no transient is present to disturb the stored beam. Switching is done by the control computer via a parallel bus. The correction signal is derived from the bunch signal in the storage ring. Two other synthesizers are referenced to the 352-MHz source, one for each of the PAR cavities (see Figure 6-5).

Since the rotation frequency, 9.8 MHz, of the PAR is not an exact multiple of 60 Hz, the linac is triggered by the PAR control system at a nominal 60-Hz rate. This ensures that the subsequent linac beam pulses are in the same place in the bucket as the first beam pulse.

Similarly, the PAR is synchronized to the synchrotron RF at extraction so the bunch is correctly placed with respect to previous bunches in the 352-MHz buckets.

7. Synchrotron RF System

The injector synchrotron RF voltage is produced by four five-cell cavities operating at the storage ring frequency of 352 MHz, the 432nd harmonic of the revolution frequency. Injection is into a stationary bucket with a peak voltage of 100 kV. The RF voltage increases to match the synchrotron radiation losses as the beam energy is increased. At extraction, the RF voltage is 10.4 MV, and the synchrotron radiation loss per turn is 6.38 MeV. The energy gain per turn is negligible compared with the synchrotron radiation losses. Table 7-1 lists the RF related parameters of the synchrotron. Figure 7-1 shows the physical layout with two cavities on each side of the synchrotron. The four cavities are driven by a single 1-MW klystron identical to those used for the storage ring.

The cavities for the 352-MHz injector synchrotron rf system are essentially copies of the LEP/PEP^{2,3} five-cell, $\lambda/2$ resonant cavity. Each cell has a 10.0-cm diameter beam hole with a reentrant nose. The cell length is $\lambda/2$ (426 mm). The radius from the center line to the inside of the outer shell is 30.2 cm. The cells are magnetically coupled with two off-axis slots. The five-cell structure is loop-

excited in the center cell using a post-coupler from the WR2300 waveguide. Tuners are located in the two cells adjacent to the center cell. Vacuum separation between the waveguide and the cavity is a cylindrical ceramic window surrounding the waveguide post. The cavity body is made from forged disks and forged seamless cylinders of copper. These are machined to close tolerances and electron-beam welded. See Figure 7-2 and Table 7-2.

The cavity is fitted with two 220 l/s ion pumps on the two outermost cells. After the cavity has been RF processed to full power, this amount of pumping capacity should maintain the beam path volume of the cavity at 10^{-10} Torr or better.

The 352-MHz system for the injector synchrotron is essentially the same as the 352-MHz RF system for the storage ring. The same kind of klystron is used, but optimized to achieve a maximum efficiency of 65-70% at 700 kW instead of 1 MW. A circulator protects the klystron from reflected power. Static phase shifters are used to adjust the phase to the four cavities.

The klystron which is used for the RF power amplifier is manufactured by two European companies and were developed by CERN in Geneva. A photo of the klystron is shown in figure 7-3. The klystron operates with a negative voltage on

the cathode in the range of 100 kV. The body and all accessible outer surfaces of the klystron are at ground potential. The RF drive power is applied to the first klystron cavity (nearest the cathode) and the output power is coupled out of the last klystron cavity, then to the waveguide which is atop the klystron.

The klystron power supply must power all the elements of the klystron; these include the cathode heater power, the modulating anode power, the focusing magnet power, and the klystron beam power. The power supply system also includes equipment and personnel protective interlocks.

The RF system is under active computer control and is continuously monitored by the main control computer. The five cells of the cavity each have field monitors. The monitors are added in phase and the resultant signal is compared with a digital phase meter to the driving signal. The digital phase information goes to the control computer, the computer adds an offset to maintain the proper voltage amplitude and phase. The computer then controls the two tuners of each cavity to keep the cavity tuned in the presence or absence of beam loading. The monitoring system also records the cavity temperature, cavity power, klystron power supply and warns of improper operating conditions.

8. Storage Ring RF System

The RF system must generate adequate voltage and power to compensate for synchrotron radiation from the dipole magnets and the insertion devices, excitation of parasitic modes by the beam, and overvoltage for an adequate beam lifetime. Design limits in the storage ring RF are: (a) 200 kW of RF power per ceramic vacuum window and (b) 800-kV peak voltage per cavity. The nominal frequency of operation for the storage ring rf system is 352 MHz.

The RF system uses 15 single-cell cavities. These are the same type of cavities used at the Photon Factory in Tsukuba⁴ and the SRS in Daresbury.⁵ Three 1-MW klystrons power the cavities. Each klystron drives five cavities. Each group of five cavities is located in a 6-m straight section. A third-harmonic cavity, operating at 1056 MHz and 1.8 MV, is located in the 30th straight section after injection. The RF parameters are listed in Table 8-1, and the parameters of the beam and RF system in Table 8-2.

Figure 8-1 shows the cross section and dimensions of the single-cell cavity used for the storage ring. Calculations with the computer program URMEL⁶ and estimates made by scaling from the Photon Factory measurements indicate that a single cavity can develop 800 kV with 62 kW of copper loss and with a peak electric field at the copper surface of 5.9 MV/m.

Each storage ring cavity has four 14-cm- and two 12-cm-diameter ports. One port is used for the coupling loop which is post-excited from a WR2300 waveguide (can be adjusted) for coupling-coefficient. The post is vacuum-sealed from the air-filler waveguide by a cylindrical ceramic window. The second port is fitted with a tuner of the plunger type (Figure 8-2) and has an 11.5-cm diameter and a ± 6.0 -cm travel as shown in the graph in Figure 8-3. This results in a frequency-tuning range of 1.0 MHz to compensate for beam loading and temperature effects. A third port is used for vacuum pumping. Two 14-cm ports are the beam ports.

An antenna and a loop coupler with a band-stop filter for the fundamental frequency are placed in two 50 cm-diameter ports, 90 apart, in order to suppress high-order modes. A list of the lowest higher-order modes with their undamped shunt impedances and Q values calculated with URMEL is given in Table 8-3. The frequencies agree closely with values scaled from measurements on the 500-MHz cavities at the Photon Factory; hybrid modes are expected at 482.3, 580.5, 749.6, 796.5 and 871.5 MHz. These modes cannot be verified with any of the cavity computer programs, since these programs do not calculate hybrid modes. The antenna- and loop-damping couplers are successful in eliminating the effects of the higher-order longitudinal and transverse modes on the stored beam.

The center-to-center spacing of the cavities is 0.852 m. The waveguide lengths are adjusted to phase the cavities with respect to the beam, and mechanically tunable phase-shifters are used for fine tuning of the cavity phase (≈ 1.0 degree).

A 1-MW klystron drives five cavities. A block diagram for the five-cavity arrangement is shown in Figure 8-4. From the klystron, the power is divided equally to the five cavities. The power is fed to the cavities in a waveguide directional coupler system.

Elevation and plan views of adjacent cavity, waveguide, and klystron systems in an RF power building are shown in Figure 8-5.

The coupling loop on each cavity is adjustable to change the coupling constant from about 1.0 to 5. Since the circulators and klystron can safely handle large amounts of reflected power, the loop is normally set for optimum operation at the highest expected beam current during the operating period. This implies that the loop is overcoupled for lower currents, which will result in reflected power. The feedback loop that drives the tuning plunger works on only the reactive element of cavity input impedance. The klystrons with circulator can handle the reflected power from overcoupling at power levels below the maximum point in the designated operating cycle.

Table 8-4 lists the operating parameters for the Thomson-CSF TH2089 klystrons. The YK 1350 klystron available from Phillips-Valvo has similar characteristics, and either tube could be used. A total of three 1-MW klystrons are required for 15 cavities.

The RF power delivered to the beam via the cavities can be much larger than that used to excite the cavity to the required voltage. The highest coupling constant between drive loop and the cavity alone, β , required is about 4.5. The cavity coupling will be adjusted to give a matched condition at the circulating current.

It is necessary to compensate for the reactive component of beam loading. This is done prior to beam injection by detuning to comply with the requirement of the Robinson instability criterion.⁷ For stability,

$$[1/(1 + \beta)] (P_b/P_c) < 1.$$

The required amount of detuning from the no-beam condition to the fully loaded condition is

$$\begin{aligned} \Delta f &= - (f_{rf}/2Q_0) \times (P_b/P_c) \times \cot(\text{phase angle}) \\ &= (352 \times 10^6/2 \times 40 \times 10^3) \times (176/39) \times \cot(51.2) = -15.91 \text{ kHz.} \end{aligned}$$

(Note that beam power is 4.5 times the cavity power.)

This detuning coverage can easily be handled by the tuning system, which has a range of 1 MHz. Detuning requires additional power. After beam filling is completed, the cavities are tuned closer to resonance, and the Robinson instability is counteracted with dynamic feedback via the low-level controls. The low-level loops are fast enough for this application.

Klystron beam power is supplied by a 95-kV, 20-A multiphase rectifier with $\pm 0.5\%$ ripple and regulation. A modulating anode supply is used to maximize efficiency. The klystron is fully protected by an electronic crowbar and arc detection circuitry.

9. Acknowledgements

The RF systems design were designed by the following people:

Robert Kustom

George Mavrogenes

James Bridges

Gilbert Nicholls

William Wesolowski

Conceptual design⁸ was complete in 1987 and detailed designs are being done until 1993. Both a Linac Test Stand and a 352 MHz RF Test Stand are being built. Two views of the RF Test Stand are shown in Figures 9-1 and 9-2. The Linac Test Stand will be built in early 1991, for testing the electron guns and one three-meter section of accelerating waveguide.

References

1. D. Boussard, "Control of Cavities with High Beam Loading," IEEE NS-32, No. 5 (Oct. 1985).
2. "LEP Design Report," Vol. II, CERN-LEP/84-01 (June 1984).
3. M. A. Allen, et al., "RF System for the PEP Storage Ring," IEEE Trans. Nucl. Sci., NS24, 229 (1977).
4. "Photon Factory Activity Report, 1982/83," National Laboratory for High Energy Physics, KEK, Japan (1983).
5. D. M. Dykes and B. Taylor, "Development of a High Power RF System for the Daresbury SRS," IEEE Trans. on Nuclear Science, NS-30, 3475 (August 1983).
6. T. Weiland, "Computer Modeling of Two- and Three-Dimensional Cavities," IEEE Trans. on Nuclear Science, NS-32, 2738 (October 1985).
7. K. W. Robinson, "Stability of Beam in Radio Frequency System," CEAL-1010, p. 8 (February 17, 1964).
8. 7 GeV/c Advanced Photon Source - Conceptual Design Report, Argonne National Laboratory, Publication ANL-87-15.

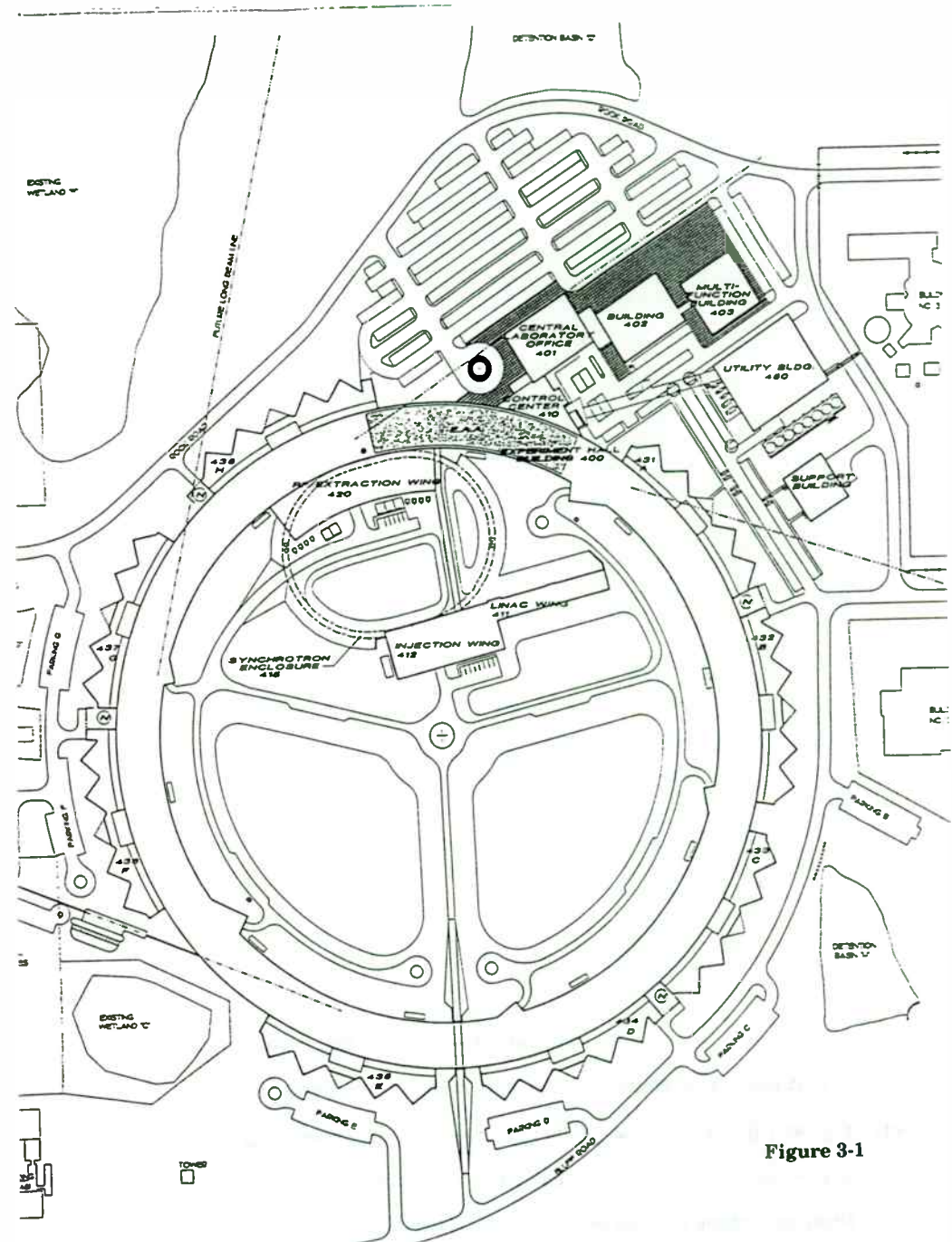


Figure 3-1

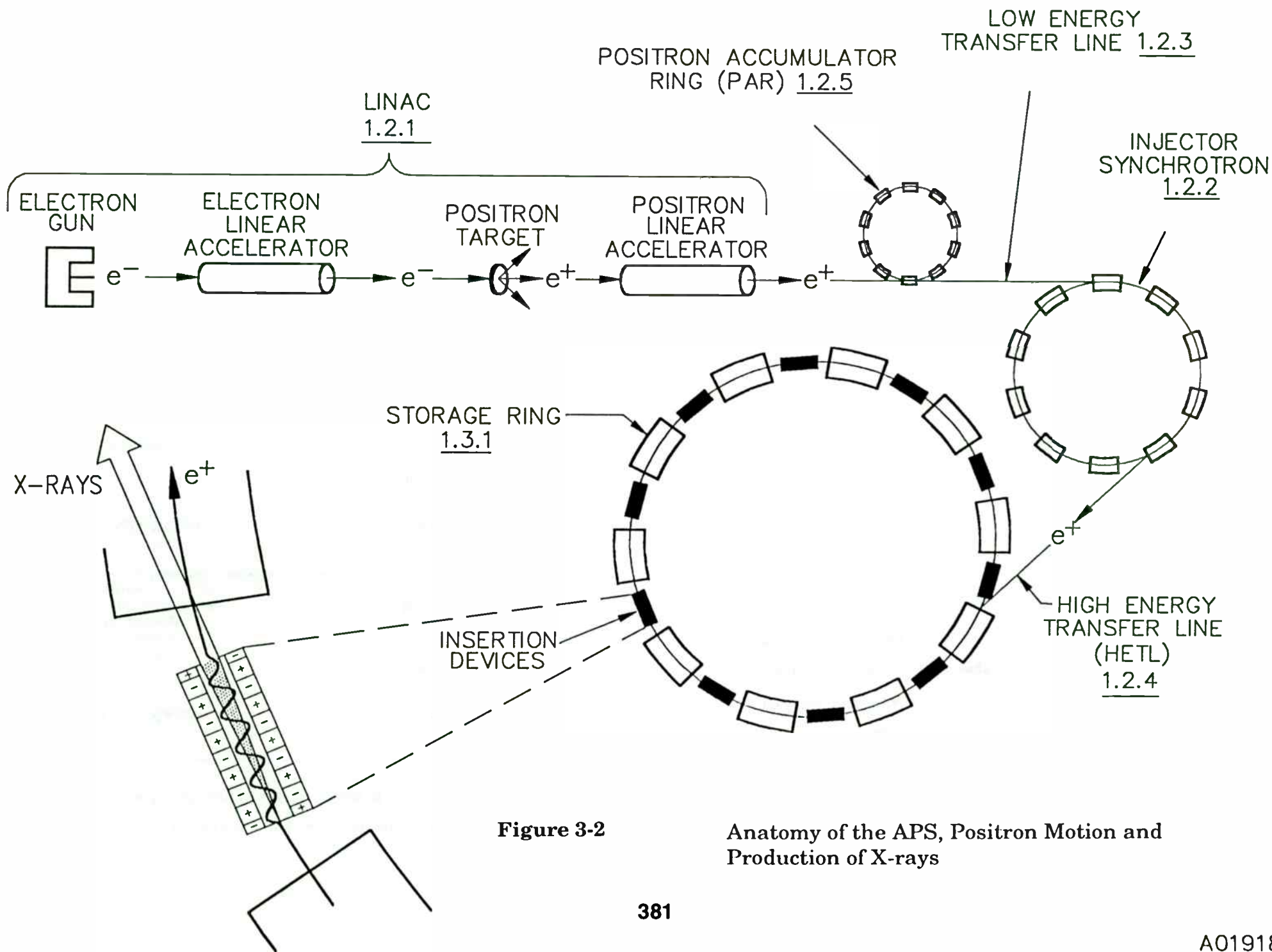


Figure 3-2

Anatomy of the APS, Positron Motion and Production of X-rays

Table 3-1

**Design Goals and Specifications for the
Technical/Facilities of the Advanced Photon Source**

<u>DESIGN PARAMETER</u>	<u>COMMISSIONING</u>	
<u>GOALS</u>		
Linac Energy (e ⁻)	200	MeV
Linac Energy (e ⁺)	450	MeV
Synchrotron Energy	7	GeV
Storage Ring Energy	7	GeV
Storage Ring Beam Current	20	mA
Beam Lifetime	>3	h
Undulator Fundamental Energy Range (Nominal)	4-14	keV
<u>DESIGN PARAMETER</u>	<u>OPERATIONAL GOALS</u>	
Beam Energy	7	GeV
Beam Current	100	mA
Beam Lifetime	>10	h
Number of Bunches	1-60	
Bunch Duration	50-100	ps
Horizontal Emittance	10	nm·rad
Number of Straight Sections	40	
Straight Section Length (for IDs)	5	m

Table 3.2

Design Performance Specifications for the Injector System

Electron Linac Output Energy	200	MeV
Positron Linac Output Energy	450	MeV
Linac Repetition Rate	60	Hz
Injector Synchrotron Output Energy	7	GeV
Synchrotron Rep. Rate	2	Hz

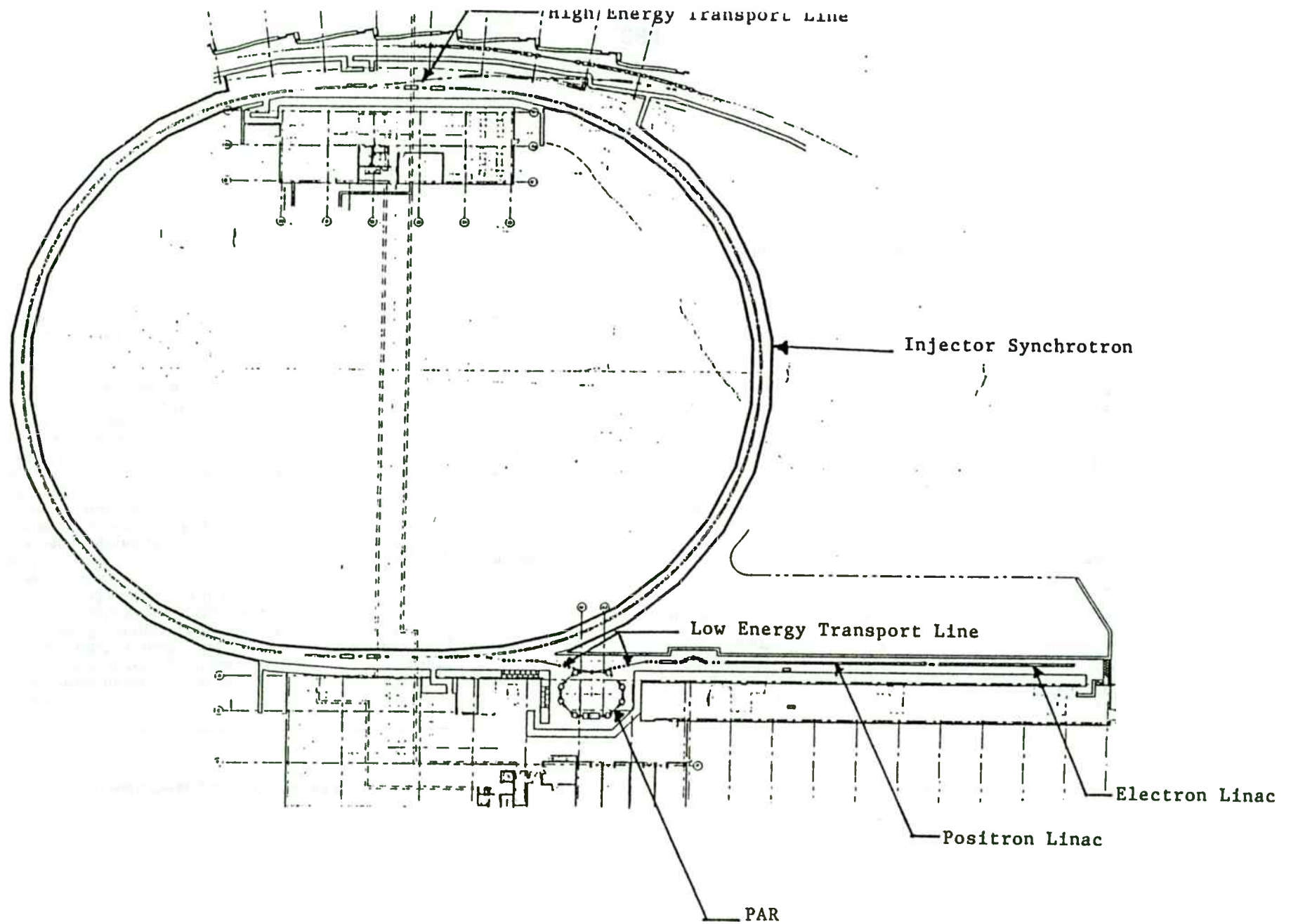


Figure 3-3 Layout of the APS Injector System

Table 3-3
Design Performance Goals and Parameters
for the Storage Ring

Nominal energy	7.0	GeV
Nominal circulating current, multibunch	100	mA
Nominal number of stored positrons, multibunch	2.3×10^{12}	
Maximum circulating current, multibunch	300	mA
Maximum number of stored positrons, multibunch	6.9×10^{12}	
Maximum circulating current, single bunch	5	mA
Number of stored positrons, single bunch	1.2×10^{12}	
Harmonic number	$2^4 \times 3^4$	= 1296
Natural emittance	8.2×10^{-9}	m-rad
Natural energy spread, rms	9.6×10^{-4}	
Energy spread, rms, at max. bunch current	2.9×10^{-3}	
Bunch length, rms, natural	5.3	mm
Bunch length, fwhm, natural	27.5	ps
Bunch length, fwhm, maximum bunch current	72.5	ps
Max energy	7.7	GeV
Beam lifetime, mean-life		
Gas scat., 8-mm vert. gap, 1 nTorr 75% H ₂ & 25% CO	76	h
Touschek, maximum bunch current	190	h
Filling rate	4.3×10^{10}	e ⁺ /s
Filling time		
Multibunch, to 100 mA	0.9	min
Single bunch, per 5 mA bunch	2.7	s

STORAGE RING
 =
40 X

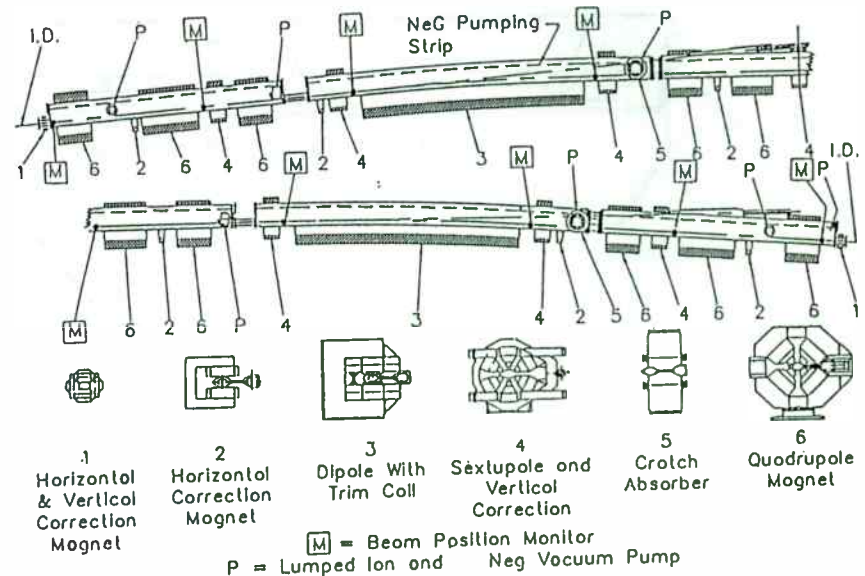


Figure 3-4 Layout of an APS Storage Ring Sector

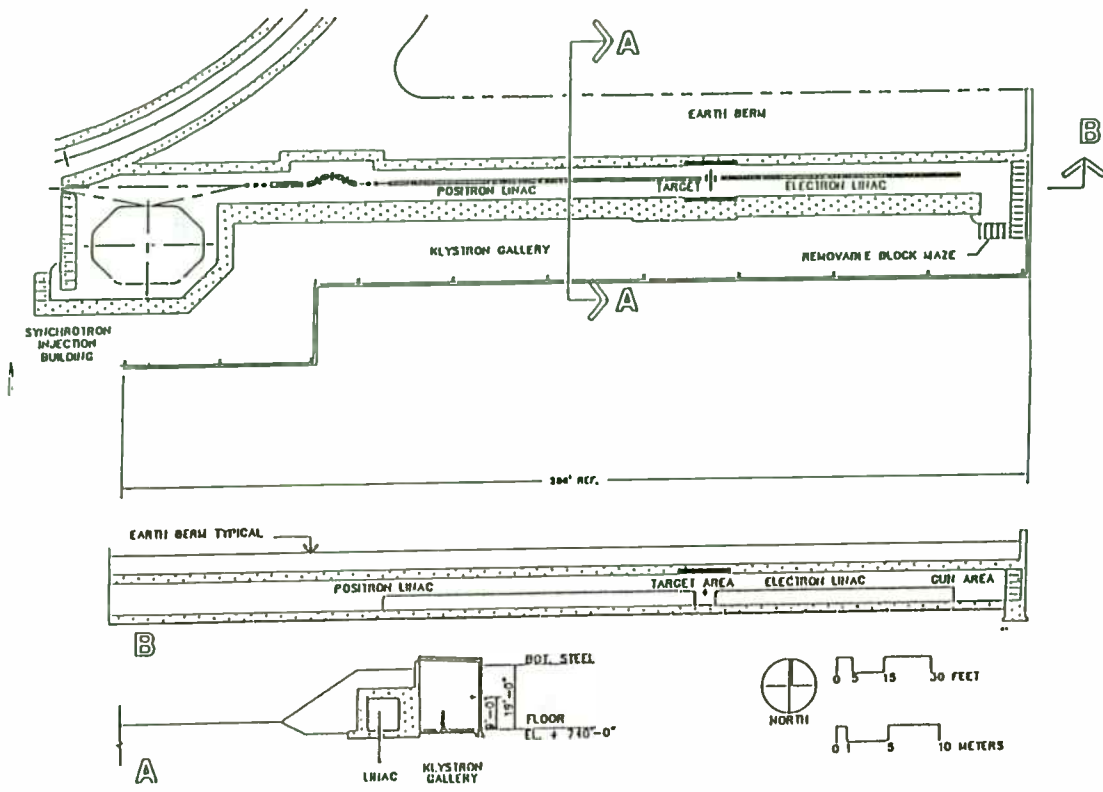
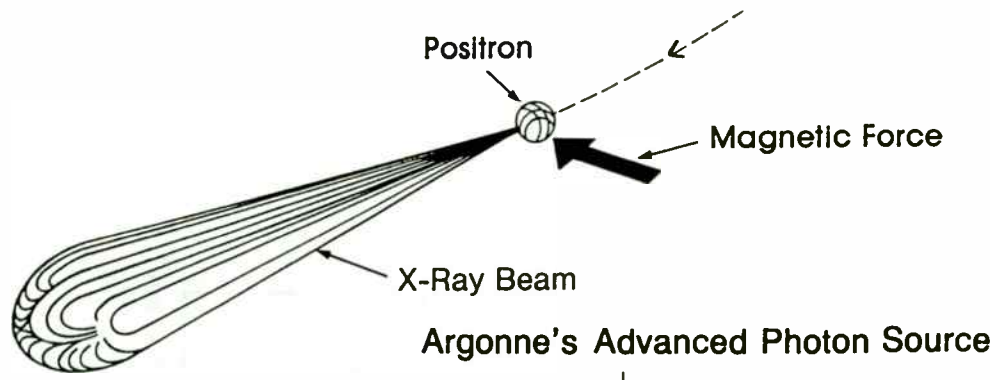


Figure 3-5 Layout of the APS Linac Building



Argonne's Advanced Photon Source

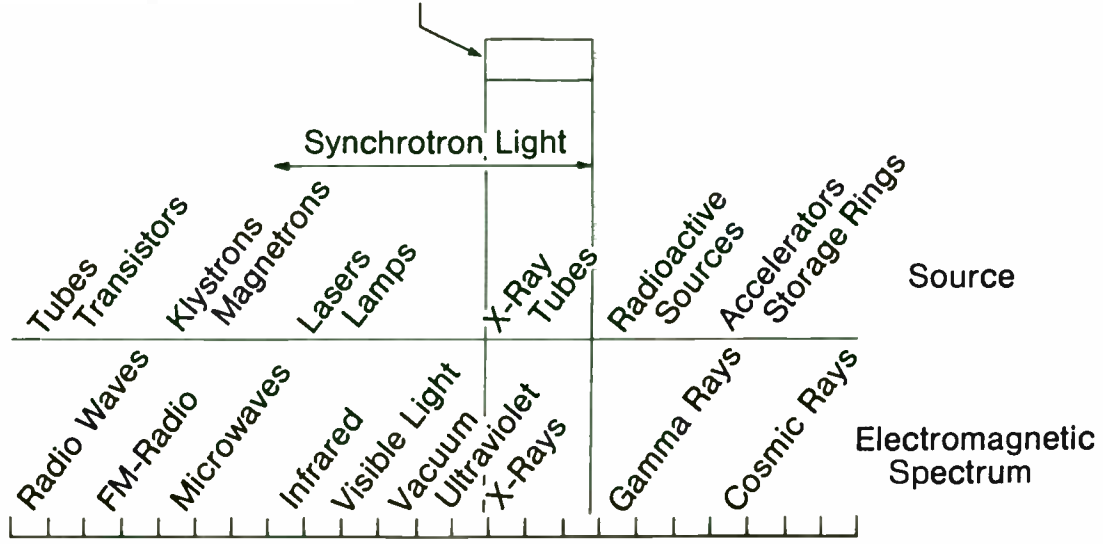


Figure 4-1

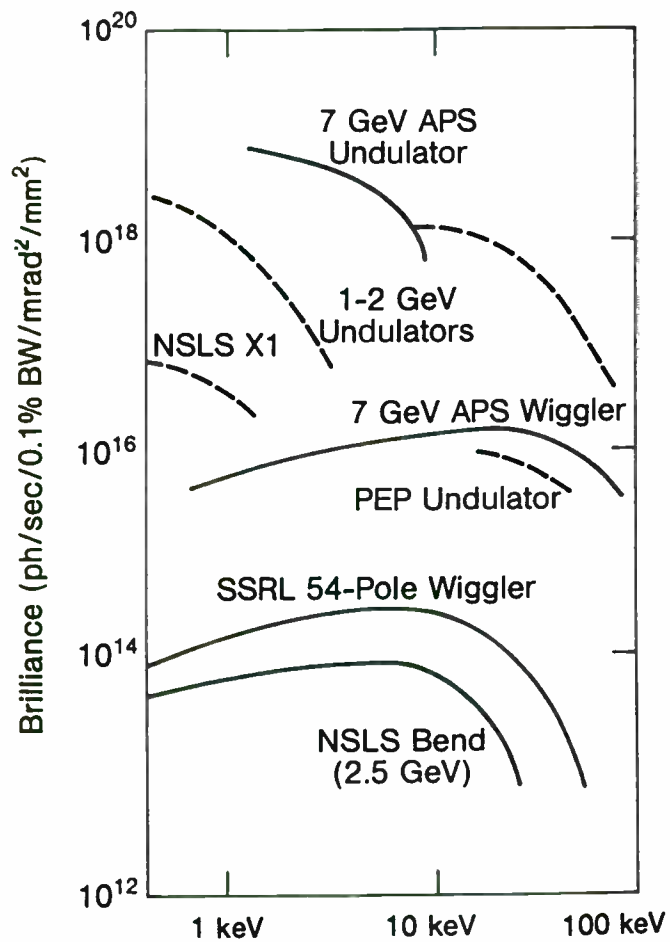


Figure 4-2

Table 5-1

Design Performance Specifications for the Linac System

<u>Electron Linac</u>		
Output Energy	>200	MeV
Output Current	1.7	A @ 30 ns
Repetition Rate	60	Hz; 24 contiguous 16.7 ms apart every 1/2 s
Spot Size	< 3	mm diameter
Longitudinal Bunch	< 15'	
Emittance (95th Percentile)	< 1.2	mm-mrad at 200 MeV
Energy Spread $\Delta E/E^*$	< $\pm 8\%$	
<u>Positron Linac</u>		
Input Energy	8	MeV
Output Energy	450	MeV
Energy Spread, $\frac{\Delta E}{E}$ (95th percentile)	< ± 0.01	
Transmission Efficiency	$\geq 60\%$	
Emittance (95th percentile)	6.6	mm-mrad

*The energy spread and the emittance are significant only to the extent that a 3 mm diameter beam spot size is not achieved at the positron converter.

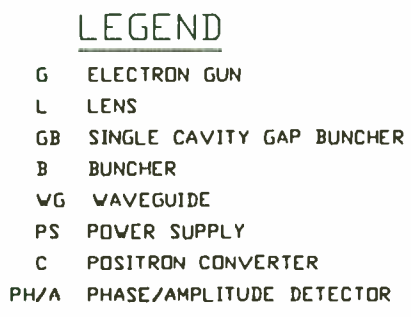
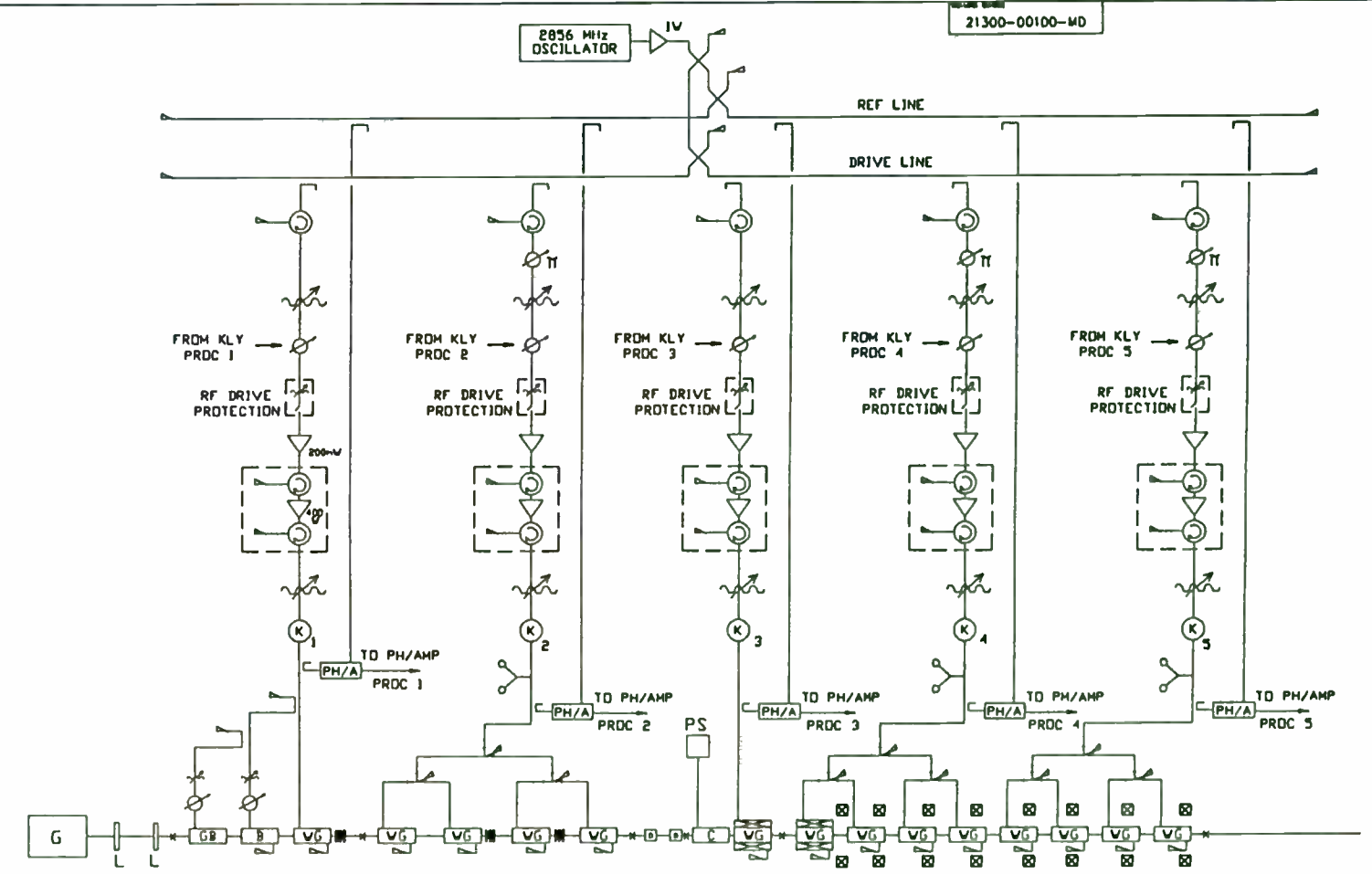
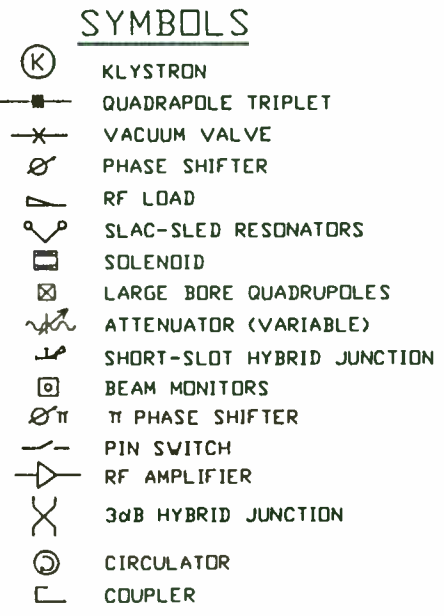
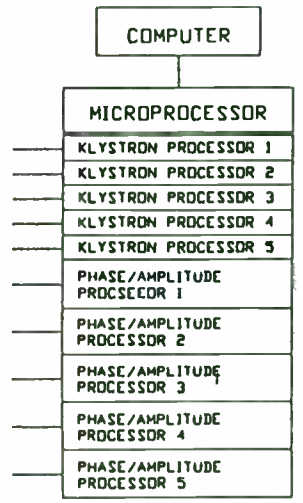
Table 5-2
Parameters of the Linacs

a. General			
Linac e ⁻	200	MeV	
Linac e ⁺	450	MeV	
Frequency	2.856	GHz	
Total number of TW accelerating sections	14		
Number of klystrons with SLEDS	3		
Number of klystrons without SLEDS	2		
b. Linac e⁻			
Gun voltage	100	kV	
Prebuncher I, type SW, single-gap re-entrant cavity			
Buncher, TW, beta = .75			
6 cavities long			
Number of TW accelerating sections	5		
Pulse repetition rate	60	Hz (24 contiguous 16.7 ms apart every 1/2 s)	
Beam pulse length	30.0	ns	
Pulse current (output)	1.7	A	
Emittance, 95 percentile	< 1.2	mm-rad	
Bunch length (90% of particles)	15°		
Energy spread ($\Delta E/E$)	± 0.08		
c. Target			
Target material	Tungsten		
Target thickness, (2X ₀)	7	mm	
e ⁻ beam diameter on target	< 3	mm	
Average incident power	500.0	W	
Pulsed solenoidal field	1.5	T	

Table 5-2 (Cont.)

Conversion efficiency e ⁺ /e ⁻	0.0083		
Mean energy of positrons from target for 200 MeV incident electrons	8	MeV	
d. Linac e⁺			
Linac output energy	450	MeV	
Linac output current	8	mA	
Emittance, 95th percentile	6.6	mm-mrad	
Energy spread, 95th percentile	± 0.01		
Transmission efficiency	≥ 60%		
Number of TW sections	9		
Overall e ⁺ /e ⁻ conversion efficiency	0.005		

2856 MHz OSCILLATOR



JOB NUMBER		DATE	
NEXT APPROVAL			
ARGONNE NATIONAL LABORATORY			
ADVANCED PHOTON SOURCE			
LINAC			
POWER DIST/LOW POWER RF CONTROL			
100 NUMBER	A01568	DATE LET OUT	
NAME OF	M. MARKINS	DATE	
CHK BY	30 W	DATE	
ALL THE PROGRAMS OPERATED AS DESCRIBED ARE IN REPORTS SECTION 1 1. 0 0 2. 0 0 3. 0 0 4. 0 0 5. 0 0 6. 0 0 7. 0 0 8. 0 0 9. 0 0 10. 0 0 11. 0 0 12. 0 0 13. 0 0 14. 0 0 15. 0 0 16. 0 0 17. 0 0 18. 0 0 19. 0 0 20. 0 0 21. 0 0 22. 0 0 23. 0 0 24. 0 0 25. 0 0 26. 0 0 27. 0 0 28. 0 0 29. 0 0 30. 0 0 31. 0 0 32. 0 0 33. 0 0 34. 0 0 35. 0 0 36. 0 0 37. 0 0 38. 0 0 39. 0 0 40. 0 0 41. 0 0 42. 0 0 43. 0 0 44. 0 0 45. 0 0 46. 0 0 47. 0 0 48. 0 0 49. 0 0 50. 0 0 51. 0 0 52. 0 0 53. 0 0 54. 0 0 55. 0 0 56. 0 0 57. 0 0 58. 0 0 59. 0 0 60. 0 0 61. 0 0 62. 0 0 63. 0 0 64. 0 0 65. 0 0 66. 0 0 67. 0 0 68. 0 0 69. 0 0 70. 0 0 71. 0 0 72. 0 0 73. 0 0 74. 0 0 75. 0 0 76. 0 0 77. 0 0 78. 0 0 79. 0 0 80. 0 0 81. 0 0 82. 0 0 83. 0 0 84. 0 0 85. 0 0 86. 0 0 87. 0 0 88. 0 0 89. 0 0 90. 0 0 91. 0 0 92. 0 0 93. 0 0 94. 0 0 95. 0 0 96. 0 0 97. 0 0 98. 0 0 99. 0 0 100. 0 0			
1 of 1	21300-00100-MD	00	00

Table 5-3
Accelerating Structures
 (SLAC Type Accelerating Structures)

Type of Construction	Constant Gradient	
Operating Frequency	2856	MHz
Number of Sections	5 e ⁻ ; 9 e ⁺	
Overall Length of Sections, l	305	cm
Number of Cavities Per Section	86	
Phase Shift	$\frac{2\pi}{3}$	
Field Attenuation, τ	.57	Np
Shunt Impedance for Fundamental r ₀	52 - 60	MΩ/m
Q	13,000	
Filling Time t _F = l/v _g	.83 x 10 ⁻⁶	s
Waveguide Diameter, 2b	8.3461 - 8.1793	cm
Iris Aperture Diameter, 2a	2.622 - 1.9235	cm
Disc Thickness	.5842	cm
Klystron Peak Output Power Rating	35	MW

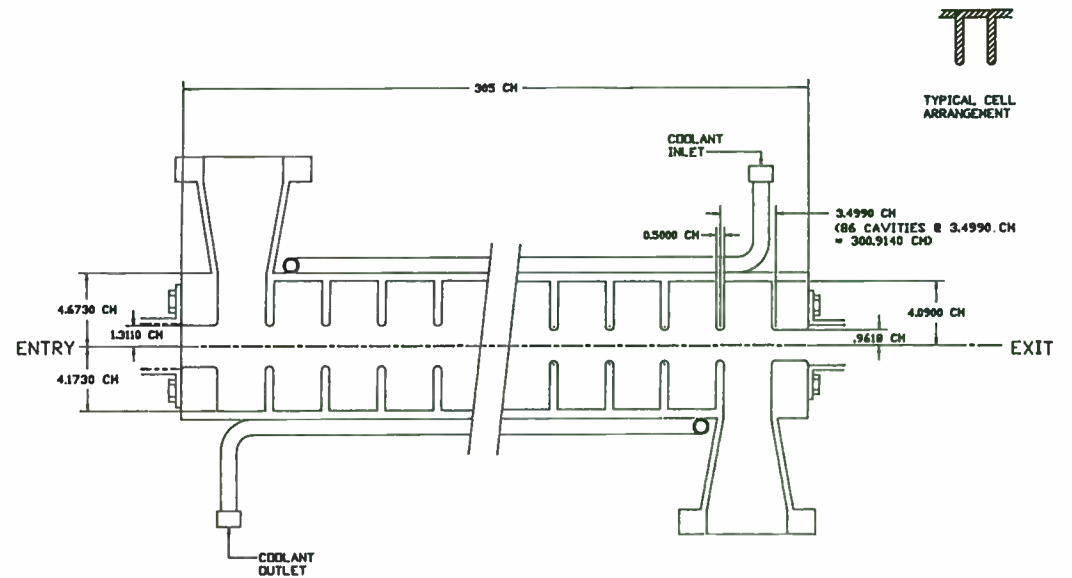


Figure 5-3 Constant Gradient T.W. Accelerating Structures (SLAC type)

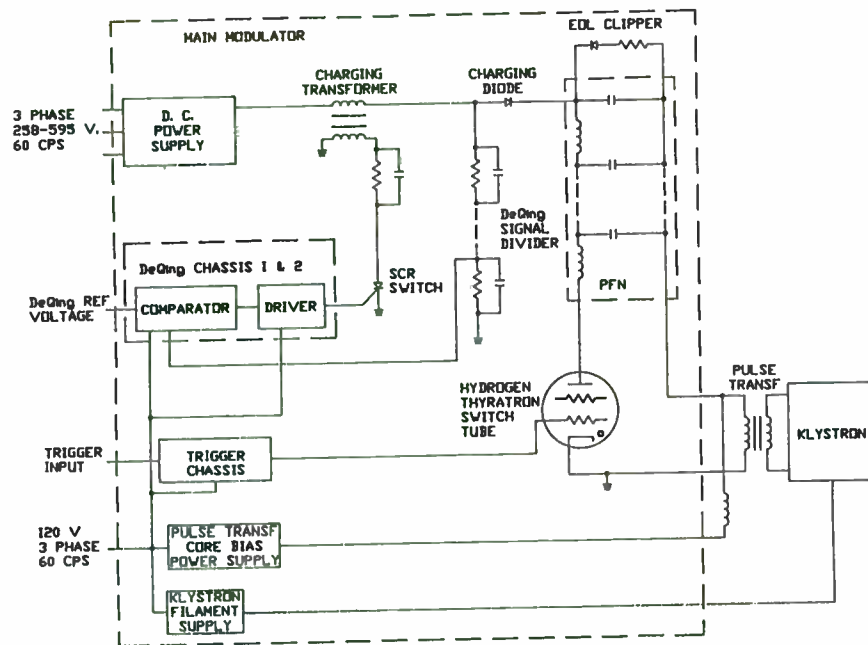


Figure 5-4 Modulator Block Diagram

Table 5-4

Power Supply Parameters

Peak Power Output	100 MW
Average Output Power	36 KW
Output Pulse Voltage Peak	315 kV
Output Pulse Current, Peak	315 A
HV Pulse Flat-top Width	5 μ s
Voltage Rise-time into klystron load	700 ns
Pulse Repetition Rate	60 Hz

Table 6-1

Parameters for PAR RF Systems

RF Systems

System I

Frequency, f	9.77584	MHz
Harmonic number, h	1	
Peak Voltage, V	40	kV
Synchrotron frequency, f_s	19.0	kHz
Natural bunch length (damped)	0.92	ns

System II

Frequency, f	117.3101	MHz
Harmonic number, h	12	
Peak voltage, V	30	kV
Synchrotron frequency, f_s	60.2*	kHz
Natural bunch length (damped)	0.29*	ns

*System I and II both ON

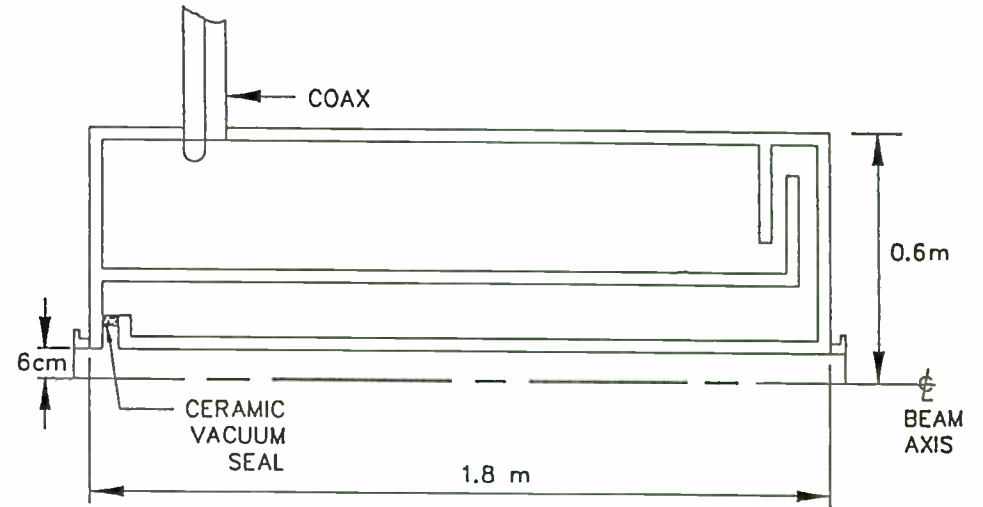


Figure 6-1 Schematic of First Harmonic (9.8-MHz) Cavity, Half Section

Table 6-2
PAR Cavity Parameters

Parameter	First-Harmonic	Twelfth-Harmonic
f (MHz)	9.7758	117.309
V (kV)	40	30
Type	$\lambda/4$, loaded	$\lambda/2$
Length (m)	1.8	0.9
Z_0 (Ω)	50	50
Power (kW)	4.70	0.222
R_g (k Ω)	170	2020
Q	7,630	25,300
τ [$= 2Q/\omega$] (μ s)	248	68

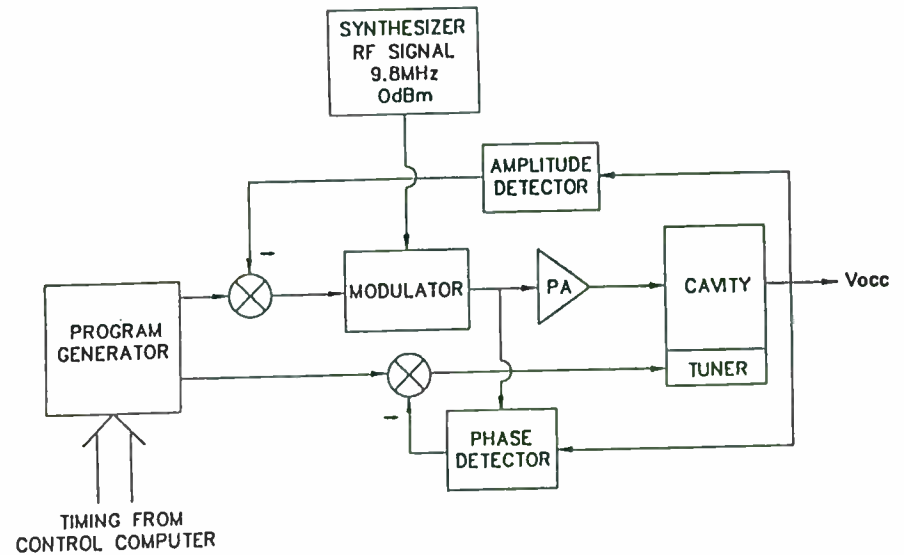


Figure 6-2 9.8-MHz RF System Block Diagram Showing Program Generator

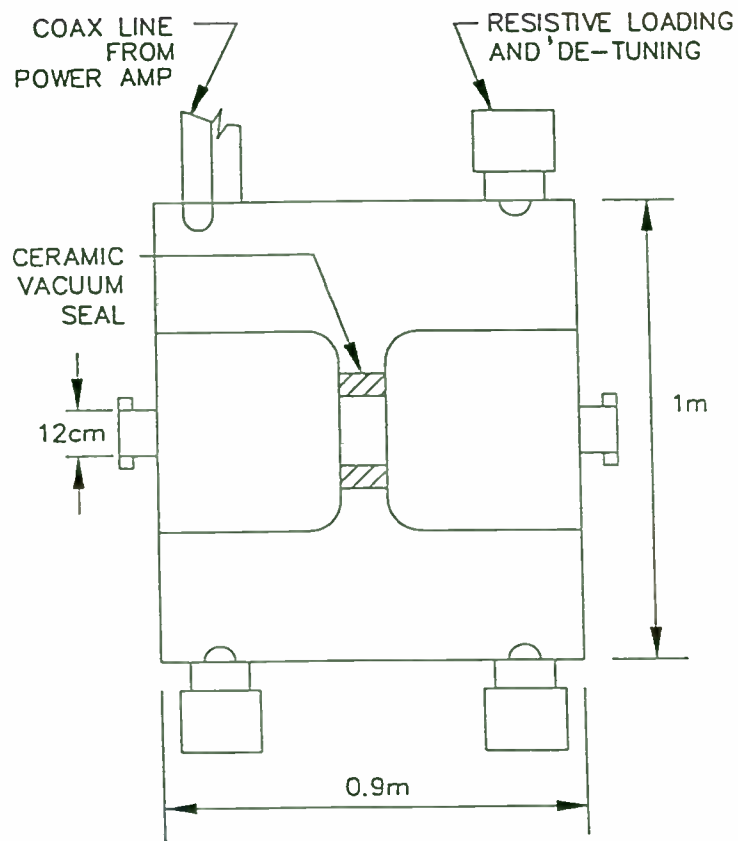


Figure 6-3 Schematic of Twelfth Harmonic (117-MHz) Cavity

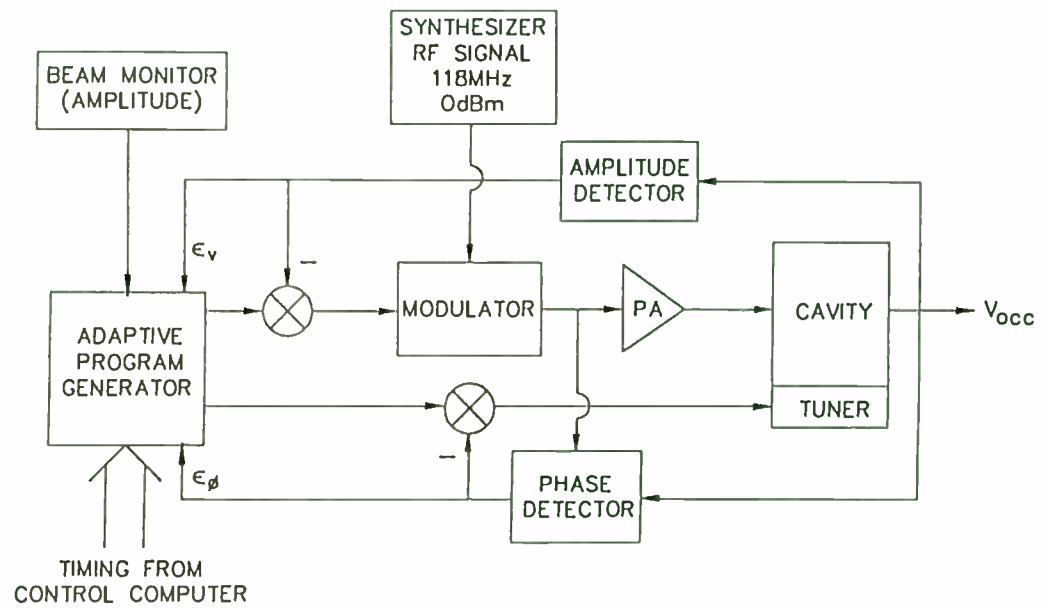


Figure 6-4 Twelfth Harmonic (117-MHz) RF System Block Diagram

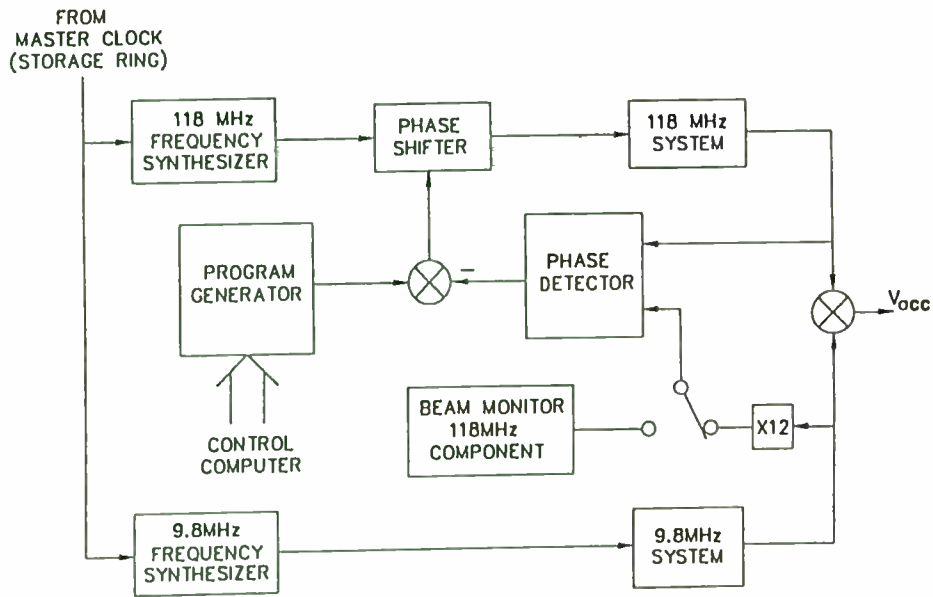


Figure 6-5 PAR RF System Showing Synchronization Scheme

Table 7-1

Injector Synchrotron RF Parameters

Parameter	Value	Unit
Circumference	368.0	m
Revolution Time	1.228	μ s
Injection Energy	0.45	GeV
Nominal Energy	7.0	GeV
Maximum Energy	7.7	GeV
Repetition Time	0.5	s
Acceleration Time	0.25	s
Energy Loss Per Turn at 7 GeV	6.38	MeV/turn
Average Beam Current	4.7	mA
Energy Gain per Turn	32.0	keV
RF Parameters		
Frequency, f	351.930	MHz
Harmonic Number	432	h
Voltage, V, at 7 GeV	9.5	MV
Synchrotron Frequency, f_s , at 7 GeV	21.1	kHz

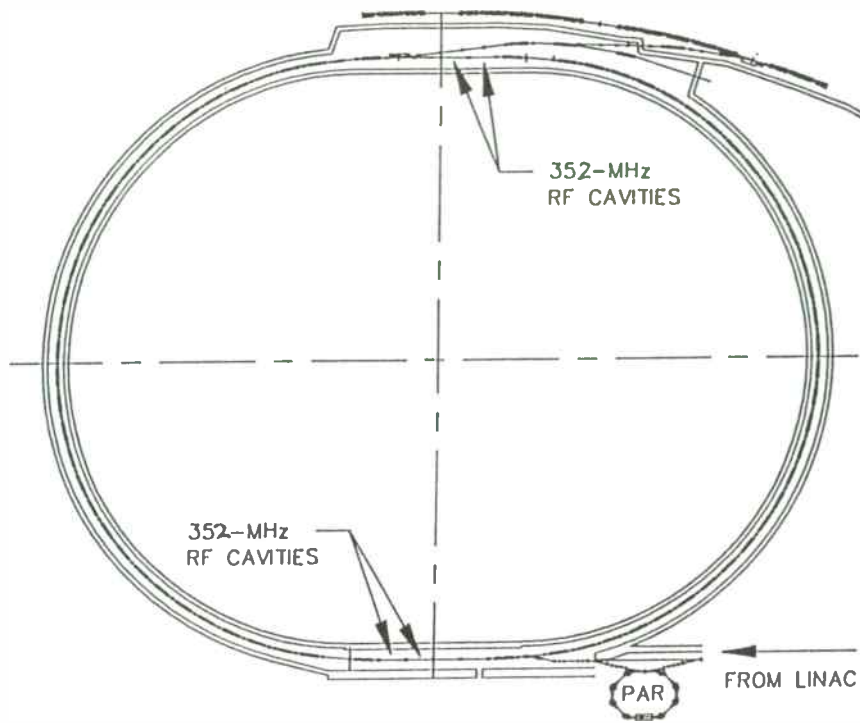


Figure 7-1 Physical Layout of the APS Injector Synchrotron

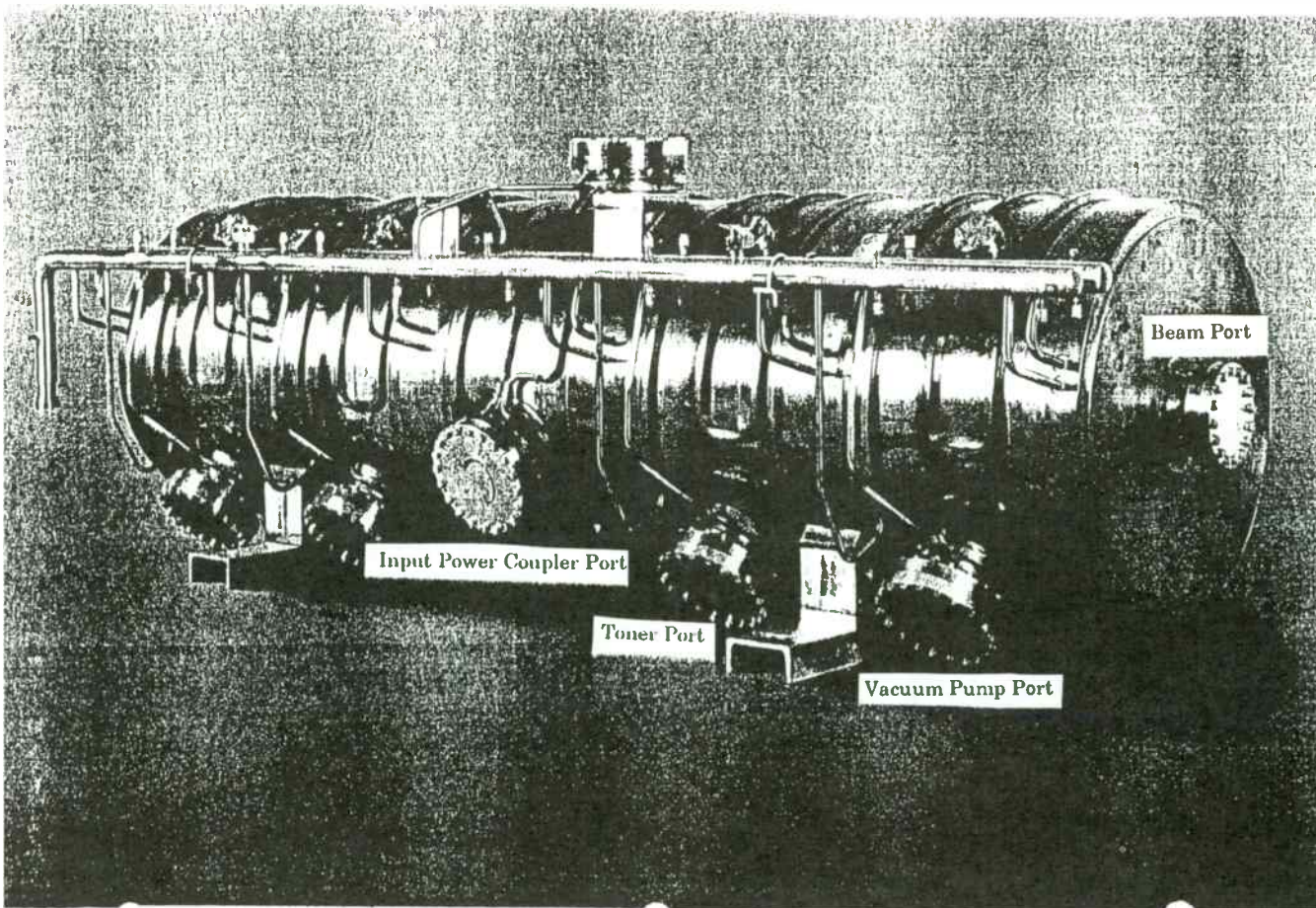


Figure 7-2 350 MHz Normal Conducting LEP Cavity/CERN

Table 7-2
Parameters for the Five-Cell, $\lambda/2$, 352-MHz Cavity

Parameter	Value	Unit
Bore-Hole Diameter	10.0	cm
Cell Length (center line to center line)	42.49	cm
Cell Length (inside of cell, wall to wall)	38.9	cm
Cell Radius	30.2	cm
Number of Cells	5	
Active Length of Cavity	2.12	m
Total Length of Cavity	2.32	m
Shunt Impedance per cavity	55.3	M Ω
Average Accelerating Voltage	1.39	MV/m
Total Power Required	546	kW
rf Power @ 2.95 MV/cavity	156.9	kW

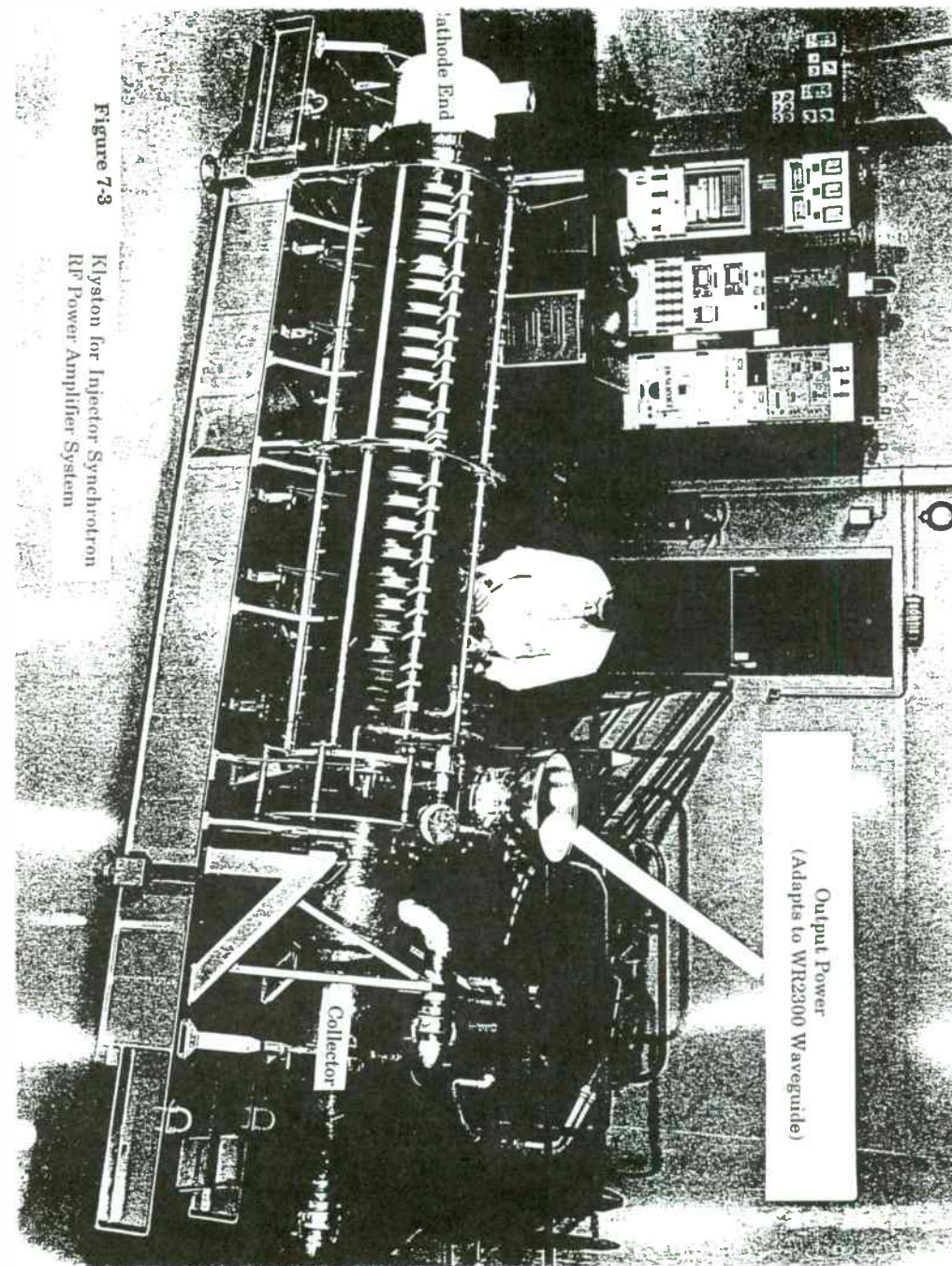


Figure 7-3

**Klystron for Injector Synchrotron
 RF Power Amplifier System**

Table 8-1

Parameters of the RF System

Harmonic number	1296			
RF frequency	351.929	MHz		
Peak voltage per turn	9.500	MV		
Number of cavities	15			
Cavity parameters:				
Max voltage (estimated)	1.00	MV		
Shunt resistance	5.60	M Ω		
Max power	89.2	kW		
Quality Factor, Q	48.6	10^3		
Operating values:				
	7 GeV	7GeV	7.5 GeV	
	<u>100 mA</u>	<u>300 mA</u>	<u>200 mA</u>	
Voltage per turn	9.5	9.5	12.0	MV
Voltage per cavity	633.3	633.3	800.0	kV
Power per cavity	35.8	35.8	57.1	kW
Total power	537.0	537.0	856.5	kW
Beam power per cavity	46.0	138.0	117.3	kW
Sum	81.0	173.0	174.3	kW
Q (loaded)	21.1	9.87	16.0	10^3
Bandwidth (loaded)	16.7	35.8	22.1	kHz
Power lost (source to cavity)	8.1	17.3	17.4	kW
Source power	1.34	2.85	2.87	MW

3dB bandwidth of cavity alone = 7.23 kHz

Table 8-2

Radio Frequency and Beam Parameters for
7-GeV and 100-mA Operation

Frequency	351.929	MHz
Harmonic Number	1296	
rf Voltage	9.5	MV
rf Voltage per Cavity	633	kV
Number of Single-Cell Cavities	15	
Synchrotron Radiation Loss per Turn (bending Magnets)	5.45	MeV
Parasitic Voltage Loss	0.20	MV
Voltage for Insertion Devices	1.25	MV
$\sin \phi_s$	0.73	
Number of Klystrons	3	
Power at 7 GeV and 100 mA	1.27	MW
Installed Power	3.0	MW
With 5.0 mA per Bunch:		
Energy Spread, σ_E/E	0.29×10^{-2}	
Bunch Length, σ	17.5	mm
rf-Bucket Height, $\Delta E_{rf}/E_0$ (with ID and estimated parasitic losses)	2.0% = 7	σ_E/E
Synchrotron Frequency	1.96	kHz

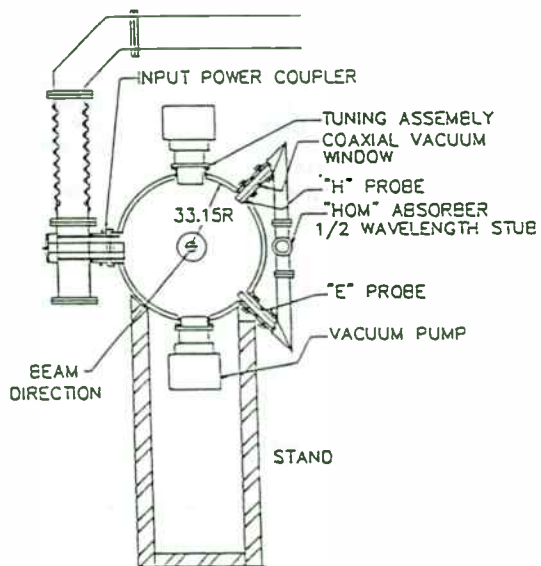
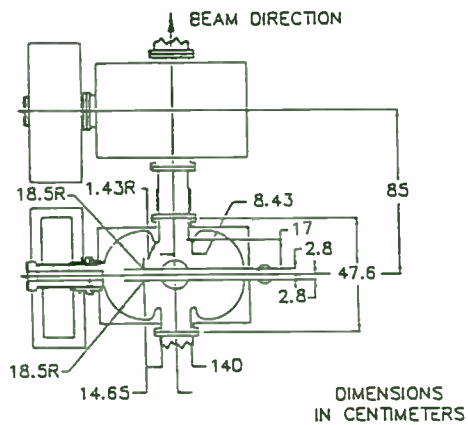


Figure 8-1 352-MHz Accelerating Structure Showing a Top View of Two Cavities and a Vertical Cross Section

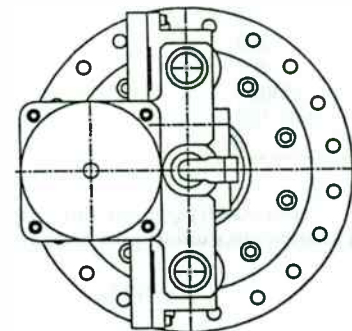
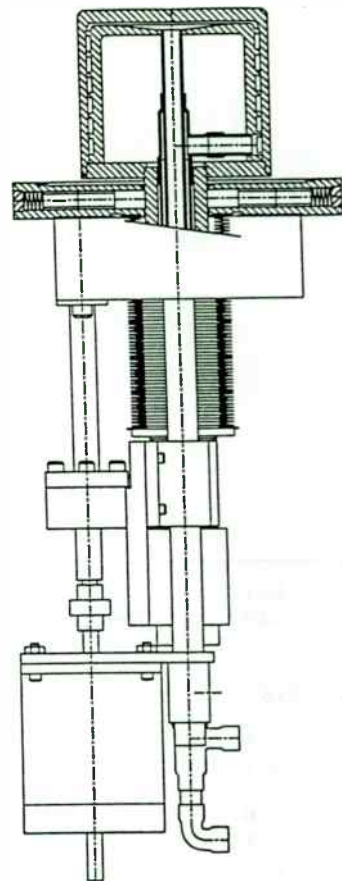


Figure 8-2 Tuner (Non-Conducting Plunger), Activated by Stepping Motor over a One MHz Range.

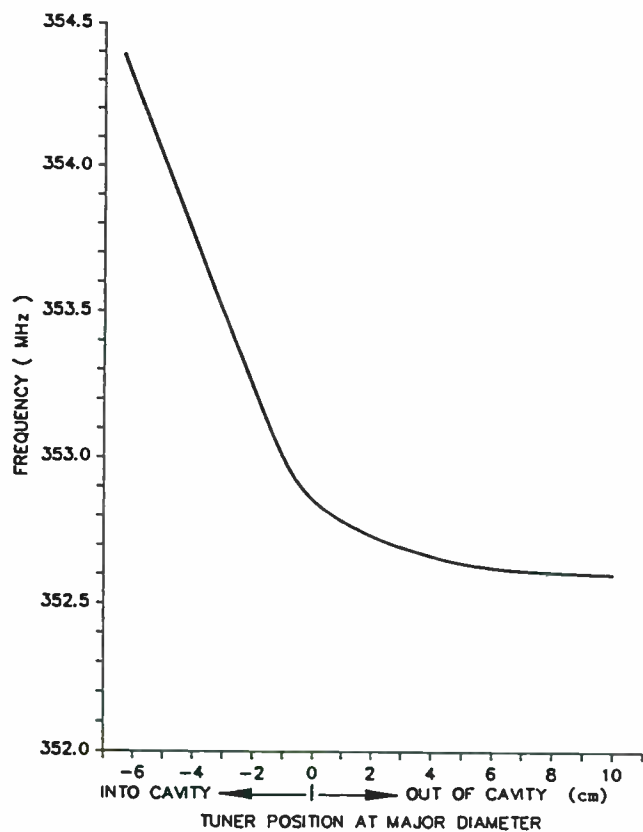


Figure 8-3 Effect of Tuner

Table 8-3

Shunt Impedances of Some of the Higher-Order Modes of the Single-Cell Spherical Cavity

Frequency MHz	Shunt Impedance (undamped) MΩ	Q (undamped)
353.0	11.23	48,600
743.0	0.03	41,630
925.0	1.25	108,800
1174	0.33	43,450
1330	0.03	129,000
1511	1.09	88,130
1654	0.07	45,770
1679	1.06	46,260
1842	0.33	121,250
1972	2.98	54,850

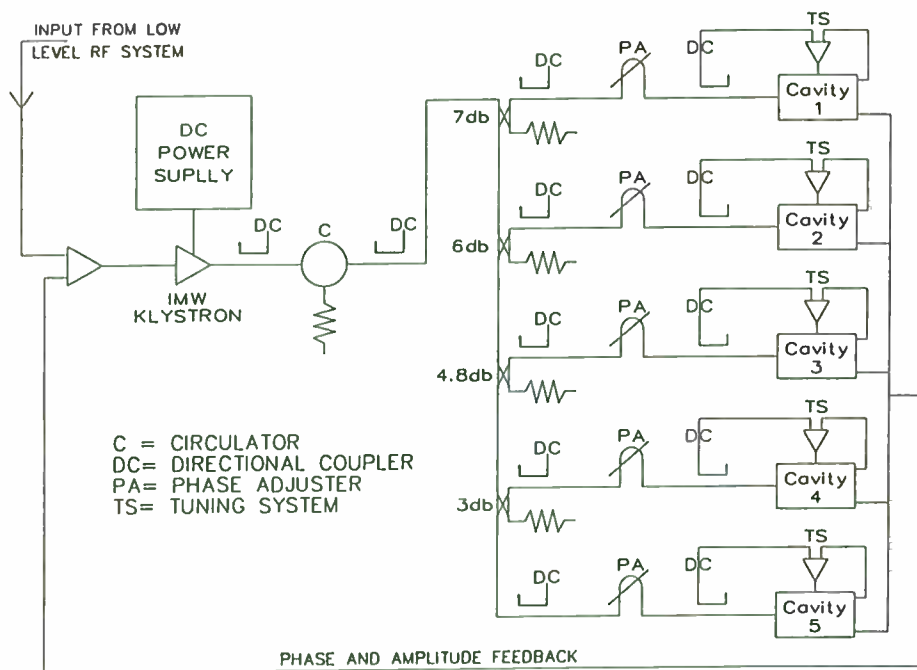


Figure 8-4 Schematic Diagram of Circuit Used to Split the Power From One 352-MHz, 1-MW Klystron and Distribute it to Five RF Cavities

Table 8-4

**Parameters for the Thomson-CSF
TH 2089 1-MW, 352-MHz Klystron**

Operating Frequency	352	MHz
Mechanical Tuning Range with Respect to Center Frequency	±3	MHz
Continuous Output Power	1.0	MW
Reflected Power, Maximum	16.6	kW
Drive Power, Maximum	200	W
Gain, Minimum	40	dB
Gain, Typical	41	dB
Efficiency	65-70	%
Beam Voltage	90	kV
Beam Current	18	A
Length (horizontal position)	4.8	m
Height (horizontal position)	1.85	m
Width	1.0	m
Output Waveguide	WR2300	

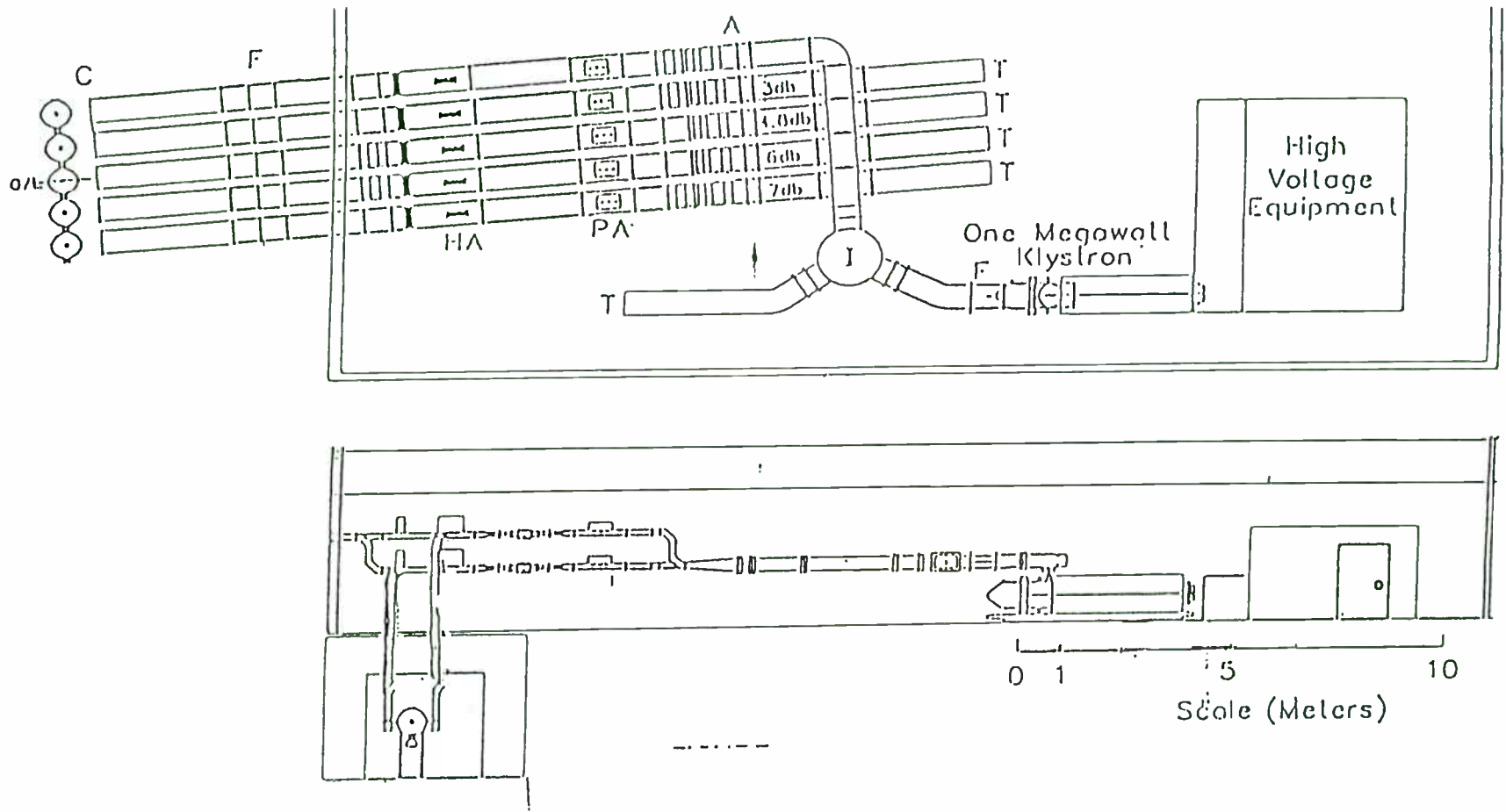
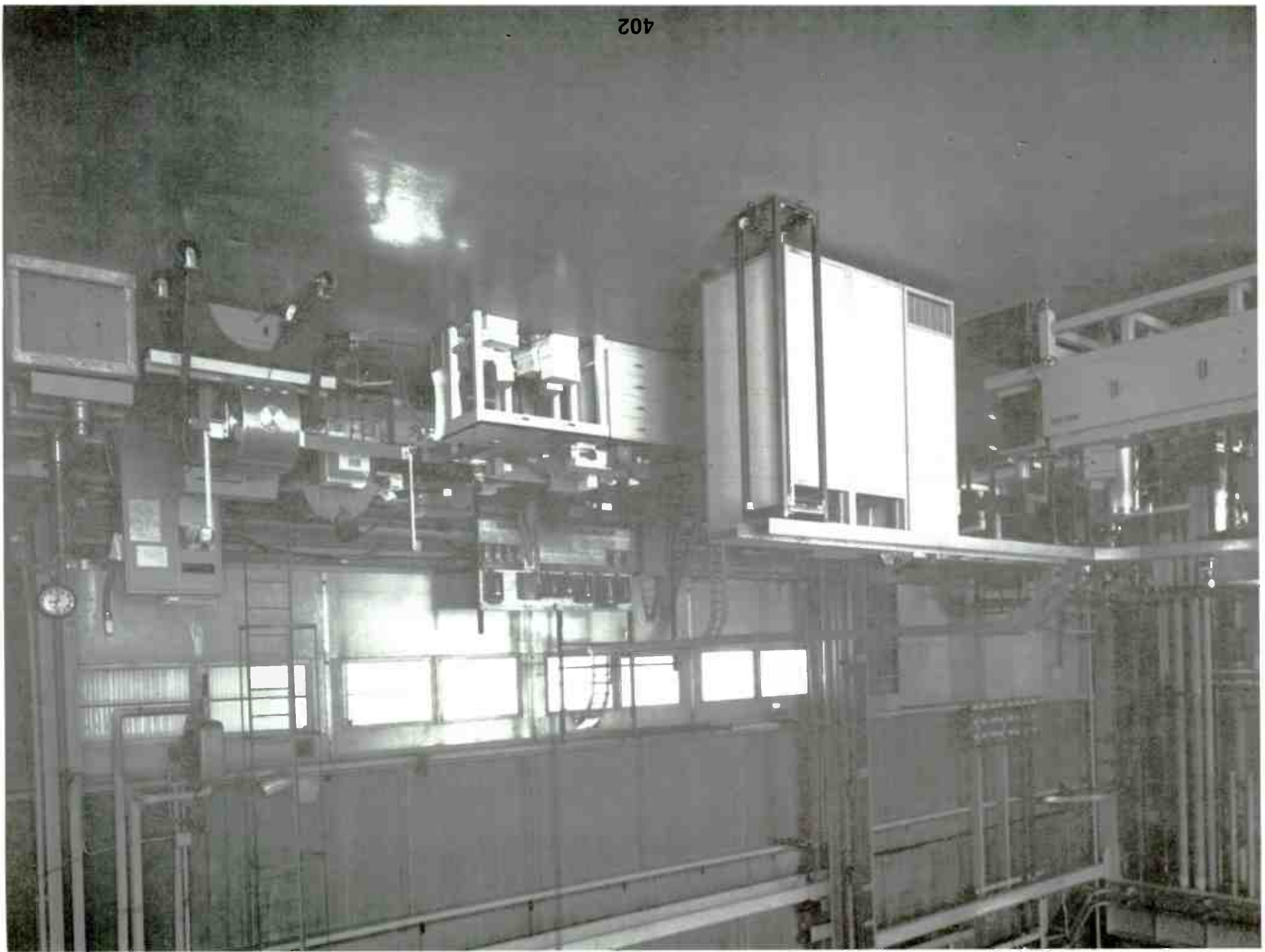
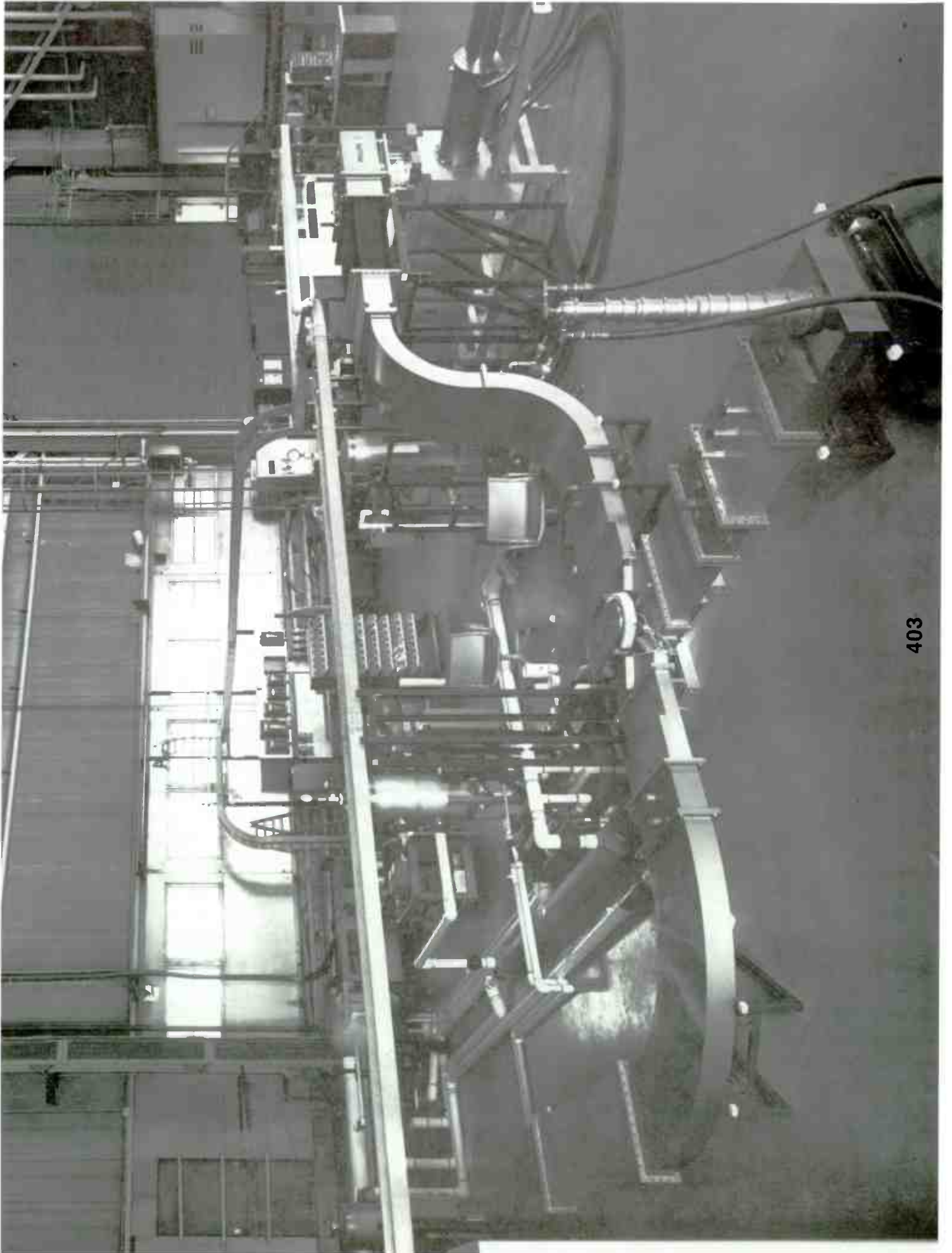


Figure 8-5 Klystron Amplifier and Cavities





RF Applications in Particle Accelerators*

Curt Hovater and Rich Abbott

Continuous Electron Beam Accelerator Facility
12000 Jefferson Avenue, Newport News, Virginia 23606

Abstract

Most particle accelerators, either for physics research or medical applications, use RF fields to accelerate the charged particles. For example, charged particles gain energy from electromagnetic fields stored in resonant structures, RF cavities, which are driven in a mode that has a strong longitudinal electric field along the particle path. The quality factor or "Q" for these cavities runs from 10,000 for a copper structure to several 10^9 for a niobium superconducting cavity. Typically, heavy ion accelerators operate below 100 MHz, proton machines below 500 MHz, and electron accelerators below 3 GHz. To successfully accelerate a charged particle the cavity RF phase and amplitude must be precisely controlled, otherwise beam quality may be degraded. To control the phase and amplitude, accelerators use feedback schemes at either a baseband or an IF frequency. Typical RF components used to accomplish this are: phase detectors, diode detectors, complex phasor modulators, varactor phase modulators, pin-diode amplitude modulators and Gilbert cell multipliers. Other areas in accelerators that use RF systems include beam position monitors and beam conditioning (bunching and modulation). This paper discusses RF control systems and the RF circuits employed by the various types of particle accelerators.

Introduction

RF technology is used in three distinct areas of particle accelerators. The most obvious is in the acceleration of particles themselves; this normally requires phase and amplitude control of both the high power amplifier and the accelerating cavity. Second is in beam conditioning which includes bunching of the beam, separation of bunches with different

*Supported by U.S. Department of Energy under contract DE-AC05-84-ER40150.

energies, and stochastic beam cooling. Lastly, beam position can be determined either through inductive coupling loops or resonated cavities using comparison techniques. While some of these terms may be new to the average RF engineer, the circuits and components used in these applications are common to many RF systems.

Accelerating Structure

In order to accelerate a charged particle, some type of cavity resonator or loaded waveguide is needed to couple the RF energy onto the beam. Accelerating structures come in many forms depending on the mass and velocity of the charged particle. For a heavy ion or proton the cavity may look like Figure 1 which has drift tubes between the acceleration gaps.¹ One drawback for this type of structure is that the drift spaces become longer as the particles speed increases. This is necessary to synchronize the particles with the RF. The solution is not as simple as increasing the frequency of the cavity and thereby reducing the driftspace. The acceleration gaps between the drift tubes conduct large displacement currents at high frequencies and would load down the power amplifier.²

Once the proton or ions attain higher energies, different types of cavities that can support a standing wave are used. In Figure 2 a coupled cavity resonator is shown that is being used to accelerate protons at LANL.³ This is a disk and washer structure with the cavities defined by the washers. The fields in the cavities are capacitively coupled through the washers. This is only one type of coupled cavity structure, and there are many other types in use. For heavy particles (protons and ions) a combination of the drift tube and the coupled cavity linacs are necessary to get the particles to relativistic energies.

Electrons on the other hand are easier to accelerate and may only require one type of structure to reach high energies. For a pulsed system such as the one used at SLAC, they use a slow wave ($V < c$) iris loaded waveguide that can support a travelling wave. A simple iris loaded waveguide is shown in Figure 3. At the downstream end of the waveguide the attenuated RF power is coupled into a load to avoid reflections. In a continuous wave accelerator, such as CEBAF, a superconducting coupled cavity that can support standing waves is used. The cavities, Figure 4, incorporate elliptical cells which help to eliminate

voltage breakdown and in turn increase the field gradient. When resonant cavities are used a feedback system is necessary to keep the cavity fields stable.

Another decision for the accelerator designer is whether to use superconducting or normal conducting materials. Copper is almost exclusively used for normal conducting accelerators. It is inexpensive and is a very good conductor at room temperature. The advantages of using superconducting cavities are higher CW gradients and lowered RF power requirements. For large machines the cost of a helium refrigeration system may be less than higher power RF amplifiers. Presently most superconducting cavities are made from niobium, which is only superconducting at liquid helium temperatures (< 9 K). An area that holds intense interest to cavity designers is the new high temperature superconductors. By going to liquid nitrogen cooling the cost of these machines would greatly decrease.

One drawback of superconducting cavities is their susceptibility to low frequency noise, i.e., vacuum pumps, vehicles, etc. This is due to the extremely high "Q"'s achieved by these cavities. With the increased Q, the bandwidth becomes of the order of 100 Hz and sophisticated feedback systems are often needed to achieve required performance.

RF Power Amplifiers

RF amplifiers used in particle accelerators have mainly been tube devices. Klystrons have been used in accelerators above 200 MHz, while tetrodes are principally used at lower frequencies. Their power ranges from a few hundred watts to a megawatt depending on the system configuration. One popular way to power low and medium accelerators is to use one huge tube to power a number of accelerating cavities. At NIST a 500 kW klystron powers four accelerating cavities through a wave guide splitter network.³ This is possible because the cavity noise is small and mainly dominated by slow temperature effects. For a superconducting cavity where errors may not be correlated, the microphonic effects limit the feedback system to one amplifier per cavity.

An interesting outcome from SDI has been research into high power solid state amplifiers. The BEAR (Beam Experiments Aboard Rockets) project uses two pulsed 60 kW

amplifiers at 425 MHz. The amplifier is made up of silicon bipolar transistors packaged in groups of four. For a pulse length of 60 microseconds, the four transistor package can produce 2 kilowatts.⁴

RF Control Systems

Phase

Upon entering a cavity the bunch of charged particles are introduced to a time varying electromagnetic field. In order to accelerate the particles the phase of the field must be precisely tuned to the bunch. The engineer must provide a system that controls phase around the amplifier/cavity and sets the phase relative to the beam. Figure 5 shows a block diagram of such a system. Assume the system operates at 1500 MHz and has a 10 kW klystron feeding a copper cavity with a loaded Q of 10,000. The first phase that needs to be set is the reference phase, PS1. This phase shifter needs to be continuous, capable of rotating 360 degrees. An easy way of accomplishing this is to use a Vector or Complex Phasor Modulator, CPM, which is programmed through two DACs. Now that the phase relative to other cavities is controlled, it is possible to synchronize the linac. To eliminate phase jitter a servo or feedback system is necessary. PS2 is used for this and is typically a varactor diode phase shifter. Rarely is there a need for more than 180 degrees to control the cavity phase. A linear feedback loop is then set up around the cavity. A reference signal is compared to the signal in the cavity through a diode ring mixer, PD1. To put the loop into quadrature with the reference signal a second CPM, PS3, is used. The video output of the mixer is then forced by the loop to operate around 0 Vdc. The video output is essentially the cavity phase error signal and is processed through inverting gain stages and applied to PS2. For example, if the cavity had a 20 degree phase error at 60 Hz and it needs to be reduced to 0.2 degrees, a voltage gain of roughly 40 dB is required at 60 Hz; i.e.,

$$40 \text{ dB} = 20 \log (20/.2)$$

Obviously, it is not quite as simple as this and system parameters such as poles and zeros need to be addressed. In this example, the cavity provides one pole at

$$150 \text{ kHz} = 1500 \text{ MHz}/Q_i$$

and the poles of PS2 and PD1 should also be considered. Therefore, it is necessary to provide a pole in the gain stages (loop filter) so the system does not become unstable.

Amplitude

The field of the cavity must remain constant, otherwise it imparts noise onto the beam. This can make the beam useable for the experimenter or its intended application. Like the phase loop the cavity needs an amplitude feedback system. Figure 5 also shows such an amplitude loop. The cavity amplitude error signal is detected by a low barrier Schottky diode, D1. The detected video signal is compared to a voltage reference in the first gain stage, which removes the dc component of the signal. What is left is the cavity error signal. This signal is then inverted, amplified and applied to a pin-diode attenuator, AM1. If the operator needs more energy imparted onto the beam he adjusts the voltage reference to a higher position. Like the phase loop the engineer must also consider loop parameters such as the cavity and the RF components when designing the feedback system.

The systems mentioned above will easily control phase to 1 degree level and reduce amplitude noise by 3 orders of magnitude. A high performance accelerator like the one being built at CEBAF poses some more challenges. To properly accelerate the beam the cavities have to be regulated to a ± 0.1 degree in phase and have amplitude variations of less than $\pm 2.5 \times 10^{-5}$. The cavities are superconducting and have a loaded Q of 6.6×10^6 . With such a high loaded Q the bandwidth is now only a couple of hundred hertz and makes the cavity sensitive to microphonics. Mechanical vibrations from vacuum, cryogenic pumps, and other sources can now perturb with the cavity resonance frequency. Long term effects such as temperature drifts that affect phase and amplitude must also be compensated to keep the cavities synchronized.

Figure 6 shows the CEBAF RF control system. The CEBAF system is a heterodyne system that has a cavity frequency of 1497 MHz and an IF frequency of 70 MHz. Because of the tight specifications signal processing is done at an intermediate frequency, using

highspeed analog function IC's. Figure 7 shows a block diagram of a CPM and its output on a network analyzer. The CPM uses high speed Gilbert cell four quadrant multipliers to modulate the sine and cos inputs. Two advantages to be gained by using high speed analog circuitry are linearity and cost. Another feature of the CEBAF control system is the ability to detect phase shifts in the feedback line. A quadrature phase detector compares the cavity signal to a reference signal and outputs the "X" and "Y" terms to a microprocessor, where the phase shift is computed. The resonance frequency of the cavity is measured in a similar manner by comparing the incident signal to the cavity signal. This allows the cavity to be tuned mechanically using a motor driven tuner.

The control system described above uses separate phase and amplitude loops. As the accelerators become more complex and specialized, control systems that use combined phase and amplitude loops may offer advantages.

Beam Conditioning

Chopping and Bunching

In many instances it is necessary to modify the charged particle beam either by removing sections of it, or decreasing the bunch length. The method of removing part of the beam is called "chopping." Upon leaving the cathode of the gun the charged particles are in a continuous stream. There needs to be a method to create a bunch so the beam can be accelerated uniformly, otherwise the beam would see different fields as it entered an accelerating cavity. One method that works well is to pass the beam through a square resonant cavity where two orthogonal modes are excited. If the modes are phased correctly, 90 degrees apart, their magnetic component will produce a time dependent deflection. Next an aperture is placed in the path of the beam. As the beam is swept across the aperture, a short pulse is created and the beam is "chopped." The deflection is cancelled after passing the bunch through another cavity and removing the transverse kick. Figure 9 shows the RF circuits involved in a chopping system. Like the modes in the cavities, the two chopping cavities need to be phased correctly, a 180 degree differential in phase, and have equal amplitudes to remove the deflection of the bunch. To properly accelerate the beam,

the bunch length has to be shortened. This is accomplished by passing the bunch through a cavity that decelerates the head and accelerates the tail. Instead of passing through the cavity at the crest of the RF it is phased to see the field go from negative to positive. The phase and amplitude for these cavities is also controlled through feedback as described previously.

Stochastic Cooling

Another form of beam conditioning that is used in proton/antiproton storage rings is stochastic beam cooling. Particles travelling around a ring have slightly different energies, an “energy spread.” Experimenters prefer a beam with a small energy spread and a way to reduce this difference is to cool the beam through feedback. The position of the particle inside the beam pipe is related to its energy. A detector senses a particle’s position at one place in the ring and gives it a cancelling kick in another. A simplified picture of such a system is given in Figure 10.⁵ The cable and amplifiers are chosen so that the signal generated in the pickup by a group of particles arrives at the kicker at the same time as the particles.⁵

In reality the pickup sees a distribution of particles with different energy offsets and positions. To cool the beam more quickly it is necessary to have the smallest sample size possible; this requires a system with a wide bandwidth. Bandwidths normally run several gigahertz.

A block diagram of a system in place at FNAL is shown in Figure 11.⁶ At first glance it looks similar to a monopulse RADAR feed and in reality it’s not much different. Because of reciprocity the pickups and kickers are identical. The simplest form of a pickup is a 1/4 wave loop pick as seen in Figure 12.⁷ Care must be taken in designing pickups because of the small signals imparted by the beam. Single loops rarely provide enough signal and must be combined and phased properly with other signals in the same quadrant. One of the limitations of the coupled loop is bandwidth. As bandwidths are increased to improve cooling, half wave slot lines may provide better coupling.

Since the weak beam noise is basically the detected signal, pre-amplifiers must have extremely low noise characteristics. Preamplifiers (GAsFET) are quite often cryogenically cooled to reduce their noise temperature.

To provide the broad band kick the power amplifier is either a travelling wave tube or a solid state device. The need for wide bandwidths almost precludes any other tubes from being used. After the amplifier, the signal is split and applied to the beam.⁵

Beam Position Monitors

In an accelerator, it is important to know where the beam is inside the vacuum pipe. The optics of an accelerator are optimized when the beam is centered. (The term optics comes from the close relationship focusing magnets (quadrupoles) have with lenses used in light optics.) If the beam is not centered when it enters an accelerating structure the field gradient in the cavity may steer it even more off center because of field asymmetry.

Beam position monitors (BPM) vary really only in their pick up electronics. All rely on similar techniques to measure relative beam position. Figure 13 shows a typical block diagram of such a system. Like the stochastic cooling electronics BPM’s also use a technique similar to mono pulse RADAR. With four pick ups (two for “X” and “Y”) and software performing the mathematical relationship,

$$(A - B)/(A + B)$$

one can map the position onto the X, Y, plane. From this information a feedback system can be set up to correct the position using steering magnets before the BPM.

Inductive Pickup

The first pick up method that works well for any accelerator with a large enough current is an inductive pickup loop. As with a current in a wire, circular magnetic field lines are produced by the charged particle beam. By modulating the beam and then looking at the modulation coupled onto four loop pickups located in the four quadrants around the beam, the position of the beam is determined. Figure 14 shows a single channel

of such a system being used at CEBAF. A coherent detection scheme is used where the phase term in the down converted signal is removed by a varactor phase shifter. A diode ring mixer is used to compare the two 100 MHz signals with only the amplitude component remaining. This is then further processed through an analog to digital converter (ADC) where the math is performed by a computer.

Quarterwave Pickup

Another pickup method uses 1/4 wave shorted stubs in the beam pipe, matched to the frequency of the charged particle bunch. The bunch frequency is the same as the accelerating cavity frequency. Figure 15 shows a circuit currently being tested at CEBAF. Because of its cavity frequency (1497 MHz), it uses an IF at 1 MHz. The detected signal (-75 dBm) is passed through a low noise preamp and then down converted to 1 MHz.

The signal is then amplified again using a high speed operational amplifier. After the OP-AMP the signal is split in two. One signal goes directly into the analog demodulator and carries the relevant amplitude information. The other signal first goes through variable phase shifter that puts the two signals in phase. Next it is phased locked to a VCO at the same frequency. This acts like a perfect limiter and keeps a constant LO into the demodulator. It has one advantage over a limiter in that it does not have any AM to PM effects arising from the different power levels the device may see. The two signals are then compared in the demodulator providing a dc output. The signal from there is handled similar to the previous BPM.

BPM's can also use resonant cavities to find beam position. A charged particle beam excites a TE110 mode in a cavity at the bunch frequency. When the particles are centered the gradient excited would be at a minimum as seen by a loop pick up. Any deviation from the center would result in a field change. This can be detected by the loop pickup and a similar receiver system, as mentioned previously, can be used to find beam position.

Summary

The number of different RF devices used in particle accelerators is immense. One has only to look into the IEEE Particle Accelerator Conference proceedings to get an idea of

the different types of cavity control systems and beam position systems that are in use today. In this paper, only a few of the more significant areas have been covered.

The future of particle accelerator projects is very bright and in turn this means more potential RF applications. The 57 mile Superconducting Super Collider (SSC) being built is one example, and it will need many of the systems mentioned in this paper. Some of the projects that are currently under construction or planned include: free electron lasers, synchrotron light sources, heavy ion fusion experiments, and heavy ion storage rings.

Acknowledgments

The authors would like to thank Stefan Simrock for his technical editing, Joe Bisognano for his discussions on stochastic cooling, and Jay Heefner for his description on beam position monitors.

Acronyms

CEBAF:	Continuous Electron Beam Accelerator Facility
SLAC:	Stanford Linear Accelerator
NIST:	National Institute of Standards and Technology (NSB)
LANL:	Los Alamos National Laboratory
FNAL:	Fermi National Accelerator Laboratory

References

1. "Partical Accelerators", Martin P. Reiser, 1972 American Institute of Physics Handbook.
2. "Principles of Charged Particle Acceleration", Stanley Humphries, Jr., 1986, John Wiley & Sons.
3. The NIST/NRL Free-Electron Laser Facility, P. H. Debenham, et. al., PAC, 1989.
4. "High Powered, Solid State RF Systems", D. W. Reid, LANL, 1987, PAC.
5. "Charged Particle Beams", Stanley Humphries, Jr., 1990, John Wiley and Sons.

6. "Performance of Tevatron I Core Stochastic Cooling Systems", W. Kells, et al., PAC, 1987.
7. "Review of the Physics, Technology and Practice of Stochastic Beam Cooling", J. Marriner, PAC, 1987.

[apd.hovater]@paper.tex

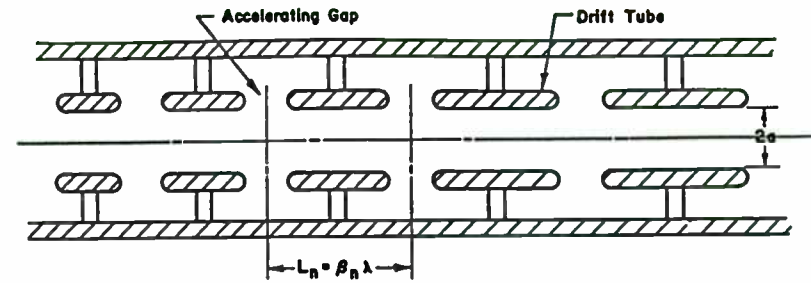


Figure 1. ACCELERATION SYSTEM OF A PROTON LINAC
Reference 1.

VG12/01

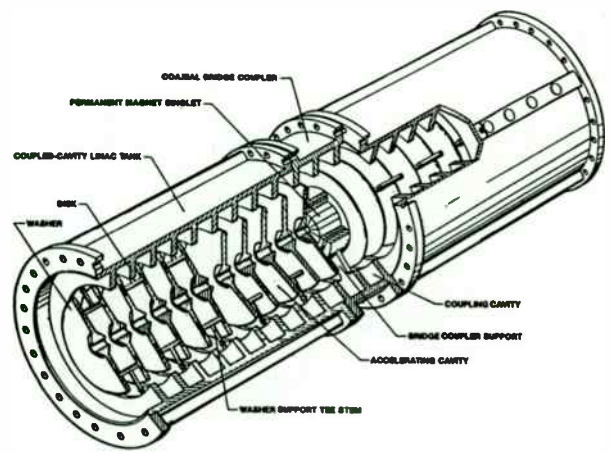


Figure 2. CUTAWAY VIEW OF A DISK-AND-WASHER ACCELERATOR STRUCTURE
Reference 2.

VG13/CH

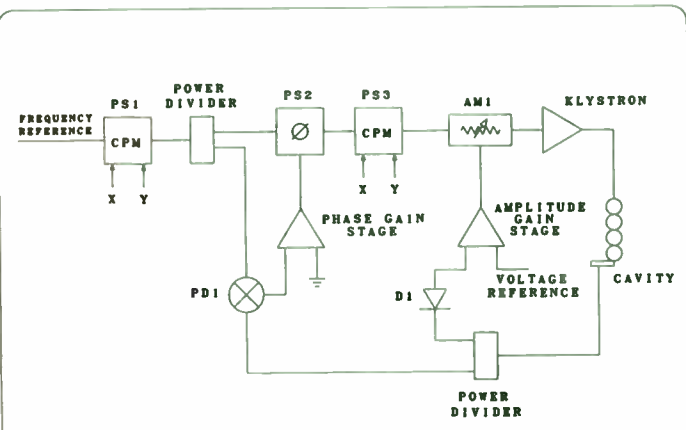


Figure 5. SIMPLE RF CAVITY CONTROLLER

Y62/CH

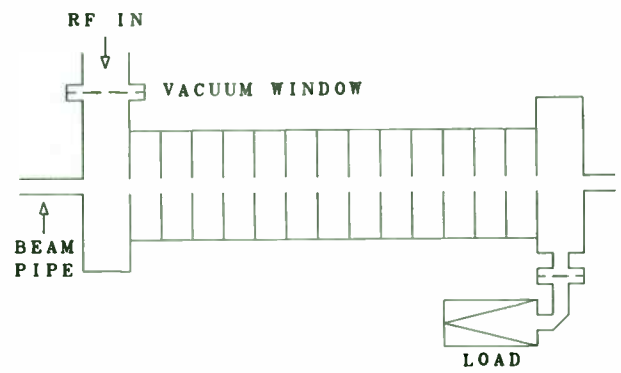


Figure 3. DISK LOADED WAVEGUIDE

Y61/CH

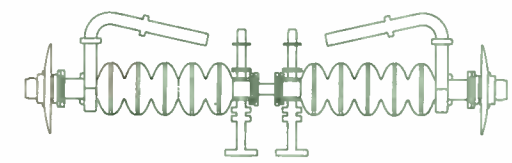
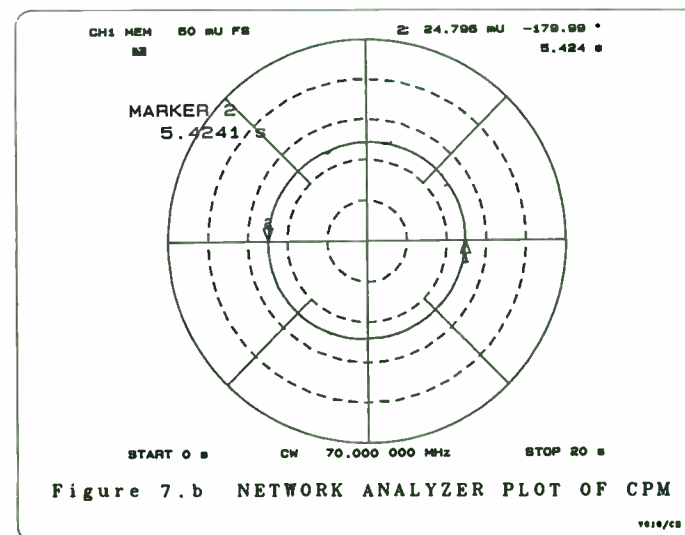
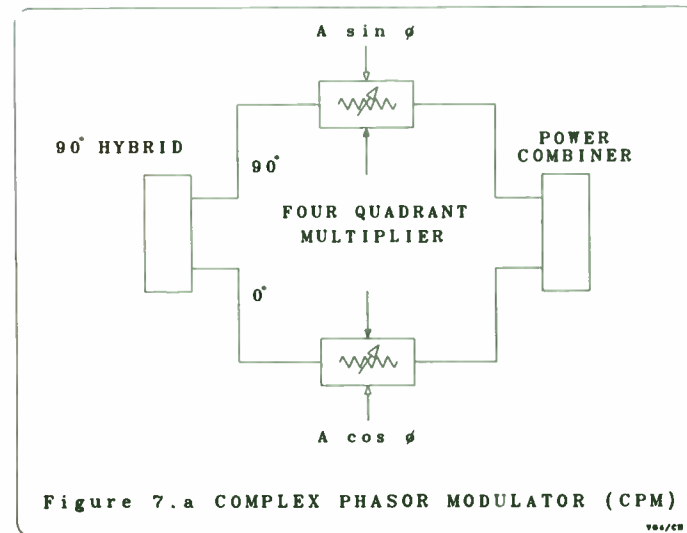
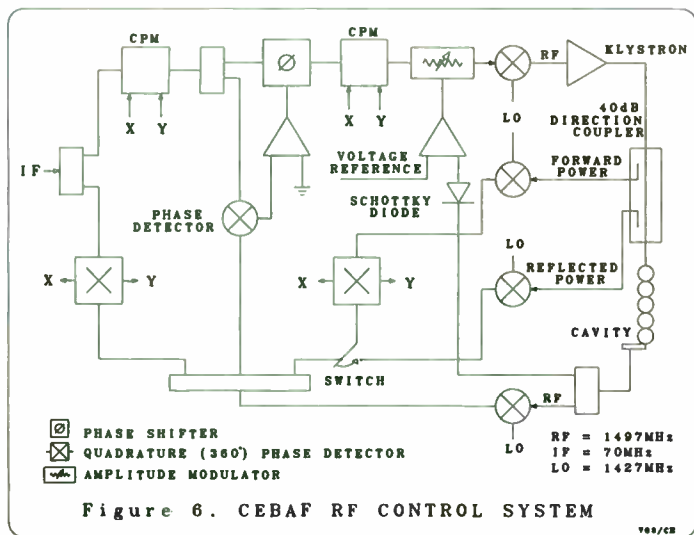
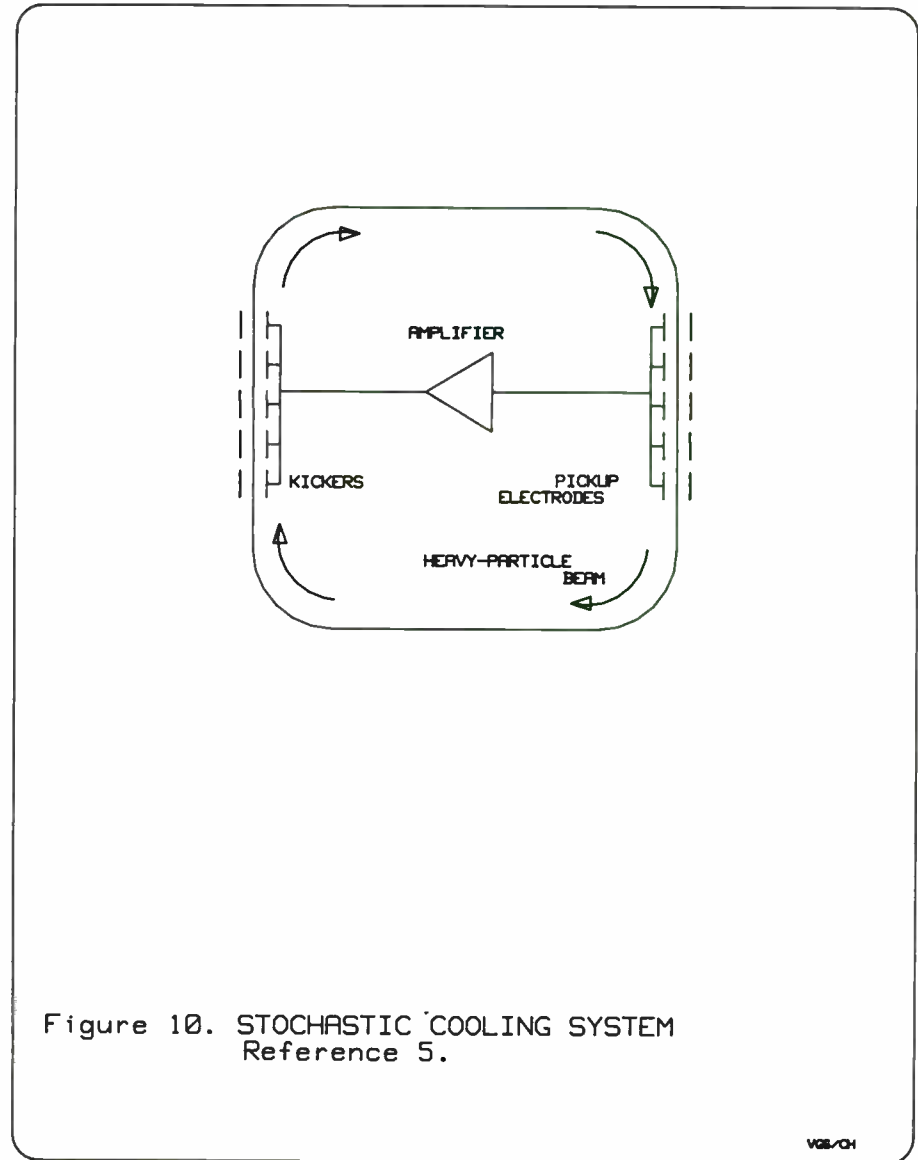
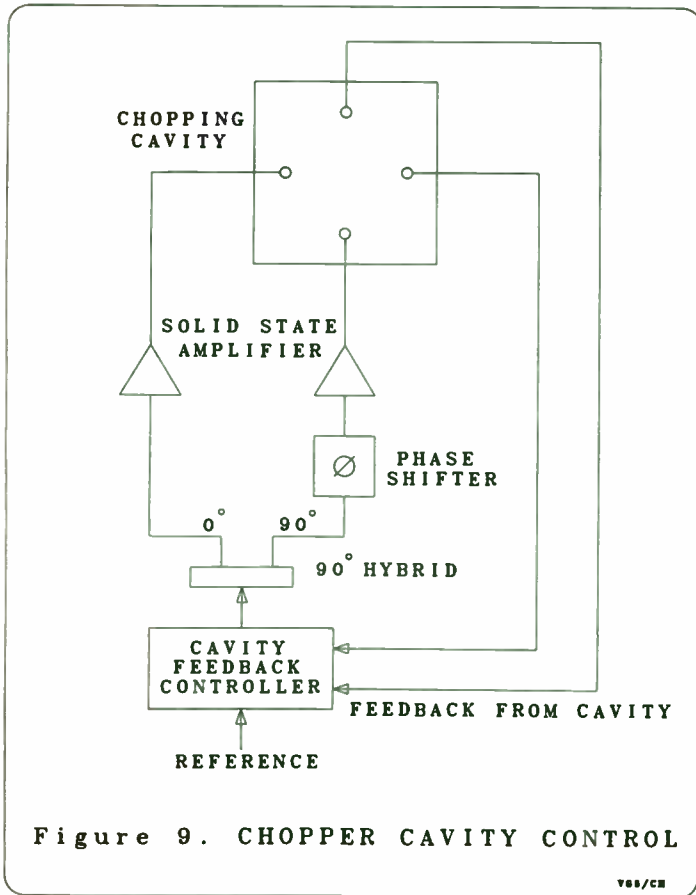
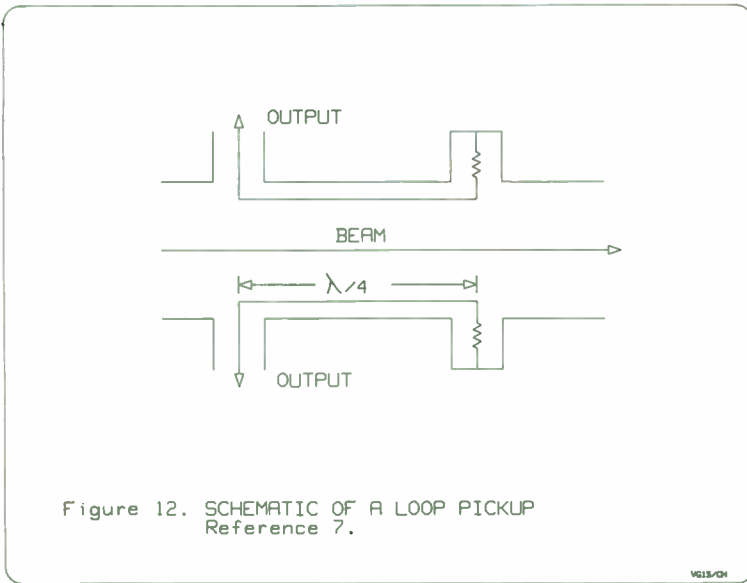
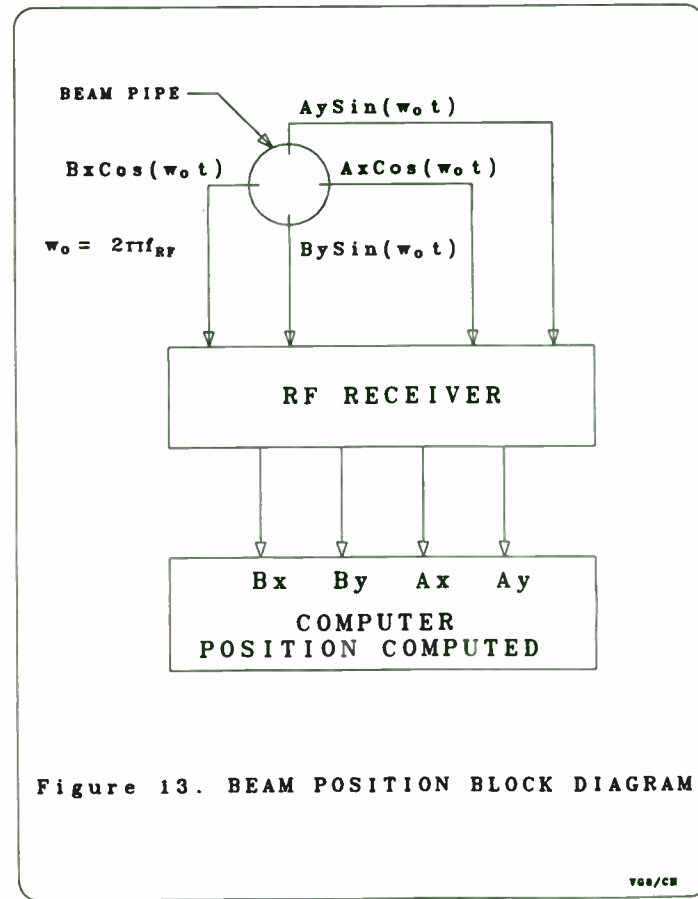
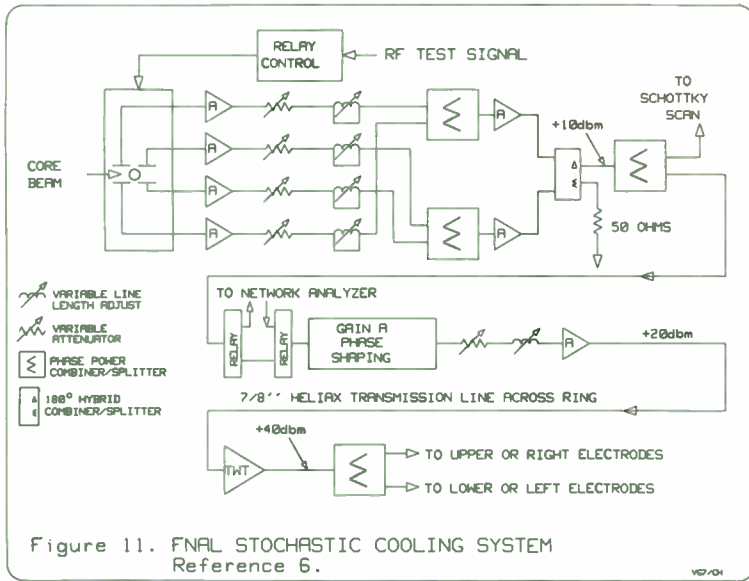


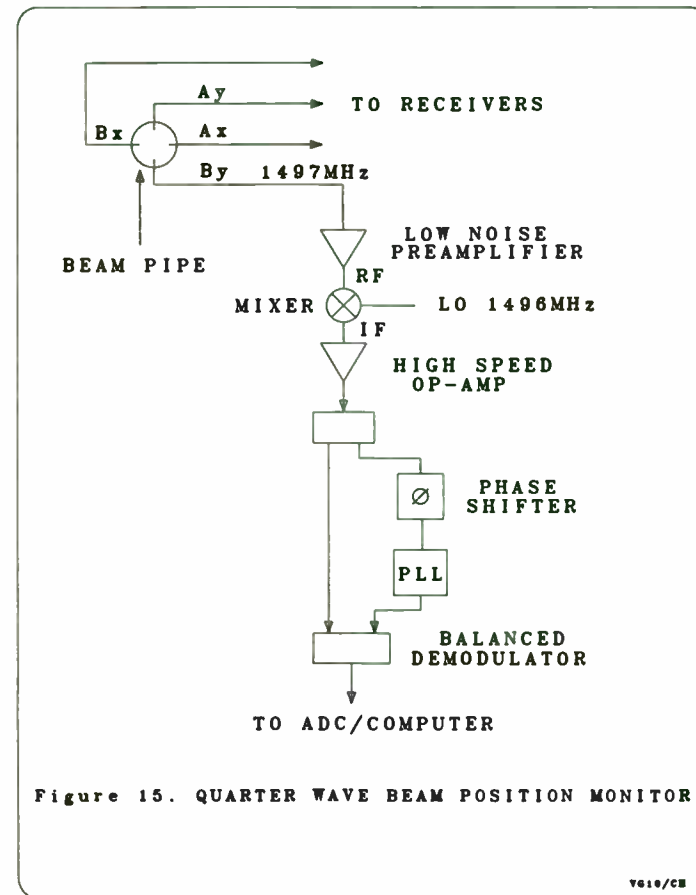
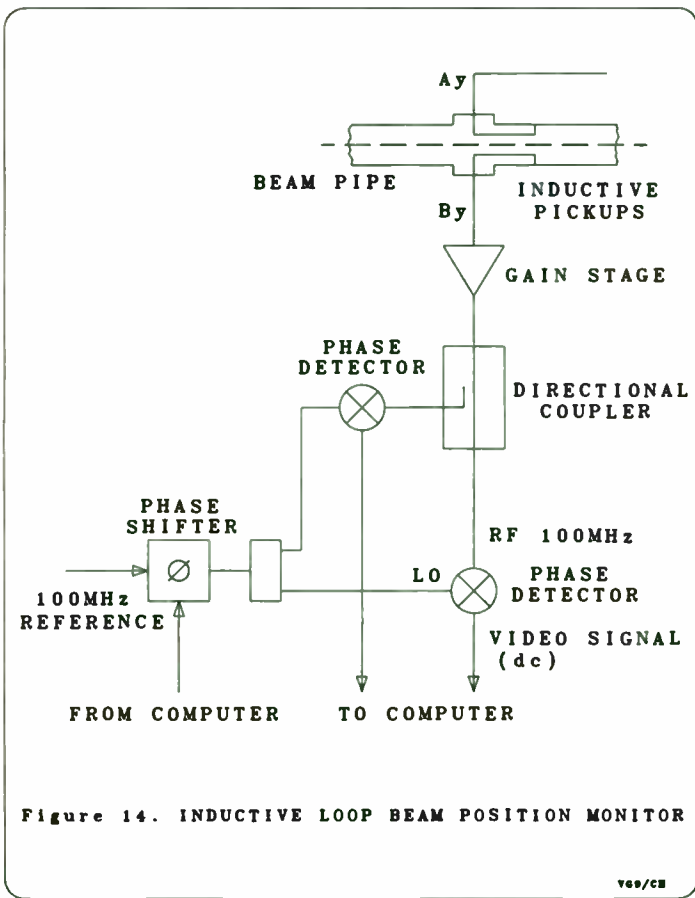
Figure 4. CEBAF SUPER CONDUCTING CAVITY

Y611/CH









A fully digital RF-signal synthesis and phase control for acceleration in the cooler synchrotron COSY

Paul Shirkey^{(a)†}, Hermann Meuth^(a), and Heinz Rongen^(b)
(a) Institut für Kernphysik, (b) Zentrallabor für Elektronik,
Forschungszentrum Jülich,
P.O. Box 1913, D-5170 Jülich 1, FRGermany

Abstract:

For rf carrier frequencies ranging up to 2 MHz, and maximum clock and sampling rates of about 25 MSPS, a fully digital real time rf-signal synthesis, phase control, and processing system is being designed for use on COSY. This new **CO**oler **SY**nchrotron accelerator ring is now under construction at the research center KFA Jülich. Lacking presently the availability of integrated processors operating at such speeds, the required performance of this digital signal processing system will be achieved by a hardware-programmed hybrid scheme, based on a binary integer algorithm. It heavily relies on parallel pipelining, with butterfly-type fast multiplier configurations as main single elements. Components for such an approach, mainly of the CMOS technology, have become available only recently.

At the core of the control system, the rf acceleration signal is synthesized by modulation of amplitude, frequency, and phase. Rf acceleration requirements call for amplitude variations in excess of 55 dB; a frequency range of 0.4 to 1.6 MHz at a max. tuning rate of 4 MHz/s; and rapid phase jumps of more than π within ten rf cycles. The system will serve as control of the sequential chain of rf power amplifiers. Its phase control part is governed by longitudinal beam-phase measurements, while the frequency modulation is given by transverse beam-position measurements and/or host provided input tables from the central control computer. The power amplifiers of ca. 50 kWatts are terminated into a ferrite-loaded frequency-tunable resonant cavity load.

The synthesis and control system basically consists of a numerically controlled digital oscillator and a phase-control loop, that includes amplitude, frequency, and phase modulation and demodulation modules. It has a linear 12 to 16-Bit dynamic range in rf-signal variation and is based on the quadrature principle, permitting a continuous and

smooth phase swing of a full 2π , with an expected phase resolution of a fraction of a degree. These features are intended to avoid frequency-to-phase and amplitude-to-phase trans-modulations, inherent to control systems of large frequency-swing and amplitude-dynamic range. It also avoids the usual "blind spots" for phase values around π and/or 2π , common to phase discriminators of more conventional design.

The scheme is presently being examined for its viability and accuracy by computer simulations, and some of the major electronic components will soon be available to us for bench tests.

1. Introduction:

Particle accelerators are employed for basic research, and for many technical and industrial applications. Depending on the type and field of use, they vary tremendously in performance characteristics and techniques. Nevertheless, electromagnetic fields are generally used to accelerate charged particles to speeds very close to the speed of light. Although dc electric acceleration fields can be used, like in Van-de-Graaf accelerators, rf fields offer many benefits. In rf accelerators, with proper phasing and timing, acceleration field strengths can greatly be reduced (to the kV range), in comparison with dc systems. Dc accelerators cannot be recirculating, and therefore use linear geometry (LINACS). Rf accelerators are both of the LINAC type and also of the circular or "race track" type. There exists a host of such recirculating schemes, requiring transverse "bending" forces to force particles onto their turns. These transverse forces are generated by dipole magnetic fields. Cyclotrons and synchrotrons are two major examples for recirculating machines. In cyclotrons, particles spiral outwards due to increasing centripetal forces during acceleration, and are finally ejected, limiting the total number of turns. However, cyclotrons have the benefit of retaining the particles' revolution frequency. In synchrotrons, particles stay on fixed tracks for millions of turns, and can therefore be used also as particle storage rings, while, when accelerated, they increase their revolution frequency. Thus, in synchrotrons, a sophisticated frequency and phase control of the rf fields is required to lock particles and rf acceleration fields together, and synchronize them with the magnetic guiding field control.

[†] permanent address Oregon State University, Corvallis, Oregon 97330

In the past few years, several proton storage-synchrotrons have been built, or are under construction, in a number of countries, that possess considerable beam quality, as reflected e.g. by the beam's focusability. As there are always many particles circulating, there is a certain statistical noisiness in their behavior, a measure of which is the beams' emittance. The lower this randomness (relative to the beam's overall velocity), the better will be the beam quality. It may be enhanced by cooling techniques, such as stochastic and/or electron cooling. On the other hand, to make these cooling efforts worth while, the demands on the tolerances of the entire control of such a cooler-synchrotron-storage ring are very high. In turn, these high beam qualities will permit experiments in intermediate energy and particle physics of hitherto unattained precision, and may be likened to optical qualities achievable since the advent of the laser for spectroscopy and diagnostics.

Such a cooler-synchrotron storage ring, called COSY, is under construction at the Research Center Jülich. With a race-track configuration of 184 m in circumference, it is one of the largest of this class of cooler devices, and is designed to achieve particle energies of 2.5 GeV, accelerated from ca. 40 MeV at injection.

2. The radio frequency acceleration structure:

The radio frequency acceleration structures of such rings are usually high power cavities of tens of kilowatts, generating maximum acceleration voltages of around ten kilovolts. Depending on particle energies and ring circumference, frequencies range from hundreds of kilohertz to a few megahertz (for COSY: 400 kHz to 1.6 MHz).

For such low frequencies, reasonably sized cavities have to be loaded with ferrites, to accommodate the wavelengths of the rf fields at these frequencies. At the same time, these ferrites serve for cavity tunability by magnetic polarization. This polarization varies the ferrites' permeability. While being dc compared with the rf frequencies, the polarization currents have to closely track the ramping of frequency (and of the guiding magnetic fields) to keep the cavity, or cavities, in resonance during the course of acceleration.

3. Overall rf control system:

The just mentioned cavity tuning is achieved by controlling the phase between the rf voltage and the rf current into the cavity, which must be in phase at all times for an ideal cavity tune.

A second, separate rf control task is to keep beam particles (gathered together in a "beam bunch") and rf cavity voltage at a predetermined phase. During acceleration, when the rf frequency has to be varied, this phase is non-zero. For particle storage, when rf frequency is kept fixed, the phase is returned to zero. The overall control scheme containing both this cavity tuning feature and the phase control between bunch and cavity is depicted in Fig. 1. It further includes some sort of rf waveform generator with frequency modulation (FM), phase modulation (ΦM), and amplitude modulation (AM) capability. While FM and AM are predetermined by the central host computer on the basis of a desired acceleration schedule, the phase modulation is governed by both the host, and an in-flight phase correction loop, the "synchrotron feedback loop" of Fig. 1.

A representative set of modulation functions, as computed from basic accelerator laws, is depicted in Fig. 2. We note amplitude variations of three orders of magnitude, rapid phase changes by 180° , and a frequency swing by more than a factor of four. The rf carrier reaches a maximum value of 1.634 MHz for $\beta=1$, i.e. for particles at the speed of light. Beam stability requirements imply the need for a very good temporal and dynamic resolution of the rf-waveform and phase control. Traditionally, in all accelerators of this type, waveform (or frequency) generator on the one hand and synchrotron feedback loop on the other are separate units. For reasons of speed performance here, however, these two functions will be integrally combined for the first time to form a monolithic, fully digital rf-signal synthesis and phase control system. It is this system, that will be the subject of the present paper. The amplitude demodulation, while being a prerequisite for the type of phase extraction discussed here, is *not* intended for amplitude control tasks. However, the amplitude information could be used for status reports to the central host computer. Such report tasks require a less demanding temporal resolution, and, consequently, would allow continuous data transfer rates at reduced speed. The same applies to the time resolution requirements for status reports on the other quantities that may result from this digital phase control system as a by-product.

The system presented here is admittedly involved. Preliminary digital-binary simulations show, that it likely will be the only choice to achieve the desired resolution, at the mentioned frequency and phase swings, and amplitude dynamic range. Such a system is definitely realistic and deserves consideration at this point, since recent developments in the field of digital signal processing have brought out suitable commercial components, that would not have been available only a short time ago. While some of the aspects of the concept still have to be worked out in more detail, its overall approach is certainly viable.

3.1 Synopsis of requirements (see also Fig. 2):

Rf signals:

Programmable (in-flight) frequency modulation and demodulation in the range of 400 kHz to 1.6 MHz. Programmable (in-flight) amplitude modulation and demodulation in the range exceeding 60 dB. Programmable (in-flight) phase modulation and demodulation in the range of 360°. Accuracy of phase determination in the range of 1/10°. (The resulting overall phase control accuracy depends largely on the characteristics of the subsequent high power rf components.) Characteristic time constants for temporal variations in these modulation functions are in the range of less than 50, and more likely ten rf periods. Precise tolerances for amplitude, frequency and phase values are presently being specified on the basis of extensive numerical beam simulations.

Digital value and time resolution:

Nominal 12 to 16 bit, at clocking frequencies of max. either ca. 13 or 25 MHz, depending on the final choice of components. This requires parallel processing of digital sequential data streams at this resolution and clock rate. Continuous (in-flight) digital signal processing is required, since total signal durations exceed several seconds, which would otherwise require real-time 100 MByte storage and transfer. While the dynamic range requirements could be alleviated by employing any kind of dynamic compression to lower the bit-requirement, this should be considered carefully in order to avoid amplitude-to-phase cross modulations that can occur in such schemes.

4. Basis and Prerequisites:

The hardware-programmed scheme calls for only a few simple (and very rapid) mathematical operations. The concept is based on real-time computations of basic trigonometric identities (sum and product rules), as, for instance: $\sin(\omega t + \phi) = \sin\omega t \cdot \cos\phi + \sin\phi \cdot \cos\omega t$. This means that, within the limits given by the bit-resolution and the timing jitter of the analog-to-digital conversion, the procedure is rigorous. The digital data are processed in parallel streams (pipelining) along bus lines. For purely harmonic signals, i.e. signals of the form of a *single term* sine (or cosine). $A(t)\sin[2\pi f_{rf}(t) + \phi(t)]$, none of the usual filtering or averaging techniques of phase discrimination schemes would have to be invoked. Here the rf carrier frequency is denoted by $f_{rf}(t) = \omega(t)/2\pi$, the phase by $\phi(t)$, and the amplitude by $A(t)$. Instead, in the language of conventional rf-phase techniques, image rejection is used as in single-side band techniques.

For such an algorithm, frequencies, phases, and amplitudes may be arbitrary functions of time. The respective time constants for AM, FM, and Φ M variations are limited in principle only by the sampling (or clock) frequency f_c of the digitizing, and/or the computational processing. On the other hand, since the rf signals are eventually terminated into a cavity with a quality factor $20 < Q < 40$, modulation time constants of both the monitor signals and the synthesized signals for the rf acceleration voltage will not exceed the order of $1/(10f_{rf})$.

A quadrature scheme, involving only sines and cosines, and not the phases themselves, guarantees a smooth and continuous 2π -periodic phase range of a full 360°.

A central design feature is the specific realization of the frequency modulation: All digital components, including both analog-to-digital and digital-to-analog converters, are to be clocked with the *n-th harmonic* of the desired final rf frequency. While this method may seem to be somewhat out of the ordinary, it offers many benefits discussed below.

For the beam phase monitor (BPM), see Fig. 1, the prerequisite of a purely harmonic signal is not well fulfilled. During acceleration, beam bunches get more and more compressed. The beam current signals show thus large variations in duty cycle, depending on the ratio of beam bunch length to ring circumference, which introduces higher harmonic contributions. Moreover, analog dynamic compression, e.g. by logarithmic amplification, before digitization may have to be used to reduce the range of input signals of both BPM and the cavity voltage. This may introduce further anharmonicity. Thus, a subsequent narrow-band filter will be needed to reject higher harmonics. This filter has to be tuned in some way, tracking the large frequency swings of the FM. To minimize phase determination errors, identical (matched) filters have to be placed in both monitor branches (BPM and cavity voltage). Another, interesting alternative is considered here. Very fast digital filters could be used *after* the signals have been digitized. This demands a larger digital amplitude dynamic range due to the wide variation of the signals' duty factor. Thus, perhaps, analog tunable filters (with wider *fixed* band pass) have to be combined with digital filters to optimize their both advantages.

5. Functional blocks

Referring to Fig. 3, the digital signal synthesis and phase control logic includes the following functional blocks: (a) local oscillator with sine and cosine output; (b) 90°-phase shifter for quadrature; (c) frequency demodulation; (d) digital filter; (e) amplitude demodulation; (f) phase discriminator; (g) phase shifter; (h) frequency modulation; and (i) amplitude modulation. It should be noted, that, with the exception of the amplitude demodulation, the 90°-phase shifters, and the digital filters, these functional tasks can all be accomplished with identical butterfly blocks, seen in more detail in Fig. 4. They accomplish four multiplications, one sum, and one difference.

The 90°-phase shifters are discussed below. The signals are periodic with the fundamental particle revolution frequency. Thus, digital filters can be implemented by full-cycle summers after the first frequency demodulation blocks. All harmonic components of the signal carry at this point a frequency components of the form $n \cdot f_{rf}$, except the (original) rf fundamental (for which $n=1$), which is the only component retained by the full cycle summing procedure. When using such a one-cycle summer, the just mentioned 90°-phase shifters can actually be dispensed with, since quadrature

can then be accomplished by the sine/cosine local oscillator alone. Of course, the use of a full cycle summer prolongs the transit time through the pipeline by one rf period, with a corresponding reduction in temporal resolution.

For speed performance of the components, the algorithm likely has to be binary integer. This has especially repercussions on the amplitude demodulation procedure, that calls for squaring of the sine and cosine inputs, with subsequent square rooting and inversion (division). The latter two tasks can only be achieved on the necessary time scales by using a look-up table. Using the truncation (or bit-shift) feature provided by the "most significant port" (MSP) and "least significant port" (LSP) of most multipliers, the input amplitude B can be brought to the maximum permissible value (given the total bits) by the "inversion" factor

$$\text{RND}_1 \{A^2/B\} = m \cdot A + \Delta_m, \quad \text{for the value range } A/(m+1) < B \leq A/m.$$

From this, the "window indicator" m is computed to $m = \text{FLOOR}_1 \{A/B\}$, and the corrector $\Delta_m = \text{RND}_1 \{A^2/B\} - m \cdot A$. RND_1 stands for rounding to the nearest integer, FLOOR_1 stands for truncation to the next lower integer. Entering for each register address "REG" the corresponding value of m and Δ_m , where $B = \text{RND}_1 \{\text{SQRT}[\text{REG} \cdot A]\}$, the resulting pair of look-up tables will perform the desired procedure. A corresponding hardware lay-out for the amplitude demodulation is shown in Fig. 5, while Fig. 6 shows characteristic graphs of the involved expressions. It is clear, that the permissible value of B has to be limited from below, say, to the order of $A/16$. At the present time, this amplitude demodulation is the weakest part in the algorithm, it sets the limit of the system's overall accuracy. This fact may, therefore, require already some dynamic compression in the analog part, ahead of the ADC.

The final amplitude modulation of our signal synthesis and phase control system is not shown in Fig. 3. Moreover, an interpolator, doubling the sampling rate at this point, may be desirable to ease the filtering requirements after digital to analog conversion.

6. Synchronization and Clock Rates:

All components are externally clocked, whereby component delays are always less than the clock period. Originally, the sequence of digital words (i.e., the sequential data stream) is generated by analog-to-digital converters (ADC) from the input monitor

signals. *The accurate synchronization of these ADC's translates directly into a corresponding phase accuracy of the procedure, and is therefore absolutely crucial.* All subsequent components have latching provisions, that reduce these tight requirements on synchronization somewhat.

As mentioned above, the clock and sample frequency is a multiple of the actually desired rf frequency modulation, f_{rf} , and thus varies with time according to the commands of the host. To ensure accurate sampling, the clock frequency f_c should, under any condition, be larger by at least a factor of ten than the rf carrier frequency f_{rf} , thus sampling every period ten times. This specific sampling method implies the following: The algorithm is independent of the respective rf frequency. Rf frequency and frequency modulation are exclusively determined by the clock rate. This clockrate is generated separately by a programmable master oscillator. A possible realisation for such a programmable master oscillator is shown in Fig. 7. For this specific clocking scheme, the sine and cosine look-up tables, used in the local oscillator/function generator block FG (Fig. 3), become rather simple; and the 90°-phase shift/quadrature operation can be realized by a simple shift register, acting as a digital delay line, as long as the clock rates harmonic number is divisible by four. A reasonable minimum harmonic number would, therefore, be eight. For instance, a clock rate of $8 f_{rf}$ would amount to a maximum sampling rate of 13 MHz at highest particle energy. Clearly, the higher the sampling rate, the less problematic becomes the filtering requirement after the DAC. The bottleneck for raising the sampling frequency are the ADC's. Presently available components performing at 12 bits are limited to 20 to 25 MSPS, and at 14 bits to 10 MSPS.

Finally, the algorithm calls for parallel pipelining of about ten sequential operations, and 20, if the digital filtering is used. This amounts to a total computation delay of one or two rf periods. If faster multipliers, summers, or adders/subtractors can be used or become available, a phased-clocking scheme can reduce the operation-caused delay even further. Filtering with a full-cycle summer requires always one full period.

7. Computer simulations:

Computer simulations are being performed in several steps of increasing realism. Presently, a floating point programming of the algorithm has been successfully

completed to check overall mathematical validity of the approach, see Fig. 8. As a second step, integer binary simulations are being written to examine, at a more realistic level, the achievable accuracy. This will eventually also include both A/D and D/A conversion. Subsequently, hardware simulation will first focus on the component level. Commercial components, first with discrete functions, such as multipliers, and later DSP chips, modeling an entire butterfly block, will be investigated. As a final step, the complete system has to be simulated at the board level, before the hardware development of the entire circuit.

Acknowledgments:

We are much indebted to H. Halling, R. Leuchter, G. Melder, K.D. Müller, R. Pape, and last, not least, to H.J. Stuckenberg, without whose encouragement this project would not have been started.

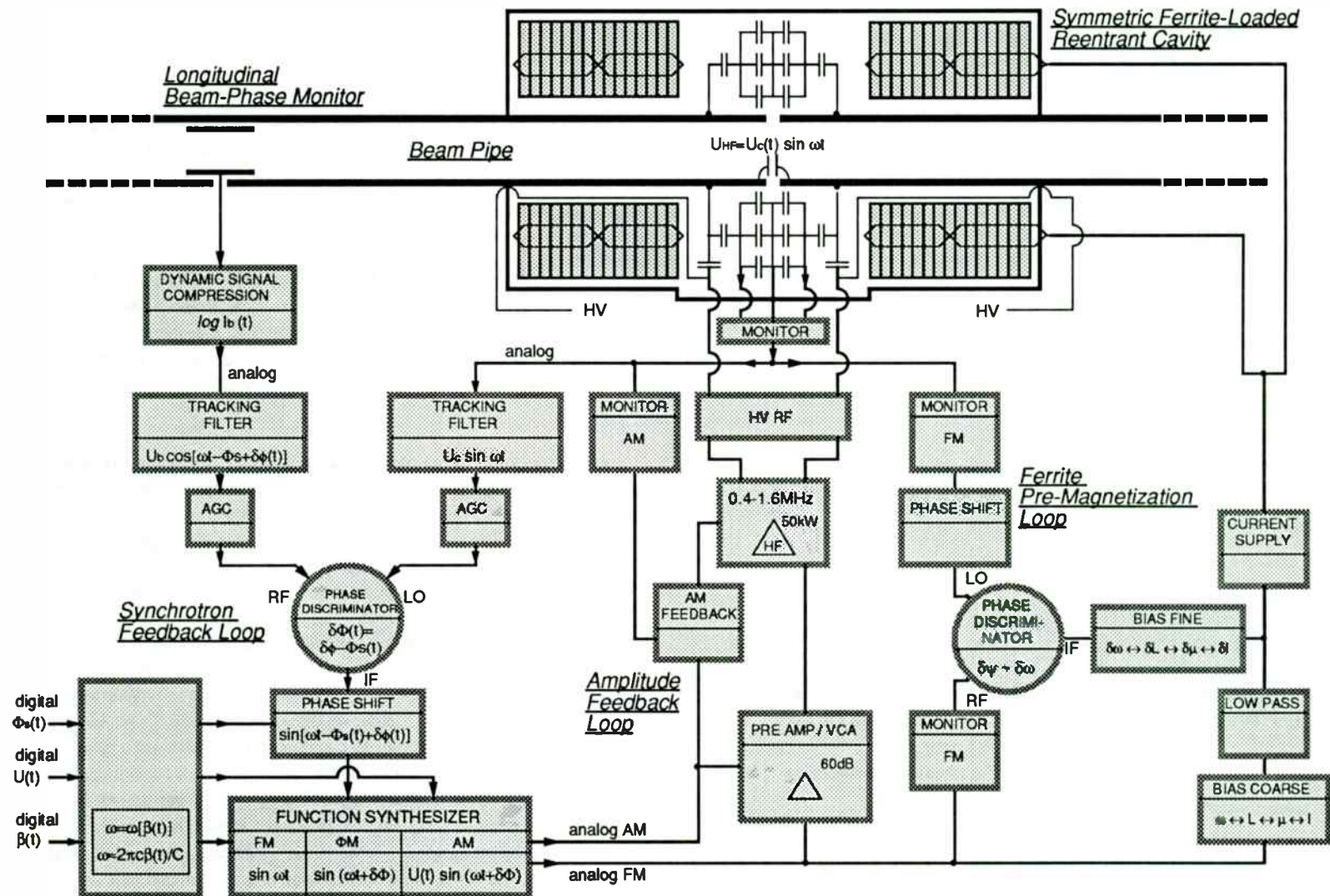


Fig. 1: COSY RF System and RF-Control System Schematic

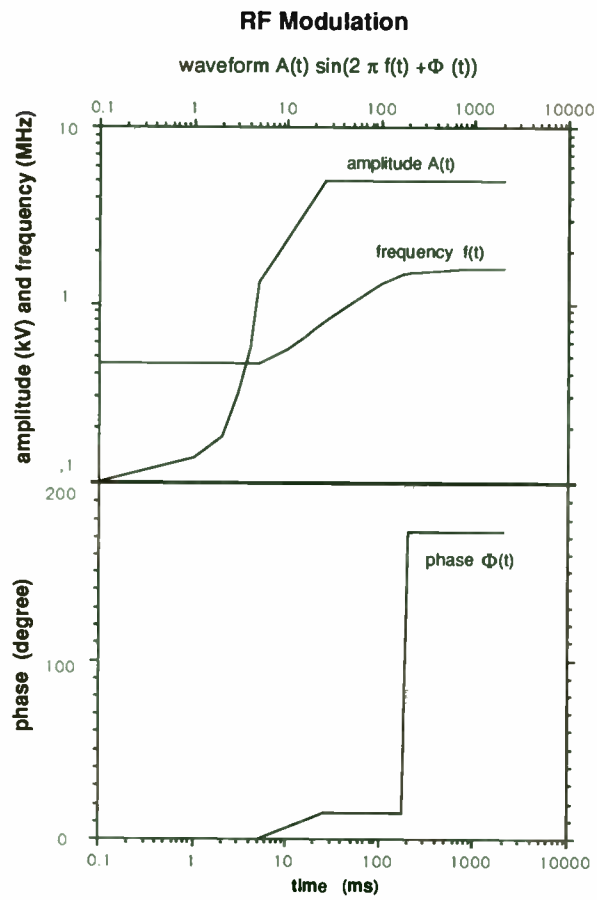


Fig. 2: Characteristic time histories for frequency, amplitude, and phase modulation of the rf-acceleration voltage

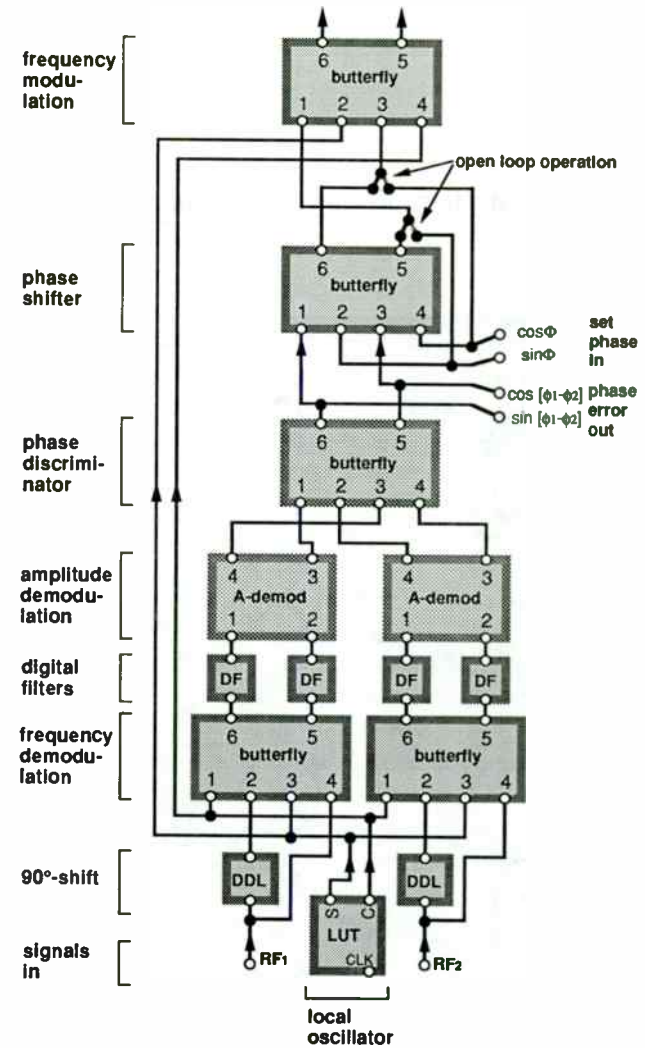


Fig. 3: Block and function diagram for the signal synthesis and phase control system

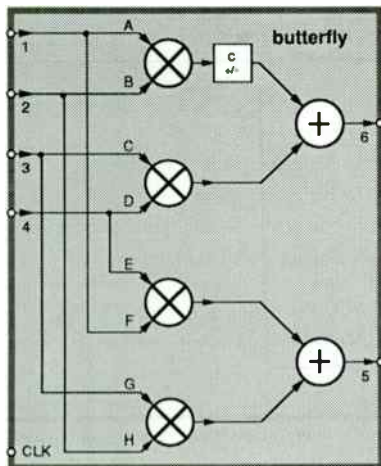


Fig. 4: Twin-butterfly configuration

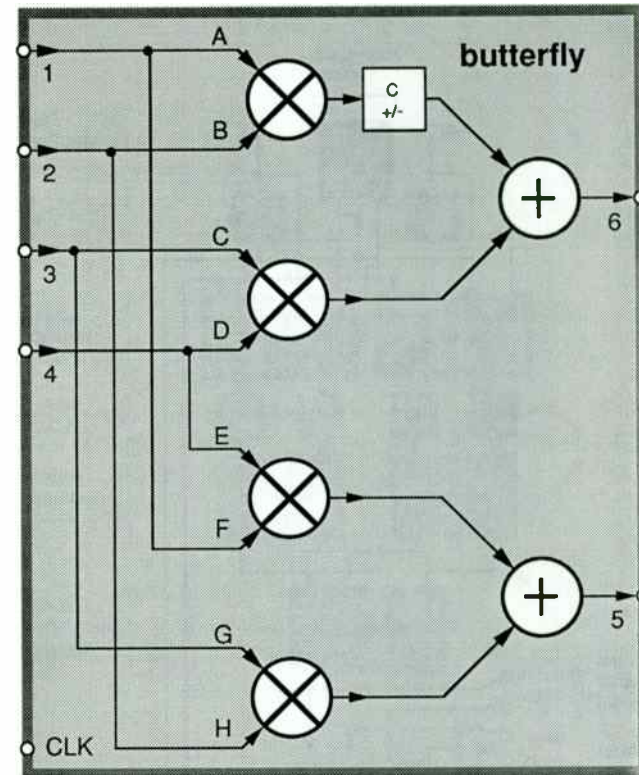


Fig. 4: Twin-butterfly configuration

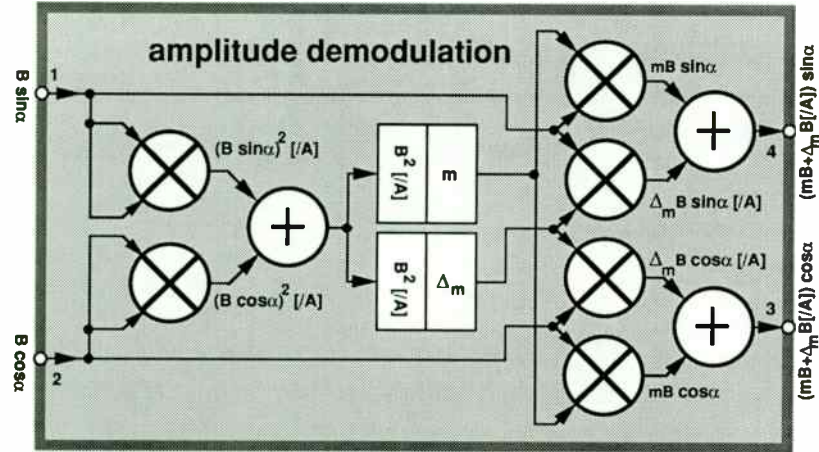


Fig. 5: Binary integer amplitude demodulation block

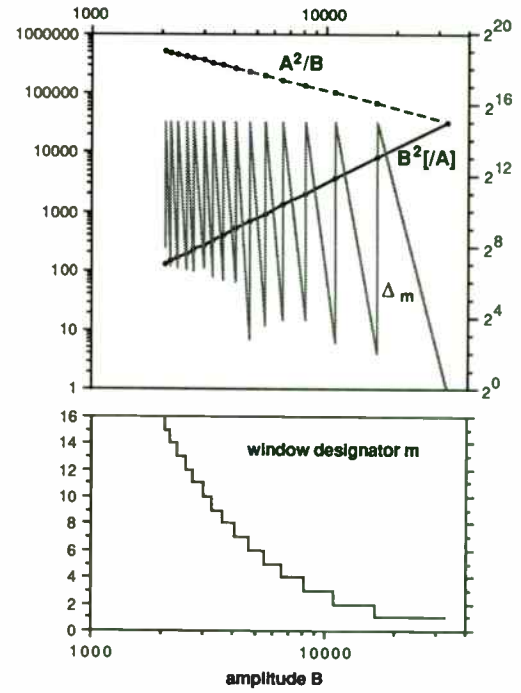


Fig. 6: Functions Δ_m and m , entering the amplitude demodulation algorithm

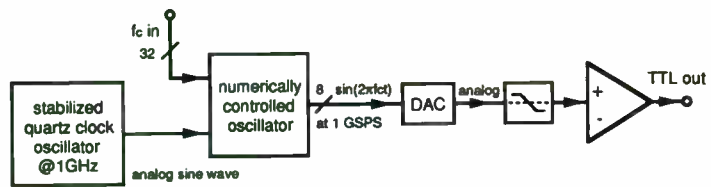


Fig. 7: Programmable clock, consisting of quartz clock, NCO, DAC, low-pass filter, and comparator

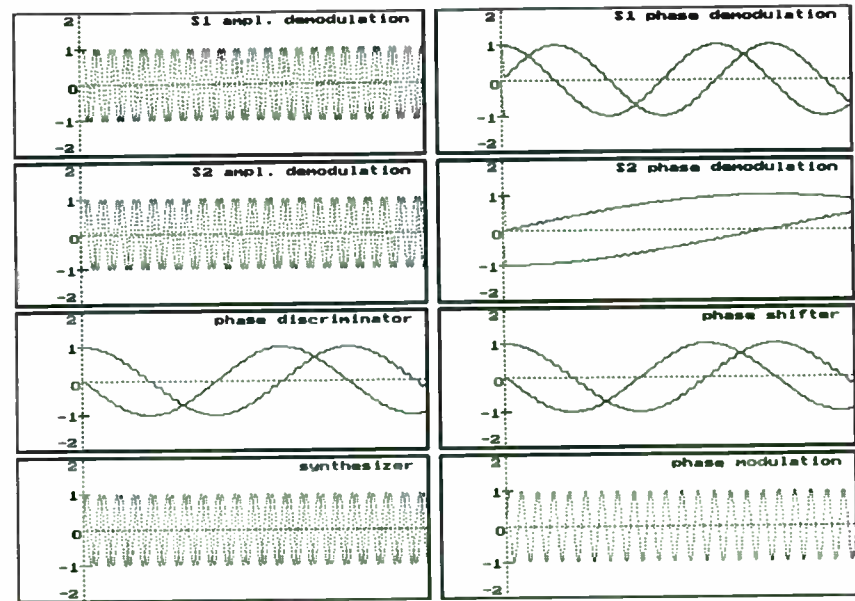


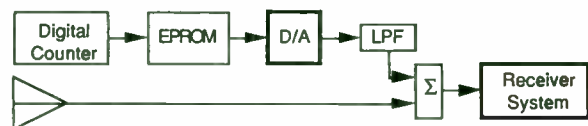
Fig. 8: Floating-point simulations

DYNAMIC EVALUATION OF HIGH SPEED, HIGH RESOLUTION D/A CONVERTERS

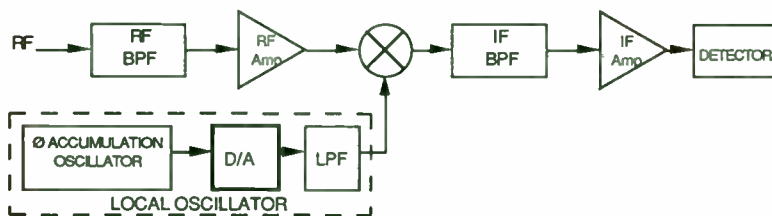
Data sheet specifications of D/A Converters often reflect performance under conditions unlike those in the considered application. However, Dynamic D/A Evaluation can uncover the necessary performance information under the appropriate conditions, guiding you past the shoals of uncertainty.

James J Colotti
 Analog Design Engineer
 CSD/Telephonics
 815 Broad Hollow Road
 Farmingdale, New York 11735

Practically speaking, the all digital receiver will never exist. Yet, as digitally uncharted waters dwindle, many traditionally analog functions are being replaced by their digital counterparts - augmenting the performance of the remaining analog components and thus the overall system. One interface device that merges these two technologies is the High Speed, High Resolution Digital-to-Analog Converter (DAC or D/A Converter), shown in two potential applications in Figure 1.



(a) Built-In-Test Tone Injection



(b) Superheterodyne Receiver with Digitally Generated Local Oscillator

Figure 1 Two Application Examples of High Speed, High Resolution DACs

While DAC applications are not limited to receiver design, in virtually all high speed/high resolution applications careful evaluation of potential candidates is required to assure that the appropriate device is selected. Although most manufacturers provide a comprehensive set of characterization data, often the device will not be specified under the specific conditions called for in your application.

To alleviate this uncertainty, the D/A dynamic evaluation techniques outlined in this article were developed. Through a trio of tests; Single Tone, Two Tone and Noise Power Ratio (NPR), the performance of a potential D/A can be comprehensively analyzed. While this article will focus on RF applications, these tests are applicable to the dynamic characterization of most any DAC.

The Test Set Up

As depicted in Figure 2, the DAC under evaluation receives digital inputs that are generated as follows; A TTL clock of the required sampling frequency, f_s , drives a counter chain which generates addresses for the high speed memory (EPROM or RAM). Contained in the memory is the Look-up table of codes that generate the appropriate test tone or tones. The sampling frequency will often dictate the memory type that is employed. EPROMs can provide a convenient storage medium, however they typically exhibit slower access times than RAMs. One drawback to using RAMs however, is the continual need for the download hardware.

Wave Generation software is used to create and download the Look Up Table data to the memory devices. The software also loads in a reset command that will clear the counter chain, once the final data point is read. This allows the counter to continuously run from 0 to some maximum value, N-1. Data outputted by the memory is latched to minimize erroneous transitional data, and then presented to the D/A converter. This look up table generation technique is preferred over other approaches by virtue of its ease of implementation and multi-tone generation capability.

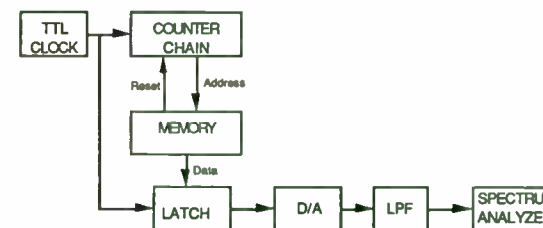


Figure 2 D/A Converter Test Set Up

The analog output of the DAC is presented to the spectrum analyzer where the frequency spectrum is monitored. Due to the high image frequencies contained in the D/A output, it is sometimes necessary to limit the bandwidth with a low pass filter depending on the test equipment limitations.

Each test of the trio is useful for examining various D/A performance parameters. For example, Harmonic Distortion (HD) and signal to quantization noise performance is readily accomplished with the single tone test. Since the resulting spectrum is relatively uncluttered, as compared to the other tests, the single tone analysis is also useful for characterizing other DAC parameters, such as power supply rejection and gain accuracy.

Harmonic Distortion is characterized by products that occur at integer multiples of the fundamental frequency. Often, the second and third products of a DAC are most prominent.

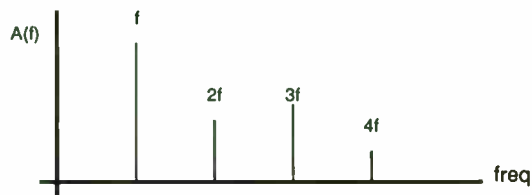


Figure 3 Harmonic Distortion

The two tone test is useful for examining intermodulation products, a nonlinearity characterized by distortion products that occur at sums and differences of integer multiples of the two primary frequencies. Typically, the dominant IM products are among the second order components located at $f_2 - f_1$ and $f_1 + f_2$, and the third order components located at $2f_1 - f_2$ and $2f_2 - f_1$. Although this test can also be used for signal to noise ratio evaluation, it is limited to less than full scale testing due to saturation problems that would arise if the instantaneous amplitude of the combined signals exceeded the full scale limit. For example, if two equal amplitude tones are considered, the level of each must be at least 6.02 dB below the D/A full scale level to avoid saturation.



Figure 4 Intermodulation Distortion

The NPR test, considered the most stringent of the three, is used to evaluate a converter's ability to replicate wide band signals such as those encountered in spread spectrum communication. This test entails generating a comb of uniformly spaced frequencies over a range dictated by the application. The comb is then characterized by a narrow notch that is usually located in the center of the frequency range.

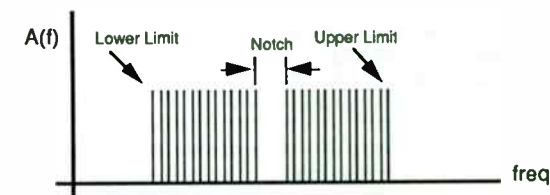


Figure 5 NPR Signal

Inside the notch, below the lower frequency limit, and above the upper frequency limit would appear the culmination of the nonlinear products generated by the converter. Often, the discrete products of these nonlinearities are so numerous that a wide band noise appearance is created - which is particularly noticeable in the notch. This test can be especially useful since manufacturers rarely evaluate the NPR performance of their devices.

The Wave Generation software mentioned earlier, also contains a Fast Fourier Transform (FFT) algorithm that allows the look up table data to be viewed in the frequency domain prior to downloading. This useful reference illustrates the performance of an ideal DAC of the desired resolution. Use of the FFT algorithm however, restricts the number of data points to powers of 2, which can yield a cumbersome resolution frequency (discussed in a following section) depending on the sampling rate.

A Focus on D/A Dynamic Errors

The transfer function of an ideal DAC is characterized by a linear relationship, where the analog output is proportional to the digital input code. For example, the transfer function of an ideal 3 bit DAC is shown below.

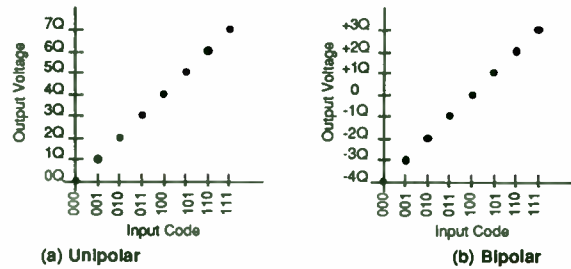


Figure 6 Ideal 3 Bit DAC Transfer Functions

Q refers to the weight or value that corresponds to 1 Least Significant Bit (LSB).

$$Q = V_{FS} / (2^{N_b})$$

Where V_{FS} = Full Scale Peak-to-Peak Voltage
 N_b = Number of bits

Due to this finite resolution, even the ideal DAC would exhibit a fundamental quantization error of $\pm Q/2$. Higher DAC resolution (ie more bits) yields a smaller quantization error, allowing greater fidelity in the reconstruction of a desired signal. Calculating the theoretical DAC noise produced by this quantization error, begins by modeling the DAC output, $F(nT)$ as the sum of the exact sequence of sampled values $G(nT)$ corrupted by an error component, $\epsilon(nT)$, which shifts the exact value to the nearest quantization level.

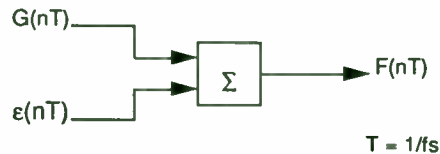


Figure 7 Ideal DAC Quantization Error Representation

The maximum sine wave mean square value that can be generated before clipping is:

$$P_{Max} = [Q (2^{N_b-1})/\sqrt{2}]^2 = 2^{2N_b-3}Q^2$$

Based on the assumption that ϵ is a uniformly distributed and uncorrelated random variable over the range of $-Q/2 \leq \epsilon \leq +Q/2$, its variance 'power' is given by:

$$P_{\epsilon} = [[Q/2 - (-Q/2)]^2] / 12 = Q^2/12$$

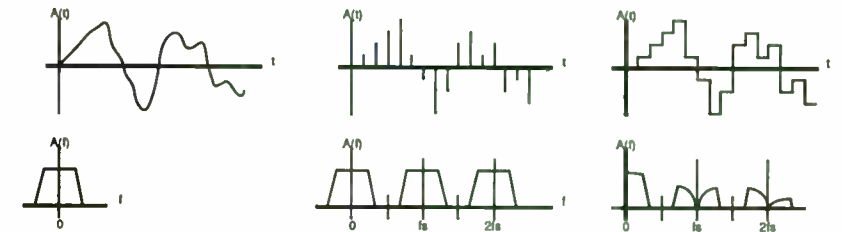
The sought after DAC dynamic range (maximum sine level to quantization noise over the Nyquist bandwidth) is calculated by simply taking the ratio of the two powers:

$$DR = 10 \text{ Log}_{10} [(2^{2N_b-3}Q^2)/(Q^2/12)] = 6.02 N_b + 1.76$$

Since the quantization noise is uniformly distributed over the Nyquist bandwidth, determination of the dynamic range in a smaller bandwidth, f_{bw} , is simply:

$$DR = 6.02 N_b + 1.76 + 10 \text{ Log}_{10} [f_s/2 f_{bw}]$$

Ideally, reconstruction of an analog signal from its samples would be represented in the frequency domain as the convolution of the original analog signal spectrum and a train of impulse functions. The resulting spectrum, as depicted below in Figure 8b, would consist of the original signal spectrum plus its images centered at integer multiples of the sampling frequency, f_s .



(a) Original Waveform (b) Sampled Representation (c) Staircased Representation

Figure 8 Time and Frequency Domain of a Sampled Signal

Since an impulse function would place unrealistic slew rate demands on a real world DAC, its output is instead characterized by a "staircased" function as depicted in Figure 8c. Although the resulting frequency spectrum of the staircased waveform also contains the original spectrum and images, the envelope is attenuated by a sine x/x roll-off;

$$\text{Atten} = 20 \text{ Log}_{10} \left[\frac{[\sin(\pi f / f_s)]}{[\pi f / f_s]} \right]$$

where f = Output Frequency
 f_s = DAC Sampling Rate

Typically in DAC applications, only the spectrum from DC to the Nyquist Frequency ($f_s/2$) would be of interest, thus the higher frequency images are filtered with a LPF.

The sine x/x roll-off however, will attenuate a signal at the Nyquist limit by 3.92 dB as compared to frequencies at the low end of the spectrum. Demanding applications would digitally correct this problem by placing an inverse sine x/x filter before the DAC.

In addition to the fundamental considerations of quantization noise and sine x/x roll-off, DACs also exhibit other characteristics which must be carefully considered in high speed applications. Some of these characteristics and their associated impact on AC performance are listed below;

<u>DAC Characteristic</u>	<u>Impact on AC Performance</u>
Monotonicity	Code dependent Spurs
Differential Non Linearity	Increased Quantization Noise
Integral Non Linearity	IM and HD Distortion
Glitch Impulse	Spurious
Digital Feed-through	Spurious
Power Supply Rejection	Spurious
Settling Time	Spurious, also dictates maximum f_s
Slew Rate	IM and HD Distortion
Gain	Amplitude error
Offset	Usually none, if AC Coupled

Table 1 DAC Characteristics and Their Associated Impact on AC Performance

Monotonicity indicates whether or not the analog output will consistently increase with increasing input code. Only when the signal passes through the non-monotonic portion of the transfer function, will it be tainted. Depending on where this discontinuity exists the resulting spurs may be signal level (code) dependent. As an example, if a non-monotonic point existed at BF0 (Hex code of a 12 bit converter), smaller signals that did not exercise this code are unaffected, while larger signals that pass through this point will be corrupted. Fortunately, monotonicity is virtually always guaranteed by DAC manufacturers over the applicable temperature range, and is not usually a consideration.

Differential non-linearity, usually expressed in LSB weights, refers to the incremental accuracy of the DAC transfer function. Since this parameter dictates an increase in spread of quantization error, the resulting noise floor increase is readily predictable. Integral non-linearity pertains to the overall deviation of the DAC transfer function. Often characterized as a "bowing" deviation, this type of error will create distortion products in the DAC output. Glitch impulse, sometimes referred to as glitch energy, is a measure of the glitch area that is created by switching transients between updates. Although it is sometimes possible to de-skew the Most Significant Bits (MSBs) to reduce the glitch impulse area, the efficacy of this technique is very limited, usually to about a 40 or 50% reduction. If needed, a much more effective method in reducing glitch area is to employ a Sample and Hold Amplifier (SHA) at the DAC output. The SHA would maintain the proper analog level while the DAC is transitioning to the next value, buffering the output from the glitch activity. The DAC-02315 and DGL-02316 manufactured by Data Device Corporation is a good example of a DAC/SHA pair which is specifically intended for this purpose.

Digital feed-through pertains to the isolation that exists between the digital signals and the analog output. This feed-through is most problematic in high speed applications where high slew rate logic often carries higher frequency ripple components. Since this parameter is very dependent on circuit layout and implementation, it is often unspecified

therefore not of significant concern in AC applications. Offset, which is also expressed as a percent of full scale output pertains to the resulting output level that would appear at the DAC output when it is instructed to output 0 volts. The offset is usually not significant, and is easily removed with AC coupling.

Test Considerations

Before discussing actual D/A test results, a few items should be addressed concerning the test parameters. The sampling window that contains the digital waveform must embody an integral number of cycles. Failure to assure this will result in discontinuities when the transition from the end of data period to the start of the new one occurs.

The frequency resolution is simply;

$$f_{res} = f_s / N$$

where; f_s = Sampling frequency

N = Length of the sampling window (number of points)

Avoiding the discontinuity requires that the fundamental frequency be an integer multiple (m) of the resolution frequency;

$$f_f = m f_{res} = m f_s / N$$

Other considerations should also be heeded. To maximize the number of DAC codes exercised, the sampling window length, N , should be as long as practical while the integer multiple, m , chosen in the above equation should be odd and prime. The problems associated with choosing a small sampling window or a non-prime multiple can be visualized by examining the following example; consider a sampling frequency of $f_s = 102.4$ MHz that generates a tone at $f_f = 12.8$ MHz. Regardless of how large the sampling length is, under these conditions there will always exist exactly 8 samples per cycle which would utilize a very limited number of DAC codes.

by manufacturers. Latching the digital data will limit coupling of extraneous noise riding on the logic signals, but will do nothing to prevent logic edge coupling. Maximizing the distance between the digital and analog circuitry will minimize capacitive coupling, while minimizing loop areas of both the analog and digital circuitry will minimize inductive coupling. Unfortunately, even the most carefully executed layout will not reduce the stray coupling capacitance that exists between the chip boundaries of the DAC, which is typically on the order of 0.2 pF. Manufacturers usually limit this capacitance by placing the digital signal pins as far away as practical from the analog pins. One method of reducing the effect of this coupling capacitance is to incorporate a Faraday shield around the DAC package - this will be discussed in more detail in the test results section.

Power Supply Rejection Ratio (PSRR), frequently specified only at DC, is expressed in terms of percent of full scale change for a DC percent change in power supply voltage. Although this is helpful for determining amplitude variation over a given supply voltage range, this DC specification will provide little information about high frequency rejection. In high speed applications, judicious use of the proper bypass capacitors and filter inductors will complement the PSRR to maintain the proper noise immunity. Providing a capacitor pair consisting of a 0.001~0.01 μ F ceramic and ~5 μ F tantalum on each supply pin helps stabilize the voltage over a wide frequency range. The capacitors can be augmented by series inductors to further cleanse the supply lines.

Settling time of a DAC is traditionally defined as the time from the digital input transition to the time the DAC output has settled to within a certain error band, usually $\pm 1/2$ LSB. A portion of this delay may be attributed to a fixed "pipeline" delay due to latch and switch propagation times, during which the analog output is unchanged. Therefore, in AC applications DAC settling time may be redefined in terms of the output alone; ie, as the time the output leaves a $\pm 1/2$ LSB error band to the time the output settles to within a $\pm 1/2$ LSB band. Ideally, a DAC should be chosen with a settling time that is much shorter than the sampling period.

The remaining DAC parameters; Slew Rate, Gain and Offset are relatively straightforward. DAC Slew rate limitations are similar to that of other analog components, where the maximum output frequency is limited to;

$$f_{max} = SR / 2\pi V_p$$

where V_p = Maximum peak voltage level
 SR = Slew Rate (V/S)

Gain error, often expressed as a percent of the Full Scale (FS) output, relates to the amplitude accuracy of the DAC output. For example a 0.1% of FS gain error would dictate an amplitude error of less than 0.01 dB. Small gain errors are common, and are

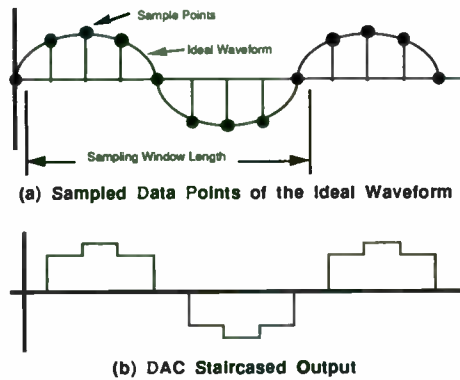
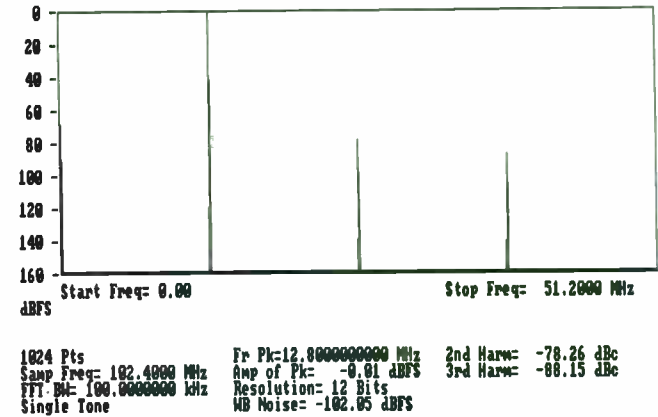
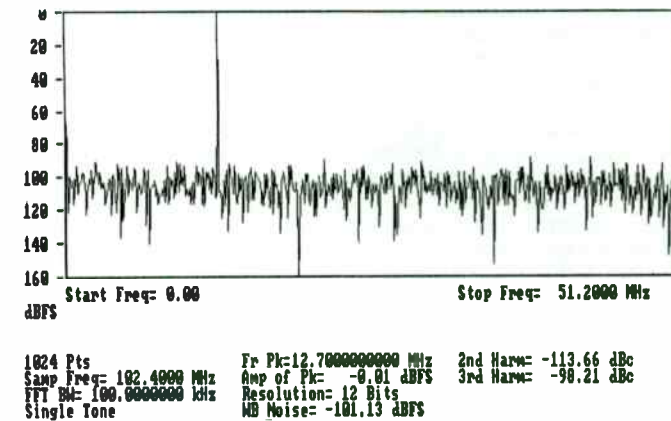


Figure 9 A limited number of DAC codes are exercised when the fundamental is a non-prime multiple of the resolution frequency

When viewed in the frequency domain, the quantization errors of the tone are concentrated at the harmonics of the fundamental as depicted in Figure 10a. This anomaly yields misleading results concerning the true HD performance of the DAC - a problem that is easily solved by allowing the largest length (N) that is practical and by selecting the fundamental to be an odd and prime multiple on the resolution frequency. This would slightly offset subsequent cycles, maximizing the number of codes exercised thus "spreading" the quantization error. Referring back to the example, by re-selecting the fundamental to be 12.7 MHz (which is an odd and prime multiple of the resolution frequency of 0.1 MHz) the resulting frequency domain plot, Figure 10b, depicts an evenly distributed quantization noise floor.



(a) Quantization Noise is not evenly distributed when the fundamental is not a prime multiple of the resolution frequency - as depicted in this extreme case



(b) Quantization noise is evenly distributed over the Nyquist bandwidth when the fundamental is a prime and odd multiple of the resolution frequency

Figure 10 FFT Spectrums of an Ideal 12 Bit DAC Demonstrating Quantization Noise Distribution

An interesting consideration that arises during DAC evaluation is the performance limitations of the test equipment. Recall that the theoretical DAC dynamic range (defined as the full scale sine amplitude to the quantization noise floor ratio) is;

$$DR = 6.02 N_b + 1.76 + 10 \text{ Log} (f_s/2f_{bw})$$

where N_b = Converter resolution (number of Bits)
 f_s = Sampling Frequency
 f_{bw} = Measurement Bandwidth

Considering, for example, a 12 bit DAC converting at 34 MHz, the resulting theoretical dynamic ranges for some typical spectrum analyzer bandwidths are listed below;

Resolution Bandwidth	Dynamic Range
100 kHz	96.3 dB
30 kHz	101.5 dB
10 kHz	106.3 dB

Table 2 Theoretical Dynamic Range of a 12 Bit DAC Converting at 34 MHz, at three typical Spectrum Analyzer Resolution Bandwidths

Measuring instantaneous dynamic ranges of greater than 80 or 90 dB generally place formidable demands on a spectrum analyzer. Therefore, some tests encountered in the evaluation of a quality high speed, high resolution DAC, will be limited by the test equipment. Fortunately, techniques frequently exist to circumvent this problem - as will be discussed in the following section.

Test Results

The AD9713A by Analog Devices was characterized at 34 MHz with the test trio to determine its suitability in various applications. The schematic of the DAC test circuit is shown in the Figure below.

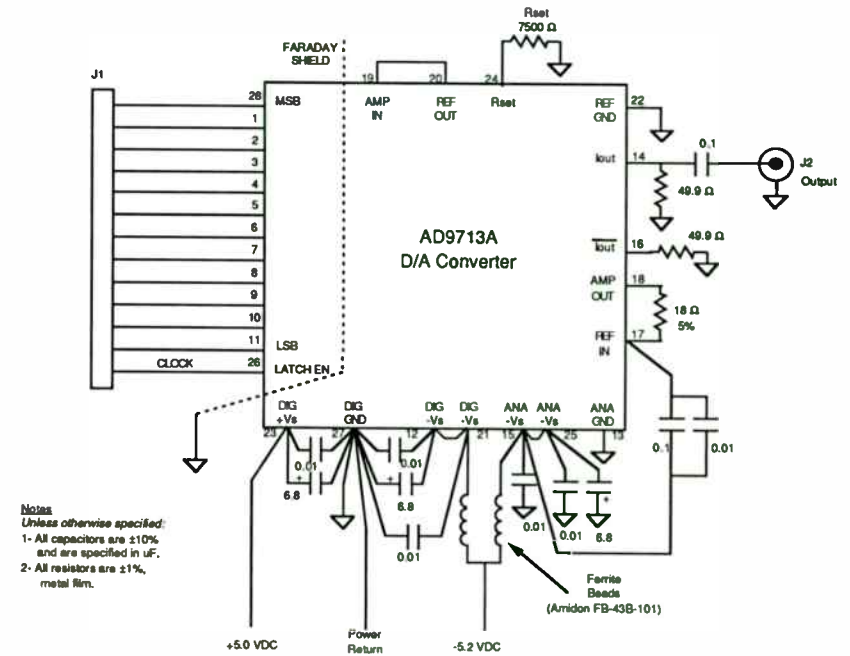


Figure 11 AD9713A Test Schematic

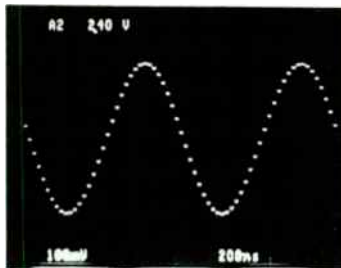
The unipolar current source DAC output is specified for a full scale level of 20.65 mA, with a set resistor of 7.5 kΩ. Placing the 50Ω resistor at the output creates a 50Ω Thevenin 1.033 unipolar voltage source. This dictates an available power of -1.8 dBm into an AC coupled 50Ω load. Applications requiring higher level outputs can be accommodated with a high speed transconductance amplifier, such as the AD9617.

The Faraday shield was constructed with 3 mil copper tape wrapped around the length of the IC package and connected to the board ground plane. Except where noted in the single tone case, the Faraday shield was used in all the following tests.

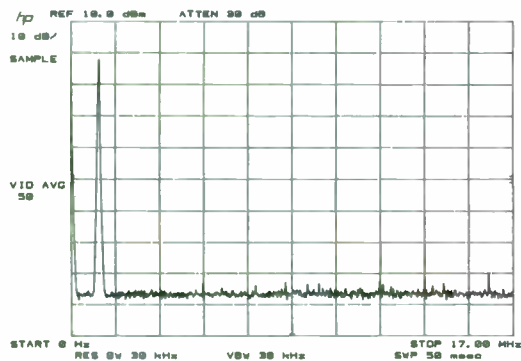
DAC characterization for a 1.0127 MHz local oscillator is accomplished with the single tone test. The time domain and frequency domain results are shown below in Figures

12 a and b respectively. Note that in the time domain, the duration of the switching transients between updates are substantially shorter than the update period. The staircased appearance is easily smoothed with a LPF. In examining the frequency domain, it is important to note that the observed noise floor is that of the spectrum analyzer which masks the quantization noise and all but the most ornery of DAC spurs. Being consistent with the data sheet specification, these spurs and HD products are observed to be at least 68 dB down from the full scale carrier. Note also that with the peak amplitude of -1.8 dBm, the theoretical quantization noise floor in the resolution bandwidth of 30 kHz will be 101.5 dB below the peak at -103.3 dBm, well below the analyzer's noise floor. Reducing the analyzer's internal attenuator from 30 to 20 dB will improve its effective noise figure, but will create misleading harmonic products as the front end of the spectrum analyzer will add distortion to the signal.

Digitally reducing the signal to -30 dBFS (below full scale) reduces the instantaneous dynamic range requirement of the spectrum analyzer, allowing for a more comprehensive observation of the DAC performance, as depicted in Figures 13 a and 13 b. However, depending on the application the digital level reduction may not be a valid test since the DAC spurious content will likely be signal level dependent. In such a case, it would be more meaningful to attenuate the fundamental in the analog domain with a notch filter, to reduce the analyzer instantaneous dynamic range requirement. However, careful implementation of the filter is required to assure that it does not generate distortion products that would create misleading test results.

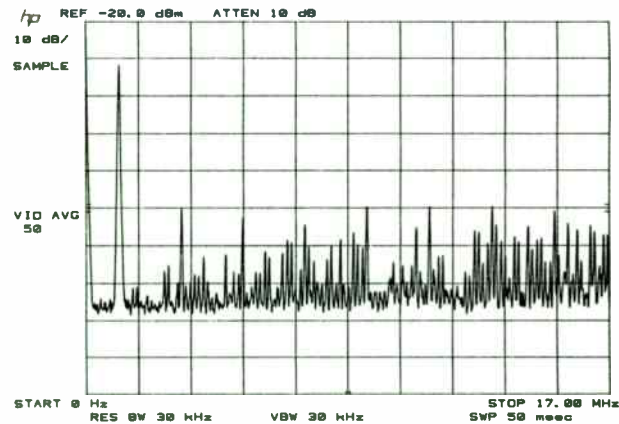


(a) Time Domain

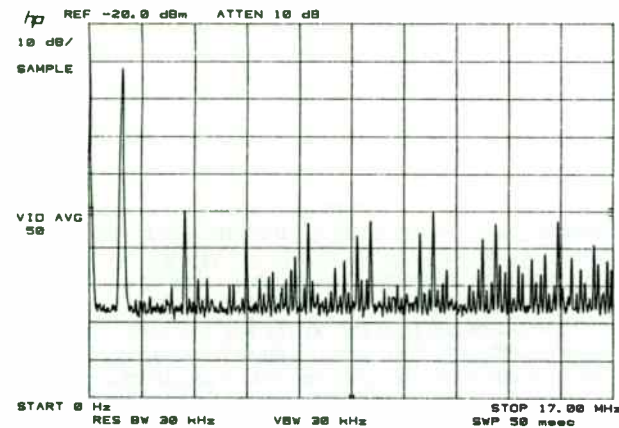


(b) Frequency Domain

Figure 12 Single Tone Full Scale Test Result



(a) Without Faraday Shield



(b) With Faraday Shield

Figure 13 Single Tone -30 dBFS Test Result

The numerous spurs are caused by both capacitive coupling of the digital data to the analog circuitry and DAC nonlinearities. Although careful layout can limit the coupling problem, it can do little for the coupling that exists within the DAC itself, as discussed in a previous section. Use of the Faraday Shield can attenuate the effect of the coupling capacitance (as illustrated in a comparison of the Figures 13a and 13b), though its efficacy is limited since its proximity to the die is constrained by the package. Nevertheless, most of the spurs and harmonics are attenuated, some by as much as 8 dB. Ignoring the discrete spurs, Figure 13 reveals a noise floor of -96 dBm which again is limited by spectrum analyzer performance.

Although many manufacturers do specify harmonic distortion, the single tone HD test is useful in situations where data sheet test conditions do not parallel the specific application. Additional uses for this test include; verifying the DAC circuit configuration and characterization of other DAC parameters such as Power Supply Rejection.

Frequently unspecified by a manufacturer, Intermodulation Distortion (IMD) is another important DAC parameter which is useful for example, in evaluating a DAC intended to inject a Built-in-Test (BIT) signal consisting of two tones. Figure 14 illustrates the DAC performance in generating a two tone signal at approximately 7.952 and 8.981 MHz. To avoid saturation, the amplitude of each signal is at -8 dBm, slightly less than half the full scale amplitude of -1.8 dBm.

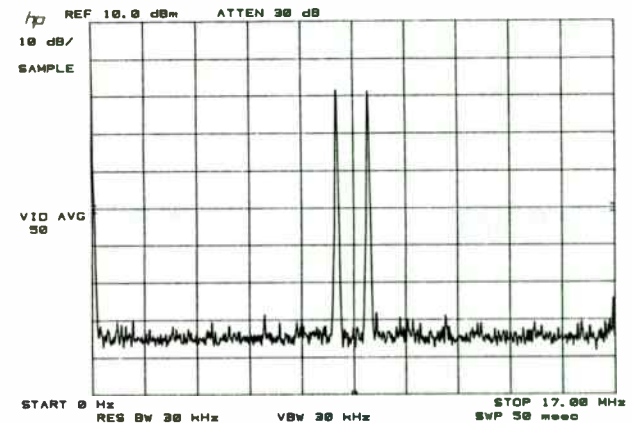
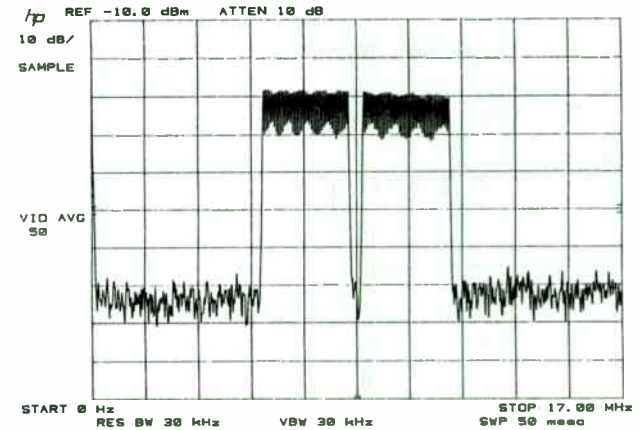


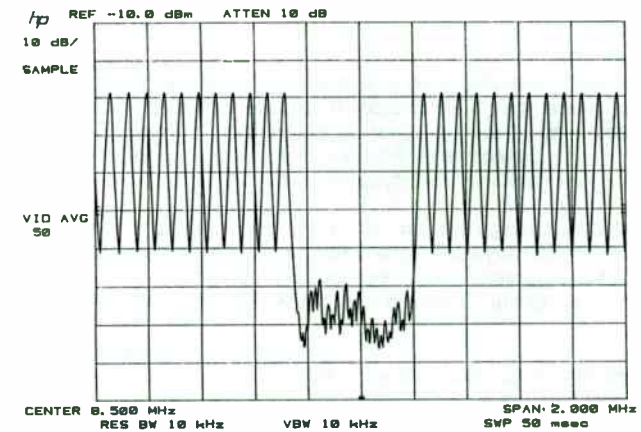
Figure 14 Two Tone DAC performance

Note that the largest of the IM components is the second order product at 16.933 MHz which is at -64 dBm (56 dBc).

The final and most stringent test of the trio is the Noise Power Ratio, which is especially useful in DAC characterization in wide band applications. In the following example, the NPR test was used to characterize potential DACs for use in the IF output generation of a ground based satellite receiving system. Since the IF consisted of a PN modulated 6 MHz bandwidth carrier centered at 8.5 MHz, the NPR test was developed using a comb of frequencies ranging from approximately 5.5 to 11.5 MHz with a void from approximately 8.25 to 8.75 MHz. The discrete frequencies were spaced at 4 times the resolution frequency of 16.6 kHz, providing about 82 components. Randomizing the phases of each signal is necessary to minimize the peak-to-RMS voltage ratio, thus maximizing the number of DAC codes exercised.



(a) DC to 17 MHz (Nyquist Frequency)



(b) Focus on Notch

Figure 15 NPR DAC Performance

Actual NPR performance of the AD9713A is depicted in Figure 15. Note the noise floor of -85 dBm depicted in Figure 15a, falls far short of the theoretical level of -103 dBm. In actuality the noise floor is a culmination of the numerous HD and IMD products of each of the frequency components that make up the NPR test, as anticipated previously. The 2 MHz frequency span of Figure 15b details the notch spectrum. Note that the individual frequency components, spaced at 66.4 kHz, are easily resolved in this Figure. Although the DAC performance is impressive, under these conditions it will only yield an instantaneous dynamic range equivalent to that of an ideal 9 Bit converter. Depending on the application requirements, this may not be a significant limitation since as the NPR signal is digitally attenuated, the noise floor decreases.

It is interesting to note the slight decline in signal amplitude at the higher NPR frequencies. This is not due to the frequency response of the physical part, but is rather a consequence of the sine x/x attenuation discussed earlier.

Summary

Most manufacturers do an excellent job specifying DAC performance. Unfortunately, data sheet specifications often reflect operation under conditions unlike those called for in a specific application - or worse a desired parameter such as IM performance, may not be specified at all. Dynamic evaluation with the Single Tone, Two Tone and NPR tests will help define DAC uncertainties, providing an efficient means to characterize and evaluate DACs for a wide variety of applications.

References

1. High Speed Design Seminar, Analog Devices 1990
2. Alen Oppenheim, Digital Signal Processing, Prentice-Hall, 1975

A HIGH PERFORMANCE LOW COST T.V. DEMODULATOR

PAULO R.M.A. CORRÊA
LYS ELECTRONIC LTDA
RIO DE JANEIRO - BRAZIL

INTRODUCTION

The transmission of a T.V. broadcast signal has to meet the modern standards of quality and reliability. The evaluation of a T.V. transmission is an important way to achieve a good reproduction of picture and sound on a domestic receiver. This evaluation is done on both RF and base band signals. The base band signals require a precision demodulator to achieve low inherent errors. Such demodulator permits the adjustment of transmitters and transposers as well as the use of the demodulated signal in services like remote monitoring or links.

The choice of a synchronous demodulator has the advantage of avoiding the quadrature distortion present in an envelope detection of a vestigial-sideband transmission. Also, the synchronous mode of detection permits an improvement of the linear distortion of the demodulated signals, and is more similar to the quasi-synchronous domestic receivers widely used today.

RF/IF CONVERTER.

The RF/IF converter shown in Fig-1 is formed basically by a band-pass filter, adjusted in any T.V. channel, a double-balanced mixer, a low-pass filter, and a local oscillator. The incoming R.F. signals are converted to the standard I.F. frequency (41 - 47 MHz). The mixer is a broadband device that covers all the T.V. VHF and UHF bandwidth. When the signal comes directly from a coupled sample of the main transmission line, after the aural and visual combiner, the band-pass filter can be disconnected. Otherwise, if the operating mode is remote or link, the channel filter is necessary and a L.N.A. may be required to improve the sensitivity of the receiving signal (Fig. 2). It is important to remember that a downconverter is usually a multi-response transducer where the signal and its image contributes to the same I.F. output (Fig. 3). When an amplifier is introduced before the mixer device, it produces noise in the signal frequency and in the image frequency, recording the IRE definition, the noise factor and the noise can be expressed by:

$$F = \frac{N_o'}{K T_o G} \quad (1) \quad \text{and} \quad N_o' = 2K (T_g + T_e) G. \quad (2)$$

Where:

N_o' = Total output noise density (per unit of bandwidth)

T_o = Standard reference temperature

K = Boltzmann Constant

G = Power gain

T_g = Noise temperature of service termination.

T_e = Noise temperature of the device.

In the case of broadband signals and cascade circuit (amplifier and mixer) the parameters are:

G_{as} = Gain of the amplifier at signal frequency

G_{ai} = Gain of the amplifier at image frequency

G_b = Gain of the mixer (assumed to be equal at both frequencies)

B = Bandwidth

The expression of the noise becomes:

$$N_o' = K.T_o. (G_{as} + G_{ai}). G_b.B \quad (3)$$

Replacing the temperature by the temperature noises of the devices and adding the noise temperature of the mixer (T_b) we have:

$$N_o = K.B. [(T_g + T_e) G_{as}. G_b + T_b G_b] + \text{Total noise in signal response}$$

$$K.B. [(T_g + T_e) G_{ai}. G_b + T_b G_b] \\ \text{Total noise in image response.}$$

As we can see, the image response is a component of the overall noise. The use of a band-pass filter after the amplifier can reduce the gain of the image frequency and provide an improvement in the total noise. Notice that this reduction would not be exactly one half of the total noise. Considerations on the impedance mismatch between the filter and the mixer-out of the filter pass band-the insertion loss (I.L.), and differences of G_{as} and G_{ai} have to be taken into account. In our case, there was

a reduction close to 1.5 dB in the noise figure of the RF/IF converter. These noise considerations are shown in reference 1.

In the remote or link modes, it also requires an automatic gain control (AGC) in the I.F. signal to maintain constant the level at the I.F. processor. This IF-AGC is shown in Fig. 4 and is composed by a gain controlled amplifier, a band-pass filter, a constant gain amplifier and an AGC circuit. This circuit performs peak detection and voltage comparison to provide a constant level I.F. output of -10 dBm for a R.F. input variation of 45dB.

The local oscillator (Fig. 5) is a synthesized PLL circuit with the channel selection programmed in an EPROM. The voltage control oscillator is divided in four bands i.e, B I , B III, B IV and B V. The spectral purity of the local oscillator is assured by avoiding the F.M. and A.M. sidebands. The F.M. sidebands may occur, for example, caused by the frequency reference present at the output of the loop-filter and depends essentially on the design of the synthesizer. These FM sidebands signals could be stronger than AM sidebands in an oscillator, but they could be minimized by a proper design. The A.M. sidebands may occur, caused by the prescale ($\div P$) and would spread spurs on a large portion of the spectrum (Multiples of P). A high-pass filter was introduced between the prescaler and the VCO to isolate the " divide by P " components from the VCO output. The importance of this consideration is to prevent signal spurs in the I.F. band (reference 2).

The VCO transfer function depends on the desired bandwidth and on the voltage to frequency transducer. For example, we will see the case of B.I. VCO:

- A) Channel 2 is from 54 to 60 MHz
- B) Channel 6 is from 83 to 88 MHz
- C) I.F. frequency is from 41 to 47 MHz.

Considering that the I.F. is inverted in frequency referred to the channel frequency, we have the L.O. for channel 2 at 101 MHz and for channel 6 at 129 MHz. This means that we have a frequency variation of 28 MHz. The DC voltage variation at the control port of the VCO was chosen to be no more than 15 V (Power Supply is 24 V) to cover the entire B I spectrum. The transfer function of the VCO was found to be:

$$KVCO = \frac{\Delta W}{\Delta V} \cong 11,7 \times 10^6 \text{ rad/S/V.}$$

The loop filter has two singularities: one low - frequency zero and a very low-frequency pole (essentially at the origin) "so that the hold-in range and acquisition range become theoretically infinite" (Ref. 2). The zero in the filter assures the necessary stability of the feedback circuit. Considering the transfer functions of the phase comparator and the amount of division ration (1/N.P), we can calculate the loop filter components. These calculations take in account that the worst case occurs in the last channel of the UHF band (C. 83) due to the division ratio. The dumping factor and the lock time were established at 0.5 and 10 mS. The analysis of the completey circuit shows a second order type 2 P.L.L. synthesizer and the

calculations can be made using the expressions and the graphics present in Ref. 3.

During the tests a presence of the reference frequency at -60 dBc was found. A non-dominant two-poles filter was placed in series with the loop filter to improve the spectral purity of the L.O.

I.F. PROCESSOR / DEMODULATOR

Now we have a television signal of any channel in I.F. band with a controlled level to be demodulated. The purpose was to design and manufacture a synchronous demodulator that could permit an access to the signal carried within a TV channel. This access has to allow a quality evaluation of the transmitted signals.

The I.F. Processor (Fig. 6) input signal is divided by three. One part of the I.F. will be used by the audio demodulator, which will be explained later. The other two parts will be used to recover the carrier, and to be processed and demodulated.

First we shall analyse the processed part. The I.F. signal is amplified and applied to the Nyquist filter (Fig. 7) to compensate the vestigial-sideband transmission. The V.S.B. transmission has a difference of power density between the lower

sideband and the upper sideband. This is a characteristic of the system which has tolerances that could provide a discontinuity in frequency response of the demodulated signal in the vicinity of 0,75 MHz. This frequency is the limit of the vestigial-sideband (Ref. 4). The Nyquist filter has to achieve the best response in this frequency without a bad performance in group delay response. Nowadays, the use of SAW vestigial-sideband filter in TV transmitters is very common and it demands the improvement of the Nyquist filter. The linearity of the demodulator allows the use of a filter without the aural notch and the Nyquist filter can have its shape optimized close to the visual carrier, i.e., a good approach to the Nyquist slope. We have chosen a Cauer band-pass filter (Ref. 5) with 5 poles and 4 zeros which assures the correct video frequency response. Further on, the group delay of this filter is well known and could be corrected by a second-order four-section all-pass filter. The I.F. is applied to a PIN diode attenuator and then to a divide-by-two splitter. The attenuator adjusts the correct level to the demodulator and it is also used to receive the zero carrier reference pulse. The I.F. signal is now prepared to be demodulated.

The circuit to recover the carrier is based on the fact that TV visual amplitude modulation does not suppress the carrier and that the maximum percentage of luminance modulation is 87.5%. The IF signal is amplified and filtered by a 300 KHz band-pass filter. The sound carrier and the high frequency components of the video signal are very attenuated. The visual carrier,

modulated by the low frequency video components, is then obtained. This signal has the amplitude modulation suppressed with diode limiters and E.C.L. integrated circuit. The limiter circuit is based in the F.M. limiters and allows the 12.5% portion of the carrier, that is not modulated, to pass through the circuit (Fig. 8). This part of the carrier has no phase variation due to the video modulation. The resulting signal is amplified and filtered and is now free of both harmonics and amplitude modulation. A phase shift circuit adjusts the phase of the carrier.

The phase shift circuit consists of a quadrature coupler constructed with a pair of twisted wires (Ref. 6 and 7) with the coupled and the transmitted ports loaded with varicaps diodes (Fig. 9). The signal output is at the isolated port. The adjustment places the carrier at the same phase of the I.F. signal at the demodulator device inputs. There is another quadrature coupler included in the original design in order to provide a quadrature video output.

This output allows the users to measure the incidental carrier phase modulation (ICPM). This distortion is the phase modulation of the video carrier caused in the modulator or in the class AB power amplifiers of the transmitter. The quadrature output is obtained with a double-balanced mixer working also as a phase detector due to the 90° phase shift of the carrier.

The demodulator device is also a double balanced mixer where the R.F. port is fed with I.F. signal. The local oscillator

port has the recovered synchronous carrier. The I.F. port is now the demodulated signal which contains the video and the 4.5 MHz audio carrier. To assure that the intermodulation beats do not appear during the demodulation process we have chosen a double-balanced mixer with high performance third-order intermodulation characteristic. (Ref. 8).

The advantages of a synchronous demodulation when compared to the envelope demodulation may be expressed mathematically as can be found on reference 9.

$$m(t) = [1 + \frac{1}{2} V(t)] \left\{ 1 + \left[\frac{1/2 V_q(t)}{1 + 1/2 V(t)} \right]^2 \right\}^{1/2}$$

This equation shows the presence of $V_q(t)$ which represents the quadrature distortion due to the envelope detection of a vestigial-sideband signal. Now a days, this problem is not negligible because the vertical blanking interval is used to transmit teletext. Quadrature distortion increases the bit-error-rate and a synchronous detection is therefore mandatory. (Ref.9).

VIDEO PROCESSOR

Figure 10 shows the block diagram of the video processor. The output signal of the demodulator is applied to an emitter-follower amplifier and then to a low-pass filter with a cut-off frequency of 4.17 MHz. (Fig.11).The purpose of the filter is to reject the 4.5 MHz frequency, and to limit the video

bandwidth. The adjustments of the group delay corrector are set to emulate the delay found in domestic receivers. (Fig. 12). The users can switch off the filter so that the frequency and the group delay response be fully correct. It allows the measurements in the colour frequency range without interference of the low-pass filter. All the circuitry in the video processor is DC coupled, with thermal stability compensation, which gives accuracy in measurements of low video frequencies.

The output signal of the demodulator is also amplified, filtered, and applied to a circuit to separate the vertical sync. The vertical sync excites a retriggerable monostable circuit located in the I.F. processor. It generates the zero carrier reference pulse which is applied to the PIN attenuator (Fig. 13).

AUDIO DEMODULATOR

The figure 14 shows the sound demodulator block diagram. It was found that a split mode demodulator could recover an audio signal free of the interferences that could appear in the intercarrier demodulation mode. The I.F. signal is amplified and passes by a 41.25 MHz band-pass filter. The filtered signal is limited to reject any amplitude modulation. The demodulator is a broadband FM detector, that recuperates the audio or the stereo base-band. When mono-mode is used, the audio signal passes by a de-emphasis circuit and if the stereo-mode is used, the de-emphasis is switched off. The audio signal has an adjustment of amplitude and an amplifier to get the specified level of the

outgoing audio. The circuit provides a balanced output used for mono-mode and an unbalanced output for stereo facilities. The output transformer is active.

The use of a split demodulator is a good choice due to the vision incidental phase modulation. This incidental phase modulation occurs either because the inadequate adjustment of the modulator or improper pre-correction of the RF output stages of the transmitter. This results in a degradation of the audio distortion and in a lower S/N when an intercarrier demodulation is used.

CONCLUSION.

To assure a good transmission of television signal, the users need an access to evaluate the quality of their transmission. The synchronous demodulator provides the necessary access to the base band signals. The high performance of the demodulator allows the evaluation of T.V. signals with high accuracy.

As examples of measured characteristics we have:

Differential phase: Less than $\pm 1\%$

Differential gain : Less than $\pm 1\%$

K factor : Less than 1%

Audio Distortion : Less than $0,3\%$

REFERENCES:

- 1) - Raoul Pettai, Noise in Receiving Systems
John Wiley & Sons, 1984
- 2) - William F. Egan, Frequency Synthesis by Phase Lock,
John Wiley & Sons, 1981
- 3) - Motorola, Phase-Locked Loop Data Book, 1973
Donald G. Fink
- 4) - Television Engineering Handbook,
Mc Graw Hill, 1957
- 5) - Anatol I. Zeverev, Handbook of Filter Synthesis,
John Wiley and Sons, 1967
- 6) - C.Y.HO, R.Furrow, "Analysis and Design of VHF Quadrature
Couplers:
Part 1, "RF Design, July/August 1979, pp 48-50
- 7) - C.Y.HO, R.Furrow, "Analysis and Design of VHF Quadrature
Couplers:
Part 2, "RF Design, September/October, 1979, pp 32-39
- 8) - Mini-Circuit, RF/IF Signal Processing Handbook
- 9) - Noel Boutin, Complex Signals:
Part IV, RF Design, May 1990, pp 65-75

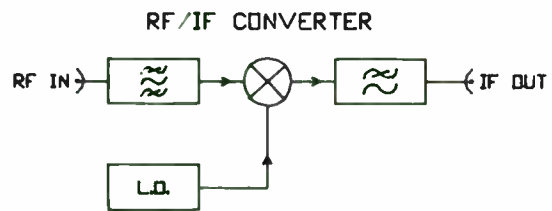


FIG. 1

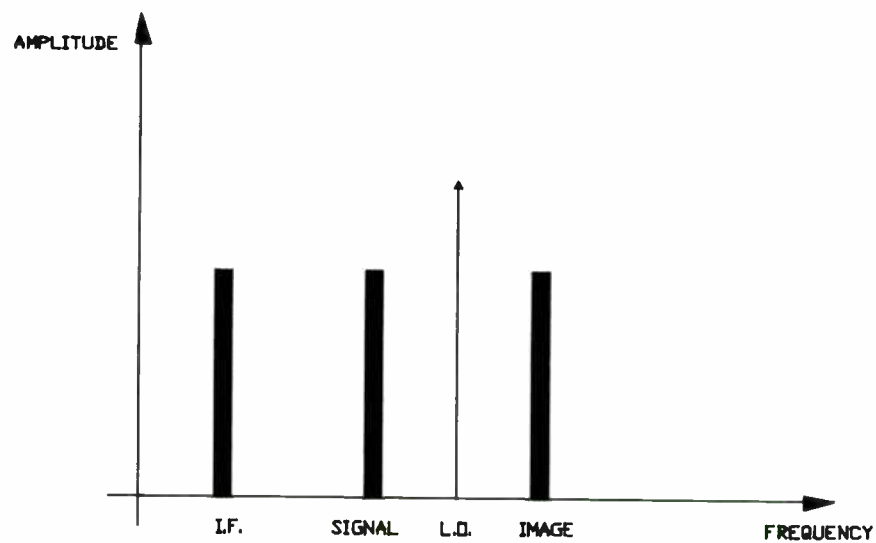


FIG.3

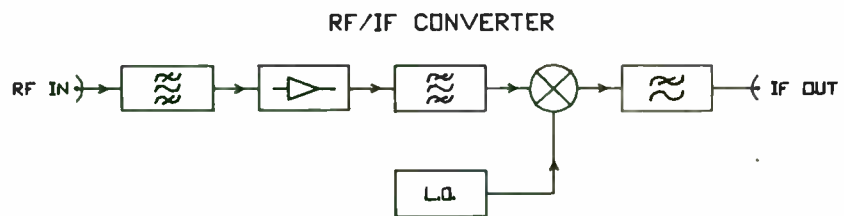


FIG. 2

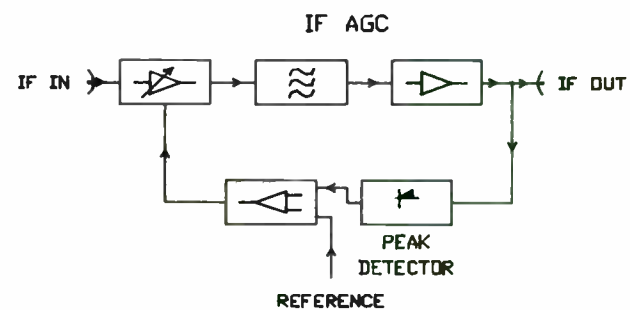


FIG. 4

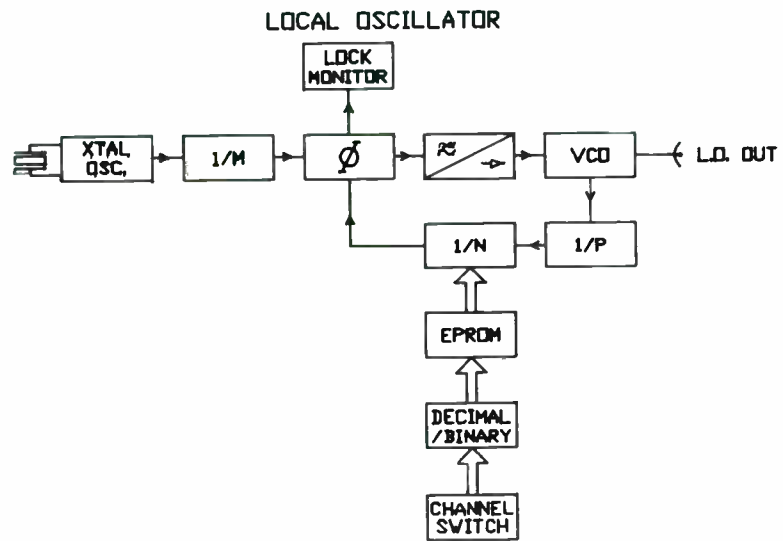


FIG. 5

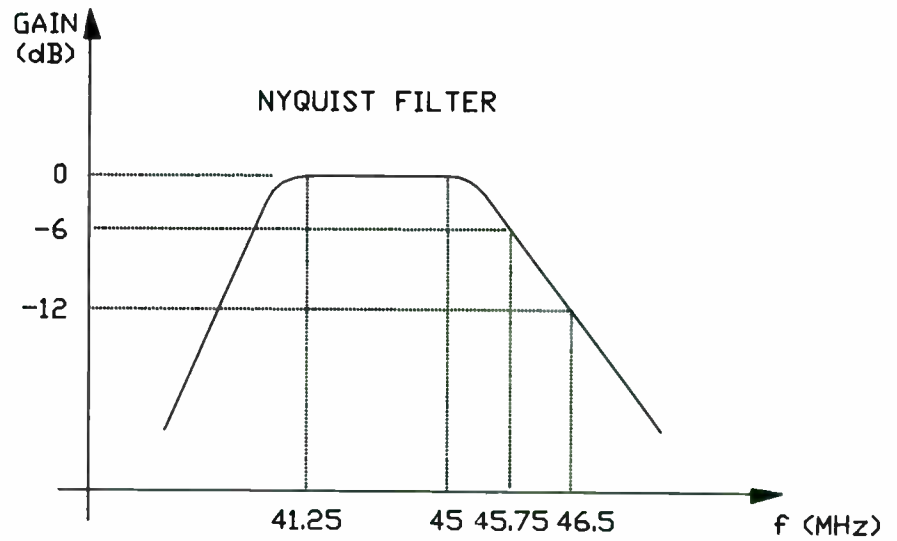


FIG. 7

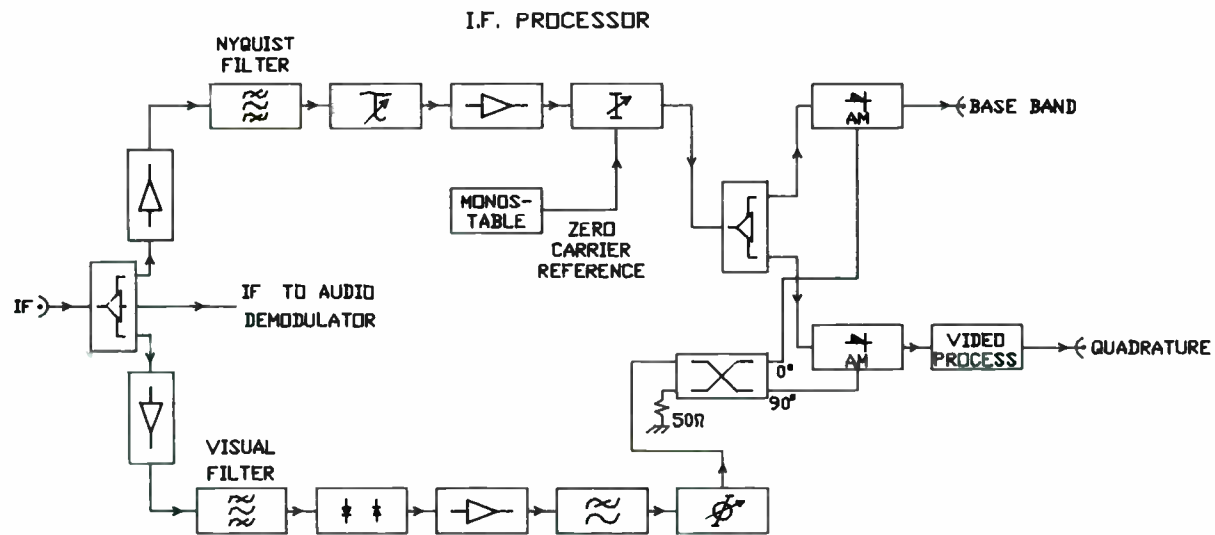


FIG. 6

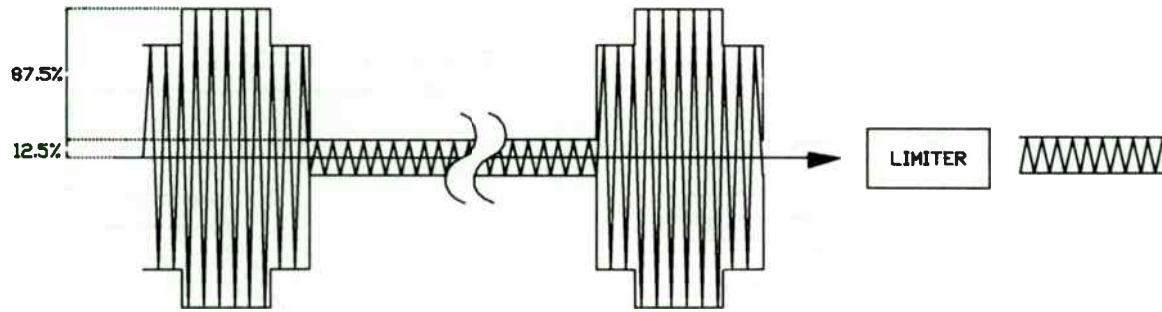


FIG. 8

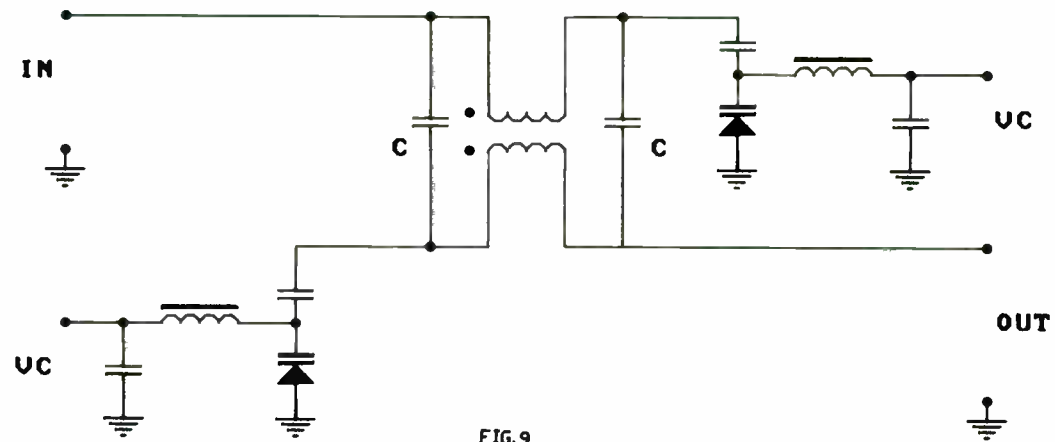


FIG. 9

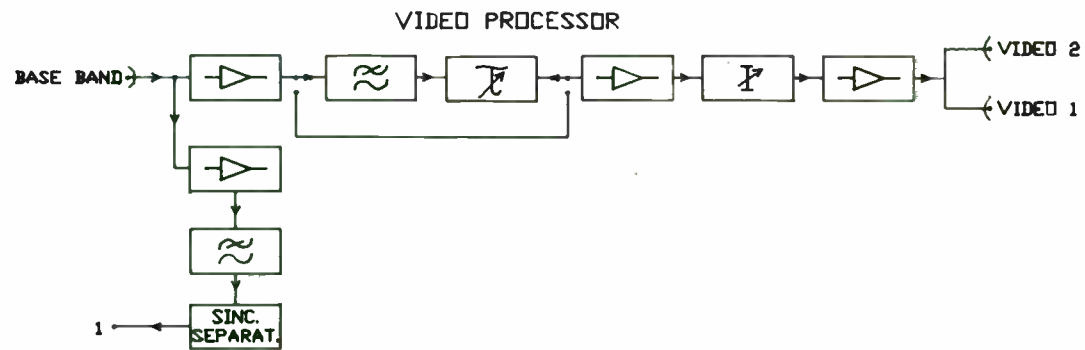


FIG. 10

VIDEO RESPONSE

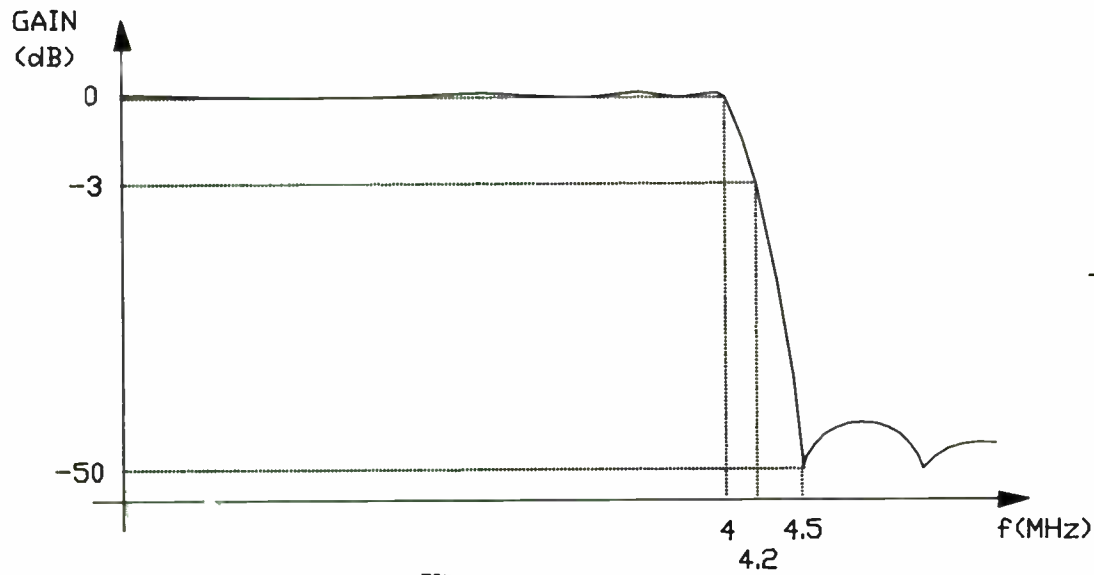


FIG. 11

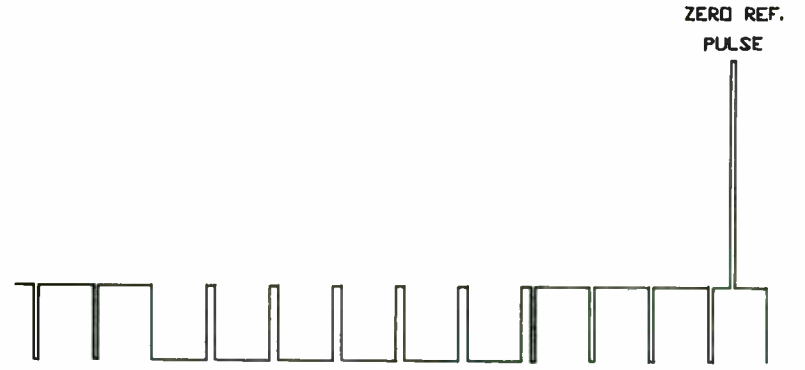


FIG. 13

DEMODULATOR/RECEIVER
DELAY RESPONSE

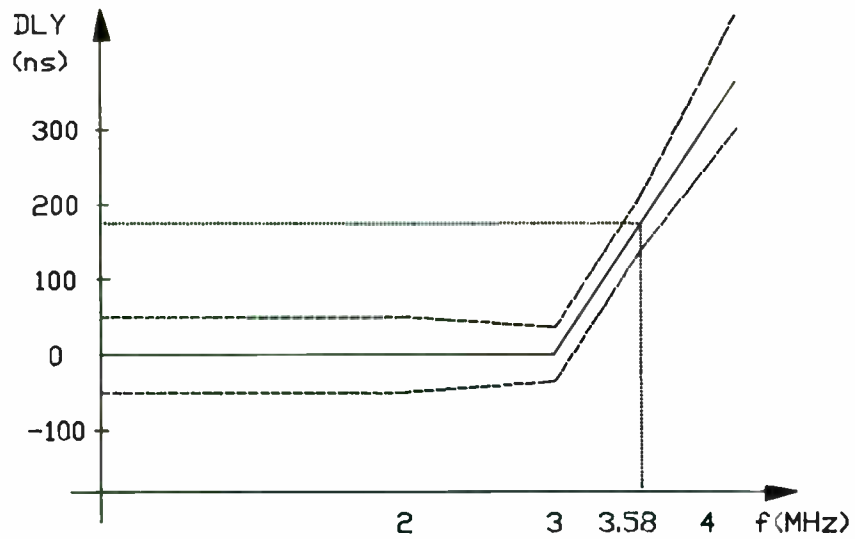


FIG. 12

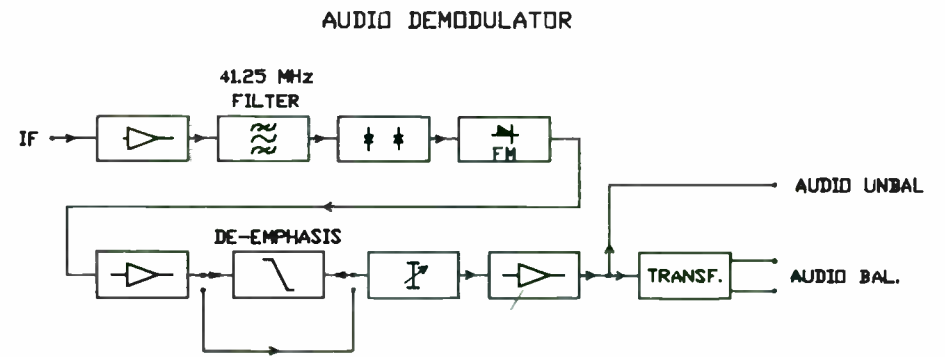


FIG. 14

**DIGITAL-SIGNAL-PROCESSING-BASED SPECTRUM-MONITORING SYSTEM
USED FOR THE EUROPEAN BROADCASTING AREA**

István Novák

Design Automation, Inc.

809 Massachusetts Avenue, Lexington, MA 02173-3992, U.S.A.

TEL.: (617) 862 8998 FAX.: (617) 862 3769

(on temporary leave from the Technical University of Budapest, Budapest, Hungary)

ABSTRACT

This paper describes a spectrum monitoring system for the 0.1 to 30 MHz frequency range. The system is based on a high-performance, synthesizer-tuned receiver and digital signal processing (FFT) of its intermediate-frequency output signal. The built-in controller of the signal analyzer allows the user to operate part or all of the system manually or according to predefined sequences.

Special features of the system are high-accuracy measurements of field-strength and frequencies of user-selected spectral components, and automatic recognition of carrier signals. By virtue of the high selectivity (bandwidth of the FFT bin can be as low as 2.5 millihertz) and frequency resolution (better than 100 microhertz), the system readily lends itself to monitoring crowded broadcasting bands with closely spaced carrier signals. A proprietary smart signal-processing algorithm provides automatic signal identification and high-resolution frequency measurements (together with confidence ranges of measured data from a single spectrum) without the penalty of increased measuring time.

I. INTRODUCTION

Ever-increasing transmitter powers and uncontrolled frequency assignments in the early decades of broadcasting resulted in an overcrowded spectrum in the European Broadcasting area in the LF (150 to 300 kHz) and MF (530 to 1620 kHz) bands. Regular and sometimes sophisticated monitoring is therefore necessary to make sure that a given transmitter can serve the geographical area it was designed and licensed for. Tight tolerances of carrier frequency and radiated bandwidth are required to reduce mutual interference and audible beat-frequency tones. These have a strong impact on both the on-site and remote monitoring equipment [1].

In particular, the monitoring of the actual service area of an operating transmitter can be extremely difficult with conventional instrumentation, since international recommendations (*e.g.*, by CCIR, the Radio Consultative Committee of the International Telecommunications Union) call for a maximum of 10-Hz frequency tolerance of carrier frequencies, making it impossible to separate measured carriers by only the selectivity of an analog receiver. The reason for the 10-Hz tolerance limit: even though this beat frequency is not audible directly, the harmonic and intermodulation products, as well as the fluctuation noise generated near the threshold of envelope detectors, tend to be annoying if the beat frequency is higher than 10 Hz. The high operating costs of super-power transmitters (up to 2 MW) can be significantly decreased by adjusting the carrier power according to the actual modulation depth (Dynamic Carrier Control), but still extensive on-site and remote monitoring is required to verify continuously the proper coverage.

Such a situation calls for monitoring systems with extremely high selectivity (to separate and measure common-channel signals individually), high

accuracy (to monitor and control quasi-synchronous broadcasting networks which have specified frequency separation among carriers of 0.1 Hz maximum and to provide data for preventive maintenance). Due to the "slowly" varying nature of broadcasting signals, the scanning speed and data throughput rate — which may be important parameters when monitoring wide-band transmissions in the VHF or UHF bands [3] — are of secondary importance.

This paper describes some of the results of the R&D effort conducted at the Technical University of Budapest since 1975. First, an analog hardware and a measuring method called Envelope Analysis Method [2] was developed, which allowed the approximate measurement of the common-channel interference of on-the-air operating transmitters. This was the first published method [2], which replaced the previously used measuring procedure that required shutting down the main transmitter while measuring the common-channel interfering signals in the background. As synthesizer-tuned receivers became common, a general-purpose, high-resolution, automated monitoring system was developed [4]. The high accuracy and resolution of the monitoring system are achieved by digital signal processing of the sampled intermediate-frequency signal [5]. The system can be operated step-by-step manually or fully automatically. Transmitter performance measurements can be made on-site or remotely. Based on several different equipment designs, the measuring principle has been in use at five monitoring stations in three countries.

II. CONFIGURATION

Fig. 1 and Table I. show the instrumentation set-up and the major specification items, respectively. The system is modular and can be used in different configurations.

Most of the special monitoring features are provided by the signal analyzer, which is at the same time the system controller, and represents the core of the system. It samples the band-limited incoming signal, evaluates it in the time and frequency domains and outputs the result of feature extraction. It controls other instruments in the system via the IEEE bus, according to the actual measuring needs. The system can be programmed, used manually, or controlled by an external controller. In the case of on-site baseband measurements, a small portion of the transmitter's output signal is rectified and connected directly to the input of the signal analyzer. Antenna and receiver are not needed. The baseband signal is evaluated, and only a hardcopy unit is needed to complete the system.

For on-site and remote radio-frequency measurements, the signal to be evaluated is fed through a receiver which provides the necessary band-limiting, and frequency translation. For calibrated level measurements it also does the leveling. A block diagram of the receiver is shown in Fig. 2. This receiver combines the advantages of a high-performance communication receiver and a measuring receiver. High sensitivity and dynamic range of signal analysis is guaranteed by the low-noise, high-level mixer, preceded by a controlled attenuator. The synthesized local oscillators have low phase noise to avoid masking of small signals and to provide high-quality reception. Dual conversion and a set of crystal, mechanical, and active filters allow selection (manually or by the system's firmware) of the optimum bandwidth of reception. This is especially useful when there are large adjacent-channel interfering signals.

A wide choice of analog-filter bandwidths and spans of digital signal processing makes it possible to select the optimum combination of filtering to reject unwanted signals. Input to the receiver is either a properly attenuated

output signal of a transmitter, output of a calibrated or uncalibrated antenna, or — to extend the frequency range by cascading — the intermediate-frequency signal of higher-band receiver(s).

Off-the-air measurements require an adequate antenna. Calibrated field-strength measurements are possible with the wide-band active loop antenna of the system, which has a constant 20-dB conversion factor (difference of dBuV/m field strength and dBuV output voltage of the antenna) over the frequency range of 0.15 to 30 MHz. The antenna is powered from the receiver.

Precise frequency measurements may require the use of an external frequency reference. With no external reference, all local oscillators and sampling clocks are locked to the oven-controlled master clock of the receiver (frequency accuracy is ± 0.1 ppm). If necessary, this is replaced by an external frequency reference.

III. OPERATION, FEATURES, ADVANTAGES

The firmware of the monitoring system offers easy-to-use, fast, and accurate measurements in all operating modes. All of the measurement functions can be controlled from the keyboard of the signal analyzer and all measurement results are displayed on its screen (see the hardcopies in Figs. 3, 5, and 6). The screen displays *living spectra* (spectra are updated automatically as they become available) of signals to be analyzed, together with the selected measurement parameters and measurement results corresponding to the spectrum shown. Easy and fast operation is provided by selecting of input parameters in simple radio-frequency terms such as channel frequency, analysis bandwidth and full-scale field strength; the optimum combination of receiver and signal analyzer parameters are set by the system firmware.

Operation of the system can be performed through different levels of commands and parameter inputs. Those of the most frequently used commands, which do not require numerical entries, are executed by single keystrokes without stopping data acquisition and evaluation. Those major measurement parameters which require numerical data entries, are accessible from the function-list mode. All of the features, operating modes and display modes of the system can also be controlled by commands incorporated into the user's operating program. Finally, if an external controller is used, the signal analyzer is switched to its talker/listener function.

Measurement outputs and data displays are similarly structured. The major setup parameters with the most-important output data are always displayed on the screen. Screen hardcopies are generated by single keystrokes. Less-frequently-used output data are available from the user RAM.

Single-keystroke commands:

- C:** initiates the calibration of receiver.
- R:** reads the actual status of the receiver.
- A:** starts the automatic setting of full-scale level of receiver.
- CLS:** clears the spectrum counter and statistics (there is a dedicated cls key).
- T:** toggles tracking of spectral lines on and off.
- P:** initiates print screen.

Function-list commands:

To the left of the displayed spectrum, the column of alphanumeric information is for data input and output. In the function-list mode, a highlighted cursor is moved around the input fields and the user is allowed to change any

of the measurement parameters, namely:

- input full-scale level in dBuV/m,
- channel frequency in Hz, analysis span in Hz,
- type of spectrum to be evaluated, type of spectrum averaging,
- numerical thresholds for spectrum evaluations.

In this menu, the operator can switch on and off input and output fields which may not be necessary in all measurements. These hidden fields are: bandwidth, AM modulation depth, and tracking of selected sinusoidal spectral components.

Output fields:

Two categories of output data appear on the screen: narrow-band cursors and wide-band characteristics.

Cursors: The *living spectra* have two kinds of cursors. A line-by-line cursor above the spectrum can be placed to any spectral line and acts as a usual line cursor in the spectrum. On the other hand, the results of spectrum post-processing are shown in two detailed fields to the left of the spectrum. These fields contain the frequencies, confidence ranges (of the frequencies) and levels of the sinusoid signals which are automatically detected in the spectrum. The field with the header **MAXIMUM** is always set to the highest-level sinusoid signal found in the spectrum. The field with the header **CURSOR** shows the parameters of the sinusoidal signal which is marked by the cursor. In contrast to the line-by-line setting of the conventional cursor, this field can be moved through the sinusoidal signals by pressing the up or down arrows. Pressing the up or down arrow moves the cursor up or down in frequency to the next

sinusoidal peak. The fields to the right of the header also indicate in brackets the actual/total number of sinusoidal signals in the spectrum. Note that the sinusoidal cursor gives the accurate frequency and level of the sinusoid signal, while the conventional cursor has inherent errors. The raw data from the FFT may have an amplitude error as high as 1.5 dB with Hanning weighting and 4.2 dB with rectangular weighting, depending on the frequency of the signal relative to the sampling frequency. The uncertainty of the frequency is half of the FFT bin. Interpolation on the spectrum allows compensation for the inherent errors [6], [7], [9]. The unique interpolation method incorporated in the high-resolution monitoring system (partly published in [8]) provides the confidence range of the measured values from a single spectrum frame.

Wide-band characteristics of the signals are based on the power spectra. The bandwidth is calculated as the difference of frequencies between which the signal power is $(1-x)$ times the total signal power, where x is defined by the operator. x is the out-of-band ratio which is symmetrically divided into two halves at the two sides of the signal's spectrum.

The AM modulation depth is proportional to the ratio of the total side-band power and carrier power. The carrier is assumed to be the largest sinusoidal signal within the specified spectral window. To lock out adjacent-channel signals, the user can set a low and high spectral-line limit for the evaluation. These are shown as **LO=XXX** and **HI=YYY** on the screen, where **XXX** and **YYY** are integers between 1 and 400.

IV. APPLICATIONS, MEASUREMENT RESULTS

A. *High-resolution remote monitoring*, to measure common-channel interference

Fig. 3 shows common-channel interference of two closely-spaced carrier signals in the LF broadcasting band. The one-Hz frequency span of the display corresponds to 2.5-milliHz digital channel spacing, which enables the clear distinction of the two carriers, which are only 60 milliHz apart. The higher-frequency carrier is marked with the dotted line of the graphic cursor, the interpolated signal strength, frequency and confidence range (of the frequency) are shown in the CURSOR field. Interpolated data for the lower-frequency peak (which, in this case has the largest level) are shown in the MAXIMUM field. The narrow effective bandwidth also results in a low background-noise level. Thus, in spite of the approximately 20-dB level difference of carriers, the smaller signal still can be accurately measured.

Note the 25-microHz and 140-microHz confidence ranges of measured frequencies. The same accuracy of frequency measurement by conventional methods would usually require an equivalent 40000 and 7000 seconds measuring time, respectively. The total sampling time for a one-Hz span is 400 seconds (the processing time is approximately 400 milliseconds), accounting to a $40000/400 = 100$ as well as $7000/400 = 17$ times reduction of measuring time.

A typical example of high-resolution measurements for the purpose of preventive maintenance is shown in Fig. 4. The carrier frequency of a high-power transmitter was measured repeatedly at one-minute intervals and the measured values were plotted against time. The extremely fine resolution of frequency measurements allows the operator to observe changes of the fre-

quency and the drift rate of frequency before it is detectable by other means. Early discovery of performance degradation (which can be a sign of an impending catastrophic failure) allows planned repairs to be done without costly and unexpected breakdowns.

B. *Wide-band remote monitoring*, to measure modulation parameters

Wide-band measurements of broadcasting channels are used to identify and measure interfering signals with large frequency offsets, and to measure the bandwidth and modulation depth characteristics of the main transmitter. Manual or programmed scanning of channels in a wide-span mode is used as a regular quick surveillance of a set of transmitters. Fig. 5 shows 20 kHz-span averaged spectrum of an AMDSB sound-broadcasting transmitter as measured off-the-air. Besides the carrier frequency and field strength, the two-sided bandwidth and the modulation depth of the transmission are also shown. The user can specify the percent out-of-band power to measure bandwidth. Together with the instantaneous AM modulation depth (calculated from one frame of power spectrum), the line below displays the minimum, average and maximum values also.

C. *On-site baseband monitoring* of transmitter modulation parameters

An optional user program extends the capabilities of the measuring system to include on-site baseband measurements of detailed transmitter parameters on calibrated, rectified signals from its output. An example is shown in Fig. 6. Some of the measured parameters (peak positive and peak negative modulation index) are based on the time function, carrier power, sideband power, effective modulation depth and the bandwidth are calculated

from the power spectra. For convenient use with Dynamic Carrier Control, the operator can enter the reference carrier power. With the exception of bandwidth, the minimum, average and maximum values are also shown. Measurements may be made on the actual audio program material or with audio-frequency sinewaves connected to the modulator input of transmitter. In this latter case the program measures and displays the modulation depth relative to the reference, together with the harmonic distortion and the signal-to-noise ratio.

ACKNOWLEDGEMENT

The research and development project described here was supported and financed mainly by the Hungarian PTT, PONT Szövetkezet (PONT Manufacturing Co.), and Mechanikai Laboratorium (ML Manufacturing Co.). The measurement results shown in Figs. 3 through 6 were taken at the Measuring Station of the PTT, Tárnok, Hungary, where a system similar to the one described here is in regular use.

REFERENCES

- [1] CCIR, *Handbook for Monitoring Stations*, Geneva, ITU, 1988.
- [2] I. Novák, "The envelope analysis method -- a new technique for measuring co-channel interference in the LF and MF bands," *E.B.U. Review -- Technical*, pp. 170-175, August 1981.
- [3] H. Petry, R. Bott, "Digital broadband scanning receiver EBD 900 for radio surveillance", *News from Rohde Schwarz*, pp. 11-15, no.129, 1990.
- [4] I. Novák, "New trends in radiomonitoring," *Telecommunications Journal*, pp. 817-823, December 1987.
- [5] High-Resolution Monitoring System, HMS-1. Data sheet, PONT Szövetkezet, Mechanikai Laboratorium, Budapest, Hungary, 1989.
- [6] Tien T. Wang, "The segmented chirp Z-transform and its application in spectrum analysis," *IEEE Trans. on Instrumentation and Measurement*, pp. 318-323, April 1990.
- [7] C. Offelli, D. Petri, "Interpolation technique for real-time multifrequency waveform analysis," *IEEE Trans. on Instrumentation and Measurement*, pp. 106-111, February 1990.
- [8] I. Novák, "Digital signal processing for radio monitoring," XXIInd General Assembly of URSI, Tel Aviv, Israel, 24 Aug. - 2 Sept. 1987. Copies are available from the author.
- [9] C. Offelli, D. Petri, "A frequency-domain procedure for accurate real-time signal parameter measurement," *IEEE Trans. on Instrumentation and Measurement*, pp. 363-368, April 1990.

Table I. MAIN SPECIFICATIONS OF THE MONITORING SYSTEM.

Receiver:

Frequency range: 0.15 to 30 MHz
 Synthesizer step: 1 Hz
 Input level: 0 to 120 dBuV full scale, in 10-dB steps
 Calibrated IF output: 10 kHz, 1 Vrms (EMF)
 Sensitivity: 0.4 uV EMF in A1 mode
 BW = 400 Hz, (S+N)/N = 10 dB
 IF bandwidths: 0.15, 0.4, 0.7, 1, 1.4, 2, 3, 6, 14 kHz
 Frequency reference input: 5 MHz, 0.1 Vrms, any waveform

Signal analyzer, system controller:

A/D conversion: 12 bits
 Frequency spans: 1, 2, 5, 10, 20, 50 Hz
 0.1, 0.2, 0.5, 1, 2, 5, 10, 20 kHz
 FFT: 1024 points, 400 lines
 Frequency reference input: 5 MHz, 0.1 Vrms, any waveform
 Built in floppy disk drive: 5.25", 360 KB
 16 Kbytes user RAM, high-level language interpreter
 IEEE bus modes: selectable controller or talker/listener
 Spectrum evaluation: non-parametric peak search
 three-point interpolation
 confidence-range calculation

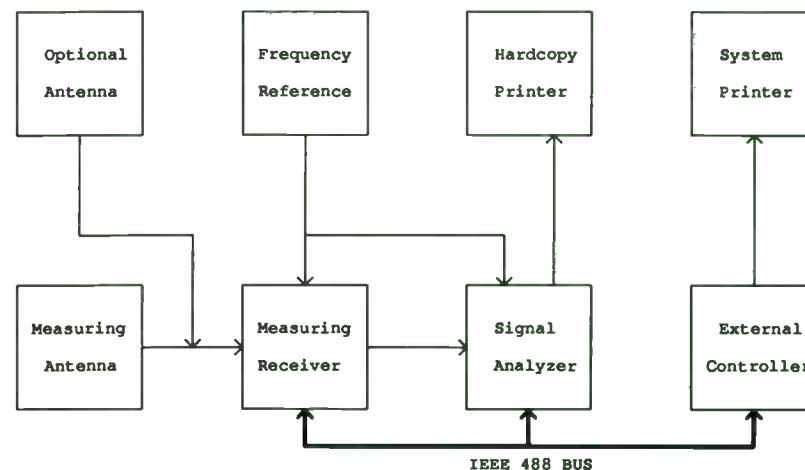


Fig. 1. System block diagram of the monitoring instrumentation.

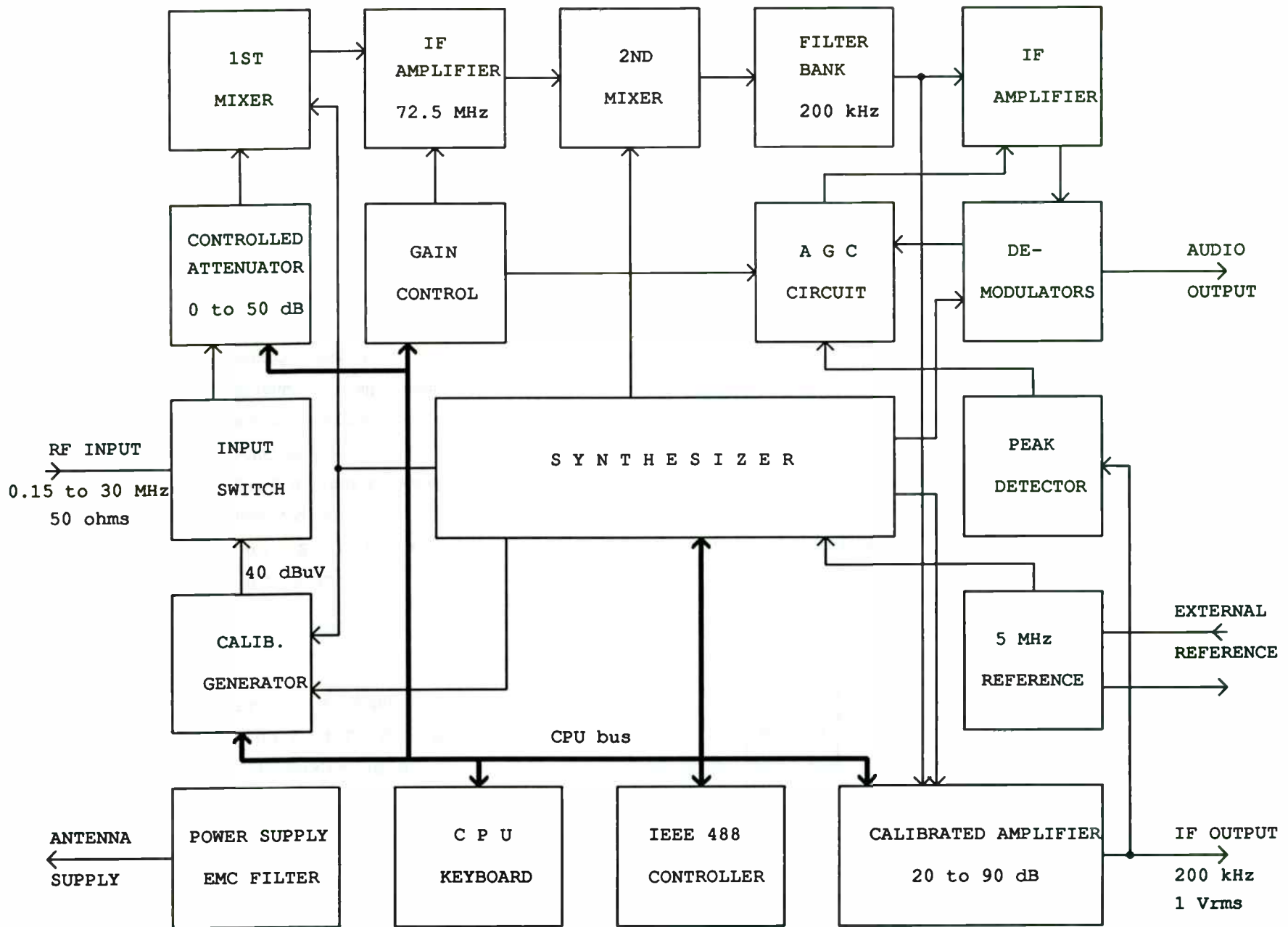


Fig. 2. Block diagram of the communications/measuring receiver.

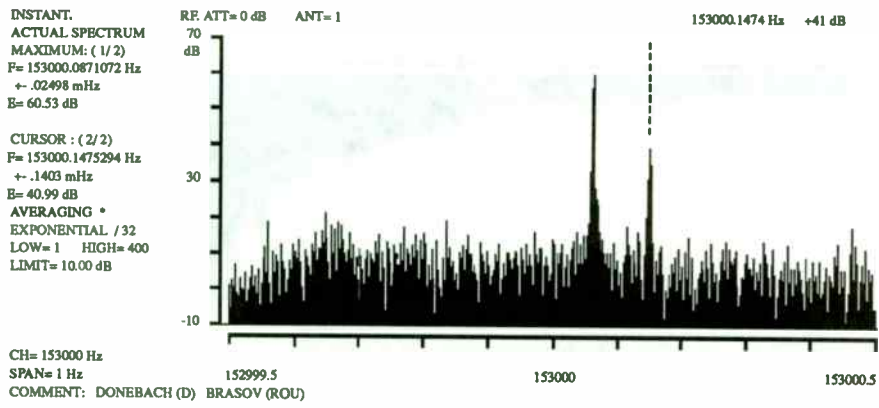


Fig. 3. Sample hardcopy of high-resolution common-channel interference measurement. Note the change of slope in the extrapolated trend.

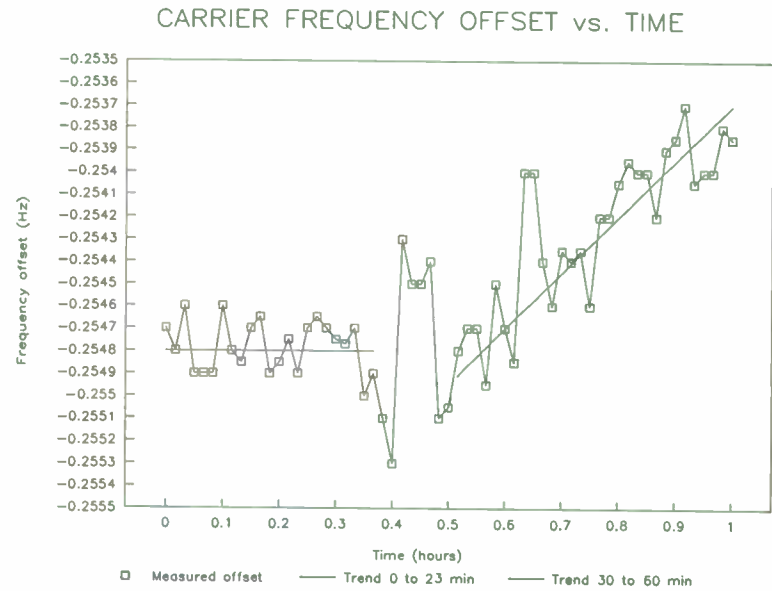


Fig. 4. Example of high-accuracy measurements for preventive maintenance.

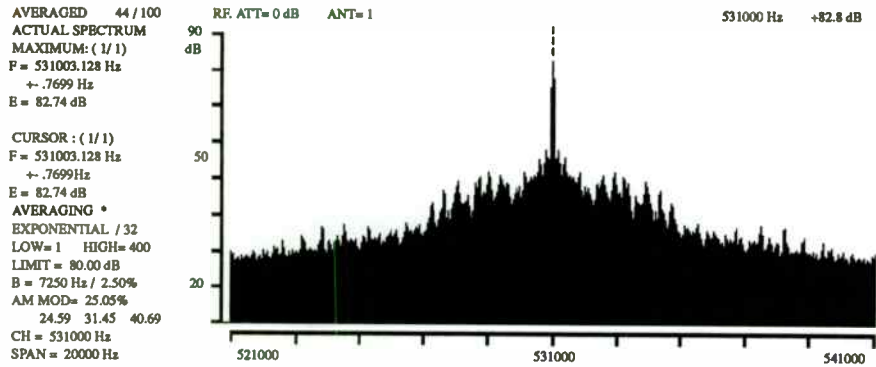


Fig. 5. Measurement of wide-band modulation characteristics.

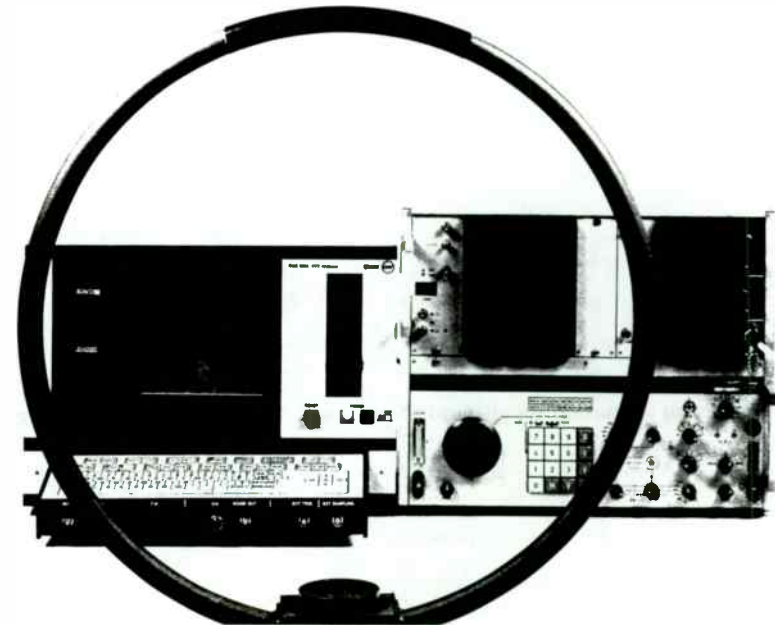


Fig. 7. Photo of the high-resolution monitoring system.

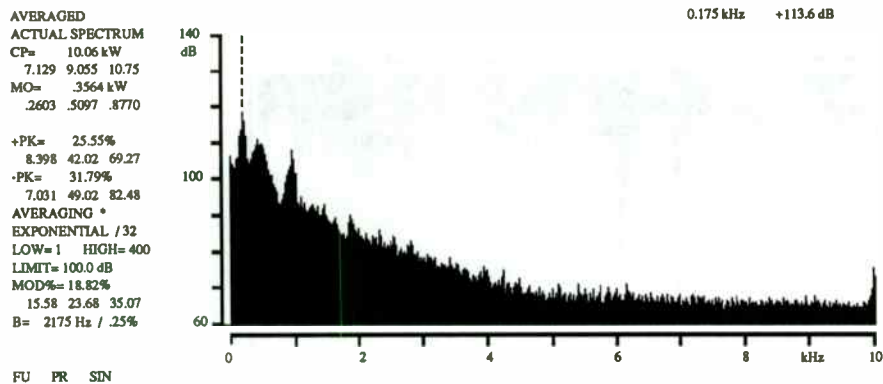


Fig. 6. Example of on-site transmitter measurement in the baseband.

Impedance-matching Transformers for RF Power Amplifiers

David N. Haupt
Erbtec Engineering, Inc.
2760 29th Street
Boulder, Colorado 80301

Introduction

As applications for RF systems require higher power levels, matching transformers become an appealing alternative to traditional lumped element impedance matching networks. This brief tutorial is intended to provide an insight into how RF transformers work, show the advantages of the transmission-line configurations, and present enough information for a designer to develop a functioning broadband transformer on the first attempt.

The need for transformer coupling - limitations of lumped-element matching

The most common configuration for an impedance matching network is the lumped element ladder or "L" network. These networks are conceptually easy to understand and design, and for small signal amplifiers can be realized with inexpensive automatically-insertable leaded components or chip components. When used at high power levels, the RF currents and voltages imposed on the components results in the use of more costly, harder to obtain components, and frequently introduces multiple adjustments to "tweak" production units. Broadband designs require multiple stages, adding a real estate problem to the high current and voltage problem. To a large extent, all of these drawbacks are

mitigated when matching transformers are used. Transformers, while tedious to build, may represent fewer components and solder joints than multiple stage lumped element networks, making them the obvious choice in most broadband design work. Transformers are frequently built with coaxial cable transmission lines, which enable them to easily handle high power levels. The inherent broadband nature of transformers reduces the need for adjustable elements, thus contributing to reduced production costs and fewer field adjustment problems. Enhanced reliability is often a desirable byproduct of using transformers, with their attendant reduction in quantity of soldered connections.

A review of the conventional transformer and its limitations for high power RF applications

In applications where lumped element L networks obviously cannot work, the next obvious candidate is a transformer. Conventional transformers work fine at low frequencies, so an investigation into their high frequency behavior may show how to use them effectively in RF systems.

A conventional transformer with its significant stray elements is shown in Figure 1. In operation, the primary winding is driven by a signal source and a load is connected to the secondary winding. The power delivered to the primary winding is converted to a magnetic field within the magnetic core of the transformer which is then converted to electrical power in the secondary winding.

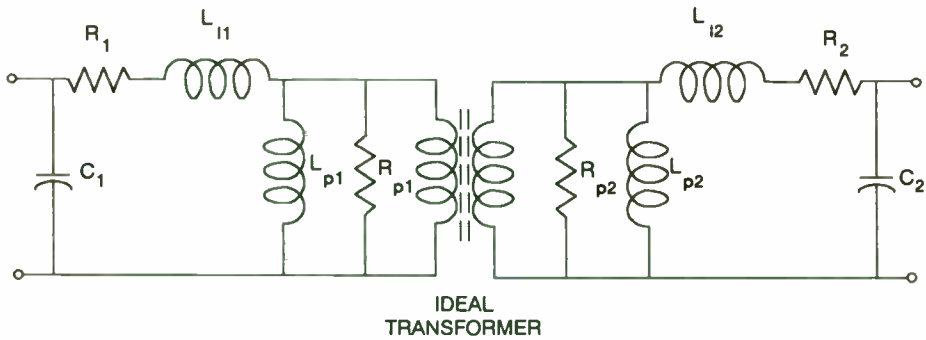


Figure 1: Electrical equivalent of a conventional transformer

The interwinding capacitances, C_1 and C_2 , come from the proximity of one turn to another in each winding, and increase with the number of turns. These capacitances interfere with high frequency performance and should be minimized if reasonable high frequency performance is required. The shunt inductances, L_{p1} and L_{p2} , represent so-called "magnetization inductance" and arise from the self inductance of each winding. These inductances cause losses at low frequencies by shunting current to ground. Leakage inductances, L_{l1} and L_{l2} are caused by incomplete linkage of the magnetic field of each winding with the core. They increase losses at high frequencies by presenting series impedances to the flow of current. They can be minimized by making the windings close to the core, using a toroid core (or other tightly-coupled core shape) and by making the magnetic core out of high- μ material.

The design of conventional transformers at low frequencies is fairly straightforward. By using enough turns on the primary and secondary, the shunt inductances are minimized, and by using a high- μ core, the leakage inductance is minimized. At low frequencies, the stray winding capacitance has negligible effect.

If operation of the transformer at RF is attempted, however, the interwinding capacitance becomes a low shunting reactance and the leakage inductance becomes a high series reactance, both contributing to poor response. Fewer turns per winding helps to minimize stray capacitance, while high- μ cores in efficient shapes such as baluns or toroid can reduce leakage inductance. Such cores are usually made of powdered iron. These techniques can work for low power transformers. Unfortunately, as power levels increase, core saturation becomes a problem. If the core material used is ferrite instead of powdered iron, saturation levels increase, but at the expense of lowered μ and increased core loss at frequencies above several tens of MHz. The lowered μ forces larger cores for the same low frequency cutoff, and can increase leakage inductance, effectively lowering the upper cutoff frequency. These tradeoffs become more severe as higher power levels are attempted. While conventional transformers can be made effective at higher power levels, they usually require "fixes" such as resonating capacitors that limit bandwidth.

The transmission-line transformer configuration

If a 1:1 conventional transformer is reconfigured as shown in Figure 2, the result is a transmission-line transformer. While it is possible to use a conventionally-wound transformer in this configuration, significant advantages accrue if the windings take the form of a transmission line rather than two separate inductive

windings. The critical difference between the two winding techniques is that the coupling between input and output of the transmission line transformer is not through a magnetic core. Instead, the power transfer from input to output is accomplished through the transmission line properties of the windings. For a 1:1 turns ratio, which always exists when a transmission line is used as the winding set, the voltage that appears across each winding is the same. Because of this, the difference voltage at the output is the same as the difference voltage at the input, leading to $V_{PRI} = V_{SEC}$, identical to the conventional 1:1 transformer.

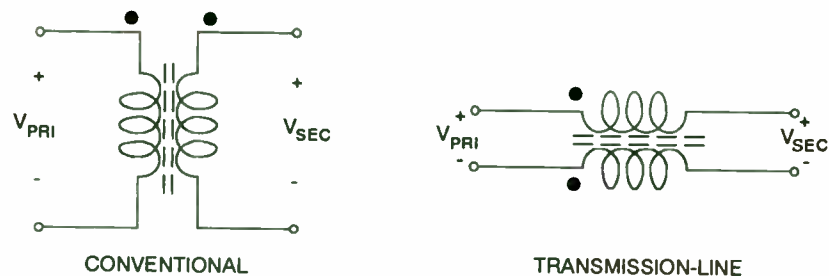


Figure 2: Conventional versus transmission line transformer configurations - 1:1 Impedance ratio

Analysis of the transmission-line transformer

A popular impedance transformation ratio is 4:1. This ratio is useful as a matching network for the input stage of a single ended bipolar transistor power amplifier. The configuration is shown in Figure 3. Note that the two windings have equal numbers of turns (frequently 1), and magnetic core material may optionally be used if extension of low frequency performance is required. Also note that the transformer is inherently an unbalanced design - that is, there is a common ground connection between the input and output ports.

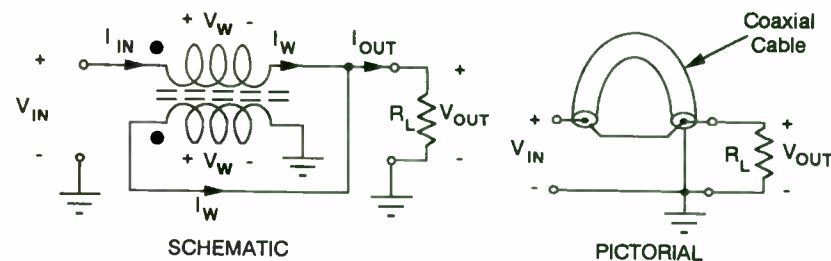


Figure 3: 4:1 Impedance ratio transmission line transformer

The 1:1 nature of the transmission line windings leads to two extremely useful results. First, the voltage across primary and secondary windings of each section are equal (labelled V_W in the schematic). Second, the current through primary and secondary windings is of equal magnitude but in opposite directions.

The output voltage has been labelled V_{OUT} and has been arbitrarily given a polarity. From the schematic, it is obvious that the lower winding of the transformer is directly in parallel with the load, and must therefore have the same voltage and polarity across it. Therefore,

$$V_{out} = V_W.$$

$$V_{OUT} = \frac{1}{2} V_{IN}$$

$$I_{OUT} = 2 I_{IN}$$

$$\therefore 4:1 \text{ Z CHANGE.}$$

$$4:1 \text{ req } 25 \times Z_0$$

Because of the 1:1 turns ratio enforced by the use of a transmission line, $V_W = V_{out}$ also exists across the upper winding. It is evident from the schematic that the input voltage V_{in} is the sum of the voltage across the upper winding, V_W and the output voltage, V_{out} . Since V_W and V_{out} are equal,

$$V_{in} = 2V_{out}.$$

Not so obvious is the current transformation ratio. For this analysis it is useful to start at the input end of the transformer. It is obvious that the current through the upper winding is identical to the input current:

$$I_W = I_{in}$$

The 1:1 turns ratio requires that the same current flows in the lower winding in the opposite direction. These two equal currents sum at the junction at the output of the transmission line, resulting in

$$I_{out} = 2I_W = 2I_{in}.$$

The impedance ratio of the overall configuration is

$$\frac{Z_{in}}{Z_{out}} = \frac{V_{in} / I_{in}}{V_{out} / I_{out}} = \frac{2V_{out} / \frac{1}{2}I_{out}}{V_{out} / I_{out}} = 4/1.$$

or, as is more commonly written,

$$4:1$$

Consideration must now be given to the characteristic impedance of the transmission line that should be used in the construction of this transformer. The correct value is determined by evaluating the terminal voltage at one end of the transmission line versus the current through one of the conductors. In this case, the terminal voltage at the output end (the right end) is obviously V_{out} . From the previous analysis, the current through one conductor is $I_{in} = \frac{1}{2}I_{out}$. The correct characteristic impedance is therefore

$$\frac{V_{out}}{\frac{1}{2}I_{out}} = 2Z_{out}.$$

If this transformer is designed to match 50Ω to 12.5Ω , then a 25Ω transmission line is required. This configuration is shown in Figure 3, using coaxial transmission line.

Other impedance matching ratios are possible, as long as they are $n^2:1$. For example, 9:1 and 16:1 transformers are shown in Figure 4.

Analysis of these higher ratio transformers is similar to the analysis presented for the 4:1 transformer. First, set the voltages across the two conductors of each transmission line section equal, then set the currents equal and opposite, and then solve the resulting simultaneous equations. Sometimes this can be performed by inspection. Note that the voltage drop across each transmission line section will not necessarily be the same. For example, the upper transformer of the 9:1 will have $2V_{out}$ dropped across the primary and secondary, while the lower transformer will have only V_{out} dropped across the primary and secondary. For this reason, separate cores must be used for the two transmission line sections when magnetic loading is required to extend low frequency response. Additionally, the amount of magnetic loading used on each transmission line section must be proportional to the voltage across the sections - in this case, two beads on the upper section and one on the lower section.

This keeps time delays equal in the parallel branches of the circuit. If this were neglected, low frequency performance would suffer. Inspection of the terminal voltages and currents for each transmission line will again provide the necessary characteristic impedances for the individual transmission lines. Additionally, the lines will not always need to be the same impedance as each other. Individual analysis of the terminal voltage and currents is required to determine appropriate line impedances.

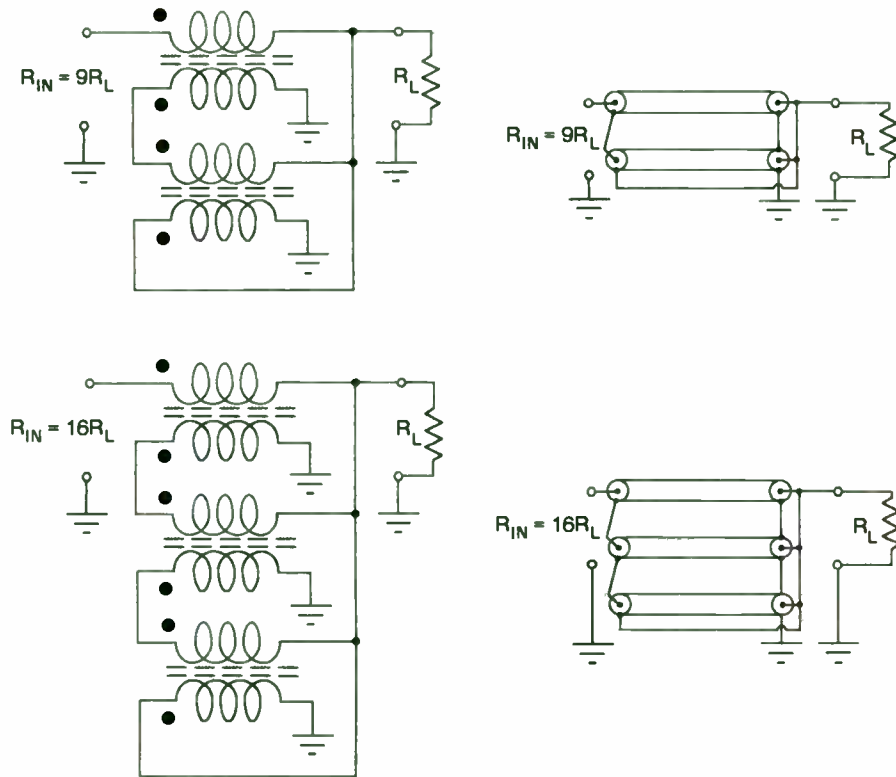


Figure 4: 9:1 and 16:1 unbalanced transformers

Transmission lines - impedances and configurations

If the transformer of Figure 3 were designed to match 12.5Ω to 50Ω , the required characteristic line impedance would be 25Ω . This impedance is available from several sources, but tends to be expensive due to low volume. An alternative is to parallel two 50Ω sections, which must exhibit the same delay. Other impedance ratios may require odd combinations of lines in parallel, for example $75\Omega || 50\Omega = 30\Omega$. This line would be required for a transformer designed to match 15Ω to 60Ω . Again, both lines must exhibit the same delay. For most coaxial lines, the velocity factor, and hence the delay in a finite length, is determined by the dielectric between the center conductor and the shield. Transmission lines of differing characteristic impedance will still have the same delay as long as they employ identical dielectrics. In the event lines with differing dielectrics are used in parallel, the physical lengths must be adjusted to achieve the same electrical length.

The preceding discussion assumes coaxial transmission line. Twisted pair lines represent an attractive alternative in many situations. Virtually any impedance may be custom made between approximately 20 and 200Ω . Thin conductors and thick insulation result in high impedance lines, while thick conductors and thin insulation (enamel) result in low impedance lines. It is possible to create even lower impedance lines by connecting two twisted pairs in parallel, but the net impedance can be expected to be half the calculated result due to extra distributed capacitances.

The effects of line length at high frequencies

Several assumptions were made in the foregoing discussion. One of them was that the total delay through the transmission line section was relatively short. Only one conductor of the transmission line is driven by the input signal, and correct operation of the transformer is dependent upon equal and opposite currents being generated in the other conductor. In general, this will cease to be true at frequencies higher than the $\lambda/8$ frequency of the line. At those frequencies, the additional delay introduced makes the secondary current lag the primary current, and the transformer input and output impedances become reactive. This effect becomes even more pronounced if the transmission line used is not of the correct impedance. For the 4:1 configuration in Figure 3, the equation for the input impedance at the low impedance end, for example, is

$$Z_{in} = Z_0 \frac{Z_L \cos \gamma l + jZ_0 \sin \gamma l}{2Z_0(1 + \cos \gamma l) + jZ_L \sin \gamma l}$$

Where Z_0 = Characteristic impedance of line used
 $\gamma = \omega/v$ where v is the phase velocity of the line
 l = physical line length in the same units as v
 Z_L = load impedance

Figure 5 is a graph of mismatch loss versus frequency calculated for a 50Ω - to - 12.5Ω transformer using the correct 25Ω transmission line and an incorrect 50Ω transmission line. The horizontal scale is in wavelengths; this is equivalent to frequency normalized to the full wavelength frequency of the transmission line length employed in the transformer.

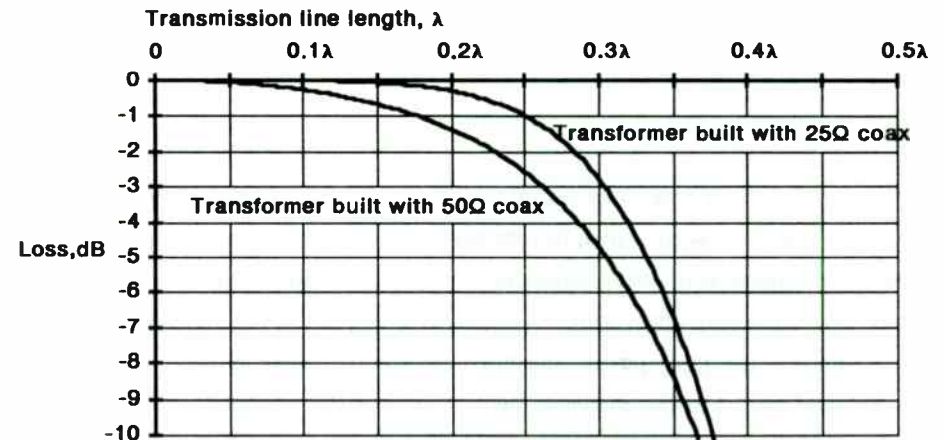


Figure 5: Mismatch loss versus frequency for 4:1 transformers

Further restrictions in high frequency performance will result if the optimum transmission line impedance is unavailable or impractical. Power amplifiers frequently require extremely low impedances, and core cross sectional area may not permit sufficient paralleling of transmission lines to achieve the desired values. One of two choices must then be made: either accept the reduced bandwidth, or somehow compensate the transformer for the line impedance. If a higher than optimum line impedance is used (frequently the case), then the input and output impedances of the transformers take on a net inductive character, which can be compensated by the addition of parallel capacitance at the input and output. The equation for Z_{in} presented earlier is used to determine the actual input impedance of the transformer. A capacitance is chosen which resonates with the inductive component near the highest frequency of operation and is placed in parallel with the input. For optimum bandwidth, the capacitor should be split into two, with the ratio of the values of the two capacitors being

equal to n^2 (where n^2 equals the impedance ratio of the transformer). The lower value capacitor belongs in the high impedance end of the transformer. The net capacitance at the input formed by the input capacitor and the transformed output capacitor (they appear in series) must be the capacitance that was earlier calculated to resonate with the net input series inductance. The additional capacitors will slightly mismatch the transformer at lower frequencies, but an exact match will be achieved at high frequencies.

Low frequency limitations

Referring again to Figure 3, it can be seen that the lower winding is in parallel with the output side of the transformer. This winding exhibits magnetizing inductance just as much as the winding of a conventional transformer would. A realistic minimum of inductive reactance to not seriously degrade transformer performance is achieved when the condition $X_L \geq 5R_L$. This value results in a transformer mismatch loss of 0.043 dB, a negligible amount even for a power amplifier. The first solution to the minimum inductance requirement might be to lengthen the transmission line, but this is in conflict with the requirements imposed at high frequencies which tend to drive the line length to a minimum. A good solution is to place magnetic material around the transmission line (iron powder or ferrite beads) to increase this inductance. This does not materially affect the performance at high frequencies, and reduces the shunting effect of the line at low frequencies. Core dimensions and μ may be chosen according to the rules found in most core manufacturers' catalogs. Although it may seem that the problems of cores have just been recreated, this is not the case. With the transmission line configuration, the power that passes through the transformer is not being coupled through the magnetic material. The flux density in the core is therefore only a result of the magnetizing current caused

by inductive reactance in shunt with an RF voltage source. In fact, as the μ of the core increases, the flux density decreases, making the problem even easier to handle. At VHF, where higher core losses cause significant heating in a conventional transformer, the inductance is so high that currents flowing on the outside of the line are negligible, and no heating occurs. Further improvements in low frequency performance may be obtained through the use of series compensation capacitors. Using the earlier equation, the input impedance of the transformer must be determined, and converted to shunt form. The appropriate capacitance is that which resonates with the shunt inductive component at the desired low frequency. The net input impedance which results has a slightly lower real part than without compensation, but the mismatch loss is substantially lowered due to elimination of the reactive part. Best results are obtained if the capacitor is split in the same manner as the high frequency compensation capacitor discussed previously. The net capacitance at the input formed by the input capacitor and the transformed output capacitor in parallel must be the capacitance that was earlier calculated to resonate with the net input shunt inductance.

Balanced transformers

Many instances require the use of balanced transformers. The 4:1 unbalanced transformer studied so far can evolve into a balanced transformer by adding a second transmission line to mirror the first. This configuration is shown in Figure 6. Note that both transmission lines may be passed through the same ferrite core, since the voltage appearing across each transmission line section (end to end, not terminal voltage) is the same.

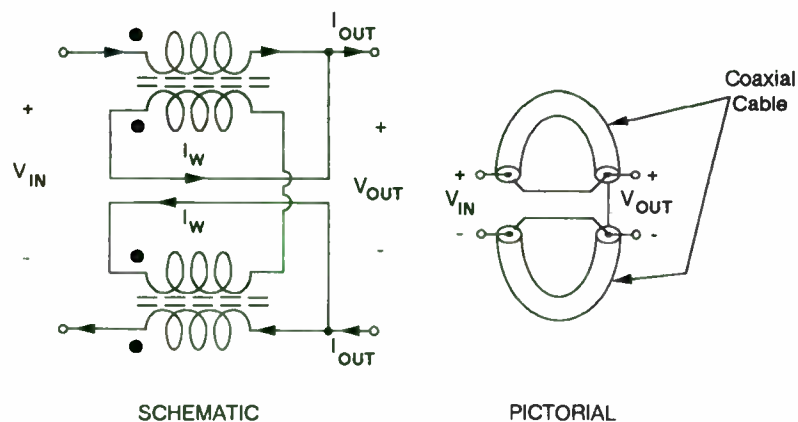


Figure 6: 4:1 Balanced transformer

Other ratio transformers may be similarly enhanced. The 9:1 and 16:1 transformers shown in Figure 4 can undergo a similar transformation and become balanced. The ground connections for the "upper" and "lower" sections are simply tied together, and the two single ended inputs are driven push-pull, with similar treatment given to the outputs.

Transforming from balanced to unbalanced,

Many times a balanced amplifier must drive an unbalanced load or vice versa. In this discussion, a balanced load is one with neither terminal grounded. The voltages at each end of the load are usually equal with respect to ground, and in opposite phase. If these voltages are not equal, the load is said not to be balanced, but floating.

The most often used method for matching between balanced and unbalanced sources and loads uses the 1:1 balanced-to-unbalanced (balun) transformer. This configuration was shown in Figure 2. It relies on establishing equal currents in opposite directions in the two conductors of the transmission line, but time delay effects caused by excess length do not exist. Line length is critical only insofar as the inductance from the input terminals to the output terminals again be larger than approximately $5R_L$. Loading ferrite beads onto the outside of a coaxial transmission line will achieve this over fairly broad bandwidths (several decades).

If this line section is made $\lambda/4$ long, the output end can float above ground. That is, the two output voltages need not be symmetric with respect to ground. If symmetry is desired, it is necessary to present the same impedance to ground to each output terminal. If a balanced amplifier or transformer is connected at these terminals, then the symmetry is established. Note also that if broad bandwidth is not required, the balun can be built with a $\lambda/4$ length line with no need for ferrite loading.

Techniques for higher frequencies

If an effective balun in a small space is desired, the 1:1 configuration can be combined with a microstrip technique to force equal impedances to be seen at each output terminal. The microstrip lines cause inductance to ground to appear at the output terminals for frequencies at which they are less than $\lambda/4$ long. A single capacitor between the output terminals can resonate with the net inductance and eliminate the mismatch loss the inductance would otherwise cause. This approach tends to narrow the bandwidth of the balun, but is useful where space is a consideration. This configuration is shown in Figure 7.

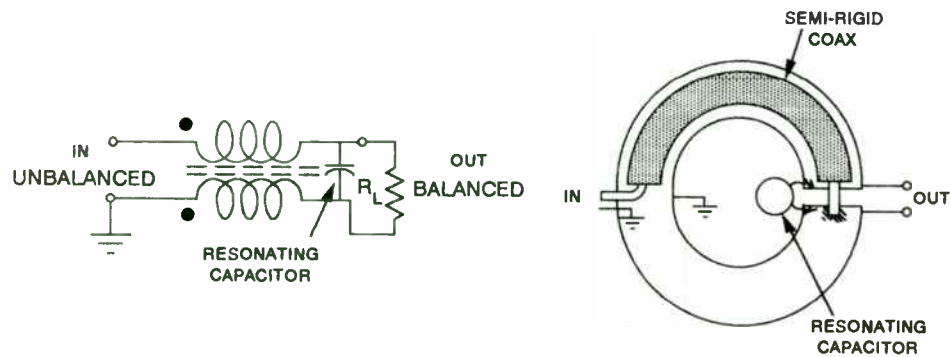


Figure 7: 1:1 balun on microstrip

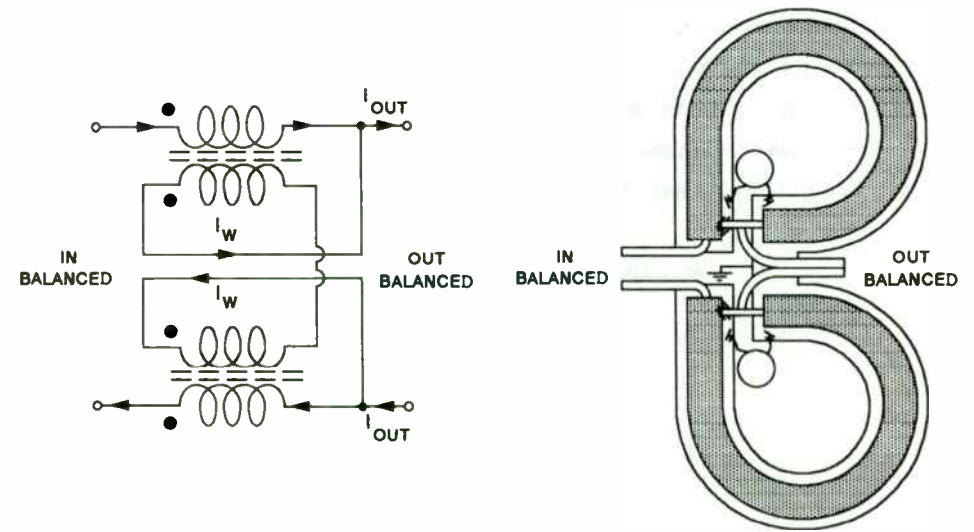


Figure 8: 4:1 transformer using the UHF microstrip technique

Other transformer configurations

With the impedance matching and balun sections thus far described, any $n^2:1$ combination may now be developed. Simply cascading an impedance matching section and a balun, if necessary, will provide the required transformation. It is also possible to cascade several impedance matching sections. For example, high power amplifiers are often built with two 4:1 transformers in cascade. One might transform 50Ω down to 12.5Ω using 25Ω coaxial cable, while a second stage transforms 12.5Ω down to 3.125Ω , using two 12.5Ω cables in parallel to create a 6.25Ω combination. Examples of this can be found in several commercial amplifiers.

Similar microstrip techniques may also be used to advantage with impedance matching transformers. Figure 8 shows a 4:1 transformer built on microstrip, with resonating capacitors. Knowing the inductance of the microstrip transmission lines, the desired resistance from output to ground, and the resonating capacitor size will give the Q of the resonant circuit, which will be the approximate Q of the overall structure.

Power combiners and push-pull balancing chokes

No discussion of coaxial broadband transformers is complete without some mention of power combiners. A 2:1 power combiner is shown in Figure 9. Analysis similar to that used on transformers will show that if the voltages presented to the two input terminals on the left are equal in magnitude and opposite in phase, then no voltage will appear at the difference terminals, and thus, no power will be dissipated in R_{diff} . The sum of the two voltages will appear across the load resistor R_L . This is useful for push-pull class A applications. Note that the load resistance R_L must be twice the output impedance of each of the driving stages.

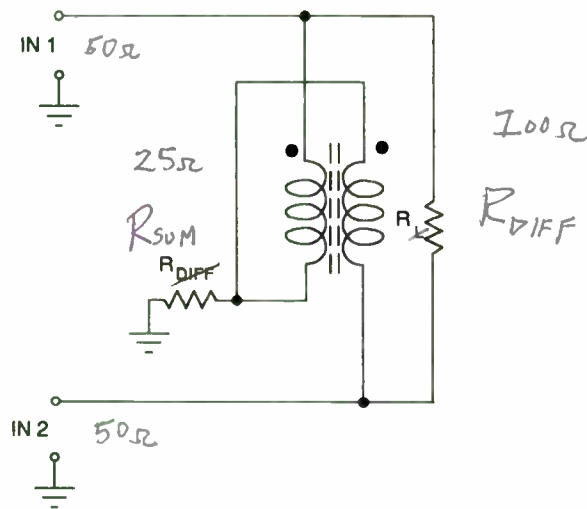


Figure 9: A 2:1 power combiner

If the difference resistor of the power combiner of Figure 9 is replaced with a connection to ground, the result is a push-pull balancing choke useful for class B or D power amplifiers. This is shown in Figure 10. In class B and D power amplifiers, two devices are driven out of phase and then combined to produce power in a load. If no balancing device is used, there is no path for return current from a load or transformer to flow.

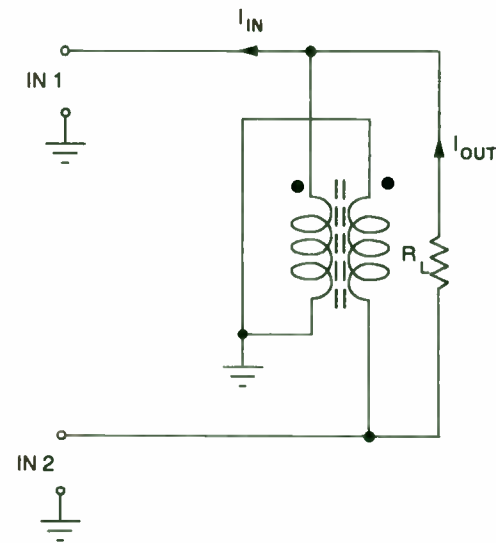


Figure 10: The push-pull balancing choke

To analyze Figure 10, assume an output current, I_{out} , flows upward through the load resistor R_L . Assume also that the device connected to the lower of the two input terminals (labelled IN 2) is in cutoff, implying that current flow into or out of that lead is zero. The source path for current to the load must then be upward through the right-hand winding of the balancing choke. Since this current must

be flowing downward, an equal current must be flowing upward in the left-hand winding. This current sums at the upper node with I_{out} flowing from the load, and therefore $I_{in} = 2I_{out}$. Observation of the voltages created by these currents will show that $V_{in} = \frac{1}{2}V_{out}$ and the resistance seen by the one device which is conducting will be $\frac{R_L}{4}$. Thus, this device provides a 4:1 impedance stepdown to each of the driving devices. Evaluation of terminal voltages and currents reveals that the proper characteristic impedance for the transmission line of which the windings are made is $\frac{1}{2}R_L$.

When the push pull balancing choke is combined with any of the balanced impedance matching transformers described so far, the net impedance transformation to each device is the product of the individual ratios.

Testing transmission line transformers

Testing an individual transformer can be very difficult. The added series inductance of soldered leads interferes with reasonable impedance measurements at any frequencies above mid VHF. The problem gets more severe with wider ratio transformers. A 12.5Ω load was connected to the output of a 4:1 balanced transformer, and the input of the transformer was measured on a Hewlett-Packard HP8753B network analyzer. The impedance as plotted on a Smith chart is shown in Figure 11. The transmission line used was a 12 inch length of 25Ω coax made from lengths of RG-174 in parallel, and was wound through a ferrite core four times. The impedance versus frequency agrees closely with that predicted by the equation given earlier. SWR versus frequency is also shown in Figure 11.

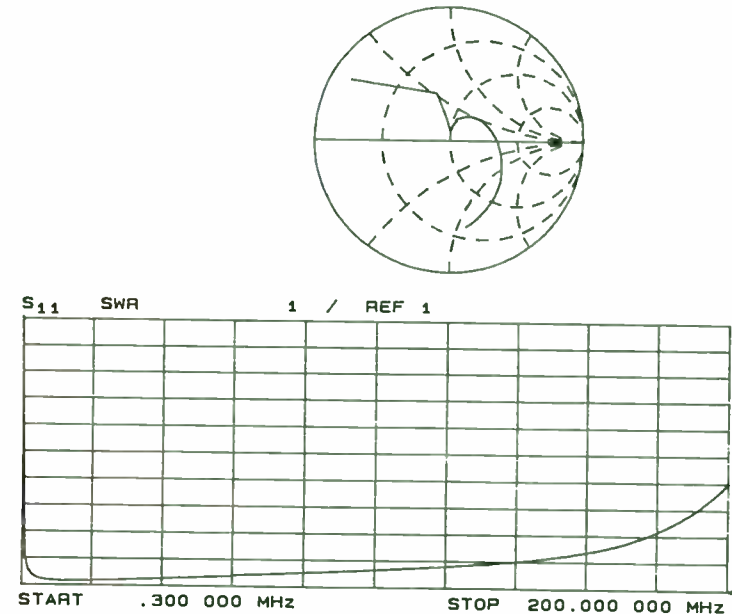


Figure 11: Input impedance and SWR of 4:1 transformer

Notably worse results occurred when an attempt was made to measure a 1:9 transformer in the same manner. In this case, a better approach would be to construct two prototype transformers and connect them back-to-back. The impedance mismatches would cause the net loss through the pair to be twice that of a single transformer. This is also the only technique that will work if the available roster of test equipment does not include an impedance meter or network analyzer. This technique was used in generating Figure 12, which shows the loss of back-to-back unbalanced 4:1 transformers, with the correct 25Ω line, and a more commonly available 50Ω line.

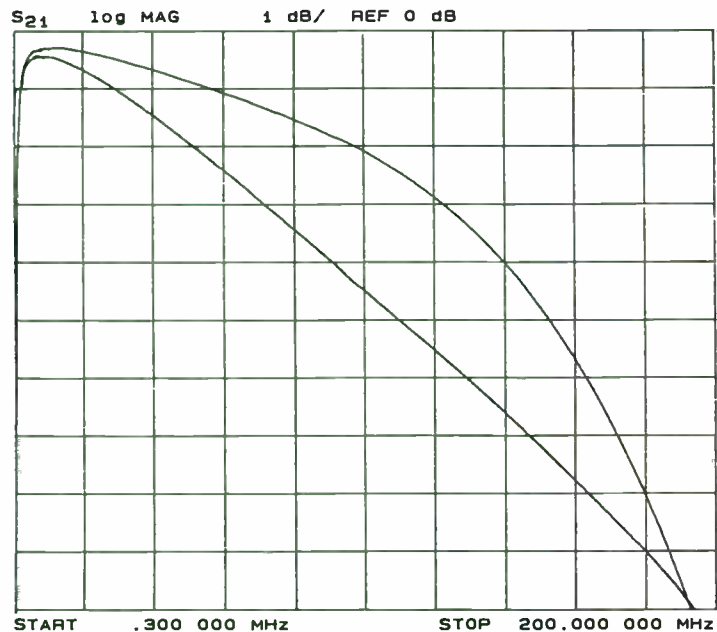


Figure 12: Loss versus frequency - two 4:1 transformers back-to-back

Summary

It has been the intent of this paper to describe broadband impedance matching transformers and related devices in enough detail to allow an experienced designer to use them effectively. Sufficient data has been presented to allow analysis of arbitrary configurations, and to predict performance of prototype transformers. While configurations other than those described do exist, including simple transformers that perform the balun function in combination with impedance matching functions, the configurations discussed are sufficient for almost any broadband design requiring high power transformers.

A case has also been made for transformers as a cost-effective alternative to traditional lumped element matching networks, and in fact the only solution for some impedance matching problems.

References:

- 1) Krauss, Bostian and Raab, **Solid State Radio Engineering**, John Wiley & Sons, ©1980
- 2) C. L. Ruthroff, **Some Broadband Transformers**, proceedings of the IRE, August 1959

*June 1990
Twisted Pair
Transmission Lines*

Temperature-Compensating Attenuators

by

Perry F. Hamlyn

M/A-COM Solid State Components - ANZAC Operations

80 Cambridge Street

Burlington, MA 01803

Abstract

Passive Temperature-Compensating Attenuators are designed using simple mathematical models. These networks can be used to compensate signal amplitude variations over a wide temperature range. Various symmetrical attenuator topologies are discussed and actual circuit performance presented.

1. Introduction

System performance over temperature can be a concern in RF design. This is especially true of systems which function over the full military temperature range of -55°C to $+85^{\circ}\text{C}$ or $+125^{\circ}\text{C}$ since signal amplitude performance of many components fluctuates over temperature. Most active circuits, such as amplifiers, exhibit higher gain at low temperatures with gain rolloff at high temperatures. To compensate for these fluctuations several options are available. One method is to use active circuits which adjust the gain or loss of the signal path over temperature. This requires the use of bias currents and could cause linearity problems in the circuit when nonlinear devices are used. An alternative is to use a completely passive circuit structure whose attenuation characteristics vary over temperature. This approach simplifies design since it requires no bias and contributes no distortion to the signal.

Attenuator design considerations include frequency bandwidth, linear temperature response, impedance mismatch, power handling capability, and packaging. This paper describes the design of a DC - 2000 MHz temperature compensating attenuator.

2. Attenuator Theory

There are four basic types of symmetrical attenuator topologies; (a) Tee Configuration (Figure 1), (b) Pi Configuration (Figure 2), (c) Bridged Tee Configuration (Figure 3), and (d) the Balanced Configuration (Figure 4).¹ Of these, the Balanced Configuration is not as easily realized on microstrip and was thus excluded from consideration for the purposes of this paper.

The analysis was conducted assuming a source impedance of Z_0 . The load impedance was left as Z_L to allow for loads other than Z_0 .

Tee Configuration Theory - Figure 1

The input impedance, Z_{in} , and current transfer ratio, (I_L/I_{in}) , can be calculated as:

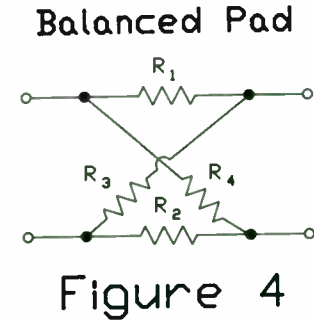
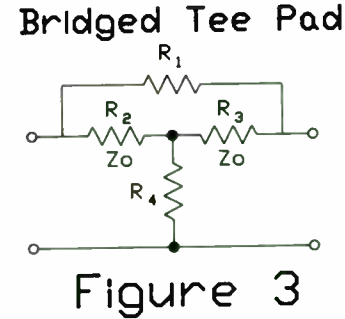
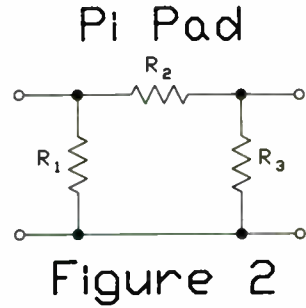
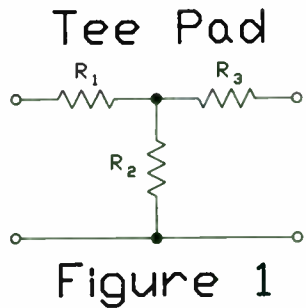
$$Z_{in} = R_1 + \frac{R_2 (R_3 + Z_L)}{R_2 + R_3 + Z_L} \quad \text{and} \quad I_L/I_{in} = \frac{(R_2)}{(R_2 + R_3 + Z_L)}$$

Attenuation including mismatch loss can be expressed as:

$$\text{Attenuation(dB)}_{\text{Tee}} = 10 \log_{10} \left[\frac{4 * Z_0 * Z_L}{(Z_0 + Z_{in})^2} * \frac{(I_L)^2}{(I_{in})^2} \right]$$

Where Z_0 is the source impedance and Z_L is the load impedance.

¹ Jordan, Edward C., Reference Data for Engineers: Radio, Electronics, Computer, and Communications, pp 11-3,11-4, Howard W. Sams, & Co., Inc., 1985.



Note that since loss is expressed as a function of the current transfer ratio (I_L/I_{in}), the loss equation will be identical for all topologies. The difference is in the calculation of Z_{in} and (I_L/I_{in}).

Pi Configuration Theory - Figure 2

The input impedance, Z_{in} , and current transfer ratio, (I_L/I_{in}), can be calculated as follows:

$$Z_{in} = \frac{R_1 \left[R_2 + \frac{(R_3)(Z_0)}{(R_3+Z_0)} \right]}{\left[R_1 + R_2 + \frac{(R_3)(Z_0)}{(R_3+Z_L)} \right]} \quad \text{and} \quad \frac{I_L}{I_{in}} = \frac{(R_1)(R_3)}{Z_L(R_1 + R_2 + R_3) + R_3(R_1 + R_2)}$$

Similarly, attenuation including mismatch loss can also be expressed as:

$$\text{Attenuation(dB)}_{pi} = 10 \log_{10} \left[\frac{4 * Z_0 * Z_L}{(Z_0 + Z_{in})^2} * \frac{(I_L)^2}{(I_{in})^2} \right]$$

Where Z_0 is the source impedance and Z_L is the load impedance.

Bridged Tee Configuration Theory - Figure 3

The input impedance, Z_{in} , is calculated from:

$$Z_{in} = \frac{R_1 [R_2(R_3+R_4+Z_L) + R_3R_4] + Z_L [R_2R_3+R_4(R_1+R_2+R_3)]}{[(R_1+R_2+R_3)(R_3+R_4+Z_L) - R_3^2]}$$

The current transfer ratio, (I_L/I_{in}), is calculated to be:

$$\frac{I_L}{I_{in}} = \frac{R_2R_3 + R_4(R_1+R_2+R_3)}{[(R_1+R_2)(R_3+R_4+Z_L) + R_3(R_4+Z_L)]}$$

And finally, the attenuation including mismatch loss, can be expressed as:

$$\text{Attenuation(dB)}_{B-Tee} = 10 \log_{10} \left[\frac{4 * Z_0 * Z_L}{(Z_0 + Z_{in})^2} * \frac{(I_L)^2}{(I_{in})^2} \right]$$

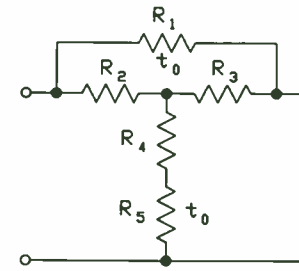
Where Z_0 is the source impedance and Z_L is the load impedance.

Design Approach

In order to vary the attenuator value over temperature, combinations of both positive and negative temperature coefficient chip thermistors were used. The design goal was to create a linear temperature response attenuator with 3dB of attenuation at room temperature (+25°C), less than 2dB of attenuation at +85°C, and greater than 4dB of attenuation at -55°C. Other constraints were; maximum impedance mismatch from 5 to 2000 MHz of 1.5:1, power handling capability of +20dBm, and TO-5 packaging.

The major limiting factor in the design was the availability of a "small" dimension, low value, negative temperature coefficient (NTC) thermistor. The chip size for values much lower than 100Ω made them impractical for use.

An analysis of the three topologies; Tee, Pi, and Bridged Tee yields the conclusion that the Bridged Tee configuration is the most temperature responsive given the high values of the NTC component. However one modification was made to the classical Bridged Tee configuration (Figure 3). Typically $R_1 = R_2 = Z_0$. For the purposes of this design, the value of R_1 and R_2 was allowed to change to set the attenuation and match based on the value of R_3 and R_4 . The final configuration is shown given in Figure 5. The circuit was modified by adding a thermistor R_5 in series with the fixed resistor R_4 . In order to obtain a negative temperature attenuation response in this circuit, R_3 and R_5 are negative and positive temperature coefficient thermistors respectively. The reverse combination could be used if a positive temperature attenuation characteristic was desired.



Modified
Bridged Tee Pad

Figure 5

Fixed resistor networks were realized in thin film on .025" thick alumina substrates. Positive and negative temperature coefficient thermistors were purchased in chip form from commercially available sources.

Experimental Results

The Temperature-Compensating Attenuator (TCP-1) was designed with values: $R_1=R_2=14\Omega$, $R_3=100\Omega$ NTC, $R_4=0$, and $R_5=220\Omega$ PTC. The 100Ω thermistor had a temperature coefficient of resistivity of -3.4%/°C at +25°C and a tolerance of 5%. The 220Ω thermistor's temperature coefficient of resistivity was +0.7%/°C at +25°C with a tolerance of 5%. Note that the elimination of R_4 , the fixed value resistor, maximizes attenuation change versus temperature. This design was built and tested in a TO-5 header. The calculated upper limits, lower limits, and measured data (■) can be found in Figure 6. The upper and lower limits were calculated using worst case analysis of the possible range of values for fixed value

resistors and thermistors assuming the maximum tolerances. The "measured" data represented in Figure 6 is actually the arithmetic average of the attenuation versus frequency from 10 MHz to 2000 Mhz. A typical frequency response curve is illustrated in Figure 7. Note that the average attenuation response versus frequency was usually less than +/- 0.1 dB from 10 Mhz to 2000 Mhz. The VSWR was less than 1.5:1 over frequency and temperature.

Additional Observations

Once the models were developed for the various configurations, it was rather simple to try various combinations of the thermistors and fixed resistors for the different topologies. By adjusting the values, different temperature characteristic curves can be developed which vary slope, linearity, and attenuation levels. Using thermistors with higher temperature coefficients of resistivity will increase the slope of the attenuation versus temperature curve, but this also tends to decrease the linearity of the change versus temperature. This leads to curves which are parabolic rather than linear, and tends to have a greater adverse impact on impedance matching.

Conclusions

Simple passive Temperature Compensating Attenuators can be designed to compensate signal levels over a wide temperature range. Simple models predict actual performance with a fair degree of accuracy and circuits can be realized using fixed resistors and thermistors.

Attenuation versus Temperature TCP-1

Measured & Theoretical Limits

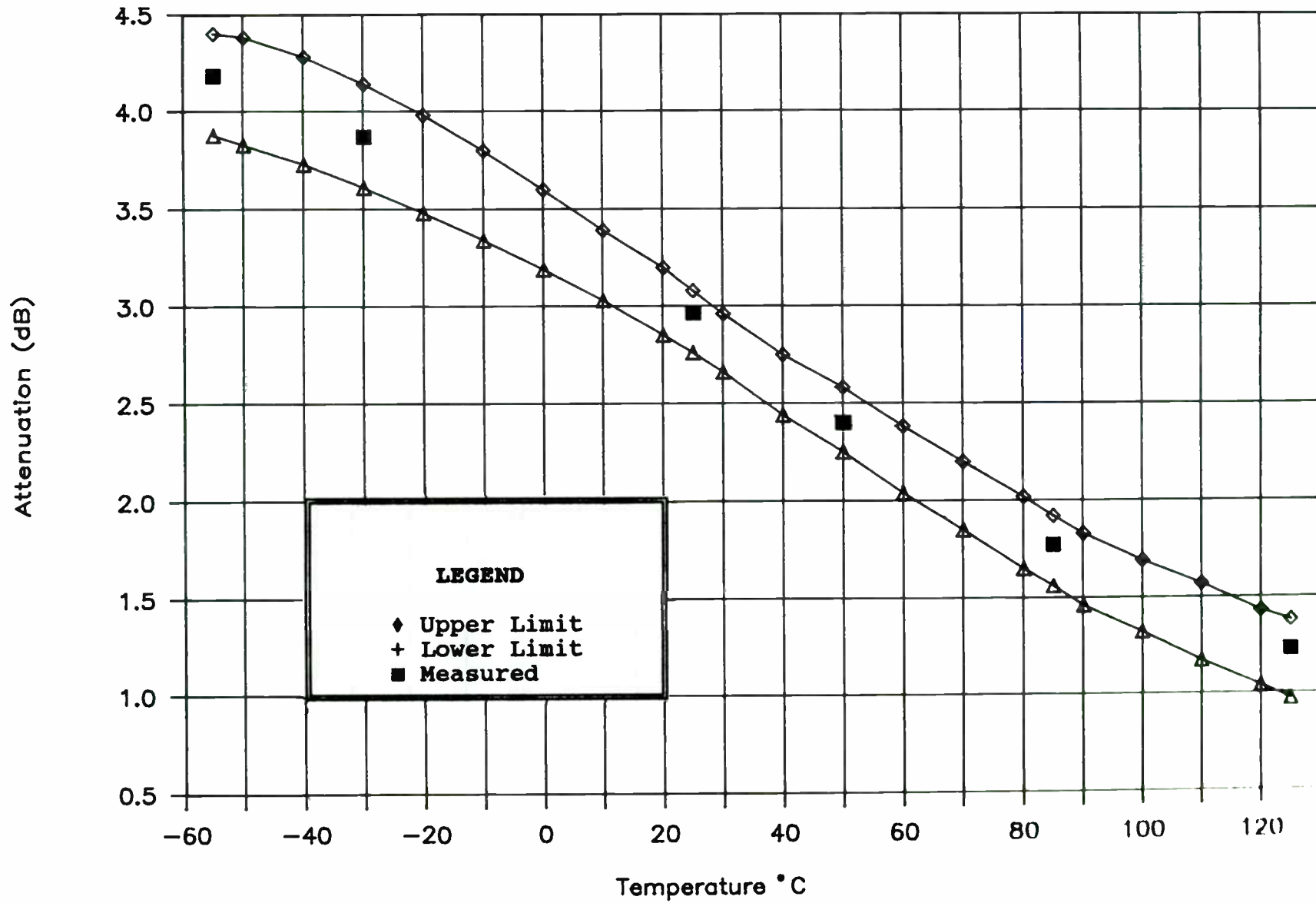


FIGURE 6

Attenuation vs Frequency

TCP-1 (Measured .01-2.0 GHz)

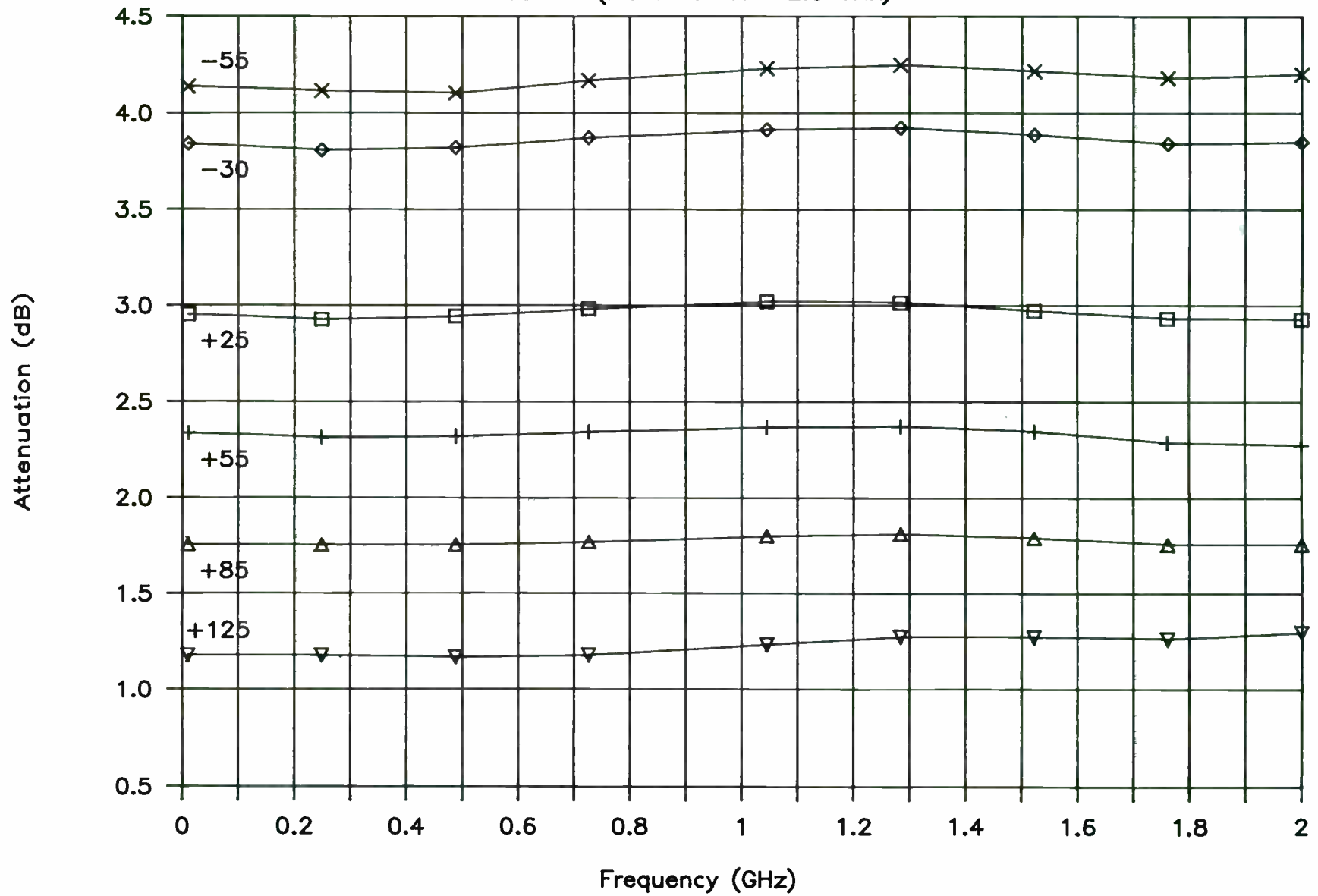


FIGURE 7

476

USEFUL NETWORK TRANSFORMATIONS IN FILTER DESIGN

WILLIAM B. LURIE, Consultant
8503 Heather Place
Boynton Beach, FL 33437

In designing R, L, C filters, it is frequently found that some of the element values become impractical. Capacitors can become exceedingly large or exceedingly small, very expensive, or difficult to realize in practice. Inductances can be so large that they can not be built with practical devices, or so small that they are approximated by their connecting or lead wires. This paper presents a number of practical methods for overcoming such difficulties.

Some of the transformations described here are exact transformations or equivalences, that is, they yield component values which are not frequency-dependent. A computer analysis of the network's performance will give the same frequency response before and after the transformation is made. The frequency dependence is not found in the equations describing the transformation. Examples of this would be the familiar Norton transformations, the substitution of one canonic form of a two-terminal network for another, and the use of a transformer to change impedance levels.

There are also transformations which are approximations, in that they may be exact at one or more frequencies, and perhaps acceptably close at all other frequencies. In these cases, the equations describing the transformed components will contain a frequency dependence which is noted by the existence of the frequency variable, ω . These are sometimes described as 'narrow-band equivalences'.

Among the 'exact equivalents', there are several classes of network configurations. If there are more than two reactive elements in a two-terminal network, then it may be realized in more than one form. If only two elements exist, an L and a C, obviously the only possible forms are series or parallel connections. With three or more elements, however, there exist more choices, and in one form or another the element values may be more practical, or the configuration may accommodate special elements (such as a quartz crystal) more conveniently.

Transformations are given for only a few of these exact equivalences; in all cases, it takes only simple mathematics to derive transformations for all element values, and simple computer programs to calculate them.

In the case of three reactive elements, there are only two cases: two L's and a C, or two C's and an L. The equivalences are in Figure 1.

Another useful set of equivalences relates the various four-element two-terminal networks to each other, but now there are more possible variations, as shown in Figure 2.

Some of these are more useful than others; for example, the networks of 2A and 2C allow L to be one winding of a transformer or autotransformer, which permits the other three elements to be stepped up or down. Only the network of 2B permits a crystal to be introduced as three of the elements the network, and only the first has a capacitor across each inductor, to inductor to 'swamp out' the inductors' parasitic (distributed) capacitance. Formulas for these have been tabulated and published, or can be derived [1,2].

It is comparatively more rare that a filter design comes about with one two-terminal branch containing, in its simplest or canonic form, more than four reactive elements. It does happen, however, and these have special and interesting characteristics and applications. Consider, for example, a branch with six elements. Here there are many possibilities, all exactly equivalent, only a few of which are shown in Figure 3.

The network of Figure 3A has some interest, in that it is a string of inductors in series, each with a capacitor in parallel. Figure 3B has considerable interest, in that it represents a number of crystals in parallel, with a parallel-resonant circuit shunting the entire array. Some types of pulse-forming networks might have some of the other combinations. The mathematical tools exist for determining the element values for all possible combinations, but are beyond the scope of this presentation.

Dual sets exist for the four- and six-element networks shown in Figures 2 and 3, and some of these are shown in Figures 4 and 5. Again, formulas for calculating all the element values, given one of the sets, can readily be derived. It should be mentioned that, in the process of synthesizing a network, perhaps from a given transfer function, the poles and zeros of the two-terminal branch impedance are derived. One or more of the sets of element values can be obtained from these by the simple method known as partial-fraction expansion.

There is another class of 'exact' equivalences, presenting some very elegant work from a mathematical point of view. These have usefulness perhaps only in very special cases, but they show how ingenious a network designer can be when the need exists. In this regard, references given [3-6] will lead to more detailed explanation, but an example is now given to show the need and the solution.

Suppose the requirement exists for a low-pass filter with very sharp cutoff, say a ratio of 1.006 for 40 dB to 3 dB, with no returns poorer than 40 dB. It is simple and straightforward to design this as an Elliptic filter, eleventh degree, but analysis with practical inductor Q's reveals two major deficiencies: the transition from passband to stopband occurs too gradually, and the close-in stopband peak does not appear, as a result of inadequate Q. Using a higher degree would, in theory, yield a narrower transition from passband to stopband, but in practice that's not the case. Instead, because the higher degree demands still higher Q near the cutoff, the corner rounding actually gets worse, the stopband peak is still gone, and nothing is gained. Another method which can be used is to add an amplitude equalizer, essentially to reduce all responses except right near the rounded corner, making the passband appear wider and flatter but somewhat attenuated. This can be quite effective, but it does nothing to bring back the vanished attenuation peak.

An exact transformation can be applied to a portion of the lowpass filter, and this time it substitutes one TWO-PORT network as an exact equivalent of another. Refer to Figures 6A and 6B.

These are obviously identical topologies, except for the addition of one series-resonant circuit, which has actually been designed in, not just 'patched' or 'fudged' in on a trial-and-error basis. The element values are given with the Figures, and as an exercise both circuits may be analyzed using Q's of 250 for all inductors, and 10,000 for the one crystal. The results should be as shown in Figures 7 and 8, where the deficiencies referred to previously have been largely overcome.

perhaps even better! At times it is even possible to design a network with more components than will fit into size or cost limitations, and then use this sort of transformation to make it practical.

There is a dual transformation, operating on a single series branch with one end grounded, as shown in Figure 14. Everything stated up to now for the Norton transformation with a branch in series, applies as well to this counterpart, and therefore no additional details will be presented. I myself, over the years, have found far fewer occasions where this one-end grounded version is useful.

Transformers can be valuable tools in converting what might be an impractical network into one which is quite practical, or perhaps more economical in size, number of components, or cost. Consider Figure 15 which illustrates one form of describing a two-winding transformer as a Tee of uncoupled inductors.

This equivalence can be shown in a number of different ways.

Usually a network will be designed, after which it is noticed that a Tee of inductors is present, which it might be desirable to build in the form of a transformer, for reasons of size or economy. In Figure 16 a Tee L_1, L_2, L_3 has been shown, with the transformer equivalent; there are three equations and three unknowns, so it is a simple matter to solve for L_p, K , and N .

$$\begin{array}{ll} L_1 + L_3 = L_p & \text{This gives } L_p. \\ L_2 + L_3 = N^2 L_p & \text{Then this gives } N \\ -L_3 & \\ K = \frac{L_3}{L_p} & \text{And this gives } K. \\ N L_p & \end{array}$$

There is no assurance, of course, that K will be a value which is realizable in a practical wound inductor. If it happens to be, that is a great convenience, because L_1, L_2 , and L_3 are all replaced by one single core containing two windings. Suppose, however, that K is an awkward value; L_3 can then be split into two parts, L_{3A} and L_{3B} , such that $L_3 = L_{3A} + L_{3B}$. Then, (See Figure 17),

$$\begin{array}{ll} \text{Now } L_1 + L_{3A} = L_p & \\ L_2 + L_{3A} = N^2 L_p & \\ -L_{3A} & \\ K = \frac{L_{3A}}{L_p} & \end{array}$$

, and as long as L_{3A} is chosen less than L_3 , L_{3B} will be positive, and L_{3A} can be chosen to make K a realizable coupling coefficient. Actually, if an acceptable value of K is known for a particular core and winding method, it can be used to pre-select a value for L_{3A} .

There is an interesting observation, in case L_p, L_s , or K can not be found to be convenient values. Note that there is no requirement that B be the grounded, or non-input/output terminal of the Tee. Suppose we simply relabel it and use the same equivalences. (Fig. 18)

$$\begin{array}{ll} L_1 = L_p (1 + KN) & \\ L_2 = -KN L_p & \\ L_3 = L_p (N^2 + KN) & \end{array}$$

There are quite a number of such transformations available for low-pass and bandpass cases as well, and by careful use of lowpass to highpass conversions etc., other classes can be realized. The references given [3-6] include some extremely complicated equivalences.

Perhaps the most frequently used of the 'exact' transformations is the Norton transformation, which in one of its most general forms, is shown in Figure 9.

In the left-hand schematic, the impedance level of the network is R , at both sides of the impedance Z , while in the right-hand schematic, an impedance transformation has caused the impedance to become $N^2 R$. There is no other restriction on the value of N , except that it must be real, positive, greater than zero and less than infinity. It can easily be seen that, in the trivial case that $N=1$, the original network is returned.

Perhaps the most common application for this transformation involves the use of a capacitor for the series element, in which case the element values are as shown in Figure 10.

Again, this obviously returns the original network in the trivial case where $N=1$. A specific numerical case will illustrate the practical use of this transformation for capacitors. Suppose there exists a simple bandpass filter derived from a Butterworth lowpass prototype, 1000Hz wide at a center frequency of 10000Hz, at an impedance level of 10000 ohms, as shown in Figure 11.

The shunt elements to ground are reasonable, acceptable values, but the inductor in the series branch is awkwardly large. Suppose it is desired to perform Norton transformations to make all three inductors identical. The steps consist of splitting the series capacitor into two equal capacitors, placing the series inductor between them, stepping the impedance DOWN using the left-hand capacitor, then stepping the impedance BACK UP using the right-hand series capacitor, and then combining capacitors which appear in parallel to ground at various nodes. This entire process is as shown in Figure 12.

Of course, recognition of the the symmetry of the network, after splitting the series capacitor and placing the series inductor between them would have allowed us to draw the completely transformed network without actually performing the second Norton transformation. One of my graduate school professors would have called this 'The Principle of Minimum Astonishment'.

The impedance Z can be any two-terminal impedance, and it is convenient at times to perform the transformation when it is an inductor and capacitor in parallel. Such a case is shown in Figure 13, where a particular bandpass filter has been designed by image-parameter methods, as a cascade of two four-element sections which has five inductors and five capacitors. It is frequently desirable to minimize the number of inductors, as they are larger, more lossy, more expensive, and poorer in performance than capacitors. In Figure 13, the first series circuit is transformed, then the second with the reciprocal impedance ratio, leaving the final network with the original terminating resistances. The ratio was chosen such that L_1 and L_A are equal in value but of opposite sign, causing them to cancel at the last step, at both ends of the network, leaving a total of only three inductors. Admittedly, this was a special case designed to show what can, under the right circumstances, be accomplished. The resultant network performs exactly like its prototype, or, with practical, lossy inductors,

Now

$L1+L2=Lp$ This gives Lp
 $L3+L2=N^2Lp$ This then gives N
 $-L2$
 $K = \frac{-L2}{NLp}$ from $L2$, N , and Lp

This gives a second set of values for Lp , N , and K , which might be preferable to the first set of values, both being equivalent. It is obvious that a third orientation exists (Figure 19), and this will give a third set of values to choose from; all three sets are exactly equivalent to each other, not approximations.

With all transformations listed as exact, the substitution of one for another does not change the network's performance, but may allow it to be implemented with elements whose values might be achieved in a more practical manner.

Among exact equivalents, the simple expedient of a Tee-to-Pi or Pi-to-Tee transformation can frequently be used to make element values more practical or realizable. As with the Norton transformations, these are frequency-independent. Referring to Figure 20, the various branches $Z1$ through $Z6$, and $Y1$ through $Y6$, need not all be L's or C's or R's, and each can in fact be any two-terminal impedance or admittance, of a type different from any or all of the rest. It is frequently found useful, with high-pass or band-pass filters, where a Tee of capacitors exists with the central one inconveniently large, to convert to a Pi, where the central element comes out quite small. Consider, for example, Figure 21, where in one circuit a 7 microfarad capacitor is present, while in its equivalent the largest capacitor is 0.37 microfarads. All three are smaller than in the original set.

So far, all of the equivalences given have been exact, but there are many occasions where a transformation can be made, advantageously, even though it is only approximate, perhaps exact at only one frequency.

Consider a two-terminal network consisting of a resistor and capacitor in parallel, and another network with a resistor and capacitor in series, as shown in Figure 22. Without going through the mathematics, which is really quite simple, two sets of relationships between $(r, C1)$ and (R, C) can be established. Note that all of these include the radian frequency ω . These are correct and exact at any one frequency, but they obviously change as ω does. What this means, in effect, is that if we substitute one set for the other at, for example, the center frequency of a bandpass filter, then at that frequency the transformation is exact, but it becomes an approximation, poorer and poorer as the frequency deviates more and more from that center frequency. With very narrow filters, it can be excellent over the entire passband, and over much of the stopbands on both sides. With wider filters, (5 to 10% wide) it can be quite acceptable but of course the effect must be determined by a computer analysis to evaluate its acceptability. An R-L transformation also exists (see Figure 23).

The advantage of this transformation is that it frequently takes a set of element values at an awkward impedance level and converts them to an eminently practical and acceptable set. Consider, for example, Fig. 24 and 25, both describing essentially the same filter, 500 KHz wide at a center frequency of 20 MHz. In Figure 24, it would be impractical to scale the entire filter to reduce the terminations to 50 ohms; the L's and C's would both be impractical. To put taps (or 'link' coupling) on the inductors would also be impractical. The transformation adds two relatively inexpensive components, but yields a practical solution.

There are a number of other 'transformations' which are, as described, exact at one frequency and approximate at other frequencies. For example, if a negative capacitance appears as an element in a synthesized or converted schematic, the positive inductance which is its equivalent at one frequency may be substituted. Similarly, a positive capacitance can be substituted for a negative inductance. Sometimes it is convenient to add a parallel-resonant L-C circuit from one node to ground, perhaps to provide enough capacitance at that node so that an effective Norton transformation may be used.

In summary, the use of network transformations, exact and approximate, offers the designer the ability to convert what might be an expensive and awkward network design into something useful and practical.

Much appreciation is due to Dick Abrahams of Radio Systems, Inc., for the many hours of diligent effort devoted to preparation of the figures accompanying this article.

REFERENCES

- [1] 'Handbook of Filter Synthesis', A. Zverev, John Wiley & Sons, 1967
- [2] 'Les Filtres a Cristaux Piezoelectriques', D. Indjoudjian et P. Andrieux, Gauthier-Villars, Paris, 1953
- [3] 'Cables et Transmission', J. E. Colin, Apr. 1962 (French publication)
- [4] 'Cables et Transmission', J. E. Colin, Jan. 1958
- [5] 'Cables et Transmission', J. E. Colin, Apr. 1961
- [6] 'Cables et Transmission', J. E. Colin, Apr. 1967
- [7] 'Reference Data for Radio Engineers', I T&T, 4th Edition, P. 142
- [8] E. L. Norton, U. S. Patents 1681554 and 1708950

FIGURE 1--TWO-TERMINAL NETWORK EQUIVALENTS (Three-element)
FIGURE 2--TWO-TERMINAL NETWORK EQUIVALENTS (Four-element)
FIGURE 3--TWO-TERMINAL NETWORK EQUIVALENTS (Six-element)
FIGURE 4--TWO-TERMINAL NETWORK EQUIVALENTS (Dual four-element)
FIGURE 5--TWO-TERMINAL NETWORK EQUIVALENTS (Dual six-element)
FIGURE 6--EXAMPLE OF TWO-PORT EXACT EQUIVALENT
FIGURE 7--RESPONSE CURVES FOR NETWORK OF FIGURE 6
FIGURE 8--FIGURE 7, EXPANDED SCALE
FIGURE 9--ONE FORM OF NORTON TRANSFORMATION, GENERALIZED
FIGURE 10--NORTON TRANSFORMATION FOR SERIES CAPACITOR
FIGURE 11--BANDPASS FILTER BEFORE NORTON TRANSFORMATIONS
FIGURE 12--NORTON TRANSFORMATIONS ON FIGURE 11
FIGURE 13--NORTON TRANSFORMATIONS ON ANOTHER FILTER
FIGURE 14--NORTON TRANSFORMATION, ALTERNATE FORM
FIGURE 15--TRANSFORMER TEE-EQUIVALENT
FIGURE 16--MORE TRANSFORMER EQUIVALENCES
FIGURE 17--MORE TRANSFORMER EQUIVALENCES
FIGURE 18--MORE TRANSFORMER EQUIVALENCES
FIGURE 19--MORE TRANSFORMER EQUIVALENCES
FIGURE 20--TEE-PI EQUIVALENCES
FIGURE 21--EXAMPLE OF TEE-PI CONVERSION
FIGURE 22--NARROW-BAND R-C SERIES/PARALLEL EQUIVALENCES
FIGURE 23--NARROW-BAND R-L SERIES/PARALLEL EQUIVALENCES
FIGURE 24--NARROW-BAND FILTER AT AWKWARD IMPEDANCE LEVEL
FIGURE 25--SAME NARROW-BAND FILTER TRANSFORMED

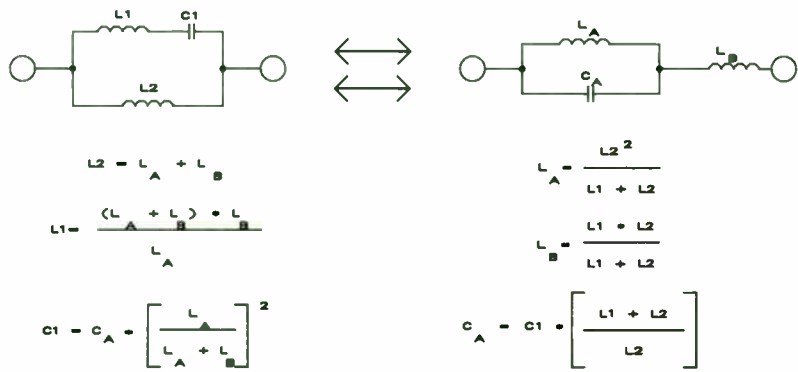


FIGURE 1A

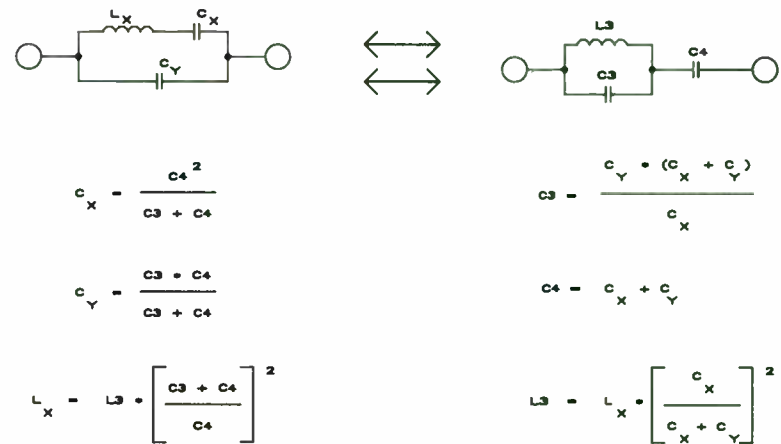


FIGURE 1B

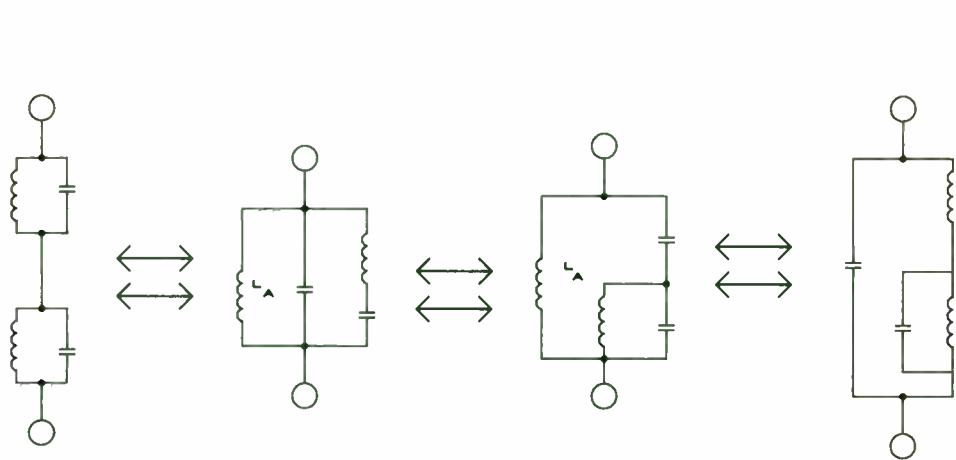


FIGURE 2

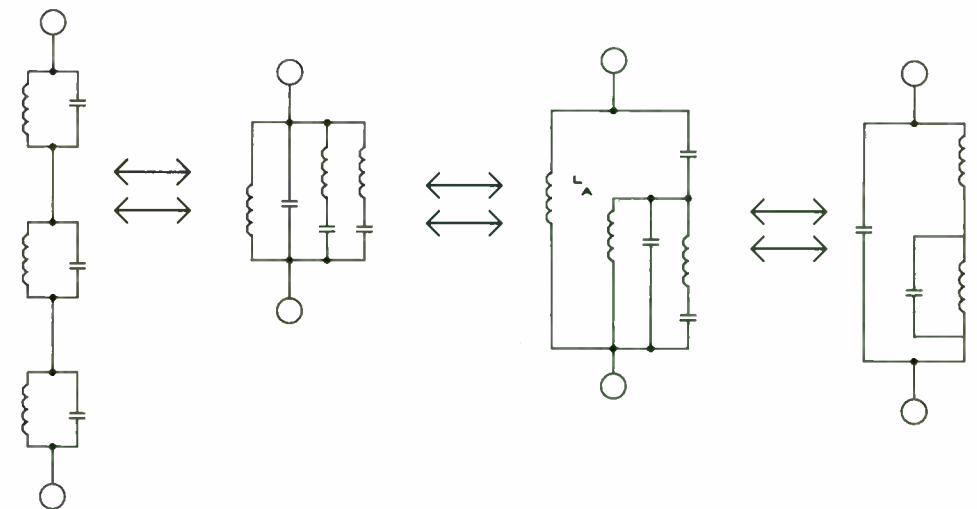


FIGURE 3

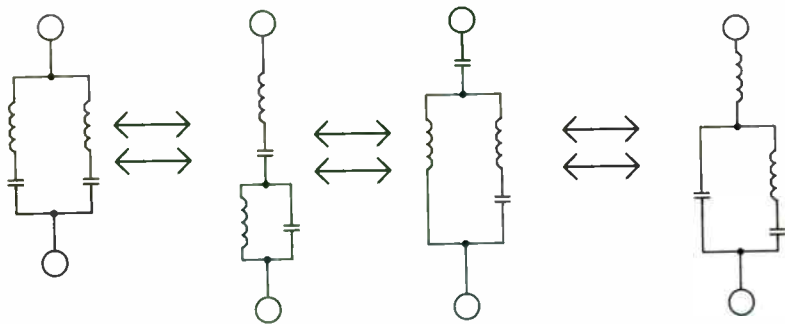


FIGURE 4

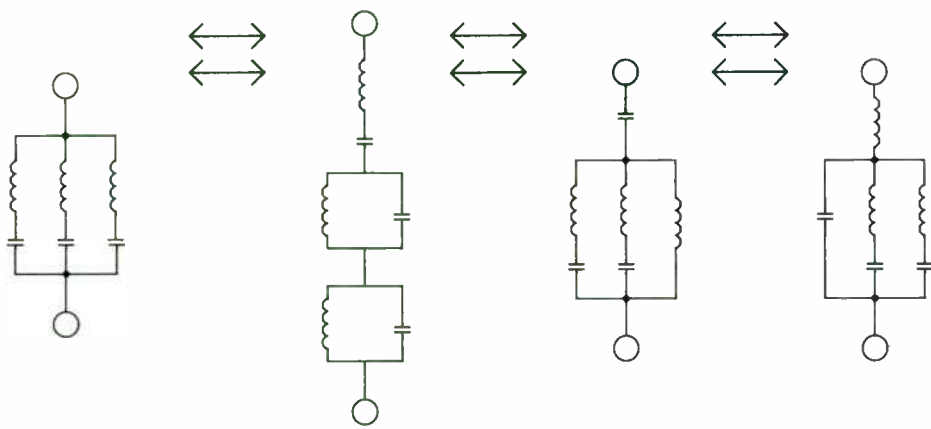
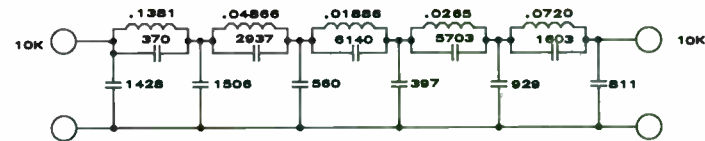


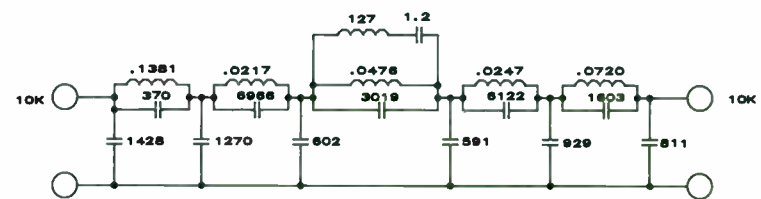
FIGURE 5



NOTE:

INDUCTORS ARE IN HENRIES
CAPACITORS ARE IN PICOFARADS

FIGURE 6A



NOTE:

INDUCTORS ARE IN HENRIES
CAPACITORS ARE IN PICOFARADS

FIGURE 6B

COLIN TRANSFORM EXAMPLE

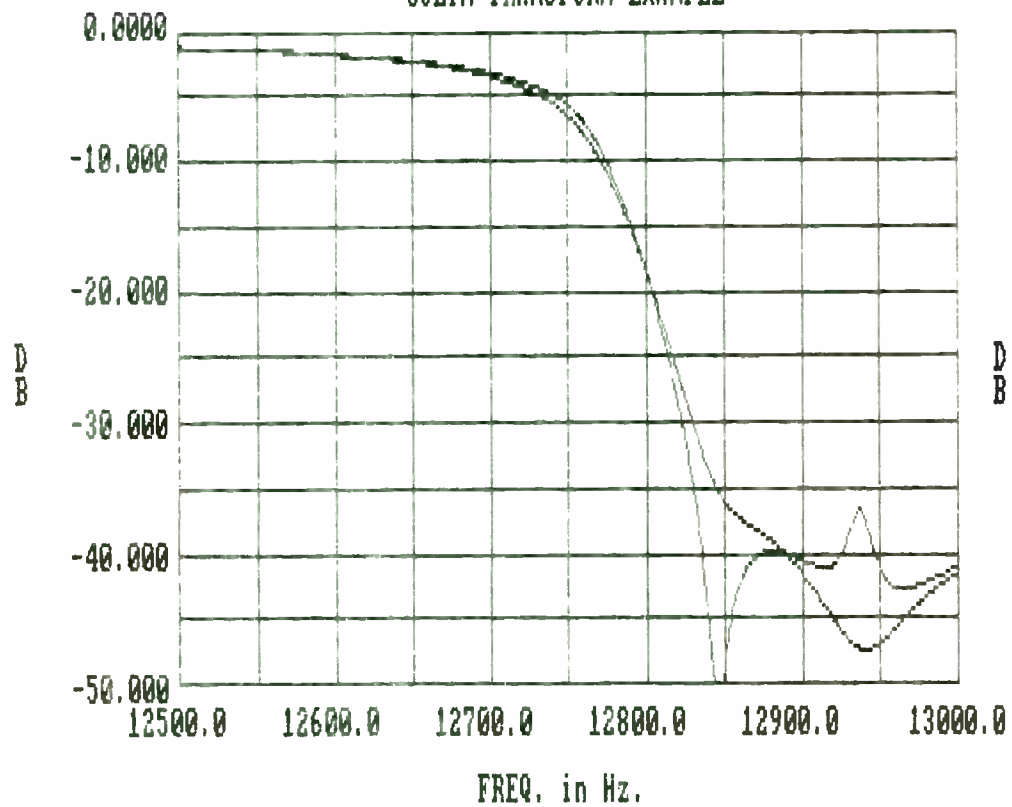


FIGURE 7

COLIN TRANSFORM EXAMPLE

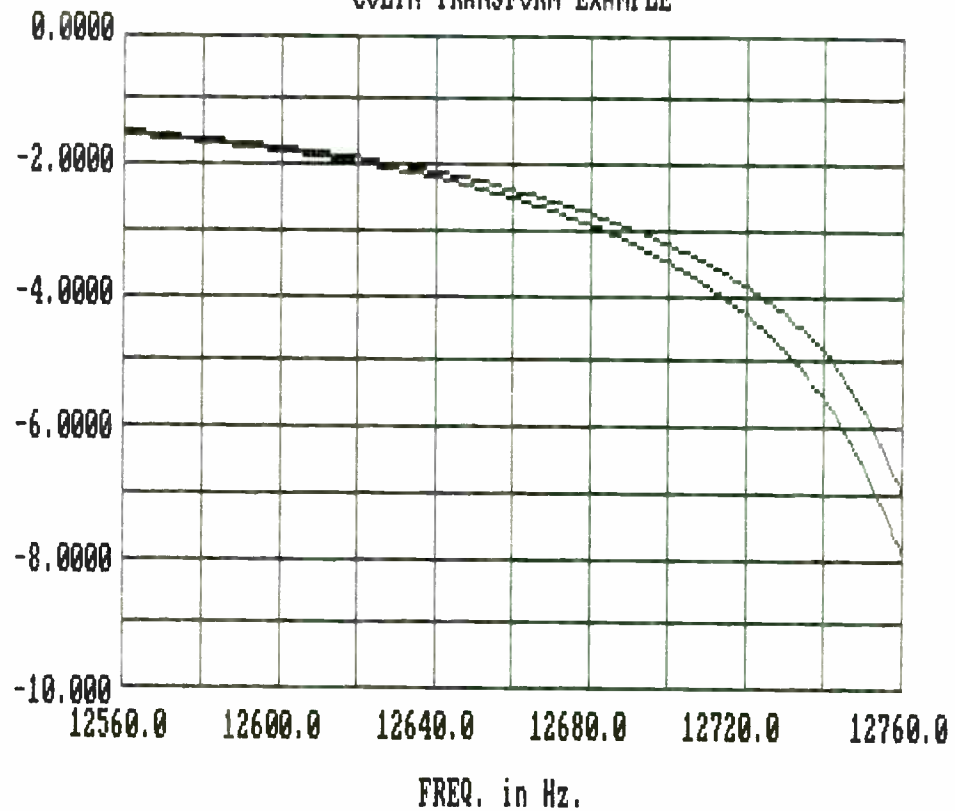


FIGURE 8



FIGURE 9

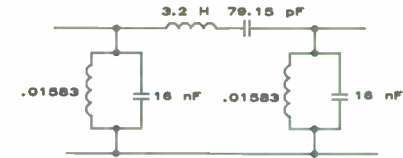


FIGURE 11



FIGURE 10

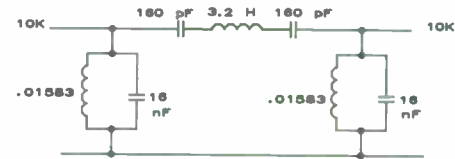


FIGURE 12A

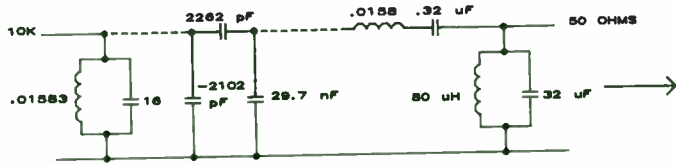


FIGURE 12B

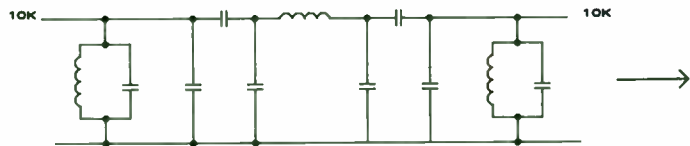


FIGURE 12C

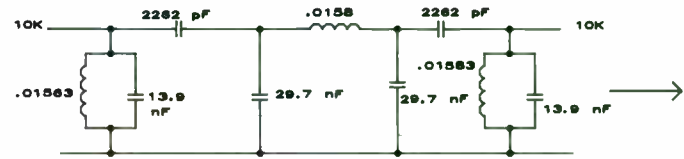


FIGURE 12D

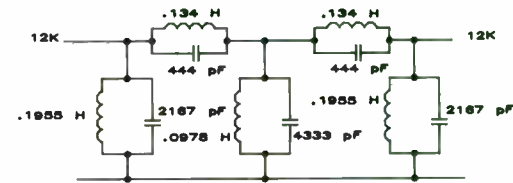


FIGURE 13A

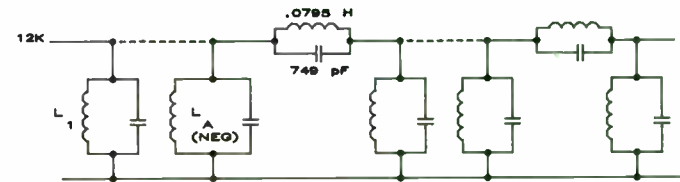


FIGURE 13B

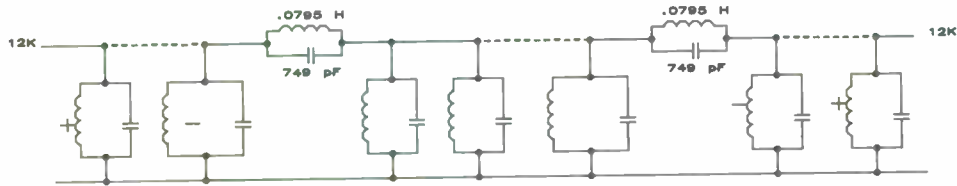


FIGURE 13C

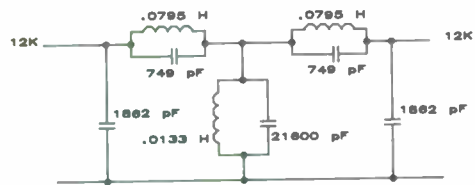


FIGURE 13D



FIGURE 14

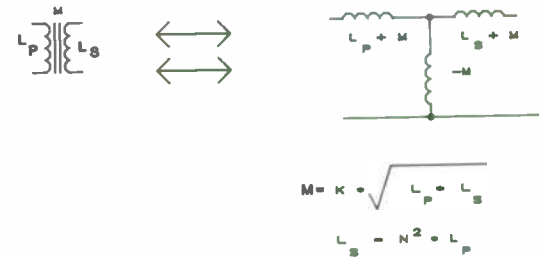


FIGURE 15

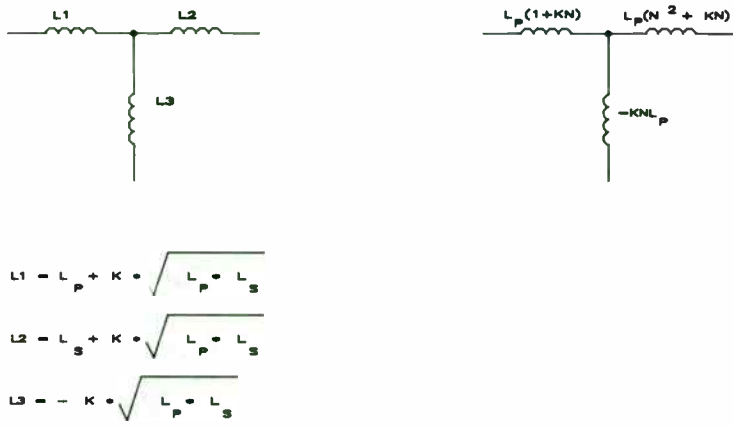


FIGURE 16

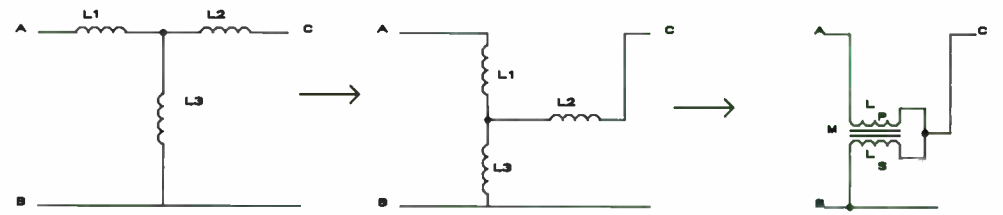


FIGURE 18

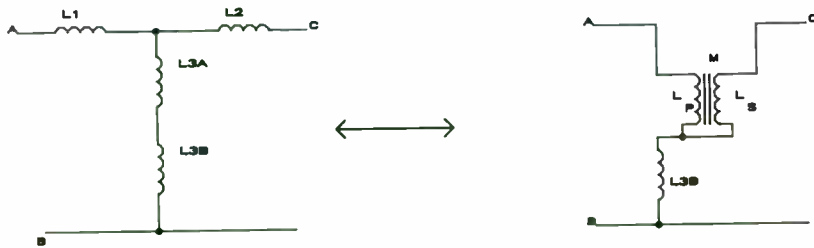


FIGURE 17

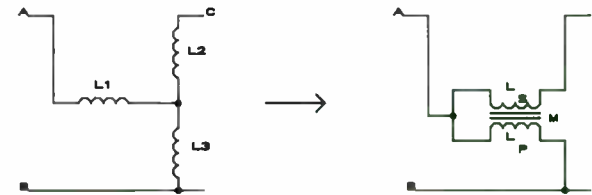
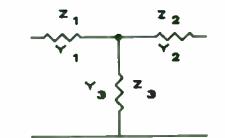
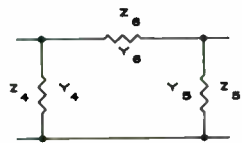


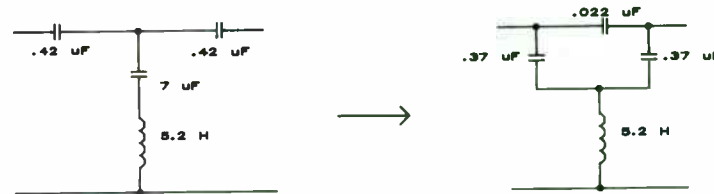
FIGURE 19



TEE NETWORK



PI NETWORK



$$Z_6 = \frac{Z_1 Z_2 + Z_1 Z_3 + Z_2 Z_3}{Z_3}$$

$$Z_4 = \frac{Z_1 Z_2 + Z_1 Z_3 + Z_2 Z_3}{Z_2}$$

$$Z_5 = \frac{Z_1 Z_2 + Z_1 Z_3 + Z_2 Z_3}{Z_1}$$

$$Z_1 = \frac{Z_4 Z_6}{Z_4 + Z_5 + Z_6}$$

$$Z_2 = \frac{Z_5 Z_6}{Z_4 + Z_5 + Z_6}$$

$$Z_3 = \frac{Z_4 Z_5}{Z_4 + Z_5 + Z_6}$$

$$Y_6 = \frac{Y_1 Y_2}{Y_1 + Y_2 + Y_3}$$

$$Y_4 = \frac{Y_1 Y_3}{Y_1 + Y_2 + Y_3}$$

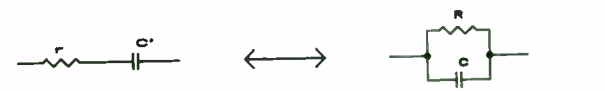
$$Y_5 = \frac{Y_2 Y_3}{Y_1 + Y_2 + Y_3}$$

$$Y_1 = \frac{Y_4 Y_5 + Y_4 Y_6 + Y_5 Y_6}{Y_4}$$

$$Y_2 = \frac{Y_4 Y_5 + Y_4 Y_6 + Y_5 Y_6}{Y_5}$$

$$Y_3 = \frac{Y_4 Y_5 + Y_4 Y_6 + Y_5 Y_6}{Y_6}$$

FIGURE 21



$$r = \frac{R}{1 + \omega^2 R^2 C^2}$$

$$C' = C \left[1 + \frac{1}{\omega^2 R^2 C^2} \right]$$

$$R = r \left[1 + \frac{1}{\omega^2 r^2 C'^2} \right]$$

$$C = \frac{C'}{1 + \omega^2 r^2 C'^2}$$

ALSO: IF A DESIRED RATIO FOR $\frac{R}{r}$ EXISTS, THEN

$$C = \frac{\sqrt{\frac{R}{r} - 1}}{\omega R} \quad \text{AND} \quad C' = \frac{C}{1 - \frac{r}{R}}$$

FIGURE 22

FIGURE 20



$$L' = L \left[\frac{R^2}{R^2 + \omega^2 L^2} \right]$$

$$r = R \left[\frac{\omega^2 L^2}{R^2 + \omega^2 L^2} \right]$$



$$L = L' \left[1 + \frac{r^2}{\omega^2 L'^2} \right]$$

$$R = r \left[1 + \frac{\omega^2 L'^2}{r^2} \right]$$

FIGURE 23

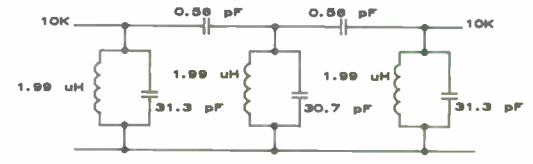


FIGURE 24

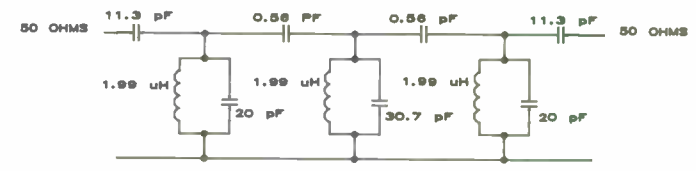


FIGURE 25

“Vibrational Sensitivity and
Phase Noise in Crystal Oscillators”

Glenn R. Kurzenkabe
Piezo Crystal Company
100 K Street, P.O. Box 619
Carlisle, PA 17013

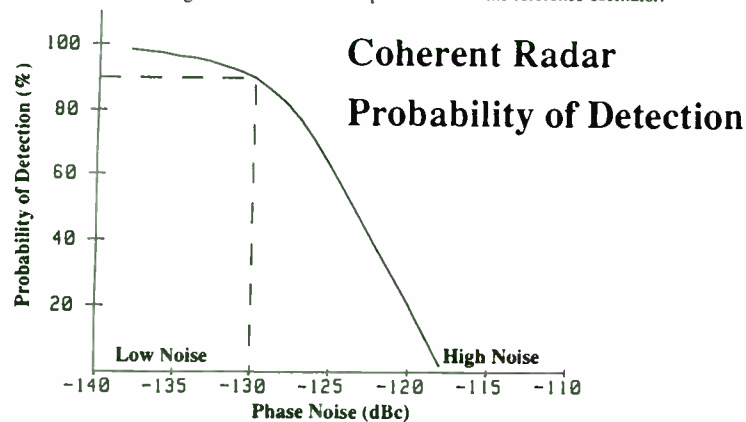
ABSTRACT

A growing concern in the radar, ECM and communications community is the effect of vibration/acceleration on the phase noise of crystal oscillators and it's degradation on overall system performance. This paper will review what phase noise is and why it is degraded with vibration/acceleration. Several types of oscillators will be discussed and possible solutions will be considered.

INTRODUCTION

Many military and aerospace systems require very low phase noise crystal oscillators. Crystal resonators are sensitive to vibration/acceleration; therefore, during use in environments such as fixed wing and rotary aircraft, shipboard and vehicle, the oscillator is FM modulated thereby degrading the phase noise performance of the oscillator. This effect has been recognized as the most limiting factor in the performance of many sophisticated systems and is assuming increasing significance in their design. Figure 1 is an example of how the capability of a Coherent Radar degrades with a rise in the phase noise of the reference oscillator.

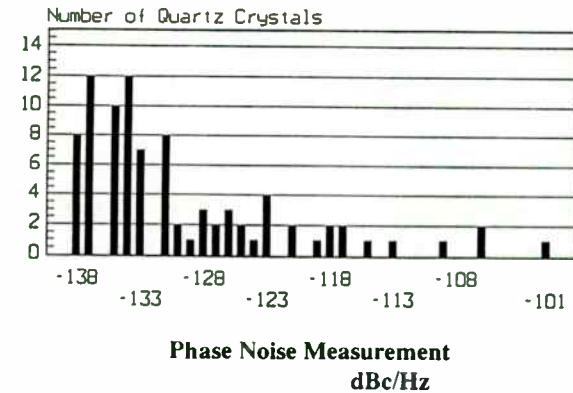
Figure 1:



PHASE NOISE

Phase noise in bulkwave quartz crystal resonators is broken down into two types; “far-out” and “close-in.” “Far-out” phase noise is generally considered to be 5-10 KHz and beyond from the carrier and is a function of semiconductor noise and drive level on the resonator. This subject will not be addressed in any detail as it is generally unaffected by acceleration spectrums as none usually extend beyond a few KHz thereby having no effect on the dynamic phase noise. “Close-in” phase noise (5-10 KHz and closer) is generally a function of resonator Q. Noise energy is filtered by the resonator. Increasing the resonator Q narrows its bandwidth and most noise is rejected resulting in better phase noise. There is a second factor that effects “close-in” phase noise. All electronic components, not just active devices, generate flicker noise. Quartz crystals can be observed to display phase noise that does not originate in the oscillator circuit and does not correlate to resonator Q. (Figure 2) This phenomenon requires care and selection of the specific resonator to be used in a given oscillator.

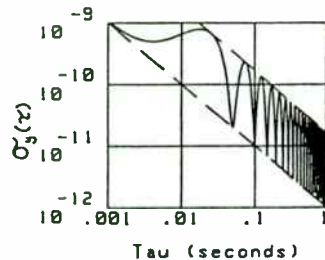
Figure 2: **PHASE NOISE FREQUENCY DISTRIBUTION
CRYSTAL FREQUENCY: 100 MHz
n = 90**



ALLAN VARIANCE

The effect of sinewave vibration on phase noise is shown in Figure 3. At rest this oscillator will exhibit 1×10^{-12} /second. The g sensitivity is $1 \times 10^{-9}/g$ and the acceleration level is 1 g. These small shifts in frequency are caused by the changing g levels on the resonator.

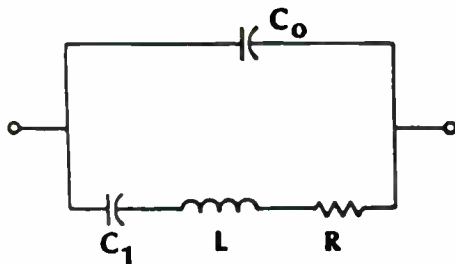
Figure 3:



IDENTIFYING THE PROBLEM

A quartz crystal resonator is often thought of as an electrical device (Figure 4). To some degree it is, as it has R, L and C components. In reality it is a mechanical device because the resonator is physically "moving" at the frequency of operation, i.e. a 1 MHz resonator, when excited, is actually vibrating 1 million times per second. Since the resonator is a mechanical device, when it is subjected to an external vibration spectrum, it will be FM modulated by the vibration spectrum. The modulation will appear in the form of sidebands resulting in degraded phase noise. These sidebands will only appear at the vibration frequency assuming the absence of mechanical resonances in the resonator mounting structure or oscillator assembly. Research done recently suggests that mechanical stretching and bending of the resonator mounting structure during acceleration will cause changes in the series inductance and shunt capacitance. These shifts in the electrical characteristics of the resonator will cause shifts in frequency.

Figure 4:

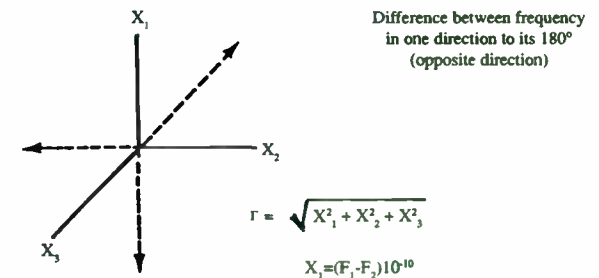


VECTOR DIFFERENCES

Acceleration sensitivity is a vector quantity in three dimensions, different in all axes. Measured differences can be as great as 10 to 1 from axis to axis. These differences are principally due to the moment of inertia acting upon the elastic coefficients of the quartz. One needs to keep in mind that quartz exhibits different coefficients of expansion and contraction in all three axes. Combining the sensitivity in each axis gives gamma (Γ). The magnitude of gamma is determined by taking the square root of the sum of each axis squared (Figure 5). The direction of gamma has little correlation from resonator to resonator even though each may be built from the same quartz using identical manufacturing processes for a given resonator design.

CALCULATIONS OF ACCELERATION SENSITIVITY

Figure 5:



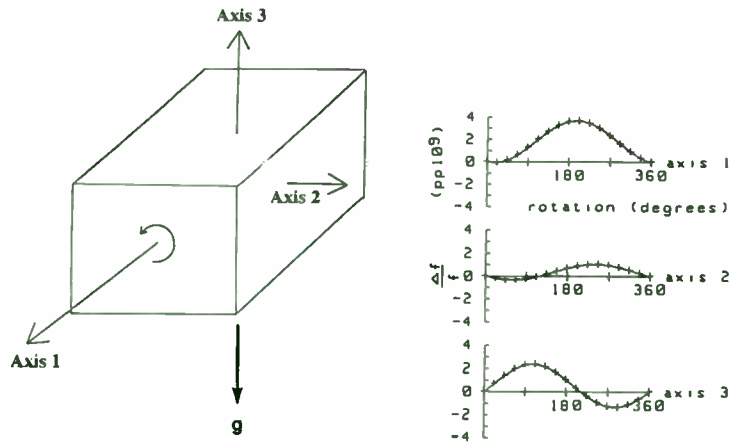
2 g TIP-OVER AND ACCELERATION

The 2 g tip-over test is a dramatic demonstration of the g effects of acceleration on a crystal oscillator. An oscillator at rest on the bench is subjected to 1 g of force toward the center of the earth. Therefore, one can assume that the actual resonator is "sagging" under the 1 g load. Physically turning the oscillator over 180 degrees will again produce a 1 g load; however, when added to the original 1 g, the result is 2 g's, hence the 2 g tip-over test. If this test is conducted in all three axes with accurate frequency measurements, significant differences can be observed depending on the oscillator type and resonator design (Figure 6). When SC cut

crystals are utilized, the frequency change will be in the area of low parts in $X10^{-9}$ or $X10^{-10}$.

Figure 6:

2-g Tipover Test



ACCELERATION SENSITIVITY

The effects of acceleration sensitivity as demonstrated with the 2 g tip-over test are of little interest to the systems designer because the conditions found in this bench test are never reproduced in actual system environments. As oscillators in their systems experience acceleration by vibration, sidebands are produced at the vibration frequency.

SINEWAVE VIBRATION

When an oscillator is subjected to sinewave vibration from such sources as ships propellers, cooling fans or transformers, sidebands will appear in the output spectrum at the vibration frequency only. It can be readily

seen that a 1 g vibration at 100 Hz will produce 100 Hz sidebands. (Figure 7) For sinewave vibration spectrums the sideband level can be calculated using the following equation:

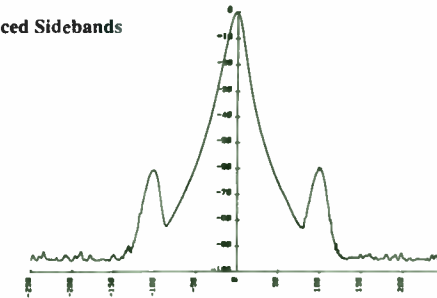
$$SSB = 20 \log \left[\frac{\Gamma \cdot g \text{ level} \cdot f_c}{2 \cdot f} \right]$$

Using this equation and assuming a "perfect oscillator" (noise-free) at rest with a g sensitivity (Γ) of 1×10^{-6} at 10 MHz, the SSB phase noise due solely to a sinewave vibration level of 1 g would be:

Vibration Frequency	SSB Phase Noise
1 Hz	-46 dBc/Hz
10 Hz	-66 dBc/Hz
100 Hz	-86 dBc/Hz
1 kHz	-106 dBc/Hz
10 kHz	-126 dBc/Hz

Note: SSB = Phase Noise in dBc
 Γ = g sensitivity in Hz/g
 f_c = carrier frequency in Hz
 f = Frequency of vibration in Hz

Figure 7: Vibration-Induced Sidebands



RANDOM VIBRATION

When an oscillator is subjected to random vibration, the results are much more dramatic and devastating. The most common source of random vibration is an aircraft. During random vibration an entire "vibration envelope" contains energy which effects the oscillator (Figure 8). For random vibration spectrums the phase noise can be calculated using the following equation:

$$SSB = 20 \log \left[\frac{\Gamma \cdot A \cdot f_c}{2 \cdot f} \right]$$

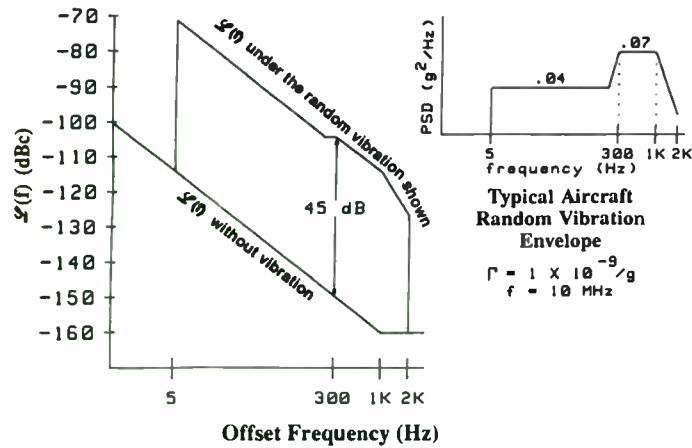
Using this equation and again assuming a "perfect oscillator" with a g sensitivity (Γ) of 1×10^{-6} /g and a power spectral density (PSD) of $0.1 \text{ g}^2/\text{Hz}$ at 10 MHz, the resulting SSB phase noise would be:

Offset Frequency (from carrier)	SSB Phase Noise
1 Hz	-53 dBc/Hz
10 Hz	-73 dBc/Hz
100 Hz	-93 dBc/Hz
1 kHz	-113 dBc/Hz
10 kHz	-133 dBc/Hz

Note: SSB = Phase Noise in dBc
 Γ = g sensitivity in Hz/g
 f_c = carrier frequency in Hz
 f = Frequency of vibration in Hz
 A = $2 \cdot$ PSD in a 1 Hz bandwidth
 f = Frequency at point of interest on PSD curve in Hz.

Note: There is a similarity to the equation used for sinewave calculations; however, the vibration frequency has been substituted with "power spectral density."

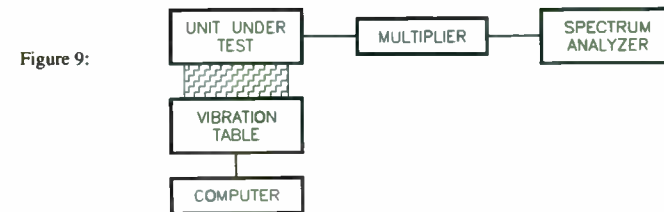
Figure 8: **Random-Vibration-Induced Phase Noise**



MEASUREMENT METHODS

There are a number of accepted methods for measuring g sensitivity and phase noise over vibration. One method is the 2 g tip-over test addressed earlier. The results of this test can be g-sensitivity (Γ) expressed in fractional frequency shift (i.e. $5 \times 10^{-10}/g$) used to calculate the sideband rise in either a sine or random condition. It is possible using this method that there may be some frequency offset during tip-over due to thermal shifts in the internal oscillator circuitry/oven of some oscillators. Caution should be observed.

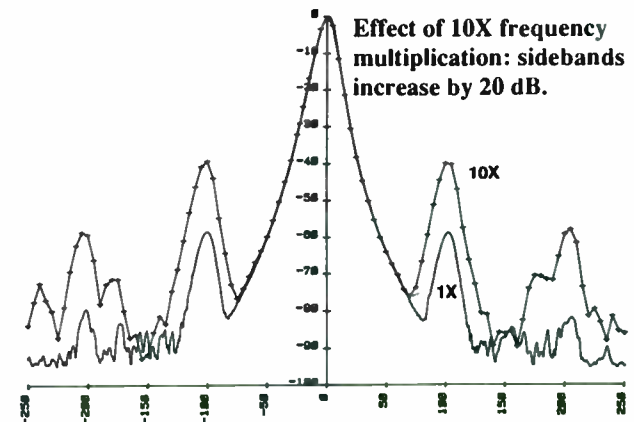
Real-time measurements can be made several different ways. The oscillator being tested can be operated on a vibration table. The oscillator is multiplied to a high frequency that will permit visual measurements of the sidebands during vibration on a spectrum analyzer (Figure 9).



This method will work for sinewave vibration. Vibration at a single frequency may produce inaccurate results as resonances may be present in the oscillator or the vibration fixture. It is suggested that several vibration frequencies be used and the results be compared for accuracy. Remember to adjust the resulting phase noise levels for $20 \log N$ due to the multiplication during the test (Figure 10).

Figure 10:

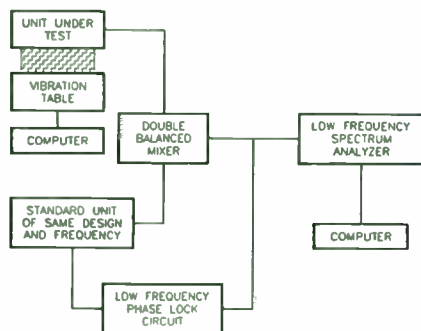
Vibration-Induced Sidebands



The third and most accurate method is to actually measure the phase noise during vibration using a computer controlled vibration table and phase noise measurement system.

The Hewlett Packard 3047/3048 are popular systems in use today. Using this method the actual system vibration profile can be introduced into the test and into subsequent calculations which are carried out by the 3047/3048 (Figure 11).

Figure 11:



THE BEST CRYSTAL CUTS

The SC cut crystal is by far the favorite for phase noise over vibration applications.

One of the more undesirable properties of quartz crystals is stress. Stress accounts for the warm-up, hysteresis and vibrational sensitivity characteristics of a resonator.

The SC cut is sometimes referred to as "Stress Compensated" which makes it more desirable compared to the more common AT cut. Other cuts sometimes used are BT, FC and IT, however, the SC is the most popular.

Figure 12 shows examples.

Figure 12:

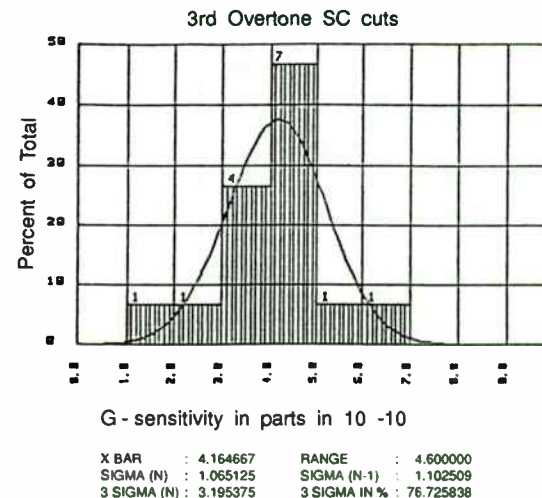
ACCELERATION SENSITIVITY MEASUREMENTS (Typical) SC cut crystals

Frequency / Mode	g-SENSITIVITY (Γ)
5 MHz/3rd Overtone	1.3 X 10 ⁻⁹ /g
10 MHz/3rd Overtone	1.5 X 10 ⁻⁹ /g
60 MHz/3rd Overtone	4.5 X 10 ⁻⁹ /g
80 MHz/3rd Overtone	3.8 X 10 ⁻⁹ /g
95 MHz/5th Overtone	5.5 X 10 ⁻⁹ /g
100 MHz/5th Overtone	4.8 X 10 ⁻⁹ /g
100 MHz/3rd Overtone	4.0 X 10 ⁻⁹ /g
118 MHz/5th Overtone	5.0 X 10 ⁻⁹ /g
135 MHz/5th Overtone	5.5 X 10 ⁻⁹ /g

Note: All of the crystals utilize a four point mounting configuration spaced at 90 degrees. This mounting appears to be optimum.

Figure 13 is a histogram showing the measured acceleration sensitivity distribution of a 106 MHz, 3rd overtone SC cut crystal. The sample group was 15 devices and the \bar{X} is 4×10^{-10} /g.

Figure 13:



COMPENSATION METHODS

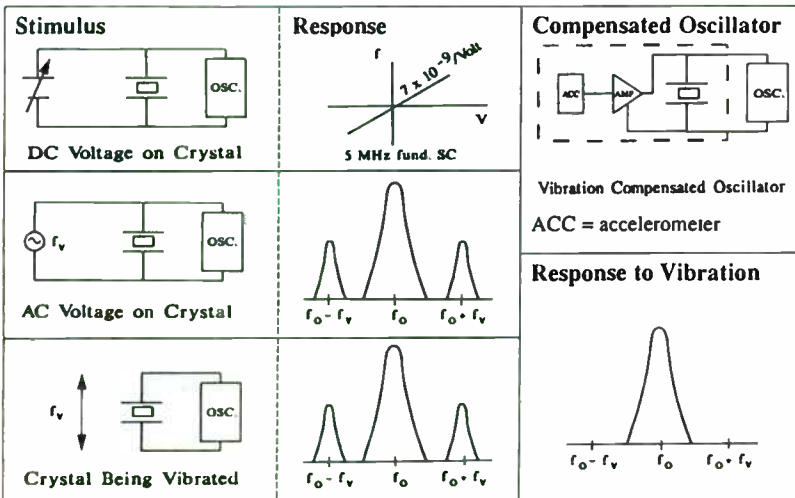
Experiments have been conducted by government and industry on a number of methods to compensate for the effects of acceleration, both electrical and mechanical, with varying results. One method was to mechanically arrange two similar resonators so that the components of their acceleration sensitivities normal to the plates were antiparallel. The resonators were connected in series and used in a single oscillator. Other experiments have utilized three and four resonators in a similar configuration.

Another method was to measure the actual acceleration g levels using an accelerometer. The output voltage from this network was fed into a varactor tuning network. This would then counter the effects of the

acceleration g levels. The limitation of this method was the linearity of the accelerometer and control circuit.

(Figure 14)

Figure 14: Vibration Compensation



Still another method used multiple accelerometers and a microprocessor to control the signals from the three accelerometers and apply it to the varactor controlled oscillator.

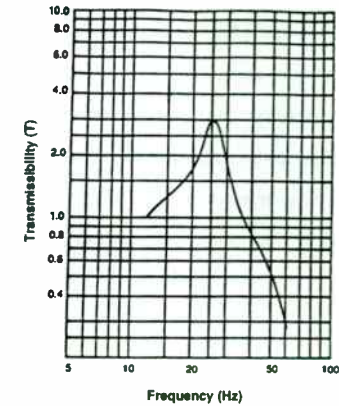
None of the electrical methods mentioned has proved to be successful on a production basis even though they have been successful in the laboratory.

The mechanical isolation system has proven to be more successful although it is not the total answer.

Mechanical isolation systems utilize springs, rubber mounts, grommets and dampers. These systems are generally large, bulky, heavy and usually ineffective at low vibration frequencies. Figure 15 indicates the

effectiveness of a mechanical isolation system.

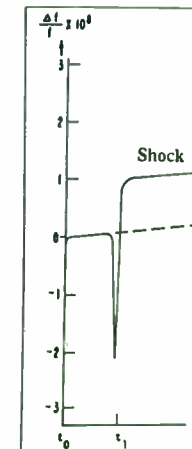
Figure 15:



THE EFFECTS OF SHOCK

The frequency excursion during a shock pulse is due to the acceleration sensitivity of the resonator. Following the shock pulse, the resonator should return to the original frequency unless a permanent frequency offset is introduced by particulate (contamination) shifts on the resonator surface or permanent changes are introduced in the circuit or resonator mounting structure (Figure 16).

Figure 16:



EXAMPLES OF CURRENT TECHNOLOGY

Figures 17, 18 and 19 indicate an example of a 10MHz oscillator incorporating a 3rd overtone SC cut resonator under random acceleration. One should be careful to note the differences between the X, Y and Z axes when subjected to the same acceleration spectrum.

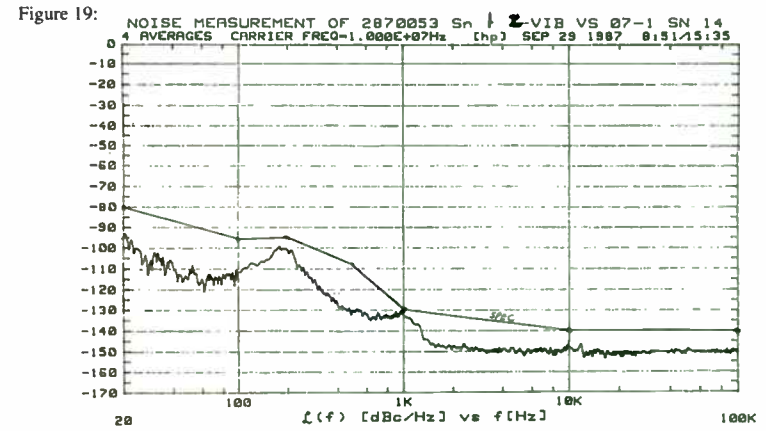
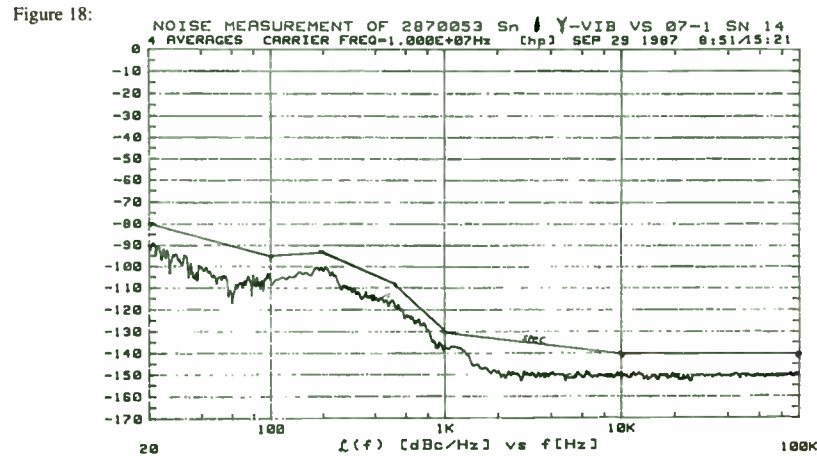
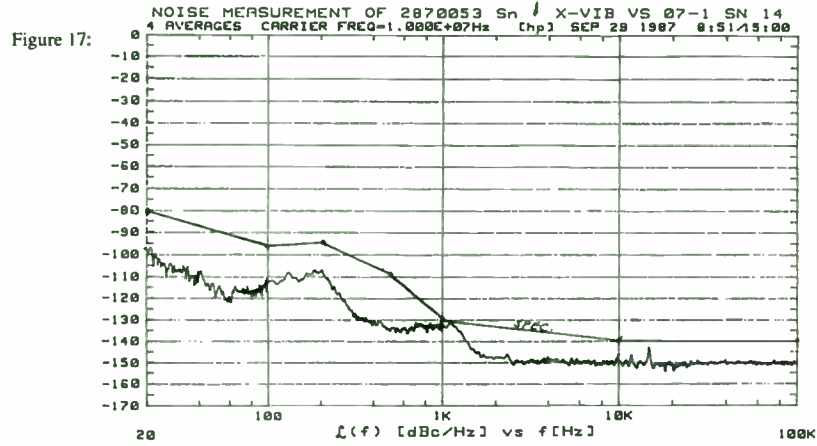


Figure 20 is the phase noise spectrum at rest of the same oscillator.

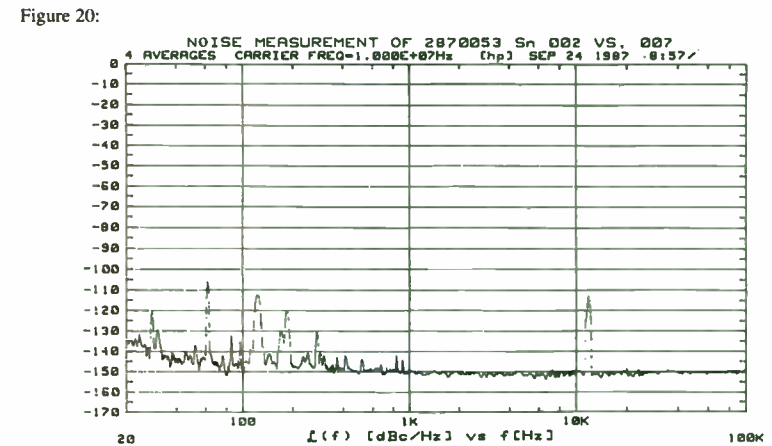
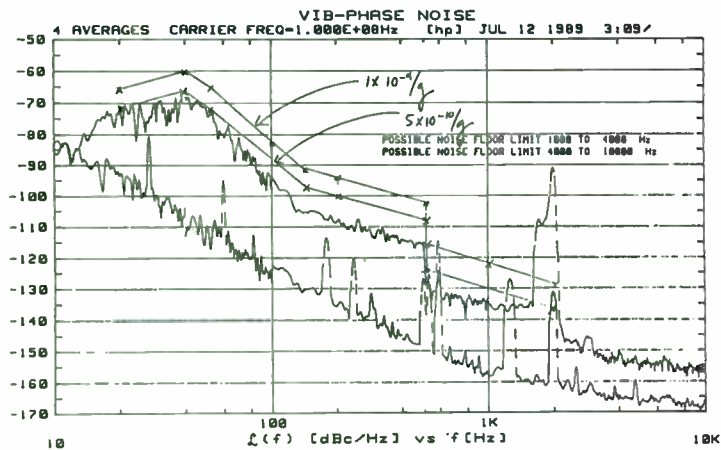


Figure 21 indicates an example of a 100 MHz oscillator incorporating a 3rd overtone SC cut resonator under random acceleration and at rest. The limits for vibrational sensitivities of $1 \times 10^{-9}g$ and $5 \times 10^{-10}g$ are also indicated.

Figure 21:



WHAT IS IN THE FUTURE

This problem has plagued the industry for many years. Today most of the research is in resonator design. Specific areas are blank geometry, mounting structures, surface finish and plating techniques. Generally at this time the industry limit is $1 \times 10^{-9}g$ for a 10 MHz, 3rd overtone SC cut crystal. Due to reduced resonator mass, $5 \times 10^{-10}g$ can be achieved with an equivalent resonator at 100 MHz.

Progress has been made in understanding vibrational/acceleration sensitivity but a full explanation has been elusive.

CONCLUSIONS

Engineers who are involved with system design where phase noise is of concern are cautioned to be sure that they clearly understand the requirements and that any oscillator manufacturer clearly demonstrate a knowledge of the subject. It is strongly suggested that vendors be requested to submit actual measured data from programs that they have participated in prior to contract award. The lack of specific details can have a serious impact on the final system performance.

USERS ARE ENCOURAGED TO ASK QUESTIONS.

ACKNOWLEDGEMENTS

I would like to thank my colleagues at Piezo Crystal Company for their guidance and support in the preparation of this paper.

REFERENCES

Vig, John, "Quartz Crystal Resonators and Oscillators", U.S. Army Electronics Technology and Devices Laboratory (LABCOM) 1990

Filler, Raymond, "The Acceleration Sensitivity of Quartz Crystal Oscillators: A Review", U.S. Army Electronics Technology and Devices Laboratory (LABCOM) 41st Annual Frequency Control Symposium 1987.

Rosati, Vincent, "Suppression of Vibration-Induced Phase Noise in Crystal Oscillators: An Update", U.S. Army Electronics Technology and Devices Laboratory (LABCOM) 41st Annual Frequency Control Symposium 1987.

Long, Bruce, "Quartz Crystals and Oscillators" Piezo Crystal Company, RF Expo 1989

Kurzenknabe, Glenn, "Phase Noise Under Vibration in Crystal Oscillators" Piezo Crystal Company 1988

Bates, Nicolas and Weaver, Gregory, "Phase Noise Frequency Distributions of SC and AT Quartz Resonators", Piezo Crystal Company, 43rd Annual Frequency Control Symposium 1989

Hanson, William, Heishman, Lynn and Meeker, Thrygve, "A New Factor Affecting the Acceleration Sensitivity of the Resonance Frequency of Quartz Crystal Resonators", Piezo Crystal Company, 44th Annual Frequency Control Symposium 1990.

QUARTZ CRYSTAL FILTERS:
A REVIEW OF CURRENT ISSUES

M.D. Howard and R.C. Smythe
Piezo Technology Inc.
Orlando, Florida

February 21, 1990

ABSTRACT

This paper discusses some of the issues facing both the user and manufacturer of crystal filters in today's dynamic RF engineering environment.

Applications for crystal filters are subject to constant update and revision. System operating frequencies are increasing while modulation and multiplexing schemes are utilizing spread spectrum and digital transmission techniques. Examples would include the recently formatted European cellular radio system and secure military communication systems. The increased operating frequencies call for corresponding higher IF frequencies, while the modulation schemes call for bandwidths that are too wide to be constructed using the traditional overtone crystal resonators.

Also, the continued development of multiple channel radar, ECM, and direction locating systems that require stringent phase and amplitude matching pushes the filter manufacturer to incorporate components that have normally been reserved for precision oscillators. As modern semiconductors have improved in power handling and linearity, crystal filters have become a dominant source of intermodulation problems. Finally, as systems have become integrated at higher levels, the crystal filter has become one of the largest components on the IF strip. Many systems houses are converting to surface mount technology and require filters to be surface mountable.

This paper will review currently available filters that use high frequency fundamental mode resonators, both single resonator and monolithic dual resonators (MDRs), and compare their performance with that of traditional overtone devices. The performance of phase- and amplitude-matched sets will be examined and some insight to the phase match problem will be presented. Factors affecting intermodulation performance and power handling will be reviewed and the advantages of SC versus AT cut will be

discussed. Finally, available surface mount options will be compared and some possible future configurations will be presented.

VHF FUNDAMENTAL MODE QUARTZ CRYSTAL FILTERS

The last decade has seen a dramatic increase in the maximum fundamental frequency of quartz crystal resonators. For the user of crystal filters, this means that crystal filters with greatly increased bandwidth and selectivity, as well as reduced size, loss, and cost, are now available through most of the VHF frequency range. While high-performance VHF crystal filters have been available since the late 60's [1,2], because they used overtone resonators, they were restricted to very narrow bandwidths. Even so, in most cases these filters required the use of extra inductors ("spreading coils") to compensate for excess circuit capacitance. These spreading coils not only add to the size of the filter, they increase its loss, limit its maximum bandwidth, and may degrade its stability over temperature. The burden imposed upon the filter network by these inductors is such that only the simplest filters are available using third-overtone resonators. Even in the 1970's and early 80's, fundamental mode crystals operating much above 30 to 35 MHz were rare and found application only in the most sophisticated military applications. Today, fundamental mode resonators are routinely used in high-volume, low-cost commercial applications at 45 MHz with an increasing number of commercial applications appearing at 70 MHz and numerous military applications from 40 to 200 MHz.

In the late 1970's and early 1980's radios were in development intended to satisfy the emerging cellular radio telephone market. These radios would operate in the 800 MHz to 900 MHz range, and the receive/transmit frequency scheme was easily and economically serviced with a 45 MHz first I.F. However, for the required bandwidth of 30 to 35 kHz, the third-overtone devices then available were quite high in impedance, typically 10,000 ohms. Attempts to reduce this level significantly by increasing the resonator electrode area results in a strongly excited crop of

analytically predictable, but nevertheless undesirable, spurious responses in the filter stopband. The best third-overtone designs still have a relatively high impedance and consequently have high insertion loss and low ultimate attenuation. The response of a typical third-overtone, two-pole filter manufactured for this application is shown in fig. 1. The combined insertion loss of the MDR and associated input and output impedance-matching networks, with most of the loss being in the latter, is 6 dB. The ultimate attenuation is 30 dB. Clearly, if the second I.F. image rejection requirement of 60 dB at 910 kHz from filter center is to be satisfied without the addition of more poles, then the filter impedance must be reduced. This can only be done through the use of fundamental mode resonators. Since the device impedance level is proportional to the cube of the overtone, using a fundamental mode MDR instead of a third-overtone MDR results in an impedance reduction of 27. For the 45 MHz cellular radio filter, this means an impedance of a few hundred ohms rather than ten thousand ohms.

The added benefits of reduced impedance are reduced insertion loss, which improves the signal-to-noise ratio, reduced sensitivity to coil tuning, and reduced size, since the required number of poles is kept to a minimum. In addition, a portion of the impedance reduction can be traded for improved spurious mode response. All of these factors suggested that a fundamental mode MDR would result in a higher performance radio. The performance of such a filter is shown in fig. 2. As can be seen there is a substantial improvement in ultimate attenuation to approximately 58 dB at +910 kHz and 75 dB at -910 kHz, while the insertion loss is less than 2 dB. The switch to a fundamental mode MDR had delivered all of the increased performance that was expected.

The higher fundamental frequencies have been made possible by improvements in wafer fabrication technology. At frequencies above about 1 MHz, crystal filters use thickness-mode resonators, primarily the well-known AT-cut. Thickness mode resonators are thin wafers, usually circular, of crystalline quartz and having suitably dimensioned thin film electrodes. The resonance frequency

is determined primarily by wafer thickness, with which it varies inversely, according to eqn. (1):

$$f_n = n \cdot K/t \quad (1)$$

where K is a constant characterizing the cut, t is the wafer thickness, n is the overtone ($n = 1, 3, 5...$) and f_n is the resonance frequency at overtone n . For example, a 30 MHz fundamental mode AT-cut resonator is approximately 2.2×10^{-3} inch thick, while a 300 MHz fundamental would be one-tenth that thickness. The thickness of a quartz wafer is reduced (and its frequency increased) by a sequence of mechanical lapping, polishing and then chemical milling techniques. As the wafer becomes thinner it requires less force to cause fracture and in addition, carriers required to support the wafer during mechanical material removal become thinner and more fragile. Consequently the highest frequency to which a crystal can be processed by mechanical means is limited. Additional material can be removed chemically, but for normal electronic grade synthetic quartz this process is limited by the formation of etch pits and channels. As more material is chemically removed the population density of these defects increases to a point where the wafer is no longer useable. The 45 MHz filters described above are manufactured by reducing wafer diameter, resulting in a more robust wafer, refining existing mechanical lapping techniques to extend their range and then finishing the wafer with an extended chemical etch, but not enough to cause pits or channels.

To extend the highest frequency fundamental much beyond 45 MHz requires a radically different approach -- the ring-supported structure. In this approach, fig. 3, only the central portion of the resonator wafer is thinned; an outer ring is left much thicker, providing support for the thin central region. Early resonators of this type were made using ion-beam milling [4]. While this process is technically satisfactory, it is slow and expensive. As an alternative, since the early 80's, PTI has been developing chemically-milled ring-supported resonators and MDR's based on the

chemical polishing techniques pioneered by Vig and co-workers at US Army LABCOM, Ft. Monmouth, NJ [5-8]. We have developed processes for both AT-cut and SC-cut devices that reduce the incidence of pits and channels to an acceptable level [9-11]. (While for filter applications, the AT-cut is of primary importance, SC-cuts are valuable when increased power handling is required, as well as in some applications requiring low intermodulation of in-band signals.)

During this period we have fabricated, in the laboratory, useful fundamental resonators at frequencies up to 1 GHz. One spectacular result was a fundamental-mode resonator at 1.6 GHz, corresponding to a thickness of 1 micrometer (39 microinches) for the central region. Results such as this are still very much a laboratory curiosity but the spin-off to the world of manufacturing is very apparent with products up to 200 Mhz now being offered.

Having drawn attention to just how thin the central resonator portion of the wafer is, it is appropriate to discuss the mechanical robustness of these devices -- a real concern of some users. To date, all of the results obtained by the authors show that these resonators are at least as robust as most conventionally fabricated lower frequency resonators. If a resonator free from cracks or defects is sealed in its protective hermetic enclosure, then the major source of force applied to the wafer is generated by its own mass when exposed to shock or vibration. As the wafer and the inverted mesa in particular have little mass the forces are also small. In addition, and perhaps more significantly, the surface of the wafer after the removal of much material by chemical milling has a very low incidence of mechanical defects left over from the use of abrasives in prior processes. The result is an extremely strong wafer. It is not unusual to be able to bend wafers in a 45 degree arc without causing fracture. Resonators at 112 MHz have been tested at shock levels of 6,400 G's without damage to the wafer. Some results on these tests are given in table 1.

Table 1

	FS (kHz)	R1 (ohms)	L1 (mH)	KQ
Start	111947.89	11.45	0.96	59
After 200 G	111947.901	11.58	0.99	60
After 400 G	111947.566	11.76	0.99	59
After 800 G	111947.631	12.03	0.98	58
After 1600 G	111947.626	12.03	0.98	57
After 3200 G	111947.690	11.89	0.98	58
After 6400 G	111946.452	16.79	0.98	41

The lower impedance of these fundamental resonators offers the major advantage of increased bandwidth. Filter requirements that are too wide to be realized using third-overtone resonators are readily realized using fundamentals. In fact, filter impedance levels reduce to the point where, in the VHF range, the designer of filter networks is no longer restricted to low-order, narrow-band designs but may explore the possibilities of multi-pole intermediate-band and wideband designs that extend the available bandwidths to over 1%. Some examples of filters recently produced is given in figs. 4 through 9. Figure 4 illustrates a 70 MHz filter assembled from discrete resonators and approximately 330 kHz wide at 3 dB. This filter is an 8-pole, two section, intermediate-band design and has a 60 dB bandwidth of 520 kHz giving a 60 dB:3 dB shape factor of less than 1.6:1. The ultimate attenuation is 90 dB and is maintained to 200 MHz. The insertion loss is only 5.6 dB at room temperature. Figure 5 illustrates a 6-pole monolithic dual resonator (MDR) filter at 125 MHz comprised of three MDR sections. The 3 dB bandwidth is 100 kHz, the 60 dB bandwidth is 250 kHz and the ultimate attenuation is 120 dB. Figs. 6 and 7 illustrate a filter close to 70 MHz intended for use in a radio employing digital modulation techniques. The filter design is based upon a four pole transitional Butterworth/Gaussian response to obtain an optimum trade-off between differential delay performance and selectivity. The passband amplitude and delay response is shown in fig. 6 and illustrates a 3 dB bandwidth of over 250 kHz and a differential delay of better than 850 nSec. The 55 dB bandwidth is

less than 1300 kHz and the ultimate attenuation is close to 70 dB (fig. 7). The entire filter can be hermetically sealed in a package 0.8 X 0.6 X 0.5 inches that provides 50 Ohm terminations. An example of an intermediate-band filter is given in figs. 8 and 9 which illustrate a filter having a 3 dB bandwidth of 1.040 MHz and a center frequency of 70.0 MHz. This a three-pole, single section filter that has a 30 dB bandwidth of 2.5 MHz, an ultimate attenuation of 60 dB and an insertion loss of 5 dB.

In the last decade, the highest frequency at which a fundamental mode filter is available in production quantities has tripled. The required techniques are subject to constant improvement and it is expected that the availability of high frequency fundamentals and the frequency of operation will both continue to increase through the next decade.

PHASE AND AMPLITUDE MATCHED FILTER SETS

Phase and amplitude matched filter sets find applications in multi-channel receivers where information is contained in the phase and amplitude difference between two or more received signals. An example would be a monopulse radar system where the resolution is directly related to the phase and amplitude match between receiver channels. Because the bandwidth of the crystal filter is normally very much narrower than that of other components in the receiver, the phase and amplitude match between the crystal filters is the most important contributor to the match between receiver channels. Because phase match is usually more critical to the user and because the amplitude match is usually somewhat easier to achieve, at least within the center 80% of the filter passband, the focus of the following discussion will be on phase match.

While filters with identical components will match perfectly, in practice, components are never identical, particularly the most critical component, the quartz resonator. Motional inductance and resistance, frequency at reference temperature and frequency shift with temperature are all factors that will affect filter amplitude

and phase response. Resonator frequency is probably the most critical of these.

The fractional bandwidth over which match is required is important. As the 3 dB bandwidth fraction over which match is required increases, match becomes increasingly difficult to achieve. As a general rule, phase and amplitude match requirements should be restricted to less than 80% of the 3 dB bandwidth. Very narrow and very wide bandwidth filters are particularly difficult to match; narrow-band filters because they are very sensitive to crystal frequency changes and wide-band filters because they are very sensitive to coil tuning and temperature compensation changes. Use of an adjustable attenuator and/or a wide band phase shifter in the using system to correct for filter differences at room temperature will often have a net cost benefit due to relaxed filter requirements.

Some specifications call for a population match where all filters must match some reference trace within specified tolerances. Population matches are usually more costly. For example, if crystals must be within 5 ppm of each other in order to satisfy a match requirement, then for a population match the entire usable distribution of crystals must be within ± 2.5 ppm of some nominal frequency performance. However, for a set match only those crystals in a set need be within ± 2.5 ppm of each other, so the total useable distribution is much greater than ± 2.5 ppm. The useable distribution may be several times greater for a set match as compared to a population match, with a corresponding impact on cost. Whenever logistics will allow, it is worth considering the use of a set rather than a population match.

As stated above, the crystal resonator frequencies are critical in narrow-band filters and, in the center portion of the filter passband, the phase match is normally the most difficult requirement. A simple analysis is to assume that all resonators in the reference filter deviate from nominal in the same direction and by the same amount, δf (Hz). The tracking filter is assumed to

deviate from nominal by an equal and opposite amount. In the center portion of the passband the frequency/phase shift response is approximately linear and is ϕ degrees over the 3 dB bandwidth. For a Butterworth filter the phase shift can be simply calculated as 90° per pole over the 3 dB bandwidth (BW_3). For other filter types ϕ must be read from low pass response curves or established by analysis. In either case, the two filter responses are assumed identical except for a difference in center frequency of $2 \cdot \delta f$. The phase difference between filters, $\delta\phi$, is estimated by equation 2 assuming a phase slope at F_{on} of ϕ / BW_3 . (Please note that equations (2), (3), (5) and (6) are good only for a first pass analysis intended to establish the order of difficulty of the required match and should be verified by a more detailed analysis.)

$$\delta\phi \approx \frac{2 \cdot \phi \cdot \delta f}{BW_3} \text{ deg.} \quad (2)$$

Where BW_3 is the 3 dB bandwidth in Hz. This can be rewritten to give the maximum allowed δf for a given phase tracking requirement.

$$\delta f \approx \frac{\delta\phi \cdot BW_3}{2 \cdot \phi} \text{ Hz} \quad (3)$$

and
$$\delta F = \delta f \cdot 10^6 / F_{on} \text{ ppm} \quad (4)$$

for Butterworth filters

$$\phi = N \cdot 90 \text{ deg.}$$

Where N is the number of poles and F_{on} is the nominal filter center frequency.

Another scenario is that all of the resonators in the reference filter deviate in such a manner that they increase the filter bandwidth and that all of the resonators in the tracking

filter deviate to reduce the bandwidth. The bandwidth would decrease, for example, if all of the low frequency resonators were high and all of the high frequency resonators were low in frequency. In this case the filters will have approximately the same center frequency and will have close to equal phase shift at center frequency. However, as the two filters have different bandwidths and corresponding different phase slopes then, as the frequency deviates from center, their phase shift will no longer track. In this instance the phase offset at $\pm F_p/2$, where F_p is the bandwidth over which phase match is required in Hz, is given by eqn. (5).

$$\delta\phi \approx \frac{\phi \cdot F_p \cdot 2 \cdot \delta f}{K \cdot BW_{32}} \quad \text{deg.} \quad (5)$$

and

$$\delta f \approx \frac{\delta\phi \cdot K \cdot BW_{32}}{2 \cdot \phi \cdot F_p} \quad \text{Hz} \quad (6)$$

Where K is a constant related to the filter type (Butterworth or Chebychev, etc.) and structure (narrow-band or intermediate-band etc.). A good estimate for K is 0.7 for most filters.

These equations can be used to estimate the degree of difficulty of a particular phase match as illustrated in the following example.

F₀ = 21.4 MHz
 BW₃ = 10 kHz
 F_p = 8 kHz
 δφ = 4 deg. max
 N = 8 poles

Design type: 0.1 dB Chebychev

From low pass design charts:

φ = 1040 deg.

Assuming a different F₀ for each filter and using eqns (3) and

(4), the maximum allowed difference in resonator frequencies is 19 Hz or 0.9 ppm. Assuming differing bandwidths and using eqns. (6) and (4) the maximum allowed difference in resonator frequencies is 16.8 Hz or 0.8 ppm. The tolerance to which crystal resonators must be matched in order to satisfy the above requirement is therefore the smaller of the two, i.e. 0.4 ppm. This match in resonator frequencies is to be maintained over the operating temperature range, over the specified range of drive levels, after exposure to shock and vibration, and over the expected life of the product. Clearly, this specification is extremely stringent and will only be satisfied by the use of resonators having low aging, smooth frequency-temperature plots and moderate hysteresis performance. In short, this requirement demands high performance tracking resonators. Fig. 10 illustrates the circuit diagram of such a filter. Note the inclusion of series trimmers with each resonator to remove the room temperature offset between resonators of reference and tracking filter. The room temperature phase and amplitude match is illustrated in fig. 11. The phase match can be seen to be less than 2°, an extremely good result that is maintained to better than 4° over temperature.

FILTERS HAVING IMPROVED INTERMODULATION AND POWER HANDLING PERFORMANCE

The power handling capability of today's semiconductors is such that the crystal filter, in many instances, is the critical component when optimum intermodulation or power handling performance is required. Intermodulation performance is usually subdivided into two types defined as in-band and out-of-band intermodulation, which reflect different phenomena within the filter as well as different applications within the using system. Out-of-band intermodulation is normally specified and measured at low levels of incident power and with the test tones situated in the filter stopband such that an intermodulation product falls within the filter passband for transmission to the load. In-band intermodulation is normally specified at comparatively high power levels with the test tones and intermodulation products both

remain constant, will have 9.5 dB lower IM products than a fundamental. Allowance would have to be made in the remaining filter specifications such as insertion loss and ultimate attenuation to allow a third-overtone filter.

Increasing the electrode area will improve the IM performance. Increased electrode area will, however, often lead to degraded spurious response performance.

Increasing the filter fractional bandwidth, since the IM ratio is related to $(BW_3/Fon)^2$, will have a significant effect.

Changing crystal cut to SC or BT will offer improvement. As both the SC and BT cut give higher motional inductances than AT, there will be a trade-off with insertion loss and probably spurious response performance. Also, both of these cuts have greater temperature coefficients than the AT-cut, which may require a reduced operating range or relaxed specifications. Even so, the SC-cut in particular has been found to present the best combination of performance for some requirements.

All of the previous discussion in this section has focused on the generation of third order IM products. This next section will briefly touch upon a relationship between power handling and IM products. If, for example, the input power of the two test tones is increased by 3 dB per tone, then the third order IM products will increase by 9 dB. The additional energy present as third order IM product is provided by the two test tones. Therefore, the total power output at the two test tones will not show an increase of 3 dB, but will be somewhat less by an amount equal to the energy converted to the third order IM product. The insertion loss at the two test tones will, therefore, appear to have increased by an amount equal to the power lost to the IM products. Equation (7) can then be used to give some insight into the power handling capability of a filter and the variation of insertion loss with input power can be estimated with some minor manipulation.

situated within the filter passband. There are three major sources of non-linearities in crystal resonators which may lead to the generation of IM products: surface contamination, non-linearly coupled modes, and the anelasticity of crystalline quartz (anelasticity refers to the failure of Hooke's law) [12- 16]. Crystal surface contamination is the most prominent source of low level intermodulation (out-of-band) and is primarily determined by manufacturing variables. Given a properly manufactured resonator, the high level intermodulation (in-band) products are primarily determined by the anelastic properties of quartz and the presence or absence of non-linearly coupled modes. The high level intermodulation products are analytically predictable and can be calculated for AT, SC and BT cuts using eqn. (7). This equation is derived for a two pole Butterworth filter but has proven useful in predicting the intermodulation products of other filter types and also for filters containing more than two poles.

$$IM_r \text{ (dBc)} = K_{CUT} + 20 \cdot \text{Log}_{10} (n \cdot A_E \cdot BW_{32}^2 / Fon^2 / P_{IT}) \quad (7)$$

where:

IM_r = the ratio of generated IM product to the incident single tone power level (P_{IT}).

A_E = the resonator electrode area in square mils.

P_{IT} = the incident test tone power, per tone in mW.

K_{CUT} is a constant dependant upon the choice of cut used to fabricate the crystal resonator.

$$K_{AT} = 130, K_{SC} = 136 \text{ and } K_{BT} = 134$$

Equation (7) defines all of the variables available to the filter design engineer that allow the filter to be designed for optimum intermodulation performance. It also serves to illustrate to the user where some of the trade-offs might be when improved in-band intermodulation performance is required. Some of the more important trade-offs are listed below:

Increasing the overtone will dramatically improve IM performance. A third-overtone filter, provided all other factors

In many instances the presence of non-linearly coupled modes will disrupt this analysis. However, if a resonator design is available that is free from these modes (this is more likely to occur with an SC-cut), then this approach can be used to estimate the power handling capability of a filter. It is realized that this analysis is somewhat simplistic as it neglects thermal effects and only includes the effects of third order non-linearities. Nevertheless, the analytical tools developed to predict the third-order IM product generated by a simple two-pole filter have been found extremely useful in predicting the power handling capabilities of filters in terms of non-linear insertion loss performance as well as the IM performance of higher order filters.

SURFACE MOUNTABLE FILTERS

Currently, surface-mount filters fall into one of three categories:

1) Complete filter networks, inclusive of impedance transforming components, can be fabricated using the traditional leaded components but assembled inside an enclosure that is suitable for surface mount.

2) MDRs and resonators can be mounted in leaded or leadless surface mount packages, but without the impedance transforming circuitry required to complete the filter network.

3) The leadless MDRs or resonators of option 2) can be incorporated, inclusive of impedance transforming components, into a miniaturized package suitable for surface mount.

Examples of these three options will be given in this section.

The first option is probably the most economical but requires more volume than the second and third options. Also, as these packages will most likely be quite large when compared to other surface mount components, special attention must be given to the mechanical attachment which may require some compromise of the intent of surface mount design. Fig. 12 illustrates some of the

mounting options and table 2 reviews the advantages and disadvantages of three mounting methods -- adhesive, large area solderable ground lugs, and screws. All of these techniques offer equivalent electrical performance to that which is available from traditional through hole mounted components.

Table 2. Surface Mountable Filters Comparison Chart

Mechanical Support Mechanism	Advantages	Disadvantages
Adhesive Bonding	Spreads load over a Gives the most efficient use of volume	Needs additional cleaning procedures Strength may be process dependent Difficult to rework May have grounding problems
Large Area Grounding Terminals	Clean Has good grounding Can be reworked with care	Uses additional board area for support
Inserts or Studs	Clean Has good grounding Can be reworked with comparative ease Is the most rugged	Uses most volume for support Needs holes in board

Examples of monolithic resonator structures mounted in ceramic LCC packages are given in figs. 13 and 14. The example in fig. 13 is described in detail in [17] and is a four-pole, single-wafer device operating at a center frequency of 21.4 MHz and with a BW₃ of ±7.5 kHz. In the past, extensive use has been made of a four-pole, single-wafer configuration [18, 19], with electrodes arranged in line. This arrangement is too long to be successfully adapted

for operation at 21.4 MHz on a wafer that can be accommodated in the chosen LCC. The approach was, therefore, modified to use a folded topology in which the signal path follows a U-shaped pattern. One feature of this approach is that acoustical coupling may exist between the first and last resonators of the four-pole and may be used to improve either selectivity [20, 21] or phase [22]. For the present application, an all pole design is appropriate and this coupling is minimized by appropriate resonator design. Because the center is inactive the wafer can be mounted on a central pedestal of conductive epoxy about 0.12 mm high which also provides the ground connection. All other connections are by wire bonds. The electrical performance of a device fabricated in this manner is shown in fig. (15).

The second example is also of a four-pole mounted in a 0.45 inch square LCC. The approach used here is less elegant and employs two wafers, each based upon a circular wafer of 0.250 inch diameter with large flats ground top and bottom to allow for the installation of two wafers within a single LCC. Because the center of each wafer is active, mounting and electrical connection are conventional and use thin nickel-ribbon mounts attached to the edge of the wafer. Having two separate wafers for the MDRs gives improved spurious performance, especially if use is made of the available design flexibility which allows the use of non-identical MDRs to obtain offset spurious responses from the two filter sections.

The LCC building blocks described above offer a substantial improvement in volumetric efficiency when compared with conventional resonator packaging. These packages have been developed to incorporate resonator designs suitable for the fabrication of four- and eight-pole filters having narrow-band, intermediate-band and wideband filter structures. The result to date of these efforts is a filter packaging structure which is truly surface mount in nature and that offers an improvement in volumetric efficiency of up to 4:1 over conventional packaging. We believe this to be the first major breakthrough in filter packaging

in over a decade. All of the filters assembled using this packaging technique have matching networks included that adapt the filter natural impedance for 50 Ohm termination.

Fig. 16 illustrates a four-pole, narrow-band filter network that is assembled in the package illustrated in fig. 17. The assembly uses a double-sided substrate with the LCC mounted on the underside. This LCC contains the two MDRs. A multi-purpose brass or kovar support frame is attached to the top side of the substrate. This frame stiffens the assembly, provides an essential solid ground plane connection down each side of the assembly by means of the side flanges and divides the top side of the assembly into shielded cavities that house the inductors, chip capacitors and trimmer capacitors needed to complete the filter network. The top side of the assembly is hermetically sealed to ensure component stability. Protruding down from the substrate and adjacent to the LCC are J-leads that are co-planar with ground flanges and provide input/output connection. The performance of a 45 MHz four-pole filter assembled using the above structure is given in fig. 18. The BW_{60} of this filter is 80 kHz, the 60 dB bandwidth is 350 Khz, the ultimate attenuation is 65 dB and the insertion loss is 3.0 dB. All of these results are comparable with what could be obtained using conventional assembly techniques and a much larger package.

Fig. 19 illustrates the network of an eight-pole filter using four MDRs. This filter has been assembled in a package similar to that described above but having two LCCs on the underside and three cavities on the top side. This package is 40% smaller than a typical conventional assembly of the same filter and is illustrated in fig. 20. The performance of a filter assembled in this package and having a center frequency of 21.4 MHz is given in fig. 21 and again is comparable with that of a conventionally assembled filter.

Finally, wide-band and intermediate-band filters having the network configuration of fig. 22 are under construction. These filters have two filter sections, each with four discrete resonators. The 0.450 inch square LCC described above is modified

to accept four 0.150 inch diameter wafers. Two of these LCCs are installed in an assembly having the same dimensions as the eight-pole MDR filter of fig. 20. The center cavity of this assembly is used to house the additional inductor and trimmer required for these filters. In this assembly eight conventional resonators are replaced with two LCC assemblies to give a dramatic reduction in volume in the ratio of 4:1.

Acknowledgements:

The authors wish to thank the Naval Air Development Center for permission to publish details of work relating to miniature surface mount filters performed under contract N62269-87-C-0025 and to acknowledge the many hours of dedicated effort by R.B. Angove and R.C. Helmbold that were required to successfully produce some of the devices discussed in this paper.

References

- [1]R.C. Smythe, "HF and VHF Inductorless Filters for Microelectronic Systems," Proc. IEEE/EIA Electronic Components Conference, pp. 115-119; 1969. Reprinted in D.F. Sheahan and R.A. Johnson, editors, Modern Crystal and Mechanical Filters, pp. 301-305, IEEE Press, New York; 1977.
- [2]R.C. Smythe, "Communications Systems Benefit from Monolithic Crystal Filters," Electronics, v. 45, no. 3, pp. 48-51; January 31, 1972.
- [3]G.K. Guttwein, A.D. Ballato, and T.J. Lukaszek, "VHF-UHF Piezoelectric Resonators," U. S. Pat. 3,694,677; 26 September, 1972.
- [4]M. Berté, "Acoustic Bulk Wave Resonators and Filters Operating in the Fundamental Mode at Frequencies Greater than 100 MHz," Proceedings of the 31st Annual Symposium on Frequency Control, 1977, pp. 122-125.
- [5]J.R. Vig, J.W. LeBus, and R.L. Filler, "Chemically Polished Quartz," Proceedings of the 31st Annual Symposium on Frequency Control, 1977, pp. 131-143.
- [6]J.R. Vig, R.J. Brandmayr, and R.L. Filler, "Etching Studies on Singly and Doubly Rotated Quartz Plates," Proceedings of the 33rd Annual Symposium on Frequency Control, 1979, pp. 351-358.
- [7]R.J. Brandmayr and J.R. Vig, "Chemical Polishing in Etching Solutions that Contain Surfactants," Proceedings of the 39th Annual Symposium on Frequency Control, 1985, pp. 276-281.
- [8]R.J. Brandmayr and J.R. Vig, "Further Results on the Use of Surfactants in Chemically Polishing Quartz Crystals," Proceedings of the 40th Annual Symposium on Frequency Control, 1985, pp. 86-90.
- [9]J.R. Hunt and R.C. Smythe, "Chemically Milled VHF and UHF Resonators," Proceedings of the 39th Annual Symposium on Frequency Control, 1985, pp. 292-300.
- [10]Smythe, R.C., M.D. Howard, and J.R. Hunt, "VHF Monolithic Filters Fabricated by Chemical Milling," Proceedings of the 39th Annual Symposium on Frequency Control, 1985, pp. 481-485.
- [11]R.C. Smythe and R. B. Angove, "Chemically-Milled UHF SC-Cut Resonators," Proceedings of the 42nd Annual Symposium on Frequency Control, pp. 73-77, 1988.
- [12]Horton, W.H. and R.C. Smythe, "Experimental Investigations of Intermodulation in Monolithic Crystal Filters," Proc. 27th Annual Symposium on Frequency Control, pp. 243-245; 1973.

[13] Smythe, R.C., "Intermodulation in Thickness-Shear Resonators," Proc. 28th Annual Symposium on Frequency Control, pp. 5-7; 1974.

[14] Smythe, R.C., "Bulk Acoustic Wave Filters," in Precision Frequency Control, Vol. 1, (E.A. Gerber and A.D. Ballato, ed.s), pp. 216-219, Academic Press, New York; 1985.

[15] Howard, M.D., R.C. Smythe, and P.E. Morley, "Monolithic Crystal Filters Having Improved Intermodulation and Power Handling Capability," Proc. 39th Annual Symposium on Frequency Control, pp. 491-503; 1985.

[16] Smythe, R.C., "Crystal Filters," Ch. 7 in Miniature Filters (S.K. Mitra and C.F. Kurth, editors), Wiley-Interscience; 1989.

[17] Smythe, R.C., "An LCC Monolithic Filter," Proc. 2nd European Frequency and Time Forum, pp. 637-644; 1988.

[18] Smythe, R.C., "Some Recent Advances in Integrated Crystal Filters," Proc. IEEE, v. 67, no. 1, pp. 119-129; January, 1979. Reprinted in Piezoelectricity, (R.E. Newnham, B.V. Hiremath, and C.Z. Rosen, editors), Am. Inst. Phys.; in preparation.

[19] Smythe, R.C., "Bulk Acoustic Wave Filters," in Precision Frequency Control, Vol. 1, (E.A. Gerber and A.D. Ballato, ed.s), pp. 188-228, Academic Press, New York; 1985.

[20] R. M. Kurzrok "General Four-Resonator Filters at Microwave Frequencies," IEEE Trans. Microwave Theory and Technique, v. MTT-14, no. 6, pp. 295-296; June, 1966.

[21] A. E. Williams, "A Four Cavity Elliptic Waveguide Filter," IEEE Trans. Microwave Theory and Technique, v. MTT-18, no. 12, pp. 1109-1114; Dec., 1970.

[22] J. D. Rhodes, "A Low Prototype Network for Microwave Linear-Phase Filters," IEEE Trans. Microwave Theory and Technique, v. MTT-18, no. 6, pp. 290-301; June, 1970.

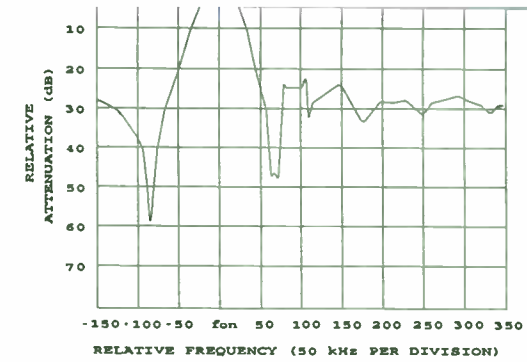


Figure 1. A Third-Overtone 45 Mhz, 2-Pole Filter.

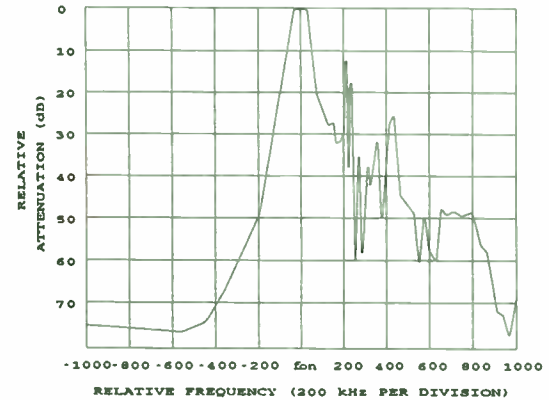


Figure 2. A Fundamental Mode 45 Mhz, 2-Pole Filter.

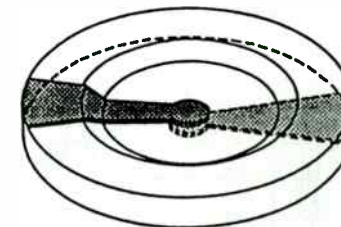


Figure 3. The Ring Supported Structure for VHF Fundamental Resonators.

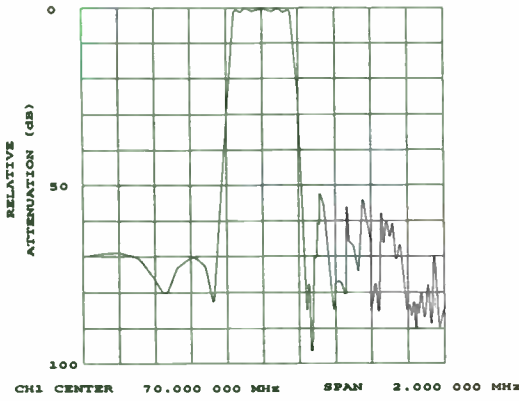


Figure 4. An 8-Pole, Intermediate-Band Filter at 70 Mhz.

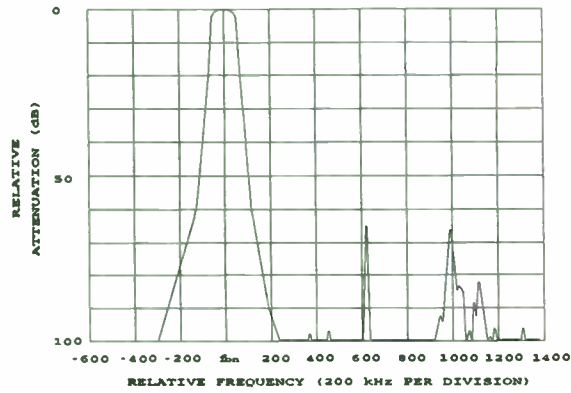


Figure 5. A 6-Pole, 3 MDR Filter at 125 Mhz.

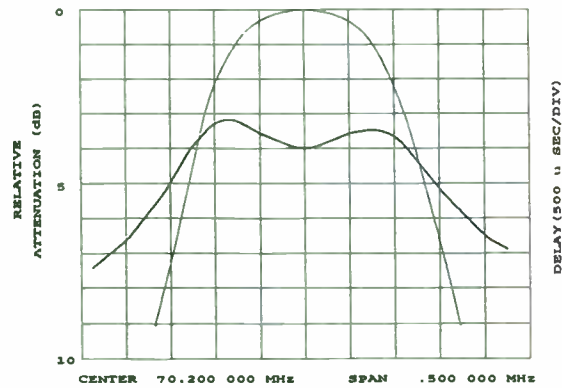


Figure 6. A 4-Pole, Transitional Filter at 70 Mhz; Passband Amplitude & Delay Response.

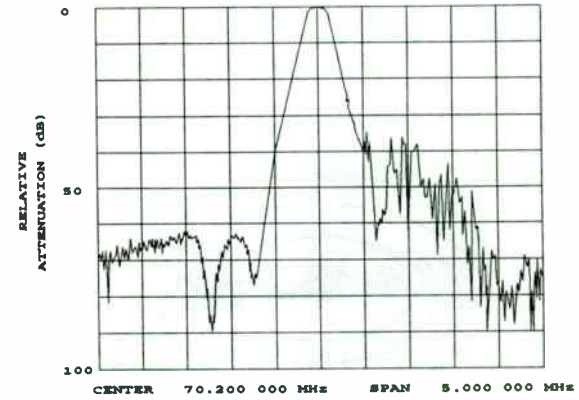


Figure 7. A 4-Pole, Transitional Filter at 70 Mhz; Stopband Response.

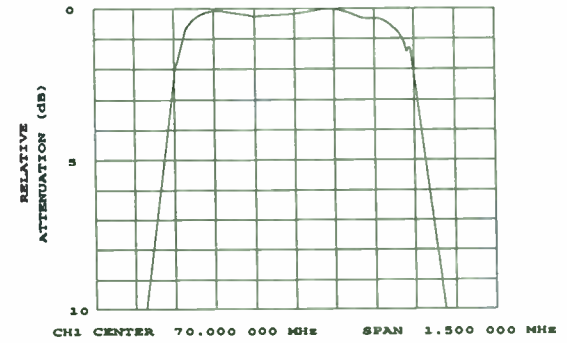


Figure 8. A 3-Pole, Intermediate-Band Filter at 70 Mhz; Passband Response.

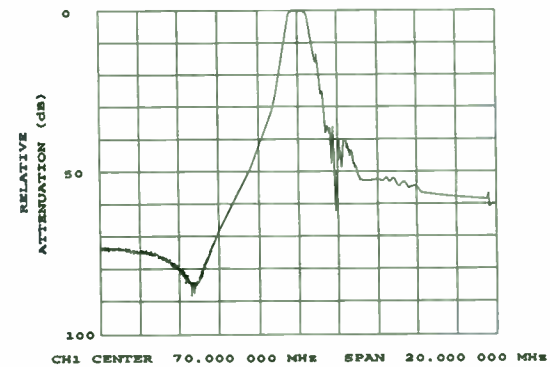


Figure 9. A 3-Pole, Intermediate-Band Filter at 70 Mhz; Stopband Response.

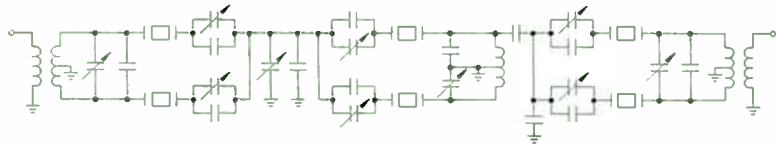


Figure 10. Schematic of an 8-Pole, Phase Matched Filter.

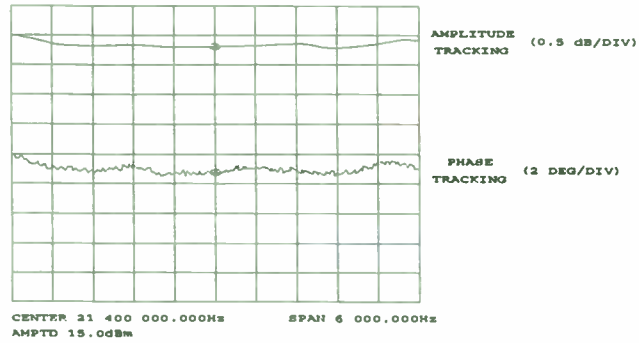
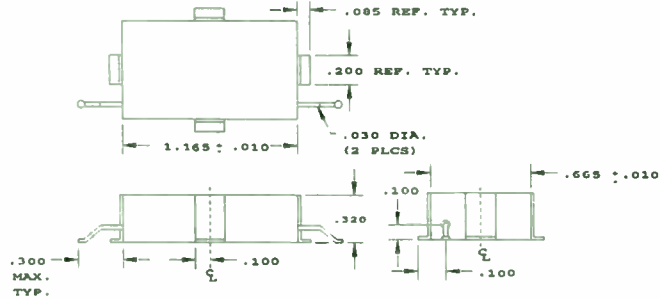
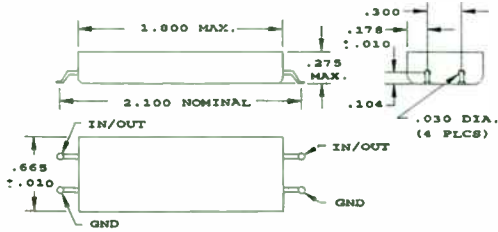


Figure 11. Phase and Amplitude Error Plot for a Matched Set.

SECURE BY SOLDERING LARGE AREA GND. TERMINALS



SECURE BY ADHESIVES



SECURE BY INSERTS

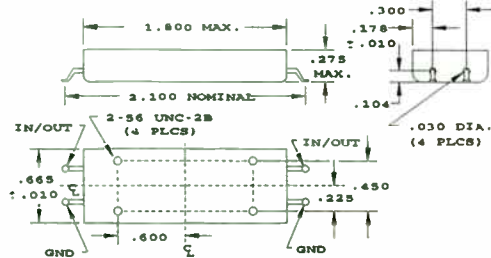


Figure 12. Mounting Styles for Conventionally Assembled Surface Mount Filters.

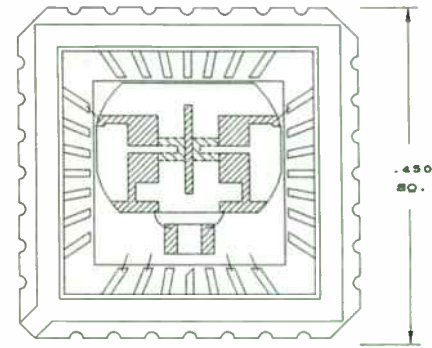


Figure 13. A 4-Pole, Single Wafer LCC Assembly.

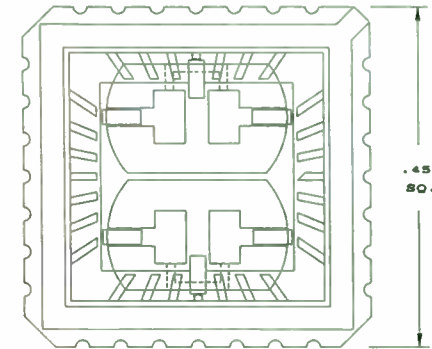


Figure 14. A 4-Pole, Dual Wafer LCC Assembly.

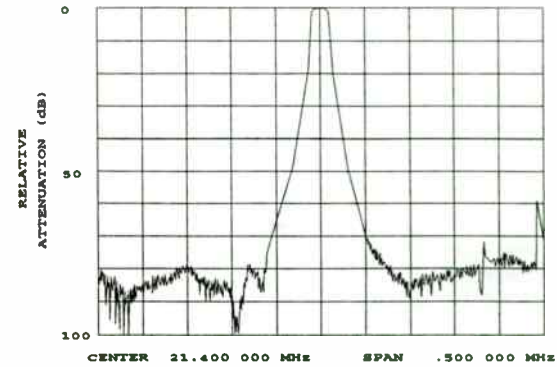


Figure 15. The Response of A 4-Pole, 21.4 Mhz, Single Wafer LCC Assembly.

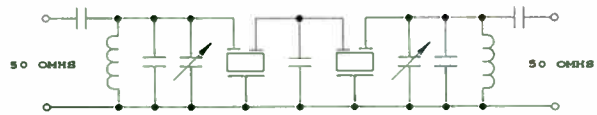


Figure 16. Schematic of a 4-Pole, 50 Ohm Terminated, Narrow Band, Surface Mountable Filter.

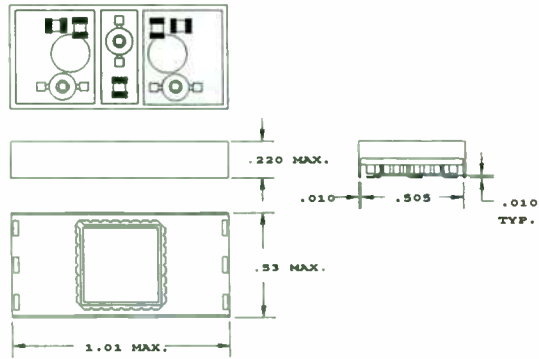


Figure 17. Mechanical Outline of a 4-Pole, 50 Ohm Terminated, Surface Mountable Filter.

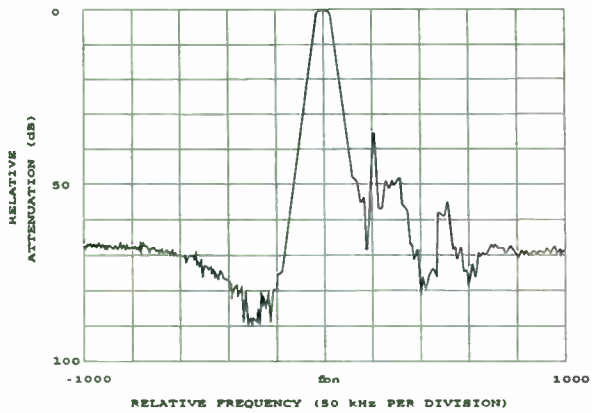


Figure 18. Response of an 4-Pole, 50 Ohm Terminated, 2 MDR, Narrow Band, Surface Mountable Filter.

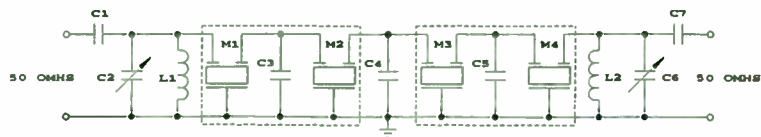


Figure 19. Schematic of an 8-Pole, 50 Ohm Terminated, Narrow Band, Surface Mountable Filter.

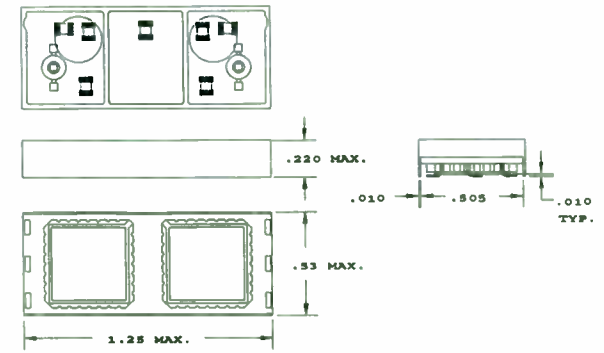


Figure 20. Mechanical Outline of an 8-Pole, 50 Ohm Terminated, Surface Mountable Filter.

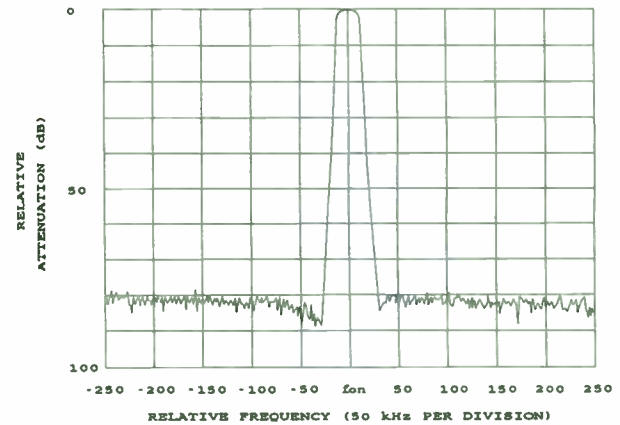


Figure 21. Response of an 8-Pole, 50 Ohm Terminated, 4 MDR, Narrow-Band, Surface Mountable Filter.

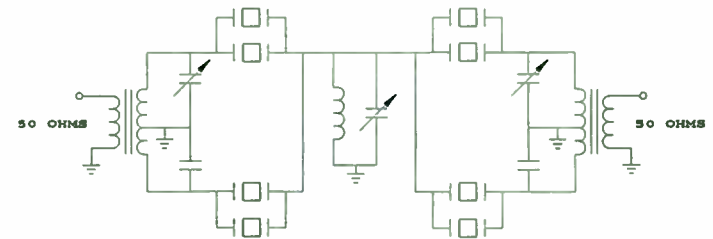


Figure 22. Schematic of an 8-Pole, 50 Ohm Terminated, Intermediate-Band, Surface Mountable Filter.

FREQUENCY CORRELATION OF QUARTZ CRYSTAL OSCILLATORS

Bruce Long
Piezo Crystal Company
100 K Street
P.O. Box 619
Carlisle, PA 17013

INTRODUCTION

Imagine a hard-pressed design engineer, up against a deadline to deliver several RF systems, each needing a stable, accurate frequency source. A quick look through a popular circuit handbook for a crystal oscillator circuit yields a likely winner and the crystals are ordered. But the handbook doesn't mention the effect of oscillator load reactance. So, the crystals are specified without a load. When the crystals are put in the circuit, they appear to be off frequency. What happened?

Quartz crystal resonators are widely used in electronics as highly stable and accurate frequency sources, but the oscillation frequency depends as much on the oscillator circuit as it does on the crystal. This presentation will clarify resonator correlation and show how correlation problems are avoided. Correlation here means correspondence between the crystal resonator frequency and oscillation frequency in a circuit.

RESONATOR PHYSICAL DESCRIPTION

A quartz crystal resonator is simply a circular piece of quartz with electrodes plated on both sides, mounted inside an evacuated enclosure. But resonator design demands knowledge of mechanics, acoustics, wave motion, piezoelectricity and electronic circuit theory. Quartz is ideal for resonators because it is hard yet flexible, dimensionally stable, non-conductive, and most important, piezoelectric.

The piezoelectric effect links the mechanical and electrical properties of the resonator. Electrode voltage causes mechanical movement. Likewise, mechanical displacement generates an electrode voltage. Therefore a crystal mechanical resonance can be treated as if it were electrical in nature. Physical displacement of an operating resonator is minuscule, generally only a few atomic diameters, but tremendous mechanical forces are in play. For example, the surface acceleration of a 50 MHz third overtone crystal exceeds five million gravities.

Making a resonator starts with slabs of quartz sawed from raw quartz crystal stock. Both natural quartz mined from the earth and cultured quartz grown artificially in high pressure autoclaves are used. The slabs are cut into squares, rounded, and ground flat. These thin pieces of unfinished quartz are called blanks. Thin blanks have high resonant frequencies, but they must remain thick enough to withstand grinding without excessive breakage. For this reason, the upper limit for mechanically ground fundamental mode resonators is approximately 35 MHz. These paper thin quartz blanks are too fragile to withstand further grinding.

High frequency resonators are made using overtone responses. This extends the upper frequency limit beyond 200 Mhz.

The frequency tolerance of a finished resonator can be as precise as plus or minus one part per million, making exact control of blank thickness critical. Grinding must stop the moment the correct thickness is reached. Fortunately, the piezoelectric effect makes possible continuous measurement of the blank thickness. Vibration occurs as abrasive slides across the crystal. That, in turn, excites the crystal resonance generating radio frequency energy - energy that is detected and measured by a simple shortwave receiver.

Polishing removes small scratches left by grinding and leaves the surface ready for plating. The electrode mass loads the resonator active region and that lowers the crystal resonant frequency. To compensate, blanks are ground for resonance slightly above the desired frequency and set exactly on frequency by adjusting the thickness of the electrode. A 10 MHz resonator shifts 5 to 7 kHz during the plating process and the amount of shift is roughly proportional to the resonator frequency. That means a 100 MHz resonator moves about 50 to 70 kHz. During the plating process, the resonator is connected to a test oscillator and the resonant frequency is monitored with a frequency counter. Plating stops the instant the correct frequency is reached.

RESONATOR ELECTRICAL DESCRIPTION

The crystal's mechanical resonance appears as a very high Q electrical resonance with the equivalent circuit shown in Figure 1. Components C, L and R make up a series resonant circuit representing the blank's mechanical resonance. Resistor R represents energy lost in the crystal and its mounting structure. The capacitance C1 varies with crystal elasticity and the crystal mass determines the inductance L. These parameters are sometimes called the motional inductance and capacitance, highlighting their mechanical origins. The electrodes also form the plates of a capacitor with a quartz dielectric. This capacitance, represented by C_0 , varies with the size of the electrodes. Resonator electrical parameters are measured with a crystal impedance bridge, a vector voltmeter, or a network analyzer. The instrument's frequency resolution must be good since circuit impedance varies sharply with frequency.

Figure 2 shows how resonator reactance changes with frequency. At F_s , the series resonant frequency, the motional capacitance and inductance cancel leaving a small capacitive component from C_0 . Resonator reactance goes to zero at a slightly higher frequency. Here the effect of C_0 is cancelled by a small inductive component coming from the resonator motional branch and the impedance is purely resistive. In practice, the series resonant frequency and the resonator zero reactance point are quite close together. Confusion comes when the distinction between the two is ignored.

Above series resonance, the motional inductance and capacitance partially cancel, leaving a high Q equivalent inductor which, when combined with the electrode capacitance C_0 , create the parallel resonant response at R_p . The parallel resonant frequency is strongly affected by circuit loading. External load capacitance adds to C_0 lowering the parallel resonant frequency. The following formulas give the resonant frequencies:

$$F_s = \frac{1}{2\pi\sqrt{LC}} \qquad F_p = F_s \left[\frac{C_0}{1 + 2(C_0 + C_{\text{external}})} \right]$$

Resonator impedance changes drastically between series and parallel resonance. At series resonance the crystal impedance is very low, limited only by the loss resistor R . But at parallel resonance - only a few parts per million higher in frequency - the impedance is quite high. The steep phase slope that accompanies the rapid impedance transition accounts for the frequency stability of quartz crystal oscillators.

Which resonance point, series or parallel, controls the oscillation frequency? That depends on the oscillator.

CONDITIONS FOR OSCILLATION

Resonators are passive. They do not oscillate without additional circuitry and a source of energy. A resonator, placed as a feedback element around an amplifier, makes an oscillator. The amplifier replaces energy lost in the resonator. The resonator

controls the frequency of oscillation.

Two conditions must exist to start and sustain oscillations. First, the phase shift around the loop must be an integer multiple of 360 degrees. This guarantees that successive cycles add constructively. Second, the sum of gain and loss around the loop must equal or exceed one. During start-up, the loop gain is more than one and the oscillation amplitude grows exponentially. However, no system can sustain unlimited exponential growth. Ultimately, the amplifier is driven into gain compression, which stabilizes the gain at a value just sufficient to overcome resonator losses. Clipping limits gain in most oscillators, but some precision oscillators use separate automatic gain control (AGC) circuitry or clipping diodes. Oscillation conditions, known as the Barkhausen criteria, are named for the German scientist who first presented them.

RESONATOR OPERATION POINT

Crystal oscillator circuits traditionally are labeled as parallel or series resonant, with the crystal specified accordingly. But a close look at oscillator theory shows this bit of conventional wisdom is too simple. Oscillators operate on the point of the crystal reactance slope that satisfies the Barkhausen criteria. This point coincides with the crystal series resonance point only if the phase shift in the rest of the circuit sums to a multiple of 360 degrees. In most oscillator circuits the crystal operates in the inductive region between series and parallel resonance.

CRYSTAL OSCILLATOR CIRCUITS

Figure 3 shows the basic equivalent circuit common to the Pierce, the Colpitts and the Clapp oscillators. The only difference between them is the location of the grounded node. Performance differences are due to changes in the amplifier input and output impedance and to the varying effect of stray capacitance as the ground node is moved. The Colpitts oscillator is used at low to medium frequencies, and is replaced by the Pierce at higher frequencies. All three circuits are parallel mode oscillators with the crystal in each acting as an equivalent inductor. These oscillators operate significantly above the crystal series resonant frequency. Therefore crystals used in these circuits are specified for the load capacitance of the oscillator.

In the Pierce circuit, the feedback path around the common emitter amplifier is obvious, starting at the transistor collector and returning to the amplifier input through the crystal. The Colpitts oscillator, in contrast, is a little obscure. Gain comes from an emitter follower amplifier. Capacitors C1 and C2, along with the crystal equivalent inductor, make up a tapped tuned circuit, which matches the low impedance amplifier output to the high impedance amplifier input. The Clapp circuit is very similar in this respect, except a common base amplifier is used.

The input impedance of a parallel resonant oscillator has two parts - a negative resistance coming from combined amplification and positive feedback, and a capacitive reactance

coming mostly from feedback capacitors C1 and C2. The former cancels resonator losses, allowing sustained oscillation. The latter makes up the oscillator load capacitance. Figure 4 shows a formula giving the input impedance of an ideal Colpitts oscillator, with the transistor represented as an ideal voltage controlled current generator. Capacitors C1 and C2 dominate the imaginary part of the expression but appear in the real portion. This equation should be used with caution because it assumes linear transistor operation. It is inaccurate for oscillators that saturate the transistor during part of each cycle. It also fails to account for stray capacitance and transistor phase shift.

SERIES MODE OSCILLATORS

In a series mode oscillator the crystal resonator operates at or near its zero reactance point. Figure 5, from page 161 of reference 3, shows a series mode oscillator consisting of two CMOS logic inverters. Bias resistors place the gates in the linear region. Load resistor RL sets the resonator loaded Q. This circuit works best at low frequencies, where the gate propagation delay can be safely neglected. At low frequencies the phase shift through the gates totals 360 degrees - 180 degrees per inverter. Zero phase shift across the feedback path meets the Barkhausen criteria so this circuit oscillates near the resonator zero reactance point.

At higher frequencies gate propagation delays start showing an effect. As the phase shift in the forward path moves past 360

degrees, the oscillation frequency drops below series resonance into the capacitive region of the crystal reactance curve. Here the crystal acts as an equivalent capacitor, forming an RC phase lead network with resistor R_L , which compensates for the gate delay. This hurts frequency stability because the resonator reactance slope is not as steep here as in the inductive region and because gate propagation delay changes with temperature. Operation below series resonance does not follow good engineering practice and such oscillators are uncommon.

Another series mode oscillator, the common collector Butler, is shown in Figure 7. It strongly resembles the Colpitts parallel resonant oscillator, but the resonator is replaced with an inductor. The crystal goes between the junction of C_1 and C_2 and the transistor emitter.

FREQUENCY ADJUSTMENT

The frequency of a crystal oscillator is easily adjusted by adding series reactance. Reactance in series with the crystal slides the operating frequency along the reactance curve -- down for an inductor -- up for a capacitor, but the adjustment range is limited. Remember the crystal motional inductance is very large. Conventional inductors of reasonable value are small by comparison and have a proportionately smaller effect on frequency. Indeed, quartz crystal oscillators are highly stable because circuit reactance is swamped by the high Q resonator.

SPECIFYING A CRYSTAL RESONATOR

Crystal oscillator designers face a dilemma. How to determine the crystal load impedance? The iterative approach is one solution. It goes:

Make an (educated) guess.

Order a sample crystal.

Try it in the oscillator.

Note the frequency offset.

Try to pull the crystal on to frequency.

Change the crystal specification.

Order another set of crystals.

Many crystal users find themselves in this situation and eventually they succeed.

Alternately the customer can do two things: provide the crystal vendor a copy of his oscillator and request the vendor use it during the electrode plating process. A correlation oscillator reduces uncertainty, but adds logistical difficulties and often is not practical.

Another approach involves breadboarding an oscillator and measuring its load impedance using one of two methods. The first is a simple, direct method. Connect the oscillator to a network analyzer, or RF impedance analyzer, and read the load impedance directly. Easy, but it has a serious limitation. Because the oscillator is not operating, the measurement fails to account for impedance shifts that occur during non-linear transistor operation. Still a "ballpark" measurement is obtained, which might be good enough in some situations. Later in this paper

there is an example of a direct measurement, taken for a test oscillator with a known load impedance so accuracy could be assessed.

The second method of oscillator load measurement is an indirect method which replicates actual oscillator operating conditions. Replace the crystal with a simple discrete component LCR equivalent circuit. For a parallel resonant oscillator, the circuit can be a single variable inductor. Adjust the inductor for the desired oscillator frequency, remove it from the circuit, and measure the reactance on an impedance bridge or a network analyzer. The inductive reactance shows the point on the crystal reactance slope at which the circuit oscillates. Equating inductive and capacitive reactance at resonance gives the load capacitance for the crystal. For accuracy, the crystal loss resistance R also is represented, keeping in mind the inductor losses provide part, if not all, of this element. Avoid inductors with self-resonant frequencies close to the oscillator frequency. Self-resonance magnifies inductance at the expense of Q . Measurement accuracy is important, but precision adjustable inductors are rare. A series resonant circuit operating above series resonance and using a precision variable capacitor as the adjustable element, is a good substitute.

COMPUTER MODELING

Computer modeling is less helpful than expected. Crystal oscillators are hard to model accurately for two reasons. First, oscillators are non-linear circuits. Oscillation amplitude

builds until some non-linear mechanism, usually clipping or gain saturation, reduces the loop gain to one. The exact stabilization point is difficult to predict. Clipping often is accompanied by large and abrupt impedance changes which dramatically affect circuit phase shifts. Model accuracy is poor unless the final operating conditions are pinpointed.

Second, all crystal resonators have Q factors as large as ten to twenty-thousand, with Q factors for precision resonators exceeding one million. The loop time constant can be a large fraction of a second. Time domain modeling programs easily accommodate circuit non-linearities, but they do so by calculating circuit parameters on a cycle-by-cycle basis. Running enough cycles to get out of the start-up transient and into the steady-state solution can take a lot of computer time. A good guess for initial conditions or a harmonic balance approach can help, but breadboarding remains a good approach due to the time and effort needed to accurately model a crystal oscillator.

EXPERIMENTAL RESULTS

This experiment is designed to show circuit loading effects in quartz crystal oscillators. Twelve third-overtone, 10 MHz, AT cut resonators are used, nearly identical except for the load capacitance used to set the resonators on frequency. Crystal frequency is defined as the zero reactance frequency for the resonator connected to an external series load. Three crystals resonate at 10 MHz with no external load capacitance. The others

are plated onto frequency connected to 20, 40, or 100 pF series load capacitors. Proportionately controlled ceramic heaters regulate resonator temperature during testing. Typical crystal parameters are: C_0 - 4.4 pF, C_1 - 2.36 femto-farads, L - 107 mH, R - 15 ohms and Q - 460,000. Table 1 lists crystal loaded and un-loaded resonant frequencies.

The first test circuit shown in Figure 6 is an unembellished Colpitts oscillator, with voltage regulation and an inexpensive hybrid buffer amplifier. A resistor couples the buffer amplifier to the oscillator. The only unorthodox feature is the unbypassed emitter resistor, which eases crystal current adjustment. It is selected to match the circuit crystal current with the current used to test the crystals. The five ohm resistor in the crystal ground leg provides a simple way to measure the current. The resistor has no measurable effect on oscillator frequency or amplitude.

As a first step, capacitor C1 is adjusted until crystal number 9 oscillates on its specified frequency. Because the load impedance of crystal number 9 is 40 pF, I chose a value for C1 which, when combined with C2, totalled approximately 40 pF. Knowing I neglected the effects of stray capacitance and transistor base capacitance, I planned to reduce C1. After several iterations of soldering iron optimization, excellent correspondence between the crystal and the oscillator frequency is achieved with a C1 value equal to 15 pF. At this point the oscillator load reactance has to be very close to 40 pF although C1 is much smaller than I expected.

The other 40 pF crystals, numbers 7 and 8, also oscillate close to their marked frequencies, but the crystals plated to frequency with loads other than 40 pF are spread across nearly 50 ppm. The 100 pF load and no-load crystals run above their marked frequencies; the 20 pF load crystals run below.

The crystal in the test oscillator acts as an equivalent inductor. So crystal current should lag behind crystal voltage. Measurements show this is the case. Figure 6 shows voltage and phase measurements at four nodes taken with a HP-8405A vector voltmeter using the transistor base node as a reference. As expected, the voltage across the crystal current sensing resistor follows the crystal voltage.

Also notice the phase shift across the transistor. For an ideal emitter follower amplifier, the input and output voltages are in phase. This amplifier, however, has significant internal phase shift at 10 MHz. One way to represent this effect, short of a full-fledged transistor model, is to treat beta as complex and assign to it a frequency dependant magnitude and a phase.

OSCILLATOR INPUT IMPEDANCE

To measure the oscillator input impedance, I connected a HP-4193A vector impedance meter in place of the crystal and the current sensing resistor. Table 2 lists the results. The Colpitts circuit generates a negative input resistance across a wide range of frequencies. At 10 MHz the input impedance is -26.2 -j324 ohms. An oscillator will start as long as the sum of the crystal loss resistance R and the real part of the oscillator

input impedance is less than zero. The imaginary part should correspond to the oscillator load reactance, but it doesn't match very well. This discrepancy arises because the transistor is not saturated during measurement as it is during oscillation.

Next I replaced the crystal with a toroidal inductor. A 40 pF load reactance amounts to $-j398$ ohms at 10 MHz. At resonance, the crystal impedance has the same magnitude, but the opposite sign. I wound an inductor on a toroidal core and adjusted it by spreading and compressing turns to get as close to $+j398$ ohms as possible while measuring reactance with a HP-4193A vector impedance meter. I got within two ohms of my target impedance and secured the windings with adhesive. The impedance measurement has to be taken at the actual operating frequency to account for the effects of inductor self resonance. Measuring impedance at 10 kHz, as is common in many LCR impedance bridges, gives poor results. Exchanging the crystal in the test oscillator with this inductor and a dc blocking capacitor transforms the Colpitts crystal oscillator into a Colpitts LC oscillator. The frequency stability is poor, but the circuit does oscillate within 50 kHz of 10 MHz without adjustment.

It should be possible to insert a crystal in the oscillator feedback path, converting the LC oscillator back to crystal control. And if a no-load series resonant crystal is used, the oscillator should oscillate on the specified crystal frequency. This series mode oscillator, shown in Figure 7, is known as a Butler crystal oscillator in honor of its inventor. Crystals, plated to frequency with no-load, run on frequency while the

100 pF, 40 pF, and 20 pF load crystals run progressively lower. Frequency correlation for crystal numbers 4 through 10 appear twice. The crystal parameter test system measures both the loaded and unloaded crystal resonant frequencies. All 12 test crystals oscillate within 1.5 ppm of their no-load series resonant frequencies. Also, the voltage phase shift across the crystal is nearly zero degrees. The eight degrees of phase lag present results from a RC phase lag network, consisting of C2 and the crystal resistance.

In summary, I built a Colpitts test oscillator and adjusted it so the 40 pF load crystals ran on frequency. Then I substituted an inductor for the crystal, creating a Colpitts LC oscillator. Breaking the feedback path and inserting a crystal restored the oscillator to crystal control. Now the no-load crystals ran on frequency.

CONCLUSION

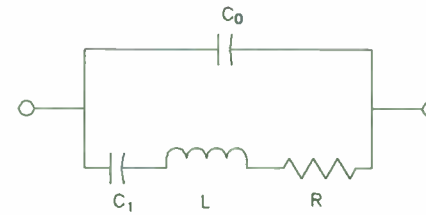
Crystals and oscillators must be designed with each other in mind.

ACKNOWLEDGEMENTS

I would like to thank the management of Piezo Crystal Company for their support of this effort. Individuals who contributed include Tim Wickard, who provided the test crystals, Denna Menges, who typed the draft, and Ron Trace, who created the drawings.

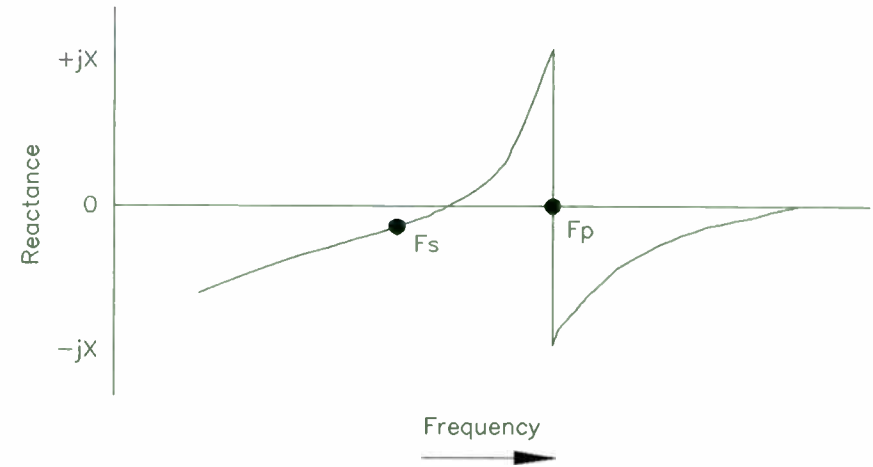
REFERENCES

- 1) Driscoll, Michael M., Low Noise Oscillator Design Using Acoustic and Other High Q Resonators, Tutorial presented at the 44th Annual Frequency Control Symposium, Baltimore, Maryland, May, 1990
- 2) Frerking, Marvin E., "Crystal Oscillator Design and Temperature Compensation", New York, Van Nostrand, 1970.
- 3) Matthys, Robert J., "Crystal Oscillator Circuits", page 161, New York. Wiley, 1983.
- 4) Parzen, B., Ballato, A., "Design of Crystal and Other Harmonic Oscillators", New York, Wiley, 1983.



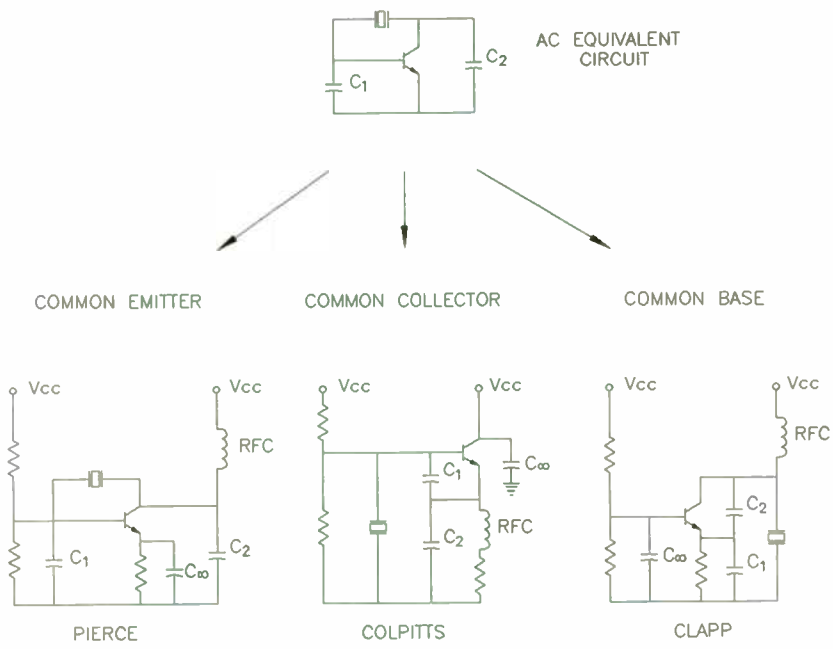
Crystal Resonator Equivalent Circuit

FIGURE 1



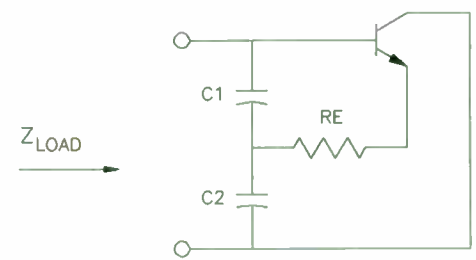
Resonator Reactance Frequency Function

FIGURE 2



Common Oscillator Configurations

FIGURE 3



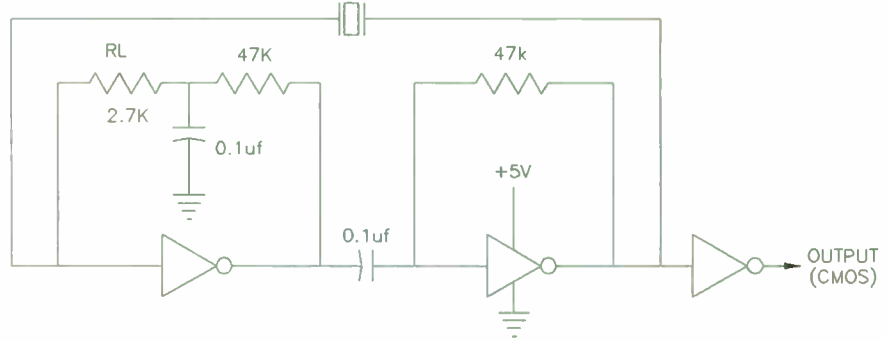
$$Z_{LOAD} = Z_1 + Z_2 + \frac{Z_1 Z_2}{R_E + 1/g_m}$$

$$Z_{LOAD} = \frac{1}{j\omega C_1} + \frac{1}{j\omega C_2} - \frac{1}{(\omega^2 C_1 C_2)(R_E + 1/g_m)}$$

From Reference 1

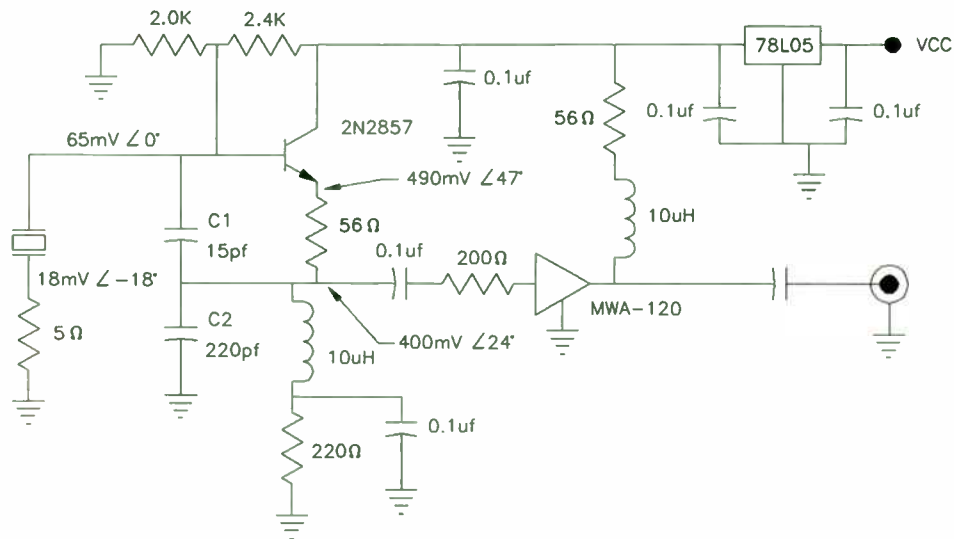
Colpitts Load Impedance

FIGURE 4



CMOS Series Mode Crystal Oscillator

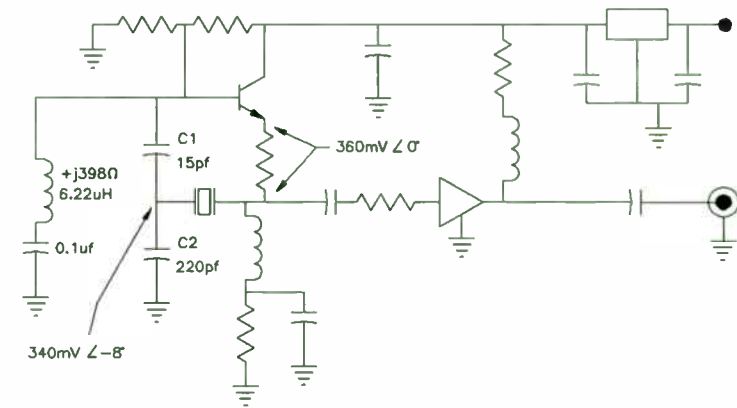
FIGURE 5



* C1 ADJUSTED TO PUT CRYSTAL #9 ON FREQUENCY
CRYSTALS TESTED IN ORDER OF INCREASING LOAD REACTANCE

CRYSTAL	CRYSTAL FREQUENCY	RESONANT LOAD CAPACITANCE	OSCILLATOR FREQUENCY	DEVIATION
01	9,999,993 Hz	NONE	10,000,264	+27ppm
02	10,000,031 Hz	NONE	10,000,293	+26ppm
03	10,000,061 Hz	NONE	10,000,329	+27ppm
10	10,000,003 Hz	100pf	10,000,161	+16ppm
11	10,000,045 Hz	100pf	10,000,197	+15ppm
12	10,000,029 Hz	100pf	10,000,176	+15ppm
07	10,000,042 Hz	40pf	10,000,045.0	-0.05ppm
08	10,000,028 Hz	40pf	10,000,031.4	+0.34ppm
* 09	10,000,017 Hz	40pf	10,000,016.5	+0.30ppm
04	10,000,052 Hz	20pf	9,999,868	-18ppm
05	9,999,983.8 Hz	20pf	9,999,786	-20ppm
06	10,000,030 Hz	20pf	9,999,845	-19ppm

Colpitts Test Oscillator
FIGURE 6



CRYSTAL	CRYSTAL FREQUENCY	RESONANT LOAD CAPACITANCE	OSCILLATOR FREQUENCY	DEVIATION
01	9,999,993.2 Hz	NONE	10,000,003.6 Hz	+1.4ppm
02	10,000,031 Hz	NONE	10,000,037.1 Hz	+0.61ppm
03	10,000,061 Hz	NONE	10,000,061.6 Hz	+0.06ppm
10	9,999,891.3 Hz	NONE	9,999,889.0 Hz	-0.23ppm
11	9,999,932.2 Hz	NONE	9,999,937.2 Hz	+0.50ppm
12	9,999,916.9 Hz	NONE	9,999,921.2 Hz	+0.43ppm
07	9,999,778.6 Hz	NONE	9,999,782.0 Hz	+0.34ppm
08	9,999,762.1 Hz	NONE	9,999,771.0 Hz	+0.89ppm
09	9,999,753.1 Hz	NONE	9,999,758.4 Hz	+0.53ppm
04	9,999,498.0 Hz	NONE	9,999,568.7 Hz	+0.30ppm
05	9,999,498.0 Hz	NONE	9,999,498.2 Hz	+0.02ppm
06	9,999,549.2 Hz	NONE	9,999,553.4 Hz	+0.42ppm
10	10,000,003 Hz	100pf	9,999,891.3 Hz	-11.2ppm
11	10,000,045 Hz	100pf	9,999,932.2 Hz	-11.3ppm
12	10,000,029 Hz	100pf	9,999,916.9 Hz	-11.2ppm
07	10,000,042 Hz	40pf	9,999,782.0 Hz	-26.0ppm
08	10,000,028 Hz	40pf	9,999,771.0 Hz	-25.7ppm
09	10,000,017 Hz	40pf	9,999,758.4 Hz	-25.8ppm
04	10,000,052 Hz	20pf	9,999,568.7 Hz	-48.3ppm
05	9,999,983.8 Hz	20pf	9,999,498.2 Hz	-48.6ppm
06	10,000,030 Hz	20pf	9,999,553.4 Hz	-47.7ppm

Butler Test Oscillator
FIGURE 7

TABLE 1

TEST CRYSTAL FREQUENCIES

CRYSTAL	NO-LOAD RESONANT FREQUENCY (Hz)	LOAD CAPACITANCE	LOADED RESONANT FREQUENCY (Hz)
01	9,999,993.2	NONE	
02	10,000,031	NONE	
03	10,000,061	NONE	
04	9,999,565.7	20pf	10,000,052
05	9,999,498.0	20pf	9,999,983.8
06	9,999,549.2	20pf	10,000,030
07	9,999,778.6	40pf	10,000,042
08	9,999,762.1	40pf	10,000,028
09	9,999,753.1	40pf	10,000,017
10	9,999,891.3	100pf	10,000,003
11	9,999,932.2	100pf	10,000,045
12	9,999,916.9	100pf	10,000,029

TABLE 2

Colpitts Test Oscillator Input Impedance

FREQUENCY	INPUT IMPEDANCE		EQUIVALENT CAPACITANCE
	POLAR	RECTANGULAR	
6.00 MHz	680 $\angle -71.0^\circ$	221 -j643	41pf
7.00 MHz	562 $\angle -80.9^\circ$	88.9 -j554	41pf
8.00 MHz	462 $\angle -87.5^\circ$	20.1 -j462	43pf
9.00 MHz	385 $\angle -87.5^\circ$	-11.4 -j385	46pf
10.00 MHz	326 $\angle -94.6^\circ$	-26.2 -j324	49pf
11.00 MHz	281 $\angle -96.4^\circ$	-31.3 -j279	52pf
12.00 MHz	245 $\angle -97.4^\circ$	-31.5 -j243	55pf
13.00 MHz	218 $\angle -98.0^\circ$	-30.3 -j215	57pf
14.00 MHz	195 $\angle -98.3^\circ$	-28.2 -j193	59pf
15.00 MHz	177 $\angle -98.4^\circ$	-25.9 -j175	60pf

New Method of Linear Amplitude Modulation

by

Li Minggang, Gan Liangcai, Zhang Suwen
Department of Radio Information Engineering
Wuhan University
Wuhan, Hubei 430072
The People's Republic of China

Abstract

Deriving from the conventional non-linear modulation method, this paper suggests a linear amplitude modulation method with mini-signals. This method exhibits a wide range of modulation. The analysis and the experiments show that the method can be applied to any oscillators.

1. Introduction

It is known that the high level amplitude modulation can be classified as the collector(anode) amplitude modulation and the base(control grid) amplitude modulation. The former whose modulation index can approach unity needs some large power signal source, the later, though can be modulated with the small power source, its whole set efficiency is low. Both of them use the non-linear character of the transistor for modulation.

This paper introduces a method of using the linear character of elements. It uses the small power modulating signal source with the advantage of the above two modulation methods to do the amplitude modulation.

2. Basic Principles

According to the principles of the oscillator, while a positive feedback transistor oscillator works, if changes are made in the circuit gain, the amplitude of the oscillating wave will change

correspondingly. By this, we can assume that if the gain of the circuit is controlled by a modulating signal, the amplitude of the output signal must be changed in correspondence with the modulating signal, only if the change can, in general, satisfy the linear relation that the amplitude modulation requires. Therefore, the problem leads to how we can control the gain of oscillator circuit to make it meets the linear relation with the modulation requires.

In any transistor oscillator circuit, when a modulating signal V_{Ω} is added to the base, the dynamic resistance between the base and the emitter will be changed correspondingly, so that the gain will change, yet the change of modulating signal V_{Ω} related to the oscillator output voltage V_o is still non-linear. An amendment can be made as negative feedback branch is introduced between the output and the input. The theoretical study is as follows: Suppose the positive feedback branch in the transistor oscillator is broken, the circuit stops oscillations, the gain of the amplifier is [2]

$$K = \frac{A}{R + r_e} \quad (1)$$

where A and R are constants.

r_e , the dynamic resistance between the base and the emitter after the modulating signal and the negative feedback between the output and input are added. Under ambient temperature

$$r_e = \frac{26}{I_e} \quad (2)$$

where I_e is the emitter current, in mA.

Assuming

$$I_e = I_{eQ} + MV_n - NV_o \quad (3)$$

where I_{eQ} is the static emitter current when the amplifier loop is open;

V_n is the modulating signal voltage;

V_o is the output signal voltage;

M is a constant which represents the emitter current produced by the modulating signal voltage V_n as V_n is 1V;

N is a constant which represents the emitter current produced by the output voltage V_o as V_o is 1V after the negative feedback branch is introduced.

Therefore (1) can be written as

$$K = \frac{A}{R + \frac{26}{I_e}} = \frac{A(I_{eQ} - MV_n - NV_o)}{R(I_{eQ} - MV_n - NV_o) + 26} \quad (4)$$

Close the positive feedback branch and adjust the feedback to make it oscillating. When the oscillation is stable, i.e. the phase-amplitude balanced condition is satisfied, $KF = 1$.

Assuming the initial gain is K_0 , thus

$$V_o = \frac{I_{eQ}}{N} - \frac{26K_0}{N(A - K_0R)} + \frac{M}{N}V_n \quad (5)$$

where the former two terms are constants, the third term shows that V_o and V_n varies with each other correspondingly.

Evidently, equation (5) expresses that amplitude V_o , the output signal of the oscillator, and V_n , the input modulating signal in oscillating circuit are linearly correlated.

If $V = V \cos \omega_m t$, substitute into (5), we have

$$V_o = \frac{I_{eQ}}{N} - \frac{26K_0}{N(A - K_0R)} + \frac{M}{N}V_m \cos \omega_m t \quad (6)$$

Equation (6) is sinusoidal envelope modulation. The condition

for equation (6) to be valid is that the positive bias voltage of the transistor $V_{be} = 0.1V$. This can be fulfilled by the transistor oscillator even if it at class C operation. Here, the critical condition is that after a negative feedback is introduced between the output and the input of the oscillator, we can make the emitter current of the transistor to satisfy equation (3). If M and N are selected to make $MV_n - NV_o \approx 0$, that is to say, to introduce a negative feedback branch to keep the emitter current I_e of the transistor stabilizing and guarantee a stable dynamic resistance between the base and the emitter. Therefore, it eliminates the non-linear influence of the modulating signal to the output amplitude of the oscillator and realizes the linear amplitude modulation.

It should be noted, as the negative feedback is introduced between the output and input of transistor, providing the negative feedback is proper, no influence can be made to the oscillating circuit. This mode of modulation can be applied to any oscillating circuit.

3. Experiment and Discussion

Based on the above analysis, the mode of modulation can be applied to any transistor oscillating circuit. For the sake of simplicity, only RC phase-shift oscillator, Seiler oscillating circuit and crystal oscillator are treated.

As in Fig.1, its oscillating frequency is $f_o = \frac{1}{2\pi\sqrt{6RC}}$. Open loop gain $K_0 = 29$ in BG1 and BG2. Operational amplifiers A1 and A2 is the emitter follower. From equation (1), we have [2]

$$K = \frac{-\alpha RL}{(RB + r_{bb'}) (1 - \alpha) + r_e}$$

take $\alpha = 0.995$, $R_L = 1000 \Omega$, $(R_E + r_{BE})(1-\alpha) = 12 \Omega$, we have [2]

$$K = \frac{995}{12 + r_e}$$

$$I_{eQ} = \frac{V_{CC} - V_{be}}{R_{b1} + R_b + R_e(1 + \frac{1}{\alpha})} = 5.1 \text{mA}$$

$$I_e = 5.1 + \frac{K V_0}{1 - K V_0}$$

take $M = N = 1.5 \text{mA/V}$, substitute into equation (5), we have

$$V_0 = 3.4 - (9.11 \times 10^{-1}) + V_{\Omega} = +2.49 + V_{\Omega} \quad (7)$$

Equation (7) predicts the linear relation between the output amplitude V_0 and the modulating signal V_{Ω} as in Fig.1 with a direct current stabilized voltage source as the modulating signal data in Fig.2 can be observed. By applying the method of LMS, a curve of

$$V_0 = 0.775V_{\Omega} + 2.43$$

is obtained. If the modulating voltage V_{Ω} is -3.12 , the output amplitude V_0 is 0V , the modulation index reaches unity. The theoretical prediction differs from the surveyed curve to a minimal value. Because the parameters of the circuit are all estimated, the conclusion derived from equation (7) coincides well with the actually surveyed.

Fig.3 is a Seiler oscillator experiment circuit with a working frequency $f_0 = 2.4 \text{MHz}$. Operational amplifiers A_1 and A_2 form an output-input negative feedback branch, where A_1 is the attenuator and A_2 is the emitter follower. In the same way, a direct current stabilized voltage is used as the modulating signal source, the data surveyed are shown as in Fig.4. Again an estimation and calculation by applying the method of LMS, a curve of

$$V_0 = 0.342V_{\Omega} + 1.08$$

is obtained. From the experiment, it is known, if V_{Ω} is -3.17V , the output voltage V_0 is 0V . Obviously, the modulation index can reach unity.

Fig.5 is a crystal oscillator experiment circuit, $f_0 = 6\text{MHz}$. A_1 is the attenuator and A_2 is the emitter follower. We use a sinusoidal signal with a frequency $f_{\Omega} = 7\text{kHz}$ as a modulating signal. Fig.6, Fig.7 and Fig.8 are the outputs with modulation index 0.25 , 0.5 and 1.0 respectively. Obviously, the outputs are the standard sinusoidal amplitude modulated waves.

4. Conclusion

The above modulation is a new mode for linear modulation. It has the advantage of obtaining a modulation index reaching unity, using small power modulating signals and a wide linear range of the amplitude modulated signals. As compared with the double-balanced mixer, this method is simpler since a careful matching of the diode characteristics and accurate balance of the transformer windings are not needed as in the double-balanced mixer circuit.

References

1. Zhang Suwen, "High Frequency Electronic Circuits", 2nd. ed. Higher Education Press, Beijing, 1984.
2. Huang Changyu, "Transistor Circuits", Qinghua University Press, Beijing, 1982.
3. N.R. Draper and H. Smith, "Applied Regression Analysis", New York, Wiley, 1966.
4. Zhen Weiming, "A Collection of System Engineering FORTRAN Programs", Qinghua University Press, Beijing, 1985.

5. David J. Comer, Micheal L. Christiansin and David K. Fox, "The Loop-gain Modulator: A New Class of Linear Amplitude Modulators", IEEE Transactions on Circuits and Systems, Vol. CAS-34, No. 10, October, 1987.

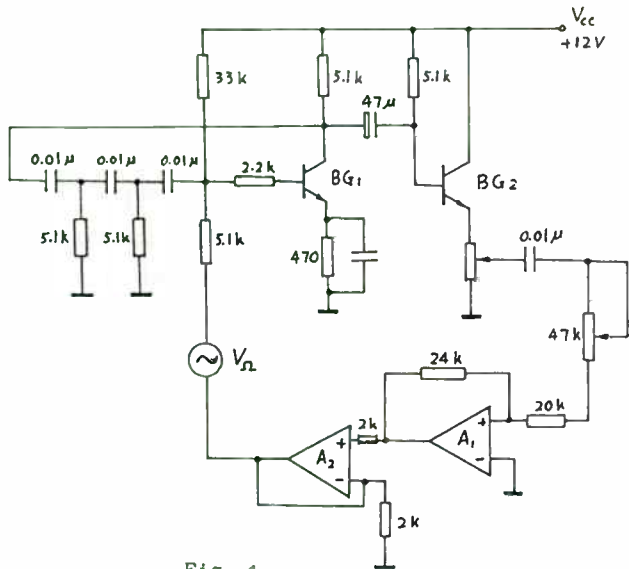


Fig. 1

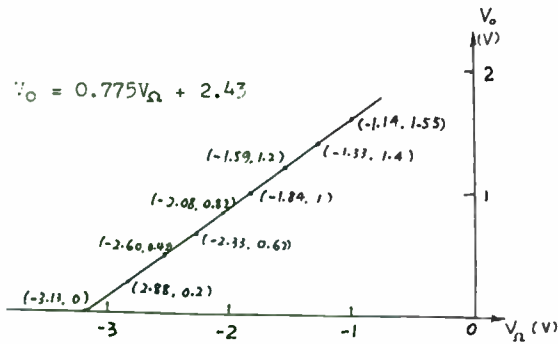


Fig. 2

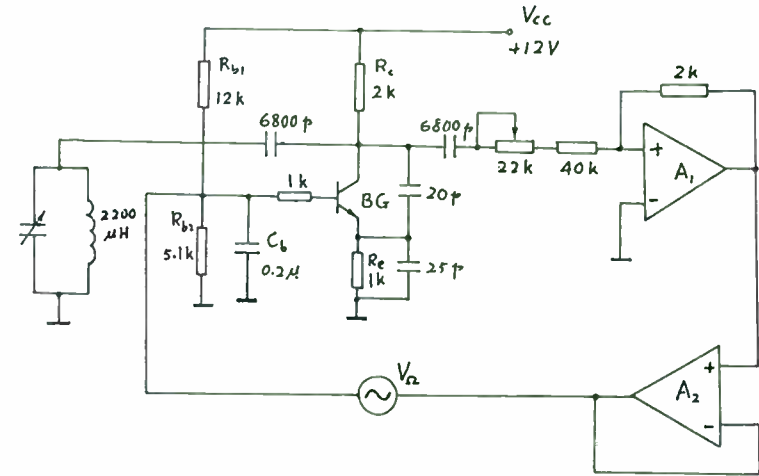


Fig. 3

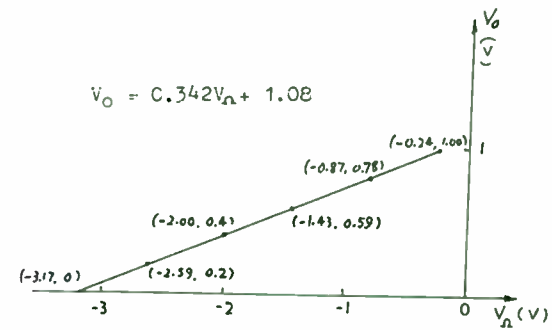


Fig. 4

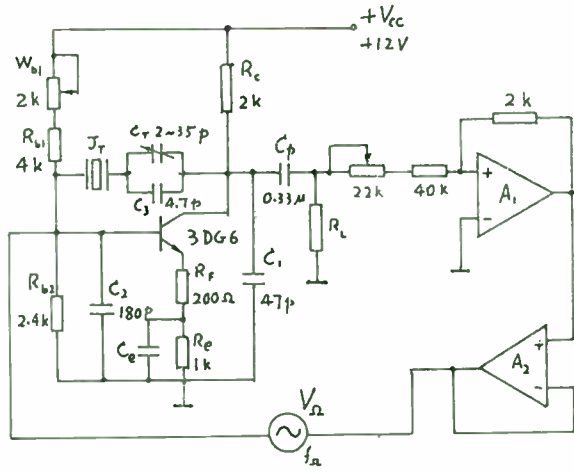


Fig. 5

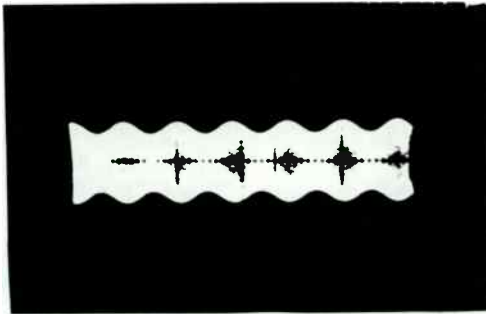


Fig. 6

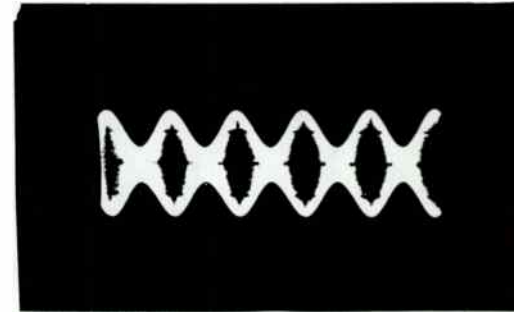


Fig. 7

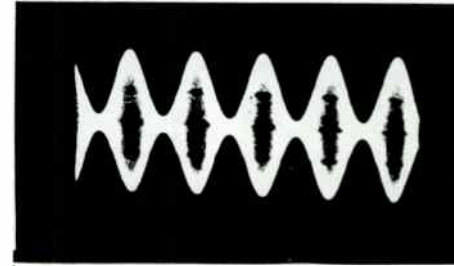


Fig. 8

4 Ghz. Multiplied Source

by

R. Daniel Balusek

Rockwell International

Network Transmission Systems Division

P. O. Box 568842

Dallas, Texas 75356-8842

ABSTRACT

The purpose of this paper is to describe a Multiplied 4 Ghz Frequency Source with performance characteristics suitable for Quadrature Amplitude Modulation (QAM) Digital Microwave Radio applications. The unit consists of a crystal reference oscillator operating in the 114 to 120 Mhz frequency range that is multiplied up to an intermediate frequency between 1850 and 2100 Mhz then doubled to produce an output frequency between 3700 and 4200 Mhz. The unit is capable of being used as either a Transmit Source when combined with an upconverter or Receive Local Oscillator when working in conjunction with a downconverter as shown in the block diagram of Figure 1. The combination of a quiet low frequency reference oscillator together with a high degree of mechanical integrity result in a unit that is a modest improvement over fundamental frequency microwave sources operating in the same frequency range.

INTRODUCTION

Microwave sources have long been a problem concern for Digital Microwave communication systems for as long as such systems have been in existence. Many people consider them to be one of the most difficult components to design, manufacture, and keep running in the field. As modulation schemes become more and more complex, the physical and electrical characteristics of microwave oscillators become more and more demanding. Frequency and power stability, low phase noise, and phase stability are some of the most important criteria that must be addressed when designing an acceptable microwave source. Before the advent of Silicon Bipolar or FET devices that were capable of operating at microwave frequencies, the concept of multiplying a lower fundamental frequency oscillator up to a usable microwave frequency was a common practice. As device operating frequencies increased and their prices decreased, fundamental frequency oscillators became an attractive alternative to their multiplied counterparts due to design simplicity and problems that sometimes occur with multipliers in general. The apparent simplicity of a fundamental frequency microwave source design seems like an attractive option when one considers electrical parameters; however, mechanical integrity can become an overwhelming obstacle at frequencies much higher than 2 Ghz.

The 4 Ghz Multiplied Source described in this paper was designed to be an elegant solution to many of the inherent problems encountered with previous designs. The module consists of five basic building blocks: 1. Crystal Reference Oscillator circuit, 2. Step Recovery Diode (SRD) Multiplier, 3. Tunable Harmonic Filter, 4. Two stage GaAs MMIC Amplifier, and 5. Doubler/Filter circuit.

PHYSICAL DESCRIPTION

The 4 Ghz Source circuitry is housed in a folded aluminum box as illustrated in Figure 2. that contains three separate compartments. The first compartment houses the Crystal Reference Oscillator and associated circuitry. Provision is made for field adjustment of the crystal frequency with a variable inductor that is accessed through a hole in the front of the module. A BNC connector also located on the front panel of the unit provides a monitor point for measuring the crystal frequency. The printed circuit board used is .060" thick "FR-4" material and is shock mounted to the chassis with rubber grommets. The second compartment contains voltage regulation circuitry, a Step Recovery Diode multiplier, a tunable harmonic filter, and two GaAs MMIC amplifiers. This board is also constructed on .060" thick "FR-4" substrate material and the components used are a combination of surface mount and through-hole technology. Provision is made for field adjustment of the tunable harmonic filter with the appropriate tuning tool through two holes in a side cover of the module.

The third compartment contains a FET doubler, microstrip bandpass filter, and FET buffer amplifier. The output from the buffer amplifier is passed to the outside world via an SMA connector located on top of the module. The substrate material used is also .060" thick "FR-4" and all of the components on this board are surface mount.

CIRCUIT DESCRIPTION

I. Crystal Reference Oscillator

The Crystal Reference Oscillator; shown in Figure 3, is composed of a single inline pin (SIP) hybrid containing a common base oscillator, buffer, and output amplifier. External to the hybrid is a field replaceable ovenized fifth overtone crystal and associated circuitry which allows operation over a range from 114 to 120 Mhz. A variable inductor in the tank circuit allows approximately ± 8 PPM mechanical adjustment range in order to set the crystal frequency and compensate for long term crystal aging. A tuning varactor which is also in the oscillator tank circuit allows ± 8 PPM electrical tuning range and can be used for locking the unit to an external reference standard. Short term frequency stability of the reference oscillator is ± 4 PPM over the temperature range of -20 to $+70$ degrees Centigrade while long term stability is specified at 3 PPM/year maximum at $+75$ degrees Centigrade. A Motorola MWA130 silicon bipolar hybrid amplifier stage provides an output signal level of approximately $+13$ dBm in order to drive the succeeding multiplier circuit.

II. SRD HARMONIC GENERATOR

The reference signal is multiplied using a Step Recovery Diode circuit that produces a comb of harmonically related frequencies extending into the 1890 to 2100 Mhz frequency range. The multiplier circuit consists of an input matching/lowpass filter section and a temperature compensated active biased SRD operating in the shunt mode. The multiplication factor of the circuit is either x15 or x16 and is dependent upon the reference crystal used and desired output frequency. Power output from the multiplier is approximately -9 dBm when driven with a +13 dBm input signal. The output of the harmonic generator is terminated in a 3 dB resistive pad in order to provide a stable load over the entire range of operating frequencies. This results in an overall output level of approximately -12 dBm at 2 Ghz.

III. TUNABLE HARMONIC FILTER

In order to select the desired harmonic frequency from among the large number of undesirable tones, a two cell harmonic filter follows the multiplier circuit. The filter is a mechanical combine Chebyshev response design constructed with round coupling rods mounted inside of a 3.4 inch length of standard 6 Ghz waveguide material. Two Johanson ceramic tuning elements provide a means by which to select the desired harmonic and at the same time reject adjacent harmonics. The filter has a nominal insertion loss of 1 dB and provides approximately 50 dB of adjacent harmonic suppression.

The filter is mechanically fastened to the "FR-4" substrate with five mounting screws and connected to 50 ohm microstrip transmission lines on the input and output using an electromechanical connection provided by two more screws. Because a good connection between the filter body and the printed circuit board and chassis ground is extremely critical for optimum performance, an aluminum bracket on the backside of the substrate provides an additional degree of mechanical integrity and insures a good ground connection between the filter body and chassis ground. The relatively high Q response of the mechanical filter requires two versions in order to cover the entire band from 1850 to 2100 Mhz with the frequency split occurring at 1975 Mhz. With 1 dB insertion loss through the filter, the 2 Ghz output level at this point is approximately -13 dBm.

IV. TWO STAGE GaAs MMIC AMPLIFIER

In order to insure adequate drive level to the Doubler/Filter circuit, two GaAs MMIC amplifiers with a combined gain of approximately 30 dB follow the tunable harmonic filter. The input stage is an NEC UPG100 GaAs MMIC with an operational bandwidth of 50 Mhz to 3 Ghz. This device is internally matched to 50 ohms and provides a typical 16 dB gain across the entire operating bandwidth with a 2.7 dB noise figure. The second MMIC, an NEC UPG101, is also internally matched to 50 ohms and is specified with 14 dB gain and a 5 dB typical noise figure across the same operating bandwidth.

A 2 dB fixed resistive pad between the two MMIC amplifier stages insures stable operation over temperature and results in an overall gain of approximately 28 dB for the combined circuitry. At this point, the 2 Ghz output signal level is approximately +15 dBm.

V. Doubler/Filter

The Doubler/Filter circuit is composed of an active FET doubler, a microstrip bandpass filter, and a FET buffer amplifier all mounted on .060" thick "FR-4" substrate material that is located in a separate compartment from the rest of the module. The doubler FET is a Mitsubishi MGF1601-01 medium power FET that is biased to provide a non-linear element and maximize the 4 Ghz second harmonic output. The bandpass filter is a microstrip edge coupled design with a -3 dB bandwidth from 3600 to 4300 Mhz and a maximum insertion loss of 1.5 dB across the 3700 to 4200 Mhz passband. The filter provides 20 dB of rejection for harmonics located at 2 and 6 Ghz respectively. A second MGF1601-01 FET is used as a buffer amplifier that provides 10 dB of gain across the 3.7 to 4.2 Ghz output range and also helps to isolate the doubler and filter from external load variations. The Doubler/Filter circuit is capable of providing a nominal +18 dBm output power level with input drive levels varying between +10 to +16 dBm.

MODULE PERFORMANCE

As mentioned previously, some of the most important design goals that were targeted in designing the 4 Ghz Source were frequency and output power stability, low phase noise, and phase stability. And since the application for this unit is for use in a commercial Microwave Radio system, it has to meet all of the required specifications over a temperature range of -20 to +70 degrees Centigrade with only a small degree of variation and performance degradation. In order to verify that the unit was capable of meeting the required performance characteristics in a production environment, a total of 25 units were constructed and tested for all parameters. One group of fifteen modules was built and tested in the Engineering Laboratory, while another group of ten units were independently built and tested in an actual production facility and then re-tested in the Engineering Laboratory to verify the final results. Specified frequency stability of the unit is ± 4 PPM maximum over the -20 to +70 degree range which translates to approximately ± 16 Khz at 4 Ghz. Frequency drift of the 25 test units ranged from ± 8 Khz to a worst case of ± 13 Khz with the average change being ± 10 Khz over temperature. Allowable output power variation over the same temperature range is ± 1.75 dB from a nominal value of +18 dBm. All 25 units met the specified variation with a nominal ± 1.25 dB power variation over temperature. Phase noise of the unit is specified as being not more than -100 dBc/Hz at 10 Khz offset from the 4 Ghz carrier with the spectrum response following a general 1/f curve as shown in Figure 4.

Typical numbers for all 25 test units were on the order of -103 dBc/Hz with no appreciable degradation over temperature. Since the unit utilizes a multiplied reference frequency in the range of 114 to 120 Mhz, the presence of harmonics at this distance away on either side of the carrier are common. In order to prevent intermodulation distortion and adjacent channel interference, these particular harmonics must be at a level no greater than -42 dB below the 4 Ghz carrier. These harmonic levels were typically -55 dB below the carrier on all of the units tested with a 3 to 6 dB worst case degradation over temperature. Phase stability is perhaps the most difficult task to accomplish and accurately measure where microwave sources are concerned. Dissimilar metals, bad solder joints, cracked or damaged parts, loose screws, and poor mechanical connections resulting in microphonic behavior are several of the major contributors to poor phase stability. Some of these problems can only be seen during temperature transitions which makes them all the more difficult to detect and solve. A special test station allows us to monitor phase perturbations of the carrier frequency in degrees while the unit is cycled over temperature both by itself and when installed in an actual system operating with 64 QAM data. The detection circuitry is designed to record all phase errors of 30 nanoseconds or greater duration. A 4 degree phase transition will cause bit errors which can result in system noise and a 10 degree phase error will cause a complete frame loss or data interruption in a 64 QAM Digital Radio.

The unit must endure two complete temperature cycles over the range of -0 to +65 degrees Centigrade and is allowed to have only five 4 degree errors of a duration not to exceed .01 seconds each and no 10 degree errors. All of the systems test units displayed a high degree of phase stability by successfully completing this trial. The units were exceptionally resistant to microphonics that are often caused by accidentally bumping into the equipment racks or by directly striking the module itself with a wrench or screwdriver. Needless to say, a judicious selection of electrical components and a thorough understanding of mechanical integrity and assembly techniques is imperative. Aside from a few minor problems that are always encountered when going through the assembly learning process for any new product, all of the units successfully passed the requirements as outlined in the equipment specification with a fair degree of margin. The unit is now in full production at our manufacturing facility and will be used in Digital Microwave Radios both here in the US and several foreign countries.

CONCLUSION

The 4 Ghz Multiplied Source described in this paper is the result of an increasing demand for cost effective, dependable, and manufacturable microwave frequency sources that will meet the stringent requirements of high capacity Digital Microwave Radio systems.

Although the basic concept of a multiplied source is not new, the demanding requirements dictated by increasingly complex modulation schemes has forced us to rethink certain performance characteristics. We have also been able to take advantage of mistakes that were made in the past while advancing the state of the art. Microwave sources that were designed for early low capacity analog FM applications would not be usable in a 64 QAM Digital Radio system today. And the next generation of sources will have to meet the even more stringent demands of 256 QAM. One of the main advantages of starting with a low fundamental frequency is the option of adding additional multiplier stages in order to extend operating frequency limits. A Tripler/Filter board is currently under development that will replace the Doubler/Filter board in the 4 Ghz Source in order to create a 6 Ghz version. By doing this, we can not only take advantage of a proven basic design, but also keep development and production costs down by not having to "re-invent the wheel".

ACKNOWLEDGMENTS

The author would like to thank Dr. Leon Jinich for his invaluable comments and discussions during the development of the 4 Ghz Multiplied Source. A special thanks is also due to Mr. Truong Nguyen for his dedicated work in assembling and testing the Engineering Prototypes mentioned in this paper.

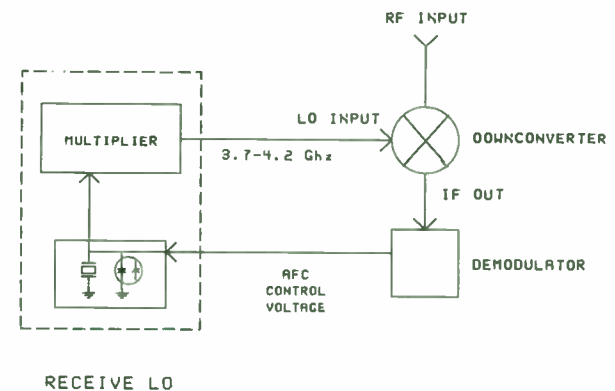
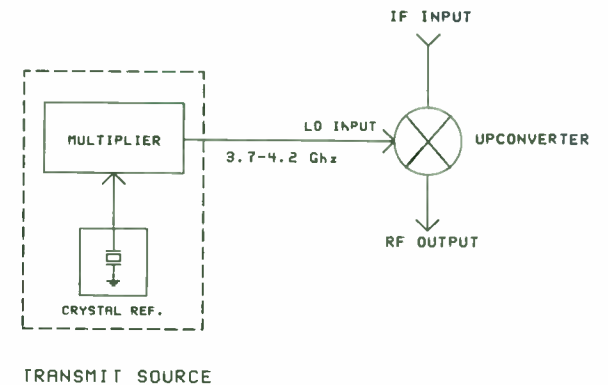


FIGURE 1.
TYPICAL APPLICATIONS

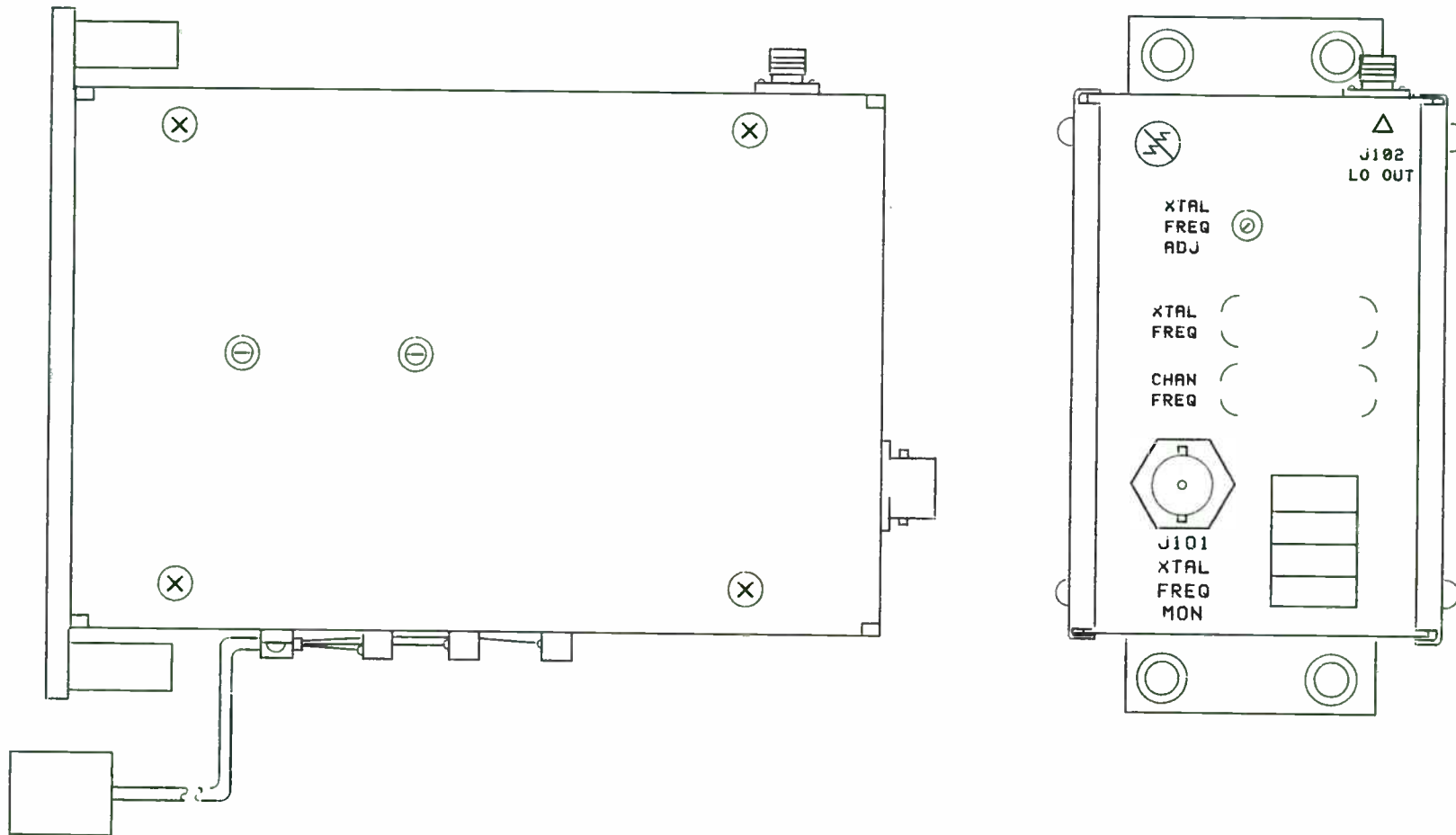


FIGURE 2.
MECHANICAL CONFIGURATION

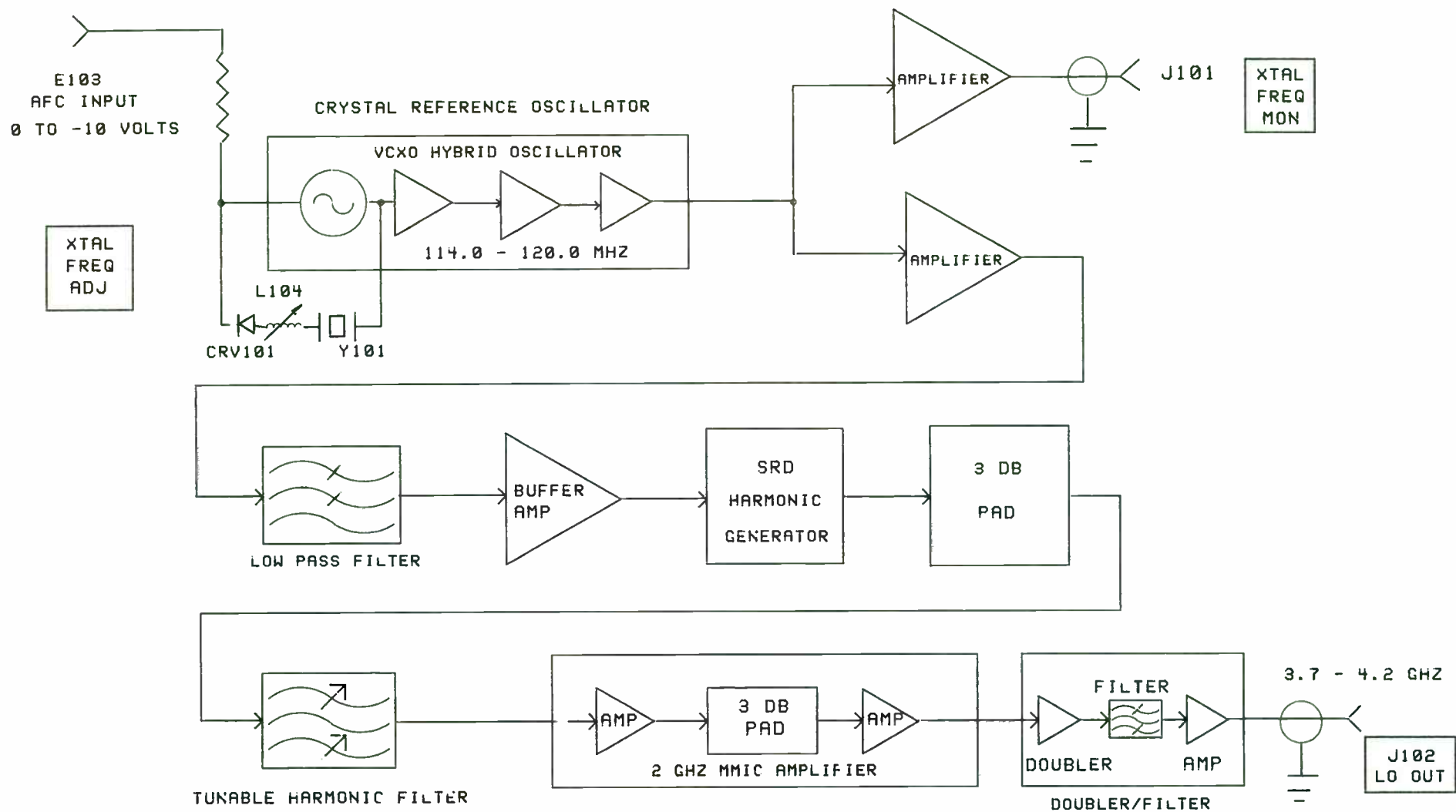


FIGURE 3.
BLOCK DIAGRAM

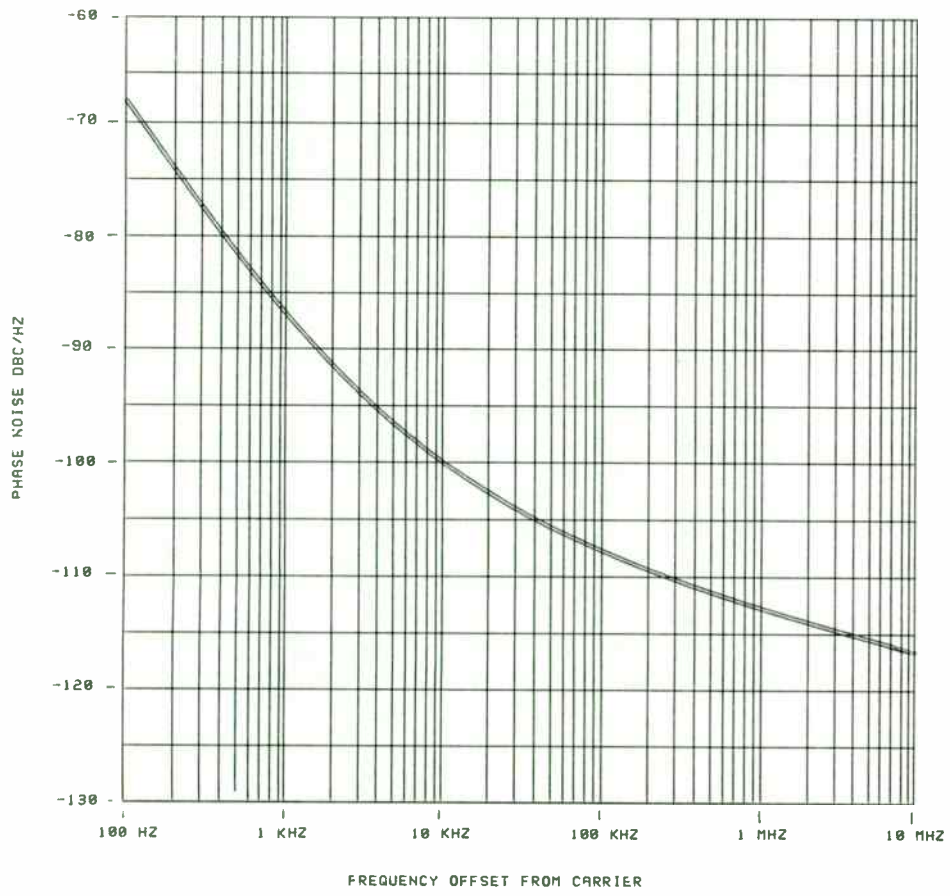


FIGURE 4.
PHASE NOISE

Techniques in Voice Compression and Synthesis

by Paul G. Beaty
Erbtec Engineering Inc.
2760 29th Boulder, Colo. 80301
Sept. 16, 1990

Introduction:

Voice compression is the art of converting an analog voice signal (as produced in a microphone) into a digital data stream and compressing/reducing this data while retaining the essence of the analog signal. The "essence" is not well defined, but includes the characteristics of the voice which identify the speaker, his/her intonation, accent, and mood. Voice synthesis is the art of generating a voice-like sound from digital data. Again, the difficulty is defining "voice-like". In the context of this paper, voice synthesis is the inverse of voice compression. It is common to evaluate a compression method by listening to its synthesized output. We would like for a synthesized voice to be indistinguishable from an actual human speaker. Researchers like Fant, Rabiner, Flanagan, Schafer, and Markel, in the early 1970's developed the art of voice synthesis/compression far beyond the level of then available inexpensive commercial electronics. Some of these methods are in use today in applications which are insensitive to price. In the last 5 years, the price and performance of microprocessors and DSP controllers has made many of these methods viable for more price sensitive commercial and consumer applications. This paper is a summary of the most common compression-synthesis methods, their advantages and weaknesses. Specific details are given which describe how each method works, and when it is applicable. This paper presents no original work. Readers are encouraged to consult the bibliography for further explanations and details.

Voice tutorial:

There are many methods of compressing/synthesizing voice. Judgment must be exercised when determining the performance of a particular method. There have been many attempts at specifying an impartial measure. In 1988, Schuyler R Quackenbush published the results of a massive computer effort to develop procedures which could compare and quantify the performance of various compression methods under controlled circumstances. This paper draws extensively

on this data.

Typical human speech contains spectral components ranging from approximately 200Hz to 4kHz. However, this includes gaps of silence between words and phrases which can impact message interpretations. The natural required band is therefore 0 Hz to 4 kHz. It is not possible to compress a band of random data by a single general technique. However, if the data is known to conform to any specific characteristic, the data can be compressed by removing the characteristic and presuming it. For example, in the case of voice, there is no energy between 0 and 200Hz. The vocal tract is quite predictable and there are some highly preferred frequencies called "formants". It is natural to look for methods of compressing the band by capitalizing on these and other features. In practice, there are several techniques which can compress a voice signal with no loss of information. These methods fall under the category of "source coding" since they exploit the characteristics of the source to achieve acceptable quality and compression.

Human hearing has some measurable limitations. Aside from the limited bandwidth, studies have shown that most people cannot distinguish phase relationships between certain frequencies. Ohm and Helmholtz allegedly speculated that speech was completely specified by its short term frequency content. No phase relationships could be identified. While this was subsequently shown to be wrong, it is close. Additionally, some frequencies cannot be identified while in the presence of others. And finally, the relative amplitude of various frequencies is often misconstrued. In situations where a synthesized signal is played to a human audience (the usual situation), there is no value in retaining the extra information. Some techniques achieve additional compression by capitalizing on these limitations.

Some of the methods for compressing speech require the sound segment be broken into discrete frames and analyzed for frequency information independently. The partition which defines the frame boundary cannot be assigned optimally without considering the entire sound segment. LPC (Linear Predictive Coding) is typical. Other methods like CVSD (Continuously Varying Slope Delta) exploit the band limitations and can easily be implemented "on the fly". These methods differ in their basic approach and present the question: What defines the limits to eligible approaches? It is normally assumed that the limit to system performance will be the method, not the hardware implementation, and that any method is acceptable which does not depend upon prior knowledge of the message. Computers (microcontrollers) may be required at both the transmitter and the receiver which are sufficiently involved that the methods can be

implemented without concessions. Fortunately, in many cases, there are single chip solutions available. Few methods demand more than a fast DSP microcontroller.

The most appropriate compression/synthesis method generally depends on the application. For example, when developing products which talk, it is possible to speak into a microphone while recording the sound and then analyze the data by various methods to determine the "best" one. Furthermore, it is usually possible to select the spoken text based on how well it processes. And often, a segment of spoken text will include duplication of vowel sounds, words, and phrases which can be exploited. This contrasts with the problem faced by the phone company, which must select the method of compression/synthesis prior to hearing the sound. The methods used in these applications are usually simpler to implement and involve the least compression. This paper addresses the methods which can be implemented in "real time" without prior knowledge of the message. Note: This allows for short (200ms or so) time delays between the data collector and the transmitter while data frames are being collected. The techniques which follow are described in the order of increasing complexity, usually decreasing voice quality and increasing compression.

Many methods of compressing/synthesizing voice are possible. Judgment must be exercised when determining the performance of a particular method. There have been many attempts at specifying an impartial measure. In 1988, Schuyler R. Quackenbush published the results of a massive computer effort to develop measures which can compare and quantify the performance of various methods under controlled circumstances. This paper draws extensively on his data. There are two general classes of voice synthesis schemes: time domain synthesis and frequency domain synthesis. The principle difference is that no effort is made to retain phase information in the frequency domain techniques.

Waveform Coding Methods:

The first category of encoding methods is called waveform coding. These are attempts at coding the time domain waveform as accurately as possible. At least initially, no attempt is made to model the voice tract or to capitalize on voice specific characteristics. These methods are easy to implement in "real time" using standard microcontrollers. Several chips exist which make these techniques even easier. The quality of the reconstructed voice using these methods is quite good, and the compression is minimal. Each of these methods which is discussed here has parameters which can be varied. These parameters are must be varied to suit the

specific application. The methods to be discussed are Pulse Coded Modulation (PCM), Differential Pulse Coded Modulation (DPCM), Delta Modulation, Adaptive Pulse Coded Modulation (ADPCM), Adaptive Delta Modulation (ADM), and Continuously Varying Slope Delta (CVSD).

PCM (Pulse Coded Modulation):

As perceived by a microphone, an acoustic signal is a continuous time varying analog signal with a continuous frequency spectrum. The compression and synthesis techniques which are discussed in this paper apply only to digital data. Therefore, the first action must be to digitize the signal. This is achieved by periodically sampling the signal. In pulse code modulation, the voltage amplitude is sampled and converted into a digital number. This number is transmitted in a series of pulses and hence, the name.

When data is sampled periodically, frequencies above $1/2$ the sampling rate cannot be distinguished from a corresponding frequency below $1/2$ the sampling rate. This phenomenon is called "aliasing". When the analog signal is reconstructed, the energy from a frequency and all of its aliases will be superimposed. Hardware filters must attenuate the undesirable frequencies prior to sampling. Commercial PCM Codecs (coders+decoders) usually contain bandlimiting and smoothing hardware filters. The corner frequencies of hardware filters are not infinitely sharp, therefore, a guard band must be created and wasted. For example, the phone industry samples the data at 8kHz, and bandlimits the signal to 3kHz.

Typical A/D converters sample an analog signal in some voltage range by partitioning the range into equal voltages and returning the corresponding digital number. This method insures that the maximum error between the actual voltage and the measured voltage has been minimized. Actual A/D converters which implement this "linear" partition are common and fairly inexpensive. Unfortunately, in speech, all voltages are not equally probable. Most of the signal is close to the DC average. Furthermore, the amplitude response of human hearing is closer to logarithmic than linear. We can hear a pin drop, but only in a quiet room. For most people, absolute amplitude perception is quite limited. Maintaining a constant signal-to-noise ratio is more important than minimizing worst case amplitude error. These statements suggest that a logarithmic A/D converter is desirable. Aside from the linear partition, there are two widely accepted standards for companding data which are commercially available; mu-law and A-law.

Pulse Coded Modulation (PCM) can be either linear or non-linear depending on the type of digitization used. Most applications require some data compression and use this method to “define” the raw uncompressed data. As such, the voice quality of this method is the standard of measure. The data rate required for high quality voice is about 8kHz with 8-bit data. This is usually expressed as 64k bits/s.

DPCM (Differential Pulse Controlled Modulation):

Sampled speech signals have a strong tendency for each data point to be near (in voltage) the previous data point. The variance of the first difference of data is less than the variance of the data itself. This can provide an advantage. Given a fixed sampling quantization, this permits a smaller error variance and therefore a better SNR. Or alternatively, given a fixed SNR, this technique permits specifying the data in fewer bits which requires a smaller bandwidth. The compression advantage of recording the successive delta rather than the actual data is achieved when the maximum delta has fewer bits than the maximum data. This is true except in the case of rapid voltage slews. If an upper limit is imposed on the voltage slew rate (similar to an op-amp) and/or the sampling rate is increased, then compression can be achieved without significant loss of data. Whenever significant compression is available with DPCM, it is also available by reducing the sampling rate (which is easier). Therefore, this method as presented is rarely used for voice encoding.

DM (Delta Modulation):

The general strategy of DPCM method was to increase the sampling rate and to record only the successive difference information. Collectively, this leads to a slight compression. Delta modulation is the result of carrying this strategy to its natural limit. This is a specific case of DPCM in which 1 bit of difference data is recorded for each sample. In most voice segments, there is little additional compression in using delta modulation over other forms of DPCM. However, there is one additional benefit. When delta data is played to a DAC, it is necessary to integrate first. It is frequently easier to implement an integrating DAC cheaper than an absolute voltage DAC. The principle advantage of delta modulators is the ease of implementation. The disadvantage is the requirement to band limit and amplitude limit the signal.

Delta modulation has a more serious problem. It replaces every sample with ± 1 . Therefore,

the best possible approximation of a DC signal is a square wave (alternating +1 and -1). This characteristic is called “granularity”. If the step size is too large, then the granularity is excessive resulting in poor SNR. Alternatively, if the step size is too small, then the slew rate limitation is excessive. Delta modulation is used extensively for compressing arbitrary waveforms. But for most voice applications, the range of unacceptable granularity overlaps the range of unacceptable slew rate. Consequently, delta modulation is rarely used for voice compression. There are several common enhancements which will be discussed which provide both significant data compression and excellent voice reproduction. These methods will all be classified together as “delta modulators”.

ADPCM (Adaptive Differential Pulse Controlled Modulation):

In some situations, it is possible to specify the step size in a DPCM stream based on previous data. For example, suppose a DPCM data point specified a large displacement, then it might be appropriate to increase the step size for subsequent data. Similarly, if the data specified a small number of steps (which forces poor resolution), then it might be appropriate to decrease the step size (which will improve resolution). These are two examples of adjusting the differential in a DPCM system dynamically. Other methods of “adapting” are possible and can depend on the character of the data. This is the easiest method to implement which has “real” applications. In typical ADPCM, the data specifies 3-4 bits of delta (1 sign + 2-3 offset). The quantum unit of offset Δn is typically a function of the previous data point and the rate of adaptation β as follows:

$$\Delta n = \beta \delta(n-1) + (1-\beta)|e(n)|$$

$$\text{data} = \delta(n)/\Delta n$$

Commercial chips are available which make ADPCM easy to implement when the parameters are sufficiently restricted. When designing an ADPCM system, it is necessary to specify β , the number of quantization levels N, and the sampling (data) rate. Table 1 charts the performance of ADPCM with several permutations of these parameters.

N	bit rate	performance
3	4.0k	speaker has nasal congestion
7	8.0k	minimum understandable
15	16.0k	private telephone quality
15	32.0k	commercial telephone quality

Table 1: Performance of ADPCM

ADM (Adaptive Delta Modulation):

This method is a special case of ADPCM in which delta is encoded with 1 bit. The method has most of the performance benefits of ADPCM and implementation benefits of delta modulators. Since $\text{data} = \pm \Delta n$, the condition of adaptation used in ADPCM won't work. A common replacement is:

$$\begin{aligned} \delta(n) &= \delta(n-1) A & \text{when } e(n)=e(n-1) & & ; A > 1 \\ &= \delta(n-1) B & \text{otherwise} & & ; B < 1 \end{aligned}$$

Like all delta modulators, the real advantage in using ADM is the ease of implementation.

CVSD (Continuously Varying Slope Delta):

This is a specific form of adaptive delta modulation in which the step size δ is a continuous function of the previous data. There are many possible implementations. Typically, function definitions depends on the "coincidence" of the previous 3 or 4 steps as follows:

$$\begin{aligned} \delta(n) &= \beta \delta(n-1) + A & \text{if } e(n-1)=e(n-2)=e(n-3) \text{ (} =e(n-3) \text{)} \\ &= \beta \delta(n-1) + B & \text{otherwise} \end{aligned}$$

The 4 step definition achieves slightly wider dynamic range at the expense of lower amplitude slew rate. When developing a CVSD design, the first variable to specify is the step integrator variable β and is equivalent to assigning the loop gain of figure xx. Next, CVSD imposes both upper and lower limits to the rate of amplitude change (step size). The minimum step size is $\frac{B}{1-\beta}$ and the maximum step size is $\frac{A}{1-\beta}$. Frequently, the maximum step is specified by defining the expansion ratio $\frac{\text{maximum step}}{\text{minimum step}}$. And finally, the sampling rate and the integration filter parameter α must be specified as in all waveform coders. If we design assuming the usual bandwidth and value for α , then there is only one independent parameter. Table 2 shows relative performance vs. sampling rate.

bit rate	performance
9.6k	minimum understandable
12.0k	moderate
16.0k	private telephone quality
32.0k	commercial telephone quality

Table 2: Performance of CVSD

All Pole Methods:

The encoding methods which have been discussed up to now apply equally well to arbitrary data packets. No effort has been made to capitalize on features or qualities of the sound which are specific to voice. In order to achieve any significant compression of the data, it is necessary to identify these features. The methods which are discussed in this section are based upon an all-pole model of the voice tract. They are attempts (like before) at estimating the original time-domain waveform. They result in significant compression but also result in perceivable loss of voice quality. The methods which will be discussed are Adaptive Predictive coding, Linear Predictive Coding, Residual Excited Linear Predictor, and Adaptive Transform Coding. These methods are significantly more complicated than the waveform coders outlined earlier and require a more extensive introduction.

The basic model which is generally used in the synthesis of voice was developed by Fant 1960 and was greatly enhanced by Wakita (1972-1975). Air in the lungs is pushed by the diaphragm through the trachea and past the vocal chords. If the vocal chords are tensed, they will vibrate at natural resonant frequencies called "formants". Vowels are the sum of formants. Depending on the location of the velum, the air either exits out the mouth or the nose. The location of the jaw, lips, and tongue determine the final sound. If the vocal chords are not tensed, then they do not vibrate and the sound is caused by the turbulence caused by passing through the mouth. These sounds are called "fricatives". The "sh" sound is typical.

The basic assumptions itemized by Wakita are: 1) The vocal tract consists of N interconnected sections of equal length. 2) The transverse dimension is small with respect to the length so that sound can be treated as a plane wave. 3) The sections are sufficiently rigid that there are no losses through the wall. 4) The elementary wave propagation equations are valid. 5) The model is linear. 6) The effect of the nasal tract can be ignored. It is important to note the linear separation of the source (the lungs and the diaphragm) from the filter (the vocal chords and the mouth). This model works fairly well for synthesizing a single human voice. A more complicated model is required for situations like two voices on a telephone.

LPC (Linear Predictive Coding):

It should be apparent from the previous discussion that the mathematics required to model to the vocal tract for estimating an acoustic waveform is quite complicated. For mathematical convenience, we would like to arbitrarily restrict our attention to linear, time

invariant models. Unfortunately, in reality, both of these assumptions fail. The vocal tract is constantly time varying and Flanagan (1968) showed that the glottis is coupled to the voice tract producing a non-linearity. For the highest quality speech reproduction, linear time invariant models are inadequate. However, over a short enough time interval, the vocal tract doesn't change much, and the non-linearity caused by the coupling of the glottis is slight. Experience has shown that acoustic waveforms can be partitioned into discrete frames of 10-50ms each and modeled independently with fairly good sounding results. In the performance data which is cited later, the frame length is 15ms.

The transfer function of any implementable linear system can be represented in the z-domain as the quotient of two finite degree polynomials. By convention, we define the transfer function

$$f(z) = \frac{p(z)}{q(z)} \quad ; \text{deg}(p)=m, \text{deg}(q)=n$$

This transfer function will be used to model or "predict" the acoustic waveform for a short interval of time called a frame. In the actual implementation, $f(z)$ will be implemented as a z-domain filter, initialized appropriately, and driven by some function. The "prediction" is this filter's transient response. A different transfer function will be used to model each frame. Clearly, for a given frame, the model will best estimate the actual waveform when the degrees of freedom, $n+m$, is as large as possible. However, when the number of freedoms is fixed, it is unclear how they should be allocated between m and n for best results. This resource allocation problem applies to every linear prediction application, not just speech synthesis. For reasons of mathematical convenience, speech is usually modeled with $m=0$. All freedoms are contained in the denominator. This assignment of freedoms is called the "all-pole" method or "maximum entropy" method. The analysis which follows demonstrates one method for determining the predictor coefficients.

Assume that a stream of periodically sampled data $s(n)$ has been received, that the driving function has been specified as the delta function, and that the degree of the filter (i.e., number of freedoms in the model) is p . The transfer function of interest can be expressed in the form

$$1) \quad H(z) = \frac{1}{1 - \sum_{i=0}^p a_i z^i}$$

and our problem reduces to determining the set $\{a_i\}$. These coefficients are known as the Maximum Entropy Method (MEM) coefficients. If $\{a_i\}$ were known, then the reconstructed data stream would be

$$2) \quad s(n) = \sum_{k=0}^{\infty} a_k s(n-k).$$

Following the usual "least squares" style, the selection of the elements a_i will be based on minimizing the total squared error

$$3) \quad E = \sum_{n=0}^{\infty} (s(n) - \hat{s}(n))^2$$

By taking the partial derivatives with respect to each coefficient, we get the following set of simultaneous equations.

$$4) \quad \sum_{k=1}^N a_k \sum_{n=1}^{\infty} s(n-k)s(n-1) = \sum_{n=1}^{\infty} s(n)s(n-1)$$

$$5) \quad \Rightarrow \quad M \bar{a} = \bar{b} \quad ; \text{ in which } M_{ij} = \sum_{n=1}^{\infty} s(n-i)s(n-j), \text{ and } b_j = \sum_{n=0}^{\infty} s(n)s(n-j)$$

This method of developing the equations is called the "autocorrelation" method since the elements of the matrix M and the vector b are all autocorrelations of the original data. The matrix M is symmetric and positive definite. Therefore, it has an inverse and the equations have a (unique) simultaneous solutions. The solution vector (the MEM coefficients) can be transmitted to the receiver which can execute this procedure in reverse and reconstruct an approximation of the original data.

The restriction to the all-pole model simplified the mathematics. Most serious enhancements to this method start by relaxing this restriction. In the current vernacular, linear prediction (or least squares linear prediction) is the set of methods involving matrix solutions to the predictor coefficients for an arbitrary linear model. Prior to determining the coefficients, it was necessary to specify several variables. The points of variation are: the pole count, the sampling frequency, the frame length, and the driving function.

The first problem is to specify the number of poles. Assuming the frame rate is fixed, the more poles which are retained in the model the more data is required to specify the set, and also

the better the reconstruction will be. We hope that a small number of poles will be sufficient to produce adequate voice and still retain reasonable compression. It is generally acknowledged that the total time delay in the filter should be $\frac{2l}{c}$ where l is the length of the vocal tract and c is the speed of sound. A typical adult male vocal tract is about 17cm long. Sound travels at about 34cm/s. Therefore, the time delay of the filter need to be about 1.0ms to maintain a reasonable low end frequency response. If the data is collected at 10kHz, there should be at least 10 poles. Experiments have demonstrated that there is little performance advantage in using more.

The next problem is addressing the issue of stability. The MEM coefficients will be used as feedback multipliers in an IIR filter. The determination of stability of a system with time-varying coefficients is mathematically complicated. This is the principle reason for the time-invariance condition. Equation 5 is guaranteed to have a unique solution. However, this solution may lead to an unstable IIR. With time invariant coefficients, the condition of stability is simple. The IIR is stable whenever all poles of the transfer function lie inside the unit circle, $|z| < 1$. The coefficients of the IIR must be transmitted to the receiver. Therefore, they must be implemented with a finite word width. It is natural to select the IIR coefficients by rounding the MEM coefficients. Even if the original equation is stable, the final IIR may not be. Finally, if the transfer function is stable, it is possible (even likely) that all frequencies rapidly attenuate to zero amplitude. Since this is undesirable, it is usually necessary to adjust the pole positions to better match the overall amplitude envelope. There are several reasonable (mathematically defensible) recipes which can be followed.

The basic voice model has two possible driving functions; an impulse function used for vowels, and a random number generator used for fricatives. If we were developing products which talk, then we could analyze the signal and know which input was required. However, if we are compressing "on the fly", we need a procedure for identifying and specifying which driving function is required. This process is normally called "buzz-hiss" detection. There are several techniques possible. The easiest technique requires monitoring the closeness of match between the reconstructed data with the actual data. A close match is declared a buzz, otherwise it is a hiss.

LPC is deficient in several areas. There are three general categories of sounds which are present in speech; vowels, plosives, and fricatives. Vowels occur from the vocal chords vibrating. Since LPC is an attempt at modeling the formant structure of the vocal tract, vowels are reconstructed quite well. Similarly, fricatives occur when sound is forced through the mouth

without vibrating the vocal chords. These reconstruct reasonably well when the random number generator is used as the drive. Unfortunately, plosives reconstruct rather poorly.

The autocorrelation development of linear prediction accurately generates the MEM coefficients. These can be treated as the forward impedance of the data through the filter. A slight alteration of the method also generates the corresponding reflection coefficients. Because of the method of calculations, these are called the partial correlation or PARCOR coefficients. A problem with using the MEM coefficients to characterize a data set is that they potentially span an indefinitely wide dynamic range. The PARCOR coefficients are limited and typically are all near ± 1 . For this reason, most LPC methods (and their derivatives) transmit the PARCOR rather than the MEM coefficients. It is possible to develop the MEM set from the PARCOR set. And because of the resolution around ± 1 , it is typical to transmit the inverse sine of each coefficients.

Given that the frame interval is fixed (at 15ms), the Hamming window is fixed (at 30ms), the number of bits allocated for encoding pitch and gain for each frame is fixed (at 7), then the only variable in LPC is the number of bits/frame allocated to encoding the PARCOR coefficients. Table 3 shows various choices and relative speech quality.

Coefficient bits/frame	Data rate	Voice quality
20	1800	very choppy
29	2400	minimum interpretable
38	3000	satisfactory
48	3666	private telephone quality
58	4333	private telephone quality

Table 3: LPC performance

There is reasonable improvement in voice quality as the bit rate increases as expected. Linear predictive coding generates marginal quality voice at about 2400 bits/sec and seems to reach a performance limit at about 3666 bit/sec. Commercial chips exist which allow easy implementation of this method and achieve compression rates significantly better than the waveform coding discussed earlier. (Recall that raw PCM data is about 64k bits/sec).

APC (Adaptive Predictive Coding):

This method requires the input sampled waveform be partitioned into frames. This frame is analyzed by the LPC methods discussed earlier to determine the MEM (predictor) coefficients,

the PARCOR (reflection) coefficients, and the gain which are all transmitted to the receiver. The transmitter also uses the MEM coefficients to predict the data stream. The predicted data is subtracted from the original data to produce a stream of error data. This data is then adaptively quantized and transmitted to the receiver using one of the waveform coding methods discussed earlier. Typically, the coding method for the error stream is ADPCM, using a small number of quantization levels.

The receiver uses the PARCOR coefficients to reconstruct the basic data then adds the error stream. This general style of construction is called "additive" synthesis and can be made quite accurate. In this formulation, APC depends on 5 parameters; the sampling rate, the frame length, the number of poles, the Hamming window, the error quantization. Quackenbush tabulates the voice quality from the following configuration: The error stream is encoded using ADPCM with 3 levels of quantization yielding an error data rate is approximately 11533 bits/s. The LPC parameters are the same as before; i.e. the frame interval is fixed (at 15ms), the Hamming window is fixed (at 30ms), and the number of bits allocated for encoding pitch and gain for each frame is fixed (at 7). The voice quality using this method is better than the corresponding quality of either ADPCM or LPC as predicted. The data rate of APC is comparable to the sum of the rates ADPCM and LPC.

VELPS and RELPS (Voice and Residual Excited Linear Predictors):

One of the problems of the linear prediction techniques is the requirement to explicitly extract and transmit pitch information. These two methods avoid the problem by transmitting pitch and gain over a narrow baseband. In the VELP system, the speech signal is applied directly to the base-band filter, whereas in the RELP system speech is passed through the inverse filter $A(z)$. See figure xx. These methods are essentially the same as APC discussed earlier with the exception that a filtered version of the error signal is transmitted. Quackenbush tabulates the quality of voice for VELP with the following configuration: the error signal is passed through a lowpass filter and is resampled at the new Nyquist frequency. The error signal is quantized by ADPCM and is transferred separately. This method has performance similar to APC with a slight rolloff at the higher frequencies and requires fewer bits.

ATC (Adaptive Transform Coder):

When a data stream is partitioned by an LPC analyzer into equal frames, it is assumed that

each frame carries an equally interesting frequency distribution and that the data between frames is uncorrelated. The second assumption is obviously false; pole locations change rapidly with plosives and slowly with vowels. When the data in a frame is subjected to LPC analysis, it is assumed that the resultant predictor (or reflection) coefficients will be quantized. The coefficients will change slightly and shift the pole locations which will degrade our estimate of the frequency spectrum and could impact the stability of the transfer function. If 1) the frame partition could be defined dynamically or 2) the pole locations could be adaptively approximated based on results from previous frames or from other pole locations within the frame, then the bits of data allocated to carrying coefficient information could be more efficiently utilized. This will result in a smaller coefficient quantization and is the basic motive behind a class of methods called "adaptive transform coding" (ATC). These methods are complicated and presently are a topic of research. The general performance is similar to unquantized LPC.

Frequency domain synthesis techniques:

The final section of this paper covers compression techniques which depend on frequency domain representations. These techniques exploit the inability of the human hearing to distinguish specific phase relationships. They effectively extract the Fourier transform of the signal and abandon the phase portion. These techniques result in significant compression. Unfortunately, the corresponding synthesized voice has marginal quality and consequently limited application. The methods which are discussed are channel vocoders, and formant synthesizers.

Channel Vocoder:

This method is conceptually simple and was probably the first attempt at generating computer voice. The frequency band required for voice is approximately 0Hz-3200Hz. This band can be partitioned into a small finite number of channels and analyzed independently. The synthesized voice will be the sum of the channels. Within any channel, the only interesting quantity is the total energy as a function of time. This energy can be approximated as a sine wave of the appropriate amplitude at the center frequency. Therefore, the full voice band can be encoded as the relative amplitude levels at these predefined channel centers. It was stated earlier that the amplitude response of human hearing is quite limited. The dynamic range is quite wide,

but the resolution is poor. This can be exploited to achieve significant data compression. The data rate is clearly proportional to the number of channels and the resolution to which amplitude is specified. The overall data rate of channel vocoders range from about 2400 bits/s to 15000 bits/s. Many studies have been made to compare voice quality with data rates. In general, performance is unacceptable for commercial use.

Formant Synthesis:

For a given voice tract, there are some natural resonances called "formants". When vowels are spoken, these resonances vibrate with center frequencies and spectral widths which can be measured reasonably accurately. For given vowels, certain formants will be played at predictable amplitudes. Conversely, when these frequencies are played out at the specified amplitudes, the resulting sound is perceived as the appropriate vowel sound. Someone showed that voice could be adequately compressed/synthesized by preserving only the relative amplitude of the formant frequencies. Formant synthesizers are similar to channel vocoders with variable channel spacing.

Conclusion:

There are many methods of encoding audio speech. The intent of this paper was not to examine each method in detail, but rather to present a representative sampling of the methods along with the general motives. Hopefully, this will help readers select appropriate methods for their applications. These methods span a wide range of complexity and have several variable control parameters. Depending on the desired quality of the synthesized speech, they can achieve compression up to about 95%. The following table (mostly from J.L.Flanagan) is a brief summary of the data:

Method	Relative Complexity	Bits/sec	Quality of speech
PCM	1	64k	exceptional (by definition)
DM	1	16k	good
ADPCM	2	20k	exceptional
CVSD	2	10k	excellent
LPC	10	3.6k	good
APC	20	12k	excellent
VELP	50	3.2k	good
Channel Vocoder	10	varies widely	usually poor
Formant Synthesis	100	varies widely	varies
ATC	500	3.6k	excellent

With the exception of some of the waveform coders discussed in the first section, these methods are too new, too complicated, or too shabby to exist in widespread commercial applications. However, as the price and performance of microprocessors becomes more favorable, many of these other methods become attractive.

Bibliography:

1. J.D. Markel, "Linear Prediction of Speech"
2. Schuyler R. Quackenbush, "Objective Measures of Speech Quality"
3. L.R. Rabiner, "Theory and application of Digital Signal Processing"
4. N.S. Jayant, "Adaptive Delta Modulator with a One Bit Memory"
5. R. Zelinski, "Adaptive Transform Coding of Speech Signals"

Amateur EME CW Signal	1 dB
GPS Signal (uncorrelated C/A)	-20 dB

Noise

Noise is a random function. Adding noise to a signal, consequently, adds some degree of randomness to the signal. The ratio of signal power to noise power (SNR) quantifies to what extent a signal is being randomized by the presence of noise:

$$\text{SNR} = S/N \quad (1)$$

where:

SNR signal-to-noise (power) ratio

S signal power

N noise power

and:

$$\text{SNR}_{\text{dB}} = 10\text{Log}_{10}(S/N) \quad (2)$$

The characteristics of a signal and its application set a lower acceptable limit on SNR. For example, an 80 dB SNR may just barely be acceptable to music aficionado for his stereo system, while a 10 dB SNR may be entirely suitable for casual BPSK packet radio link. Here are some generally accepted SNR limits:

Sound Studio Recording	80 dB
Network TV Signal	60 dB
Telephone Signal	40 dB
BPSK Data Transmission, 10^{-4} BER	10 dB

Most discussions of RF system noise focus on the receiver input, where signal power is at its lowest level, and a given amount of added noise will reduce the SNR to the greatest extent. Noise is characterized as external if it is added to the signal before it reaches the receiver, or internal if it is added by the receiver circuitry. External noise is heavily dependent on system operating frequency, and to some extent location. Below 30 MHz, external noise caused by lightning and manmade electrical systems is usually so high that internal receiver noise is of little concern. On the other hand, most of the noise added to a satellite downlink signal at 1.6 GHz will be due to the receiver itself, unless the receiver is very carefully designed for low internal noise.

The most ubiquitous type of internal receiver noise is broadband thermal noise. It occurs naturally in all resistors. Available (thermal) noise power is proportional to the absolute temperature of the resistor, and the bandwidth of the noise power measurement:

$$P_n = kTB \quad (3)$$

where:

P_n available noise power in watts

k Boltzmann's constant, $1.38\text{E-}23$ watts/kelvin-Hz

T absolute temperature in kelvins

B measurement bandwidth in Hz

Thermal noise sources must be conjugately matched for maximum power transfer, hence the term *available noise power*. An alternate way of characterizing thermal noise is in terms of open circuit mean square voltage or short circuit mean square current:

$$\overline{V_n^2} = 4kTB R \quad (4)$$

$$\overline{I_n^2} = 4kTB/R \quad (5)$$

where:

$\overline{V_n^2}$ open circuit mean square noise voltage

$\overline{I_n^2}$ short circuit mean square noise current

The $\overline{V_n^2}$ and $\overline{I_n^2}$ models can be used to assess noise power transfer in unmatched conditions. Semiconductor devices are subject to several noise generation mechanisms in addition to thermal noise. The overall noise behavior of a semiconductor device is often modeled using mean square voltage and current sources, with values of T representing equivalent, rather than actual physical temperatures. Values of T in excess of 1000 K are not uncommon in semiconductor noise modeling, especially at low frequencies.

Definitions

Device Under Test (DUT)– a device that will be tested to characterize its noise behavior. The DUT may be a completed RF system, a receiver, or a subassembly such as an amplifier, mixer, etc.

Noise Bandwidth– the bandwidth of an ideal (brick wall) band-pass filter that would transmit the same noise power as a given filter. The insertion loss of a filter does not directly affect its noise bandwidth. (Filter insertion loss is handled in noise modeling as a separate issue.)

$$B_n = (1/V_p^2) \int_0^\infty |V(f)|^2 df \quad (6)$$

where:

B_n Noise Bandwidth

$V(f)$ Filter voltage transfer function

V_p Peak value of $V(f)$

Noise Factor– the signal-to-noise ratio at the input of a DUT divided by the signal-to-noise ratio at the output of the DUT, in a thermal environment of 290 kelvins.

$$F = (S_i/N_i)/(S_o/N_o) \quad (7)$$

where:

F Noise Factor

Noise Figure– the decrease, in dB, of the signal-to-noise ratio from the input of a DUT to the output of the DUT, in a thermal environment of 290 kelvins.

$$NF = (S_i/N_i)_{dB} - (S_o/N_o)_{dB} \quad (8)$$

or

$$NF = 10\text{Log}_{10}(F) \quad (9)$$

where:

- NF Noise Figure
- F Noise Factor
- S_i/N_i signal-to-noise (linear ratio) at the DUT input
- S_o/N_o signal-to-noise (linear ratio) at the DUT output

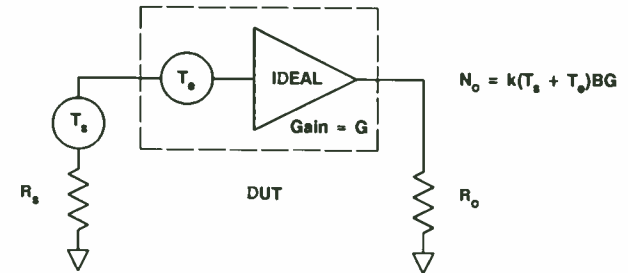
Noise Temperature— in defining noise temperature, a DUT is modeled as a noise free component (amplifier, mixer, receiver, etc.) plus a noise generator representing the internal noise of the DUT. The noise generator is connected at the input of the component such that when an external signal source is connected to the DUT, the noise power of the source and the noise power of the DUT add to produce (through the gain of the DUT) the total noise observed at the output. The noise power added by the DUT noise generator is modeled by an equivalent physical temperature.

$$N_o = k(T_s + T_e)BG \quad (10)$$

where:

- N_o DUT output noise power
- k Boltzmann's constant
- T_s source equivalent noise temperature
- T_e DUT equivalent noise temperature
- B measurement bandwidth
- G DUT gain, linear ratio

Noise temperature is a somewhat more abstract concept than noise factor or noise figure. However, noise temperature is a more flexible concept as its definition is not confined to a 290 K thermal environment. The concept of noise temperature is especially useful in space communications, including satellite RF links.



RF Component Noise

Passive Devices

The primary types of noise in passive devices are thermal noise and low frequency flicker noise. Except in low phase noise oscillator design, flicker noise in passive devices is usually of little concern. On the other hand, broadband thermal noise in passive devices can have a major effect on system noise performance.

The noise factor of an attenuator, filter, transmission line or other passive component is a function of the component's loss and physical temperature:

$$F = 1 + ((1/G)-1)(T_a/T_o) \quad (11)$$

where:

F noise factor of attenuator (passive device)

G attenuator "gain" (power out/power in)

T_a attenuator physical temperature

T_o noise factor reference temperature, 290 K

when T_a = T_o:

$$F = (1/G)$$

$$F = F_1 + ((F_2-1)/G_1) \quad (12)$$

where:

F overall noise factor of the two cascaded stages

F₁ noise factor of the first (input) stage

F₂ noise factor of the second (output) stage

G₁ gain of the first stage (power out/power in)

The noise factor for a cascade of more than two stages can be calculated by applying this formula repeatedly. For example, the noise factor for a three stage cascade is calculated by first determining the noise factor of the last two stages. The noise factor for the last two stages is then used as F₂ in a second calculation with F₁ and G₁ of the first stage to determine the overall noise factor for all three stages.

By repeatedly applying formula 12, the noise factor of an entire receiver can be determined. The noise factor and gain of the first several stages generally set the noise factor for the overall receiver, unless one of the stages deeper in the receiver exhibits a very high loss or noise factor.

Noise Performance Measurement

The noise performance of a DUT is generally measured using the functional equivalent of the Y-factor (hot/cold source) technique. The DUT input is connected to a "hot" source of a known (equivalent) temperature and the output power measured. The DUT input is then connected to a "cold" source, and the output power measured again. The ratio of the hot source to cold source DUT output power is referred to as

Active Devices

There are many noise mechanisms in addition to thermal noise and flicker noise found in active devices, including diodes. (Reference 2 covers these mechanisms in considerable detail.) Noise performance is generally a function of device type, operating frequency, bias conditions, and source and load impedances. In some cases, the noise behavior of an active device can be modeled (at a given frequency and set of bias condition) with noise voltage and current sources. This approach is commonly used to characterize low frequency devices. In general, the device manufacturer will recommend a set of operating conditions for best noise performance.

Noise In Cascaded RF Stages

The noise factor of two RF stages in cascade can be calculated from the noise factor of each stage, and the gain of the first stage:

the Y-factor. If the DUT added no noise, the Y-factor would be the same as the ratio of the absolute temperatures of the two test sources. The DUT will add some noise, so the Y-factor will be a smaller number. The noise factor of the DUT is given as:

$$F = 1 + ((T_H - Y T_C) / T_o (Y - 1)) \quad (13)$$

where:

- F DUT noise factor, referenced to 290 K operation
- T_H "hot" source (equivalent) noise temperature
- T_C "cold" source (equivalent) noise temperature
- Y Y-factor, DUT hot-to-cold source output power ratio
- T_o noise factor reference temperature; 290 K

Frequently, the "cold" source will be a resistor at 290 K. In this case it is convenient to define the term *excess noise ratio* (ENR) as:

$$ENR = (T_H / 290) - 1 \quad (14)$$

then equation (13) becomes:

$$F = ENR / (Y - 1) \quad (15)$$

and:

$$NF = ENR_{dB} - 10 \log_{10}(Y - 1) \quad (16)$$

RF System Noise Performance

Returning to our original discussion of signal-to-noise ratio (SNR), the noise performance of an RF system is determined by how much the SNR of a signal is

degraded by transmission through the RF system. To determine system noise performance, the following information must be known:

- a. the SNR of the signal before transmission
- b. signal power at the receiver input
- c. external noise power at the receiver input
- d. noise factor, referenced to the receiver input
- e. noise bandwidth of the receiver (usually set by the noise bandwidth of the most narrow filter in the receiver)
- f. the SNR characteristic of the receiver demodulator (some demodulators can provide a significant SNR improvement; e.g., a wideband FM detector operating above threshold)

example:

A data communication system for overland freight dispatch and tracking is being developed, based on a constellation of low earth orbit satellites. The system will operate at a nominal frequency of 1.6 GHz. The satellites have an EIRP of 5 watts. Data is transmitted with a SNR greater than 40 dB. The maximum required transmission range is 3000 km. The data is transmitted using BPSK modulation. To meet system bit error rate (BER) objectives, a SNR of 10 dB is required by the receiver BPSK demodulator. The receiver noise bandwidth is 3 kHz. The receiver antenna is an omnidirectional stripline design, with a gain of 1.5 dB. The antenna is mounted directly on the receiver module. What is the maximum receiver noise figure (antenna input to demodulator) allowed to meet system BER objectives?

solution:

The satellites transmit an EIRP of 5 watts, or +37 dBm. Path loss over 3000 km at 1.6 GHz is 166 dB. With 1.5 dB of antenna gain, the signal strength delivered to the receiver input is:

$$S = 37 - 166 + 1.5 = -127.5 \text{ dBm}$$

Given the omnidirectional nature of the receiver antenna and the system operating frequency, external noise can be reasonably assumed to be from a 290 K thermal environment. This validates the use of noise figure to characterize the receiver's noise performance. The external noise received by the antenna in a 3 kHz bandwidth is:

$$N = kTB = -139 \text{ dBm @ 3 kHz}$$

The transmitted SNR is 3 orders of magnitude better than required by the BPSK demodulator, so the noise transmitted with the signal can be safely ignored. The SNR at the receiver input is:

$$\text{SNR}_{\text{dB}} = -127.5 - (-139) = 11.5 \text{ dB}$$

Recalling the definition of NF:

$$\text{NF} = (\text{SNR}_{\text{in}})_{\text{dB}} - (\text{SNR}_{\text{out}})_{\text{dB}}$$

the maximum allowed receiver noise figure is:

$$\text{NF} = 11.5 - 10 = 1.5 \text{ dB}$$

While a 1.6 GHz receiver with a noise figure of 1.5 dB can be designed for volume production, it is a challenging project.

Basic Noise Programs

NF-F-TMP.BAS

This program provides conversions between noise figure, noise factor and noise temperature.

NF-CASC.BAS

This program provides the overall noise figure for two or more cascaded stages.

When the program is run, it first asks for the noise figure of the "output stage". This is the last stage in the cascade. The program then asks for the noise figure and gain of the "input stage". If there are just two stages, input the noise figure and gain of the 1st stage to complete the calculation. If there are more than two stages in the cascade, input the noise figure and gain of the next to the last stage and answer Y to the CASCADE ANOTHER INPUT STAGE(Y/N). Then input the noise figure and gain of the 3rd to last stage, etc. until the 1st stage of the cascade is input. The overall noise figure is progressively compiled on each iteration. Filters, pads, double balanced mixers, transmission lines, etc. which exhibit an insertion loss have a gain in dB less than zero. A filter with a 3 dB insertion loss has a gain of -3 dB!

example:



STAGE:	PREAMP	FILTER	MIXER	I-F
Stage NF:	0.5 dB	3.0 dB	7.0 dB	10.0 dB
Stage Gain:	30.0 dB	-3.0 dB	-6.5 dB	—
Casc. NF:	0.83 dB	19.55 dB	16.55 dB	10.0 dB

PREAMP.BAS

This program tabulates the improvement in overall NF provided by a preamp ahead of a receiver, over a range of receiver noise figures.

YTAB.BAS

This program tabulates noise figure vs Y factor (voltage and power) for a noise source with a given ENR (linear and dB) or noise temperature. Useful for manual noise figure measurements.

CAL_ENR.BAS

This program characterizes (calibrates) a homebrew noise source using data from a DUT with a known noise figure.

NS-T-ENR.BAS

This program converts between noise source ENR (both dB and linear ratio) and noise temperature.

ATTN-ENR.BAS

On occasion you may want to put an attenuator in series with your noise source to improve source VSWR or to increase measurement resolution for very low NF DUT's. This program computes the overall ENR of your noise source-attenuator combination.

ATTN-T-F.BAS

At 290 K the noise figure of a resistive attenuator is the same as its insertion loss. This program computes an attenuator's noise figure, noise factor and noise temperature for any (reasonable) kelvin temperature. Try it on your 1.00 dB coax run on a hot August afternoon...you may be surprised!

KELVINS.BAS

OK, you know the temperature of you coax run is 140 degrees F. What is its temperature in kelvins? This program tells.

N_POWER.BAS

Input source equivalent noise temperature, bandwidth, and resistance and you get available noise power/noise floor in watts and dBm, plus equivalent open circuit mean square noise voltage and short circuit mean square noise current.

References

1. Hayward, W.H., *Introduction to Radio Frequency Design*, Prentice-Hall, Inc., Englewood, New Jersey, 1982.
2. Ambrozy, Andras, *Electronic Noise*, McGraw-Hill International Book Company, New York, 1982.
3. Stanley, William D., *Electronic Communications Systems*, Reston Publishing Company, Inc., Reston, Virginia, 1982.
4. Kuhn, Nicholas J., "A Survey of Transistor Noise Characterization," Hewlett-Packard, Palo Alto, California, 1988.
5. Iseli, Jerry, "A Basic Tutorial on Noise Figure," RF Expo Proceedings, Anaheim, California, 1987

PROGRAM LISTINGS

```
10 REM ***NF-F-TMP.BAS VER 1.1PC 27DEC87***
20 CLS : PRINT
30 PRINT "CONVERSIONS: NOISE FIGURE(dB), NOISE FACTOR, NOISE TEMPERATURE"
40 PRINT "PRINT " NOISE FIGURE(dB) - 1"
50 PRINT " NOISE FACTOR - 2"
60 PRINT " NOISE TEMPERATURE - 3"
70 PRINT : INPUT "INPUT DATA TYPE (1, 2 OR 3)";M : PRINT
80 IF M=1 THEN GOSUB 160
90 IF M=2 THEN GOSUB 190
100 IF M=3 THEN GOSUB 220
110 PRINT "NOISE FIGURE: "; : PRINT USING "#####.##";NF; : PRINT " dB"
120 PRINT "NOISE FACTOR: "; : PRINT USING "#####.##";F; : PRINT " (LN. RATIO)"
130 PRINT "NOISE TEMP: "; : PRINT USING "#####.##";T; : PRINT " KELVINS"
140 REM RUN "B:NOISE.BAS"
150 END
160 INPUT "NOISE FIGURE(dB)";NF : PRINT : PRINT
170 F = 10^(NF/10) : T = (F-1)*290
180 RETURN
190 INPUT "NOISE FACTOR";F : PRINT : PRINT
200 T = (F-1)*290 : NF = 4.34295*LOG(F)
210 RETURN
220 INPUT "NOISE TEMP (KELVINS)";T : PRINT : PRINT
230 F = 1 + (T/290) : NF = 4.34295*LOG(F)
240 RETURN
```

```
10 REM ***NF-CASC.BAS VER 1.1PC 27DEC87***
20 CLS : PRINT : PRINT "NOISE FIGURE OF CASCADED STAGES:" : PRINT
30 INPUT " NOISE FIGURE OF OUTPUT STAGE (dB)"; N2
40 INPUT " NOISE FIGURE OF INPUT STAGE (dB)"; N1
50 INPUT " GAIN OF INPUT STAGE (dB)"; G1
60 F1 = 10^(N1/10)
70 F2 = 10^(N2/10)
80 G = 10^(G1/10)
90 F = F1 + ((F2-1)/G)
100 N = 4.34295*LOG(F)
110 PRINT : PRINT "CASCADED NOISE FIGURE = ";
120 PRINT USING "###.##"; N;
130 PRINT " dB"
140 PRINT : INPUT "CASCADE ANOTHER INPUT STAGE (Y/N)"; D$
```



```

150 IF D$= "N" THEN GOTO 180
160 N2=N : PRINT
170 GOTO 40
180 REM RUN "B:NOISE.BAS"
190 END

```

```

10 REM ***PREAMP.BAS VER 1.1PC 27DEC87***
20 CLS : PRINT: INPUT "PREAMP NOISE FIGURE IN dB";N
30 INPUT "PREAMP GAIN IN dB";G
40 F= 10^(N/10)
50 R= 10^(G/10)
60 LPRINT : LPRINT "NOISE FIGURE IMPROVEMENT FROM PREAMP" : LPRINT
70 LPRINT " PREAMP NOISE FIGURE ";
80 LPRINT USING "###.###";N;
90 LPRINT " dB"
100 LPRINT " PREAMP GAIN ";
110 LPRINT USING "###.###";G;
120 LPRINT " dB" : LPRINT
130 LPRINT "NF PREAMP + RCVR NF RCVR ALONE" : LPRINT
140 FOR K= 3 TO 20
150 S= 10^(K/10)
160 T= F+((S-1)/R)
170 A= 4.34295*LOG(T)
180 LPRINT " ";
190 LPRINT USING "###.###";A;
200 LPRINT " dB ";
210 LPRINT USING "###.###";K;
220 LPRINT " dB"
230 NEXT K
240 REM RUN "B:NOISE.BAS"
250 END

```

```

10 REM ***YTAB.BAS VER 1.1PC 27DEC87***
20 CLS : PRINT : PRINT "Y FACTOR TABULATION" : PRINT : T= 1280
30 PRINT " NOISE SOURCE TEMPERATURE - 1"
40 PRINT " NOISE SOURCE ENR(dB) - 2"
50 PRINT " NOISE SOURCE ENR (RATIO) - 3" : PRINT
60 INPUT "INPUT DATA TYPE (1, 2 OR 3)";M
70 IF M=1 THEN GOSUB 330
80 IF M=2 THEN GOSUB 360
90 IF M=3 THEN GOSUB 390
100 LPRINT "THE TABULATION BELOW IS BASED ON THE Y FACTOR"
110 LPRINT "TECHNIQUE OF NOISE FIGURE MEASUREMENT"

```

```

120 LPRINT : LPRINT "HOT SOURCE TEMPERATURE IS";T;"KELVINS"
130 LPRINT "ENR ="; : LPRINT USING "###.###";EN; : LPRINT " (";
140 LPRINT USING "###.###";ER; : LPRINT " dB )" : LPRINT
150 LPRINT "NOISE FIGURE RMS VOLTAGE RATIO POWER RATIO"
160 LPRINT
170 FOR N= 0 TO 6 STEP .5
180 GOSUB 250
190 NEXT N
200 FOR N= 7 TO 20
210 GOSUB 250
220 NEXT N
230 REM RUN "B:NOISE.BAS"
240 END
250 X= 10^(N/10) : P= (EN/X)+1 : R= SQR(P)
260 LPRINT " ";
270 LPRINT USING "###.###";N;
280 LPRINT " ";
290 LPRINT USING "###.###";R;
300 LPRINT " ";
310 LPRINT USING "###.###";P
320 RETURN
330 INPUT "NOISE SOURCE TEMPERATURE IN KELVINS";T
340 EN= ((T/290)-1) : ER=4.34295*LOG(EN)
350 RETURN
360 INPUT "NOISE SOURCE ENR IN dB";ER
370 EN=10^(ER/10)
380 RETURN
390 INPUT "NOISE SOURCE ENR (L/N. RATIO)";EN
400 ER=4.34295*LOG(EN)
410 RETURN

```

```

10 REM ***CAL_ENR.BAS VER1.1PC 27DEC87***
20 CLS : PRINT : PRINT "ENR(dB) CALIBRATION:" : PRINT
30 INPUT " DUT OUTPUT VOLTAGE WITH HOT SOURCE"; VH
40 INPUT " DUT OUTPUT VOLTAGE WITH 290 K SOURCE"; VC
50 INPUT " DUT NOISE FIGURE (dB)"; N
60 Y=(VH*VH)/(VC*VC)
70 EN=N+4.34295*LOG(Y-1)
80 ER=10^(EN/10)
90 PRINT : PRINT "ENR(dB) ="; : PRINT USING "###.###";EN;
100 PRINT " dB (ENR ="; : PRINT USING "###.###";ER; : PRINT ")
110 REM RUN "B:NOISE.BAS"
120 END

```

```

10 REM ***NS-T-ENR.BAS VER 1.1PC 27DEC87***
20 CLS : PRINT
30 PRINT "NOISE SOURCE CONVERSIONS: TEMPERATURE, ENR(dB), ENR"
40 PRINT : PRINT " NOISE SOURCE TEMPERATURE - 1"
50 PRINT " NOISE SOURCE ENR (dB) - 2"
60 PRINT " NOISE SOURCE ENR - 3" : PRINT
70 INPUT "INPUT DATA TYPE (1, 2 OR 3)";M : PRINT
80 IF M=1 THEN GOSUB 190
90 IF M=2 THEN GOSUB 220
100 IF M=3 THEN GOSUB 250
110 PRINT : PRINT
120 PRINT "NOISE SOURCE TEMPERATURE "; : PRINT USING "#####.##";T;
130 PRINT " KELVINS"
140 PRINT "NOISE SOURCE ENR(dB) "; : PRINT USING "#####.##";ER;
150 PRINT " dB"
160 PRINT "NOISE SOURCE ENR (LIN. RATIO) "; : PRINT USING "#####.##";EN
170 REM RUN "B:NOISE.BAS"
180 END
190 INPUT "NOISE SOURCE TEMPERATURE IN KELVINS"; T
200 EN=((T/290)-1) : ER=4.34295*LOG(EN)
210 RETURN
220 INPUT "NOISE SOURCE ENR IN dB"; ER
230 EN=10^(ER/10) : T=290*(EN+1)
240 RETURN
250 INPUT "NOISE SOURCE ENR (LIN. RATIO)";EN
260 T=290*(EN+1) : ER=4.34295*LOG(EN)
270 RETURN

```

```

10 REM ***ATTN-ENR.BAS VER 2.1PC 30MAY88***
20 CLS : PRINT : PRINT "NOISE SOURCE ATTENUATION" : PRINT
30 PRINT " NOISE SOURCE TEMPERATURE - 1"
40 PRINT " NOISE SOURCE ENR (dB) - 2"
50 PRINT " NOISE SOURCE ENR - 3" : PRINT
60 INPUT "INPUT DATA TYPE (1, 2 OR 3)";M : PRINT
70 IF M=1 THEN GOSUB 260
80 IF M=2 THEN GOSUB 280
90 IF M=3 THEN GOSUB 310
100 INPUT "WHAT IS THE INSERTION LOSS OF ATTENUATOR (dB)"; A
110 INPUT "WHAT IS TEMPERATURE OF ATTENUATOR (USUALLY 290K)"; TA
120 IF TA=0 THEN TA=290
130 AR=10^-ABS(A/10)
140 TE=(TS*AR) + (1-AR)*TA
150 EN= (TE/290)-1
160 ED= 4.34295*LOG(EN)

```

```

170 PRINT : PRINT "NOISE TEMPERATURE AT ATTENUATOR OUTPUT IS";
180 PRINT USING "#####"; TE
190 PRINT "ENR =";
200 PRINT USING "##.##";EN;
210 PRINT " (";
220 PRINT USING "##.##";ED;
230 PRINT " dB )"
240 REM RUN "B:NOISE.BAS"
250 END
260 INPUT "NOISE SOURCE TEMPERATURE IN KELVINS"; TS
270 RETURN
280 INPUT "NOISE SOURCE ENR IN dB"; ER
290 EN=10^(ER/10) : TS=290*(EN+1)
300 RETURN
310 INPUT "NOISE SOURCE ENR (LIN. RATIO)";EN
320 TS=290*(EN+1)
330 RETURN

```

```

10 REM ***ATTN-T-F.BAS VER1.1PC 27DEC87
20 CLS : PRINT
30 PRINT "ATTENUATOR NOISE TEMP, NOISE FACTOR AND NOISE FIGURE"
40 PRINT : INPUT " ATTENUATION IN dB";A
50 INPUT " ATTENUATOR PHYSICAL TEMPERATURE (290 K TYPICAL)";TA
60 AR=10^-ABS(A/10)
70 TE=((1/AR)-1)*TA
80 F=1 + (TE/290)
90 NF=4.34295*LOG(F)
100 PRINT
110 PRINT "ATTENUATOR NOISE TEMP "; : PRINT USING "#####.##";TE;
120 PRINT " KELVINS"
130 PRINT "ATTENUATOR NOISE FACTOR "; : PRINT USING "#####.##";F;
140 PRINT "ATTENUATOR NOISE FIGURE "; : PRINT USING "#####.##";NF;
150 PRINT " dB"
160 PRINT "ATTENUATOR LINEAR GAIN "; : PRINT USING "#####.##";AR
170 REM RUN "B:NOISE.BAS"
180 END

```

```

10 REM ***KELVINS.BAS VER 1.1PC 27DEC87***
20 CLS : PRINT : PRINT "CONVERSION TO KELVINS:" : PRINT
30 INPUT " INPUT TEMPERATURE, SCALE (C OR F)"; T, AS
40 IF AS="C" THEN K=T+273.16
50 IF AS="F" THEN K=(5/9)*(T-32)+273.16
60 PRINT : PRINT "TEMPERATURE IS"; : PRINT USING "#####.##";K;

```

```
70 PRINT " KELVINS"  
80 REM RUN "B:NOISE.BAS"  
90 END
```

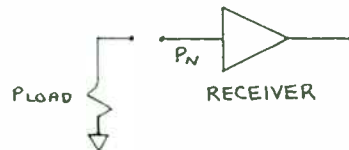
```
10 REM ***N_POWER.BAS VER 1.3PC 15JUL90***  
20 CLS : PRINT  
30 PRINT "AVAILABLE NOISE POWER:": PRINT  
40 INPUT " SOURCE TEMPERATURE IN KELVINS (290 K TYPICAL)": T  
50 INPUT " SYSTEM BANDWIDTH IN kHz (3 kHz TYPICAL)": B  
55 INPUT " SOURCE RESISTANCE (50 ohms DEFAULT)": R: PRINT  
58 IF R = 0 THEN R = 50  
60 P = (1.38E-20) * T * B: PD = 4.34295 * LOG(1000 * P)  
65 V = 4 * P * R: VR = SQR(V): I = 4 * P / R: IR = SQR(I)  
70 PRINT "AVAILABLE NOISE POWER "; : PRINT USING "#.###~~~~~"; P;  
80 PRINT " WATTS ("; : PRINT USING "#####.##"; PD; : PRINT " dBm)"  
90 PRINT "OPEN CIRCUIT MEAN SQUARE VOLTAGE "; : PRINT USING "#.###~~~~~"; V;  
100 PRINT " Vrms ("; : PRINT USING "#.###~~~~~"; VR; : PRINT " Vrms)"  
110 PRINT "SHORT CIRCUIT MEAN SQUARE CURRENT "; : PRINT USING "#.###~~~~~"; I;  
120 PRINT " Arms ("; : PRINT USING "#.###~~~~~"; IR; : PRINT " Arms)"  
130 REM RUN "B:NOISE.BAS"  
140 END
```


RF SYSTEM NOISE BASICS PART II
by Al Ward

1. RECEIVER SENSITIVITY CALCULATION

The previous section covered the calculation of RF system noise performance with the assumption that the antenna temperature is equivalent to 290 kelvins; the standard temperature at which noise figure is measured. In this case it is a simple matter to determine sensitivity improvement when noise figure is lowered. A 1 dB decrease in noise figure results in a sensitivity improvement of 1 dB. With a directional antenna at the microwave frequencies, it is possible to obtain antenna temperatures down to 25 kelvins or less. How is sensitivity calculated when T_a is other than 290 kelvins? Let us revisit some of the basic noise equations.

Consider a receiver whose input termination is P_{load}



Recall the equation for the noise power generated by the receiver referenced to its input as:

$$P_n = K T_e B = K T_o B (NF - 1)$$

In the actual system, the receiver is terminated by P_{load} . In the case of a noise figure measurement, P_{load} is 290 kelvins. In the case of a typical satellite system at L band it is possible that P_{load} be in the region of 25 kelvins. The resultant noise power of the system referenced to its input is now:

$$P_{total} = P_{load} + P_n$$

$$\text{where } P_{load} = P_{ant}$$

$$= K T_a B$$

Substituting:

$$P_{total} = K T_a B + K T_o B (NF - 1)$$

Rearranging:

$$P_{total} = K T_o B (T_a / T_o + NF - 1)$$

P_{total} actually represents the noise floor of the system.

Converting to dBm results in the following:

Sensitivity (dBm)

$$= 10 \log K T_o + 10 \log B + 10 \log (T_a / T_o + NF - 1)$$

$$= -114 \text{ dBm} + 10 \log B + 10 \log (T_a / T_o + NF - 1)$$

where

B is bandwidth in MHz

NF is noise factor expressed as a ratio

T_a is antenna temperature in kelvins

T_o is 290 kelvins

Note that if T_a is equal to T_o , the equation simplifies to the form used in the exercise in the first section.

EXAMPLE

Consider a 1691 MHz WEFAX receiving system. Assume T_a is 25 kelvins. An Avantek AT-41485 bipolar LNA sets the overall receiver noise figure at 1.7 dB. Assuming a bandwidth of 30 kHz the

sensitivity calculates to be

$$\begin{aligned} &= -114 + -15 + 10 \log(.0862 + 1.479 - 1) \\ &= -131.5 \text{ dBm} \end{aligned}$$

Substituting in an Avantek ATF-10135 low noise GaAsFET sets the overall receiver noise figure at 0.7 dB. The sensitivity is now

$$\begin{aligned} &= -114 + -15 + 10 \log(.0862 + 1.175 - 1) \\ &= -134.8 \text{ dBm} \end{aligned}$$

which corresponds to a 3.3 dB improvement which is equivalent to doubling effective antenna area.

2. G/T PERFORMANCE

The preceding section developed an equation that calculates receiver sensitivity based on bandwidth, noise figure and antenna temperature. For a given transmitter power, transmit and receive antenna gains, and a given receiver sensitivity, it then follows that there is a maximum range that can be covered for a specified signal to noise ratio. It also follows that for improving received signal strength, that either receiver sensitivity can be improved or receiver antenna gain can be increased. It is possible for a smaller gain antenna and a lower noise figure receiver to actually provide a higher signal to noise ratio than a larger dish and a higher noise figure receiver. In order to better analyze which system may be better, the term G/T was devised.

G/T is simply the ratio of antenna gain to receiver temperature. The antenna gain should be expressed as a ratio. Receiver sensitivity is expressed in kelvins and includes the

summation of several terms, such as receiver noise temperature (T_r) plus the apparent noise temperature of the transmission line (T_l) connecting the antenna to the receiver plus the antenna noise temperature (T_a).

$$G/T = \frac{\text{ANTENNA GAIN}}{T_r + T_l + T_a}$$

From the previous section:

$$T_r = T_o (NF - 1)$$

$$T_l = T_o (L - 1)$$

where both noise factor(NF) and transmission line loss(L) are expressed as ratios.

The antenna temperature, T_a , is a function of the antenna pattern. Although the main lobe may be aimed off in space to a relatively cold part of the sky, a few of the sidelobes and especially the backlobe will be looking at a portion of warm earth. Computer simulation programs such as NEC-II analyze the effective antenna temperature by integrating the noise power over all angles in the three principal planes.

EXAMPLE #1

Compare the G/T performance of a 10 ft. parabolic reflector and an LNA with a noise temperature of 120 kelvins at C band versus a 6 ft. parabolic reflector and an LNA noise temperature of only 35 kelvins. Assume an antenna temperature of 25 kelvins and no coax cable loss between the LNA and antenna feed.

DISH DIAMETER	ANTENNA GAIN dBi	GAIN ratio	Ta	Tl	Tr	Ttot	G/T
6 ft.	35.0 dBi	3162	25°	0°	35°	60°	+17.2 dB
10 ft.	39.5 dBi	8912	25°	0°	120°	145°	+17.9 dB

The results show comparable receive performance for both systems

EXAMPLE #2

Consider a similar analysis between two systems where both systems have a 10 ft. parabolic reflector antenna and one system has a 120 degree LNA and the second system has a 35 degree LNA.

DISH DIAMETER	ANTENNA GAIN dBi	GAIN ratio	Ta	Tl	Tr	Ttot	G/T
10 ft.	39.5 dBi	8912	25°	0°	35°	60°	+21.7 dB
10 ft.	39.5 dBi	8912	25°	0°	120°	145°	+17.9 dB

The analysis shows a 3.8 dB improvement in G/T and therefore signal to noise ratio for the lower noise LNA.

3. COOLING A GaAs FET LNA

It has already been shown that with the low antenna temperatures that are typical of the microwave frequencies, noise figures less than 1 dB can provide a significant increase in system sensitivity. Typically the best noise figures that can be obtained with today's MESFETs operating at room temperature are in the 0.5 dB region. Lowering the LNA noise figure below 0.5 dB

typically requires that the device or the entire LNA be physically cooled in some fashion.

Some low noise devices appear to cool better than others. Most device noise figures will decrease with decreasing temperature, however, some device's noise figures will improve more for a given temperature change. Some of this may be due to bias changes or even matching network changes which are hard to evaluate when the entire LNA is at cold temperatures.

A colleague of mine, Tom Henderson, built and tested two 1300 MHz low noise amplifiers similar to those described in the February 1989 RF Design article on Low-noise VHF and L-band GaAsFET amplifiers. One of the LNAs uses the Avantek ATF-10135 and the other LNA uses an Avantek ATF-13284. The ATF-10135 is a 500 micron FET typically used at C band while the ATF-13284 is a 250 micron FET typically used in Ku band applications. Tom was able to perform noise figure tests at 295 kelvins, 200 kelvins and 100 kelvins. The ATF-10135 LNA was further tested by Bill Lakatos at the NRAO who was able to cool the LNA down to 18 kelvins. The results of the tests are as follows:

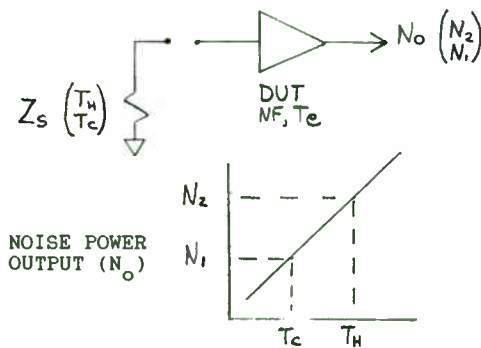
DEVICE	Noise Figure	Gain	Kelvins
ATF-10135	0.52 dB	13.5 dB	298
	0.33 dB	14.4 dB	100
	0.28 dB	14.7 dB	18
ATF-13284	0.60 dB	15.0 dB	295
	0.43 dB	16.1 dB	200
	0.38 dB	16.5 dB	150

Assuming an antenna temperature of 25 kelvins, cooling the ATF-10135 from 298 kelvins to 18 kelvins results in a sensitivity improvement of 1.45 dB. Of course the cost of cooling the LNA must

be weighed against the cost of increasing antenna gain by a like number of dB.

4. NOISE FIGURE MEASUREMENT UNCERTAINTIES

THE NOISE FIGURE MEASUREMENT-Y FACTOR METHOD REVIEWED



Th=SOURCE TEMP. ON (K)
 Tc=SOURCE TEMP. OFF (K)
 Te=RECEIVER TEMP. (K)
 K=BOLTZMANN'S CONSTANT
 =1.38E-23 JOULE/K
 G=GAIN
 B=BANDWIDTH (Hz)
 DUT= DEVICE UNDER TEST

NOISE SOURCE TEMPERATURE (T_x)

$$Y = \frac{N_2}{N_1} = \frac{kGB (T_h + T_e)}{kGB (T_c + T_e)}$$

$$T_e = \frac{T_h - Y T_c}{Y - 1}$$

OR SINCE $NF = \frac{T_e + T_o}{T_o}$

$$F = \frac{((T_h/T_o)-1) - Y ((T_c/T_o)-1)}{Y - 1}$$

IF $T_c = T_o$ THEN

$$F = \frac{(T_h/T_o)-1}{Y - 1}$$

CONVERTING TO NOISE FIGURE (dB) YIELDS

$$NF(dB) = 10 \text{ LOG } ((T_h/T_o)-1) - 10 \text{ LOG } (Y-1)$$

$$= \text{E.N.R.} - 10 \text{ LOG } (Y-1)$$

EXAMPLE

E.N.R. = 5.2 dB
 $Y = 6 \text{ dB OR } 4 \text{ EXPRESSED AS A RATIO}$

$$NF (dB) = 5.2 \text{ dB} - 10 \text{ LOG } (4-1)$$

$$= .43 \text{ dB}$$

Gain is calculated from the slope of the noise power versus noise source temperature curve.

$$G = \text{SLOPE} = \frac{N_2 - N_1}{T_h - T_c}$$

Factoring out the second stage noise figure yields DUT noise figure.

$$NF = NF_{\text{total}} - \left\{ \frac{NF_{\text{second stage}} - 1}{\text{GAIN}_{\text{dut}}} \right\}$$

EXCESS NOISE SOURCES

I Excess Noise Ratio - ENR

HP346B 15.2 dB NOMINAL
 HP346A 5.2 dB NOMINAL

RSS UNCERTAINTY +/- .09 dB 10 MHz - 12 GHz
 +/- .11 dB 12 GHz - 18 GHz

RSS = ROOT SUM OF THE SQUARES

HIGHER ENR NOISE SOURCE MORE APPROPRIATE FOR HIGH NOISE FIGURE DUTs

II MAXIMUM VSWR (REFLECTION COEFFICIENT Γ_o)

	10-30 MHz	30-5000 MHz	5-18 GHz
HP346B	1.3:1(0.13)	1.15:1(0.07)	1.25:1(0.11)
HP346A	1.3:1(0.13)	1.15:1(0.07)	1.25:1(0.11)

III CHANGE IN REFLECTION COEFFICIENT WITH SOURCE ON OR OFF

- 346B NOT SPECIFIED-TYPICALLY 0.02 - 0.035
- 346A SPECIFIED AT 0.01 MAXIMUM

AFFECTS NOISE AND GAIN MEASUREMENTS ON MOST AMPLIFIERS
SINCE AMPLIFIERS WITHOUT ISOLATORS ARE GENERALLY
SENSITIVE TO SOURCE VSWR

IV ADDING AN ATTENUATOR TO HP346B NOISE SOURCE TO IMPROVE
ON/OFF VSWR CHANGE

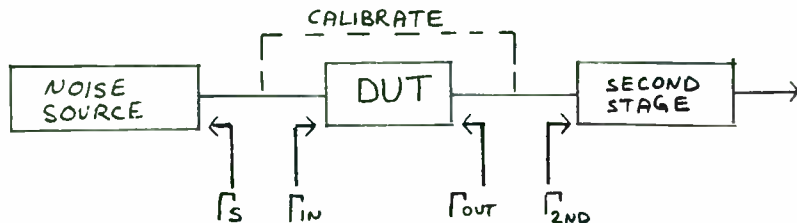
$$\text{ADJUSTED ENR} = \text{INITIAL ENR} - \text{ATTENUATOR LOSS(dB)}$$

@ $T_a = 290$ KELVINS

OR $T_e(\text{adjusted}) = T_h/L + (1-(1/L)) * T_a$
WHERE L IS GREATER THAN OR EQUAL TO 1
AND LOSS(dB) = 10 LOG L
AND T_h = SOURCE TEMPERATURE WHEN SOURCE
IS ON

$$\text{ADJUSTED ENR} = 10 \text{ LOG } \frac{T_e - T_o}{T_o}$$

EFFECT OF VSWR ON NOISE FIGURE MEASUREMENT



The noise figure equipment is calibrated by bypassing the DUT and measuring the second stage noise figure. Both noise figure and gain are then measured after the DUT is substituted back into the system.

The technique of "DUT substitution" uses the available gain technique whereby the result takes into account the mismatch that

occurs at the input and output of the DUT. As an example, consider the noise source that is emitting T_h into the DUT. If the DUT input VSWR is 1.0:1 then all of the available noise power is dissipated in the DUT. If the DUT input VSWR is not 1.0:1 then some of the noise power is reflected back into the noise source. If the noise source has a 1.0:1 VSWR, then all of the reflected power is absorbed in the noise source. If, however, the noise source does not have a 1.0:1 VSWR, then the residual reflected power is rereflected back to the DUT. The result is uncertainty in the noise figure measurement due to multiple reflections due to both the source and load VSWRs and their interaction with the DUT input and output VSWR. Depending on the phase angle of the reflection coefficients, they may add in phase or out of phase. The result again is uncertainty in both the gain and noise figure measurements.

By only measuring reflection magnitude, the worst case uncertainty is the mismatch loss (ML) where:

$$ML = 20 \text{ LOG } (1 +/\- \Gamma_s \Gamma_2)$$

$$\text{where } \Gamma_x = \frac{VSWR_x - 1}{VSWR_x + 1}$$

EXAMPLE

Γ_s	=	.07	(1.15:1 VSWR)
Γ_{in}	=	.33	(2.0:1 VSWR)
Γ_{out}	=	.20	(1.5:1 VSWR)
Γ_{2nd}	=	.33	(2.0:1 VSWR)

$$ML (\text{input}) = +.198 \text{ dB} \quad \sim \text{+/- } .2 \text{ dB}$$

$$- .202 \text{ dB}$$

$$ML (\text{output}) = +.555 \text{ dB} \quad \sim \text{+/- } .57 \text{ dB}$$

$$- .593 \text{ dB}$$

RSSing suggests that the gain uncertainty be +/- .6 dB. The mismatch also affects the noise figure measurement since DUT gain

is used in factoring out the effect of the second stage noise figure. However, most of the noise figure uncertainty is due to the input mismatch loss.

Solutions to minimize errors:

- *Use isolators on input to DUT and input to second stage
- *Alternative is to use an attenuator at input to second stage
- *Design DUT with as low an input VSWR and output VSWR as possible.

ABOVE ALL !!!! Use a noise source with as low a VSWR as possible to minimize the rereflection of noise energy back into the DUT. This will help guarantee the most accurate noise figure measurement on a DUT with high input VSWR.

The following table shows the effect of noise source and DUT input VSWR on mismatch loss. The mismatch loss directly relates to noise figure uncertainty.

MISMATCH LOSS	NOISE SOURCE VSWR	DUT INPUT VSWR
+/- .19 dB	1.05:1 (.024)	17.0:1 (.89)
+/- .11 dB	1.05:1 (.024)	3.0:1 (.50)
+/- .07 dB	1.05:1 (.024)	2.0:1 (.33)
+/- .81 dB	1.23:1 (.100)	17.0:1 (.89)
+/- .45 dB	1.23:1 (.100)	3.0:1 (.50)
+/- .29 dB	1.23:1 (.100)	2.0:1 (.33)

An input VSWR of 17.0:1 which corresponds to an input return loss of 1 dB was actually measured on a low noise GaAs FET LNA at VHF frequencies. The table clearly shows that the uncertainty in measuring a high input VSWR LNA is reduced to an acceptable value when using a low VSWR noise source.

The graphs that follow show graphically the effect of source and

DUT VSWR on measurement accuracy. They are from HP Application Note 64-3 and are courtesy of Hewlett Packard.

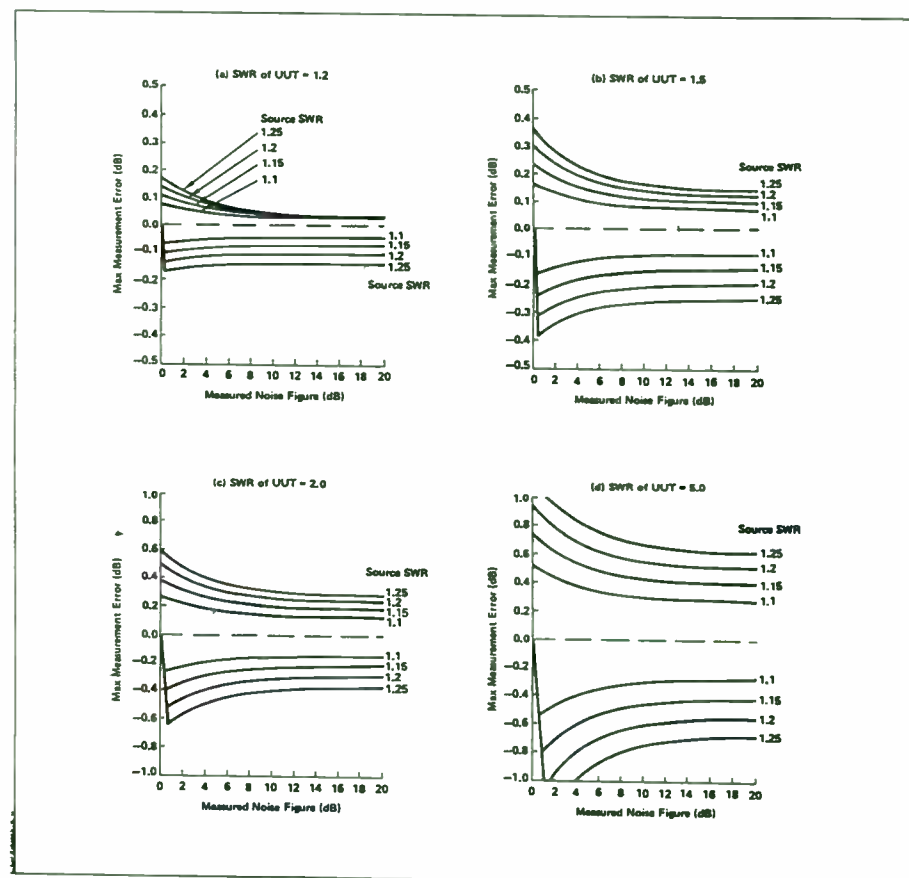


Figure 1-4. The worst case errors in the measured noise figure caused by rereflections between the noise source and UUT. Each graph is for a different UUT input SWR.

From HP Application Note 64-3, Hewlett-Packard

EFFECT OF MISMATCH ON ACTUAL NOISE FIGURE OF DUT

PROBLEM: How sensitive is the noise figure of an LNA to a change in source impedance?

DISCUSSION: This depends on the type of semiconductor device and the topology of the input matching network. As the impedance of the noise source changes between T_h and T_c , the apparent LNA noise figure and gain may vary, causing measurement errors. Having a low VSWR noise source with minimal change in VSWR between states will minimize the problem.

Another variation of the problem occurs when the LNA is connected to the antenna. Is the VSWR of the antenna known? How much different is it as compared to the noise source? At frequencies below 1 GHz, the VSWR of the HP346A is less than 1.05:1. What effect does the different source impedance of the antenna have on LNA performance? This question is a two part problem. First off, the LNA which was optimized with a noise source with a near perfect 1.05:1 VSWR is now connected to an antenna with a VSWR of 1.23:1 as an example. Since the LNA was optimized on a near perfect system there is the potential for an increase in mismatch loss between the antenna and the LNA. Like the uncertainty terms discussed earlier, if the phase of the reflections are known, then the precise effect on noise figure can be calculated. Otherwise, all that can be done is to calculate the magnitude of the uncertainty associated with using a higher VSWR antenna.

Consider the example of an LNA with an input VSWR of 2.0:1.

Consulting the mismatch loss table in the previous discussion, reveals an increase in mismatch loss of 0.29 dB - 0.07 dB = 0.22 dB. 0.22 dB of noise figure may seem like a trivial amount until the effect on receiver sensitivity is calculated assuming a quiet antenna. In a typical space application, the 0.22 dB increase in noise figure from 0.4 dB to 0.62 dB could result in a system sensitivity loss of 1.2 dB! The solution is to tune the antenna for less than a 1.1:1 VSWR.

The second part of the problem relates to how sensitive the amplifier is to source VSWR changes. With the help of gain /noise figure contour curves, the sensitivity of the device to various impedances is understood. Generally the input matching network is designed to transform the 50 ohm source impedance to the reflection coefficient that produces minimum noise figure within the device. Now that matching networks are installed around the low noise device, the sensitivity of the LNA to source impedance changes is desired. As the source impedance departs from the design impedance of 50 ohms, the noise figure will increase but by how much?

The equation that will predict the change in amplifier noise figure with varying source impedance is identical to the formula that generates the familiar noise figure contour curves for the devices.

$$NF = F_{min} + 4 r_N \left[\frac{|\Gamma_s - \Gamma_0|^2}{|1 + \Gamma_0|^2 \cdot (1 - |\Gamma_s|^2)} \right]$$

Fmin is the noise figure of the amplifier when Γ_s is equal to 0.0. Γ_o is the reflection coefficient required for minimum noise figure. r_n for the entire LNA, which is the rate of change in noise figure as the impedance varies from 50 ohms, must be calculated or measured. r_n is normalized to 50 ohms and will vary depending on the type of matching network chosen.

EESOF has incorporated a routine in Touchstone version 2.1 that calculates noise parameters at the circuit level. The NPAR routine will generate a similar set of noise parameters for both the device and the circuit consisting of the device plus matching networks. This information can be extremely important to the design engineer in determining the optimum input matching network.

Consider the 1300 MHz LNA described in Feb 1989 RF Design that uses the Avantek ATF-10135. This circuit was analyzed by Touchstone 2.1 and the following set of noise parameters was obtained. Compare the circuit parameters to those of the device by itself. The noise figure circles project that a 3.0:1 VSWR source impedance will deteriorate the LNA noise figure by only 0.25 dB. This analysis shows the insensitivity of this amplifier to varying source impedance. How does this compare to other LNAs?

NOISE PARAMETERS	NFo dB	Gamma Mag	Opt Ang	Rn/50
DEVICE	0.40	.805	30.9	.628
CIRCUIT	0.44	.107	-5.8	.094

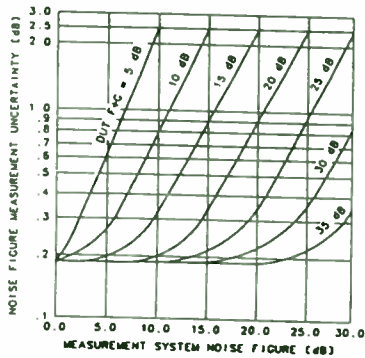
EFFECT OF SECOND STAGE NOISE FIGURE ON MEASUREMENT UNCERTAINTY

Second stage or system noise figure directly affects the uncertainty of the DUT noise figure. The system consists of the noise figure meter and in some cases a downconverter. Generally the system components are calibrated out by the noise figure meter as in the case of the HP8970. However, high second stage noise figure does add to the uncertainty of the measurement. In order to minimize the uncertainty, it is important to insure that the noise power output from the DUT be at a level significantly above the noise floor of the measuring system. According to Hewlett Packard for the HP8970, the noise figure of the system should be atleast as low as Fmin to minimize measurement error.

$$F_{min} = NF_{dut} + GAIN_{dut} - 15 \text{ dB}$$

If the NF_{dut} plus GAIN_{dut} is less than 15 dB, then a low noise amplifier should be added in front of the measurement system, i.e. something in the 2 to 3 dB noise figure range with enough gain to set the noise figure of the measurement system.

The following graph will help determine the required system noise figure to minimize uncertainty. As an example, when using the noise figure meter at frequencies less than 1600 MHz, with its typical 5 to 9 dB noise figure, amplifiers with a combined noise figure plus gain of atleast 20 dB can be measured with almost negligible degradation in uncertainty due to second stage effects. An example might be an LNA with a noise figure of 1 dB with atleast 19 dB of gain.



Noise Figure Measurement Uncertainty versus Measurement System Noise Figure

This is a graph of overall noise figure measurement uncertainty versus measurement system noise figure. "DUT F + G" is the device under test noise figure plus gain in dB. The curves are based on typical values of noise figure instrumentation uncertainty (0.1 dB), gain instrumentation uncertainty (0.15 dB), noise source ENR uncertainty (0.1 dB), measurement system SWR (1.7), noise source SWR (1.15), DUT input SWR (1.5) and DUT output SWR (1.9).

EXAMPLE

The difference in noise figure reading between Tc at 74.3 degrees F versus 84.3 degrees F is simply the ratio

$$\begin{aligned} \text{ERROR (dB)} &= 10 \text{ LOG } \frac{302.1}{296.5} \\ &= .08 \text{ dB} \end{aligned}$$

An additional error that needs to be accounted for when attempting to reproduce reliable measurements is the absolute temperature of the noise source as it warms up. Tests run on an HP346A noise source indicate that after the noise source has been on and the temperature stabilized for several hours that the body temperature rose 3.9 degrees over the ambient air temperature. At an ambient air temperature of 296.5 kelvins, this equates to an apparent noise figure degradation of .057 dB. To take this into account, the HP8970 needs to be updated. (SPECIAL FUNCTION 6.0)

IMAGE REJECTION

A lack of image rejection will result in an apparent (but not realistic) improvement in noise figure over a system that has adequate image rejection. The best place to put an image reject filter is at the input to the mixer. This will insure a SSB type measurement by rejecting image noise from the LNA. The following table shows the effect of image rejection on measurement error.

OTHER SUBTLE EFFECTS

EFFECT OF AMBIENT TEMPERATURE ON MEASUREMENT

Nout from a resistor varies as a function of temperature

$$N_{out} = KToB$$

Noise figure measurements with the HP8970 are based on a Th/Tc ratio where Tc is assumed to be at 296.5 kelvins unless it is instructed differently. (Special Function 6.0)

If the ambient temperature is other than 296.5 kelvins then Tc should be adjusted per the following table.

TEMPERATURE TABLE	
°F	K
62.6	290
74.3	296.5
84.3	302.1

IMAGE REJECTION	NF ERROR
0 dB	3.00 dB
6	1.25
10	0.46
13	0.22
20	0.04

NOISE FIGURE MEASUREMENT UNCERTAINTIES

CONCLUSIONS

SATURATION/RECEIVER LINEARITY

When measuring a broadband receiver, care should be taken to insure that no stage of the DUT is being driven to compression. The noise source is a broadband source generating noise from a few kHz to beyond 18 GHz. Appropriate frontend preselection and IF filters should be utilized.

SPURIOUS SIGNALS

Any spurious signals generated in the receiver either from the local oscillator or an unstable amplifier will give erroneous noise figure measurements. Any extraneous signals radiating in the lab will also effect the measurement, hence a shielded screen room is desirable.

1. Use a noise source that has a low VSWR, i.e. less than 1.1:1 and preferably 1.05:1. It is important that there be very little change in reflection coefficient between the ON and OFF states, preferably 0.01 maximum. The HP346A is preferred but the HP346B with an attenuator will do fine for measuring low noise amplifiers. Isolators are convenient for test but lossy and bulky for the actual system.

2. Using a noise source with a 1.05:1 VSWR reduces the uncertainty in noise figure due to mismatch loss to about 0.1 dB assuming that the DUT input VSWR is no greater than 3.0:1.

3. Taking into account ENR uncertainty, instrumentation uncertainty, mismatch uncertainty (with dut input vswr of 2.0:1), an overall uncertainty can be estimated. Since all of the variables are random and independent from each other, it is possible to RSS the quantities to determine the typical error.

ENR	+/- .09dB
INSTRUMENTATION	+/- .10 dB
MISMATCH	+/- .15 dB
RSSing YIELDS	+/- .20 dB

4. In order to realize the low noise performance of an amplifier when installing in the system, the antenna VSWR must be as low as possible, i.e. 1.1:1 or better. A 1.23:1 VSWR may contribute up to 0.22 dB additional loss resulting in an additional 1.2 dB of

sensitivity degradation in a typical satellite receiving system.

5. Design an LNA with a matching network that minimizes the source impedance's effect on device noise figure.

6. Insure that the second stage noise figure is low enough to minimize its' effect on measurement accuracy.

7. Adjust T_c as necessary to offset changes in ambient air temperature. Can amount to over 0.1 dB of error if not taken into account.

8. Require a minimum of 20 dB of image rejection to insure less than 0.05 dB of noise figure uncertainty. Prefer 30 dB.

SPICE Modeling And Simulation Of An 800MHz, Class-AB Push-Pull Amplifier (1)

Richard LaLau
Mobile Data International Inc.
11411 Number 5 Rd.
Richmond, B.C.
V7A 4Z3
(604) 277 - 1511

ABSTRACT

For years, RF and microwave designers have done a large portion of their design work on the lab bench with a soldering iron and tuning tools. Recent developments of powerful software simulation programs, which accurately predict circuit performance, have reduced dependence on prototyping to determine design functionality.

A design procedure for a linear, Class-AB, 5 Watt, single stage push-pull amplifier is presented utilizing BJT power transistor SPICE modeling and circuit simulation using EEsof's Touchstone®, Libra® and mwSPICE®. Two-tone third order intermodulation, AM/AM, and frequency response is predicted. Simulation results are verified by measured data from the fabricated amplifier. The SPICE model was developed using simple equipment available in any RF lab. Satisfactory results are achieved even though the model does not perfectly represent the selected transistor.

1. INTRODUCTION

The design of Class-AB amplifiers is an inexact art. The reason for the uncertainty is the lack of impedance data measured at the intended operating power levels and bias conditions. The impedance data can be obtained either from direct measurement, rule-of-thumb approximations from Class-C values, or SPICE (Simulation Program with Integrated Circuit Emphasis) modeling. Since large-signal terminal impedances are difficult to measure and approximations are too inexact, the best alternative is modeling which can predict circuit performance at any power level or bias. A possible design procedure might consist of these steps

1. The work detailed in this article was performed entirely at Simon Fraser University, Burnaby B.C. as partial fulfillment for the degree Bachelor of Applied Science (Engineering). None of this work, or the circuits described, are or will be used by Mobile Data International Inc., Richmond B.C.

- perform system design, select amplifier topology and a suitable transistor,
- model the transistor,
- design a bias circuit to provide for constant collector current over temperature,
- determine optimum matching networks for maximum gain,
- calculate microstrip dimensions,
- simulate performance, try alternatives,
- perform a thermal analysis to determine heat-sinking requirements,
- fabricate, tune and test.

This paper will show that even with a model developed using simple equipment available in any RF lab, satisfactory results can still be achieved. A power transistor will be modeled by a small-signal transistor's model and an area scaling factor.

2. SPICE MODELING

A Bipolar Junction Transistor (BJT) can be described using both linear and nonlinear models. Linear models enable frequency-domain simulators to predict small signal performance of the device at fixed bias points. Changing the bias point requires new model parameters measured under the new bias conditions to accurately simulate transistor performance. Nonlinear models, like the classic Gummel-Poon (G-P) large-signal transport BJT model shown in Figure 1, include bias dependence and can simulate devices under large-signal and transient conditions (Bunting 1989).

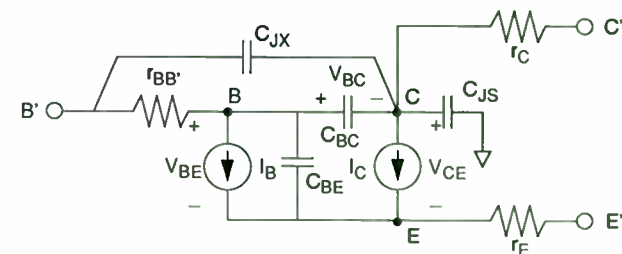


Figure 1 Gummel-Poon large-signal transport equivalent circuit.

The purposes of the G-P model parameters are summarized as follows (EESof 1989)

- I_S , β_F , I_{KF} , n_F , I_{SE1} , and n_{EL} determine the high and low forward-current gain characteristics,
- β_R , I_{KR} , n_R , I_{SC} , and n_{CL} determine the high and low reverse-current gain characteristics,
- V_A and V_B determine output conductances for forward and reverse regions,
- r_B , r_C , and r_E model the ohmic resistances between the active base, collector, and emitter regions and the actual device terminals. r_B can have a high current dependence which is described by r_{BM} and I_{rB} ,
- τ_F , τ_R , I_{TF} , V_{TF} , and P_{TF} model the base charge storage effects, τ_F may be bias dependent,
- C_{JE} , C_{JC} , C_{JS} , V_{JE} , V_{JC} , V_{JS} , M_{JE} , M_{JC} and M_{JS} describe the non-linear depletion capacitances for base-emitter, base-collector and collector-substrate junctions.

Complete definitions and derivations are available in Getreu (1976).

2.1 PARAMETER EXTRACTION

The procedure for determining DC parameters of the G-P model involves gradient inspection of logarithmic collector current, ($\ln I_C$), versus base-emitter voltage, V_{BE} , and logarithmic base current, ($\ln I_B$), versus V_{BE} , for $V_{BC} = 0$ V, as shown in Figure 2. These measurements are repeated for both forward and reverse biases to determine forward and reverse current gain data and the dependence of current gain on collector current.

In practice, evaluating the DC model parameters is not a trivial matter. Several measurements must be performed with $V_{BC} = 0$ V; achieved by adjusting base and collector supplies, not by shorting the base and collector terminals.

A correction must also be applied to the high current portion of the $\ln I_B$ and $\ln I_C$ curves to eliminate the effects of r_B and r_E . These ohmic resistances eliminate the straight-line portion of

the $\ln I_B$ curve and prematurely roll-off the $\ln I_C$ curve shown in Figure 3. A typical correction consists of

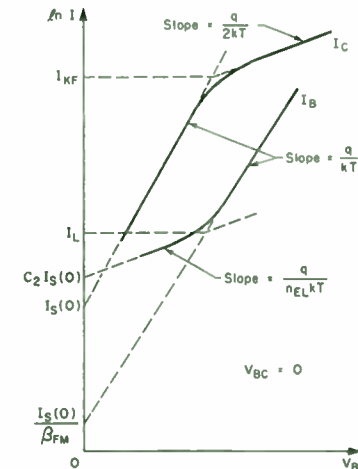


Figure 2 Plot of $\ln I_C$ and $\ln I_B$ versus V_{BE} for $V_{BC} = 0$ (Massobrio and Antognetti 1988).

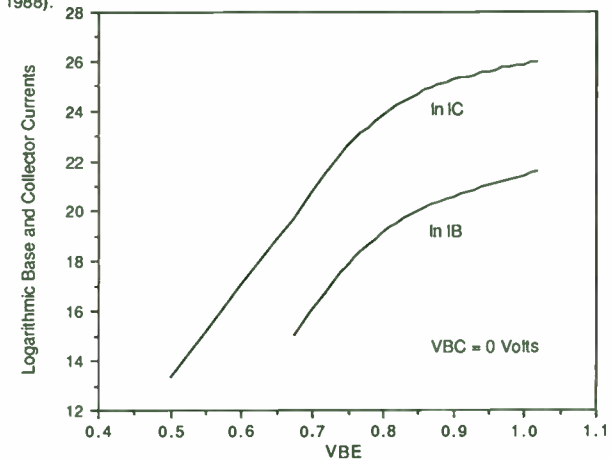


Figure 3 High current ohmic resistance effects as measured for the MRF581A transistor.

1. Extrapolating the ideal straight-line portion of the $\ln I_B$ curve with slope q/kT .

1. In older versions of SPICE C_2 and C_4 are sometimes used in place of $I_{SE} (= C_2 \times I_S)$ and $I_{SC} (= C_4 \times I_S)$.

- Assuming that the horizontal distance from the extrapolated ideal $\ln I_B$ curve is due to $I_B r_B + I_E r_E$, subtract this amount from the $\ln I_C$ curve to determine the true high collector current roll-off (Getreu 1976).

Once the correction has been applied, transistor parameters can be calculated using simple algebra as suggested in Figure 2.

The emitter ohmic resistance, r_E , can be obtained by determining the slope of the base current plot as a function of collector-emitter voltage, V_{CE} , with the collector open-circuited.

A problem associated with measuring the collector ohmic resistance, r_C , is determining which value to use. The value for r_C depends strongly on how the transistor is used or which aspect of the device's behavior needs modeling. An adequate approximation of r_C is the slope of the saturation region of the characteristic I-V curve.

The base ohmic resistance, r_B , has traditionally been the most difficult parameter to measure accurately, mainly because it is modeled as a lumped constant resistance when it is actually a distributed, variable resistance (Hauser 1964). The value for r_B depends on the measurement technique used and the device's operating conditions. r_B should be determined by the method closest to the actual operating conditions. A few possible methods include noise, pulse, input impedance circle, and phase cancellation measurement techniques (Getreu 1976).

Zero-bias junction and substrate capacitances can be measured with a capacitance bridge. Capacitance values are measured for several voltages, plotted and the zero-bias value determined by extrapolating the curves to zero volts. This method is sufficiently accurate at RF frequencies to produce reliable results. At frequencies above 1 GHz parasitic effects introduce significant errors. Default values for barrier potentials V_{JE} , V_{JC} , and V_{JS} , and gradient factors M_{JE} , M_{JC} and M_{JS} provide suitable estimates for most applications.

Transit time parameters can be approximated from the data sheet value of f_T . For greater accuracy, this parameter must also be characterized at the bias value specified by the circuit application.

To build a complete parameter set, valid over a broad temperature range, the entire measurement process must be repeated for forward and reverse conditions at the upper, lower and mean temperatures to calculate temperature coefficients. These coefficients model parameter variations as the device heats up or is subjected to changes in ambient conditions. However, from

experience, forward and reverse parameters measured at room temperature adequately predict circuit performance.

For more background on SPICE modeling and parameter extraction read Getreu (1976) and Antognetti and Massobrio (1988).

Before performing any measurements, every effort should be made to convince the vendor to supply the device model. In a few years, device models should become available in data books.

2.2 PARAMETER VERIFICATION

Before a device's parameter set is accepted as gospel it should be tested. DC model parameters can be verified by comparing SPICE generated characteristic I-V curves with measured curves, as shown in Figure 4. Some deviation from the high current I_C curve can be expected since the model used did consider the effects of junction heating.

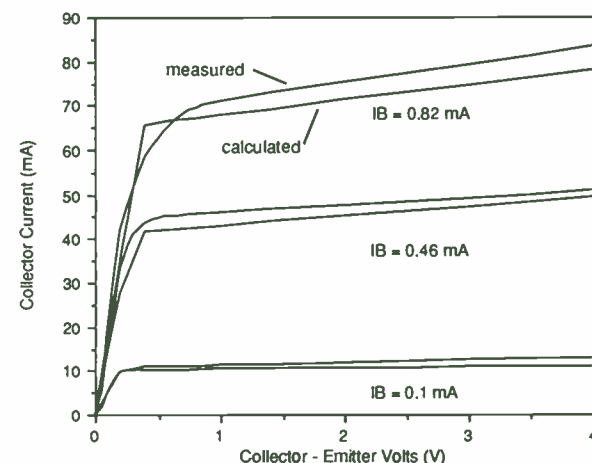


Figure 4 Comparison of calculated and measured characteristic I-V curves for MRF581A transistor.

The AC model parameters can be tested by calculating the device's S-Parameters and comparing with the manufacturer's quoted values as shown in Table 1. Values for S_{12} and the magnitude of S_{22} are not within acceptable error (recall that published data book specifications are averages taken over several lots; hence, if calculated values are within 30% of data sheet values

and show the same trends, the model parameters are probably valid). However, for amplifier design, S_{12} can be ignored. The error in S_{22} will reduce the software's ability to accurately predict frequency response. To test the model further and check the effects of S-Parameter error the model was also tested in a design for the Class-A amplifier shown in Figure 5. Libra1 linear and harmonic balance predicted performance closely agrees with measured results as shown in the following figures. The circuit file may be found at the back of this article.

Frequency (MHz)	S_{11}	S_{21}	S_{12}	S_{22}
300	0.66 -172	8.46 93	0.05 49	0.30 -134
500	0.68 174	5.06 82	0.07 56	0.25 -147
800(2)	0.68 164	3.61 72	0.10 61	0.24 -162
1000	0.68 157	2.64 65	0.12 64	0.23 -172
mwSPICE Calculated				
300	0.85 -167	7.33 98	0.04 9.1	0.66 -158
500	0.86 -172	4.44 93	0.04 5.5	0.66 -166
800	0.87 -175	2.79 88	0.04 3.4	0.66 -171
1000	0.87 -176	2.23 86	0.04 2.7	0.66 -172

Table 1 Comparison between simulated S-Parameters and data book values for the MRF581A transistor for $I_C = 100$ mA and $V_{CE} = 10$ V.

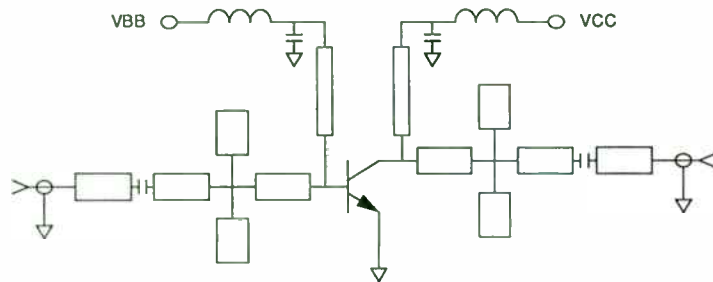


Figure 5 MRF581A, Class-A amplifier (See circuit file for component values).

1. mwSPICE, Touchstone, Libra and LineCalc are products of EEsos Inc., Westlake Village, CA, USA.
2. Linearly approximated by Touchstone

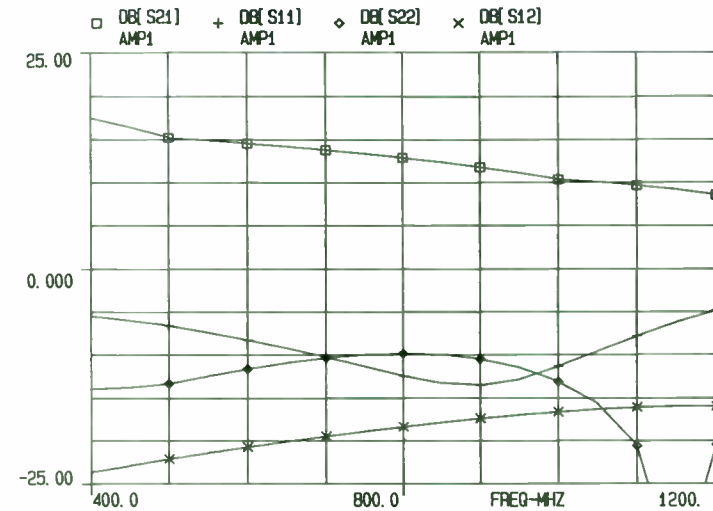


Figure 6 Touchstone predicted Class-A amplifier S-Parameters using the MRF581A transistor.

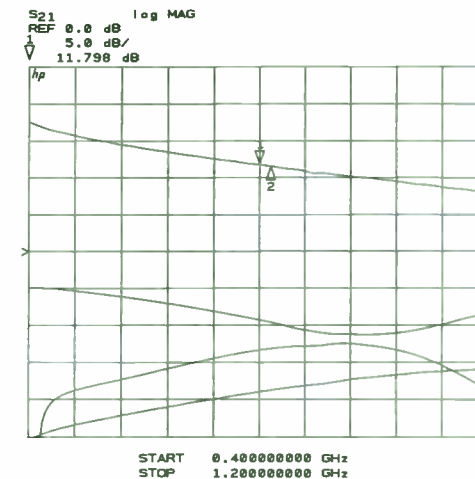


Figure 7 Measured (HP8510A) Class-A amplifier S-Parameters using the MRF581A transistor.

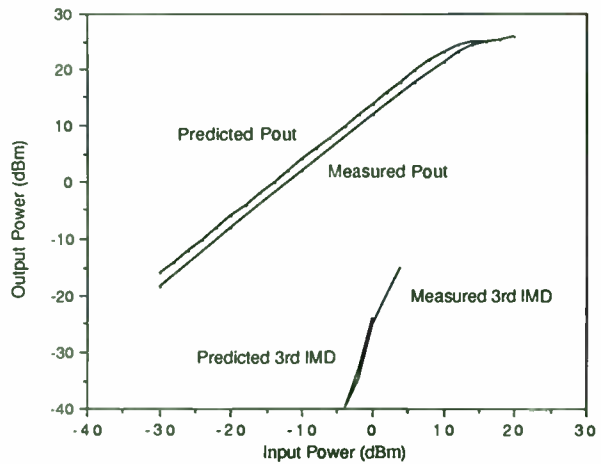


Figure 8 Libra predicted and measured AM/AM and third order intercept.

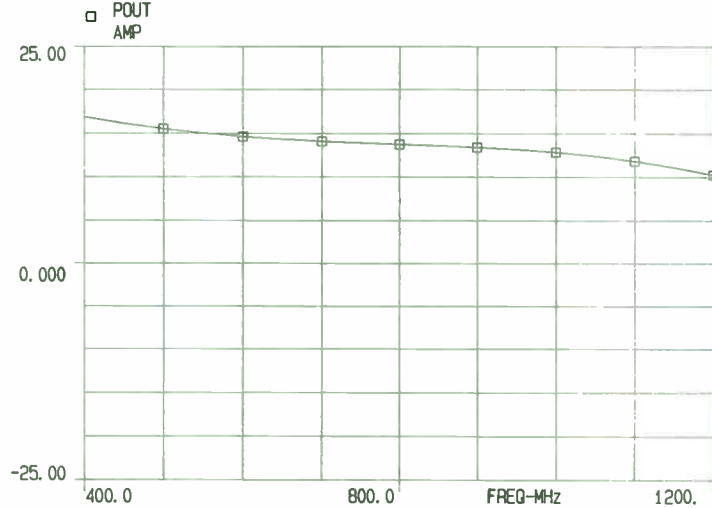


Figure 9 Libra predicted frequency response.

From these tests, in spite of the poor agreement in S_{22} , the model adequately predicts circuit performance of the MRF581A transistor. Based on this known performance, and the fact that the MRF581A is approximately a one quarter scaled version of the MRF839F power transistor, the model will be used to predict its terminal characteristics and in-circuit performance.

2.3 ADVANTAGES AND DISADVANTAGES

The primary advantage of this form of transistor modeling is equipment simplicity; apart from the measurement of base ohmic resistance, r_B , most parameters are easily measured. Disadvantages include the several different equipment set-ups required to build a complete data set, prolonged characterization times and the likelihood of an error.

3. CLASS-AB AMPLIFIER DESIGN AND SIMULATION

MRF839F impedance data were calculated from the SPICE model of the MRF581A transistor in mwSPICE at the anticipated quiescent point using a four times area scaling factor. With this data in consideration, the matching networks were designed with a Smith Chart (Abrie 1985, Bowick 1982, Gonzales 1984), transferred to microstrip using LineCalc and verified/optimized in Touchstone. Finally, the entire amplifier design was simulated in Libra.

The circuit file was built up in sections. First a single ended, Class-AB amplifier was simulated. Libra did not produce the expected clipped output waveform even with a large number of harmonics, instead, an undistorted amplified sine wave resulted. It was hypothesized that the undistorted output was due to the resonant characteristics of the matching circuitry. Next, two single ended amplifiers were paralleled and driven from an ideal 180° splitter. Libra could not handle the coaxial splitter used in the actual amplifier so a centre tapped transformer element was used instead. Lastly, an output combiner was included to complete the amplifier topology shown in Figure 10.

Based on this initial simulation, the amplifier was built and tested. The fabricated amplifier's performance differed considerably from predicted. The difference was attributed to unaccounted parasitics, inexactness of the four times area scaling factor and initial inaccuracies in the small-signal model (S_{22}). Inclusion of some estimated parasitics into the circuit file significantly reduced the difference between predicted and measured results. In the end, the software did give a good indication of how the circuit would perform, but the match between measured and predicted performance was not as good as with the Class-A amplifier.

The following figures summarize the final results.

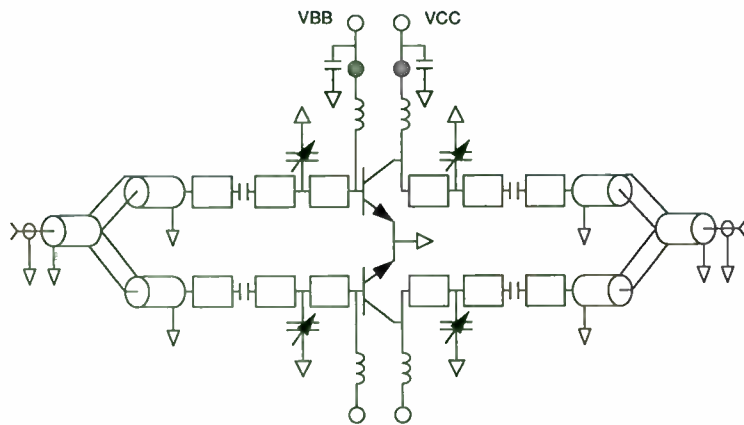


Figure 10 MRF839F, Class-AB amplifier (See circuit file for component values).

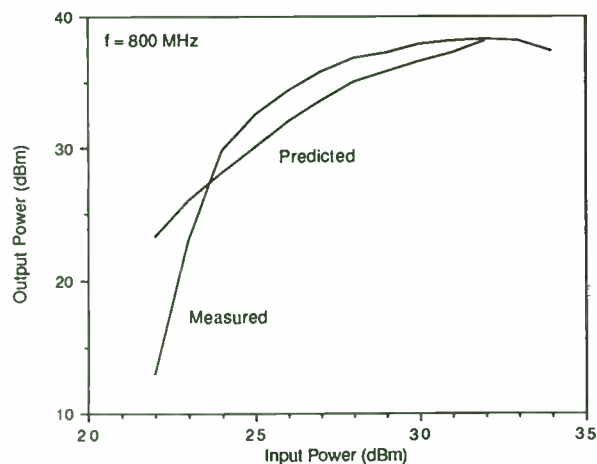


Figure 11 Libra predicted and measured AM/AM.

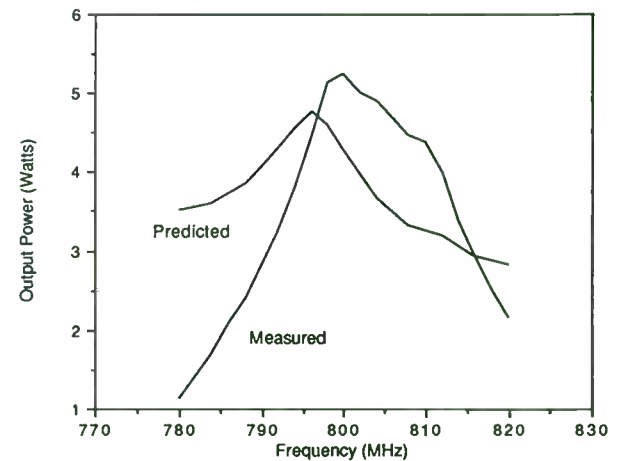


Figure 12 Libra predicted and measured frequency response.

4. CONCLUSION

This paper has discussed power amplifier simulation using the G-P BJT SPICE model. An overview of some critical model parameters and three tests used to verify the device model were presented. Lastly, the model was used to predict performance of a Class-AB push-pull power amplifier.

Considerable effort is needed to develop and verify a transistor's SPICE model. If a suitable model library is not available, simulation should not be considered unless accompanied by a willingness to put this effort into device modeling and testing.

Non-linear simulation is not a one shot effort. An initial simulation will give preliminary indication of circuit function. Once the circuit has been built, subsequent simulation is used to locate differences between the desired and actual circuit. Based on this second simulation, improvements to the design can be predicted.

The availability of simulation tools does not lessen the requirement for good circuit design, a great deal of interpretation is still required to understand what is happening at the component level and to appreciate software limitations.

5. ACKNOWLEDGEMENTS

I am indebted to Dr. Shawn Stapleton of Simon Fraser University for initiating this paper, contributing helpful insight, ideas and funding and to Mr. Ron Vanderhelm of Mobile Data International for his time and willingness to review the work.

6. REFERENCES

- Abrie, P.L.D., Design of Impedance Matching Networks for Radio Frequency and Microwave Amplifiers. Artech House, 1985.
- Antognetti, P. and G. Massobrio, Semiconductor Device Modeling With SPICE. McGraw Hill, 1987.
- Bowick, C., RF Circuit Design Theory. Howard W. Sams, 1982.
- Bunting, J., "Nonlinear BJT model accurately simulates microwave operation," Microwaves and RF, vol.28, no. 11, pp. 77-87, Nov. 1989.
- EEsof, Elements Catalog, February 1989.
- Getreu, I., Modeling the Bipolar Transistor. Elsevier Scientific, 1976.
- Gonzalez, G., Microwave Transistor Amplifiers Analysis and Design. Prentice Hall, 1984.
- Goyal, R. and S.S. Bharj, "Microwave circuit analysis using SPICE," Microwave Journal, August 1989.
- Granberg, H.O., "Building push-pull, multioctave, vhf power amplifiers," Microwaves & RF, November 1987.
- Hauser, J.R., "Effects of distributed base potential on emitter-current injection density and effective base resistance for stripe transistor geometries, the," IEEE Trans. Electron Devices, vol. ED-11, pp. 238-242, May 1964.
- Krauss, H.L., D.W. Bostian and F.H. Raab, Solid State Radio Engineering. John Wiley & Sons, 1980.
- LaLau, R. Y., 800 MHz, 5 Watt, Class-AB Power Amplifier Simulation And Design, Simon Fraser University, April 1990, To Be Published.
- Motorola, RF Device Data, Volume 1, DL 110, Revision 3, 1988.
- Pitzalis, O., and T.P. Couse, "Practical design information for broadband transmission line transformers," Proc. of the IEEE, vol. 56, no. 4, pp. 738-739, Proc. Letters, April 1968.
- Scholten, J.G.A., "Modelling RF transistors when the heat's on," Microwaves & RF, February 1984.
- Sechi, F.N., "Linearized class-B transistor amplifiers," IEEE Journal of Solid-State Circuits, vol. SC-11, No. 2, April 1976.
- Turkoz, H., "Operation of linear class AB amplifiers," RF Design, January 1989, pp. 41-45.

SIMULATION FILES

```
! NAME:          SPAR1.CKT
!
!              Richard LaLau
!              RF Design Engineer,
!              Mobile Data International Inc.
!              11411 Number 5 Road
!              Richmond, B.C. V5A 4Z3
!
! DESCRIPTION:  File to generate S-Parameter data for the MRF581A to
!              compare against data book parameters.
!              This file also generates I-V characteristic curves for
!              comparison against measured results.
!
DIM
  FREQ MHZ
  RES  OH
  IND  KH
  CAP  NF
  LNG  HIL
  ANG  DEG
!
CKT
S2PA_Q1  1  2  0  (MODEL = MRF581A)
DEF2P    1  2          TRAN

TRAN_X1  1  2
DEF2P    1  2          AMP

MODEL
MRF581A  NPN  IS=2.65E-15  BF=120  NF=1  IKR=0.035  IKF=0.120  6
          ISE=2.79E-14  NE=1.74  BR=0.8  NR=1.02  NC=1.06  6
          ISC=1.9E-15  VAF=20  RB=3  RC=1.2  RE=1.11  6
          RBM=1.3E-3  IRB=0.011  CJE=8E-12  VJE=0.989  CJC=4E-12  6
          TPF=13E-12  XTF=0.676  ITP=2.68E-5  VTF=0.890  PTF=35  6
          TR=1.0E-9  VJC=0.568  HJE=0.714  HJC=0.223

SOURCE
AMP      ICS_IBB  0  1  DC=1.5M AC=1.0M
AMP      IVS_VCE  2  0  DC=10

CONTROL
AMP DC  IVS_VCE  0  4  0.2  ICS_IBB  0.1M  0.82M  0.36M
AMP AC  LIM     13  300MEG  1500MEG
AMP OPTIONS  ACCT LIST NODE
AMP OPTIONS  RELTOL=1.0E-5  ABSTOL=0.01P  VNTOL=0.5U  CHGTOL=1E-9

SPICEOUT
AMP DC  V(ALL)  I(ALL)
AMP AC  V(ALL)  I(ALL)
AMP SP  TRAN_X1  SPAR.S2P  50

OUT
DC
AMP RE[I[X1.Q1.C]] GR1

GRID
DC
RANGE 0  4  0.5
GR1  0  0.1  0.01
```

```

! File:          1CLASSAB.CKT
!
! Author:       Richard LaLau
!              RF Design Engineer,
!              Mobile Data International Inc.
!              11411 Number 5 Road
!              Richmond, B.C.
!              V7A 4Z3
!
! Description:  Libra circuit file to simulate a Class-AB, power amplifier
!              using the SPICE model for the MRF839.

```

```

DIM
  FREQ  MHZ
  RES   OH
  IND   nH
  CAP   pF
  LNG   MIL
  TIME  ns
  COND  /OH
  ANG   DEG
  CUR   MA
  PWR   DBM
  VOL   V

```

```

VAR
  W  = 110.3
  L  = 316.0
  L1 = 174.8
  L2 = 623.0
  C  = 68
  C1 = 26
  C2 = 12.8

```

```

EQN
  F2 = F1 + 1

```

```

CKT
  MSUB          ER=4.8 H=62.5 T=0 RHO=1 RGH=0
  XFERTAP 200 1 0 19 0 N12=1.414 N13=1.414 L1=800 K=1.0

```

```

MLIN  1  2  W^W L^L
CAP    2  3  C^C
MLIN  3  4  W^W L^L
CAP    4  0  C^C1
MLIN  4  5  W^W L^L1
S2PA_Q1 5  6  0  [MODEL=MRF581 AREA=4]
MLIN  6  7  W^W L^L2
CAP    7  0  C^C2

```

```

MLIN  7  8  W^W L^L
CAP    8  9  C^C
MLIN  9 10  W^W L^L
MLIN 19 20  W^W L^L
CAP   20 30  C^C
MLIN 30 40  W^W L^L
CAP   40 0  C^C1
MLIN 40 50  W^W L^L1
S2PA_Q2 50 60 0  [MODEL=MRF581 AREA=4]
MLIN 60 70  W^W L^L2
CAP   70 0  C^C2
MLIN 70 80  W^W L^L
CAP   80 90  C^C
MLIN 90 100 W^W L^L

```

```

XFERTAP 300 10 0 100 0 N12=1.414 N13=1.414 L1=800 K=1.0
DEF2P 200 300 AMP

```

```

MODEL ! The DIM block does not apply to the MODEL block.
MRF581 NPN IS=2.65E-15 BF=120 NF=1 IKR=0.035 IKF=0.120 &
ISE=2.79E-14 NE=1.74 BR=0.8 NR=1.02 NC=1.06 &
ISC=1.9E-15 VAF=20 RB=3 RC=1.2 RE=1.11 &
RBM=0.0013 IRB=0.011 CJE=8E-12 VJE=0.989 CJC=4E-12 &
TF=13E-12 XTF=0.676 ITF=2.68E-5 VTF=0.890 PTF=35 &
TR=1.0E-9 VJC=0.568 MJE=0.714 MJC=0.233

```

```

SOURCE
AMP P_GEN1 110 0 R=RES_RSRC P^PWR F^F1
! AMP P_GEN2 110 111 R=RES_RSRC P^PWR F^F2
AMP RES_RSRC 110 200 R=50
AMP RES_RLD 300 0 R=50
AMP VS_VCC1 14 0 DC=12
AMP IND_LC1 14 6 L=10
AMP CAP_CC1 14 0 C=68
AMP VS_VCC2 140 0 DC=12
AMP IND_LC2 140 60 L=10
AMP CAP_CC2 140 0 C=68
AMP VS_VBB1 12 0 DC=.3
AMP IND_LB1 12 5 L=10
AMP CAP_CB1 12 0 C=68
AMP VS_VBB2 120 0 DC=.3
AMP IND_LB2 120 50 L=10
AMP CAP_CB2 120 0 C=68

```



```

FREQ
STEP      800
NH=       1

POWER
STEP      15 16 17 18 19 20 21 22 23 23.5 24 24.5 25 25.4 25.8 26.2 26.6
27
STEP      27.4 27.8 28.2 28.6 29 29.4 29.8 30.2 30.6 31 31.4 31.8 32

OUT
AMP       V_VOUT2  300                GR1
AMP       PT_POUT  300 0  R=RES_RLD  GR2
AMP       PT_POUT  300 0  R=RES_RLD  GR4
! AMP     PS_IMD   300 0  R=RES_RLD  GR3

GRID
TIME      0  4  0.5
GR1       -20 20  5
POWER     15 35  1
GR2       20 40  1
RANGE     0 4000 500
GR3       -120 40 10
FREQ      700 900 50
GR4       15 45  5

```

```

! File:      1CLASSA.CKT
! Author:    Richard LaLau
!            RF Design Engineer,
!            Mobile Data International Inc. (A Motorola Company)
!            11411 Number 5 Road
!            Richmond, B.C.
!            V7A 4Z3
!
! Description: File to simulate a Class-A, small-signal amplifier using
!              an S-Parameter file and harmonic balance using a SPICE
!              model of the MRF581A transistor.
!

```

```

DIM
FREQ      MHZ
RES       OH
IND       nH
CAP       pF
LNG       MIL
TIME      ns
COND      /OH
ANG       DEG

```

```

VAR
L1 # 100 498.54 5000
L2 # 100 477.23 5000
L3 # 100 402.13 5000
L4 # 100 419.83 5000
W = 110.3
W2 = 24.2
L = 217.4

```

```

EQN
F2 = F1 + 1.0

```

```

CKT
MSUB
MLIN      1  2                ER=4.8 H=62.5 T=0 RHO=1 RGH=0
CAP       2  3                W^W L^L
          C=33 SPAC L=80
MLIN      3  4                W^W L^L
MCROS     4  5  6  7          W1^W W2^W W3^W W4^W
MLOC      5                    W^W L^L1
MLOC      7                    W^W L^L1
MLIN      6  21               W^W L^L2

MTEE      22 21 23            W1^W W2^W W3=24.2
MLIN      22 35                W^W L=75
MLIN      23 40                W^W2 L=700
MBEND2    40 41                W^W2

```

```

MLIN      41  42          W^W2 L=700
MBEND2    43  42          W^W2
MLIN      43  44          W^W2 L=200
MBEND2    45  44          W^W2
MLIN      45  46          W^W2 L=488
CAP        46  0          C=68 SPAC L=50

S2PA_Q1   35  30  0      MRF581A [MODEL=MRF581A AREA=1] SPAC L=200

MLIN      30  36          W^W L=341
MTEE      31  36  32      W1^W W2^W W3=24.2
MLIN      32  50          W^W2 L=700
MBEND2    51  50          W^W2
MLIN      51  52          W^W2 L=700
MBEND2    52  53          W^W2
MLIN      53  54          W^W2 L=200
MBEND2    54  55          W^W2
MLIN      55  56          W^W2 L=488
CAP        56  0          C=68 SPAC L=50

MLIN      31  10          W^W L^L3
MCROS     10  11  12  13  W1^W W2^W W3^W W4^W
MLOC      11              W^W L^L4
MLOC      13              W^W L^L4
MLIN      12  14          W^W L^L
CAP        14  15          C=33 SPAC L=80
MLIN      15  16          W^W L^L

DEF2P     1   16          AMP

MODEL      ! The DIM block does not apply to the MODEL block.
MRF581A    NPN IS=2.65E-15 BF=120 NF=1 IKR=0.035 IKF=0.12 &
           ISE=2.79E-14 NE=1.74 BR=0.8 NR=1.02 NC=1.06 &
           ISC=1.9E-15 VAF=20 RB=3 RC=1.2 RE=1.11 &
           RBM=1.3E-3 IRB=0.011 CJE=8E-12 VJE=0.989 CJC=4E-12 &
           TFF=13E-12 XTF=0.676 ITF=2.68E-5 VTF=0.980 PTF=35 &
           TR=1.0E-9 VJC=0.568 MJE=0.714 MJC=0.233

SOURCE
AMP        VS_DVCC  56  0      DC=12
SMP        VS_DVBB  47  0      DC=5
AMP        RES_RB   47  46      R=3800

AMP        P_PIN1   60  0      R=RES_RSRC P^PWR F^F1 ! Change 60 to 61 for
IMD.
! AMP      P_PIN2   60  61      R=RES_RSRC P^PWR F^F2 ! Remove "!" for IMD.
AMP        RES_RSRC  60  1      R=50
AMP        RES_RLD   16  0      R=50

```

FREQ

```

SWEEP     400  1200  50
! SWEEP   800  830   1
! STEP    806  814  821  830
STEP      800
NH=       1                                     ! Increase for IMD.

POWER
! SWEEP   -30  20  2
STEP      0

OUT
AMP       DB[S21]                               GR1   ! Linear Analyses
AMP       DB[S11]                               GR1
AMP       DB[S22]                               GR1
AMP       DB[S12]                               GR1

AMP       V_VIN   1                               GR2   ! Harmonic Balance Analyses
AMP       V_VOUT  16                              GR2
AMP       PT_POUT 16  0  R=RES_RLD SCN
AMP       PT_POUT 16  0  R=RES_RLD GR3
! AMP     PS_IMD  16  0  R=RES_RLD GR4

GRID
RANGE     400  1200  100
GR1       25  -25   5
TIME      0   5   1
GR2      -6   6   1
POWER    -30  20   5
GR3      -20  30   5
RANGE    795  805   2
GR4      -40  -20   2

OPT
RANGE     806  821
AMP       DB[S21] > 10.5
AMP       DB[S21] < 14
AMP       DB[S11] < -10
AMP       DB[S22] < -10
RANGE    100  2000
AMP       DB[S11] < 0
AMP       DB[S22] < 0

```

**COMPUTER PROGRAMS DESIGN, SIMULATE, AND OPTIMIZE
HIGH-EFFICIENCY SWITCHING-MODE (CLASS E) RF POWER AMPLIFIERS**

Nathan O. Sokal, President and István Novák, Project Engineer

Design Automation, Inc.
809 Massachusetts Ave.
Lexington, MA 02173-3992
U.S.A.

TEL (617) 862-8998
FAX (617) 862-3769

Abstract — Single-ended switching-mode RF power amplifiers (Class E) offer high efficiency, low power dissipation, and low sensitivity to component variations (including transistors). Despite these desirable features, the exploitation of these amplifiers has been hindered by the lack of simple accurate design equations. Complicated interactions among the many component parameters and design variables yield a set of nonlinear implicit design equations which is infeasible to solve without a computer.

Previous circuit-simulation programs such as SPICE and MICROCAP III were not designed for the needed function of simulating the *steady-state periodic response* of a highly nonlinear circuit having periodic excitation. Such programs are too slow to be used effectively for designing RF power amplifiers. The new programs described here are *2-3 orders of magnitude faster than MICROCAP III* and include many more functions needed for designing RF power amplifiers. These new programs make it feasible and economical to *design and optimize* high-efficiency switching-mode RF power amplifiers.

OUTLINE

- I. NEED FOR THESE PROGRAMS
- II. COMPUTER SIMULATION OF THE RF POWER AMPLIFIER
 - A. Why Use a Computer Program to Simulate the RF Power Amplifier?
 - B. Previously Available Programs and Their Shortcomings
 - C. Summary of the New Programs and Their Capabilities
- III. MATHEMATICAL BACKGROUND
 - A. Computing Capabilities Needed for Design
 - B. Reason for Slow Computation with SPICE-like Programs
 - C. Previous Efforts to Meet the Requirements
 - D. The Chosen Mathematical Method
 - E. Mathematical Assumptions About the Switch, and Switch Model
 - F. Implementation of the Chosen Mathematical Method
- IV. CIRCUIT TOPOLOGY
 - A. Load in Series with the Series Resonator
 - B. Load in Series with the Parallel Resonator
 - C. Load in Parallel with the Parallel Resonator
 - D. Load in Parallel with the Series-Resonance Inductor
 - E. Load in Parallel with the Series-Resonance Capacitor
 - F. Load in Parallel with a Portion of a Split Series-Resonance Capacitor
- V. MODELING INPUT-PORT IMPEDANCE AND ATTENUATION OF IMPEDANCE-MATCHING/HARMONIC-SUPPRESSION NETWORK
- VI. PROGRAM FUNCTIONS
 - A. Simulation of Steady-State Periodic Response
 - B. Optimization
 - C. Transfer Functions
 - D. Required Variation of One Circuit Parameter vs. a Second Parameter to Achieve a Desired Result
 - E. Graph-Plotting
- VII. USING THE PROGRAM
 - A. Data and Command Inputs
 - B. Making Parametric Studies
 - C. Automatic Preliminary Design
- VIII. DESIGN EXAMPLES AND COMPARISON WITH MEASUREMENTS
 - A. 10-MHz 3-Watt Amplifier
 - B. 200-MHz 20-Watt Amplifier
 - 1. Choice of switching transistor
 - 2. Choice of circuit topology to provide required bandwidth
 - 3. Optimization of component values
 - 4. Accommodating excessive transistor output capacitance
 - 5. Measurement results
- IX. FUTURE PLANS
- REFERENCES

I. NEED FOR THESE PROGRAMS

A. Benefits of Switching-Mode RF Power Amplifiers

Single-ended switching-mode RF power amplifiers (Class E) offer high efficiency, low power dissipation, and low sensitivity to component variations (including transistors) [1], [2], [3]. The low sensitivity results in good reproducibility in production, without need for "tweaking." Fig. 1 is a circuit diagram for this family of amplifiers. A pair of these amplifiers driven in push-pull can be combined in a 180° combiner to double the output power and cancel the even-harmonic spectral output components.

Despite these desirable features, the exploitation of these amplifiers has been hindered by the lack of accurate design equations applicable to wide-band amplifiers or to amplifiers using finite-Q inductors and capacitors, and power transistors with parasitic loss resistances. Complicated interactions among the many component parameters and design variables yield a set of nonlinear implicit¹ design equations which is infeasible to solve without a computer. Simplified equations usable for manual design cannot account accurately for the complicated interactions among the variables. *Optimizing* the design cannot even be considered without a set of accurate design or analysis equations which can be solved in only a few seconds. *Simulation* is needed to evaluate the circuit operation under *off-nominal* operating conditions.

Previous circuit-simulation programs such as SPICE and MICROCAP III were not designed for the needed function of simulating the *steady-state periodic*

response of a highly nonlinear circuit having periodic excitation. Such programs are too slow to be used effectively for designing high-efficiency RF power amplifiers, and they lack needed functions *other than* simulation.

The new programs described here are *2-3 orders of magnitude faster than MICROCAP III* and include many more functions needed for designing RF power amplifiers. The new programs make it feasible and economical to *design and optimize* high-efficiency power amplifiers.

B. What Makes an Amplifier Class E?

Gradually, RF-power engineers are becoming aware of the considerably improved efficiency which can be obtained by operating the transistor in the switching mode. Those who have studied the theory of Class-E operation [1], [2], [3], [10] understand the physical and mathematical basis for the high efficiency which is achieved, and can use design equations or this computer program to proceed *directly* to high-efficiency amplifiers without "cut and try." Other engineers, more inclined to develop designs by experimental methods, have achieved high efficiency by driving the transistor hard (putting it into the switching mode) and varying the load-network components experimentally until they find a combination which yields good efficiency. If they try all possible combinations, they can eventually find a combination which works well, although they will expend more labor time and schedule time than would be the case for the engineer who proceeds directly to the end result. Even though the experimenter might not have known the Class-E principles for achieving high efficiency, and might not have used the published Class-E design equations, his amplifier is Class E, and falls within the scope of the Class-E patent [10], if it has the following characteristics:

¹ An "implicit" equation is one in which the variable is a function of itself, (i.e., $x = f(x)$). Solving simultaneously a set of strongly coupled nonlinear implicit equations is a task feasible only by numerical solution with the help of a computer.

- The transistor is operated in the switching mode: "off" for a substantial part of the RF cycle (typically about 50% of the cycle), "on" with a low conducting voltage drop for another substantial part of the RF cycle (also typically about 50% of the cycle), and making *fast transitions* between those two states during the remainder of the RF cycle. These "on" and "off" conditions yield low power dissipation during those portions of the RF cycle. Transition times (discussed further below) each of up to 15% of the RF cycle yield acceptable efficiencies; faster is better. The speed of the turn-off transition has more effect on efficiency than that of the turn-on transition.
- The load-network topology and component values are such that (a) the transistor collector-emitter or drain-source voltage rises slowly enough during the turn-off transient that the voltage has not increased much by the time that the transistor is fully "off" (*e.g.*, has not yet reached 30% of V_{CC}), and (b) after transistor turn-off, the transistor collector-emitter or drain-source voltage rises and then returns back to nearly zero (*e.g.*, less than 30% of V_{CC}) at the time the transistor will next be turned "on." Conditions (a) and (b) yield low power dissipation during the turn-off and turn-on transitions, respectively.
- The *slope* of the voltage waveform is nearly zero at turn-on time (*e.g.*, less than 30% of the slope existing just after the transistor turns "off"). That yields low power dissipation during the turn-on transient, for another reason, independent of condition (b) above.

In the above description, the waveform voltage and slope at transistor turn-on time are zero for a nominal Class E amplifier and are nearly zero for an amplifier which is slightly off-nominal. The Class E amplifier has low sensitivities to

deviations from nominal; details are in [3]. References [1], [2], [3], and [10] explain in detail why the above-listed characteristics result in high efficiency.

Optionally, the circuit can include one or more harmonic resonators or a voltage clamp, to reduce the peak/rms ratio of the voltage and/or current waveforms. That can reduce the power dissipation in the transistor "on" resistance, for a given transistor die area, at the cost of additional circuit components.

The programs to be described here, which are derived directly from the basic theory of Class-E operation, lead *directly* to a working design and *accurate predictions* of the performance which will be obtained. The circuit *can be optimized before it is built*. The advantages over "cut-and-try" design are faster and lower-cost product development, and probably a better product. Other useful program features will be discussed.

II. COMPUTER SIMULATION OF THE RF POWER AMPLIFIER

A. Why Use a Computer Program to Simulate the RF Power Amplifier?

The Class E circuit has been well characterized analytically, for operation with the nominal waveforms with lossless components and a switch with nonzero turn-off time [1], [2], [3]. The analyses have been extended to include deviations from nominal inductance, capacitance, and frequency [3], [4] and additional effects of nonzero switch turn-off time [5] and the switch resistance [6]. Another extension gives computed waveforms for operation with several off-nominal load impedances, but does not include the effects of parasitic resistances, nonzero switching times, and the body diode of a MOSFET switch [7]. Further work [8] adds the effects of the parasitic resistances of the switch output capacitance and of the circuit inductors and capacitors and the func-

tional dependence of output power on network loaded Q , and corrects errors in previous publications.

With the help of the published simplified analyses, and using only a hand calculator, a skilled RF engineer can design a reasonable first approximation to a final power-amplifier product. At the nominal design values of frequency and load, the amplifier will deliver somewhat less than the expected output power (depending on the chosen value of network loaded Q), at somewhat less than the expected efficiency (depending on the inductor and capacitor quality factors and the unspecified quality factor of the transistor output capacitance). The engineer will not have *a priori* quantitative information on the effects of variations of load impedance or operating frequency. The design will work, but it will not necessarily be the best possible design for the particular application. To achieve the best design, the engineer must make many trade-off decisions. For example, the engineer should consider the effects of

- all parasitic resistances, including those of the "on" transistor and the transistor output capacitance,
- transistor nonzero turn-off and turn-on switching times,
- off-nominal load impedance, resulting in off-nominal operating waveforms,
- operating at any frequency within a specified band, usually with fixed tuning, and
- all component tolerances.

Unfortunately for analytical design, the equations which include most of the important parasitic effects, or the important off-nominal operating conditions, are a complicated set of strongly interacting nonlinear implicit equations. An explicit analytical solution is not possible when including the important parasitic effects. The equations can be solved only by iterative numerical techniques.

In principle, how does one optimize a design, *e.g.*, to minimize the power loss? *In principle*, the engineer could minimize the total power loss by choosing the circuit parameters to trade increases of some power losses for larger *decreases* of other power losses. That requires many predictions of circuit performance, with different combinations of circuit parameter values. In the absence of complete analytical solutions for the optimum design, the engineer must depend on computer numerical performance predictions. To be a practical design tool, such performance predictions must take not more than a few seconds each. Until now, that has not been possible with the computers and programs available to most engineers. In projects with constraints on design schedule and cost, the engineers have been unable to evaluate fully the complicated trade-offs and to choose the optimum combination of trade-off decisions. As a result, power amplifiers have been some combination of less efficient, larger, heavier, less reliable, and more expensive than they might have been with a better set of trade-off decisions.

Fast circuit simulation (*i.e.*, not more than a few seconds per simulation) is the only practical way to optimize an amplifier design. Hence, fast computer simulation should be of interest to engineers designing RF power amplifiers, and to their managers who are concerned with having competitive products and with product-development schedule and cost.

B. Previously Available Programs and Their Shortcomings

The readily available general-purpose time-domain simulation programs (e.g., SPICE and its clones) were not designed for the types of analysis needed for switching-mode RF power amplifiers. The shortcomings of SPICE-like programs for this application are:

1. SPICE *et al* were not designed to find the *steady-state periodic response* for a circuit driven with *periodic excitation*. As a consequence, the steady-state periodic response must be found by letting the simulation run for many cycles of the periodic excitation, until the circuit response settles to its steady-state periodic solution. Fig. 2 shows the results of such a simulation using the SPICE-like MICRO-CAP III. The graph shows the build-up of current in the dc-feed inductor of the 1.5-MHz 40-W dc/dc power converter described in [9]. The simulation required *41 cycles of the switching frequency* to settle to within 1% of its steady-state periodic behavior.
2. SPICE-like programs usually have no provisions for computing an "objective function" from the computed circuit response. (An "objective function" is a weighted sum of several measures of the quality of the circuit performance. It is used as an overall measure of the quality of the circuit performance, during manual or automatic design optimization.) For example, the objective function could be defined as a certain weighted combination of the desirable features of high efficiency and conformance to a specification on output power.
3. Beyond the need for simulation, the SPICE-like programs do not include the capabilities of *designing* a circuit to meet the user's

requirements (as distinguished from *simulating* a circuit designed by the user), *optimizing* a design automatically, or making an *a priori evaluation* of the performance which can be provided by a candidate RF power transistor.

As a result of its inherent shortcomings for this type of application, SPICE provides very slow simulations of RF power amplifiers, and a large amount of manual intervention is required to complete a design. For example, the MICRO-CAP III simulation shown in Fig. 2 took 420 seconds on an 8-MHz AT clone with one wait state in memory. (The simulation was speeded-up by using ideal switches, at the sacrifice of all information about transistor switching power losses. Modeling the switches as transistors would have provided higher accuracy, but would have made the simulation run much slower.) Additional time would be used in post-processing the results to compute the power input and output, and all of the components of power dissipation. (The engineer needs that information to evaluate the circuit performance, and to make the trade-off decisions.) Because a careful trade-off evaluation requires *many* such simulations and evaluations, design optimization is infeasible with the SPICE-like programs because of the required large computing time. The engineer needs a better tool for this type of design.

Fortunately, the better tool has become available. Analyzing the circuit used for the MICRO-CAP example, the program to be described in this paper took only 1.67 seconds instead of 420 seconds, *including* all of the post-processing. The speed-up factor in this case was greater than 250; more generally, measured values are between 100 and 1000, depending on the circuit-parameter values.

C. Summary of the New Programs and Their Capabilities

The "High Efficiency Power Amplifier" (**HEPA**) series of computer programs now makes it easy and quick to design and optimize these otherwise desirable circuits — about 1.7 seconds for a simulation on a PC-AT, instead of about seven minutes. The programs can accommodate single-ended circuits or pairs of such circuits combined in push-pull. **HEPA-PLUS** integrates all of the following programs which are available individually:

- **Transistor EVALuator (HEPA-TEV)** evaluates, *a priori*, the performance achievable with a candidate RF power transistor used in a switching-mode high-efficiency (Class E) RF power amplifier having a user-specified relative bandwidth (bandwidth/center frequency). This saves the considerable work and schedule time associated with building and testing experimental amplifiers for evaluating candidate transistors. The calculation includes the effects of the transistor nonzero resistances, capacitances, and switching times, and the finite quality factors of the circuit inductors and capacitors and of the transistor output capacitance. The program predicts the achievable drain or collector efficiency *vs.* frequency and RF output power, over user-specified ranges of frequency and output power.
- **HEPA DESIGN (HEPA-DES)** computes the component values required to provide a user-specified output power and bandwidth, and computes the overall circuit efficiency, accounting for all effects listed above for **HEPA-TEV**. In a fraction of a second, the program supplies an excellent circuit design. No initial design is needed from the user; in fact, the user needs no knowledge of design procedures or design equations. The program solves rapidly a complicated set of strongly interacting nonlinear implicit design equations. This design program

can pass its design to the input of the simulation program **HEPA-SIM**, described below.

- **HEPA SIMulator (HEPA-SIM)** simulates very rapidly the circuit's steady-state periodic time-domain waveforms. It then computes the dc input power, RF output power, and all of the power dissipations. Using a unique mathematical method, *the entire computation* takes only about 1.7 seconds on an IBM AT, *vs.* typically about 7 minutes for only the simulation with a conventional time-domain simulator such as MICROCAP III or SPICE. **HEPA-SIM** can perform a series of analyses, sweeping any of the ten major circuit parameters, and plot the computed results *vs.* the swept parameter. The program can also compute the spectrum of the waveform of any capacitor voltage or inductor current. Voltage and current waveforms can be plotted, and numerical data can be displayed, on the monitor screen; the same data can be printed on a dot-matrix or laser printer.
- **HEPA-OPTimizer (HEPA-OPT)** optimizes a design very rapidly (usually about two minutes on an IBM PC/AT), minimizing a user-specified objective function of efficiency and output power. It is a very fast gradient-following constrained optimizer, using adaptive step size and direction. The optimizer program requires the use of its companion simulator program **HEPA-SIM**. The optimizer receives, from the simulation program, the computed dc input power, RF output power, and total power dissipation. The optimizer directs the simulator to perform a series of circuit analyses with sets of circuit-component values chosen by the optimizer, so as to find quickly the design which best meets the user-specified definition of "optimum." **HEPA-OPT** improves the efficiency by trading increases of some components of power dissipation to achieve larger *decreases* of other components of

power dissipation. The result is essentially to achieve the user-specified output power with the best possible efficiency. **HEPA-OPT** can receive a starting-point design from its companion program **HEPA-DES** which designs a nominal-waveform circuit to provide a user-specified output power and bandwidth.

The programs apply to the broad class of single-ended switching-mode RF power amplifiers shown in Fig. 1, and to push-pull pairs of such stages whose outputs are combined in a push-pull (180°) combiner. Most known Class E RF power amplifiers [1], [2], [3], [10] are included within the topology of Fig. 1. That topology allows for the series combination of a series resonator and a parallel resonator, with *any type of loading of either resonator*: By choosing appropriate values for C_2 , L_2 , C_3 , and L_3 (see Fig. 1), the load can be (a) in series with either or both resonator(s) or (b) in parallel with any of the following: the resonant capacitor, the resonant inductor, both of them, or a *portion* of the resonant capacitor or inductor (the resonator is split; one part is loaded and the other part is unloaded). Components not needed in a particular simulation can be removed by the user.

The programs do not sacrifice numerical robustness or accuracy to attain their high speed. They attain their high speed by using a unique mathematical method which is especially well-suited to the task of simulating the operation of a switching-mode RF power amplifier. The mathematical approach is completely different from that used in the SPICE-like programs.

All of the programs include the date and time and a user-typed title on the screen displays and printed output, enhancing the quality of record-keeping and design documentation.

Hardware requirements: The programs run on IBM PC, XT, AT, PS-2, and compatible computers. **HEPA-PLUS**, which includes all of the above individual programs, uses 300 kB of RAM (kB = 1000 bytes; KB = 1024 bytes). Providing an additional 20 kB for the DOS (3.30) operating system results in a requirement for 320 kB total RAM. The usual built-in 512 KB or more of RAM is more than sufficient, leaving 204 kB or more available for other uses and/or future expansion. A floating-point numeric coprocessor is recommended, but not required.

III. MATHEMATICAL BACKGROUND

A. Computing Capabilities Needed for Design

To design an optimized circuit of this type, the engineer must do the following:

1. Obtain the steady-state periodic response of the circuit to periodic drive, with a given set of component values.
2. From the known circuit response, compute a target function to be minimized, such as a combination of power dissipation and deviation from a target value of output power.
3. Change the values of the "adjustable" parameters in a way which is expected to reduce the value of the target function.
4. Repeat Steps 1-3 until the "best" design has been achieved.

B. Reason for Slow Computation with SPICE-like Programs

As noted above, SPICE was not designed for the type of simulation needed for Step 1 above. The reason for the slow computation is as follows: The transient-analysis routine must integrate the circuit differential equations numerically step-by-step in time until the circuit reaches nearly its final periodic response, *i.e.*, the last computed cycle of the switching frequency is nearly the same as the solution would be after computing for an infinite number of cycles. Typically, that takes of the order of 10-100 cycles of the switching frequency. The number of integration steps needed – and hence the computing time – is proportional to the ratio of the largest and smallest time constants in the circuit. For a typical RF power amplifier, the resulting number of integration steps is so large that the computing time becomes inconveniently long, *e.g.*, of the order of seven minutes per simulation on a 80286-class computer, as noted above.

C. Previous Efforts to Meet the Requirements

Several researchers, *e.g.*, [11]-[13], have addressed the problem of computing rapidly the steady-state periodic response of a circuit driven by periodic excitation. (Their papers referenced here contain references to other papers.) Their programs were experimental and/or used a large amount of memory and/or executed relatively slowly and/or have not been made available to the RF-power community at a generally acceptable price. (Although the researchers have published their basic mathematical approaches, the detailed implementations and the source and object codes are not available. Anyone wishing to use those mathematical approaches must evaluate them and choose one, work out the details of the implementation, and design, code and debug the entire program. That is a several-man-years job requiring experienced professionals with

expertise in user needs, electronics, mathematical methods, numerical analysis, programming, and the peculiarities of the specific computer being used. That is not an appropriate project for a group which does not include specialists in all of those subjects.)

D. The Chosen Mathematical Method

The first step in achieving a program with the needed capabilities is to change from a continuous nonlinear circuit model (as in SPICE and similar programs) to a piecewise-linear model, containing switches and linear *R-L-C* circuit elements. That allows the use of mathematical techniques which yield a *fast solution for the steady-state periodic response of the circuit*. Such a circuit model is well suited for switching-mode power amplifiers, where the power transistor is operated as a switch for which it is not necessary to model the fine details *within* the switching transitions.

The second step is to choose the appropriate mathematical technique for computing the steady-state periodic response. *The third step* is to design a software system which provides user-oriented capabilities based on the chosen mathematical technique. *The last step* is to implement the technique in robust and reliable software.

Our company developed software using an improved mathematical method for *computing directly* the circuit's steady-state periodic response. The method is applicable to a wide range of circuit topologies, in addition to the specific topology shown in Fig. 1.

Using the chosen mathematical method, the complete time-domain solution is computed about 2-3 orders of magnitude faster than by solving the differential equations as is done in the SPICE-like programs.

E. Mathematical Assumptions About the Switch, and Switch Model

The switch is modeled as a mathematically ideal switch to which are added the following parasitic components: series resistance, nonzero turn-on and turn-off switching times, parallel capacitance which has parasitic series resistance, and (optionally) a reverse-polarity diode connected in parallel with the switch ("anti-parallel diode"). Fig. 3 shows the switch model. A silicon MOSFET or a junction-isolated bipolar transistor (BJT) in a monolithic integrated circuit has such a diode built-in (the MOSFET body diode or the BJT collector-to-substrate isolation diode). A gallium-arsenide MESFET or a discrete BJT does not have an anti-parallel diode, but the circuit designer can choose to add one externally.

The switch non-idealities are discussed further in **F.** below. [14] gives experimental data and further information on modeling a transistor switch.

A diode can be modeled as a switch which turns "on" and "off" when the circuit response causes the diode voltage to pass through a threshold voltage, *e.g.*, 0.8 V. However, those times are not known *a priori* because the times at which diodes switch are implicit variables. (The times that the diode switches "on" and "off" depend on the circuit response, while the circuit response, in turn, depends on the times that the diode switches "on" and "off.") If an antiparallel diode conducts, its effect is the same as increasing the switch "on" time. Rarely does the circuit designer know, *a priori*, if and when the diode conducts. With **HEPA-SIM**, the designer need not know or estimate the times that the diode

switches "on" and "off." The program determines it automatically and includes the effects of the diode conduction in the simulation.

F. Implementation of the Chosen Mathematical Method

1. *Network Topologies and Parasitic Effects:* The program includes the following circuit topologies and parasitic effects (refer to Fig. 1):

- parasitic resistance in series with every component,
- user-specified switch turn-on time (during the turn-on time, the switch conductance increases linearly from zero to the static value),
- user-specified switch turn-off time (during the turn-off time, the switch current decreases linearly from its initial value to zero),
- a finite-value dc-feed inductor with different series resistances at dc and at the switching frequency (to account for dc winding resistance and for ac skin effect, proximity effect, and core and dielectric losses), and
- series and/or parallel resonators with series and/or parallel loading of any of the resonator components, or loading of a *portion* of a resonator component (split resonator). For example, R_3 - L_3 - C_3 in Fig. 1 can represent an arbitrary load impedance connected as a load in series with the series resonator L_2 - C_2 , or in parallel with the parallel resonator L_3 - C_3 . For an RF power amplifier, the arbitrary load impedance can represent the input-port impedance of the network usually provided between the power amplifier and the load, for

impedance matching and for low-pass filtering (harmonic suppression) of the carrier-frequency output. The filter/matching-network parasitic losses can be absorbed into the equivalent parallel resistances of L_3 and C_3 . Section IV gives further details of resonator loading.

2. Numerical Robustness: During the development and evolution of the program, from 1977 through 1990, the developers located and circumvented numerous potential causes of numerical error. As a result, the programs in the **HEPA** series avoid or minimize the numerical problems which frequently plague circuit-simulation programs: incorrect results caused by near-singular matrices, incorrect results and/or long computing time caused by "stiff" matrices (resulting from a wide range of eigenvalues), and failure to converge to a correct solution. The programs' reliable performance results from using robust numerical algorithms, mathematical formulations which avoid recognized types of potentially troublesome computations, internal error-checking, adaptive adjustment of computation controls, and judicious use of double-precision arithmetic. The program reliably produces accurate results quickly, even when the circuit parameter values would cause numerical instability with a less-robust program.

IV. CIRCUIT TOPOLOGY

Fig. 1 shows the circuit topology of a generic single-ended switching-mode RF power amplifier. This topology includes almost all known members of the family of switching-mode RF power amplifiers. A specific member of the family is generated by (a) indicating to the program whether the load is located at R_2 or at R_3 and (b) retaining wanted components and deleting unwanted components. (A component can be deleted by making its value negligibly large or

negligibly small.) The program can accommodate a push-pull amplifier comprising a pair of amplifiers of a topology generated from Fig. 1, combined in a push-pull (180°) combiner. Subsequent explanations will be for the single-ended amplifier (or one side of a push-pull amplifier).

L_2-C_2 is a series resonator and L_3-C_3 is a parallel resonator.

Listed below are examples of seven different topologies in this circuit family, all of which can be generated from the generic topology of Fig. 1 by choosing the load location and deleting unwanted components. The topologies A through G in the list below are discussed in the corresponding text Sections A. through G. below.

- A. load in series with the series resonator,
- B. load in series with the parallel resonator,
- C. load in parallel with the parallel resonator,
- D. load in parallel with the series-resonance inductor,
- E. load in parallel with the series-resonance capacitor,
- F. load in parallel with a portion of a split series-resonance capacitor, or
- G. load in parallel with a portion of a split series-resonance inductor.

The sections which follow give the details of those component choices. Refer to Fig. 1 for following the topological descriptions in Sections A. through G.

A. Load in Series with the Series Resonator

L_2 and C_2 are the series resonator. R_3 - L_3 - C_3 is an arbitrary-impedance load in series with the series resonator. Usually, R_3 - L_3 - C_3 is used to represent the input-port impedance of a load-matching/harmonic-suppression network chosen by the designer. The designer specifies the values of the four parameters (R_3 , L_3 , C_3 , and the parallel combination of the EPRs (equivalent parallel resistances) of L_3 and C_3) to represent any four chosen characteristics of the network. For example, the four parameters could be chosen to represent the following four characteristics of the network:

- The parallel combination of R_3 and the two EPRs represents the input-port conductance. This conductance receives the output power of the amplifier.
- The apportioning of the total conductance between R_3 and the two EPRs in parallel is chosen to duplicate the sharing of the power delivered by the amplifier: R_3 receives the power transmitted through the network to the load, and the EPRs receive the power dissipated in the attenuation of the network. A simple example: if the network input resistance is 10 ohms and the attenuation is 3 dB, $R_3 = 20$ ohms and the two EPRs in parallel are 20 ohms (e.g., each is 40 ohms).
- C_3 and L_3 in parallel represent the input-port susceptance at the carrier (switching) frequency.
- The apportioning of the total susceptance between C_3 and L_3 is chosen to duplicate the rate of change of susceptance with frequency in the vicinity of the operating frequency.

B. Load in Series with the Parallel Resonator

L_3 and C_3 are the parallel resonator. The load is R_2 in series with reactances L_{2A} and C_{2A} . The series resonator (if any) is L_{2B} and C_{2B} . L_2 and C_2 of Fig. 1 represent, respectively, $(L_{2A} + L_{2B})$ and $(C_{2A}$ in series with $C_{2B})$. The apportioning of total resistance between R_2 and the ESRs (equivalent series resistances) of L_2 and C_2 duplicates the sharing of amplifier output power between the load and the network attenuation, as in A. above.

C. Load in Parallel with the Parallel Resonator

L_3 and C_3 are the parallel resonator. The input-port inductance and/or capacitance of the matching/filtering network comprise part of L_3 and/or C_3 . R_3 and the EPRs receive and share the output power of the amplifier as in A. above.

D. Load in Parallel with the Series-Resonance Inductor

Here, L_{3A} is the series-resonance inductor. The arbitrary-impedance load is the parallel combination of L_{3B} , C_3 , R_3 , and the two EPRs. L_3 is the parallel combination of L_{3A} and L_{3B} . The amplifier output power is shared between R_3 and the two ESRs as in A. above. L_2 is made small enough to be negligible.

E. Load in Parallel with the Series-Resonance Capacitor

C_3 comprises two paralleled capacitors: C_{3A} and C_{3B} . C_{3A} is the series-resonance capacitor. The arbitrary-impedance load is the parallel combination of

C_{3B} , R_3 , L_3 , and the two EPRs. C_2 is a dc-blocking capacitor, usually chosen to have a capacitance larger than that of C_3 by a factor of 10 to 100. The choice of R_3 and the two EPRs is as in **A.** above.

F. Load in Parallel with a Portion of a Split Series-Resonance Capacitor

C_3 comprises two paralleled capacitors: C_{3A} and C_{3B} . The split series-resonance capacitor is C_2 and C_{3A} in series. C_2 is the unloaded portion. C_{3A} is the loaded portion, loaded by the load $R_3-L_3-C_{3B}$. All other components are as in **A.** above.

G. Load in Parallel with a Portion of a Split Series-Resonance Inductor

L_3 comprises two inductors in parallel: L_{3A} and L_{3B} . The split series-resonance inductor is L_2 and L_{3A} in series. L_2 is the unloaded portion. L_{3A} is the loaded portion, loaded by the load $R_3-L_{3B}-C_3$. All other components are as in **A.** above.

V. MODELING INPUT-PORT IMPEDANCE AND ATTENUATION OF IMPEDANCE-MATCHING/HARMONIC-SUPPRESSION NETWORK

As illustrated in Section **IV.A.** above, any four characteristics of the load can be modeled by choosing the four parameters L_3 , C_3 , R_3 , and the two EPRs, or the four parameters L_2 , C_2 , R_2 , and the two ESRs, depending on whether the load is at the R_3 or R_2 location.

VI. PROGRAM FUNCTIONS

All of the program functions are summarized in the main menu, reproduced in Fig. 4.

A. Simulation of Steady-State Periodic Response

The simulation by *HEPA-SIM* generates the time-domain waveforms of

- all inductor currents and capacitor voltages vs. time
- switch voltage and current vs. time

and then computes the following results from those waveforms:

- dc input power
- RF output power
- all of the components of power dissipation:

in each of the parasitic resistances

in the switch during the full-conduction interval

in the switch during turn-on switching

in the switch during turn-off switching

- the ratios of output power to input power (efficiency) and total power dissipation to input power (inefficiency).
- upon user request, the spectrum of switch voltage, switch current, any capacitor voltage, or any inductor current.

Fig. 5 shows the simulator input screen. Figs. 6 and 7 show typical simulation outputs. Fig. 6 shows waveform plots; Fig. 7 shows a tabulation of efficiency and powers.

The simulator can operate in "swept" mode: any circuit parameter can be swept over a user-specified range, with the computed powers and efficiency being written to a buffer in memory or to a disk file. From there, the results can be plotted and printed, or can be used as input to an external program.

B. Optimization

HEPA-OPT can optimize the design automatically, according to a user-specified trade-off between output power and efficiency. To give the capability of generating circuits which operate with the nominal Class-E waveforms, the optimizer also includes criteria of switch voltage and switch current at turn-on time; in the nominal Class-E circuit, those variables are both zero [1]. The optimizer minimizes the objective function

$$w_1(P_{out}/P_{target} - 1)^2 + w_2(P_{diss}/P_{in}) + w_3v_{sw}(0)^2 + w_4i_{sw}(0)^2. \quad (1)$$

In that function,

- P_{out} is the computed output power,
- P_{target} is the "target" value of output power specified by the user.
- The variable inside the first parentheses is the fractional deviation of the output power from the target value.
- P_{diss} is the computed total power dissipation.
- P_{in} is the computed dc input power.
- P_{diss}/P_{in} is the power inefficiency.
- $v_{sw}(0)$ and $i_{sw}(0)$ are the values at time zero (when the switch is turned "on") of the switch voltage and the current injected into the circuit node at the top of the switch.
- w_1 and w_2 are user-specified weighting factors which designate the relative importances of achieving the specified output power and achieving the best possible efficiency, i.e., the criterion for the trade-off between output power and efficiency.
- w_3 and w_4 are weighting factors for the switch voltage and current at turn-on time (both zero in a nominal-waveform Class E amplifier).

When w_1/w_2 is of the order of 1000 and $w_3 = w_4 = 0$, the output power is usually equal to the target value, to the fifth digit in the numerical value, and the efficiency is the best possible at that output power.

The program performs a series of circuit analyses, adjusting automatically the circuit parameters chosen by the user from a menu of the ten major circuit parameters. The optimizer trades increases of some power losses for larger *decreases* of other power losses. It uses a gradient-following method, with adaptive step size and direction. It constrains the choices of parameter values to lie within physically realizable ranges.

Figs. 8 and 9 show the optimizer input screens. The output screens are the same as for the simulator, Figs. 6 and 7.

C. Transfer Functions

The program can be used to compute any desired transfer function: the dependence of any chosen computed variable on any chosen circuit parameter, *e.g.*, output power *vs.* switch duty ratio, or power dissipated in the transistor *vs.* frequency. This is done by making a series of analyses while varying the chosen circuit parameter. The process is automatic for the two computed variables of most interest: output power and objective function. In that case, the user first defines the objective function at the optimizer input screen (Fig. 8). Then the user sweeps the chosen input variable, using *HEPA-SIM's* "Sweep" capability. The program automatically plots the output power and the objective function *vs.* the swept variable. Examples are output power or amplifier inefficiency ($1 - \text{efficiency}$) *vs.* frequency, load resistance, load capacitance, or switch duty ratio. Fig. 10 shows, for example, a plot of output power and inefficiency *vs.* frequency for a 20-watt amplifier designed for operation in the frequency band 190-230 MHz (discussed further in Section **VIII.B**).

D. Required Variation of One Circuit Parameter *vs.* a Second Parameter to Achieve a Desired Result

The optimizer can compute the *required* variation of one circuit parameter *vs.* a second parameter to achieve a desired result. For example, the optimizer can find the required variation of switch duty ratio with operating frequency, to maintain a specified output power across a specified range of operating frequency. (The user instructs the optimizer to vary the switch duty ratio as needed to maintain the output power at the user-specified value. Then the user varies the frequency over the range to be investigated, and observes how the optimizer sets the duty ratio at each frequency.) If two parameters are varied, two criteria can be satisfied, *e.g.*, maintain output power while providing the best possible efficiency. In the example given, the second variable parameter could be, for example, the dc supply voltage or C_2 .

E. Graph-Plotting

The program can display and print one or two plots on the same screen or sheet of paper, of any of the following variables plotted *vs.* time: switch voltage, switch current, any capacitor voltage, or any inductor current. As noted in Section C above, the program can also display and print graphs of output power and the objective function *vs.* a swept variable such as frequency, load resistance, *etc.*

VII. USING THE PROGRAM

A. Data and Command Inputs

The program provides "user-friendly" prompts for command and data inputs. As illustrated previously, Fig. 4 shows the main menu at which the user selects a program function. Fig. 5 shows the input-data screen for the simulation of Figs. 6 and 7, and Figs. 8 and 9 show the optimizer input screens.

B. Making Parametric Studies

The structure of the input routine makes it easy for the user to do parametric studies of circuit operation. For example, the user might wish to vary one design parameter while keeping other parameters fixed. We give below a few examples of design parameters which the user might choose to vary during a parametric study:

- Impedance level at which the circuit operates (load resistance),
- loaded Q of the load network,
- volume allocated to the resonant-circuit components L_2 and/or C_2 ,
- volume allocated to the dc-feed inductor L_1 ,
- inductance of the dc-feed inductor, or
- frequency.

The input routine is designed to facilitate such studies, accounting for the relationships among the physical and electrical parameters of high-frequency components and circuits. For example, as one changes the value of an inductance or a capacitance of a given type, keeping its physical volume fixed, its quality factor (Q) at a given frequency remains essentially constant. If one allocates a larger volume to the inductor or capacitor, Q increases. Additionally, an inductor's Q increases approximately as the square root of frequency and a capacitor's Q decreases approximately inversely with frequency.

For each inductor and capacitor, the user specifies Q at a chosen frequency (not necessarily the operating frequency). The program automatically calculates and uses corresponding values for the ESRs of those components at the operating frequency. If an inductance, capacitance, or frequency is changed by the user or by the optimizer routine during the parametric studies, the program automatically inserts an appropriate new value for the ESR, retaining the Q value originally specified by the user at the originally specified frequency and extrapolating that Q for the new inductance or capacitance and frequency. If the user specifies new Q data, the program uses the new data for calculating ESR values.

The user can easily evaluate the effects of allocating a larger or smaller physical volume to an inductor or capacitor, or of changing to a different type of inductor or capacitor: the user specifies an appropriate larger or smaller value of Q and repeats the circuit simulation. Again, the program will insert the appropriate new values of ESR to use in the circuit analyses, as the inductance, capacitance, or frequency is varied by the user or the optimizer.

C. Automatic Preliminary Design

Before optimizing a circuit, the engineer must have a starting-point design for input to the optimizer. Such a circuit is difficult to design manually. The interactions among the many component parameters and design variables yield a complicated set of nonlinear implicit design equations. As a result, manual design is tedious, time-consuming, and error-prone, and it cannot account accurately for these complicated interactions. It is appropriate to relegate this design task to the computer.

HEPA-DES is an "Automatic Preliminary Design" routine. The user input to this routine is the desired operating frequency range, the electrical parameters of the switching transistor, the quality factors of each inductor and capacitor, and any two of the parameters output power, dc supply voltage, and load impedance. Fig. 11 shows the data-input screen. The design routine solves rapidly the complicated set of interacting nonlinear implicit equations which characterize the circuit behavior. The output of the computation is the set of component values required to provide the user-specified performance. The computation includes the effects of nonzero transistor switching times and parasitic resistances of all components. The program computes also the expected circuit efficiency, accounting for all causes of power dissipation. The design is passed to the circuit-parameters array in the simulation module, from where the circuit can be simulated and optimized.

If the switch output capacitance is *larger* than the total capacitance needed in parallel with the switch, the program automatically chooses the best method of accommodating the excess capacitance, according to the user's specification of whether the supply voltage and/or the load resistance can be varied by the design routine.

VIII. DESIGN EXAMPLES AND COMPARISON WITH MEASUREMENTS

During the development of the programs and of Class-E technology, many Class-E circuits were designed, built, and tested, and the simulated performances were compared against actual measurements. The power transistors used in the various circuits were silicon BJTs, silicon MOSFETs, and GaAs MESFETs. The simulations were always in good agreement with the experimental measurements. Two examples are shown here: a 10-MHz 3-watt amplifier and a 200-MHz 20-watt amplifier, both using bipolar junction power transistors.

A. 10-MHz 3-Watt Amplifier

Fig. 5 shows the input data for the simulation and analysis of a 10-MHz 3-watt amplifier which was also built and tested. Fig. 12(a) shows the computed waveform of voltage across the switch and C_1 . In this example, C_1 was made slightly larger than optimum, and C_2 was made slightly smaller than optimum, to demonstrate the discharge of a charged capacitor by a turning-on switch, which occurs when the nominal Class-E zero-voltage-switching condition is not met. In this example, the capacitor is discharged from 4 V to zero at 95 ns. Fig. 12(b) shows an oscilloscope photograph of the corresponding waveform in the actual circuit. The computed waveform is the same as the measured waveform. The transistor was a 2N3725 BJT.

B. 200-MHz 20-Watt Amplifier

A 20-watt amplifier was designed for operation across the frequency band of 190-230 MHz. The areas of particular concern were: choice of the switching

transistor, choice of the proper circuit topology to provide the required bandwidth, and optimization of the component values.

1. Choice of switching transistor

The Class-E circuit inherently is tolerant of "slower-than-ideal" switching speeds. Turn-off and turn-on switching times as long as 10% of the RF cycle cause little penalty of decreased efficiency. However, faster-switching transistors are advantageous: they reduce the already low switching power losses, and they are easier to drive at the input port (base-emitter or gate-source port). Switching times are inversely proportional to f_T ; f_T is usually about an order of magnitude higher than the advertised operating frequency in Class-C operation. Turn-off time and turn-on time are usually about the same; in case a trade-off is necessary, note that turn-off time is more important than turn-on time. (*HEPA-SIM* simulations can predict the dependence of efficiency on turn-off and turn-on times, to give quantitative data for trade-off evaluations.)

At present, the choice of an appropriate transistor is hindered by the lack of data for transistor parameters needed for assessing the capability of the transistor for use in a switching-mode power amplifier. [14] specifies the data needed, but manufacturers of RF power transistors have not yet provided such data. For now, the designer must measure or estimate the needed transistor parameters. We hope that eventually customer pressure will convince the transistor manufacturers to provide the needed data.

For the intended application of this 190-230-MHz power amplifier, transistor cost was of low priority because only a few amplifiers of this design were to be made. The engineering cost would exceed the transistor purchase cost by a large factor. Therefore it would be a good trade-off to pay more for the transistor if the higher-cost transistor would save as little as a few hours of engineer-

ing. With that criterion, we searched for the highest-frequency transistor we could obtain easily, with an appropriate output-power capability.

MOSFET vs. BJT: Although MOSFETs are advertised as being suitable for operation at 1 GHz, we knew from previous evaluations that these MOSFETs could not provide as high efficiency as do BJTs in switching-mode UHF amplifiers. Therefore, the choice would be among UHF BJTs.

Choice among UHF BJTs: After considering technical and delivery factors among several manufacturers and product lines, we decided to investigate Motorola's highest-frequency product line, the MRF20xx series (formerly the TRW20xx series). From that product line, we chose the MRF2020 as having an appropriate output-power capability. To check the feasibility of using the MRF2020 at 190-230 MHz, we used the Transistor Evaluation routine, *HEPA-TEV*. Fig. 13 shows the input data for the prediction. Fig. 14 shows the predicted amplifier efficiency over the frequency range of 100 to 500 MHz, at 10, 15, 20 and 25 watts of output power. We can expect about 85% collector efficiency at 210 MHz at 20 watts output.

2. Choice of circuit topology to provide required bandwidth

The grounded-emitter configuration is preferable for higher gain and easier impedance-matching at the input port. However, the MRF2020 is available in only a grounded-base package, so we designed the input-drive circuit to provide the needed drive into a 0.5-ohm input resistance.

The input drive was to be obtained from an external 50-ohm source. An impedance-matching network with a large impedance-transformation ratio is inherently narrow-band. In this case, we needed a network to match 50 ohms

to 0.5 ohms, a 100:1 transformation ratio. The limitation on the amplifier bandwidth was almost entirely in the input network because the amplifier output network is easily capable of octave bandwidth if needed. To achieve the required 19% bandwidth (190-230 MHz), we used a two-section low-pass pi matching network.

3. Optimization of component values

Using the simulation, optimization and sweep features of the **HEPA** software, we designed the "best" design trade-off for achieving the desired output power with good efficiency across the specified frequency band. Fig. 10 shows the predicted variation of output power and inefficiency vs. frequency, for the amplifier as optimized for operation across the frequency band of 190-230 MHz.

4. Accommodating excessive transistor output capacitance

A problem frequently encountered at high switching frequencies (VHF for silicon MOSFETs or high UHF for BJTs) is that the transistor output capacitance exceeds the value which is required at that point in the circuit. Such excess capacitance can be accommodated in either or both of two ways:

- decrease the inductance of the dc-feed choke (L_1) and change the values of other components accordingly ([15] gives partial data), or
- scale all impedance values by the ratio of the desired capacitance to the existing capacitance, and reduce the dc supply voltage to provide the desired output power.

The first method can accommodate capacitance up to about four times the desired amount; the exact amount depends on the circuit parasitic power losses. The second method can accommodate any amount of capacitance up to a limit which is higher than that of the first method. Both methods pay a penalty of decreased efficiency compared with what could be obtained with a lower-capacitance transistor, if such a transistor could be obtained. Which method will yield superior efficiency depends on the particular set of design parameters in the case at hand. **HEPA-DES** knows how to use both methods; it chooses the appropriate one for a particular case.

In this design, the method of reducing L_1 was used.

5. Measurement results

The circuit was built and its performance was measured. Figs. 15 (a) and (b) show the simulated and measured collector-voltage waveforms. The slight differences between those waveforms result from the nonlinearity of the transistor output capacitance and uncertainties of some measured component values (a component used in the hardware might not have been exactly what was called for in the design). Above about 100 MHz, the distributed nature of components becomes increasingly evident. This effect can be modeled by stray inductances and capacitances which depend strongly on the physical layout. Good UHF layout reduces parasitic effects; parasitic inductance is usually more important than capacitance. The collector-voltage waveform deviates slightly from the nominal Class-E waveform because of trade-offs made among conflicting design criteria.

Figs. 16 and 17 show the measured output power and collector efficiency vs. frequency at $V_{CC} = 16$ Vdc. The simulation results in the two graphs of Fig. 10

are in good agreement with the corresponding graphs of measured data in Figs. 16 and 17. Table I lists the output power and collector efficiency at 210 MHz, $V_{CC} = 16$ Vdc, and 20 W RF output, obtained from the transistor *a priori* evaluation program, the simulation program, and laboratory measurements on an amplifier built to the design which was simulated. All three sets of data agree very well.

TABLE I.
COMPARISON OF MEASURED, SIMULATED, AND "TRANSISTOR EVALUATION"
RESULTS AT 210 MHz, 16 Vdc, AND 20 W OUTPUT

	Transistor Evaluation	Simulation	Measurement
Output power	20 W	20.3 W	20.0 W
Efficiency	85%	84.8%	88.3%

The measured collector efficiency is 3.5 percentage points higher than the efficiency obtained from the simulation. In a grounded-base circuit, a few per cent of the RF output power comes from the emitter-input drive instead of from the dc collector-voltage supply; that increases the measured collector efficiency by the same few per cent.

IX. FUTURE PLANS

Our company plans to generalize **HEPA-SIM** to accept *any circuit topology* input by the user, as in the SPICE-like programs. Potential users are invited to contact the first author for further information.

REFERENCES

- [1] N. O. Sokal and A. D. Sokal, "Class E — A new class of high-efficiency tuned single-ended switching power amplifiers," *IEEE J. Solid-State Circuits*, vol. SC-10, no. 3, pp. 168-176, June 1975. Reprinted in Japanese translation in *Nikkei Electronics*, March 22, 1976, pp. 127-141.
- [2] F. H. Raab, "Idealized operation of the Class E tuned power amplifier," *IEEE Trans. Circuits & Systems*, vol. CAS-24, no. 12, pp. 725-735, Dec. 1977.
- [3] N. O. Sokal and A. D. Sokal, "Class E switching-mode RF power amplifiers - low power dissipation, low sensitivity to component tolerances (including transistors), and well-defined operation," *IEEE Electro/79, Session 23*, New York, NY, April 1979, reprinted in *R.F. Design*, vol. 3, no. 7, pp. 33-38, 41, July/Aug. 1980.
- [4] F. H. Raab, "Effects of circuit variations on the Class E tuned power amplifier," *IEEE J. Solid-State Circuits*, vol. SC-13, no. 2, pp. 239-247, April 1978.
- [5] M. K. Kazimierczuk, "Effects of the collector current fall time on the Class E tuned power amplifier," *IEEE J. Solid-State Circuits*, vol. SC-18, no. 2, pp. 181-193, April 1983.
- [6] F. H. Raab and N. O. Sokal, "Transistor power losses in the Class E tuned power amplifier," *IEEE J. Solid-State Circuits*, vol. SC-13, no. 6, pp. 912-914, Dec. 1978.

- [7] F. H. Raab, "Effects of VSWR upon class E power amplifier," *Proc. RF Expo East*, Philadelphia, PA, Oct. 25-27, 1988.
- [8] N. O. Sokal, "Class-E high-efficiency RF power amplifier: prediction of efficiency and output power vs. frequency, and circuit optimization," unpublished manuscript, Sept. 1988.
- [9] R. Redl, B. Molnár, and N. Sokal, "Class-E resonant regulated dc/dc power converters: analysis of operation, and experimental results at 1.5 MHz," *IEEE Trans. Power Electronics*, vol. PE-1, no. 2, pp. 111-120, April 1986 (reprinted from *PESC '83 Record of 14th Annual IEEE Power Electronics Specialists Conf.*, IEEE Catalog No. 83CH1877-0, June 1983, pp. 50-60).
- [10] N. O. Sokal and A. D. Sokal, "High-efficiency tuned switching power amplifier," U. S. Patent 3,919,656, Nov. 1975.
- [11] Muhammet Köksal, "A fast convergent method for the analysis of nonlinear systems with periodic excitations," *Proc. 1984 IEEE International Symp. on Circuits & Systems*, vol. 3, IEEE Catalog No. 84CH1993-5, May 1984, pp. 1361-1364.
- [12] S. Skelboe, "Computation of the periodic steady-state response of nonlinear networks by extrapolation methods," *IEEE Trans. Circuits & Systems*, vol. CAS-27, no. 3, pp. 161-175, March 1980.
- [13] F. R. Colon and T. N. Trick, "Fast periodic steady-state analysis for large-signal electronic circuits," *IEEE J. Solid-State Circuits*, vol. SC-8, no. 2, pp. 260-269, June 1973.
- [14] N. O. Sokal and R. Redl, "Model for switching power transistor output port, for analyzing high-frequency resonant power converters and RF power amplifiers," *R.F. Design*, vol. 10, no. 6, June 1987.
- [15] R. E. Zulinski and J. W. Steadman, "Class E power amplifiers and frequency multipliers with finite dc-feed inductance," *IEEE Trans. Circuits & Systems*, vol. CAS-36, no. 9, pp. 1074-1087, Sept. 1987.

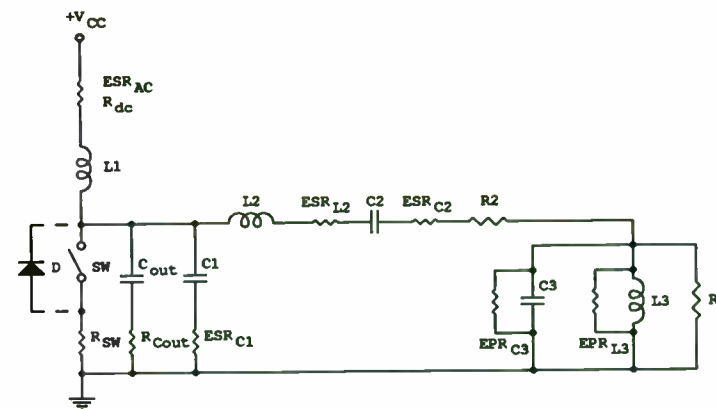


Fig. 1. Circuit diagram of generic single-ended RF power amplifier.

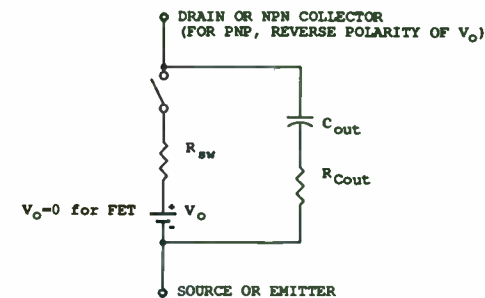


Fig. 3. Switch model.

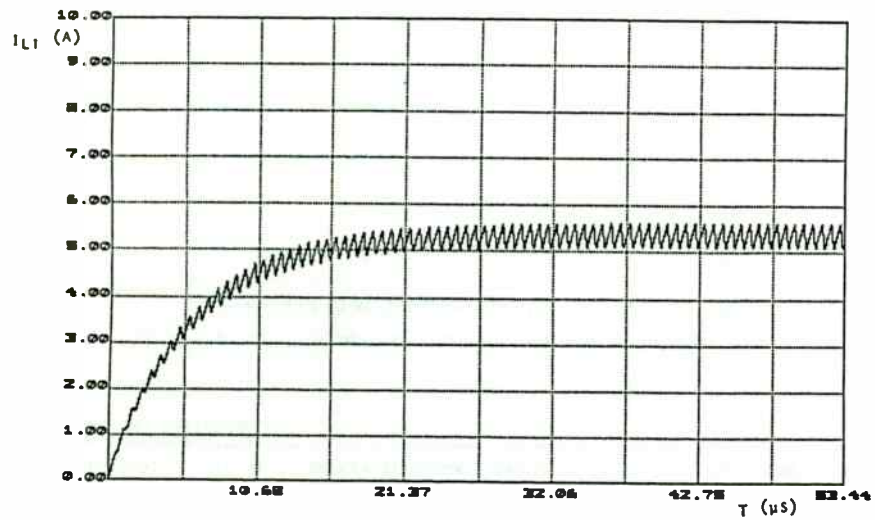


Fig. 2. MICRO-CAP III simulation of 1.5-MHz 40-W circuit reported in [9].

```

High Efficiency Power Amplifier PLUS (HEPA-PLUS) — Aug. 20, 1990 14:26
Type title on this line, up to 78 characters; then press <ENTER>.

                                MAIN MENU

LOAD CIRCUIT FROM DISK
CHANGE CIRCUIT PARAMETERS and/or TITLE
SIMULATE AND ANALYZE
OPTIMIZE
DISPLAY RESULTS
WRITE CIRCUIT ON DISK
MODIFY DEFAULTS, OPTIONS, OR PARAMETER LIMITS
PRINT INPUT OR OUTPUT
READ DEFAULTS, OPTIONS, AND PARAMETER LIMITS FROM DISK
AUTOMATIC PRELIMINARY DESIGN
TRANSISTOR EVALUATION

SELECTION: <1,1>      EXECUTE: <ENTER> or FIRST LETTER      EXIT TO DOS: <ESC>
SELECTING FUNCTION...

```

Fig. 4. Main menu.

```

High-Efficiency Power Amplifier PLUS (HEPA-PLUS) — Aug. 20, 1990 14:26
10.5-MHz Class E, detuned to show effects of nonzero (4 V) turn-on voltage.
ENTER CIRCUIT PARAMETERS and/or TITLE

```

SWITCH		LOAD	
Switching freq.(f)..[Hz]:	1.05E+07	Load location:	R2 R3
Duty ratio.....	0.5	Load resistance..[ohms]:	50
"On" resistance...[ohms]:	0.25	R3/Rload.....	1
Switching times: turn-on,turn-off[sec]		L3.....[henries]:	7.5788E-07
on: 5E-09 off: 5E-09		Qu: 180 at freq: 1.05E+07	
Cout.....[farads]:	1E-11	C3.....[farads]:	3.0315E-10
Cout series resis.[ohms]:	0.25	Qu: 1800 at freq: 1.05E+07	

LOAD NETWORK			
DC supply.....[volts]:	12.2	C2.....[farads]:	7.3E-11
L1.....[henries]:	8.2E-05	Qu: 1300 at freq: 1.05E+07	
Qu: 1082 at freq: 1.05E+07		L2 or Network loaded Q?:	L2 Q
Rdc.....[ohms]:	0.1	L2.....[henries]:	3.972E-06
C1 external to switch		Qu: 161 at freq: 1.05E+07	
capacitance...[farads]:	5.8E-11	Network loaded Q.....	5.0725
Qu: 2613 at freq: 1.05E+07			

```

SELECTION: (T,I,*,>)   ENTRY: ALPHANUM.,(ENTER)   RETURN TO MAIN MENU: (ESC)

```

SELECTING PARAMETER...

Fig. 5. Simulation input screen (input data for simulation and analysis of 10-MHz 3-watt circuit).

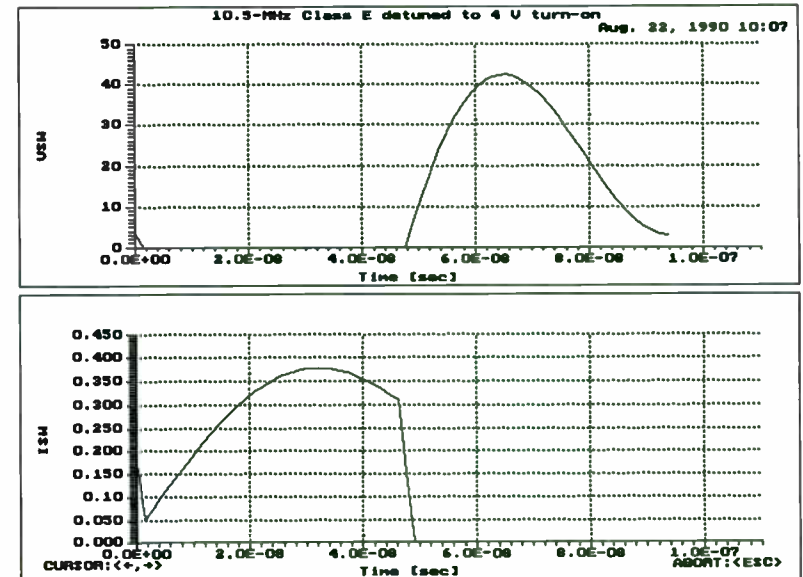


Fig. 6. Typical simulation output, waveforms of switch voltage and current.

High Efficiency Power Amplifier PLUS (HEPA-PLUS) — Aug. 20, 1990 14:26
 User title here, entered in the ENTER CIRCUIT PARAMETERS screen.

EFFICIENCY AND POWERS

Efficiency.....[Pout/Pin]	89.327%
Inefficiency.....[(Pin-Pout)/Pin]	10.673%
Power input.....[watts]	112.97
Power output.....[watts]	100.91
Power loss in L1.....[watts]	0.50606
Power loss in L2.....[watts]	1.3253
Power loss in L3.....[watts]	1.4372
Power loss in external C1.....[watts]	0.032379
Power loss in C2.....[watts]	0.74166
Power loss in C3.....[watts]	1.3224
Resistive power loss of switch and Cout..[watts]	5.6653
Turn-off power loss of switch.....[watts]	1.0265
Turn-on power loss of switch.....[watts]	0.00027602

"DISPLAY RESULTS" MENU: <ESC>

DISPLAYING COMPUTED POWERS...

Fig. 7. Typical simulation output, tabulation of efficiency and powers.

High Efficiency Power Amplifier PLUS (HEPA-PLUS) — Aug. 20, 1990 14:26
 User title here, entered in the ENTER CIRCUIT PARAMETERS screen.

INPUTS TO OPTIMIZER, SCREEN 1 - OBJECTIVES OF OPTIMIZATION

The optimizer minimizes a user-defined "objective function"; press <F1> for explanation. Choose the target output parameter with the cursor or by typing (P, V or U, or C or I). Then enter the numerical value.

Choose target output parameter: Power Voltage Current
 Target value.....[watts]: 105

Pout, Vout, and Iout are output power, voltage, and current; Pdiss is total power dissipation; Pin is input power. The "objective function" is:

$$w1*(Pout/Ptarget - 1)^2 + w2*Pdiss/Pin + w3*Vsw(0)^2 + w4*[I11(0)+I12(0)]^2$$

w1 = Weighting Factor for deviation from target value.... 1
 w2 = Weighting factor for inefficiency..... 1
 w3 = Weighting Factor for switch voltage at t=0..... 0
 w4 = Weighting Factor for switch current at t=0..... 0

SELECTION: <↑,↓,←,→> ENTRY: ALPHANUM.,<ENTER> NEXT SCREEN: <PgDn>

SELECTING PARAMETERS, ENTERING VALUES...

Fig. 8. Optimizer input, first screen.

```

High Efficiency Power Amplifier PLUS (HEPA-PLUS)  Aug. 20, 1990 14:26
User title here, entered in the ENTER CIRCUIT PARAMETER screen.

INPUTS TO OPTIMIZER, SCREEN 2 - CIRCUIT PARAMETERS TO BE VARIED BY OPTIMIZER

Choose parameters to be varied simultaneously by the optimizer (suggested
to be five or less, for fast optimization).

Duty ratio      Yes  No      min.:      current:  max.:
L1              Yes  No
C1              Yes  No
C2              Yes  No      1E-09      7.7E-09   1E-8
Load resistance Yes  No      0.1        1.5       100
L2              Yes  No
L3              Yes  No
C3              Yes  No
Frequency       Yes  No      1E+07      1.4E+07   3E+07
DC supply voltage Yes No

Press <ENTER> and change min, max values to set limits for optimization.
SELECTION: <↑,↓>  CHOICE: <←,→> or Y,N  OPTIMIZE: <PgDn>  MAIN MENU: <ESC>
SELECTING PARAM(S) TO BE OPTIMIZED...

```

Fig. 9. Optimizer input, second screen.

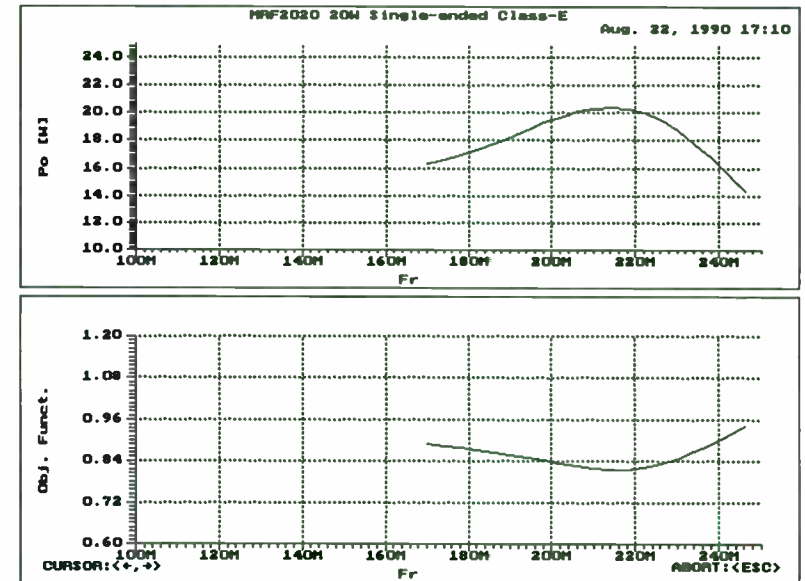


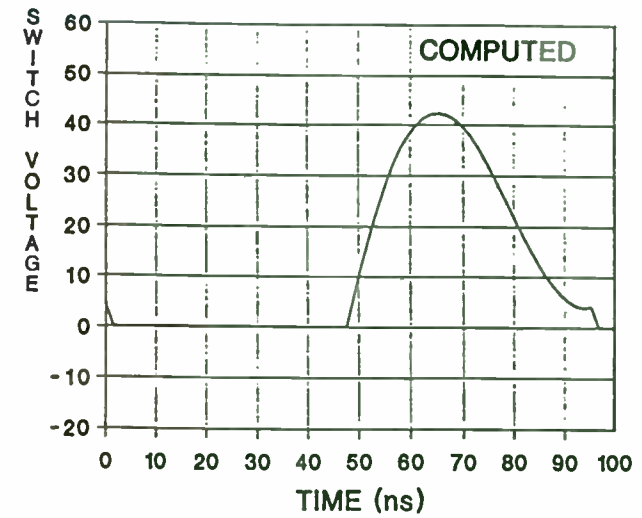
Fig. 10. Predicted output power and inefficiency vs. frequency, from a series of simulations with frequency as the swept variable.

```

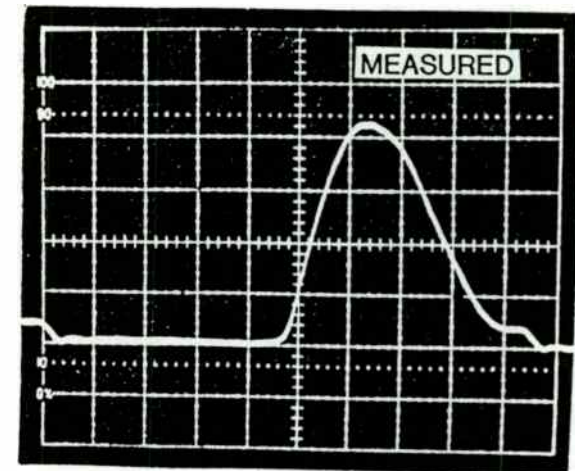
High Efficiency Power Amplifier PLUS (HEPA-PLUS)  Aug. 20, 1990 14:26
Type title on this line, up to 78 characters; then press <ENTER>.
      AUTOMATIC PRELIMINARY DESIGN
      Single-ended
Frequency limits....[Hz]:      Lower: 1.1E+07      Upper: 1.7E+07
Specify any two of the following three items:
  Output power.....[watts]:      100
+DC supply voltage.....[volts]:    22
*AC load resistance.....[ohms]:    1.8324
Predicted efficiency.....[Pout/Pin]: 89.8%
Specify as many of the following as you wish.
*Switch turn-off and turn-on times, each....[sec]: 4.2857E-09
*Switch resistance.....[ohms]:      0.06
*Switch output capacitance.....[farads]: 5.1E-10
*Series resistance of switch capacitance...[ohms]: 0.3
  Unloaded Q of L1 at arithmetic mean frequency... 100
  Unloaded Q of L2 at arithmetic mean frequency... 100
  Unloaded Q of L3 at arithmetic mean frequency... 100
  Unloaded Q of C1 at arithmetic mean frequency... 3000
  Unloaded Q of C2 at arithmetic mean frequency... 3000
  Unloaded Q of C3 at arithmetic mean frequency... 3000
*The program supplies a value for this input parameter, which you can change.
SELECTION: <↑,↓>  ENTRY: ALPHANUM.  CALC.: <PgDn>  EXIT: <PgUp>  ABORT: <ESC>
SELECTING PARAMETER...

```

Fig. 11. Automatic Preliminary Design data-input screen.



(a)



(b)

Fig. 12. Collector-voltage waveform, 10.5 MHz. (a) Computed. (b) Measured. Horizontal: 10 ns/div.; Vertical: 10 V/div.

```

High Efficiency Power Amplifier PLUS (HEPA-PLUS) — Aug. 20, 1990 14:26
Type title on this line, up to 78 characters; then press <ENTER>.
TRANSISTOR EVALUATION

Transistor application
Frequency range....[Hz]:  Min.: 1E+07      Max.: 2E+07
Power range.....[watts]:  Min.: 10        Max.: 100
Amplifier relative bandwidth... [f(max)/f(min)]: 1.5

Transistor characteristics
Peak switch voltage at nominal tuning...[volts]: 75
Switch turn-off and turn-on times, each...[sec]: 4.2857E-09
Switch resistance.....[ohms]: 0.06
Switch capacitance.....[farads]: 5.1E-10
Series resistance of switch capacitance...[ohms]: 0.3

Passive component characteristics
Unloaded Q of L1 at operating frequency..... 100
Unloaded Q of L2 at operating frequency..... 100
Unloaded Q of L3 at operating frequency..... 100
Unloaded Q of C1 at operating frequency..... 3000
Unloaded Q of C2 at operating frequency..... 3000
Unloaded Q of C3 at operating frequency..... 3000

SELECTION: <T,I>      ENTRY: ALPHANUM.      CALC.: <PgDn>      ABORT: <ESC>
SELECTING PARAMETER...

```

Fig. 13. Input screen for transistor evaluation, MRF2020 transistor.

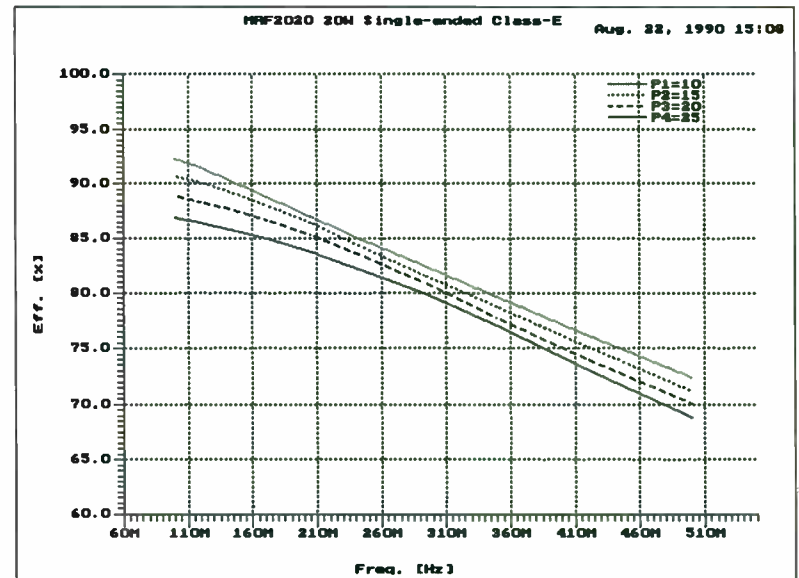
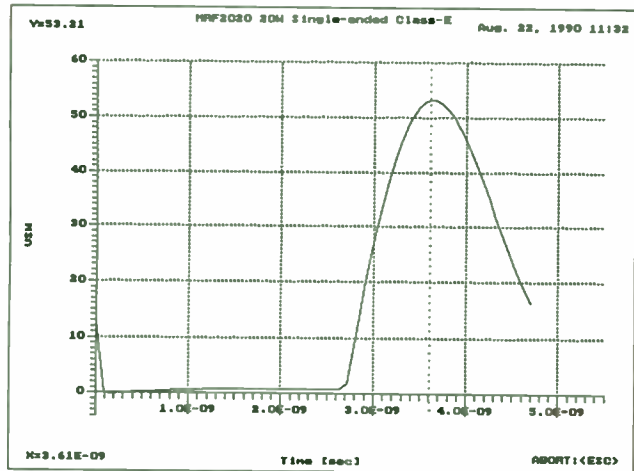
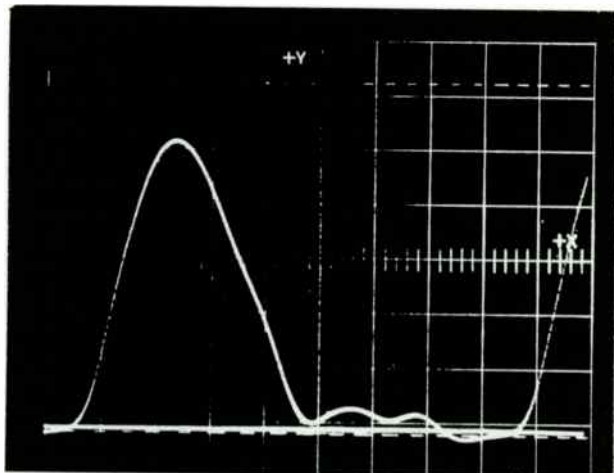


Fig. 14. Transistor evaluation results: predicted efficiency vs. frequency and output power for amplifier using MRF2020 transistor.



(a)



(b)

Fig. 15. Collector-voltage waveform, 210 MHz. (a) Simulated.
(b) Measured. Horizontal: 0.6 ns/div. Vertical: 10 V/div.

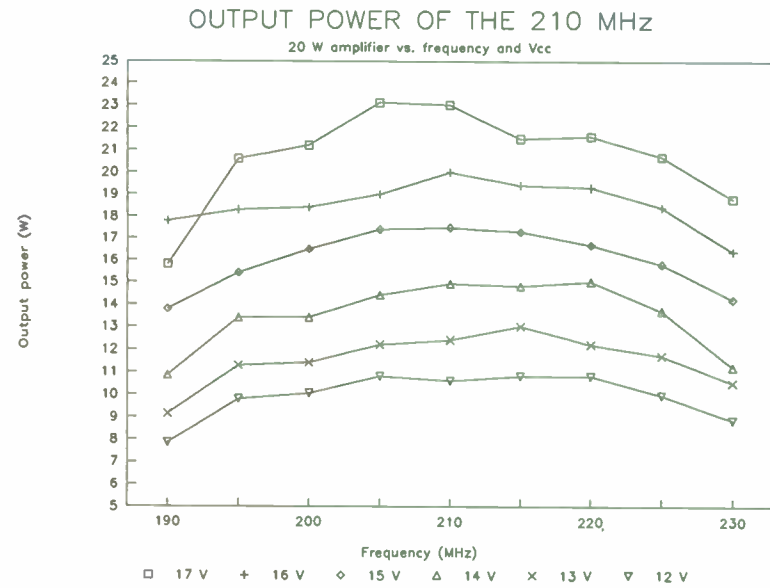


Fig. 16. Measured output power vs. frequency and dc supply voltage, amplifier using MRF2020 transistor.

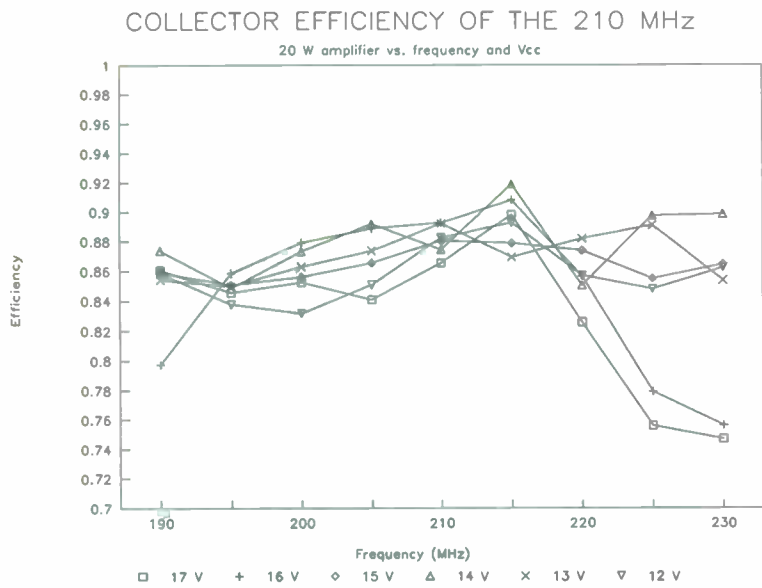


Fig. 17. Measured collector efficiency vs. frequency and dc supply voltage, amplifier using MRF2020 transistor.

**A QUASI-LINEAR DETERMINATION OF UHF
POWER DEVICE OPERATION
FROM A SPICE SIMULATED NON-LINEAR BJT MODEL**

by
Dr. Pablo E. D'Anna
Microwave Modules & Devices, Inc.
550 Ellis Street
Mt. View, California 94043

INTRODUCTION

The current methods for designing RF and microwave transistor power amplifiers are largely trial and error types of situations where the engineer mixes linear methods of network analysis with actual device measurements.

A method is proposed here by which it can be predicted, with a reasonable amount of accuracy, the RF performance of a bipolar device by using large-signal y-parameters obtained from D.C. and low frequency A.C. measurements. This type of approach was first proposed by Houselander et al. (1) and further developed by Kotzebue (2, 3). The present approach differs from these previous ones in the sense that elaborated methods of y-parameter measurements at large power and high frequencies are not used. Instead, the y-parameters for the transistor are computationally generated from a non-linear Gummel-Poon model utilizing the transient analysis mode of the circuit simulation program SPICE (the version used is PSpice v4.02 by the MicroSim Corporation) (4). PSpice utilizes the enhanced Gummel-Poon model of the bipolar transistor shown in Figure 1 which includes the following characteristics:

- Effects of basewidth modulation
- High injection effects
- Variation of forward transit time (T_f) with collector current (I_C)
- Split collector-base junction capacitance across R_B

The device used is a 1-cell, MMD fabricated, L-Band device (ME6) in a common-base configuration.

DEVICE PARAMETER EXTRACTION

Device DC measurements were made using a Tektronix Model 576 curve tracer. The methods used to extract the Gummel-Poon model parameters are outlined by Getreu (5). A listing of the parameters and values determined from the D.C. measurements is given in Table 1.

**Table 1
Gummel-Poon Model Parameters Determined From D.C. Measurements**

<u>Symbol</u>	<u>Definition</u>	<u>Value</u>
R_B	Base Spreading Resistance	0.4 ohm
R_E	Emitter Resistance	1.4 ohm
R_C	Collector Resistance	1.8 ohm
B_F	Forward Beta	1E6
B_R	Reverse Current Gain	0.9434
V_A	Forward Early Voltage	23.5 volt
V_{AR}	Reverse Early Voltage	6.8 volt
I_S	Transport Saturation Current	20 E-11 amp
I_{SE}	Base-emitter Leakage Saturation Current	0.165 E-6 Amp

Small signal A.C. capacitances were measured using a Boonton Model 72B capacitance meter. Measurement methods for these parameters are also found in Getreu (5). A listing of the parameters and values obtained is given in Table 2.

Table 2
Gummel-Poon Model Parameters Determined From A.C. Measurements

<u>Symbol</u>	<u>Definition</u>	<u>Value</u>
C _{JE}	Base-Emitter zero-bias p-n capacitance	22.52 E-12 F
C _{JC}	Base-Collector zero-bias p-n capacitance	12.62 E-12F
V _{JC}	Collector-Base Built-in Voltage	0.75 Volt
V _{JE}	Collector-Emitter Built-in Voltage	0.75 Volt
M _{JC}	Collector-Base Junction Grading Factor	0.486
M _{JE}	Base-Emitter Junction Grading Factor	0.278

From the data obtained, the Parts sub-program of PSpice was used to generate some of the Gummel-Poon parameters for the bipolar transistor model. A list of the parameters used and their computed values for the device model is given in Table 3.

Table 3
Gummel-Poon Model Parameters for ME6 Device

<u>Symbol</u>	<u>Definition</u>	<u>Value</u>
B _F	Forward Beta	1 E-6
B _R	Reverse Beta	0.943
V _{AF}	Forward Early Voltage	23.5 Volt
V _{AR}	Reverse Early Voltage	6.8 Volt

I _S	Transport Saturation Current	0.2 E-9 Amp
I _{SE}	Base-Emitter Leakage Saturation Current	165.6 E-9 Amp
I _{KF}	Corner For Forward-Beta High-Current Roll-Off	49.38 E-6 Amp
N _E	Base-Emitter Leakage Coefficient	3.614
N _F	Forward Current Emission Coefficient	1.345
R _E	Emitter Resistance	1.4 Ohm
R _C	Collector-Resistance	1.8 Ohm
R _B	Base Resistance	1.0 Ohm
R _{BM}	Minimum Base Resistance	0.8 Ohm
I _{RB}	Current At Which R _B Falls Halfway To R _{BM}	0.5 Amp
C _{JC}	Base-Collector Zero-Bias P-N Capacitance	12.62 E-12 F
M _{JC}	Base-Collector P-N Grading Factor	0.486
C _{JE}	Base-Emitter Zero-Bias P-N Capacitance	22.52 E-12 F
M _{JE}	Base-Emitter P-N Grading Factor	0.278
T _F	Ideal Forward Transit Time	90 E-12 Sec.
T _R	Ideal Reverse Transit Time	30 E-12 Sec.
P _{TF}	Prep Excess Phase	50 Degree

Some of the Gummel-Poon model parameter values obtained from Parts were adjusted slightly in order to better represent the performance of the actual device that was tested. In going through and adjusting the parameters, each had a different effect on the family of collector current curves vs. V_{ce}. The circuit netlist and schematic used to generate a family of collector current curves is given in Figure 2. Table 4 is a partial list of some Gummel-Poon model parameters and the effect of their variation on device performance.

Table 4

Effect of Variations of G.P Model Parameters on Device Performance

Parameter	Sensitivity
I_{KF}	Increasing I_{KF} will decrease the slope of the $I_{C(sat)}$ region, increasing I_{KF} will move out the knee of the H_{FE} vs. I_C curve, decreasing I_{KF} will increase the slope of the $I_{C(SAT)}$ region, decreasing I_{KF} will move in the Knee of the H_{FE} vs. I_C curve.
N_F	Increasing N_F will increase the slope of the $I_{C(SAT)}$ region, increasing N_F will decrease the DC gain, increasing N_F will decrease the roll-off rate of the H_{FE} vs. I_C curve, decreasing N_F will decrease the slope of the $I_{C(SAT)}$ region, decreasing N_F will increase the DC gain, decreasing N_F will increase the roll-off rate of the H_{FE} vs. I_C curve.
R_C	Increasing R_C will increase the slope of the $I_{C(SAT)}$ region, decreasing R_C will decrease the slope of the $I_{C(SAT)}$ region.
I_S	Increasing I_S will decrease the slope of the $I_{C(SAT)}$ region, increasing I_S will increase the DC gain, decreasing I_S will increase the slope of the $I_{C(SAT)}$ region, decreasing I_S will decrease the DC gain
I_{SE}	Increasing I_{SE} will increase the slope of the $I_{C(SAT)}$ region, increasing I_{SE} will decrease the DC gain, decreasing I_{SE} will decrease the slope of the $I_{C(SAT)}$ region, decreasing I_{SE} will increase the DC gain.
B_F	Increasing B_F will increase the DC gain, increasing B_F will increase the slope of the $I_{C(SAT)}$ region, decreasing B_F will decrease the DC gain, decreasing B_F will decrease the slope of the $I_{C(SAT)}$ region.

Using the input file from Figure 2, PSpice predicted a DC common emitter current gain relative to collector current for the test device as shown in Figure 3. The figure illustrates the correlation obtained between the predicted and measured responses.

The large-signal enhanced Gummel-Poon model obtained from the measurement and computations described above for the MMD ME6 bipolar transistor is shown in Figure 4. The transistor is shown in a common-base configuration. The model takes into account the bond wire inductances coming from the die to the package as well as some parasitic package capacitances. The values for the bond wire inductances were assumed using nominal values for 1 mil gold wire.

LARGE SIGNAL ANALYSIS

In order to obtain large signal y-parameter values from the model of the ME6 device the circuit diagrams shown in Figures 5 and Figure 6 were created. The circuit net lists entered into the SPICE simulation are shown in Tables 5 and 6.

It is not possible to directly obtain the y-parameters from the SPICE analysis because the model used is non-linear due to the large-signal conditions of operation. By doing a Fourier analysis of the voltages and currents at the input and output ports at the device, the y-parameters for the fundamental frequency can be calculated. In determining the correct y-parameters, many Gummel-Poon model parameter values were tested in order to determine the resulting computed y-parameter sensitivities. Because the input of the transistor is relatively insensitive to changes in the output, it is easier to obtain the output y-parameters first. Later on, after the input y-parameters are determined, the output parameters can be adjusted, if needed, accordingly to changes caused by the input y-parameters.

Kotzebue (3, 4) has shown that this quasi-linear method of characterization of a device provides adequate data to design "Class C" power amplifiers as long as the output of the device is not operated in a highly

non-linear fashion and at sufficiently high frequency. However, this approximation of near linear behavior of the output port of a microwave transistor under large-signal operation is not valid at low frequencies (low compared to f_T , for example), as it is well known that the efficiency of a low frequency transistor amplifier is highly dependent on the value of the load impedance at harmonic frequencies. One basic difference between the low-frequency case and the high-frequency case may be summarized as follows. At low frequencies, the gain is high, small signals are present at the transistor input port, and saturation occurs primarily as a result of the clipping of the large signals present at the output port. At high frequencies, the gain is low and large-amplitude signals are present at the transistor input. Because of this low gain, saturation effects will occur first at the input, while the output voltage is below the level necessary to generate significant additional nonlinearity.

In the procedure reported here, fixed-bias operation is used to obtain the large signal y-parameter values from the SPICE test circuits; under common-base operation both the collector bias voltage and collector bias current are held constant, even in the presence of large RF signals. This mode of operation is similar to "Class A" operation, although that does not imply that only small RF signals are involved here, or that saturation effects are excluded. Fixed-bias operation is used as the basis of the procedure presented here to reduce the degrees of freedom, and to make possible the use of linear circuit theory previously developed for the design of microwave transistor power amplifiers. However, the device was tested under "Class C", with self-bias operation.

From the formulations derived by Kotzebue (3), it can be shown that:

$$(P_a)_{\max} = |V_1|^2 \frac{|Y_{21}|^2 + |Y_{12}|^2 + 2\text{Re}(Y_{21} Y_{12}) - 4g_{11} g_{22}}{4 g_{22}} \quad (1)$$

Where $(P_a)_{\max}$ is the maximum added output power for the device, operating at the collector bias and input signal voltage corresponding to the values that the large signal y-parameters were obtained.

The load termination corresponding to this value of maximum output added power for the device in an amplifier circuit can be determined by using the following formula:

$$(Y_L)_{\text{opt}} = \frac{2Y_{21}}{Y_{21} + Y_{12}^*} - Y_{22} \quad (2)$$

The input admittance for this optimum load termination is given by

$$(Y_{in})_{\text{opt}} = Y_{11} - \frac{Y_{21} Y_{12} + |Y_{12}|^2}{2g_{22}} \quad (3)$$

This value for $(Y_{in})_{\text{opt}}$, coupled with the r.m.s. value for the fundamental frequency input voltage, is used to determine the calculated input power

$$P_{in} = |V_1|^2 \text{Re} \{Y_{in}(\text{opt})\} \quad (4)$$

From (1) and (4), the maximally efficient gain (G_{ME}), a figure of merit for high frequency active two-port devices, can be determined by the following equation:

$$G_{ME} = 10 \log \frac{\text{Output Added Power}}{\text{Input Power}} \quad (5)$$

The G_{ME} is defined as the power gain which maximizes the two-port added power for a given value of the input port independent variable (3).

RF AMPLIFIER PERFORMANCE

Large signal y-parameters for the ME6 device were obtained by the proposed method at 850 MHz. Figure 7 shows the variation of the output parameters (y_{12} and y_{22}) with output signal voltage (for a constant frequency and D.C. voltage bias). Figure 8 shows the corresponding situation for the input port parameters (y_{21} , y_{11}). From this data and utilizing equations (1), (4) and (5) predictions about the maximum added power and its associated gain for the device were made. This calculated performance was compared to actual data taken from an operating amplifier. Figure 9 shows the test set up used to measure the RF performance of the device. The device test fixture was designed for easy disassembly in order to facilitate actual measurement of input and output admittances.

In Table 7 computed and measured results are given for one set of input/output operating points. Figures 10 and 11 show the correlation obtained between measured and calculated added output power and gain for the test device over a range of input power conditions. The agreement between both curves was considered good as long as the device was operated below heavy collector saturation conditions.

Table 7
Comparison of Measured and Predicted Performance of ME6 Device

<u>Parameter</u>	<u>Calculated</u>	<u>Measured</u>
Input Power (P_{in})	0.303 Watt	0.304 Watt
Output Added Power (P_o) Max	2.06 Watt	2.04 Watt
Maximum Added Gain (G_{ME})	8.22 dB	8.25 dB

Input Admittance (Y_{in})	0.146 + j0.0592	0.157 + j0.08467
Output Admittance (Y_{out})	0.00744 + j0.0277	0.0184 + j0.02226
V_{CB}	= 30 Volt	
I_C	= 163 mA	

Acknowledgements: The author would like to thank Earl Lum and Robinder Virk for the computational results provided. This work was sponsored by the Electronic Technology Laboratory - Wright Research and Development Center - Aeronautical System Division - USAF - Wright - Patterson ABF.

References

- [1] L.S. Houselander, H.Y. Chow, and R. Spence, "Transistor Characterization By Effective Large-Signal Two-Port Parameters," IEEE J. Solid-State Circuits, Vol. SC-5. pp.77-79, April 1970
- [2] K. L. Kotzebue, "A Quasi-Linear Approach to the Design of Microwave Transistor Power Amplifiers," IEEE Trans. Microwave Theory Tech., pp. 975-978, Dec. 1976.
- [3] K. L. Kotzebue, "Maximally Efficient Gain: A Figure of Merit for Linear Active 2 Ports," Electronics Letters, Vol. 12, No. 19, pp.490-491, Dec. 16, 1976.
- [4] Paul W. Tuinenga, Spice: A Guide to Circuit Simulation and Analysis Using PSpice, Prentice Hall, 1988.
- [5] Ian Getreu, Modeling The Bipolar Transistor, Tektronix Inc., 1976.

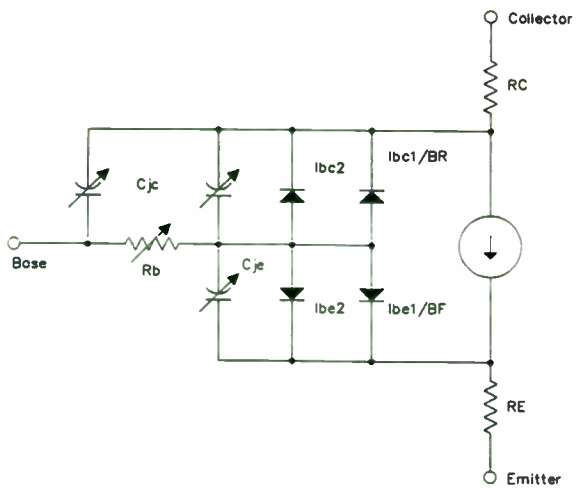
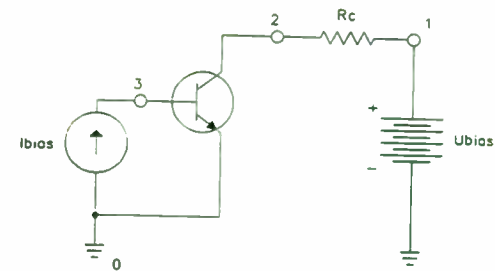


Figure 1. Enhanced Gummel-Poon BJT



```

VBIAS 1 0 30 V
IBIAS 0 3 50 mA
RC 1 2 1 OHM
Q1 2 3 0 ME6
o MODEL QME6 NPN (BF=1E6 VAF=23.5 IS=20E-11 IKF=49.38E-6 ISE=165.6E-9
+ NE=3.614 BR=.9434 VAR=6.8 NF=1.345 RE=1.5 RC=1.8 RB=.4)
o DCVBIAS 0 10V IBIAS 0 50 mA 5 mA
o PROBE
o END

```

Figure 2. PSPice Circuit File Used to Generate Collector Current Curves as a Function of Collector-Emitter Voltage

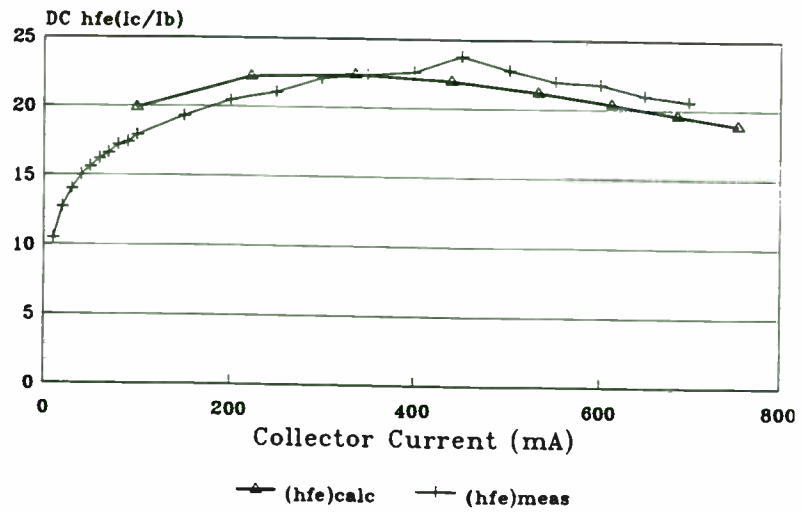


Figure 3. D.C. Current Gain as a Function of Collector Current. (Common-Emitter)

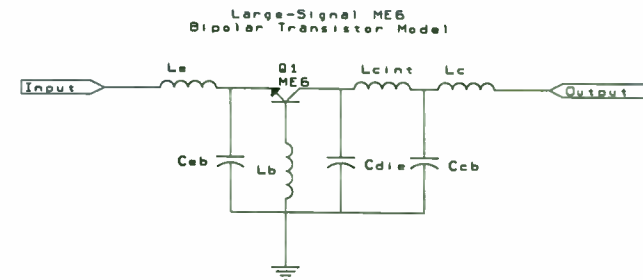


Figure 4. Common-Base Model of ME6 Device Used in Simulations.

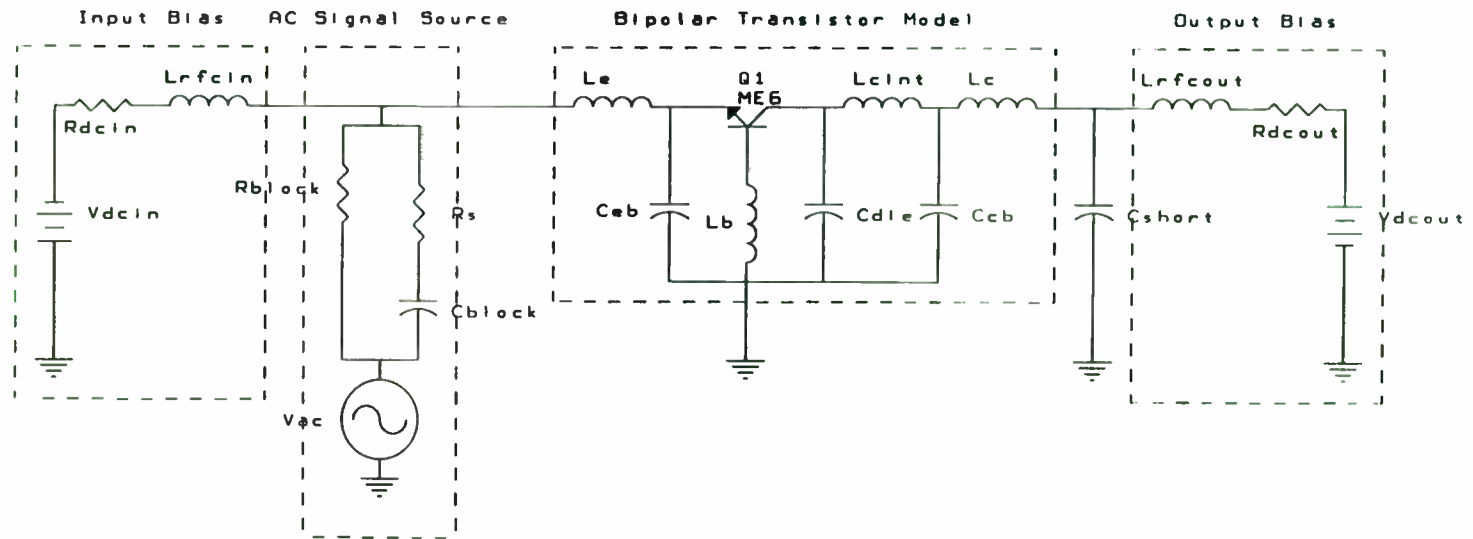


Figure 5. Circuit Used to Determine Y_{11} and Y_{21} .

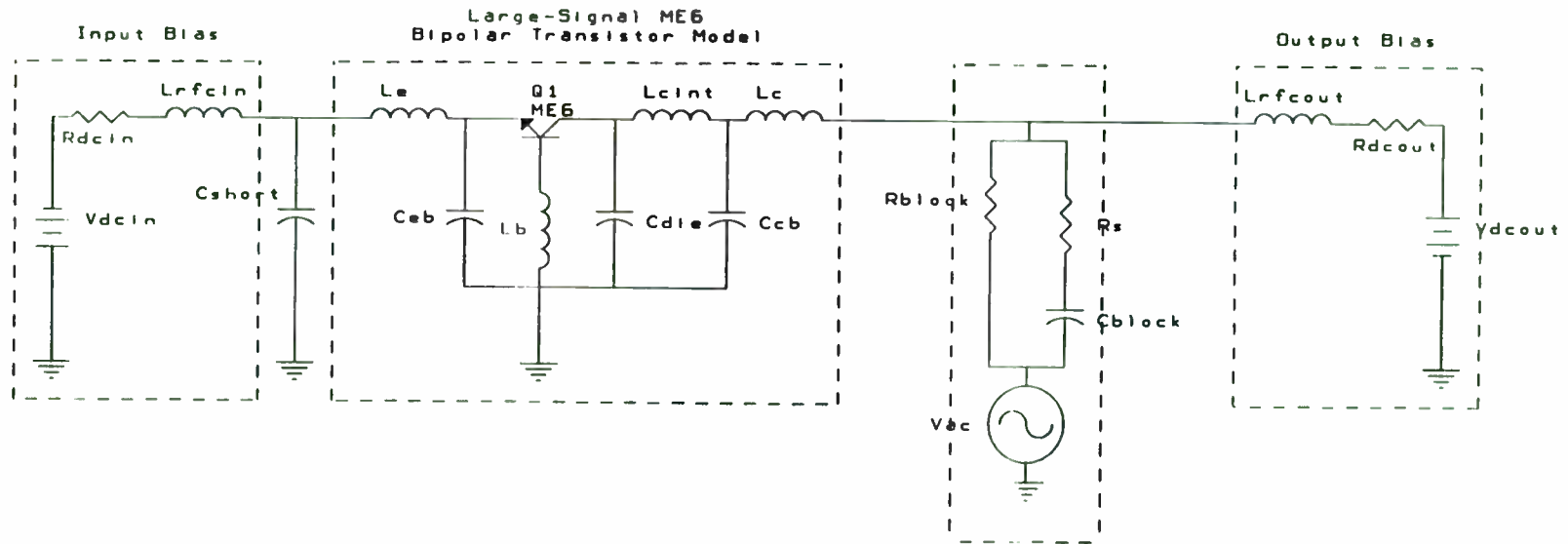


Figure 6. Circuit Used to Determine Y_{22} and Y_{12} .

***** 08/28/90 ***** PSpice 4.02 - 1989 ***** 11:08:00 *****

Prediction of ME-6 input/output impedance

**** CIRCUIT DESCRIPTION

```

**pkg: 440023
**die: ME-6 1-cell
**Common-Base Configuration
*Input DC Bias Circuit*
vdcin 0 1 dc 1.55
rdcin 1 2 1
lrfcin 2 3 5m
*Output DC Bias Circuit*
vdcout 9 0 dc 30.5
rdcout 9 8 1
lrfcout 8 7 5m
*Input AC Signal Source*
vac 10 0 sin(0 26 850meg 0 0 0)
cblock 3 100 1u
rx 100 10 50
rblock 3 10 10meg
cshort 7 0 100u
*Bond Wire Inductances*
le 3 4 .3n
lb 5 0 .3n
lc 7 6 .5n
lcint 6 11 .4n
*Parasitic Package Capacitances*
cbc 6 0 1.5p
cbe 0 4 2.12p
cdie 11 0 .26p
*ME6 Device Model*
q1 11 5 4 qme6
.model qme6 npn (is=200.000p bf=1.000meg nf=1.345
+ vaf=23.5 ikf=49.380u ise=165.600n ne=3.614 br=.943 var=6.8
+ rb=1 rbm=.8 irb=.5 re=1.4 rc=1.8 cje=22.520p
+ mje=.278 cjc=12.620p mjc=.486 tf=90.000p ptf=50 tr=30.000n ) ; *ipsp*
*Anaysis Section*
.four 850meg i(le) i(1c) v(3,0)
.tran 50p 10n 8.82353n 50p
.options tnom=120
.end

```

Table 5. Input Circuit File used to Determine Y_{21} and Y_{11} .

***** 08/28/90 ***** PSpice 4.02 - 1989 ***** 11:15:05 *****

Prediction of ME-6 input/output impedance

**** CIRCUIT DESCRIPTION

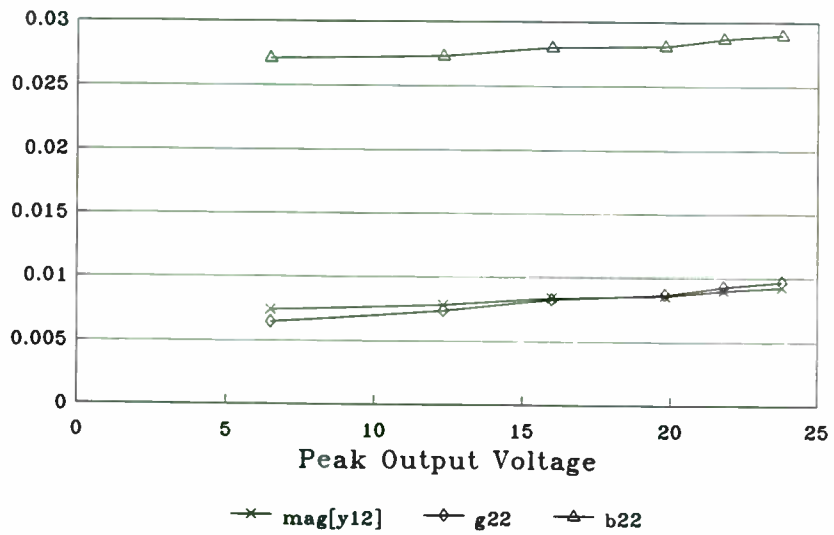
```

**pkg: 440023
**die: ME-6 1-cell
**Common-Base Configuration
*Input DC Bias Circuit*
vdcin 0 1 dc 1.61
rdcin 1 2 1
lrfcin 2 3 5m
*Output DC Bias Circuit*
vdcout 9 0 dc 32
rdcout 9 8 1
lrfcout 8 7 5m
*Output AC Signal Source*
vac 10 0 sin(0 32 850meg 0 0 0)
cblock 7 100 1u
rx 100 10 50
rblock 7 10 10meg
cshort 0 3 100u
*Bond Wire Inductances*
le 3 4 .3n
lb 0 5 .3n
lc 7 6 .5n
lcint 6 11 .4n
*Parasitic Package Capacitances*
cbc 6 0 1.5p
cbe 0 4 2.12p
cdie 11 0 .26p
*ME6 Device Model*
q1 11 5 4 qme6
.model qme6 npn (is=200.000p bf=1.000meg nf=1.345
+ vaf=23.5 ikf=49.380u ise=165.600n ne=3.614 br=.943 var=6.8
+ rb=1 rbm=.8 irb=.5 re=1.4 rc=1.8 cje=22.520p
+ mje=.278 cjc=12.620p mjc=.486 tf=90.000p ptf=50 tr=30.000n ) ; *ipsp*
*Analysis Section*
.four 850meg i(le) i(1c) v(7,0)
.tran 50p 10n 8.82353n 50p
.options tnom=120
.end

```

Table 6. Output Circuit File Used to Determine Y_{12} and Y_{22} .

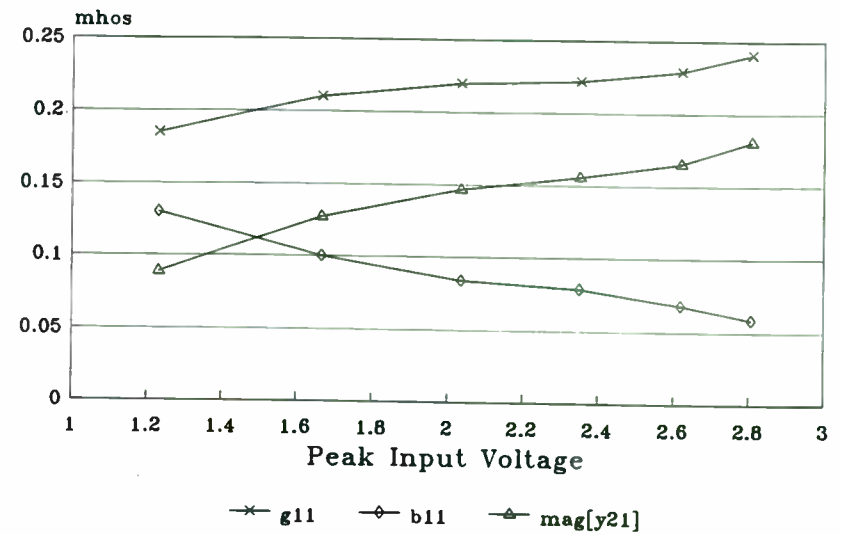
Predicted y_{12} and y_{22}



f=850MHz, Vcc=30V

Figure 7. Predicted Output Y-Parameter Values from GP Model of ME6 Device

Predicted y_{11} and y_{21}



f=850MHz, Vcc=30V

Figure 8. Predicted Input Y-Parameter Values from GP Model of ME6 Device

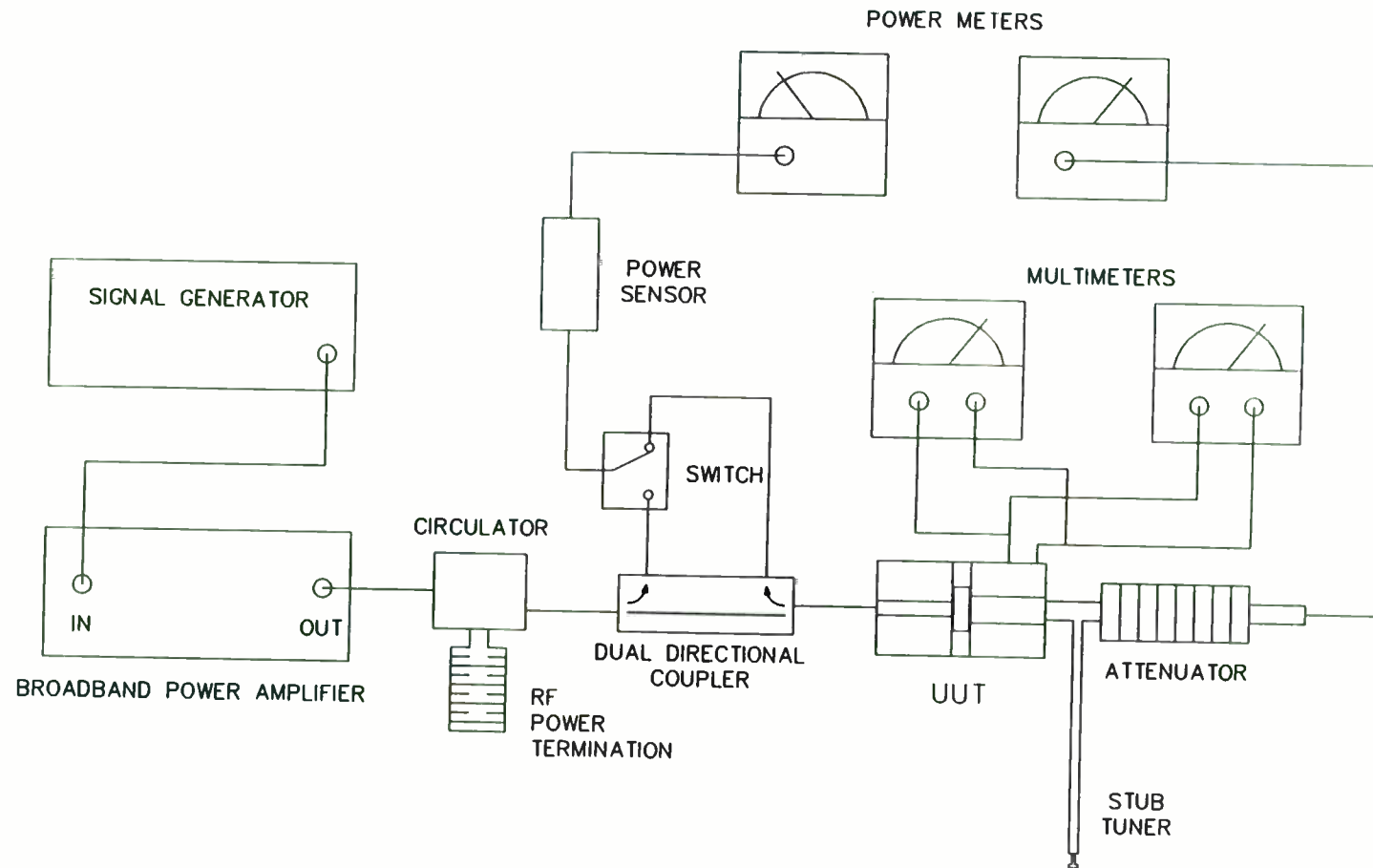
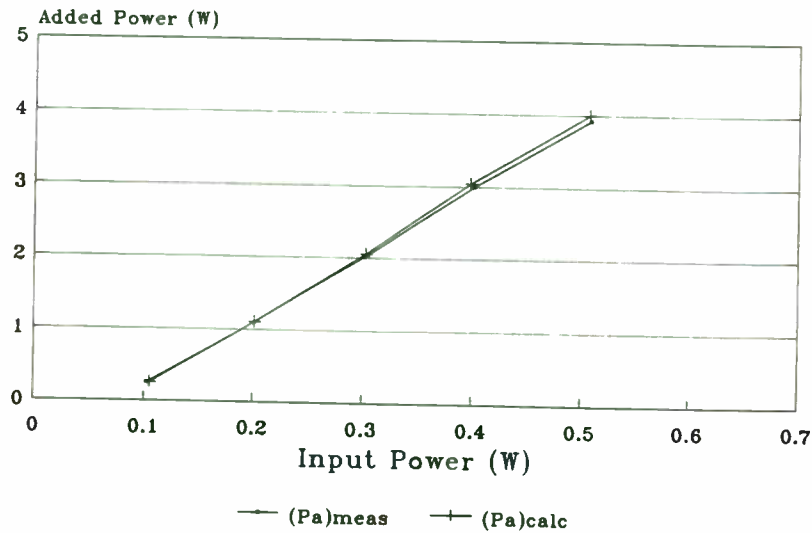


Figure 9. Test Set-Up Used to Measure Performance of ME6 Device

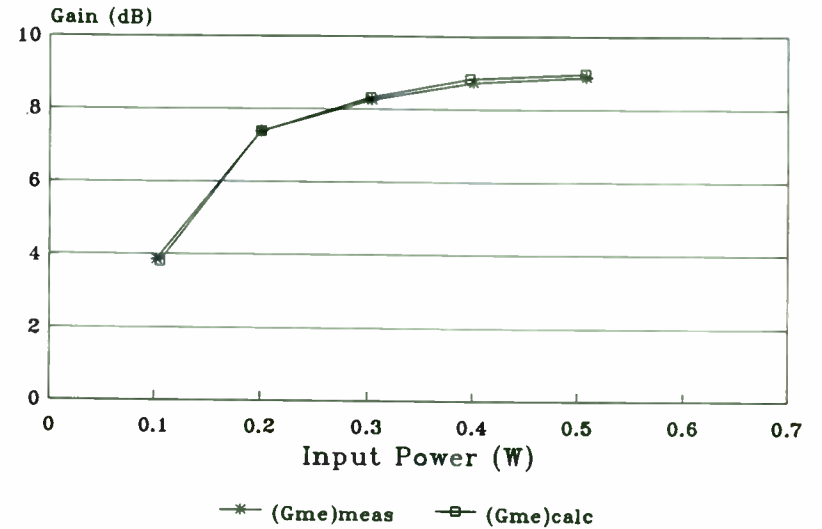
Added Power vs. Input Power



f=850MHz, Vcc=30V

Figure 10. Correlation Between the Measured Added Power and the PSpice Predicted Maximum Added Power as a Function of Input Power.

Gain vs. Input Power



f=850MHz, Vcc=30V

Figure 11. Correlation Between the Measured Gain and the PSpice Predicted Gain as a Function of Input Power.

DESIGNING WITH DIRECT DIGITAL FREQUENCY SYNTHESIZERS

FRANCISCO A. B. CERCAS
M. TOMLINSON A. A. ALBUQUERQUE

*Instituto Superior Técnico (IST), DEEC/CAPS
Av. Rovisco Pais, P-1096 Lisboa, PORTUGAL
Tel. + 351 1 802045 ext. 1450 Telex: 63423 ISTUTL P
FAX: + 351 1 899242*

SUMMARY

The aim of this article is to provide all the necessary information to analyse and design any Direct Digital Frequency Synthesizer (DDFS or simply DDS) with ease and precision. The principle of operation of a basic DDS is described and its main sources of degradation are pointed out. A complete characterization of DDS's is then made in both the time and frequency domain with presentation of useful and original expressions on this subject. As an application example of the derived expression for the power spectrum density with phase quantization, an extremely simple algorithm is described that sequentially computes the frequency and magnitude of each spur component and gives exactly the same result as a FFT. Expressions for the signal-to-noise ratio, including phase and amplitude quantization, a summary of its general spectral properties and general design rules, including a design example, are also presented. An ECL hardware prototype was built and its performance is shown to be in good agreement with both theoretical and simulation results.

1. INTRODUCTION

DDS's are taking an ever increasing role in the frequency synthesis field with the advent of Very High-Speed Integrated Circuits (VHSIC). DDS's have several advantages over conventional types of synthesizers. Their main advantages are:

- Extremely fast frequency switching, limited only by the speed of available logic circuits, specially the access time of the memory, and by the delay of the low-pass filter.
- Continuity of the phase when the frequency is changed which minimizes transients and allows to control the phase of the generated signal.
- Capability of very fine resolution increasing exponentially with the hardware.
- Low cost and small size made possible by a high level of digital integration.
- High immunity against external noise.

Although these are excellent properties that can suit most applications, DDS's only became practical in the late 1960s by some advances made in semiconductor technology applied to Read-Only-Memories (ROM's). The maximum output frequency of the early prototypes was limited to some kilohertz, even with a very efficient use of memory [5]. Nowadays, single dedicated chips excluding only the DAC and LPF are readily available which can generate frequencies approaching the gigahertz and frequency switching times in the order of a nanosecond!

There is a wide range of applications, namely very high speed frequency hopped sources, single sideband converters, phase control, baseband receivers, digital signal processors and so on. For some applications where present state-of-the-art technology is still a limiting factor, as for example the maximum synthesizable frequency, DDS's can be used in conjunction with other types of synthesizer to get the best of both worlds.

2. OPERATING PRINCIPLE

Figure 1 shows the block diagram of a DDS. It is composed essentially by a m bit adder working as a phase accumulator, a $N \times n$ bit ROM containing $N = 2^i$ values of the \sin or \cos of the corresponding phase, a n bit DAC to convert the signal to analogue form and a low-pass filter to cut the undesired spurious components. Usually the accumulator's length m is large in order to provide a good frequency resolution, but only the i most significant bits address the ROM. The m bit accumulator and associated registers can then be thought as having i integer plus f fractionary bits. So, the m bit integer value stored in the input setting register L , $L \in [1 .. 2^{m-1} - 1]$ can also be thought as a fractionary number L_f , $L_f = L \times 2^{-f}$ whose minimum non-zero value is 2^{-f} occurring for $L = 1$.

For a given desired frequency f_d , a phase step $\Delta\phi = (2\pi/N) \times L_f$ is stored in the input setting register. At every clock cycle $T_c = 1/f_c$ the accumulator will increment the output by that amount and therefore the corresponding sample of the sinewave is decoded and outputted. Whenever the accumulator overflows only the most significant bits are lost and since its maximum value corresponds to a phase of 2π , a modulo 2π operation is automatically performed. So, the

rate of overflow is the generated frequency f_d . When a new frequency is desired, a new phase increment is loaded in the input setting register and this will be added to the existing phase in the next clock cycle. This means that the continuity of the phase is always maintained.

For a given configuration of the m bits at the input, the generated frequency f_d is given by :

$$f_d = \frac{L_f}{N} f_c = \frac{L 2^{-f}}{N} f_c = L \frac{f_c}{2^m} = L f_{res} \quad (1)$$

where f_{res} is the minimum synthesizable frequency or frequency resolution. This equation also shows that all generated frequencies are integer multiples of f_{res} . This value can be made arbitrarily small by just increasing the accumulator's length m which in turn will also increase the number of synthesizable frequencies 2^{m-1} . This assumes that the maximum generated frequency is $f_c/2$ but in practice we have to reduce this number in order to build a realisable low-pass filter, with a maximum synthesizable frequency $f_{dmax} < f_c/2$.

3. SOURCES OF DEGRADATION

Among the several mechanisms that contribute for degrading the signal in a DDS, phase quantization is inherent to this particular type of implementation and can appear whenever the number of bits i addressing the ROM is less than the number of bits in the accumulator m , which is common practice. This means that sometimes the accumulator will output a phase value $2\pi/2^m$ for which there is not a corresponding stored value in ROM as the actual phase resolution is $\phi_{res} = 2\pi/2^i$. The resulting phase error is then converted to an amplitude error and the sequence of phase errors is periodic with period P . For any frequency the generated sequence of samples is also periodic and their magnitudes repeat with period M , which is always an integer multiple of P . This is a more general property of a signal generated by a DDS, which also has odd half-wave symmetry¹ defined by :

$$y \left[\left(k + \frac{M}{2} \right) T_c \right] = -y(kT_c) \quad (2)$$

Table 1 shows how to determine the expressions for these periods as a function of the number L representing the binary word at the input setting register that controls the generated frequency.

Since the frequencies for which the f least significant bits of the accumulator are always zero, will never have phase quantization, it is easy to deduce an expression for this important class of frequencies :

¹ This property will only be truth when the distribution of values in the ROM table, the amplitude quantization law and the active elements of the circuit do not alter that symmetry.

$$f_{dunq} = K 2^f f_{res} \quad K = 1 \dots K_{max} \quad (3)$$

where

$$K_{max} = \frac{f_{dmax}}{2^f f_{res}} \quad (4)$$

is the number of frequencies with this property and increases for lower f , which means a higher ROM table size. If $f = 0$ there will be never phase quantization and K_{max} will represent the total number of generated frequencies.

Other sources of degradation are amplitude quantization resulting from the fact that only 2^i discrete amplitudes can be outputted, DAC transients or "glitches", that will corrupt the output pulses and generate components at harmonics of f_c/M thus being responsible for even-order harmonic distortion, the DAC hold effect that will transform the input sample sequence in a staircase-like waveform introducing frequency nulls at all multiples of the clock frequency, therefore attenuating the highest generated frequencies by a few dB, and aliasing, as in any other sampled system, since the low-pass filter is not ideal. Phase noise is not of concern since the stability of a DDS depends only on that of its system clock.

4. TIME AND FREQUENCY MODEL

Modeling the signal at the input of the DAC as :

$$y(t) = \sum_{k=-\infty}^{+\infty} \sin[\phi_{res} \times \text{int}(kL_f)] \delta(t - kT_c) \quad (5)$$

where $\text{int}(kL_f)$ accounts for the truncation that originates phase quantization, it is shown[1] that in the passband considered as the interval $[0 \dots f_c/2]$, all generated frequencies with exception of those which are direct submultiples of the clock frequency or its odd harmonics will be phase quantized and P frequency components are then generated including the signal. In that case P is always an even number so the passband can be divided in $P/2$ frequency slots of width f_c/P numbered from $s = 0$ to $s = P/2 - 1$ as shown in figure 2.

All P components are symmetrically located in pairs, designated by (f_{1s}, f_{2s}) , around the center frequency of each slot s . The frequency of each of these pair of components in the slot s , where eventually $f_{1s} \geq f_{2s}$ depending on the value of f_d , can be determined by the expressions :

5. SIGNAL-TO-NOISE RATIO

Integrating $|Y_{LP}(f)|^2$ over the passband it is also shown [1] that the total power is constant and has the value :

$$\int_{-\frac{B}{2}}^{\frac{B}{2}} |Y_{LP}(f)|^2 df = \frac{1}{2T_c^2} \quad (14)$$

The power in the signal component can also be derived from equation 10 with $s = s_0$:

$$S = |Y_{LP}(f)|_{f=f_d}^2 = \frac{1}{2P^2T_c^2} \frac{\sin^2(\frac{\pi}{N})}{\sin^2(\frac{\pi}{NP})} \quad (15)$$

and therefore the signal-to-noise ratio due only to phase quantization is given by :

$$\left(\frac{S}{N}\right)_{PQ} = 10 \log_{10} \left[\frac{\sin^2(\frac{\pi}{N})}{P^2 \sin^2(\frac{\pi}{NP}) - \sin^2(\frac{\pi}{N})} \right] \text{ dB} \quad (16)$$

A worst-case function (the worst-case occurs for $P = 2$ with a penalty of 1.25 dB) can be easily deduced to be :

$$\left(\frac{S}{N}\right)_{PQ} = 6i - 5.17 \text{ dB} \quad (17)$$

Assuming uniform distribution for the amplitude quantization errors, a general expression for the signal-to-noise ratio including both amplitude and phase quantization effects is :

$$\left(\frac{S}{N}\right)_Q = 10 \log_{10} \left[\frac{\sin^2(\frac{\pi}{N})}{P^2 \sin^2(\frac{\pi}{NP}) \left[1 + \frac{1}{1.5(2^n - 1)^2} \right] - \sin^2(\frac{\pi}{N})} \right] \text{ dB} \quad (18)$$

As we can see the factor $\left[1 + \frac{1}{1.5(2^n - 1)^2} \right]$ accounts for the amplitude quantization effect so that when $n \gg 1$ this equation becomes SNR_{PQ} . On the other hand when $P \rightarrow \infty$ or $N \rightarrow \infty$ the well known formula for the amplitude quantization noise is obtained :

$$\lim_{N \rightarrow \infty} \left(\frac{S}{N}\right)_Q = 6.02n + 1.76 \text{ dB} \quad (19)$$

$$\begin{aligned} f_{1s} &= f_d \text{modr} \frac{f_c}{P} + \frac{s}{P} f_c \quad s \in [0 \dots \frac{P}{2} - 1] \\ f_{2s} &= (f_c - f_d) \text{modr} \frac{f_c}{P} + \frac{s}{P} f_c \end{aligned} \quad (6)$$

where the functions *divi* and *modr* are defined as follows :

$$a \text{ divi } b = \text{int}(a/b) \quad (7)$$

$$a \text{ modr } b = \text{frac}(a/b) * b \quad (8)$$

a and b can be any real numbers. The function *divi* returns an integer while *modr* returns a real number. The frequency slot containing f_d will be called s_0 and is given by :

$$s_0 = f_d \text{divi} \frac{f_c}{P} \quad s_0 \in [0 \dots \frac{P}{2} - 1] \quad (9)$$

The power spectrum density in the considered bandwidth is given by :

$$\begin{aligned} |Y_{LP}(f)|^2 &= \sum_{s=0}^{P/2-1} \{ A(s) [\delta(f - f_{1s}) + \delta(f + f_{1s})] \\ &+ B(s) [\delta(f - f_{2s}) + \delta(f + f_{2s})] \} \end{aligned} \quad (10)$$

where :

$$A(s) = \frac{\sin^2[\pi(s+p)]}{P^2 \sin^2[\frac{\pi}{P}(s+p)]} \quad (11)$$

$$B(s) = \frac{\sin^2[\pi(s-p+1)]}{P^2 \sin^2[\frac{\pi}{P}(s-p+1)]} \quad (12)$$

$$p = \frac{1}{N} - s_0 \quad (13)$$

For frequencies having $M \ll N$ only a few values in the ROM table will be used and therefore the amplitude quantization noise is highly dependent on the initial phase of the signal which then determines the associated errors contributing for that noise. Since these frequencies are only a small fraction, we can consider the average value given by equation 19 as a good approximation.

The graph shown in figure 3 represents these expressions as a function of i . As we observe the signal-to-noise ratio, SNR, due to phase quantization with i bits, $SNR_{PQ}(i)$, is comparable to the SNR due to amplitude quantization for $n = i - 1$ bits, $RAQ(n = i - 1)$, the two upper curves, resulting in a global SNR about 3 dB lower as expected, $SNR(n = i - 1)$. However an improvement of about 2 dB can still be achieved if we use $n = i - 2$, as we see comparing $SNR(n = i - 2)$ with $SNR(n = i - 1)$.

6. COMPUTER ALGORITHM

An algorithm for calculating the power spectrum affected by phase quantization is described as follows :

1. DETERMINE $N = 2^i$, P (from table 1) and s_0 (equation 9).

2. COMPUTE

$$f_1 = f_d \bmod \frac{f_c}{P} \quad (20)$$

$$f_2 = (f_c - f_d) \bmod \frac{f_c}{P} \quad (21)$$

3. IF $f_1 < f_2$ THEN

REPEAT FROM $s = 0$ TO $s = \frac{P}{2} - 1$:

Compute the frequency and magnitude of the two components in the slot s by :

$$f_{1s} = f_1 + s \frac{f_c}{P} : \text{magnitude} = A(s) \quad (22)$$

$$f_{2s} = f_2 + s \frac{f_c}{P} : \text{magnitude} = B(s) \quad (23)$$

OTHERWISE repeat the same calculation interchanging f_{1s} with f_{2s} in order to obtain the sequential components existing in the passband, as defined.

As we can see this algorithm is extremely simple and can be programmed in any computer or even a pocket calculator. It gives the exact value of all $(P - 1)$ spurious components due to phase quantization and the signal, and by increasing order, without having to use an FFT.

7. GENERAL SPECTRAL PROPERTIES

The frequency spectrum of an ideal DDS contains only odd harmonics or subharmonics of the generated signal which agrees with the fact that the signal has odd half-wave symmetry as defined in equation 2.

It is also shown[1] that all generated frequencies affected by phase quantization with the same P value, have exactly the same phase and amplitude quantization spurious components, and therefore the same signal-to-noise ratio. According to the particular frequency being generated those spurious will just permute their locations.

We saw that the amplitude quantization errors are periodic with period M , given in table 1, therefore originating a line spectrum with $M/4$ spurious components which will coincide with the signal and other existing phase components, at frequencies :

$$f_k = \frac{2k+1}{M} f_c, \quad k = 0, 1, 2, \dots, \frac{M}{4} - 1 \quad (24)$$

All these spurious, generated either by phase quantization or by amplitude quantization, are then odd harmonics or subharmonics of the generated signal and have a frequency separation of $f_{sep} = 2f_c/M$. This property allows a dramatic reduction in the number of points needed to analyze the signal by means of an FFT without any loss of information.

The spectral properties just described apply to an ideal frequency synthesizer. In a practical realization more components are present including even harmonics and intermodulation products between the generated frequency and the clock frequency. These extra components are due mainly to the DAC output glitches and slew rate limiting and to non-linearities introduced by the active components.

8. DESIGN RULES

1. The relation between the maximum frequency you want to synthesize, f_{dmax} , and f_c is essentially a function of the low-pass filter roll-off. Choosing a filter with, at least, SNR dB of attenuation at the image frequency of f_{dmax} , $f_c - f_{dmax}$, a first approximation of the clock frequency will be given by :

$$f_{c1} = (\Omega_s + 1) f_{dmax} \quad (25)$$

Since f_c must verify the equation :

$$f_c = 2^m f_{res} \quad (26)$$

we use first f_{c1} to determine the number of accumulator bits m which is the lower integer verifying the equation :

$$m \geq \log_2 \left[\frac{f_{c1}}{f_{res}} \right] \quad (27)$$

and then determine the exact value for f_c .

2. Choose the number of DAC bits n as the nearest integer that verifies the equation :

$$n \geq \frac{SNR + \Delta_{dB}}{6} \quad (28)$$

where SNR is the desired global value and Δ_{dB} is a corrective factor, $\Delta_{dB} \in [2 \dots 8]$, which accounts for other noise sources, like DAC glitches, is proportional to the bandwidth in use and depends also on the care taken with the practical implementation (layout,etc.).

3. The number of bits addressing the ROM is then given by :

$$i = n + 2 \quad (29)$$

9. DESIGN EXAMPLE

Suppose we want to implement a DDS with the following parameters :

- $f_{dmax} = 17.5$ MHz
- $f_{res} = 2.5$ Hz
- $SNR \geq 40$ dB

Applying the design rules as described and using a 7th order elliptical low pass filter with $\Omega_s = 1.37$ we have :

1.
 - $f_{c1} = 41.475$ MHz
 - $m \geq 23.98$ or $m = 24$ bits
 - $f_c = 41.94304$ MHz

2. Assuming $\Delta_{dB} = 3$ dB we have :

- $n \geq 7.1$

so we can use a common 8 bit DAC.

3. The number of lines addressing the ROM will be :

- $i = 10$

which means that the ROM will have $N = 1024 \times 8$ bit words.

Using equation 4 we see that this synthesizer can generate 427 frequencies free of phase quantization out of $f_{dmax}/f_{res} = 7000000$ possible frequencies.

10. HARDWARE PROTOTYPE

A complete prototype of s DDS was implemented using the design parameters of the example above, with a few extras like a pseudo-random generator which could program the synthesizer to hop randomly from one frequency to another. The input could also be programmed manually or through a computer by a serial or parallel interface. The accumulator was implemented using 100K ECL. The memory was the limiting factor in frequency since the accumulator and associated registers have been successfully tested up to 100 MHz. The DAC was also an ECL chip with $n = 8$ bit resolution and a settling time of 5 ns in order to minimise spurious components. The low-pass filter was an 7th order passive elliptical filter with amplitude equalization and a cut-off frequency of 17.5 MHz.

Figure 4 shows the synthesizer's output spectrum for $f_d = f_c/2$ with a very low level of spurious. Figure 5 shows a sample of the synthesizer's output taken with a memory scope which gives evidence of the continuity of the phase when the frequency is changed. Figure 6 shows the output of this synthesizer using the pseudo-random generator and hopping at about 10 Khop/s.

A general software simulator was also developed for this type of synthesizers including a 2048 point FFT which was applied to the sampled waveform in order to generate the frequency spectrum.

Figure 7 shows the simulated spectrum for a frequency close to the upper limit of this synthesizer, $f_d = 17.03936$ MHz. Since this is one of the frequencies free of phase quantization we intentionally reduced the value of i to 3 in order to introduce that source of noise. From table 1 we have $P = 4$ and $M = 32$ which means that in the passband we have 8 components: the signal, 3 due to phase quantization and the others due to amplitude quantization. Using the algorithm described we have $f_{s0} = 3.93216$ MHz, $f_{s10} = 6.5536$ MHz, $f_{s21} = 14.41792$ MHz and

$f_{20} = f_d$. These are exactly the major four components given by the FFT and their relative amplitudes are respectively -20.132 dB, -16.221 dB and -17.937 dB. The noise contribution of these components gives a SNR of 13.04 dB which is exactly the value given by equation 16. This situation was also simulated in the hardware prototype by disconnecting the 7 lower significant bits addressing the ROM and the measured spectrum is shown in figure 8. As we can see the frequency and magnitude of these phase spurious is remarkably similar to the computed values, also showing the predicted symmetry in the two frequency slots. The amplitude quantization spurious are not as well behaved and we can observe some even harmonics, but these are due mainly to the active components, specially for generated frequencies close to the upper bound, like this one.

Figure 9 shows the output spectrum for $f_d = 1.31072$ MHz. This frequency is also free from phase quantization and it is interesting to note that all 7 noise components existing in the passband are exactly the ones predicted for amplitude quantization, as they are all odd harmonics and their amplitudes have the expected average magnitude for a 8 bit DAC. The measured SNR was 42 dB which perfectly verifies the project requests. Figure 10 shows an expansion of figure 9 centered at f_d which gives evidence of the excellent close-to-carrier noise level.

11. CONCLUSIONS

In this paper we presented a complete characterization of a DDS, deducing exact expressions and general properties of these synthesizers not mentioned in previous works [6,7]. Very recent publications [10] show that they are still not known, leading to a vague choice of parameters concerning the project of a DDS. Based on these results we also presented an extremely simple, but accurate, algorithm for the calculation of all the frequency spurious components due to phase quantization and general design rules. It was also shown that there is a very good agreement between the measured performance of a hardware prototype, a dedicated software simulator and those theoretical results, therefore reinforcing their validity.

References

- [1] F. A. B. Cercas, "Direct Digital Frequency Synthesizer for a Frequency Hopped Spread Spectrum System", Thesis, Masters of Science in Electrotechnical and Computer Engineering, IST - Lisbon, 1988.
- [2] F. A. B. Cercas, M. Tomlinson, A. A. Albuquerque, "Direct Digital Frequency Synthesizer for a FH Spread Spectrum System: Analysis and Design", SBT / IEEE ITS'90 : International Telecommunications Symposium, Rio de Janeiro, Brazil, p. 434-8, 3-6 September 1990.
- [3] F. A. B. Cercas, M. T., A. A. A., J. M. P., "Phase Continuous Frequency Synthesizer for a Frequency Hopping Spread Spectrum System", IEEE MELECON'89, Lisbon, p. 403-6, 11-13 April 1989.
- [4] R. E. Ziemer, R. L. Peterson, "Digital Communications and Spread Spectrum Systems", Macmillan Publishing Company, 1985.
- [5] J. Gorski-Popiel, Ed., "Frequency Synthesis - Techniques and Applications." New York : IEEE, Press, 1975.
- [6] James Olsen, Philip M. Fishman, "Truncation Effects in Direct Digital Frequency Synthesis", IEEE Conference Record : Twentieth Asilomar Conference on Signals, Systems and Computers, Pacific Grove, CA, USA, p. 186-90, 10-12 November 1986.
- [7] Henry T. Nicholas, III and Henry Samuelli, "An Analysis of the Output Spectrum of Direct Digital Frequency Synthesizers in the Presence of Phase-Accumulator Truncation", IEEE, Proceedings of the 41st Annual Frequency Control Symposium, Philadelphia, PA, USA, p. 495-502, 27-29 May 1987.
- [8] B. A. Wittman, S. H. Early, and D. G. Messerschmitt, "A Hardware Multitone Digital Frequency Synthesizer", IEEE Trans. on Acoustics, Speech, and Signal Processing, vol. ASSP-27, no. 6, p. 804-9, December, 1979.
- [9] J. Tierney, C. M. Rader, and B. Gold, "A Digital Frequency Synthesizer", IEEE Trans. Audio and Electroacoustics, vol. AU-19, p. 48-57, 1971.
- [10] R. Gilmore, and R. Kornfeld, "Hybrid PLL/DDS Frequency Synthesizers", RF Design, p. 41-5, July, 1990.

L	ODD ($L=L_1$)	EVEN ($L=L_1 2^f$)	
		$j < f$ $j = 1 \dots f-1$	$j \geq f$ $j = f \dots m-1$
P	2^f	2^{f-j}	1
M	2^m	2^{m-j}	2^{m-j}
PHASE QUANTIZATION NOISE	yes	yes	no

Table 1: Expressions for determining the periodicity of the phase errors P and the periodicity of the samples at the output M expressed in terms of clock cycle units (T_c).

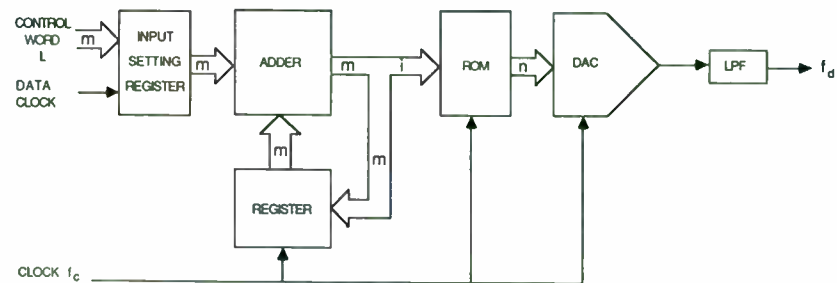


Figure 1: Basic block diagram of a DDS.

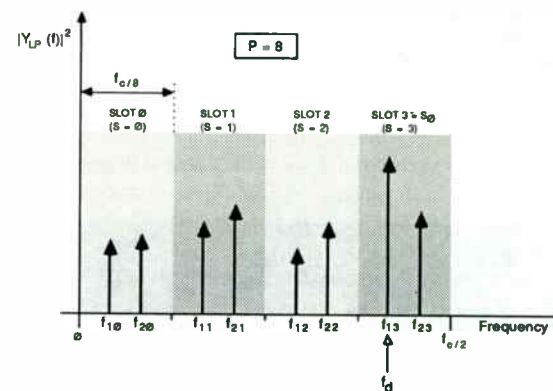


Figure 2: Frequency slot division and numbering for $P = 8$ and $s_0 = 3$.

SIGNAL-TO-NOISE RATIO

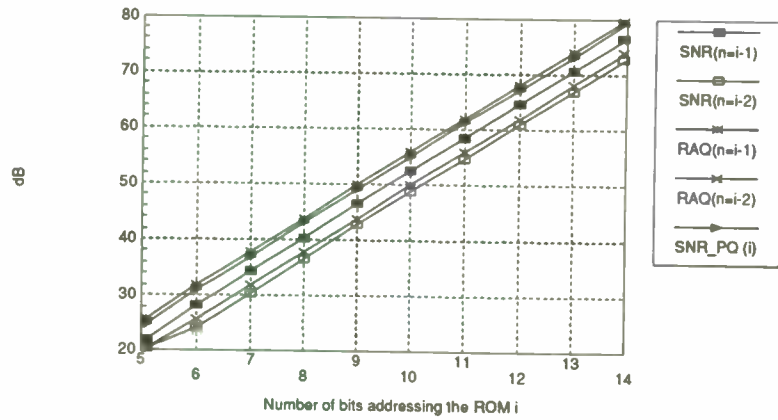


Figure 3: SNR as a function of i for different values of n .

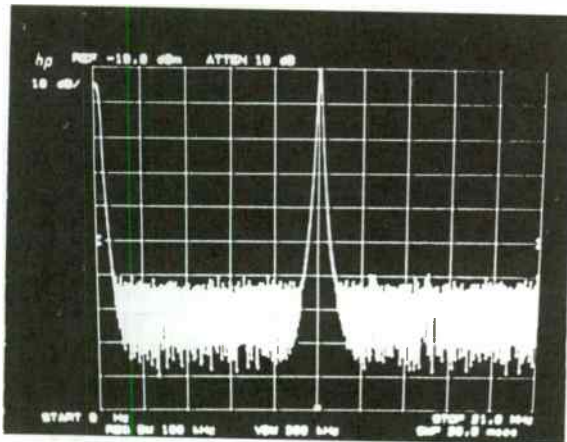


Figure 4: Generated frequency with very low level of spurious in the passband.

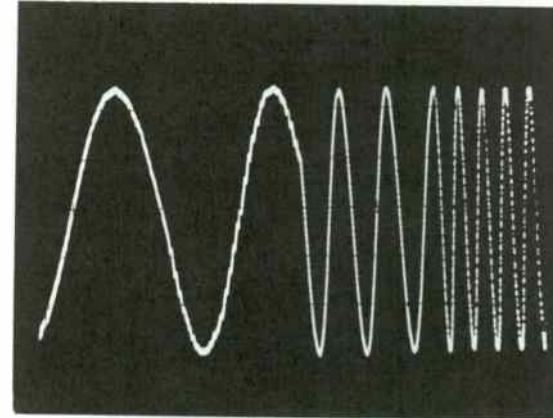


Figure 5: Photo showing the continuity of the phase.

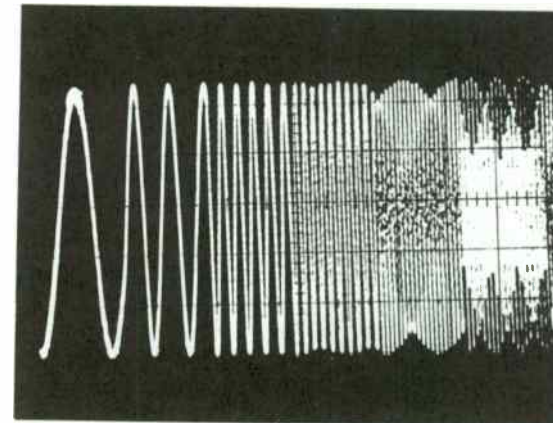


Figure 6: Output of the DDS in frequency hopping mode.

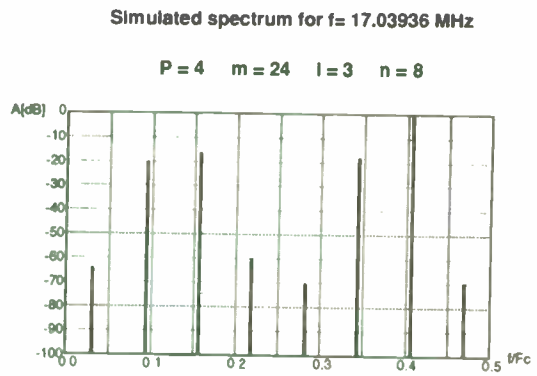


Figure 7: Simulated spectrum for $f_d = 17.039360$ MHz with $P = 4$.

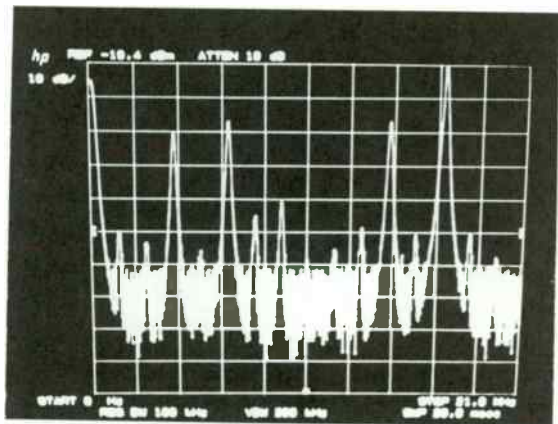


Figure 8: Measured spectrum for $f_d = 17.039360$ MHz with $P = 4$.

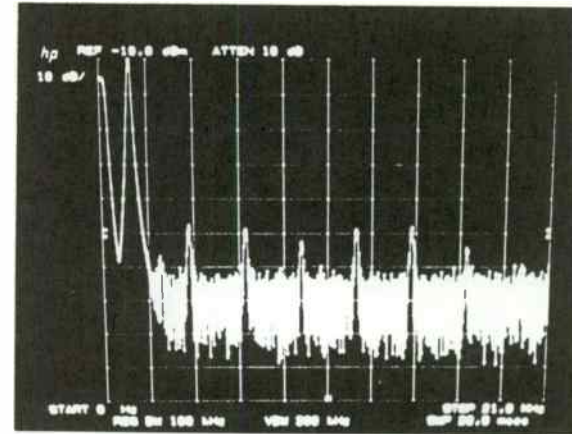


Figure 9: Measured spectrum for $f_d = 1.31072$ MHz.

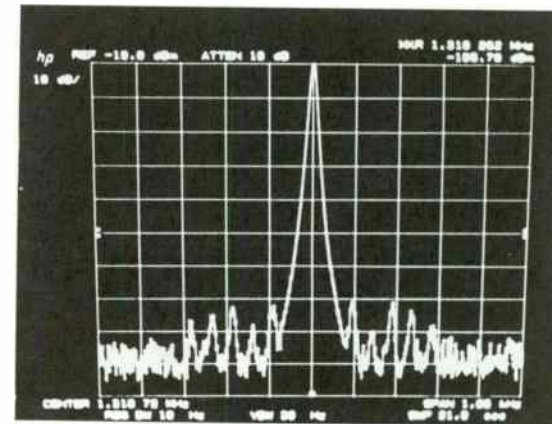


Figure 10: Expanded version of the previous figure showing close-to-carrier noise.

DIRECT-DIGITAL WAVEFORM GENERATION USING ADVANCED
MULTI-MODE DIGITAL MODULATION

Bar-Giora Goldberg, MSEE
Sciteq Electronics, Inc.
8401 Aero Drive
San Diego, CA 92123

Abstract

This paper defines methods by which a direct-digital synthesizer (DDS) can provide precise all-digital manipulation of every characteristic and modality of the output signal. It presents an architecture that integrates all these capabilities, and then identifies system categories that benefit from such all-mode waveform control.

Introduction

Compared to direct-analog (mix/filter) or phase-locked loop (PLL), the DDS has intrinsic advantages. In one sense, it is the only real "synthesizer" because others manipulate and control the output of oscillators that begin operating at arbitrary points in phase, while the DDS literally constructs the waveform by defining rigid relationships between time and signal amplitude. Because the DDS process is deterministic, with its output having a specific starting point and remaining under control of a purely numerical process, the signal can be managed in ways that are not otherwise possible. The DDS covers its operating range in fine steps, with good phase noise, and because it is a digital device with little inertia it can change aspects of its operating mode or output frequency very quickly. This paper addresses that exploitation of digital signal processing techniques in a DDS, and explains the result in theory and practice.

DDS Basics

Figure 1 shows the basic architecture of a traditional DDS, and the mechanism by which the output signal is constructed. Nyquist and Shannon agree that the desired output waveform must be sampled at a rate equal to twice the highest frequency present in it, so it is evident that bandwidth of the DDS depends only upon the speed of the logic, memory, and data conversion devices used in the design.

Density of the digital circuitry determines the accuracy to which the desired waveform is constructed, but that density also limits the speed at which the system can be operated. Bandwidth and spectral purity are therefore inversely related, and that relationship approximates $20 \cdot \log f$, or 6dB per octave. A DDS with 50MHz BW and -45dBc spurs is operationally equivalent to one with 25MHz BW and -51dBc spurs or another with 100MHz BW and -39dBc spurs. For an improvement in DDS performance to be real, it must depart from that $20 \cdot \log f$ relationship. That requires improvements in speed and circuit density.

In the accumulator and memory portions of the circuitry it is now trivial to achieve spurious suppression of 90dB. While that figure is academically interesting, of all the DDS functional components the principal antagonist to spectral purity appears later in the signal path, as the digital-to-analog converter (DAC). Quantization error in the DAC generates spurs in the output, and that factor alone swamps all other contributors to degradation of the desired signal. For that reason, it is not practical to evaluate a DDS unless measurements are made after the DAC; in this paper, all data relating to spectral purity will have been taken only at that point.

DDS Waveform Manipulation

Figure 2 shows a DDS with waveform control (modulation) ports added. The additional circuitry is not complex and imposes only modest penalties on speed and cost.

Frequency *control* becomes frequency *modulation* (FM) when the signal is digitized and then integrated into the digital signal generation process. The modulation signal is converted to a digital word using a conventional analog-to-digital converter (ADC), and the output of the ADC varies the frequency control word accordingly (**Figure 3**). In a DDS, digital FM performance is excellent and the FM can vary to DC.

Phase is controlled by interrupting the digital path between the accumulator and memory, and introducing a digitized signal to shift the accumulator's output, as shown in **Figure 4**. Note that the phase change occurs without any non-programmed waveform discontinuity (**Figure 5**). The performance of this phase-shifting capability, in a BPSK application, is shown in **Figure 6**. Because the DDS-1 provides excellent rise/fall time and nearly total control of the waveform, side lobes can be suppressed and spectral control optimized.

Many DDS products and techniques exploit the FM and ϕ M processes described above, but amplitude modulation (AM) is more difficult. AM is ordinarily achieved by placing a multiplier between the memory and the DAC (**Figure 7**). Regardless of the multiplier design (which might output 16 bits, for instance) the number of amplitude steps usable is one bit less than the amplitude quantization of

the DAC. With a 12-bit DAC that limitation is not significant because 11 bits of amplitude modulation is sufficient for virtually all applications.

It is evident that the inclusion of well-planned digital signal processing supports precise control over the waveform generated by the DDS.

Optimized DDS Design

The optimum multi-mode DDS begins with good spectral purity across sufficient bandwidth for the specific application. Because most DDS applications involve integration with either direct-analog or PLL circuitry, a few MHz is usually sufficient. Once the frequency plan is satisfied by a usable combination of bandwidth and spectral purity, waveform control can be addressed. Most DDS plus PLL and DDS plus direct-analog frequency plans require that the DDS operate at 10MHz, with good spurious suppression.

The optimum DDS will operate over at least 10MHz bandwidth with at worst -60dBc spurs, and will provide digital control of frequency, phase, and amplitude, plus a digital high-isolation ON/OFF switch to support pulse modulation.

Finally, such a DDS must be easy to integrate into the system, considering power, control, and footprint. Sciteq has incorporated those capabilities in a CMOS hybrid designated the DDS-1 (**Figure 8**), which has the characteristics shown in the following table:

DDS-1

Maximum clock.....	>25MHz
Maximum bandwidth.....	>11MHz
Step size.....	32 bits
Switching speed.....	<1µsec
Spurious.....	-65dBc (worst case)
Phase control.....	16 bits
Amplitude control.....	11 bits
Auto-FSK toggle.....	1-bit (user sets F_1 and ΔF)
Gating (ON/OFF).....	1 bit control, >100dB isolation
Size.....	1" x 1" (one square inch), 84-pin CLCC
Power.....	1.5W, ±5VDC

Whether used in baseband by itself, as a modulation source, or as a building block in the frequency plan of a microwave synthesizer, the DDS-1 is a highly optimized design. It is one of the very few direct-digital synthesizer architectures to provide such complete waveform control, and in fact may be the only one at this time. This range of capabilities should be available from any well-planned DDS, because the block diagram shown in Figure 8 can be executed by any competent design center and foundry.

Applications

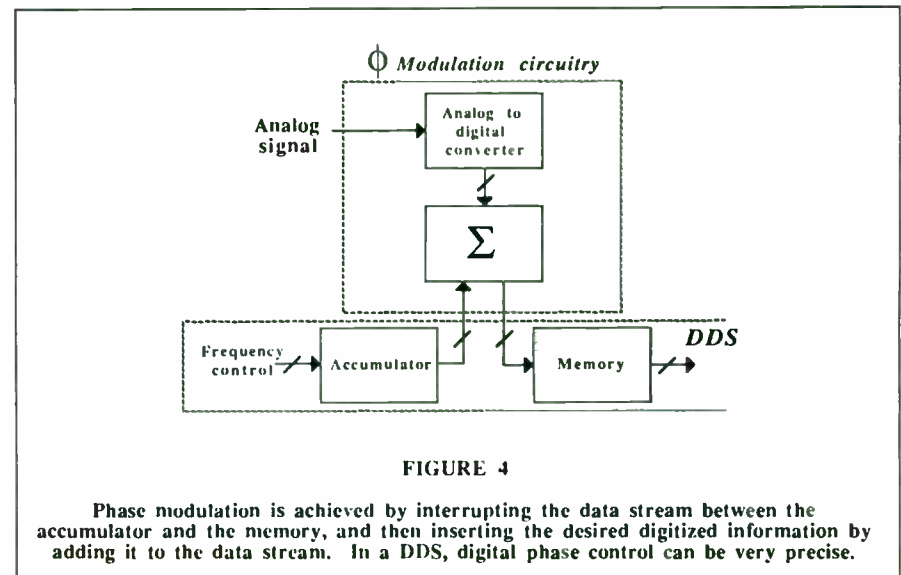
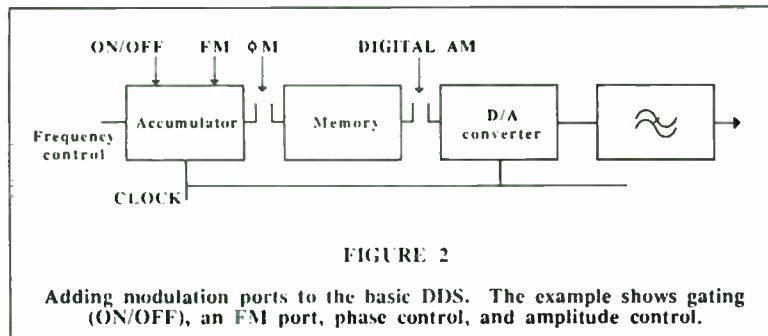
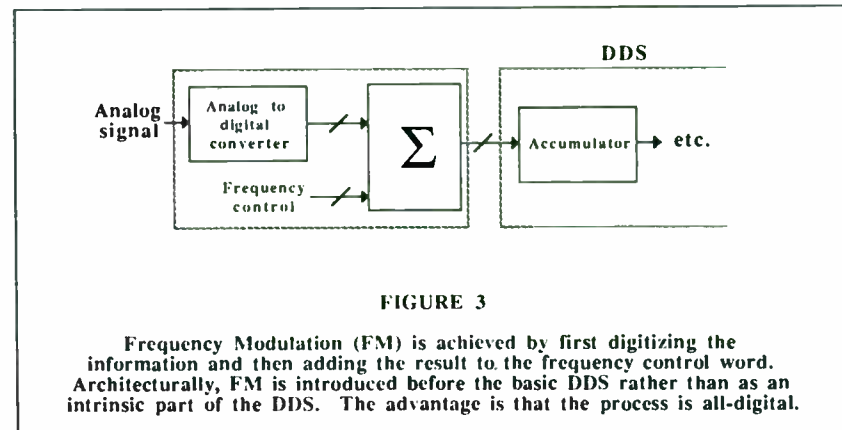
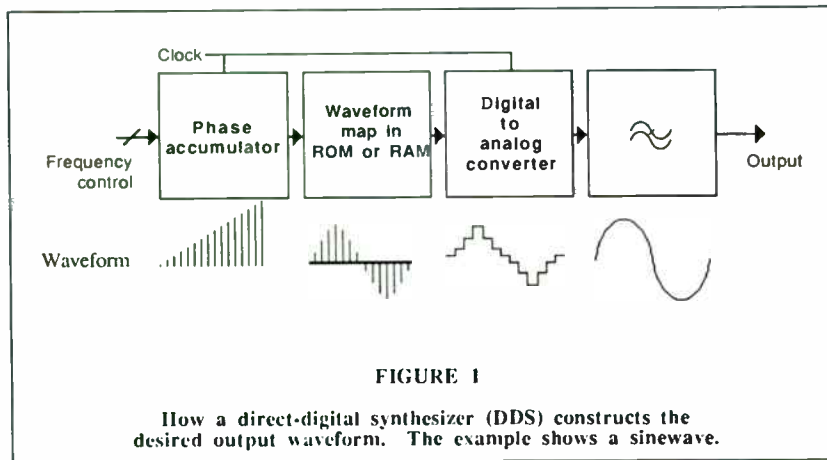
Any system that requires good spectral purity plus a variety of waveform manipulation capabilities will benefit from the complete solution provided by an optimized DDS.

In telecommunications, QAM with high-resolution phase and amplitude control support high-accuracy modulated QAM signals. In communications, the subsystem's digital AM and FM, plus digital SSB (with additional circuitry), support high-accuracy digital modulation, including very sophisticated modulation schemes. In simulation, the speed and versatility of the system's digital control permits an extensive menu of simulated waveforms, limited only by bandwidth and the software that controls the system. As an FSK or MSK modulator, the transitions are smooth and glitch-free, and the automatic function simplifies the system interface. In linear FM and magnetic resonance imaging, the ability to sweep while changing amplitude makes this approach a total solution.

In general, the ability of the direct-digital synthesizer to operate beyond sinewave generation can contribute significantly to the absolute performance of the system and reduce its relative complexity and cost.

Summary

The DDS is growing in importance as a design resource for the system architect. While the signal is in the digital domain, it is easy to manipulate using conventional digital signal processing techniques. In an optimized DDS, the result is complete control over all parameters of the waveform, with digital precision not attainable by analog means.



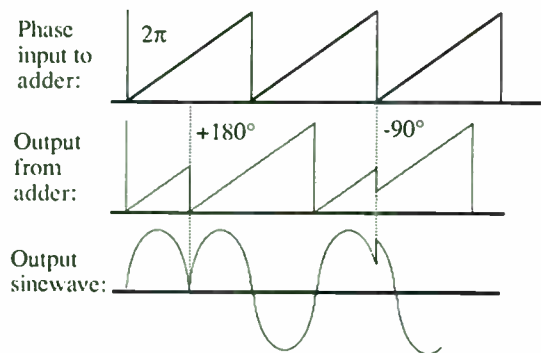


FIGURE 5

This shows what happens when a phase control command is added to the DDS data stream between the accumulator function and the waveform memory function.

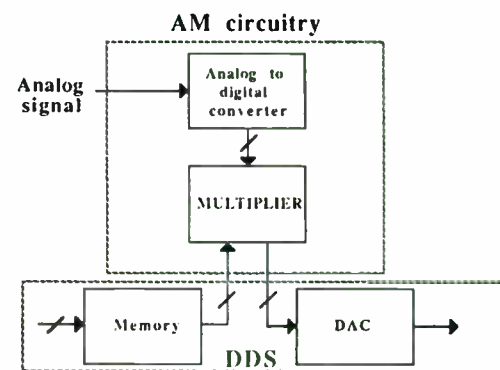
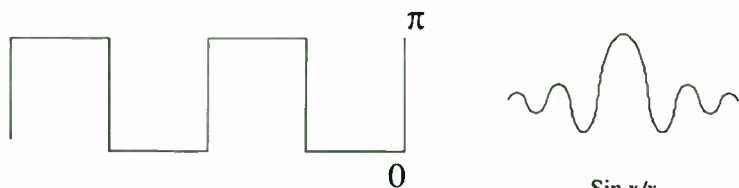


FIGURE 7

Amplitude of a DDS' output can be controlled by placing a multiplier between the waveform memory map and the data converter. If the second input to the multiplier is a digitized analog signal, then the result is digital amplitude modulation with extreme accuracy.

Conventional BPSK:



With DDS-1:



FIGURE 6

In BPSK and other modulation schemes, sidelobe suppression is improved by using a DDS with phase control.

DDS-1 WAVEFORMER™

Max clock >25MHz
Bandwidth >11MHz
Step size 32 bits
Spurious -65dBc
Switching speed <1μsec
Size one square inch
Power ~1.5W, ±5VDC

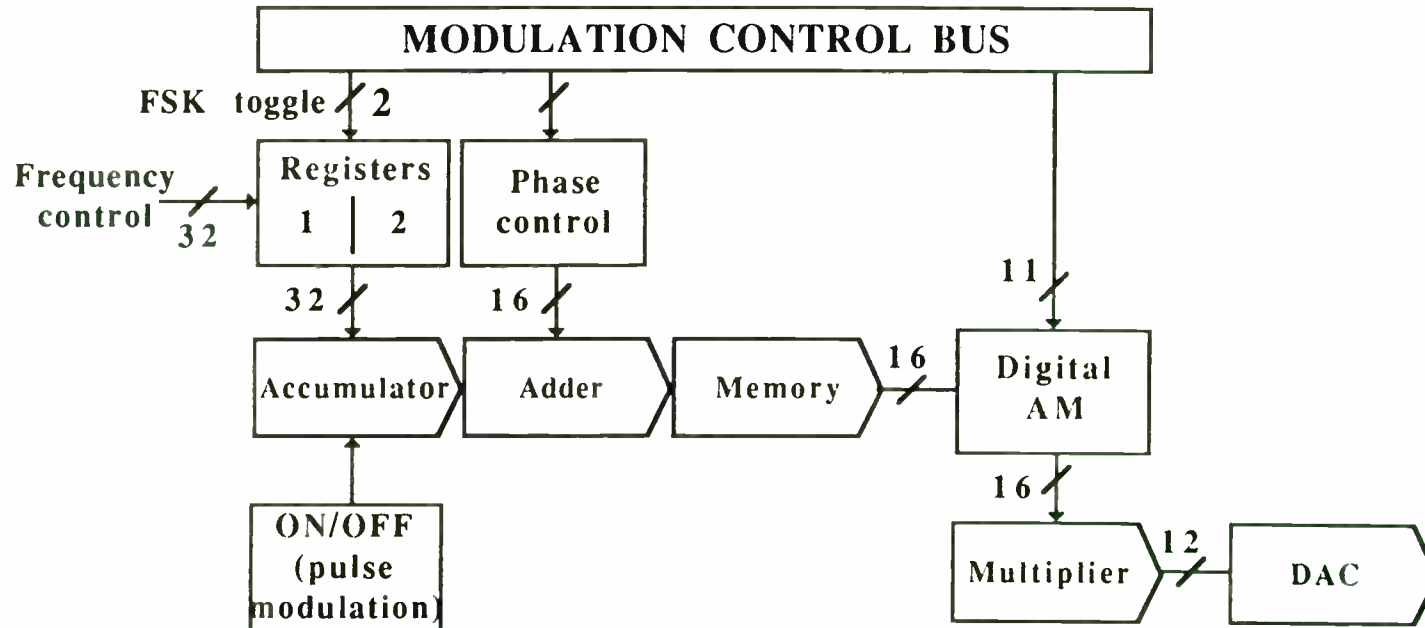


FIGURE 8

Sciteq's DDS-1 is one example of a highly optimized DDS with complete waveform control.



Optimum PLL Design for Low Phase Noise Performance

Stanley Goldman
Engineering Specialist
E-Systems Inc, Garland Division
P.O. Box 660023
M/S 4-43210
Garland, Texas 75266-0023

Introduction

Electronic warfare receivers, test instruments, and radar systems often require low phase noise performance from PLLs. Receivers need low phase noise PLLs to prevent large signals from degrading small signal detection levels. Test instruments need low phase noise PLLs to make measurements over a large dynamic range and to improve the accuracy of measurements. Radar systems need low phase noise PLLs to detect small signals from ground clutter or chaff. In designing a PLL, the general practice has been to select damping factor and loop bandwidth for switching time². This article shows that switching time design goals are different from low phase noise level design goals. In designing a PLL for switching time requirements, references recommend using a 0.7 damping factor for minimum settling time and a bandwidth greater than the inverse of the switching time. This article will determine the optimum damping factor and bandwidth goals for low phase noise PLL design.

PLL Phase Noise Equations

To design low phase noise PLLs requires equations that mathematically describe phase noise in PLLs. Making these equations a function of the damping factor and loop bandwidth design goals will ease the study of optimum phase noise design goals. From reference 1, Equation 1 computes phase noise at the output of the PLL with control systems variables:

$$L_{pll}(f_m) = L_{ref}(f_m) \left(\frac{G(f_m)}{1 + G(f_m)H(f_m)} \right)^2 + \frac{L_{vco}(f_m)}{(1 + G(f_m)H(f_m))^2} \quad (1)$$

where:

- f_m = Offset frequency from the carrier (Hz),
- $L(f_m)_{ref}$ = Single sideband phase noise ratio from the reference oscillator (rad/Hz),
- $L(f_m)_{vco}$ = Single sideband phase noise ratio from the voltage controlled oscillator (rad/Hz),
- $L(f_m)_{pll}$ = Single sideband phase noise ratio at the output of the PLL (rad/Hz),
- $G(f_m)$ = Forward transfer function,
- $H(f_m)$ = Feedback transfer function, and
- $G(f_m)H(f_m)$ = Open loop transfer function.

Converting Equation 1 to a function of damping factor and natural frequency will produce an equation of damping factor and loop bandwidth because Equation 2 relates loop bandwidth to natural frequency¹:

$$f_n = \frac{B_{pll}}{\sqrt{1 + 2\xi^2 + \sqrt{(1 + 2\xi^2)^2 + 1}}} \quad (2)$$

where:

- B_{pll} = Three dB bandwidth of the PLL (Hz),
- ξ = Damping factor ratio of the PLL, and
- f_n = Natural frequency of the PLL (Hz).

To convert Equation 1 to a function of damping factor and natural frequency requires an equation for the open loop transfer function and the forward transfer function in terms of damping factor and natural frequency. Equations for a type 2, second order PLL with an active integrator provide the starting point for the derivation and the result of the derivation is Equations 3 and 4. Equation 3 computes the open loop transfer function in terms of damping factor and natural frequency¹:

$$1 + G(f_m)H(f_m) = \sqrt{\left(1 - \left[\frac{f_n}{f_m}\right]^2\right)^2 + \left(\frac{2\xi f_n}{f_m}\right)^2} \quad (3)$$

Equation 4 computes the forward transfer function in terms of damping factor and natural frequency¹:

$$|G(f_m)| = n_{mf} \frac{f_n^2}{f_m^2} \sqrt{1 + \left(\frac{2\xi f_m}{f_n}\right)^2} \quad (4)$$

where:

- n_{mf} = Multiplication factor of PLL.

Combining Equations 1 to 4 mathematically describes the output phase noise of a PLL in terms of damping factor and PLL bandwidth. To complete the model of output phase noise in a PLL requires an equation for modeling the phase noise of the oscillators in the PLL. Equation 5 models phase noise for the oscillators in the PLL¹:

$$L(f_m) = a f_m^b \quad (5)$$

where:

$$a = \exp_{10}\left(\frac{L(f_a) - 10b \log(f_a)}{10}\right)$$

$$b \leq 0$$

$$b = \frac{L(f_a) - L(f_b)}{10[\log(f_a) - \log(f_b)]}$$

f_a = Start frequency of slope (Hz), and

f_b = Stop frequency of slope (Hz).

Equations 1 through 5 model the output phase noise of a PLL. Consequently, these equations allow damping factor effects and loop bandwidth effects on the output phase noise of a PLL to be studied.

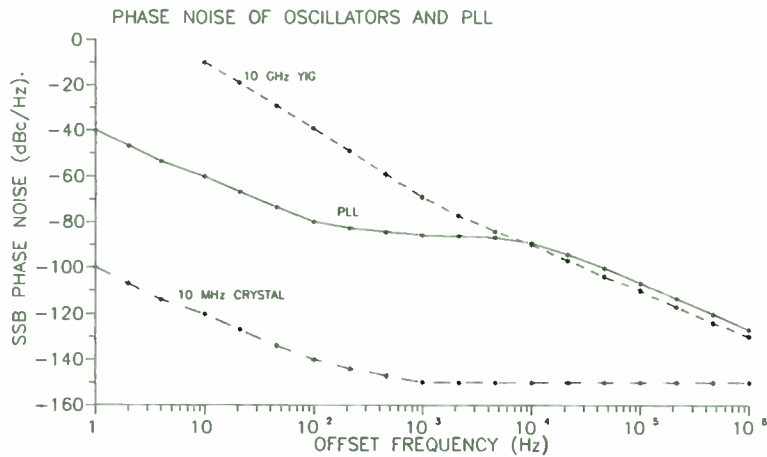


Figure 1. Example 10 GHz PLL

Damping Factor Effect

Studying an example PLL shows the effect of damping factor on phase noise. For the example, a 10 MHz crystal oscillator and 10 GHz YIG oscillator are combined to form a PLL with a multiplication factor of 1000 [3]. Figure 1 shows the desired optimum phase noise performance for the PLL combination of the 10 MHz crystal oscillator and the 10 GHz voltage controlled YIG oscillator. Varying the damping factor in Figure 2 shows the

peaking effect that damping factor has on phase noise. In Figure 2, a damping factor less than 1 adds a significant amount of phase noise. Consequently, a damping factor range of 1 to 1.5 minimizes the amount of additive phase noise. However, a damping factor of 1 to 1.5 degrades optimum switching time to a slower over damped response. Consequently, one has to choose between optimum phase noise design and optimum switching time design. Now setting the damping factor to within the range of optimum damping factors for phase noise performance allows us to study the dependence of phase noise performance with the variation of PLL bandwidth.

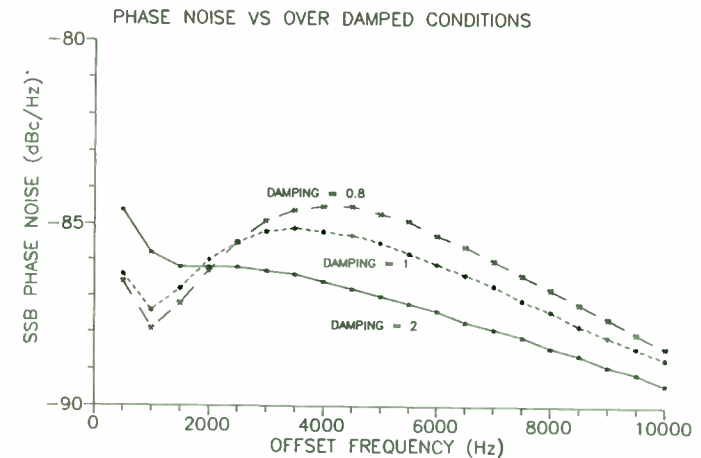


Figure 2. Damping Factor vs Phase Noise

PLL Bandwidth Effect

Again, the example PLL can be used to study the effects of bandwidth on the output phase noise of a PLL. Figures 3 and 4 show the effect of varying the bandwidth on the output phase noise of the PLL. The bandwidths below optimum in Figure 3 follows the far from the carrier phase noise of the VCO. However, these bandwidths add phase noise to the multiplied close to the carrier phase noise of the reference oscillator. The bandwidths above optimum in Figure 4 follow the multiplied close to the carrier phase noise of the reference oscillator. However, these bandwidths add phase noise to the far from the carrier phase noise by shifting the phase noise curve of the VCO. From these figures, any switching time performance requirement faster than the inverse of the optimum loop bandwidth will have to be sacrificed in order to obtain optimum phase noise performance.

Up until now, the general practice has been to select the loop bandwidth to be the phase noise response intersection of the multiplied reference oscillator and the VCO (between 5 and 20 kHz in the example). However, Figures 3 and 4 show a different

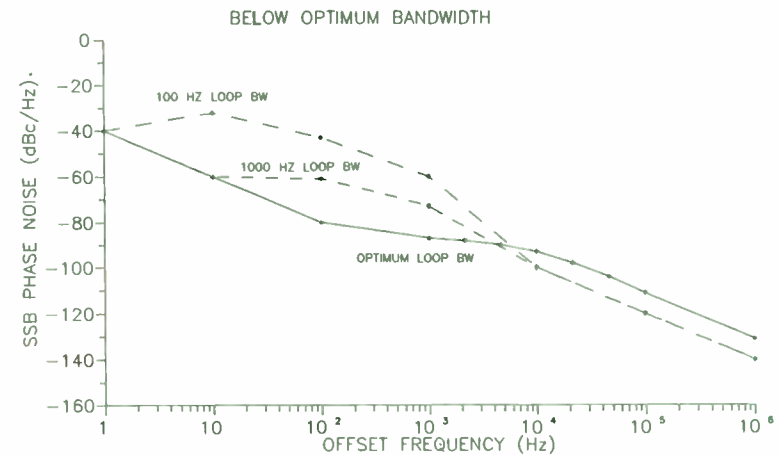


Figure 3. Below Optimum Bandwidth

critereon to achieve optimum loop bandwidth. At optimum bandwidth, the PLL has output phase noise that follows the multiplied close to the carrier phase noise of the reference oscillator. In addition, the optimum loop bandwidth adds a phase noise contribution from the multiplied phase noise of the reference oscillator equal to the far from the carrier phase noise of the VCO. This last bit of information will be used to compute the optimum bandwidth for the PLL.

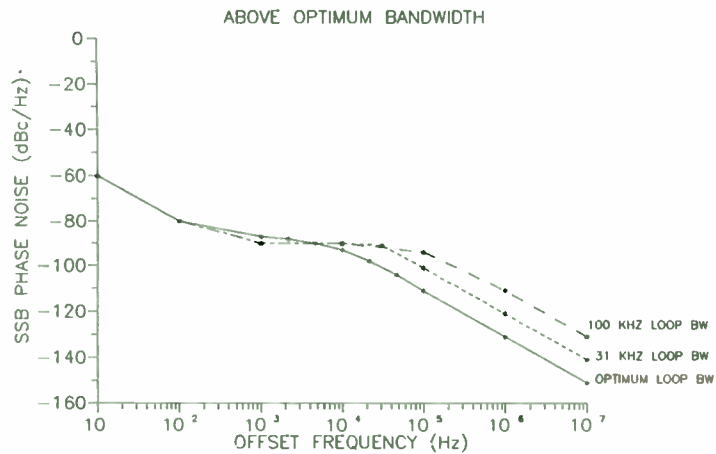


Figure 4. Above Optimum Bandwidth

Equations to Compute PLL Bandwidth

From the previous section, the equal phase noise contribution characteristic for the optimum bandwidth provides one of the ingredients in solving for the optimum phase noise bandwidth. Now, making assumptions about the phase noise of the VCO and reference oscillator provides the final ingredients for calculating the optimum bandwidth. A 20 dB per decade roll off for the phase noise of the VCO and a constant phase noise for the multiplied reference oscillator are assumed to compute the opti-

mum bandwidth of the PLL. Substituting a 20 dB per decade phase noise roll off into Equation 5 produces Equation 6 for modeling the phase noise of the VCO:

$$L(f_m)_{vco} = \alpha_{vco} f_m^{-2} \quad (6)$$

where:

$L(f_m)_{vco}$ = Phase noise response of VCO (rad/Hz) and

α_{vco} = VCO power slope.

A constant phase noise in Equation 5 produces Equation 7 for modeling the phase noise of the reference oscillator:

$$L(f_m)_{ref} = constant \quad (7)$$

Returning to the results of the study on bandwidth, optimum bandwidth produces equal phase noise contributions from the reference oscillator and the VCO for phase noise far from the bandwidth of the PLL. Consequently, Equation 8 mathematically describes this optimum PLL bandwidth condition:

$$L(f_m)_{pll} = L(f_m)_{vco} L(f_m)_{add} \quad \text{for } f_m \gg B_{pll} \quad (8)$$

where:

$L(f_m)_{pll}$ = Output phase noise level of PLL (rad/Hz) and

$L(f_m)_{add}$ = Amount of phase noise added to VCO phase noise far from the bandwidth of the PLL.

Studying the output phase noise of the PLL for frequencies greater than the bandwidth of PLL allows several mathematical simplifications to be made. Equation 1 can be simplified for high frequencies because the numerator of Equation 1 reduces to 1:

$$\frac{1}{1 + G(f_m)H(f_m)} = 1 \quad (9)$$

Then, substituting Equations 8 and 9 into Equation 1 reduces Equation 1 to Equation 10:

$$L(f_m)_{vco} L(f_m)_{add} = L(f_m)_{ref} G^2(f_m) + L(f_m)_{vco} \quad (10)$$

Equation 4 can also be simplified for frequencies much greater than the bandwidth of the PLL. For high frequencies, Equation 4 reduces to Equation 11:

$$G(f_m) = n_{mf} \frac{f_n^2}{f_m^2} \sqrt{1 + \left(\frac{2\xi f_m}{f_n}\right)^2} \sim \frac{n_{mf} 2\xi f_n}{f_m} \quad (11)$$

Now, a few more algebraic steps with Equations 6, 10, and 11 will produce an equation for optimum bandwidth. Substituting Equation 11 into Equation 10 produces Equation 12:

$$L(f_m)_{vco} (L(f_m)_{add} - 1) = L(f_m)_{ref} \left(\frac{n_{mf} 2\xi f_n}{f_m}\right)^2 \quad (12)$$

Substituting Equation 6 into Equation 12 produces Equation 13:

$$\alpha_{vco} f_m^{-2} (L(f_m)_{add} - 1) = L(f_m)_{ref} \left(\frac{n_{mf} 2\xi f_n}{f_m}\right)^2 \quad (13)$$

Cancelling the frequency variable and solving for the natural frequency produces Equation 14:

$$f_n = \sqrt{\frac{\alpha_{vco} (L(f_m)_{add} - 1)}{L(f_m)_{ref} (n_{mf} 2\xi)^2}} \quad (14)$$

Equation 14 computes the optimum natural frequency, which has a relatively simple conversion to loop bandwidth.

Now however, the vco slope constant and additive phase noise constant must be determined to compute the optimum natural frequency in Equation 14. From Equations 5 and 6, Equation 15 computes the VCO constant in Equation 14 from one data point on the phase noise curve for the VCO:

$$A_{vco} = 10^{\left\{ \frac{L(f_a)_{vco} - 10(-2)\log(f_a)}{10} \right\}} \quad (15)$$

where:

$L(f_a)_{vco}$ = Phase noise at f_a (dBc/Hz) and
 f_a = Frequency of data point on VCO phase noise curve (Hz).

Next, Equation 16 computes the amount of additive phase noise in Equation 14 by assuming equal reference oscillator phase noise and VCO phase noise:

$$L(f_m)_{add} = \frac{1}{10^{-3/20}} = 1.4142 \quad \text{for } 3 \text{ dB} \quad (16)$$

The 3 dB amount of additive phase noise provides a good compromise between close to the carrier phase noise performance and far from the carrier performance. However, the amount of additive phase noise can be adjusted to lower values to improve

far from the carrier phase noise at the expense of higher close to the carrier phase noise. Conversely, the amount of additive phase noise can be adjusted to higher values to improve close to the carrier phase noise at the expense of higher far from the carrier phase noise.

Now all the equations are present to solve for the optimum loop bandwidth. First, Equations 14 through 16 solve for the optimum natural frequency. Then, Equation 2 converts optimum natural frequency to optimum 3 dB PLL bandwidth. These equations are new and provide a more accurate solution than the general practice of the past. For instance, Equations 2 and 14 through 16 compute a 10000 Hz 3 dB bandwidth and a 8291 Hz crossover frequency for the example PLL with a 1.5 damping factor. Computing this optimum bandwidth is more accurate than graphically estimating between 5 and 20 kHz, which has been the practice in the past for determining the loop bandwidth for optimum phase noise performance.

Summary

To summarize, low phase noise damping factor and loop bandwidth design goals have been shown to be different than switching time design goals. For low phase noise design goals, a damping factor

of 1 to 1.5 has been graphically shown to minimize additive phase noise in a PLL. For loop bandwidth, equations have been derived that compute the optimum loop bandwidth. Now, engineers can compute the optimum bandwidth instead of graphically estimating at the loop bandwidth.

Bibliography

- 1) Stan Goldman, Phase Noise Analysis in Radar Systems, John Wiley, New York, 1989.
- 2) Vadim Mannasewitsch, Frequency Synthesizers Theory and Design, John Wiley, New York, 1980.

DESIGN AND DEVELOPMENT OF AN RF DATA ACQUISITION SYSTEM

BY

Thomas H. Jones
Dynetics, Inc.
P. O. Box Drawer B
Huntsville, AL 35814-5050

Madjid A. Belkerdid
University of Central Florida
Electrical Engineering Dept.
Orlando, FL 32816

ABSTRACT

Using an automatic network analyzer to test devices allows the user to view device frequency responses, but does not allow the user the ability of acquiring accurate data and using the data with IBM formatted software. This paper discusses many other limitations to using an automatic network analyzer to obtain accurate measurements and the development of an RF Data Acquisition System that greatly enhances the ability of a Hewlett-Packard 8753c automatic network analyzer. The network analyzer is interfaced with an IBM AT computer via an IEEE 488 card from National Instruments. Data from the network analyzer is acquired in a user friendly environment that allows the user to obtain over 20,000 points of complex data in an IBM format (IEEE floating point or ASCII). It allows the user to rapidly view acquired data in a desired format, and to view the impulse response of a device and calibration errors in the test fixture. The development of the system is discussed, including special features of the system and use with other software. Actual measured data of a bandpass SAW device and verification of the calibration is presented.

I. INTRODUCTION

The ability of quickly obtaining accurate measurements of the scattering parameters (S-parameters) using an automatic network analyzer and an S-parameter test set is a viable tool that should be available to the engineer. There are, however, some limitations to using an automatic network analyzer to obtain accurate measurements.

One limitation is that it is difficult to obtain a permanent record of the measurements which could be used in with IBM software. Although a Hewlett-Packard computer could be purchased and utilized for a data acquisition system, it would be quite difficult to convert the data to an IBM format for use with other software. The only permanent record that can be obtained when using the network analyzer alone is a plot obtained using the HP plotter [4].

A second limitation is that the network analyzer is limited to measuring only 1601 points in a frequency sweep [4]. It is impossible to perform a wideband frequency sweep without losing resolution.

Another problem is that, although it is possible to perform a twelve term error correction calibration, it is impossible to graphically view the calibration coefficients [4]. Without the ability to view the calibration coefficients, the user cannot determine the causes and effects of inherent measurement errors in the test fixture. Moreover, in order to obtain accurate data, the network analyzer must be recalibrated every time the machine is used. Ideally, calibrating the 8753 before each use would be desirable. However, if the same frequency span, number of points, sweep time, and resolution bandwidth are desired; recalibration is a redundant drudgery.

Also, the network analyzer does not have the ability to allow the user to view the impulse response of the acquired data unless a special option is purchased for the network analyzer from Hewlett-Packard [4].

The purpose of this paper is to solve all of the above mentioned problems by developing a completely computer controlled Data Acquisition System that would interface an HP 8753c automatic network analyzer and an HP 85046A S-parameter test set with an IBM AT computer via an IEEE 488 interface card from National Instruments.

A. Basic Approach

The following discussion explains the priorities that dominated the design of the Data Acquisition System. The first priority was that the system should be completely computer controlled. It should set up the Network analyzer to take the desired measurements with a specified frequency span, number of points, number of averaging runs, resolution bandwidth, sweep time, and input power. It should allow the user the freedom to control the network analyzer manually if desired. The system should prompt the user to connect the proper terminations on each port of the network analyzer for measurements required in a full two port calibration. Moreover, all data measurements should be stored either on a hard drive or floppy drive of an IBM personal computer in either binary or ASCII format.

The second priority was that the system be able to measure more than 1601 points. The ability to measure a large number of points gives the user the opportunity to measure a device over a wide band of frequencies while retaining good resolution.

A third priority was that the system be able to perform calibration measurements and calculate calibration coefficients that can be stored on the hard drive of the IBM computer. This gives the user the ability to use the same calibration data in the future for data measurements that require the

same frequency span, number of points, sweep time, and resolution bandwidth. Saving the calibration data also gives the user the ability to graphically view the calibration coefficients to verify the integrity of the test fixture.

A fourth priority was that the system be able to easily create user specified files containing the measured scattering parameters, the calibrated scattering parameters, and the calibration coefficients. The system should also have the versatility to be able to store the data in either polar or rectangular format and to create ASCII files for use with other software.

A fifth priority was that the system be able to perform a Fast Fourier Transform on any of the acquired data [6].

The system should also have the ability to graph the acquired data on the computer screen to allow the user to verify the data.

B. General Solution To the Data Acquisition System

In order to satisfy the priorities stated in the previous section, the heart of the data acquisition system was a program that interfaced the IBM AT computer with the HP 8753C Network Analyzer and an HP 85046A S-parameter test set by using an IEEE 488 GPIB card from National Instruments and the HP-IB bus. A block diagram of the system is shown in Figure 1.

In designing the data acquisition system, the most efficient method for writing the program was to use Microsoft Quickbasic for the main program and all the subroutines that involved communicating with the network analyzer. The main reason for this was that the IEEE 488 GPIB card from National Instruments was purchased with software that included assembly language subroutines that were already designed to interface with Quickbasic [5]. Moreover, it made the task of programming the menus very easy by using Quickbasic's "SELECT" statement [3].

In order to solve the problem of performing all of the complex math required for calibration, Microsoft Fortran was used [8]. Fortran subroutines were also used to perform all of the reading and writing to the data files, and perform data format conversions [8]. In order to perform the inverse Fast Fourier transform, a mixed radix FFT algorithm was used.

After writing the two separate sets of software, the Basic and Fortran modules of the program were compiled separately and then linked with the object files from the GPIB software using the Microsoft link operation [8]. The following three sections of this paper describe in detail all of the important functions of the program. The general order of the discussion is the same as the main functions listed in the main menu of the program. The actual main menu of the program is shown in Figure 2.

II. CONTROLLING THE HP8753c NETWORK ANALYZER

A. Items 1 & 2 of the Main Menu

The first two items in the main menu of the program enable the user to setup the network analyzer with the proper network analyzer measurement parameters and allow the user the option to directly interact with the network analyzer from the front panel.

Item 1 of the main menu (Reset 8753c) allows the user to use the Network Analyzer front panel controls by pressing the 'local' button on the front panel [4]. Then, when the user is ready to return to operating the network analyzer with the Data Acquisition System, this option should be selected.

The second item in the main menu (Network analyzer Parameters Menu) controls setting up the network analyzer with the desired parameters and also sets up the desired data directory and filenames that will be used to store the acquired data. When item number 2 of the main menu is selected the "Network Analyzer Parameters Menu" is activated. This menu is shown in Figure 3.

B. Setting the Network Analyzer Measuring Parameters

The Network Analyzer Parameters menu (Figure 3) allows the user to set up the desired measuring parameters and to save the desired measurement parameters in a specified data directory. All corresponding data files will be stored in this same data directory. The Data Acquisition System creates a user friendly environment by giving the user the ability to easily create new directories for new sets of measurement data and provides for altering filenames of the data. Moreover, the system keeps track of all the measurement parameters for a given directory. The Data Acquisition System also keeps track of all of the data that has been taken, and only the data that has been stored appears on any of the menus.

C. Other Features built into the Network Analyzer Menu

Although the previous section describes the user interaction with the Network Analyzer Parameter menu, there are two important features built into the subroutine that controls this menu that should be discussed.

The first feature that has been added by the data acquisition system is that the program was designed to handle up to 20,013 data points whereas the network analyzer can only measure a maximum of 1601. The Data Acquisition System accomplishes this feat by breaking up the desired frequency span into smaller frequency spans that can be measured in 1601 point sweeps. The program then compiles the various chunks of data into one data file that represents the entire frequency span. In this manner, a file management system allows the only limitation to the number of points that can be measured to be the available memory of the hard disk drive on the computer. A BASIC subroutine controls the network analyzer menu and controls the number of points to be

measured with two variables 'npt' and 'n'. The variable 'npt' represents the number of points that the network analyzer will take, and the variable 'n' represents the number of sweeps that the network analyzer will have to perform.

Throughout the program, whenever any operation is performed on any data, it is performed in increments of 1601 points (if the number of points is greater than 1601). This is done merely for memory considerations. For example, in order to perform a twelve term error correction on the four measured scattering parameters of 1601 points using single precision calculations, it requires 256 kilobytes of memory.

Another feature is the creation of a file containing the frequencies that are measured. The program automatically creates a file listing of the frequencies measured and saves it on disk with the file name being a concatenation of the calibration filename and 'FREQ'.

III. ACQUIRING AND CALIBRATING DATA

Items 3-5 of the main menu allow the user to perform a calibration run, a measurement run, and to calibrate the data. The Data Acquisition System prompts the user for all of the proper terminations and automatically creates binary files containing the measured data. At the conclusion of a measurement run, the measured data will be stored in a single file in a two dimensional array format in rectangular form. The four S-parameters are the columns and the different frequency measurements are the rows. When a calibration run is performed, a similar file is produced in an array format with the 12 error coefficients as the columns. Then, when these calibration and measurement runs have been completed, the user can calibrate the data by selecting the proper option to create the file containing the calibrated data. It should be noted that all of the above functions are performed in increments of 1601 points. If the number of points is greater than 1601

points, however, the data acquisition system will still retain a single file containing all of the necessary frequency sweep measurements. For a complete discussion on the development of calibration procedure, see references [1],[2], & [4].

IV. DATA FORMAT AND SPECIAL FUNCTIONS

The main purpose of this section is to discuss items 6 through 12 of the main menu which allow the user to view the data and to store the data in the desired format. It should be noted that all menus only display the data that has been taken, and they always indicate whether the data is presently stored in polar or rectangular format.

The purpose of Item 6 (Convert Data Polar/Rect. Format Menu) is to allow the user to change the format of any of the data that is desired. All files are originally stored in rectangular format for calculational speed, but this option will convert any of the present files to polar format.

The purpose of Item 7 (Print menu) is to allow the user to print out any of the acquired data or the network analyzer parameters. The menu allow the user to print the data either to the screen or to the printer. The data is printed in the present format. If a change in format is desired, the user must convert the data using item 6, the data format menu.

The purpose of Item 8 (Graph menu) is to allow the user to graphically view the data. The data will be graphed in its present data format. However, if the user specifies that the data be graphed in log magnitude format, then the program will automatically convert the data for graphing purposes. The data is not stored on the disk in log magnitude format. Since the program has the ability to measure a great number of points and the resolution of Quickbasic graphics only allows for 640 pixels to be graphed, the program automatically sorts the data and only plots the necessary number of points for graphing [3]. Moreover, it should be noted that the graphs in this program

are to allow the user a quick view of the data. In order to obtain more accurate plots of the acquired data, other software packages should be utilized. Examples of use with other software will be discussed in the section entitled "Test Examples and Use With Other Software."

The purpose of Item 9 (ASCII menu) is to allow the user to create ASCII files for use with other software. Unless created by this menu, all of the data files that the system uses are binary files that do not include the measured frequencies. However, this option of the program allows the user to create ASCII files that contain frequency information and the desired data for use with other software.

The purpose of Item 10 (Impulse Response menu) is to allow the user to calculate the impulse response of the acquired data using a mixed radix FFT. Since the network analyzer only has a frequency span from 300 KHz to 3 GHz, the program allows the user to pad the frequency response with zeros from DC to the lower end of the measured frequency spectrum. The FFT algorithm that is used is a mixed radix FFT and will only accept a number of points that have factors of prime numbers less than 23. Since the network analyzer only performs frequency sweeps in increments that are prime numbers (Ex. 201,401,1601), the program corrects for the proper number of points by adjusting the number of points that will be sent to the FFT subroutine or by padding the frequency response with zeros.

The purpose of Items 11 and 12 are to allow the user the freedom to view the current directory files and to perform DOS operations without exiting the program. Item 11 uses the Quickbasic function to display current directory files [8]. Item 12 uses the Quickbasic DOS shell function [8].

V. TEST EXAMPLES AND VERIFICATION OF CALIBRATION

In order to verify the accuracy of the data acquisition system, there were several measurements taken using data acquired with the Data Acquisition System and data measured directly from

the front panel of the network analyzer. Figures 4-12 demonstrate the system's ability to accurately graph acquired data. Tables 1-4 contain examples of the data taken for verification of the calibration. All data was taken using a bandpass SAW device.

A. S11 and S12 Measured Using the Data Acquisition System

Figures 4-8 represent data acquired and plotted using the plot routines built into the data acquisition system and plots taken by importing the data into Quatro Pro. Figure 9 is the impulse response of the system. Both real and imaginary components are present in the time response because the inverse FFT is performed using only positive frequencies. Figures 10-12 demonstrate the ability to perform wideband sweeps and to use the data in conjunction with other software.

B. Verification of the Calibration Using Numeric Results

In order to verify the accuracy of the calibration, data was compared using the network analyzer alone and the calibration of the Data Acquisition System.

The data shown in Tables 1-4 displays the scattering parameters S11 and S12 taken from a bandpass SAW device. The network analyzer measurement parameters are shown below:

Center Frequency	60 MHz
Frequency Span	40 MHz
Number of Points	201
Resolution Bandwidth	10 Hz
Input Power	+10 dB
Averaging runs	1

The purpose of Tables 1-4 is not to provide a complete analysis of the accuracy of the network analyzer calibration technique, but to demonstrate that the Data Acquisition System calibration equations in the program are correct and that the Data Acquisition System is capable of providing

very accurate results of measured data. By increasing the sweep time, decreasing the resolution bandwidth, and performing averaging runs, the percent error shown in the tables could have been greatly improved. The equations used in the calibration of the Data Acquisition System are the same equations that are used by the network analyzer to perform a front panel calibration [1] [4]. There are two types of residual errors that are not accounted for in the calibration equations. Random residual errors are due to trace noise, noise floor, and connector repeatability [4]. There are also residual drift errors that are due to frequency drift and instrumentation drift. Other residual systematic errors that remain after calibration can be due to imperfections in the calibration standards, the connector interface, the test fixture, and the interconnecting cables [12]. The low percent errors of the measurements and the fact that the calibration equations are the same as the equations used by the network analyzer is a testament that the calibration of the Data Acquisition System is functioning properly [1].

VI. MODIFICATIONS FOR USE WITH OTHER NETWORK ANALYZERS

Although this data acquisition system was specifically developed for the Hewlett-Packard 8753c network analyzer, it would be relatively easy to modify the program to be used with other network analyzers.

The main limitation that must be considered to convert the data acquisition program to work with other network analyzers is the ability of the network analyzer to be controlled by the HP-IB bus. Moreover, if the network analyzer does not support IEEE floating point format data transfers then the data transfers must be performed in ASCII which will greatly slow down the data transfers.

All of the subroutines that communicate with the network analyzer must be converted to the proper analyzer commands for a given network analyzer. The program must also be modified to accept different network analyzer measurement parameters depending on the network analyzer requirements.

VII. CONCLUSIONS

The Data Acquisition System allows the user to retain a permanent record of data. Since all of the data is stored in either binary or ASCII files, the acquired data can easily be used in conjunction with other software. The calibration coefficients can be used at a later date as long as none of the network analyzer parameters are changed between measurements. The following files are stored for future use:

1. A file containing the network analyzer parameters. (Note: this file is an ASCII file that can be easily altered.)
2. A frequency file containing the measured frequency points.
3. A file containing the measured data.
4. Files of the calibrated data and the calibration coefficients. (Note: these files only exist if the data was calibrated.)
5. Optional files such as:
 - a. Impulse response files.
 - b. ASCII files for use with other software.

The data acquisition system creates a user friendly environment by placing all of the data files in given directory and completely controlling the network analyzer via the HP-IB bus. All of the data acquisition system functions are menu driven and prompt the user for necessary inputs.

The data acquisition system is capable of performing wideband frequency sweeps without losing resolution by enabling the user to measure a large number of points.

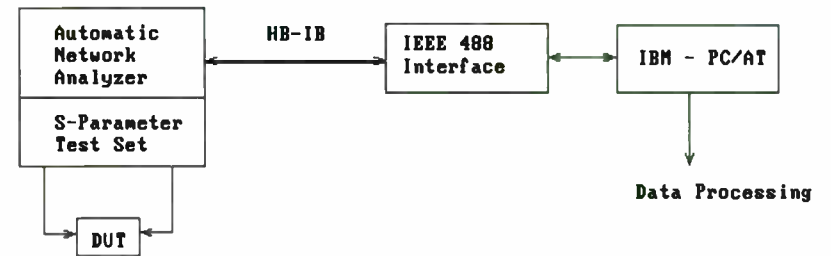
The data acquisition system is also capable of calculating and viewing the impulse response of a device.

In summary, the data acquisition system is a useful engineering tool. It allows the user to obtain quick, accurate results that can be permanently stored or used with other software such as Quatro Pro. Using the Data Acquisition System is much easier and faster than using the network analyzer alone because the menus are easy to follow the binary data transfers are very fast. The limiting factor on time when using the Data Acquisition System is still the settling time of the Network Analyzer. With these advantages the system solves all of the problems mentioned in the abstract and greatly enhances the usefulness of an automatic network analyzer.

VIII. TABLES AND FIGURES

A. Figures

RF Data Acquisition System



Network Analyzer - HP 8753C
 S-Parameter Test Set - HP 85046A
 IEEE 488 Interface - National Instruments
 IBM PC\AT (EGA required)

Figure 1. System Block Diagram. This figure represents the general solution to the Data Acquisition System.

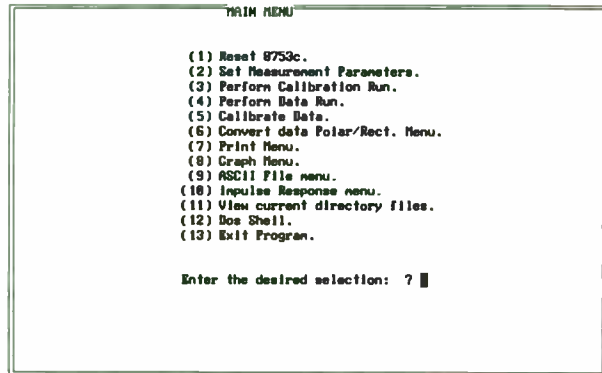


Figure 2. Main menu of the Data Acquisition System.

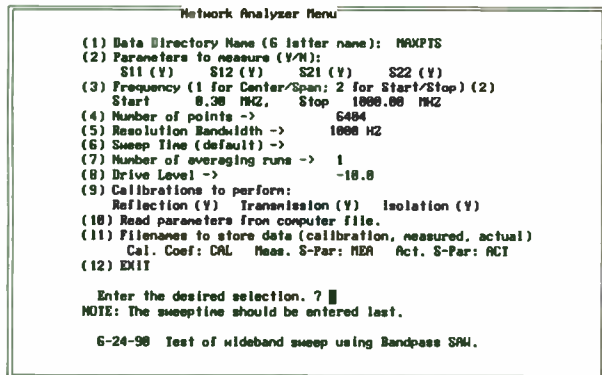


Figure 3. The Network Analyzer Parameters Menu.

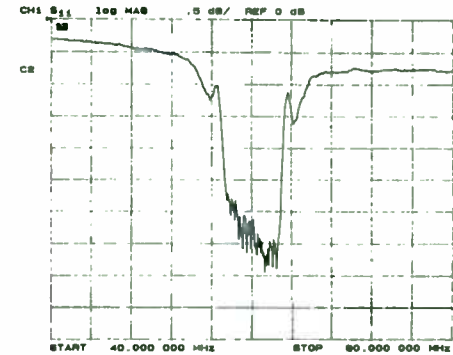


Figure 4. Calibrated S11 data acquired using Network Analyzer and HP plotter.

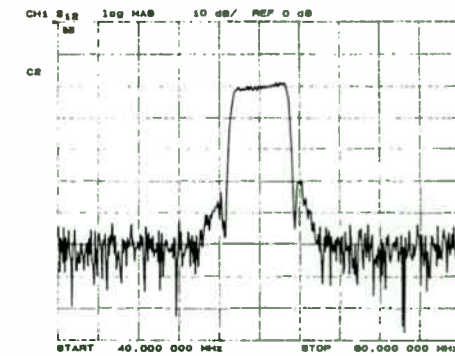


Figure 5. Calibrated S12 data acquired using Network Analyzer and HP plotter.

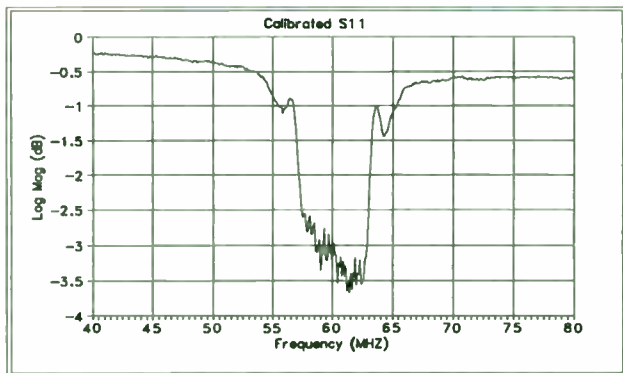


Figure 6. Calibrated S11 data acquired using the data acquisition system. Note: This file was converted into an ASCII file and subsequently into QUATRO PRO for graphing.

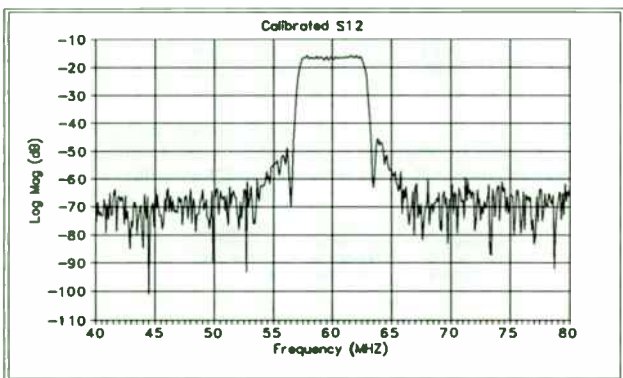


Figure 7. Calibrated S12 data acquired using the data acquisition system. Note: This file was converted into an ASCII file and subsequently into QUATRO PRO for graphing.

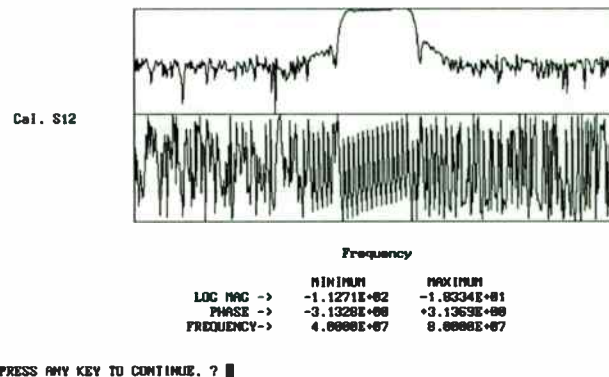


Figure 8. This figure merely displays the results that are obtained directly from Data Acquisition System. This is a direct copy of the computer screen that would be viewed by the user.

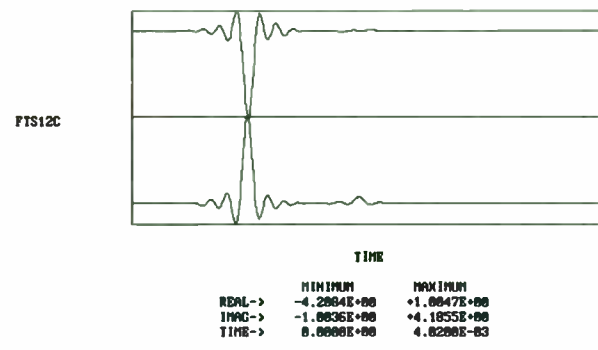


Figure 9. This figure demonstrates the graph obtained by calculating the impulse response of the measured data. Note: Only positive frequencies were used to calculate the FFT, therefore, an imaginary portion results.

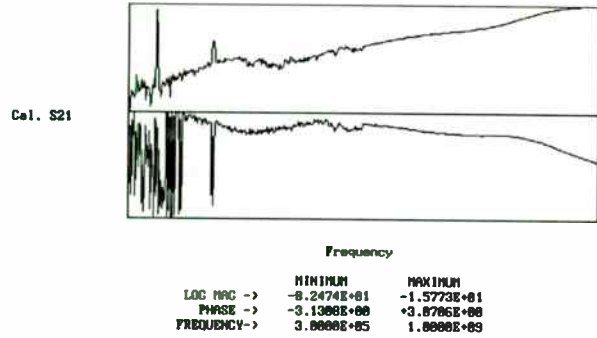


Figure 10. Graph of calibrated S21 of a bandpass SAW device measured with a wide-band frequency sweep. This graph is taken directly from the computer screen when using the data acquisition system.

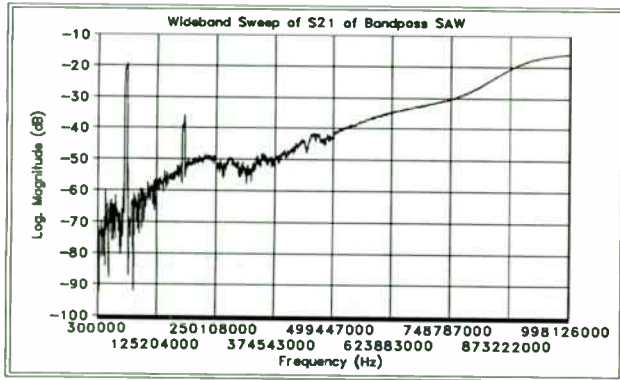


Figure 11. Graph of calibrated S21 of a bandpass SAW device measured with a wide-band frequency sweep. This graph was measured with the data acquisition system and converted into an ASCII file and imported into Quatro Pro for graphing.

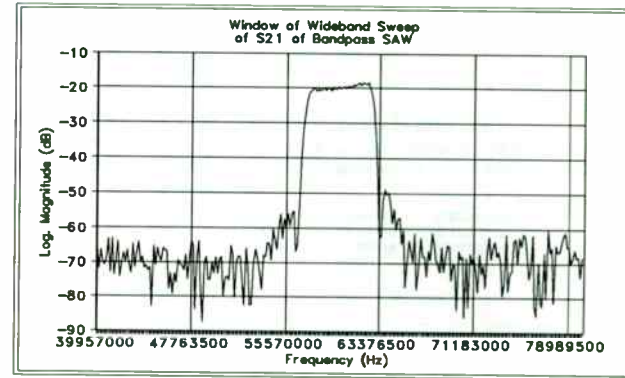


Figure 12. Graph of calibrated S21 of a bandpass SAW device measured with a wide-band frequency sweep. This graph was measured with the data acquisition system, converted into an ASCII file, and imported into Quatro Pro for graphing. Only a window of the measured device was graphed.

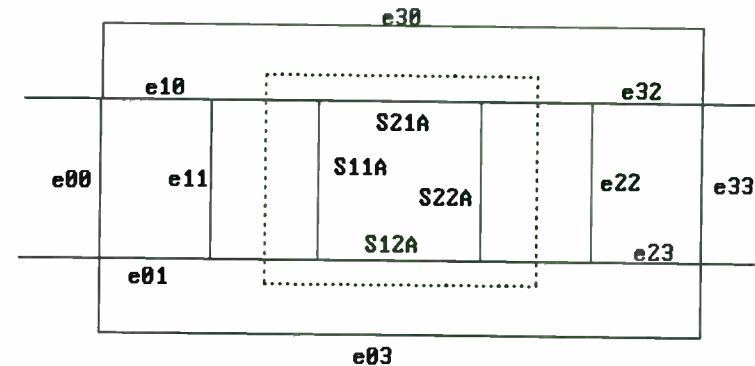


Figure 13. Error model used for the 12 term error correction. (Note: frequency tracking error in port 1 is e10e01)

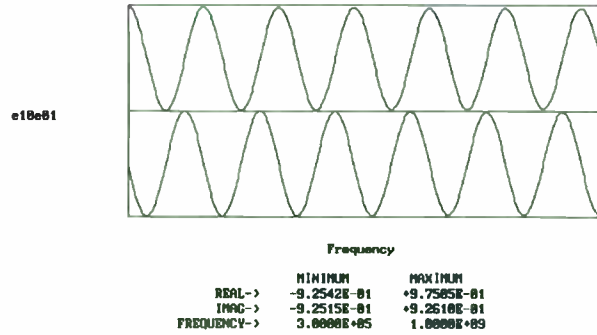


Figure 14. Graph of the error coefficient e10e01 over a wideband sweep. Error e10e01 represents the frequency tracking error in the cable connected to port one of the network analyzer.

B. Tables

TABLE 1
COMPARISON OF CALIBRATED S11 DATA

Calibrated Data: Freq. MHZ	S11 Data from Acquisition System.		S11 Data from Front panel.	
	Log Mag.	Phase (Rad)	Log Mag.	Phase (Rad)
40	-.2954	-.8774	-.3084	-.8933
45	-.3600	-.9914	-.3734	-1.0083
50	-.4522	-1.1173	-.4672	-1.1350
55	-.9653	-1.3035	-.9767	-1.3210
58	-2.7916	-1.3548	-2.7753	-1.3719
60	-3.3090	-1.2533	-3.3028	-1.2678
62	-3.5336	-1.1340	-3.5582	-1.1514
65	-1.2398	-1.1223	-1.2534	-1.1416
70	-.7454	-1.3122	-.7602	-1.3312
75	-.7595	-1.4731	-.7736	-1.4448
80	-.7779	-1.5304	-.7910	-1.5475

TABLE 2
COMPARISON OF CALIBRATED S11 DATA

S11 Percent Error in Data Acquisition System Calibration.		
Freq. MHZ	% Error Mag.	% Error Phase
40	4.22	1.78
45	3.59	1.68
50	3.21	1.56
55	1.17	1.32
58	.587	1.25
60	.188	1.14
62	.691	1.51
65	1.16	1.71
70	1.95	1.43
75	1.82	1.96
80	1.66	1.11

TABLE 3
COMPARISON OF CALIBRATED S12 DATA

Calibrated Data: Freq. MHZ	S12 Data from Acquisition System.		S12 Data from Front panel.	
	Log Mag.	Phase (Rad)	Log. Mag.	Phase (Rad)
40	-88.63	-.5171	-88.00	-2.429
45	-83.77	-.5194	-82.12	-2.782
50	-73.67	-2.666	-73.73	-2.765
55	-57.05	-2.892	-58.65	-2.795
58	-19.37	1.649	-20.35	1.781
60	-18.80	2.155	-19.12	2.303
62	-18.39	2.688	-17.98	2.853
65	-58.82	-.8073	-58.69	-.8116
70	-68.55	3.139	-69.30	3.127
75	-65.57	-2.967	-66.59	-3.082
80	-63.72	-2.191	-65.19	-3.138

TABLE 4
COMPARISON OF CALIBRATED S12 DATA

S12 Percent Error in Data Acquisition System Calibration (*-noise)		
Freq. MHZ	% Error Mag.	% Error Phase
40	.716	78*
45	2.01	81*
50	.081	3.58
55	2.73	3.47
58	4.82	7.43
60	1.67	6.35
62	2.28	5.78
65	.222	.530
70	1.08	.377
75	1.53	3.73*
80	2.26	30.2*

IX. LIST OF REFERENCES

- [1] Bryant, G.H. Principles of Microwave Measurement. London, United Kingdom: Peter Peregrinus Ltd., 1988.
- [2] Somlo, P.I. and Hunter, J.D. Microwave Impedance Measurement. London, United Kingdom: Peter Peregrinus Ltd., 1985.
- [3] Goldstein, Larry Joel. Hands on Quickbasic. New York: Simon & Schuster, Inc. 1988.
- [4] Hewlett-Packard Company. HP8753c Network Analyzer Operating Manual. Santa Rosa, California: Hewlett-Packard Company, 1988.
- [5] National Instruments Corporation. NI-488 Software Reference Manual. Austin, Texas: National Instruments Corporation, 1988.
- [6] Proakis, John G. and Dimitris G. Manolakis. Introduction to Digital Signal Processing. New York: Macmillan Publishing Company. 1988.
- [7] Douglas, Sallie L. Remote Data Acquisition and Error Analysis of the Scattering Parameters of Quartz Crystal Devices. University of Central Florida. 1987.
- [8] Microsoft Corporation. Microsoft Fortran 4.1 Optimizing Compiler, Language Reference and Mixed Language Programming Guide. U.S. and Canada: Microsoft Corporation, 1987.

**Handheld Probing Techniques for RF-PCB and Hybrid-Circuit
Characterization**

Young Dae Kim, Project Manager
Hewlett-Packard Company
1400 Fountain Grove Parkway
Santa Rosa, CA 95403

Abstract

In-circuit probing using a handheld probe is the traditional method of quickly verifying electronic circuits during circuit design as well as manufacturing. At RF frequencies, however, the confidence level of this method suffers rapid deterioration due to non-repeatable test results associated with probe parasitics. Since the key benefit of handheld probing is the ability to probe quickly and easily, this paper will discuss, from a practical aspect, the issues of probe parasitics and measurement accuracy-enhancing techniques.

Introduction

In general terms, the most basic measurement parameters in electrical circuits are voltages, currents, and impedances, where an impedance is defined as the ratio of a voltage and a current. Since two out of the three parameters determine the rest in a linear circuit, usually only the two most convenient parameters need to be measured to fully describe a circuit in operation.

At high frequencies, achieving high impedances for voltage probes and low reactances for current probes to minimize measurement error becomes extremely challenging. Moderate success has been achieved in high-impedance voltage probes using GaAs technology. But, due to the difficulty of controlling probe parasitics, the impedances are not measured in terms of voltages and currents but measured in terms of voltage waves launched into a well-defined transmission line. This method is called an S-parameter measurement and has provided a means of stable, wideband impedance measurement [1]. All modern wideband network analyzers are based on S-parameter technology. In this article we are concerned about the high-frequency handheld probes for S-parameter measurements.

Limitations of Error Correction in Network Analyzers

One of the most powerful features of a modern network analyzer is its ability to correct errors introduced by the measurement system [1,2,3]. In principle, it is possible to totally eliminate measurement errors including that of a probe as long as the measurement is repeatable and, therefore, the error can be removed mathematically with known impedance references. However, for the calibration to be accurate, it is also implied that the system environment during calibration and measurement must be maintained. In the case of handheld probing, these conditions are often violated. In fact, the most difficult accuracy problem for this type of probe is the breakdown of calibration during the

course of measurement by changes in the probe impedance; e.g., common-mode coupling due to ground lead inductance (Fig. 1), mutual inductance or capacitance coupling by the probe tip to the adjacent ground (Fig. 2), and tip-to-circuit contact resistance. Another significant factor is the probe cable which introduces phase variations as the probe is moved around during measurement. This can cause considerable error, especially for a reactance measurement. These will be discussed in more detail. Assuming calibrations are done at frequent enough intervals, the effects of temperature and humidity variation can be ignored.

Effect of Probe Leads

A typical handheld probe needs to have a short length of high-impedance leads at the tip in order to connect the test probe to the circuit under test. This creates a couple of problems as shown in Fig. 1 and 2. First, the ground lead inductance introduces coupling of undesirable common-mode impedance. The common-mode impedance is made up of the probe grip and probe cabling impedances, and it tends to vary widely depending on the operator's probe holding method and the instrument ground return impedance. Next, the input loop made of probe leads can cause an E-M field to extend far into the adjacent circuits. This is shown in Fig. 2. The reflected impedance will show up as unpredictable changes in probe input impedance. These effects become most serious when the parasitic impedances resonate at high frequencies, making it impossible to make a reliable measurement.

The following observations can be made regarding the probe impedance variation due to probe lead parasitics:

1. Common-mode coupling can be minimized either by reducing ground impedance, Z_g , or increasing common-mode impedance, Z_{cm} .
2. Common-mode coupling can also be reduced if the common-mode impedance, Z_{cm} , is isolated from Z_g by using a common-mode choke or balun.
3. Probe impedance variations by E-M coupling of the input loop to adjacent ground can be minimized by reducing the loop size and maintaining probe orientations constant relative to ground during calibration and measurement. This effect cannot be helped by a common-mode choke.

Effects of Phase Change in Probe Cable

Any mechanical stress applied to the cable will deform its dielectric and, therefore, change its propagation constant or phase (Fig.3). Impedance discontinuities at both ends of the cable can also change by the cable stress. The resulting multiple reflections may introduce large periodic ringing in frequency domain. Although these effects are calibrated out before the measurement, the calibration can be upset easily by small changes in the cable. For large deformation the release time constant can also be quite long due to the complex mechanical property of the cable.

Since the phase and amplitude are equally important in determining an impedance value from an S-parameter, the phase uncertainty should be small enough over the expected probe cable movement. This is achieved by choosing the right type of cable, the length, the connection method, and an ergonomic design which minimizes the stress between probe and the probe cable during measurement. High-quality cables with heavy braid and jacket materials may be better in stationary conditions, but thinner, more flexible, low-cost cable may do equally well with regard to the total phase change. It seems that the lower local stress in a smaller diameter cable tends to counter-balance the advantage of absolute dielectric stability in a thicker, heavier cable. Furthermore, the rigidity of thicker cables often seriously limits the usability of the handheld probe, defeating its original purpose.

Probe Tip Selection

One must also take into account the mechanical properties of probe tips. These will include not only the selection of tip material and tip shapes for low contact resistance, but also the ergonomic aspect of achieving repeatable, precise contacts. For minimum contact resistance, gold plating is desired to prevent oxidations. Since the circuit contact must be made at two or more points at the same time, the probe tips must have some compliance. Using a spring-loaded probe tip such as [4] allows very comfortable circuit probing although care must be taken to ensure that the

spring probe itself does not introduce RF reactance variation due to its internal sliding contacts.

Calibration Standards

A typical method of calibrating an impedance measurement is to use 3 known impedance standards, e.g., open, short, and load (OSL), to mathematically solve for 3 measurement unknowns, which are source mismatch, source tracking, and directivity [2,3]. Therefore, the accuracy of calibration standards directly affects the results of measurement. However, for a typical handheld impedance measurement, the major part of the calibration error still comes largely from the differences in calibration and measurement environments rather than from the absolute accuracy of the references used. As for the 50 ohm load standard, the most ideal device for a two-prong probe would be a carefully designed microstrip termination which duplicates the measurement environment. A commercial SMA termination can also be used, understanding that there is a potential inductive frequency response which limits the accuracy of the termination at frequencies above 3 GHz. But, for most practical applications, an SMA termination mounted on a calibration plate as in Fig. 8 should provide a good alternative, considering the magnitude of inaccuracy imposed by the repeatability of a typical probe system.

Measuring Large Components and Defining Impedance Reference Ground

At high frequencies where the physical size of a component under test is no longer negligible when compared with the wavelength, the transmission line effects begin to take place. To minimize uncertainty, the impedance of a component must be uniquely defined with regard to ground reference. Fig. 4 explains this.

Experimental Probe Design

Sample Design of a Probe

As discussed before, there are several steps one can take to improve the electrical performance of a handheld probe. First, reduce probe parasitics by bringing the coaxial connection points as close to the circuit as possible and, second, isolate the probe from common-mode impedance using a common-mode choke. The latter is especially effective to prevent wild impedance variations caused by parasitic resonances (Fig 5). Third, and more important to the successful handheld probe design, is to devise ergonomically sound probes which are easy to use.

Fig. 6 shows the construction of a very inexpensive probe made of .085" semi-rigid coax cable as the probe body. The length of the probe pins has been compromised to minimize parasitics but are still long enough for easy target location. A spring-loaded pin [4] is used for ground connection to help maintain good contact against rocking motion. The tip of the center conductor determines the calibration reference plane. Ferrite beads [5] are used to isolate and damp potential common-mode coupling and resonances.

Fig. 7 also shows another version of an inexpensive probe

designed to measure impedances between two widely spaced points. This construction provides a low impedance ground connection for good common-mode rejection. Nevertheless, the maximum usable frequency of the probe is much lower due to resonance at the probe input.

Probe Cable

The probes were tested with several industry standard microwave flexible cables, RG-142 B/U, RG-223/U, and RG-188 A/U [6], and in-house general purpose mini-RF coaxial cables (.110" OD double and triple shielded coax cables with tinned copper braid). The length of the cables was 17 inches. RG-142 B/U was superior with respect to signal attenuation and phase stability, but it was too stiff for easy positioning of the probe. The cables were compared for phase shift while applying 90 degree torque. (See Fig. 8). The resulting phase shifts were nearly the same for the 3 microwave flexible cables. Although the very flexible in-house RF cables were most usable, they were too unstable in phase and too lossy. The smallest diameter microwave cable tested, RG-188 A/U, was found to be the best compromise for usability and performance.

Calibration Standard

The experimental probe #1 was tested on an HP8753C, 300 KHz to 6 GHz network analyzer. To remove system errors associated with a reflection measurement, an OSL (Open Short Load) [2,3] calibration was done on the test port. The 50 ohm load was built with a commercial SMA termination mounted on a machined aluminium block for convenience. (See Fig. 9). When tested against a precision microstrip load as the reference, the SMA coaxial load showed nearly constant 30dB return loss across the measurement band, 300 KHz to 3 GHz, showing inductive error is still relatively small.

A short circuit was achieved by touching the center portion of the calibration block with the probe. Due to mutual impedance coupling to ground, the short calibration was somewhat sensitive to where and how the short was obtained; i.e., the calibration changed visibly depending on where the probe was shorted on the block and what angle the probe was oriented. The effect was more pronounced at the high frequency end. It was also found necessary to gold plate the aluminium block to prevent surface oxidation. The open calibration was much less sensitive and was done simply by pressing the probe tip against any non-metallic surface.

Probe Evaluation

One way to evaluate the resulting accuracy is to measure a short circuit. A short circuit provides the maximum sensitivity

condition for detecting the probe contact resistance variation and the phase change due to the probe cable. The result is displayed in Smith Chart form on the network analyzer. By observing the size of the convergence circle around 1 /180 after probe calibration, one can predict the performance of the probe. The probe is moved around randomly to simulate an actual measurement while the maximum excursion of the convergence circle is observed to judge the quality of the probe under test. A quicker, more convenient method is to test only the probe repeatability by using the "data-memory" function of the network analyzer. This measurement does not need a full calibration, and the error limit is directly shown on a polar display. A sample measurement result is shown in Fig. 10. In order to see the effects of probing angle, the phase shift is monitored while probing a short circuit as a function of tilt direction and tilt angle (Fig. 11). The result shows that the main problem is due to the electrical length variation of the spring loaded ground pin. The worst case phase shift error is about 5 degrees at 3 GHz.

Computer Simulation of Probe Behavior

To understand the effect of electro-magnetic coupling, the probe tip parasitics were modeled on a computer either as small stray inductors and capacitances or as a short length of coupled transmission line. (See Fig. 12). The coupled transmission line model approximates the behavior of the high impedance region at the tip as two parallel transmission lines over a ground plane. The sensitivity study was performed for different even- and odd-mode

impedances as well as the length as parameters while observing the effect of common-mode impedances. The model suggests that in addition to reducing the length of the tip, keeping the odd- and even-mode impedances small will improve frequency performance by pushing the tip resonance frequency higher. The results support our previous observations; tighter coupling between two probe tips (to lower odd-mode impedance), thicker probe tips (to lower even-mode impedance), and isolation of common-mode parasitic impedances.

Test Results

With this experimental probe system, 3 GHz measurements were routinely made with better than ± 10 percent accuracy on a Smith Chart. To obtain better accuracies, the following measures can be taken:

1. Further downsize the probe and reduce the probe tip lead inductances.
2. Improve the probe cable assembly method.
3. Improve RF impedance variation of the spring probe pin.
4. Minimize the changes between the calibration and measurement environments;
 - Use calibration standards that have an electrical environment very similar to that of the measurement.
 - Maintain the same probe hand grip position and probe angle.

- Minimize the stress changes in the probe cable.
5. Repeat calibration as often as practical.

Conclusions and Future Directions

The issues related to handheld impedance probes and the several techniques to improve the accuracy have been discussed. It was shown that a simple experimental two-prong probe with an error-correcting network analyzer can be used for impedance measurements well into microwave frequencies.

Although only an one-port reflection measurement has been discussed in this paper, the same probing technique can be applied to a two-port measurement with a full two-port calibration. Some of the additional issues one will need to consider are:

1. Probe holder/positioner to hold the second probe.
2. Reduced measurement dynamic range due to increased cross-talks between the exposed tips of the probes.
3. Additional standards for two-port calibration.
4. The probes can exhibit significant reactive impedances at high frequencies. One should be aware certain active circuits may become unstable when terminated only with these probes.

Another key issue in handheld impedance probes is the difficulty of designing a multi-purpose probe that can handle

various sizes of test targets. This challenge could be met with an adjustable-tip probe but performance inevitably would be compromised. A much better approach would be to adopt an industry standard for RF in-circuit test such that high-quality probing can be done consistently with a standard set of probes [7].

Finally, it would be worthwhile to comment briefly on high impedance probes that can contribute in certain in-circuit test applications. For example, when probing a delicate active circuit, a standard 50-ohm probe may change the operating condition of the circuit so much that the use of the probe may cause large measurement errors. To reduce this loading problem, the probe impedance could be made to a higher value, such as 200 ohms, using a broadband balun transformer or a series resistor. If the accuracy degradation by the signal loss is not the prime concern, a series resistor could be used. With a set of 200 ohm calibration standards and built-in error correction algorithms in a network analyzer, the higher-impedance probe should provide adequate accuracy measurement.

Acknowledgement

The author would like to express sincere appreciation to those who helped him during the preparation of this paper; reviewing manuscripts, Larry Stratford and Jim Curran, valuable technical discussion, Julius Botka and Doug Rytting. I also thank Everett/Charles Inc. who provided materials for the experiment, and Mr.

Robert Kornowski of Motorola who shared his valuable original work.

References

- 1] "Measurement of Complex Impedances", Hewlett-Packard Application Note 77-3
- 2] "Accuracy Enhancement Fundamentals for Vector Network Analyzers", Joe Williams, Microwave Journal, March 1989, pp. 99 - 114
- 3] "Specifying Calibration Standards for the HP8510 Network Analyzer", Hewlett-Packard Product Note 8510-5A
- 4] Everett/Charles Contact Products Inc., Pomona, CA91767
- 5] Ferronics Inc., Fairport, NY14450
- 6] "Coaxial Cable, The Complete Catalog & Handbook", Times Microwave Systems, Inc., Wallingford, Connecticut 06492
- 7] "Kornowski Probe", Private Communication, Robert R. Konowski, Motorola Inc., September 1989

Figures

- Fig. 1 Ground Lead Inductance and Common-mode Coupling
- Fig. 2 Effect of E-M Coupling on Probe Tip Impedance
- Fig. 3 Cable Phase Shift due to Stress
- Fig. 4 Measurement of Physically Large Component
- Fig. 5 Cable Common-Mode Effect
- Fig. 6 Experimental Probe #1
- Fig. 7 Experimental Probe #2
- Fig. 8 Phase Shift in Typical Flexible Cable
- Fig. 9 Probe Calibration Fixture
- Fig.10 Probe Repeatability
- Fig.11 Effect of Probing Angle
- Fig.12 Computer Simulation

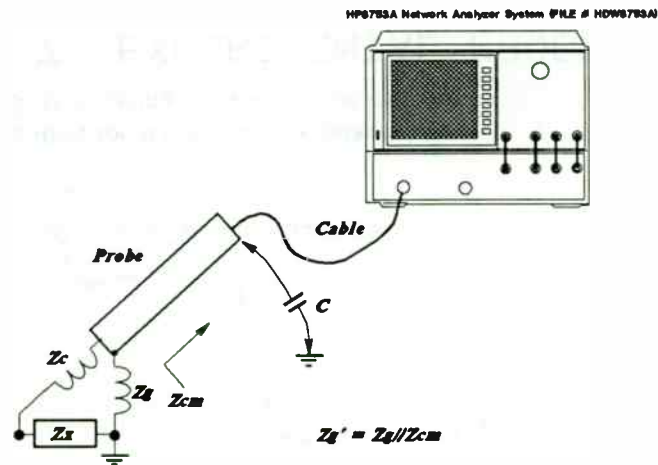


Figure 1. GROUND LEAD INDUCTANCE AND COMMON-MODE COUPLING *RFEXPO-NOV90*

1. INDUCTIVE COUPLING
LOOP SIZE
DISTANCE/ANGLE
2. CAPACITIVE COUPLING
CONDUCTOR SIZE
DISTANCE/ANGLE

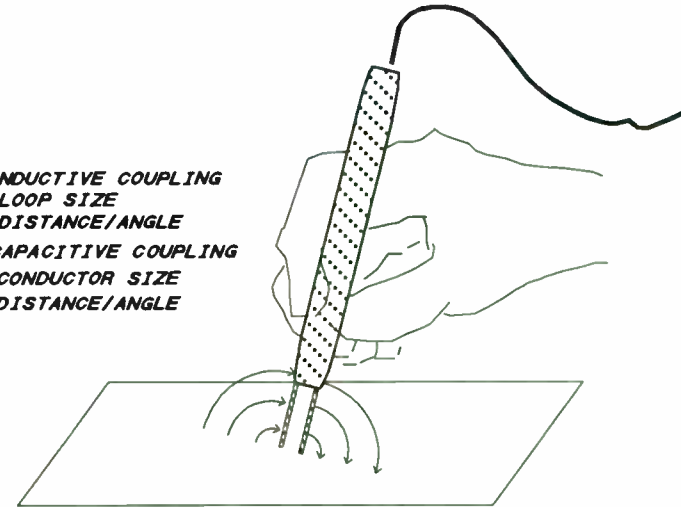


Figure 2. EFFECT OF E-M COUPLING ON PROBE TIP IMPEDANCE *RFEXPO-NOV90*

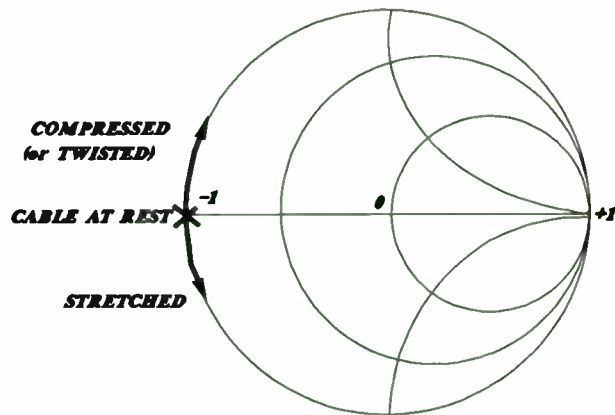
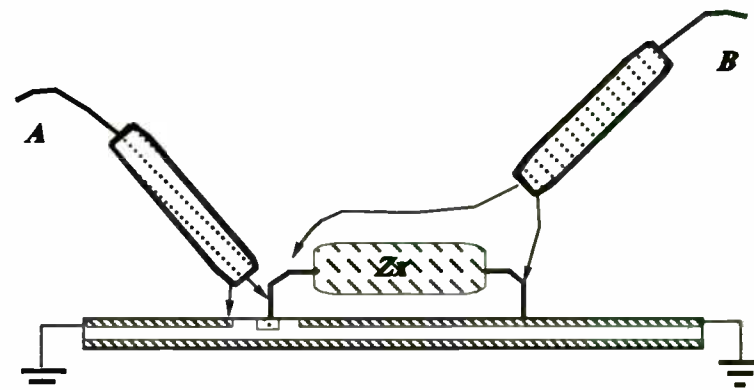


Figure 3. CABLE PHASE SHIFT DUE TO STRESS

RFEXPO-NOV90



* Probe A is a better set-up for Z_x measurement

Figure 4. MEASUREMENT OF PHYSICALLY LARGE COMPONENT *RFEXPO-NOV90*

RFEXPO-NOV90

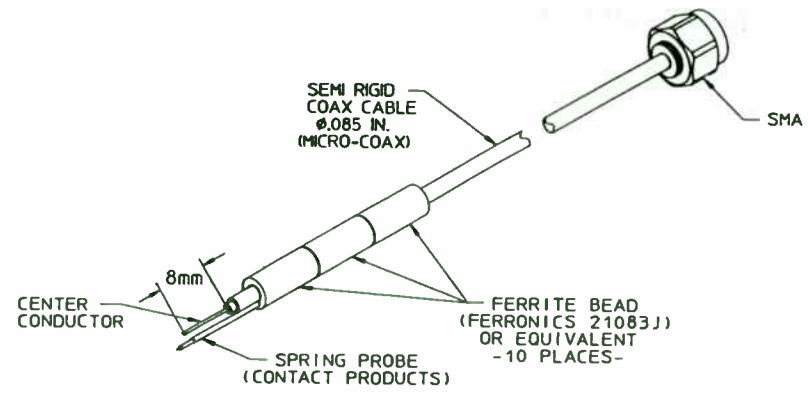
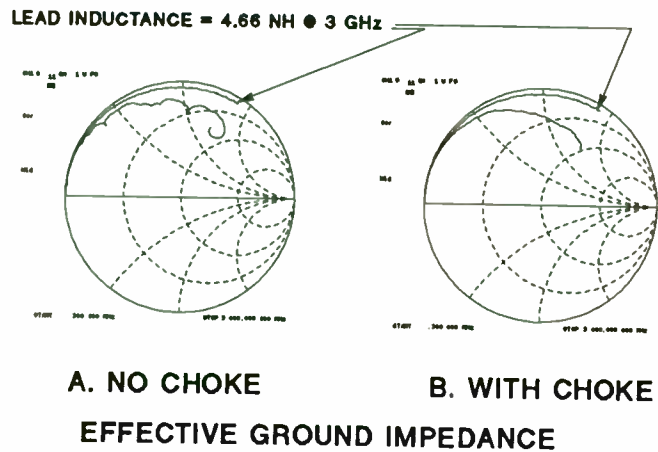
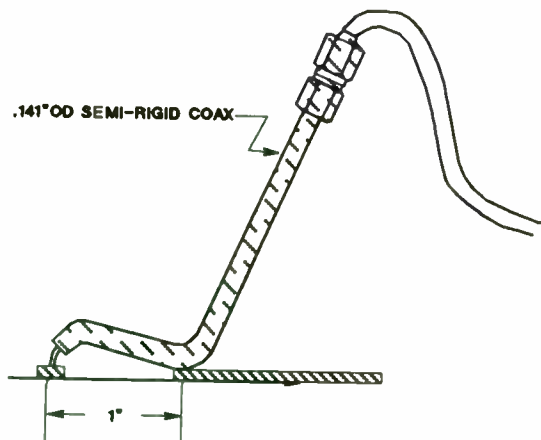


Figure 5. CABLE COMMON-MODE EFFECT Figure 6. EXPERIMENTAL PROBE #1

RFEXPO-NOV90

RFEXPO-NOV90



Suggestion for large spacing measurement
Low C-M coupling by low ground impedance

Figure 7. EXPERIMENTAL PROBE #2

RFEXPO-NOV90

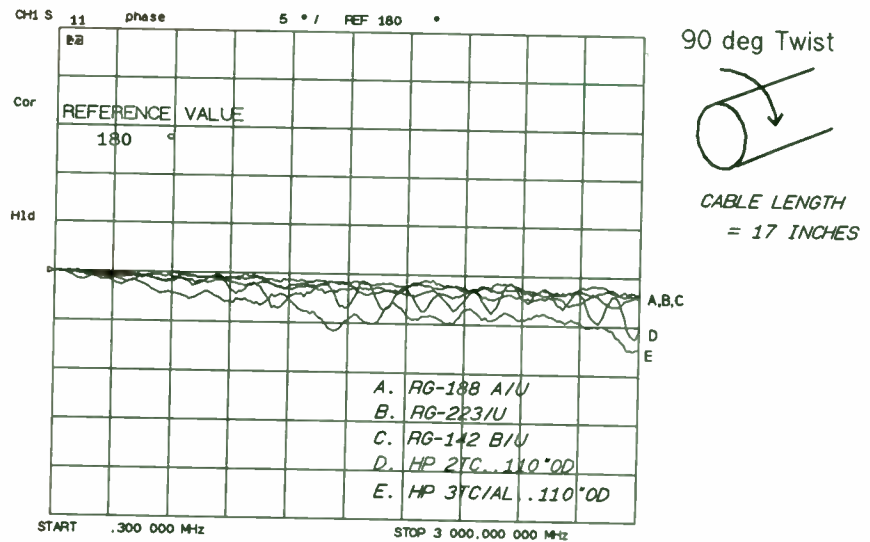


Figure 8. PHASE SHIFT IN TYPICAL FLEXIBLE CABLES

RFEXPO-NOV90

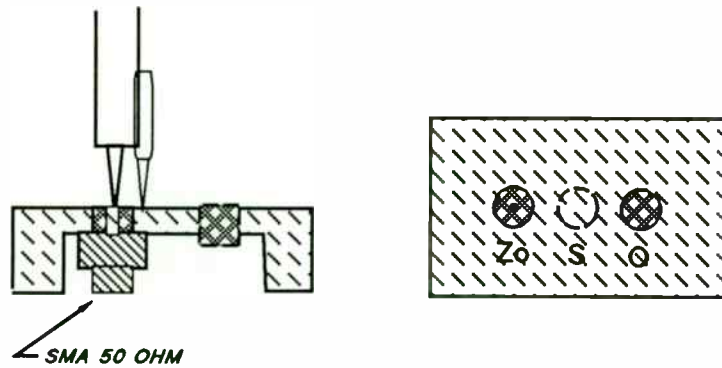


Figure 9. PROBE CALIBRATION FIXTURE

RFEXPO-NOV90

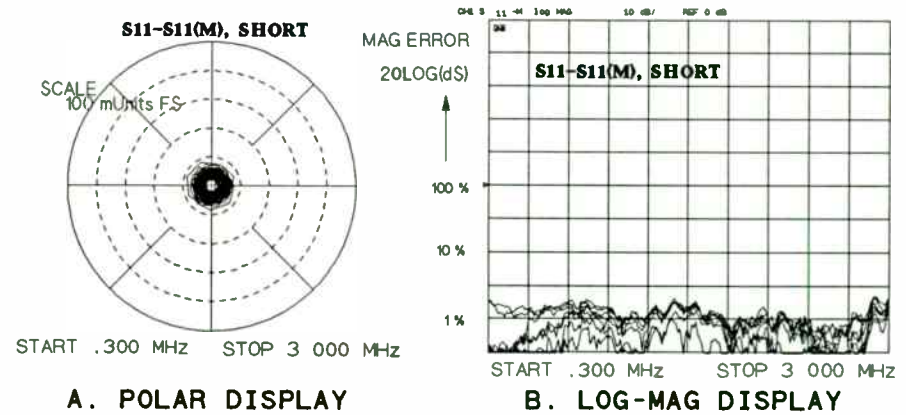
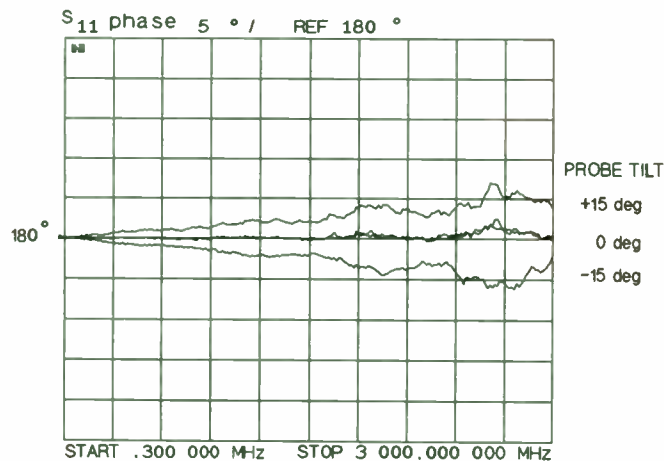


Figure 10. PROBE REPEATABILITY (PROBE #1 WITH 20" RG-188A/U CABLE)

RFEXPO-NOV90

* REPEATABILITY MEASURED BY PROBING AN AREA OF GROUND PLANE N TIMES AND RECORDING THE DEVIATIONS FROM AN INITIAL S-PARAMETER VALUE.



SHORT TERMINATION PHASE ERROR

Figure 11. EFFECT OF PROBING ANGLE

RFEXPO-NOV90

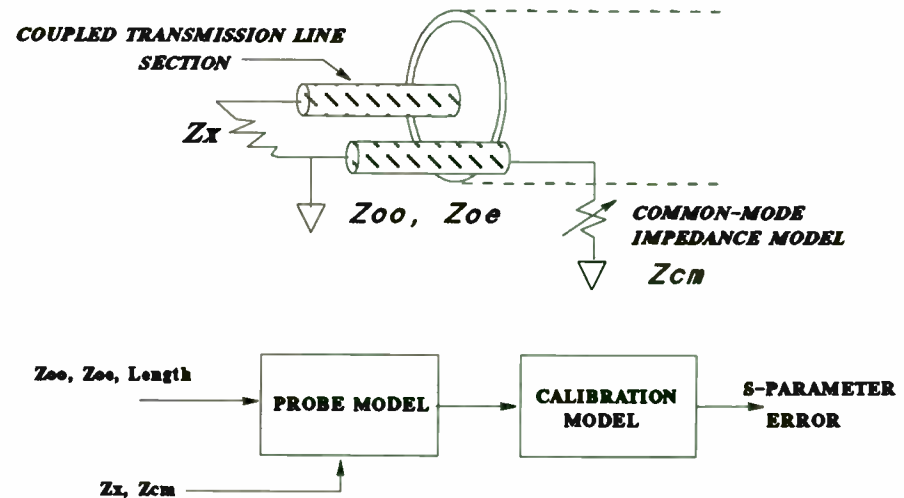


Figure 12. COMPUTER SIMULATION

RFEXPO-NOV90

USING VXIBUS-BASED PRODUCTS FOR RF TEST SYSTEMS

By

Malcolm E. Levy
Racal-Dana Instruments Inc.
4 Goodyear Street
Irvine, CA 92718

INTRODUCTION

Despite its infancy, the VXIbus has already proven to be a major contender for automatic testing requirements. Many VXIbus systems are now providing their owners with time, size, power consumption and money saving benefits. The range of applications is wide, from simple to complex, industrial to military, and development to test. However, there have been some reservations as to VXI's suitability for all applications, particularly high performance RF and Microwave. A number of companies have now shown there are no inherent weaknesses in VXI as the platform for an RF or a Microwave system. The introduction, in 1989, of a 20 GHz counter in a VXIbus format began to dispel doubts but the route to a comprehensive solution to RF VXI instrumentation required more radical and innovative developments.

This paper describes the special areas of concern relating to RF and Microwave issues and how VXIbus products can now achieve the necessary performance.

FUNDAMENTAL ISSUES

The fundamental issues relating to instruments-on-a-card and RF must first be understood. These can be classified as EMC, Noise (internal to the system), Input/Output Connections, and Cooling.

EMC

There are two aspects of EMC to be considered: the system as a whole and the performance between cards.

The performance of the individual modules is fully described in the VXIbus Specification, Rev. 1.3. Radiated emissions and radiated susceptibility performance is quantified with the aim of ensuring that if these limits are adhered to, then no card to card interference will occur from one manufacturer to the rest. It also allows a manufacturer of a super low noise module to design his circuits to be immune to expected levels. Conducted susceptibility and emissions bring into play the performance of the VXIbus chassis, the environment the modules sit in. Unlike instruments of the past, the VXIbus instruments share common power supplies, backplane communications and cooling. To a greater extent the task here is placed on the filtering performance on the module. DC to DC converters offer the best immunity to power supply related issues and improved isolation between the backplane bus and the RF compartment can also be realized. This is described later.

Once the modules are built into the chassis and become a system some of the more meaningful tests must be made. MIL-STD-461 in its various forms describes how a system performs with respect to electromagnetic compatibility. We must now consider the collection of modules enclosed in the chassis as a total system. Does the system operate correctly when subjected to high energy EM fields?

Does the system leak or radiate to the extent that meaningful tests on low noise UUT's are null and void? This is graphically identified in Table 1 and Figure 1.

EMC CHECKS	
Configuration	Standards
Module to Module	VXibus Rev. 1.3
Single Instrument Module in Chassis	MIL-STD-461D
System in Chassis	MIL-STD-461D

Table 1

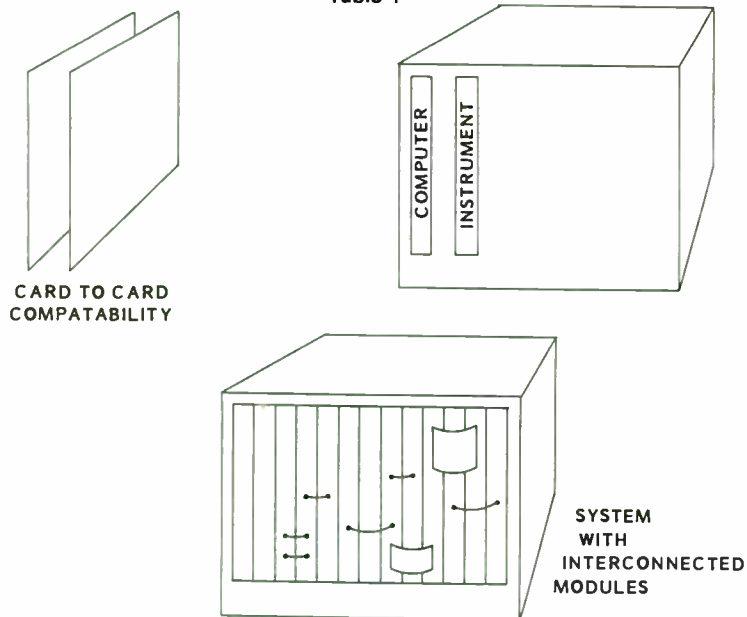


Figure 1

The operation of a single instrument and its performance relative to EMC can be somewhat meaningless as it is subject to other factors, the chassis it is in, the slot 0 performance and the interface. For this reason the most meaningful check is on the system as a whole, complete with all the instrument-to-instrument cabling. With a small VXibus test system it becomes much more feasible to take it to an anechoic chamber to carry out full EMC checks. Consider trying to do this with two six-foot racks of test equipment. An RF subsystem comprising of power meters, synthesizers, switches and analyzers can be configured and tested for full compliance. A description of how such a system would look follows later in this paper.

A point to note here is that the chassis and individual modules cannot meaningfully be compliant with MIL-STD-461 as they need other products around them to enable operation. Consider the case of product A, slot 0 B, plugged into chassis C. EMC checks show that product A's sensitivity was reduced during the radiated susceptibility tests. Where is the problem? Did the chassis power supplies collapse? Did the clock in slot 0 move frequency? Or was there a genuine desensitization of the instrument? You can see the problem, and therefore what meaning can be placed in one particular EMC test. The only real test is the final system test.

NOISE

When discussing noise in a stand-alone RF instrument, control of which is maintained by a single manufacturer, the levels are easy to define. In the VXIbus test system, noise comes from other areas. This is not dissimilar to noise problems associated with a rack of test equipment, but in the VXIbus system, it is much easier to control.

The sources of noise are: power supply, backplane busses, vibration (fans), and external fields.

Switch Mode or Linear?

In general, switch mode supplies tend to generate noise and transients due to their high speed switching nature. At full load, they tend to be very good and can be made to perform with low noise/spurious characteristics. However, when lightly loaded, they have a very narrow conduction angle giving rise to ringing and poor noise performance. Due to the wide range of load variations in a VXIbus RF ATE system, a switch mode supply is not an ideal solution.

Linear supplies do not suffer these problems and are able to cope with a wide range of varying load conditions. The only noise problem is the magnetic field, but this can be cured with toroidal transformers and ferro-magnetic shielding. The other penalty is increased weight.

Backplanes

The backplane has no way of generating noise, but it does play a key role in helping reduce noise. The VME databus can operate quite happily up to 20 MHz with fast edges producing frequencies to many GHz.

Careful screening of the databus within layers of copper ground planes, built into the backplane, can significantly reduce radiation. This concept can be continued into the module by utilizing shields around the backplane edge connector. The VXIbus specification allows for this.

This noise is very localized around the backplane, so that any low noise circuits should be built at the opposite side of the module to the bus. Such a method is also optimum for the analog I/O connections as these are then kept away from the noise source.

Vibration

Vibration and Microphony can be a problem in modular systems. Some VXIbus chassis with their fans running at high speed have vibration performance that is unsuitable for RF and Microwave applications without some module damping. An RF and Microwave chassis must have low vibration fans adequately mounted to ensure that vibration does not compromise performance.

External Fields

The environment the system is operating in may be relatively benign as far as

external RF fields are concerned, but consider some of the possible locations: On site radar testing, high energy research labs, high output power transmitter testing, etc. To ensure these fields are eliminated from accessing the instruments and, therefore the system, the first line of defense is to use a "bomb" proof chassis. Much of the external field discussion was covered in EMC performance of VXIbus.

Noise from all of the sources described can and will induce itself onto the cabling of an RF ATE system. Long cable runs in some of the six-foot rack systems need to be triple screened as well as being carefully routed away from possible interference sources. Cable runs between products in a VXIbus system are at the most one or two feet and can be adequately contained within a screened chassis environment.

Input/Output Connections

As described earlier, cabling and I/O connections must be optimized. Impedance matching is crucial in order to limit return loss which results in wasted power or inaccurate measurements. In addition, cable lengths must be kept as short as possible to avoid undue signal loss and reduce the effect of E.M. coupling of noise or unwanted signals. This performance is easy to achieve when all the instruments are enclosed in the same RF VXIbus chassis. With VXIbus, the interface to the UUT can be an integral part of the chassis. Such an arrangement is shown for a high performance RF and Microwave chassis.

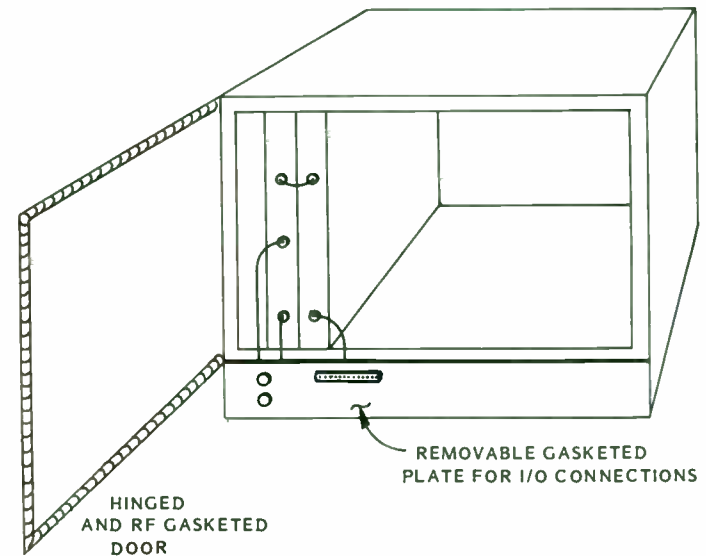


Figure 2

COOLING

The main problem in cooling RF modules relates to the very rigorous shielding requirements of such circuits, the drilling of holes for cooling is undesirable. Other techniques must be used such as a machined aluminum compartment with an heatsink fin. A more detailed description is covered in product availability.

SOLUTIONS

Now that the fundamental issues are understood, where do we go to find the products?

RF and Microwave VXibus Products

There are already hundreds of VXibus products available with many companies producing RF and Microwave products. Without producing an endless list, the following are a few of the major companies with known RF VXibus products.

EIP Microwave
Hewlett Packard
Racal-Dana Instruments Inc.
Tektronics/CDS
Wavetek

The key to ultimate VXibus performance in RF and Microwave is having a chassis able to meet the demands identified earlier. Such a chassis should look something like Figure 3. The chassis is double-screened, with an easily removable front shielded door, and should offer performance similar to that of a screened room with shielding effectiveness of typically 100 dB.

A prototyping module suitable for building low noise amplifiers or synthesizers looks something like Figure 4. This module is so designed that its applications could extend beyond its use in an EMI "quiet" mainframe. Hence, it offers a shielded RF compartment on a card. Power and I/O lines are fed into this compartment and are fully decoupled. Included on the card is a VXibus interface so the RF designer only has to worry about his or her own part of the assembly.

The RF compartment can be expanded in size, forming a multiple slot module, in order to accommodate more bulky items such as YIG oscillators. Circuits built inside the module would typically be subject to an interference level that is 80 - 100 dB down on an open card (dependent on frequency).

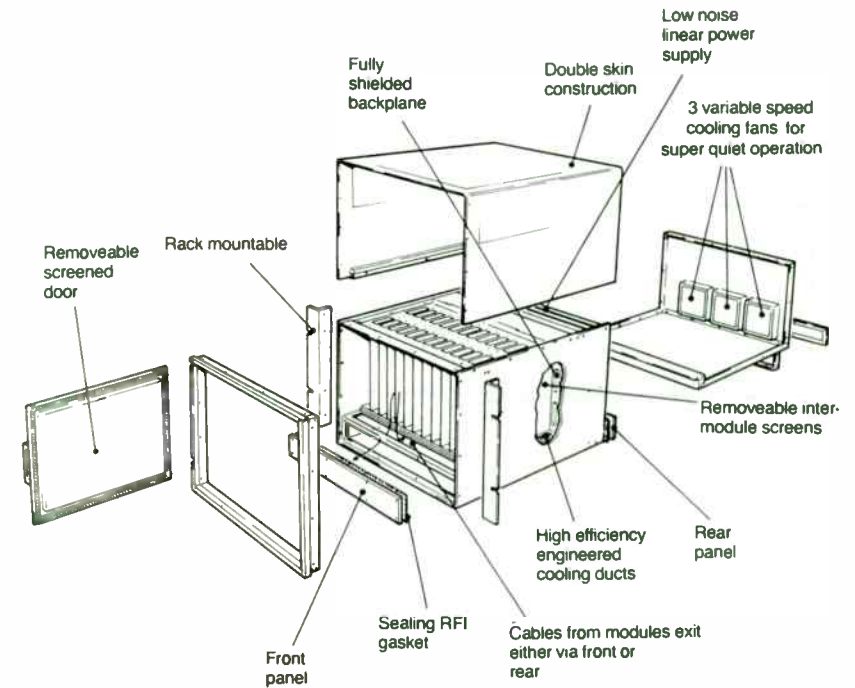


Figure 3

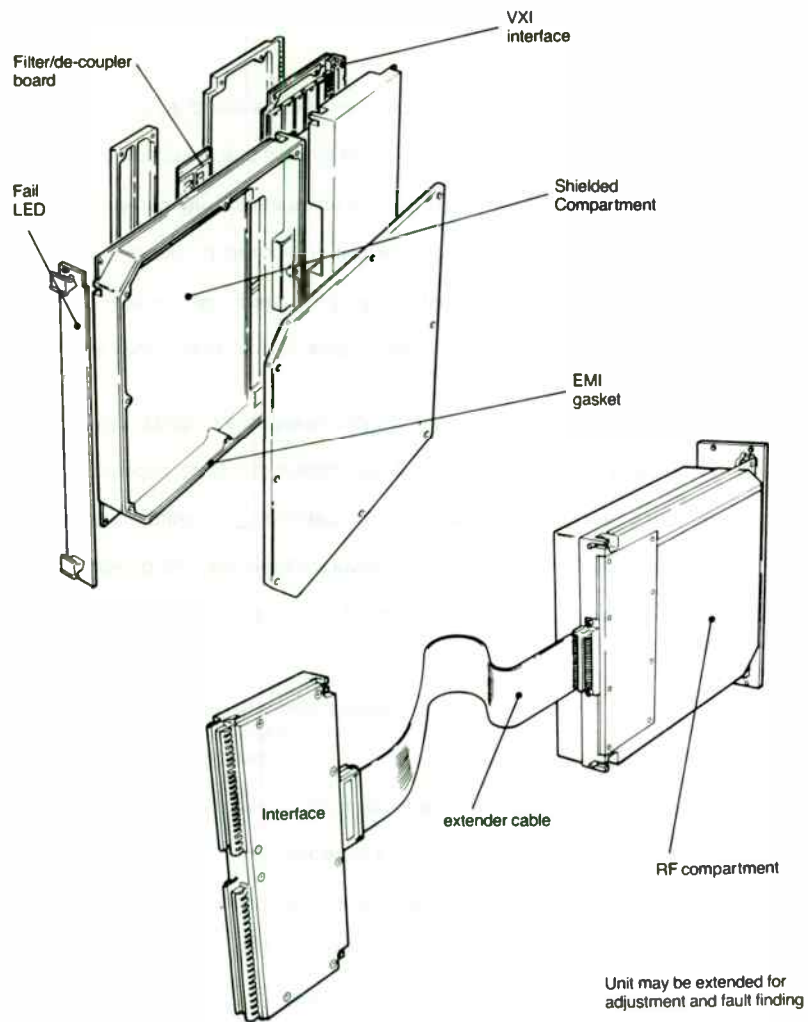
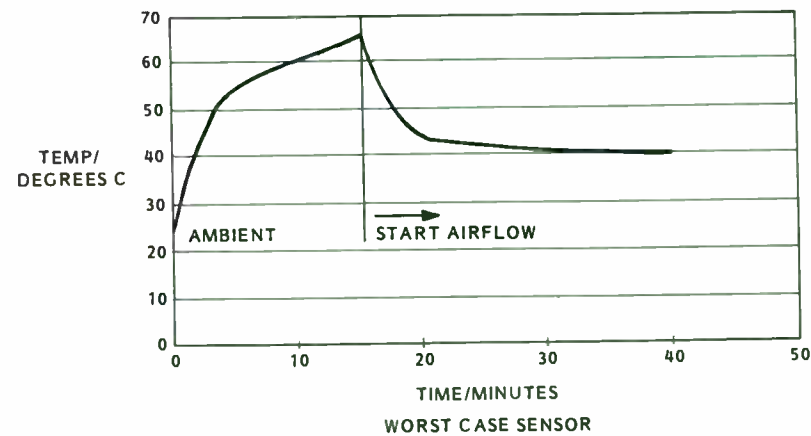


Figure 4

This product does not incorporate through module cooling and is dependent on convection/air cooling. Tests show that the module has excellent cooling performance, allowing 40 watts of power dissipation with acceptable increases in temperature for both the interface and RF compartment. See Figure 5 below.



The unit was allowed to heat up for 15 mins. before air flow was applied.

Figure 5

Applications

Many companies have already started to build RF VXIbus test systems. Lockheed-Sanders in Nashua, NH have designed a fully portable RF test system comprising of a 20 GHz synthesizer and 20 GHz wideband receiver. The product, which would have previously taken up a 6-foot rack, can now easily be wheeled onto a flight line.

Portable and reconfigurable Radar Test Systems have been shown for use in commercial airline applications.

New digital cellular radio standards both in Europe and the United States have demanded the development of a new test system. This has been achieved by the utilization of modular instrumentation. The digital cellular VXIbus test system from Racal-Dana provides an economical way of testing next generation mobile stations without the problems and costs associated with using either a system simulator or a specially modified test base station.

The system consists of six plug-in modules housed in a C-size VXIbus chassis and operates through a system controller via a GPIB link. It contains a receiver and two independently programmable signal sources. The first signal source is used to emulate a base station. The second can be configured as an interfering source, a delayed version of the first source, or a second base station. This enables performance testing in the presence of an interfering signal and in a simple 2-ray multipath environment.

CONCLUSION

VXIbus has received widespread acceptance as an excellent means of improving performance and downsizing automatic test and measurement systems. However, there has been some reluctance to adopt it for all applications, particularly high performance RF and Microwave. Now Racal-Dana, as well as others, has put those doubts to rest with the release of an RF chassis and RF prototyping card. These are low-noise, high shielding designs which offer the user a new spectrum of potential VXIbus applications. The user of high performance test systems can now benefit from the size, speed, versatility and financial advantages of VXIbus technology.

REFERENCES

1. VXIbus System Specification Revision 1.3, 14 July 1989.
2. The New Standard for Test and Measurement (Third Edition), Racal-Dana, June 1990.



RF Design Magazine Presents

Fifth Annual

RF expo

EAST

EAST

EAST

EAST

*November 13-15, 1990
MARRIOTT's
Orlando World Center
Orlando, Florida*

NEW

PTS 1000

DIRECT 1GHz SYNTHESIZER WITH PROVEN PTS QUALITY

Good Sines & Bad Signs

Looking for a low-noise, fast-switching signal source?

Good Sines

Whether it's automatic test equipment, satellite uplinks, EW communications or imaging systems, Programmed Test Sources has a frequency synthesizer to fit your needs. GE MRI units, Teradyne Testers, Varian Spectrometers... all use PTS synthesizers.

Bad Signs \$\$\$

And while other manufacturers have big dollar signs, PTS synthesizers start as low as \$1,950.

PTS manufactures a complete line of precision synthesizers covering the 100 KHz to 500 MHz frequency range with switching times as fast as 1 μ second for our *direct digital* models. And plenty of other options as well, like resolution down to .1 hertz (millihertz available as special order), GPIB and digital phase rotation.

Just as importantly, along with every PTS synthesizer comes our "absolutely everything covered" 2-year warranty. At the end of two years comes our flat \$350 service charge for any repair up to the year 2000! PTS has a commitment to quality you won't find anywhere else.

Find out how PTS synthesizers used the world over can help you in your application today. Call for our complete catalog, or to talk to an applications engineer.

Call (508) 486-3008 Fax (508) 486-4495

PTS

PROGRAMMED TEST SOURCES, Inc.
9 Beaver Brook Road, P.O. Box 517, Littleton, MA 01460



If you think that ultra-low phase noise and μ s switching cost a bundle, we have a pleasant surprise for you!

The **PTS 1000**, our new direct synthesizer with 0.1 Hz resolution and low-noise standard (1×10^{-9} /day) costs only \$11,500

WELCOME

Welcome to RF Expo East, 1990!



While the majority of the rest of the electronics industry is flat or worse, the RF industry is a true bright spot. Because this market is so diverse...with applications that include everything from simple handheld communications devices to the most complex applications in space systems, it remains strong and promising. And because of increased support by both exhibitors and attendees, Cardiff publishing has been able to expand the content of Expo East 1990.

RF Expo East 1990 is the busiest, most exciting Expo East yet. This year, more than 100 of the most exciting RF product manufacturers will be demonstrating components, sub systems and system products in the "sold-out" exhibit hall. Not only will attendees be treated to the best selection of products and services available, but because

the booths are staffed by both marketing professionals and engineers, attendees are able to discuss custom capabilities, specific specifications and application-specific requirements. In three short days, attendees can make an equivalent "field visit" to more than 100 RF manufacturers located across the United States and overseas.

Our special thanks to the Expo East 1990 program chairman Dr. Frederick Raab of Green Mountain Radio Research Company, for organizing this year's outstanding session schedule. An estimated 1,500 engineering attendees will enjoy more than 60 different technical papers and design tutorials on everything from Power Amplification techniques to RF Systems Research in Particle Physics. Copies of almost every paper were received in time to include them in the nearly 700 page Expo East Proceedings...be sure to purchase a copy for your reference library. And new for 1990, we have offered an additional day-long tutorial, on Modern Cad Techniques.

On behalf of everyone at Cardiff Publishing, and especially *RF Design* magazine, thank you for helping to make this the most exciting RF Expo East ever!



Kathi Walsh
Publisher



Kathy Kriner
Vice President



Kristin Hohn
Convention Manager

TABLE OF CONTENTS

General Information.4
Schedule of Events.4
Exhibitor Giveaways.5
Advisory Board.5
Program at a Glance.6
Presentation Briefs.8
Speakers and Session Chairmen.15
Exhibitor List.17
Exhibit Hall Map.21
Session Room Map.22
New Product Highlights.23
RF Expo East Staff.26

GENERAL INFORMATION

Registration

Location: Outside Sable and Sago Rooms, Palms Ballroom

Phone: (407) 239-2998

Hours:

Monday, November 12	7:00a.m. - 6:00p.m.
Tuesday, November 13	7:00a.m. - 6:00p.m.
Wednesday, November 14	7:00a.m. - 6:00p.m.
Thursday, November 15	8:00a.m. - 2:00p.m.

Exposition

Location: Sable and Sago Rooms, Palms Ballroom
Marriott's Orlando World Center

Hours:

Tuesday, November 13	11:00a.m. - 6:00p.m.
Sponsored Cocktail Party	5:00p.m. - 6:00p.m.
Wednesday, November 14	11:00a.m. - 6:00p.m.
Sponsored Cocktail Party	5:00p.m. - 6:00p.m.
Thursday, November 15	10:00a.m. - 2:00p.m.

Special Courses

Monday, November 12

Fundamentals of RF Circuit Design: Part I

8:00a.m. - 5:00p.m.

Grand Ballroom, Section VIII

Computer Aided Filter Design

8:00a.m. - 5:00p.m.

Crystal Ballroom, Section A & B

Tuesday, November 13

Fundamentals of RF Circuit Design: Part II

8:00a.m. - 5:00p.m.

Grand Ballroom, Section VIII

Wednesday, November 14

Oscillator Design Principles

8:00a.m. - 5:00p.m.

Grand Ballroom, Section VIII

Thursday, November 15

Introduction to Modern CAD Techniques

8:30a.m. - 4:30p.m.

Grand Ballroom, Section III

Pre-registration for these courses is mandatory. No registrations will be accepted on-site. Badges and tickets need to be called for at the RF Expo East registration counter during registration hours on Monday, November 12, Tuesday, November 13, and Wednesday, November 14.

Conference Proceedings

Location: Registration area, Marriott World Center

Proceedings of the RF Expo East are printed and available for purchase at the registration area. The cost to attendees is \$60. The cost for non-participants is \$125.

Message Center

Location: Registration area, Marriott World Center

Phone: (407) 239-2999

Any message received for attendees or exhibitors during the show will be posted at the message center. If you want to leave a number with someone back at the office, they can call in and leave a message for you. Messages will be posted alphabetically by last name. Please check daily for messages.

Speaker Ready Room

Location: New Orleans Room,
Conference Level

Convention Badges

Attendees	Red
Exhibitors	Blue

Hotel

Marriott's Orlando World Center
World Center Drive
Orlando, Florida 32821
(407) 239-4200

Future Shows

RF Expo West
February 5-7, 1991
Santa Clara Convention Center
Santa Clara, California

RF Expo East
October 29-31, 1991
Stouffer Orlando Resort
Orlando, Florida

RF Expo West

March 18-20, 1992
San Diego Convention Center
San Diego, California

SCHEDULE OF EVENTS

Tuesday, November 13

7:00a.m. - 6:00p.m.

Registration Open
Outside Sable and Sago Rooms
Marriott World Center

8:00a.m. - 5:00p.m.

Fundamentals of RF Circuit Design: Part I
Grand Ballroom, Section VIII
Marriott World Center

8:30a.m. - 4:30p.m.

Technical Program Sessions

11:00a.m. - 6:00p.m.

EXHIBITS OPEN
Palms Ballroom, Sable and Sago Rooms
Marriott World Center

11:30a.m. - 1:30p.m.

Deli Lunch
Exhibit Hall

5:00p.m. - 6:00p.m.

Sponsored Cocktail Party
Exhibit Hall

Wednesday, November 14

7:00a.m. - 6:00p.m.

Registration Open
Outside Sable and Sago Rooms
Marriott World Center

8:00a.m. - 5:00p.m.

Oscillator Design Principles
Grand Ballroom, Section VIII
Marriott World Center

8:30a.m. - 4:30p.m.

Technical Program Sessions

11:00a.m. - 6:00p.m.

EXHIBITS OPEN
Palms Ballroom, Sable and Sago Rooms
Marriott World Center

5:00p.m. - 6:00p.m.

Sponsored Cocktail Party
Exhibit Hall

6:00p.m. - 7:30p.m.

Ham Radio Reception
Anaheim/Atlanta/Boston Rooms
Marriott World Center

(Continued on page 5.)

SCHEDULE OF EVENTS continued

Thursday, November 15

8:00a.m. - 2:00p.m.
 Registration Open
 Outside Sable and Sago Rooms
 Marriott World Center

8:30a.m. - 11:30a.m.
 Technical Program sessions

8:30a.m. - 4:30p.m.
 Introduction to Modern Cad Techniques
 Grand Ballroom, Section III
 Marriott World Center

10:00a.m. - 2:00p.m.
EXHIBITS OPEN

Palms Ballroom, Sable and Sago Rooms
 Marriott World Center

EXHIBITOR GIVEAWAYS

Stop by these booths and enter your name for the following giveaways:

Eagleware Corporation in booth 213 will give away the new version 3.3 =Superstar= a general purpose circuit simulation tuning and optimization program for IBM PC's (a \$695 value) on Thursday, November 15, at 12 noon.

Hewlett-Packard in booths 410, 412, 414 and 416 will be giving away an E2373A RF Voltmeter on Tuesday, November 13, at 5:30p.m., a E2377A Voltmeter on Wednesday, November 14, at 5:30p.m. and a E2378A Voltmeter on Thursday, November 15, at 12:30p.m.

BOARD OF ADVISORS

The Board of Advisors actively contributes to the success of both RF Expo East and RF Expo West by sharing exhibitor and attendee needs with Show Management. We encourage you to contact them with your input during the show.



Malcom Levy
 Racal-Dana
 Instruments



Earl Olsen
 John Fluke
 Manufacturing



Frank Perkins
 RF Monolithics



Tony Ramsden
 Merrimac
 Industries



Jim Reeve
 Wavetek
 Corporation



David Strand
 M/A-COM
 Anzac Division

Program at a Glance

Program Chairman: Dr. Frederick H. Raab, Green Mountain Radio Research Co.

TUESDAY, NOVEMBER 13

A-1 Receivers I (Tutorial) Room: Crystal K/L	8:30-11:30	<ul style="list-style-type: none"> • Design of Receivers for Electronic Warfare
A-2 Power Amplifiers Room: Crystal A/B	8:30-9:30 9:30-10:30 10:30-11:30	<ul style="list-style-type: none"> • VSWR Performance of Transistor RF Power Amplifiers • A Novel Technique for Analyzing High-Efficiency Switched-mode Amplifiers • RF Power Transistors for 200-W Multicarrier Cellular Base Station
A-3 PLLs and Synthesizers Room: Crystal M/N	8:30-9:30 9:30-10:30 10:30-11:30	<ul style="list-style-type: none"> • The "Approximation Method" of Frequency Synthesis • A Comparison of Phase Stability Measurement Techniques • Ten-bit 300-MHz DAC for Direct Digital Synthesis
A-4 Microwaves Room: Crystal P/O	8:30-9:30 9:30-10:30 10:30-11:30	<ul style="list-style-type: none"> • System Design Considerations for Line-of-Sight Microwave Radio Transmission • Phase Shifter Based Upon Reflectively Terminated Multiport Coupler • Instrumentation for Radar Reflectively Measurement
B-1 Receivers II (Spread Spectrum) Room: Crystal K/L	1:30-2:30 2:30-3:30 3:30-4:30	<ul style="list-style-type: none"> • Spread Spectrum with Digital Signal Processing • Receivers for GPS and GLONASS Spread-spectrum Navigation Systems • Detection and Sorting of Frequency-hopped Signals
B-2 MMICS Room: Crystal A/B	1:30-2:30 2:30-3:30 3:30-4:30	<ul style="list-style-type: none"> • Ku-band MMIC Transceiver for Mobile Satellite Communication • Silicon MMICs: 35 dB - 35 dBm - \$35 • Some Design Considerations for L-band Power MMICs
B-3 Filters Room: Crystal M/N	1:30-2:30 2:30-3:30 3:30-4:30	<ul style="list-style-type: none"> • Capabilities and Applications of SAW-coupled Resonator Filters • At Long Last: Modular, Digitally Tuned RF Filters as Easy as Amplifiers and Mixers • Narrow-band SAW Filters for IF Applications
B-4 Antennas and Propagation Room: Crystal P/O	1:30-2:30 2:30-3:30 3:30-4:30	<ul style="list-style-type: none"> • Large Loop Antennas • VHF Multipath Propagation: Causes and Cures • Radio-Frequency Identification Systems for Commercial and Industrial Applications

Exhibits Open 11:00 a.m. - 6:00 p.m.

S. R. Vincent, <i>Raytheon</i>
R. W. Brounley, <i>Brounley Engineering</i>
K. Siwiak, <i>Motorola</i>
K. Vennema, <i>Phillips</i>
A. D. Helfrick, <i>TIC</i>
L. Moder, <i>Erbtec Engineering</i>
P. Jordan, <i>Analog Devices</i>
G. M. Kizer, <i>Rockwell (Dallas)</i>
M. H. Kori, <i>Centre for Development of Telematics</i>
D. J. Kozakov, C. W. Sirls, D. A. Thompson, and R. S. Banks, <i>Millimeter Wave Technology</i>
R. J. Zavrel, Jr., <i>Stanford Telecom</i>
J. Danaher, <i>Structured Systems</i>
J. E. Dunn and S. P. Russell, <i>Iowa State University</i>
R. Gilmore, <i>QUALCOMM</i>
T. Boles and D. Osika, <i>SGS-Thomson</i>
R. Weber, <i>ISU Microelectronics Research Center</i>
A. Coon, <i>RF Monolithics</i>
E. A. Janning, <i>Pole-Zero</i>
B. Horine and S. Gopani, <i>Sawtek</i>
R. P. Haviland, <i>Minitab Instruments</i>
D. R. Dorsey, <i>DocSolt</i>
J. Eaglesley, <i>Allen-Bradley</i>

WEDNESDAY, NOVEMBER 14

C-1 Receivers III (Digital) Room: Crystal K/L	8:30-9:30 9:30-10:30 10:30-11:30	<ul style="list-style-type: none"> • IF Frequency-response Considerations for the Digital Radio Environment • DSP Demodulation • A DSP PSK Modem for SATCOM SCPC Voice/Data
C-2 Transmitters Room: Crystal A/B	8:30-9:30 9:30-10:30 10:30-11:30	<ul style="list-style-type: none"> • RF Power Amplifier Using Adaptive Interface/ Distortion Cancellation • Digital-feedback Techniques for a Pulse-width-modulated Power Supply for RF Power Amplifiers • Operation of Static Induction Transistors at Cryogenic Temperatures
C-3 SAW Tutorial Room: Crystal M/N	8:30-11:30	<ul style="list-style-type: none"> • Surface Acoustic Wave (S.A.W.) Technology
C-4 RF Systems for Research in Particle Physics Room: Crystal P/O	8:30-9:30 9:30-10:30 10:30-11:30	<ul style="list-style-type: none"> • RF Systems for the Advanced Photon Source • RF Applications in Particle Accelerators
D-1 Receivers IV (Applications) Room: Crystal K/L	1:30-2:30 2:30-3:30 3:30-4:30	<ul style="list-style-type: none"> • A Fully Digital RF-signal Synthesis and Phase Control for Acceleration in COSY • Dynamic Evaluation of High-speed, High-resolution D/A Converters • A High-performance Low-cost TV Demodulator • Digital-signal-processing-based Spectrum-monitoring System for the European Broadcasting Area
D-2 Components Room: Crystal A/B	1:30-2:30 2:30-3:30 3:30-4:30	<ul style="list-style-type: none"> • Impedance-matching Transformers for RF Power Amplifiers • Temperature-compensating Attenuators • Useful Network Transformations in Filter Design
D-3 Quartz Crystals and Applications Room: Crystal M/N	1:30-2:30 2:30-3:30 3:30-4:30	<ul style="list-style-type: none"> • Vibrational Sensitivity and Phase Noise in Crystal Oscillators • Quartz-crystal Filters: A Review of Current Issues • Frequency Correlation of Quartz-crystal Resonators
D-4 Modulation Room: Crystal P/O	1:30-2:30 2:30-3:30 3:30-4:30	<ul style="list-style-type: none"> • New Method of Linear Amplitude Modulation • 4-GHz Multiplied Source for Digital Modulation • Techniques in Voice Compression and Synthesis

Exhibits Open 11:00 a.m. - 6:00 p.m.

R. Roberts, <i>Harris</i>
S. F. Russell, <i>Iowa State University</i>
Y. S. Rao, R. Asokan, and K. Reela, <i>Centre for Development of Telematics (India)</i>
P. Finman, <i>LCF Enterprises</i>
H. Direen, <i>ETO</i>
M. Abdollahian, R. J. Regan, S. J. Butler and R. J. Gage, <i>GTE Laboratories</i>
C. A. Erikson, Jr., <i>Oakmont Enterprises</i>
J. F. Bridges, <i>Argonne National Laboratory</i>
C. Hovater, <i>Continuous Electron Beam Accelerator Facility</i>
A. Schnase, <i>Forschungszentrum KFA Julich (FRG)</i>
J. Colotti, <i>CSD/Telephonics</i>
P. R. M. Correa (BRAZIL)
I. Novak, <i>Design Automation, Technical Univ of Budapest</i>
D. N. Haupt, <i>Erbtec</i>
P. F. Hamlyn, <i>ANZAC</i>
W. Lurie, <i>Consultant</i>
G. Kurzenknebe, <i>Piezo Crystal</i>
M. D. Howard and R. C. Smythe, <i>Piezo Technology</i>
B. Long, <i>Piezo Crystal</i>
L. Minggang, G. Liangcai, and Z. Suwen, <i>Wuhan University (PRC)</i>
D. Balusek, <i>Rockwell (Dallas)</i>
P. G. Beaty, <i>Erbtec</i>

THURSDAY, NOVEMBER 15

E-1 Noise Tutorial Room: Crystal K/L	8:30-11:30	<ul style="list-style-type: none"> • Noise Fundamentals
E-2 CAD and Simulation Room: Crystal E/F	8:30-9:30 9:30-10:30 10:30-11:30	<ul style="list-style-type: none"> • Spice Modeling and Simulation of an 800-MHz, Class-AB Push-pull Amplifier • Computer Programs Design and Optimize High-efficiency Switching-mode RF Power Amplifiers • A Quasi-linear Determination of UHF Power Device Operation from a Spice-simulated Nonlinear BJT Model
E-3 PLLs and Synthesizers II Room: Crystal M/N	8:30-9:30 9:30-10:30 10:30-11:30	<ul style="list-style-type: none"> • Designing with Direct Digital Frequency Synthesizers • Direct-digital Waveform Generation Using Advanced Multi-mode Digital Modulation • Optimum PLL Design for Low Phase-noise Performance
E-4 Test and Measurement Room: Crystal P/O	8:30-9:30 9:30-10:30 10:30-11:30	<ul style="list-style-type: none"> • Design and Development of an RF Data Acquisition System • Handheld Probing Techniques for RF-PCB and Hybrid-circuit Characterization • Using the VXI Bus for RF Test Equipment

Exhibits Open 10:00 a.m. - 2:00 p.m.

F. H. Perkins, Jr., and A. Ward, <i>RF Monolithics, AvanteK</i>
R. Y. LaLau, <i>Mobile Data</i>
N. O. Sokal and I. Novak, <i>Design Automation</i>
P. E. D'Anna, <i>MMD</i>
F. A. B. Cercas, A. A. Albuquerque, and M. Tomlinson, <i>Instituto Superior Tecnico (Portugal)</i>
B.G. Goldberg, <i>Sciteq</i>
S. Goldman, <i>E-Systems</i>
T. H. Jones and M. A. Belkerdid, <i>Univ of Central Florida</i>
Y. D. Kim, <i>Hewlett-Packard</i>
M. Levy, <i>Racal-Dana</i>



Look what's just surfaced!

If your microwave designs are moving to surface mount—or if your surface mount designs are approaching microwave speeds—California Eastern Labs has the NEC parts you need.

Discrete Bipolars. FETs. PIN, Schottky and Varactor Diodes. Prescalers. MMIC Amplifiers, PLL Frequency Synthesizers and Down Converters. And a variety of transistor arrays.

You get the quality and reliability you'd expect from the world's largest semiconductor manufacturer. And on-time delivery from CEL's local stock.

So call, write, or circle the number below and we'll send you a free *Surface Mount Product Selection Guide*.

NEC and CEL. It's a combination that works for you.

NEC

California Eastern Laboratories

CEL Headquarters, #590 Patrick Henry Drive, Santa Clara, CA 95054; (408) 988-3500 FAX (408) 988-0279 □ Santa Clara, CA (408) 988-7846 □ Los Angeles, CA (213) 645-0985
Bellevue, WA (206) 455-1101 □ Scottsdale, AZ (602) 945-1381 or 941-3927 □ Richardson, TX (214) 437-5487 □ Shawnee, KS (913) 962-2161 □ Burr Ridge, IL (708) 655-0089 □ Cockeysville, MD (301) 667-1310
Peabody, MA (508) 535-2885 □ Hackensack, NJ (201) 487-1155 or 487-1160 □ Palm Bay, FL (407) 727-8045 □ St. Petersburg, FL (813) 347-8066 □ Norcross, GA (404) 446-7300 □ Nepean, Ontario, Canada (613) 726-0626

©1990, California Eastern Laboratories

See us at the RF Expo East, Booth #407.

PRESENTATION BRIEFS



Dr. Frederick H. Raab



Vincent



Siwiak



Kizer



Kori

Program Chairman Welcome

I wish to take this opportunity to welcome you to the fifth annual RF Expo East.

The outstanding response to the "call for papers" enabled us to put together the largest RF Expo East with more technical papers than ever before. We also have more foreign participation than ever before. The technical papers cover receivers, transmitters, communications, and components at levels ranging from tutorial to new technology, and should provide something for everyone with interests in RF. In addition, the latest in equipment and components will be on display in the exhibit area.

The RF Expos serve the unique needs of our RF community. It has been both a pleasure and an honor to serve as your Program Chairman.

I also wish to thank the authors and session chairmen, as well as the staff of *RF Design* for their cooperation and assistance. All had to work under very tight schedules in order to have everything ready on time.

Frederick H. Raab
 Program Chairman

Editor's Comments

Many things have contributed to the building of this technical program. The hard work and enthusiasm of Program Chairman Fred Raab is first on the list. The desire of engineers around the world to participate in this unique forum was the best we've seen at any RF Expo, East or West. The willingness of session chairpersons to help evaluate papers and stay in contact with speakers is another major contribution. Finally, the entire engineering community, especially in Florida and the surrounding area, is to be congratulated for support and encouragement.

Gary A. Breed
 Editor, *RF Design*

**Tuesday, November 13 —
 8:30 to 11:30 a.m.**

Session A-1: Receivers I (Tutorial)
Chair: Peter Chadwick
Plessey Semiconductor
Room: Crystal Ballroom K/L

8:30 - Design of Receivers for Electronic Warfare
Sherman R. Vincent, Raytheon

The sophistication of radar and weapons guidance systems requires quick detection of possible threats at the earliest stage of a military mission. This tutorial provides a review of the characteristics of the five basic EW receiver architectures and a review of the basic analysis equations and calculations used by the EW receiver designer.

Sherman Vincent received his MSEE degree in Electrical Engineering from the University of California in 1976 and is currently section manager of Receiver Design at Raytheon.

Session A-2: Power Amplifiers
Chair: Steven J. Samay, Trontech
Room: Crystal Ballroom A/B

8:30 - VSWR Performance of Transistor RF Power Amplifiers
Richard W. Brounley
RF Engineering Consultant

The ability of an RF power amplifier to operate into a SWR depends upon a number of factors including the reflection coefficient, magnitude and phase, transistor power dissipation, and amplifier stability. These factors, along with protection methods, will be discussed with emphasis on applications which have severe VSWR requirements.

Richard W. Brounley is a full time RF engineering consultant specializing in the design of RF power amplifiers and associated equipment, with particular emphasis on integration with RF excited lasers.

9:30 - A Novel Technique for Analyzing High-Efficiency Switched-Mode Amplifiers
Kazimierz Siwiak, Motorola

A novel circuit analysis technique was developed for investigating the performance of high efficiency amplifiers operating in the switched mode. The analysis gives insight into the practical implementations of high efficiency RF amplifiers, particularly at high frequencies.

Kazimierz Siwiak is currently a Principal Staff Engineer in the Motorola Paging Division and an adjunct Faculty Staff Member in the State University System of Florida. He received his BSEE and MSEE from the Polytechnic Institute of Brooklyn.

10:30 - RF Power Transistors for 200 W Multicarrier Cellular Base Station
Korne Vennema, Philips Components

The new generation of cellular systems requires multi-channel amplifiers with a high

peak power capability. This paper describes the design and application of new common-emitter class-AB transistors with output power levels up to 200 W for 860-960 MHz base-station transmitters.

Session A-3: PLLs and Synthesizers I
Chair: Rob Gilmore, Qualcomm
Room: Crystal Ballroom M/N

8:30 - The "Approximation Method" of Frequency Synthesis
Albert D. Helfrick
Tel-Instrument Electronics Corp.

There is a method of frequency synthesis which uses a phase locked loop with a reference frequency significantly greater than the minimum frequency resolution. The improvement in resolution is achieved using a unique method of direct digital synthesis to vary the reference frequency of the phase locked loop by minute amounts.

Albert Helfrick is Director of Engineering at Tel-Instrument Electronics Corporation.

9:30 - Ten-Bit 350 MHz DAC for Direct Digital Synthesis
Perry Jordan, Analog Devices

A ten bit 300 MHz DAC has been tailored to the direct Digital Synthesis (DDS) Market. This DAC combined with a 300 MHz phase accumulator and the appropriate RAM will yield a complete DDS system.

10:30 - A Comparison of Techniques for Phase-Stability Measurement
Lisa M. Moder, Erbtac Engineering

Phase shift across a pulse in an amplifier offers a measurement challenge. This paper compares three techniques for making such a measurement.

Session A-4: Microwaves
Chair: R.M. Livingston
Rockwell International
Room: Crystal Ballroom P/Q

8:30 - System Design Considerations for Line-of-Sight Microwave Radio Transmission
George M. Kizer, Rockwell (Dallas)

This tutorial will focus on four major areas: System performance objectives, both national and international; Analog and digital radio transmitter/receiver performance characteristics; Site location considerations such as frequency planning and antenna charac-

PRESENTATION BRIEFS



Zavrel



Danaher



Boles



Osika



Deiss



Weber

teristics; and Path Considerations. Typical system allocation of performance degradations will also be discussed.

George Kizer earned his BSEE and MSEE degrees from Oklahoma State University and Iowa State University. He is currently a product manager in the Network Transmission Systems Division of Rockwell.

9:30 - Phase Shifter Based Upon Reflectively Terminated Multiport Coupler
M.H. Kori, Centre for Development of Telematics (India)

A reflection phase shifter, which is comprised of a reflection circuit and coupler, conventionally has the two parts designed separately. A comprehensive analysis which takes both units together reveals that the coupler also introduces phase error, making the design of a reflection phase shifter a delicate task of balancing the various parameters to obtain optimal performance.

M.H. Kori has worked for C-DOT since 1989 and is presently working as the Program Manager of the Digital Microwave Group. He received his B.E. from Mysore University, his M.E. from University of Roorkee and his Ph.D. from Indian Institute of Technology.

10:30 - Instrumentation for Radar Reflectivity Measurement

D.J. Kozakoff, C.W. Sirls, D.A. Thompson and R.S. Banks

Millimeter Wave Technology

This paper focuses on the design criteria implemented to develop a portable reflectometer instrument.

Tuesday, November 13 —

1:30 to 4:30 p.m.

Session B-1: Receivers II (Spread-Spectrum)

Chair: David Krautheimer, RHG Electronics
Room: Crystal Ballroom K/L

1:30 - Spread Spectrum with Digital Signal Processing

Robert J. Zavrel, Jr., Gwyn Edwards, and David Tahmassebi
Stanford Telecommunications

This paper will explain how several existing custom ASIC devices perform in spread spectrum systems. Although several SS techniques will be discussed, the direct sequence method is the most applicable to this design solution. Emphasis will be placed

on the fundamentals of SS, particularly relating to the RF link.

2:30 - GPS and GLONASS Spread-Spectrum Navigation Systems
James Danaher

Structured Systems & Software

The Soviet Global Navigation Satellite System (GLONASS) will provide highly accurate, world-wide position and timing information when the satellite constellation is complete in the mid-1990s. The operation of GLONASS, details of the GLONASS spread spectrum signal structure, comparison between GLONASS and GPS, and results of using GLONASS/GPS signals from satellites currently in orbit will be discussed.

Jim Danaher co-founded 3S in 1981, where he is Director, 3S Navigation. He has participated in development of GPS receivers since 1985 and currently leads 3S GPS/GLONASS receiver and simulator development.

3:30 - Detection and Sorting of Frequency-Hopped Signals

J. Eric Dunn and Steve F. Russell
Iowa State University

Frequency hopping modulation provides protection against accidental or intentional interference, detection, and signal interception. Advances in high speed digitizers and processors make feasible a digital system designed to detect and dehop or "sort" frequency hopping signals. A theoretical system is developed where signal detection is accomplished using a combination of wide and narrowband FFTs.

Session B-2: MMICS

Chair: Sheryl S. Johnson, Motorola
Room: Crystal Ballroom A/B

1:30 - Ku-band MMIC Transceiver for Mobile Satellite Communication
Rob Gilmore, Clarence Bruckner, and Doug Dunn, QUALCOMM

2:30 - Silicon MMICs: 35 dB - 35dBm - \$35
T.E. Boles, D. Osika, and M. Deiss
SGS-Thomson

The need for an inexpensive, easily constructed, high gain, medium power CW, power/gain block at frequencies approaching 1.0 GHz has been established within the RF and microwave industry. SGS-Thomson has developed a line of a combination of silicon MMICs with a discrete output device to

achieve the technical goals of 35 dB of RF gain and an output power level of +35dBm. This was accomplished while staying within the market driven cost goal of \$35.

Timothy Boles is Manager of the Silicon MMIC Engineering Department at SGS-Thomson Microelectronics. He has recently been working in the design and development of a number of silicon MMICs capable of application through 3 GHz. David Osika received his BSEE from Drexel University and works in the Silicon MMIC Department where his responsibilities are in device design, modeling, pilot wafer fabrication and packaging. Mark Deiss received his BS and MS degrees from Rensselaer Polytechnic Institute. He is a design engineer in the Silicon MMIC Department at SGS-Thomson.

3:30 - Some Design Considerations for L-Band Power MMICs

Robert J. Weber

ISU Microelectronics Research Center

Technology advances over the past decade have resulted in a large number of small signal MMICs becoming commercially available. It should also be possible to produce high power (>10 Watts) MMICs. However, several design constraints and tradeoffs concerning thermal limitations, chip size, available components, market, etc. are considerations whenever a power MMIC is considered.

Robert Weber received his BSEE, MSEE and Ph.D. in Electrical Engineering from Iowa State University. He is a member of various professional societies and has eight U.S. patents and three patents pending.

Session B-3: Filters

Chair: Maura Fox, Thomson-ICS
Room: Crystal Ballroom M/N

1:30 - Capabilities and Applications of SAW Coupled-Resonator Filters

Allan Coon

RF Monolithics

Problems associated with SAW Coupled Resonator filters are addressed with a practical selection guide of filter technologies in the VHF and UHF frequency ranges. Generalized guidelines are developed for the optimal selection of filter technology during system design. SAW CR filters are emphasized and compared with other filter technologies.

PRESENTATION BRIEFS



Janning



Dorsey



Roberts



Direen



Erikson



Bridges

2:30 - At Long Last; Modular, Digitally Tuned RF Filters as Easy as Amplifiers and Mixers

Eugene A. Janning, Pole-Zero

The design of a new family of digitally tuned bandpass filters covering 10 MHz to 1 GHz is discussed. These modular filters tune within a 3:1 frequency band in microseconds under full digital control. Their excellent selectivity and wide dynamic range make them ideally suited for receiver preselection, synthesizer postselection, or transmitter noise cleanup.

Eugene Janning received his BSEE from the University of Dayton and his MSEE from the University of Cincinnati. He co-founded Xetron Corporation and recently formed Pole/Zero Corporation.

3:30 - Narrow Band SAW Filters for IF Applications

B. Horine and S. Gopani, Sawtek

Because of the wide selection of narrow-band SAW techniques now available, the receiver design can flow smoothly from system requirements to choice of architecture and filter specifications. Several different typical receiver requirements will be discussed and SAW solutions developed for each. The factors which call for a SAW approach will be pointed out.

Session B-4: Antennas and Propagation

Chair: Alan Victor, Monicor Electronics
Room: Crystal Ballroom P/Q

1:30 - Large Loop Antennas

Robert P. Haviland, Mini Lab Instruments

This paper examines loop antennas of large size (one and two wavelength circumference) using various geometries and feed methods. Larger loops, arrays, and non-planar configurations are also discussed.

2:30 - VHF Multipath Propagation Causes and Cures

D.R. Dorsey, Jr., DocSoft Enterprises

This paper will explore the phenomenon of MultiPath Propagation at VHF frequencies and above. It will attempt to define the basic physical causes of multipath propagation and some of the means that may be used to overcome it on line-of-sight radio links. Special attention is paid to digital radio and land mobile radio systems.

Bob Dorsey is president and owner of DocSoft enterprises. He is currently a con-

sultant with Control Data Corporation at Edwards Air Force Base, CA for computer systems performance analysis at the Air Force Flight Test Center.

3:30 - Radio Frequency Identification Systems — Industrial and Commercial Applications

James Eagleson, Allen-Bradley Company

RF systems can avoid problems that can prevent proper operation of other methods of ID "tagging," such as bar codes: obstructions, distance, or environmental effects. Methods currently used to implement RFID systems are presented, including performance characteristics, advantages, and difficulties.

Wednesday, November 14 —

8:30 to 11:30 a.m.

Session C-1: Receivers III (Digital)

Chair: Madjid A. Belkerdid
Univ. of Central Florida
Room: Crystal Ballroom K/L

8:30 - IF Frequency-Response Considerations for the Digital Radio Environment
Richard Roberts, Harris Corp., and Mark A. Webster, Florida Inst. of Technology

This presentation includes a review of Nyquist filtering, eye patterns, and SER curves and their use in digital radio systems. Following this introduction, the relationships between IF bandpass performance and intersymbol interference are discussed, including effects of phase and amplitude, group delay, impulse response, and symmetry.

Richard Roberts is with the Government Communications Systems Division of Harris Corporation, where he works in the area of high data rate adaptive modems. He is currently a doctoral candidate doing research in adaptive algorithms for IF transversal filters.

9:30 - DSP Demodulation
Steve Russell and J. Eric Dunn
Iowa State University

Digital radio theory and techniques are becoming increasingly important due to the current design trends towards digital implementation of as many signal processing functions as practical. The basic design issues involved in choosing a digitization method will be presented and an important new technique called sigma-delta analog-to-digital converters will be described.

10:30 - A DSP PSK Modem for Satcom SPCPC Voice/Data

Y.S. Rao, R. Asokan, K. Reeta
C-DOT (India)

Narrowband DSP modems implemented at baseband frequencies pose problems with regards to adjacent channel and image rejection when upconverted and worked in the 52-88 MHz IF range for SPCPC applications. A hybrid approach is presented for implementation of the modulator directly at 45 MHz and brought to 52-88 MHz range and the demodulator through DSP at 20 kHz (Baseband frequency) after single down conversion.

R. Asokan has a BS in Physics from the University of Madras, India, and a B. Tech Degree in Electronics Engineering from Madras Institute of Technology. He presently works as a research engineer at C-DOT Telecom Research Centre, India.

Session C-2: Transmitters

Chair: Michael B. Steer, North Carolina State University
Room: Crystal Ballroom A/B

8:30 - High Efficiency, Low Distortion, RF Power Amplifier Using Adaptive Interference/Distortion Cancellation

Paul F. Finman, LCF Enterprises

Paul Finman is Technical Director for LCF Enterprises, where his work includes non-linear modeling and development of RF power amplifiers. He holds an S.B. in Physics from MIT, M.S., Engineers and Ph.D. EE degrees from Stanford University.

9:30 - Digital-Feedback Techniques for a Pulse-Width-Modulated RF Power Amplifier

Harry Direen

Erhorn Technological Operations

The output of an RF power supply will vary with load variations, AC line variations, duty cycle of pulse width modulation, temperature, and other factors. This paper presents a microprocessor based feedback loop that stabilizes the RF power output at any given level.

Harry Direen is a senior design engineer at Erhorn Technological Operations Inc., where his primary efforts are in the development of control systems for high power RF amplifiers. He is pursuing a doctorate in control systems engineering.

PRESENTATION BRIEFS



Hovater

Abbott

9:30 - RF Applications in Particle Accelerators
C. Hovater, R. Abbott, Continuous Electron Beam Accelerator Facility

Most particle accelerators, either for physics research or medical applications, use RF fields to accelerate the charged particles. This paper discusses RF control systems and the RF circuits employed by the various types of particle accelerators.

Curt Hovater is employed at the Continu-

ous Electron Beam Accelerator Facility (CEBAF) where he designs and implements the RF/IF controls for the superconducting accelerating cavities. Rich Abbott designs and builds RF components at CEBAF. Previously he was employed by the U.S. Navy as a nuclear reactor operator.

10:30 - A Fully Digital RF Synthesis and Phase Control for Acceleration in the Cooler Synchrotron COSY

10:30 - High-Frequency, High-Power Operation of Static Induction Transistors at Cryogenic Temperatures
 M. Abdollahian, R.J. Regan, S.J. Butler, and R.J. Gage
 GTE Laboratories

Session C-3: SAW Tutorial
 Chair: James Yolda
 U.S. Army Center for Signals Warfare
 Room: Crystal Ballroom M/N

8:30 - Surface Acoustic Wave (SAW) Technology
 C.A. Erikson, Jr.
 Oakmont Enterprises, Messiah College

This 3-hour tutorial provides an overview of the fascinating technology of surface acoustic wave devices. It is geared to a practical understanding of all aspects of SAW device design, fabrication and testing.

Carl Erikson is Assistant Professor of Engineering at Messiah College, helping to develop a new four year program leading to a Bachelor of Science in Engineering degree. He is also a consultant with Oakmont Enterprises.

Session C-4: RF Systems for Research in Particle Physics
 Chair: Otward Mueller
 General Electric Co.
 Room: Crystal Ballroom P/Q

8:30 - Overview of RF Systems for the Advanced Photon Source
 James F. Bridges
 Argonne National Laboratory

The Advanced Photon Source (APS) is a positron storage ring from which x-ray beams of energies up to hundreds of keV are emitted as the positrons pass through a series of magnets. The energy emitted as x-rays is replaced through a RF accelerating system operating at 352 MHz at a maximum power level of 3 MW. The RF system will be described as well as several lower-power systems at frequencies of 9.8 MHz, 117 MHz and 2.8 GHz.

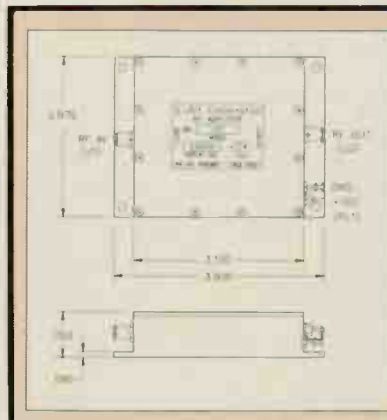
Jim Bridges is in the RF Group of the Advanced Photon Source Project at Argonne National Laboratory. He has worked on NMR devices, both for spectroscopy of solids and for NMR Imaging and holds a patent on RF resonators for whole body imaging systems.



High Dynamic Range Receiver Design Just Got Easier...

Q-bit presents the QB-101 Amplifier

Guaranteed 0°C to +50°C Performance



- IP₃ +55 dBm¹**
- IP₂ +110 dBm¹**
- Frequency Range 2-70 MHz
- DC Power +24 V/400 mA
- Output Power +31 dBm
- Noise Figure 4.5 dB
- Gain 21.9 ± 0.7 dB
- Flatness 0.5 dB p-p
- VSWR 1.5:1
- Reverse Isolation 31 dB
- Package Size 3.9" x 2.975" x 0.750"
- SFDR² 93 dB**
- DR³ 116 dB**

No matter how you calculate your dynamic range, Q-bit comes out on top! Come to us with your toughest RF amplifier requirements and we will work with you to solve them.

¹ Measurement limited by test equipment.
² Spurious Free Dynamic Range, SFDR = 2/3 * (174 + IP₃ - 10 * Log (BW) - NF - X - G)
 (Reference: "Microwave Transistor Amplifiers" by Guillermo Gonzalez).

³ Dynamic Range, DR = 174 + P_{1dB} - 10 * Log (BW) - NF - X - G
 (Reference: "Microwave Transistor Amplifiers" by Guillermo Gonzalez). x is the number of the dB above the noise floor, 3 dB used here. BW is the bandwidth, 1 MHz used here.



Q-BIT CORPORATION

2575 PACIFIC AVENUE NE, PALM BAY, FL 32905

TELEPHONE (407) 727-1838 ■ TWX (510) 959-6257 ■ FAX (407) 727-3729

PRESENTATION BRIEFS



Colotti



Correa



Haupt



Long



Zhang



Balusek

P. Shirkey, H. Meuth, and H. Rongen, Forschungszentrum KFA Julich

For carrier frequencies up to 2 MHz and maximum clock and sampling rates of about 40 MSPS, a fully digital real time RF signal synthesis, phase control and processing system is being designed for use on the new cooler synchrotron accelerator ring, COSY. Lacking present availability of integrated processors operating at such speeds, the required performance of this digital signal processing system will be achieved by a hardware programmed hybrid scheme, based on a binary integer algorithm.

**Wednesday, November 14 —
 1:30 to 4:30 p.m.**

Session D-1: Receivers IV (Applications)

**Chair: Mahesh Kumar, AEL
 Room: Crystal Ballroom K/L**

**1:30 - Dynamic Evaluation of High-Speed, High-Resolution D/A Convertors
 James Colotti, CSD/Telephonics**

While DAC applications are not limited to receiver design, in virtually all high speed/high resolution applications careful evaluation of candidates is required to assure that the appropriate device is selected. Although most manufacturers provide a comprehensive set of data, often the device will not be specified under the conditions called for in the application. However, dynamic D/A evaluation can uncover the necessary performance information under the appropriate conditions.

Jim Colotti is an Analog Design Engineer for the Communications department of the Command Systems Division of Telephonics. His design responsibilities are the analog sections of predominately digital communications systems.

**2:30 - TV Demodulator to Evaluate TV Transmission Quality
 P.R.M. Correa, LYS Electronic LTDA**

This work is based on the development of a synchronous demodulator for use in television service. Its main purpose is to obtain a demodulation of TV signals, which could assure all measurements, or the utilization of that signal in any other service. The principle goals were: high linearity, excellent frequency response, easy operation, group delay and low cost.

Paulo R. Correa received his engineering

degree from the Federal University of Rio de Janeiro. He is Development and Engineering Manager for Lys Electronic Ltd. where he works on the development of TV transmitters, FM transmitters and microwave links.

**3:30 - Digital Signal Processing Based Spectrum Monitoring System Used for the European Broadcasting Area
 Istvan Novak, Design Automation Technical University of Budapest**

This paper describes a spectrum monitoring system for the 0.1 to 30 MHz frequency range. The system is based on a high-performance, synthesizer tuned receiver and the digital signal processing (FFT) of its IF output signal. The built-in controller of the signal analyzer allows the user to operate part or all of the system according to predefined sequences.

Session D-2: Components

**Chair: Sam M. Richie
 University of Central Florida
 Room: Crystal Ballroom A/B**

1:30 - Impedance-Matching Transformers for RF Power Amplifiers

David N. Haupt, Erbtect Engineering

As RF power amplifiers proliferate, alternatives to the lumped element reactive matching networks traditionally used for small-signal amplifiers become necessary. Impedance matching transformers are an attractive alternative for many applications. Unfortunately, transformer behavior at RF, and especially transmission line transformers, are poorly understood topics to many designers.

David Haupt has been involved with RF in some fashion for 16 years, the last eight of them as a designer. He is pursuing a Masters degree in the Interdisciplinary Telecommunications program at the University of Colorado.

2:30 - Temperature-Compensating Attenuators

Perry F. Hamlyn, ANZAC

In RF systems design, one concern is performance over temperature, particularly in systems which have to perform over the military specified temperature range. This paper will describe the use of passive positive and negative coefficient thermistors in simple resistive networks to compensate for signal level variations over temperature.

3:30 - Useful Network Transformations in Filter Design

**William B. Lurie
 Consultant**

To get practical element values in filters, exact or approximate transformations, or equivalences, can be used to achieve realizable designs.

Session D-3: Quartz Crystals and Applications

**Chair: Murat Eron, Compact Software
 Room: Crystal Ballroom M/N**

1:30 - Vibrational Sensitivity and Phase Noise in Crystal Oscillators

**Glenn R. Kurzenknabe
 Piezo Crystal**

A growing concern in the radar, ECM and communications community is the effect of vibration on the phase noise of crystal oscillators as it degrades systems performance. This paper will review what phase noise is and why it is degraded with vibration.

2:30 - Quartz-Crystal Filters: A Review of Current Issues

**M.D. Howard and R.C. Smythe
 Piezo Technology**

This paper discusses some of the issues facing both users and manufacturers of crystals filters, including performance required for new applications, and special requirements for wide bandwidths, monolithic dual resonators, plus phase and amplitude matching.

Michael Howard is Manager of Filter and Subsystems Engineering with Piezo Technology. Robert Smythe is Senior Vice-President, Research and Engineering for Piezo Technology. He holds BA and MSEE degrees from Rice University and an MSE in EE from the University of Florida.

3:30 - Frequency Correlation of Quartz-Crystal Resonators

**Bruce Long
 Piezo Crystal**

Quartz Crystal resonators intended for oscillator applications must be specified for a specific oscillator load capacitance. Otherwise a considerable difference between the crystal frequency and the frequency of oscillation can occur. Crystal series and parallel resonance are discussed in terms of the resonator equivalent circuit as well as implications for oscillator design.

PRESENTATION BRIEFS



Beaty



Perkins



LaLau



Sokal



D'Anna



Cercas

Bruce Long has a BSEE and an MSEE from The Pennsylvania State University. He currently designs commercial, military, and space qualified RF products for Piezo Crystal Company.

Session D-4: Modulation

Chair: Brian D. May
 NASA Lewis Research Center
 Room: Crystal Ballroom P/Q

1:30 - New Method of Linear Amplitude Modulation

Li Minggang, Gan Linagcai and Zhang Suwen, Wuhan University (PRC)

Deriving from the conventional non-linear modulation method, this paper suggests a linear amplitude modulation method with mini-signals. This method exhibits a wide range of modulation. The analysis and the experiments show that the method can be applied to any oscillator.

S. Zhang is professor of the Department of Radio Information Engineering, Wuhan University, People's Republic of China. He has published several textbooks and has been engaged in teaching and scientific research in radio techniques since 1948. M. Li is a graduate student and L. Gan is associate professor in the Department of Radio Information Engineering.

2:30 - 4-GHz Multiplied Source for Digital Modulation

D. Balusek, Rockwell (Dallas)

This paper describes a multiplied 4 GHz source with very low microphonic susceptibility. This source is suitable for use in Digital Radio Systems using 64 Quadrature Amplitude Modulation. The design approach is described which includes the reference standard/fundamental frequency generation circuitry, step recovery diode multiplier circuit and the tunable pick-off filter for selecting the desired harmonic.

Danny Balusek is a Technical Staff Member in the Network Transmission Systems Division of Rockwell International. He has worked with a variety of analog and digital products with concentration on microwave frequency sources and related projects.

3:30 - Techniques in Voice Compression and Synthesis

Paul G. Beaty, Erbttec Engineering

There are several methods for compressing and synthesizing voice. The quality of speech which can be produced from these methods varies from being suitable for children's toys to being suitable for a telephone conversation. This paper discusses the implementation details of such methods. Emphasis will be placed on methods suitable for radio broadcast.

Paul Beaty is currently the Director of engineering at Erbttec Engineering in Boulder, Colorado. He has a Bachelors degree in Mathematics from the University of Colorado and is currently pursuing a Masters degree in Mathematics.

**Thursday, November 15 —
 8:30 to 11:30 a.m.**

Session E-1: Noise Tutorial

Chair: Michael J. Willis
 Georgia Tech Research Institute
 Room: Crystal Ballroom K/L

8:30 - Noise Fundamentals

Frank Perkins and Albert J. Ward III
 RF Monolithics/Avantek

This tutorial paper discusses the nature of RF noise and reviews the concepts of noise power, noise bandwidth, noise factor, noise figure, and noise temperature. Noise calculations for cascaded RF stages are reviewed in the context of RF system design. Noise measurement techniques are discussed along with facts that affect measurement accuracy.

Al Ward III is a microwave semiconductor applications engineer for Avantek. He received his BSEE from the University of Illinois in 1973.

Session E-2: CAD and Simulation

Chair: Mehdy Abdollahain
 GTE Laboratories
 Room: Crystal Ballroom E/F

8:30 - Spice Modeling and Simulation of an 800 MHz, Class-AB Push-Pull Amplifier
 R.Y. LaLau, Mobile Data

A design example of a Class-AB amplifier is used to illustrate the methodology and results of modeling RF amplifiers using SPICE and SPICE-based computer tools. Also presented is a comparison with measured results.

Richard LaLau is currently working as an RF Engineer with Mobil Data International. He received a Diploma of Technology from

British Columbia Institute of Technology and a B.A.Sc. in Electrical Engineering from Simon Fraser University.

9:30 - Computer Programs Design and Optimize High-Efficiency Switching-Mode (Class E) RF Power Amplifiers
 Nathan Sokal and Istvan Novak
 Design Automation

Single-ended switching-mode RF power amplifiers offer high efficiency, high reliability and low sensitivity but circuits are difficult to design accurately for wideband operation or when using non-ideal components. Complicated interactions among the many component parameters and design variables yield a set of nonlinear implicit design equations which can be solved only by computer.

Nathan Sokal is the founder of Design Automation, Inc., an electronics consulting company. He is a Member and Technical Adviser in RF power amplification, to the American Radio Relay League, and a member of Eta Kappa Nu and Sigma Xi honorary professional societies.

10:30 - A Quasi-linear Determination of UHF Power Device Operation From a Spice Simulated Nonlinear BJT Model
 P.E. D'Anna, MMD

Pablo D'Anna is the Director of Research and Development for Microwave Modules and Devices. He received his PhD and MS in Electrical Engineering from the university of California at Santa Barbara and his BSEE from the University of New Mexico.

Session E-3: PLLs and Synthesizers II

Chair: William A. Davis
 Virginia Polytechnic Institute
 Room: Crystal Ballroom M/N

8:30 - Designing With Direct Digital Frequency Synthesizers

F. Cercas, A. Albuquerque and M. Tomlinson, Institute Superior Tecnico (Portugal) and Plymouth Polytechnic (England)

A complete characterization of Direct Digital Frequency Synthesizers is made in both the time and frequency domain. As an application example of the derived expression for the power spectrum density with phase quantization, an extremely simple algorithm is described that sequentially computes the frequency and magnitude of each component and gives exactly the same result as an FFT.

PRESENTATION BRIEFS



Jones



Kim

Francisco Cercas is a lecturer/researcher in the Department of Electrical and Computer Engineering at the Instituto Superior Tecnico. He is currently working on his Ph.D. theses in the area of coding for spread spectrum communications via satellite with VSATs.

9:30 - Direct Digital Waveform Generation Using Advanced Multi-Mode Digital Modulation
B.G. Goldberg, Sciteq

This presentation defines an optimum waveform generation device, the performance of which has just been validated. In one square inch, it is a complete DDS (with DAC), that covers up to 10 MHz with -65dBc spurs, yet provides true digital AM, PM and FSK -while consuming a bit over one watt. This is a third generation DDS, and the first to include complete waveform manipulation capabilities and functionality.

Bar-Giora Goldberg earned his BSEE and MSEE at Israel's Technion and is currently Chief Scientist at Sciteq. He holds three frequency synthesis patents and has several others pending.

10:30 - Optimum PLL Design for Low Phase Noise Performance
Stan Goldman, E-Systems

Electronic warfare receivers, test instruments, and radar systems often require low phase noise performance from PLLs. In designing a PLL, the general practice has been to select damping factor and loop bandwidth for switching time. But, switching time design goals are different from low phase noise level design goals. Optimum damping factor and bandwidth goals for low phase noise PLL design will be determined.

Session E-4: Test and Measurement
Chair: Sara Mussman, Wavetek
Room: Crystal Ballroom P/Q

8:30 - Design and Development of an RF Data Acquisition System
Thomas H. Jones, Dynetics, and Madjid A Belkerid, University of Central Florida

The ability to quickly obtain accurate measurements of the scattering parameters of a device using an automatic network analyzer and S-parameter test set is a viable tool that should be of great value to the engineer. There are several limitations to using a network analyzer however. These

problems can be solved by developing a completely computer controlled data acquisition system.

Thomas Jones received his BSEE from Tennessee Technological University and his MS from the University of Central Florida. He is presently working for Dynetics Inc. doing research on mathematical modelling and analysis techniques for phased array radar antennas.

9:30 - Handheld Probing Techniques for RF PCB and Hybrid Circuit Characterization
Young Dae Kim, Hewlett-Packard

There are many traditional non-coaxial RF applications in which measurements need to be done quickly and simply by handheld probes but there hasn't been any commercial solution yet for these types of problems. This paper will address the issues related to handheld probing in RF network analysis

such as source of error, calibration, and practical performance limitations.

Young Dae Kim received his BSEE from Seoul National University, his MSEE from South Dakota State University and a PhD in EE from Stanford University. He is presently a Project Manager at Hewlett-Packard's Network Measurement Division.

10:30 - Using the VXIbus-Based Products for RF Test Systems
Malcolm Levy, Racal-Dana

RF testing is becoming more and more automated. New ATE standards such as the VXIbus are ideal for RF test systems as they allow the measurement devices, switches and interfaces to sit in one small compact unit. VXIbus RF chassis performance, RF modules for use in the chassis and interfaces suitable for test systems up to 18 GHz will be discussed.

A few good reasons to attend RF Expo West:

Communications Testing Testing of a Communications Satellite Repeater Interoperability Testing of FED-STD-1045 HF Radios	Power Amplifier Design RF Power Transistor Impedances: Myth and Truth High Power, High Voltage Static Induction Transistor Power Amplifier Class E Power Amplifier Design	Digital Techniques Embedded Microcontroller Applications for RF Data Collection Considerations for Analog Signals Modeling and Simulation of Microstrip Lines in High Speed ICs
Oscillators Comparison of VHF/UHF Sources Using Overtone AT and SC Cut Crystal Oscillators Simulation and Optimization of an 18.5 GHz DRO	RF Diode Tutorial Tutorial on the Schottky Diode Mixer The PIN Diode — A Tutorial A Low-Distortion PIN Diode Switch Using SMT Devices	High Power Amplifiers Solid State kW Linear Amplifier for 2-50 MHz 2.45 GHz Microwave Heater System
GaAs MMIC Tutorial 3-hour tutorial on circuits developed for applications under 3 GHz	Test Instrumentation Radiated Emissions Test Performance of the GHz TEM Cell High Power RF Calibration Using VXIbus Products for RF Test Systems	Modulation MSK Generation Using ILO Techniques Digital Cellular Modulation and Its Measurement QPSK Modulator in Thick Film at X-Band
Power Amplifier Performance Determination of M.T.T.F. for Microwave Transistors Synthesis of Test Signals for Linearity Testing	Microwave Amplifiers Low Phase Noise in a 10 kW L-Band Amplifier Solid State Amplifiers for V-Band Pulsed Response of a TWT	Frequency Synthesizers Timing Issues in Direct Digital Synthesis Interference Problems in Frequency Synthesizers Direct Digital Waveform Generation Using Advanced Multi-Mode Digital Modulation
Analysis and Simulation Improving Productivity With Design Tools Symbolic Circuit Analysis Generalize Modulation Mathematics Applied to RF/Microwave System Simulation	Filters SAW Filters With Low Loss for Mobile Radio Capabilities and Applications of SAW Coupled-Resonator Filters Linear Phase High Pass Digital Filter	Passive Circuits Flexible Construction Delay Lines X-Band 16-Way Radial Power Divider/Combiner

SPEAKERS AND CHAIRMEN

Dr. Mehdy Abdollahian
 GTE Laboratories Inc.
 40 Sylvan Road
 Waltham, MA 02254
 (617) 466-2438

R. Asokan
 C-DOT Telecom Research Centre
 Sneha Complex
 71/1 Miller Road
 Bangalore - 560 052
 India
 91-812-262890

Danny Balusek
 Rockwell International
 Network Transmission Systems
 Division
 P. O. Box 568842
 Dallas, TX 75356-8842
 (214) 996-5666

Paul G. Beaty
 Erbtex Engineering
 2760 29th Street
 Boulder, CO 80301
 (303) 447-8750

Dr. Madjid A. Belkerid
 Electrical Engineering Department
 University of Central Florida
 Orlando, FL 32816
 (407) 275-2318

Timothy E. Boles
 SGS-Thomson Microelectronics
 211 Commerce Drive
 Montgomeryville, PA 18936-1002
 (215) 362-8500

James F. Bridges
 Argonne National Laboratory
 9700 South Cass Avenue
 Argonne, IL 60439
 (708) 972-3966

Richard W. Brounley
 Brounley Engineering
 10341 Nicaron Court
 Largo, FL 34648-3415
 (813) 393-8177

Francisco A. B. Cercas
 Instituto Superior Tecnico
 Departamento de Engenharia
 Electrotecnica e de Computadores
 Av. Rovisco Pais 1
 1096 Lisboa Codex
 Portugal
 +351-1-802045 x 1450

Peter Chadwick
 Plessey Semiconductor
 Cheney Manor
 Swindon, Wiltshire SN2 2QW
 United Kingdom
 (44) 793-518080

James Colotti
 CSD/Telephonics
 815 Broad Hollow Road
 Farmingdale, NY 11735
 (516) 755-7352

Allan Coon
 RF Monolithics
 4441 Sigma Road
 Dallas, TX 75244
 (214) 233-2903

Paulo R. M. Correa
 R. Clarisse Indio do Brasil
 SIL 38, Apto 1404
 Rio de Janeiro RJ 22230
 Brazil

Dr. Paublo E. D'Anna
 Director of Research and
 Development
 Microwave Modules and Devices
 550 Ellis Street
 Mountain View, CA 94043
 (415) 961-1473

James Danaher
 Structured Systems
 23141 Plaza Pointe Dr.
 Laguna Hills, CA 92653-1425
 (714) 830-3777

Dr. William A. Davis
 Department of Electrical Engineering
 Virginia Polytech Institute
 and State University
 Blacksburg, VA 24061-0111
 (703) 231-6307

Harry Direen
 Erhorne Technological Operations
 4975 N. 30th St.
 Colorado Springs, CO 80919
 (719) 260-1191

Daniel R. (Bob) Dorsey, Jr.
 P. O. Box 2020
 Lancaster, CA 93534
 (408) 732-2912

J. Eric Dunn
 Department of Electrical and
 Computer Engineering
 Iowa State University
 Ames, IA 50011
 (515) 294-1273

James Eagleson
 W271 N732 Jill's Dr.
 Waukesha, WI 53188
 (414) 382-3929

Carl A. Erikson, Jr.
 Oakmont Enterprises
 P. O. Box 648
 Dillsburg, PA 17019
 (717) 432-1487

Dr. Murat Eron
 Compact Software
 483 McLean Blvd & Corner of
 18th Avenue
 Paterson, NJ 07054
 (201) 881-1200

Paul F. Finman
 LCF Enterprises
 621 Barrington Court
 Newbury Park, CA 91320-5117
 (805) 388-8454

Maura Fox
 Thomson-ICS
 P. O. Box 1088
 Southwick, MA 01077
 (203) 651-0211

Rob Gilmore
 QUALCOMM, Inc.
 10555 Sorrento Valley Road
 San Diego, CA 92121-1617
 (619) 587-1121 x151

Bar-Giora Goldberg
 Sciteq Electronics
 8401 Aero Drive
 San Diego, CA 92123
 (619) 292-0500

Stan Goldman
 E-Systems
 12705 Montfort
 Dallas, TX 75230
 (214) 272-0515 x3448

Perry F. Hamlyn
 ANZAC, A Division of Adams-Russell
 80 Cambridge Street
 Burlington, MA 01803
 (617) 273-3333

David N. Haupt
 Erbtex Engineering
 2760 29th Street
 Boulder, CO 80301
 (303) 447-8750

Robert P. Haviland
 Mini Lab Instruments
 1035 Green Acres Circle North
 Daytona Beach, FL 32019

Albert D. Helfrick
 Consulting Engineer
 5 Banta Road
 Kinnelon, NJ 07405
 (201) 933-1600

B. Horine
 Sawtek, Inc.
 P. O. Box 609501
 Orlando, FL 32860-9501
 (407) 886-8860

Curt Hovater
 Continuous Electron Beam
 Accelerator Facility
 12000 Jefferson Avenue
 Newport News, VA 23606
 (804) 249-7100

Mike Howard
 Piezo Technology
 2525 Shader Road
 P. O. Box 549049
 Orlando, FL 32854-7859
 (407) 298-2000

Eugene A. Janning
 Pole-Zero Corporation
 P. O. Box 43369
 4280 Willow Hills Lane
 Cincinnati, OH 45243
 (513) 271-3119

Sheryl Johnson
 Product Development and
 Applications Engineer
 Motorola, Inc.
 RF & Optoelectronics Products
 Division, MD B320
 5005 East McDowell Road
 Phoenix, AZ 85008
 (602) 244-4172

Thomas H. Jones
 Electrical Engineering Department
 University of Central Florida
 Orlando, FL 32816
 (407) 275-2318

Perry Jordan
 Analog Devices
 7910 Triad Center Drive
 Greensboro, NC 27409-9605
 (919) 668-9511

Young Dae Kim
 Hewlett-Packard Company
 Network Measurement Division
 1400 Fountain Grove Parkway
 Santa Rosa, CA 95403
 (707) 577-4951

George M. Kizer
 Rockwell International
 Network Transmission Systems
 Division
 P. O. Box 568842
 Dallas, TX 75356-8842
 (214) 996-2822

M. H. Kori
 Centre for Development of Telematics
 C-DOT
 Shena Complex
 71/1 Miller Road
 Bangalore 560 052
 India
 (91) 812-263399

D. J. Kozakov
 Millimeter Wave Technology
 Building 700
 1395 Marietta Parkway
 Marietta, GA 30067
 (404) 425-9382

David Krautheimer
 RHG Electronics Laboratory
 161 E. Industry Court
 Deer Park, NY 11729
 (516) 242-1100

Mahesh Kumar
 American Electronic Laboratories, Inc.
 305 Richardson Road
 Lansdale, PA 19446-1429
 (215) 822-2929 x2839

Glenn Kurzenknabe
 Piezo Crystal Company
 100 K Street
 P. O. Box 619
 Carlisle, PA 17013
 (717) 249-2151

Richard Y. LaLau
 Mobile Data International
 11411 Number Five Road
 Richmond, BC V7A 4Z3
 Canada
 (604) 277-1511

Li Minggang
 Department of Radio Information
 Engineering
 Wuhan University
 Wuchang, Hubei
 People's Republic of China

Malcolm Levy
 Racal-Dana Instruments, Inc.
 4 Goodyear Street
 Irvine, CA 92718
 (714) 859-8999

Robert M. Livingston
 Rockwell International
 Network Transmission Systems
 Division

SPEAKERS AND CHAIRMEN

P. O. Box 568842
 Dallas, TX 75356-8842
 (214) 996-7573

Bruce Long
 Piezo Crystal Company
 100 K Street
 P. O. Box 619
 Carlisle, PA 17013
 (717) 249-2151

William B. Lurie
 Consultant
 8503 Heather Place
 Boynton Beach, FL 33437
 (407) 369-3218

Brian D. May
 NASA LeRC
 21000 Brookpark Road, MS 54-6
 Cleveland, OH 44135
 (216) 433-3573

Dr. Hermann Meuth
 (COSY PL-TPL 19)
 IKP
 KF Julich
 Postfach 1913
 D-5170 Juelich 1
 Federal Republic of Germany
 (49) 2461-61-4739

Lisa M. Moder
 Erbtex Engineering
 2760 29th Street

Boulder, CO 80301
 (303) 447-8750

Dr. Ottward Mueller
 General Electric Company
 Corporate Research & Development
 NMR Building
 P. O. Box 8
 Schnectady, NY 12301
 (518)-387-5064

Sara Mussman
 317-788-9351
 Wavetek
 5808 Churchman Bypass
 Indianapolis, IN 46203-6109
 (317) 788-9351

Istvan Novak
 Design Automation, Inc.
 809 Massachusetts Avenue
 Lexington, MA 02173
 (617) 862-8998

David Osika
 SGS-Thomson Microelectronics
 211 Commerce Drive
 Montgomeryville, PA 18936
 (215) 362-8500

Frank Perkins
 RF Monolithics
 4441 Sigma Road
 Dallas, TX 75244
 (214) 233-2903

Dr. Frederick H. Raab
 Green Mountain Radio Research
 Company
 50 Vermont Avenue, Fort Ethan Allen
 Colchester, VT 05446
 (802) 655-9670

Y. S. Rao
 Centre for Development of Telematics
 C-DOT
 Shena Complex
 71/1 Miller Road
 Bangalore 560 052
 India
 (91) 812-27890

Dr. Sam M. Richie
 Assistant Professor
 Electrical Engineering Department
 University of Central Florida
 Orlando, FL 32816
 (407) 275-2786

Richard D. Roberts
 1586 Norman St. NE
 Palm Bay, FL 32907
 (407) 729-7957

Dr. Steven F. Russell
 Department of Electrical and
 Computer Engineering
 Iowa State University
 Ames, IA 50011
 (515) 294-1273

Stephen J. Samay
 Trontech Corporation
 63 Shark River Road
 Neptune, NJ 07753
 (201) 922-8585

Alexander Schnase
 (COSY PL-TPL 19)
 IKP
 K F Julich
 Post fach 1913
 D-5170 Juelich 1
 Federal Republic of Germany
 (49) 2461-61-4739

Kazimier Siwiak
 Motorola, Inc.
 10958 NW 14th Street
 Coral Springs, FL 33071
 (407) 364-3443

Nathan O. Sokal
 Design Automation, Inc.
 809 Massachusetts Avenue
 Lexington, MA 02173
 (617) 862-8998

Dr. Michael B. Steer
 Department of Electrical Engineering
 North Carolina State University
 Box 7911
 Raleigh, NC 27695-7911
 (919) 737-2336

Korne Vennema
 c/o Michel Pradille
 Phillips Components
 45 George Washington Highway
 Smithfield, RI 02917
 (401) 232-0500

Alan Victor
 Monicor Electronics Corp.
 2964 Northwest 60th Street
 Ft. Lauderdale, FL 33309
 (305) 979-1907

Sherman R. Vincent, Manager
 Receiver Design and
 Development
 Raytheon Company
 Electromagnetic Systems
 Division
 Goleta, CA 93117-3197
 (805) 967-5511

Al Ward
 AvanteK
 101 W. Renner Road
 Suite 180
 Richardson, TX 75080
 (214) 437-5694

Dr. Robert J. Weber
 ISU Microelectronics Research Center
 1925 Scholl Road
 Ames, IA 50011
 (515) 294-7763

Michael J. Willis
 Georgia Tech Research Institute
 Atlanta, GA 30332
 (404) 894-7146

James Yolda
 U. S. Army Center for Signals Warfare
 ATTN: AMSEL-RD-SW-TRE
 Vint Hill Farms Station
 Warrenton, VA 22186-5100
 (703) 349-7313

R. J. Zavrel, Jr.
 Stanford Telecom
 2421 Mission College Blvd.
 Santa Clara, CA 95054
 (408) 748-1010

Zhang, Suwen
 Department of Radio Information
 Engineering
 Wuhan University
 Wuchang, Hubei 430072

**Why engineers have
 relied on TTE filters for
 over 35 years**

- Over 1,239,580 standard filters
- Custom designs at stock filter prices
- 10 day shipment guaranteed
- 72 hour prototype service is available
- Unconditional factory guarantee

Got a problem? Call our Engineering Hotline.

(206) 821-8779



TTE®

America's Filter Specialist

TTE, Inc.
 Kirkland, WA

(206) 821-5952
 FAX: (206) 821-0992

EXHIBITOR LIST

Adams Russell (A M/A-COM Company)

5 Omni Way-Bldg. 22
 Chelmsford MA 01824
 617-272-3000

Booth: 315,317

Products: IF/RF/Microwave and millimeter wave; connectors & adaptors, cable assemblies, semiconductors, devices, switches, mixers, low noise amplifiers, and transistors. Custom and standards products available in all categories.

Advantest America, Inc.

300 Knightsbridge Pkwy.
 Lincolnshire IL 60069

708-634-2552

Booth: 609

Products: RF spectrum analyzers, microwave spectrum analyzer and RF network analyzer.

AEL Defense Corp.

305 Richardson Road
 Lansdale PA 19446

215-822-2929

Booth: 311

Products: AEL manufactures custom hybrid/microwave components with expertise in engineering capabilities straight through to high quality manufacturing.

Alan Industries, Inc.

745 Greenway Drive P.O. Box 1203
 Columbus IN 47201

812-372-8869

Booth: 517

Products: Attenuators: programmable, continuously variable, rotary, fixed cam actuated, toggle switch, rocker switch, push button; also terminations, directional couplers, RF fuses, resistive dividers, impedance matching pads.

Alessi Inc.

35 Parker
 Irvine CA 92718

714-830-0660

Booth: 525

Products: Manual and automatic microwave probe stations for on-wafer measurements. Adaptable to all brands of microwave probes.

American Technical Ceramics Corp.

One Norden Lane
 Huntington Station NY 11746-2102

516-547-5700

Booth: 418

Products: ATC manufactures RF/microwave multilayer and single layer high performance capacitors for critical applications around the world.

Amphenol RF/Microwave Operations

One Kennedy Avenue
 Danbury CT 06810

203-743-9272

Booth: 601

Products: RF/microwave coaxial, twinaxial, triaxial connectors and cable assemblies.

Amplifier Research

160 School House Road
 Souderton PA 18964-9990

215-723-8181

Booth: 504,506

Products: Broadband, high power amplifiers and accessories for general RF and RFI susceptibility testing. Amplifiers from 10 kHz to 1000 MHz frequency range and 1 to 10,000 watt power output. Accessories include TEM cells, antennas, field-strength monitors and leveling pre-amplifiers.

Analog Devices, Inc.

One Technology Way
 Norwood MA 02062

617-329-4700

Booth: 610

Products: A/D, D/A converters, op amps, references, sample/hold amplifiers, switches, multiplexers, instrumentation and isolation amplifiers, comparators, log/anti-log amplifiers, digital signal processors, special function components.

Anritsu America, Inc.

15 Thornton Road
 Oakland NJ 07436

201-337-1111

Booth: 123

Products: RF and microwave spectrum analyzers.

Anzac (A M/A-COM Company)

5 Omni Way-Bldg. 22
 Chelmsford MA 01824

617-272-3000

Booth: 315,317

Products: IF/RF/microwave and millimeter wave, connectors & adaptors, cable assemblies, semiconductors, devices, switches, mixers, low noise amplifiers, and transistors. Custom and standards products available in all categories.

Apex Systems

2400 Central Ave. Suite A
 Boulder CO 80301

303-443-3393

Booth: 303

Products: Apex Systems is a design engineering consulting firm specializing in the fields of RF design, low power digital communications, and microprocessor based control systems.

Applied Engineering Products

P.O. Box 510
 New Haven CT 06513

203-776-2813

Booth: 419

Products: Subminiature coaxial connectors in series SMA, SMB, SMC (MIL-C-39012); 7000 series (SSMB) microminiature connectors; flexible and semi-rigid cable assemblies.

Applied Specialties Inc.

10101 F Bacon Drive
 Beltsville MD 20705

301-595-5395

Booth: 620

Products: Semi-rigid bending tools, coaxial connectors.

Avantek, Inc.

481 Cottonwood Drive
 Milpitas CA 95035

408-432-3080

Booth: 417

Products: High-frequency ICs, RF and microwave products including transistors, MMIC amplifiers and frequency converters for spread spectrum, DBS, fiber-optic and other communications applications.

Bipolarics Inc.

108 Albright Way
 Los Gatos Business Park

Los Gatos CA 95030

408-438-0806

Booth: 121

Products: High performance silicon bipolar products (to 15 GHz): low noise/small signal/medium power transistors, RF ICs, MMICs, semicustom, full custom, and foundry service.

Boonton Electronics Corporation

791 Route 10 East
 Randolph NJ 07869

201-584-1077

Booth: 423

Products: B.E.C. designs and manufactures RF, microwave and impedance test measuring instruments including power meters, voltmeters, capacitance and inductance measuring instruments, audio oscillators and analyzers, distortion analyzers, modulation meters and analyzers, signal generators and calibrators.

Brennan Associates

211 Ewing Ave.
 Clearwater FL 34616

800-365-5006

Booth: 115,117

Products: Manufacturers representatives for components and systems companies from DC to daylight: amps, attenuators, couplers, crystal devices, enclosures, filters, hybrids, mixers, oscillators, splitters, switches, and test gear.

BTI

150 Mill St.
 Carleton Place, Ontario, Canada

K7C3P3

613-257-7131

Booth: 115, 117

Products: Microstrip integrated thin film devices on "feather-weight" soft flexible substrates: power divider/combiners, directional couplers, 90° hybrids, and networks. To millimeter wave frequencies, from 1/4 gram up.

Burr-Brown

6730 S. Tucson Blvd.
 Tucson AZ 85706

602-746-1111

Booth: 104

Products: High performance, high accuracy data converters and ADC test systems including new ADC614 5MHz, 14-bit sampling A/D converter featuring 85dB SFDR and 78dB SNR.

BWS Microwave Marketing

1290 Highway A1A Suite 206
 Satellite Beach FL 32937

407-773-6170

Booth: 101, 103

Products: Consulting firm specializing in RF and microwave components sub-systems DC up to 50 Ghz.

California Eastern Labs

4590 Patrick Henry Drive
 Santa Clara CA 95054

408-988-3500

Booth: 407

Products: Exclusive North American agent for NEC microwave and RF semiconductors, including: small signal & power bipolars, low noise & power FETs, GaAs & silicon prescalers, GaAs & silicon MMICs, GaAs & silicon ICs, diodes and surface mount devices.

Ceramic Devices, Inc.

8145 Ronson Road
 San Diego CA 92111

619-560-7575

Booth: 106

Products: EMI/RFI filters and feed thru capacitors. QPL supplier to MIL-F-28861 and MIL-F-15733. "S" level screening available.

Compac Development Corp.

1320-13 Lincoln Ave.
 Holbrook NY 11741

516-585-3400

Booth: 510

Products: RF/EMI shielded enclosures standard and custom-500 sizes off-the-shelf with attenuation greater than 80 dB at 20 GHz in the new SRF series. Gasketing, attenuators, and RF connectors.

Complex Corporation

238 Taunton Blvd.
 Medford NJ 08055

609-596-9388

Booth: 606

Products: Single layer ceramic parallel plate microwave chip capacitors. Gold or tin metalization. Split electrode, binary, arrays and custom electrode configuration available in Class I and II dielectrics.

Component Distributors Inc.

312 S. Harbor City Blvd. #3
 Melbourne FL 32901

407-724-9910

Booth: 126

Products: Distributors for RF/microwave products including Avantek, Coiltronics, Comlinear, Crystek, E.F. Johnson, K & L Microwave, Mini-Circuits, Monitor Products, Precision Tube, Schaffner, Telstone, Aires, Virginia Plastics, Zenith.

Cougar Components

2225-K Martin Avenue
 Santa Clara CA 95050

408-492-1400

Booth: 115,117

Products: Cascadable intermediate frequency amps from DC to 3 GHz in TO-8 or connectorized packages, volt-

EXHIBITOR LIST

age controlled attenuators, automatic gain controllers, and limiting amps.

CTS Corporation-Frequency Control Div.
 400 Reimann Ave.
 Sandwich IL 60548
 815-786-8411
 Booth: 323
 Products: Manufacturer of Knights® crystals and oscillators. Crystals, clock oscillators, TCXO's, VCXO's and OCXO's. Contractual surface mount assembly services.

DB Products
 253 N. Vinedo Ave.
 Pasadena CA 91107
 818-449-3790
 Booth: 115,117
 Products: Manufacturers a wide variety of coaxial microwave switches from DC to 18 GHz. Custom applications are welcome. Price and delivery are very competitive.

Dynawave Inc.
 94 Searle St.
 Georgetown MA 01833
 508-352-7800
 Booth: 101,103
 Products: Connectors. SMA, SSMA, field replaceable MIC packages, blindmate connectors, adapters, interconnect components.

Eagleware/Circuit Busters
 1750 Mountain Glen
 Stone Mountain GA 30087
 404-923-9999
 Booth: 213
 Products: RF/microwave engineering software for standard IBM PC and compatible computers. Demonstrated is a family of high-speed simulators and synthesis software.

EDSI
 320 Riggs Ave.
 Melbourne Beach FL 32951
 407-952-1240
 Booth: 321
 Products: Manufacturers representative, representing RF and microwave companies. Telecommunications.

EEsof, Inc.
 5601 Lindero Canyon Road
 Westlake Village CA 90291-4020
 818-991-7530
 Booth: 404,406
 Products: Software for linear/nonlinear circuit and system simulation; electromagnetic circuit and structure simulation; filter design and network synthesis; CAE; and layout tools for high-frequency printed circuit boards, hybrids, MICs and MMICs.

Ehrhorn Technological Operations, Inc. (ETO)
 4975 N. 30th St.
 Colorado Springs CO 80919
 719-260-1191
 Booth: 514
 Products: RF power supplies and amplifiers: ETO has supplied RF power solutions to the industrial, medical and

communications marketplace for over 20 years. ETO specializes in cost-effective solutions for your total RF system needs to 20 kW and 200 MHz.

ENI
 100 Highpower Road
 Rochester NY 14623
 716-427-8300
 Booth: 422
 Products: Unconditionally stable solid state RF power amplifiers, 9 KHz to 1 GHz, 1-5 KW.

Erbtec Engineering, Inc.
 2760 29th Street
 Boulder CO 80301
 303-447-8750
 Booth: 110
 Products: 20 KW, 64 MHz, linear, pulsed amplifier used in magnetic resonance imaging (MRI) applications. Features include: longer RF pulse capability, high reliability and internal diagnostics.

Florida RF Labs
 P.O. Box 2643
 Stuart FL 34995
 407-286-9300
 Booth: 608
 Products: Custom RF cable assemblies. Resistor products: flange & pill termination, high power chip & power termination.

GEC Plessey Semiconductors
 1500 Greenhills Road
 Scotts Valley CA 95066
 408-438-2900
 Booth: 111,113
 Products: Radio frequency (RF) products with communication applications in cellular radio, pagers, military radios and satellite/cable/TV.

Gentry Electronics & Instrumentation Inc.
 2447 Orlando Central Parkway
 Orlando FL 32809
 407-859-7450
 Booth: 525
 Products: Manufacturers representatives for general purpose and RF and microwave test equipment and RF and microwave components.

Harris Semiconductor
 P.O. Box 883
 Melbourne FL 32902
 1-800-4-HARRIS
 Booth: 318,320
 Products: Integrated circuits and discrete semiconductors covering analog, digital, power, military, custom and semicustom requirements for signal processing and power control applications.

Hewlett-Packard Company
 1400 Fountaingrove Parkway
 Santa Rosa CA 95403
 707-577-4749
 Booth: 410,412,414,416
 Products: 5 Hz to 500 MHz high performance vector network analyzer. 5 Hz to 500 MHz network/spectrum/impedance/impedance analyzer. Fully

integrated 75 ohm RF network analyzer. RF antenna measurement software. High frequency linear and non-linear circuit design and simulation software includes schematic entry, artwork generation and documentation utilities. Three-dimensional simulator for RF structures.

Huber & Suhner Inc.
 One Allen Martin Drive P.O. Box 400
 Essex VT 05451
 802-878-0555
 Booth: 119
 Products: Complete line of RF coaxial connectors: "sucoflex" high performance microwave cable assemblies; microwave components; lightning and nuclear EMP protectors.

IFR Systems, Inc.
 10200 W. York St.
 Wichita KS 67215
 316-522-4981
 Booth: 421
 Products: Manufacturer of communications service monitors and spectrum analyzers.

Instruments for Industry, Inc.
 731 Union Parkway
 Ronkonkoma NY 11779
 516-467-8400
 Booth: 218
 Products: EMI/RFI test equipment including, high power amplifiers, leveling preamplifiers, E-field sensors, TEM cells, E-field generating antennas, testing software and anechoic chambers.

Insulated Wire Inc.
 P.O. Box 37
 Long Island MacArthur Airport
 Ronkonkoma NY 11779
 516-981-7424
 Booth: 101,103
 Products: Microwave high performance cable and assemblies.

Integrated Microwave Corporation
 3422 Tripp Court
 San Diego CA 92121-1009
 619-259-2600
 Booth: 112
 Products: Integrated Microwave designs and manufactures RF/IF microwave filters, multiplexers and integrated subsystems in the DC to 26.5 GHz frequency range.

Inter-Continental Microwave
 2370-B Walsh Ave.
 Santa Clara CA 95051
 408-727-1596
 Booth: 525
 Products: Microwave test fixtures for chip or packaged devices, MMICs, and multi-port circuits. De-embedding with TRL, LRL, and TOSL calibration methods.

ITT Seallectro
 585 E. Main St.
 New Britain CT 06320
 203-223-2700
 Booth: 612
 Products: Manufacturer of RF and microwave coaxial connectors and

cable assemblies including SMA, SMB/SMC, slide-on SSMB/SSMC, precision N & TNC, K, solderless, adaptors and special configurations.

JCA Technology
 3529 Old Conejo Rd. #118
 Newbury Park CA 91320
 805-498-6794
 Booth: 115,117
 Products: Manufacturer of high quality thin film hybrid microwave amplifiers, switches and subassemblies for the defense and communications market. Custom requirement easily and quickly accommodated.

JFW Industries Inc.
 5134 Commerce Square Drive
 Indianapolis IN 46237
 317-887-1340
 Booth: 618
 Products: Fixed, rotary, pushbutton and programmable attenuators. Thick film microstrip attenuators and terminations. Detectors. Matching pads and RF switches.

John Fluke Mfg. Co. Inc.
 P.O. Box 9090 6920 Seaway Blvd.
 Everett WA 98206
 206-347-6100
 Booth: 611,613
 Products: Test and measurement equipment, including a full line of high purity and general purpose RF signal generators, frequency counters, and digital storage oscilloscopes covering the frequency spectrum up to 2,000 MHz.

LCF Enterprises
 651 Via Alondra #710
 Camarillo CA 93010
 805-388-8454
 Booth: 605
 Products: High power RF amplifiers covering frequencies between 2 MHz-2 GHz with powers between 1W-1KW. High efficiency and small size. High dynamic range. Customization available.

Lindgren RF Enclosures
 400 High Grove Blvd.
 Glendale Heights IL 60139
 708-307-7200
 Booth: 115,117
 Products: EMI/RFI shielding systems and accessories: screen rooms, shield rooms, MRI, TEMPEST, and tabletop systems. Modular, demountable, lightweight enclosures, feedthru line filters and shielding integrity monitors.

Loral Microwave-FSI Semiconductor
 16 Maple Road
 Chelmsford MA 01824
 508-256-4113
 Booth: 309
 Products: Silicon abrupt junction tuning varactors, VHF/UHF tuning varactors, frequency linear tuning varactors, GaAs tuning varactors, PIN and NIP diodes, limiter diodes, mesa and planar beam leads, UHF/VHF PIN diodes, chip capacitors, planar spiral inductors, step recovery diodes, har-

EXHIBITOR LIST

monic generator varactors, multi-chip high power generator varactors, noise diodes, power generation, multiplier varactors.

M/A-COM

5 Omni Way-Bldg. 22
 Chelmsford MA 01824
 617-272-3000
 Booth: 315,317

Products: IF/RF/microwave and millimeterwave; connectors & adaptors, cable assemblies, semiconductors, devices, switches, mixers, low noise amplifiers, and transistors. Custom and standards products available in all categories.

M/A-COM Passive Microwave Div.

21 Continental Boulevard
 Merrimack NH 03054
 Booth: 608

Products: Coaxial attenuators, terminations, detectors, couplers, power dividers & switches.

Marconi Instruments

3 Pearl Court
 Allendale NJ 07401
 201-934-9050
 Booth: 212,214

Products: RF signal generators and sweepers, spectrum analyzers, microwave sweepers, scalars, power meters, counters and the 6580 transmission line measurement system.

Marubeni International Electronics

20 William St.
 Wellesley MA 02181
 617-237-2115
 Booth: 521

Products: EMSCAN-a computer aided EMI scanning engineering test tool used to map the RFI noise on EGA color monitor and store as DOS text files.

Megacity Tool & Die

349 Progress Road
 Dayton OH 45449
 513-859-8251
 Booth: 321

Products: MIL 45208, large & short run stampings. Tools, dies, jigs and fixtures.

Merrimac Industries, Inc.

41 Fairfield Place
 West Caldwell NJ 07007
 201-575-1300
 Booth: 304,306

Products: IF & microwave devices, components, and subsystems; using lumped element and stripline designs, power amplifiers, IF integrated assemblies and Hi-Rel networks.

Micro-Dynamics Inc.

10 Sonur Dr.
 Woburn MA 01801
 617-729-9450
 Booth: 101, 103

Products: PIN-diode control devices of passive TR limiters, switches, integrated microwave subsystems, digital attenuators, coaxial high power limiters, passive TR limiters.

Microlab/FXR

10 Microlab Road
 Livingston NJ 07039
 201-992-7700
 Booth: 115,117

Products: Complete line of passive components for ECM, radars and fire control equipment. Specialties include high power waveguide, coax and tubular filters, multiplexors, and diplexors.

Micronetics Inc.

26 Hampshire Drive
 Hudson NH 03051
 603-883-2900
 Booth: 226

Products: Micronetics, Inc. is an established U.S. supplier of RF and microwave components to the defense and communications industries for over 15 years. The products of our three divisions include noise sources, waveguide and coaxial switches and terminations, semiconductor control components and a wide range of custom integrated circuits operating in 10 MHz to 94 GHz frequency range.

Micronics Technology Inc.

7 Alexander Place
 Glen Cove NY 11542
 516-759-5600
 Booth: 321

Products: Synthesizers, oscillators and custom sub-systems.

Microwave Components, Inc.

3171 S.E. Dominica Terrace
 Stuart FL 34997
 407-286-4455
 Booth: 608

Products: Florida RF Labs' custom RF cable assemblies, delay lines, and resistive products. M/A-COM Omni Spectra's RF connectors, attenuators, couplers, power dividers, detectors and coaxial terminations.

Microwave Engineering Corp.

1429 Osgood St.
 North Andover MA 01845
 508-685-2776
 Booth: 321

Products: Rectangular, double ridge, flexible & rigid custom waveguide and assemblies.

Microwave Marketing Inc.

7530 Citrus Ave.
 Winter Park FL 32769
 407-678-2141
 Booth: 211

Products: Manufacturer's representative with emphasis in the RF components arena. RF oscillators, crystal control devices, ceramic materials, filters, amplifiers.

Millimeter Wave Technology Inc.

1395 S. Marietta Pkwy. Bldg. 700
 Marietta GA 30067
 404-425-9382
 Booth: 313

Products: The portable reflectometer is a frequency tunable instrument for measuring the RF reflectivity of radar absorbing material. The instrument consists of the base unit and handheld

guns and covers all frequency bands from 2 GHz to 95 GHz.

Motorola Discrete & Materials Technology Group

5005 East McDowell Road
 Phoenix AZ 85008
 602-244-3818
 Booth: 102,201,200,202

Products: RF bipolar and FET transistors designed to supply up to 600 watts output power at frequencies from 2 MHz to 4 GHz. Wide-band linear amplifier modules and integrated assemblies operating to 1 GHz with output power levels to 100 watts.

Motorola RF Linear IC Division

2100 E. Elliot Rd.
 Tempe AZ 85084
 602-897-3951
 Booth: 102,201,200,202

Products: Linear integrated circuits for RF transmitter and receiver applications.

Murata Erie North America, Inc.

2200 Lake Park Drive
 Smyrna GA 30080
 404-436-1300
 Booth: 210

Products: Discs, multilayer, microwave and trimmer capacitors, resistor networks, potentiometers, piezo alarms, RFI/EMI filters, resonators, power supplies, oscillators, flyback transformers, posistors, sensors, and associated electronic components.

Nedrud Data Systems

P.O. Box 27020
 Las Vegas NV 89126
 702-255-8080
 Booth: 615

Products: Dragonwave is linear microwave analysis/optimization software for Macintosh computers featuring integrated schematic capture, interactive graphics (continuous zoom, cursor readout, etc.) and an intuitive interface.

Newport Electro-Optics Systems, Inc. (NEOS)

4451-B Enterprise Court
 Melbourne FL 32934
 407-259-2090
 Booth: 116

Products: NEOS will be displaying our new microwave laser photo plotter, model N524000-MLPP and software package AutoCAT, automatic computer aided test.

Olektron Corp.

61 Sutton Road
 Webster MA 01570
 617-943-7440
 Booth: 115,117

Products: Signal processing components from DC thru UHF: complex phase modulators, polar phase comparitors, mixers, transformers, directional couplers, power dividers, attenuators, phase shifters, and integrated products.

Omni Spectra/M/A-COM Co.

140 Fourth Ave.
 Waltham MA 02254
 617-890-4750
 Booth: 608

Products: RF connector SMA, SMB, SMC, N, TNC & BNC series, between series adaptors, and blind mate connectors.

Philips Components Discrete Products Division

20001 W. Blue Heron Blvd.
 P.O. Box 10330
 Riviera Beach FL 33404
 407-881-3200
 Booth: 203,205

Products: Philips Components offers a broad range of: circulators, isolators, CATV, video & RF modules, RF small signal transistors, RF & microwave power transistors.

Philips Components-Signetics

811 E. Argues, P.O. Box 3409
 Sunnyvale CA 94088-3409
 408-991-2000
 Booth: 204,206

Products: Philips Components-Signetics is a world leader in RF. Product line offers solutions for cellular radio, cordless phones, two way communications and a variety of other applications.

Phonon Corporation

7 Herman Drive P.O. Box 549
 Simsbury CT 06070
 203-651-0211
 Booth: 513

Products: Surface acoustic wave products, signal processing components and subsystems including filters, dispersive delay lines and non-dispersive delay lines, convolvers and SAW spectrum analyzer subsystems.

Piezo Crystal Company

100 K Street
 P.O. Box 619
 Carlisle PA 17013
 717-249-2151
 Booth: 526

Products: Quartz crystals and crystal oscillators for commercial, military and aerospace applications especially utilizing SC cut crystals.

Piezo Technology

2525 Shader Rd. P.O. Box 547859
 Orlando FL 32854-7859
 407-297-8107
 Booth: 114

Products: Frequency control products consisting of monolithic and discrete crystal filters, LC filters, cavity band-pass filters, interdigital and combine filters, precision resonators, crystal oscillators and RF subassemblies.

Polyflon Company

35 River Street
 New Rochelle NY 10801
 914-636-7222
 Booth: 509

Products: High voltage, high power, high Q, nonmagnetic fixed, variable and trimmer capacitors, virgin Teflon

EXHIBITOR LIST

dielectric substrates and finished circuit boards, custom coil/antenna designs.

Power Systems Tech. Inc.
 63 Oser Ave.
 Hauppauge NY 11788
 516-435-8597
 Booth: 101, 103
 Products: Solid state RF power amplifiers and sub-systems 1 MHz to 4000 MHz. RF power output 2 watts to 2000 watts.

Q-bit Corporation
 2575 Pacific Ave., N.E.
 Palm Bay FL 32905
 407-727-1838
 Booth: 305
 Products: High dynamic range amplifiers featuring high reverse isolation and very low input and output VSWR in the .1 to 3 GHz frequency band. These amplifiers utilize our patented Power Feedback™ technology. Hybrid micro-electronic and coaxial packaging available.

Racal-Dana Instruments Inc.
 4 Goodyear Street
 Irvine CA 92718
 714-859-8999
 Booth: 216
 Products: Racal-Dana will show its latest range of VXIbus based RF products. These will include an RF and microwave chassis, microwave prototyping cards as well as the latest high performance time interval analyzer for VXI.

Retconn
 199 W. Pearl Road
 Torrington CT 06790
 203-489-1220
 Booth: 321
 Products: D-subminiature contacts. RDM, RDM-HF coaxial, high power and high voltage.

RF Design
 6300 S. Syracuse Way #650
 Englewood CO 80111
 303-220-0600
 Booth: 314
 Products: Sponsor of RF Expo East. Magazine serves RF engineers and engineering managers.

RF Monolithics, Inc.
 4441 Sigma Road
 Dallas TX 75244
 214-233-2903
 Booth: 225,227
 Products: SAW resonators, SAW filters and delay lines, SAW-stabilized frequency sources, high-frequency digital clocks, low power UHF transmitters and receivers.

RHG (A M/A-COM Company)
 5 Omni Way-Bldg. 22
 Chelmsford MA 01824
 617-272-3000
 Booth: 315,317
 Products: IF/RF/microwave and millimeter wave; connectors & adaptors,

cable assemblies, semiconductors, devices, switches, mixers, low noise amplifiers, and transistors. Custom and standards products available in all categories.

RLC Electronics
 83 Radio Circle
 Mt. Kisko NY 10549
 914-241-1334
 Booth: 321
 Products: Coaxial switches, filters, attenuators, couplers, detectors, high power switches and filters.

Sawtek Incorporated
 1818 South Hwy. 441
 Apopka FL 32703
 407-886-8860
 Booth: 107,109
 Products: SAW devices which include bandpass filters, low-loss filters, resonator filters, oscillators, delay lines, pulse expanders/compressors and custom subsystems that use SAW components. Sawtek also provides technical assistance for new design and production requirements at frequencies from 10 MHz to 2 GHz.

Sciteq Electronics, Inc.
 8401 Aero Drive
 San Diego CA 92123
 619-292-0500
 Booth: 209
 Products: Frequency synthesizers, including DDS, PLL, and combination designs.

SGS-Thomson Microelectronics Inc.
 211 Commerce Drive
 Montgomeryville PA 18936
 215-361-6400
 Booth: 403,405
 Products: RF and microwave power transistors (2 MHz - 4 GHz), RF and microwave power amplifiers & subsystems, silicon MMIC's, solid state noise sources.

Sokol Crystal Products Inc. (Sales)
 3001 Latham Drive
 Madison WI 53713
 608-273-0222
 Booth: 505
 Products: Fundamental crystals to 125 MHz, tubular filters, tubular crystals, monolithic crystal filters, VCXO's, VCO, MiL clock Osc, ECL clock oscillators, TCVCXO's, high frequency clock oscillator, surface mount packaging.

Sokol Crystal Products, Inc. (Manufacturing)
 121 Water Street
 Mineral Point WI 53565
 608-987-3363
 Booth: 505
 Products: Fundamental crystals to 125 MHz, tubular filters, tubular crystals, monolithic crystal filters, VCXO's, VCO, MiL clock Osc, ECL clock oscillators, TCVCXO's, high frequency clock oscillator, surface mount packaging.

Sprague-Goodman Electronics
 134 Fulton Avenue
 Garden City Park NY 11040
 516-746-1385
 Booth: 215
 Products: Trimmer capacitors (including air, ceramic, film, glass, mica, quartz, and sapphire dielectric); precision inductors; and surface mounted trimmer capacitors and inductors.

Stetco Inc.
 3344 Schierhorn Ct.
 Franklin Park IL 60131
 708-671-4208
 Booth: 105
 Products: Chip inductors, chip capacitors, feed-through capacitors and feed-through arrays, variable capacitors, high frequency coaxial connectors and connector/cable assemblies, choke coils, chip LED's.

Tampa Microwave Lab, Inc.
 8742 N. Mobley Rd.
 Odessa, FL 33556
 813-920-8822
 Booth: 424
 Products: Tampa Microwave Lab, Inc. manufactures phase locked oscillators, DRO's, and related products including phase locked satellite LNB's, for C and Ku band.

Thunderline-Z
 544 Route 111
 Hampstead NH 03841
 603-329-4050
 Booth: 101,103
 Products: Glass to metal sealing and microcircuit packaging.

Toko America Inc.
 1250 Feehanville Dr.
 Mt. Prospect IL 60056
 708-297-0070
 Booth: 515
 Products: Inductors: variable, molded, surface mount. Filters: fixed, noise, SAW, LC, helical; ceramic & dielectric filters & resonators. Audio/video filters, active, high definition. Power supplies, DC-DC converters, ICs/modules.

Toshiba America Electronic Components, Inc.
 One Parkway North Suite 500
 Deerfield IL 60015
 708-945-1500
 Booth: 527
 Products: SAW devices; filters 32.7 MHz-282 sMHz, SAW resonators 91.22 MHz-345 MHz. GaAs FETs; low noise FETs, HEMT FET, C-Band internally matched FET from 3.7-8.4 GHz.

TRAK Microwave Corp.
 4726 Eisenhower Blvd.
 Tampa FL 33634
 813-884-1411
 Booth: 503
 Products: Microwave synthesizers, oscillators (XCO, PLO, DSO, VCXO, VCO, TCXO), frequency multipliers, comb generators, switched filter banks, isolators, circulators, GPS station clock.

Trilithic Inc.
 9202 E. 33rd St.
 Indianapolis IN 46236
 800-344-2412
 Booth: 308
 Products: RF and microwave components, test equipment, and subsystems, including surface and PC mount miniature filters, coaxial, rotary, and programmable attenuators.

TRM, Inc.
 401 Kelly Ave., Grenier Field
 Manchester NH 03103
 603-627-6000
 Booth: 614
 Products: Directional couplers, power dividers, hybrids, phase comparators and custom components and subsystems using lumped elements and stripline designs.

Trontech, Inc.
 63 Shark River Road
 Neptune NJ 07753
 201-922-8585
 Booth: 616
 Products: RF & microwave amplifiers from 1 KHz to 6 GHz. Products include LNA's, broadband medium power and high power to 500 watts class AB.

TTE, Incorporated
 12016 115th Ave. N.E.
 Kirkland WA 98034
 206-821-5952
 Booth: 222,224
 Products: Active and passive electrical wave filters, including anti-aliasing, delay equalized video filters, programmable filters, filter systems, duplexers and duplexers covering the frequency range of 0.1 Hz to 500 MHz.

United Microwave Products Inc.
 22129 S. Vermont Ave.
 Torrance CA 90502
 213-320-1244
 Booth: 321
 Products: SMA, SSMA, SMB, SMC, TNC, BNC, adapters, cable assemblies and special connectors.

VARI-L Company, Inc.
 1101 E. 51st Avenue
 Denver CO 80239
 303-371-1560
 Booth: 211
 Products: Hi-performance VCO's, RF mixers, power dividers and impedance transformers. State-of-the-art thin film hybrid materials capability.

Vectron Laboratories, Inc.
 166 Glover Avenue
 Norwalk CT 06850
 203-853-4433
 Booth: 512
 Products: Crystal and non-crystal controlled oscillators from 0.1 Hz to 2 GHz; sinewave, TTL, CMOS, HCMOS, ACMOS, ECL, and ECLIPS, for commercial, military and space applications.

EXHIBITOR LIST

Voltronics Corporation
 West Street, P.O. Box 476
 East Hanover NJ 07936
 201-887-1517
 Booth: 516
 Products: Precision trimmer capacitors and tuners for DRO's and microwave cavity filters. QPL'D to MIL-C-14409. Wide variety of surface mount trimmers.

W.L. Gore & Associates
 1901 Barksdale Rd. P.O. Box 9236
 Newark DE 19714-9236
 302-368-3700
 Booth: 604
 Products: Gore microwave cable assembly DC-40 GHz RFI-EMI shielding and gasket material. Digital coax cable and assembly.

Wavetek
 9045 Balboa Avenue
 San Diego CA 92123
 619-450-9971
 Booth: 500,501
 Products: RF and microwave signal generators for both the field and lab work. RF and microwave power measurements, in swept, pulsed, peak or CW. Components and attenuators calibration system.

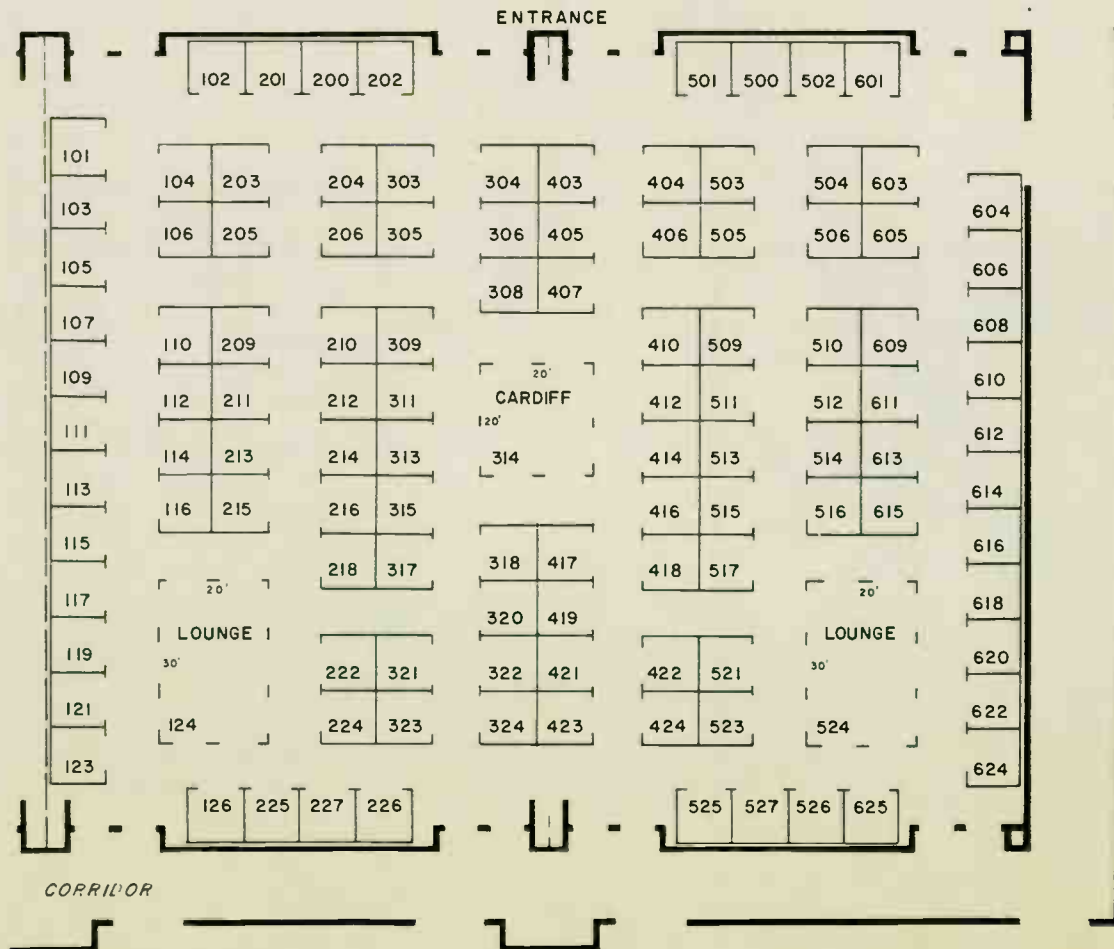
Webb Laboratories
 139 E. Capital Drive, Suite 4
 Hartland WI 53029
 414-367-6823
 Booth: 523
 Products: PC-based RF/microwave CAE tools for receiver/system simulation, network signal and noise optimization, filter synthesis, and transmission line synthesis.

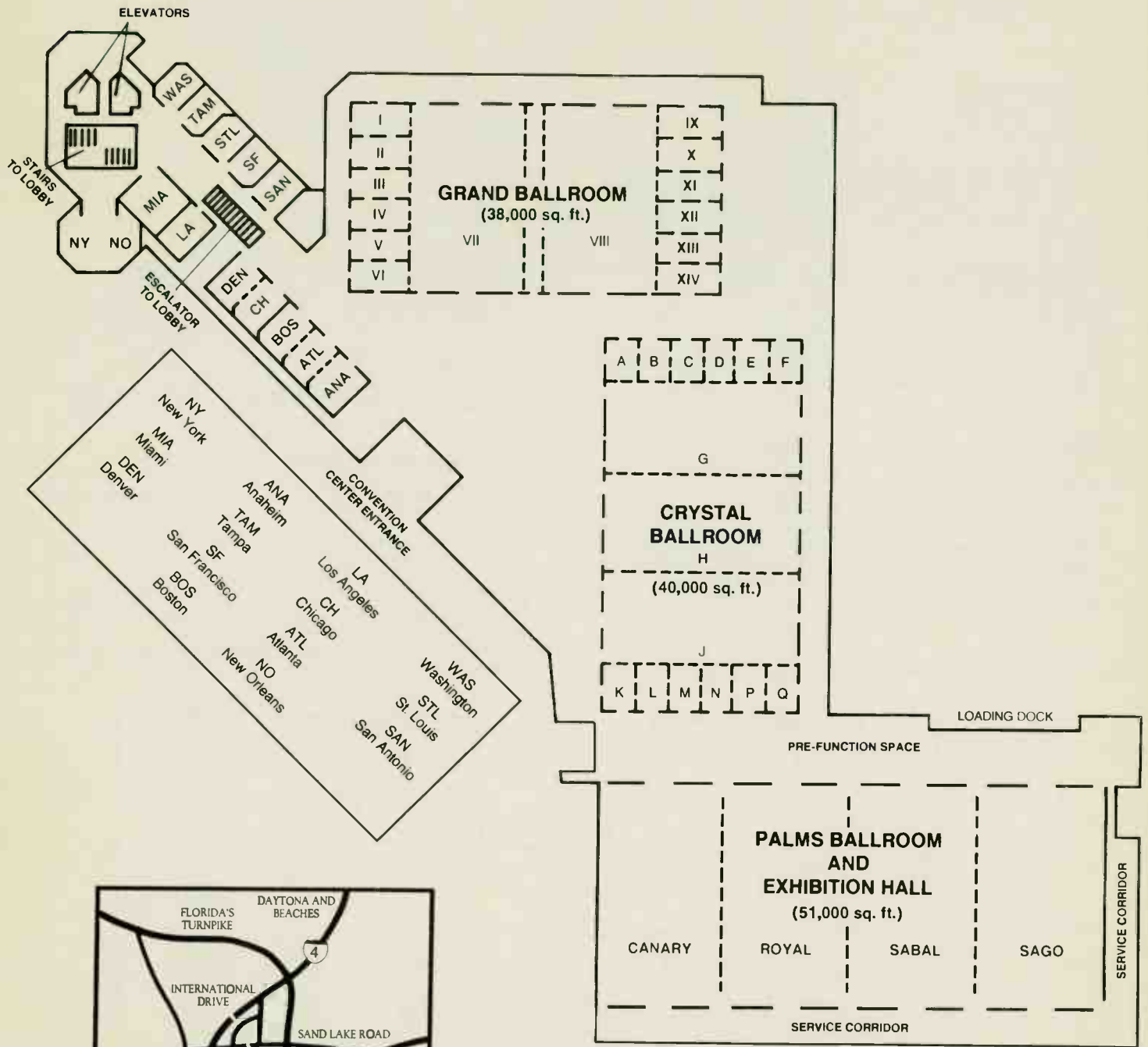
Wiltron Company
 490 Jarvis Drive
 Morgan Hill CA 95037-2809
 408-778-2000
 Booth: 525
 Products: RF and microwave test instrumentation including vector and scalar networks analyzers, synthesizers, and precision measurement components.

XL Microwave Inc.
 5811 Racine Street
 Oakland CA 94609
 415-428-9488
 Booth: 525
 Products: Microwave counters-3 GHz, 8 GHz, 12.4 GHz, 20 GHz, 26.5 GHz. Source locking counter-26.5 GHz with 1 Hz lock capability.

Advertising Index

Advantest America, Inc.	27
Amplifier Research	28
California Eastern Laboratories	7
Ford Motor Co., Electronics Division	25
Programmed Test Sources	2
Q-Bit Corp.	11
TTE, Inc.	16





Easily Accessible From Interstate 4
Take Exit 26A then 536 East



8701 World Center Drive
Orlando, Florida 32821

NEW PRODUCTS

Digital Signal Processing/ADC Test and Development System

Burr-Brown Company
 Booth 104
 The new Burr-Brown DSP-SYS604 PC-based DSP system offers designers a cost-effective way to test, evaluate and develop applications for the high dynamic range ADC604 A/D converter. The system may be used to analyze device performance, measure specification profiles, or for high speed signal conversion for a DSP processor. The DSP-SYS604 system comes complete with analog signal input system, 50 MHz DSP32C processor board, digital input buffer, dynamic signal analysis software, DSP code generation software, and power supply.

Class AB Linear Amplifier

Power Systems Technology, Inc.
 Booth 101,103
 Model BHE 4819-500 is a solid state, 500 watt amplifier operating in the 400-1000 MHz frequency range featuring class AB operation, 600 MHz bandwidth, 57 dB of overall minimum gain and is fully protected. AM distortion at 85 percent depth of modulation is 10 percent maximum and two-tone intermode is -20 dBc referenced to 500 watts PEP.

Miniature Surface Mount Filter Packages

Piezo Technology, Inc.
 Booth 114
 Piezo Technology has developed miniature, leaded and leadless surface mount filter packages. The user is required to supply the input and output impedance matching networks. The leadless packages may contain two to four poles of selectivity, and the leadless technology has been integrated into a leaded configuration that incorporates the matching networks.

Long Pulse Microwave Power Transistor

Motorola
 Booth 102,201,200,202
 Motorola has released the MRF10120, a long pulse microwave power transistor. It will deliver 120 watts of peak power for typically less than 15 watts of peak RF input power over the frequency band from 960 to 1215 MHz. The MRF10120 is supplied in a hermetic metal-ceramic package and is aimed at both military applications (specifically JTIDS) and commercial applications such as Mode S transmitters.

Microwave Reflection Analyzer

Millimeter Wave Technology, Inc.
 Booth 313
 The BEKISCAN[®] CP from Millimeter Wave Technology quantifies shielding effectiveness of conductive stainless steel fibre loaded plastic parts. It has an operating frequency of 10.525 GHz with frequency stability of ±25 MHz. It can also be used to characterize microwave absorption of RAM com-

posites, and determine paint and/or coating effects on surfaces.

Low Phase Noise OCXO

Piezo Crystal Company
 Booth 526
 Part Number 2900082 is a low profile, low phase noise OCXO that utilizes Piezo's SC cut crystals. The frequency range is 5 to 15 MHz, and typical phase noise at 10 MHz is -110 dBc/Hz at 10 Hz, -140 dBc/Hz at 100 Hz, and -160 dBc/Hz at 1 kHz. The size is 2" x 2" x 0.75".

Hybrid Plug-In Programmable Attenuators

JFW Industries, Inc.
 Booth 618
 JFW Industries has introduced a new line of hybrid plug-in programmable attenuators available in 50 ohm terminations in the frequency range of 50 to 500 MHz. The attenuation range for these items are 0-31 dB in 1 dB steps, and their switching speed is 5 microseconds.

75 Ohm Component Analyzer

Hewlett Packard Company
 Booth 410,412,414,416
 The HP 8752B RF Network Analyzer is a fully integrated RF component test system for 75 ohm applications, including CATV components and cables. It gives the characterizations of gain, impedance, phase and group delay for components in the 300 kHz to 3 GHz frequency band.

EMI Suppression Filter Sample Kit

Murata Erie North America
 Booth 210
 Murata Erie has released sample kit EK115A, which contains 220 chip EMI filter components for filtering EMI/RFI. Included are a wide variety of Murata Erie's BLM series solid ferrite devices and the NFM series of EMI filters.

Microwave IC Design Libraries

EEsof, Inc.
 Booth 404,406
 EEsof's SMART libraries combine an electrical simulation model for MMIC circuit elements with the corresponding element's physical layout model, linking simulation and layout. SMART libraries work with EEsof's Touchstone[®] and Libra[®] circuit simulators operating within the ACADEMY graphical design environment.

Variable Voltage Switching Power Supplies

Component Distributors, Inc.
 Booth 126
 Component Distributors has released a line of three and four output variable voltage switching power supplies manufactured by Zenith. Also available are switching power supplies with five and six outputs.

Multi-layer Adjustable Chip Capacitor Kit

American Technical Ceramics Corporation

Booth 418

American Technical Ceramics is offering a design kit for STA-TUNE[™] Multilayer Adjustable Chip Capacitors. The kit contains 3 pieces each of 22 values ranging from 1 to 68 pF, with adjustment ranges of 0.15 pF to 3 pF. The kit (ST2001) is priced at \$199.95.

140 MHz SAW Filters

Sawtek Inc.
 Booth 107,109
 Sawtek has announced a new line of 31 standard SAW filters at a center frequency of 140 MHz in addition to its line of 70 MHz devices. These filters feature excellent amplitude and phase linearity with steep skirts and high out-of-band rejection. Bandwidths range from 0.25 MHz to 80.0 MHz. They are available for off-the-shelf delivery.

Circuit Simulation Software

Eagleware Corporation
 Booth 213
 SuperStar Professional Extension is a high speed real-time circuit simulation, tuning and optimization package. The professional extension version includes Monte Carlo statistical analysis, use equation definitions, and microwave models.

High-Frequency Digital Clock

RF Monolithics
 Booth 225,227
 The HC1253 is a high-frequency digital clock for computer graphics by RF Monolithics. This clock operates at 262.074 MHz and is designed for applications in graphics cards supporting high-resolution 2048 x 1536 pixel displays. Small quantity pricing for the HC1253 is \$150 each.

Surface Mount Trimmer Capacitors

Sprague-Goodman Electronics, Inc.
 Booth 215
 Sprague-Goodman Electronics has announced the addition of gull-wing leaded models to their line of Surftrim[®] surface mounting ceramic dielectric trimmer capacitors. Models in the series are available in bulk pack and carrier-and-reel pack on 700 and 3,000 piece reels. Seven capacitance ranges (from 1.7-3.0 pF to 13.0-50 pF) are available.

Two-way Power Divider

TRM Incorporated
 Booth 614
 Model SDL 260 is a two-way power divider which operates over the 1 MHz - 600 MHz frequency range. Maximum insertion loss is 0.6 dB; minimum isolation is 26 dB, and VSWR (output) is 1.4:1. Amplitude balance is 0.2 dB, and phase balance is 2 degrees maximum. It comes in a surface mount package.

High Power Amplifier

Trontech
 Booth 616
 Part number P1020-43-PS is a 20 Watt, class A, linear power amplifier

covering the 1000 to 2000 MHz range. Specifications for the unit include output power at 1 dBc of 43 dBm minimum and VSWR of 1.5:1 typical. Applications include EMI testing, communications transmitter, and general RF and microwave laboratory equipment for research.

Miniature Low Noise Ultra-Stable Crystal Oscillator

Vectron Laboratories, Inc.
 Booth 512
 Type CO-705SL2 provides aging of 5 x 10⁻¹⁰ per day and 1 x 10⁻⁷ per year. Temperature stability is ±1 x 10⁻⁹ over the 0 to +50 degree Celsius range and ±1 x 10⁻⁸ over the -55 to +85 degree Celsius range. Phase noise is -130 dBc/Hz at 10 Hz with a floor better than -168 dBc/Hz. Standard output in the 4-34 MHz range is +7 dBm with HCMOS/TTL optional.

Monolithic Ceramic EMI Filters

Ceramic Devices
 Booth 106
 Ceramic Devices is offering a line of monolithic ceramic EMI filters in both solder-in and screw-in configurations. These filters provide a case diameter of 0.086 inches in C, L, Pi, and T circuits with up to 10,000 pF of capacitance at 50 VDC.

Feed-Through Capacitors and Pi-Filter Arrays

Stetco Incorporated
 Booth 105
 Stetco now manufactures a wide assortment of ceramic feed-through capacitor and Pi-filter arrays which are used in a variety of RFI suppression applications. These arrays are built to meet each customer's requirements and engineering specifications.

Programmable Attenuator

Trilithic Incorporated
 Booth 308
 Trilithic has released a programmable attenuator that covers the DC to 1 GHz range for 50 ohm loads and the DC to 650 MHz range for 75 ohm loads. It has insertion loss as low as 0.15 dB per cell and accuracy as good as ±0.1 dB. Prices start at \$138 each in quantities of 1-9.

Linear Voltage Variable Attenuator

Q-bit Corporation
 Booth 305
 The QBH-723 is a high reliability, hybrid, linear voltage variable attenuator in a 5-pin, TO-8 package. The unit operates over a frequency range of 20 to 500 MHz with a typical VSWR of 1.5:1 on the input and output ports and a linear range (dB/V) of at least 11.0 dB. Deviation from linearity is typically less than ±0.6 dB.

RF Circuit Optimizer Update

Nedrud Data Systems
 Booth 615
 Nedrud Data Systems has released DragonWave 2.0, a graphical design and optimizing software package for

NEW PRODUCTS

RF circuits on Macintosh computers. Black box data can be entered in Y- and Z-parameters as well as S-parameters. The element library includes stripline elements, coupled lines, tees, and other components. It works in kHz, MHz, and GHz.

Direct Digital Synthesizer Sciteq Electronics, Inc. Booth 209

Sciteq Electronics has introduced the DDS-1, a multi-mode DDS on one square inch, with digital phase and amplitude control. The waveform generator dissipates 1.5 watts and fits a standard 84-pin chip carrier.

750 Watt Amplifier Amplifier Research Booth 504,506

Model 750HB is a broadband amplifier that delivers a minimum of 750 watts CS through a bandwidth of 400 to 1000 MHz. Minimum gain is 58 dB, flatness is ± 1.5 dB at 1 mW input, input and output impedance is 50 ohms, VSWR is 2.0:1, and third-order intercept point is 66 dBm typically. It includes a front panel power meter for monitoring forward and reflected power an internal/external automatic level control sensing capability.

Low Cost Modulation Meter Boonton Electronics Corporation Booth 423

The Boonton Model 8220 Modulation meter has a carrier range of 10 MHz to 1.3 GHz and a level meter from -27 to +19 dBm with 0.01 dB resolution. Carrier acquisition and modulation display are totally automatic, and RMS detection is also available for residual modulation measurements. The Model 8220 is priced at \$5,995.

Miniature Diplexers TTE Incorporated Booth 222,224

TTE has just released a line of miniature diplexers that cover the frequency range of 20 kHz to 100 MHz. They are available with contiguous or noncontiguous passbands and are available in lowpass, highpass, or bandpass configurations. The lowpass frequency cased is $2'' \times 5.75'' \times 0.75''$ while the packages for units above 100 kHz is $2'' \times 4.75'' \times 0.5''$.

RF Prototyping Card for VXIbus Racal Dana Instruments, Inc. Booth 216

Model 7065 allows RF and microwave instruments and subsystems to be designed into the VXIbus format. The card features a carefully engineered enclosure which ensures an EMI sealed environment while providing highly-efficient heat dissipation. Prices begin at \$2495.

Ultrafast GaAs MMIC Switch M/A-COM, Anzac Division Booth 315,317

Anzac's newest GaAs MMIC switch (SW-256) works in the 5-1000 MHz

frequency range and switches in 50 nsec typically. It consumes 2.2 mA of DC power typically, and isolation is 35 dB minimum from 5-1000 MHz and 50 dB minimum from 5-500 MHz. The SW-256 is priced at \$129.95.

Four Channel Simultaneous Sampling ADC Analog Devices Booth 610

The AD7874, a monolithic four-channel simultaneous sampling ADC from Analog Devices, has 71 dB minimum SNR at 29 ksp/s. Maximum aperture delay deviation is 40 ns, and maximum peak spurious noise, intermodulation distortion, and total harmonic distortion are each 80 dB. Prices begin at \$28 in 100s.

Lightweight Coaxial Cable Assemblies W. L. Gore & Associates, Inc. Booth 604

W. L. Gore & Associates has introduced the CX Series GORE-TEX[®] RF coaxial cable assemblies for low-frequency applications to 1000 MHz. These assemblies are 30 percent lighter than RG type cables and have VSWR of 1.2:1. Optical power measurement range is +5 to -25dBm.

800 MHz Si MMIC Amplifier Avantek, Inc. Booth 417

Avantek is now offering an advanced silicon bipolar low noise, high gain amplifier with a 3 dB bandwidth of DC to 800 MHz. The INA-02184 and INA-02186 amplifiers offer 31 dB gain, 2 dB noise figure, and +11 dBm output power at 1 dB compression.

Spectral Linewidth Analyzer Anritsu America, Inc. Booth 123

The MS9602A is an optical linewidth analyzer from Anritsu that measures the spectral width of light sources operating in the 1.3 and 1.55 μ m bands. The analyzer has resolution of 20 kHz and has light receiver flatness of 0.3 dB. Linewidth measurement range is 20 kHz to 100 MHz for heterodyne measurements and 1 to 500 MHz for homodyne measurements. The MS9602A costs \$45,090.

Resistors, Terminations, and Attenuators Florida RF Labs, Inc. Booth 608

Florida RF Labs introduces a new line of Acrian equivalent resistors, terminations, attenuators. Manufactured using high-temperature brazing, these new components meet or exceed Acrian power ratings while maintaining low VSWR and capacitance.

Extended Range NMR Amplifier ENI Booth 422

The NMR-300L/50M produces 300 watts of pulse power over the frequency range of 5-220 MHz, reducing

to 150 watts up to 250 MHz, and 50 watts from 200-600 MHz. Rise time is less than 1 μ s and fall time is less than 150 ns. It is available for \$12,500.

Industrial RF Power Supply Ehrhorn Technological Operations, Inc. Booth 514

ETO has introduced the PG-5DW, a fully automatic, water cooled 5 kW industrial RF power supply/amplifier for excitation of CO₂ lasers and other plasma applications. It operates on any factory set frequencies between 10 and 90 MHz.

Shielding Integrity Monitor Lindgren RF Enclosures Booth 115,117

Lindgren RF Enclosures has released a self-testing automatic RF integrity tester for permanent installation, with fiber optic control and status lines, and an optional search loop antenna for RF leakage source location.

MIC Hybrid Amplifiers JCA Technology Booth 115,117

JCA Technology has released a MIC hybrid 20-22 GHz amplifier line. The amplifiers can be manufactured to military specifications with bandwidth ranges from 500 MHz to 2 GHz. Gain levels range from 15 dB to 40 dB and output power is +10 dBm at 1 dB compression.

Microwave Laser Photo Plotter Newport Electro-Optics Systems, Inc. Booth 116

The model N524000-MLPP system plots a microwave mask from an AutoCAD drawing file in less than one-half hour, with no post processing. It accommodates up to a 6'' x 6'' substrate size and plots a 0.001'' line and space. The system includes software with pull-down menus and conversion of AutoCAD drawing file to photo mask.

Dielectric Filters Toko America, Inc. Booth 515

Toko America has introduced 2-pole and 3-pole dielectric bandpass filters for spread spectrum applications. These filters feature a passband from 902-928 MHz. Insertion loss is 1.8 dB max, VSWR is 2.0 max and 20 dB attenuation is at FO +77.5 MHz. Product applications include wireless electronics, RF data/control, and LANs.

1 GHz Attenuator Merrimac Industries, Inc. Booth 304,306

Merrimac Industries has released a new attenuator, AEF-35A, that covers the 2 to 1000 MHz frequency range and provides a minimum of 35 dB of attenuation across the frequency band. The AEF-35A can be supplied screened to meet military and space applications.

MMIC LED Driver California Eastern Laboratories, Inc. Booth 407

The UPC1684 MMIC LED Driver from NEC has high speed current switching — to 300 Mb/s NRZ, 1.4 nsec fall time, and 1.0 nsec rise time. It accepts standard ECL level inputs and is available in a hermetically sealed package or in chip form.

Clock Oscillator with Tri-State Capability CTS Corporation Booth 323

The CXO-63GAU clock oscillator from CTS is available up to 110 MHz and offers CMOS/TTL compatible output with tri-state capability. Symmetry is 48 percent/52 percent typical (at 50 percent level). The oscillator features an internal pull-up resistor allowing for standard clock operation.

Wideband Variable Gain Amplifier Philips Components—Signetics Booth 204,206

The NE5209 wide band variable gain amplifier from Signetics has a gain bandwidth out to 1.5 GHz and a linear gain control range that allows precise AM modulation. It can be used to simplify automatic gain control applications.

RF Series Attenuators Compac Development Corporation Booth 510

This series of attenuators from Compac Development has attenuation at or above 80 dB out to 20 GHz. The attenuators are available off the shelf or can be customized to client specifications.

Miniature 200 Watt Amplifier LCF Enterprises Booth 605

LCF Enterprises has released a miniature 200 Watt amplifier featuring 55 percent efficiency over the 150-250 MHz frequency band. Compressed gain is 37 dB with variable control. The package size is 4.84'' x 2'' x 1'' without a heat sink.

Low Cost Switches Micronetics, Inc. Booth 226

Micronetics Electronics Division has introduced low cost SP1T and SP2T switches for commercial applications. Typical isolation is 50 dB with insertion loss of 0.75 dB up to 4 GHz. Prices are \$49 and \$69 in quantities.

Spectrum Analyzers Advantest America, Inc. Booth 609

The R3261/R3361 Series of synthesized spectrum analyzers offer frequency ranges of 9 kHz to 2.6 GHz and 9 kHz to 3.6 GHz, depending on the model. The analyzers have a display dynamic range of 120 dB and an overall accuracy level of 1 dB.

Experienced Design Engineers:

Technology Moves Fast At Ford

At Ford Electronics Division, we don't wait for technology, we move it forward. Our engineers are employing the most advanced resources available to design and develop innovations in automotive electronics. If you're an Electrical or Mechanical Engineer with 3 or more years experience looking for a variety of technical challenges, join us at Ford Electronics Division.

CELLULAR TELEPHONE ENGINEERS

Electronics Packaging

We prefer a BS/MSME and a background in:

- Mobile electronics/communications systems
- Decorative plastics and lighting
- SMD board layout
- Knowledge of Design for Assembly methods, SPC and other statistical methods
- Working knowledge of ergonomics

RF Design

We prefer a BS/MSEE and a background in:

- Cellular design methods
- EMI/EMC
- Mobile communication equipment
- SMD and RF devices

Systems/Audio

We prefer a BS/MSEE and a background in:

- Vehicle applications of cellular telephones, including systems integration with IP and Audio Systems
- EMI/EMC and suppression
- Audio system development
- Knowledge of cellular system operation and transceiver software requirements

VEHICLE NAVIGATION/REMOTE ENTRY SYSTEMS ENGINEERS

We prefer a BS/MSEE or BS/MSME and a background in:

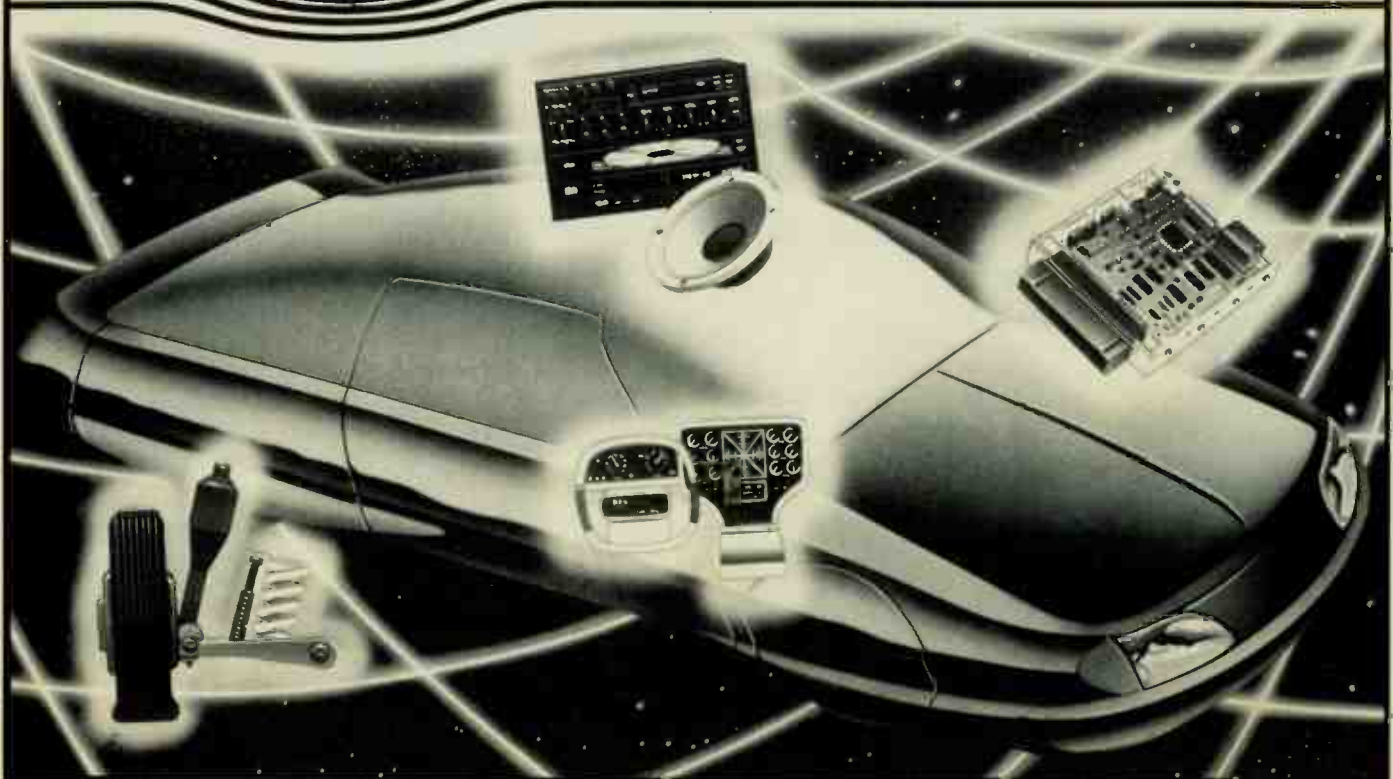
- Digital transmission transmitter/receiver design, test, and proveout to prepare for high volume manufacturing
- Antenna evaluation and characterization
- Design of input receiver circuitry
- Vehicle communications products design using RF or IR, including printed circuit board layout considerations, with design and production responsibilities.

We will provide you with a competitive salary, comprehensive benefits, and opportunities for advancement. If you would like a career with a company that moves technology forward, submit your resume in confidence to:

Ford Motor Company
Electronics Division
Product Engineering Office
Room E-130, RF1190-DK
Post Office Box 6010
Dearborn, Michigan 48121

By choice, we are an Equal Opportunity Employer.

Electronics Division



STAFF



Kathy Kriner
Vice President



Kathi Walsh
Publisher



Gary Breed
Editor



Kristin Hohn
Convention Manager



Liane Pomfret
Assistant Editor



Charles Howshar
Technical Editor



Bill Pettit
Account Executive



Cindy Wieland
Account Executive



Maryanne Averill
Account Executive



Theresa Maier
Administrative
Assistant



LeAnn Nowacki
Customer Service
Representative



Barb Binge
Registration
Coordinator



Dick Purcell
Marketing
Manager



One Card for EMI Measurements



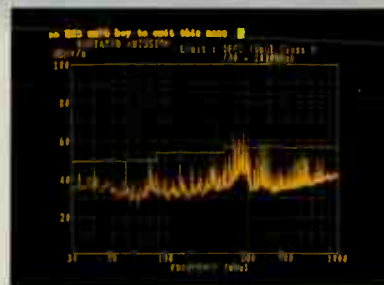
Photo: R2542B EMI Receiver System, connected to R3261/3361 Series Spectrum Analyzer with R3551 Preselector Antenna, and Plotter.

The R3261/3361 Series Spectrum Analyzers are ideally suited for RF signal analysis and offer superior functions and capabilities for EMI measurements.

Featuring the unique Advantest quasi-peak detection scheme, these analyzers offer a full 70dB dynamic range.

The IC memory card function simplifies operation and reduces the time required for routine measurements.

Difficult tasks are made easy by taking full advantage of the IC memory card and instrument controller. Using these two powerful features together allows the user to:



- Enter antenna correction factors
- Display measurements in a log/log format
- Display limit lines for FCC, VDE and VCCI standards
- Add the R3551 preselector for additional sensitivity, selectivity and protection from noise

ADVANTEST®

Advantest America, Inc.

300 Knightsbridge Parkway,
Lincolnshire, IL 60069, U.S.A.

Phone: (708) 634-2552 Facsimile: (708) 634-2610

Advantest UK Limited

Cl Tower, St. Georges Square, High Street,
New Malden, Surrey, KT3 4HH, U.K.

Phone: (01) 336-1606 Facsimile: (01) 336-1657

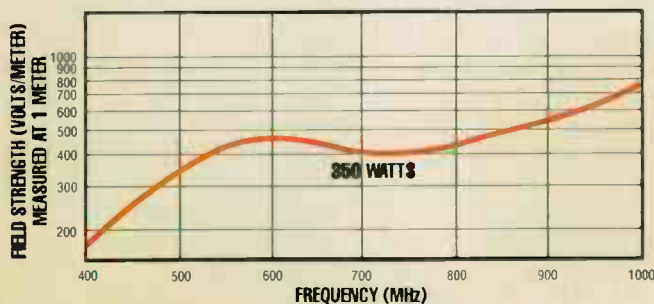
See us at the RF Expo East, Booth #609.

World Radio History



Testing for rf susceptibility to 200 volts/meter? You need the power to do it.

If you're lining your shielded room with anechoic material to avoid multipath reflections, you already know you need an amplifier with infinite-VSWR tolerance. But you also



need an amplifier/antenna marriage made in heaven.

Here is one of our many matched systems specifically designed to assure you reliable field levels as high as 1,000 V/m.

Our new Model 300HB power amplifier delivers a *minimum* of 350 watts through a bandwidth of 400 to 1,000 MHz. And our Model AT4001 horn antenna dis-

plays the happy faculty of putting out more V/m as the frequencies rise.

Other matched systems of AR amplifiers and antennas cover the frequency spectrum from 10 kHz to 1 GHz with reliable power from one to 2,000 watts. Systems that give you the reserve power you're bound to need sooner than you may think. Systems that let you sweep clean through the band of interest without the headache and delay of changing antennas.

Why not chat—on our nickel—with one of our applications engineers about *your* rf susceptibility-testing situation? He'll answer the phone himself when you dial

1-800-933-8181

AR **AMPLIFIER
RESEARCH**

160 School House Road, Souderton, PA 18964-9990 USA
215-723-8181 • TWX 510-661-6094 • FAX 215-723-5688

See us at the RF Expo East, Booths #504, 506.

World Radio History

